

FINAL RESEARCH REPORT

Defense Coastal/Estuarine Research Program (DCERP1)
Final Research Report

SERDP Project RC-1413

MAY 2013

Dr. Pat Cunningham
RTI International

This document has been cleared for public release



This report was prepared under contract to the Department of Defense Strategic Environmental Research and Development Program (SERDP). The publication of this report does not indicate endorsement by the Department of Defense, nor should the contents be construed as reflecting the official policy or position of the Department of Defense. Reference herein to any specific commercial product, process, or service by trade name, trademark, manufacturer, or otherwise, does not necessarily constitute or imply its endorsement, recommendation, or favoring by the Department of Defense.

REPORT DOCUMENTATION PAGE			Form Approved OMB No. 0704-0188	
Public reporting burden for this collection of information is estimated to average 1 hour per response, including the time for reviewing instructions, searching existing data sources, gathering and maintaining the data needed, and completing and reviewing this collection of information. Send comments regarding this burden estimate or any other aspect of this collection of information, including suggestions for reducing this burden to Department of Defense, Washington Headquarters Services, Directorate for Information Operations and Reports (0704-0188), 1215 Jefferson Davis Highway, Suite 1204, Arlington, VA 22202-4302. Respondents should be aware that notwithstanding any other provision of law, no person shall be subject to any penalty for failing to comply with a collection of information if it does not display a currently valid OMB control number. PLEASE DO NOT RETURN YOUR FORM TO THE ABOVE ADDRESS.				
1. REPORT DATE (DD-MM-YYYY) 10-05-2013		2. REPORT TYPE Final Technical Report		3. DATES COVERED (From - To) November 2007-September 2012
4. TITLE AND SUBTITLE DCERP1 Final Research Report		5a. CONTRACT NUMBER W912HQ-07-C-0002.		
		5b. GRANT NUMBER		
		5c. PROGRAM ELEMENT NUMBER		
6. AUTHOR(S) Drs. P. Cunningham, I. Anderson, K. Baumann, M. Brush, N. Christensen, C. Currin, J. Fraser, M. Fonseca, S. Karpanty, J. Morris, J. McNinch, H.Paerl, P.Piebler, A. Rodriguez, C. Tobias, and. J Walters.		5c. PROJECT NUMBER SERDP RC-1413		
		5e. TASK NUMBER		
		5f. WORK UNIT NUMBER		
7. PERFORMING ORGANIZATION NAME(S) AND ADDRESS(ES) RTI International Building 09 3040 Cornwallis Road PO Box 12194 Research Triangle Park, NC 27709-2194		8. PERFORMING ORGANIZATION REPORT NUMBER		
9. SPONSORING / MONITORING AGENCY NAME(S) AND ADDRESS(ES) SERDP/ESTCP 4800 Mark Center Drive Suite 17D08 Alexandria, VA 22350-3605		10. SPONSOR/MONITOR'S ACRONYM(S)		
		11. SPONSOR/MONITOR'S REPORT NUMBER(S)		
12. DISTRIBUTION / AVAILABILITY STATEMENT Approved for public distribution; distribution is unlimited.				
13. SUPPLEMENTARY NOTES				
14. ABSTRACT The Defense Coastal/Estuarine Research Program (DCERP) is a research-based program that was sited at Marine Corps Base Camp Lejeune (MCBCL), NC. The overall objective of DCERP was to help ensure that MCBCL sustains military training and testing activities using adaptive management based on a relevant and applied monitoring and research program. This program provides a unique opportunity to integrate the results of broadly scoped ecological research to understand the structure and function of diverse coastal ecosystems, while directly integrating this research to address the Base's management needs. To facilitate an understanding of the ecosystem state and dynamics of MCBCL, the following five ecosystem modules were established for monitoring, modeling, and research: the Aquatic/Estuarine, Coastal Wetlands, Coastal Barrier, Terrestrial, and Atmospheric modules and a Data Management Module. This report includes the results and conclusions from the 13 research projects conducted at MCBCL during the first cycle of the DCERP (July 2007 to September 2012).				
15. SUBJECT TERMS Military training impacts, ecosystem-based management, coastal wetlands, coastal barrier, atmospheric, aquatic-estuarine, terrestrial, RCW, prescribed burning, longleaf pine				
16. SECURITY CLASSIFICATION OF:			17. LIMITATION OF ABSTRACT	18. NUMBER OF PAGES 1156
a. REPORT Unclassified	b. ABSTRACT Unclassified	c. THIS PAGE Unclassified		
				19a. NAME OF RESPONSIBLE PERSON Pat Cunningham
				19b. TELEPHONE NUMBER (include area code) 919-316-3722

Table of Contents

Abstract.....	v
Executive Summary	ES-1
Chapter 1. Introduction	1-1
Chapter 2. Significant Findings and Management Implications.....	2-1
Chapter 3. Develop and Deploy Microalgal Indicators as Measures of Water Quality, Harmful Algal Bloom Dynamics, and Ecosystem Condition (Research Project AE-1).. 3-1	
Chapter 4. Quantifying and Predicting Watershed Inputs of Nutrients, Sediments, and Pathogens to Tributary Creeks on Marine Corps Base Camp Lejeune (Research Project AE-2)	4-1
Chapter 5. Developing Indicators of Ecosystem Function for Shallow Estuaries: Benthic Functional Responses in the New River Estuary (Research Project AE-3).....	5-1
Chapter 6. Development and Application of Watershed and Estuarine Simulation Models for the New River Estuary (Research Projects AE-2 and AE-3)	6-1
Chapter 7. Drivers and Forecasts of the Responses of Tidal Salt Marshes to Sea Level Rise (Research Project CW-1).....	7-1
Chapter 8. Forecasting Influence of Natural and Anthropogenic Factors on Estuarine Shoreline Erosion Rates (Research Project CW-2).....	8-1
Chapter 9. Hydraulic Exchange and Nutrient Reactivity in the New River Estuary Wetlands (Research Project CW-3).....	9-1
Chapter 10. Short-Term Barrier Evolution: Overwash at Onslow Beach Through Assessment of Training Activities and Model Predictions (Research Project CB-1) ...	10-1
Chapter 11. Long-Term Barrier Evolution Related to Variations in Underlying Geology and Land Use (Research Project CB-2).....	11-1
Chapter 12. Understanding the Top-Down and Bottom-Up Drivers of Shorebird Nest Success and Habitat Use in Relation to Beach Management Practices on MCBCL (Research Project CB-3).....	12-1
Chapter 13. Effects of Different Understory Restoration Management Options on Terrestrial Ecosystem Structure and Function (Research Project T-1).	13-1

Chapter 14. Effects of Habitat Management for Red-Cockaded Woodpeckers on Bird Communities (Research Project T-2).....	14-1
Chapter 15. Optimization of Prescribed Burning by Considering Mechanical Thinning as a Viable Land Management Option (Research Project Air-1	15-1
Chapter 16. Nitrogen Deposition to Terrestrial and Aquatic Ecosystems (Research Project Air-2).....	16-1

Abstract (DCERP1 Research Report)

Objectives

Critical military training and testing on lands along the nation's coastal and estuarine shorelines are increasingly placed at risk because of development pressures in surrounding areas, impairments due to other anthropogenic disturbances, and increasing requirements for compliance with environmental regulations. The U.S. Department of Defense (DoD) intends to enhance and sustain its training and testing assets and to optimize its stewardship of natural resources through the development and application of an ecosystem-based management approach on DoD installations. To accomplish this goal, particularly for installations in estuarine/coastal environments, the Strategic Environmental Research and Development Program (SERDP) launched the Defense Coastal/Estuarine Research Program (DCERP) as a minimum 10-year effort at Marine Corps Base Camp Lejeune (MCBCL) in North Carolina. The results of the first six years of the program (DCERP1) are presented here.

The overarching objectives of DCERP are to: (1) understand the effects of military training activities, infrastructure development, and other anthropogenic stressors, as well as natural disturbances, on the coastal ecosystems at MCBCL and other coastal military installations; (2) develop models, tools, and indicators to evaluate ecosystem health; and (3) recommend adaptive management strategies to sustain ecosystem natural resources within the context of an active military installation.

Technical Approach

DCERP1 was implemented in two phases. Phase I of the program was a planning period that was conducted between November 2006 and June 2007 and resulted in the development of the *DCERP Strategic Plan*, the *DCERP Baseline Monitoring Plan*, and the *DCERP Research Plan*, which collectively serve as the foundation for DCERP activities at MCBCL. Implementation of these plans (Phase II) began in July 2007 and resulted in the establishment of more than 350 monitoring and research sites, completion of 13 research projects, and development of the Data Information and Management System (DIMS). DIMS currently archives DCERP1 monitoring and research data and provides a standard data format that optimizes data storage and retrieval for integrated analysis, allowing for exchange of information among the various DCERP1 partners and other interested researchers and stakeholders.

During Phase I, the DCERP1 Team developed the overall approach that was implemented during Phase II and used to meet the program's objectives. This approach started with identifying ecosystem processes and stressors and developing an overarching conceptual model for DCERP1 that included four ecological modules: the Aquatic/Estuarine Module, the Coastal Wetlands Module, the Coastal Barrier Module, and the Terrestrial Module. Because the atmosphere has an overarching influence on all four ecosystem modules, it was treated as a fifth ecosystem module (i.e., the Atmospheric Module). After developing the overall conceptual model (and conceptual models for individual modules), the DCERP1 Team identified knowledge gaps in the models, worked with the installation staff to identify the needs of MCBCL management, and then

determined potential research questions to address these basic knowledge gaps and management needs.

Because DCERP1 was designed to be an adaptive program, the *DCERP Baseline Monitoring Plan* was developed to gather environmental data to address MCBCL's management concerns and support the 13 research projects. The monitoring activities established important baseline conditions in each of the modules against which changes in ecosystem processes from both military training activities, other non-military stressors, and natural phenomena (i.e., extreme events including hurricanes, droughts) could be measured. The monitoring activities also provided data at the temporal frequencies and spatial extents needed to assess variability in the environmental parameters of importance and were used to inform and validate ecosystem models. Results from the research projects fed back into the adaptive monitoring efforts so that changes in sampling frequency, spatial scale of sampling locations, or parameters to be sampled could be adapted as necessary. Results were used to identify ecosystem indicators and develop associated threshold values, tools, or design models that address MCBCL's management needs. This information was communicated to MCBCL personnel to assist them in making decisions about what type of management actions could be taken to mitigate the effects of military-related activities on the ecosystems.

Results

Key Scientific Findings

The first objective of DCERP1 was to provide basic scientific information needed to help understand the physical, chemical, and biological processes associated with the coastal ecosystems of MCBCL. The main findings associated with these processes included the hydrodynamics of the New River Estuary (NRE) and the adjacent coastal system, sediment transport among all four MCBCL ecosystems (i.e., terrestrial lands, streams and estuary, coastal wetlands, and coastal barrier island), and nutrient cycling (particularly nitrogen) within the aquatic/estuarine and marsh ecosystems, as well as the role of atmospheric deposition of nitrogen to the ecosystems.

The NRE is a semi-lagoonal estuary with a long history of water quality degradation resulting from loadings of nutrients, particularly nitrogen, resulting in phytoplankton blooms, extended periods of hypoxia or anoxia, and resultant fish kills. Our results indicate that anthropogenic nutrient-driven eutrophication and resulting algal bloom dynamics are controlled by climatically driven hydrologic variability in the NRE. When the water residence time within the estuary is too short to allow for nutrient assimilation by the phytoplankton, then bloom development is constrained. Freshwater discharge is of critical importance from both ecological function and ecosystem "health" perspectives because it controls nitrogen inputs and rates of nitrogen cycling.

In contrast to the NRE, which receives inputs of nutrients (particularly nitrogen from the New River watershed), the marshes of the lower NRE and Intracoastal Waterway (ICW) are, by comparison, nitrogen starved. Shallow groundwater from the uplands contains almost no nitrates, and much of the source inputs from the New River watershed to the upper estuary are completely assimilated by phytoplankton in the upper estuary. The intertidal salt marshes of MCBCL were

found to be overwhelmingly large sinks for nitrogen, and nitrogen sink strength was dominated by nitrogen burial during sediment accretion (80 to 90%) and by denitrification (10 to 20%).

Wind- and wave-driven hydrodynamic movement were responsible for both NRE shoreline erosion and sediment resuspension in this shallow estuary. Transport of sediments from erosion of sediment banks was found to provide at least half of the sediment required by the lower NRE and ICW marshes to keep pace with sea level rise (SLR) through accretion. Although wind and wave energy were most important as erosional forces in the estuary, within the confined channel of the ICW, boat wake energy became a more important factor affecting shoreline erosion processes. Wave energy from wind and boat wakes, compounded by the effects of routine dredging of the ICW, are the main erosional processes responsible for doubling the width of the ICW channel over the past 70 years. In addition, the very presence of the ICW traps the landward transport of sand from overwash events and aeolian transport across the barrier island, depriving marshes to the west of the ICW of this sand subsidy. As a result, salt marshes on the eastern side of the ICW were found to have a higher elevation above mean sea level than the marshes on the western (landward) side of the ICW. This finding has implications for the sustainability of the marshes landward of the ICW at MCBCL and also in other coastal areas along the ICW's extent.

A comparison of washover extent across the barrier island suggests that the primary forcing mechanism generating overwash processes has been tropical storm activity. Transgressive barriers exemplified by the southwestern portion of Onslow Island may be overwashed more frequently as sea level rises in the future, producing further erosion of dunes and creating more washover fans. Studies of the two most substantial washover deposits generated by Hurricane Irene (in 2011) found that these areas had not been overwashed in the past 70 years, and thus were not just reoccurrences of overwash of previously breached dunes as occurred at several other sites towards the middle of Onslow Island. This suggests that overwash occurs along the barrier both in new areas and those that have previously overwashed.

Longleaf pine (*Pinus palustris*) forest habitat at many southeastern installations are managed to promote habitat quality for the endangered red-cockaded woodpeckers (RCWs; *Picoides borealis*). A basic question of concern was whether forest management practices to improve habitat for RCWs were beneficial or detrimental to other avian species. Research findings from MCBCL suggest that these practices in general appear to benefit the avian community as a whole. This is reflected in measures of community composition. Both species richness (the number of species) and species diversity, which takes into account the relative abundance of the species present, increased as RCW habitat quality increased. This was especially true for another open pine habitat species of concern, Bachmann's sparrow (*Peucaea aestivalis*).

The relationship between vegetation and avian communities was assessed on 45 pine plots and was found to be highly correlated. Both vegetative composition and avifaunal communities were compositionally different among longleaf pine, loblolly pine (*Pinus taeda*), and high-pocosin sites. The overlap between the two communities suggests that the composition of avifaunal communities is correlated with differences in understory vegetative composition that can emerge in the different mature pine stands. Future efforts aimed at recovering avifaunal species may depend upon the recovery of the understory plant communities.

Models, Tools, and Indicators to Assess Ecosystem Health

The second objective of DCERP was the development of ecosystem models, decision-support tools, and environmental indicators that could be used to evaluate ecosystem health. For example, the Estuarine Simulation Model (ESM) predicted hydrodynamic exchanges in the NRE and included components such as eelgrass (*Zostera marina*), the most abundant species of submerged aquatic vegetation in the NRE, and total suspended solids (TSS). The ESM was used to examine the changes in point and non-point source inputs on estuarine water quality variables and ecosystem processes. The Marsh Equilibrium Model (MEM) was applied to MCBCL to forecast changes in the relative elevation of the marsh surface and biomass response to different rates of SLR possible in a climate changed future. Model simulations of different SLR scenarios showed that the marsh vegetation survived 100 years only when the SLR was less than 60 cm (24 in); otherwise, the marsh vegetation rapidly declined. This model can be transferred to other locations, but requires local accretion rates, standing biomass, TSS, and water level data. Finally, the Run-up and Overwash Model (ROM) was used to predict where overwash would occur on Onslow Beach. This model correctly identified the four overwash areas resulting from the passage of Hurricane Irene (in 2011) illustrating its use in forecasting vulnerable areas.

As previously discussed, there was a strong relationship discovered between hydrological flow of the New River and phytoplankton biomass production. Freshwater flow of 27 cubic meters per second (590 cubic feet per second) was identified as a tipping point for the estuary. At freshwater flows above this threshold, which occurs approximately 22 days a year, the water residence time in the NRE was too short for nutrient assimilation by phytoplankton in the water column; thereby restricting algal bloom development. Benthic chlorophyll *a* concentration was also found to be an excellent indicator of the effectiveness of the benthic microalgae to act as a nutrient filter. When chlorophyll *a* ranged from 70 to 83 mg m⁻² or above, benthic microalgal biomass increased, and nitrogen was sequestered from the water column. When conditions restricted photosynthesis (chlorophyll *a* ranged from less than 70 to 83 mg m⁻²), the microalgae released nitrogen into the water column. In shallow estuaries such as the NRE, hydrologic changes can modify both phytoplankton primary production and affect benthic microalgal production, which modulates internal nutrient cycling.

Recommended Adaptive Management Strategies to Sustain Ecosystems

DCERP's third objective was to recommend adaptive management strategies to sustain ecosystem natural resources within the context of an active military installation. These strategies are most applicable to the coastal wetlands, coastal barrier, and terrestrial ecosystems. More than 80% of the NRE shoreline is contained within the boundary of MCBCL. Only 19% of this shoreline has been hardened with revetments, sills, and seawalls. This constrained shoreline development has water quality benefits with respect to reduced nutrients and sediment runoff and allows ecosystem services (e.g., storm surge protection, fish and shellfish nursery areas) of the unhardened shorelines to be preserved. Although historic MCBCL practices of hardening NRE shoreline in high-energy areas are appropriate, marshes and sediment banks, which supply sediment vital for marsh accretion, will be needed in the future to help mitigate for rising sea level. MCBCL managers should consider whether additional shoreline hardening is needed, and if so, new shoreline hardening should be offset with marsh restoration in hardened areas where wave energy is low and marsh restoration efforts would be successful. These restoration efforts

will promote sustainability by allowing the marshes to migrate landward as sea level rises and continue to provide shoreline ecosystem services not provided by hardened structures.

Marshes along the lower NRE and ICW are an integral part of amphibious training and are a conduit for moving amphibious vessels between mainland training areas and the barrier island. Reinforced splash points within the ICW have a lower shoreline change compared to unmodified splash points. MCBCL managers should consider strategies to reduce erosion rates and enhance sustainability of splash points for future training, including reinforcing splash points with concrete ramps, implementing marsh restoration, or diverting some military training activities from overused splash points to underused ones.

Similar to the ICW and coastal marshes, the barrier island provides essential beach for the Marines to conduct amphibious assault training. At current training levels (frequency and intensity), military training did not have a measurable impact on the landscape (e.g., sediment texture, topography, habitat) or biology of Onslow Beach. For example, the installation's constraint of training to existing egress and ingress areas along the barrier island and restricting vehicular and pedestrian traffic on the dunes and backbarrier marshes also prevents impacts to the barrier. Our studies overall found that natural processes (wind and wave actions) overshadow anthropogenic effects.

Forest management at MCBCL and other installations along the coastal, southeastern United States is directed toward returning hardwood-pine lands to open canopy longleaf pine-wiregrass communities. Installation restoration goals were better achieved by the combined use of understory/midstory thinning in pine-hardwood plots followed by prescribed burning. Used in combination, these practices removed more woody material and consumed more than three times the fuel of prescribed burning alone. Thinning during the growing season was more effective in reducing the understory/midstory woody plants than dormant season thinning or prescribed burning alone. If these differences persist, they would indicate a possible benefit of growing season thinning that could be implemented at other installations with longleaf pine restoration goals. In either case with or without thinning, continued suppression of woody growth requires regular prescribed burns. Additionally, the use of understory/midstory thinning appears to have a secondary benefit in reducing PM_{2.5} emissions, thus providing improved smoke management for installations.

The recovery of RCWs at installations in the southeastern United States drives forestry management strategies. Forest management that specifically targets improving habitat conditions for the RCWs was found to result in habitat changes that benefit the biodiversity of terrestrial ecosystems in general and the total avian community specifically; therefore, this management practice should be encouraged. Installation managers also should maintain the availability of nesting substrate (e.g., live pines, pine snags, hardwood snags) for the wide variety of cavity-nesting avian species because that determines the strength of interactions among these species. Specifically, a shortage of dead or dying pine snags would likely result in negative impacts on RCWs due to the takeover of their cavities in live pines by other cavity nesting species.

Benefits

The research conducted as part of DCERP1 has resulted in a greater understanding of MCBCL's biologically diverse ecosystems and their interactions with military training activities. In addition, the research results provide an understanding of what on- and off-installation activities affect these ecosystems and what management actions could be implemented to best sustain MCBCL military training and testing resources. Through the research projects, the DCERP1 Team developed a series of indicators, models, and tools designed to benefit installation managers by providing support for environmental decision making. Knowledge gained from DCERP1 research will provide benefits to other military installations in coastal settings and to the scientific community and general public at large.

DCERP1 Final Research Report

Executive Summary

Critical military training and testing on lands along the nation's coastal and estuarine shorelines are increasingly placed at risk because of development pressures in surrounding areas, impairments due to other man-made disturbances, and increasing requirements for compliance with environmental regulations. The U.S. Department of Defense (DoD) intends to enhance and sustain its training assets and to optimize its stewardship of natural resources through the development and application of an ecosystem-based management approach on DoD installations. To accomplish this goal, the Strategic Environmental Research and Development Program (SERDP) launched the Defense Coastal/Estuarine Research Program (DCERP) in 2006 (originally planned as a 10-year program) at Marine Corps Base Camp Lejeune (MCBCL) in North Carolina. The *DCERP1 Final Research Report* covers research conducted from November 2007 through September 2012. MCBCL provides an ideal research platform for DCERP because it integrates a wide variety of coastal ecosystems—aquatic/estuarine, coastal wetlands, coastal barrier, and terrestrial—all within the boundaries of DoD properties (**Figure ES-1**).

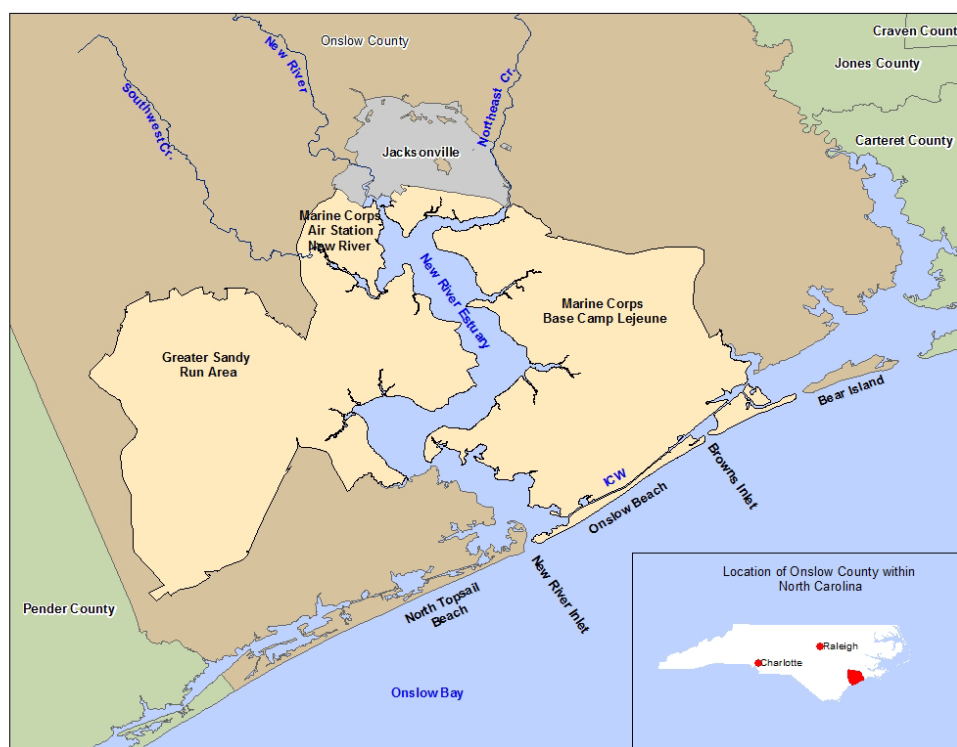


Figure ES-1. DCERP is located at MCBCL in the Lower Coastal Plain of North Carolina.

The overarching objectives of DCERP are to understand the effects of military training activities and infrastructure development, as well as other natural and anthropogenic stressors on these coastal ecosystems; to develop models, tools, and indicators to evaluate ecosystem health; and to recommend adaptive management strategies to sustain ecosystem natural resources within MCBCL's operational goals. The DCERP Team consisted of researchers from seven academic

institutions, three governmental agencies, and three private companies. Final results from 13 research projects conducted by the DCERP Team and reported here provide an understanding of the composition, structure, and function of the aquatic/estuarine, coastal wetlands, coastal barrier, and terrestrial ecosystems as they relate to MCBCL's military training mission, but these projects also have broader applicability for other DoD installations in similar coastal settings. Because the baseline monitoring program and research projects were closely integrated, the results presented here reflect input from the monitoring effort; however, the DCERP Team will produce a separate *DCERP1 Final Monitoring Report* by January 2013. An important part of DCERP's goal is to develop tools that MCBCL natural resource managers can use to implement ecosystem-based management strategies and to prepare this information for dissemination to diverse stakeholder groups.

As part of our Strategic Plan, the overarching conceptual model for DCERP at MCBCL (**Figure ES-2**) was subdivided into four ecosystem modules (i.e., the Aquatic/Estuarine, Coastal Wetlands, Coastal Barrier, and Terrestrial Modules). Because the atmosphere and its physical-chemical processes influence all four ecosystem modules, it is treated as a fifth module. In addition, a sophisticated Data and Information Management System was developed as part of the Data Management Module. This system, known as the Monitoring and Research Data and Information Management System (MARDIS), was designed to facilitate communication and collaboration among the team researchers, to archive all DCERP research and monitoring data, final DCERP reports, reports to MCBCL, geographic information systems (GIS) data files, and various models and tools developed under DCERP.

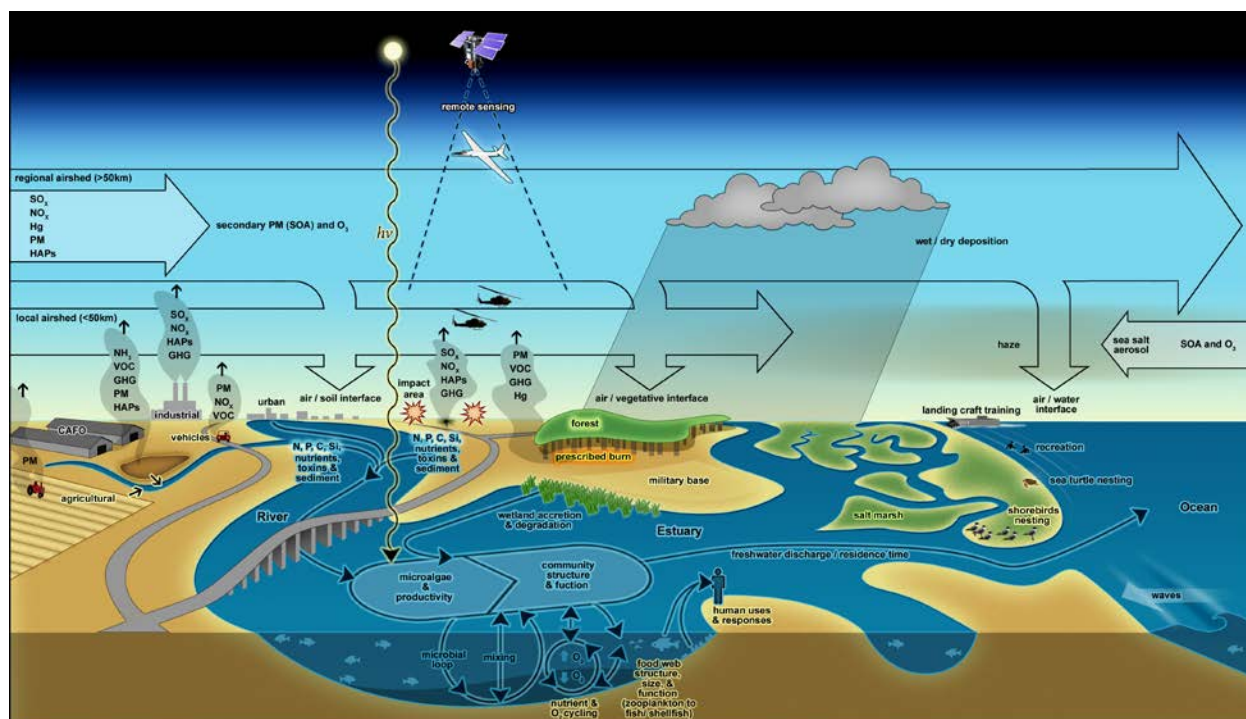


Figure ES-2. Overarching conceptual model for the DCERP at MCBCL.

For each of the five ecosystem modules, this Executive Summary delineates the context in which the research was conducted, briefly discusses the environmental processes studied and the

methods applied or developed, and the major findings of the research. In addition, recommendations are provided for MCBCL managers to use to sustain ecosystem health and at the same time enhance sustainability of the military training mission.

Programmatic Overview

DCERP was established as a highly integrated temporal and spatial monitoring and research program in which monitoring data provided information that validated models and research data provided feedback on whether the monitoring was adequate to support research hypotheses. The DCERP Team selected several major cross-module integrative processes to study. These processes included the hydrodynamics of the New River Estuary (NRE) and adjacent coastal system; sediment transport among MCBCL ecosystems (i.e., terrestrial lands, streams and estuary, coastal wetlands, and coastal barrier island); and nutrient cycling (particularly nitrogen) within the aquatic/estuarine and marsh ecosystems, and the role of atmospheric deposition of nitrogen to the ecosystems. In addition to understanding these ecosystem processes, one of the main goals of DCERP was to evaluate the impact of military training and associated land management activities on these ecological systems. Specifically, the DCERP Team evaluated water quality in watersheds with a wide range of land uses; assessed the impacts of amphibious vehicles and vessels on the coastal wetlands and the barrier island; studied differences among the various use zones (i.e., recreational, training, and off-road vehicle) of the barrier island; and quantified the effects of forestry management practices on forest recovery goals, the avian community, and smoke emissions during prescribed burning. The results from these studies are summarized at a program level in Chapter 2 and within each module section of this report.

Aquatic/Estuarine Module

The Aquatic/Estuarine Module examined the tidal reaches of the NRE, from the freshwater head of the estuary near Jacksonville, NC, to the tidal inlet at Onslow Bay, including 10 tributary creeks within MCBCL lands. Research efforts were directed at ecosystem scale effects of MCBCL and regional man-made activities and climatic stressors on microalgal production and community structure in the NRE. These projects focused on identifying the physical and chemical conditions affecting the development of phytoplankton communities and harmful algal blooms (HABs), evaluating how water quality and nutrient cycling within the NRE are regulated by benthic microalgae (BMA), and identifying and quantifying the contribution of MCBCL tributary creeks to loadings of nutrients, sediment, and bacteria to the estuary from watersheds with representative levels of military activities (e.g., training maneuvers, associated infrastructure development).

Numerical models were developed and used to

- Integrate historical, monitoring, and research data to characterize the NRE
- Scale project-level results to the entire estuarine system
- Understand the effects of natural and anthropogenic stressors on watershed inputs to the NRE
- Understand the NRE's structure, function, and response to natural and anthropogenic stressors

- Provide decision-support tools that can be used by MCBCL for making complex management decisions.

The modeling effort focused on the application of a range of Watershed Simulation Models (WSMs) to predict loads of freshwater, nutrients, and sediments from the MCBCL watersheds. The modeling effort also focused on the development of an Estuarine Simulation Model (ESM) to understand and predict responses to natural (e.g., inter-annual hydrologic variability) and man-made (e.g., nutrient and sediment loading) stressors within the NRE.

The NRE, surrounded by MCBCL and the City of Jacksonville at its head, is a shallow, semi-lagoonal system with more than half of the estuary less than 2-m deep. Shallow estuaries such as the NRE are vulnerable to man-made disturbances, including inputs of nutrients (e.g., nitrogen, phosphorus) and sediments, and natural disturbances due to episodic storms. To assist MCBCL in understanding how to sustain the water quality of the estuary, the DCERP Team determined the relative importance of off-Base versus on-Base sources of nutrients and sediment to the NRE and calculated loads produced within the NRE. DCERP demonstrated that nitrogen was the primary nutrient driving eutrophication in the estuary. On an annual basis, off-Base watersheds (i.e., New River and Southwest Creek) contributed 64% of the total external nitrogen load to the NRE, whereas MCBCL watersheds and the MCBCL wastewater treatment facility (WWTF) contributed a combined 15% of the load (**Figure ES-3**). Onslow Bay (i.e., the Atlantic Ocean) and atmospheric deposition accounted for 15% and 6% of the external N load, respectively. Although this current picture of nutrient sources points heavily toward management of nutrients in the New River watershed upstream of MCBCL, increasing infrastructure development and training needs are rapidly modifying land uses on MCBCL that could impact the future delivery of nutrients to the NRE.

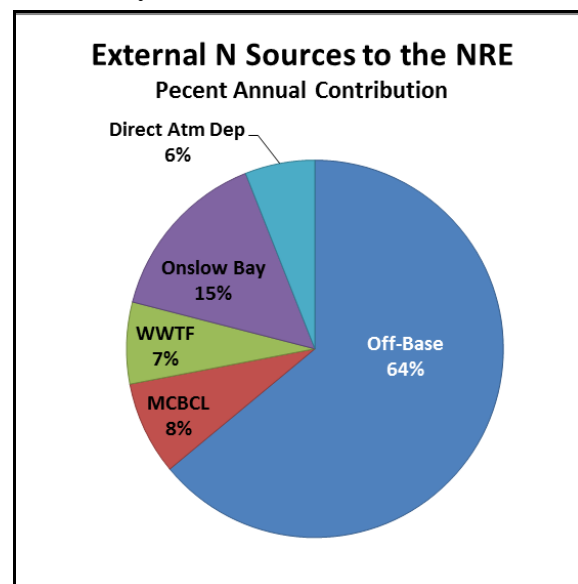


Figure ES-3. The annual contribution of external nitrogen (N) sources to the NRE.

Coastal streams are both the receiving waters and transport conduits for land-derived materials (e.g., nutrients, sediment, bacteria). This high level of connectivity to the surrounding watershed makes headwater streams sentinels of impacts that may occur due to changing land uses. Determining the impacts of land use and rainfall patterns on material delivery by streams is necessary for quantifying and reducing degradation resulting from watershed development. Headwater streams on MCBCL were investigated for 5 years during baseflow and storm events. Flow was measured continuously and samples were analyzed for nutrient and total suspended solids (TSS) concentrations and bacterial contamination. Research results show that in more developed watersheds with a higher percentage of impervious surfaces (e.g., paved roads, parking lots), loading of most constituents increased when compared to less developed watersheds with lower percentages of impervious surfaces. Regression modeling found a linear

relationship between the percentage of imperviousness of the watershed and nitrogen loading to the tributaries. This positive correlation suggested a possible tipping point of 15% of impervious cover, above which there was considerably higher nutrient runoff into the tributary creeks, except in instances in which best management practices (BMPs) were involved (**Figure ES-4**).

Additionally, comparison of the loading from a drier year (2008–2009) to two wetter years (i.e., 2009–2010 and 2010–2011) revealed increased loads of most constituents in wetter years. Somewhat surprisingly, this comparison showed that developed watersheds had similar proportional increases in loading compared with less developed watersheds.

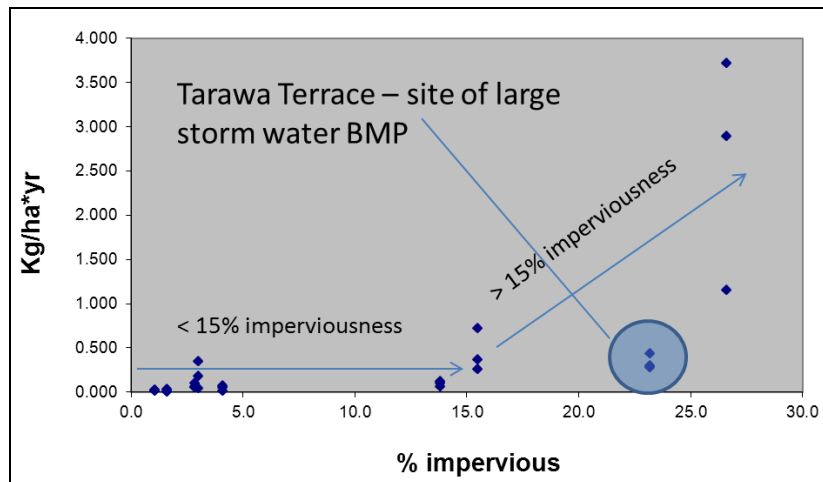


Figure ES-4. Tributary creek loading of nitrate versus percent watershed imperviousness.

Loading patterns of fecal indicator bacteria (FIB) in coastal streams have not received significant attention in the past. FIB, which are used as proxies for pathogens of fecal origin, were frequently found at elevated concentrations above regulatory standards for fecal contamination in headwater portions of 10 study streams. Total loads of 10 million to 10 trillion bacteria cells per storm event were released into the creeks, and storm loadings were 30–37 times greater than baseflow loadings. To determine whether the elevated FIB concentrations detected were from human or other mammalian sources, several indicators of human fecal contamination were assessed in a subset of four of the 10 creeks. Within those four creeks, human fecal contamination was detected in only two creeks, with the highest frequency of positive results (50%) for human contamination detected in a tributary to Southwest Creek near the New River Air Station. Although the high FIB concentrations detected in tributary creeks were significantly diluted when creek effluents enter the estuary, this dilution is likely not enough in all cases for the waterbody to meet regulations for certain uses such as shellfish harvesting.

The vast majority of the primary production in the NRE, which forms the base of the estuarine food chain for shellfish, fish, and other organisms, is contributed by the pelagic (water column dwelling) phytoplankton and BMA. Other photosynthesizing components of the system (e.g., salt marshes, sea grasses, macroalgae) contribute very little to total system production due to their limited areal extent in the NRE. Phytoplankton and BMA production appear to be of comparable magnitude on an estuary-wide basis. Phytoplankton production dominates at the head of the estuary, whereas BMA production dominates in the lower estuary nearer to the New River Inlet. These trends relate to the underlying controls on productivity of each microalgal component. For example, BMA production is limited by the amount of light reaching the estuarine bottom, which is determined by water depth and clarity. Phytoplankton biomass, suspended sediments, and chromophoric (colored) dissolved organic matter reduce water clarity and inhibit light from reaching the bottom of the estuary and the BMA particularly in upper estuary areas.

Phytoplankton biomass and production are strongly controlled by river flow. As freshwater and its nutrient load enter the head of the estuary, phytoplankton assimilate the load and accumulate biomass. It takes 1–2 weeks for the phytoplankton to completely assimilate the riverine nutrient load and develop maximum bloom biomass. Where this time point is reached along the riverine-marine continuum is determined by how fast the freshwater is moving down the estuary, which is a function of river flow. Under low river flow conditions, riverine nutrient loads are completely assimilated by

phytoplankton within the upper estuary fueling phytoplankton growth and bloom formation. Both bioassay and productivity data suggest that intense nutrient limitation, particularly nitrogen limitation, occurs as riverine loads are depleted by phytoplankton growth within the upper estuary. During intermediate flow conditions, increased flushing rates preclude bloom development within the upper estuary, but blooms are observed within mid-estuarine reaches. High flows can prevent bloom formation along the entire extent of the estuary. Specifically, a threshold river flow or tipping point of approximately 27 cubic meters per second (590 cubic feet per second) results in freshwater flowing down the entire estuary at a rate too fast for bloom development (**Figure ES-5**). Periods when this hydrologic flow tipping point are achieved are rare (on average 22 days a year) and are usually associated with intense rainfall events associated with storms or hurricanes.

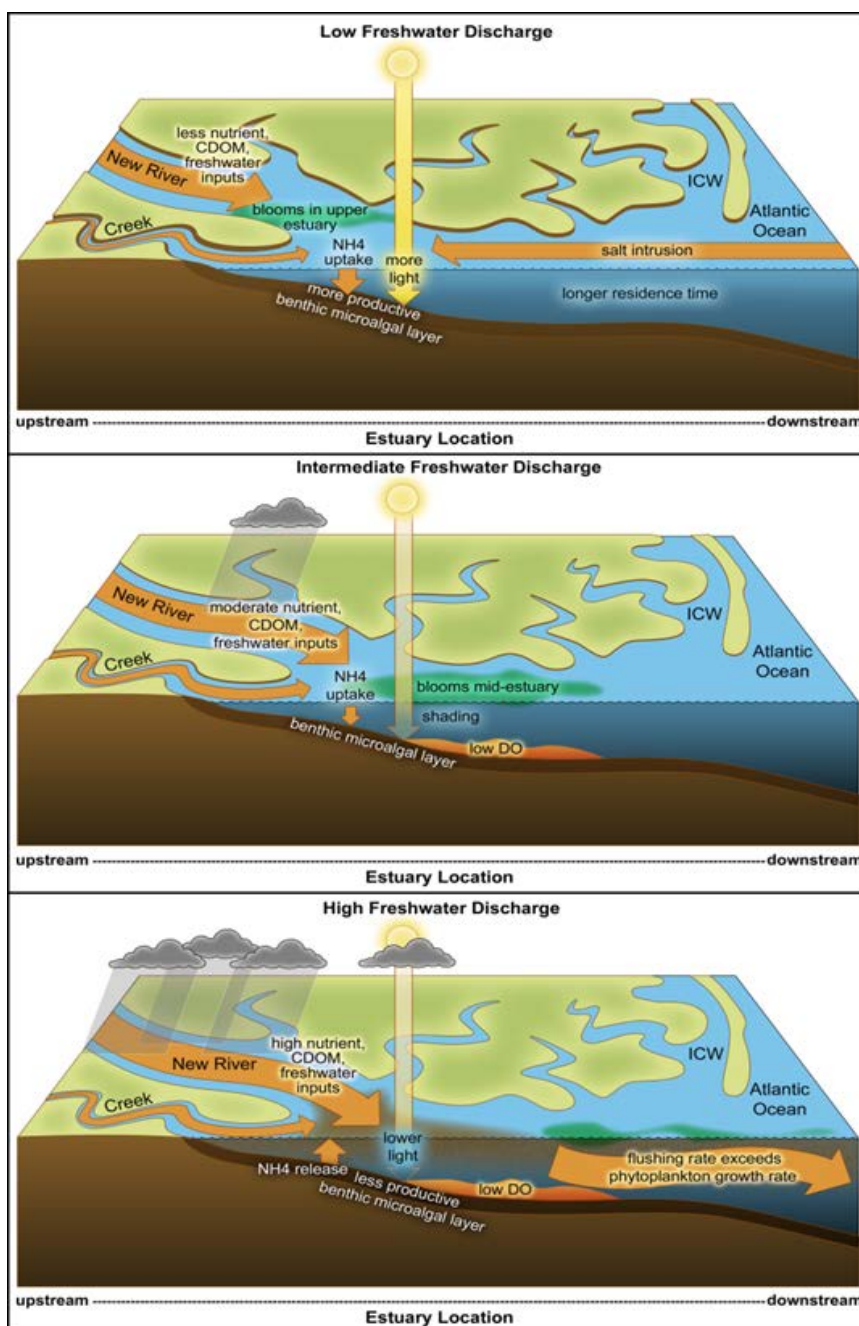


Figure ES-5. Linkage between bloom events in the NRE and riverine discharge.

Because phytoplankton have too little time to assimilate nutrients during these high flow conditions, a large fraction of the nutrient inputs are flushed directly into the ocean without producing any algal blooms. In effect, this phenomenon represents a “purge valve” for the estuary and prevents the accumulation of nutrients during periods when nutrient inputs are at their highest level. The results indicate that the NRE is highly sensitive to nutrient inputs and that any increases in riverine nutrient loads (i.e., increased riverine nutrient concentration or point source inputs directly to the estuary) that are not accompanied by flows in excess of 27 cubic meters per second are likely to lead to higher phytoplankton production and blooms in the estuary.

In addition to those phytoplankton that provide food for estuarine organisms, there are several groups that contain harmful algae species, including cyanobacteria, dinoflagellates, and raphidophytes. HABs dominated by raphidophytes (a group of flagellated phytoplankton) found in the NRE, displayed a distinct seasonality and were much more common during the warm period from late spring through early fall. In addition, although most phytoplankton blooms occurred during moderate river flow periods, raphidophyte blooms often occurred during droughts when riverine inputs were greatly reduced. The source of nutrients fueling these drought period blooms was not immediately apparent, although internal nutrient loading from the sediments may have played a critical role in bloom development of raphidophytes that can move vertically in the water column each day and may have migrated into the bottom sediment layer to obtain nutrients during the night. Although raphidophytes are known to produce toxins that can kill fish, the toxin production potential of these HABs and other harmful algal groups remains to be determined in the NRE. However, these HABs may have important consequences for the ecological health of the NRE if warming temperatures and intermittent drought and wet periods occur as projected with future climate change.

Although the productivity of the estuary is determined by both the pelagic phytoplankton and the BMA, it is the BMA that play the more important role in controlling the amount of nutrients available within the estuary. BMA acts as a “nutrient filter,” which plays an important role in regulating nutrient exchanges between the sediment and water column. When the BMA are photosynthesizing, they remove nutrients from the water column and sequester them in their biomass and in the sediments. In contrast, when the BMA are not receiving adequate light for photosynthesis, they release nutrients back into the water column and that, in turn, fuels additional phytoplankton blooms (**Figure ES-6**). BMA stabilize bottom sediments and provide some protection against nutrient enrichment and accompanying eutrophication of the overlying estuarine water column.

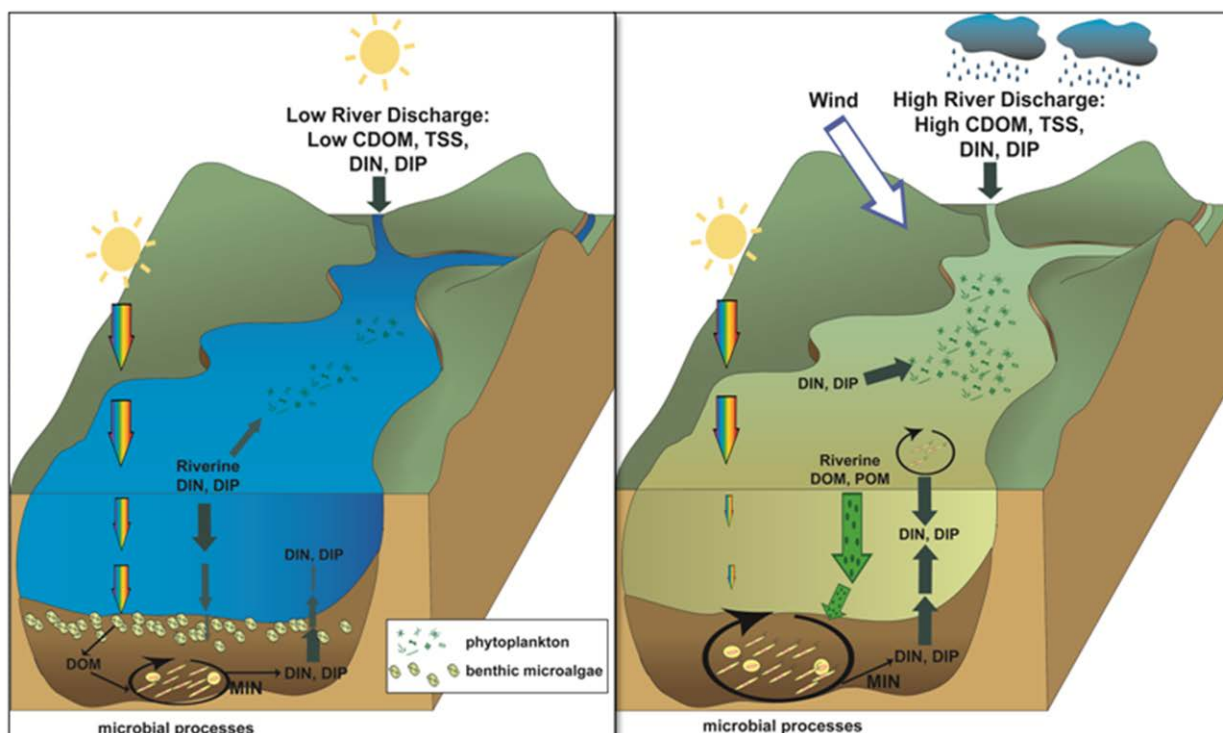


Figure ES-6. A conceptual model showing the impacts of freshwater discharge on estuarine processes, including the BMA and phytoplankton communities.

(Left) Panel shows low freshwater discharge; (right) panel illustrates high freshwater discharge.

To determine the effectiveness of the BMA as a nutrient filter, we measured seasonal variation along the estuarine gradient of sediment characteristics, benthic chlorophyll *a* biomass, metabolic rates, N cycling rates, and sediment–water nutrient fluxes. The results demonstrated that the NRE is moderately eutrophic (fairly rich in nutrients) with benthic production responsible for approximately 41% of total estuarine productivity. The benthos served as a source of internal nutrients supporting phytoplankton production and as a benthic nutrient filter, sequestering and removing nutrients from the water column. Effectiveness of the BMA was dependent upon light availability and that area of the estuary bottom receiving light otherwise referred to as the photic area. Both light availability and photic area varied as a function of freshwater discharge. Over the study period, the photic area in the NRE varied from 46–97% of the total estuarine bottom area being greatest during drought periods when water clarity was the highest. When light availability was low, the benthos switched from photosynthesizing their food to using organic compounds for food, and from being a net sink for N to being a net source of N to the water column.

Overall, benthic chlorophyll *a* is an excellent indicator of the effectiveness of the BMA as a nutrient filter. During the summer, the threshold for benthic chlorophyll *a* ranged from 70–83 mg m⁻², below which the BMA was a source of nutrients supporting phytoplankton production and above which the BMA was a sink, sequestering nutrients from the water column. During periods of high river discharge with high nutrient inputs, high pelagic phytoplankton production, and a small photic area, the BMA nutrient filter was less effective due to light limitation and low BMA biomass. In the upper estuary near Jacksonville, tannins or

chromophoric (colored) dissolved organic matter and sediment loads were dominant factors controlling light attenuation, benthic metabolism, and nutrient exchange. In contrast, in the lower estuary, resuspension of sediments and phytoplankton abundance were more important drivers controlling the benthic nutrient filter. Due to the positive effects of the BMA nutrient filter on limiting sediment fluxes of N to the water column (thereby reducing phytoplankton blooms) and on providing food for valuable fisheries resources, regional watershed management actions should aim to maintain or shift the balance toward BMA production and away from phytoplankton production. To accomplish this, both nutrient loads (which stimulate phytoplankton blooms) and riverine sediment loads (which can reduce water clarity, thus impairing photosynthesis of the BMA) should be targeted for reduction.

Recommendations to Installation Managers for Aquatic/Estuarine Ecosystems

1. Decreasing tributary nutrient concentrations and/or reducing point source loadings (e.g., wastewater treatment plant discharge) to the estuary should be a major priority of MCBCL managers to reduce phytoplankton biomass. Reductions in phytoplankton biomass resulted from upgrades made to the WWTF in 1989. This offers proof of the sensitivity of the NRE phytoplankton assemblage to flow-independent changes in nutrient loading.
2. The Estuarine Simulation Model (ESM) was validated during DCERP1 and can be used by MCBCL water quality management staff for scenario testing. For example, the ESM can predict responses of the estuary (e.g., changes in chlorophyll *a*) resulting from changes in nutrient inputs (or other parameters such as water clarity, riverine flow, or temperature) to predict changes in water quality condition of the NRE.
3. Future facilities planning strategies on MCBCL should include careful selection of the location of new infrastructure development. Proactive site selection to minimize runoff potential will be more cost effective than having to retrofit a site after construction to remedy stormwater runoff.
4. The percent imperviousness of a watershed should be a consideration in siting additional facilities, especially if the percent of impervious surface area is already approaching or exceeding 15%.
5. Maintaining significant riparian buffers along tributary creeks and the NRE shoreline should be encouraged to help reduce runoff of nutrients and sediment. Vegetated buffers are valuable for maintaining water quality, increasing resilience to climate change by decreasing damage from flooding and providing space for the marshes to migrate as sea level rises (see Recommendations to Installation Managers for Coastal Wetland Ecosystems #6).

Coastal Wetlands Module

The Coastal Wetlands Module investigated factors affecting the sustainability of coastal marshes relative to military training impacts, projected SLR, and shoreline erosion by wind waves and boat wakes, as well as the role of salt marshes in cycling nutrients within the MCBCL coastal ecosystem. Coastal wetlands are defined as the vegetated and non-vegetated intertidal habitats in salt and brackish waters and include marshes and adjacent mudflats, sandflats, and tidal creeks. Salt marshes within the MCBCL region occur in the lower NRE and along both shores of the

Intracoastal Waterway (ICW). These marshes are typically dominated by smooth cordgrass (*Spartina alterniflora*) and black needle rush (*Juncus roemerianus*). They are also the only wetlands on MCBCL that adjoin and occasionally intercept amphibious military training exercises and that play a role in barrier island stabilization. Given the importance of the estuarine shoreline for military training activities and the role of the marshes in protecting MCBCL infrastructure, our research addressed shoreline erosion within the NRE and the ICW. The increase in the number and size of vessels and their resultant wakes has complicated our ability to predict and mitigate estuarine shoreline erosion.

Several models were used to understand processes affecting these coastal marshes. The Marsh Equilibrium Model (MEM) was used to determine marsh response to projected SLR and to predict when the marshes at MCBCL might be inundated and collapse in the future. A customized version of the National Oceanic and Atmospheric Administration's (NOAA's) Wave Energy Model (WEMo) was used to classify estuarine shorelines exposed to wave energy, to identify shorelines where boat wake energy significantly increased total wave energy, and to determine shoreline erosional hotspots. A new component also was added to WEMo to determine estuarine areas prone to resuspension of sediments along the estuary bottom. Lastly, water budgets (including shallow groundwater inflows to the marshes) derived from a Salt Balance Model, and drainage fluxes derived from the Darcy Model were used for analyzing three sites at the French Creek (mid-estuary), Traps Bay (lower estuary), and Freeman Creek (ICW) marshes.

Marsh Response to Projected SLR

Some of the most sensitive ecosystems to global climate change are coastal marshes, but the future of these marsh ecosystems and their responses to accelerating SLR are uncertain. Coastal marshes maintain equilibrium with sea level by adding elevation by accretion. Marsh accretion can occur as a result of two processes: accumulation of sediments trapped from the water column and production of organic matter by marsh plants. Marsh accretion rates were measured at three salt marshes located in the lower NRE and ICW and were determined to be keeping pace with or exceeding the current rate of SLR. The accretion rate was greatest at salt marsh sites on the west side of the ICW (9 mm/y) and exceeds the current mean rate of SLR in North Carolina (2.7 mm/y; NOAA, 2004) by at least 6 mm/y.

Experimental fertilization of marsh plots with nitrogen and phosphorus increased aboveground biomass of marsh vegetation and sediment accretion rates. Treatment with these nutrients raised the rate of elevation gain 4 mm/y and 5.1 mm/y on the western and eastern sides of the ICW, respectively. These increases were sustained over the course of the 4-year study and showed no evidence of abating.

Both empirical results and the MEM predictions indicate that the Freeman Creek marsh (west of the ICW) is not in equilibrium with SLR; although the Freeman Creek marsh had the highest rate of sediment accretion, it has the lowest elevation. We can explain the apparent contradiction between the high accretion rate and low elevation by considering the effects of dredging the ICW. The ICW has been repeatedly dredged to a box cut-shaped channel on a 5-year cycle. We have developed a conceptual model for this process, which we refer to as the “dredge and slump model” (**Figure ES-7**). This conceptual model describes a cycle consisting of

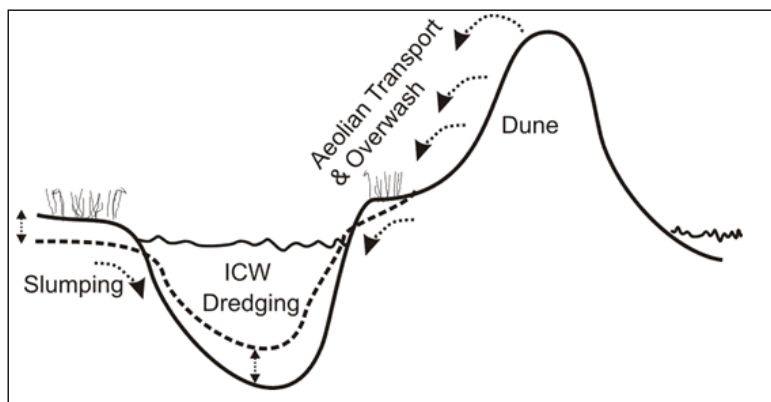


Figure ES-7. The conceptual “dredge and slump” model, which explains how marshes west of the ICW could be currently far below the equilibrium elevation.

the episodic lowering of marsh elevation, coincident with dredging, followed by a rapid recovery. We hypothesize that when this occurs, the vertical walls of the channel begin to collapse, and the adjacent marsh slumps into the channel. In addition, the proximity of Freeman Creek to Browns Inlet likely increases both the frequency and magnitude of dredging impacts, as well as the sediment supply for recovery. The ICW adjacent to Browns Inlet is

dredged more frequently than other portions of the ICW, which may increase the slumping of the marsh adjacent to the ICW channel in this vicinity relative to other areas. However, the increased sediment supply, which results in the more frequent dredging, also results in a higher sediment accretion rate to maintain marsh surface elevation. At present, the balance of these processes has resulted in a lower marsh surface at Freeman Creek, despite the high sediment accretion rates. Similar processes likely occur on both sides of the ICW, but over time, the sediment supply to the marshes on the eastern shore of the ICW will be replenished, from overwash and aeolian transport from the dunes on Onslow Island, in addition to tidal transport of suspended sediment. The ICW acts as a trap for sand and sediment eroded from the barrier island, and this dune-derived sand and sediment never reach the western shore marshes. This suggests that marshes west of the ICW (Freeman Creek) are more vulnerable to a future rise in sea level than marshes east of the ICW.

MEM simulations of marsh elevation and standing biomass were made for different SLR scenarios ranging from an assumption of a constant rate of SLR equivalent to 2.7 mm/y (0.1 in/y) to an assumption of a rapidly accelerating rate of SLR that raised mean sea level to 200 cm (7 in) by the end of the century (**Figure ES-8**). Model simulations of control sites showed that marsh vegetation survived 100 years only when sea level was assumed to rise either 24 cm (9 in) or 60 cm (24 in). Fertilized marshes fared better than controls because they were predicted to survive a 100-cm (39 in) rise in sea level, although biomass was beginning to decline rapidly by the end of the century.

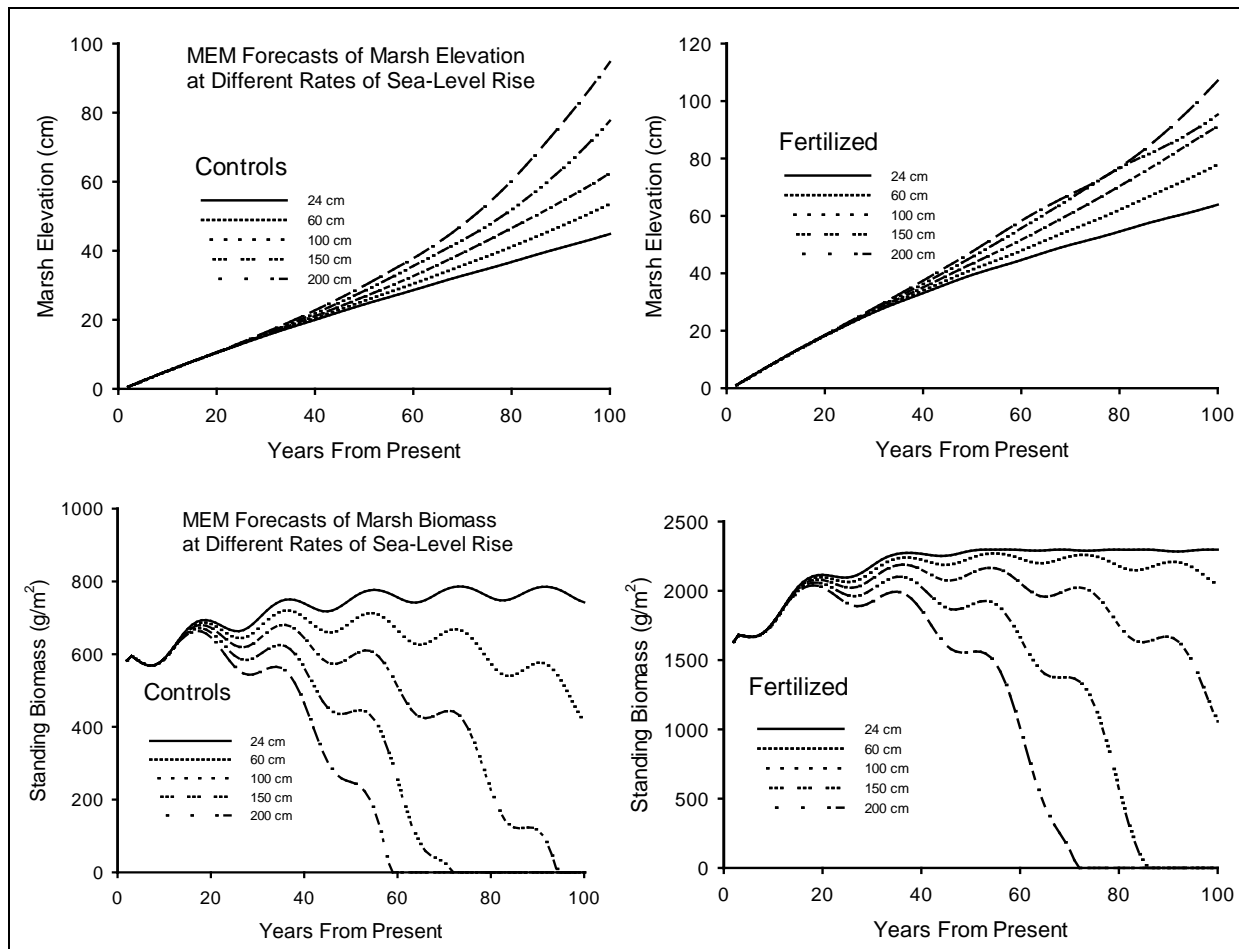


Figure ES-8. MEM forecasts of marsh elevation and standing biomass for different SLRs.

The survival times for the various MEM simulations ranged from less than 60 years for ambient marshes that experience a 200 cm (7 ft) rate of SLR to greater than 100 years, depending on the SLR scenario and nutrient treatment selected. We predicted that control sites would survive no more than a century if the sea level was to rise 80 cm (32 in) in the next century. Fertilized marshes tolerate a higher rate of SLR; only at the highest rates of SLR (i.e., 150 and 200 cm [59 and 79 in, respectively]) did the marshes succumb before the end of the century.

NRE Shoreline

The Coastal Wetlands Module utilized WEMo to evaluate the wind wave and sediment erosion potential of the NRE shoreline. Several creek mouths were found to be points of high wave energy, suggesting that any discharge from these tributary creeks would pass into an area of high resuspension capacity, which could enhance distribution of sediments and/or nutrients into the remainder of the estuary. Sediment and nutrient loading into these creeks should receive special attention from MCBCL natural resource managers. In addition to the creek mouths, other shoreline zones or “hotspots” of potential sediment resuspension were identified (**Figure ES-9**). The locations of these hotspots should be given consideration as sites where military training activities, such as splash points, should be limited.

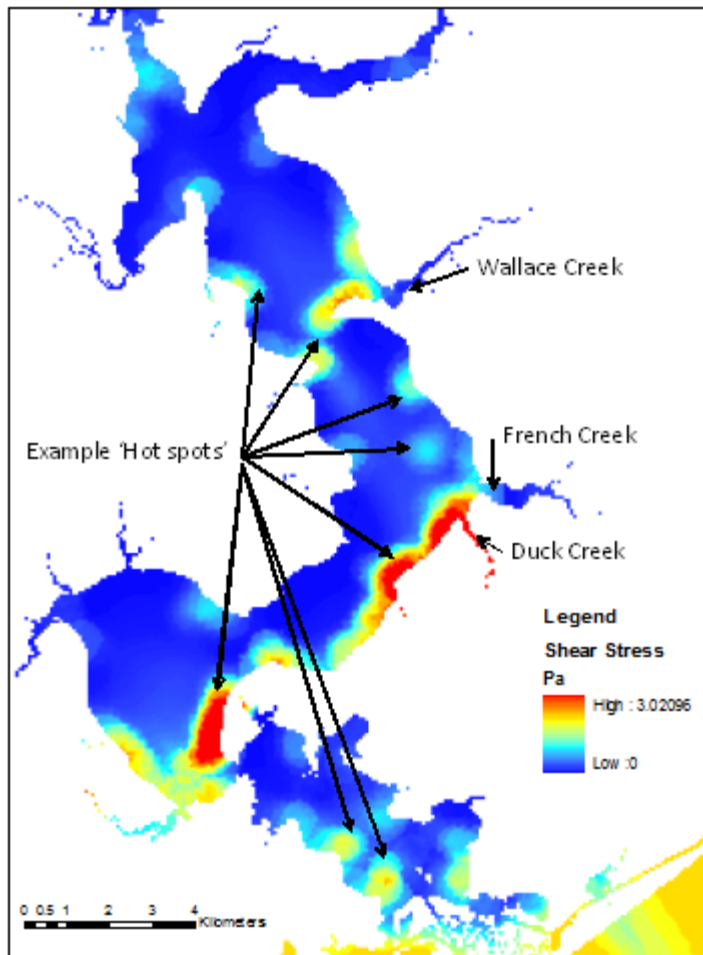


Figure ES-9. Seafloor shear stress (Pa) for the NRE with some sediment resuspension “hot spots” indicated.

Before we could determine the impact of wind and wave energy on shorelines, we conducted a detailed field survey in 2009 and found that 53% of the NRE shoreline could be characterized as Sediment Banks, 21% was Marsh, 6% was Swamp Forest, and 19% had been Modified or hardened with construction material, bulkheads, and stone sills. Shoreline change rates (SCRs) were determined from analysis of historical aerial imagery and divided into Early (1956–1989) and Recent (1989–2004) periods. Over the entire time period from 1956 to 2004, the NRE sediment bank SCR averaged -0.45 m y^{-1} . Erosion rates from the Recent period were found to be higher than for the Early period, which may be related to the increase in hurricane frequency and SLR, but may also be influenced by increased boating activity. With the exception of the Sediment Bank shoreline with marsh fringe, all shorelines demonstrated increased erosion with increased wave energy. In contrast to other shoreline types, SCR for most of the Modified shorelines decreased during the Recent period. We suspect that this was due to modifications that occurred post-1989,

so the Early period erosion rates include what were then unmodified shorelines.

To understand the potential influence of waves impacting the shoreline, shoreline-type specific SCRs were compared with Representative Wave Energy (RWE; J m^{-1} wave crest) values determined using WEMo. For this exercise, we used WEMo to calculate wave energy at the shoreline considering both local bathymetry and wind data along the entire NRE shoreline. Salt Marsh shorelines exhibited net erosion and Sediment Banks without a salt marsh fringe had more erosion in every wave class as compared to Sediment Banks with fringing marsh. Swamp Forest shorelines were few, did not exist in the highest wave classes, and in some cases, showed accretion. The existence of salt marshes across all wave classes and their mitigative effect on sediment bank erosion suggests that salt marshes are providing important stabilization services and should receive high priority for shoreline erosion protection. We have identified several erosion hotspots where salt marsh restoration may provide erosion protection.

Through SCR analysis, we also determined that the average annual volume of sediment eroded from NRE shorelines was approximately $35,300 \text{ m}^3 \text{ y}^{-1}$ ($1,236 \text{ ft}^3 \text{ y}^{-1}$), assuming a vertical shore

face. A more conservative estimate, assuming a 45-degree angle shore face, would be nearly half of that amount, or approximately $17,500 \text{ m}^3 \text{ y}^{-1}$ ($600 \text{ ft}^3 \text{ y}^{-1}$). Given that the current average rate of SLR along the North Carolina coast is 2.7 mm y^{-1} (NOAA, 2004), and this rate is expected to accelerate, for the approximately 11 million m^2 of salt marsh on MCBCL to keep pace with SLR, approximately $32,100 \text{ m}^3$ ($1,130 \text{ ft}^3 \text{ y}^{-1}$) of sediment must be accreted annually. This amount is close to the higher estimates of annual sediment volume released by vertical shore face bank erosion, but almost twice the conservative estimate, assuming a 45-degree angle shore face. These estimates demonstrate the potential importance of NRE bank erosion as one of the sediment sources important to sustain the coastal wetlands on MCBCL.

We also identified many hardened shoreline segments in areas of low forecast wind wave energy. These locations are strong candidates for marsh restoration by removal of the modified structures and transplanting marsh grasses. Shorelines with wave regimes up to approximately 340 J m^{-1} are good candidates for restoration, while shorelines with wave regimes above 340 J m^{-1} represent areas where installation of living shoreline would be more experimental. We documented a number of shoreline locations where high wave energy can be expected and special attention should be given to maintaining the status of existing shoreline structures.

ICW Shoreline

Our analysis of historical aerial imagery showed that the ICW has doubled in width since its construction (i.e., from 70 m in 1938 to more than 145 m in 2009). The SCR needed to provide this rate of channel widening is -0.5 m y^{-1} (-19.7 in y^{-1}). Analysis of SCR in the ICW from 1989 to 1999 revealed a reduction in SCR of -0.21 m y^{-1} (-8.27 in y^{-1}). Together, these data suggest that although the channel has widened substantially since its construction, shoreline erosion rates have been reduced in more recent years.

Wave energy from wind and boat wakes are the main erosional forces in the ICW. Our research in the portion of the ICW that passes through MCBCL is, to our knowledge, the first quantitative assessment of boat wakes in the ICW that evaluates historical shoreline erosion. Our research also conducted a comparative analysis among wind waves and boat wakes to define the potential tipping point where boat wake impacts would be eclipsed by the natural, wind wave environment for effects on shoreline stability. An automated video surveillance system and wave sensor were used to capture the passage of several hundred vessels on videotape. From this sampling, we detected 528 V-hull vessels. Because these V-hull vessels are responsible for most of the boat wakes that cause shoreline erosion, we focused analysis solely on this hull type. During the peak season (April and May), we detected an average of 14 V-hull vessels per day. Overall, during the 16-month period of this study, we detected 4,824 boat wakes. Although both the median and 95th percentile of wind waves were larger than those wakes caused by the V-hull vessels (i.e., boat wakes), the top few percentages of boat wake wave events exceeded the top few percentages of wind waves (**Figure ES-10**). Given that the natural shorelines in the NRE exposed to wind wave heights of approximately 0.35 m (1.15 ft) are eroding from year to year, it is not surprising that larger waves from vessels would be responsible for similar levels of shoreline erosion that we documented along the ICW.

To understand where the tipping point between wind and boat wake wave effects may occur in the estuary, we computed the relative contribution of wind wave versus potential boat wake wave energies in a test section of the lower NRE near the ICW. We found that 43% of the test bed locations would not experience boat wakes greater than that of the background (95th percentile) wind wave conditions. Based on this approach, it appears that boat wake effects will diminish rapidly with distance away from the ICW in situations where the NRE is widening. In contrast, small bays that communicate exclusively with the ICW are forecast to experience substantial boat wake waves and thus potential ecological shifts in shoreline composition and stability.

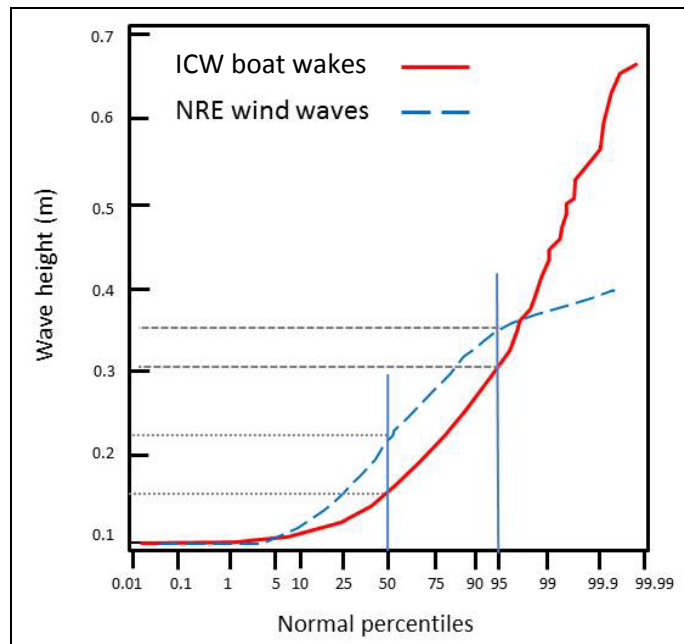


Figure ES-10. Cumulative frequency distributions comparing both ICW boat wakes and NRE wind wave heights.

Military Training Impacts on Coastal Wetlands

Our research focused on the potential impacts associated with military access to the ICW and lower NRE. There are a variety of amphibious crafts that enter and exit the ICW at many designated splash points. Observations and discussions with MCBCL personnel suggest that many of these splash points are particularly active. None of these splash points are hardened with concrete ramps, and three of them exhibited higher erosion rates between 1989 and 2009 than the average ICW SCR. We recommend that these three splash points be considered for modification, reinforcement, or marsh habitat restoration or that training activities be relocated to other underused splash points.

Finally, based on the analysis of marsh-to-water area ratio over time and the aerial record of Landing Craft Air Cushion (LCAC) tracks showing visible disturbances in the marshes adjacent to Mile Hammock Bay, we concluded that the historic rate of LCAC training events does not have a lasting impact (greater than 3 years) on salt marsh production, elevation, or marsh fragmentation (**Figure ES-11**). However, experimental passages of a LCAC vehicle over the marshes in the lower NRE area would be required to directly test the hypothesis that LCAC utilization lowers marsh elevation.

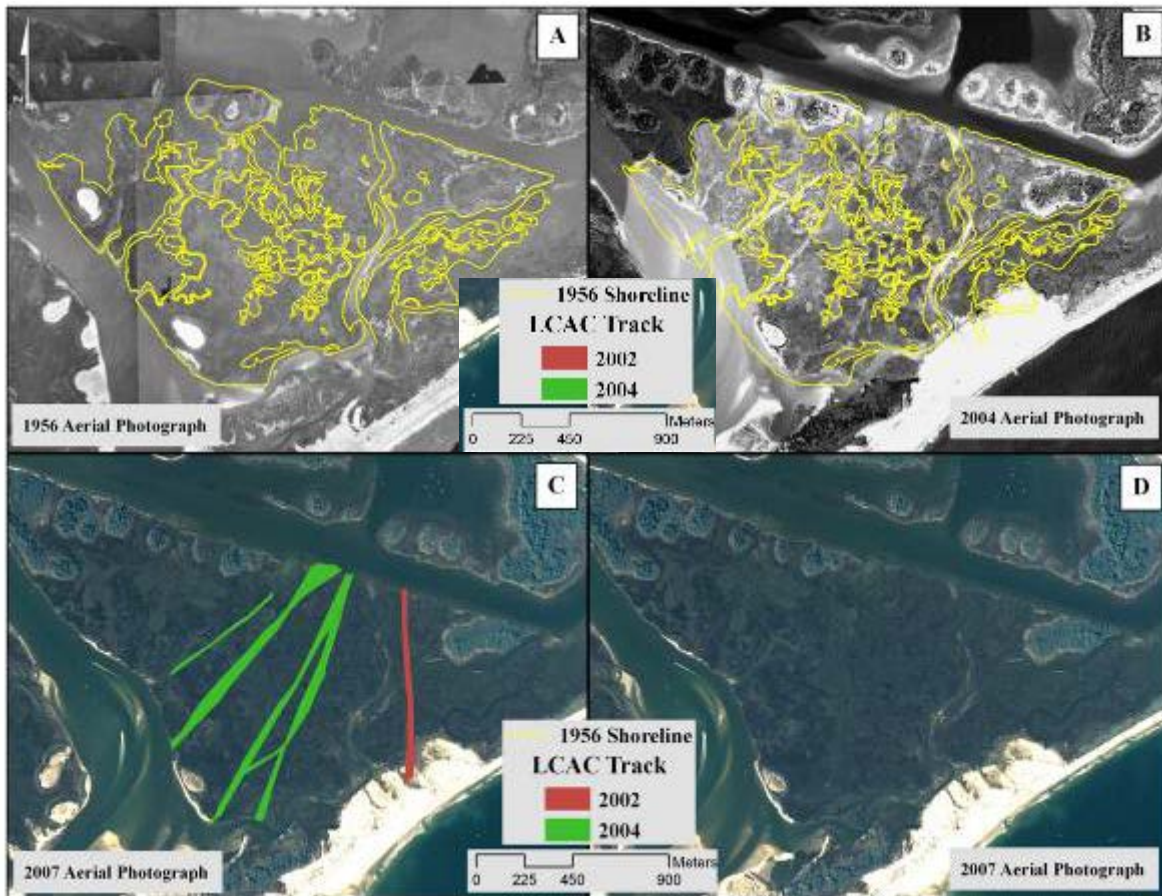


Figure ES-11. Maps of the coastal wetlands near Mile Hammock Bay.

The 1956 shoreline (mapped in yellow) on the (A) 1956 imagery and (B) 2004 imagery. Note that in the 2004 image (B), LCAC tracks are visible across the salt marsh. In the 2007 imagery (C), digitized LCAC tracks are mapped from the 2002 and 2004 imagery. In the 2007 imagery (D), the digitized tracks are not shown, illustrating the tracks are no longer visible.

Nutrient Cycling in Coastal Wetlands

Studies were conducted to determine the magnitude of N exchanges among intertidal marshes and adjacent watersheds and marine and estuarine waters within MCBCL. The work was conducted in three marshes (i.e., French Creek [mid-NRE], Traps Bay [lower NRE], and Freeman Creek [ICW]) that represent a gradient in tidal amplitude and marsh ecotypes common to MCBCL. Routes of nitrogen exchange focused on groundwater discharge to marshes, marsh drainage to the NRE and ICW, and denitrification (conversion of nitrates and nitrites to nitrogen gas [N₂]) and burial. The net nitrogen source or sink capacity of the marshes was quantified.

Groundwater inputs to MCBCL were found to be an important source of freshwater to the root zone of marsh plants, but not an important source of nitrogen to the marshes principally because groundwater dissolved inorganic nitrogen (DIN) concentrations are very low. We estimated a factor of a 5 to 10 buffer for rising groundwater DIN concentrations before the groundwater nitrogen flux to the marshes could be deemed significant.

The nitrogen inputs from marsh drainage to open waters of the NRE are trivial, relative to other sources. However, nitrogen inputs are not trivial from the marshes to the waters of the ICW. Dissolved N inputs from marsh drainage was estimated for different tidal amplitudes because higher tidal amplitudes were found in marshes along the ICW and translated into a factor of 10 to 50 higher rates of nitrogen delivery to adjacent surface waters through marsh porewater drainage. The higher tidal amplitude and greater marsh perimeter-to-area ratio in these ICW marshes resulted in these systems being a local source of nitrogen to the waters of the lower NRE and ICW.

Ambient denitrification rates in the MCBCL marshes are also low and dominated by coupled denitrification (nitrates converted to N_2) because tidal nitrate concentrations are low and there is no groundwater source of nitrates. MCBCL marshes have a huge denitrification capacity and show linear increases in rates up to nitrate concentrations two orders of magnitude higher than current concentrations. With respect to the nitrogen source/sink budget of the marsh, denitrification is one to two orders of magnitude larger than marsh nitrogen export through marsh drainage and inputs of groundwater nitrogen via groundwater.

When all exchange routes for nitrogen were considered, the intertidal marshes of MCBCL should be considered overwhelmingly large sinks for nitrogen. The nitrogen sink strength is dominated by sediment nitrogen burial during sediment accretion (80–90%) and denitrification (10–20%). Scaling-up these measured rates of sediment nitrogen burial to the respective total marsh area, we estimated that $9,660 \text{ kg N y}^{-1}$ (20 lb N y^{-1}) is buried in the marshes bordering the NRE, and $23,460 \text{ kg N y}^{-1}$ (51 lb N y^{-1}) is buried in the marshes bordering the ICW. These estimates show that NRE and ICW marshes function as a net sink for nitrogen (**Figure ES-12**). The magnitude of the nitrogen sinks within the marshes would have to decrease on the order of 20-fold before the marshes would switch from being a net sink to a net source of N. Barring any extreme changes in marsh geomorphology or severe increases in tidal amplitude, if the existing marshes continue to accrete at rates keeping pace with SLR, then they will remain as a net nitrogen sink.

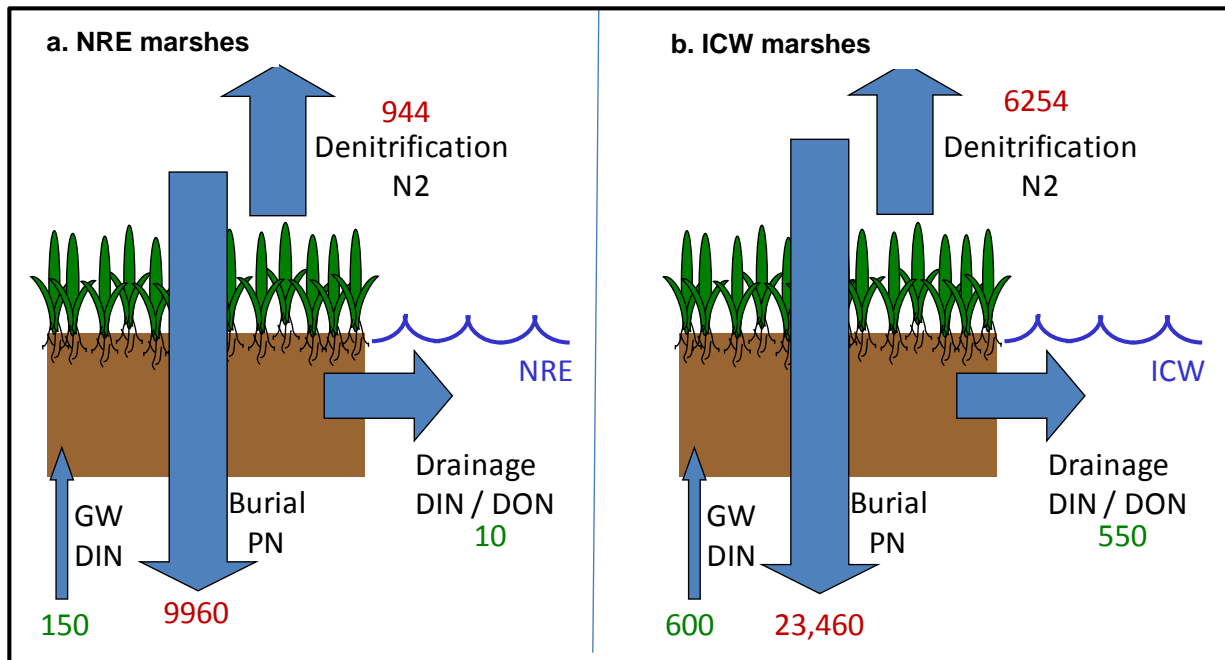


Figure ES-12. Nitrogen source/sink summary for NRE marshes (A) and ICW marshes (B) with respect to adjacent surface waters.

All fluxes are in kg N y⁻¹.

Recommendations to Installation Managers for Coastal Wetland Ecosystems

1. In the NRE, several tributary creek mouths were found to be points of high wave energy, suggesting that any discharge of materials from these creeks would enter an area of high resuspension capacity, which could enhance the release of any water column sediments or nutrients emerging from these creeks into the estuary. This release of sediments into the water column could inhibit the photosynthesis and subsequent nutrient retention by the BMA, thus spurring phytoplankton production. Thus, we recommend that sediment and nutrient loading into these creeks in particular be constrained by using BMPs (i.e., riparian buffers or stormwater detention ponds) as much as possible in the respective watersheds.
2. In the ICW, several (unreinforced) splash points have exhibited higher shoreline erosion rates than the average for the ICW. We recommend that these areas be considered for modification, reinforcement, marsh habitat restoration, or that military training activities be relocated to other underused splash points to reduce erosion rates and enhance sustainability of these splash points for future training maneuvers.
3. For any given vessel, its speed determines the size of its wake. If the speed, particularly of large V-hulled vessels, were reduced to pre-plowing levels (approximately 20 knots down to 7 knots) vessel wakes will be sufficiently small so as to not create sediment-eroding waves as they encounter shallow water at the margins of the waterway. We recommend that MCBCL consider requesting the establishment of no-wake zones in the ICW to reduce boat wake erosion of the marshes. If properly constructed, a 2-mile no-wake zone in the ICW study area would increase transit time by only 10 minutes. These

longer transit times (and smaller wakes) would substantially reduce the creation of erosion-generating boat wakes in both the ICW and small bays adjacent to the ICW.

4. The MEM forecasts a 95-year survival time for MCBCL area marshes should sea level rise 100 cm (39 in) by the end of the century. There are two management strategies that could mitigate the effect of the ICW on the surrounding marshes and enhance their sustainability: (1) nutrient enrichment to enhance biomass production and sediment accretion of the marshes, and (2) thin-layer disposal of dredge spoils on the marsh surface. Each option is described as follows:
 - Considering the option for nutrient sources for nutrient enrichment as a management strategy, the effluent from a WWTF is typically enriched with both macronutrients, N and P. Having a wetland treatment site with vegetation that is co-limited by both nutrients is desirable from the standpoint of nutrient removal. However, the possibility of unintended adverse effects needs to be investigated before nutrient enrichment for marsh survival is put into practice because there could be negative consequences for estuarine water quality.
 - Thin-layer disposal of dredge material is another alternative to the current practice of removing the dredged sediment from the system. This practice has been tested experimentally by the U.S. Army Corps of Engineers (USACE) and has been shown to promote growth of healthy marshes. *S. alterniflora* appears to be adapted to burial with sediment and thrives; however, there likely would be negative consequences for the benthic organisms that live in the marsh sediment, but these negative effects would likely only be temporary.
5. There are a large number of shoreline segments currently modified (hardened) that have potential to be converted into living shorelines based on their location in areas of low wave energy. Based on our surveys, salt marshes can readily persist on shorelines where WEMo forecasts wave energy values of 300 j m^{-1} or less. We recommend these shoreline segments as strong candidates for ecological restoration by removing the modified structures and transplanting marsh grasses. If there is any remaining vegetation after removal of the modified structures, this may be used to supplement the revegetation process and jump-start the re-establishment of the ecosystem services provided by the marshes.
6. For long-term Base planning, besides that for storm surge and wave runup, the rise in sea level should also be considered. Future placement of MCBCL facilities should consider plausible future SLR scenarios and allow for the ability of marshes to grow shoreward to keep pace with this SLR. This planning would affect the construction of MCBCL facilities and would require planning space for the landward migration of existing marshes to sustain ecosystem services such as shoreline stabilization and wildlife habitat.

Coastal Barrier Module

The Coastal Barrier Module examined the coastal barrier island ecosystem that lies at the interface between the continental shelf and the protected NRE. This barrier island ecosystem encompasses the shallow subtidal and intertidal shore face, tidal inlet, backshore beach, aeolian dune, shrub zone, maritime forest, and washover sand flat habitats. These habitats are defined by intrinsic ecological processes, but are linked by sediment transport, nutrient exchange, and biological uses, each of which undergoes substantial changes over multiple time scales. All habitat areas of the barrier, Onslow Island, were studied during DCERP from the New River Inlet to Browns Inlet, which encompasses approximately 12 km (8 mi) of island coastline (**Figure ES-13**). Research efforts were designed to support the long-term sustainability of the island as an important coastal resource necessary for amphibious military training, recreation for MCBCL staff, and maintaining critical habitats for protected species.

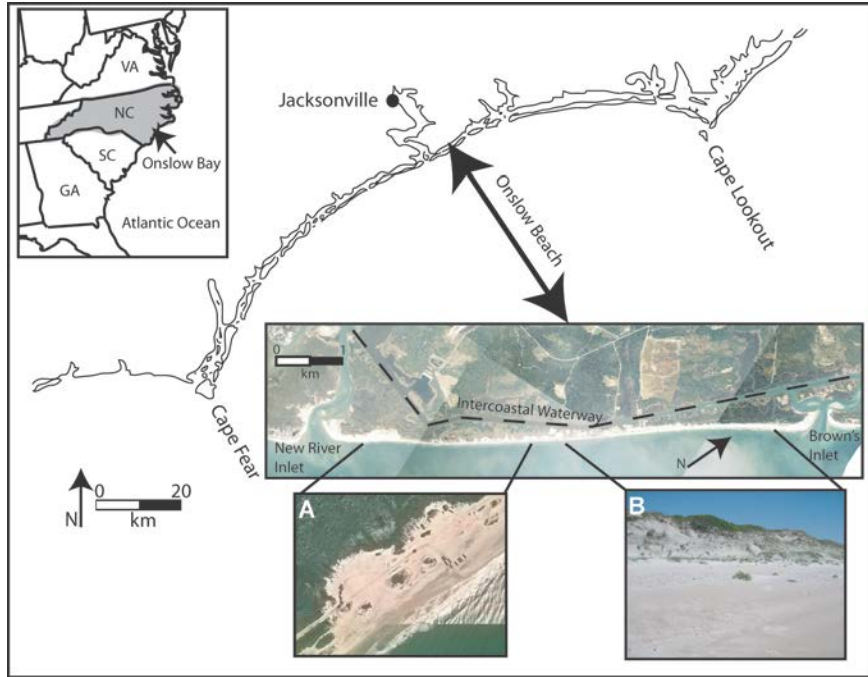


Figure ES-13. Onslow Island.

This barrier island experiences frequent overwash events in the southwestern half of the island. (A) Numerous washover fans on the southwestern portion of the island (aerial view); (B) a high primary dune field on the northeastern end of the island with no evidence of overwash.

Onslow Beach is a critical asset to MCBCL as the primary Atlantic Coast location where amphibious military training maneuvers occur. Future sustainability and effective management of this resource depend on a better understanding of the evolution of the island in terms of shoreline movement and landscape changes. Coastal Barrier Module research focused both on an improved understanding of the long-term barrier evolution related to variations in underlying geology and inlet dynamics that have shaped the island over geologic time and short-term hydrodynamic evolution related to land use and impacts of storm events. Studies examined the evolution of Onslow Beach over millennial to yearly time scales to help better manage future landscape changes that may occur in response to changes in future storminess and SLR. Modeling focused on the development of a hydrodynamic wave runup and overwash model to predict future overwash locations from storm events.

Geologic Evolution of the Coastal Barrier Island

Shoreline movement (eroding landward or accreting seaward) at decadal and yearly time scales was measured from examining historic aerial photography and laser scanning, and the evolution of the barrier at millennial to centennial time scales was reconstructed from sediment cores and radiocarbon dating. These data show that Onslow Beach is a transgressive barrier island that moved from approximately 300-m (1,000-ft) seaward of its current location around 200 Anno Domini (A.D.) to its current position principally through overwash processes and washover fan formation. Overwash processes occur during storms when sediment-laden water is carried over the dune crest, which typically results in the deposition of a fan-shaped feature (a washover fan) behind the dunes (**Figure ES-14**). The oldest washover fan deposits preserved in the sediment layers of the island are from approximately 200 A.D. and at that time an open-water lagoon separated Onslow Beach from the mainland, in contrast to the marshes and tidal channels that have characterized the backbarrier landscape since at least 1850 A.D. The number and landward extent of washover fans increased sharply along the entire island at approximately 1850 A.D., which corresponds to an increase in the rate of relative SLR to 3.2 mm/y based on foraminifera sampled in two North Carolina salt-marsh cores (Kemp et al., 2009) and a low number of tropical hurricanes in the Atlantic Ocean region. The increase in number and landward extent of washover fans at that time also implies that the rate of island movement landward increased. The increase in the rate of SLR likely lowered the elevation of the island through erosion of the dunes and made the island more vulnerable to overwash. These data suggest that Onslow Beach is extremely sensitive to increases in the rate of SLR, which causes an immediate decrease in the elevation of the island and its resistance to overwash processes. This sensitivity is likely the result of the island being sediment starved, a product of its framework geology (limestone outcropping near the shoreface release little sediment) and its location at the center of a coastal embayment (**Figure ES-14**).

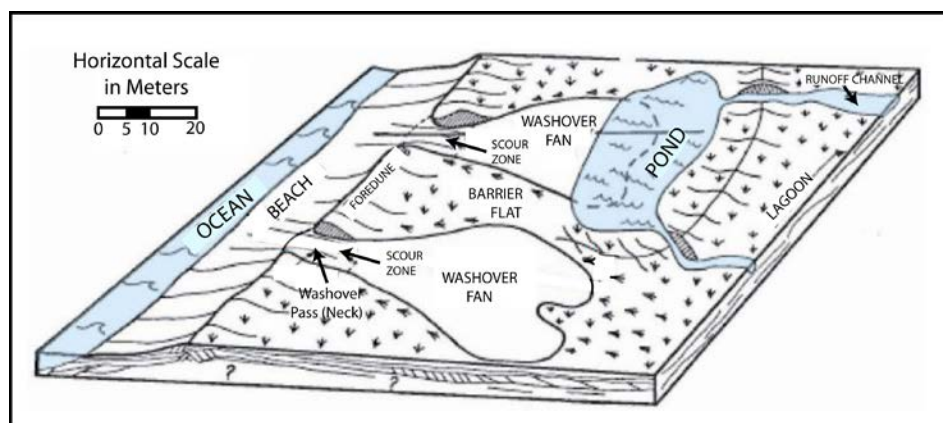


Figure ES-14. The process of overwash creates washover fans on the barrier island.

Amphibious military training activities have had little impact on island evolution because both the geological and decadal records of shoreline movement of island evolution show that the military training zone has been vulnerable to overwash and has experienced high rates of shoreline erosion since at least 1850 A.D., long before MCBCL was established. High rates of shoreline erosion in the military training zone are due to the low sediment supply as compared to the northeastern end of the island where nearshore sand thicknesses are greater. The short-term

evolution of Onslow Island has also been driven by overwash processes particularly along the southwestern half of the island. Our research focused on: (1) assessing whether current military training activities on Onslow Beach have measurably changed the occurrence of overwash, and (2) developing an analytical model that can accurately predict the location of overwash areas associated with storm events. Changes in the spatial extent of washover deposits since 1938, prior to development of MCBCL as a military installation, were measured for each decade from 1930 to 2010 from aerial photographs and field mapping. During this 80-year period, results suggest that a linkage exists between the amount of overwash and the number of tropical hurricanes that impacted the region in a given decade. Neither an increase nor a decrease in washover deposits were discernible as a linear trend, suggesting that MCBCL training activities did not measurably influence overwash processes.

Hydrodynamic Evolution of the Barrier Island

A wave runup and overwash model was developed to predict future overwash locations on Onslow Island. The boundary conditions required for this model included high-resolution beach and dune topography, nearshore bathymetry, and surf-zone waves and water level data. A new observational technique (i.e., CLARIS [Coastal LiDAR and Radar Imaging System]) was developed to measure beach and dune topography and wave runup during storms (**Figure ES-15**). Modeled wave runup, which is defined as the elevation reached by the upper 2% of wave movement on the beach foreshore, and projected locations of overwash, which is defined as where runup exceeded the elevation of the primary dune crest, demonstrated strong predictive ability of the model during Hurricane Irene (August 2011). The wave runup and overwash model correctly predicted all four overwash locations along Onslow Beach (**Figure ES-16**). Results of model simulations imply that runup elevations vary along Onslow Beach as a function of beach slope and nearshore bathymetry such that overwash and inundation predictions based solely on regional tide and surge data would likely be poor at predicting overwash except for the most extreme storm events. Therefore this tool could be used to identify areas vulnerable to wave runup and overwash, so that MCBCL managers better understand the vulnerability of existing and planned infrastructure development on Onslow Beach.

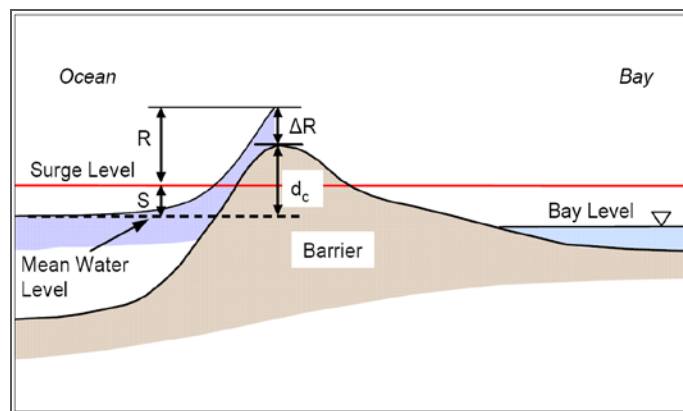


Figure ES-15. Diagram of the wave crest breaching the primary dune (d_c), which is driven by runup (R) well above the regional surge water level (S).

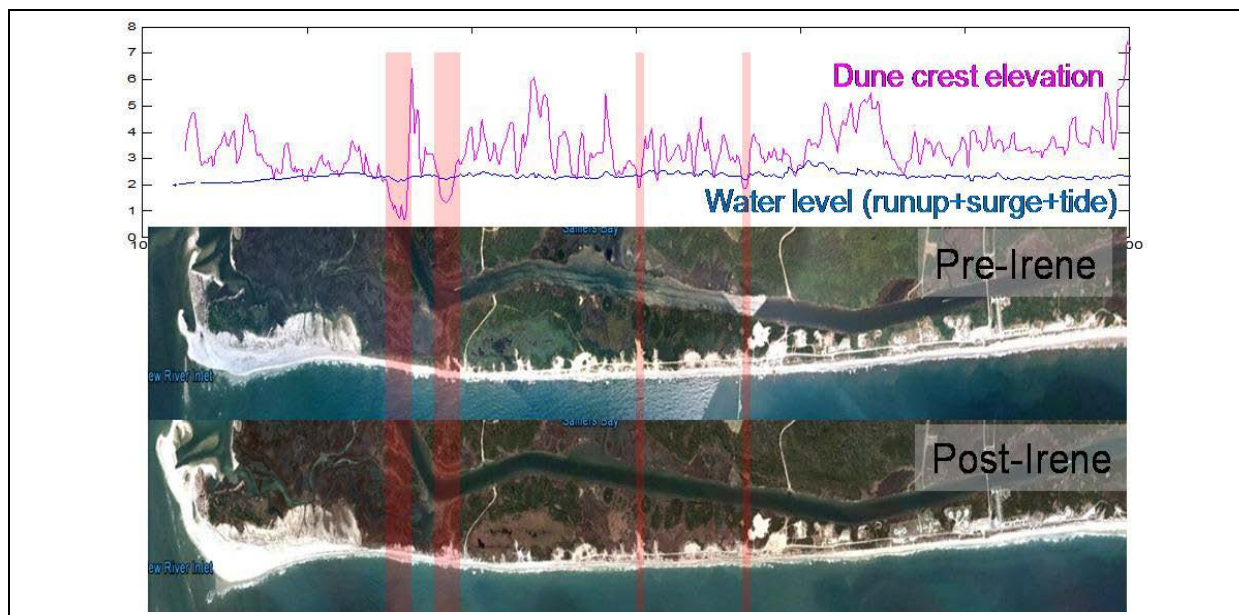


Figure ES-16. Modeled water level and overwash prediction.

Dune crest elevation (purple line; top panel) and predicted water level (runup+surge+tide) along Onslow Beach during Hurricane Irene. The bottom two panels show washover deposits before and after Hurricane Irene.

Avian Species and the Barrier Island as an Important Habitat

In addition to the geological and hydrodynamics research, the Coastal Barrier Module Team also studied the utilization of the island by an important shorebird indicator species (i.e., Wilson's plover [*Charadrius wilsonia*]), selected as a surrogate for the endangered piping plover (*C. melodus*). The team selected Wilson's plover as the focal species for this study because it is a species of concern in this region, and Onslow Beach appeared to be an important breeding location for the species in North Carolina. Research on the breeding ecology of Wilson's plovers at Onslow Beach was conducted from March through August of 2008 and 2009. Researchers resighted Wilson's plovers banded in those first two seasons in 2010 to calculate adult survival. Researchers also surveyed all shorebirds, terns, and predators at Onslow Beach during 2008–2009 concurrently with the breeding studies to understand predator-prey linkages associated with the ecology of the island.

Despite its conservation status, Wilson's plover population trends are poorly understood, and little research has been conducted on the habitat factors affecting the bird's breeding and foraging ecology. We collected Wilson's plover demographic data and explored which habitat characteristics influenced breeding success and foraging site selection among three coastal habitat types (i.e., fiddler crab [*Uca* spp.] mud flats, beach front, and interdune sand flats). We observed little difference between years in nest success (≥ 1 egg hatched), failure, and overall nest survival. The majority of nest failures were caused by mammalian predators (primarily opossums and raccoons). For those nests that hatched successfully, greater proportions of nests were located in clumped vegetation than on bare ground or sparsely vegetated areas. In-season chick survival for both years was higher for nests that hatched earlier in the season and for nests farthest from the broods' final foraging territory. Productivity estimates (chicks fledged per breeding pair) were not significantly different between years (0.88 ± 0.26 fledged per pair in 2008, 1.00 ± 0.25 fledged per pair in 2009). This was despite a shift in foraging behavior,

possibly related to habitat alterations caused by a sea level anomaly in 2009 that produced exceptionally high tides and resulted in flooding of some of the intertidal areas such that they could not be used for foraging by chicks.

Apparent survival of Wilson's plovers banded as adults was high (i.e., 82%), whereas apparent survival of plovers banded as chicks was low (13%). These survival rates calculated for both adults and first-year birds were very similar to other studies of piping plovers on the Atlantic Coast from populations that were shown to be stable over time. Our findings indicate that Wilson's plover adults and broods were flexible in establishing final foraging territories. In 2008, all final brood foraging territories were on fiddler crab flats, whereas in 2009, final foraging territories were split between fiddler crab flats, beach front, and interdune sand flats because many of the fiddler crab flats remained flooded. For those Wilson's plovers establishing territories on fiddler crab flats, spatial extent of the flat (flats $\geq 1,250$ m² were the preferred size) was the most important feature explaining use versus non-use of a particular flat. Close proximity to water and vegetative cover were also important habitat features in foraging site selection on fiddler crab mud flats and in all habitat types combined.

Recommendations to Installation Managers for Coastal Barrier Ecosystems

1. Geological structure of the surf-zone near the military training zone will likely continue to induce higher elevations of wave runup in that area than in surrounding areas. BMPs designed to minimize erosion of the primary dune crest should be considered, and anticipating likely inundation of sea turtle nests in this region should be countered with relocating nests to less overwash prone areas of the beach.
2. Given that the rate of SLR is predicted to increase over the next 100 years, one could use our data showing island response to the increase in the rate of relative SLR that occurred around 1850 A.D. to help forecast future morphologic changes. Based on these geological data, MCBCL managers should plan for an increase in the frequency and magnitude of overwash events, (regardless of future changes in frequency and magnitude of storm events), which will occur as higher sea levels cause waves to increase dune erosion and lower the elevation of the island, making it more vulnerable to overwash processes. Currently, the southwestern end of the island is most vulnerable to overwash because the elevation is lowest, annual erosion rates are high, and the offshore sediment supply is low.
3. The distance between the Atlantic Ocean and the ICW is smallest in the southwestern portion of the barrier island, indicating that the ICW may be impacted by overwash in the near future. Given the high rates of landward shoreline movement at the center of the island and the narrow dunes, the island will likely overwash in this area again within the next 20 years. We recommend that if MCBCL has plans to build additional permanent structures or to modify existing structures located on the dunes, MCBCL managers recognize that the vulnerability of these sites to inundation will increase in the near future (the next 10 to 20 years). Depending on the nature of specific construction projects, it may be prudent for MCBCL managers to plan additional infrastructure development further landward of where the existing bathhouses and cottages are located today. Looking to the future, MCBCL managers also should anticipate and plan for increased costs for post-storm infrastructure repair and clean up on the barrier island.

4. MCBCL managers have the results from the wave runup and overwash model, which projects locations of overwash areas under various storm and sea level scenarios. Overwash predictions during Hurricane Irene from this model correctly predicted all four overwash locations.
5. MCBCL managers have been proactive in posting symbolic signs and fencing to protect shorebird nesting areas of Onslow Beach. If possible, MCBCL staff should continue to identify and protect newly formed and ephemeral habitats (e.g., overwash areas, sand accretion areas, ephemeral tidal pools) that help support Wilson's plover nesting pairs and broods, as well as other breeding shorebirds with similar habitat requirements (e.g., piping plovers, American oystercatchers [*Haematopus palliatus*], least terns [*Sterna antillarum*], willets [*Catoptrophorus semipalmatus*]).
6. Although MCBCL has met with public objections about restricting access to the southwestern end of Onslow Island during shorebird breeding season, alternative measures to signs and fencing could be implemented. For example, posting interns or volunteers during high-use periods (on weekends and especially during holiday weekends) for educational outreach and to monitor critical foraging areas might be a less confrontational and more effective approach to habitat management and improving conservation knowledge of shorebirds.

Terrestrial Module

The Terrestrial Module's ecosystem-based research was conducted along the gradient of vegetation from the salt marsh at the estuary margin, through brackish/freshwater marsh, to the longleaf pine (*Pinus palustris*) savannas and pocosins (i.e., shrub bogs) that dominate the upland terrestrial environments on MCBCL. Variation in the biota and ecosystem processes along this gradient is driven by variation in hydrology, soils, and fire behavior. Most of the rare plant species characteristic of coastal terrestrial ecosystems, including species of concern on MCBCL, are found in the transitional zones of these gradients. The Terrestrial Module's research focused on the critical knowledge gaps related to efforts to restore longleaf pine ecosystems on sites across MCBCL that have been modified by past management practices. The research examined the effects of alternative midstory restoration strategies (e.g., mechanical thinning, prescribed burning [PB]) on understory plant, arthropod, and avian communities, particularly the federally protected red-cockaded woodpecker (RCW; *Picoides borealis*). In addition, the research provided information regarding whether management for a single species (i.e., the RCW) is beneficial or detrimental to other avian species.

Changing patterns of land use and forest management have greatly altered forest ecosystems across much of the mid-Atlantic Lower Coastal Plain. In particular, vast areas that were once dominated by open longleaf pine savanna now support closed canopy stands of loblolly pine (*Pinus taeda*) with a dense understory and midstory of broadleaved shrubs and trees. The absence of fire on these landscapes has exacerbated this trend, and this situation is typical of large parts of MCBCL lands. In recent years, longleaf pine restoration at MCBCL has focused on the use of understory and midstory thinning to produce savanna-like conditions and allow restoration of historical fire regimes using PB (**Figure ES-17**). The Terrestrial Module's research has also focused on providing data on fuel characteristics to complement research conducted by

the Atmospheric Module comparing the effects of PB on emissions of gases and aerosols in unthinned control and dormant season midstory-thinned loblolly pine stands.



Figure ES-17. A typical loblolly pine site prior to understory and midstory thinning (A), thinning of the site (B), and a typical site following understory and midstory thinning treatment (C).

Experimental vegetation plots were established using a randomized block design consisting of eight blocks with three treatments in each block. Individual blocks were located on MCBCL so as to represent a range of soil site conditions. Treatments included an unthinned control, dormant season thinning, and growing season thinning. All experimental plots (including controls) received dormant season PB between 6 and 18 months following treatment. As expected, the density of understory woody stems was decreased in all treatments following thinning and PB, and the density was significantly lower in the plots thinned during the growing season as compared to the plots thinned during the dormant season (**Figure ES-18**). In just 1 year following thinning and PB, understory plant species richness was significantly higher in both thinned plots compared to control plots, but no treatment effect was evident for arthropods or birds. These treatment effects may take longer to appear; therefore, additional future sampling will be required to confirm or detect any trends.

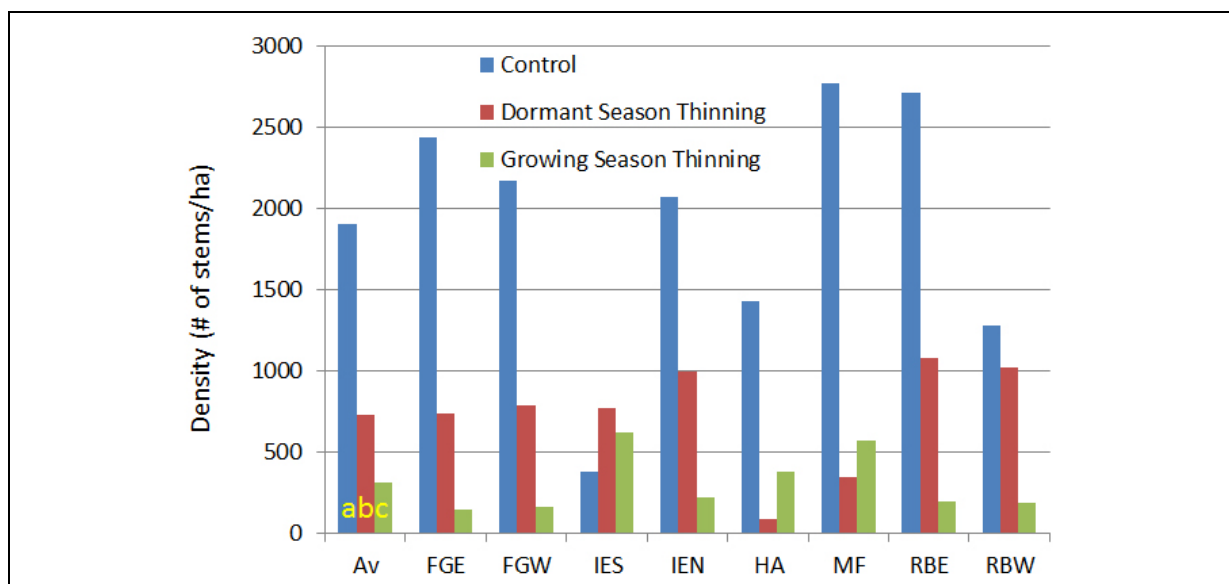


Figure ES-18. Post-treatment stem density by block and treatment.

Blocks are ordered left to right as high pocosin (FGE, FGW, and IES), wet mesic (IEN, HA, and MF), and mesic (RBE and RBW). There are no significant differences among blocks. Treatments, however, are significantly different from one another ($P < 0.05$, Duncan's Multiple Range Test) as indicated by the lowercase yellow letters in the Av (average) bars.

Thinning also significantly increased amounts of fine (1-hour) fuel and decreased amounts of coarse (1,000-hour) fuel. This treatment also diminished canopy cover and increased exposure of understory fuels, resulting in dryer fuels in thinned plots as compared to control plots. As a consequence, greater amounts of forest floor fuel were consumed in thinned than in unthinned plots. Thus, consumption of accumulated litter and forest floor organic matter may be a very important effect of thinning treatments. Taken together, these results indicate that, after a single growing season, thinning treatments are producing changes consistent with restoration objectives. Furthermore, because growing season thinning produces a greater reduction in the growth of the woody understory, it may accelerate the restoration process compared to thinning during the dormant season.

The Terrestrial Module also wanted to determine whether improving the quality of upland pine savanna and pine flatwood habitats for RCWs also benefited the remainder of the avian community characteristic of these MCBCL habitats (**Figure ES-19**). Our analysis involved a two-stage approach for determining the linkage between RCW habitat quality and the presence and abundance of other avian species. We divided RCW habitat quality scores derived from the RCW foraging habitat matrix tool developed by the U.S. Fish and Wildlife Service into four categories, from a low-quality (2) to a high-quality (5) habitat. We first looked at the probability that each species occurs at a point across these four habitat quality categories. In the analysis, we used formal occupancy models to produce these estimates. Second, we used Distance 6.0 (a computer package to estimate abundance of wildlife species) to estimate the density of each species at points within each habitat quality category in which that species occurred. Thus, our two-stage analysis indicates first how likely a species is to occur, and second how abundant it is where it occurs, as a function of RCW habitat quality.

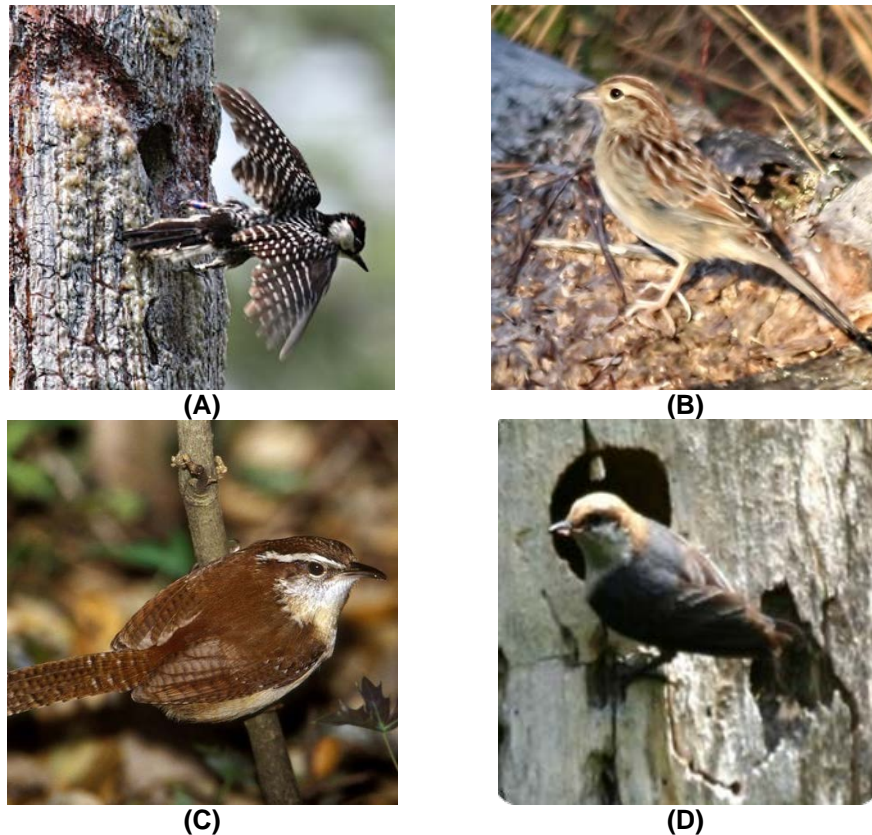


Figure ES-19. Common avian species in pine forests at MCBCL.

Red-cockaded woodpecker (A), Bachman's sparrow (B), Carolina wren (C), and brown-headed nuthatch (D).

The Bachman's sparrow (*Peucaea aestivalis*) is an at-risk species of special concern to MCBCL that is associated with open pine habitat, similar to the RCW. It is particularly important that management for the RCW should also benefit Bachman's sparrow. Our analysis indicated that this is the case: the occurrence of Bachman's sparrows increased markedly as RCW habitat quality improved, and density at points of occurrence also increased across RCW habitat quality (**Figure ES-20**). Similar trends were also found with other species associated with open pine stands. Both the red-headed woodpecker (*Melanerpes erythrocephalus*) and the Eastern bluebird (*Sialia sialis*) tended to occur more often in a high-quality RCW habitat. Thus, the open pine habitat species appear to be benefitting from habitat management for RCWs.

It is less obvious if canopy species associated with pine habitat would benefit from management for RCWs because this management affects the ground cover and midstory in more dramatic

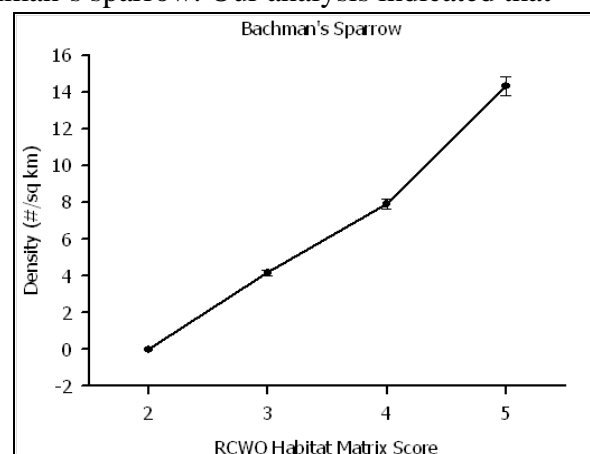


Figure ES-20. Estimated density of Bachman's sparrow at point count locations at which it occurs as a function of RCW habitat quality.

ways than it affects the canopy, but RCW management does favor larger and older pines, and this could impact canopy species. The two pine canopy species we examined during our analysis (i.e., the brown-headed nuthatch [*Sitta pusilla*] and the pine warbler [*Dendroica pinus*]) occurred at a high proportion of points and in high densities, but both were still more likely to be present in a higher quality RCW habitat and exhibited a slight tendency to occur at higher densities in a higher quality habitat. Thus, pine canopy species appear to also respond positively to management for RCWs. Species associated with hardwood habitats or shrubby understory might be expected to be adversely affected by management of habitat for RCWs because such management greatly reduces hardwood midstory and the woody understory component. We censused birds in two other habitat types (i.e., bottomland hardwood and pocosin) to provide a context for interpreting results from upland pine habitat. Species associated with shrubby understory (e.g., the Carolina wren [*Thryothorus ludovicianus*]) in pine habitat were also common in pocosins. The density and abundance of these species tended to be negatively related to RCW habitat quality score. This appears to reflect their preference for wetter conditions (i.e., pocosin) of the dry–wet soil moisture gradient in pine habitats. However, RCW management does not necessarily negatively affect these species overall: it may push them farther toward the wetter end of the gradient, but these species are known to respond positively to fire, so burning habitat for RCWs likely benefits them when the fire penetrates into these wetter habitats. We determined that two groups of hardwood-associated species occur in bottomland hardwood habitat: those that are restricted to such habitat (e.g., Acadian flycatcher [*Empidonax vireescens*] and those that are common both in this habitat and pine uplands. The Acadian flycatcher contributes to avian diversity on MCBCL, but is unaffected by RCW habitat management because this species rarely uses even a poor RCW habitat. The presence and/or abundance of those that are common both in this habitat and pine uplands (e.g., blue-gray gnatcatcher [*Poliophtila caerulea*]) are actually positively associated with RCW habitat quality with only a couple of exceptions. Thus, even hardwood-associated species appear to benefit from the management of pine habitat for RCWs.

Overall, the results of our avian research showed that avian diversity increased with RCW habitat quality. That is, the average number of species detected at a point increased as RCW habitat quality improved (**Figure ES-21**). This was especially true for species associated with upland pine habitat. Those few species exhibiting negative relationships with RCW habitat quality in their abundance were mostly species associated with shrubby understories that are common in wetter pine habitats (i.e., pocosin) on MCBCL.

We also conducted research on the cavity-nesting bird community on MCBCL because it is quite similar in structure and function to that previously studied on Eglin Air Force Base in Florida. However, the MCBCL species densities are approximately twice as high as those found on Eglin. Our results indicate that the relative availability of nesting substrates (e.g., live pines, pine snags, hardwood snags) is similar between

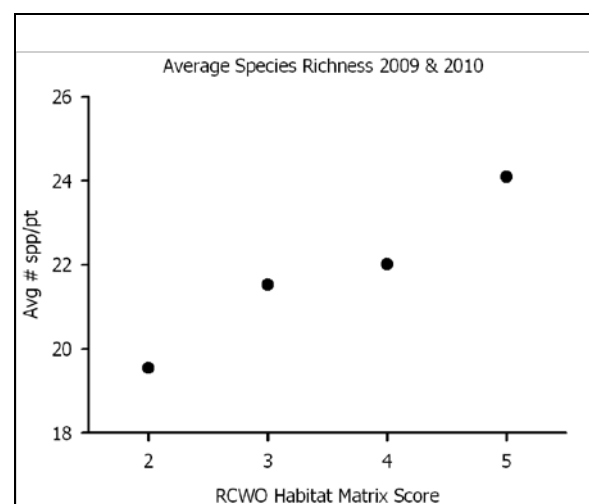


Figure ES-21. Species diversity as a function of RCW habitat quality.

the two sites, suggesting that cavity nesters are not limited by cavity availability. Cavity-nesting species tend to partition themselves among nesting substrates, and a shortage of pine or hardwood snags intensifies competition among species.

Recommendations to Installation Managers for Terrestrial Ecosystems

These research results have a number of implications for MCBCL and for other installations in the Southeast and Gulf Coast areas with similar forest restoration and RCW restoration programs.

1. Understory and midstory thinning followed by PB produces significant changes in plant species richness and composition after a single growing season. These changes are consistent with MCBCL's restoration objectives.
2. Midstory thinning of pine stands on sites with moderately organic soils (10–50% organic matter) may provide benefits for enhancing MCBCL training usage, but such stands appear to have low potential for restoration of plant and animal composition associated with longleaf pine savannas.
3. Although PB without thinning reduces the density of understory shrubs and trees, understory and midstory thinning during the growing season is significantly more effective. In either case with or without thinning, continued suppression of woody growth will require the application of regular prescribed burns.
4. In the short term, there appears to be no significant differences between applying thinning treatments during the growing season or dormant season with regard to impacts on fuels and on the composition and diversity of plants, arthropods, and birds. Growing season thinning did, however, reduce the number of live woody stems in the understory in the first post-treatment year compared to dormant season thinning. This provides MCBCL managers with greater flexibility by expanding the time frame for application of thinning treatments. However, additional research is needed to determine the longer term effects.
5. Forest management that specifically targets habitat conditions for the RCW results in habitat changes that benefit the biodiversity of terrestrial ecosystems in general and the total avian community and should be continued. This is especially true when prescribed fires penetrate into wet pocosin habitat. That is, the primary tool used to improve the quality of pine habitat for RCWs appears to produce benefits for the bird community along the ecotone between pine habitat with the other habitat type (pocosin) with which it is most commonly juxtaposed on MCBCL.
6. MCBCL should maintain, whenever possible, the availability of nesting substrate (e.g., live pines, pine snags, hardwood snags) for the wide variety of cavity-nesting avian species because that determines the strength of interactions among species. Specifically, a shortage of these dead or dying pine snags would likely result in negative impacts on RCWs due to the takeover of their cavities in live pines by other species.

Atmospheric Module

The Atmospheric Module's research focused on quantifying emissions from forest management practices, including mechanical thinning and PB, and estimating the net N deposition to MCBCL lands. In conjunction with the research conducted by Terrestrial Module researchers, the PB

research informs MCBCL's smoke management planning by quantifying emissions from different pine restoration treatments. In addition, this module collected data to estimate the total atmospheric N loading, which is information needed for developing an N budget for the NRE. This second research effort assessed and quantified the degree of atmospheric loading of N and other nutrients from wet and dry deposition to terrestrial ecosystems at MCBCL.

Mechanical thinning of the pine forest midstory prior to PB is believed to be effective in reducing wildfire risk and restoring longleaf pine savannas in the fire-dependent forest ecosystems of the Southeast (**Figure ES-22**). In situ measurements of PB emissions from the combustion of pine-dominated forest understory were conducted in conjunction with detailed before and after fuel inventory surveys. Fuel consumption was characterized in experimental research plots that underwent a understory and midstory thinning treatment (dormant season) followed by PB along a moisture gradient from semi-mesic loblolly and longleaf pine forest to wet-mesic loblolly pine forests to loblolly and pond pine pocosins. In general, the understory and midstory thinning yielded greater availability and consumption of fuels, especially woody material, regardless of fuel moisture.



Figure ES-22. Emissions were measured from control plots (left) and thinned plots (right).

Innovative mobile aerosol composition monitors were deployed to quantify emissions from plots that were mechanically thinned with those from control plots. Measured compounds included reactive gases (i.e., ammonia, nitrous acid, nitric acid, hydrogen chloride, sulfur dioxide, and light organic acids) and particulate organic compounds (POC), water-soluble ionic species, organic carbon (OC) and elemental carbon (EC), and total mass of $PM_{2.5}$ (particulate matter with a diameter of less than or equal to 2.5 microns). More than 100 POC species, including key molecular markers, were quantified, and more than 40 volatile organic compounds, including certain compounds that are important $PM_{2.5}$ precursors, were measured. Applying the carbon mass balance, emission factors were calculated for the suite of aerosol species measured.

Results indicate that the variation in site vegetation is not driving the observed emission factor differences, which are not confounded by either soil characteristics or vegetation differences on the treatment plots, thus allowing direct comparison of treatment effects on the emission factors. Gaseous emission factor averages from the control fuel and thinned fuel types are similar, and emission factor variability is highest for acidic gases and isoprene. However, $PM_{2.5}$ mass and

most PM_{2.5} species emission factors from mechanically thinned plots are significantly lower than those from control plots. Understory and midstory thinning achieves an almost 20% reduction in primary PM_{2.5} emissions per kilogram of fuel removed. Organic carbon is the dominant PM_{2.5} constituent in emissions from both fuel types, followed by EC, nitrate, potassium, and chloride (**Figure ES-23**). Employing PM_{2.5} mass closure to average control and mechanically thinned plot emissions yields total organic mass contribution of 97.2% and 95.7%, respectively. Figure ES-23 shows the lower 5% of PM_{2.5} mass fraction of species other than organics to allow for a better visual comparison of the minor species' contributions. More volatile organic carbon compounds are being emitted from both fuel types under less efficient smoldering conditions as opposed to more efficient flaming conditions. Smoldering also promotes higher emissions of inorganic constituents such as major ions (especially chloride and nitrate sulfate), major metal oxides, and non-sulfate sulfur. Removing a certain targeted amount of fuel by understory and midstory thinning prior to PB results in significant air quality benefits due to lower total PM_{2.5} emissions, although carbon monoxide, methane, and non-methane hydrocarbons emissions would be slightly enhanced.

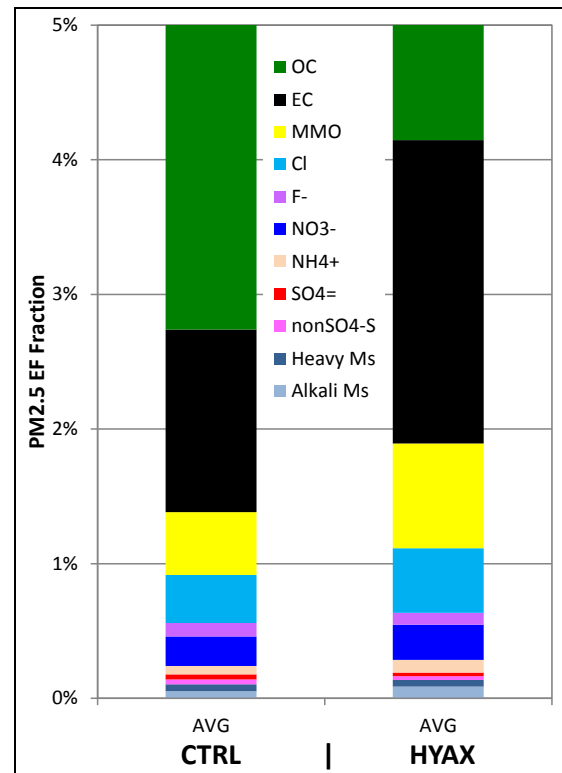


Figure ES-23. Mass fraction of major organic and inorganic compound groups emitted with PM_{2.5} from PB of both treatment types (Control [CTRL] and thinned by HydroAx machine [HYAX]).

To minimize air quality impacts of PB, MCBCL natural resource managers routinely consult the fire weather forecast released twice daily by NOAA's National Weather Service. Although the early morning version provides a 24-hour forecast, the late afternoon version looks 48 hours ahead. To determine the sensitivity of ambient PM_{2.5} to MCBCL PB activities relative to these different forecasts, we analyzed a data set from 1999 to 2007. As expected, the analysis showed that PB had the greatest impact on PM_{2.5} concentrations; however, there was also a correlation with the forecasted inversion burn-off temperature (i.e., the temperature required to dissolve remnants of the nocturnal inversion layer), suggesting that the stronger the nocturnal inversion, the more PM_{2.5} accumulates. This analysis also showed that the greater the mixing height and ventilation rate, the lower the PM_{2.5} concentrations, which points to the diluting effect of these parameters on ambient PM_{2.5} concentration. Therefore, these parameters should be used by managers to minimize air quality impacts. The analysis also determined that there was no significant difference on the projected concentrations of PM_{2.5} from PB activities using either the morning and afternoon weather forecasts, suggesting that MCBCL natural resource managers can plan their PB activities the evening before without having to wait for the morning forecast and still meet the objective to conduct PB with minimal impact on local air quality.

To inform the Aquatic/Estuarine Module's research efforts of estimating the magnitude of nitrogen inputs to the NRE, the Atmospheric Module researchers focused on determining whether atmospheric deposition represents a significant source of new nitrogen to the MCBCL ecosystems. Wet deposition (rainfall) was measured from July 2009–June 2011 using solar-powered Mercury Deposition Network wet deposition collectors at four locations across MCBCL. In 2010, the average wet deposition from the four locations was $4.3 \pm 0.7 \text{ kg N ha}^{-1} \text{ y}^{-1}$ for total nitrogen and $3.2 \pm 0.4 \text{ kg N ha}^{-1} \text{ y}^{-1}$ for DIN. Wet deposition of DIN at MCBCL was comparable to the 9-year average of $3.7 \text{ kg N ha}^{-1} \text{ y}^{-1}$ calculated for the National Trends Network (NTN) collector NC29 located at the nearby Hofmann Forest northeast of Jacksonville, NC. The highest deposition of DIN wet deposition occurred in the summer during June, July, and August. Dissolved organic nitrogen (DON, measured as the difference between total nitrogen and DIN) in wet deposition was substantial (approximately $1 \text{ kg N ha}^{-1} \text{ y}^{-1}$), with the highest percentage (approximately 40%) of nitrogen inputs observed in the fall.

A network of 28 tipping bucket rain gauges found no apparent latitudinal gradient in rainfall amounts across MCBCL due to the proximity of the ocean. There was, however, a measureable gradient in wet and dry deposition of chloride, sodium, and sulfate moving inland. Throughfall collectors were used to measure inputs of nitrogen and other nutrients into the forest floor under the dominant forested canopies (e.g.,

longleaf pine savanna [*Pinus palustris*], mixed pines and hardwoods [loblolly pine, *Pinus taeda*, and predominantly oak, *Quercus* spp.], and hardwoods [predominantly oak, *Quercus* spp]; **Figure ES-24**). Inputs of total nitrogen under these forested canopies were approximately two times greater than those found in wet deposition alone, a substantial fraction of which appeared to be in the form of DON. Calculation of net throughfall (throughfall minus wet deposition) indicated the presence of dry deposition of nitrate-nitrogen and to a lesser extent ammonium-nitrogen, but also loss of nitrogen from wet deposition during the summer and fall months due to

interaction with the overhead canopy. Therefore, nitrogen loading estimates to the NRE were likely lower than actual loadings due to the absence of direct measures of dry deposition of nitrogen. Agreement between our measured amounts of the wet deposition of nitrogen at MCBCL to the nearby NTN collector NC29 at Hofmann Forest indicate that atmospheric loading of nitrogen to MCBCL has been relatively constant for at least the past 10 years.



Figure ES-24. An example of deployed throughfall collectors under longleaf pine canopy.

To compare potential nutrient loss via PB emissions with redeposition from the forest canopy's retaining effect and washout of nutrients in subsequent rain events, throughfall samples were collected during post-PB rain events at two different times and at two different locations. One site was a mesic loblolly–longleaf pine stand close to the estuary, and the other was a semi-mesic loblolly pine stand farther inland with soil moisture levels about half those of the mesic stand.

Due to proximity to the estuary, more salt was deposited to the mesic stand close to the estuary, and the semi-mesic stand received more potassium, sulfate, and nitrogen. Relative to deposition, emissions of cations from PB on both stands were insignificant except for potassium and ammonium. For both tests, nutrient export via PB emissions was significantly smaller than subsequent nutrient input from throughfall deposition, except for reduced nitrogen under wetter stand conditions in which nutrient export approximately equaled input. These results suggest that long-term soil nutrient levels remain unaffected by PB, causing only a short-term disturbance. However, additional observations are needed to develop statistically robust conclusions.

Recommendations to Installation Managers for Atmospheric Systems

1. $PM_{2.5}$ mass and most $PM_{2.5}$ species emission factors from mechanically thinned plots are significantly lower than from untreated control plots. Employing mechanical thinning practices to a targeted amount of fuel prior to PB leads to significant air quality benefits due to lower total $PM_{2.5}$ emissions.
2. Understory and midstory thinning in stands targeted for longleaf pine restoration make two times more fuel available for combustion and help consume almost three times more fuel, especially woody material, regardless of fuel moisture, relative to unthinned, control plots. MCBCL natural resource managers should consider using understory and midstory thinning prior to PB to reduce smoke emissions as part of their Smoke Management Plan.
3. MCBCL natural resource managers can plan their PB activities using the NWS evening meteorological forecast before a PB without having to wait for the A.M. forecast. This will continue to meet the objective of conducting the PB with minimal impact on local $PM_{2.5}$ air quality.
4. MCBCL natural resource managers routinely consult the fire weather forecast released by NOAA's National Weather Service. Our analysis of MCBCL data revealed that the greater the mixing height and ventilation rate, the lower the resulting $PM_{2.5}$ concentrations, which points to the diluting effects of these parameters on ambient $PM_{2.5}$ concentration. Natural resource managers should use these parameters in their smoke management planning to help minimize air quality impacts of PB on both installation lands and on adjacent properties.
5. The NTN collector NC29 located at the nearby Hofmann Forest northeast of Jacksonville can serve as a surrogate monitoring site for MCBCL and wet deposition of N data collected as part of the National Atmospheric Deposition Program–NTN.

Next Steps

DCERP1 concluded in January 2013. The next 5 years of the program (referred to as DCERP2) began in November 2012 and will continue until November 2017. During a 3-month planning period, the DCERP Team prepared a new Research Plan that focused on several new themes: evaluation of the carbon cycle of the estuary, coastal marshes, and the barrier island; identification the impacts of climate change on physical, chemical, and biological processes in select ecosystems of MCBCL; and translation of research findings as tools and products that can be easily transferred or used by a variety of stakeholders. Many of the DCERP1 researchers are building on the knowledge gained from DCERP1 research results to develop monitoring and research programs for DCERP2. To turn science into practice, the DCERP Team will use models

developed during DCERP1 and DCERP2 to project current ecosystem processes through climate change scenarios to future conditions. These future climate change conditions are likely to include warming temperatures, wide variability in the hydrological cycle (drought/wet periods), increased magnitude of storms, and SLR.

The Data and Information Management System developed during DCERP1 will continue to support the program by storing structured monitoring and research data in the Monitoring and Research Data and Information System (MARDIS) and by archiving final products in the Document Database. A new Web-based Decision-Support System (DSS) framework (based on a prototype system developed during DCERP1) will be implemented during DCERP2 using data from MARDIS, MCBCL, and other publicly available sources to develop decision-support tools to better inform installation management decisions. This DSS framework will allow models and other decision-support tools to be easily accessible for wide distribution to interested installation managers and to the scientific community and other stakeholders.

Literature Cited

- Kemp, A.C., B.P. Horton, D. Reide Corbett, S.J. Culver, R.J. Edwards, and O. van de Plassche. 2009. The relative utility of foraminifera and diatoms for reconstructing late Holocene sea-level change in North Carolina, USA. *Quaternary Research* 71:9–21.
- NOAA (National Oceanic and Atmospheric Administration). 2004. *North Carolina Bathymetry/Topography Sea Level Rise Project: Determination of Sea Level Trends*. NOAA Technical Report NOS CO-OPS 041. Available at <http://tidesandcurrents.noaa.gov/publications/techrpt41.pdf>.

Chapter 1

Introduction

SERDP Project Number: RC-1413

Principal Investigator:
Dr. Patricia Cunningham
RTI International
Research Triangle Park, NC 27709
E-mail: patc@rti.org

May 10, 2013

Final

This report was prepared under contract to the U.S. Department of Defense (DoD) Strategic Environmental Research and Development Program (SERDP). The publication of this report does not indicate endorsement by DoD, nor should the contents be construed as reflecting the official policy or position of DoD. References herein to any specific commercial product, process, or service by trade name, trademark, manufacturer, or otherwise, do not necessarily constitute or imply its endorsement, recommendation, or favoring by DoD.

Table of Contents

List of Acronyms	1-v
Introduction.....	1-1
Background.....	1-1
Site Selection for DCERP.....	1-1
Integration of DCERP with MCBCL's Natural Resources Management	1-3
Program Organization.....	1-4
DCERP Management.....	1-4
DCERP Team.....	1-5
Overarching DCERP Strategy	1-6
DCERP Research Strategy.....	1-8
Research and Monitoring.....	1-11
Research Projects	1-11
Integration of DCERP Research and Monitoring	1-13
Report Organization.....	1-15
Literature Cited	1-16
Appendix 1-A: Prioritized List of MCBCL's Conservation and Water Quality Needs	1-A-1

List of Figures

1-1.	Site map of MCBCL	1-2
1-2.	Organization of DCERP.	1-5
1-3.	Overall DCERP process.....	1-8
1-4.	Overarching conceptual model for DCERP at MCBCL.....	1-10
1-5.	Generic roadmap of the integrated DCERP Baseline Monitoring Plan and <i>DCERP Research Plan</i> and the development of model tools and indicators.	1-14

List of Tables

1-1.	MCBCL–Specific Military Drivers	1-3
1-2.	Examples of Military, Non-Military, Legacy, and Natural Stressors to an Ecosystem	1-9
1-3.	Summary of the 13 Research Projects of DCERP	1-11
1-4.	Summary of Module-Specific DCERP Baseline Monitoring Program Activities.....	1-13

List of Acronyms

AE	Aquatic/Estuarine Module
Air	Atmospheric Module
CB	Coastal Barrier Module
CW	Coastal Wetlands Module
CWA	Clean Water Act
DCERP	Defense Coastal/Estuarine Research Program
DCERP1	first cycle of the Defense Coastal/Estuarine Research Program
DCERP2	Second cycle of the Defense Coastal/Estuarine Research Program
DIMS	Data and Information Management System
DoD	U.S. Department of Defense
EMD	Environmental Management Division
ESA	Endangered Species Act
INRMP	<i>Integrated Natural Resources Management Plan</i>
MCBCL	Marine Corps Base Camp Lejeune
NAVFAC ESC	Naval Facilities Engineering Command/Engineering Service Center
NRE	New River Estuary
OSC	On-site Coordinator
PI	Principal Investigator
PNA	Primary Nursery Area
RCC	Regional Coordinating Committee
RCCC	Resource Conservation and Climate Change (Program)
SERDP	Strategic Environmental Research and Development Program
RCW	red cockaded woodpeckers
T	Terrestrial Module
TAC	Technical Advisory Committee

[This page intentionally left blank.]

Introduction

The overall intent of the Defense Coastal/Estuarine Research Program (DCERP) “is to develop the knowledge required to assess the interaction between military activities and ecological resources in a coastal/estuarine setting, monitor those interactions, and identify adaptive, ecosystem management approaches for sustainment of military lands and adjacent waters,” as stated in the initial *DCERP Strategy Report* (SERDP, 2005). This purpose of this *DCERP1 Final Research Report* is to summarize the DCERP research activities and results from July 2007 to September 2012.

Chapter 1 of this *DCERP1 Final Research Report* provides a general introduction to DCERP conducted at Marine Corps Base Camp Lejeune (MCBCL) in North Carolina, briefly highlights the overall program objectives, and describes the activities conducted during Phases I and II of the program. Chapter 1 also describes how the DCERP Team engaged with other team members and MCBCL staff during DCERP1’s initial planning period (i.e., Phase I) from November 2006 to June 2007 to develop three key documents to guide implementation of DCERP. These documents are the overarching research strategy (the *DCERP Strategic Plan* [RTI, 2007a]), the design of an ecosystem-based monitoring program (the *DCERP Baseline Monitoring Plan* [RTI, 2007b]), and the identification of detailed research projects (the *DCERP Research Plan* [RTI, 2007c]). This chapter also discusses another Phase I activity, the development of the Data and Information Management System (DIMS) design for the program.

Chapter 1 also highlights the activities slated during the program’s subsequent implementation period (i.e., referred to as DCERP1 Phase II from July 2007 to January 2013. For instance, during Phase II, the team members carried out the *DCERP Research Plan* through field research and the operation of the long-term baseline monitoring program. The Research Plan was also implemented through the collection, management, analyses, and archiving of data from both the research and monitoring activities into the DCERP DIMS. Most of the field work for the research projects concluded in November 2011; although some of the baseline monitoring activities continued through 2012. Therefore, the last year of the DCERP1 was dedicated primarily to synthesizing and reporting the results and to disseminating the important information and data to MCBCL, local stakeholders, the scientific community, and the general public. In addition, DCERP1 research and monitoring activities laid the foundation for the follow-on contract activities proposed for DCERP2 (planned for implementation from February 1, 2013, through October 31, 2017).

Background

Site Selection for DCERP

Critical military training and testing on lands along the nation’s coastal and estuarine shorelines are increasingly placed at risk because of development pressures in surrounding areas, impairments due to other anthropogenic disturbances, and increasing requirements for compliance with environmental regulations. The U.S. Department of Defense (DoD) intends to enhance and sustain its training and testing assets and to optimize its stewardship of natural resources through the development and application of an ecosystem-based management approach

on DoD facilities. DoD's policy has established ecosystem-based management as the preferred approach for military lands (Goodman, 1996). This approach will focus on sustaining and enhancing military training and testing activities by monitoring and managing the interdependent natural resource assets on which the future of these activities depend. To expand its commitment to improving military readiness while demonstrating the science behind this approach, the Strategic Environmental Research and Development Program (SERDP) has made a commitment of at least 10 years to fund research and monitoring projects that support the sustainability of military training and testing in ecologically and economically important ecosystems. To accomplish this goal, SERDP launched DCERP at MCBCL in North Carolina (**Figure 1-1**).

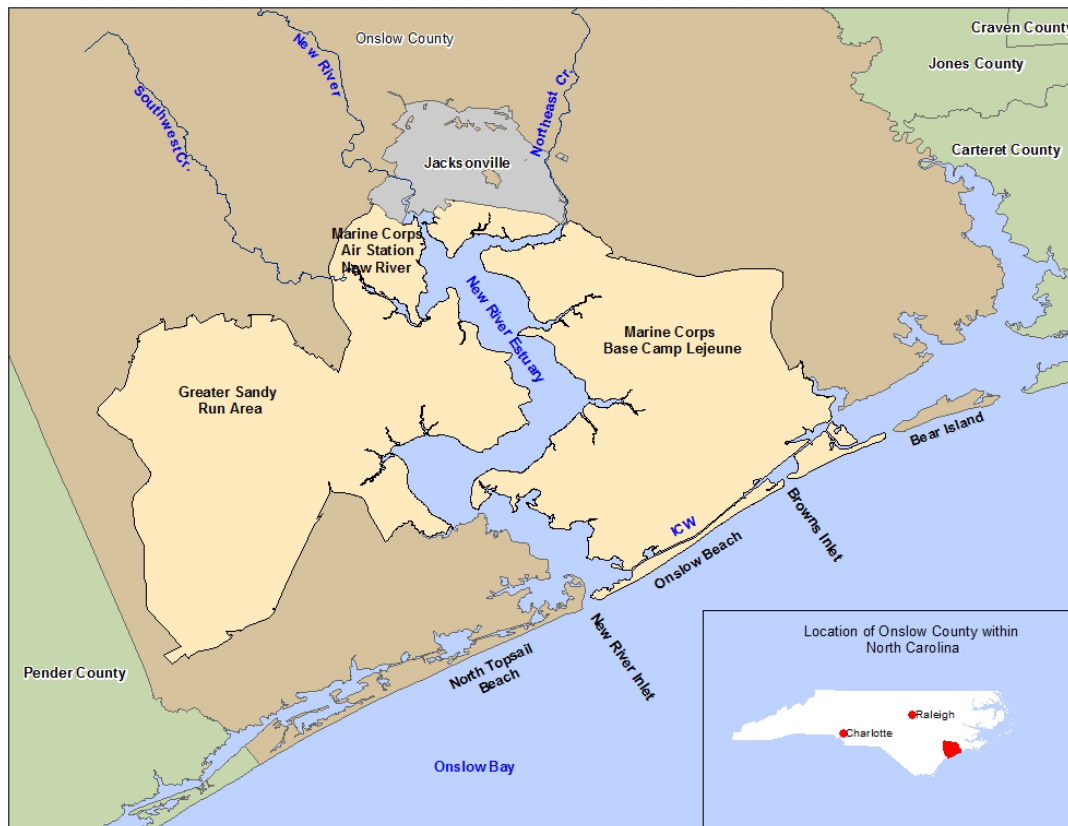


Figure 1-1. Site map of MCBCL.

As a U.S. Marine Corps installation, MCBCL has a single and exclusive mission: military preparedness. MCBCL provides an ideal platform for DCERP because it integrates aquatic/estuarine, coastal wetlands, coastal barrier, and terrestrial ecosystems, all within the boundaries of DoD properties.

MCBCL was chosen as the DCERP site for a variety of reasons, including the following:

- The New River Estuary (NRE) watershed, which borders the site, is relatively small and, therefore, a manageable study site.
- MCBCL occupies a substantial portion (approximately 80%) of the NRE shoreline.
- A barrier island and coastal dune system occurs within MCBCL's boundary that provides a unique amphibious assault training environment.

- The variety of ongoing military operations at MCBCL enables researchers to examine training impacts on a broad range of ecosystems, from upland pine savannas to aquatic and estuarine waters to coastal barriers.

Integration of DCERP with MCBCL's Natural Resources Management

MCBCL's mission is to provide military training that promotes the combat readiness of operating forces, and all MCBCL natural resources management activities on the Base must support this mission. As a military installation, MCBCL has needs, or drivers, that must be satisfied to meet its readiness mission to continue without significant disruption. MCBCL must also comply with related environmental laws and regulations, such as the federal Endangered Species Act (ESA) and the Clean Water Act (CWA), to ensure continuance of its mission. To ensure such compliance, MCBCL developed and adopted an *Integrated Natural Resources Management Plan* (INRMP; MCBCL, 2006a), which outlines the Base's conservation efforts and establishes procedures for fiscal years 2007 through 2011. One goal of the INRMP is to minimize future training restrictions (i.e., no net loss in the ability to train) by increasing the integration between natural resources management planning, training, and operations. One of DCERP's objectives is to assist MCBCL in achieving this goal. As such, Base natural resource and environmental management personnel were involved throughout the DCERP planning process by participating in all planning workshops and reviewing the *DCERP Strategic, Research, and Baseline Monitoring Plans* that were the final products from Phase I.

Unique to MCBCL are installation-specific drivers that are defined by the Base's mission and geographic location, land uses to support the mission, and natural resources affected by the mission. Identifying the primary military drivers at the MCBCL provided the basis for establishing seven natural resources management objectives for the Base. The objectives are presented in **Table 1-1**.

Table 1-1. MCBCL-Specific Military Drivers

Driver 1	Preserving the integrity of the amphibious maneuver areas, including Onslow Bay, the NRE, and the adjoining training areas and airspace of the MCBCL
Driver 2	Preserving the integrity of MCBCL as a combined-arms training Base by ensuring the continued viability of its impact areas and associated training ranges
Driver 3	Enhancing future training uses of MCBCL ranges, training areas, and airspace by fully integrating the Land Use Master Plan (MCBCL, 2005) and Range Transformation Plan (MCBCL, 2006b)
Driver 4	Ensuring that MCBCL supports all required military training activities, while complying with the ESA and other wildlife requirements
Driver 5	Ensuring that MCBCL supports continued military training use of the NRE and Onslow Bay, while complying with the CWA
Driver 6	Ensuring the viability of the New River Air Station as an aviation facility through the elimination of bird and wildlife strike hazards to aircraft, while complying with the ESA and other wildlife regulatory requirements
Driver 7	Ensuring the viability of MCBCL military training activities, while supporting mission-critical infrastructure development

In addition to these military drivers, MCBCL natural resources management staff identified a prioritized list of conservation and water quality needs that will support implementation of the INRMP (**Appendix 1-A**). Throughout DCERP, every effort was made to include the Base's areas of concern that were not currently being investigated under existing programs and to inform Base staff of DCERP activities and results.

Program Organization

DCERP is a collaborative effort between SERDP, the Naval Facilities Engineering Command/Engineering Service Center (NAVFAC ESC), MCBCL, and RTI International, which is headquartered in Research Triangle Park, NC. RTI led the DCERP research and monitoring effort at MCBCL and assembled a diverse team of experts from several federal agencies, academia, and the private sector (henceforth referred to as the DCERP Team). The Management Team and the Research Team are discussed in the following two subsections.

DCERP Management

SERDP is an environmental research and development program that is planned and carried out by DoD in full partnership with the U.S. Department of Energy and the U.S. Environmental Protection Agency. The SERDP Resource Conservation and Climate Change (RCCC) Program Manager, Dr. John Hall, ensured that DCERP activities provide for the enhanced knowledge of ecosystem and military interactions within approved scopes of work and budgets. The overarching federal management for DCERP was assigned to the NAVFAC ESC. Dr. Hall served as the Contracting Officer's Representative. In that capacity, he ensured that tasks identified in the Statement of Work were properly performed by the DCERP Principal Investigator (PI), Dr. Patricia Cunningham of RTI. The DCERP PI was responsible for the overall scientific quality, cohesiveness, and relevance of DCERP monitoring and research activities. The DCERP PI was also the primary point of contact for SERDP and MCBCL and coordinated all DCERP activities conducted at MCBCL through the DCERP On-site Coordinator (OSC), Dr. Susan Cohen.

At MCBCL, the DCERP OSC, the Director of the Environmental Management Division (EMD; Mr. John Townson), and the Head of the Environmental Conservation Branch (Mr. Bill Rogers) assisted the DCERP PI with coordinating the environmental monitoring and research activities on the Base. The DCERP OSC was the primary point of contact between MCBCL and the DCERP Team..

Two committees provided guidance and input to the DCERP. The first, the Technical Advisory Committee (TAC), was a group of discipline experts from academia, industry, government, and the military that was assembled by the SERDP RCCC Program Manager to provide scientific and technical review and guidance to ensure the quality and relevance of DCERP. The second committee, the Regional Coordinating Committee (RCC), was a group of local and regional stakeholders that served as one of the recipients of outreach from MCBCL, the DCERP PI, the DCERP OSC, and the SERDP RCCC Program Manager, thereby fostering relationships among the representative organizations and DCERP.

Figure 1-2 illustrates the program's overall organization and lines of communication.

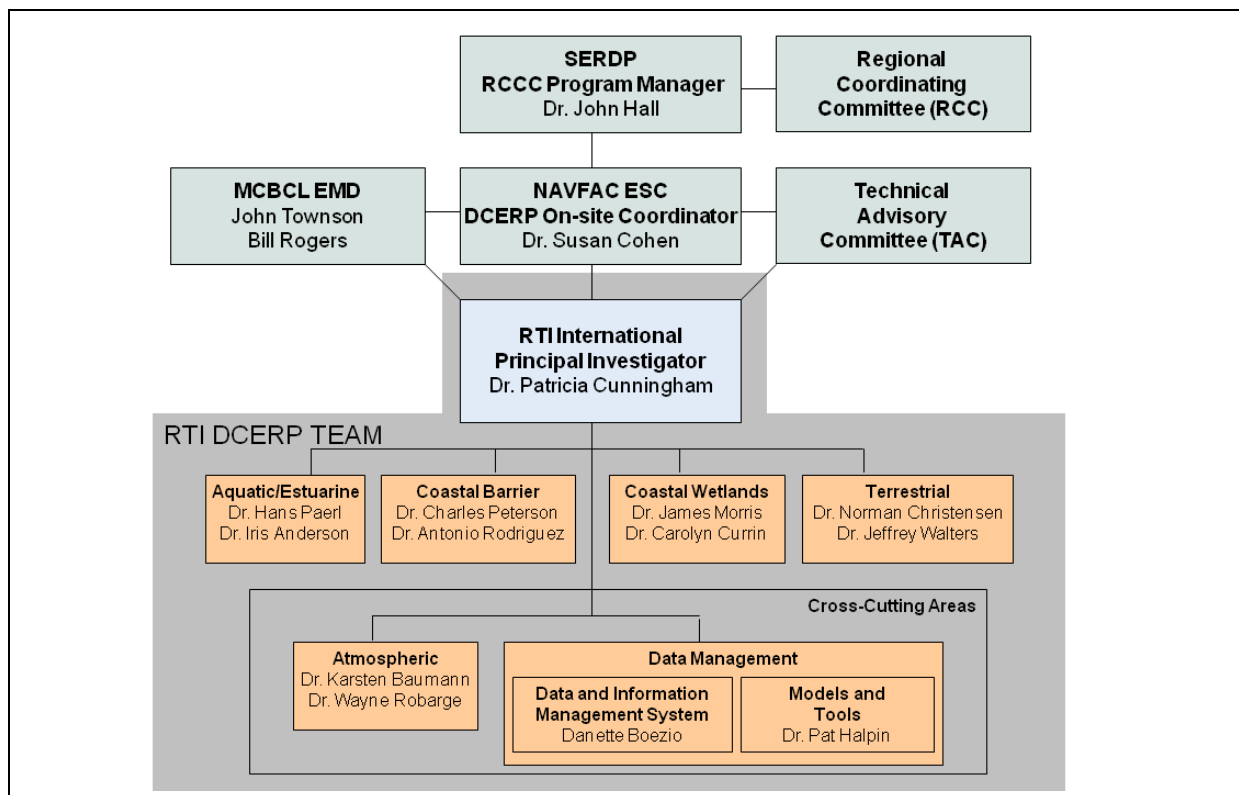


Figure 1-2. Organization of DCERP.

DCERP Team

RTI selected members of the DCERP Team because of their expertise in relevant environmental science disciplines and substantial experience in working together on interdisciplinary aquatic/estuarine, coastal, and terrestrial ecosystem projects. The DCERP Team included the DCERP PI, other environmental scientists from RTI, and researchers from seven academic institutions, three governmental agencies, and two private companies.

The DCERP Team was organized into six Module Teams based on the ecosystem-based management objective for the program. Each Module Team was directed by a Module Team Leader and Co-Leader. The DCERP PI and the Module Team Leaders and Co-Leaders composed an Executive Board, which provided input on technical decisions and helped prioritize program needs such as identifying areas of knowledge needing supplemental research and funding support. These Module Teams conducted monitoring and

DCERP Team

RTI has assembled a diverse team of researchers from the following organizations, collectively referred to as the DCERP Team:

- Atmospheric Research and Analysis, Inc.
- Duke University
- National Oceanic and Atmospheric Administration
- North Carolina State University
- Porter Scientific, Inc.
- RTI International
- University of Connecticut
- University of North Carolina at Chapel Hill
- University of South Carolina
- U.S. Army Corps of Engineers
- U.S. Geological Survey
- Virginia Institute of Marine Science
- Virginia Tech

research activities for DCERP's five ecosystem modules (i.e., Aquatic/Estuarine, Coastal Wetlands, Coastal Barrier, Terrestrial, and Atmospheric) and a Data Management Module.

The DCERP Team addressed the initial DCERP objectives of developing monitoring approaches and identifying key ecological processes through research and modeling studies, all with the goal of supporting the practice of ecosystem-based management for all coastal DoD installations in similar ecological settings.

Overarching DCERP Strategy

DCERP's primary overarching objective was to enhance and sustain MCBCL's military training mission by developing an understanding of estuarine, coastal wetlands, coastal barrier, and terrestrial ecosystem composition, structure, and function within the context of a military training environment. Specific DCERP objectives were to

- Develop the *DCERP Strategic Plan* (overarching strategy) that includes appropriate conceptual and mechanistic ecosystem models to guide monitoring, research, and adaptive management (Phase I)
- Identify significant ecosystem stressors¹ (i.e., military, non-military, legacy, and natural), their sources (on and off Base), and their level of impact on MCBCL's ecological systems through space–time coordinated monitoring and research (Phase II)
- Incorporate information about stressors and other environmental factors into ecosystem models to develop effective indicators of potential changes to ecosystem condition and state, which may require more effective management guidelines to achieve sustainability (Phase II).

During the planning period (Phase I), the DCERP Team designed an integrative monitoring, modeling, and research strategy for MCBCL that is consistent with guidance on ecosystem-based management from the Ecological Society of America (Christensen et al., 1996) and recommendations of the U.S. Commission on Ocean Policy (2004), including principles of adaptive management (Walters, 2001). This strategy transcended air–land–water boundaries to better understand the causes and nature of ecological and environmental changes across the region and locally at MCBCL. Based on interconnectivity, this strategy helped separate the underlying natural (e.g., climatic, biogenic) and anthropogenic–regional processes from locally driven processes, identify stressor-specific indicators of ecosystem status that provide early warnings of ecosystem degradation, and specify the critical thresholds for indicators of potential state shifts that could threaten sustainability. DCERP adapted the following elements of ecosystem-based management described by Christensen et al. (1996):

¹ For DCERP, stressors are defined as activities or events that alter natural ecological processes. Natural ecosystem stressors include natural forces (e.g., hurricanes, sea level rise) whose effects are enhanced by anthropogenic activity (e.g., global warming). The increased frequency and intensity of natural events, in combination with anthropogenic contributions, could cause ecosystem perturbations outside the range of natural variation.

- ***Sustainability***—The underlying premise is that military usability will persist indefinitely under a well-conceived ecosystem-based management plan.
- ***Explicit goals***—Ecosystem-based management identifies specific measurable goals for which management is conducted and which can serve as indicators of success.
- ***Sound science and ecological models***—The success of ecosystem-based management depends upon the quality and completeness of the scientific understanding of the system and models that are required to synthesize information to make sound judgments.
- ***Complexity and connectedness***—Ecosystem-based management recognizes explicitly that important interconnections exist among elements of an ecosystem and that these need to be understood to model the system properly and thereby provide tools to gauge the attainment of sustainability.
- ***Dynamic nature of ecosystems***—Because of both extrinsic drivers and intrinsic interactions, components of ecosystems are not static, and this natural variability must be understood to detect signals from other stressors and to set realistic management goals.
- ***Context and scale***—Ecosystems are driven by processes at multiple spatiotemporal scales, and recognizing the regional setting of these processes is critical for modeling locally driven impacts.
- ***Humans as ecosystem components***—Rather than ignoring humans, ecosystem-based management explicitly places humans in the system as one important element that can play an active role in achieving sustainable management goals.
- ***Adaptability and accountability***—Ecosystem-based management realizes that existing models are always incomplete and predictions are uncertain; therefore, management actions must be treated as hypotheses and tested as a practical means of ensuring success and providing feedback to improve the models.

To successfully meet the objectives previously listed, the DCERP Team

- Ensured relevance of the program to MCBCL's operations
- Ensured that outcomes reflect an adaptive management approach to ecosystem sustainability
- Developed and applied models that incorporate regional and local military drivers to support the sustainability or enhancement of military operations
- Used ecosystem-based models, including mission drivers, to identify methods and tools to support the sustainability or enhancement of ecosystem function and health
- Ensured implementation of essential monitoring, high-quality research, and data management procedures
- Conducted effective outreach and communication of information to the scientific community, MCBCL, other military facilities, other stakeholders, and the general public.

Details about the specific activities performed by the DCERP Team are presented in the following section.

DCERP Research Strategy

During the earliest stages of DCERP, the DCERP Team developed the overall process (**Figure 1-3**) that was used to meet the program's objectives. This process started with identifying ecosystem processes and stressors, developing these into an overarching conceptual model of DCERP, and then creating individual ecological models.

An important part of the DCERP process was to ensure that the ecological models developed for each individual module were designed to integrate the ecological processes and stressors with the Base's military drivers and conservation and water quality needs, as determined by MCBCL for the management of natural resources. The following subsections (Ecosystem Stressors, Overarching Conceptual Model, and Individual Ecological Models) describe each of these activities performed by the DCERP Team.

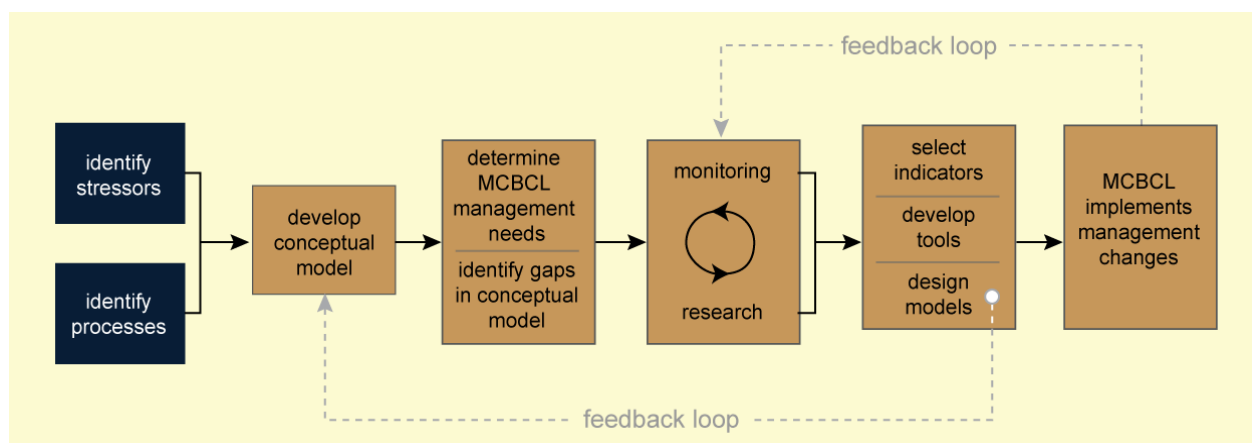


Figure 1-3. Overall DCERP process.

Ecosystem Stressors

Although the main processes are generally understood, the biological, chemical, and physical ecosystem processes at MCBCL had not been researched extensively, especially within the context of outside stressors. The DCERP Team defined stressors as activities or events that alter ecological processes. The DCERP Team grouped stressors into four major categories: military, non-military, legacy, and natural. **Table 1-2** provides a definition for each category and specific examples relevant to DCERP.

Table 1-2. Examples of Military, Non-Military, Legacy, and Natural Stressors to an Ecosystem

Stressors	Examples
Military	Military stressors are unique activities or events that are associated with military training and testing at MCBCL. Some examples of military stressors include the use of military tracked vehicles and amphibious watercraft troop movements on the Base and the use of firing ranges and impact areas.
Non-military	Non-military stressors are any anthropogenic activities that can occur on or off Base. Some examples of non-military stressors include runoff of nutrients from confined animal feeding operations, agricultural practices, or urban lands; industrial and municipal discharges; atmospheric deposition of nutrients and contaminants; local residential or commercial development; groundwater withdrawals; and prescribed burning activities.
Legacy	Legacy stressors are anthropogenic activities that have occurred in the past, but whose effects are continuing today. Some examples of legacy stressors include construction of the Intracoastal Waterway, early ditching activities to drain land, historic use of fire, agricultural activities, and timber harvesting.
Natural	Natural ecosystem stressors include natural forces (e.g., hurricanes, sea level rise) whose effects are enhanced by anthropogenic activity (e.g., global warming). The increased frequency and intensity of natural events, in combination with anthropogenic contributions, could cause ecosystem perturbations outside the range of natural variation.

Overarching Conceptual Model

Once the DCERP Team members defined and grouped the stressors into the four major categories, they developed the overarching conceptual model of DCERP for the MCBCL region. This region includes the terrestrial lands of MCBCL, the NRE, associated coastal wetlands, and the coastal barriers along Onslow Bay, as well as the overarching influence of local and regional atmospheric conditions. **Figure 1-4** presents the overarching conceptual model for DCERP.

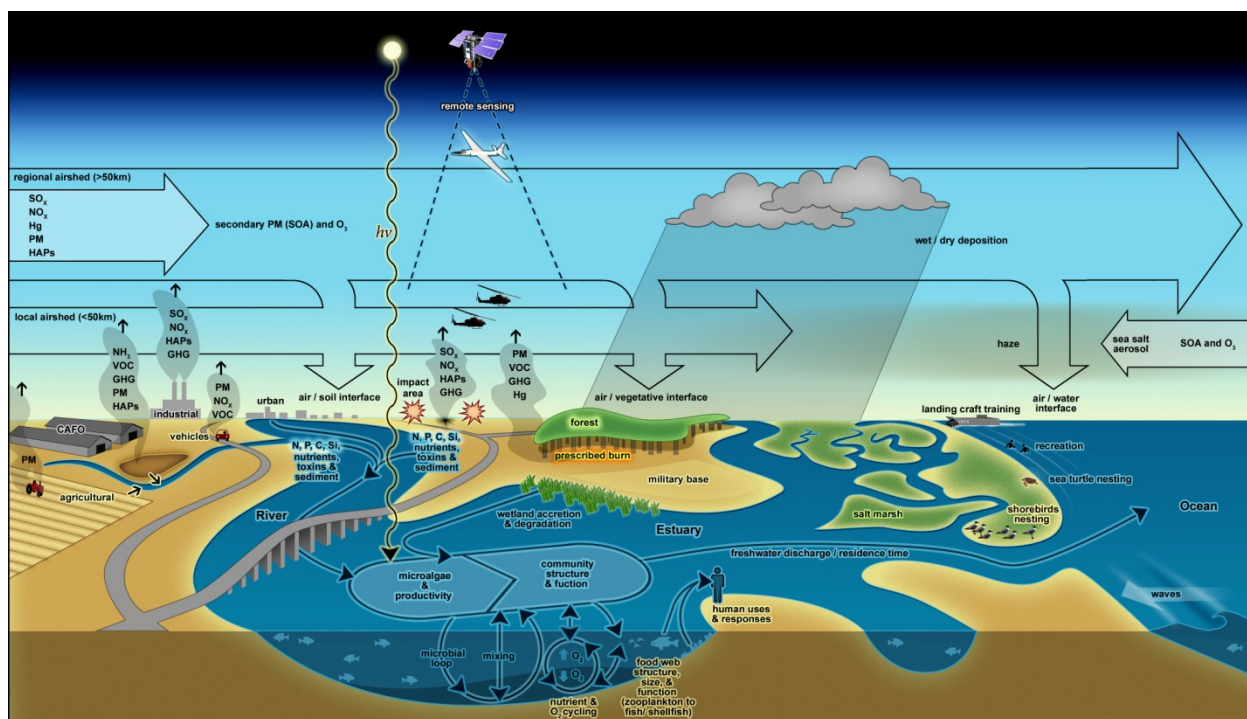


Figure 1-4. Overarching conceptual model for DCERP at MCBCL.

Individual Ecosystem Modules

To facilitate an understanding of the state of the ecosystems and dynamics of the MCBCL region, during the strategic planning process, each of the ecosystem Module Teams then divided the overarching conceptual model of DCERP into four ecosystem modules for monitoring, modeling, and research. These four modules are as follows: Aquatic/Estuarine, Coastal Wetlands (land–estuary margin), Coastal Barrier, and Terrestrial. These modules were linked to each other and to local and regional disturbances and pollutant sources of anthropogenic origin via atmospheric and aquatic transport mechanisms. Because the atmosphere has an overarching influence on all four ecosystem modules, it was treated as a fifth ecosystem module (i.e., the Atmospheric Module). All of the modules developed conceptual models for their respective ecosystems. After developing the overarching conceptual model and the individual ecosystem conceptual models, the DCERP Module Teams identified knowledge gaps in the conceptual models, worked with the Base staff to identify the needs of MCBCL management, and then determined potential research questions to fill these basic knowledge gaps and address these needs. Individual ecological models are presented in Chapter 2 of this *DCERP1 Final Research Report*.

A sixth module, the Data Management Module, involved a diverse group of data management and analysis specialists who have expertise in the development of data management procedures for the DCERP DIMS, including coordination of geospatial data, statistical analysis, and model integration. The Data Management Module involved the following two components: (1) a database and information management system and (2) model and tool development component.

SERDP envisioned the database and information management system component to be a dynamic system to facilitate the collection, integration, and exchange of environmental data

among the DCERP Team and serve as the permanent repository for research and monitoring data and for associated information (e.g., documents, reports, maps, photographs) collected during DCERP's implementation. The model and tool development component provides the ultimate cross-cutting function of incorporating the simple models, which were developed by the individual research projects, into integrated management tools and models. All data and products produced by DCERP were archived in the DCERP DIMS. A summary of this system will be provided in a separate report.

Overall, DCERP has provided basic scientific information needed to develop management plans to modulate the impacts of military training activities and to sustain both the natural resources and use of the Base for military training now and in the future.

Research and Monitoring

The main purpose of DCERP was to gain a better understanding of ecosystem, processes, and impacts of stressors on these processes, which is critical for implementing ecosystem-based management strategies. DCERP was designed to be an adaptive program; therefore, the DCERP Team developed the *DCERP Baseline Monitoring Plan* to gather environmental data to address MCBCL's management concerns and support the research projects identified in the *DCERP Research Plan*. The research projects and baseline monitoring activities of DCERP are described in the following subsections.

Research Projects

To support MCBCL's objectives, the DCERP Team conducted 13 research projects (**Table 1-3**), which focused on understanding knowledge gaps identified through the development of each ecosystem module's conceptual model, including innovative techniques for addressing these knowledge gaps. Specifically, the DCERP Team tested ecosystem response to the previously mentioned four stressors (i.e., military, non-military, legacy, and natural), examined potential indicators of ecosystem change, and evaluated various management practices to help sustain MCBCL ecosystems and their natural resource assets.

Table 1-3. Summary of the 13 Research Projects of DCERP

Research Project Title	Senior Researcher; Project Duration
AE-1: Develop and Deploy Microalgal Indicators as Measures of Water Quality, Harmful Algal Bloom Dynamics, and Ecosystem Condition	Hans Paerl; 7/2007–9/2012
AE-2: Quantifying and Predicting Watershed Inputs of Nutrients, Sediments, and Pathogens to Tributary Creeks on Marine Corps Base Camp Lejeune	Mike Piehler; 7/2007–9/2012
AE-3: Developing Indicators of Ecosystem Function for Shallow Estuaries: Benthic Functional Responses in the New River Estuary	Iris Anderson; 7/2007–9/2012

(continued)

Table 1-3. Summary of the 13 Research Projects of DCERP (continued)

Research Project Title	Senior Researcher; Project Duration
CW-1: Drivers and Forecasts of the Responses of Tidal Salt Marshes to Sea Level Rise	Jim Morris; 7/2007–9/2012
CW-2: Forecasting Influence of Natural and Anthropogenic Factors on Estuarine Shoreline Erosion Rates	Mark Fonseca; 9/2007–9/2012
CW-3: Hydraulic Exchange and Nutrient Reactivity in the New River Estuary Wetlands	Craig Tobias; 7/2008–9/2012
CB-1: Short-Term Barrier Evolution: Overwash at Onslow Beach Through Assessment of Training Activities and Model Predictions	Jesse McNinch; 7/2009–9/2012
CB-2: Long-Term Barrier Evolution Related to Variations in Underlying Geology and Land Use	Tony Rodriguez; 7/2009–9/2012
CB-3: Understanding the Top-Down and Bottom-Up Drivers of Shorebird Nest Success and Habitat Use in Relation to Beach Management Practices on MCBCL	Sarah Karpanty and Jim Fraser; 7/2007–12/2011
T-1: Effects of Different Understory Restoration Management Options on Terrestrial Ecosystem Structure and Function	Norman Christensen; 1/2008–9/2012
T-2: Effects of Habitat Management for Red-Cockaded Woodpeckers on Bird Communities	Jeffrey Walters; 1/2008–9/2012
Air-1: Optimization of Prescribed Burning by Considering Mechanical Thinning as a Viable Land Management Option	Karsten Baumann; 7/2008–9/2012
Air-2: Nitrogen Deposition to Terrestrial and Aquatic Ecosystems	Wayne Robarge; 7/2007–9/2012

Results from research projects feed back into the adaptive *DCERP Baseline Monitoring Plan* so that changes in sampling frequency, spatial extent of sampling locations, or parameters to be sampled could be adapted as necessary. The DCERP Team used results from the research and monitoring efforts to identify ecosystem indicators and develop associated threshold values, tools, or design models that address MCBCL's management needs. Team members then communicated this information to MCBCL personnel to assist them in making decisions about what management actions should be taken. After implementing these changes, the DCERP Team monitored the effects of these management changes (via feedback loops) to ensure that the desired outcomes were achieved and revised the conceptual models as appropriate. The adaptive nature of DCERP, therefore, was not fueled solely by the monitoring and research programs, but by researchers working in concert with the Base staff.

Baseline Monitoring Program

For the purposes of DCERP1, baseline monitoring was defined to include the monitoring of basic (fundamental) parameters that support the broader research agenda, that provide data that are useful to more than one ecosystem module, that must be monitored for a minimum of

5–10 years, and that will likely be transitioned in a scaled-down form to MCBCL to monitor directly at the end of DCERP efforts. The DCERP1 baseline monitoring program included the activities presented in **Table 1-4**. Final results of all DCERP baseline monitoring activities are summarized in the *DCERP1 Final Monitoring Report*.

Table 1-4. Summary of Module-Specific DCERP Baseline Monitoring Program Activities

Modules	Activities
Aquatic/ Estuarine ^a	<u>Hydrodynamics</u> : Stream flow and discharge (New River, tributary creeks) <u>Chemistry</u> : Nutrients, salinity, pH, oxygen, temperature (New River, NRE, tributary creeks) <u>Sedimentology</u> : Total suspended solids (New River, tributary creeks), turbidity (NRE) <u>Biology</u> : Primary productivity, phytoplankton, fluorescence (NRE)
Coastal Wetlands	<u>Land cover and shoreline erosion</u> : Location, elevation <u>Hydrodynamics</u> : Tide gauges (hydroperiod) <u>Chemistry</u> : Nutrients, salinity, hydraulic conductivity (shallow groundwater) <u>Sedimentology</u> : Accretion rates, organic content, particle size
Coastal Barrier	<u>Hydrodynamics</u> : Wave velocity, wave heights/period, currents, shoreline position, morphology <u>Meteorology (ocean)</u> : Air temperature, wind velocity, barometric pressure, humidity, solar radiation <u>Sedimentology</u> : Texture, compaction, composition, sediment volume <u>Biology</u> : Benthic invertebrates, fish, shorebirds/seabirds, dune/shrub/marsh vegetation, sea turtles
Terrestrial	<u>Land cover/land use</u> : Determine changes in land cover/land use (vegetation types, buildings, roads) <u>Biology</u> : Vegetative community assessment, fuel load <u>Soil</u> : Soil bulk density, pH, organic matter content
Atmospheric	<u>Meteorology (air)</u> : Wind speed, wind direction, relative humidity, temperature, photosynthetically active radiation, precipitation <u>U.S. Environmental Protection Agency criteria pollutants</u> : Ozone, fine and coarse particulate matter (mass)

^a Sedimentology, chemistry, and biology of the NRE benthic zone were characterized in Research Project AE-3.

Integration of DCERP Research and Monitoring

DCERP's approach closely integrated the *DCERP Baseline Monitoring Plan* and the *DCERP Research Plan* so that the outcomes of research projects were used to modify the adaptive *DCERP Baseline Monitoring Plan*. In turn, the monitoring data were used to develop, refine, and verify the models, tools, and indicators created as part of the research effort; therefore, the models, tools, and indicators were modified and refined as additional research and monitoring data became available.

The research projects also incorporated data from MCBCL's environmental monitoring activities, and other local, state, federal, and private monitoring activities to provide an integrated approach to ecosystem-based management and alleviate redundancy in data collection activities.

All research projects did not start simultaneously during DCERP; they were phased in to integrate research linkages among the various modules.

To achieve integration and synthesis of DCERP results within and among the six Module Teams, the DCERP Team initiated a variety of program activities, including monthly reporting of activities, Webinars, and in-person meetings. Team members also worked closely with their respective module researchers, with researchers from other modules, and with Base staff to prepare various publications and presentations for the scientific community, MCBCL, local stakeholders, and the general public.

Figure 1-5 shows how the models, tools, and indicators that are designed, developed, tested, and verified can be transitioned to MCBCL to assist in monitoring and forecasting ecosystem changes. The models, tools, and indicators developed from the research projects should also help to streamline the baseline monitoring to a limited set of key parameters that will easily be transitioned to MCBCL at the end of DCERP. A goal of DCERP is to disseminate monitoring and research results and information from associated models, decision-support tools, and indicators to MCBCL and to other users groups, including other DoD installations in similar ecological settings, the scientific community, other stakeholders (e.g., the New River Roundtable or the Onslow Bight Conservation Forum), and the general public.

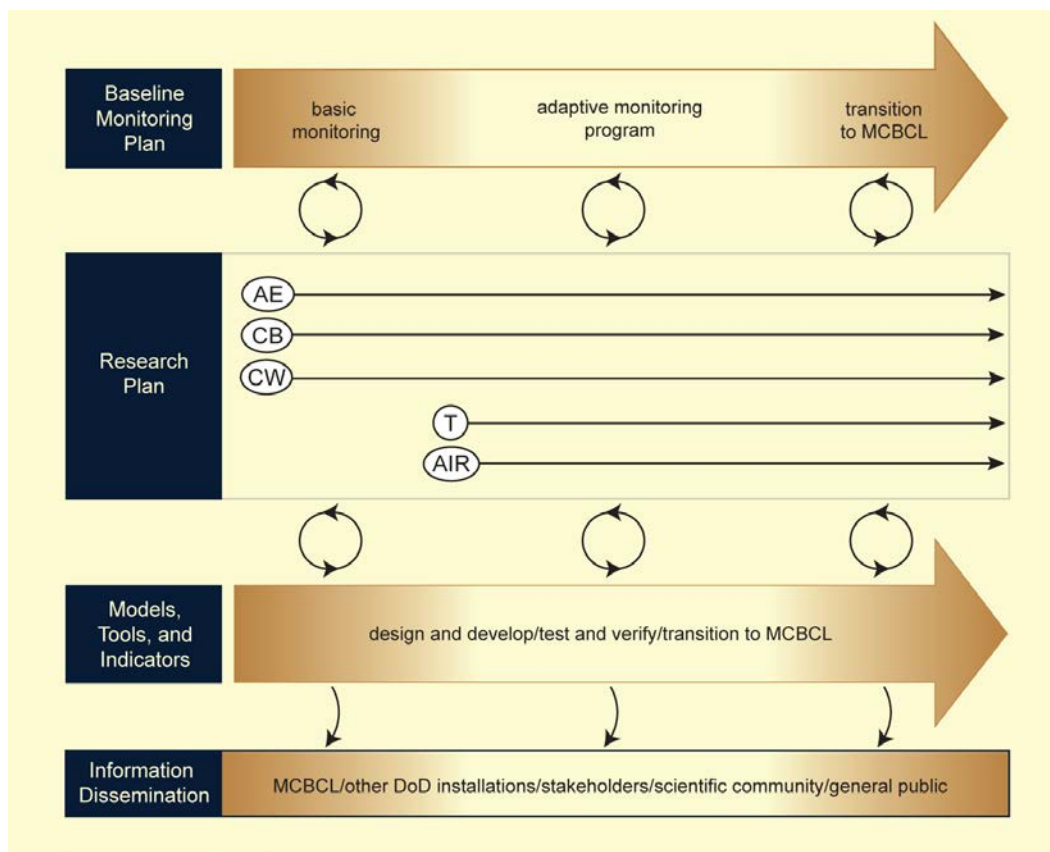


Figure 1-5. Generic roadmap of the integrated DCERP Baseline Monitoring Plan and DCERP Research Plan and the development of model tools and indicators.

Note: AE = Aquatic/Estuarine Module; CB = Coastal Barrier Module; CW = Coastal Wetlands Module; T = Terrestrial Module; AIR = Atmospheric Module

In 2009, 2010, and 2011, SERDP provided additional funding for activities not anticipated in the original *DCERP Baseline Monitoring Plan* and the *DCERP Research Plan* if the activity met specified criteria. The request for additional funding could be made if the activity: (1) needed immediate funding to prevent a negative effect on DCERP, (2) was supported by a TAC recommendation, or (3) supported a new requirement based upon new monitoring or research results or enhanced work that was already funded. This further enabled the program to adapt to new findings and management needs.

Report Organization

This *DCERP I Final Research Report* summarizes the DCERP research activities and results during the Phase II implementation period (July 2007 to January 2013). Chapter 2 of this *DCERP Research Report* summarizes the major research finding results and conclusions of the 13 research projects of DCERP and provides a brief assessment of monitoring results and a description of each ecosystem. Chapters 3 through 16 provide detailed research project reports for each of the 13 research projects listed in Table 1-3 of this chapter. As part of each final research project report, the researchers restated their initial hypotheses to be tested, provided background to their research project to set it within the context of the previous state of science, described the methods and materials used, and provided results, discussions, and conclusions, including whether they accept or reject their original hypotheses.

In addition, an Executive Summary is provided that will serve as a stand-alone summary document prepared as an outreach tool for MCBCL. The Executive Summary covers the same time period described here and specifically highlights significant results and trends applicable to MCBCL's natural resources management staff, the Base's environmental mission drivers, and direct benefits to MCBCL that were derived from DCERP.

Literature Cited

- Christensen, N.L., A. Bartuska, J.H. Brown, S. Carpenter, C. D'Antonio, R. Francis, J.F. Franklin, J.A. MacMahon, R.F. Noss, D.J. Parsons, C.H. Peterson, M.G. Turner, and R.G. Woodmansee. 1996. The scientific basis for ecosystem management. *Ecological Applications* 6:665–691.
- Goodman, S.W. 1996. Ecosystem management at the Department of Defense. *Ecological Applications* 6:706–707.
- MCBCL (Marine Corps Base Camp Lejeune). 2006a. *Integrated Natural Resource Management Plan (INRMP)*. U.S. Marine Corps, Camp Lejeune, NC. Available at <http://www.lejeune.usmc.mil/emd/INRMP/INRMP.htm>.
- MCBCL (Marine Corps Base Camp Lejeune). 2006b. *2020 Range Transformation Plan, Version 4*. Range Development, Training and Operations Department. Integrated Geographic Information Repository. Marine Corps Base Camp Lejeune, NC.
- MCBCL (Marine Corps Base Camp Lejeune). 2005. *Land Use Master Plan*. Prepared by Eagan McAllister Associates, Inc. Integrated Geographic Information Repository. Marine Corps Base Camp Lejeune, NC.
- RTI (RTI International). 2007a. *Defense Coastal/Estuarine Research Program (DCERP) Strategic Plan*. Prepared for Strategic Environmental Research and Development Program (SERDP), Arlington, VA.
- RTI (RTI International). 2007b. *DCERP Baseline Monitoring Plan*. Prepared for Strategic Environmental Research and Development Program (SERDP), Arlington, VA.
- RTI (RTI International). 2007c. *DCERP Research Plan*. Prepared for Strategic Environmental Research and Development Program (SERDP), Arlington, VA.
- SERDP (Strategic Environmental Research and Development Program). 2005. *DCERP Strategy Report*. U.S. Department of Defense, Defense Coastal/Estuarine Research Program, Marine Corps Base Camp Lejeune, NC.
- U.S. Commission on Ocean Policy. 2004. *An Ocean Blueprint for the 21st Century*. Final Report. Washington, DC.
- Walters, C. 2001. *Adaptive Management of Renewable Resources*. The Blackburn Press: Caldwell, NJ.

Appendix 1-A

Prioritized List of MCBCL's Conservation and Water Quality Needs

MCBCL Conservation and Water Quality Needs
High-Priority Needs
Primary Nursery Area (PNA) mitigation/delineation
Onslow Beach erosion
Air quality/smoke management
Measuring good quality habitat for red cockaded woodpeckers (RCW)
N1/BT3 monitoring for whales and marine mammals
RCW flexibility for Range Development—Regional RCW credit
Stormwater runoff reduction and water quality studies
Near field water quality studies
Distinguish and quantify effects of point and non-point inputs nutrient, sediment and pathogen inputs
Water quality/primary nursery areas
Physical-chemical-biological interactions and their control on water quality/habitat
Medium-Priority Needs
Wetland (marsh) restoration opportunities in the New River Estuary
Species at risk—beach amaranth
Species at risk—sea turtles
Species at risk—shorebirds
Species at risk—RCW
Fire effects on vegetation and quantifying/qualifying prescribed burns
Species at risk—rough-leaved loosestrife
Habitat restoration and tactical vehicle off-road impacts
Northern pocosin in the Great Sandy Run Area (GSRA)
RCW monitoring
Additional military effects/RCW study
Longleaf /loblolly decline
Benthic organism Index of Biological Integrity
Benthic-water column exchange and hypoxia research
Blue crab studies
Determine nutrient, sediment and pathogens loadings from the watershed; determine transformations of nutrients within the estuary; and the determine interactive role of climatic/hydrologic roles
Identify and quantify nutrients controlling primary production and excess production and algal blooms

MCBCL Conservation and Water Quality Needs
Determine causes and effects of harmful algal blooms; link nutrient-productivity to hypoxia potentials
Low-Priority Needs
Coliform counts—Freeman Creek (and other 303[d] Total Maximum Daily Load–identified tributaries)
Invasive species: alligator weed and <i>Phragmites</i>
Habitat restoration and tactical vehicle off-road impacts—maritime forest

[This page intentionally left blank.]

Chapter 2

Significant Findings and Management Implications

SERDP Project Number: RC-1413

Principal Investigator:
Dr. Pat Cunningham
RTI International
Research Triangle Park, NC 27709
E-mail: patc@rti.org

May 10, 2013

Final

This report was prepared under contract to the U.S. Department of Defense (DoD) Strategic Environmental Research and Development Program (SERDP). The publication of this report does not indicate endorsement by DoD, nor should the contents be construed as reflecting the official policy or position of DoD. References herein to any specific commercial product, process, or service by trade name, trademark, manufacturer, or otherwise, do not necessarily constitute or imply its endorsement, recommendation, or favoring by DoD.

Table of Contents

List of Acronyms	2-v
Introduction.....	2-1
Programmatic Overview	2-1
Hydrodynamics of the NRE and Coastal Area	2-1
Sediment Transport.....	2-2
Nitrogen Cycling and Primary Productivity	2-3
Military Training and Land Management.....	2-5
Development and Application of Models	2-7
Aquatic/Estuarine Module	2-8
Summary of the Ecosystem	2-8
Aquatic/Estuarine Module's Monitoring Program	2-11
Conclusions and Implications from the Aquatic/Estuarine Module	2-12
Coastal Wetlands Module	2-14
Summary of the Ecosystem	2-14
Coastal Wetlands Module's Monitoring Program	2-17
Conclusions and Implications from the Coastal Wetlands Module.....	2-18
Coastal Barrier Module.....	2-20
Summary of the Ecosystem	2-20
Coastal Barrier Module's Monitoring Program.....	2-23
Conclusions and Implications from the Coastal Barrier Modules	2-25
Terrestrial Module	2-27
Summary of the Ecosystem	2-27
Terrestrial Module's Monitoring Program.....	2-30
Conclusions and Implications from the Terrestrial Module	2-30
Atmospheric Module	2-33
Summary of Atmospheric Conditions	2-33
Atmospheric Module's Monitoring Program.....	2-35
Conclusions and Implications from the Atmospheric Module	2-36
Literature Cited	2-38

List of Figures

2-1.	Conceptual model for the Aquatic/Estuarine Module.	2-9
2-2.	Conceptual model for the Coastal Wetlands Module.	2-15
2-3.	Conceptual model for the Coastal Barrier Module.	2-21
2-4.	Conceptual model for the Terrestrial Module.....	2-28
2-5.	MCBCL terrestrial vegetation monitoring plots arrayed on non-metric scaling Axes 1 and 2.....	2-30
2-6.	Conceptual model for the Atmospheric Module.....	2-34

List of Tables

2-1.	MCBCL management strategies for reducing impacts of military training activities on MCBCL ecosystems.	2-5
2-2.	Models developed and/or applied by the RTI DCERP Team.....	2-7
2-3.	Aquatic/Estuarine Module Research Project Titles, Senior Researchers, and Summaries of Findings	2-10
2-4.	Coastal Wetlands Module Research Project Titles, Senior Researchers, and Summaries of Findings	2-16
2-5.	Coastal Barrier Module Research Project Titles, Senior Researchers, and Summaries of Findings	2-22
2-6.	Terrestrial Module Research Project Titles, Senior Researchers, and Summaries of Findings	2-29
2-7.	Atmospheric Module Research Project Titles, Senior Researchers, and Summaries of Findings	2-34

List of Acronyms

AAV	amphibious assault vehicle
A.D.	Anno Domini
ADCIRC	Advanced Circulation (Model)
AVP	autonomous vertical profiler
BBN	Bayesian Belief Network
BOMO	Boat Wake Model
CAFO	confined animal feeding operation
CDOM	chromophoric (colored) dissolved organic matter
CLARIS	Coastal LiDAR and Radar Imaging System
cm	centimeter
dbh	diameter at breast height
DCERP	Defense Coastal/Estuarine Research Program
DCERP1	first cycle of the Defense Coastal/Estuarine Research Program
DCERP2	second cycle of the Defense Coastal/Estuarine Research Program
DoD	U.S. Department of Defense
E. coli or EC	<i>Escherichia coli</i>
EF	emission factor
ENT	<i>Enterococcus</i> spp.
ESM	Estuarine Simulation Model
GSRA	Greater Sandy Run Area
ha	hectare
ICW	Intracoastal Waterway
J m^{-1}	joules per meter
kg N y^{-1}	kilograms of nitrogen per year
$\text{kg N ha}^{-1} \text{y}^{-1}$	kilograms of nitrogen per hectare per year
km	kilometer
km^2	square kilometer
LAV	light armored vehicle
LCAC	Landing Craft Air Cushion
m	meter
m^2	square meter
$\text{m}^3 \text{s}^{-1}$	cubic meters per second
MCBCL	Marine Corps Base Camp Lejeune
MEM	Marsh Equilibrium Model
mg m^{-2}	milligrams per square meter
mi	mile
mi^2	square mile

mm/y	millimeters per year
NOAA	National Oceanic and Atmospheric Administration
NRE	New River Estuary
NRESE	New River Estuary Shoreline Erosion
PB	prescribed burning
PM _{2.5}	particulate matter with a diameter of less than or equal to 2.5 microns
PM ₁₀	particulate matter with a diameter of less than or equal to 10 microns
PM _c	the coarse fraction of PM ₁₀ from the difference between the measured PM ₁₀ and PM _{2.5}
ppt	parts per thousand
RCW	red-cockaded woodpecker
ROM	Runup and Overwash Model
SERDP	Strategic Environmental Research and Development Program
SLR	sea level rise
SWAN	Simulating Waves Nearshore (Model)
WEMo	Wave Exposure Model
WSM	Watershed Simulation Model
WWTF	wastewater treatment facility

Introduction

This chapter of the *DCERP1 Final Research Report* provides a brief summary of the significant findings and management implications of the Defense Coastal/Estuarine Research Program (DCERP) conducted at Marine Corps Base Camp Lejeune (MCBCL), at both the programmatic and individual module levels. At the programmatic level, our overarching objective was to enhance and sustain MCBCL's military training mission by conducting installation-relevant and basic and applied research in support of an ecosystem-based management approach. The DCERP team focused on developing an understanding of ecosystem composition, structure, and function within the context of a military training environment. DCERP was established as a unique, highly integrated temporal/spatial monitoring and research program whereby monitoring data provided information that validated models and research data provided feedback on whether the monitoring was adequate to support research hypotheses. The RTI DCERP Team selected several major cross-module integrative processes to study, including the hydrodynamics of the New River Estuary (NRE) system, sediment transport, and nitrogen cycling and primary production, as well as military land management effects on the landscape. Although other processes were also studied, these are the major processes that are important in this estuarine/coastal system across all ecosystems.

The remainder of Chapter 2 is organized according to the five ecosystem modules: Aquatic/Estuarine, Coastal Wetlands, Coastal Barrier, Terrestrial, and Atmospheric Modules. Each module section contains short descriptions of the key biological, chemical, and physical processes and stressors that impact each ecosystem as presented in the conceptual models; the overall findings of the research program; and brief discussions of the monitoring program and assessments of data generated to support the module research and modeling efforts. Finally, the major findings and implications of the DCERP1 research within each module are discussed in the context of three categories: Key Scientific Findings, Findings with Implications for MCBCL Management Practices, and Findings with Implications for DCERP2. It should be noted that some findings may fit into more than one of these categories; however, we have tried to minimize duplication and therefore have put the findings in the most appropriate category.

Programmatic Overview

Hydrodynamics of the NRE and Coastal Area

Hydrodynamics of the NRE and adjacent coastal area include those of the estuary proper and the various inputs from the New River, tributary creeks, and exchange with the coastal ocean; the Intracoastal Waterway (ICW) and its adjacent marshes that span the southern boundary of MCBCL between the New River Inlet and Browns Inlet; and the 12-km (8-m) coastal barrier island, Onslow Island, that is separated from the mainland by the ICW. The New River is located within the Coastal Plain in southeastern North Carolina and flows 70 km (43 mi) through mostly forested and agricultural land before entering the NRE near the City of Jacksonville. The NRE is a shallow, semi-lagoonal estuary that flows southward and empties directly into the Atlantic Ocean through the narrow New River Inlet.

The hydrodynamics of the estuarine section of the New River watershed are highly complex. Freshwater can enter the NRE system through direct deposition as rain; fresh water runoff at

diffuse land and water (marsh) boundaries; groundwater; and riverine input from the New River, Southwest and Northeast Creeks, and numerous small tributary creeks. The predominant riverine input creates gravitational flow towards the ocean. The heavier saltwater, introduced into the system at the inlet, moves saline water up-estuary along the bottom towards the head of the estuary. The two water layers of different densities cause vertical stratification of differing strengths along the length of the estuary. Atmospheric events, including major storms and daily wind patterns, as well as the semi-diurnal tidal cycle are the major mechanisms producing vertical mixing of the estuarine water column. Residence time in the upper estuary is typically longer than in the lower estuary near the inlet and is influenced primarily by the flow of the New River in the upper estuary and by semi-diurnal tides in the lower estuary. The upper estuary is oligohaline, with salinity ranging from 0.5 ppt to 5 ppt, whereas the salinity in the middle and lower estuary typically ranging from 5 ppt to 30 ppt. Since the start of DCERP, hydrologic flow extremes driven by both drought conditions and storm events have led to large fluctuations in freshwater flow. Under drought conditions with low freshwater flow, high salinity tidal waters penetrated further up-estuary increasing salinity at the estuary head near Jacksonville. On the other extreme, Tropical Storm Nicole brought 57 cm (22.5 inches) of rain over 4 days and the salinity at the head of the NRE near Jacksonville declined from 25 ppt to 0 ppt as a result of this storm event. Water circulation in the lower estuary near the NRE Inlet is complicated further by exchanges with both the Atlantic Ocean and the ICW. The existence of the ICW, a man-made navigation channel, has resulted in differences in the tidal amplitude occurring in the marshes bordering the ICW.

The hydrodynamics of the offshore, coastal ocean and its influence on Onslow Beach are typically determined by semi-diurnal tides, low-frequency wind-induced flow, higher frequency wind waves, and storm surge. Seasonal variability in the offshore wind and wave climate influences the nearshore area adjacent to Onslow Beach, but the influence is constrained by the geomorphology and bathymetry of the area. Seasonal analysis indicates that the wind and wave climate of Onslow Island during the autumn and winter are driven more towards beach erosion, and the summer wind and wave climates enhance beach accretion. Overall, winds are variable from the northeast and southwest, and waves are primarily from the southeast and are strongest in the winter and autumn. Wind-induced waves can result in overwash events on the coastal barrier. In addition to the hydrodynamics of the wind and wave environment, there is also a strong bilateral component to the long-shore current flow that parallels the shoreline of Onslow Beach. On an annual basis, approximately 30–40% of the total long-shore current flow is northeast towards Browns Inlet, 20% is southwest towards the NRE Inlet, and 10% is offshore, leaving the remaining 30–40% of flow onshore. These complex hydrodynamic flows of the New River, NRE, ICW, and the coastal ocean mediate transport of sediment and nutrients among the various coastal ecosystems of MCBCL.

Sediment Transport

Hydrodynamic processes associated with both wind and water are responsible for sediment transport among the various MCBCL component ecosystems and for resuspension of sediments. A combination of hydrodynamic processes and sediment supply determine whether an area will experience erosion or accretion. Sediment can be transported into the estuary via runoff from upland agricultural lands or from MCBCL lands into tributary creeks. Areas of the New River watershed in agricultural use are vulnerable to sediment runoff, especially during high rainfall

events. In contrast, the largely undeveloped training and forest lands of MCBCL help limit surface runoff to the tributary creeks and reduce stream sediment loads. These creek loads are much lower than other southeast Coastal Plain systems. In addition to sediment input from the New River watershed, waves cause erosion of the NRE shoreline, especially sediment banks, and this sediment source provides approximately half of the sediment required for the salt marshes in the lower estuary to keep pace with sea level rise (SLR) through accretion. Wind-driven shear-stress forces on the bottom of this shallow estuary result in the resuspension of bottom sediments, which can be carried down-estuary to marshes in the lower NRE and ICW, transported to the New River Inlet and Atlantic Ocean, or redeposited to the bottom of the estuary. Within the estuary, resuspended bottom sediments can reduce light availability reaching the benthic microalgae, restricting the benthic microalgae from photosynthesizing and sequestering nutrients from the water column.

The ICW was constructed in the mid-1930s and substantially changed the hydrodynamics of sediment movement. The construction and routine maintenance of the ICW is a legacy stressor to the salt marsh ecosystems adjacent to the ICW. Marshes on the eastern side of the ICW are higher in elevation because they receive sediment replenishment from both overwash events and wind-driven aeolian sand transported across Onslow Island. In contrast, marshes on the western side of the ICW are sediment starved because they are deprived of these sediment sources by the physical presence of the ICW, which also intercepts and traps sediment carried by tidal flow through the inlets. Additionally, the number and speed of commercial, recreational, and military vessels using the ICW have also resulted in increased boat wake erosion of the ICW shoreline. This erosion leads to slumping of sediments into the ICW, which further necessitates dredging to maintain the channel. However, the dredged sediment is often lost from the marsh ecosystem as it is removed or deposited on Onslow Beach.

Sediment transport along Onslow Beach is driven by daily wind, wave, current, and semi-diurnal tidal patterns and by more severe, seasonal, episodic storm events, particularly during autumn and winter, that are responsible for overwash and the formation of substantial washover fans composed of beach and dune sand. Large storm events such as hurricanes and tropical storms have caused significant overwash and sediment re-working on the barrier island; however, sub-tropical storms and nor'easters have had similar effects. At the northeastern, regressive end of the island, the combination of high dunes (7–9 m in height) and well-developed plant communities constrain overwash and almost completely block aeolian sediment transport from the beach to the backbarrier marshes. At the southwestern, transgressive end of the island, overwash is a more dominant process due to the lower dune height (less than 2 m in height). However, even at this end of the island, the plant communities limit across-island aeolian sediment transport. After storms, when vegetation density is reduced by overwash events, the efficiency of aeolian sediment transport between the beach, dunes, and backbarrier marsh increases.

Nitrogen Cycling and Primary Productivity

A main focus of DCERP was to identify the sources, transport mechanisms, processes, and fate of nitrogen across the MCBCL landscape because it is often this nutrient that limits primary production and determines rates of other material (carbon, nutrients, and oxygen) cycling. Like sediments, nitrogen is transported by hydrodynamic processes among various components of the

New River watershed and MCBCL estuarine/coastal systems. The largest source of nitrogen enters the NRE system from the upper New River watershed, with lesser contributions from the Atlantic Ocean, MCBCL tributary creeks, the MCBCL wastewater treatment plant, and atmospheric deposition. Because the NRE is a shallow, microtidal system with a relatively long residence time (greater than 69 days [median]), the estuary responds very differently to nutrient enrichment than deeper, tidally dominated estuaries with shorter residence times.

In the coastal marshes, terrestrial forest, and barrier island systems, higher plants (macrophytes, woody plants) dominate primary production, whereas in the NRE, the bulk of the primary production is mediated by planktonic and benthic microalgae. Nutrient inputs (nitrogen and phosphorus), light availability (mediated by turbidity and chromophoric [colored] dissolved organic matter [CDOM]) and advective processes (freshwater flow, tides, and flushing) interactively control the rate of primary production and the community composition of primary producers in the NRE. Although nutrient inputs are essential for supporting primary producers, excessive nutrients can lead to eutrophication, which adversely affects both water quality and habitat conditions. Examples of adverse effects include production of harmful (toxic) algal blooms that can alter food webs, the development of hypoxia and anoxia resulting from decaying algal material that can result in fish kills, decreased light availability resulting from a reduction in water clarity (essential to support benthic primary production and nutrient uptake and sequestration), loss of habitat for finfish and shellfishing, and reduction in recreational, commercial, and military training uses of the estuary.

Although nitrogen supplies from external (i.e., atmospheric deposition, riverine loading, and ocean water) and internal sources play key regulatory roles, physical factors such as freshwater discharge, flushing (water residence time), and transparency (water clarity) modulate primary production. In the NRE, freshwater discharge and resulting flushing rates play fundamentally important roles in controlling the amount and composition of planktonic primary producers. Freshwater discharge is of critical importance from both ecological function and ecosystem “health” perspectives because it controls nitrogen inputs and rates of nitrogen cycling. Clearly, there is a strong interaction between nitrogen delivery and flushing characteristics of the estuary in terms of the types (species composition) and amounts (biomass) of microalgal production. The primary responses to nitrogen enrichment in deep estuaries are phytoplankton blooms and resulting eutrophication; however, the shallow NRE is more resilient because of the other major primary producers—the benthic microalgae. Benthic microalgal production, accompanied by denitrification and annomox, modulates the effects of nutrient enrichment by constraining the release of nitrogen back into the water column; however, these processes are regulated by light availability, residence time, and salinity, all of which vary during episodic storm events. Light availability, in particular, is affected by erosion and resuspension of sediment and CDOM in response to both natural (storm) and anthropogenic perturbations such as MCBCL training activities and infrastructure development. Light availability is also vital to allow the benthic microalgae to undergo photosynthesis, thereby sequestering nutrients such as nitrogen from the water column into benthic microalgal biomass and the sediments.

In contrast to the NRE, which receives inputs of nutrients (particularly nitrogen from the New River watershed), the marshes of the lower NRE and ICW are, by comparison, nitrogen starved. Groundwater from the upland pine forests that flows through these marshes is nitrogen poor. Therefore, the marshes of MCBCL do not function to remove large groundwater-derived

nitrogen fluxes from the watershed because there is little to remove. Nitrogen is also produced by decomposition of organic matter in intertidal marshes. However, 10–20% of the nitrogen is converted to nitrogen gas via denitrification and is lost from the coastal landscape to the atmosphere. The more dominant fate (80–90%) of nitrogen in the MCBCL marshes is burial in sediment during marsh accretion, which provides nitrogen storage over varying time scales (from decades to centuries). This further illustrates that intertidal marshes of MCBCL are overwhelmingly sinks for nitrogen in the coastal landscape.

A fertilization study that artificially added nitrogen and/or phosphorus revealed that the salt marsh vegetation (*Spartina alterniflora*) at MCBCL is co-limited by both nitrogen and phosphorus. This increase in biomass production on plots fertilized with both nitrogen and phosphorus significantly raised the marsh elevation. Singular additions of nitrogen or phosphorus did not elicit a statistically significant increase in biomass production, but the combined effects of the two nutrients raised the standing biomass by a factor of 2.8 above the controls and raised the average rate of sediment accretion by 4.6 mm/y. Therefore, nutrient additions of both nitrogen and phosphorus may have potential for use in marsh restoration efforts to increase accretion rates of the marshes to help them keep pace with SLR and continued provisioning of ecosystem services.

Military Training and Land Management

Based on the landscape of MCBCL, the type of training maneuvers and equipment in use, and the current intensity of the training, the RTI DCERP Team was able to design its research and monitoring programs and select appropriate research sites that allowed for comparison of results from both training and non-training locations. This also allowed the team to develop an understanding of the ecosystem composition, structure, and function within the context of a military training environment. MCBCL managers are proactive about the sustainability of the ecosystems at MCBCL (**Table 2-1**). At the current level (types and intensity) of military training employed at MCBCL from 2007 through 2012, the impacts of this training were not significant ecosystem stressors in comparison to the magnitude of natural disturbances from storms, hurricanes, droughts, and flooding.

Table 2-1. MCBCL management strategies for reducing impacts of military training activities on MCBCL ecosystems.

MCBCL Management Strategies
Tanks and tracked vehicles are not permitted to maneuver except on designated tank trails or tank training ranges, and this practice constrains soil erosion and minimizes impacts of sediment and nutrient runoff to receiving waters.
Intersections or other areas of high training use are maintained routinely by grading these areas and placing signage and guard rails to keep vehicles out of areas where restoration is ongoing.
Amphibious vehicle impacts are constrained by restricting their entry and exit from the water via specified splash points (often, these are hardened with concrete pads) on the NRE or ICW and via designated ingress/egress points on Onslow Beach.

(continued)

Table 2-1. MCBCL management strategies for reducing impacts of military training activities on MCBCL ecosystems (continued).

MCBCL Management Strategies
Landing Craft Air Cushions (LCACs) train over marshes in the lower estuary and barrier island; however, various paths through the marshes are used, and thus the marshes appear to be able to withstand and recover within 3 years, assuming the current intensity and types of training continues.
Tactical landing zones used in helicopter and fixed-wing aircraft training exercises become rutted with use, and these are routinely graded and reseeded with native grasses, and then closed for 1–2 years to allow vegetation to recover before use is reinitiated.

With more than 35,000 ha (86,500 acres) of forest land at MCBCL, forest managers strive to achieve sustainability for continued provisioning of ecosystem services and support of the military training mission. A key component of that management is the restoration of longleaf pine (*Pinus palustris*) ecosystems. Areas once dominated by open, longleaf pine now support closed canopy stands of loblolly pine (*Pinus taeda*) with a dense understory and midstory of broad-leaved shrubs and trees. These mixed hardwood-pine forests are not readily useable for training because of the dense understory, and they are of poor habitat quality to support the endangered red-cockaded woodpecker (RCW; *Picoides borealis*). The suppression of fire on these landscapes has also exacerbated these conditions. Although land management prescriptions are frequently motivated by single-species management for threatened and endangered species, the land management approach at MCBCL (perhaps initiated by RCW management) ultimately addresses multiple issues by taking a holistic, ecosystem recovery approach. Forestry management practices (i.e., midstory thinning followed by prescribed burning [PB]) used at MCBCL to create more open pine savanna-like communities were found to be addressing long-term forestry restoration goals, created more useable land for military training activities, supported the recovery goals for the RCWs and other species of concern, and offered the benefit of lower PM_{2.5} emissions during PB events.

Amphibious capabilities are key to MCBCL's mission and Onslow Island, adjacent marshes, and water crossings provide critical training environments. Amphibious assault training takes place on a relatively small portion of Onslow Island and marshes, and uses splash points to launch amphibious assault vehicles (AAVs) and light armored vehicles (LAVs) across the ICW to and from the main side of the installation. Additionally, the lower NRE is used to launch landing craft air cushion (LCAC) vehicles across the marshes to transport personnel and materials to offshore vessels, and then to ferry them to the assault beaches on the central training area of Onslow Island. With respect to the barrier island, military training did not produce a significant impact at current training levels in comparison to natural forces associated with overwash from storm surge and wind and wave processes. Similarly, LCAC trails in marshes were visible in aerial photographs, but within 3 years, these tracks were no longer distinguishable. In comparative analyses, LCACs did not have a lasting impact on the marsh, either in terms of marsh surface elevation, vegetation biomass, or marsh fragmentation.

Shoreline erosion of the ICW was measurable over the period from 1956 through 2009 from analysis of historic aerial photographs. Waves created by boat wakes in the ICW that erode the marsh shoreline are primarily a result of commercial and recreational vessel traffic rather than military training vessels. Minimal erosion was detected at splash points along the ICW, and those

isolated incidences where erosion was occurring might be reduced at some currently used splash points by shifting some of the training pressure to the underutilized splash points, by reinforcing existing splash points with concrete ramps, or implementing marsh restoration around the more impacted sites.

Development and Application of Models

To understand ecosystem processes and identify indicators of potential changes to ecosystem state that would require more effective management to achieve sustainability, the RTI DCERP Team developed and/or applied a variety of models. These models were validated using extensive monitoring and research data and were used to test different scenarios representing natural and anthropogenic stressors. For example, the Estuarine Simulation Model (ESM) was used to predict the effect of changing loads of nitrogen on chlorophyll *a* concentrations in the NRE and the Marsh Equilibrium Model (MEM) was used to predict the response of coastal marshes to changes in sea level. More information on each model is contained within the individual research project chapter (see **Table 2-2**).

Table 2-2. Models developed and/or applied by the RTI DCERP Team.

Model Name	Chapter/Research Project	Objective
Bayesian Belief Network (BBN)	Chapter 3, Research Project AE-1	To examine the variables critical to eutrophication and guide monitoring and assessment procedures
Watershed Simulation Models (WSMs)	Chapter 6, Research Project AE-2	To understand the effect of natural and anthropogenic stressors on watershed loads to the NRE
Estuarine Simulation Model (ESM)	Chapter 6, Research Project AE-3	To scale up results to the entire NRE system and understand the effect of natural and anthropogenic stressors on the NRE
Bio-optical model (for the NRE)	Chapter 5, Research Project AE-3	To guide monitoring and assessment procedures and understand the effects of water quality parameters on light attenuation in the NRE
Marsh Equilibrium Model (MEM)	Chapter 7, Research Project CW-1	To forecast changes in marsh elevation and inform efforts to stabilize NRE shoreline
Wave Exposure Model (WEMo)	Chapter 8, Research Project CW-2	To classify shorelines by wind wave energy; identify areas where boat wake energy significantly increases total wave energy; predict distribution of storm waves on top of surge under different storm scenarios; determine seafloor shear stress to predict areas of high sediment resuspension in the NRE; and identify vulnerable Installation assets
Boat Wake Model (BOMO)	Chapter 8, Research Project CW-2	To perform boat wake impact forecasting and geographic assessments

(continued)

Table 2-2. Models developed and/or applied by the RTI DCERP Team (continued).

Model Name	Chapter/Research Project	Objective
New River Estuary Shoreline Erosion (NRESE)	Chapter 8, Research Project CW-2	To illustrate dominant shoreline erosion processes in different NRE locations
Runup and Overwash Model (ROM)	Chapter 10, Research Project CB-1	To predict changes in the beach in response to short-term storms and/or changes in the physical parameters (e.g., beach slope, removal of dunes) and forecast locations of wave runup and overwash
Advanced Circulation (ADCIRC) Model	Coastal Barrier Module Monitoring Program	To simulate the velocity flow field and pathways of sediment transport
Simulating Waves Nearshore (SWAN) Model		

Aquatic/Estuarine Module

Summary of the Ecosystem

Estuaries integrate inputs from terrestrial habitats, freshwater rivers and streams, the coastal ocean, and atmospheric systems. Accurate assessment and management of estuarine water quality necessitates consideration of the interconnections to, and interactions with, these other systems. Many estuaries also exist in regions of rapid population growth and diversifying human activity that can impact natural ecosystem processes. In the context of the MCBCL region, the Aquatic/Estuarine Module studied the tidal reach of the NRE from the head of the estuary near Jacksonville, NC, to the tidal inlet at Onslow Bay, including 10 tributary creeks within MCBCL lands that flow into the NRE or the ICW.

The NRE is a relatively small (88 km² [34 mi²]), shallow (approximately 3 m [9.8 ft] mean depth) Coastal Plain estuary. Most of the estuary resides within MCBCL. The NRE is comprised of a series of lagoons and is confined by barrier islands restricting water exchange with the Atlantic Ocean. Flushing time in the NRE varies seasonally with storm and runoff events, ranging from 8 to 187 days, with an average of 70 days (Ensign et al., 2004). The semi-lagoonal nature of the NRE plays a significant role in its sensitivity to nutrient inputs because long flushing times allow more time for algal nutrient assimilations, growth, and internal nutrient recycling. Principal tributaries discharging into the NRE include the blackwater New River and Southwest and Northeast Creeks. In addition, numerous small creeks, whose catchment areas lie within MCBCL boundaries, also discharge into the NRE. Land use in both the New River and Southwest Creek watersheds is dominated by agriculture and includes numerous swine confined animal feeding operations (CAFOs). Prior to 1998, discharges from CAFOs, a wastewater treatment facility (WWTF) in the City of Jacksonville, and seven WWTFs on MCBCL resulted in massive

phytoplankton blooms, widespread hypoxia, and fish kills, such that the estuary was named one of the most eutrophic in the Southeastern United States (Bricker et al., 1999; Mallin et al., 2005). In 1998, the Jacksonville WWTF was upgraded to secondary treatment and the MCBCL facilities were consolidated, which markedly improved water quality (Mallin et al., 2005). However, the NRE continues to receive high nutrient loads from the New River watershed and episodic WWTF spills. In addition, development on MCBCL, with attendant increases in imperviousness, buildings, and forest clearing also has the potential to impact the small tributaries discharging into the NRE.

The Aquatic/Estuarine Module investigated how anthropogenic loadings (nutrient and sediment inputs) from the New River watershed and MCBCL tributaries affected the benthic microalgae and pelagic phytoplankton. Phytoplankton production and community structure are controlled by nutrient inputs, residence time, and the degree of stratification in the estuary. In contrast, benthic microalgae production is controlled by water clarity that allows the benthic microalgae to sequester nutrients under autotrophic conditions, but causes a release of nutrients back into the water column under heterotrophic conditions. Water clarity that controls benthic microalgae production is reduced by the presence of suspended sediments, CDOM, and pelagic phytoplankton biomass—all parameters regulated by climate-driven hydrologic flows from the New River and from forcings from tidal activity and wave energy. Furthermore, the effects of climatic variability, including acute or episodic events (e.g., tropical hurricanes, floods, droughts) and longer term trends (e.g., warming, precipitation patterns), on estuarine structure and function were characterized and quantified to better understand the interactive and potentially confounding impacts of climate (change) on water quality and habitat condition (Figure 2-1).

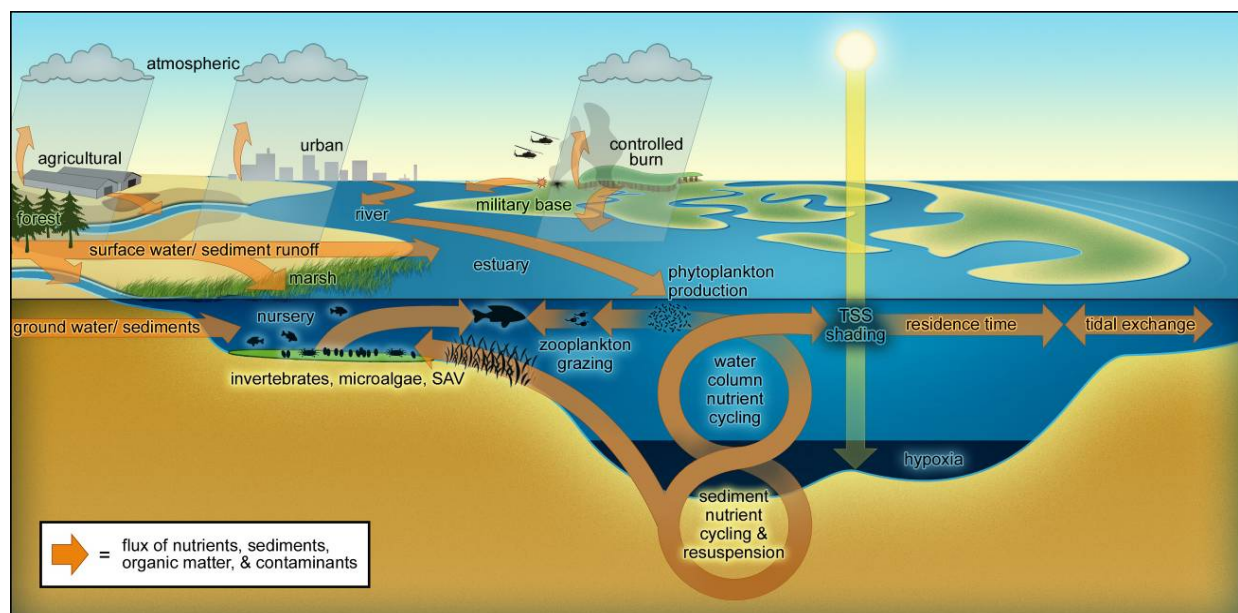


Figure 2-1. Conceptual model for the Aquatic/Estuarine Module.

The Aquatic/Estuarine Module conducted three research projects listed in **Table 2-3** to address the stressors associated with both on- and off-Base anthropogenic activities and from natural stressors associated with extreme episodic events. Research Projects AE-1 and AE-3 identified the

important processes and interactions ongoing within the NRE between the pelagic and benthic communities, respectively. Research Project AE-2 tracked the relationship between land use and precipitation events to quantify loadings of nutrients, sediments, and bacteria under baseflow and stormflow conditions to MCBCL tributary creeks. A variety of watershed simulation models were applied to predict current watershed loads to the NRE and potential changes in those loads due to installation development. The ESM was developed and implemented to integrate stressors and ecosystem processes ongoing in the estuary to inform development of a water quality management tool.

Table 2-3. Aquatic/Estuarine Module Research Project Titles, Senior Researchers, and Summaries of Findings

Research Project	Research Project Title	Senior Researcher
AE-1	<i>Develop and Deploy Microalgal Indicators as Measures of Water Quality, Harmful Algal Bloom Dynamics, and Ecosystem Condition</i>	Senior Researcher: Hans Paerl
	<p>Findings: Research Project AE-1 determined that phytoplankton biomass was strongly impacted by river flow variations due to its dual influence on nutrient delivery and residence time. Nutrient addition bioassays showed that nitrogen was the primary limiting nutrient controlling phytoplankton production. Hydrologic forcing plays an important role in determining phytoplankton biomass and community structure. System-wide primary productivity is nearly evenly split between phytoplankton and benthic microalgae. Management actions should maintain this ecologically healthy balance by limiting excessive nitrogen and suspended sediment loads that tend to favor phytoplankton over benthic microalgal production. Currently, most of the nutrient and sediment loading to the estuary occurs upstream of MCBCL, and thus upstream sources should be the focus of load reduction efforts. However, future growth and development within MCBCL watersheds may increase the importance of MCBCL tributaries as sources of nutrients and suspended solids to the NRE.</p>	
AE-2	<i>Quantifying and Predicting Watershed Inputs of Nutrients, Sediments, and Pathogens to Tributary Creeks on Marine Corps Base Camp Lejeune</i>	Senior Researcher: Mike Piehler
	<p>Findings: Overall loadings from MCBCL tributary creeks were very low compared to other East Coast Coastal Plain streams. Loads of nutrients and total suspended solids were positively correlated with increasing impervious cover in the watershed. The pattern in nutrient loading suggested a threshold in impervious cover of 15% as a tipping point, above which considerably higher nutrient loading occurred. Comparison of the loadings from a drier year (2008–2009) to two wetter years (2009–2010 and 2010–2011) revealed increased loads of most constituents in wetter years and that developed watersheds had similar proportional increases in loading, as did less developed watersheds. Loading patterns of fecal indicator bacteria (<i>Enterococcus</i> spp. [ENT] and <i>Escherichia coli</i> [E. coli (EC)]) frequently exceeded regulatory standards for fecal contamination in headwater portions of the study streams. EC and ENT in storm loading was as much as 30 to 37 times greater than baseflow loading.</p>	

(continued)

Table 2-3. Aquatic/Estuarine Module Research Project Titles, Senior Researchers, and Summaries of Findings (continued)

Research Project	Research Project Title	Senior Researcher
AE-3	<i>Developing Indicators of Ecosystem Function for Shallow Estuaries: Benthic Functional Responses in the New River Estuary</i>	Senior Researcher: Iris Anderson
	<p>Findings: Benthic microorganisms (e.g., the benthic nutrient filter) play an important role in retention and removal of remineralized nutrients, regulation of benthic–pelagic nutrient exchanges, and stabilization of bottom sediments. Benthic microorganisms also provide some protection against nutrient enrichment and accompanying eutrophication of the estuary. The NRE is moderately eutrophic with benthic gross primary production responsible for 41% of total estuarine productivity. Effectiveness of the benthos as the benthic nutrient filter is dependent on light availability and photic area of the estuary which varied as a function of freshwater discharge ranging between 46–97% of total estuarine bottom area. Benthic chlorophyll <i>a</i> was an excellent indicator of the effectiveness of the benthic microalgal nutrient filter. During summer, a threshold for benthic chlorophyll <i>a</i> was observed that ranged from 70–83 mg m⁻², below which the benthos was a source of nutrients and above which was a sink for nutrients. In high discharge periods with high nutrient inputs, high pelagic primary production, and low photic area, the benthic microalgal “filter” is likely to be less effective due to light limitation and low biomass.</p>	
AE Synthetic Modeling	<i>Development and Application of Watershed and Estuarine Simulation Models for the New River Estuary</i>	Senior Researcher: Dr. Mark Brush
	<p>Findings: A range of watershed models was applied to predict current material loads to the NRE and potential changes in those loads due to MCBCL development. The models differed in their ability to accurately predict annual and monthly loads, and no single model provided the best predictions for all parameters (fresh water, nitrogen, phosphorus, and sediments). An inter-model comparison indicated that the simpler models and the more complex models often predicted loads and could therefore be useful management tools for the MCBCL. An ESM was applied in nine spatial elements down the axis of the NRE and reproduced the annual cycles and key events for surface chlorophyll <i>a</i>, nutrient and dissolved oxygen concentrations, benthic microalgal biomass, and key rate processes. A series of model simulations indicated that the key controls on NRE response to watershed nutrient loads include flushing time via freshwater loading, nutrient sequestration by benthic microalgae, nutrient removal by denitrification, and strong light attenuation in large part due to CDOM. A series of simulations with varying watershed nutrient inputs indicated minimal effects of the MCBCL wastewater treatment plant and loads originating from MCBCL, but strong effects of loads from the upland, off-Base watershed; this response is modulated by inter-annual hydrologic variability.</p>	

Aquatic/Estuarine Module’s Monitoring Program

The Aquatic/Estuarine Module monitoring program was designed to capture and link hydrologic, nutrient, and sediment inputs from the New River watershed and MCBCL tributary creeks with phytoplankton community growth (productivity) and biomass (chlorophyll *a* and diagnostic pigments) responses in the NRE. Differentiating the stressors affecting processes in the estuary

included the consideration of extreme weather-related events, such as hurricanes, nor'easters, floods, and droughts, which have been shown to be important drivers whose impacts vary greatly inter-annually.

Inputs to the NRE were collected from two locations on the New River and from 10 tributary creeks located on MCBCL. Flow measurements and nutrient and sediment data were used to characterize changes in hydrologic flow and to determine loadings to the estuary. Tributary creek monitoring stations were distributed throughout the estuarine gradient to capture the impacts of various land uses on nutrient and sediment loadings. As watershed development increased, creeks draining them showed reduced seasonality in typical flow pattern (elevated in winter, depressed in summer), increases in the ratio of nitrogen to phosphorus loaded to the estuary, and increases in the proportion of nutrients and sediments delivered during storms.

In the NRE, water quality measurements were made using eight fixed sampling stations, two continuous autonomous vertical profilers (AVPs), and monthly Dataflow transects to capture hydrologic and nutrient inputs. These measurements were linked with phytoplankton community growth (productivity) and biomass (chlorophyll *a* and diagnostic pigments) responses from the research effort. AVP data enabled researchers to characterize vertical stratification in the upstream microtidal and downstream tidal components of the estuary. These data are essential for understanding the seasonal and inter-annual interplay of physical–chemical forcing features (e.g., freshwater discharge, salinity regimes, temperatures and stratification, water transparency, nutrient inputs and concentrations, dissolved oxygen conditions) with trophic and biogeochemical responses in the NRE. The monitoring data revealed that the NRE is functionally divided into two estuaries, with dramatically different biological responses noted in each, including contrasting sensitivities to the development and proliferation of harmful algal blooms, hypoxia potentials, and external inputs versus internal releases of nutrients from the BMA.

Conclusions and Implications from the Aquatic/Estuarine Module

Key Scientific Findings—Fundamental Cause-and-Effect Relationships

- The New River watershed is the major source (approximately 64%) of the external nitrogen loadings to the NRE. External nitrogen is the primary nutrient driving phytoplankton and benthic microalgae production. Both bioassay and productivity data suggest that intense nutrient limitation, particularly nitrogen limitation, occurs as riverine loads are depleted by phytoplankton growth within the upper estuary. The bathymetry and hydrodynamics of this system create significant down-estuary gradients in a number of physical parameters (i.e., CDOM, nitrogen and phosphorus concentrations, and sediment concentrations) that directly impact estuarine productivity.
- The pelagic phytoplankton and benthic microalgae in the NRE together account for the overwhelming proportion of the primary production. Other primary producer groups (e.g., marsh grasses, sea grasses, macroalgae) are of minor importance because of their limited areal extent in the NRE.
- Benthic chlorophyll *a* can serve as an excellent indicator of the effectiveness of the benthic microalgae as a nutrient filter. During the summer, the threshold for benthic chlorophyll *a* ranged from 70–83 mg m⁻². Below this range, the benthic microalgae were

a source of nutrients to the water column supporting phytoplankton production; above this range, the benthic microalgae were a sink, sequestering nutrients from the water column, thereby reducing the potential for phytoplankton blooms to develop.

- There is a strong hydrological control of phytoplankton biomass production in the NRE. For total phytoplankton biomass, there is a threshold river flow or tipping point of approximately $27 \text{ m}^3 \text{ s}^{-1}$. Above this flow rate, water residence time within the estuary is too short to allow for assimilation of nutrients by the phytoplankton to occur and therefore restricts algal bloom development.

Findings with Implications for MCBCL Management Practices

- Current nutrient loadings from MCBCL watersheds to the tributary creeks have extremely low nitrogen concentrations relative to other estuarine watersheds along the East Coast, suggesting that current land uses for military training and infrastructure development are not impairing water quality. A lack of development along the majority of the shoreline of the NRE and ICW has reduced landscape disturbance, thus protecting estuarine water quality.
- Future development planning for MCBCL should include comprehensive evaluation of locations for new infrastructure projects or training areas. Proactive site selection to minimize runoff potential of nutrients and sediments will be more cost effective than having to retrofit a site after construction to remedy stormwater runoff. The percent imperviousness of a watershed should be a key consideration in siting additional facilities, especially if the percent of impervious surface area is already approaching or exceeding 15%. This 15% imperviousness value appears to be a tipping point for these watersheds above which greater nutrient loading occurs.
- Benthic microalgae act as a “nutrient filter” regulating nutrient exchanges between the sediment and water column. When the benthic microalgae are photosynthesizing, they retain and remove nutrients from the water column and sequester them in their biomass and sediments. In contrast, when the benthic microalgae are not photosynthesizing because of reduced water clarity, they release nutrients back into the water column that fuels phytoplankton blooms in the NRE. MCBCL management actions to reduce nutrient and sediment runoff through maintenance of riparian buffers and implementation of stormwater management practices on MCBCL lands should aim to maintain or shift the balance toward benthic microalgae production and away from phytoplankton production. These actions will be especially important as MCBCL land use changes and as future climate change impacts the hydrologic cycle (the wet/dry periods).

Findings with Implications for DCERP2

- Understanding the role of the creeks as conduits for nutrient and sediment loading to the NRE under baseflow and stormflow conditions and varying land uses will help in understanding the potential for increased loadings of these constituents from MCBCL lands under climate change scenarios that project increased rainfall during storms.
- Both the phytoplankton and benthic microalgae populations in the NRE are modulated by factors (nutrients, sediment, CDOM) associated directly with the hydrologic cycle and its impacts on the hydrodynamics of the New River. Understanding future climate change

conditions (changed hydrologic cycle associated with wet/dry periods and warming temperatures) will be important in understanding the climate change impacts to the estuarine carbon cycle.

- Raphidophytes, a harmful algal bloom group that produces toxins known to kill fish, have been prevalent in algal blooms in the NRE and are the singular algal group linked to bloom development during drought periods. Future climate change conditions may alter the hydrologic cycle and occurrence of wet/dry period and severe drought could increase opportunities for bloom development of this group and their potential to impact fish populations. Although drought may promote raphidophyte development, changes in extreme rainfall events projected for the future could also flush nutrients and phytoplankton from the estuary, thereby transporting carbon from the estuary to the coastal ocean.

Coastal Wetlands Module

Summary of the Ecosystem

Coastal wetlands are a vital component of the estuarine landscape that links terrestrial and freshwater habitats with the sea. Marshes provide a variety of ecosystem services, including improving water quality by transforming nutrients and trapping sediment, attenuating wind wave and boat wake energy on shorelines, stabilizing the coastal barriers, accreting sediments and building land, and providing recreational opportunities for people. Marshes provide important habitat area for a diverse group of estuarine organisms, including commercially important fish and shellfish species (**Figure 2-2**). The Coastal Wetlands Module investigated factors affecting the sustainability of coastal marshes relative to military training impacts, projected SLR, and shoreline erosion by wind waves and vessel wakes, as well as the role of salt marshes in cycling nutrients within the MCBCL coastal ecosystem. Salt marshes within the MCBCL region occur in the lower NRE and along both shores of the ICW and are typically dominated by smooth cordgrass (*Spartina alterniflora*) and black needle rush (*Juncus roemerianus*). *Spartina* and *Juncus* are the dominant plant species in salt marshes of the Atlantic and Gulf Coasts, making these research results readily transferrable to other locations. The ICW bisects the backbarrier island salt marsh system on MCBCL, providing an opportunity to examine the potential impact of boating activity and dredging operations on coastal wetlands. The distribution of salt marsh relative to elevation, which is a key predictor of resilience to SLR, differs on either side of the ICW. Salt marshes on the west, or mainland side, of the ICW are lower in elevation than those on the east side of the ICW. The ICW channel may act as a trap that intercepts sand and sediment eroded from the barrier island. Routine maintenance dredging of the ICW channel removes this sediment from the system, depriving the mainland marshes of this sediment subsidy for accretion. The lower surface elevation of the mainland marshes, in combination with erosion from boat wakes, makes these marshes susceptible to the predicted acceleration in SLR. Salt marshes are also the only wetlands on MCBCL that adjoin and occasionally intercept amphibious military training exercises and that play a role in coastal barrier island stabilization.



Figure 2-2. Conceptual model for the Coastal Wetlands Module.

The Coastal Wetlands Module conducted three research projects listed in **Table 2-4** to address the stresses imposed as a consequence of MCBCL military training activities and other direct anthropogenic activities and of global climate change, particularly SLR on coastal marshes. Two of these research projects (i.e., CW-1 and CW-2) addressed changes in geomorphology driven by sea level change, impacts from amphibious training maneuvers, and wind wave and boat wake erosion. Research Project CW-1 used the MEM to determine marsh response to projected SLR and to predict when the marshes at MCBCL might be inundated and collapse in the future. Research Project CW-2 developed a customized version of the National Oceanic and Atmospheric Administration's (NOAA's) Wave Exposure Model (WEMo) to classify estuarine shorelines exposed to wave energy, identify shorelines where boat wake energy significantly increased total wave energy, and determine shoreline erosional hotspots. A new component was added to WEMo to determine estuarine areas prone to resuspension of sediments along the estuary bottom. The third project, Research Project CW-3, addressed the flux of water (upland and tidal) through the marshes and the transformation of nutrients in the water cycling through the marsh. Research sites were strategically chosen to take advantage of significant activity (e.g., amphibious military training operations, splash points), proximity to upland land uses (e.g., groundwater, nutrient flux), research and monitoring activities by other modules (e.g., coastal barrier island migration), or other significant attributes (e.g., shoreline stabilization structures).

**Table 2-4. Coastal Wetlands Module Research Project Titles,
Senior Researchers, and Summaries of Findings**

Research Project	Research Project Title	Senior Researcher
CW-1	<i>Drivers and Forecasts of the Responses of Tidal Salt Marshes to Sea Level Rise</i>	Senior Researcher: Jim Morris
	<p>Findings: The salt marshes of MCBCL provide some evidence in support of the concept that the relative elevations of marsh landscapes vary and demonstrate skewness in a direction that is diagnostic of their position. Both the empirical results and the MEM predictions indicate that the marshes west of the ICW are not in equilibrium with SLR. The elevation of these marshes is significantly lower than marshes east of the ICW, yet the marshes west of the ICW had the highest rate of sediment accretion. We concluded that the ICW causes loss of sediment from the margins of the marshes and traps sediment from the backbarrier marshes of Onslow Island. Without the presence of the ICW, the backbarrier marshes would be subsidizing the sediment supply of the marshes west of the ICW. The fertilization experiments indicated that the salt marsh vegetation at MCBCL is co-limited by nitrogen and phosphorus, and this increased the biomass, thus raising the elevation of the marsh plots. In summary, the MEM predicts a collapse of the ICW marshes within 95 years depending upon the rate of SLR and other factors such as sediment supply, tidal amplitude, and biomass.</p>	
CW-2	<i>Forecasting Influence of Natural and Anthropogenic Factors on Estuarine Shoreline Erosion Rates</i>	Senior Researcher: Mark Fonseca
	<p>Findings: Wave energy along the NRE is primarily from wind waves, whereas wave energy on ICW shorelines is primarily from boat wakes. In the NRE, marsh shorelines exhibited lower erosion rates than sediment bank shorelines; however, erosion rates were significantly lower when a narrow fringing marsh (less than 5 m in width) was present. The annual input of sediment into the NRE via sediment bank erosion is approximately half the amount needed for salt marshes to keep pace with current rates of SLR. This estimate also demonstrates the potential importance of coastal marshes in trapping sediments and maintaining water quality in the NRE. In the ICW, the shoreline is predominately salt marshes; however, the average width of the ICW has increased from approximately 70-m wide in 1938 to more than 145-m wide in 2009 from the combined effects of wave and boat wake erosion and repeated dredging of the ICW to maintain navigability.</p>	

(continued)

Table 2-4. Coastal Wetlands Module Research Project Titles, Senior Researchers, and Summaries of Findings (continued)

Research Project	Research Project Title	Senior Researcher
CW-3	<i>Hydraulic Exchange and Nutrient Reactivity in the New River Estuary Wetlands</i>	Senior Researcher: Craig Tobias
	Findings: Groundwater inputs to coastal marshes were found to be an important source of fresh water to the root zone of the marsh plants, but not an important source of nitrogen because groundwater nitrogen concentrations are low. The nitrogen inputs from marsh drainage to the NRE are trivial, but are not trivial from the marshes to the ICW. When all exchange routes for nitrogen are considered, the intertidal marshes of MCBCL are overwhelmingly large sinks for nitrogen. The nitrogen sink strength is dominated by sediment nitrogen burial during accretion (80–90%) and denitrification (10–20%). We estimated that 9,660 kg N y ⁻¹ is buried in the marshes bordering the NRE, and 23,460 kg N y ⁻¹ is buried in the marshes bordering the ICW. The magnitude of the nitrogen sinks within the marshes would have to decrease on the order of 20-fold before the marshes would switch from being a net sink to a net source of nitrogen. Barring any extreme changes in marsh geomorphology (e.g., marsh edge to area ratio) or severe increases in tidal amplitude, if the existing marshes continue to accrete at rates keeping pace with SLR, then they will remain as a net nitrogen sink.	

Coastal Wetlands Module’s Monitoring Program

The Coastal Wetlands Module monitoring effort provided crucial baseline information to support the three research projects of the Coastal Wetlands Module and established and maintained tide gauges, which provided the first recognized tidal datums for MCBCL. The Coastal Wetlands Module monitoring effort also measured marsh surface elevation and sediment accretion in *Spartina* and *Juncus* marshes, annually measured marsh above-ground primary production, and monitored nutrients in shallow groundwater within the marsh zone.

Overall, the Coastal Wetlands Module’s monitoring stations ranged from the upper portion of the NRE (Wallace Creek), to mid-estuary (French Creek), to the lower portion of the NRE (Traps Bay, Mile Hammock Bay), and finally to the salt marshes that border either side of the ICW (Freeman Creek, Onslow Beach). These monitoring stations included sites dominated by *Spartina alterniflora* in the lower estuary and *Juncus roemerianus* in the mid to upper estuary. This spatial coverage allowed us to demonstrate how changes in marsh geomorphology, tidal amplitude, wave energy exposure, and surface elevation affect the processes (nutrient exchange, sediment accretion, shoreline erosion, marsh primary production) being studied. Our analysis of current monitoring data demonstrates significant site variability in the relationship between marsh biomass and surface elevation and in the relationship between tidal inundation and sedimentation rates. Some of this site variability is due to differing tidal amplitude, which was observed in the tide gauge data, whereas changes in salinity, dominant plant vegetation, and proximity to sediment sources also influence the measured site-specific responses.

The frequency of sampling ranged from annual measures of primary production to close interval (6–15 minutes) sampling of water level. In addition, long-term (more than 50 years) rates of shoreline erosion for the NRE and ICW shorelines were determined using aerial photography.

Sampling frequency has proven adequate to detect significant site and annual variability. However, several of the processes of interest to the Coastal Wetlands Module's research effort are long-term processes (marsh response to SLR, shoreline erosion) that require fairly long-term (5 to 10 years) monitoring to distinguish short-term variability from long-term trends and to increase the likelihood of capturing storm events that may be important.

Conclusions and Implications from the Coastal Wetlands Module

Key Scientific Findings—Fundamental Cause-and-Effect Relationships

- The MEM describes plant productivity and sediment accretion in marshes and forecasts changes in marsh elevation as a function of primary productivity, suspended sediments, and flooding, and primary production as a function of relative elevation. The model forecasts a 95-year survival time for MCBCL area marshes given a scenario where sea level rises 100 cm by the end of the century.
- Wave energy from wind and boat wakes are the main erosional forces in the ICW. Our research is the first quantitative assessment of boat wakes in the ICW that evaluates historical shoreline erosion. Our research also conducted a comparative analysis among wind waves and boat wakes to define the potential tipping point where boat wake impacts would be eclipsed by the natural, wind wave environment for effects on shoreline stability. The majority of the boat wakes that exceeded wind waves (31.7%) were approximately 0.45 m larger than wind waves; this difference is larger than the top 5% of wind waves normally observed throughout the entire NRE. The top 5% of boat wake waves exceeded wind waves by greater than 0.75 m, with a few percent exceeding ambient wind conditions by almost 0.9 m.
- The history and effects of dredging the ICW to a box-shaped channel on a 5-year cycle, led to the development of a conceptual model for this process, which we refer to as the “dredge and slump model.” This conceptual model describes the adverse impact of dredging operations in the ICW on adjacent salt marshes, via removal of sediment from the system, and slumping of the marsh edge as a result of erosion into the navigation channel. This slumping process has widened the ICW channel from a width of 70 m in 1938 to more than 145 m in 2009 and may have implications for the sustainability of the ICW at MCBCL and in other areas along its extent. The next research steps include the following: (1) an assessment of suspended sediment concentration and transport in marshes adjacent to the ICW to fill a data gap and refine predictive models of marsh response to SLR, and (2) assessment of adaptive management practices (such as thin-layer spreading of dredge spoil material over marsh plots) to minimize the adverse impacts of maintenance dredging of the ICW on coastal marshes.
- The intertidal marshes of MCBCL should be considered overwhelmingly large sinks for nitrogen. The nitrogen sink strength is dominated by nitrogen burial during sediment accretion (80–90%) and denitrification (10–20%). Scaling up measured rates to total marsh area; we estimated that 9,660 kg N y⁻¹ and 23,460 kg N y⁻¹ are buried in the marshes bordering the NRE and ICW, respectively. These estimates show that the marsh functions as a net sink for nitrogen for both the NRE and ICW marshes.

Findings with Implications for MCBCL Management Practices

- In the ICW, several unreinforced splash points have exhibited higher shoreline erosion rates than the average rate for the ICW. Reinforced splash points within the ICW have a lower shoreline change rate as a result of boat wake or wave erosion compared to unmodified splash points. MCBCL managers should give consideration to many strategies to reduce erosion rates and enhance sustainability of splash points for future training maneuvers. These strategies include reinforcing splash points with concrete ramps, implementing marsh habitat restoration, or diverting some military training activities from splash points showing the most erosion to underused splash points to reduce training pressure on overused splash points.
- Only 19% of the NRE shoreline has been modified through hardened revetments, sills, and seawalls. This constrained development/use of the shoreline has water quality benefits with respect to reduced runoff of nutrients and sediment and allows ecosystem services (e.g., aquatic habitat, storm surge protection) of these shorelines (i.e., sediment banks, swamp forests, and marshes) to be preserved.
- Historic MCBCL practices have hardened NRE shoreline areas in high-energy areas which are appropriate; however, marshes and sediment banks, which supply sediment vital for marsh accretion, will be needed in the future to help mitigate for SLR impacts on the marshes. MCBCL managers should consider whether additional shoreline hardening is needed, and if so, offset new shoreline hardening with habitat restoration in hardened areas where wave energy is low. This will help sustain the marshes by allowing the release of sediment required for the marshes to keep pace with SLR.
- Based on our surveys, salt marshes can readily persist on shorelines where WEMo forecasts wave energy values $\leq 300 \text{ J m}^{-1}$. We recommend these NRE shoreline segments as strong candidates for habitat restoration by removing the modified structures and transplanting marsh grasses. If there is any remaining vegetation after the removal of the modified structures, then this may supplement the revegetation process significantly. These restoration efforts will promote sustainability by allowing the marshes to migrate landward as sea level rises and will continue to provide shoreline ecosystem services not achieved with hardened structures.
- If the speed of large V-hulled vessels was reduced in the ICW (from 20 knots to 7 knots), then vessel wakes would be sufficiently small so as not to create sediment-eroding waves. MCBCL managers should consider requesting the establishment of a no-wake zone in the ICW. If properly placed, a 2-mile no-wake zone would increase transit time by only 10 minutes along the southern MCBCL boundary. However, this longer transit time would provide the benefit of substantially reducing the creation of erosion-generating boat wakes.
- For long-term planning in addition to that for storm surge and wave runup, the rise in sea level should also be a primary consideration. Future placement of MCBCL infrastructure and facilities should consider SLR. This planning could affect the construction of new facilities and require setback space allowances to accommodate the future landward migration of existing marshes with SLR to sustain marsh ecosystem services such as shoreline stabilization and wildlife habitat.

Findings with Implications for DCERP2

- During DCERP1, the MEM was applied to the *Spartina alterniflora* marshes of MCBCL. For DCERP2, preliminary work started in DCERP1 on *Juncus roemerianus* marshes will be expanded at MCBCL, where both marsh plant species exist. In addition, the Coastal Wetlands Module Team will gather sediment cores at Eglin Air Force Base in Florida to supplement information collected at MCBCL with the aim of parameterizing a model for this second species that is widely distributed in the Gulf Coast area.
- The RTI DCERP Team will use results from the marsh experimental biomass studies (both above ground [shoot] and below ground [root]) and measured sediment accretion rates to support the development of a spatially explicit numerical model of marsh accretion. The MEM will predict how carbon sequestration and marsh vulnerability change across the marsh landscape and throughout the next century in response to SLR.
- Based on MEM forecast scenarios, there are two management strategies that could mitigate the effect of the ICW on the surrounding marshes and enhance their sustainability: (1) nutrient enrichment to enhance biomass production of marsh plants and sediment accretion, and (2) thin-layer disposal of dredge spoils on the marsh surface. As part of DCERP2, consideration will be given to evaluating these management strategies as potential options to help enhance sustainability. Results of these tests would inform the use of such management strategies in sustaining marshes in similar ecological settings.
- Currently, salt marshes on MCBCL are a net nitrogen sink. Provided that the MCBCL marshes keep pace with SLR, this function is likely to remain intact. DCERP1 also demonstrated that the productivity of *Spartina alterniflora* marshes on MCBCL is co-limited by nitrogen and phosphorus. These results will inform efforts to model marsh production, sediment accretion, and, ultimately, carbon burial across the MCBCL landscape.

Coastal Barrier Module

Summary of the Ecosystem

Onslow Beach is a northeast-southwest trending, wave-dominated barrier island located just south from where the Outer Banks barrier-island chain ends. This 12 km (8 mi)–long barrier fronts saltmarsh and is bounded by the New River Inlet to the southwest and Browns Inlet to the northeast. The shoreline of Onslow Beach is sinusoidal with a central headland separating two shallow, cusped embayments. The northern embayment has a wide beach (approximately 80-m) with multiple well-developed dune ridges (7–9 m in height) and is similar to other barrier islands to the northeast such as Bear Island and Bogue Banks. The central headland area has a narrow beach (approximately 20-m wide) with a single discontinuous dune ridge less than 4 m in height. The beach widens significantly along the southern embayment from 20 m in the northeast to 80 m in the southwest, and the morphology of this part of the beach is very similar to barrier islands to the south such as Topsail Island. The discontinuous dunes along the southern end are less than 2 m in height, and washover fans can be extensive (250-m wide) and extend across backbarrier marshes. The highly variable morphology along Onslow Beach is unique; however, this allows DCERP results to be applicable to many other barrier islands worldwide.

The Coastal Barrier Module examined the coastal barrier island ecosystem that lies at the interface between the continental shelf and the protected NRE. This barrier island ecosystem encompasses the shallow subtidal and intertidal shore face, tidal inlet, backshore beach, aeolian dune, shrub zone, maritime forest, and washover sand flat habitats. These habitats are defined by intrinsic ecological processes, but are linked by sediment transport, nutrient exchange, and biological uses, each of which undergoes substantial changes over multiple time scales (**Figure 2-3**). Research efforts were designed to support the long-term sustainability of the island as an important coastal resource necessary for amphibious military training, for recreation for MCBCL personnel, and for maintaining important habitats for protected species.

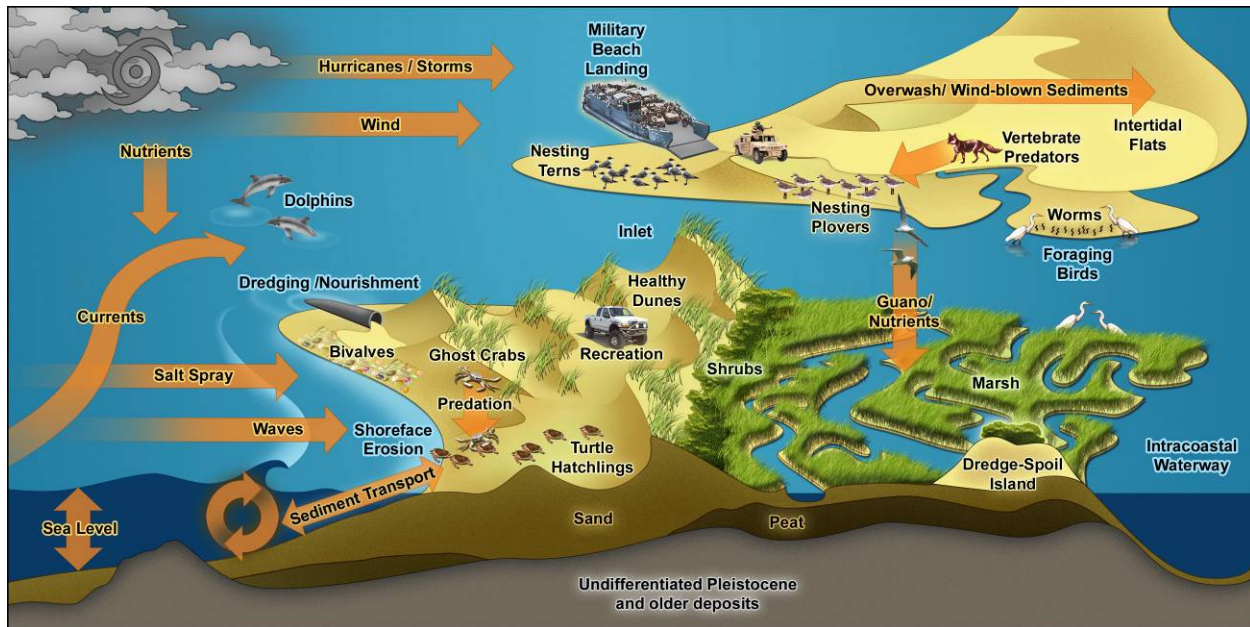


Figure 2-3. Conceptual model for the Coastal Barrier Module.

Onslow Beach is a critical asset to MCBCL as the primary Atlantic Coast location where amphibious military training maneuvers occur. Research projects for the Coastal Barrier Module (**Table 2-5**) studied geological and hydrodynamic evolutions of the coastal barrier island and the response of avian species. Future sustainability and effective management of the coastal barrier island depend upon a better understanding of the evolution of the island in terms of shoreline movement and landscape change. Coastal Barrier Module research focused on an improved understanding of the short-term hydrodynamic evolution related to land use and impacts of storm events (Research Project CB-1) and on long-term barrier evolution related to variations in underlying geology and inlet dynamics that have shaped the island over geologic time (Research Project CB-2). Studies examined the evolution of Onslow Beach over millennial to yearly time scales and the contribution of aeolian sand to backbarrier marshes to help better manage future landscape changes that may occur in response to changes in future storminess and SLR. Modeling focused on the development of a hydrodynamic Runup and Overwash Model (ROM) to predict future overwash locations from storm events. Research Project CW-3 addressed the population dynamics of Wilson's plover (*Charadrius wilsonia*), a regional species of concern that was selected as a surrogate for the endangered piping plover (*Charadrius melodus*) and assessed this species' habitat requirements and success in nesting and foraging in various barrier

habitats. Results from examining predator top-down influences have been provided to MCBCL staff so they can design the most efficient predator-trapping program and determine how to manage habitat availability.

Table 2-5. Coastal Barrier Module Research Project Titles, Senior Researchers, and Summaries of Findings

Research Project	Research Project Title	Senior Researcher
CB-1	<i>Short-Term Barrier Evolution: Overwash at Onslow Beach Through Assessment of Training Activities and Model Predictions</i>	Senior Researcher: Jesse McNinch
	Findings: Results suggest a relationship exists between the amount of overwash and the number of tropical hurricanes that impact the barrier island in a given decade. Neither an increase nor a decrease in washover deposits were discernible as a linear trend, suggesting that MCBCL training activities did not measurably influence overwash processes. Modeled wave runup and projected locations of overwash demonstrated strong skill during Hurricane Irene. ROM simulations correctly predicted four overwash locations along Onslow Beach. Model results imply that runup elevations vary along Onslow Beach as a function of beach slope and nearshore bathymetry such that overwash and inundation predictions based solely on regional tides and surge would likely have poor skill in predicting overwash locations except for the most extreme storm events. Furthermore, hard bottom outcrops in the surf zone in the central portion of the island (military training zone) will likely continue to induce higher elevations of runup in these areas.	
CB-2	<i>Long-Term Barrier Evolution Related to Variations in Underlying Geology and Land Use</i>	Senior Researcher: Tony Rodriguez
	Findings: Onslow Beach is a transgressive barrier island that moved from approximately 300 m seaward of its present location in approximately 200 A.D. to its present position during the late Holocene, principally through overwash processes and washover fan formation. Around 1850 A.D., the number and landward extent of washover fans increased sharply along the entire island. This corresponded to an increase in the rate of SLR and a low number of annual tropical hurricanes in the Atlantic Ocean. The increase in the rate of SLR resulted in more frequent wave erosion of the backshore and aeolian dunes, which likely lowered the elevation of the island and made the island more vulnerable to overwash. This sensitivity is likely the result of the island being sediment starved, a product of its framework geology (limestone outcropping near the shoreface) and its location at the center of a coastal embayment (Onslow Bay). Military training activities have had little impact on island evolution because the decadal record of shoreline movement and the geological record of island evolution show that the military training zone has been vulnerable to overwash and experienced high rates of shoreline retreat in 1850 A.D., long before MCBCL existed.	

(continued)

**Table 2-5. Coastal Barrier Module Research Project Titles,
Senior Researchers, and Summaries of Findings (continued)**

Research Project	Research Project Title	Senior Researcher
CB-3	<i>Understanding the Top-Down and Bottom-Up Drivers of Shorebird Nest Success and Habitat Use in Relation to Beach Management Practices on MCBCL</i>	Senior Researchers: Sarah Karpanty and Jim Fraser
	<p>Findings: Results of a 2-year study of Wilson’s plovers (<i>Charadrius wilsonia</i>) at Onslow Beach indicated little differences between years in nest success (≥ 1 egg hatched), nest failure, and overall nest survival. The majority of nest failures were caused by mammalian predators. For those nests that hatched successfully, greater proportions were located in clumped vegetation than on bare ground or sparsely vegetated areas. In-season chick survival for both years of the study was higher for nests that hatched earlier in the season and for nests farthest from the broods’ final foraging territory. The survival rate of adult Wilson’s plover was high (82%) and was consistent with studies of other plover species on the Atlantic Coast. Our findings indicate that Wilson’s plover adults and broods were flexible in establishing final foraging territories. In 2008, all final brood foraging territories were on fiddler crab (<i>Uca</i> spp.) flats, whereas in 2009, final foraging territories were sometimes split between fiddler crab flats, beach front, and inter-dune sand flats. For those Wilson’s plovers establishing territories on fiddler crab flats, the size of the flat was the most important feature explaining the use versus non-use and the area of the fiddler crab flats; $\geq 1,250$ m² was preferred. Close proximity to water and vegetative cover were also important habitat features in foraging site selection on fiddler crab mud flats and in all habitat types combined.</p>	

Coastal Barrier Module’s Monitoring Program

The goal of the Coastal Barrier Module’s monitoring activities was to make those necessary measurements and observations that allow isolation and integration of human-derived (including military training activities) and natural processes to understand the dynamics of the coastal barrier ecosystem. The focus was on outputs that served to identify how those components of the ecosystem of greatest concern to MCBCL in sustaining the coastal barrier for training and for its natural resource assets can be successfully managed and optimized. Fulfilling this goal required not only measurement of various conditions and processes, but also analysis, synthesis, integration, and use of a wide variety of hydrodynamic models used by the research projects. The components of Coastal Barrier Modules’ monitoring program supporting the three coastal Barrier Module research projects included measurements of ocean meteorology; ocean and near shore hydrodynamics; beach topography, geomorphology, and sedimentology (including aeolian sand); dune, shrub and marsh plants cover and height; and avian abundance.

Ocean meteorology and hydrodynamics were measured continuously at two NOAA buoy stations 5 and 25 mi seaward of the New River Inlet and an additional station 500 m off Onslow Beach. These measurements provided information to develop seasonal wind and wave climates for the barrier and were used to validate the coupled Advanced Circulation (ADCIRC) + Simulating Waves Nearshore (SWAN) Models that were used to determine shoreline position

changes in response to storms including erosion and habitat changes. Tide data were acquired from NOAA's sites in Wilmington and Beaufort (both in North Carolina) and from two gauges at Mile Hammock Bay and Wallace Creek maintained by the Coastal Wetlands Module. Accurate tidal frequency data were needed for ADCIRC Model set up of the Onslow Bay region. Shoreline position, sandbar position, and morphology were measured along the entire length of Onslow Beach every 3 years, as well as semiannually and before and after storm events at specific sites. These data also were used to validate the coupled ADCIRC + SWAN Model (Research Project CB-1) and to understand barrier migration. The ocean meteorology, offshore and nearshore hydrodynamics data, and tide data and shoreline position data were used to understand the seasonal variability of wind and wave fields across the barrier and in conjunction with beach profile data to determine seasonal accretion and erosion rates (Research Project CB-2). Baseline bathymetry data were collected in 2007 for the entire coastal barrier shoreface, including the New River Inlet, backbarrier, and portions of the NRE. This updated information when integrated with hydrodynamic wind, wave, tide and longshore current measurements and constrained by shoreface bathymetry and barrier island morphology was used to calibrate the hydrodynamic barrier models to forecast shoreline change for both long-term morphologic responses of the beach (erosion over decades) studied in Research Projects CB-2 and modeling of short-term storm events CB-2.

Monitoring of avian species temporal and spatial occurrence across Onslow Island and tidal information supported the species specific research of Research Project CB-3 by providing an overall perspective of shorebird utilization of habitat availability on Onslow Island. Monitoring data identified a tidal anomaly in 2009 that caused flooding of backbarrier marshes used by the indicator species, Wilson's plovers, for foraging. Identification of the tidal anomaly supported the research observation of changes in the foraging behaviors of Wilson's plovers that illustrated the plasticity of this species' habitat utilization in response to this natural phenomenon.

As DCERP evolved, monitoring procedures used by the Coastal Barrier Module were modified to generate better results by using more accurate and efficient equipment (e.g., changing method to measure sediment compaction, introducing state-of-the-art equipment such as the Coastal LiDAR and Radar Imaging System [CLARIS] to measure inshore hydrodynamic processes); and by sampling during unscheduled times to respond to episodic anthropogenic activities (e.g., military training events, pier removal, and dredge-spoil disposals) as well as episodic natural events (e.g., hurricanes, nor'easters). These new procedures and measurements were introduced to enhance our ability to fill data gaps (e.g., measuring aeolian wind transport using a new sand capturing sampler, quantifying shorebird activity to direct human interference). Information on barrier island vegetation was used in concert with the aeolian transport measurements to determine sand movement at three locations along the barrier. This information helped determine the rate of shoreline retreat in various locations along the barrier, thus refining model predictions. In August 2011, the region was affected by Hurricane Irene, a Category 2 hurricane that caused significant overwash on the island. Researchers were finally able to document changes to island morphology and ecology and to test their hypotheses, predicting how the island would respond to a major storm event. The results of all of these analyses are included in detail in the *DCERP I Final Baseline Monitoring Report*.

Conclusions and Implications from the Coastal Barrier Modules

Key Scientific Findings—Fundamental Cause-and-Effect Relationships

- The two most substantial washover deposits generated by Hurricane Irene in 2011 had not been overwashed at least since 1938, and thus are not just a reoccurrence of overwash at a previously breached dune (as occurred at two other overwash locations toward the middle of the island). This suggests that overwash occurs both at new areas and at those areas previously impacted.
- Sand thickness offshore of Onslow Island varied from 3 m at the northeastern part of the island to less than 1.5 m at middle and southwestern portions of the island. This confirms the relatively sand-starved conditions of the middle and especially the southwestern most portions of the barrier where erosion is higher.
- A comparison of washover extent, obtained from aerial photographs from 1938–2010, suggests that the primary forcing mechanism generating overwash processes on Onslow Beach has been tropical storm activity.
- Sand beds preserved within backbarrier marsh deposits are commonly thought to have been emplaced rapidly during a storm; however, post-storm aeolian transport should also be considered as an important mechanism for forming sand beds over a longer period of time within salt marsh strata. The percent volume of the marsh originating from aeolian sand, based on the upper 1 cm of marsh sediment, decreased by an order of magnitude only approximately 20 m from the dune–marsh boundary. Sandy beds sampled in every marsh core at depth are composed of aeolian sand and were likely placed over time after storms deposited a sandy washover fan near the marsh and/or reduced vegetation cover across the island.
- For Wilson’s plovers, 80% of nests laid in clumped grasses or mixed vegetation were successful, compared to only 41% of nests laid in low-growing sparse vegetation or on open sand. Additional research is needed to determine if habitat availability or preference of Wilson’s plovers is driving these results.
- The size (area) of a fiddler crab mud flat was the most important habitat feature influencing whether a Wilson’s plover brood established a territory on it. The ideal fiddler crab mud flat for Wilson’s plover brood territory establishment would be one that is greater than 1,250 m², within 10 m of water, subject to regular tidal flooding, and within 4 m of vegetation cover. A next research step would be to determine the areas that meet these requirements or could be managed to meet these requirements to improve available habitat for Wilson’s plovers.
- Wilson’s plover broods exhibited a change in foraging behavior between years that may reflect a change in environmental conditions. Similarly, broods established final foraging territories in all available foraging habitats (i.e., fiddler crab flats, inter-dune sand flats, and beach front) in 2009, but they only used fiddler crab flats in 2008. In 2009, Wilson’s plover access to fiddler crab mud flats was limited due to a coast-wide sea level anomaly that flooded the flats. However, sand accretion occurring between the two study seasons increased the beach front foraging opportunities during this same period. Despite this observed habitat shift by foraging adults and broods, no evidence was found of decreased

chick survival between years. This suggests that some plasticity exists in foraging behavior of this species if a range of alternative habitats are available for exploitation.

Findings with Implications for MCBCL Management Practices

- Overwash processes peaked both in 1950 and again in 1990, but a clear linear trend (either an increase or a decrease) was not evident. This suggests that MCBCL amphibious training activities did not have a measurable effect on overwash processes at Onslow Beach.
- MCBCL's strict use of designated ingress and egress points on the barrier island to move troops and equipment from the beach to the backbarrier areas is a protective strategy for sustaining dune structure and reduces the number of areas where overwash can penetrate behind the dunes. When first established, the ingress and egress points were selected because they were overwash areas. MCBCL managers should be cautious when considering the development of additional ingress and egress points because these provide conduits for overwash to penetrate more deeply into the barrier dune structure.
- Based on historical data, MCBCL managers should plan for an increase in the frequency and magnitude of overwash events, which will occur as higher sea levels increase dune erosion and lower the elevation of the island, making it more vulnerable to overwash processes. Additionally, future changes in extreme events such as tropical storms may further enhance overwash processes. Currently, the southwestern end of the island is most vulnerable to overwash because the elevation is lowest, annual erosion rates are high, and the offshore sediment supply is low. Given the high rates of landward shoreline movement at the center of the island and the narrow dunes, the island will likely overwash in this area again within the next 20 years. This makes sustainability of the marshes to the west (landward) of the ICW important particularly if the barrier island is breached.
- We recommend that if MCBCL has plans to build additional permanent structures or to modify existing structures located on the dunes, MCBCL managers recognize that the vulnerability of these sites to flooding and inundation will increase during the next 10 to 20 years. Depending on the nature of specific construction projects, it may be prudent for MCBCL managers to plan additional infrastructure development further landward of where the existing bathhouses and cottages are currently located. Looking to the future, MCBCL managers should also anticipate and plan for increased costs for post-storm infrastructure repair and clean up on the barrier island.
- The geological structure of the surf zone near the military training zone will likely continue to induce higher elevations of wave runup in that area than in surrounding areas. Best management practices designed to minimize lowering of the primary dune crest should be considered, and anticipating likely flooding of sea turtle nests in this area of the beach should be countered with continuing to relocate nests to less overwash-prone areas.
- MCBCL managers have been proactive in posting signage and fencing to protect shorebird nesting areas of Onslow Beach. MCBCL staff should continue to identify and protect newly formed and ephemeral habitats (e.g., overwash areas, sand accretion areas, ephemeral tidal pools) that help support Wilson's plover nesting pairs and broods and other breeding shorebirds with similar habitat requirements (e.g., piping plovers,

American oystercatchers [*Haematopus palliatus*], least terns [*Sterna antillarum*], willets [*Catoptrophorus semipalmatus*]). MCBCL managers should also aim to provide a variety of potential nesting and foraging sites from the beach front to sound-side mud flats to allow for flexible habitat use by breeding Wilson's plovers and foraging broods.

- An optimal range of 11–18% vegetation cover per 1 m² of beach front habitat was favorable for Wilson's plover foraging broods. This goal can be achieved by protecting newly formed washover areas and beach front sand accumulation that results in habitat relatively free of vegetation, except for sparse low-growing plants (i.e., sea rocket [*Cakile edentula*], new growth seashore-elder [*Iva imbricate*], and seaside pennywort [*Hydrocotyle bonariensis*]).
- Wilson's plover hatching success is positively related to the presence of a specific vegetation density around the nest site (i.e., successful nests have 8–22% vegetated cover within 0.5–1 m² of nest bowl) and a gradient of vegetation growth form (i.e., low-growing sparse vegetation and clumped grasses) beginning at the nest bowl and extending up to 1 m². Management of Wilson's plovers should attempt to achieve this density of vegetation in sandflat areas.
- Although MCBCL has met with public objections about restricting access to the southwestern end of Onslow Island during shorebird breeding season, alternative measures to signs and fencing could be implemented that might be more effective. For example, interns or volunteers could be used during high-use periods (i.e., on summer weekends and especially on Memorial Day, Independence Day, and Labor Day holiday weekends) for educational outreach to the general public and to monitor important foraging areas. Utilizing interns or volunteers might be a less confrontational and more effective approach to habitat management and improving conservation knowledge of shorebirds.

Findings with Implications for DCERP2

- The results from the ROM used during DCERP1 will be modified to project the barrier island's response to SLR and overwash events in the wake of projected increased incidence and magnitude of storm events which will be derived from Strategic Environmental Research and Development Program (SERDP) Research Project RC-1702 and from other sources.
- The ROM and the island transgression results from SERDP Research Project RC-1702 will be used to project the rate of exposure of the peat outcropping on the forebeach that can release carbon and the rate of carbon burial in the backbarrier marshes.

Terrestrial Module

Summary of the Ecosystem

The Terrestrial Module's ecosystem-based research was conducted along the gradient of vegetation from the salt marsh at the estuary margin, through brackish and freshwater marsh, to the longleaf pine savannas and pocosins (i.e., shrub bogs) that dominate the upland terrestrial environments on MCBCL. Variation in the biota and ecosystem processes along this gradient are

driven by variation in hydrology, soils, and fire behavior. Most of the rare species that are characteristic of coastal terrestrial ecosystems, including species of concern on MCBCL, are found in the transitional zones of these gradients. Changing patterns of land use, agriculture, and forest management have greatly altered forest ecosystems across much of the mid-Atlantic lower Coastal Plain. In particular, vast areas that were once dominated by open longleaf pine savanna now support closed canopy stands of loblolly pine with a dense understory and midstory of broadleaved shrubs and trees. The absence of fire on these landscapes has exacerbated this trend. This situation is typical for large portions of MCBCL. In recent years, longleaf pine restoration at MCBCL has focused on the use of understory and midstory thinning to produce savanna-like conditions and allow restoration of historical fire regimes using PB. **Figure 2-4** presents the conceptual model for the Terrestrial Module and illustrates the complementary nature of these critical physical, chemical, and biotic processes, disturbances, and interactions.

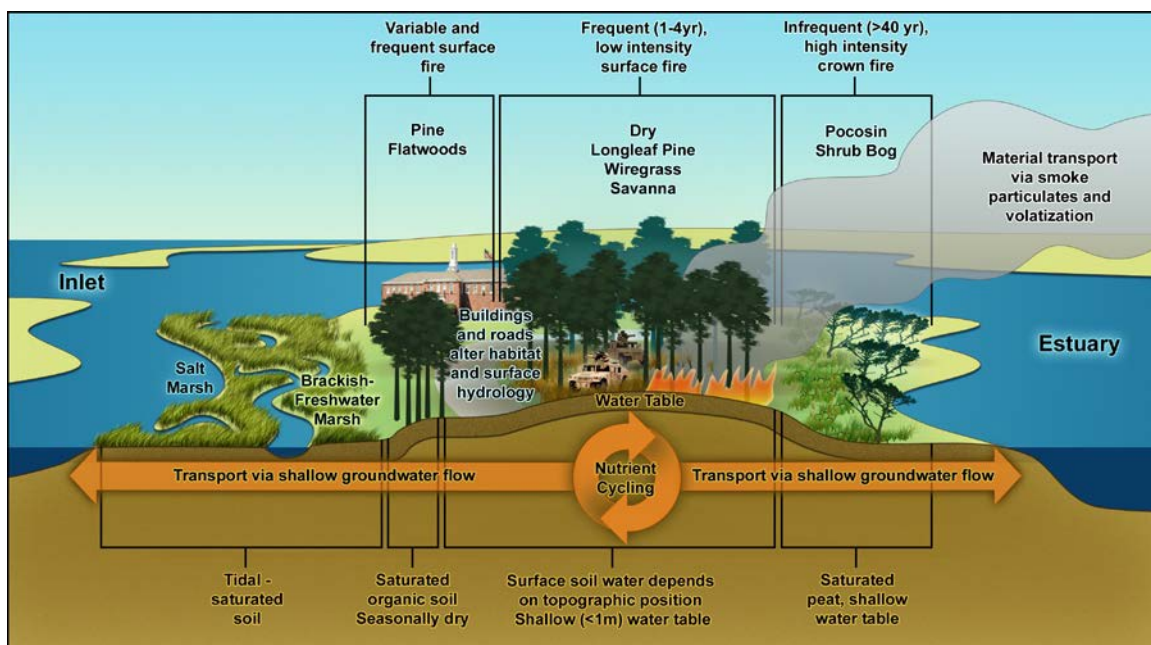


Figure 2-4. Conceptual model for the Terrestrial Module.

The locations of transitions from one ecosystem to another along this gradient are often influenced by disturbance (fire) history (Christensen, 1981; Garren, 1943). Fire is a natural part of this landscape, and natural fire regimes (frequency and intensity) change across this soil–hydrology–vegetation gradient, from frequent surface fires in longleaf pine savannas to relatively infrequent and intense crown fires in pocosins. The Terrestrial Module’s research focused on the critical knowledge gaps related to efforts to restore longleaf pine ecosystems on sites across MCBCL that have been modified by past management practices. The research examined the effects of alternative midstory restoration strategies (e.g., mechanical thinning, PB) on understory plant, insect, and avian communities, particularly the federally protected, RCW. In addition, the research provided information regarding whether management for a single species (i.e., RCW) is beneficial or detrimental to other avian species.

The two research projects of the Terrestrial Module (**Table 2-6**) constitute an integrated program designed to provide a greater understanding of how forest restoration treatments affect the

interrelationships among the vegetation, arthropod, and avifaunal communities across sites representing a wide range of soil conditions and RCW foraging habitat qualities. The relationship between RCW foraging habitat quality and community composition was an outcome of these projects. The Terrestrial Module's research also focused on providing data on fuel characteristics to complement research conducted by the Atmospheric Module comparing the effects of thinning on PB emissions.

Table 2-6. Terrestrial Module Research Project Titles, Senior Researchers, and Summaries of Findings

Project	Research Project Title	Senior Researcher
T-1	<i>Effects of Different Understory Restoration Management Options on Terrestrial Ecosystem Structure and Function</i>	Senior Researcher: Norman Christensen
	Findings: As expected, the density of understory vegetation decreased following mechanical thinning and PB, and the density was significantly lower in the plots thinned during the growing season as compared to the plots thinned during the dormant season. In 1 year following thinning and PB, understory plant species richness was significantly higher in both thinned plots compared to control plots, but no treatment effect was evident for arthropods or birds. Greater amounts of forest floor fuel were consumed in thinned than in unthinned plots. Thinning reduces the amount of coarse fuels and increases the amount of fine fuels, leading to higher consumption of accumulated litter and forest floor organic matter during the PB, which is consistent with restoration objectives. Furthermore, in comparison to dormant season thinning, growing season thinning produced a greater reduction in the growth of woody understory stems that might limit growth of plant species associated with longleaf pine ecosystems. Thus, growing season thinning may accelerate the restoration process compared to thinning during the dormant season. However, additional sampling is needed to determine whether this difference persists beyond the first growing season.	
T-2	<i>Effects of Habitat Management for Red-Cockaded Woodpeckers on Bird Communities</i>	Senior Researcher: Jeffrey Walters
	Findings: Overall, the results of our avian research showed that avian diversity increased with RCW habitat quality, and most avian species exhibited a positive relationship with RCW habitat quality in their abundance, habitat occupancy, or both. This was especially true for species associated with upland pine habitat, even for the Bachman's sparrow (<i>Peucaea aestivalis</i>), which is a species of special concern on MCBCL. Those few species exhibiting negative relationships with RCW habitat quality in their abundance and occupancy were mostly species associated with shrubby understories and are common in habitat types other than pine savanna, pocosin, and bottomland hardwoods on MCBCL. The results of research on the cavity-nesting bird community on MCBCL indicate that the relative availability of nesting substrates (e.g., live pines, pine snags, hardwood snags) determines the strength of interactions between species. Cavity-nesting species tend to partition themselves among nesting substrates, and a shortage of pine or hardwood snags intensifies competition among species. Therefore, MCBCL should maintain the availability of nesting substrates for the wide variety of cavity-nesting avian species.	

Terrestrial Module's Monitoring Program

The Terrestrial Module's monitoring program provided a detailed understanding of the variation in plant species diversity and composition associated with variations in soil physical and chemical characteristics, as well as patterns of disturbance. The monitoring program was based a network of permanent vegetation monitoring plots across the MCBCL landscape. Experimental treatment plots were included among these monitoring plots, and analysis of these plots thus provides a context for understanding the vegetation and environmental gradients across which terrestrial and atmospheric experimental studies (Research Projects T-1, T-2, and Air-1) were conducted.

The vegetation monitoring plots were established across a broad range of stand characteristics, particularly those that are of greatest interest to MCBCL management. Forest types include both longleaf and loblolly pine forests across a wide range of age classes, soil conditions and properties, and disturbance histories (i.e., fire). Significant data were also collected on high pocosin systems, which cover much of the installation, compared to other land-cover types on MCBCL. The non-metric scaling and soil comparisons (**Figure 2-5**) indicate that the numbers of plots and species are sufficient to reveal relatively subtle correlations among vegetation composition, diversity, and the environment.

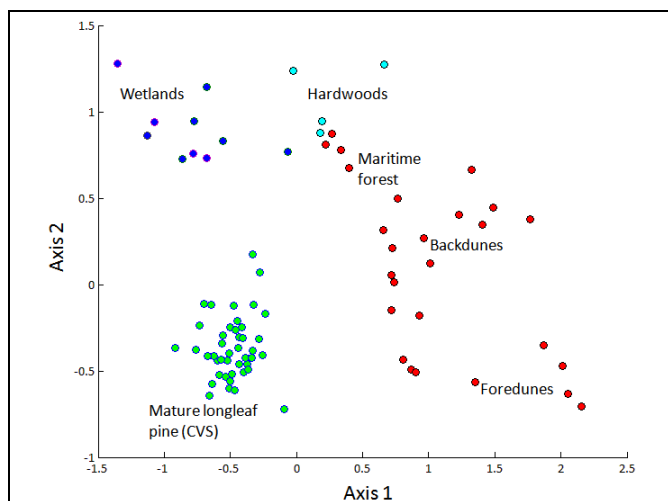


Figure 2-5. MCBCL terrestrial vegetation monitoring plots arrayed on non-metric scaling Axes 1 and 2.

Distances among points reflect relative differences in plant species composition.

Conclusions and Implications from the Terrestrial Module

Key Scientific Findings—Fundamental Cause-and-Effect Relationships

- Although PB without thinning reduced the density of understory shrubs and trees, the mechanical thinning treatments during the growing season were significantly more effective. PB alone reduced the density of understory/midstory woody plants (1–20 cm dbh) by an average of 88%. However, dormant season thinning resulted in 63% fewer woody stems (for a total of 95% reduction), and growing season thinning resulted in 81% fewer woody stems (total of a 98% reduction) than PB alone. In either case with or without thinning, continued suppression of woody growth will require the application of regular prescribed burns. If these differences persist, they would indicate a possible benefit of growing season thinning compared to dormant season thinning that could be implemented at other U.S. Department of Defense facilities with longleaf pine restoration efforts in ecosystems currently dominated by loblolly pine.

- Midstory thinning followed by PB produced significant change in plant species richness and composition after a single growing season. These changes are consistent with MCBCL's restoration objectives. Across treatment plots, there were very strong correlations between soil characteristics and vegetation composition and between vegetation composition and bird community composition. Correlations with arthropod community composition were much weaker.
- Vegetation species composition in MCBCL pine stands is highly correlated with a complex site and soil moisture gradient from comparatively wet, organic soils with low bulk densities to well-drained sandy soils with high bulk densities. Plant species richness also increases along this same gradient. Additional variation in species composition was related to the effects of disturbance (fire).
- In the 45 plots where both vegetation and bird communities were sampled, plant and avian species composition was found to be highly correlated. Both vegetative composition and avifaunal communities showed partitioning and were compositionally different among longleaf pine, loblolly pine, and high-pocosin sites. The overlap between the two communities suggests that the composition of avifaunal communities is tightly correlated to the differences in understory vegetative composition that can emerge in the different mature pine stands. This indicates that future efforts aimed at recovering avifaunal species of concern may depend upon the recovery of understory plant communities.

Findings with Implications for MCBCL Management Practices

- Regardless of treatment season, thinning treatments greatly reduced the number of live understory hardwood stems in the first growing season. Growing season thinning had a small, but significantly greater impact on understory hardwood stem number than dormant season thinning. Additional sampling is needed to determine whether this difference will persist beyond the first growing season or if it is large enough to influence restoration success.
- Midstory thinning generally increases fuel amounts and, therefore, the total amount of fuel consumed in prescribed fires. Furthermore, mechanical thinning redistributes fuels to the forest floor and facilitates surface fires that are consistent with overall restoration objectives.
- Although PB without thinning reduces the density of understory shrubs and trees, mechanical thinning treatments during the growing season are significantly more effective. Irrespective of thinning treatments, continued suppression of woody growth in pine stands will depend upon the maintenance of regular prescribed burns.
- In the short term, there appears to be no significant differences between applying thinning treatments during the growing season or the dormant season with regard to impacts on fuels and on the composition and diversity of plants, arthropods, and birds. This provides MCBCL managers with greater flexibility by expanding the time frame for application of thinning treatments. However, additional research is needed to determine the longer term effects.

- Comparison of longleaf pine plots sampled in both 1993 and 2009–2010 indicated that these ecosystems tend to become more diverse and species composition becomes more characteristic of sites with increased soil moisture and regular PB. This supports continuation of PB for meeting longleaf pine restoration goals.
- Midstory thinning of pine stands on sites with moderately organic soils (10–50% organic matter) may provide additional benefits for enhancing military training usage, although such use may have adverse effects on these sites. In any case, stands on such sites appear to have low potential for restoration of plant and animal composition associated with longleaf pine savannas.
- MCBCL should maintain, whenever possible, the availability of nesting substrate (e.g., live pines, pine snags, hardwood snags) for the wide variety of cavity-nesting avian species because that determines the strength of interactions among species. Specifically, a shortage of these dead or dying pine snags likely would result in negative impacts on RCWs due to the takeover of their cavities in live pines by other species.
- Forest management that specifically targets habitat conditions for the RCWs results in habitat changes that benefit the biodiversity of terrestrial ecosystems in general and the total avian community specifically; therefore, this should be continued.

Findings with Implications for DCERP2

- Research Project T-1 gathered vegetation, soil, and fuel data in such a way as to provide a basis for the assessment of future changes in carbon storage. Thinning and PB represent major manipulations of ecosystem carbon pools and likely influence subsequent carbon fluxes. These experimental plots will provide ideal test sites for future studies of these changes.
- The relatively early results from the thinning treatment followed by PB versus PB without thinning suggest that significant treatment effects are likely to emerge when these plots are resampled in 2 to 3 years. The unique patterns observed in arthropod species composition and diversity compared to either plants or birds demand further investigation. Further analysis of these data may reveal correlations within particular ecological guilds of insects and such results would be an important guide to the refinement of sampling protocols for these insects.
- Thinning and PB treatments are only the first steps in a long-term process to recover longleaf pine ecosystems. Continued sampling of these experimental plots in DCERP2 will allow us to determine whether promising short-term changes persist and are consonant with long-term restoration goals (i.e., replacement of the loblolly pine canopy with an uneven aged population of longleaf pine).
- In the intermediate term (next 30 years), MCBCL hopes that these understory and midstory thinning treatments, coupled with regular (3 year) prescribed fires, will restore habitat conditions similar to longleaf pine savannas (e.g., conditions favorable for sustainable populations of RCW and other endemic species) in these stands. Such restoration will depend on the re-establishment of important plant species associated with longleaf pine savannas. During DCERP2, we will continue to examine the effects of PB with and without thinning on plant, arthropods, and breeding bird communities and

determine whether these organisms have shifted toward the composition of fire-maintained longleaf pine savannas. We will also evaluate changes in fuel composition and distribution that will allow us to determine whether higher intensity ground fires will remove litter and soil organic matter without propagating a crown fire. Such a shift could further promote the restoration of the habitat characteristics of fire-maintained longleaf pine savannas.

Atmospheric Module

Summary of Atmospheric Conditions

The input of nutrients and potential pollutants via atmospheric deposition interacts with most key terrestrial and aquatic ecological processes occurring at MCBCL as illustrated in **Figure 2-6**. Atmospheric deposition is a direct source of inputs onto the open-water surfaces of the aquatic ecosystem and onto the vegetation surfaces of the terrestrial ecosystem, with the frequency, level, and composition of these inputs posing an important influence on flora diversity. In addition to direct sources of atmospheric input, the aquatic ecosystem is impacted by atmospheric deposition after it is filtered and altered by passage through the terrestrial ecosystem. This impact occurs during all time scales, ranging from rapid inputs following large rainfall events (runoff) to slow, but critical, changes in baseflow from the superficial aquifer (Hunsaker et al., 1994; Osgood and Zieman, 1998). Similarly, terrestrial ecosystem impacts might be due to exposure to a complex combination of long-term climatological stress (e.g., temperature, drought) and shorter term air pollutant stress (oxidants and metals).

Fire is a natural part of the terrestrial landscape in the Southeast in general and MCBCL in particular, and natural fire regimes (e.g., frequency, intensity, season) vary across a soil–hydrology–vegetation gradient, from frequent surface fires in longleaf pine savannas to relatively infrequent and intense crown fires in pocosins. MCBCL managers use PB to reduce wildfire risk, maintain training areas, and restore habitat for the federally protected RCW. Despite these benefits, PB is a major source of PM_{2.5} and other air pollutants because of its incomplete and largely uncontrolled combustion process, which involves flaming and smoldering phases with different effective fuel consumption. Certain fuel and fire meteorological parameters influence the emissions from the different combustion phases of PB, which in turn participate in transport processes within the atmospheric boundary layer, causing air quality impacts on local and regional scales (Friedli et al., 2007; Lee et al., 2005). Coarse particles (PM_c) in the size fraction between 2.5 and 10 microns receive special attention in conjunction with local impacts because gravitational settling accelerates their deposition to the surrounding aquatic and terrestrial surfaces. One of the more important conditions enhancing PM_c involves the proximity of MCBCL to the Atlantic Ocean, which provides an environment conducive to sulfate formation. Another PM_c enhancing factor is the reaction of nitric acid with sea-salt aerosol to form coarse mode sodium nitrate particles, potentially increasing the PM_c mass. Resulting consequences and implications for land management practices are discussed extensively in the *DCERP1 Final Monitoring Report*.

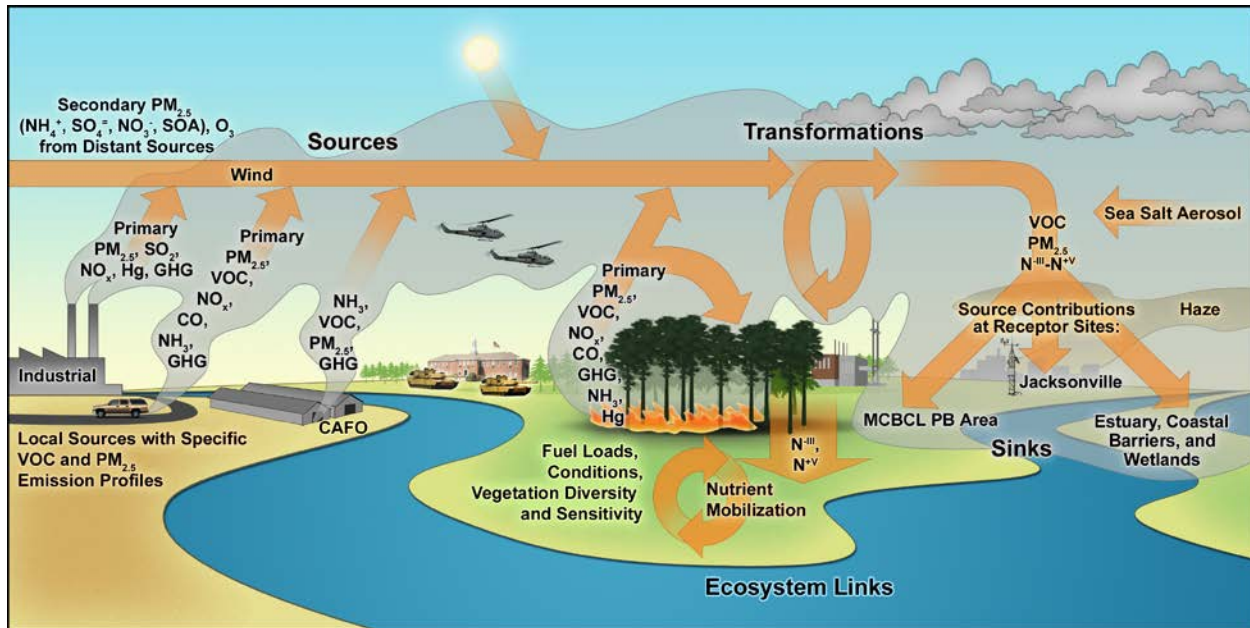


Figure 2-6. Conceptual model for the Atmospheric Module.

The Atmospheric Module's research program focused on the areas of quantifying emissions from forest management practices, including midstory thinning and PB, and estimating the net nitrogen deposition to MCBCL lands (**Table 2-7**). In conjunction with the ecological research of the Terrestrial Module, Research Project Air-1 can inform MCBCL's smoke management planning by quantifying PB emissions from different pine restoration treatments. In addition, Research Project Air-2 estimated the total atmospheric nitrogen loading, which was used to develop a nitrogen budget for the NRE by the Aquatic/Estuarine Module. This second research effort assessed and quantified the degree of atmospheric loading of nitrogen and other nutrients from wet and dry deposition to terrestrial ecosystems at MCBCL.

Table 2-7. Atmospheric Module Research Project Titles, Senior Researchers, and Summaries of Findings

Research Project	Atmospheric Module Research Project Title	Senior Researcher
Air-1	<i>Optimization of Prescribed Burning by Considering Mechanical Thinning as a Viable Land Management Option</i>	Senior Researcher: Karsten Baumann
	Findings: In general, fuel consumption was greater in experimental plots that incorporated a midstory thinning treatment followed by PB, especially woody material regardless of fuel moisture. Innovative mobile aerosol composition monitors were used to measure and distinguish emissions from mechanically thinned plots with those from control plots. Our results indicate that site vegetation variation is not driving the observed emission factor (EF) differences, which are, therefore, not confounded by either soil characteristics or vegetation differences, allowing direct comparison of treatment effects on the EF. Gaseous EF averages from the two fuel types were similar, and EF variability was highest for acidic gases and isoprene. However, PM _{2.5} mass and most PM _{2.5} species EF from mechanically thinned plots were significantly lower than those from untreated control plots. Organic	

(continued)

Table 2-7. Atmospheric Module Research Project Titles, Senior Researchers, and Summaries of Findings (continued)

Research Project	Atmospheric Module Research Project Title	Senior Researcher
Air-1 (cont)	carbon was the dominant PM _{2.5} constituent in emissions from both fuel types, followed by elemental carbon, nitrate, potassium, and chloride. More volatile organic compounds were emitted from both fuel types under less efficient (smoldering) combustion conditions, which also promote higher emissions of inorganic constituents. Episodic comparison of PB emissions with throughfall-deposition suggests that long-term soil nutrient levels remain unaffected by PB, causing only a short-term disturbance.	
Air-2	<i>Nitrogen Deposition to Terrestrial and Aquatic Ecosystems</i>	Senior Researcher: Wayne Robarge
	<p>Findings: The average annual wet deposition of total nitrogen was $4.3 \pm 0.7 \text{ kg N ha}^{-1} \text{ y}^{-1}$; for dissolved inorganic nitrogen, it was $3.2 \pm 0.4 \text{ kg N ha}^{-1} \text{ y}^{-1}$. Wet deposition of dissolved inorganic nitrogen at MCBCL in 2010 was comparable to the 9-year average of $3.7 \text{ kg N ha}^{-1} \text{ y}^{-1}$ calculated at nearby Hofmann Forest, NC. Dissolved inorganic nitrogen wet deposition was highest in the summer months, and dissolved organic nitrogen was highest in the autumn months. A network of up to 28 tipping bucket rain gauges found no apparent latitudinal gradient in rainfall amounts across MCBCL due to the proximity of the nearby marine environment. There was, however, a measureable gradient in wet and dry deposition of chloride, sodium, and sulfate moving inland. Throughfall collectors were used to measure inputs of nitrogen and other nutrients into the forest floor under the dominant forested canopies at MCBCL. Inputs of total nitrogen under forested canopies were approximately two times greater than those observed from wet deposition alone, a substantial fraction of which appeared to be in the form of dissolved organic nitrogen. Calculation of net throughfall (throughfall minus wet deposition) indicated the presence of dry deposition of nitrate and to a lesser extent ammonium, but also loss of nitrogen from wet deposition during the summer and autumn months due to interaction with the overhead canopy. For 2012, nitrogen loading to different land-cover classes at MCBCL was estimated at 360 metric tons of total nitrogen and 210 metric tons of dissolved inorganic nitrogen. Agreement between measured amounts of the wet deposition of nitrogen by this project to the nearby collector at Hofmann Forest indicates that this amount of atmospheric loading of nitrogen to MCBCL has been relatively constant for at least the past 10 years.</p>	

Atmospheric Module's Monitoring Program

The monitoring activities and research projects of the Atmospheric Module are helping to describe and improve the understanding of critical pollutant transport and advection processes that are subject to complex land-sea breeze circulation patterns and their effects on the atmospheric abundance and composition of a variety of air pollutants. The Atmospheric Module monitoring program measured a variety of meteorological parameters (including wind speed and direction, air temperature, rainfall) and concentrations of particulate matter and ozone. Data on these parameters were collected in a coordinated manner from sites on MCBCL and compared with data from the regional airshed.

Results indicate that rainfall does not vary significantly across MCBCL, whereas ozone concentrations were higher nearer the beach and decreased moving inland toward the City of Jacksonville. In contrast, PM_{2.5} was lowest at the beach and increased farther inland likely

resulting from the addition of PM_{2.5} from residential heating and wood burning in urban areas especially during the winter months. Differences were found for PM_{2.5} and PM_c (fine and coarse PM) on short time scales between the Onslow Beach site and the Greater Sandy Run Area (GSRA) Tower site located 20-km (12-mi) inland. The differences measured between these two sites seem to be governed by air mass transport and distinct localized source activities such as PB or military training involving the movement of heavy equipment in proximity to the GRSA Tower site. Meteorological and particulate matter monitoring data also provided an in-depth historic reference, which is needed in making forest management decisions associated with application of various forest management practices (investigated by Research Projects T-1 and Air-1) and in smoke management planning.

Conclusions and Implications from the Atmospheric Module

Key Scientific Findings—Fundamental Cause-and-Effect Relationships

- Considering the possible effects from the fuel treatment (mechanically thinned and control) alone, average gaseous emissions factors from the two treatment types were similar. However, PM_{2.5} mass and most PM_{2.5} species EFs from mechanically thinned plots were significantly lower than those from untreated, control plots. Therefore, removing a certain targeted amount of fuel by employing mechanical thinning prior to PB results in significant air quality benefits due to lower total PM_{2.5} emissions, although emissions of carbon monoxide, methane, and non-methane hydrocarbons are slightly enhanced.

Findings with Implications for MCBCL Management Practices

- Mechanical thinning in loblolly dominated pine stands makes two times more fuel available for combustion and helps consume almost three times more fuel (especially woody material) regardless of fuel moisture, compared to untreated controls. This is especially the case for stands growing red bay (*Persea palustris*), red maple (*Acer rubrum*), tulip poplar (*Liriodendron tulipifera*), and titi (*Cyrilla racemiflora*), with the latter dominating the more pocosin-like stands. MCBCL managers should continue using mechanical thinning prior to PB to reduce smoke emissions as part of their smoke management planning.
- Based on 2009 MCBCL data, the PB emissions (i.e., PM_{2.5}, carbon monoxide, methane, and volatile organic compounds) were significantly higher on an annual basis than any other combustion source category operated on MCBCL. These include Jet Engine Test stands, fire training pits, diesel generators, and boilers. Relative to the untreated plots, the emissions from mechanically thinned plots were significantly reduced for PM_{2.5} by almost 48 tons (18%). However, there was a 19%, 11%, and 5% increase in the EF for carbon monoxide, methane, and volatile organic compounds from mechanically thinned plots over the fuels from control plots, which translates to 144, 3.2, and 2.4 tons of additional annual emissions, respectively. These results show the importance of PB as a source for PM_{2.5} and gases that should be considered in carbon management.

Findings with Implications for DCERP2

- During DCERP1, the Atmospheric Module established a network of meteorological stations to monitor MCBCL lands to determine whether there were gradients in rainfall and air quality parameters. The results suggested that information already being captured by the meteorological station at the New River Air Station is generally representative of the entire MCBCL at annual time scales. Therefore, during DCERP2, the RTI DCERP Team will use data from the New River Air Station and other regional sites as appropriate to assess variability in meteorological parameters that could inform climate change scenarios.
- Data from Hofmann Forest, approximately 20 miles northeast of MCBCL, can serve as a proxy for nitrogen deposition data for MCBCL lands and for other meteorological data. Use of this information by the installation is encouraged because it reduces redundancy and produces a cost savings to MCBCL that can be directed to other monitoring efforts.

Literature Cited

- Bricker, S.B., C.G. Clement, D.E. Pihalla, S.P. Orlano and D.R.G. Farrow. 1999. *National Estuarine Eutrophication Assessment: Effects of Nutrient Enrichment in the Nation's Estuaries*. NOAA, NOS, Special Projects Office and the National Centers for Coastal Ocean Science, Silver Spring, MD. 71 pages.
- Christensen, N.L. 1981. Fire regimes in southeastern ecosystems. Pp. 112–136 in *Fire Regimes and Ecosystem Properties*. Edited by H.A. Mooney, T.M. Bonnicksen, N.L. Christensen, J.E. Lotan, and W.A. Reiners. General Technical Report WO-26. U.S. Department of Agriculture, Forest Service.
- Ensign, S.H., J.N. Halls, and M.A. Mallin. 2004. Application of digital bathymetry data in an analysis of flushing times of two North Carolina Estuaries. *Computers and Geosciences* 30:501–511.
- Friedli, H.R., L.F. Radke, N.J. Payne, D.J. McRae, T.J. Lynham, and T.W. Blake. 2007. Mercury in vegetation and organic soil at an upland boreal forest site in Prince Albert National Park, Saskatchewan, Canada. *Journal of Geophysical Research* 112(G1):G01004.
- Garren, K.H. 1943. Effects of fire on vegetation of the southeastern United States. *Botanical Review* 9:617–654.
- Hunsaker, C.T., C.T. Garten, and P.J. Mulholland. 1994. Modeling nitrogen cycling in forested watersheds of Chesapeake Bay. Pp. 481–491 in *Proceedings of the Water Environment Federation 67th Annual Conference & Exposition 4*, Chicago, IL. October 15–19.
- Lee, S., K. Baumann, J.J. Schauer, R.J. Sheesley, L.P. Naeher, S. Meinardi, D.R. Blake, E.S. Edgerton, A.G. Russel, and M. Clements. 2005. Gaseous and particulate emissions from prescribed burning in Georgia. *Environmental Science and Technology* 39:9049–9056.
- Mallin, M.A., M.R. McIver, H.A. Wells, D.C. Parsons, and V.L. Johnson. 2005. Reversal of eutrophication following sewage treatment upgrades in the New River Estuary, North Carolina. *Estuaries* 28:750–760.
- Osgood, D.T., and J.C. Zieman. 1998. The influence of subsurface hydrology on nutrient supply and smooth cordgrass (*Spartina alterniflora*) production in a developing barrier island marsh. *Estuaries* 21(4B):767–783.

Chapter 3

Develop and Deploy Microalgal Indicators as Measures of Water Quality, Harmful Algal Bloom Dynamics, and Ecosystem Condition

SERDP Project Number: RC-1413

Aquatic/Estuarine Module

Research Project AE-1

Lead Researchers:

Hans W. Paerl

Nathan S. Hall

Benjamin L. Peierls

Karen L. Rossignol

Alan R. Joyner

Timothy Otten

University of North Carolina at Chapel Hill

Institute of Marine Sciences

Morehead City, NC

Kenneth H. Reckhow

Cardno ENTRIX

Raleigh, NC

Farnaz Nojavan

Duke University

Durham, NC

May 10, 2013

Final

This report was prepared under contract to the U.S. Department of Defense (DoD) Strategic Environmental Research and Development Program (SERDP). The publication of this report does not indicate endorsement by DoD, nor should the contents be construed as reflecting the official policy or position of DoD. References herein to any specific commercial product, process, or service by trade name, trademark, manufacturer, or otherwise, do not necessarily constitute or imply its endorsement, recommendation, or favoring by DoD.

Table of Contents

List of Acronyms	3-vii
Acknowledgements.....	3-ix
Abstract.....	3-1
Results and Applications to Water Quality Management.....	3-1
Objectives of the Research Project	3-2
Hypotheses.....	3-2
Technical Goals	3-2
Background.....	3-3
Characteristics of the NRE.....	3-5
Phytoplankton as Indicators of Ecological Change	3-6
The Phytoplankton Community of the NRE.....	3-7
Materials and Methods.....	3-10
Measurements of Physical and Chemical Environmental Conditions.....	3-10
Measurement of Freshwater Inputs and Flushing Time	3-11
Measurements of Phytoplankton Biomass and Community Composition	3-12
Assessment of Hydrological Impacts on Phytoplankton Biomass and Composition	3-14
Measurement of Phytoplankton Primary Productivity	3-14
Assessment of Nutrient Limitation via Nutrient Enrichment Bioassays	3-15
Bayesian Belief Network Model.....	3-16
Results and Discussion	3-16
Climatic Controls on the Phytoplankton.....	3-16
Harmful Algal Blooms.....	3-30
Phytoplankton Primary Production.....	3-33
Assessment of Nutrient Limitation	3-40
Comparison of Chlorophyll <i>a</i> with State and National Water Quality Assessment Criteria	3-43
Conclusions and Implications for Future Research	3-50
Literature Cited	3-52
Appendix 3-A: Prediction and Uncertainty Analysis of Eutrophication in the New River Estuary: An Integrated Bayesian Network Approach.....	3-A-1
Appendix 3-B: Supporting Data	3-B-1
Appendix 3-C: List of Scientific Publications	3-C-1
Appendix 3-D: List of Students	3-D-1

List of Figures

3-1.	Map of the NRE study site and sampling stations.	3-4
3-2.	The role of microalgal indicators in assessing the impacts of human and climatic stressors on estuarine structure and function.	3-5
3-3.	Schematic diagram and photograph of the AVPs.	3-11
3-4.	Diagram showing the methodology for determining algal community composition using diagnostic photopigment analyses by high-performance liquid chromatography.	3-13
3-5.	Photograph of the bioassay incubation setup in the seawater pond at the UNC-IMS in Morehead City, NC.	3-16
3-6.	Physical, chemical, and phytoplankton biomass response to changes in discharge and temperature in the NRE from October 2007 through December 2011.	3-18
3-7.	Temperature, river discharge, and contour plots of the space-time distributions of accessory photopigments indicative of major phytoplankton taxonomic groups.	3-19
3-8.	Photomicrographs of algal blooms from NRE surface waters.	3-20
3-9.	Relationship between flushing time and salinity in the NRE from October 2007 through December 2011.	3-23
3-10.	Relationship between flushing time and photopigment concentrations indicative of total phytoplankton biomass (chl <i>a</i>) and major phytoplankton classes within the NRE.	3-24
3-11.	Space–time location of HAB and non-HAB blooms in relation to freshwater discharge within the NRE from October 2007 through December 2011.	3-25
3-12.	Chl <i>a</i> in vivo fluorescence and salinity data from the AVP at Morgan Bay over a 10-day period in September 2008.	3-27
3-13.	Occurrence of DVM patterns of phytoflagellates in relation to water column stratification.	3-28
3-14.	Down-stream gradients of light attenuation and concentrations of optically active constituents.	3-35
3-15.	Relationship between New River discharge and instantaneous loads of total dissolved nitrogen and total dissolved P at Gum Branch.	3-36
3-16.	Annual average areal phytoplankton production versus annual volumetric DIN load from the NRE and other estuarine systems.	3-36

3-17.	(A) Linkage between chl <i>a</i> and primary productivity within NRE surface waters. Results are plotted log-log for visualization purposes but the regression was performed on non-transformed values. R^2 and p values are from a Pearson's correlation. Identity of the dominant phytoplankton class within bloom samples (chl <i>a</i> greater than 40 $\mu\text{g L}^{-1}$) is indicated by symbol color. (B) Biomass normalized productivity (P^b) versus chl <i>a</i> . R_s and p values are from a Spearman's rank correlation. N=432 for both panels.	3-38
3-18.	Comparison of phytoplankton photosynthetic performance (P^b) of samples incubated on the day of collection and day after collection.....	3-40
3-19.	Example results from an in situ nutrient addition bioassays conducted on NRE natural phytoplankton assemblages from stations on June 3, 2008.	3-41
3-20.	Frequency of observed phytoplankton biomass stimulation by nutrient amendments across all six bioassay time points, at Stations 3 and 5, and on Days 2 and 4 of each bioassay experiment (N=24).	3-42
3-21.	Phytoplankton biomass response to nutrient additions in water collected from Station 7 on June 14, 2010.....	3-42
3-22.	Chl <i>a</i> concentrations ($\mu\text{g L}^{-1}$) in surface waters for each station in the NRE, October 2007–December 2011..	3-45
3-23.	Chl <i>a</i> concentrations ($\mu\text{g L}^{-1}$) for each station in the NRE, October 2007–December 2011.	3-46
3-24.	Percentages of chl <i>a</i> samples that were rated good, fair, or poor from each station based on criteria from EPA's <i>National Estuary Program Coastal Condition Report IV</i> (U.S. EPA, 2012).....	3-48
3-25.	Overall site ratings for chlorophyll <i>a</i> conditions in the NRE based on criteria adopted from EPA's <i>National Estuary Program Coastal Condition Report</i> (U.S. EPA, 2012).....	3-49

List of Tables

3-1.	The 10 most common phytoplankton photopigments contained within classes microscopically identified in the NRE.....	3-7
3-2.	Comparison of annual average freshwater inflows into the NRE from 2008–2011 with average flows from the long-term record produced by the USGS Gaging Station number 0209303205 near Gum Branch.....	3-17
3-3.	Summary of phytoplankton bloom composition in the NRE from October 2007 through December 2011.....	3-21
3-4.	Pearson's correlation (<i>R</i>) matrix for 8 of the 10 most common phytoplankton photopigments contained within algal divisions microscopically identified in the NRE.....	3-22

3-5.	Coefficients for regressions of temperature and flushing time on photopigment concentrations.	3-26
3-6.	Concentrations of total microcystin toxins in surface waters of the upper NRE during late summer–early fall 2008.	3-31
3-7.	Annual areal phytoplankton primary production for segments of the NRE ($\text{g C m}^{-2} \text{ y}^{-1}$).	3-33
3-8.	Comparison of phytoplankton, BMA, and salt marsh production for segments of the NRE over the study period ^a (10^6 g C y^{-1}).	3-34
3-9.	Percent of samples greater than NCDENR’s water quality criterion for chl <i>a</i>	3-43
3-10.	Chl <i>a</i> based water quality assessment criteria adopted from EPA’s <i>National Estuary Program Coastal Condition Report IV</i> (U.S. EPA, 2012) for rating monthly chl <i>a</i> levels, and annual or multi-year site conditions.	3-46

List of Acronyms

°C	degrees Celsius
$\Delta\rho$	bottom surface density
$\mu\text{g/L}$, $\mu\text{g L}^{-1}$	micrograms per liter
μm	micrometer
μM , μmol	micromole
$\mu\text{mol L}^{-1}$	micromoles per liter
19-hex	19'hexanyloxyfucoxanthin
Allo	alloxanthin
ANOVA	analysis of variance
AU	arbitrary unit
AVP	autonomous vertical profiler
BBN	Bayesian Belief Network (model)
BMA	benthic microalgae
chl <i>a</i>	chlorophyll <i>a</i>
chl <i>b</i>	chlorophyll <i>b</i>
chl <i>c</i>	chlorophyll <i>c</i>
CAFO	concentrated animal feeding operation
CDOM	chromophoric dissolved organic matter
CI	confidence interval
cm	centimeter
CWA	Clean Water Act
CyanoHAB	cyanobacterial harmful algal bloom
d	day
DCERP	Defense Coastal/Estuarine Research Program
Diad	diadinoxanthin
DIN	dissolved inorganic nitrogen, sum (NO_3^- , NO_2^- , and NH_4^+)
DoD	U.S. Department of Defense
DVM	diel vertical migration
ELISA	enzyme-linked immunosorbent assay
EPA	U.S. Environmental Protection Agency
Fuco	fucoxanthin
FWD	Fresh water discharge
$\text{g C m}^{-2} \text{ y}^{-1}$	grams of carbon per square meter per year
GFF	glass fiber filter
HAB	harmful algal bloom
HPLC	high-performance liquid chromatography
K_d	light attenuation coefficient for photosynthetically active radiation
km	kilometer
km^2	square kilometer

kPa	kilopascal
L	liter
m	meter
m h ⁻¹	meters per hour
m ⁻² s ⁻¹	square meters per second
m ⁻³ s ⁻¹	cubic meters per second
MA	microalgae
MCBCL	Marine Corps Base Camp Lejeune
mg/L	milligrams per liter
mL	milliliter
mm	millimeter
mph	miles per hour
N	nitrogen
NCDENR	North Carolina Department of Environment and Natural Resources
NO ²⁻	nitrite
NO ³⁻	nitrate
NRE	New River Estuary
P	phosphorus
P ^b	primary productivity normalized to chlorophyll <i>a</i>
PAR	photosynthetically active radiation
PCR	polymerase chain reaction
Peri	peridinin
PO ₄ ⁻³	orthophosphate
SD	standard deviation
SERDP	Strategic Environmental Research and Development Program
SiO ₃ ⁻²	silicate
SD	Standard deviation
TDN	total dissolved nitrogen
TMDL	total maximum daily load
TSS	total suspended solids
UNC-IMS	University of North Carolina at Chapel Hill's Institute of Marine Sciences
USGS	U.S. Geological Survey
Viol	violaxanthin
Zea	zeaxanthin

Acknowledgements

We would like to thank co-workers in the Paerl Laboratory, including J. Braddy, L. Kelly, M. Hoffman, B. Abare, and R. Sloup, who assisted with field and laboratory work.

[This page intentionally left blank.]

Abstract

Research Project AE-1 identified and quantified ecosystem-scale effects of Marine Corps Base Camp Lejeune (MCBCL) and regional anthropogenic activities and climatic stressors on microalgae, with an emphasis on phytoplankton, which are useful indicators of water quality and ecological condition. The New River Estuary (NRE) has a history of excessive anthropogenic nitrogen (N) and phosphorus (P) inputs and resultant eutrophication, while also experiencing the effects of climatic variability, including record rainfall events and droughts. Research Project AE-1's working hypothesis was: *microalgae are the dominant primary producers in the NRE and changes in their abundance, community composition, and productivity are under strong control by these climatic and anthropogenic factors*. The overarching objective of Research Project AE-1 was to *characterize and quantify the interactive effects of freshwater discharge and associated nutrient loading on the biomass, composition and bloom potentials of the phytoplankton*.

Through monthly transect surveys, phytoplankton biomass and community composition were determined by a combination of diagnostic algal photopigments, microscopy, and molecular methods. Seasonal nutrient addition bioassays were performed to identify growth-limiting nutrients. Flushing times within the estuary were calculated to determine effects of variability in NRE flow and seawater inflows on total phytoplankton biomass and the biomass of major algal classes. Results were used to identify hydrologic and nutrient input controls on phytoplankton production and composition and for evaluating microalgal impacts on water quality in the NRE. This information was used to assess compatibility of MCBCL activities with desirable water, sediment, and habitat quality. Data were used to calibrate and validate the NRE Estuarine Simulation Model and Bayesian Belief Network models aimed at predicting estuarine productivity and phytoplankton responses to hydrologic and nutrient drivers.

Results and Applications to Water Quality Management

Phytoplankton biomass was strongly impacted by river flow variations due to its dual influence on nutrient delivery and residence time. Phytoplankton biomass increased rapidly up to a threshold flushing time of approximately 10 d and then declined slowly at longer flushing times. This unimodal relationship indicates a balance between advective losses due to flushing and nutrient stimulation of biomass by riverine loading. Findings from the Bayesian Belief Network model corroborate the strong influence of riverine flow on phytoplankton biomass due to its impact on nutrient delivery, flushing, and stratification. The model shows that stratification is a key factor determining occurrence of harmful algal bloom species with higher likelihoods of their occurrence under moderately stratified conditions. Nutrient addition bioassays showed that N was the primary limiting nutrient controlling phytoplankton production. Significant differences in threshold salinities/flushing times and rates of decline at higher salinities/longer flushing times suggest that hydrologic forcing plays an important role in determining phytoplankton composition. Temperature additionally controlled composition with picocyanobacteria and harmful algal bloom forming raphidophytes occurring predominantly during the summer. Microcystin-producing cyanobacteria were detected, but microcystin levels were far below the World Health Organization's $10 \mu\text{g L}^{-1}$ recommended limit for recreational waters.

System wide primary productivity is nearly evenly split between phytoplankton and benthic microalgae (BMA). Management actions should maintain this ecologically healthy balance by limiting excessive N and suspended sediment loads that tend to favor phytoplankton over BMA production. Currently, most of the nutrient and sediment loading to the estuary occurs upstream of MCBCL and thus upstream sources should be the focus of load reduction efforts. However, future growth and development within MCBCL may increase the importance of within Base tributaries as sources of nutrients and suspended solids.

Keywords: Bioassay, diagnostic photopigments, eutrophication, flushing time, harmful algal blooms (HABs), high-performance liquid chromatography, benthic microalgae, light attenuation, nitrogen, nutrient limitation, nutrient load, phosphorus, photosynthetically active radiation, phytoplankton, primary productivity, raphidophytes, residence time

Objectives of the Research Project

Hypotheses

1. Microalgae dominate primary production in the New River Estuary (NRE).
2. Human (e.g., nutrients, sediments) and climatic (e.g., hydrologic) environmental factors control microalgae (MA) production, community structure, and fate and determine water quality, ecological condition, and sustainability of the NRE.
3. Climatic variability and extremes (e.g., hurricanes) play a central, and at times a dominant role, in determining MA production and harmful algal bloom (HAB) potentials.
4. Recently developed diagnostic MA indicators for shallow estuaries, coupled with a Bayesian Belief Network (BBN), will provide a regulatory (e.g., total maximum daily load [TMDL], Clean Water Act [CWA]) tool for Defense Coastal/Estuarine Research Program (DCERP) researchers and Marine Corps Base Camp Lejeune (MCBCL) managers to identify, distinguish, and predict local (Base) and regional stressors of ecological condition or change in the NRE.

Technical Goals

Research conducted during Research Project AE-1 will identify and quantify ecosystem-scale effects of Base and regional anthropogenic activities and climatic stressors on MA within the NRE (**Figure 3-1**). As key primary producers and indicators of estuarine water quality, understanding how anthropogenic and climatic factors impact the MA community is critical for evaluating the ecological health of the NRE (**Figure 3-2**). This research will facilitate the adaptive management of the NRE with the help of a BBN, using data from monitoring and experimental projects. Results will verify the use of diagnostic photopigments coupled to molecular analyses as broadly applicable, sensitive indicators of water and habitat quality and HAB potentials in estuaries. Results will be communicated to management on estuarine-wide time-space contour plots and data will be used to determine compliance with the State of North Carolina's and the U.S. Environmental Protection Agency's water quality criteria (e.g., nutrient-

sensitive waters, TMDL, CWA). Predictive, probabilistic models of MA and HAB dynamics will be developed for long-term adaptive water quality management of the NRE.

Background

Estuaries integrate inputs from terrestrial, freshwater, oceanic, and atmospheric systems (Day and Kemp, 1989; Hobbie, 2000; Paerl, 1997; Valiela et al., 1997), and the accurate assessment and management of estuaries necessitates consideration of their connections to, and interactions with, these other systems. Many estuaries also exist in regions of rapidly expanding and diversifying human activity (Boesch et al., 2001; Cloern, 2001; Nixon, 1995). In the context of the Marine Corps Base Camp Lejeune (MCBCL) region, the Aquatic/Estuarine Module is examining the tidal reach of the New River Estuary (NRE) from near Jacksonville, NC, to the tidal inlet at Onslow Bay (**Figure 3-1**). Understanding and sustaining the function of the NRE cannot occur without quantifying and distinguishing natural processes from human-influenced watershed- and airshed-based impacts, as well as human activities that occur in the estuary (Boesch et al., 2001; Malone et al., 1999; Nixon, 1995; Paerl, 1997; **Figure 3-2**). Furthermore, the effects of climatic variability, including acute or episodic events (tropical cyclones, floods, droughts), as well as longer term trends (e.g., warming, precipitation patterns) on estuarine structure and function must be characterized and quantified to understand and take into consideration the interactive and potentially confounding impacts of climate (change) on water quality and habitat condition (Cloern and Jassby, 2010; Kennish and Paerl, 2010; Paerl et al., 2010).

Estuarine responses to physical, chemical, and biological processes may serve as indicators of ecological change (Cloern, 2001; Niemi et al., 2004; NRC, 2000; Peierls et al., 2003). Inputs of nutrients, sediments, organic matter, and contaminants reach the NRE from multiple sources, including watershed inputs, precipitation and dry deposition from the atmosphere, and tidal exchanges with Onslow Bay. Watershed inputs include sources from the New River at Jacksonville, NC; creeks that drain into the NRE; surface runoff; and groundwater as baseflow. These inputs influence the biological and chemical cycling within the NRE's water column and sediments (e.g., nutrient cycling and sediment transport; Anderson et al., 2003; Cloern, 2001). Nutrients stimulate both phytoplankton and benthic microalgae (BMA) (primary production), thereby providing food for zooplankton and benthic invertebrates (secondary production), respectively (Hobbie, 2000; Sundbäck et al., 2003). The zooplankton and benthic invertebrates provide food for fish, and phytoplankton is the primary food source for shellfish.

An overgrowth of phytoplankton and excessive sediment inputs, however, can reduce light penetration, leading to declines in important nursery area attributes, such as submerged aquatic vegetation and BMA abundance (Gallegos et al., 2005), thereby reducing the food supply for benthic-feeding fish and interfering with the role of BMA in modulating water column nutrient enrichment. Additionally, excessive amounts of phytoplankton (e.g., algal blooms) sink from surface to bottom waters within the estuary and, together with watershed inputs of organic matter, lead to depleted oxygen conditions (hypoxia or anoxia) in bottom waters. Such hypoxic and anoxic events can have critical negative impacts on shellfish, other invertebrates, and finfish (Paerl et al., 1998; Rabalais and Turner, 2001). These processes may be influenced by water exchanges with Onslow Bay, which have the potential to remove excess nutrients, organic matter, and phytoplankton. The NRE's response to natural and anthropogenic impacts depends in

part on physical and biological interactions, such as wave activity, which lead to the resuspension of bottom sediments, and freshwater discharge and exchange, which affects the estuary's water residence time and degree of stratification (Luettich et al., 2000). These conditions strongly influence the biomass and composition of the autotrophic communities within the NRE, the estuary's susceptibility to hypoxia or anoxia, and the relative importance of microbial processes that may remove nutrients from both the water column and benthos.

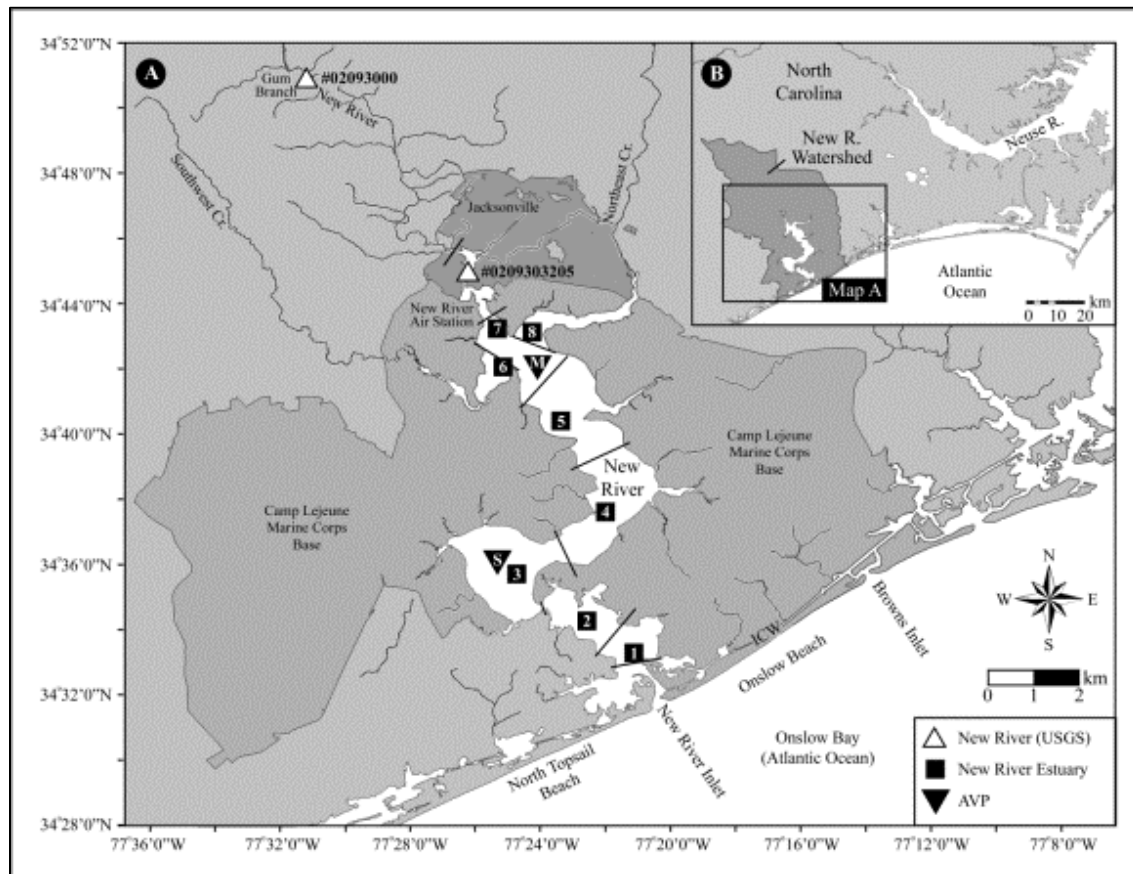


Figure 3-1. Map of the NRE study site and sampling stations.

Lines across the estuary show segments used to determine flushing time for each station.

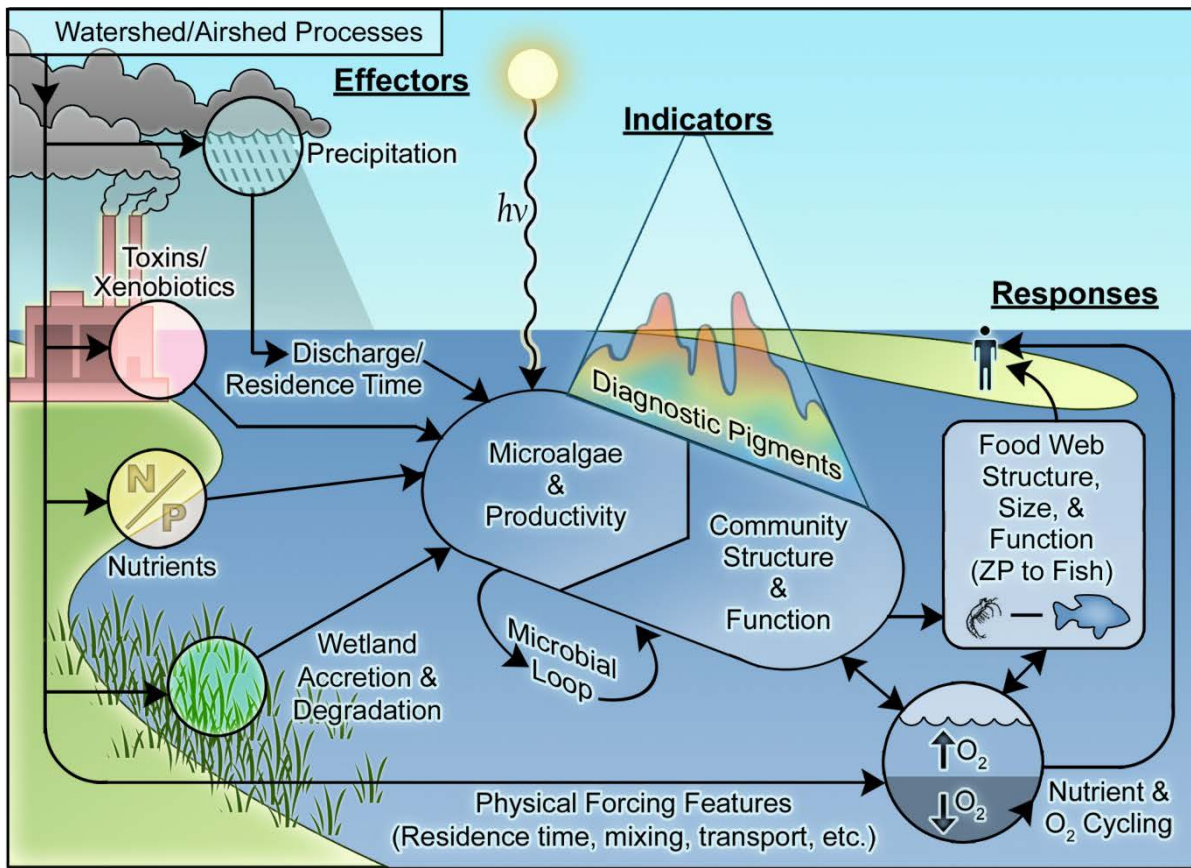


Figure 3-2. The role of microalgal indicators in assessing the impacts of human and climatic stressors on estuarine structure and function.

Characteristics of the NRE

The NRE is a relatively small (88 km²), shallow (approximately 3 m mean depth) coastal plain estuary, located in Onslow County, southeastern North Carolina (**Figure 3-1**). Most of the estuary resides within the MCBCL. Jacksonville, a moderate-sized city (2009 population of 80,500), is located on the upper part of the estuary on Wilson Bay (**Figure 3-1**). The NRE is comprised of a series of lagoons, and confined by barrier islands restricting water exchange with the Atlantic Ocean (Mallin et al., 2005). Flushing time in the NRE varies seasonally with storm and runoff events, ranging from 8 to 187 days, with an average of 70 days (Ensign et al., 2004). The semi-lagoonal nature of the NRE plays a significant role in its sensitivity to nutrient inputs because long flushing times allow more time for algal nutrient assimilation, growth, and “internal” nutrient recycling. Similar to its neighboring semi-lagoonal estuaries to the north—the Neuse River Estuary and Pamlico Sound—the NRE experiences periodic phytoplankton blooms, including harmful species (Tomas et al., 2007) and periods of bottom water hypoxia seasonally (Mallin et al., 2005; Paerl et al., 2007 and 2010).

Non-point nutrient sources dominate New River discharge to the estuary (Paerl et al., unpublished data). The NRE watershed is dominated by agricultural activities, including row crop and concentrated animal feeding operations (CAFOs; Mallin et al., 2005). The other major source of nutrient input to the NRE is the City of Jacksonville, which has had a history of

nutrient inputs from its municipal wastewater treatment plant. From the 1970s to the 1990s, partially treated waste was discharged to the New River at Jacksonville, which promoted highly eutrophic conditions in the Wilson Bay area in the upper reaches of the NRE (Mallin et al., 1997 and 2005). Improved wastewater treatment, starting in the late 1990s greatly decreased the nutrient (both nitrogen [N] and phosphorus [P]) load at Jacksonville, which had a beneficial impact on eutrophication potential of the NRE (marked declines in chlorophyll *a* [chl *a*] concentrations in the upper estuarine regions [Mallin et al., 2005]). Meanwhile, non-point source nutrient inputs associated with burgeoning CAFO and row crop operations have increased significantly over the past several decades, leading to sustained eutrophication, including phytoplankton concentrations in excess of the State of North Carolina's "acceptable" chl *a* concentration ($40 \mu\text{g L}^{-1}$; NCDENR, 2007), and harmful algal bloom (HAB) outbreaks (Mallin et al., 2005; Tomas et al., 2007).

Research conducted during Research Project AE-1 was aimed at quantifying ecosystem-scale effects of Base and regional anthropogenic activities and climatic stressors on phytoplankton production and composition. Phytoplankton are key primary producers and indicators of estuarine water quality and ecological condition. Because phytoplankton community composition is an important determinant of the fate of phytoplankton production (i.e., transferred up the food chain, accumulating in the water column, or settling to the benthos fueling bottom water hypoxia), determining factors that govern phytoplankton community composition is critical to understanding the relationship between nutrient inputs and the symptomatic expression of estuarine eutrophication (Cloern, 2001).

Phytoplankton as Indicators of Ecological Change

All phytoplankton contain chl *a*, which is the primary light harvesting photosynthetic pigment and is used as a metric of total phytoplankton biomass within aquatic systems. In addition to chl *a*, each phytoplankton class contains a specific suite of accessory photosynthetic pigments that serve to enhance light uptake or protect the cell from excessive irradiance (Lewitus et al., 2005). These pigments can be used as biomarkers (**Table 3-1**) to identify and quantify the biomass of the classes that comprise the phytoplankton assemblage (Pinckney et al., 1998).

The research efforts of Research Project AE-1 included developing these user-friendly photopigment indicators of phytoplankton biomass and composition for use in the NRE. These indicators provide an efficient means to assess phytoplankton responses to external stressors impacting water quality and habitat condition; information that is critical for adaptive management of the NRE. These indicators were used to determine phytoplankton group specific responses to climatic factors over the course of the study and to determine impacts of anthropogenic nutrient enrichment on phytoplankton community structure via nutrient enrichment bioassays. Results have been communicated to management as estuarine-wide, time-space contour plots and have been used to compare NRE water quality with the State of North Carolina's and the U.S. Environmental Protection Agency's (EPA's) water quality assessment criteria (e.g., nutrient-sensitive waters, total maximum daily load [TMDL], Clean Water Act [CWA]). Predictive, probabilistic models of phytoplankton and HAB dynamics have been developed for long-term adaptive water quality management of the NRE.

Table 3-1. The 10 most common phytoplankton photopigments contained within classes microscopically identified in the NRE

Pigment	Abbreviation	Classes Represented by Pigment
Chlorophyll <i>a</i>	chl <i>a</i>	All classes
Fucoxanthin	Fuco	Diatoms, raphidophytes , chrysophytes, dinoflagellates ^a , haptophytes
Peridinin	Peri	Dinoflagellates
Diadinoxanthin	Diad	Same as for fucoxanthin plus dinoflagellates
Zeaxanthin	Zea	Cyanobacteria , chlorophytes, chrysophytes, raphidophytes, cryptophytes
Chlorophyll <i>b</i>	chl <i>b</i>	Chlorophytes
Chlorophyll <i>c</i>	chl <i>c</i>	Same as for fucoxanthin plus dinoflagellates and cryptophytes
Alloxanthin	Allo	Cryptophytes and ciliophora containing cryptophyte chloroplasts
Violaxanthin	Viol	Raphidophytes , chlorophytes, chrysophytes
19'hexanyloxyfucoxanthin	19-hex	Dinoflagellates ^a , haptophytes

^a These dinoflagellates are a small group of HAB-forming genera that contain chloroplasts of haptophyte origin and thus lack peridinin. Genera include Karlodinium, Karenia, and Takayama (Daughjerg et al., 2000). Classes in **bold type** indicate the dominant contributors to the pigment in the NRE.

The Phytoplankton Community of the NRE

The phytoplankton community of the NRE consists of a diverse assemblage of phytoplankton species represented primarily by six classes: diatoms, dinoflagellates, cryptophytes, chlorophytes (including euglenoids), raphidophytes, and cyanobacteria (Mallin et al., 2005; Tomas et al., 2007). Other minor classes represented include the haptophytes and chrysophytes, but these appear in low abundance and their small (nano-plankton to picoplankton) size and relatively low cell abundances lead to low contributions to total phytoplankton biomass in the NRE. The dinoflagellates, cryptophytes, raphidophytes, haptophytes, chrysophytes, and some chlorophytes bear flagella that propel the cells through the water. Collectively, these flagellated phytoplankton are called phytoflagellates. Mallin et al. (2005) stated that diatoms and dinoflagellates were responsible for most of the blooms observed during their study. The addition of raphidophytes to the list of dominant bloom-forming classes by Tomas et al. (2007) may reflect a temporal change in bloom composition as observed in the Skidaway Estuary, GA (Verity, 2010). Alternatively, it may simply reflect differences in identification and quantification methods used to determine biomass of these notoriously fragile cells (Tomas, 1997).

Many diatom species are fast growing, opportunists that commonly out-compete other groups when nutrient inputs are high (Smayda, 1997; Willen, 1991). As such, they commonly dominate phytoplankton communities of nutrient rich estuaries (Adolf et al., 2006; Cloern and Dufford, 2005). Diatoms readily assimilate dissolved inorganic nitrogen (DIN; nitrate, ammonium, and urea) and phosphorus (P; phosphate) forms and some simple organic compounds (Willen, 1991).

In contrast to other phytoplankton classes with polysaccharide or peptidoglycan cell walls, the outer shell of diatom cells, the frustule, is composed of a silica impregnated organic matrix (Hoek et al., 1997). As a result, diatom growth requires dissolved silica uptake in quantities similar to N uptake (Dortch and Whitedge, 1992). Because other phytoplankton groups lack this high silica requirement, silica limitation can play a key role in determining dominance by other phytoplankton groups when silica concentrations are below 2 μM and the silica to DIN ratio is less than 1 (Conley and Malone, 1992; Dortch and Whitedge, 1992; Justic et al., 1995). The primary accessory photopigment in diatoms is fucoxanthin (**Table 3-1**).

Diatoms have no flagella and only a weak ability for depth regulation in the water column by buoyancy regulation via regulation of the ionic content of the cytoplasm (Waite et al., 1997). The silica shell generally makes diatom cells denser than seawater (Boyd and Gracmann, 2002). Thus, diatoms require turbulent mixing to keep them within the euphotic zone of turbid estuaries (Margalef, 1978). Many diatoms are considered benthic and live along well-lit sediment surfaces of estuaries where they often form the dominant component of the BMA assemblage. Planktonic diatoms often settle to the sediments during periods of weak vertical mixing and benthic diatoms are commonly entrained in the water column during strong vertical mixing (Tester et al., 1995). As such, the distinction between benthic and planktonic diatom forms in shallow estuaries is not well defined (Tester et al., 1995). Generally, diatoms are considered highly palatable to higher organisms such as crustacean zooplankton and oysters (Willen, 1991) and dominance by diatoms is rarely regarded as a water quality concern. However, upon bloom termination, diatom cells often settle rapidly (Alldredge and Gotschalk, 1989; Smetacek, 1985), which can lead to a large pulse of fresh organic matter to the sediments (Alldredge and Gotschalk, 1989). If bottom waters are isolated from the atmosphere by stratification, the biological oxygen demand from these bloom termination events can result in hypoxia (Conley and Malone, 1992).

The dinoflagellates have two flagella and average swimming speeds (approximately 1 m h^{-1}) sufficient for effective depth regulation under weakly mixed conditions. Photosynthetic dinoflagellates use this swimming ability to vertically migrate up to the surface during the day toward favorable light conditions and deeper into the water column at night where nutrient concentrations are often higher (Jephson et al., 2011). This diel vertical migration (DVM) pattern provides access to growth limiting light and nutrient resources, a distinct growth advantage over a uniform vertical distribution (Ault, 2000; Watanabe et al., 1995). The nutritional modes of dinoflagellates are diverse and poorly understood. As alluded to above, some are strictly heterotrophic and are therefore not technically phytoplankton. These rarely cause water quality problems and will not be addressed further.

Most photosynthetic dinoflagellates contain peridinin, an accessory pigment contained in no other phytoplankton class (**Table 3-1**). Although light is required for growth, all photosynthetic dinoflagellates studied, have been shown to subsidize their energy and nutrient requirements by ingesting other plankton including bacteria and even similarly sized phytoplankton (Hansen et al., 1994; Jeong et al., 2005). Thus, in addition to being important autotrophs, they are considered mixotrophs, and are often a dominant component of the microzooplankton assemblage. Additionally, the dinoflagellates are capable and in some cases dependent (Tang et al., 2010) on the osmotrophic uptake of a wide range of organic macromolecules. The advantages gained from vertical migrations, mixotrophy, and osmotrophy are believed to be important aspects of the survival, competition, and bloom strategies of the dinoflagellates

(Smayda, 1997). Many harmful algal species exist within this class that produce an array of potent toxins that hinder grazing, kill fish and make shellfish unsafe for human consumption (Hallegraeef, 1993). However, many species are also considered excellent food sources for higher trophic levels (Ban et al., 1997; Mallin and Paerl, 1994; Sellner et al., 1991). In the NRE, *Karlodinium veneficum* is the most common toxin producing dinoflagellate (Tomas et al., 2007). This species is a member of small group of toxic dinoflagellates that lack the pigment peridinin and contain fucoxanthin as their primary accessory pigment. Fortunately, the minor accessory pigment 19'-hexanyloxyfucoxanthin (19-hex) is shared only by the haptophytes (Hoek et al., 1997), which are relatively uncommon in the NRE.

Often reflected in their distributions with respect to salinity, cyanobacteria in estuaries are composed of a mix of marine and freshwater species (Phlips et al., 2010). Most water quality problems associated with cyanobacteria in estuaries are due to freshwater, brackish-tolerant species (Moisander et al., 2002; Paerl, 1988). Through strong buoyancy regulation via intracellular gas vesicles, blooms often float to the surface. The resultant unsightly surface scums can completely shade out other phytoplankton, benthic algae, and submerged aquatic vegetation resulting in severe degradation of impacted aquatic systems (Paerl, 1988). A variety of toxins are produced by these harmful bloom-forming cyanobacterial (CyanoHAB) genera that disrupt grazer communities, contaminate drinking water sources, and can cause contact dermatitis in humans (Chorus and Bartram, 1999). In contrast, the cyanobacteria of marine origin are predominantly non-toxic, picoplanktonic (less than 2 μm in diameter) species that do not contain gas vesicles and are generally not a concern from a water quality perspective. Despite their extremely small size, high cell abundances (often 10–100 fold higher than eukaryotic autotrophs) of picocyanobacteria can make them an important contributor to total phytoplankton biomass and productivity of estuaries (Gaulke et al., 2010; Murrell and Lores, 2004). Although often observed microscopically in the NRE (Hall personal observation), the small size picocyanobacteria makes them difficult to quantify using inverted microscopy. Although other phytoplankton classes do contain trace amounts of zeaxanthin, levels of zeaxanthin within picocyanobacteria are much higher which makes zeaxanthin a reliable indicator of picocyanobacterial abundance (Gaulke et al., 2010).

The raphidophytes commonly reported in estuaries are brackish tolerant marine species that often bloom in poorly mixed, nutrient rich conditions (Lewitus et al., 2003; Tomas et al., 2007). Similar to the dinoflagellates, they are bi-flagellated and their DVM patterns are believed to be a critical component of their growth and survival strategy (Handy et al., 2005; Watanabe et al., 1995). All of the marine raphidophytes are considered HABs (Moestrup et al., 2011) due to toxin production and association with fish kills that are distributed globally at tropical to temperate latitudes (Jeong, 2011). Mixotrophic feeding upon bacteria and picocyanobacteria has recently been documented for several genera (Jeong, 2011). Similar to diatoms, the dominant accessory pigment of the raphidophytes is fucoxanthin. However, in the NRE, raphidophytes are the major group containing the minor accessory pigment violaxanthin which is a reliable indicator for changes in their biomass (see the *Harmful Algal Bloom* section).

The cryptophytes, indicated by the diagnostic pigment alloxanthin, are also mixotrophic phytoflagellates and undergo DVMs (Hall and Paerl, 2011). However, no species of cryptophyte is known to produce toxins (Moestrup et al., 2011), and they are generally considered excellent food sources for higher trophic levels (Burkhill et al., 1987).

The chlorophytes found in estuaries are usually a mix of nanoplanktonic, marine (often flagellated) and larger, microplanktonic, freshwater (often non-flagellated) species. Although they are common, they rarely form blooms in estuaries and are usually a minor component of the phytoplankton assemblage (Mallin et al., 2000). Euglenophytes, which are often grouped with the chlorophytes, are an exception to this generality because they do occasionally form dense blooms in nutrient rich estuaries including the NRE (Mallin et al., 2000; Tomas et al., 2007). The pigment chlorophyll *b* (chl *b*) is a reliable measure of chlorophyte biomass.

Materials and Methods

Measurements of Physical and Chemical Environmental Conditions

Monthly samples for measuring physical and chemical conditions, phytoplankton biomass, and phytoplankton community composition were collected along an eight station downstream transect (**Figure 3-2**) from October 11, 2007 through December 6, 2011. At each station, surface (0.2-m depth) and bottom (0.5 m above bottom) samples were collected using a non-destructive diaphragm pump and dispensed into 4-L polyethylene bottles. Bottles were immediately placed in coolers to maintain dark, in situ temperature conditions for the duration of each sampling trip (less than 6 h) prior to laboratory sample processing at the University of North Carolina at Chapel Hill's Institute of Marine Sciences (UNC-IMS). At each sampling station, vertical profiles of temperature, salinity, dissolved oxygen, conductivity, chlorophyll fluorescence, turbidity, pH, and photosynthetically active radiation (PAR) were measured at each station using a YSI 6600 multi-parameter water quality instrument (YSI, Yellow Springs, OH). Light attenuation (K_d) was calculated as the slope of natural log transformed PAR versus depth according to Beer's law.

In addition to the eight monthly sampling stations, biweekly to monthly samples were also collected from surface waters with pre-cleaned polyethylene bottles at two U.S. Geological Survey (USGS) gaging stations that continuously monitor water level, temperature, salinity, and flow velocity. Gaging Station number 0209303205 (**Figure 3-2**) is at the head of the NRE near Jacksonville. Gaging Station number 02093000 near Gum Branch is the only gaging station along the freshwater reaches of the New River. Discrete sampling at Gum Branch occurred throughout the study period, but sampling at Gaging Station number 02093205 began April 2008.

Nutrient analyses were conducted on water collected from the eight monthly estuarine stations and from the two USGS gaging stations. All water samples were gently filtered (less than 20 kPa) through 25 mm in diameter Whatman glass fiber filters (GFF; 0.7 μm nominal pore size). Total dissolved nitrogen (TDN), nitrate (NO_3^- + nitrite [NO_2^-], labeled as NO_3^-), ammonium (NH_4^+), orthophosphate (PO_4^{3-}) and silicate (SiO_3^{2-}) concentrations were determined using colorimetric flow injection analyses (Lachat QuikChem 8000, Lachat Instruments, Milwaukee, WI) and standard protocols (Lachat QuikChem methods 31-107-04-3-B, 31-107-04-1-C, 31-107-06-1-A, and 31-115-01-3-C, respectively). Detection limits for TDN, NO_3^- , NH_4^+ , PO_4^{3-} , and SiO_3^{2-} were 2.53, 0.04, 0.18, 0.06, and 0.75 $\mu\text{mol L}^{-1}$, respectively.

Concentrations of chromophoric dissolved organic matter (CDOM), a key determinant of light attenuation, were measured at the eight monthly estuarine stations fluorometrically according to

methods detailed in Lunetta et al. (2009) and are expressed as quinine sulfate equivalents ($\mu\text{g L}^{-1}$). Water samples were vacuum filtered (less than 25 kPa) using pre-combusted Whatman glass fiber filters (GFFs) on the day after water sampling. The filtrate was stored in scintillation vials in the dark at 4°C until fluorometric analysis on a Turner Designs TD-700. Total suspended solids (TSS) were measured according to Standard Methods 2540 D (American Public Health Association, 1998): Water samples were filtered on pre-rinsed, pre-dried, tared Whatman GFFs. Filters were dried at 105°C and then weighed using a calibrated Mettler Toledo AB-S analytical balance. Solids concentration is the difference in filter weights before and after filtration divided by volume of water filtered.

Physical and chemical conditions within the NRE were additionally assessed by two autonomous vertical profilers (AVPs, for complete description, see Reynolds-Fleming et al., 2002) deployed at one upstream (Morgan Bay near Station 6) and one downstream (Stones Bay near Station 3) location (**Figure 3-1**). The AVPs consist of a floating platform that contains a solar powered computer and winch mechanism that casts a datasonde at programmable time intervals (**Figure 3-3**). The AVPs were outfitted with YSI 6600 datasondes and were configured to produce a full water column profile of temperature, salinity, turbidity, pH, dissolved oxygen, and chlorophyll fluorescence every 0.5 hour with approximately 10 cm depth resolution. Anemometers (RM Young Marine Wind Monitor 0510) mounted to each AVP measured 6-minute average wind speed and direction every 0.5 hour. Because the AVPs were deployed in June 2008, they have provided a nearly continuous record of basic water quality at the two mooring locations.

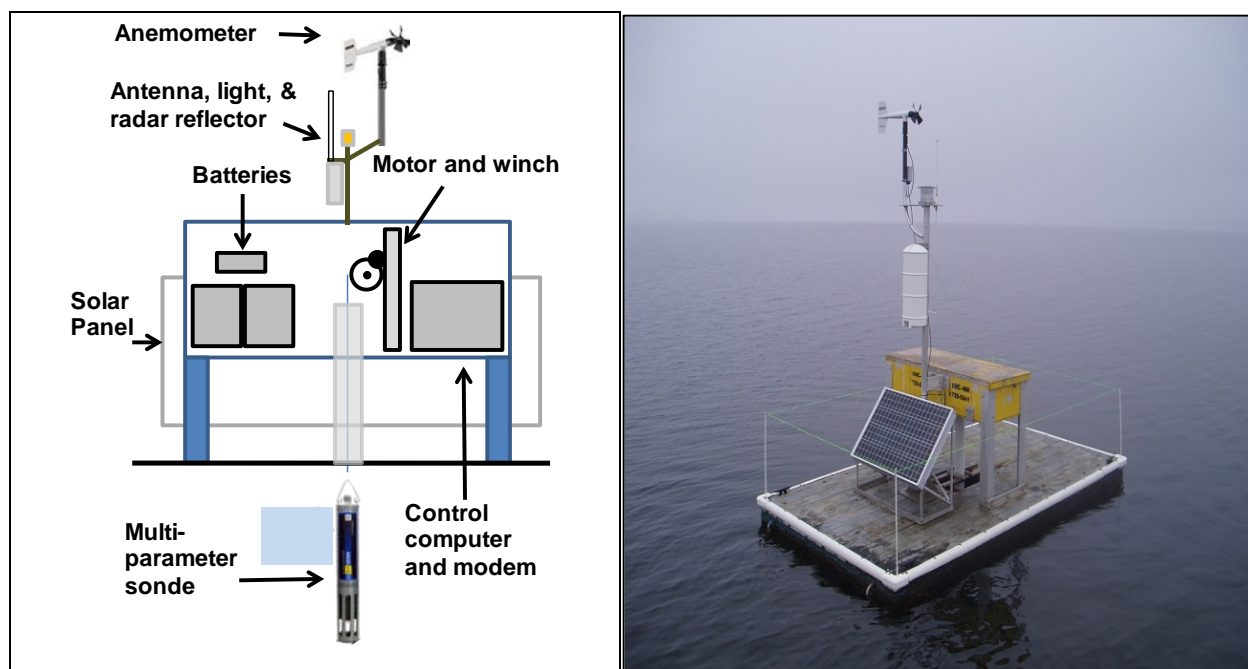


Figure 3-3. Schematic diagram and photograph of the AVPs.

Measurement of Freshwater Inputs and Flushing Time

Freshwater discharge to the NRE was continuously quantified by the USGS near Gum Branch (**Figure 3-2**; USGS gage number 02093000). Approximately 78% of the watershed of the NRE

is ungaged (Ensign et al., 2004). Ungaged freshwater inputs were estimated by multiplying the gauged freshwater discharge by the ratio of ungaged: gaged watershed area, exclusive of the estuary water surface (Ensign et al., 2004).

Flushing time was calculated using the date-specific freshwater replacement method (Alber and Sheldon, 1999). Flushing time is the amount of time necessary for the combination of riverine discharge and seawater inflows to replace the volume of an estuary or estuarine segment (Sheldon and Alber, 2006). The date-specific version of this traditional measure of transport time scale was chosen because it accounts for changing river flow conditions and the time lags between river gage and downstream locations (Alber and Sheldon, 1999). Flushing time, as calculated here, is also correctly interpreted as the average age of freshwater within an estuary (Sheldon and Alber 2006). This interpretation is utilized to provide time scales for the biological transformation of riverine nutrient loads into phytoplankton biomass as freshwater is advected and mixed downstream within the NRE.

The estuary was divided into nine segments encompassing sampling Stations 1–8 and the USGS station near Jacksonville (number 0209303205; **Figure 3-2**). Volumes for each segment were estimated using raster bathymetry data from the National Geophysical Data Center's Coastal Relief Model according to methods detailed by Ensign et al. (2004). Salinity of each segment was taken as the vertically averaged salinity of the monthly profiles at each of the eight monthly sampling stations. For the most upstream segment, encompassing the USGS Station number 0209303205, salinity at the approximately 1-m instrument depth was assumed representative of the entire water column. Flushing time for each segment was taken as the cumulative flushing times upstream of the downstream boundary of each segment, and represents the average time freshwater spent upstream of each segment (i.e., average freshwater age within the estuary). Calculating the cumulative flushing times from the head to the exit of the estuary in this manner allows use of the discretely sampled snapshots of phytoplankton biomass and nutrient concentrations to reconstruct the time course of phytoplankton biomass development and nutrient draw down during downstream transport within the estuary.

Measurements of Phytoplankton Biomass and Community Composition

Chl *a* was determined from all water samples collected at the routine monthly transect stations and from the two USGS gaging stations. (**Figure 3-1**). Fifty mL aliquots were filtered onto 25 mm in diameter Whatman GFFs. Storage, extraction, and fluorometric analyses follow those described by Wetz et al. (2011a).

Accessory photopigments representing major phytoplankton divisions were measured using high-performance liquid chromatography (HPLC; **Figure 3-4**) from surface and bottom water samples at the eight monthly sampling stations but not at the USGS gaging stations. Samples were filtered, sonicated, and extracted in 100% acetone and pigment extracts were separated and quantified by using HPLC (Shimadzu model LC-20AB) equipped with a photodiode array spectrophotometric detector (Shimadzu SPD-M20AC). The HPLC procedures are described by Pinckney et al. (1998 and 2001). Photopigments were identified according to their absorption spectrum, which was determined using a commercially obtained pigment standard (DHI, Denmark).

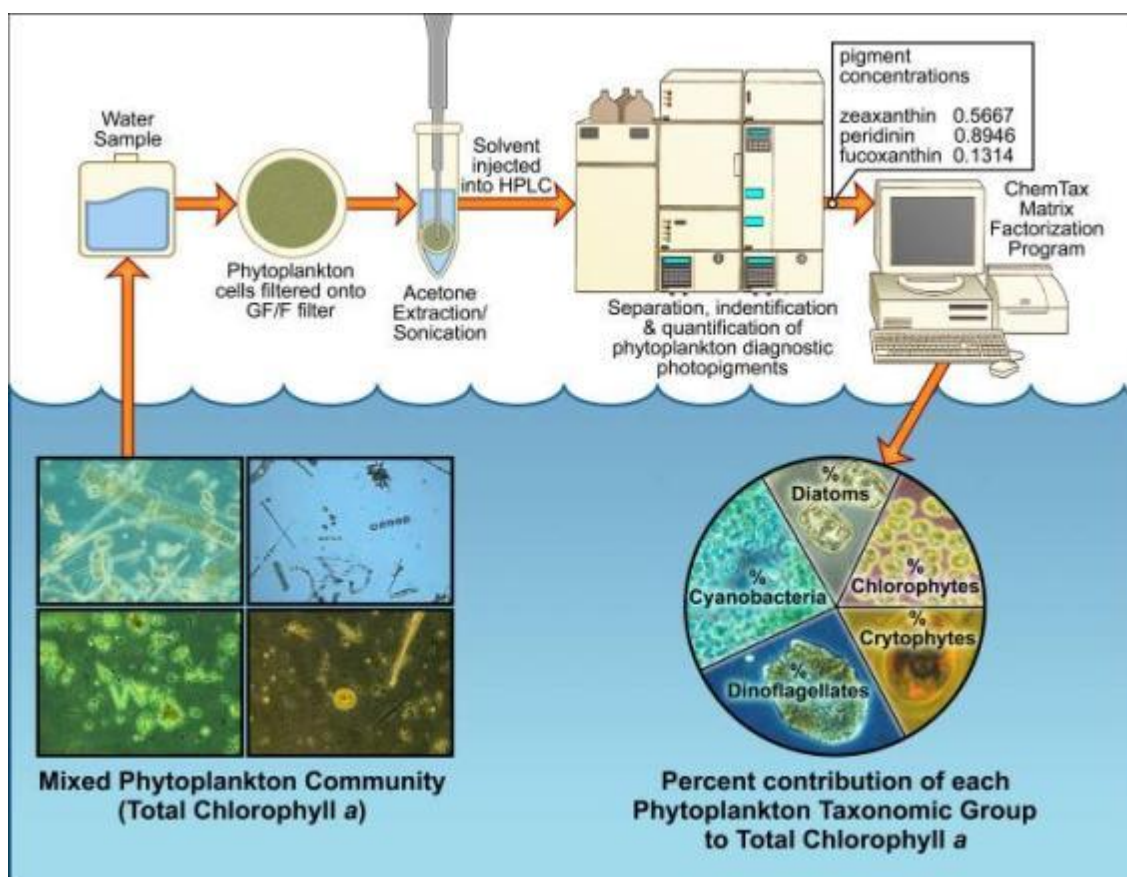


Figure 3-4. Diagram showing the methodology for determining algal community composition using diagnostic photopigment analyses by high-performance liquid chromatography.

Causative species of phytoplankton blooms at the eight monthly transect stations were identified and quantified from preserved samples (1% Lugols solution) using inverted microscopy (Utermöhl, 1958). A bloom sample was defined as a sample in excess of the $40 \mu\text{g L}^{-1}$ chl *a* water quality standard adopted by the North Carolina Department of Environment and Natural Resources (NCDENR; 2007). When multiple bloom samples were collected at spatially contiguous stations on the same sampling date, only the surface water sample with the highest chl *a* concentration was examined. Cell abundances and biovolume estimates of the major taxa followed methods detailed in Hall and Paerl (2011). Because Lugol's solution distorts the shape of raphidophytes (Tomas, 1997), identification of raphidophytes beyond the class level was not possible.

For molecular identification of potentially toxic CyanoHAB species, selected sub-samples from the eight monthly transect stations (during spring–summer bloom periods) were filtered on Pall Supor® filters, placed in 2-mL tubes, and maintained at -80°C until further processing. DNA extraction was performed by chemical and mechanical lysis (glass bead beating), using GeneRite RWoC3 kits per the manufacturer's instructions. Extracted DNA was then amplified via polymerase chain reaction (PCR) using primers designed to detect the 16S rDNA of CyanoHAB genera and the microcystis toxin producing gene *mcyB*. The *mcyB* primers were specific to major

microcystin-producing genera (*Planktothrix*, *Anabaena* and *Microcystis*) and were utilized to assess the toxin production potential of CyanoHABs in the NRE.

The actual quantity of cyanobacterial toxins in the estuary was also determined by direct measurements of total microcystins via enzyme-linked immunosorbent assays (ELISA) according to methods detailed in Otten et al. (2012). Total microcystin concentration is a measure of a broad class of structurally similar microcystin toxins produced by several CyanoHAB genera, including *Microcystis*, *Anabaena*, and *Planktothrix*. Measurements were made from surface waters over the period August through November of 2008 at monthly sampling Stations 5–8 and two additional samples from the USGS gaging stations.

Assessment of Hydrological Impacts on Phytoplankton Biomass and Composition

Vertically averaged (mean of surface and bottom water samples) photopigment concentrations indicative of total phytoplankton biomass (chl *a*) and of individual algal classes were compared against flushing time. Prior to analyses, photopigment and flushing time data were log₂ transformed. In cases where a pigment concentration was undetectable, a minimal value (0.5 times the lowest measured concentration) was assigned. Transformed pigment concentrations were binned into 30 equally spaced log₂ (flushing time) bins. Mean pigment concentrations within each bin were then compared against the center of each flushing time bin. Relationships between flushing time and pigment concentrations were fitted using a segmented linear regression analysis consisting of two segments. Continuity of the segments was assured by defining the start of the second modeled segment as the end of the first segment. The breakpoint at which the two model segments meet was determined by iteratively fitting the segmented model with each observed flushing time and retaining the model with the breakpoint that minimized the sum squared error of the residuals. Because the breakpoint location was allowed to vary between all flushing time bins, a single-segment linear regression was possible. Model fitting was performed using the least squares curve fitting “lsqcurvefit” function in MATLAB v.7.1, the Mathworks (Natick, CT).

The full segmented empirical model is defined by four parameters: (1) the y-intercept of the first segment, (2) the slope of the first segment, (3) the breakpoint flushing time, and (4) the slope of the second segment. Confidence intervals for these parameters were estimated by standard bootstrapping (Hall et al., 2004). The binning, and segmented regression procedures described above were repeated with 1,000 resampled data sets each of the same size as the original. The upper and lower bounds for the 95% confidence interval (CI) are then defined as the 26th and 975th rankings of each parameter estimate (Hall et al., 2004) and used to infer differences in class-level phytoplankton community responses.

Measurement of Phytoplankton Primary Productivity

Primary productivity was measured via the ¹⁴C method (Paerl, 2002) for surface waters from the eight monthly sampling stations from approximately 09:00 a.m.–13:00 p.m. on the day following sample collection. Water samples were maintained overnight and incubations were performed under ambient light and temperature conditions in an outdoor pond at the UNC-IMS with circulating sea water (Mallin and Paerl, 1992). Light conditions associated with vertical mixing were simulated using a field light simulator (Mallin and Paerl, 1992). Light availability was

measured throughout each incubation period with a Li-Cor 2 π PAR meter. The average PAR flux during the incubations was 234 $\mu\text{mol photons m}^{-2} \text{ s}^{-1}$ (SD=94). Light-dark ^{14}C assay methods followed those described in Paerl (2002) with the exception that activity of samples was measured on a Beckman Coulter LS 6500 liquid scintillation counter and dissolved inorganic carbon concentration was measured on a Shimadzu total organic carbon analyzer (TOC-5000A).

Assessment of Nutrient Limitation via Nutrient Enrichment Bioassays

Nutrient addition bioassays were used to evaluate microalgae (MA) responses to nutrient enrichment at levels reflecting tributary inputs to the NRE (**Figure 3-5**). These highly replicated (quadruplicate treatments), bioassays are designed to identify growth-limiting nutrients and bloom-threshold input levels, below which water quality (e.g., the State of North Carolina's chl *a* water quality standard and nutrient-sensitive water designation; NCDENR, 2007), EPA and CWA, and HAB criteria can be met for the NRE (Paerl et al., 1995).

Surface water was collected from Stations 3 and 5 during June and September of 2008–2010. Subsamples were dispensed into 4-L cubitainers and were amended with a factorial design of ammonium, nitrate, and phosphate additions to achieve total DIN and P amendments of 20 μM N and 5 μM P. The two forms of DIN were used to determine the impact of DIN form on phytoplankton growth response. An unamended quadruplicate set of cubitainers served as a control for all bioassays. Phytoplankton assemblages were incubated in the outdoor circulating pond at UNC-IMS under a single layer of neutral density screening to simulate in situ temperature and light conditions (Piehler et al., 2002). Cubitainers were subsampled on Days 2 and 4 of the incubation and MA photopigments that are indicative of class-level phytoplankton biomass and primary productivity measurements (as described for the monthly transects) were used to determine MA growth responses to nutrient enrichment.

Statistical significance of differences in growth responses to experimental treatments were tested using the Kruskal-Wallis rank sum test (the non-parametric alternative to analysis of variance [ANOVA]). In cases in which a significant treatment effect was determined, a non-parametric, multiple comparison test was used to compare treatment effects to the control (Siegel and Castellan, 1988).



Figure 3-5. Photograph of the bioassay incubation setup in the seawater pond at the UNC-IMS in Morehead City, NC.

Bayesian Belief Network Model

A Bayesian Belief Network (BBN) Model was constructed to probabilistically identify linkages between climatic and anthropogenic physical and chemical drivers and water quality responses within the NRE. Physical drivers investigated were light attenuation, wind speed and direction, temperature, river flow, and vertical water column stratification. Chemical drivers included concentrations of DIN, phosphate, and the DIN to phosphate ratio. Water quality responses investigated were total phytoplankton biomass (*chl a*), four accessory photopigments indicative of HAB species (peridinin, 19-hex, gyroxanthin, and violaxanthin), and benthic dissolved oxygen. Detailed descriptions of model methodology and output are provided in **Appendix 3-A**.

Results and Discussion

Climatic Controls on the Phytoplankton

The study period from October 2007 through December 2011 was a period of dramatic climatic variability due to extended droughts and rainy periods, and two tropical storm systems that impacted the region. As a result of this extreme climatic variability, the range of New River discharge to the NRE encompassed the 0.5% to 99.99% quantiles of daily average freshwater discharge documented over the past 63 years at Gum Branch. The past few months of 2007 and most of 2008 and 2011 were exceptionally dry periods (**Table 3-2**). Due to an extended rainy

period that extended from fall 2009 through winter 2010 and Tropical Storm Nicole in 2010, 2009 and 2010 had river flows that were closer to long-term average conditions. The extreme level of hydrologic variability during this period along with seasonal temperature fluctuations allowed assessment of nutrient and hydrologic effects on the phytoplankton across nearly the full range of environmental conditions that would be expected within the NRE.

Table 3-2. Comparison of annual average freshwater inflows into the NRE from 2008–2011 with average flows from the long-term record produced by the USGS Gaging Station number 0209303205 near Gum Branch.

Year	2007 ^a	2008	2009	2010	2011	1949–2011
Average Flow (m ³ s ⁻¹)	2.56	6.84	12.42	15.34	7.20	14.61

^a Data from 2007 is the average flow for the period October 7–December 31, 2007. Data are scaled to account for ungaged, freshwater inputs downstream of the gaging station (see *Methods and Materials*).

Water samples analyzed for diagnostic photopigments to quantify the major algal taxonomic groups show distinct seasonal patterns and shifts in algal community composition and biomass. Diagnostic photopigments allowed us to detect, quantify, and locate phytoplankton biomass distribution (as chl *a*) and functional groups responsible for primary production and algal bloom formation (cf., Paerl et al., 2003). Results demonstrate differential sensitivities to external forcings, including freshwater discharge, tidal exchange, water temperature, and nutrient loads.

Temporal and spatial variability of biomass, community composition, and blooms in relation to the physical–chemical environment

Figures 3-6 and 3-7 show the responses of salinity, nutrients, and phytoplankton indicators to two principal drivers (e.g., temperature and river discharge) over the period from October 2007 through December 2011. Results are plotted along a transect ranging from near the mouth of the estuary (Station 1) to the estuarine headwaters near Jacksonville (Stations 7 and 8) using space-time contour plots, where the space axis is distance upstream from Station 1 (see **Figure 3-1** for exact station locations).

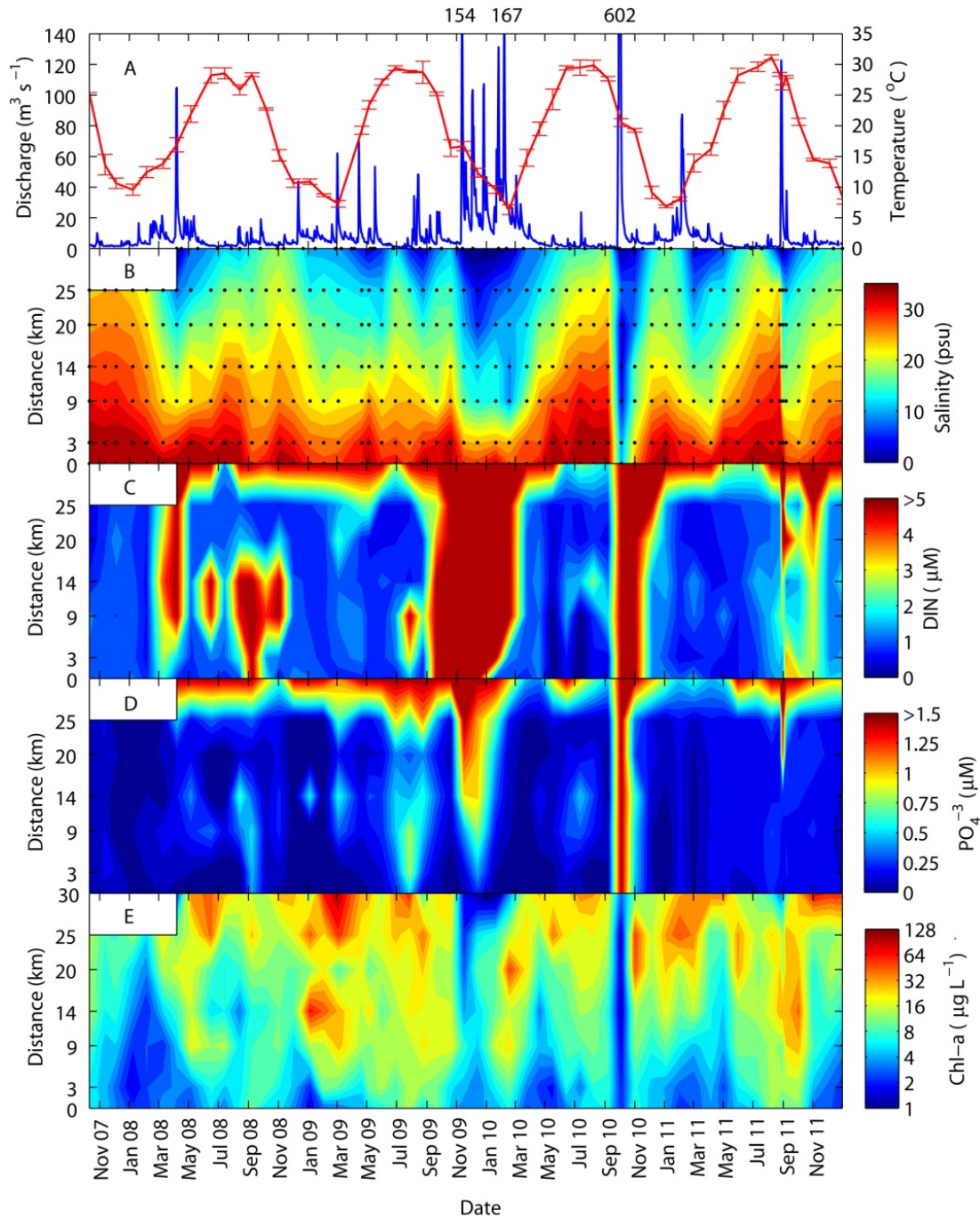


Figure 3-6. Physical, chemical, and phytoplankton biomass response to changes in discharge and temperature in the NRE from October 2007 through December 2011.

(A) Time series of daily average freshwater discharge (blue line), and mean (SD) of average surface and bottom water temperature (red line with error bars) from all stations. Off-scale flows are written above the panel. The x-axis tick marks represent the first day of every other month. Data in panels B–E are averages of surface and bottom water conditions except for data from the USGS Station number 0209303205 at 30 km where bottom water data were not collected. (B) Space-time contour plot of surface water salinity. The y-axis is the distance from New River Inlet (Station 1). Data at 25 km are means from Stations 6, 7, and 8. Black dots in salinity panel show sampling locations and times. Rectangular white patches on contour plots represent the unsampled period for the USGS Station number 0209303205. (C) Dissolved inorganic nitrogen, (D) phosphate, and (E) chl *a*.

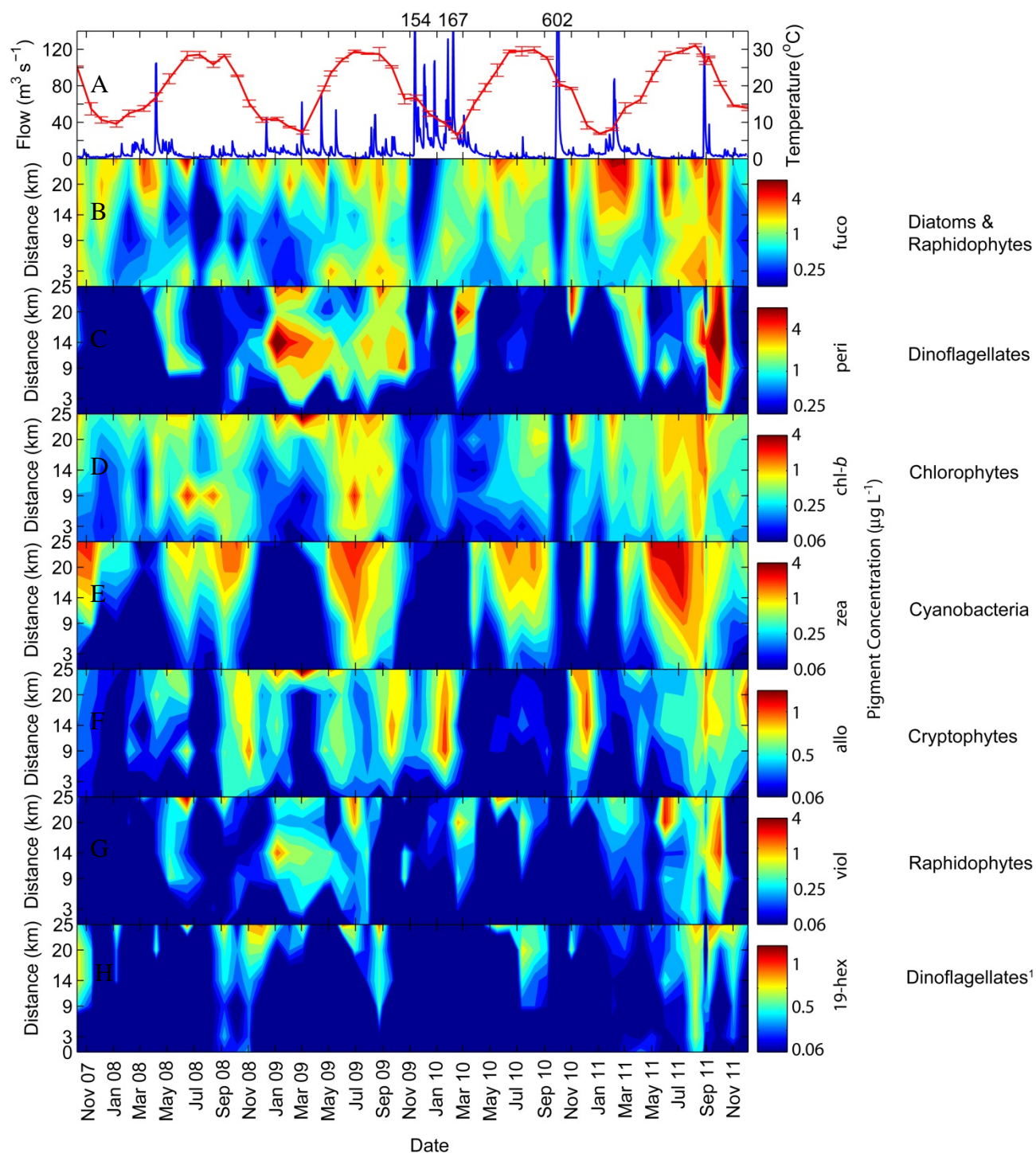


Figure 3-7. Temperature, river discharge, and contour plots of the space-time distributions of accessory photopigments indicative of major phytoplankton taxonomic groups.

Pigment abbreviations follow Table 3-1. Format and data treatment are identical to Figure 3-6.

Phytoplankton biomass varied substantially, and the spatial and temporal scales of chl *a* variability suggest a strong dependence on river discharge and associated nutrient loading

(**Figure 3-6**). Riverine chl *a* at Gum Branch was low (mean 1.1 $\mu\text{g chl } a \text{ L}^{-1}$, standard deviation [SD]=1.2, data not shown) and thus riverine inputs do not appear to be a significant source of phytoplankton biomass to the estuary. Chl *a* was generally highest and bloom events (greater than 40 $\mu\text{g L}^{-1}$ chl *a*) occurred more frequently at upstream stations that were more directly impacted by riverine nutrient supplies.

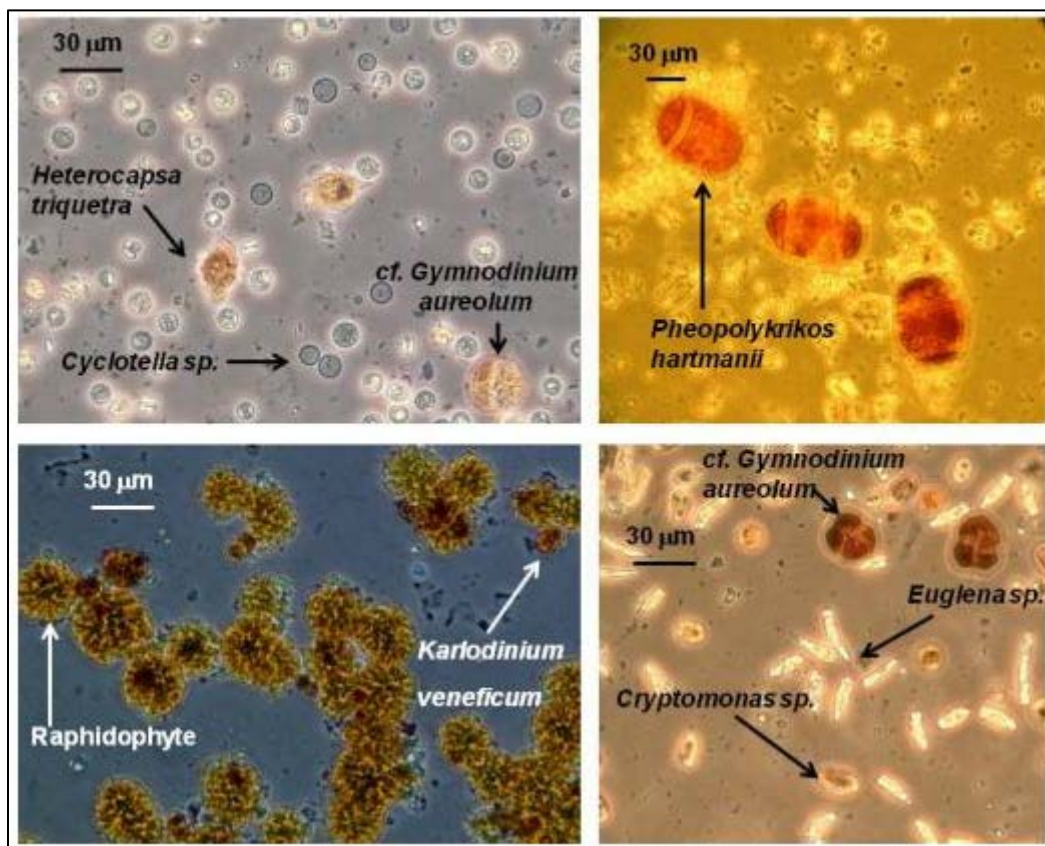


Figure 3-8. Photomicrographs of algal blooms from NRE surface waters.

Top left: Mixed diatom and dinoflagellate bloom on 1 February 2011, Station 7. Bottom left: Raphidophyte bloom on June 16, 2008 at Station 6. The shape of the raphidophyte cells has been severely distorted by preservation in Lugol's solution and the cells have clumped together. Top right: Dinoflagellate bloom on October 3, 2011, Station 3. Bottom right: Mixed euglenophyte and cryptophyte bloom on March 4, 2009, Station 7.

Biomass was generally lowest and only two blooms were observed during the prolonged drought periods of 2008 (**Figure 3-6**). Both blooms occurred 25 km or more upstream of the inlet. The bloom in June was dominated by raphidophytes (**Table 3-2, Figure 3-8**) and the one in September was dominated by raphidophytes and a large dinoflagellate (**Table 3-2**). Compared to 2008, phytoplankton biomass was considerably higher in 2009 which corresponded with both higher discharge and N inputs (**Figure 3-6**). There were 5 bloom events in 2009, with the highest concentration of chl *a* observed during the study period (224 $\mu\text{g L}^{-1}$) occurring 25-km upstream from the inlet (Station 7) in March 2009 (**Figure 3-8**). This bloom was dominated by two flagellates, the euglenophyte *Euglena sp.*, and the cryptophyte *Cryptomonas sp.* (**Table 3-2, Figure 3-9**). Other blooms in 2009 were similarly comprised of dinoflagellates, euglenophytes, and raphidophytes, all flagellated groups (**Table 3-2**).

Table 3-3. Summary of phytoplankton bloom composition in the NRE from October 2007 through December 2011.

Date	Stations Impacted	Division or Class	Species	% Biovolume	Abundance (cells L ⁻¹)
June 16, 2008	6,8	Raphidophyte	Undeterminable	92	2.0×10^7
September 8, 2008	7	Raphidophyte Dinoflagellate	Undeterminable Gymnodinoid	53 27	2.3×10^6 2.2×10^5
January 5, 2009	6,7,8	Dinoflagellate Euglenophyte	<i>Akashiwo sanguinum</i> <i>Eutreptia</i> sp.	51 25	8.2×10^5 4.5×10^6
February 2, 2009	4	Dinoflagellate Dinoflagellate	<i>Akashiwo sanguinum</i> <i>Heterocapsa triquetra</i>	74 18	8.5×10^5 1.7×10^6
March 4, 2009	7	Euglenophyte Cryptophyte	<i>Euglena</i> sp. <i>Cryptomonas</i> sp.	47 29	3.1×10^7 1.8×10^7
June 29, 2009	6,7	Raphidophyte Euglenophyte	Undeterminable <i>Euglena</i> sp.	70 6	1.3×10^6 1.6×10^5
August 24, 2009	5,6,7,8	Dinoflagellate Dinoflagellate	<i>Gyrodinium instriatum</i> <i>Karlodinium veneticum</i>	68 11	7.3×10^5 1.1×10^7
February 17, 2010	5	Dinoflagellate	<i>Heterocapsa triquetra</i>	96	8.5×10^6
May 17, 2010	6,8	Raphidophyte	Undeterminable	94	2.6×10^6
June 14, 2010	7	Raphidophyte	Undeterminable	82	2.7×10^6
November 1, 2010	5,7,8	Dinoflagellate Ciliophora Euglenophyte	<i>Gyrodinium instriatum</i> <i>Myrionecta rubra</i> <i>Eutreptia</i> sp.	50 22 10	9.9×10^5 8.4×10^6 1.8×10^6
February 1, 2011	7	Diatom Dinoflagellate Dinoflagellate	<i>Cyclotella</i> sp. cf. <i>Gymnodinium aureolum</i> <i>Heterocapsa triquetra</i>	39 30 28	2.2×10^7 1.1×10^6 1.5×10^6
March 2, 2011	6,7	Diatom	<i>Cyclotella</i> sp.	83	2.3×10^7
May 31, 2011	5,6,7	Raphidophyte	Undeterminable	99	5.9×10^6
August 8, 2011	6	Raphidophyte	Undeterminable	87	4.4×10^6
August 31, 2011	4	Dinoflagellate	<i>Pheopolykrikos hartmanii</i>	97	6.6×10^5
September 7, 2011	3	Dinoflagellate	<i>Pheopolykrikos hartmanii</i>	99	1.7×10^5
September 7, 2011	5,7	Euglenophyte Dinoflagellate Raphidophyte Dinoflagellate Chrysophyte	<i>Eutreptia</i> sp. <i>Gyrodinium instriatum</i> Undeterminable <i>Pheopolykrikos hartmanii</i> <i>Apedinella radians</i>	32 21 18 8 6	2.1×10^6 1.6×10^5 1.6×10^6 1.1×10^4 1.0×10^6
October 3, 2011	3,4	Dinoflagellate	<i>Pheopolykrikos hartmanii</i>	98	3.2×10^5

Taxa listed comprised greater than 70% of total phytoplankton biovolume.

Despite large nutrient pulses to the estuary, chl *a* biomass was low during the peak discharge periods in late fall 2009. Chl *a* was low throughout the estuary during the drought period in spring 2010 (**Figure 3-7**). Similar to the peak discharge period in fall 2009, biomass was extremely low (chl *a* less than $2 \mu\text{g L}^{-1}$) in the period immediately following the remnants of

Tropical Storm Nicole (**Figure 3-6**). These periods of high flushing and low phytoplankton biomass are dominant drivers of variability of chl *a* in the NRE and result in a weak, but significant negative correlation between discharge and chl *a* (Pearson's $R=-0.10$, $p=0.04$). Periods of elevated phytoplankton biomass and blooms generally occurred weeks to a month after periods of elevated freshwater discharge (**Figure 3-6**). Thus, blooms appear to follow pulses of nutrient enriched freshwater inputs to the NRE. For example, blooms were observed from 20–25 km upstream of the inlet several weeks after the late September 2010 freshwater discharge event from the remnants of Tropical Storm Nicole. This storm delivered more than 50 cm of rain to the watershed over a 3-day period and resulted in peak daily average river flows in excess of $600 \text{ m}^3 \text{ s}^{-1}$, a flow level seen on only 4 days since the gaging station near Gum Branch was established in 1949. As in 2008 and 2009, all blooms in 2010 were dominated by phytoflagellates (**Table 3-2**). The flagellate dominated character of NRE blooms has been previously documented by other researchers (Tomas et al., 2007) and the data presented here from 2007 through 2010 is currently in review for publication (Hall et al., in review). Throughout the study period, no blooms occurred at the two stations closest to the inlet (**Figure 3-6** and **Table 3-2**). As a result of upstream phytoplankton uptake and dilution with shelf waters, nutrient concentrations at these stations were too low to support bloom development except during the exceptionally high flows during fall 2009 and following Tropical Storm Nicole in 2010.

Table 3-4. Pearson's correlation (*R*) matrix for 8 of the 10 most common phytoplankton photopigments contained within algal divisions microscopically identified in the NRE.

	Chl <i>a</i>	Fuco	Peri	Zea	Chl <i>b</i>	Allo	Viol
Chl <i>a</i>							
Fuco	0.79						
Peri	0.49	0.13					
Zea	0.24	0.18	-0.01				
Chl <i>b</i>	0.43	0.16	0.31	0.20			
Allo	0.34	0.07	0.31	0.07	0.72		
Viol	0.83	0.79	0.22	0.21	0.11	0.07	
19-hex	0.50	0.48	0.17	0.32	0.34	0.24	0.42

All of the major accessory photopigments were significantly and positively correlated with chl *a* (**Table 3-3**). The high correlation between fucoxanthin and violaxanthin indicates that raphidophytes are the dominant fucoxanthin containing phytoplankton in the NRE (**Table 3-3**). The strong correlations between both fucoxanthin and peridinin with chl *a* also confirms the microscopic analyses which indicate raphidophytes and dinoflagellates are the dominant bloom forming organisms. Most of the class-level photopigments showed significant, positive relationships with each other, which suggests a common dominant regulating factor or set of factors that controls the biomass of most phytoplankton classes.

Assessment of Hydrologic Control

Comparison of these photopigments with flushing time indicates that one common controlling mechanism for all phytoplankton groups in the NRE is freshwater discharge. Increases in freshwater discharge lead to decreases in flushing time that were often associated with rapid decreases in salinity (**Figure 3-9**). For each photopigment analyzed, a segmented regression with an initial increase and subsequent decrease with increasing flushing time resulted in a better fit than a single, monotonic regression (**Figure 3-10**).

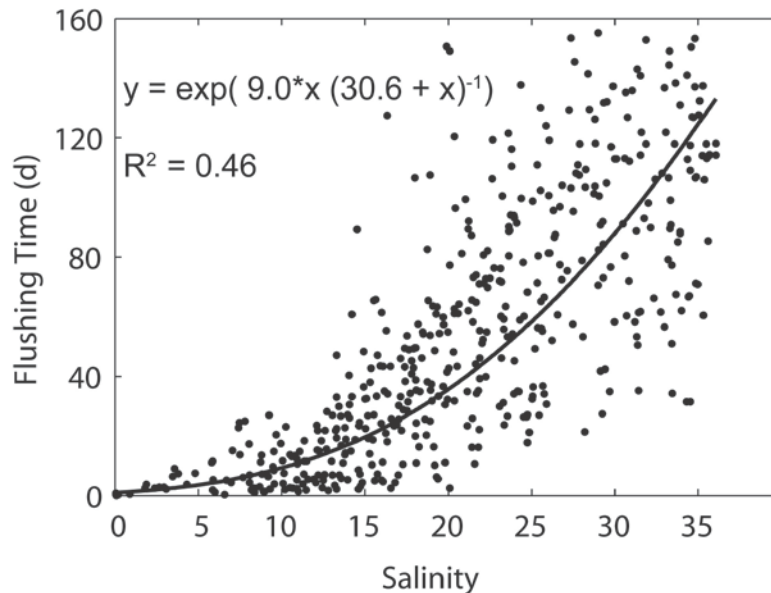


Figure 3-9. Relationship between flushing time and salinity in the NRE from October 2007 through December 2011.

This non-monotonic response to hydrologic forcing is driven by the dual influences of decreases in biomass losses due to flushing from the estuary with concomitant decreases in growth stimulating nutrient delivery as river flow decreases. Higher nutrient loads associated with increased flow enhance nutrient availability within the estuary, which favors biomass accumulation of all algal classes. However, under high flow conditions flushing time becomes too short to allow biomass to accumulate. Total phytoplankton biomass (chl *a*) increased rapidly from a flushing time of approximately 1 day, up to a flushing time of approximately 9 days (95% CI 4.0–11.3 days; **Figure 3-10** and **Table 3-5**), and declined slowly at flushing times greater than this breakpoint (note the log₂ scale of the *x*-axis in **Figure 3-10**).

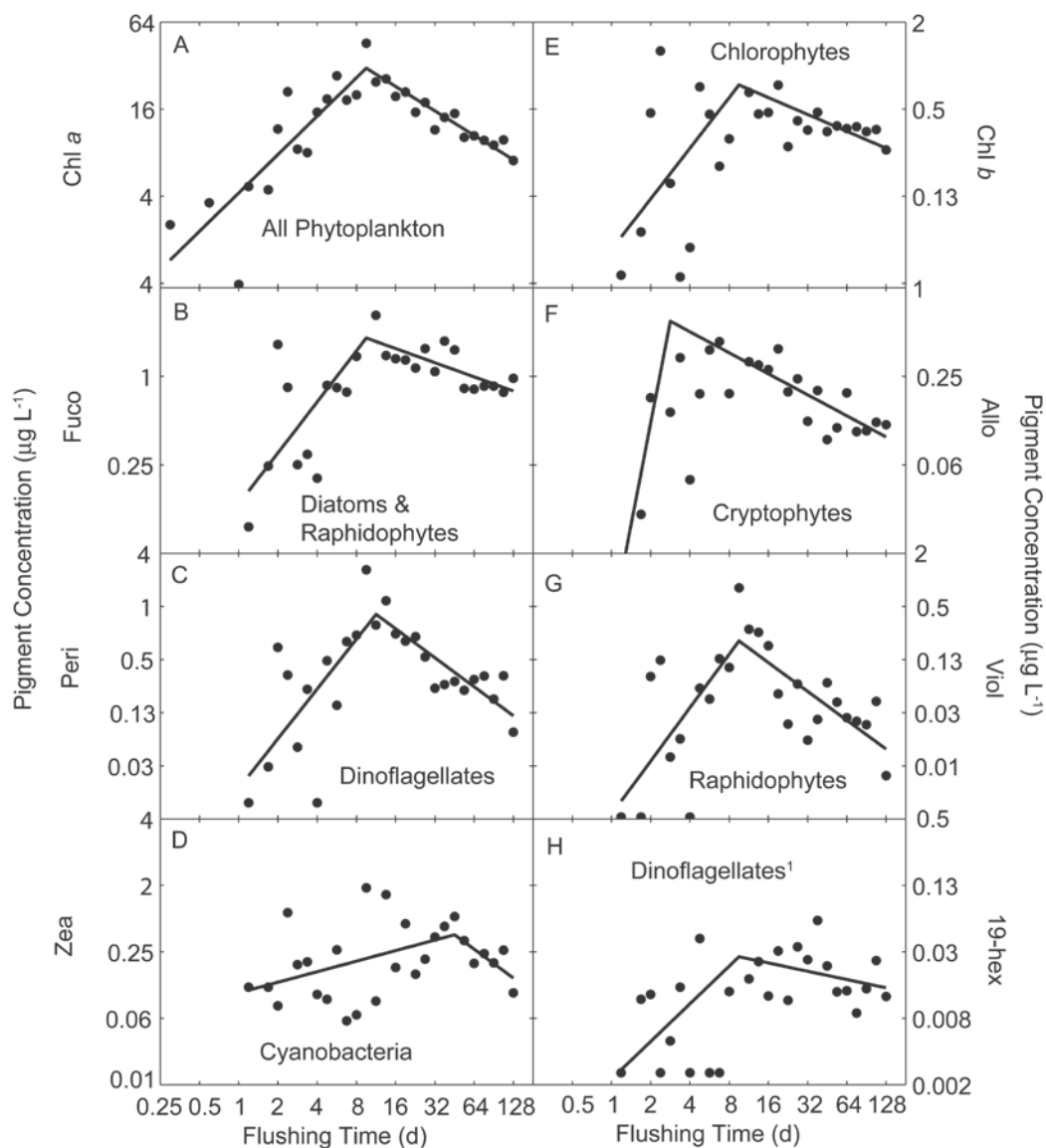


Figure 3-10. Relationship between flushing time and photopigment concentrations indicative of total phytoplankton biomass (chl *a*) and major phytoplankton classes within the NRE.

Pigment abbreviations and phytoplankton groups represented by each pigment are shown in Table 3-1. Data points are mean \log_2 pigment concentrations within each flushing time bin. Solid lines represent segmented linear regressions. ¹19-hex is indicative of dinoflagellates that lack peridinin, primarily *Karlodinium veneticum* in the NRE.

The decline in biomass at longer flushing times is likely due to nutrient limitation (particularly N limitation, see the *Assessment of Nutrient Limitation* section) driven by nutrient uptake near the head of the estuary where maximum biomass was usually observed (Stations 6, 7, and 8 and USGS Station number 0209303205). This strong hydrologic control of phytoplankton biomass points to the need to consider both freshwater discharge and its nutrient load on seasonal and inter-annual time scales because the combined effects of these drivers determine whether blooms, including HABs, develop and where in the estuary blooms are likely to occur. **Figure**

3-11 shows the space-time distribution of blooms in relation to freshwater discharge. Blooms occurred within flows of $0.8\text{--}26.8\text{ m}^3\text{ s}^{-1}$. Flows on the low end of this range tended to allow bloom formation further upstream near Jacksonville and conversely flows on the higher end of this range forced bloom development further downstream.

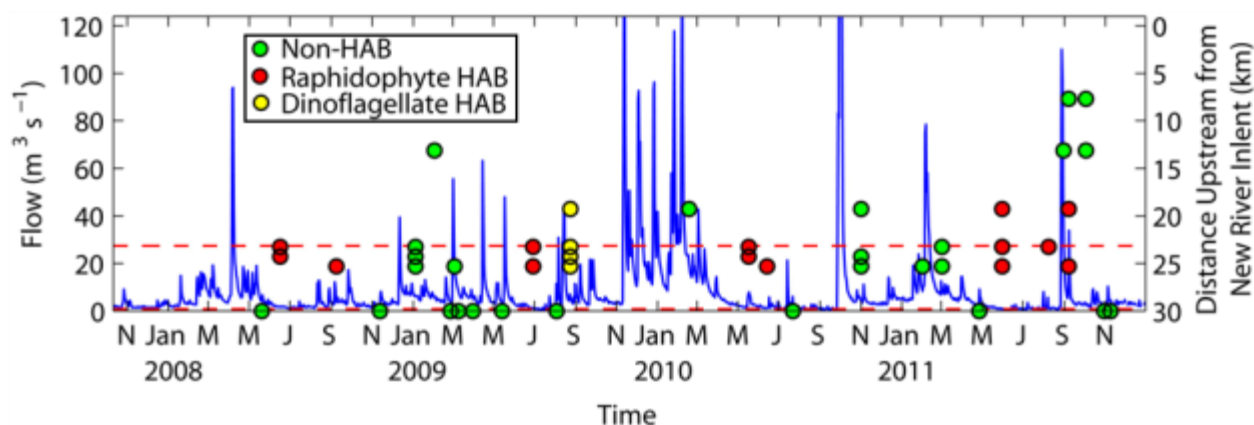


Figure 3-11. Space–time location of HAB and non-HAB blooms in relation to freshwater discharge within the NRE from October 2007 through December 2011.

Red dashed lines indicate the range of flows ($0.8\text{--}26.8\text{ m}^3\text{ s}^{-1}$) under which blooms occurred.

Diagnostic pigments responded in a similar non-monotonic fashion to increases in flushing time. Maximum concentrations of all pigments occurred at flushing times ranging from approximately 2 d to 45 d (**Figure 3-10**). Significant differences in the slopes and breakpoints of these segmented regressions indicate that these flow effects or additional factors that covary with flow have differential impacts across phytoplankton groups (**Table 3-5**). Similar to total phytoplankton biomass and other phytoplankton groups, biomass of the dominant bloom forming classes, dinoflagellates and raphidophytes was restricted at short flushing times (**Figure 3-11C and G**).

These short flushing time conditions (less than 1 week) were accompanied by salinities that are generally lower than approximately 10 (**Figure 3-9**). Because the observed dinoflagellate and raphidophytes species were brackish-tolerant, marine species, it is likely that low salinity would have restricted their biomass accumulation even in the absence of restrictive flushing effects (Sellner et al., 2001). However, as time within the estuary increased (**Figure 3-10**) and salinity conditions became more conducive for growth (**Figure 3-9**), these dominant bloom formers responded more rapidly to the improved growth conditions than other phytoplankton groups. This can be seen in the significantly steeper initial slope of the break point regression of violaxanthin against flushing time (**Figure 3-10 and Table 3-5**) compared to chl *a*. Peridinin exhibited an initial slope that was almost significantly higher than chl *a* (**Table 3-5**).

The fact that these groups were consistently the dominant bloom formers suggests some suite of competitive advantages over other phytoplankton groups that lead to larger net population growth rates. Intrinsic growth rates of these bloom forming flagellates are generally slower than other groups and are generally poor competitors under most growth conditions (Smayda, 1997). However, some species, especially HAB species, may experience lower grazing pressure due to chemical defenses (Graham and Strom, 2010) or their relatively large size (generally greater than

20 μm in diameter; Demir et al., 2008), which can enhance net population growth rates. One commonality among all the observed bloom forming flagellate species is that each species has well documented DVM patterns (Amano et al., 1998; Hall and Paerl, 2011; Jephson et al., 2011).

Table 3-5. Coefficients for regressions of temperature and flushing time on photopigment concentrations.

Pigment	Temperature Effect Linear Regression		Flushing Time Effect Segmented Linear Regression			
	β_{temp} $\log_2(\mu\text{g L}^{-1}) \text{ } ^\circ\text{C}$	R^2_{temp}	Intercept (95% CI)	Slope1 (95% CI)	Breakpoint (95% CI)	Slope2 (95% CI)
Chl <i>a</i>	0.13	0.04*	2.1 (1.5, 2.9)	0.83 (0.60, 1.35)	9.4 (4.0, 11.3)	-0.50 (-0.67, -0.34)
Fuco	0.037	0.04*	-2.9 (-5.0, -1.3)	1.15 (0.49, 5.03)	9.6 (2.0, 26.9)	-0.33 (-0.60, -0.08)
Peri	-0.009	0.02*	-5.9 (-8.1, -4.1)	1.94 (1.18, 2.92)	10.3 (8.0, 13.5)	-0.99 (-1.33, -0.69)
Chl <i>b</i>	0.013	0.12*	-4.2 (-16.8, -2.5)	1.16 (0.38, 15.6)	9.5 (2.0, 19.0)	-0.39 (-0.59, 0.19)
Zea	0.051	0.43*	-3.2 (-4.1, -2.5)	0.32 (0.07, 0.60)	45.3 (19.5, 108)	-0.87 (-9.67, -0.14)
Allo	-0.006	0.004	-8.3 (-22.0, -2.4)	3.25 (0.24, 19.8)	2.4 (1.7, 11.3)	-0.20 (-0.87, -0.01)
Viol	0.017	0.04*	-8.8 (-11.6, -7.5)	2.01 (1.38, 6.51)	9.5 (2.8, 11.3)	-1.09 (-1.41, -0.47)
19-hex	0.005	0.05*	-8.8 (-10.6, -5.3)	1.13 (-1.33, 2.69)	9.5 (2, 38.1)	-0.25 (-1.21, 0.56)

β_{temp} and R^2_{temp} values are the slopes and coefficients of determination from the regressions of pigments on temperature. Asterisk superscripts over R^2_{temp} values indicate significance at $\alpha=0.001$. The regression of temperature against alloxanthin was not significant at $\alpha=0.05$. Intercept, Slope1, Break Point, and Slope2 represent the y-intercept of the first segment, slope of the first segment, flushing time at the break point, and slope of the second segment, respectively. For the segmented linear regression coefficients, values in bold indicate a significant difference between the coefficient for that pigment and total phytoplankton biomass (chl *a*).

Data from the AVPs confirm that DVM is a dominant mode of variability in the depth distribution of chl *a* in the NRE. **Figure 3-12** shows high resolution vertical profiles of density and phytoplankton biomass (in vivo chlorophyll fluorescence) for a 10-day period containing the raphidophyte bloom detected on September 8, 2008 (**Table 3-2**). The up (daytime) and down (nighttime) pattern of DVM is obvious.

To examine the full record of AVP chlorophyll fluorescence profiles, the depth of the chlorophyll maximum in the water column was used as a metric of temporal changes in phytoplankton depth distribution. The depth of the chlorophyll maximum is a useful metric of phytoplankton distribution that is independent of the total phytoplankton biomass within the water column (Denman, 1977). We analyzed the time series of the depth of the chlorophyll maximum with a time series analysis technique called wavelet analysis to identify daily cycles in the depth of the chlorophyll maximum that are indicative of DVM. Similar to traditional Fourier analysis methods, the relatively new wavelet analysis method provides estimates of the power

contained within periodic signals contained within a time series. The advantage of the wavelet analysis method is that it shows where in time a period signal, such as the up-down movements indicative of DVM, occurred in the data record. Through the use of the Morlet wavelet function, it also retains the phase information of each frequency component. The phase information of the diel signal component was processed in a manner such that a phase near zero hours indicates that the phase of the diel signal has the appropriate phase (up during the day, down at night) indicative of DVM (Hall, 2009). In the adjacent Neuse River and Newport River estuaries, much of the variability in physical and biological properties of the water column occur in the semidiurnal to diurnal band, or in the synoptic scale (2–7 d band) (Hall, 2009; Litaker et al., 1987; Reynolds-Fleming and Luettich, 2004). Based on these findings, we investigated a range of frequencies that represent periods from hour up to 14 days to encompass the band likely to be most important for structuring depth distributions of the phytoplankton community.

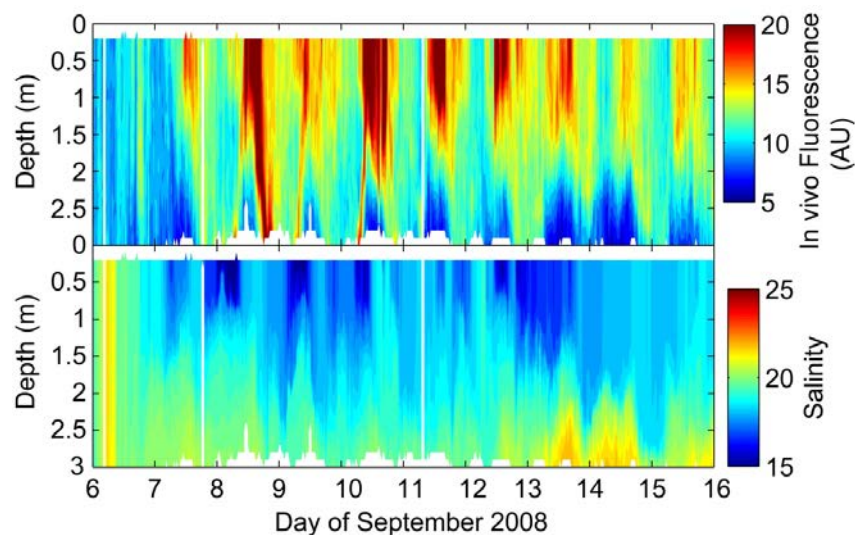


Figure 3-12. Chl *a* in vivo fluorescence and salinity data from the AVP at Morgan Bay over a 10-day period in September 2008.

The *x*-axis tick marks represent midnight of each day. Blank spaces in contour plots represent data gaps. Bottom of data record is approximately 0.25 m above the bottom of the estuarine floor. Chl *a* in vivo fluorescence values are presented as arbitrary units (AUs) because they were not post-calibrated against in vitro chl *a* values.

Figure 3-13 shows a wavelet power spectrum of the time series of the depth of the chl *a* maximum from AVP profiles at Morgan Bay. Most of the time, the dominant frequency component of the depth of the chlorophyll maximum was the diel component (**Figure 3-13**). During periods of high power at the diel frequency, the phase of the signal was close to zero, indicative of the phase expected from DVM (**Figure 3-13**). This indicates that DVM is a very common occurrence in the upper NRE where flagellates are a dominant component of the phytoplankton community.

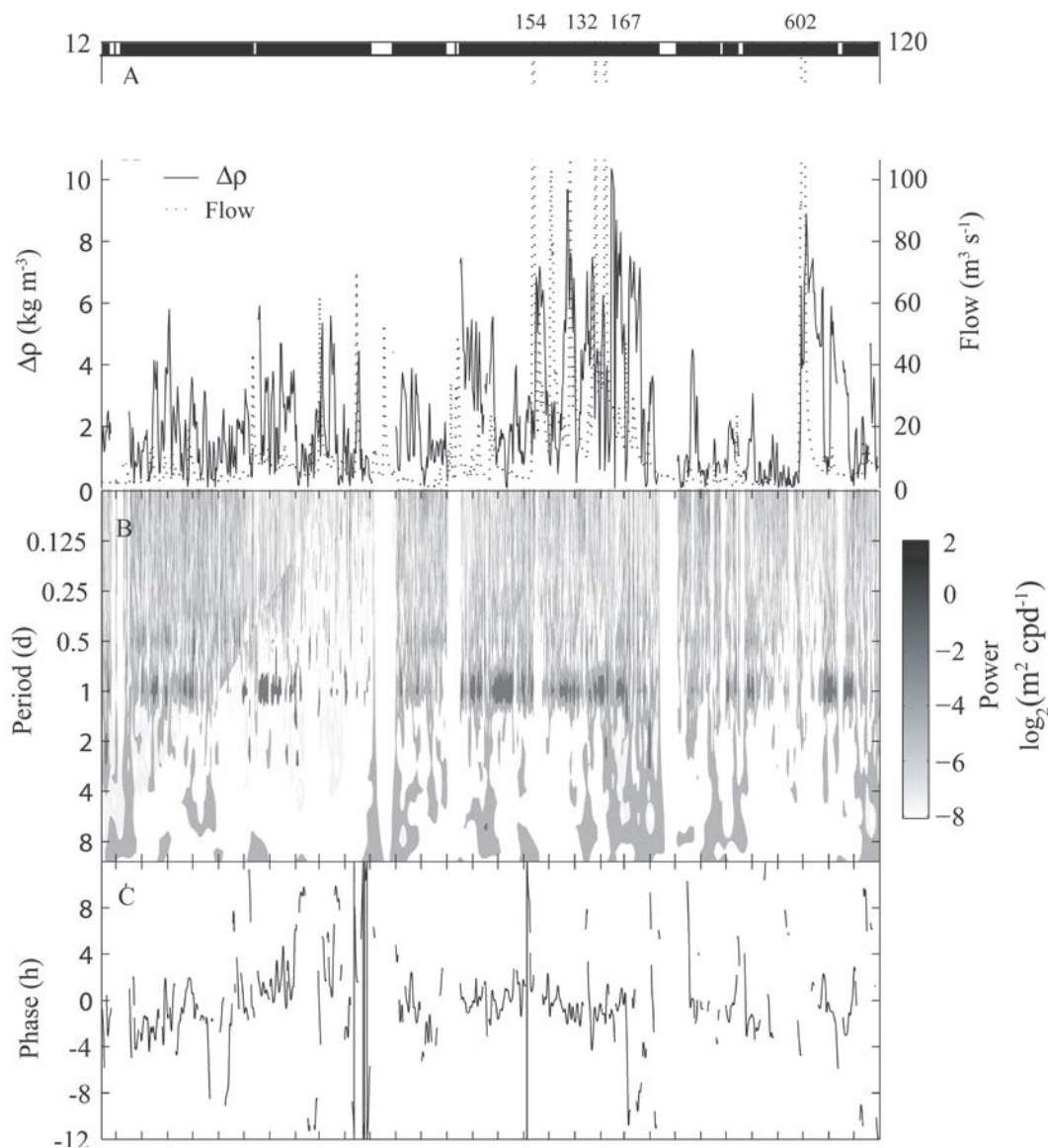


Figure 3-13. Occurrence of DVM patterns of phytoflagellates in relation to water column stratification.

(A) Water column stratification ($\Delta\rho$ = bottom surface density) at the Morgan Bay AVP location from September 2008–December 2010, (B) wavelet power spectrum of the depth of the fluorescence maximum, and (C) the phase of the diel frequency component. A phase near zero is consistent with DVM. White areas in black bar at top of figure represent periods of missing data.

Periods when the DVM signal was weak or not apparent coincided with periods of weak stratification (e.g., October–November 2008 and August–September 2010) or periods of extremely high river discharge (e.g., early November 2009, early October 2010) despite the high degrees of stratification that occurred during these flood events. These results are not surprising because the: (1) swimming velocities of these phytoflagellates are incapable of overcoming the strong vertical mixing necessary to destratify the water column (Hall, 2009) and, (2) biomass of these phytoflagellate groups was severely restricted by flushing losses during the highest flow periods (**Figure 3-10**).

Bloom potentials of raphidophytes and other large motile flagellates are enhanced by the ability to access nutrient rich bottom water or even sediment pore waters at night via their DVM behaviors (Amano et al., 1998; Handy et al., 2005; Watanabe et al., 1995). These DVM patterns, coupled with elevated DIN concentrations deeper in the water column, may mitigate nutrient limitation of the dominant bloom forming groups during periods when riverine nutrient loads are minimal such as during the observed droughts of 2008 and 2011. Maintaining a relatively high biomass during periods of low riverine nutrient input may provide these large flagellate groups a higher inoculum concentration that allows for rapid proliferation following periods of higher riverine nutrient input. Under nutrient-rich, moderate-flow conditions, their ability to vertically migrate can still significantly enhance intrinsic growth rates by providing access to saturating light conditions near the surface (Ault, 2000).

At the population level, daily vertical migration of the dinoflagellates in the water column allows them to maintain their spatial position in the estuary longer by migrating to the deeper bottom waters and riding the more saline water upstream (Anderson and Stolzenbach, 1985; Chang and Carpenter, 1985). In contrast, non-motile drifting species are at the mercy of the surface currents and can more quickly be swept out of the estuary. Our flushing time estimates are representative of the flushing of non-motile drifters but do not capture these more complex interactions between stratified flows and variations in the vertical distribution of motile phytoplankton (Monsen et al., 2002). The observed co-variations between river discharge, flushing time, and stratification, indicate that: (1) nutrient concentrations capable of stimulating biomass accumulation, (2) poor vertical mixing permissive of vertical migration, and (3) two-layer flow conducive to this type of advective loss reduction mechanism often occur simultaneously. Thus, the physical dynamics of the NRE likely plays a large role in determining the dominance of blooms by large, highly motile flagellate species. Results from the BBN model corroborate this assertion by showing a significantly higher probability of occurrence of HAB species under moderately stratified conditions when HABs would be capable of vertically migrating but not under the highest stratification conditions which are accompanied by overwhelming advective losses and prohibitively low salinities in the surface waters (see **Appendix 3-B**).

Prior to sewage treatment upgrades, silica was, at times, potentially limiting (approximately $0.5 \mu\text{mol L}^{-1}$) for the growth of diatoms (Mallin et al., 1997), and silica limitation was suggested as an explanation for flagellate dominance of the NRE. Current silica concentrations ($3\text{--}92 \mu\text{mol L}^{-1}$) are unlikely to limit diatom growth (Dortch and Whitledge, 1992), yet blooms are still dominated by flagellates, including some HAB species. Rather than nutrient stoichiometry, it seems more likely that selective advantages gained by motility explain why blooms in this estuary are dominated by flagellates. These advantages allow such bloom forming flagellates to assimilate a large portion of the riverine nutrient load. Nutrient reduction strategies should limit the levels of biomass attained by these bloom-formers, but phytoflagellates, including some HAB species, are still likely to be dominant members of the phytoplankton community.

The picocyanobacteria, indicated by the pigment zeaxanthin, reached a maximum at a significantly longer flushing time than most groups (**Figure 3-11D**). The small size and low nutrient demands of picocyanobacteria make them particularly well suited for growth on low concentrations of regenerated nutrients that existed under higher salinity and longer flushing time conditions in the NRE (Wetz et al., 2011b). Cryptophytes, indicated by alloxanthin, were a

significant, though rarely dominant, component of the phytoplankton community. Cryptophytes showed maxima under relatively fresh conditions associated with short flushing times (**Figure 3-11F**). This is consistent with results from the nearby Neuse River Estuary where cryptophyte biomass is generally highest during high river flow conditions (Valdes-Weaver et al., 2006). Chlorophytes, indicated by chl *b*, were relatively minor components of the NRE community and their response to changes in flushing time was weaker than many of the other groups (**Figure 3-11E**). This may be due to the wide variety of physiological characteristics exhibited by the mix of freshwater and marine species within the NRE.

Assessment of Temperature Control

A weak but positive relationship with temperature was also common among phytoplankton classes as determined by class-level photopigments (**Table 3-4**). Alloxanthin (cryptophytes) was the only pigment that did not show a significant temperature relationship (**Table 3-4**) and peridinin (dinoflagellates) was the only pigment with a significant negative relationship with temperature. The positive correlation of zeaxanthin (primarily picocyanobacteria) with temperature was exceptionally strong, accounting for 42% of its variability, a pattern clearly visible in the space-time contour plots shown in **Figure 3-7E**. These results are consistent with geographically diverse observations that cyanobacteria prefer warmer waters for optimal growth (Paerl and Huisman, 2009). However, there is some evidence from the nearby Neuse River Estuary that seasonal changes in grazer populations may produce observed summertime increases in picocyanobacteria through a trophic cascade mechanism. Summertime increases in the crustacean mesozooplankton populations (primarily copepods) substantially deplete microzooplankton grazers of picocyanobacteria with resultant alleviation of grazing pressure and enhanced population growth of the picocyanobacteria (Wetz et al., 2011b).

Raphidophyte blooms also demonstrated a distinct seasonality with blooms occurring only during the warmer months from late May through September (**Table 3-2** and **Figure 3-11**). This is corroborated by the positive relationship between temperature and the pigment violaxanthin (**Table 3-4**). During each of the 4 years, the period from mid-May through mid-June exhibited a raphidophyte bloom (**Table 3-2**). This repeatable timing likely results from the seasonal inoculation of the water column by germination of cysts in the sediments as water temperatures increase during the spring (Imai and Yamaguchi, 2012; Yamaguchi et al., 2008).

Harmful Algal Blooms

The raphidophytes and the dinoflagellate, *Karlodinium veneficum*, are considered HAB species (Moestrup et al., 2011) due to the ability of some strains to produce toxins that negatively impact growth and reproduction of filter feeders and can kill fish (Bourdelaïs et al., 2002; Lewitus et al., 2003). *K. veneficum* produces karlotoxins that cause asphyxiation in fish by destroying the epithelial cells of the gills (Deeds et al., 2002). *K. veneficum* was found in low abundances throughout the NRE but was only a prominent component of an algal bloom on one occasion, August 29, 2009 (**Table 3-2** and **Figure 3-11**). Even during this bloom, concentrations of *K. veneficum* were less than half of the 30×10^7 cells L⁻¹ typically associated with fish kills in North Carolina estuaries (Fensin, 2004).

The cell abundances of raphidophytes and regularity of their occurrence within the NRE are of particular concern. Marine raphidophytes contain an assortment of poorly characterized toxins that have been responsible large-scale fish-kill events in coastal waters around the world (Jeong, 2011). The highest observed bloom concentration of greater than 20×10^6 cells L⁻¹ observed on June 16, 2008 is 2- to 10-fold higher than concentrations associated with fish kills in Delaware's inland bays (Bourdelaïs et al., 2002).

Cellular toxin levels of *Karlodinium veneficum* and raphidophyte species vary greatly by strain and with changes in physiological condition (Adolf et al., 2009; Powers et al., 2012). We are unaware of any incidences of fish kills or human illness caused by these blooms which may indicate low levels of toxins within the particular bloom strains. However, fish kills possibly caused by HABs have occurred in the past within the upper (near Jacksonville) region of the NRE (Tomas et al., 2007).

Table 3-6. Concentrations of total microcystin toxins in surface waters of the upper NRE during late summer–early fall 2008.

Date	Site	Total Microcystins (µg L ⁻¹)
August 7, 2008	USGS number 02093000	0.030 ±0.017
August 7, 2008	USGS number 020903205	0.095 ±0.054
August 14, 2008	New River Station 5	0.179 ±0.060
August 14, 2008	New River Station 6	0.231 ±0.040
August 14, 2008	New River Station 7	0.110 ±0.029
August 14, 2008	New River Station 8	0.090 ±0.014
September 8, 2008	New River Station 5	0.122 ±0.025
September 8, 2008	New River Station 6	0.123 ±0.022
September 8, 2008	New River Station 7	0.093 ±0.038
September 8, 2008	New River Station 8	0.142 ±0.023
October 7, 2008	New River Station 5	0.111 ±0.045
October 7, 2008	New River Station 6	0.108 ±0.022
October 7, 2008	New River Station 7	0.241 ±0.026
October 7, 2008	New River Station 8	0.195 ±0.039
November 3, 2008	New River Station 5	0.201 ±0.030
November 3, 2008	New River Station 6	0.251 ±0.037
November 3, 2008	New River Station 7	0.236 ±0.033
November 3, 2008	New River Station 8	0.255 ±0.026

Bloom potentials of CyanoHAB genera were assessed using high sensitivity PCR amplification and sequencing of cyanobacterial 16S rDNA from samples collected from summer through fall 2008 within the upper estuary (Stations 5–8). The resulting 16S rDNA sequence analyses revealed that potentially toxigenic cyanobacteria, such as *Anabaena* sp. and *Microcystis* sp. exist within the upper reaches of the NRE. *Microcystis* is a common freshwater bloom forming cyanobacterial genus that is also relatively salt tolerant, being able to survive in waters with

salinities up to 17 (Tonk et al., 2007). *Anabaena* strains are differentially tolerant of salinity, with some strains being very sensitive to increases in salinity, whereas others thrive in brackish waters (Fernandes et al., 1993). PCR amplification of the microcystin production gene, *mcyB*, routinely failed to amplify DNA extracted from samples collected from these NRE Stations 5–8, even during the peak summer months. The apparent discrepancy that the 16S rRNA analysis detected potential microcystin-producing genera, while the *mcyB* PCR assays failed to yield a positive result can likely be attributed to differences in copy numbers of these genes within the cells. Many copies of “housekeeping” genes such as 16S rRNA are present, but only one or two copies of the *mcyB* generally occurs (Klappenbach et al., 2000; Tanabe et al., 2004).

The failure to amplify the *mcyB* gene provides a useful means to quantify the maximum cell abundances of these CyanoHABs. The limit of detection for *mcyB* primer sets is approximately 10 cells. On average, 100 mL of NRE water is passed through each filter. Therefore, the primers’ failure to amplify suggests that these potentially toxic CyanoHAB species are present at concentrations less than 100 cells L⁻¹. CyanoHAB concentrations less than 100 cells L⁻¹ pose little risk of negative ecological impacts and no documented human health hazard (Chorus and Bartram, 1999). *Microcystis* and *Anabaena* were not observed during microscopic examination of blooms (Hall, personal observation), which further corroborates the conclusion that these CyanoHAB genera are rare in the NRE. However, *Anabaenopsis* sp., a microcystin containing CyanoHAB genus closely related to *Anabaena* (Chorus and Bartram, 1999), was observed at low concentrations during the raphidophyte bloom detected on June 14, 2010 at Station 7 (**Table 3-3**) (Altman and Paerl, 2012).

The average total microcystin concentrations observed at the four least saline stations (5–8) was 0.15 ±0.08, 0.12 ±0.03, 0.16 ±0.06, and 0.24 ±0.04 µg l⁻¹, respectively. These values are remarkably similar considering that they encompass both wet and warm months (August and September) and cool and dry months (October and November). The highest one time microcystin value observed was 0.275 µg L⁻¹ and occurred in October 2008 at Station 7 (**Table 3-5**). All of the values collected during the late summer–early fall period to date have been well below 1 µg l⁻¹, the World Health Organization’s recommended maximum exposure limit for microcystins in drinking water, and far below the 10 µg L⁻¹ limit for recreational waters (Chorus and Bartram, 1999). Due to the low observed concentrations, measurement of microcystin toxin concentration was not continued further. Although these toxin producing CyanoHAB groups are rare, results suggest that there is the potential for toxic blooms to form because these genera exist within the NRE system. They are consistently present at very low cell concentrations and their bloom potentials are presumably controlled by factors other than temperature and rainfall, such as flushing time, nutrient (N and P) availability, and/or salinity.

Many of the other observed bloom forming species within the dinoflagellates (other than *Karlodinium veneficum*), the euglenophytes, the cryptophytes, and the diatoms are not listed as HAB species (Moestrup et al., 2011). However, high biomass blooms of any type can have major detrimental consequences on estuarine ecosystems including reduced light penetration (important for BMA and seagrass communities), and enhanced vertical carbon flux, which fuels bottom water hypoxia (Paerl et al., 1998).

Phytoplankton Primary Production

Spatial and inter-annual variability in phytoplankton primary production

Over the period from October 2007 through December 2011, annual average phytoplankton production for the NRE was $146 \text{ g C m}^{-2} \text{ y}^{-1}$ (**Table 3-7**). This level of phytoplankton production is comparable to other systems with similar N loads (**Figure 3-14**). Between years and between sections of the NRE, productivity varied approximately 2 fold (**Table 3-7**). As will be shown below, both the spatial and inter-annual variability are largely governed by levels of phytoplankton biomass which is largely governed by the counteractive effects of biomass stimulating riverine nutrient loads and biomass losses due to enhanced flushing rates.

Table 3-7. Annual areal phytoplankton primary production for segments of the NRE ($\text{g C m}^{-2} \text{ y}^{-1}$).

Section of NRE	Phytoplankton					
	2007	2008	2009	2010	2011	Average 2007–2011
Whole estuary	85	102	154	156	186	146
Lower (Stations 1–2)	45	64	74	70	122	80
Middle (Stations 3–4)	74	89	123	132	168	125
Upper (Stations 5–USGS Gage number 020903205)	96	123	201	198	217	179

Comparison of Phytoplankton Production with Benthic Microalgal and Salt Marsh Production

Estimates of annual primary productivity of the three major primary producer categories, phytoplankton, BMA, and salt marsh were produced for the lower, middle, and upper estuary segments. Production by sea grasses and macroalgae were not measured because their areal coverage is negligible within the NRE. BMA production estimates were produced by Research Project AE-3. Salt marsh production was estimated by the Coastal Wetlands Module (Research Projects CW-1 and CW-2) based on measured marsh area and areal production for the two dominant marsh grasses, *Spartina alterniflora* ($396 \text{ g C m}^{-2} \text{ y}^{-1}$) and *Juncus roemerianus* ($450 \text{ g C m}^{-2} \text{ y}^{-1}$). The lower estuary is dominated by *Spartina alterniflora* while the upper and middle estuary marshes are dominated by *Juncus roemerianus*. Estimates of marsh production assume 100% dominance by either of the two species within the three estuarine segments, and include aboveground and belowground production.

On an estuary-wide basis, phytoplankton primary production (12,848 metric tons per year) is ~40% higher than BMA production (9,152 metric tons per year) (**Table 3-8**). Marsh area is greater in the lower estuary where it constitutes a sizeable fraction (12%) of total primary production (**Table 3-8**). However, the small areal coverage of marshes in the middle and upper

sections result in salt marshes producing only about 1% of total production for these sections and only about 3% of the total estuarine production (**Table 3-8**). It is important to note that only 13% of the total marsh area within MCBCL lies upriver of the Intracoastal Waterway (i.e. within the NRE) and that the relative importance of marsh production is much higher along the Intracoastal Waterway and inlet region.

Table 3-8. Comparison of phytoplankton, BMA, and salt marsh production for segments of the NRE over the study period^a (10^6 g C y^{-1}).

Section of NRE	Phytoplankton Production	BMA Production	Salt Marsh Production
Whole estuary	12,848 (57)	9,152 (40)	605 (3)
Lower (Stations 1–2)	760 (26)	1,777 (62)	348 (12)
Middle (Stations 3–4)	4,654 (56)	3,537 (43)	113 (1)
Upper (Stations 5–USGS Gage number 020903205 ^b)	7,357 (58)	3,329 (31)	144 (1)

Values in parentheses are the percentages of total production by each producer type.

^a Average production for the period October 2007 –December 2011.

^b Phytoplankton productivity at USGS station number 0209303205 was estimated based on measured chl *a* values and the regression between primary productivity and chl *a* shown in Figure 3-17a.

Collectively, the data indicate that microalgal production (phytoplankton and BMA) constitutes the vast majority (greater than 99%) of total primary production within the NRE. Spatially, areal phytoplankton production is nearly double BMA production in the upper sections of the estuary (**Table 3-8**) where phytoplankton biomass is higher due to the direct influence of riverine nutrient inputs. BMA production is more than double phytoplankton production in the lower estuary (**Table 3-8**) where waters are clearer and adequate light levels reach a greater portion of the benthos (**Figure 3-14**).

Downstream increases in water clarity are the result of decreases in both phytoplankton biomass and CDOM (**Figure 3-14**). TSS are highest at the most downstream stations where tidal velocities are strongest and cause frequent resuspension events (Hall et al., in review). However, the most upstream stations exhibit higher TSS than mid-estuarine stations which indicates riverine-derived TSS is also important. Riverine inputs of CDOM occur naturally due to the swampy head waters of the New River. Tidal resuspension of sediment is also beyond the control of Base managers. However, chl *a* and riverine derived suspended sediments may be mitigated by management actions (on the Base or upstream) that reduce nutrient and sediment loads to the New River upstream of the NRE.

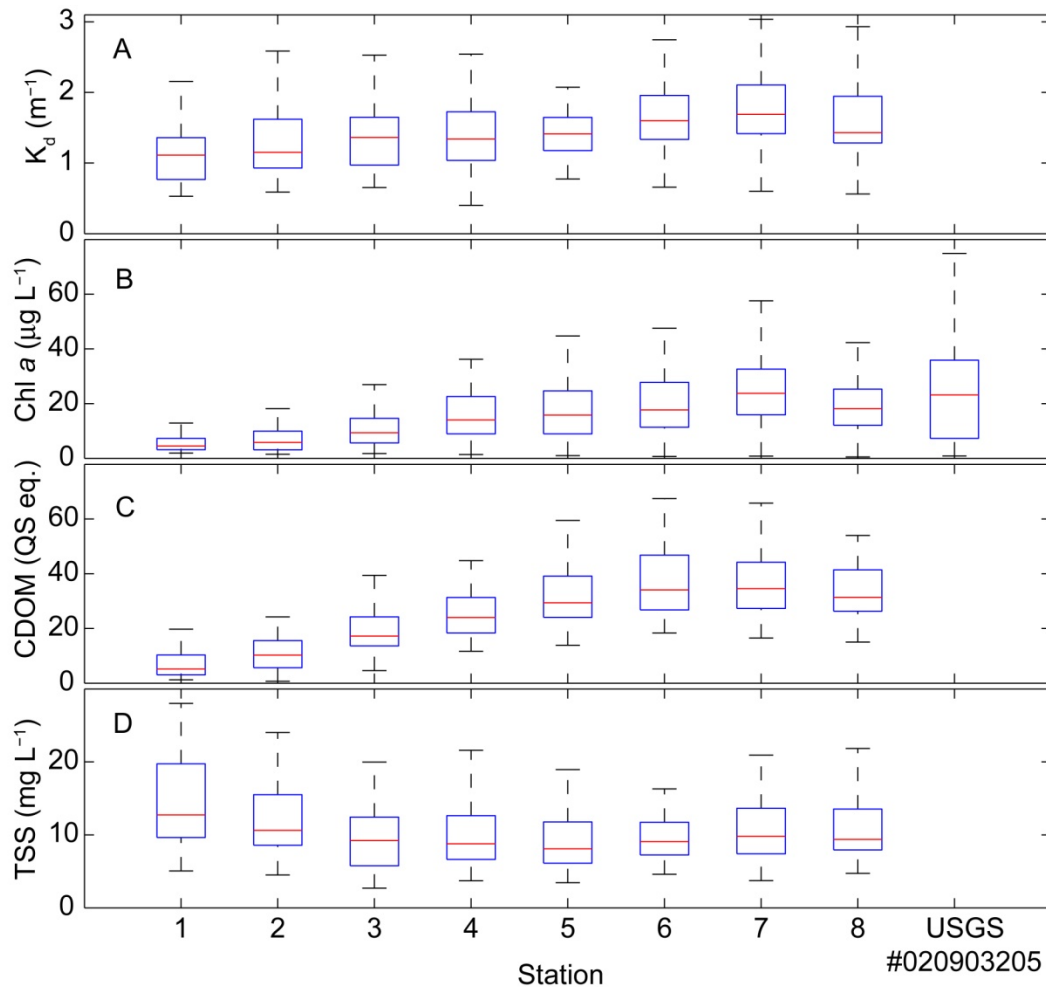


Figure 3-14. Down-stream gradients of light attenuation and concentrations of optically active constituents.

Box plots of (a) the light attenuation coefficient (K_d) and the optically active constituents that contribute to light attenuation, (b) chl *a*, (c) CDOM in units of quinine sulfate equivalents ($\mu\text{g L}^{-1}$), and (d) TSS. Red lines represent median values. Boxes represent interquartile range and whiskers are 1.5 times the interquartile range.

Relationship Between Phytoplankton Production and Nutrient Loading

River discharge largely controlled N and P loading to the estuary (**Figure 3-15**), and inter-annual variability in nutrient loading can partly explain observed inter-annual variability in phytoplankton productivity. Years of higher flow and loading generally had higher areal production (**Figure 3-16**). The exception to this trend was 2011 which had higher productivity than all other years despite lower N loads (**Figure 3-16**). This suggests that internally generated nutrient loads are also highly important, a feature common of shallow eutrophic estuaries (Fisher et al., 1982). Spatially, upstream regions of the NRE exhibited higher production than downstream regions (**Table 3-7**). This trend is directly linked to the higher levels of riverine nutrient loads that fuel higher phytoplankton biomass in this upstream region (**Figure 3-6**).

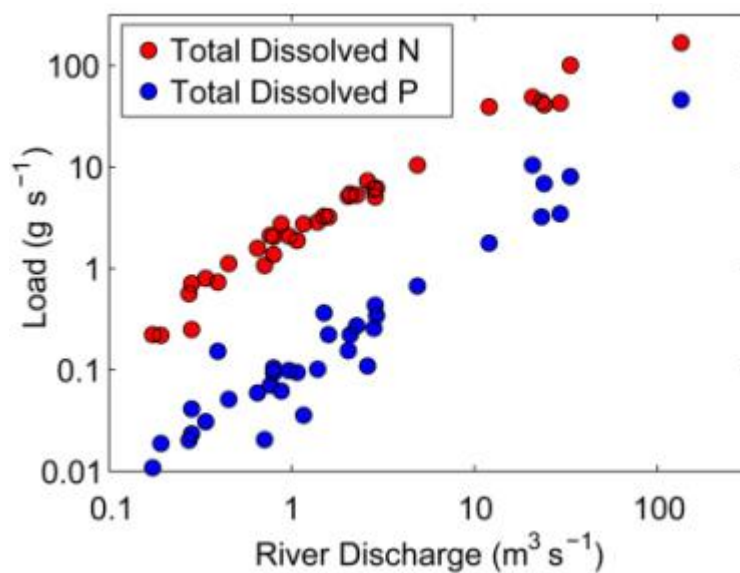


Figure 3-15. Relationship between New River discharge and instantaneous loads of total dissolved nitrogen and total dissolved P at Gum Branch.

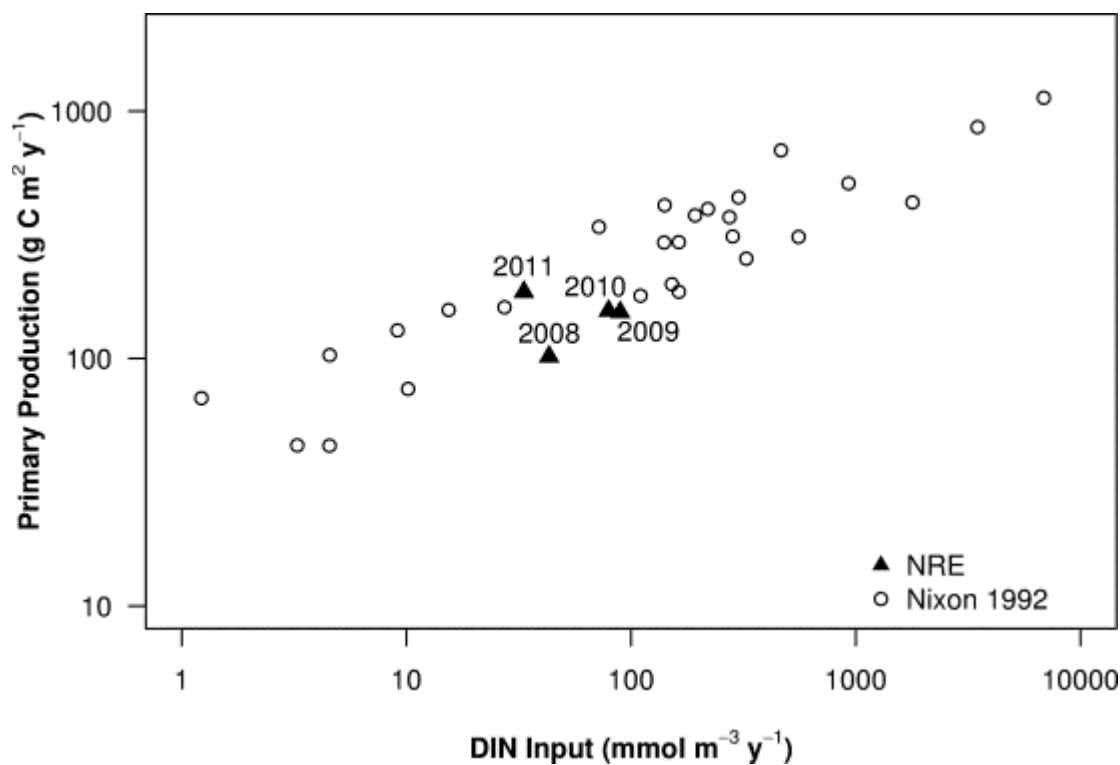


Figure 3-16. Annual average areal phytoplankton production versus annual volumetric DIN load from the NRE and other estuarine systems.

Data other than from the NRE were compiled by Nixon (1992).

Relationship Between Phytoplankton Productivity and Phytoplankton Biomass

Primary productivity showed a reasonably linear relationship ($R^2=0.54$) with chl *a* (**Figure 3-17A**). The slope of the relationship between primary productivity (P^b) provides a measure of the biomass specific productivity of the phytoplankton. The average P^b determined by the regression in **Figure 3-17A** ($P^b=1.2 \text{ g C g chl } a^{-1} \text{ h}^{-1}$) is within the range of biomass normalized productivity of other estuarine systems under near light-saturated incubation conditions (Boyer et al., 1993; Hall and Paerl, 2011). Because phytoplankton primary production was so closely tied to biomass (chl *a*; **Figure 3-17A**), understanding the factors that control phytoplankton biomass accumulation is critical for a first order understanding of pelagic primary production of the NRE. Variability in river flow and its dual impact on nutrient delivery and flushing losses of the phytoplankton community are thus key determinants of both phytoplankton biomass and primary productivity.

Although it is difficult to see in **Figure 3-17A**, part of the unexplained variability in productivity is a trend toward a reduction in P^b (productivity normalized to chl *a*) as chl *a* increases. This trend is evident in a plot of P^b versus chl *a* (**Figure 3-17B**). This type of reduced photosynthetic efficiency has been previously observed during *Cochlodinium polykrikoides* (Dinophyceae) blooms in the lower Chesapeake Bay (Mullholland et al., 2009), where it was also suggested that the cells may have been severely light limited due to self-shading and possibly satisfied their carbon demand through mixotrophic feeding upon other phytoplankton. Due to the small size of the productivity incubation bottles (maximum light transmission length of approximately 10 cm) even large changes in light attenuation associated with bloom biomass would have a minimal effect on photon flux density. Therefore, it is unlikely that self-shading caused these decreases in photosynthetic performance. It seems more likely that the reduction in P^b is due to an increasing level of nutrient limitation under high biomass conditions.

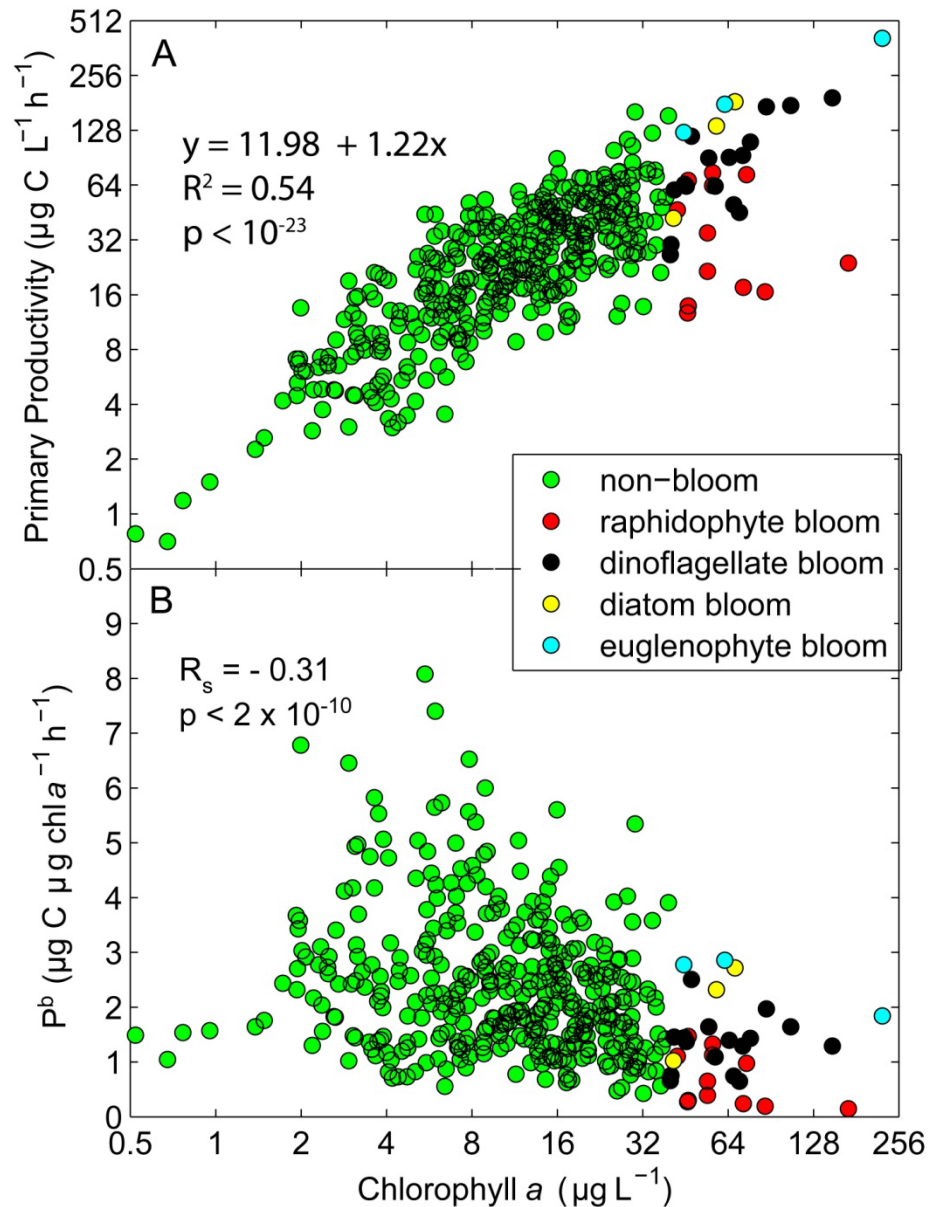


Figure 3-17. (A) Linkage between chl a and primary productivity within NRE surface waters. Results are plotted log-log for visualization purposes but the regression was performed on non-transformed values. R^2 and p values are from a Pearson's correlation. Identity of the dominant phytoplankton class within bloom samples (chl a greater than $40 \mu\text{g L}^{-1}$) is indicated by symbol color. (B) Biomass normalized productivity (P^b) versus chl a . R_s and p values are from a Spearman's rank correlation. $N=432$ for both panels.

Compared to blooms dominated by other phytoplankton classes, blooms dominated by raphidophytes showed the greatest degree of depression of P^b (**Figure 3-17A**). It is unclear what caused the anomalously low photosynthetic performance of these raphidophyte blooms. In culture, maximum P^b of the raphidophyte *Heterosigma akashiwo* is approximately $4 \text{ g C g chl } a^{-1} \text{ h}^{-1}$ (Fredrickson et al., 2011). This is much higher than what we observed and also suggests that low photosynthetic performance is not a trait common to the class. Artifacts due to handling and

isolation from the remainder of the water column may be responsible. Raphidophytes are notoriously fragile, and cells may have been damaged during collection, transport, or dispensing into bottles associated with ^{14}C incubations (Connell and Catollico, 1996; C. Tomas personal communication). Additionally, isolation of raphidophytes from the remainder of the water column over the period from sample collection to productivity determination (a time span of up to 24 hours) may have particularly exacerbated nutrient limitation of the raphidophytes which vertically migrate deeper into the water column at night where nutrient availability is generally higher. Within the productivity assay methodology, an extended period of isolation from the remainder of the water column is unavoidable, due to the fact that only a short period of weak daylight remains after a sampling trip. However, this artificial isolation of the phytoplankton community from regenerated nutrient supplies from deeper in the water column may be an important factor determining the decrease in P^b with increasing biomass that was exhibited on a community level by the phytoplankton.

To determine whether this nearly 24-hour isolation from the remainder of the water column causes a decrease in P^b , a modified primary productivity assay experiment was performed on May 3, 2012. Surface water samples were collected from Stations 6, 7, and 8 at 07:00, 07:15, and 06:45 in the morning, respectively. This early morning collection allowed sufficient time for setting up the midday (10:00 a.m. to 14:00 p.m. EST) ^{14}C primary productivity assays on the same day as the water was collected. Sample water was stored in 4-L polyethylene bottles in the same manner as would be performed after a routine monthly sampling expedition. On the following day, productivity assays were performed again on the day old water. The comparison of P^b from the freshly collected sample water against P^b from the day-old sample water allowed a direct comparison of the impacts of the nearly day-long storage that accompanies the routine productivity assay methodology.

A two-way ANOVA with station and day as factors was used to determine whether there were significant differences in the means of triplicate values of P^b produced by the productivity assays performed on the day of collection (Day 1) and day following collection (Day 2). ANOVA results showed that the time lapse effect was not a significant factor ($p > 0.05$). Additionally, the response between stations was not consistent. At Stations 6 and 7, P^b actually increased slightly after a day of sample storage, whereas at Station 8, there was a slight decrease. Light levels between the 2 days were similar and were actually slightly higher on Day 1 when two of the three stations had a slightly lower P^b . This indicates that differences in light regime were unlikely to have masked changes in photosynthetic efficiency between the 2 days. In general, the experiment demonstrated that a 24-hour isolation of the phytoplankton community from the water column had no significant effect on the photosynthetic efficiency of the phytoplankton community. However, it should be noted that the samples collected for this experiment were not bloom samples. Chl *a* ranged from 9-14 $\mu\text{g L}^{-1}$ between the three stations and did not change significantly between the 2 days (p value from ANOVA of station and day on chl *a* > 0.05). At this level of chl *a*, P^b values (approximately 4 g C g chl *a* $^{-1}$ h $^{-1}$) are consistent with those observed during the routine monthly productivity assays (**Figure 3-17B**) and depressions in photosynthetic efficiency are not observed. Similar experiments that capture true bloom conditions will be necessary to further examine this issue.

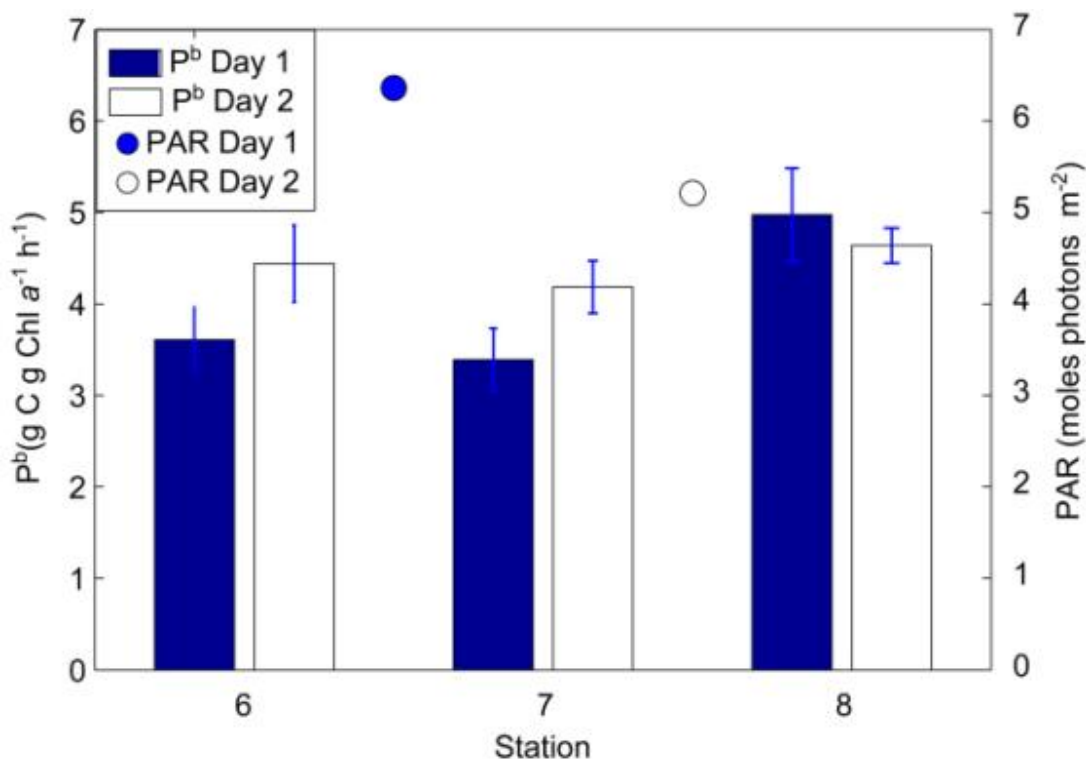


Figure 3-18. Comparison of phytoplankton photosynthetic performance (P^b) of samples incubated on the day of collection and day after collection.

Error bars represent one standard deviation of triplicate values. Circles represent total flux of PAR during the incubations.

Assessment of Nutrient Limitation

In situ nutrient addition bioassays were conducted during the maximum productivity and bloom periods, June and September 2008–2010. A complete display of the chl *a* responses to nutrient addition bioassays is located in the Supplementary Information. Results indicated that N was the nutrient most consistently controlling phytoplankton growth (**Figures 3-19 and 3-20**). At times (see example data from June 2008, **Figure 3-19**), N and P additions together yielded slightly higher degrees of algal biomass stimulation than N alone. However, N usually had to be added first to obtain co-stimulation with P (**Figure 3-19**). P additions alone never stimulated algal production at these bioassays that were conducted from water collected from Stations 3 and 5 (**Figure 3-20**). However, a single bioassay performed using water collected at Station 7 showed that heterocystous cyanobacteria (*Anabaenopsis sp.*) became dominant in the P addition treatment (**Figure 3-21**, for further details, see Altman and Paerl, 2012). In this experiment, cyanobacterial dominance due to P addition was observed only after a lengthy 8-day incubation period which is consistent with a low original concentration of the cyanobacterium. Results from this experiment suggest that increases in P loading to this predominantly N-limited estuary may stimulate growth of these N-fixing cyanobacteria that are currently low in abundance (Altman and Paerl, 2012).

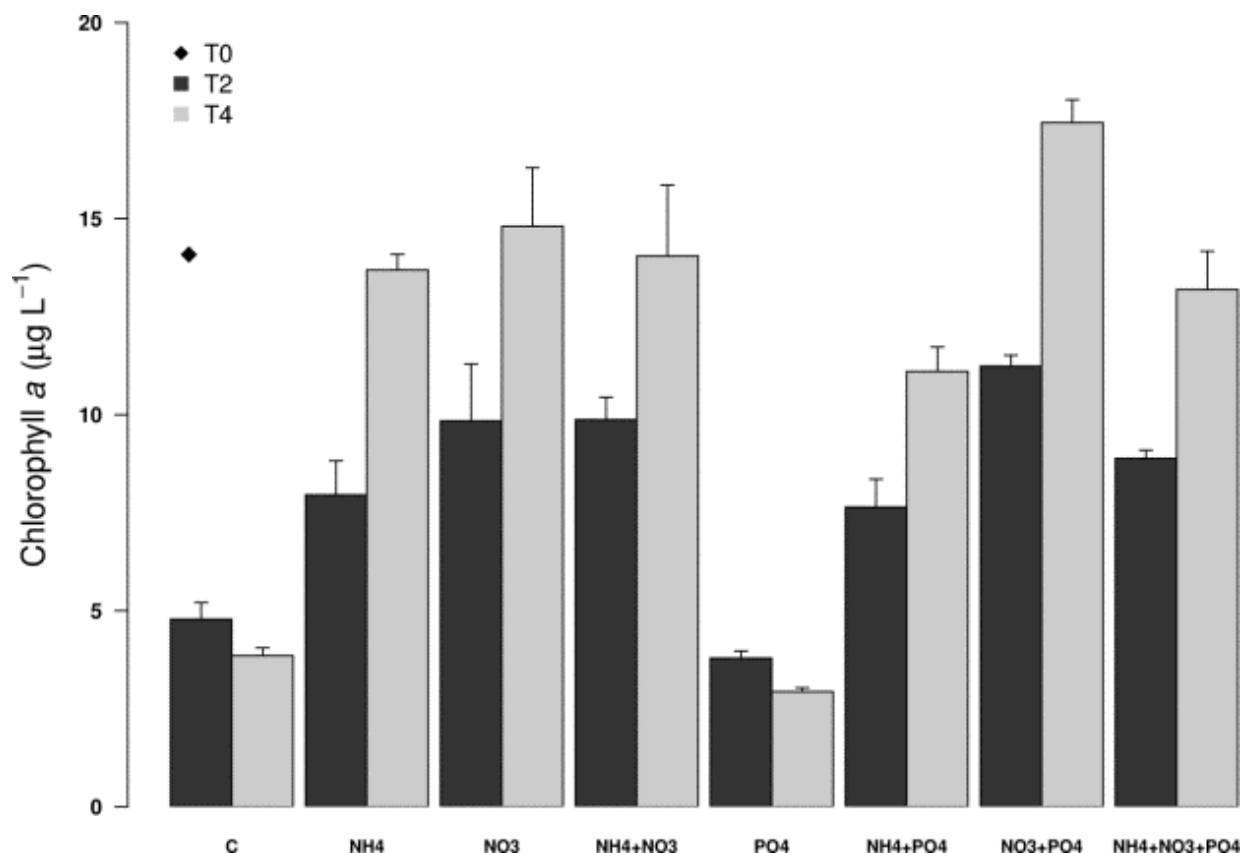


Figure 3-19. Example results from an in situ nutrient addition bioassays conducted on NRE natural phytoplankton assemblages from stations on June 3, 2008.

Bars represent means of each treatment. Error bars are standard error of the mean. Growth responses to various individual and combined N and P additions were measured as chl *a* concentrations. Results from all six bioassays were similar.

Additionally, it is also possible that P limitation occurred during cooler months and therefore was not detected with the June and September bioassays. Water and surface sediment temperatures during these warm periods lead to large releases of P from the sediments of shallow estuaries which can enhance N limitation (Fisher et al., 1982). Seasonal P co-limitation may occur during winter and spring months as in other shallow, temperate estuaries (Paerl et al., 1995; Rudek et al., 1991). However, the consistent N limitation during the warm months does suggest that N reductions will be most effective at mitigating the occurrence of HABs which were most common during warm months. This result is of particular relevance to inputs from the NRE watershed upstream of the Highway 17 bridge at Jacksonville, which dominate overall nutrient loading to the NRE.

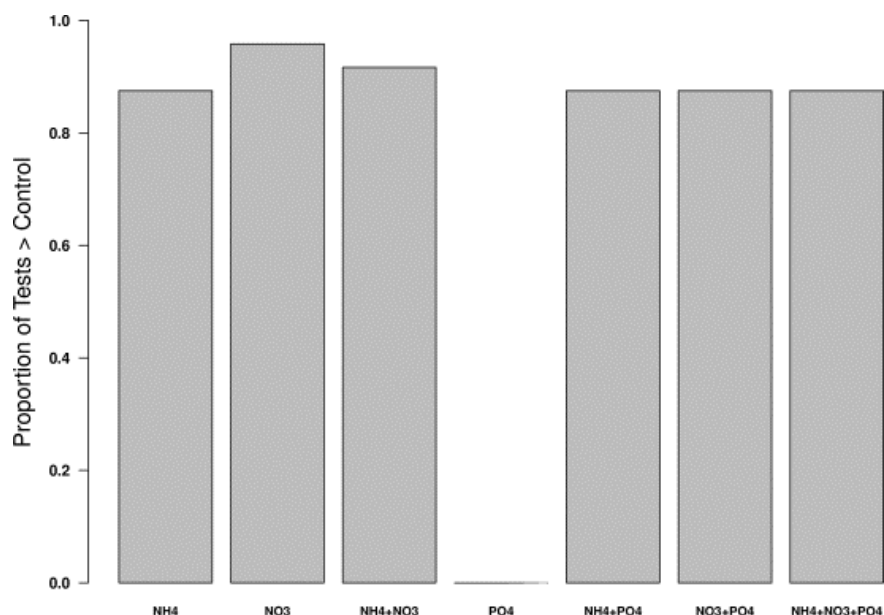


Figure 3-20. Frequency of observed phytoplankton biomass stimulation by nutrient amendments across all six bioassay time points, at Stations 3 and 5, and on Days 2 and 4 of each bioassay experiment (N=24).

Significant stimulation responses were defined as a significant ($\alpha < 0.05$) Kruskal-Wallis comparison of between group versus within group variability followed by a significant post-hoc comparison of median values of treatment versus control.

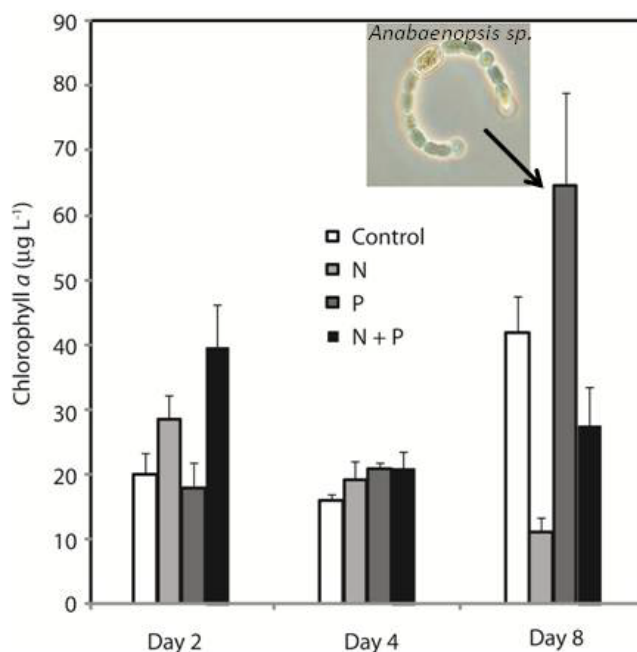


Figure 3-21. Phytoplankton biomass response to nutrient additions in water collected from Station 7 on June 14, 2010.

Inset image is a photomicrograph of the heterocystous cyanobacteria that dominated the P addition treatment on Day 8 of the bioassay incubation.

Comparison of Chlorophyll *a* with State and National Water Quality Assessment Criteria

North Carolina Criteria

The North Carolina “acceptable” water quality standard for chl *a* is 40 µg L⁻¹ (NCDENR, 2007). Occasional blooms that exceed this standard are likely to occur, even in pristine surface waters. Recognizing this fact, NCDENR has adopted the 10/40 criterion for chl *a*, which allows 10% of samples from a water body to exceed 40 µg L⁻¹ chl *a* without determining that the water body is in violation of the standard. Statistical confidence in determining whether observed exceedance percentages are greater or less than the 10% criterion is not currently considered by NCDENR. However, statistical confidence is readily calculated from the binomial distribution and is a valuable tool for assessing the robustness of any compliance determination (McBride and Ellis 2001; Smith et al., 2001).

For samples collected throughout the whole estuary from October 2007 through December 2011, 53 of the total 866 (6.0%) surface and bottom water samples contained a chl *a* concentration greater than 40 µg L⁻¹. This frequency (6.0%) is significantly lower ($p < 0.05$) than the 10% criterion established by NCDENR (**Table 3-9**). However, if just the surface water samples are considered, the frequency rises to 7.9%, a frequency that is not significantly different from 10%.

Significant spatial variability in the proportion of chl *a* samples greater than 40 µg L⁻¹ existed. Middle and lower stations (Stations 1–4) met the State standard. However, for the middle estuary stations, statistical confidence that chl *a* levels were below the state standard was generally low. For the upper stations (Station 5 [i.e., USGS Station 0209303205]) during 2009 and 2011, the percentages of samples above 40 µg L⁻¹ were significantly greater than 10% ranging from 15.8% to 22.1% during 2009 and 14.5% to 17.7% dependent upon whether surface only, surface and bottom, or average surface and bottom water chl *a* values were used in the calculation. Surface waters contained a greater number of values in excess of the 40 µg L⁻¹ standard. As a result, for the entire study period, the percent of samples from the upper estuary with chl *a* in excess of 40 µg L⁻¹ was significantly greater than 10% if only surface water samples are considered but was not significantly greater than 10% if either the combination of surface and bottom water samples or the average of the surface and bottom values were used.

Table 3-9. Percent of samples greater than NCDENR’s water quality criterion for chl *a*.

Section of NRE	Depth	2007 ^a	2008	2009	2010	2011	2008–2011
Whole estuary Stations 1–8 and USGS Station number 0209303205	S	0	4.7	13.3	7.3	12.9	9.3
	S and B	0	3.3	11.7	5.5	10.9	7.6
	Avg (S,B)	0	3.8	10.8	5.5	10.5	7.4
Lower estuary Stations 1–2	S	0	0	0	0	0	0
	S and B	0	0	0	0	0	0
	Avg (S,B)	0	0	0	0	0	0

(continued)

**Table 3-10. Percent of samples greater than NCDENR's water quality criterion for chl *a*.
(continued)**

Section of NRE	Depth	2007 ^a	2008	2009	2010	2011	2008–2011
Middle estuary Stations 3–4	S	0	0	3.9	0	14.3	4.6
	S and B	0	0	7.7	0	10.7	4.6
	Avg (S,B)	0	0	7.7	0	3.6	2.8
Upper estuary Stations 5–8 and USGS Station number 0209303205	S	0	8.6	22.1	12.9	17.7	14.9
	S and B	0	4.7	15.8	10.0	14.5	11.0
	Avg (S,B)	0	6.9	16.2	9.7	17.7	12.3

Percent of chl *a* samples greater than 40 µg L⁻¹ for surface samples (S), the combination of surface and bottom water samples (S and B), and the set of means of the surface and bottom water concentrations for each sampling point (Avg[S,B]). Bold values indicate a significant difference from 10% based on the binomial cumulative probability distribution function ($\alpha=0.05$).

^a Only includes samples from October 7–December 31, 2007.

These results indicate that instances of chl *a* elevated above the state standard are spatially variable within the NRE with upstream stations being more likely to have elevated levels (**Figure 3-22**). Additionally, compliance determinations are influenced by sampling biases associated with vertical gradients of phytoplankton biomass. Assessment of the 10/40 criterion based only on surface samples will lead to higher exceedance percentages and increase the likelihood of violations. This is not unexpected given the observed commonality of vertical migration patterns and the flagellate-dominated character of the NRE phytoplankton community. These types of potential sampling biases are not currently considered within the NCDENR's water quality assessment protocols (NCDENR, 2007).

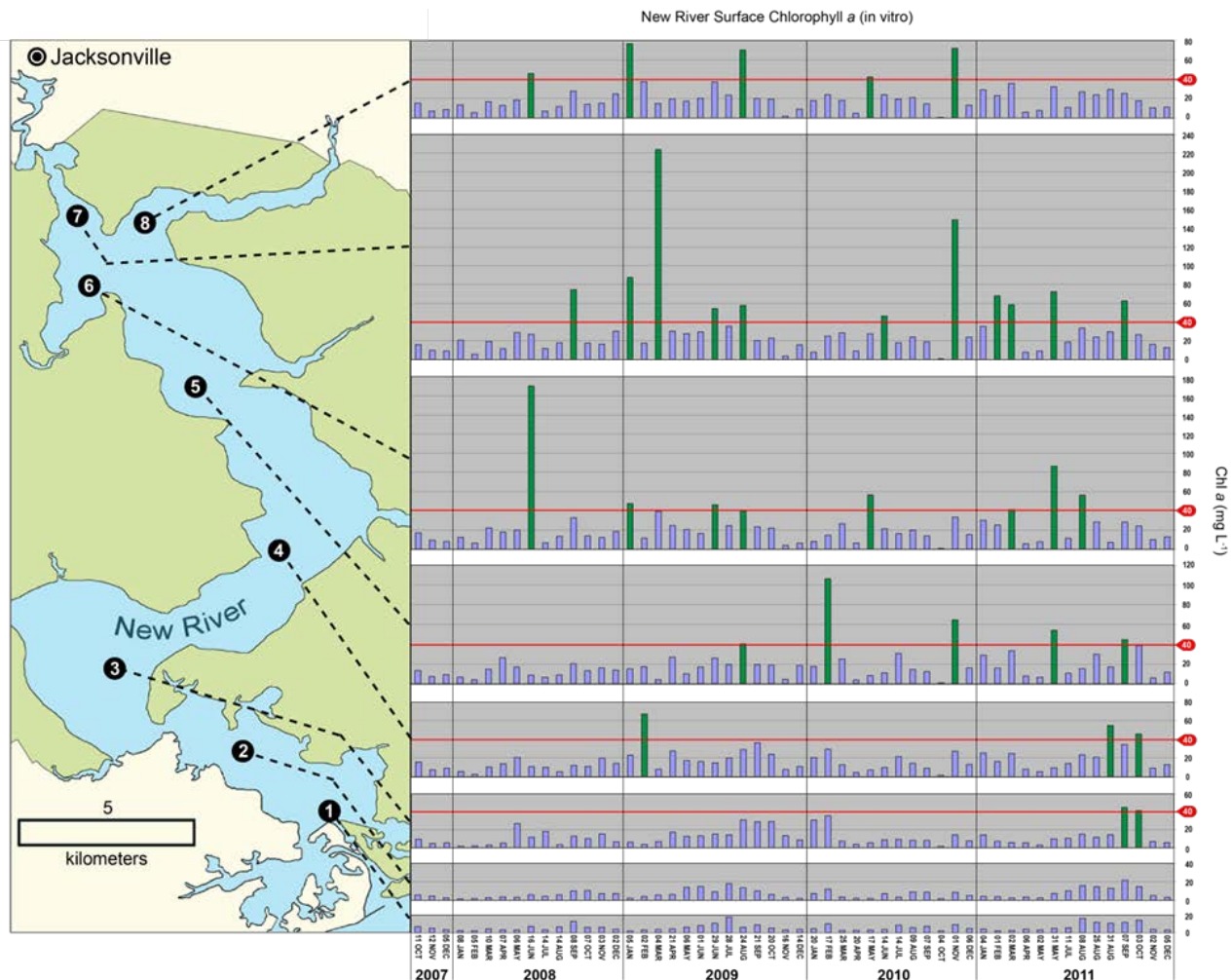


Figure 3-22. Chl *a* concentrations ($\mu\text{g L}^{-1}$) in surface waters for each station in the NRE, October 2007–December 2011.

Red bars indicate when concentrations were elevated above the State of North Carolina's acceptable chl *a* concentration of $40 \mu\text{g L}^{-1}$.

National Criteria

As part of the National Estuary Program, EPA has adopted a set of region (e.g., East Coast, West Coast, Puerto Rico) specific chl *a* criteria designed to rate estuarine water quality as good, fair, or poor (U.S. EPA, 2012). The East Coast criteria that are applicable to the New River Estuary were used. Conditions at each site were rated monthly based on monthly chl *a* samples and EPA's criteria (**Table 3-10**). Note that the use of the $20 \mu\text{g L}^{-1}$ cutoff for a poor rating provides a more stringent standard for water quality than the current State of North Carolina standard of $40 \mu\text{g L}^{-1}$. **Figure 3-23** shows the time series of monthly chl *a* concentrations by station along the downstream transect. Note that instances when chl *a* exceeded $20 \mu\text{g L}^{-1}$ are very common throughout the upper and middle sections (Stations 3–8 and USGS Station number 209303205) of the estuary.

Table 3-11. Chl *a* based water quality assessment criteria adopted from EPA's *National Estuary Program Coastal Condition Report IV* (U.S. EPA, 2012) for rating monthly chl *a* levels, and annual or multi-year site conditions.

Criteria	Good	Fair	Poor
Monthly site condition criteria	$<5 \mu\text{g L}^{-1}$	$5\text{--}20 \mu\text{g L}^{-1}$	$>20 \mu\text{g L}^{-1}$
Annual or multi-year overall site condition criteria	Less than 10% of the monthly samples were in poor condition and more than 50% of samples were in good condition	10–20% of the monthly samples were in poor condition or more than 50% of the samples were in fair or poor condition (combined)	More than 20% of the monthly samples were in poor condition

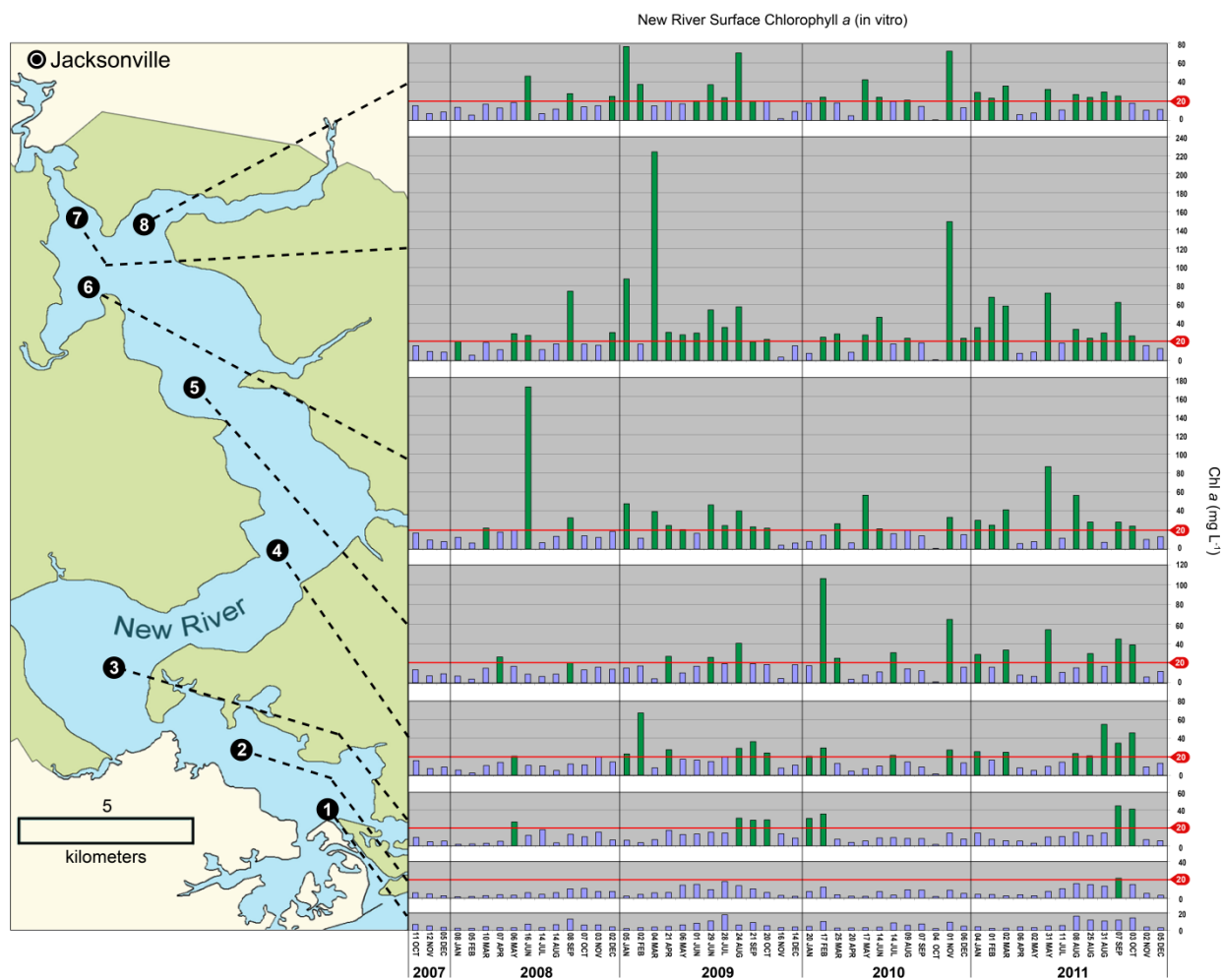


Figure 3-23. Chl *a* concentrations ($\mu\text{g L}^{-1}$) for each station in the NRE, October 2007–December 2011.

Red bars indicate when concentrations were elevated above EPA's $20 \mu\text{g L}^{-1}$ criterion for identifying estuarine waters in poor conditions with respect to elevated chl *a* concentrations.

The percentages of total monthly surface water chl *a* samples that were rated as good, fair, or poor according to the criteria in **Table 3-10** are shown in **Figure 3-24** for 2008 through 2011 and for the combination of all samples collected from 2008 through 2011. The downstream gradient in water quality is clearly apparent with Stations 1 and 2 near the New River Inlet having the highest percentage of monthly samples ranked as good. However, during most years, the majority of monthly chl *a* samples at these downstream stations were only given an annual rating of fair condition. Stations 6–8 and USGS station #209303205 consistently showed the highest proportion of poor chl *a* conditions. During 2008 and 2011, Stations 6–8 exhibited no good chl *a* conditions and during 2009 and 2010 these stations experienced good conditions only 8–17% of the time. This resulted in very low (4–6%) frequencies of good conditions at these stations when the whole study period is considered. USGS Station number 209303205 experienced better chl *a* conditions than Stations 6–8 due to the aforementioned effects of high flow periods where flushing prevents biomass accumulation at this most upstream site.

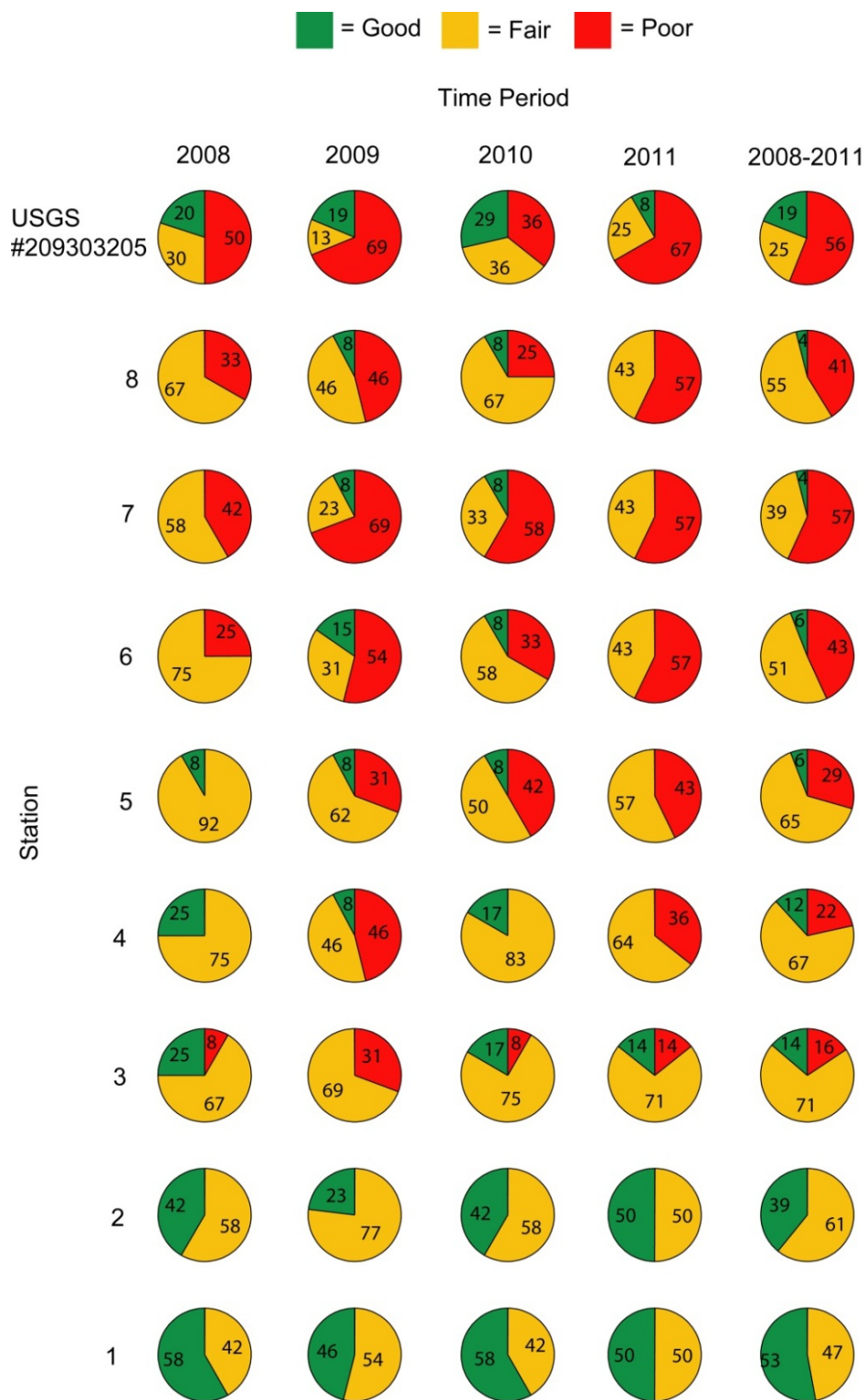


Figure 3-24. Percentages of chl *a* samples that were rated good, fair, or poor from each station based on criteria from EPA's *National Estuary Program Coastal Condition Report IV* (U.S. EPA, 2012).

Based on the above rating percentages, criteria designed to provide an overall annual or multi-year site rating of good, fair, or poor chl *a* conditions for each station were adapted from the *National Estuary Program Coastal Condition Report IV* (U.S. EPA, 2012) as shown in **Table 3-10**. The original design of the EPA criteria for determining an overall site rating was based on the percent surface area of an estuary rated as good, fair, or poor over a single sampling time typically June through September. The sampling design for which the criteria were designed utilized a probabilistic, spatial sampling scheme designed to minimize sampling biases that may occur with more structured sampling designs (U.S. EPA, 2012). The data from this DCERP project are comprised of a highly-structured, mid-channel, downstream transect of stations with data collected on a monthly basis year-round. Therefore, the methods used here were modified to establish annual ratings of the percentage of time each station was in good, fair, and poor conditions based on monthly samples and an overall rating for each site based on annual conditions. This method substitutes the percent of monthly ratings over a year or multi-year period rather than percent of surface area of the estuary represented by each sampling site as defined by the EPA method.

These overall site ratings for each year and for the entire study period are shown in **Figure 3-25**. The upper stations, from Station 6 through USGS Station number 0209303205, consistently received an overall site rating of poor. Mid and lower estuary Stations 2–5 were generally rated fair or poor, and only the station closest to the inlet (Station 1) was generally rated as having an overall good site rating for chl *a*. In 2008, Site 2 was rated as good despite having only 50% of the monthly samples rated as good rather than the required greater than 50% rated as good prescribed by the EPA method. This determination was made due to the fact that there were no instances of poor conditions at these stations during 2008 at this site, and a strict interpretation of the EPA criteria (**Table 3-10**) would provide no site rating for the case of an exact 50:50 % split of good and fair monthly samples.

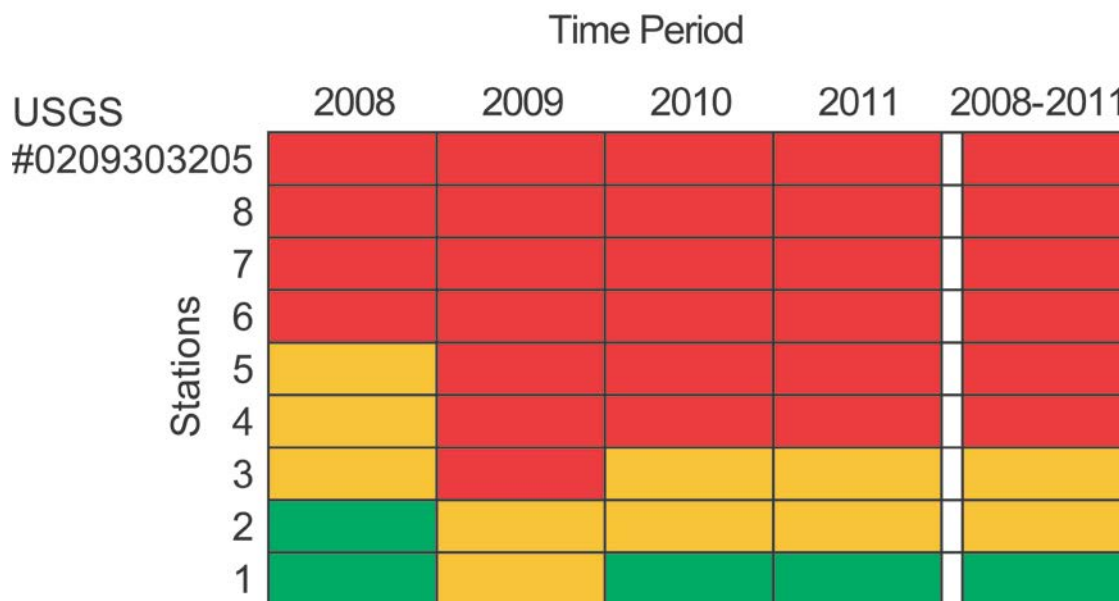


Figure 3-25. Overall site ratings for chlorophyll *a* conditions in the NRE based on criteria adopted from EPA's *National Estuary Program Coastal Condition Report* (U.S. EPA, 2012).

Conclusions and Implications for Future Research

Collectively, water column (phytoplankton) and BMA contribute more than 99% of total estuarine primary production in the NRE. Other autotrophic components of the system such as saltmarshes, seagrasses, and macroalgae contribute very little to total system production due to their limited areal extent. Within the microalgae, phytoplankton production and BMA production appear to be of comparable magnitude on an estuary wide basis. Spatially, however, phytoplankton production contributes a greater fraction of total production upstream near Jacksonville and BMA production is comparably greater nearer the inlet. These trends relate to the underlying controls on productivity of each microalgal component. BMA community production is largely limited by light availability to the benthos, which is determined by depth and water clarity. Phytoplankton biomass, suspended sediments, and CDOM concentrations govern water clarity and all of the light absorbing and scattering constituents of the water column are higher at the head of the estuary. The naturally high colored dissolved organic matter concentrations derived from upland swamps exacerbates light limitation within the NRE. Due to the positive effects of BMA on limiting sediment fluxes of N and P to the water column, and providing food for valuable fisheries resources, management actions should aim to maintain or shift this balance toward BMA production and away from phytoplankton production. To promote BMA production over phytoplankton production, both nutrient loads which stimulate phytoplankton and riverine sediment loads should be targeted for reduction.

The upper estuarine region is particularly prone to phytoplankton blooms, especially during moderate flows. Although blooms occasionally occurred during droughts, very high river flows always impeded bloom development. This underscores the strong hydrological control of phytoplankton biomass production in this estuary. For total phytoplankton biomass and for all phytoplankton classes there is a threshold river flow of approximately $27 \text{ m}^3 \text{ s}^{-1}$ above which the residence time within the estuary is too short to allow for bloom development. Under these high flow conditions, there is insufficient time for phytoplankton to assimilate and process riverine nutrient inputs and a large fraction of the nutrient inputs are flushed directly into the ocean. In effect, this phenomenon represents “a purge valve” for the estuary and prevents the accumulation of nutrient inputs during periods when nutrient inputs are at their highest level. It is worth noting that periods when this flow threshold is achieved are rare and are usually associated with intense precipitation events such as the observed tropical cyclones.

Under most flow conditions, riverine nutrient loads are completely assimilated within the estuary. Both the bioassay data and productivity data suggest that intense nutrient limitation, particularly N limitation, occurs as riverine loads are depleted by phytoplankton growth within the upper estuary. Although only one instance of P limitation was observed, this may have been due to the timing of the experiments to coincide with periods of high internal P loading from the sediments as seen in other shallow estuaries (Fisher et al., 1982; Rudek et al., 1991). Similar bioassays during cooler periods would be necessary to determine whether seasonal P limitation occurs within the NRE. Thus, we caution that this study should not be used to conclude that N is always the limiting nutrient in an effort to thwart efforts at limiting external P load. In fact, increased P loading may favor undesirable N-fixing cyanobacteria. In total, this study indicates that the estuary is highly sensitive to nutrient inputs and that any increases in riverine nutrient loads that are not accompanied by increased flow (i.e., increased riverine nutrient concentration or point source inputs directly to the estuary) are likely to lead to higher phytoplankton

production and bloom potentials in the estuary. Conversely, decreases in riverine nutrient concentrations or elimination of direct point source loading to the estuary should reduce phytoplankton biomass. The reductions in phytoplankton biomass following sewage treatment upgrades in the late 1990s offer further (Mallin et al., 2005) proof of the dramatic sensitivity of the NRE phytoplankton assemblage to flow-independent changes in nutrient loading.

Phytoplankton blooms in general show little seasonality but are generally linked to elevated nutrient inputs related to moderate river flow periods. However, HABs, dominated by raphidophytes, displayed a distinct seasonality being much more common during the warm period from late spring through early fall. Although enhanced flow and associated loading generally precedes blooms, some of the HABs occurred during droughts when riverine inputs were greatly reduced. The source of nutrients fueling these drought period blooms is not immediately apparent. Mixotrophic feeding on bacteria or picocyanobacteria is a possibility (Jeong, 2011). Internal nutrient loading from the sediments may also play a critical role in bloom development of this HAB-forming group. Evidence from Delaware's inland bays suggests that raphidophytes undergoing DVMs may even swim into the surficial sediment layer during their nocturnal descent (Handy et al., 2005). Nutrient concentrations in the surficial sediment layer of the organic rich silts and muds that dominate much of the NRE bottom are likely to be several orders of magnitude higher than in the water column (Luettich et al., 2000). Determining whether these raphidophytes species actually vertically migrate into the sediments is a critical knowledge gap that deserves further investigation. Additionally, the toxin production potential of raphidophytes blooms remains to be determined but may have important consequences for the ecological health of the NRE.

Over the course of this study, it was difficult to clearly separate anthropogenic effects (i.e., nutrient, sediment loads) from climatically driven, hydrological effects on the MA community. This is likely because over a short (4.5-year) duration, nutrient loading is so strongly related to the extreme variability in freshwater inflow that effects of changes in nutrient or sediment concentrations due to changes in human activity constitute a negligible component of the variation in load (Stow and Borsuk, 2003). However, the observed relationships derived between flushing time and phytoplankton biomass may be useful indicators of the current functional response of the phytoplankton community to changes in inputs from the watershed (Swaney et al., 2008). As in-stream concentrations of nutrients or sediments change with alterations in land use or other anthropogenic activities, the shape of the flushing time- phytoplankton response curve is predicted to change. For example, higher flow-independent nutrient loads should result in higher peak biomass that occurs at a longer flushing time (Swaney et al., 2008). Thus the observed phytoplankton biomass and community compositional responses to flushing times provides a valuable baseline for detecting future changes in the structure and function of the MA assemblage. This is particularly important in light of the difficulty of quantifying some of the diffuse, yet increasingly important sources of nutrients to the estuary-like atmospheric deposition and ground water inputs (Paerl, 1997).

Literature Cited

- Adolf, J.E., T.R. Bachvaroff, and A.R. Place. 2009. Environmental modulation of karlotoxin levels in strains of the cosmopolitan dinoflagellate, *Karlodinium veneficum* (Dinophyceae). *Journal of Phycology* 45:176–192.
- Adolf, J.E., C.L. Yeager, W.D. Miller, M.E. Mallonee, and L.W. Harding Jr. 2006. Environmental forcing of phytoplankton floral composition, biomass, and primary productivity in Chesapeake Bay, USA. *Estuarine, Coastal and Shelf Science* 67:108–122.
- Alber, M., and J.E. Sheldon. 1999. Use of a date-specific method to examine variability in the flushing times of Georgia estuaries. *Estuarine, Coastal and Shelf Science* 49:469–482.
- Allredge, A.L., and C.C. Gotschalk. 1989. Direct observations of the mass flocculation of diatoms blooms: Characteristics, settling velocities and formation of diatom aggregates. *Deep Sea Research* 36:159–171.
- Altman, J.C., and H.W. Paerl. 2012. Composition of inorganic and organic nutrient sources influences phytoplankton community structure in the New River Estuary, North Carolina. *Aquatic Ecology* 46(3):269–282.
- Amano, K., M. Watanabe, K. Kohata, and S. Harada. 1998. Conditions necessary for *Chatonella antiqua* red tide outbreaks. *Limnology and Oceanography* 43:117–128.
- American Public Health Association. 1998. *Standard Methods for the Examination of Water and Wastewater*. American Public Health Association: Washington, DC.
- Anderson, D.M., and K.D. Stolzenbach. 1985. Selective retention of two dinoflagellates in a well-mixed estuarine embayment: The importance of diel vertical migration and surface avoidance. *Marine Ecology Progress Series* 25:39–50.
- Anderson, I.C., K.J. McGlathery, and A.C. Tyler. 2003. Microbial mediation of “reactive” nitrogen in a temperate lagoon. *Marine Ecology Progress Series* 246:73–84.
- Ault, T.R. 2000. Vertical migration by the marine dinoflagellate *Prorocentrum triestinum* maximizes photosynthetic yield. *Oecologia* 125:466–475.
- Ban, S., C. Burns, J. Castel, Y. Chaudron, E. Christou, R. Escibano, S.F. Umani, S. Gasparini, F.G. Ruiz, M. Hoffmeyer, A. Ianora, H. Kang, M. Laabir, A. Lacoste, A. Miralto, X. Ning, S. Poulet, V. Rodrigues, J. Runge, J. Shi, M. Starr, S. Uye, and Y. Wang. 1997. The paradox of diatom-copepod interactions. *Marine Ecology Progress Series* 157:287–293.
- Boesch, D.F., E. Burreson, W. Dennison, E. Houde, M. Kemp, V. Kennedy, R. Newell, K. Paynter, R. Orth, and W. Ulanowicz. 2001. Factors in the decline of coastal ecosystems. *Science* 293:629–638.

- Bourdelaïs, A., C. Tomas, J. Near, J. Kubanek, and D. Baden. 2002. New fish-killing alga in coastal Delaware produces neurotoxins. *Environmental Health Perspectives* 110:465–470.
- Boyd, C.M., and E.D. Gradmann. 2002. Impact of osmolytes on buoyancy of marine phytoplankton. *Marine Biology* 141:605–618.
- Boyer, J.N., R.R. Christian, and D.W. Stanley. 1993. Patterns of phytoplankton primary productivity in the Neuse River Estuary, North Carolina, USA. *Marine Ecology Progress Series* 97:287–297.
- Burkhill, P.H., R.F. Mantoura, C.A. Llewellyn, and N.J.P. Owens. 1987. Microzooplankton grazing and selectivity of phytoplankton in coastal waters. *Marine Biology* 93:581–590.
- Chang, J., and E.J. Carpenter. 1985. Blooms of the dinoflagellate *Gyrodinium aureolum* in a Long Island Estuary: Box model of bloom maintenance. *Marine Biology* 89:83–93.
- Chorus, I., and J. Bartram. 1999. *Toxic Cyanobacteria in Water: A Guide to Their Public Health Consequences, Monitoring, and Management*. E&FN Spon, London. St. Edmundsbury Press: Bury St. Edmunds, Suffolk. (416 pages).
- Cloern, J.E. 2001. Our evolving conceptual model of the coastal eutrophication problem. *Marine Ecology Progress Series* 210:223–253.
- Cloern, J.E., and A.D. Jassby. 2010. Patterns and scales of phytoplankton variability in estuarine-coastal ecosystems. *Estuaries and Coasts* 33:230–241.
- Cloern, J.E., and R. Dufford. 2005. Phytoplankton community ecology: principles applied in San Francisco Bay. *Marine Ecology Progress Series* 285:11–28.
- Conley, D.J., and T.C. Malone. 1992. Annual cycle of dissolved silicate in Chesapeake Bay: implications for the production and fate of phytoplankton biomass. *Marine Ecology Progress Series* 81:121–128.
- Connell, L., and R.A. Cattolico. 1996. Fragile algae: axenic culture of field-collected samples of *Heterosigma carterae*. *Marine Biology* 125:421–426.
- Daugbjerg, N., G. Hansen, J. Larsen, and O. Moestrup. 2000. Phylogeny of some of the major genera of dinoflagellates based on ultrastructure and partial LSU rDNA sequence data, including the erection of three new genera of unarmoured dinoflagellates. *Phycologia* 39:302–417.
- Day, J.W., and W.M. Kemp (Eds.). 1989. *Estuarine Ecology*. Wiley Interscience: New York, NY.

- Deeds, J.R., D.E. Terlizzi, J.E. Adolf, D.K. Stoecker, and A.R. Place. 2002. Toxic activity from cultures of *Karlodinium micrum* (= *Gyrodinium galatheanum*) (Dinophyceae) a dinoflagellate associated with fish mortalities in an estuarine aquaculture facility. *Harmful Algae* 1:169–189.
- Demir, E., K.J. Coyne, M.A. Doblin, S.M. Handy, and D.A. Hutchins. 2008. Assessment of microzooplankton grazing on *Heterosigma akashiwo* using a species-specific approach combining quantitative real-time PCR (QPCR) and dilution methods. *Microbial Ecology* 55:583–594.
- Denman, K.L. 1977. Short-term variability in vertical chlorophyll structure. *Limnology and Oceanography* 22:434–441.
- Dortch, Q., and T.E. Whitledge. 1992. Does nitrogen or silicon limit phytoplankton production in the Mississippi River plume and nearby regions? *Continental Shelf Research* 12:1293–1309.
- Ensign, S.H., J.N. Halls, and M.A. Mallin. 2004. Application of digital bathymetry data in an analysis of flushing times of two North Carolina Estuaries. *Computers and Geosciences* 30:501–511.
- Fensin, E.E. 2004. Occurrence and ecology of the dinoflagellate *Karlodinium micrum* in estuaries of North Carolina, USA. Pp. 62–67 in *Harmful Algae 2002*. Edited by K.A. Steidinger, J.H. Landsberg, C.R. Tomas, and G.A. Vargo. Florida Fish and Wildlife Conservation Commission, Florida Institute of Oceanography, and Intergovernmental Oceanographic Commission of the United Nations Educational, Scientific, and Cultural Organization, St. Petersburg, FL.
- Fernandes, T.A., V. Iver, and S.K. Apte. 1993. Differential responses of nitrogen-fixing cyanobacteria to salinity and osmotic stresses. *Applied and Environmental Microbiology* 59:899–904.
- Fisher, T.R., P.R. Carlson, and R.T. Barber. 1982. Sediment nutrient regeneration in three North Carolina estuaries. *Estuarine Coastal and Shelf Science* 14:101–116.
- Fredrickson, K.A., S.L. Strom, R. Crim, and K.J. Coyne. 2011. Interstrain variability in physiology and genetics of *Heterosigma akashiwo* (Raphidophyceae) from the West Coast of North America. *Journal of Phycology* 47:27–35.
- Gallegos, C.L., T.E. Jordan, A.H. Hines, and D.E. Weller. 2005. Temporal variability of optical parameters in a shallow, eutrophic estuary: seasonal and inter-annual variability. *Estuarine, Coastal Shelf Science* 64:156–170.
- Gaulke, A.K., M.S. Wetz, H.W. Paerl. 2010. Picophytoplankton: A major contributor to planktonic biomass and primary production in a eutrophic, river-dominated estuary. *Estuarine, Coastal and Shelf Science* 90:45–54.

- Graham, S.L., and S.L. Strom. 2010. Growth and grazing of microzooplankton in response to the harmful alga *Heterosigma akashiwo* in prey mixtures. *Aquatic Microbial Ecology* 59:111–124.
- Hall, N.S. 2009. *Effects of the Vertical Structure of the Water Column on the Phytoplankton in a Shallow, Lagoonal Estuary*. Ph.D. dissertation. University of North Carolina at Chapel Hill, Chapel Hill, NC.
- Hall, N.S., and H.W. Paerl. 2011. Vertical migration patterns of phytoflagellates in relation to light and nutrient availability in a shallow, microtidal estuary. *Marine Ecology Progress Series* 425:1–19.
- Hall, N.S., B.L. Peierls, H.W. Paerl, A.C. Whipple, and K.L. Rossignol. In review. Effects of climatic variability on phytoplankton community structure and bloom development in the eutrophic, microtidal, New River Estuary, North Carolina, USA. *Estuarine Coastal and Shelf Science*.
- Hall, M.J., H.F.P. Van den Boogaard, R.C. Fernando, and A.E. Mynett. 2004. The construction of confidence intervals for frequency analysis using resampling techniques. *Hydrology and Earth System Sciences* 8:235–246.
- Hallegraeff, G.M. 1993. A review of harmful algal blooms and their apparent global increase. *Phycologia* 32:79–99.
- Handy, S.M., K.J. Coyne, K.J. Portune, E. Demir, M.A. Doblin, C.E. Hare, S.C. Cary, and D.A. Hutchins. 2005. Evaluating vertical migration behavior of harmful raphidophytes in the Delaware Inland Bays utilizing quantitative real-time PCR. *Aquatic Microbial Ecology* 40:121–132.
- Hansen, B., P.K. Bjornsen, and P.J. Hansen. 1994. The size ratio of planktonic predators and their prey. *Limnology and Oceanography* 39:395–403.
- Hobbie, J.E. (Ed.). 2000. *Estuarine Sciences—A Synthetic Approach to Research and Practice*. Island Press: Washington, DC.
- Hoek, C.V., D.G. Mann, and H.M. Jahns. 1997. *Algae, an introduction to phycology*. Cambridge University Press: Cambridge, UK.
- Imai, I., and M. Yamaguchi. 2012. Life cycle, physiology, ecology and red tide occurrences of the fish-killing raphidophytes *Chattonella*. *Harmful Algae* 14:46–70.
- Jeong, H.J. 2011. Mixotrophy in red tide algae raphidophytes. *Journal of Eukaryotic Microbiology* 58:215–222.

- Jeong, H.J., Y.D. Yoo, J.Y. Park, J.Y. Song, S.T. Kim, S.H. Lee, K.Y. Kim, and W.H. Yih. 2005. Feeding by phototrophic red-tide dinoflagellates: five species newly revealed and six species previously known to be mixotrophic. *Aquatic Microbial Ecology* 40:133–150.
- Jephson, T., T. Fagerberg, and P. Carlsson. 2011. Dependency of dinoflagellate vertical migration on salinity stratification. *Aquatic Microbial Ecology* 63:255–264.
- Justic, D., N.N. Rabalais, and R.E. Turner. 1995. Stoichiometric nutrient balance and origin of coastal eutrophication. *Marine Pollution Bulletin* 30:41–46.
- Kennish, M.J., and H.W. Paerl (Eds.). 2010. *Coastal Lagoons: Critical Habitats of Environmental Change*. CRC Marine Science Series. CRC Press: Boca Raton, FL.
- Klappenbach, J.A., J.M. Dunbar, and T.M. Schmidt. 2000. rRNA operon copy number reflects ecological strategies of bacteria. *Applied Environmental Microbiology* 66:1328–1333.
- Lewitus, A.J., D.L. White, R.G. Tymowski, M.E. Geesey, S.N. Hymel, and P.A. Noble. 2005. Adapting the Chemtax taxonomic composition method for assessing phytoplankton in Southeastern U.S. estuaries. *Estuaries* 28:160–172.
- Lewitus, A., L. Schmidt, L.J. Mason, J.W. Kempton, S.B. Wilde, J.L. Wolny, B.J. Williams, K.C. Hayes, S.N. Hymel, C.J. Keppler, and A.H. Ringwood. 2003. Harmful algal blooms in South Carolina residential and golf course ponds. *Population and Environment* 24:387–413.
- Litaker, R.W., C.S. Duke, B.E. Kenney, and J. Ramus. 1987. Short-term variability and phytoplankton abundances in a shallow tidal estuary. I. Winter and summer. *Marine Biology* 96:115–121.
- Luetlich, Jr., R.A., J.E. McNinch, H.W. Paerl, C.H. Peterson, J.T. Wells, M. Alperin, C.S. Martens, and J.L. Pinckney. 2000. *Neuse River Estuary Modeling and Monitoring Project Stage I: Hydrography and Circulation, Water Column Nutrients and Productivity, Sedimentary Processes and Benthic-Pelagic Coupling*. Report UNC-WRRI-2000-325B. Water Resources Research Institute of the University of North Carolina System, North Carolina State University, Raleigh, NC.
- Lunetta, R.S., J.F. Knight, H.W. Paerl, J.J. Streicher, B.L. Peierls, T. Gallo, J.G. Lyon, T.H. Mace, and C.P. Buzzelli. 2009. Measurements of water colour using AVIRIS imagery to assess the potential for an operational monitoring capability in the Pamlico Sound Estuary, USA. *International Journal of Remote Sensing* 30:3291–3314.
- Mallin, M.A., and H.W. Paerl. 1994. Trophic transfer in an estuary: Seasonal, diel, and community structure effects. *Ecology* 75:2168–2184.
- Mallin, M.A., and H.W. Paerl. 1992. Effects of variable irradiance on phytoplankton productivity in shallow estuaries. *Limnology and Oceanography* 37:54–62.

- Mallin, M.A., M.R. McIver, H.A. Wells, D.C. Parsons, and V.L. Johnson. 2005. Reversal of eutrophication following sewage treatment upgrades in the New River Estuary, North Carolina. *Estuaries* 28:750–760.
- Mallin, M.A., Burkholder, J.M., Cahoon, L.B., Posey, M.H., 2000. North and South Carolina coasts. *Marine Pollution Bulletin* 41:56–75.
- Mallin, M.A., L.B. Cahoon, M.R. McIver, D.C. Parsons, and G.C. Shank. 1997. *Nutrient Limitation and Eutrophication Potential in the Cape Fear and New River Estuaries*. Report number 313. Water Resources Research Institute of the University of North Carolina System, North Carolina State University, Raleigh, NC.
- Malone, T.C., A. Malej, L.W. Harding Jr., N. Smodlaka, and R.E. Turner (Eds.). 1999. Coastal and estuarine studies. *Ecosystems at the Land-Sea Margin: Drainage Basin to Coastal Sea (Volume 55)*. American Geophysical Union: Washington, DC.
- Margalef, R. 1978. Life-forms of phytoplankton as survival alternatives in an unstable environment. *Oceanologica Acta* 1:493–509.
- McBride, G.B., and J.C. Ellis. 2001. Confidence of compliance: A Bayesian approach for percentile standards. *Water Research* 35:117–1124.
- Moestrup, Ø., R. Akselman, G. Cronberg, M. Elbraechter, S. Fraga, Y. Halim, G. Hansen, M. Hoppenrath, J. Larsen, N. Lundholm, L.N. Nguyen, and A. Zingone (Eds.). 2011. *IOC-UNESCO Taxonomic Reference List of Harmful Microalgae*. Available at <http://www.marinespecies.org/HAB>.
- Moisander, P.H., E. McClinton, and H.W. Paerl. 2002. Salinity effects on growth, photosynthetic parameters, and nitrogenase activity in estuarine planktonic cyanobacteria. *Microbial Ecology* 43:432–442.
- Monsen, N.E., J.E. Cloern, L.V. Lucas, and S.G. Monismith. 2002. A comment on the use of flushing time, residence time, and age as transport time scales. *Limnology and Oceanography* 47:1545–1553.
- Mullholland, M.R., R.E. Morse, G.E. Boneillo, P.W. Bernhardt, K.C. Fillipino, L.A. Procise, J.L. Blanco-Garcia, H.G. Marshall, T.A. Egerton, W.S. Hunley, K.A. Moore, D.L. Berry, and C.J. Gobler. 2009. Understanding causes and impacts of the dinoflagellate, *Cochlodinium polykrikoides*, blooms in the Chesapeake Bay. *Estuaries and Coasts* 32:734–747.
- Murrell, M.C., and E.M. Lores. 2004. Phytoplankton and zooplankton seasonal dynamics in a subtropical estuary: importance of cyanobacteria. *Journal of Plankton Research* 26:371–382.

- Niemi, G., D. Wardrop, R. Brooks, S. Anderson, V. Brady, H. Paerl, C. Rakocinski, M. Brouwer, B. Levinson, and M. McDonald. 2004. Rationale for a new generation of indicators for coastal waters. *Environmental Health Perspectives* 112:979–986.
- NCDENR (North Carolina Department of Environment and Natural Resources) 2007. “Redbook” *Surface Water and Wetland Standards*. NCDENR, Division of Water Quality. May 1. Available at <http://portal.ncdenr.org/web/wq/ps/csu>.
- Nixon, S.W. 1995. Coastal marine eutrophication: A definition, social causes, and future concerns. *Ophelia* 41:199–219.
- Nixon, S.W. 1992. Quantifying the relationship between nitrogen input and the productivity of marine ecosystems. Pp. 57–83. In *Proceedings of Advanced Marine Technology Conference (AMTEC)*, Tokyo, Japan. Edited by M. Takahashi, K. Nakata, and T.R. Parsons.
- NRC (National Research Council). 2000. *Clean Coastal Waters: Understanding and Reducing the Effects of Nutrient Pollution*. National Academy Press: Washington, DC.
- Otten, T.G., H. Xu, B. Qin, G. Zhu, and H.W. Paerl. 2012. Spatiotemporal patterns and ecophysiology of toxigenic *Microcystis* blooms in Lake Taihu, China: Implications for water quality management. *Environmental Science & Technology* 46:3480–3488.
- Paerl, H.W. 2002. Primary productivity and producers. Pp. 329–341 in *Manual of Environmental Microbiology (2nd edition)*. Edited by C.J. Hurst. ASM Press: Washington, DC.
- Paerl, H.W. 1997. Coastal eutrophication and harmful algal blooms: Importance of atmospheric deposition and groundwaters as “new” nitrogen and other nutrient sources. *Limnology and Oceanography* 42:1154–1165.
- Paerl, H.W. 1988. Nuisance phytoplankton blooms in coastal, estuarine, and inland waters. *Limnology and Oceanography* 33:823–847.
- Paerl, H.W., and J. Huisman. 2009. Climate change: A catalyst for global expansion of harmful cyanobacterial blooms. *Environmental Microbiology Reports* 1:27–37.
- Paerl, H.W., K.L. Rossignol, N.S. Hall, B.L. Peierls, and M.S. Wetz. 2010. Phytoplankton community indicators of short- and long-term ecological change in the anthropogenically and climatically impacted Neuse River Estuary, North Carolina, USA. *Estuaries and Coasts* 33:485–497.
- Paerl, H.W., L.M. Valdes-Weaver, A.R. Joyner, and V. Winkelmann. 2007. Phytoplankton indicators of ecological change in the eutrophying Pamlico Sound system North Carolina. *Ecological Applications* 17:S88–S101.

- Paerl, H.W., L.M. Valdes, J.L. Pinckney, M.F. Piehler, J. Dyble, and P.H. Moisander. 2003. Phytoplankton photopigments as indicators of estuarine and coastal eutrophication. *BioScience* 53:953–964.
- Paerl, H.W., J.L. Pinckney, J.M. Fear, and B.L. Peierls. 1998. Ecosystem responses to internal and watershed organic matter loading: Consequences for hypoxia in the eutrophying Neuse River Estuary, North Carolina, USA. *Marine Ecology Progress Series* 166:17–25.
- Paerl, H.W., M.A. Mallin, C.A. Donahue, M. Go, and B.L. Peierls. 1995. *Nitrogen Loading Sources and Eutrophication of the Neuse River Estuary, NC: Direct and Indirect Roles of Atmospheric Deposition*. UNC Water Resources Research Institute Report number 95-291. (119 pages). Available at <http://repository.lib.ncsu.edu/dr/bitstream/1840.4/1851/1/NC-WRRI-291.pdf>.
- Peierls, B.L., R.R. Christian, and H.W. Paerl. 2003. Water quality and phytoplankton as indicators of hurricane impacts on a large estuarine ecosystem. *Estuaries* 26:1329–1343.
- Phlips, E.J., S. Badylak, M.C. Christman, and M.A. Lasi. 2010. Climatic trends and temporal patterns of phytoplankton composition, abundance, and succession in the Indian River Lagoon, Florida, USA. *Estuaries and Coasts* 33:498–512.
- Piehler, M.F., J. Dyble, P.H. Moisander, J.L. Pinckney, and H.W. Paerl. 2002. Effects of modified nutrient concentrations and ratios on the structure and function of the native phytoplankton community in the Neuse River Estuary, North Carolina, USA. *Aquatic Ecology* 36:371–385.
- Pinckney, J.L., T.L. Richardson, D.F. Millie, and H.W. Paerl. 2001. Application of photopigment biomarkers for quantifying microalgal community composition and in situ growth rates. *Organic Geochemistry* 32:585–595.
- Pinckney, J.L., H.W. Paerl, M.B. Harrington, and K.E. Howe. 1998. Annual cycles of phytoplankton community-structure and bloom dynamics in the Neuse River Estuary, North Carolina. *Marine Biology* 131:371–381.
- Powers, L., I.F. Creed, and C.G. Trick. 2012. Sinking of *Heterosigma akashiwo* results in increased toxicity of this harmful algal bloom species. *Harmful Algae* 13:95–104.
- Rabalais, N.N, and R.E. Turner (Eds.). 2001. Coastal hypoxia: Consequences for living resources and ecosystems. *Coastal and Estuarine Studies* 58. American Geophysical Union: Washington, DC.
- Reynolds-Fleming, J.V., and R.A. Luettich. 2004. Wind-driven lateral variability in a partially mixed estuary. *Estuarine Coastal and Shelf Science* 60:395–407.
- Reynolds-Fleming, J.V., F.G. Fleming, and R.A. Luettich. 2002. Portable autonomous vertical profiler for estuarine applications. *Estuaries* 25(1):142–147.

- Rudek, J., H.W. Paerl, M.A. Mallin, and P.W. Bates. 1991. Seasonal and hydrological control of phytoplankton nutrient limitation in the lower Neuse River Estuary, North Carolina. *Marine Ecology Progress Series* 75:133–142.
- Sellner, K.G., R.V. Lacouture, S.J. Cibik, A. Brindley, and S.G. Brownlee. 1991. Importance of a winter dinoflagellate-microflagellate bloom in the Patuxent River Estuary. *Estuarine, Coastal and Shelf Science* 32:27–42.
- Sellner, K.G., S.G. Sellner, R.V. Lacouture, and R.E. Magnien. 2001. Excessive nutrients select for dinoflagellates in the stratified Patapsco River Estuary: Margalef reigns. *Marine Ecology Progress Series* 220:93–102.
- Sheldon, J.E., and M. Alber. 2006. The calculation of estuarine turnover times using freshwater fraction and tidal prism models: A critical evaluation. *Estuaries and Coasts* 29:133–146.
- Siegel, S., and N.J. Castellan. 1988. Nonparametric Statistics for the Behavioral Sciences. (Pp. 213–214). McGraw Hill International: New York.
- Smayda, T.J. 1997. Harmful algal blooms: Their ecophysiology and general relevance to phytoplankton blooms in the sea. *Limnology and Oceanography* 42:1137–1153.
- Smetacek, V.S. 1985. Role of sinking in diatom life-history cycles: ecological, evolutionary and geological significance. *Marine Biology* 84:239–251.
- Smith, E.P., K. Ye, C. Hughes, and L. Shabman. 2001. Statistical assessment of violations of water quality standards under section 303d of the clean water act. *Environmental Science and Technology* 35:606–612.
- Stow, C.A., and M.E. Borsuk. 2003. Assessing TMDL effectiveness using flow-adjusted concentrations: A case study of the Neuse River, North Carolina. *Environmental Science and Technology* 37:2043–2050.
- Sundbäck, K., A. Miles, S. Hulth, L. Pihl, P. Engstrom, E. Selander, and A. Avenson. 2003. Importance of benthic nutrient regeneration during initiation of macroalgal blooms in shallow bays. *Marine Ecology Progress Series* 246:115–126.
- Swaney D.P., D. Scavia, R.W. Howarth, and R.M. Marino. 2008. Estuarine classification and response to nitrogen loading: Insights from simple ecological models. *Estuarine, Coastal and Shelf Science* 77:253–263.
- Tanabe, Y., K. Kaya, and M.M. Watanabe. 2004. Evidence for recombination in the microcystin synthetase (*mcy*) genes of toxic cyanobacteria *Microcystis* spp. *Journal of Molecular Evolution* 58:633–641.
- Tang, Y.Z., F. Kock, and C.J. Gobler. 2010. Most harmful algal bloom species are vitamin B₁ and B₁₂ auxotrophs. *Proceedings of the National Academy of Sciences* 107:20756–20761.

- Tester, P.A., M.E. Geesey, C. Guo, H.W. Paerl, and D.F. Millie. 1995. Evaluating phytoplankton dynamics in the Newport River Estuary (North Carolina, USA) by HPLC-derived pigment profiles. *Marine Ecology Progress Series* 124:237–245.
- Tomas, C.R. (Ed.). 1997. *Identifying Marine Phytoplankton*. Academic Press: New York, NY.
- Tomas, C.R., J. Peterson, and A.O. Tatters. 2007. *Harmful Algal Species from Wilson Bay, New River, North Carolina: Composition, Nutrient Bioassay and HPLC Pigment Analyses*. North Carolina Water Resources Research Institute Report number 369. (31 pages). Available at <http://repository.lib.ncsu.edu/dr/bitstream/1840.4/2002/1/NC>.
- Tonk, L., K. Bosch, P.M. Visser, and J. Huisman. 2007. Salt tolerance of the harmful cyanobacterium *Microcystis aeruginosa*. *Aquatic Microbial Ecology*. 46:117–123.
- U.S. EPA (U.S. Environmental Protection Agency). 2012. *National Estuary Program Coastal Condition Report IV*. Report number EPA-842-R-10-003. Washington, DC. April.
- Utermöhl, H., 1958. Zur Vervollkommnung der quantitativen phytoplanktonmethodik. *Mitteilung Internationale Vereinigung fuer Theoretische unde Amgewandte Limnologie* 9:1–38
- Valdes-Weaver, L.M., M.H. Piehler, J.L. Pinckney, K.E. Howe, K. Rossignol, and H.W. Paerl. 2006. Long-term temporal and spatial trends in phytoplankton biomass and class-level taxonomic composition in the hydrologically variable Neuse-Pamlico estuarine continuum, North Carolina, USA. *Limnology and Oceanography* 51:1410–1420.
- Valiela, I., G. Collins, J. Kremer, K. Lajtha, M. Geist, B. Seely, J. Brawley, and C.H. Sham. 1997. Nitrogen loading from coastal watersheds to receiving estuaries: New method and application. *Ecological Applications* 7:358–380.
- Verity, P.G. 2010. Expansion of potentially harmful algal taxa in a Georgia Estuary (USA). *Harmful Algae* 9:144–152.
- Waite, A., A. Fisher, P.A. Thompson, and P.J. Harrison. 1997. Sinking rate versus cell volume relationships illuminate sinking rate control mechanisms in marine diatoms. *Marine Ecology Progress Series* 157:97–108.
- Watanabe, M., K. Kohata, T. Kimura, T. Takamatsu, S. Yamaguchi, and T. Ioriya. 1995. Generation of a *Chattonella antiqua* bloom by imposing a shallow nutricline in a mesocosm. *Limnology and Oceanography* 40:1447–1460.
- Wetz, M.S., E.A. Hutchinson, R.S. Lunetta, H.W. Paerl, and J.C. Taylor. 2011a. Severe droughts reduce estuarine primary productivity with cascading effects on higher trophic levels. *Limnology and Oceanography* 56:627–638.

- Wetz, M.S., H.W. Paerl, J.C. Taylor, and J.A. Leonard. 2011b. Environmental controls upon picophytoplankton growth and biomass in a eutrophic estuary. *Aquatic Microbial Ecology* 63:133–143.
- Willen, E. 1991. Planktonic diatoms-an ecological review. *Algological Studies* 62:69–106.
- Yamaguchi, M., H. Yamaguchi, G. Nishitani, S. Sakamoto, and S. Itakura. 2008. Morphology and germination characteristics of the cysts of *Chatonella ovata* (Raphidophyceae), a novel red tide flagellate in the Seto Island Sea, Japan. *Harmful Algae* 7:459–463.

Appendix 3-A

Prediction and Uncertainty Analysis of Eutrophication in the New River Estuary: An Integrated Bayesian Network Approach

Prediction and Uncertainty Analysis of Eutrophication in the New River Estuary: An Integrated Bayesian Network Approach

SERDP Project Number: RC-1413

Aquatic/Estuarine Module

Research Project AE-1

Lead Researcher:

Kenneth H. Reckhow

Cardno ENTRIX

Raleigh, NC

Supporting Researcher:

Farnaz Nojavan

Duke University

Durham, NC

August 3, 2012

Final Report

Table of Contents

List of Acronyms	3-A-viii
Abstract	3-A-1
Objectives	3-A-2
Background	3-A-2
Materials and Methods.....	3-A-2
BBN Nodes	3-A-3
Building Conditional Probability Tables	3-A-9
BBN Validation	3-A-12
Results and Discussion	3-A-23
Freshwater Discharge.....	3-A-23
Wind.....	3-A-25
Stratification.....	3-A-26
Temperature	3-A-28
Phosphorus Concentrations.....	3-A-30
Nitrogen Concentrations	3-A-31
Chl <i>a</i> Concentrations.....	3-A-33
Benthic Oxygen Concentrations	3-A-35
Conclusions and Implications for Future Research	3-A-37
Literature Cited	3-A-37

List of Figures

3-A-1.	Structure of the BBN with its Components.	3-A-4
3-A-2.	Bivariate scatter plots below the diagonal, histograms on the diagonal, and the Pearson correlation above the diagonal for chl <i>a</i> ($\mu\text{g/lit}$) and its regulating factors: light attenuation coefficient ($1/\text{m}$), stratification ($\Delta\rho$), DIN ($\mu\text{g/lit}$), orthophosphate ($\mu\text{g/lit}$), temperature ($^{\circ}\text{C}$).	3-A-5
3-A-3.	Bivariate scatter plots below the diagonal, histograms on the diagonal, and the Pearson correlation above the diagonal for freshwater discharge and its regulating factor.	3-A-6
3-A-4.	Bivariate scatter plots below the diagonal, histograms on the diagonal, and the Pearson correlation above the diagonal for stratification (upper left), K_d (upper right), dissolved inorganic nitrogen (lower left), orthophosphate (lower right) and their regulating factors.	3-A-7
3-A-5.	Bivariate scatter plots below the diagonal, histograms on the diagonal, and the Pearson correlation above the diagonal for benthic dissolved oxygen and its regulating factors.	3-A-8
3-A-6.	BBN structure, the nodes represent variables of interest, and the existence of a link between two nodes means informational and/or causal dependency.	3-A-11
3-A-7.	BBN for the NRE to investigate ecosystem-scale effects of regional anthropogenic activities and natural stressors on NRE's water quality and ecological condition using chl <i>a</i> concentrations, bottom water oxygen, and formation of HABs as major indicators of its ecological health.	3-A-12
3-A-8.	A low freshwater discharge ($\text{FWD} < 31 \text{ m}^3/\text{s}$) scenario for the NRE.	3-A-24
3-A-9.	A high freshwater discharge ($\text{FWD} > 142 \text{ m}^3/\text{s}$) scenario for the NRE.	3-A-24
3-A-10.	A low wind (wind $< 1.2 \text{ mph}$) scenario for the NRE.	3-A-25
3-A-11.	A high wind ($3.80 \text{ mph} < \text{wind}$) scenario for the NRE.	3-A-26
3-A-12.	A stratified water column ($3.6 < \Delta\rho$) scenario for the NRE.	3-A-27
3-A-13.	A well-mixed water column ($\Delta\rho < 1.04$) scenario for the NRE.	3-A-27
3-A-14.	A partially stratified water column ($1.04 < \Delta\rho < 3.60$) scenario for the NRE.	3-A-28
3-A-15.	A high temperature (temperature $> 25.80^{\circ}\text{C}$) scenario for the NRE.	3-A-29
3-A-16.	A low temperature (temperature $< 12^{\circ}\text{C}$) scenario for the NRE.	3-A-29
3-A-17.	A low phosphorus concentration (phosphorus $< 5.29 \mu\text{g/L}$) scenario for the NRE.	3-A-30
3-A-18.	A high phosphorus concentration (phosphorus $> 36.75 \mu\text{g/L}$) scenario for the NRE.	3-A-31
3-A-19.	A low nitrogen concentration (nitrogen $< 56.29 \mu\text{g/L}$) scenario for the NRE.	3-A-32
3-A-20.	A high nitrogen concentration (nitrogen $> 334.20 \mu\text{g/L}$) scenario for the NRE.	3-A-33

3-A-21. A low chlorophyll <i>a</i> concentration (chlorophyll <i>a</i> <40.70 µg/L) scenario for the NRE.....	3-A-34
3-A-22. A high chlorophyll <i>a</i> concentration (chlorophyll <i>a</i> >40.70 µg/L) scenario for the NRE.....	3-A-35
3-A-23. A low benthic dissolved oxygen concentration (benthic dissolved oxygen <4.03 mg/L) scenario for the NRE.....	3-A-36
3-A-24. A high benthic dissolved oxygen concentration (benthic dissolved oxygen >4.03) scenario for the NRE.	3-A-37

List of Tables

3-A-1. The station information for data downloaded on precipitation and wind speed.	3-A-10
3-A-2. Conditional probability for DIN node and parent nodes FWD and Stratification.	3-A-10
3-A-3. BBN validation for chl <i>a</i> node, confusion matrix, error rate, and Area under Curve representing matching between the actual states and the predicted, % of cases matching the predictions, the goodness of the BBN as a classifier for the node.	3-A-13
3-A-4. BBN validation for Benthic Dissolved Oxygen node, confusion matrix, error rate, and Area under Curve representing matching between the actual states and the predicted, % of cases matching the predictions, the goodness of the BBN as a classifier for the node. Average Euclidian distance and average Kulbach-Leibler divergence are also reported. On the ROC, X-axis is the false positive rate, and the Y-axis is the true positive rate.	3-A-14
3-A-5. BBN validation for 19'-hexanoyloxyfucoxanthin node, confusion matrix, error rate, and Area under Curve representing matching between the actual states and the predicted, % of cases matching the predictions, the goodness of the BBN as a classifier for the node. Average Euclidian distance and average Kulbach-Leibler divergence are also reported. On the ROC, X-axis is the false positive rate, and the Y-axis is the true positive rate.	3-A-15
3-A-6. BBN validation for Gyroxanthin node, confusion matrix, error rate, and Area under Curve representing matching between the actual states and the predicted, % of cases matching the predictions, the goodness of the BBN as a classifier for the node. Average Euclidian distance and average Kulbach-Leibler divergence are also reported. On the ROC, X-axis is the false positive rate, and the Y-axis is the true positive rate.	3-A-16
3-A-7. BBN validation for Peridinin node, confusion matrix, error rate, and Area under Curve representing matching between the actual states and the predicted, % of cases matching the predictions, the goodness of the BBN as a classifier for the node. Average Euclidian distance and average Kulbach-Leibler divergence are also reported. On the ROC, X-axis is the false positive rate, and the Y-axis is the true positive rate.	3-A-17
3-A-8. BBN validation for Vialoxanthin node, confusion matrix, error rate, and Area under Curve representing matching between the actual states and the predicted, % of cases matching the predictions, the goodness of the BBN as a classifier for the node. Average Euclidian distance and average Kulbach-Leibler divergence are also reported. On the ROC, X-axis is the false positive rate, and the Y-axis is the true positive rate.	3-A-18

- 3-A-9. BBN validation for Growth Rate node, confusion matrix, error rate, and Area under Curve representing matching between the actual states and the predicted, % of cases matching the predictions, the goodness of the BBN as a classifier for the node. Average Euclidian distance and average Kulbach-Leibler divergence are also reported. On the ROC, X-axis is the false positive rate, and the Y-axis is the true positive rate.3-A-19
- 3-A-10. BBN validation for PPR node, confusion matrix, error rate, and Area under Curve representing matching between the actual states and the predicted, % of cases matching the predictions, the goodness of the BBN as a classifier for the node. Average Euclidian distance and average Kulbach-Leibler divergence are also reported. On the ROC, X-axis is the false positive rate, and the Y-axis is the true positive rate.....3-A-20
- 3-A-11. BBN validation for Nitrogen node, confusion matrix, error rate, and Area under Curve representing matching between the actual states and the predicted, % of cases matching the predictions, the goodness of the BBN as a classifier for the node. Average Euclidian distance and average Kulbach-Leibler divergence are also reported. On the ROC, X-axis is the false positive rate, and the Y-axis is the true positive rate.....3-A-21
- 3-A-12. BBN validation for Phosphorus node, confusion matrix, error rate, and Area under Curve representing matching between the actual states and the predicted, % of cases matching the predictions, the goodness of the BBN as a classifier for the node. Average Euclidian distance and average Kulbach-Leibler divergence are also reported. On the ROC, X-axis is the false positive rate, and the Y-axis is the true positive rate.3-A-22

List of Acronyms

BBN	Bayesian Belief Network
Chl a	Chlorophyll a
CPT	Conditional Probability Table
DCERP	Defense Coastal/Estuarine Research Project
DIN	Dissolved Inorganic Nitrogen
DoD	U.S. Department of Defense
FWD	Freshwater Discharge
HAB	Harmful Algal Bloom
Kd	Light Attenuation Coefficient
MARDIS	Monitoring and Research Data Information System
NPC	Necessary Path Condition
NRE	New River Estuary
PPR	Primary Productivity
SERDP	Strategic Environmental Research and Development Program

Abstract

Estuaries are amongst the most productive environments on earth due to their semi-enclosed nature, riverine inflow of nutrients, extensive intertidal plant communities, and shallow depth. Human population growth and human activities along the estuaries have accelerated the accumulation of the nutrients, altering estuarine watersheds dynamics throughout the world. High rates of nutrient input into estuaries can contribute to low dissolved oxygen, toxic algal blooms, fish kills, and benthic habitat degradation. The New River Estuary located near the largest Marine Corps base on the East Coast of the U.S., in Onslow County, North Carolina is a shallow estuary draining a catchment area of 1,436 km². The NRE was considered one of the most eutrophic estuaries in the south eastern United States during the 1980s and 1990s (Burkholder et al., 1997; Mallin, McIver, Wells, & Parsons, 2005; NOAA, 1996); hence it is crucial to develop a quantified understanding of the scientific and management factors impacting eutrophication in the New River Estuary.

This study identifies and quantifies ecosystem-scale effects of regional anthropogenic activities and natural stressors on chlorophyll *a* concentrations, harmful algal blooms presence/absence, and benthic dissolved oxygen concentrations, indicators of estuarine water quality and ecological condition, using a Bayesian Belief Network (BBN). A BBN consists of a graphical model with probabilistic relationships encoded among variables in a system. The graphical model is built based on an understanding of the causal relationships in the system. Using the data from ongoing monitoring and experimental projects along the New River Estuary, we identify and quantify the factors affecting water quality indicators. This will provide a regulatory tool for researchers, managers and policy makers to evaluate the impact of local and regional stressors of ecological condition in the New River Estuary. Furthermore BBN will enable us to quantify uncertainties associated with predictions.

Our results indicate that physical forcings play a significant role in regulating chlorophyll *a* concentrations, harmful algal bloom presence/absence, and benthic dissolved oxygen concentrations. Among the physical forcings, freshwater discharge plays a triple role in the dynamics of the system by delivering nutrients, impacting water column stratification, and regulating the residence time of water in the estuary.

Keywords: Bayesian belief network, BBN, Estuarine ecosystem modeling, Eutrophication, Harmful algal blooms, HABs, benthic dissolved oxygen concentrations, chlorophyll *a* concentrations

Objectives

In this study, we analyze drivers and effects of eutrophication in the New River Estuary (NRE) by quantifying the impact of eutrophication on ecological health utilizing water quality indicators, i.e. surface chlorophyll *a* concentrations, presence/absence of harmful algal blooms (HABs) and benthic dissolved oxygen (DO).

Background

We investigate the eutrophication dynamics in the New River Estuary (NRE), located at Onslow county North Carolina, with a surface area of 32.8 mi², and an average depth of 5.2 ft.. Surrounded by Marine Corps Base Camp Lejeune, the largest Marine Corps in east coast US and yet to be expanded, the NRE is at risk of anthropogenic disturbances. The NRE was once considered one of the most eutrophic estuaries in the USA, however the symptoms have alleviated after the upgrade of sewer systems in its watershed (M. A. Mallin et al. 1997; M. Mallin et al. 2005). The NRE experiences moderate to high levels of chlorophyll *a*, nitrogen, phosphorus, and turbidity, with occasional presence of bottom water hypoxia, and nuisance and toxic algae (NOAA 1996). Eutrophication is spatially extended all along the NRE; however extreme events tend to occur in Morgan Bay near the head of the estuary (NOAA 1996).

The interaction of physical, chemical, and biological processes that lead to eutrophic symptoms is complex and partially ecosystem specific. Furthermore, as in many other ecosystems, estuaries have diverse stakeholders. In order to quantify the impact of eutrophication on ecological health and present results readily communicable with stakeholders, we investigate drivers and effects of eutrophication in the NRE using a Bayesian belief networks (BBN) approach on water quality indicators, i.e. surface chlorophyll *a* concentrations, presence/absence of harmful algal blooms and benthic dissolved O₂ (Ryther 1971; Strobl & Robillard 2008; Conley et al. 2009; Sheldon & Alber 2011). BBNs are directed acyclic graphs, composed of nodes and links, with embedded conditional probability tables associated with each node (Jensen & Nielsen 2007; Heckerman 2008). The interaction between BBN's variables is of an informational and/or causal dependency. BBNs' visualization makes them a valuable tool to communicate research with stakeholders with variety of knowledge background. Applying object oriented approach in a developed BBN facilitates reusing it in other ecosystems by accommodating ecosystem specific variability (Jensen & Nielsen 2007; Koller & Pfeffer 1997; Johnson et al. 2010). BBN, a tool to reason under uncertainty, suits predicting future, investigating climate change scenarios, and dealing with small dataset (Uusitalo 2006).

Materials and Methods

We examined the impact of human and climatic environmental factors' on water quality criteria in the NRE utilizing a Bayesian Belief Network (BBN). The first step in developing a BBN is setting the modeling boundary, and identifying its components. Based on aforementioned objectives, the BBN has five components (i.e., physical environment, nutrients, chlorophyll *a* [chl *a*] concentration, HABs, and hypoxia/anoxia) representing environmental factors (precipitation [in], wind intensity [mph], freshwater discharge [m³/s], temperature [°C], stratification, and light [m]); human impacts (dissolved inorganic nitrogen [DIN; µg/L], orthophosphate [PO₄; µg/L]); chl *a* concentration (µg/L); harmful algal blooms presence/absence; and benthic dissolved oxygen levels (mg/L), respectively (**Figure 3-A-1**). The

three later components are the water quality indicators of interest, and it is of critical importance to study how they respond to changes in environmental factors and anthropogenic perturbations. Further, we need to identify the important variables within each component and how these variables interact within our model's boundary. The interaction between BBN's components is of an informational and/or causal dependency. In the following section we explain the variables within BBN and justify their connections.

BBN Nodes

Freshwater discharge brings nutrients into the estuary (Paerl, Valdes, Peierls, Adolf, & Lawrence, 2011). Hence chl *a* concentrations depend on the levels of freshwater discharge. Further, discharge regulates residence time which means that high freshwater discharges also flushes chl *a* and nutrients from the estuary to the open ocean. In contrast, low freshwater discharges are associated with lower nutrient inflow. Freshwater discharge also plays an important role in stratifying and mixing the water column which impacts both benthic oxygen concentrations and light availability for phytoplankton photosynthesis. The main factor regulating freshwater discharge is precipitation (**Figure 3-A-3**).

In estuarine ecosystems, major drivers of water column mixing are freshwater discharge, wind and tidal energy (Cloern 2001). In the NRE, the tidal energy is constrained by the geomorphology and shallow depth of the NRE inlet as well as the narrowing of the estuary at the Highway 17 bridge. Hence the main mixing energies for the upper and middle estuary are wind and freshwater discharge (**Figure 3-A-4**) (Ensign, Halls, & Mallin, 2004). In our study, stratification was calculated as the difference between bottom water salinity and surface water salinity. The most important factor for phytoplankton photosynthesis is light availability (Domingues, Anselmo, Barbosa, Sommer, & Galvão, 2011; Gameiro, Zwolinski, & Brotas, 2011; Keller, 1989). Freshwater discharge and stratification regulate light availability by impacting turbidity and chromophoric dissolved organic matter, through delivery or suspension (**Figure 3-A-4**).

Main sources of nutrients (in our study DIN and PO₄) in the NRE are delivered through freshwater discharge or resuspension from sediments. The resuspension occurs when the water column is mixing, hence the degree of water column stratification impacts nutrient concentrations (**Figure 3-A-4**).

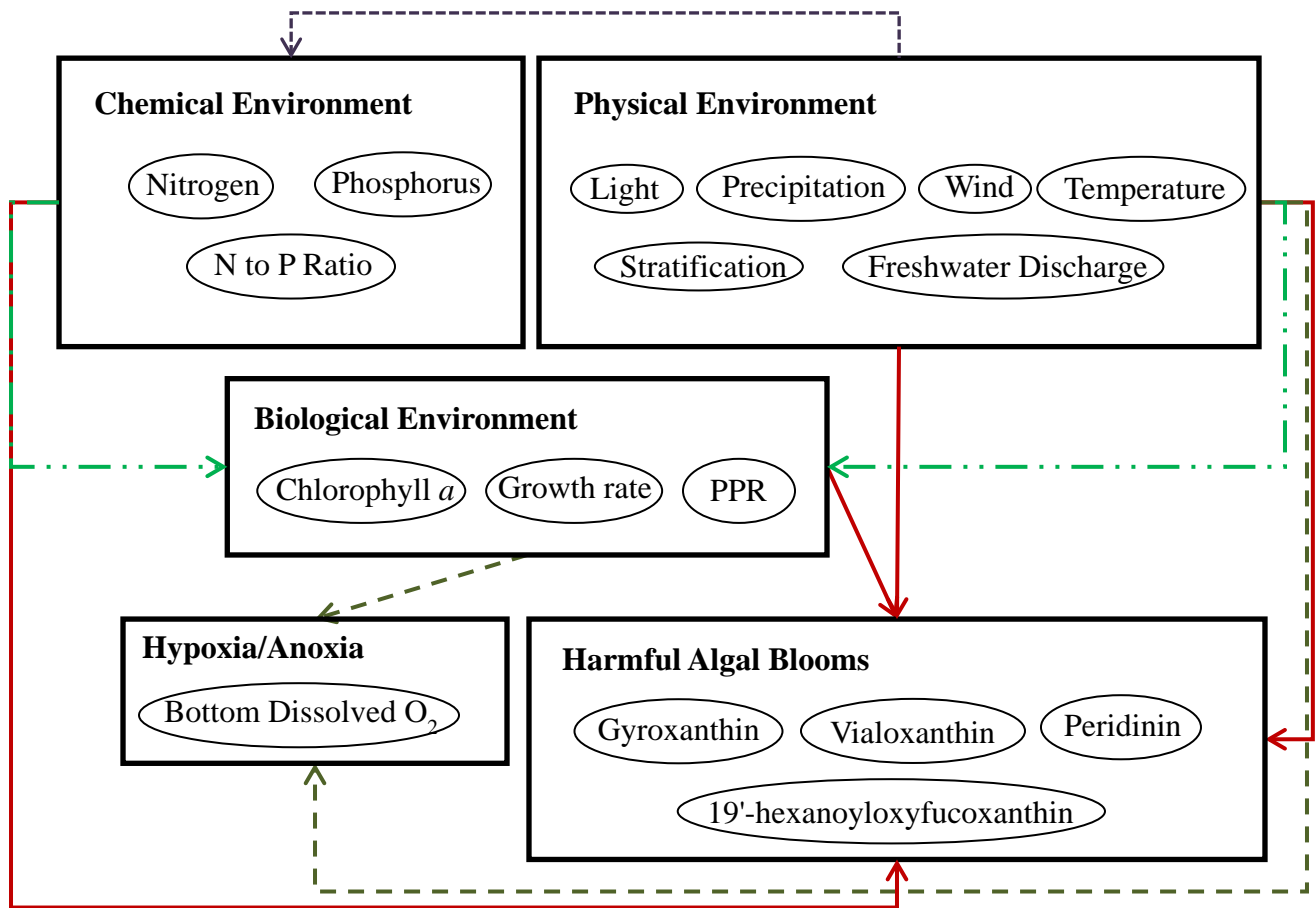


Figure 3-A-1. Structure of the BBN with its Components.

The “Physical Environment” will include variables representing climatic forcings, and the “Harmful Algal Blooms” will feature the pigments characterizing HABs. Other components are typical of an eutrophication model.
 Abbreviations: N = nitrogen, P = phosphorus, PPR = primary productivity; O₂ = oxygen

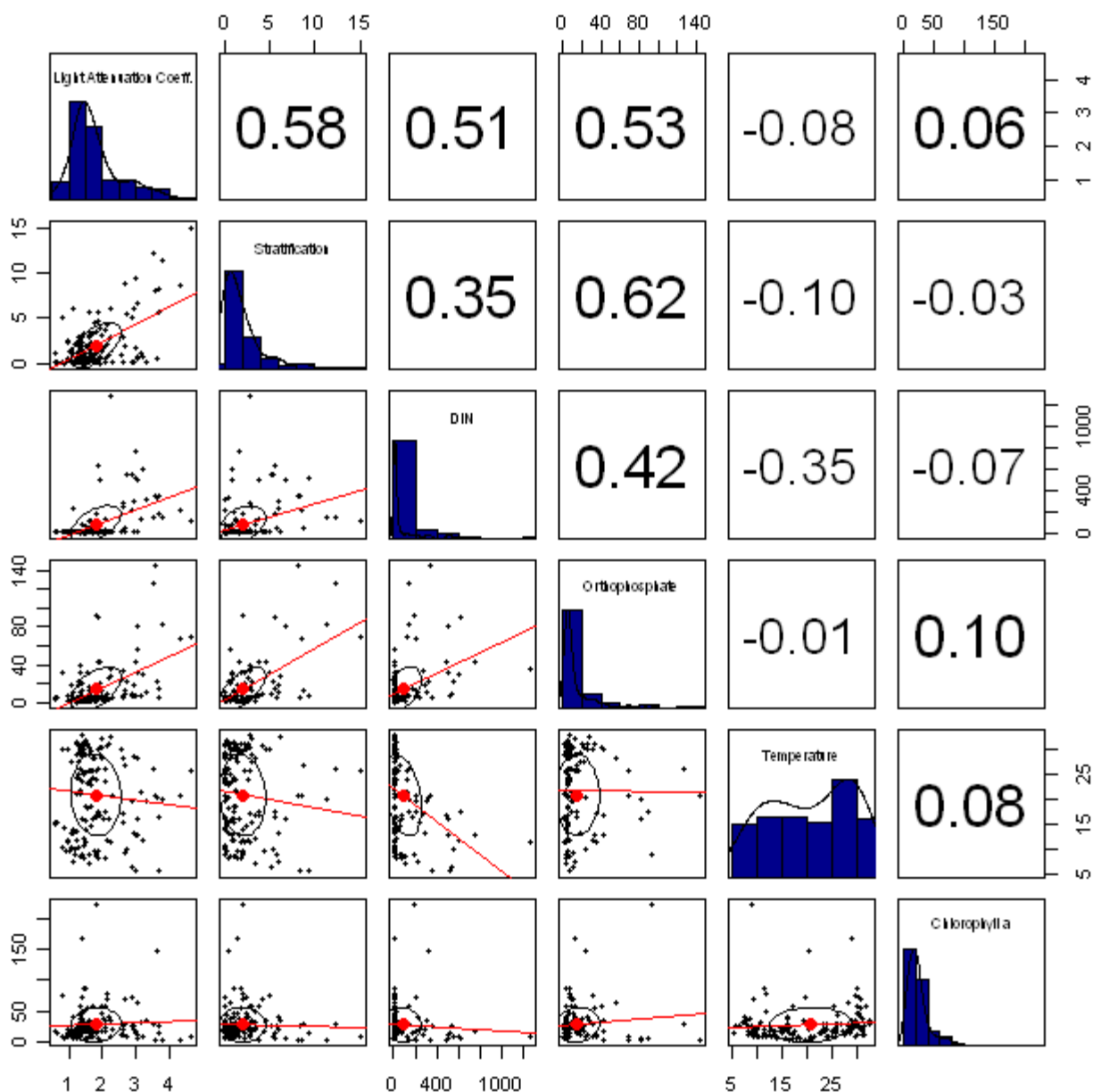


Figure 3-A-26. Bivariate scatter plots below the diagonal, histograms on the diagonal, and the Pearson correlation above the diagonal for chl a ($\mu\text{g/lit}$) and its regulating factors: light attenuation coefficient ($1/\text{m}$), stratification ($\Delta\rho$), DIN ($\mu\text{g/L}$), orthophosphate ($\mu\text{g/L}$), temperature ($^{\circ}\text{C}$).

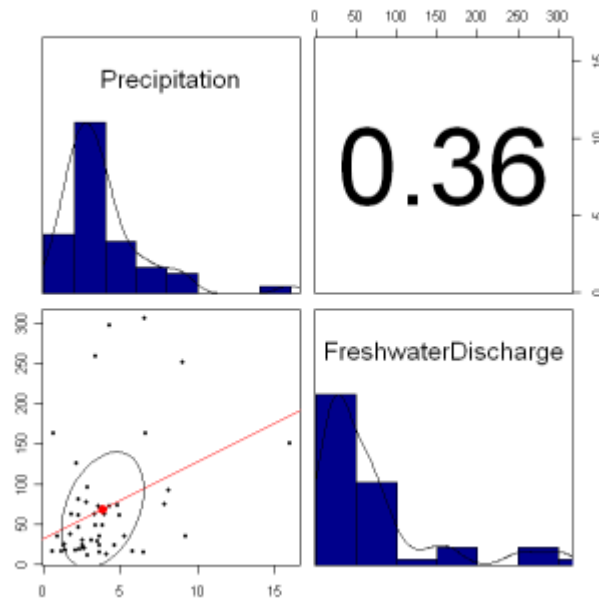


Figure 3-A-3. Bivariate scatter plots below the diagonal, histograms on the diagonal, and the Pearson correlation above the diagonal for freshwater discharge and its regulating factor.

Chl *a* concentration is a measure of algal biomass in water. Factors regulating chl *a* concentrations within the NRE are light, stratification, nutrients (nitrogen and phosphorus), and temperature. **Figure 3-A-2** shows bivariate scatter plots below the diagonal, histograms on the diagonal, and the Pearson correlation above the diagonal. The variables are chl *a* and its regulating factors. The factors are quantified by means of the light attenuation coefficient (*K*), the difference between bottom and surface water density, DIN (i.e., nitrate + nitrite + ammonium), and PO₄ concentrations, respectively. Parallel to chl *a* concentrations, we also investigated the PPR (primary productivity) and growth rate. The PPR and the “Growth Rate” variable evaluate whether the system is top-down or bottom-up controlled. High PPR with high “Growth Rate”, means the system is controlled bottom-up, whereas high PPR but low Growth Rate, indicates the system is controlled by grazing (top down). We calculated the “Growth Rate” using the following equation:

$$\text{Growth Rate} = \frac{\text{PPR}}{[\text{Chl } a] \times \left[\frac{C}{[\text{Chl } a]} \right]}, \text{ PPR}$$

In order to calculate $\left[\frac{C}{[\text{Chl } a]} \right]$ we utilized the following empirical relationship (Cloern et al. 1995):
 Chl: $C = 0.003 + 0.0154[\exp(0.050T)] \times \langle \exp \left\{ -0.059 \left(\frac{I_0}{kH} \right) [1 - \exp(-kH)] \right\} \rangle \times [N/(K_N + N)]$,
 where:

T: temperature, I_0 : daily irradiance, *k*: light attenuation coefficient, *H*: depth of mixed layer, *N*: concentration of the most limiting nutrient (DIN in our study) and *K_N*: half saturation constant. Chl *a* concentrations were measured at eight water column monitoring stations along the main channel of NRE by Dr. Paerl.

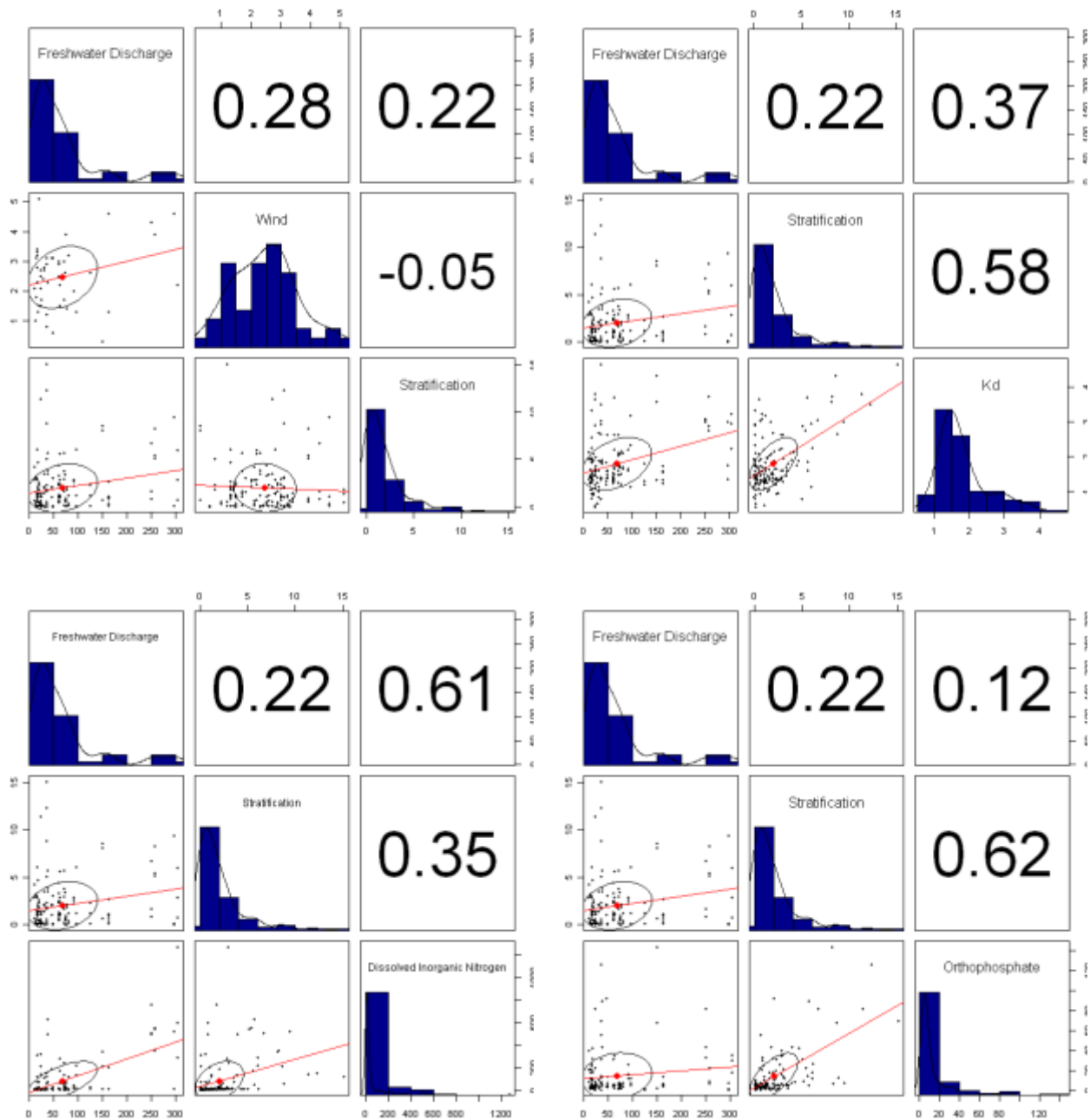


Figure 3-A-4. Bivariate scatter plots below the diagonal, histograms on the diagonal, and the Pearson correlation above the diagonal for stratification (upper left), Kd (upper right), dissolved inorganic nitrogen (lower left), orthophosphate (lower right) and their regulating factors.

Benthic dissolved oxygen concentration is an important factor to investigate in an estuarine ecosystem. Low bottom water oxygen concentrations may result in limiting or loss of habitat and fish kills due to hypoxia. High chl *a* concentrations in the water column consume oxygen from the water by respiration or microbial decomposition. Low bottom water oxygen concentrations can also be the result of a stratified water column. Stratification severely dampens mixing in the vertical dimension of the water column, and the sediment oxygen demand gives rise to hypoxic or anoxic conditions (**Figure 3-A-5**).

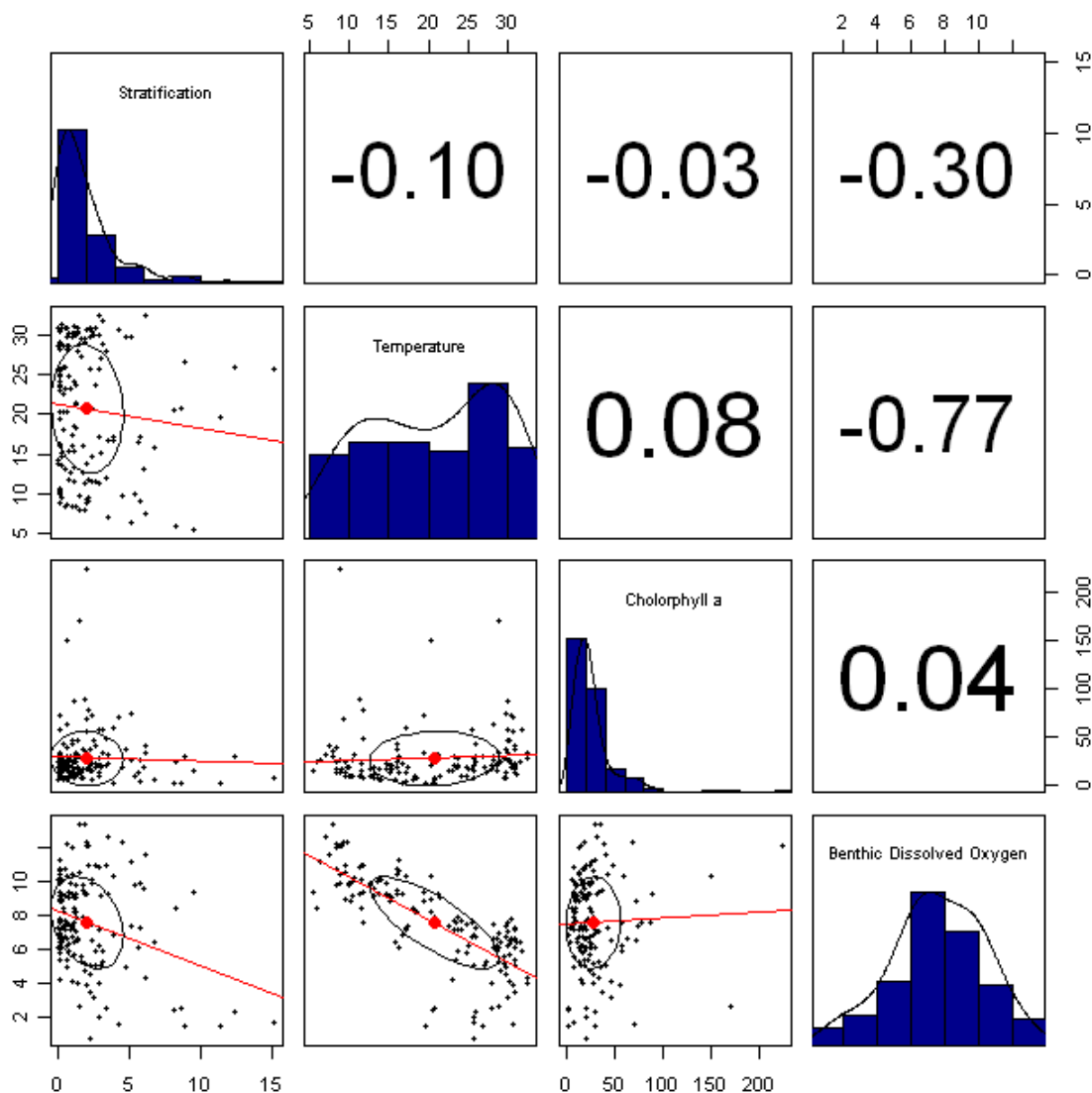


Figure 3-A-27. Bivariate scatter plots below the diagonal, histograms on the diagonal, and the Pearson correlation above the diagonal for benthic dissolved oxygen and its regulating factors.

For HABs, we did not have data at the species level; therefore, we utilized accessory photopigments that are indicative of dominant HAB taxa as biomarkers for the presence or absence of HAB species. Gyroxanthin and 19' hexanoyloxyfucoxanthin were used as indicators for the toxic dinoflagellate, *Karlodinium veneticum*. Peridinin was used as a class-level indicator of dinoflagellates which contain some HAB species, and violaxanthin was used as a class level indicator for toxic marine raphidophytes.

Building Conditional Probability Tables

The next step in developing the BBN is building the conditional probability tables (CPTs). We utilized the data from the monthly water column samples along the mainstem of the NRE from October 2007 to September 2011. We use the BBN softwares Hugin Educational 7.0 (Madsen et al., 2003). Hugin 7.0 has a Learning wizard embedded within the software that can be utilized to develop the CPTs based on the data. The settings we used to develop the CPTs were as follows: level of significance: 0.001; algorithm: Necessary Path Condition (NPC) and the EM (Expectation-Maximization) Learning algorithm (Dempster and Laird, 1977; Madsen et al., 2003), and the time line for the data: 10/2007–9/2011. For the data on precipitation and wind speed, we downloaded the data from the North Carolina State Climate Office of North Carolina for the modeling period. The details of the station information are described in **Table 3-A-1**.

Variables in BBN are discrete; hence, we needed to represent a quantity or series using a discrete quantity or quantities of the data prior to building the CPTs. We utilized several discretization methods depending on the variable. Mainly we used the Moment Matching Method to discretize all variables except chl a and BO. In this method, we try to match as many as possible of the lower statistical moments of the initial distribution. The “moment matching approach lets us correctly represent the first few moments of the assessed input distributions, so that we can often easily and accurately compute the moments of the output distribution” (Smith, 1993). Discretizing with n points will result in matching 2n-1 moments of a given distribution. In this study we have discretized the raw data, using two points into three intervals. Three or more points result in too many states for the child nodes (Alameddine et al., 2011).

The first three moments of the data are calculated as follows:

$$\begin{aligned} p_1x_1 + p_2x_2 &= \mu, p_1(x_1 - \mu)^2 + p_2(x_2 - \mu)^2 = \sigma^2, \\ p_1(x_1 - \mu)^3 + p_2(x_2 - \mu)^3 &= \mu_3, \end{aligned}$$

where $x_1, x_2, p_1, p_2, \mu, \sigma^2, \mu_3$ are the first and second breaking points, first and second probability associated with breaking points, mean, variance and skewness of data respectively.

The two points are calculated using the following equation:

$$x_i = \mu + \frac{\mu_3}{2\sigma^2} + (-1)^i \sqrt{\left(\frac{\mu_3}{2\sigma^2}\right)^2 + \sigma^2}, i = 1, 2$$

For chlorophyll a and benthic dissolved oxygen concentrations, the State of North Carolina has set standards of 40 µg/L and 4 mg/L, respectively. Hence discretization was based on those standards.

Table 3-A-1. The station information for data downloaded on precipitation and wind speed.

State Climate Office of North Carolina North Carolina State University	
Data Base	CRONOS
Station ID	KNCA
Station Type	AWOS
Station Name	New River MCAS
City, State	Jacksonville, NC
County	Onslow County
Latitude	34.7073361
Longitude	-77.4451639
Elevation	26 feet above sea level
Climate Division	NC06 - Southern Coastal Plain
Supported by	US Military

Table 3-A-2. Conditional probability table for DIN node and parent nodes FWD and Stratification.

FWD		Low			Medium Low			Medium High			High		
Stratification		L	M	H	L	M	H	L	M	H	L	M	H
DIN	L	0.9	0.92	0.75	1	0.8	0.375	0.8	0.8	0.3	0.7	0.5	0
	M	0.1	0.08	0.25	0	0.2	0.375	0.2	0.2	0.7	0.1	0	0.25
	H	0	0	0	0	0	0.25	0	0	0	0.2	0.5	0.75
Experience		34	25	4	16	18	8	11	13	3	9	4	8

Experience is the number of real measurements from the dataset that are in that specific status. These nodes, their states, probabilities and relationships are visible in the Bayesian network in Figure 3-A-7. Note: L = low, M = medium, and H = high

The number of intervals was chosen depending on the variable. For HABs and Growth Rate only two intervals were defined since only presence/absence or $>0.01/<0.01$ (1/day) were important; however for other variables three intervals were defined since that is the minimum intervals that can best represent the shape of the underlying distribution. For environmental variables (i.e., precipitation, FWD, wind intensity, and temperature), four intervals were chosen to capture detailed impacts of them on the NRE.

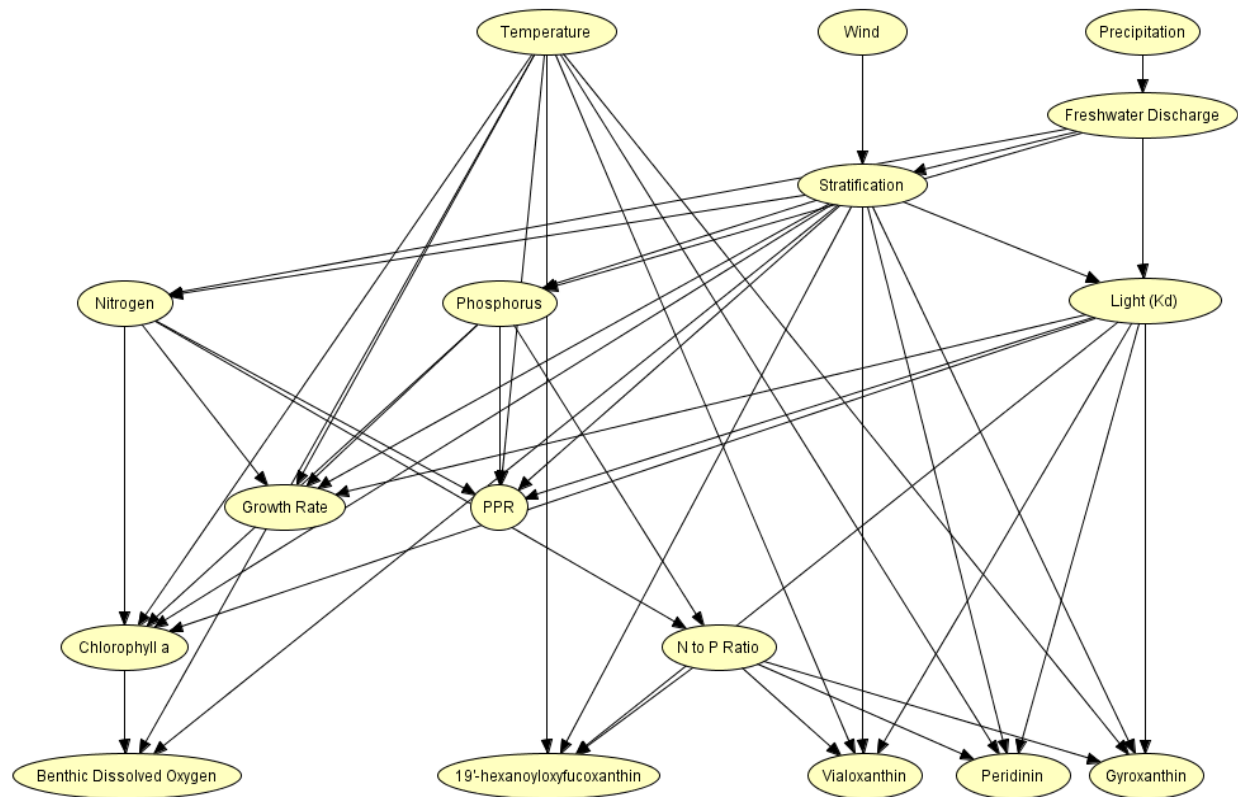


Figure 3-A-6. BBN structure, the nodes represent variables of interest, and the existence of a link between two nodes means informational and/or causal dependency.

Note: PPR = primary productivity

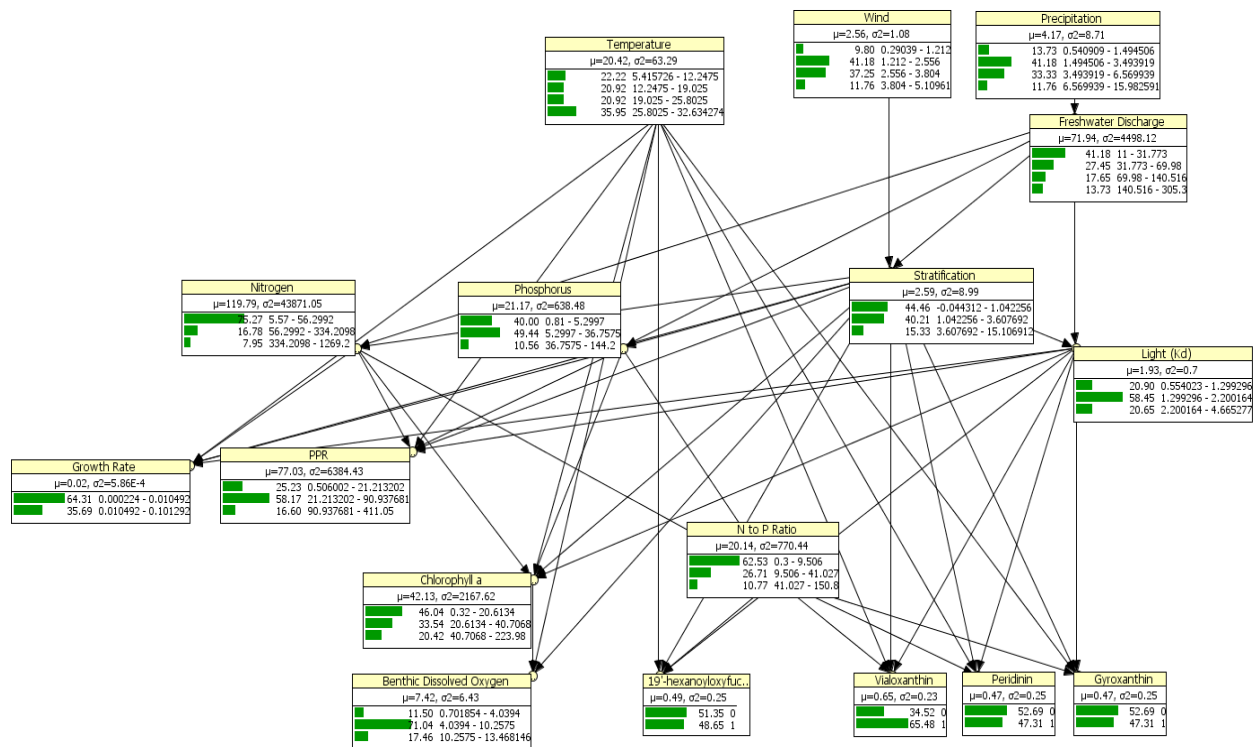


Figure 3-A-7. BBN for the NRE to investigate ecosystem-scale effects of regional anthropogenic activities and natural stressors on NRE's water quality and ecological condition using chl *a* concentrations, bottom water oxygen, and formation of HABs as major indicators of its ecological health.

Green bars represent probability of each defined state; the numbers next to bars are probability of the variable being in that state, and the numbers represented as intervals to the right of the probabilities are the interval defined for the status of the variables of interest.

BBN Validation

We utilized Area Under Curve (AUC; Receiver Operator Characteristic models sensitivity as a function of (1-specificity), and the area under the ROC curve is called AUC) to validate the BBN (Marcot and Steventon, 2006). Using the analysis wizard embedded in Hugin 7.1 software, we generated 10,000 cases, with 5% of the values Missing at Random. The results are summarized in **Table 3-A-3 through 3-A-12**. In the case of all water quality indicator variables the AUC is larger than 0.80, which demonstrates the good predictability of the BBN. Without exception the confusion matrices show that the model is capable of distinguishing between states of water quality indicator variables.

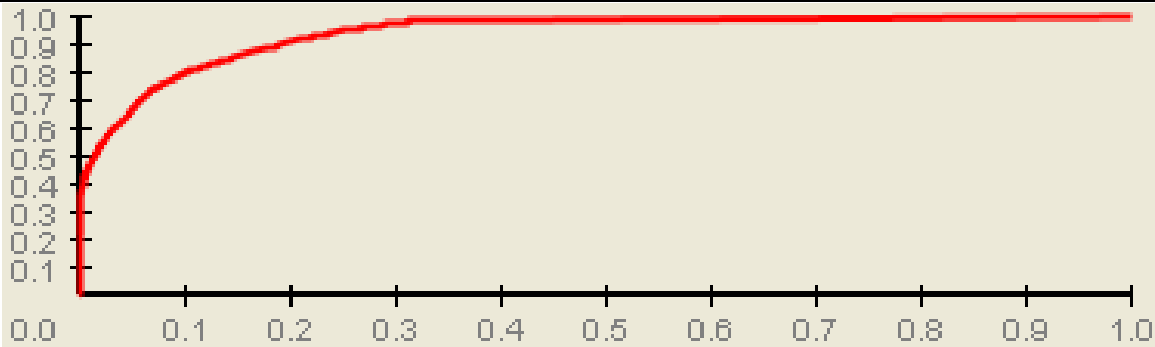
Table 3-A-3. BBN validation for chl *a* node, confusion matrix, error rate, and Area under Curve representing matching between the actual states and the predicted, % of cases matching the predictions, the goodness of the BBN as a classifier for the node.

Node	Chlorophyll <i>a</i>	Number of cases	10,000	
Confusion Matrix				
[actual]	0.32–20.6134	20.6134–40.7068	40.7068–223.98	[predicted]
	681	0	0	0.32–20.6134
	0	200	0	20.6134–40.7068
	0	0	182	40.7068–223.98
	Error rate	Avg. Euclidian distance	Avg. Kulbach-Leibler divergence	Area Under the Curve
	89.37	0.32922	0.53551	0.90999

Average Euclidian distance and average Kulbach-Leibler divergence are also reported. On the ROC, *x*-axis is the false positive rate, and the *y*-axis is the true positive rate.

Table 3-A-4. BBN validation for Benthic Dissolved Oxygen node, confusion matrix, error rate, and Area under Curve representing matching between the actual states and the predicted, % of cases matching the predictions, the goodness of the BBN as a classifier for the node.

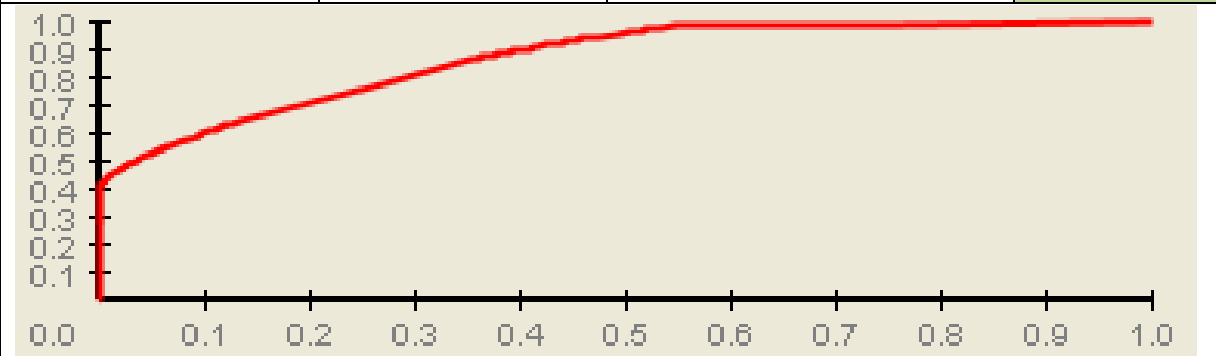
Node	Benthic dissolved oxygen	Number of cases	9,328	
Confusion Matrix				
[actual]	0.70185381–4.0394	4.0394–10.2575	10.2575–13.468146	
	35	0	0	0.70185381–4.0394
	0	820	0	.0394–10.2575
	0	0	65	10.2575–13.468146
	Error rate	Avg. Euclidian distance	Avg. Kulbach-Leibler divergence	Area Under the Curve
	90.14	0.26615	0.40402	0.94582



Average Euclidian distance and average Kulbach-Leibler divergence are also reported. On the ROC, *x*-axis is the false positive rate, and the *y*-axis is the true positive rate.

Table 3-A-5. BBN validation for 19'-hexanoyloxyfucoxanthin node, confusion matrix, error rate, and Area under Curve representing matching between the actual states and the predicted, % of cases matching the predictions, the goodness of the BBN as a classifier for the node.

Node	19'-hexanoyloxyfucoxanthin		Number of cases	10,000
Confusion Matrix				
[actual]	0	1	[predicted]	
	1044	0	0	
	0	621	1	
Error rate	Avg. Euclidian distance	Avg. Kulbach-Leibler divergence		Area under Curve
83.35	0.27597	0.39041		0.87375



Average Euclidian distance and average Kulbach-Leibler divergence are also reported. On the ROC, x -axis is the false positive rate, and the y -axis is the true positive rate.

Table 3-A-6. BBN validation for Gyroxanthin node, confusion matrix, error rate, and Area under Curve representing matching between the actual states and the predicted, % of cases matching the predictions, the goodness of the BBN as a classifier for the node.

Node	Gyroxanthin		Number of cases	10,000
Confusion Matrix				
[actual]	0	1	[predicted]	
	715	0	0	
	0	269	1	
Error rate	Avg. Euclidian distance	Avg. Kulbach-Leibler divergence		Area Under the Curve
90.16	0.33118	0.46540		0.80782

The figure is a Receiver Operating Characteristic (ROC) curve for the Gyroxanthin node classification. The x-axis represents the False Positive Rate (FPR) and the y-axis represents the True Positive Rate (TPR), both ranging from 0.0 to 1.0. A red curve is plotted, starting at (0,0) and rising steeply to a TPR of about 0.8 at an FPR of 0.1. The curve then continues to rise more gradually, reaching a TPR of 1.0 at an FPR of approximately 0.6. The area under the curve is shaded in light green, indicating a good classifier performance. The Area Under the Curve (AUC) value is 0.80782, which is displayed in the table above.

Average Euclidian distance and average Kulbach-Leibler divergence are also reported. On the ROC, x -axis is the false positive rate, and the y -axis is the true positive rate.

Table 3-A-7. BBN validation for Peridinin node, confusion matrix, error rate, and Area under Curve representing matching between the actual states and the predicted, % of cases matching the predictions, the goodness of the BBN as a classifier for the node.

Node	Peridinin	Number of cases	9,780
Confusion Matrix			
[actual]	0	1	[predicted]
	704	0	0
	0	233	1
Error rate	Avg. Euclidian distance	Avg. Kulbach-Leibler divergence	Area Under the Curve
90.42	0.32796	0.46233	0.81614

Average Euclidian distance and average Kulbach-Leibler divergence are also reported. On the ROC, x -axis is the false positive rate, and the y -axis is the true positive rate.

Table 3-A-8. BBN validation for Vialoxanthin node, confusion matrix, error rate, and Area under Curve representing matching between the actual states and the predicted, % of cases matching the predictions, the goodness of the BBN as a classifier for the node.

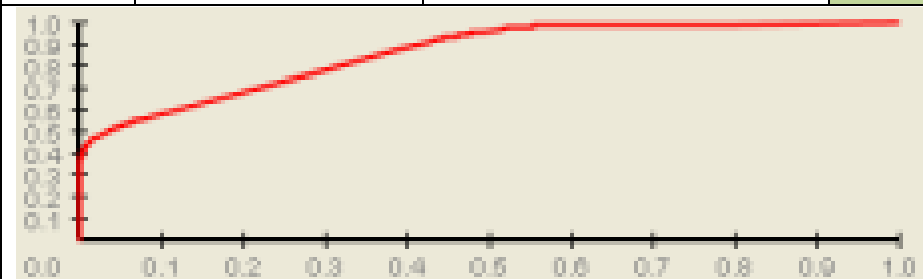
Node	Vialoxanthin		Number of cases	10,000
Confusion Matrix				
[actual]	0	1	[predicted]	
	354	0	0	
	0	552	1	
Error rate	Avg. Euclidian distance	Avg. Kulbach-Leibler divergence		Area under Curve
90.94	0.26803	0.38482		0.868

Average Euclidian distance and average Kulbach-Leibler divergence are also reported.

On the ROC, x -axis is the false positive rate, and the y -axis is the true positive rate.

Table 3-A-9. BBN validation for Growth Rate node, confusion matrix, error rate, and Area under Curve representing matching between the actual states and the predicted, % of cases matching the predictions, the goodness of the BBN as a classifier for the node.

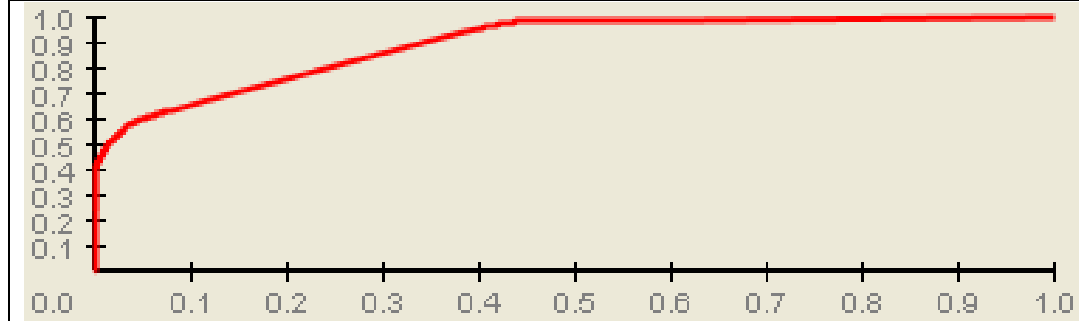
Node	Growth Rate		Number of cases	10,000
Confusion Matrix				
[actual]	2.2380388E-4 - 0.010491825	0.010491825 - 0.10129176		[predicted]
	941	0		2.2380388E-4 - 0.010491825
	0	333		0.010491825 - 0.10129176
Error rate	Avg. Euclidian distance	Avg. Kulbach-Leibler divergence		Area under Curve
87.26	0.28083	0.40147		0.86457



Average Euclidian distance and average Kulbach-Leibler divergence are also reported.
On the ROC, x-axis is the false positive rate, and the y-axis is the true positive rate.

Table 3-A-10. BBN validation for PPR node, confusion matrix, error rate, and Area under Curve representing matching between the actual states and the predicted, % of cases matching the predictions, the goodness of the BBN as a classifier for the node.

Node	PPR	Number of cases	10,000	
Confusion Matrix				
[actual]	0.5060018– 21.213202	21.213202–90.937681	90.937681–411.05	[predicted]
	147	0	0	0.5060018– 21.213202
	0	1089	0	21.213202– 90.937681
	0	0	124	90.937681–411.05
	Error rate	Avg. Euclidian distance	Avg. Kulbach-Leibler divergence	Area Under the Curve
	86.40	0.32872	0.52603	0.89992



Average Euclidian distance and average Kulbach-Leibler divergence are also reported. On the ROC, x -axis is the false positive rate, and the y -axis is the true positive rate.

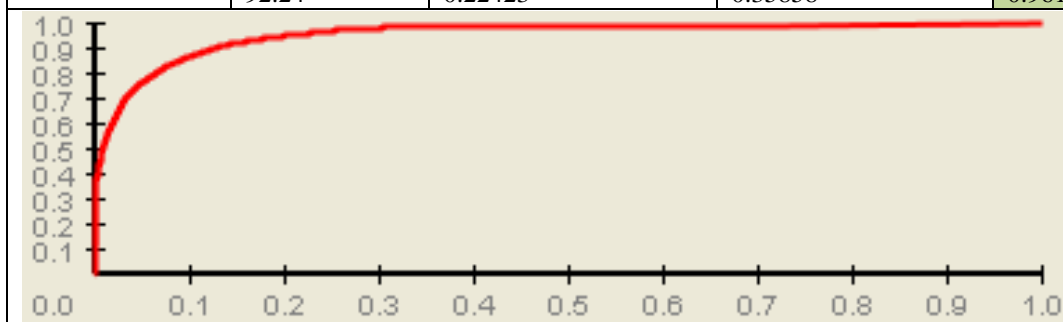
Table 3-A-11. BBN validation for Nitrogen node, confusion matrix, error rate, and Area under Curve representing matching between the actual states and the predicted, % of cases matching the predictions, the goodness of the BBN as a classifier for the node.

Node	DIN	Number of cases	10,000	
Confusion Matrix				
[actual]	5.57–56.2992	56.2992–334.2098	334.2098–1269.2	[predicted]
	2623	0	0	5.57–56.2992
	0	293	0	56.2992–334.2098
	0	0	155	334.2098–1269.2
	Error rate	Avg. Euclidian distance	Avg. Kulbach-Leibler divergence	Area Under the Curve
	69.29	0.07558	0.12335	0.99547

Average Euclidian distance and average Kulbach-Leibler divergence are also reported. On the ROC, x -axis is the false positive rate, and the y -axis is the true positive rate.

Table 3-A-12. BBN validation for Phosphorus node, confusion matrix, error rate, and Area under Curve representing matching between the actual states and the predicted, % of cases matching the predictions, the goodness of the BBN as a classifier for the node.

Node	Phosphorus (PO4)	Number of cases	8,768	
Confusion Matrix				
[actual]	0.81–5.2997	5.2997–36.7575	36.7575–144.2	[predicted]
	226	0	0	0.81–5.2997
	0	265	0	5.2997–36.7575
	0	0	189	36.7575–144.2
	Error rate	Avg. Euclidian distance	Avg. Kulbach-Leibler divergence	Area Under the Curve
	92.24	0.22423	0.35858	0.96133



Average Euclidian distance and average Kulbach-Leibler divergence are also reported. On the ROC, x -axis is the false positive rate, and the y -axis is the true positive rate.

Results and Discussion

The BBN enabled us to quantitatively assess the impact of climatic variability on nutrients, chl *a*, and benthic dissolved oxygen concentrations, as well as presence/absence of HABs. Our results support the crucial role played by water column stratification on estuarine water quality. As expected, the stratification is impacted by the freshwater discharge and wind intensity. Tidal forces have minimal impact on mixing the water column of the upper NRE due to the geomorphology and hydrodynamics of the New River Inlet and estuary. However, our study goes beyond the qualitative description. In a stratified water column ($3.6 < \Delta\rho$ [density gradient] < 15.1), the NRE's probability of experiencing chl *a* concentrations greater than 40 $\mu\text{g/L}$ increases by 5%. Hence high freshwater discharge ($> 140 \text{ m}^3/\text{s}$) causes both more stratified water column (0.41, 0.28, 0.30, probabilities of water column status being stratified from low to high) and higher nutrient levels P: (0.27, 0.53, 0.18), N: (0.41, 0.12, 0.46), probabilities of nutrient concentrations taking values of low, medium, high) which ultimately results in higher chlorophyll *a* concentration (0.41, 0.36, 0.22, probabilities of chlorophyll *a* concentration being low, medium, high).

The pigments representative of HABs specific to the NRE enabled us to investigate the potential and extent of influence of physical/chemical variables (i.e., freshwater discharge, light attenuation coefficient, temperature, stratification, and N:P ratio) on the formation of HABs. Our analysis shows that the probability of the presence of violaxanthin, peridinin, gyroxanthin, and 19'hexanoyloxyfucoxanthin under current conditions shown in Figure A17 in the NRE are 0.6548, 0.4731, 0.4731, and 0.4865 respectively. Whereas if the NRE always had a partially mixed water column ($1 < \Delta\rho < 3.6$), HABs have a higher probability of being present (probability of violaxanthin, peridinin, gyroxanthin, and 19'hexanoyloxyfucoxanthin being present, 0.7256, 0.5652, 0.5652, and 0.5172 respectively).

In the following section we examine the impact of scenarios of interest such as changes in physical environment, or nutrient concentrations on the NRE water quality criteria:

Freshwater Discharge

Freshwater discharge in the NRE is regulated by precipitation. Low precipitation results in low freshwater discharge which results in low nutrient loading to the estuary, and ultimately lowers concentrations of chlorophyll *a* **Figure 3-A-8**.

High freshwater discharge is a result of high precipitation. As shown in **Figure 3-A-9** high freshwater discharge delivers more nutrients to the NRE. Furthermore, high FW discharge results in high light attenuation coefficients due to high concentrations of organic matter, dissolved organic carbon (DOC) and chromophoric dissolved organic matter (CDOM). Furthermore higher freshwater discharge results in lower benthic dissolved oxygen concentrations as it introduces higher stratification levels in the water column. Using high freshwater discharge rates ($> 140 \text{ m}^3/\text{s}$) we can examine how the NRE reacts to high precipitation events (Wetz and Paerl, 2008).

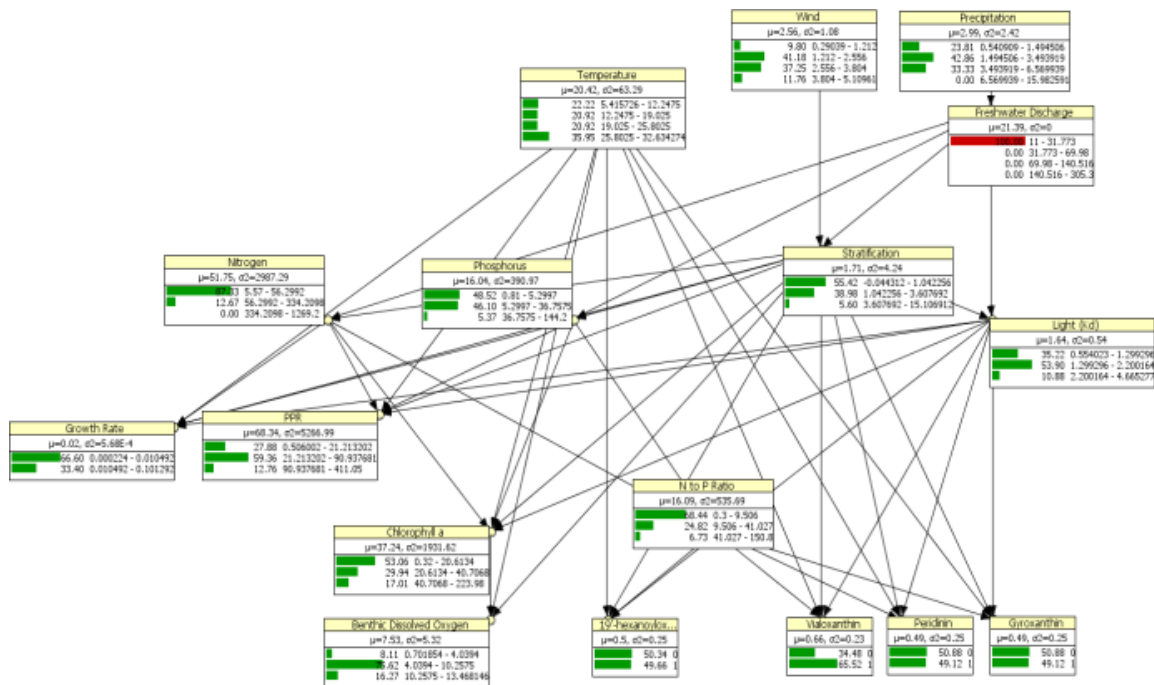


Figure 3-A-8. A low freshwater discharge (FWD < 31 m³/s) scenario for the NRE.

Green bars represent probability of each defined state; red bars are evidence for a dominant state for scenarios of interest; the numbers next to bars are probability of the variable being in that state, and the numbers represented as intervals to the right of the probabilities are the interval defined for the status of the variables of interest.

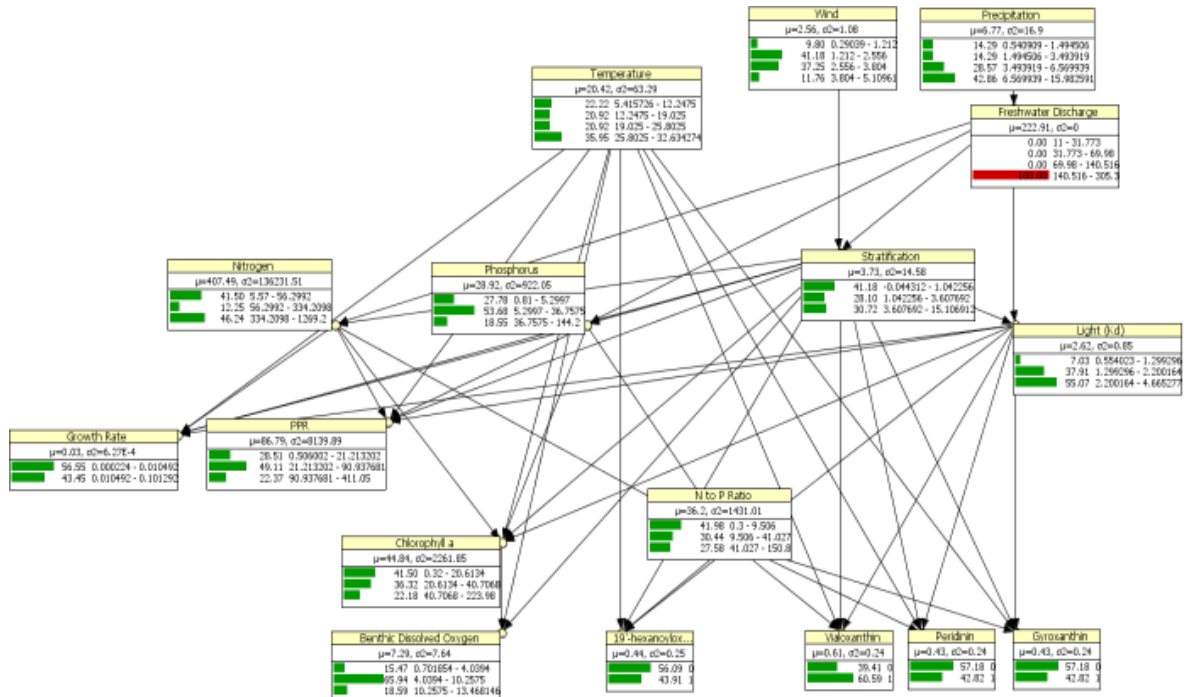


Figure 3-A-9. A high freshwater discharge (FWD > 142 m³/s) scenario for the NRE.

Green bars represent probability of each defined state; red bars are evidence for a dominant state for scenarios of interest; the numbers next to bars are probability of the variable being in that state, and the numbers represented as intervals to the right of the probabilities are the interval defined for the status of the variables of interest.

Wind

We examined high wind scenarios for hurricanes and tropical storms (Wetz and Paerl, 2008) by setting the wind intensity status to its high interval (**Figures 3-A-10 and 3-A-11**).

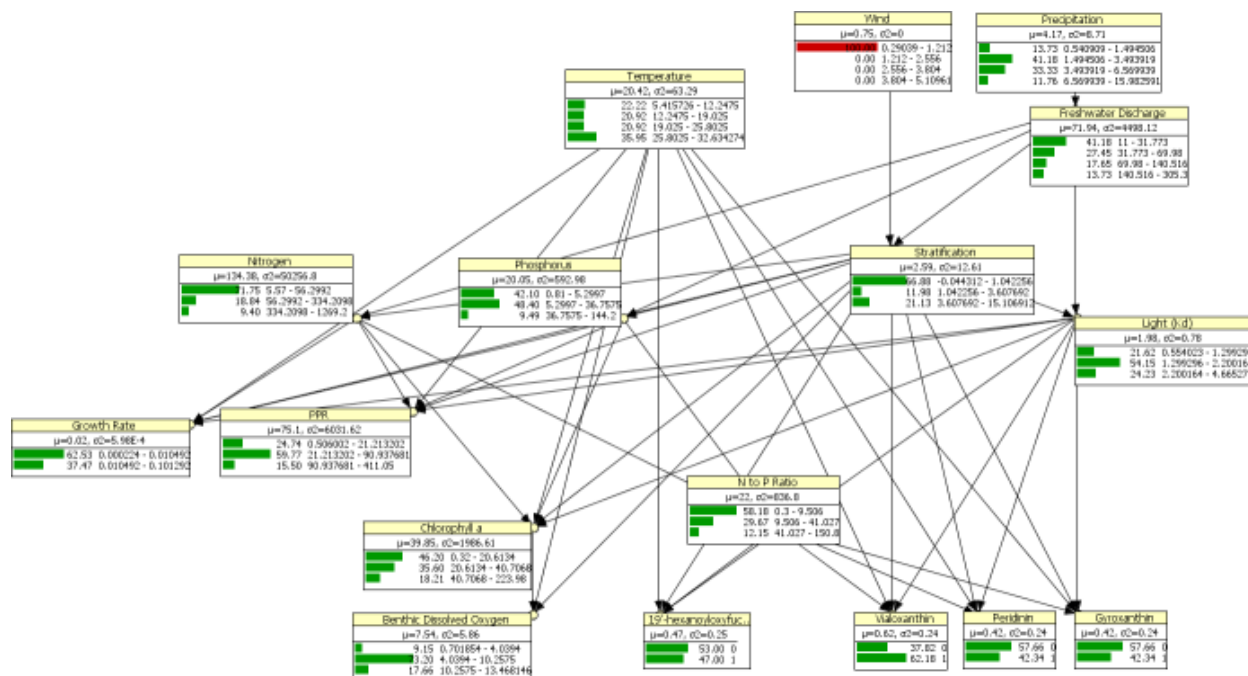


Figure 3-A-10. A low wind (wind <1.2 mph) scenario for the NRE.

Green bars represent probability of each defined state; red bars are evidence for a dominant state for scenarios of interest; the numbers next to bars are probability of the variable being in that state, and the numbers represented as intervals to the right of the probabilities are the interval defined for the status of the variables of interest.

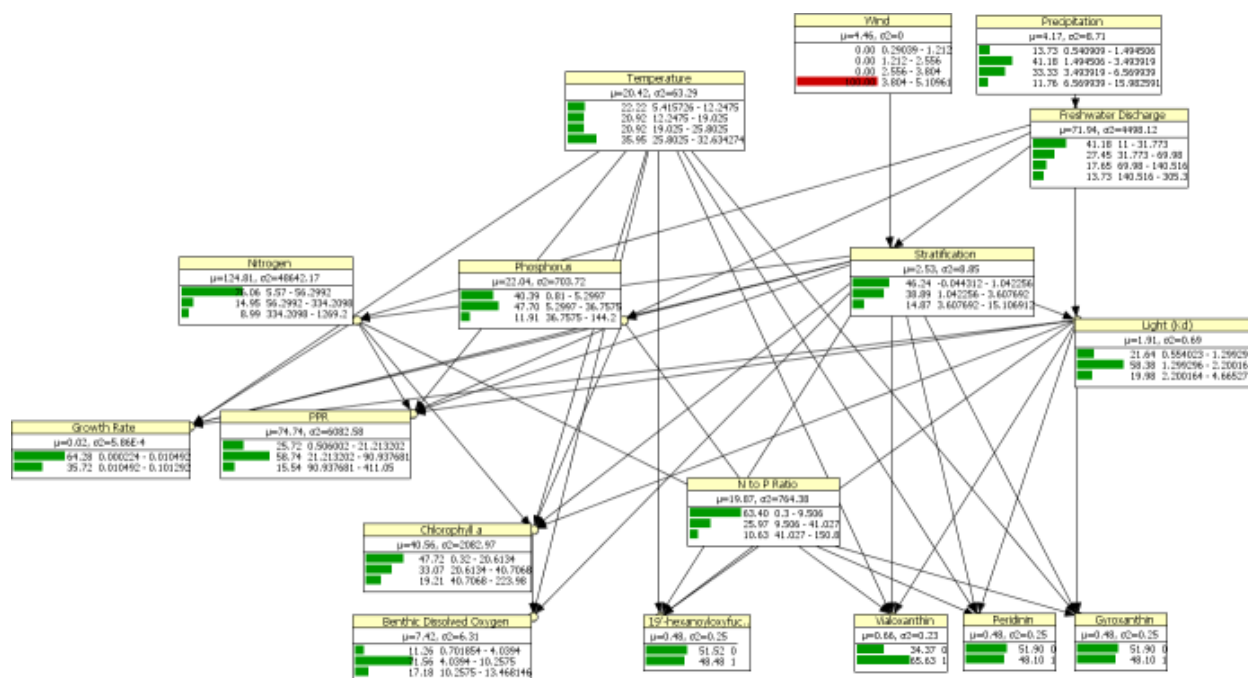


Figure 3-A-11. A high wind (3.80 mph <wind) scenario for the NRE.

Green bars represent probability of each defined state; red bars are evidence for a dominant state for scenarios of interest; the numbers next to bars are probability of the variable being in that state, and the numbers represented as intervals to the right of the probabilities are the interval defined for the status of the variables of interest.

Stratification

A stratified water column is the result of low mixing energy in the NRE. In a stratified water column, phytoplankton biomass is typically high since they can photosynthesize for longer periods due to increased light exposure. When the water column is stratified, bottom oxygen decreases since surface water with higher oxygen concentrations is not mixing with the bottom water (**Figure 3-A-12**). The high nutrient concentrations in this scenario may be associated with high freshwater discharges rather than the degree of stratification. Stratified water columns decrease the presence probability of pigments associated with HABs.

High mixing energy in the NRE results in a well-mixed water column. In a well-mixed water column, phytoplankton biomass decreases, since the phytoplankton is not exposed to light long enough to undergo photosynthesis. Bottom water oxygen concentrations increase due to mixing of surface and bottom water (**Figure 3-A-13**). It is worth noting that medium levels of stratification ($1.04 < \Delta\rho$ [density gradient] < 3.61) results in higher presence probability of pigments associated with HABs (**Figure 3-A-14**).

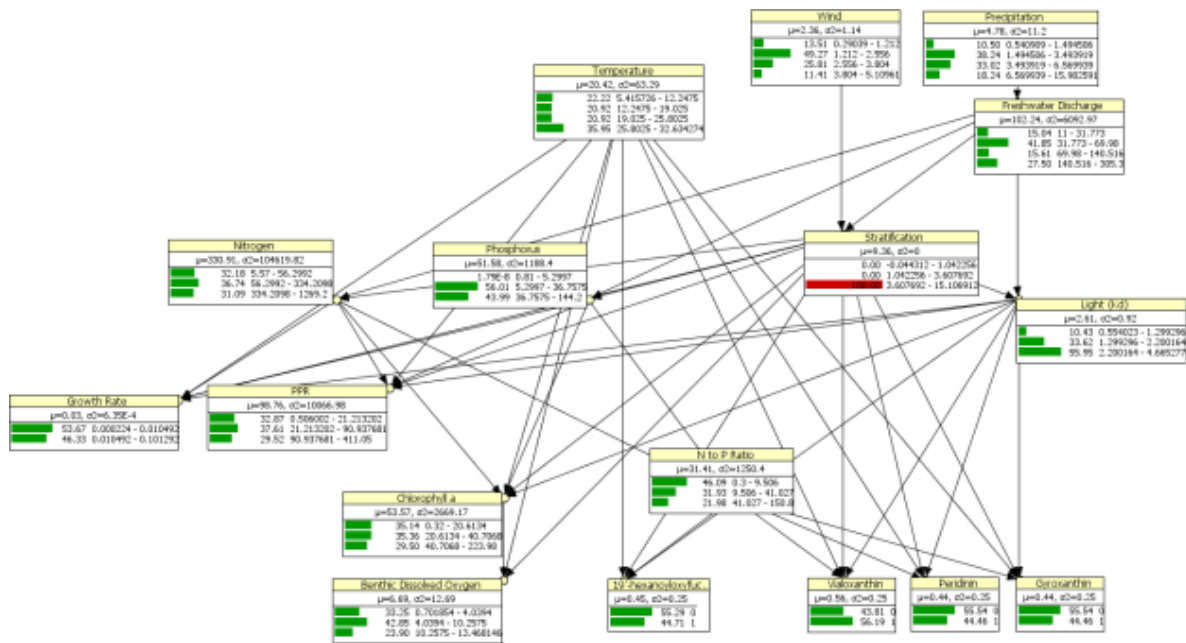


Figure 3-A-12. A stratified water column ($3.6 < \Delta\rho$) scenario for the NRE.

Green bars represent probability of each defined state; red bars are evidence for a dominant state for scenarios of interest; the numbers next to bars are probability of the variable being in that state, and the numbers represented as intervals to the right of the probabilities are the interval defined for the status of the variables of interest.

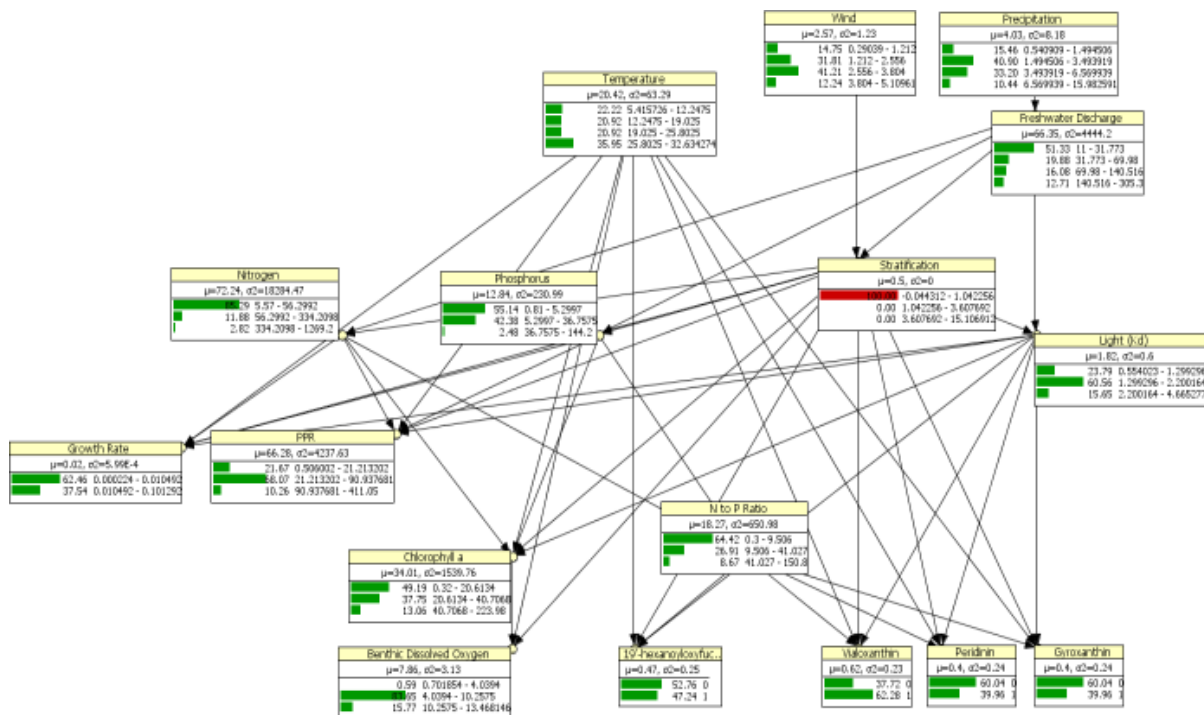


Figure 3-A-13. A well-mixed water column ($\Delta\rho < 1.04$) scenario for the NRE.

Green bars represent probability of each defined state; red bars are evidence for a dominant state for scenarios of interest; the numbers next to bars are probability of the variable being in that state, and the numbers represented as intervals to the right of the probabilities are the interval defined for the status of the variables of interest.

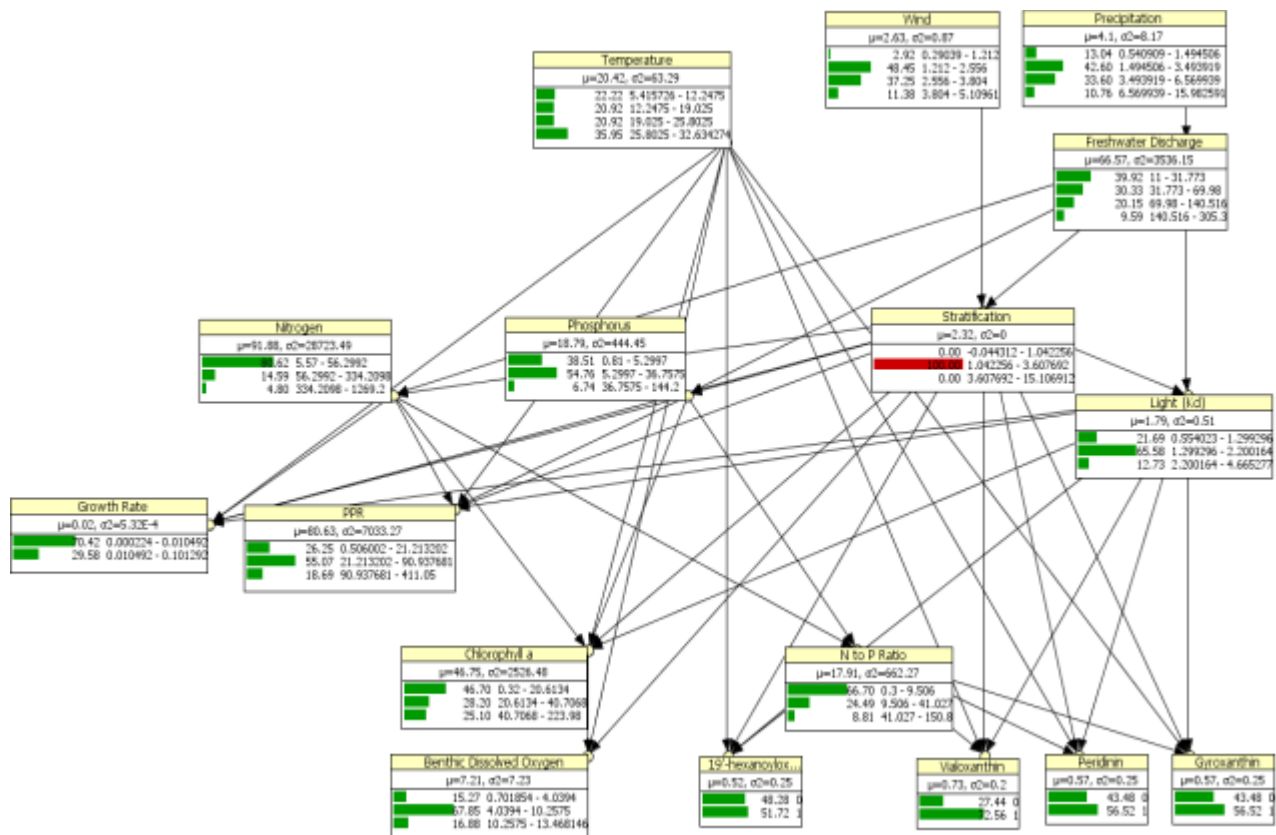


Figure 3-A-14. A partially stratified water column ($1.04 < \Delta\rho < 3.60$) scenario for the NRE.

Green bars represent probability of each defined state; red bars are evidence for a dominant state for scenarios of interest; the numbers next to bars are probability of the variable being in that state, and the numbers represented as intervals to the right of the probabilities are the interval defined for the status of the variables of interest.

Temperature

In a low water temperature scenario bottom water oxygen concentrations increases due to more solubility, and only less than 3% of the time bottom water oxygen concentrations are below 4 (mg/L) (**Figures 3-A-15 and 3-A-16**). Also based on the BBN results, lower water temperatures result in higher presence probability of 19'hexanoxyfucoxanthin pigment associated with *Dictyocha speculum*.

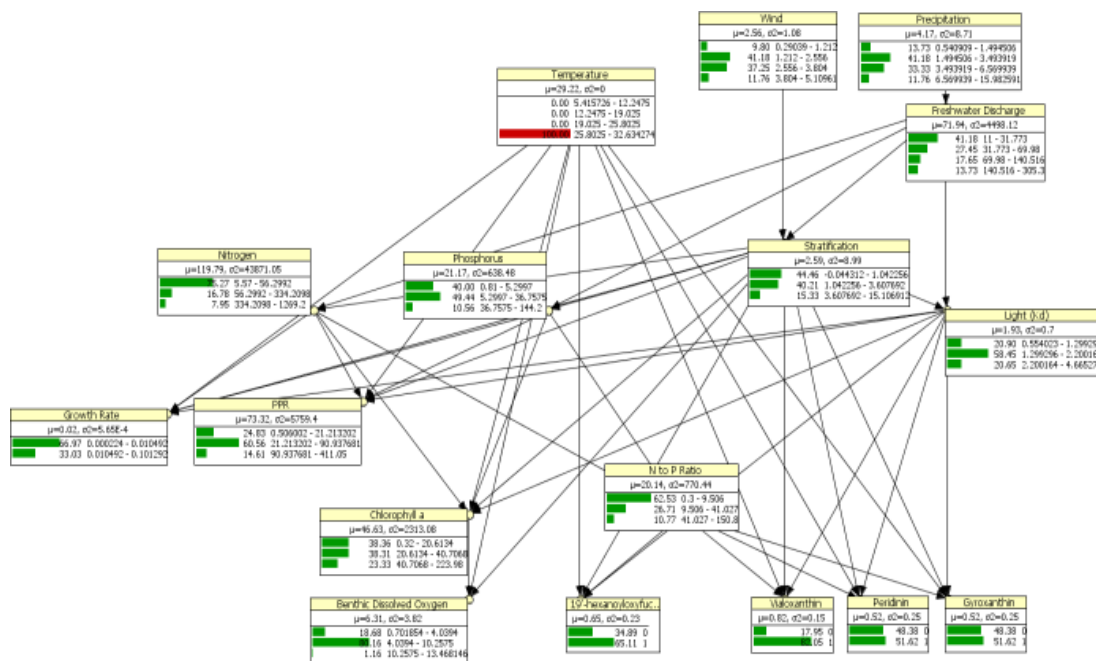


Figure 3-A-15. A high temperature (temperature >25.80°C) scenario for the NRE.

Green bars represent probability of each defined state; red bars are evidence for a dominant state for scenarios of interest; the numbers next to bars are probability of the variable being in that state, and the numbers represented as intervals to the right of the probabilities are the interval defined for the status of the variables of interest.

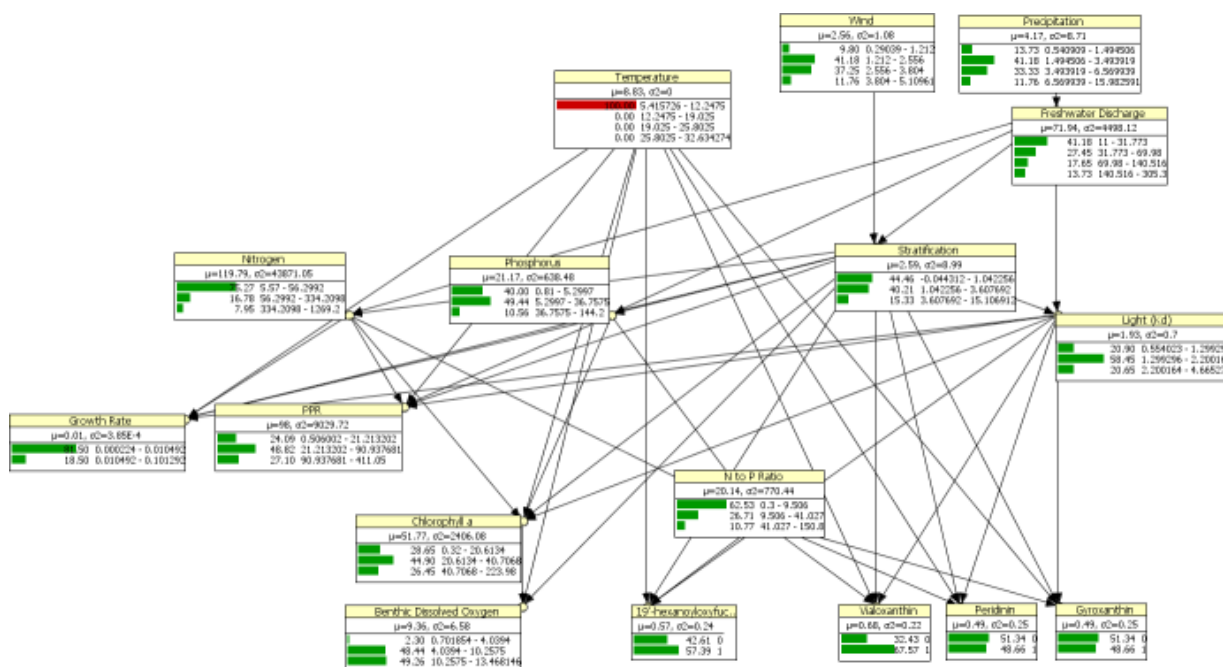


Figure 3-A-16. A low temperature (temperature <12°C) scenario for the NRE.

Green bars represent probability of each defined state; red bars are evidence for a dominant state for scenarios of interest; the numbers next to bars are probability of the variable being in that state, and the numbers represented as intervals to the right of the probabilities are the interval defined for the status of the variables of interest.

Phosphorus Concentrations

Low phosphorus levels mean fewer nutrients available for phytoplankton to uptake. As chl *a* concentrations decrease, benthic dissolved oxygen levels will increase (**Figure 3-A-17**). Conversely, high phosphorus levels mean excess nutrients are available for phytoplankton to uptake. As a result chl *a* levels increase (**Figure 3-A-18**) which increases in oxygen demand, hence benthic oxygen concentrations decrease. The presence/absence of pigments associated with HABs does not show a significant change.

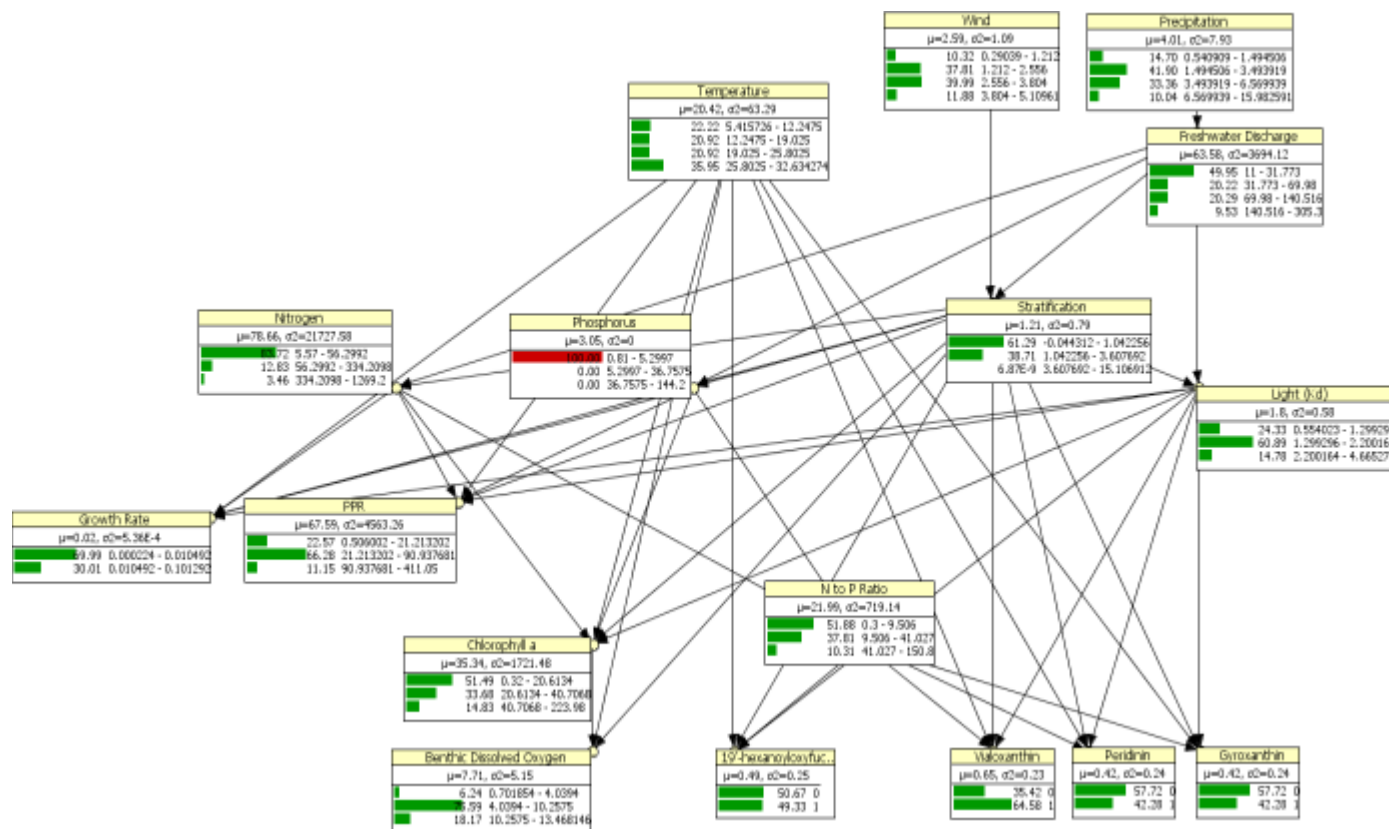


Figure 3-A-17. A low phosphorus concentration (phosphorus<5.29 $\mu\text{g/L}$) scenario for the NRE.

Green bars represent probability of each defined state; red bars are evidence for a dominant state for scenarios of interest; the numbers next to bars are probability of the variable being in that state, and the numbers represented as intervals to the right of the probabilities are the interval defined for the status of the variables of interest.

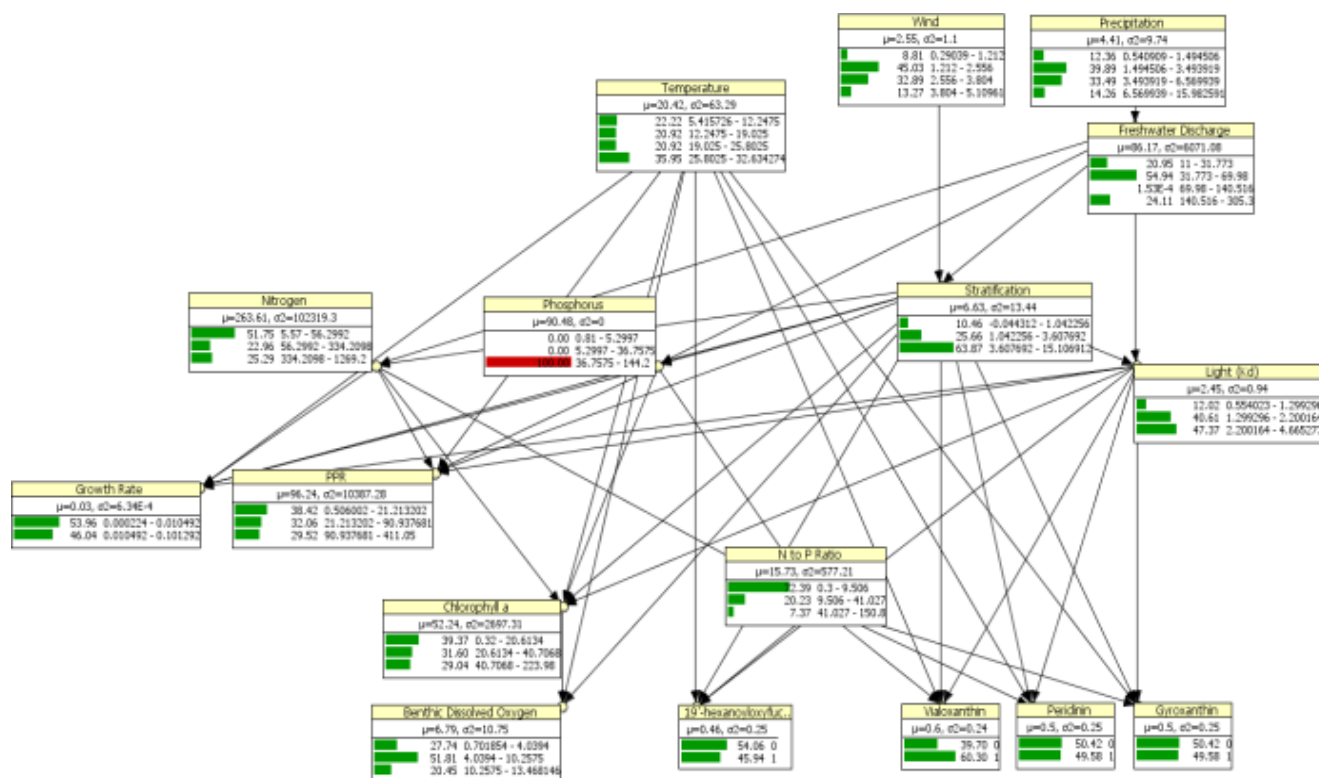


Figure 3-A-18. A high phosphorus concentration ($p < \text{phosphorus} > 36.75 \mu\text{g/L}$) scenario for the NRE.

Green bars represent probability of each defined state; red bars are evidence for a dominant state for scenarios of interest; the numbers next to bars are probability of the variable being in that state, and the numbers represented as intervals to the right of the probabilities are the interval defined for the status of the variables of interest.

Nitrogen Concentrations

Decrease in the nitrogen available for phytoplankton to uptake results in lower level of chl *a* concentration; however, presence probability of pigments associated with HABs show a slight increase. The probability of presence is 0.45, 0.60, 0.49, 0.49 for 19'-hexanoyloxyfucoxanthin, vialoxanthin, peridinin, and gyroxanthin respectively (**Figure 3-A-19**). High nitrogen concentrations ($>334.20 \mu\text{g/L}$) mean additional nutrients available for phytoplankton to utilize; hence, chl *a* concentrations increase (**Figure 3-A-20**).

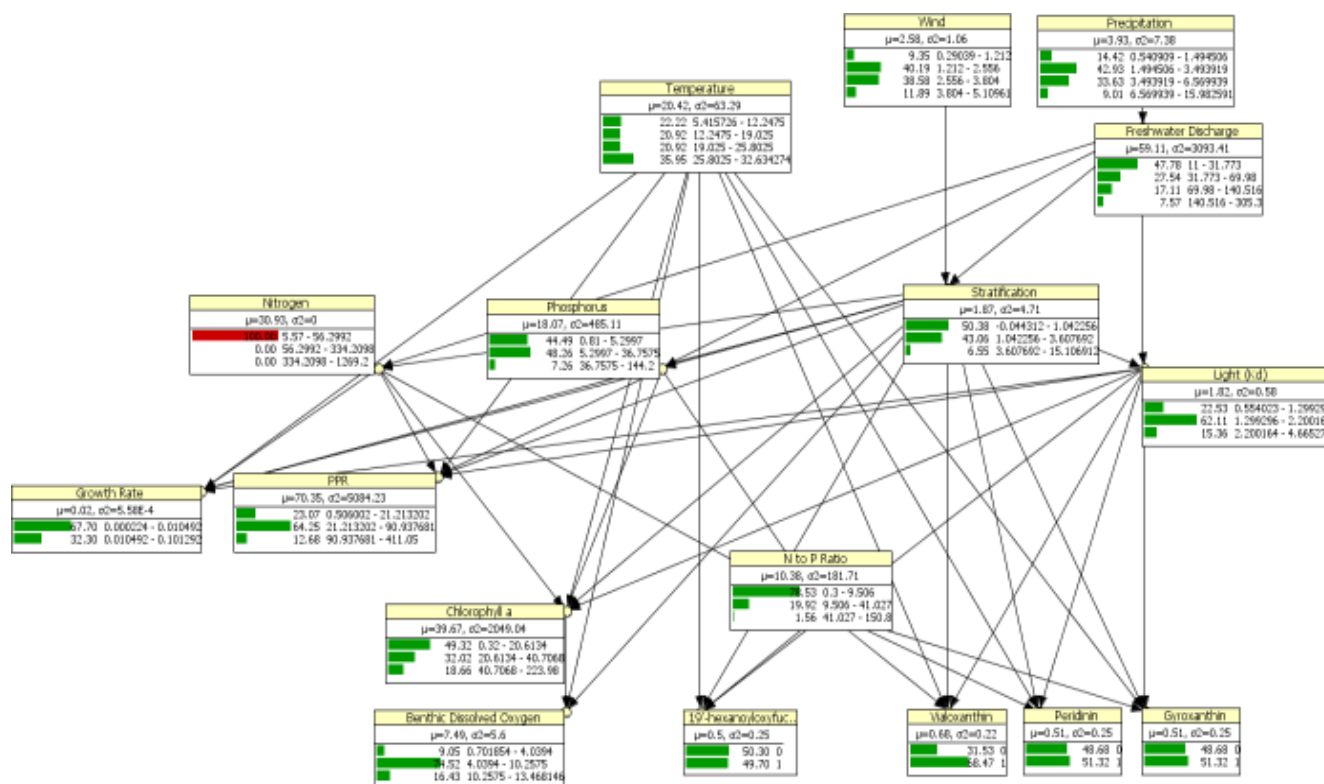


Figure 3-A-19. A low nitrogen concentration (nitrogen <56.29 $\mu\text{g/L}$) scenario for the NRE.

Green bars represent probability of each defined state; red bars are evidence for a dominant state for scenarios of interest; the numbers next to bars are probability of the variable being in that state, and the numbers represented as intervals to the right of the probabilities are the interval defined for the status of the variables of interest.

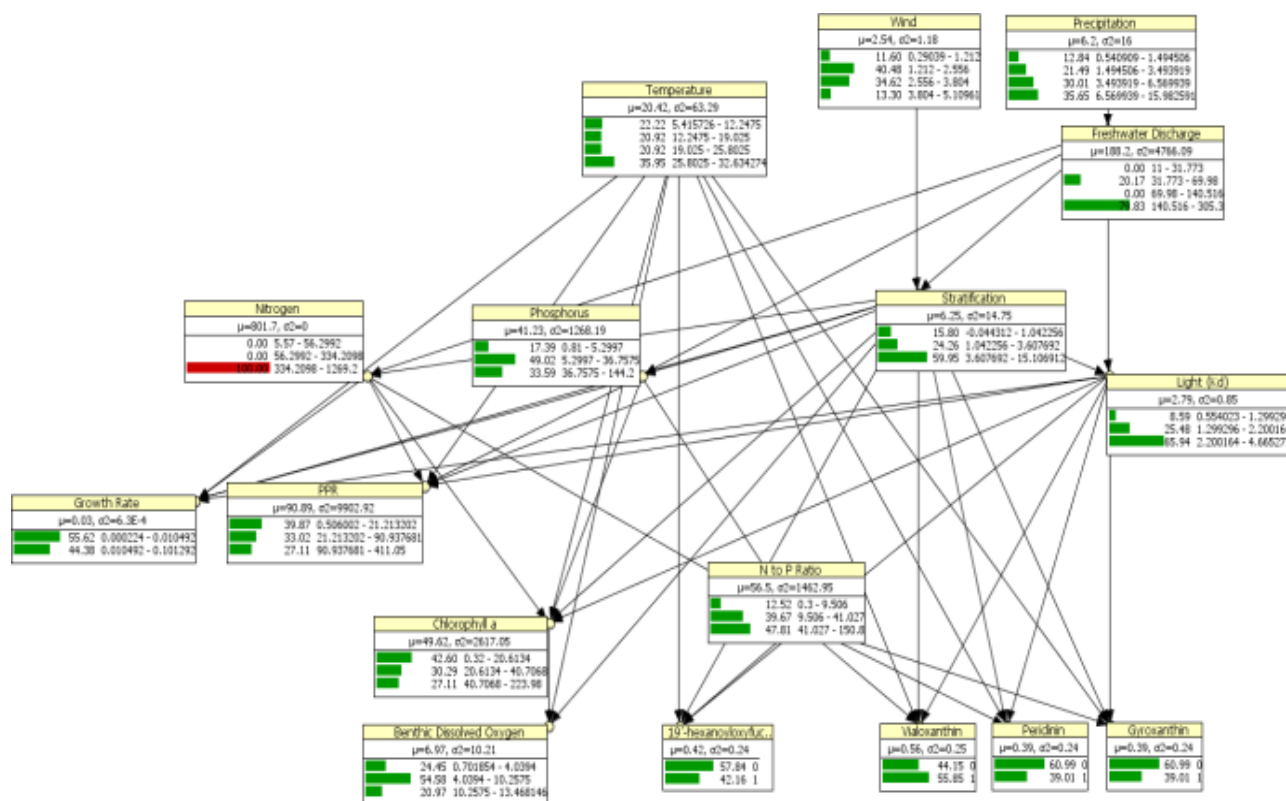


Figure 3-A-20. A high nitrogen concentration (nitrogen >334.20 µg/L) scenario for the NRE.

Green bars represent probability of each defined state; red bars are evidence for a dominant state for scenarios of interest; the numbers next to bars are probability of the variable being in that state, and the numbers represented as intervals to the right of the probabilities are the interval defined for the status of the variables of interest.

Chl *a* Concentrations

Lower concentrations of chl *a* are associated with low nutrient concentrations, mixed water column and low light attenuation (*K_d*) (**Figure 3-A-21**). Higher levels of chl *a* are associated with high nutrient concentrations, stratified water column and higher *K_d* (**Figure 3-A-22**).

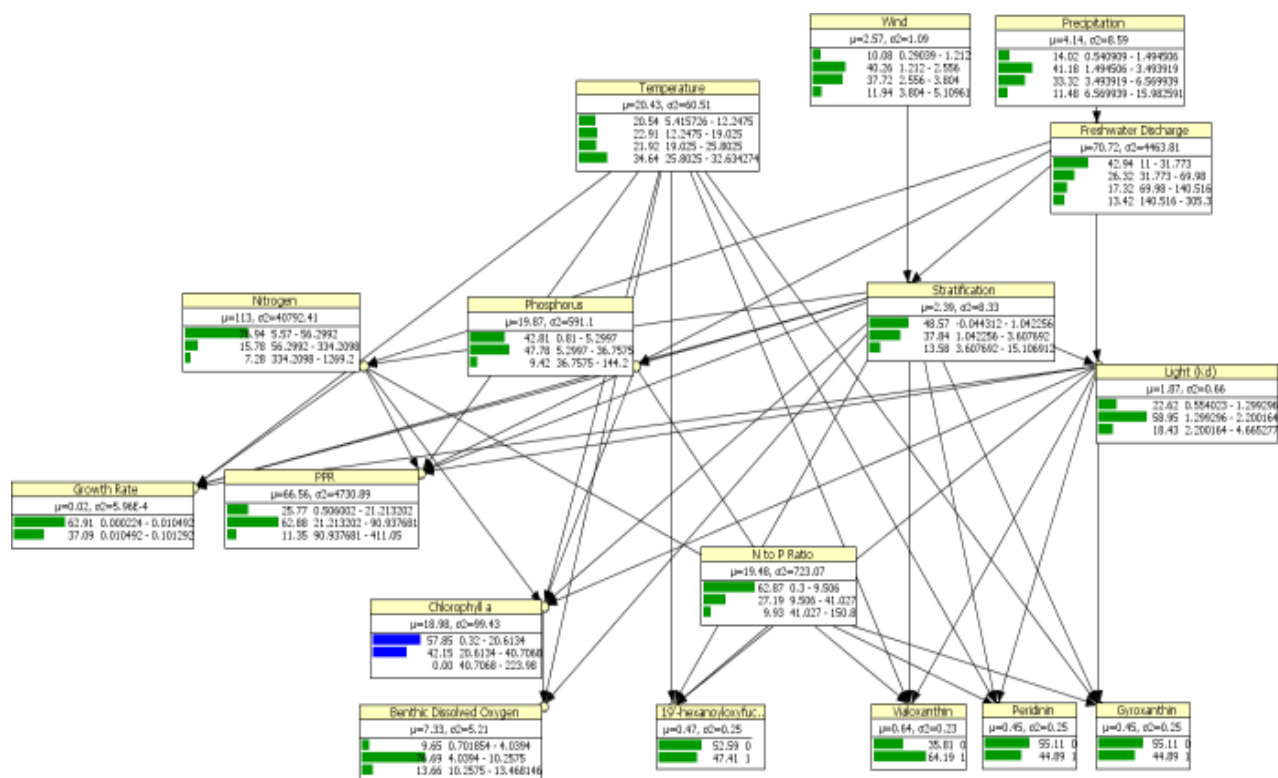


Figure 3-A-21. A low chl *a* concentration (chl *a*<40.70 $\mu\text{g/L}$) scenario for the NRE.

Green bars represent probability of each defined state; red bars are evidence for a dominant state for scenarios of interest; the numbers next to bars are probability of the variable being in that state, and the numbers represented as intervals to the right of the probabilities are the interval defined for the status of the variables of interest.

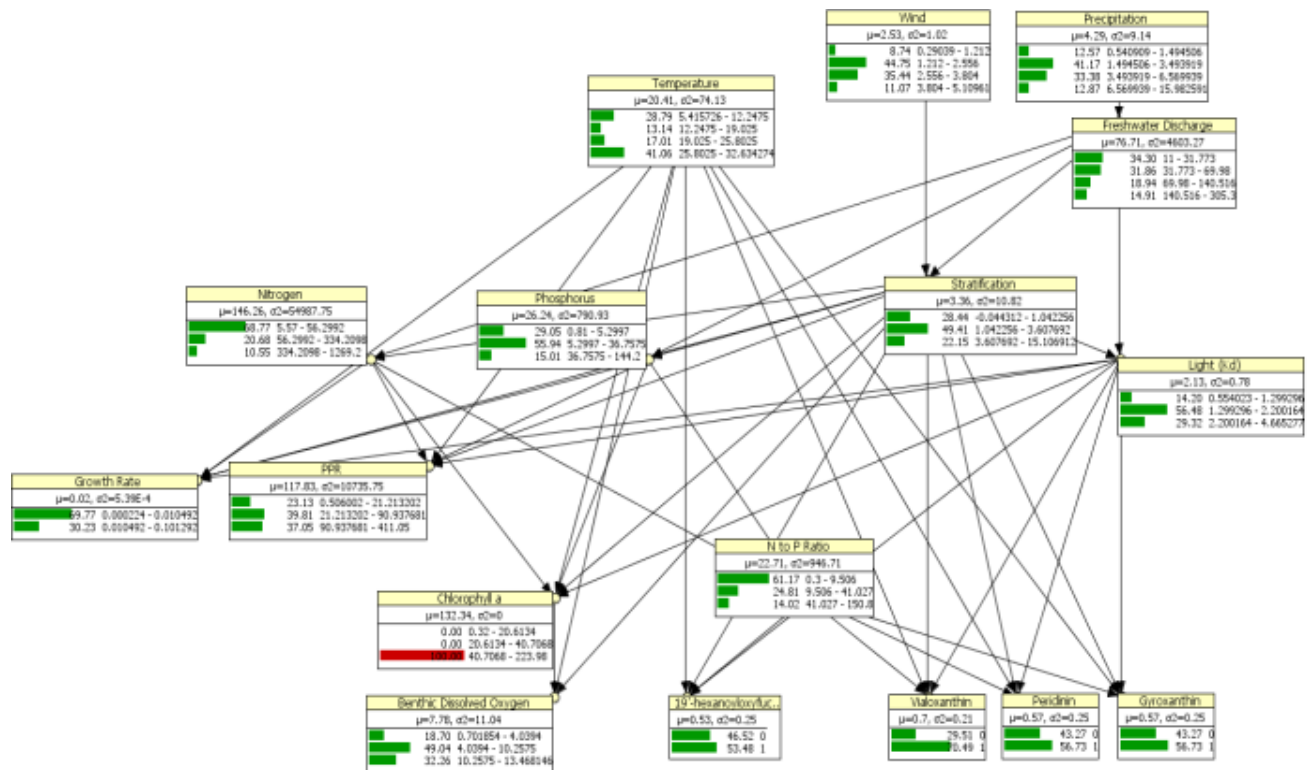


Figure 3-A-22. A high chl *a* concentration (chl *a* > 40.70 $\mu\text{g/L}$) scenario for the NRE.

Green bars represent probability of each defined state; red bars are evidence for a dominant state for scenarios of interest; the numbers next to bars are probability of the variable being in that state, and the numbers represented as intervals to the right of the probabilities are the interval defined for the status of the variables of interest.

Benthic Oxygen Concentrations

Low bottom water dissolved oxygen concentrations are the result of high chl *a* biomass, stratified water column, and high water temperatures (**Figure 3-A-23**). Mixed water column, lower chl *a* concentrations, and low water temperatures result in higher bottom oxygen concentrations (**Figure 3-A-24**).

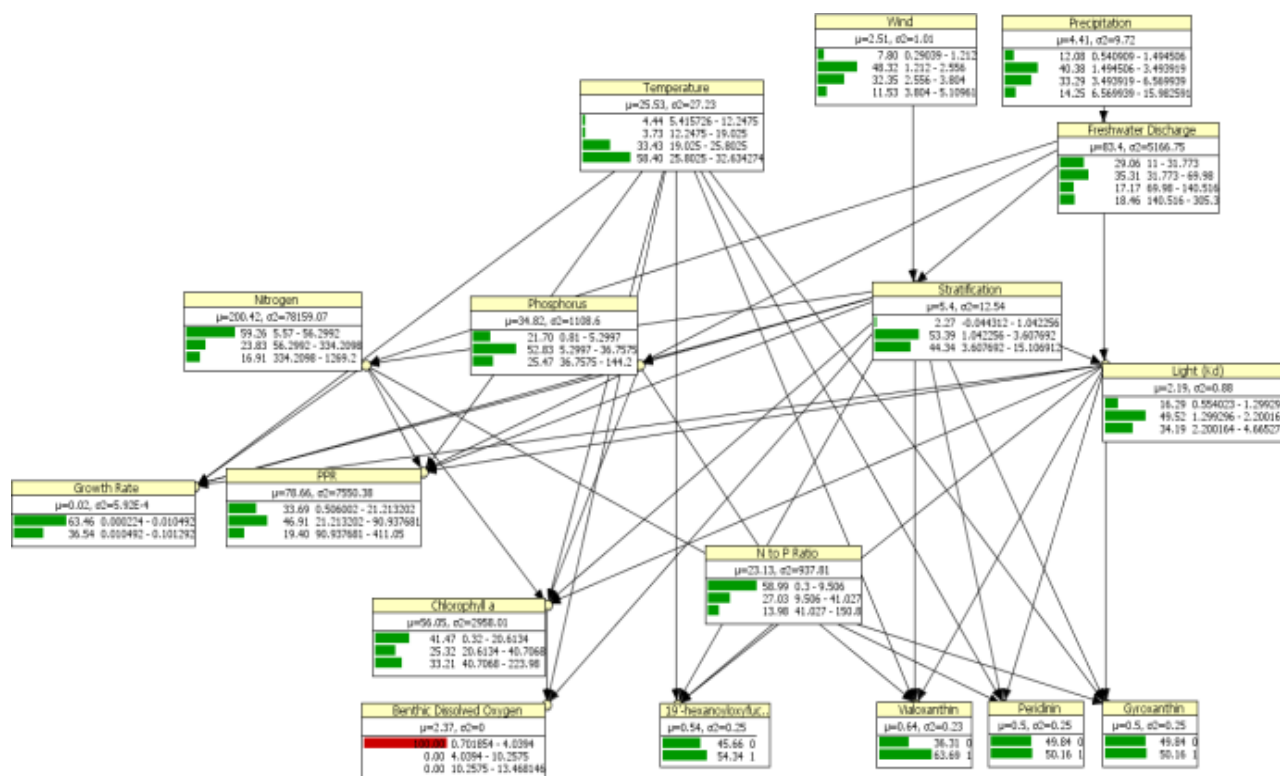


Figure 3-A-23. A low benthic dissolved oxygen concentration (benthic dissolved oxygen <4.03 mg/L) scenario for the NRE.

Green bars represent probability of each defined state; red bars are evidence for a dominant state for scenarios of interest; the numbers next to bars are probability of the variable being in that state, and the numbers represented as intervals to the right of the probabilities are the interval defined for the status of the variables of interest.

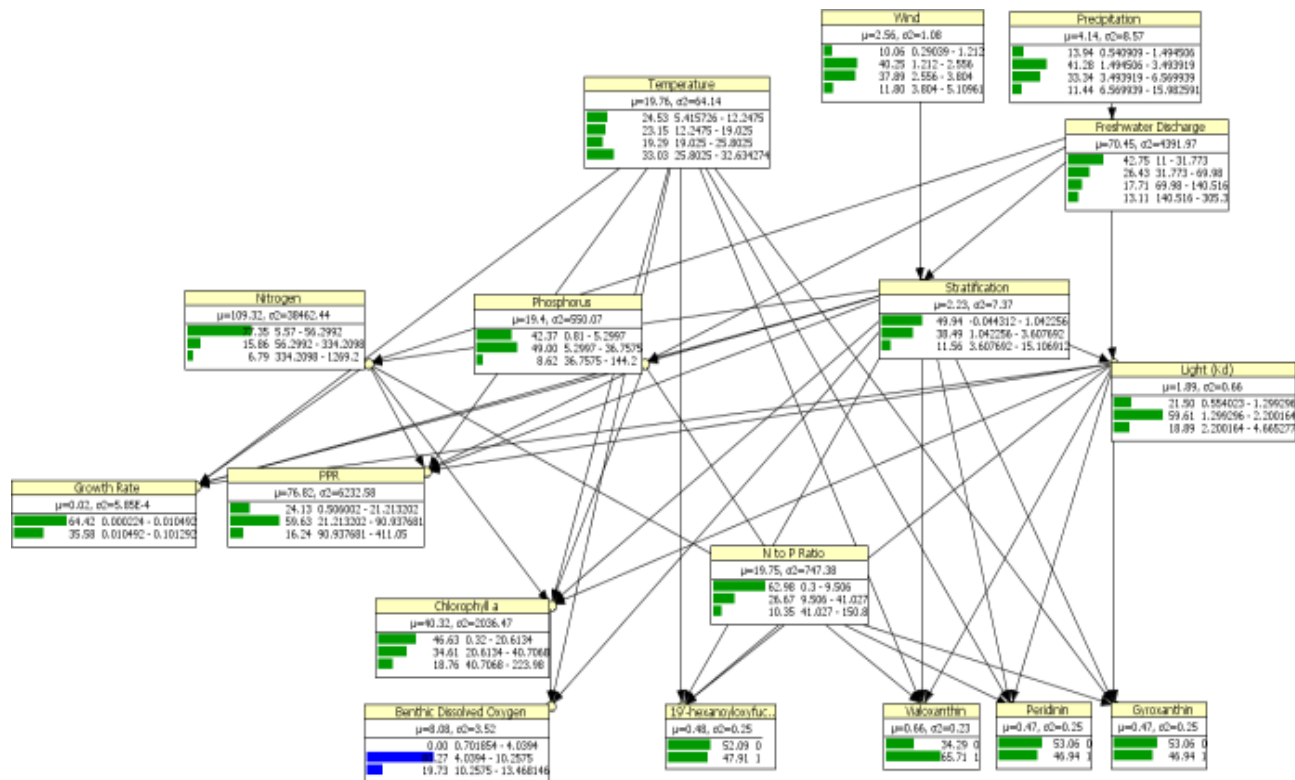


Figure 3-A-24. A high benthic dissolved oxygen concentration (benthic dissolved oxygen >4.03) scenario for the NRE.

Green bars represent probability of each defined state; red bars are evidence for a dominant state for scenarios of interest; the numbers next to bars are probability of the variable being in that state, and the numbers represented as intervals to the right of the probabilities are the interval defined for the status of the variables of interest.

Conclusions and Implications for Future Research

Our results show that both climatic variability and anthropogenic enrichment impact water quality indicators; however in the short term managers can only control nutrient concentrations. The BBN enables the managers to decide which variables' concentration to restrict.

As future work adding land use / land cover variable to the BBN would improve our prediction ability and enables us to investigate scenarios of land use change on water quality. Further discretizing the data imposes a restriction which can be resolved by using other softwares such as R. Hence future work needs to be done to construct a network with continuous nodes.

Literature Cited

Alameddine, I., Cha, Y., & Reckhow, K. H. (2011). An evaluation of automated structure learning with Bayesian networks: An application to estuarine chlorophyll dynamics. *Environmental Modelling & Software*, 26(2), 163–172.

- Burkholder, J., Mallin, M. A., Glasgow Jr, H. B., Larsen, L. M., McIver, M. R., Shank, G. C., Deamer-Melia, N., et al. (1997). Impacts to a coastal river and estuary from rupture of a large swine waste holding lagoon. *Journal of Environmental Quality*, 26(6), 1451–1466.
- Cloern, J. (2001). Our evolving conceptual model of the coastal eutrophication problem. *Marine Ecology Progress Series*, 210, 223–253.
- Cloern, J. E., Grenz, C., & Videgar-lucas, L. (1995). chlorophyll : carbon An empirical model of the phytoplankton rate and growth factor between productivity ratio-the conversion. *Limnology and Oceanography*, 40(7), 1313–1321.
- Dempster, A., & Laird, N. (1977). Maximum likelihood from incomplete data via the EM algorithm. *Journal of the Royal Statistical Society.*, 39(1), 1–38.
- Domingues, R. B., Anselmo, T. P., Barbosa, A. B., Sommer, U., & Galvão, H. M. (2011). Light as a driver of phytoplankton growth and production in the freshwater tidal zone of a turbid estuary. *Estuarine, Coastal and Shelf Science*, 91(4), 526–535.
- Ensign, S. H., Halls, J. N., & Mallin, M. A. (2004). Application of digital bathymetry data in an analysis of flushing times of two large estuaries. *Computers & Geosciences*, 30(5), 501–511.
- Gameiro, C., Zwolinski, J., & Brotas, V. (2011). Light control on phytoplankton production in a shallow and turbid estuarine system. *Hydrobiologia*, 669(1), 249–263. doi:10.1007/s10750-011-0695-3
- Keller, A. (1989). Modeling the effects of temperature, light, and nutrients on primary productivity: An empirical and a mechanistic approach compared. *Limnology and oceanography*, 34(1), 82–95.
- Madsen, A. L., Lang, M., Kjærulff, U. B., & Jensen, F. (2003). The Hugin Tool for Learning Bayesian Networks. *Learning*, 594–605.
- Mallin, M., McIver, M., Wells, H., & Parsons, D. (2005). Reversal of eutrophication following sewage treatment upgrades in the New River Estuary, North Carolina. *Estuaries and*, 28(5), 750–760.
- Marcot, B., & Steventon, J. (2006). Guidelines for developing and updating Bayesian belief networks applied to ecological modeling and conservation. *Canadian Journal of Forest Research*.
- NOAA. (1996). *NOAA's Estuarine Eutrophication Survey Volume 1: South Atlantic Region*.
- Paerl, H. W., Valdes, L. M., Peierls, B. L., Adolf, J. E., & Lawrence, W. (2011). Anthropogenic and Climatic Influences on the Eutrophication of Large Estuarine Ecosystems Source : *Limnology and Oceanography*, Vol. 51, No. 1, Part 2: Eutrophication of Freshwater and

Marine Ecosystems (Jan., 2006), pp. 448-462 Published by : Am. *Limnology*, 51(1), 448–462.

Smith, J. (1993). Moment methods for decision analysis. *Management science*, 39(3), 340–358.

Wetz, M. S., & Paerl, H. W. (2008). Estuarine Phytoplankton Responses to Hurricanes and Tropical Storms with Different Characteristics (Trajectory, Rainfall, Winds). *Estuaries*, 419–429.

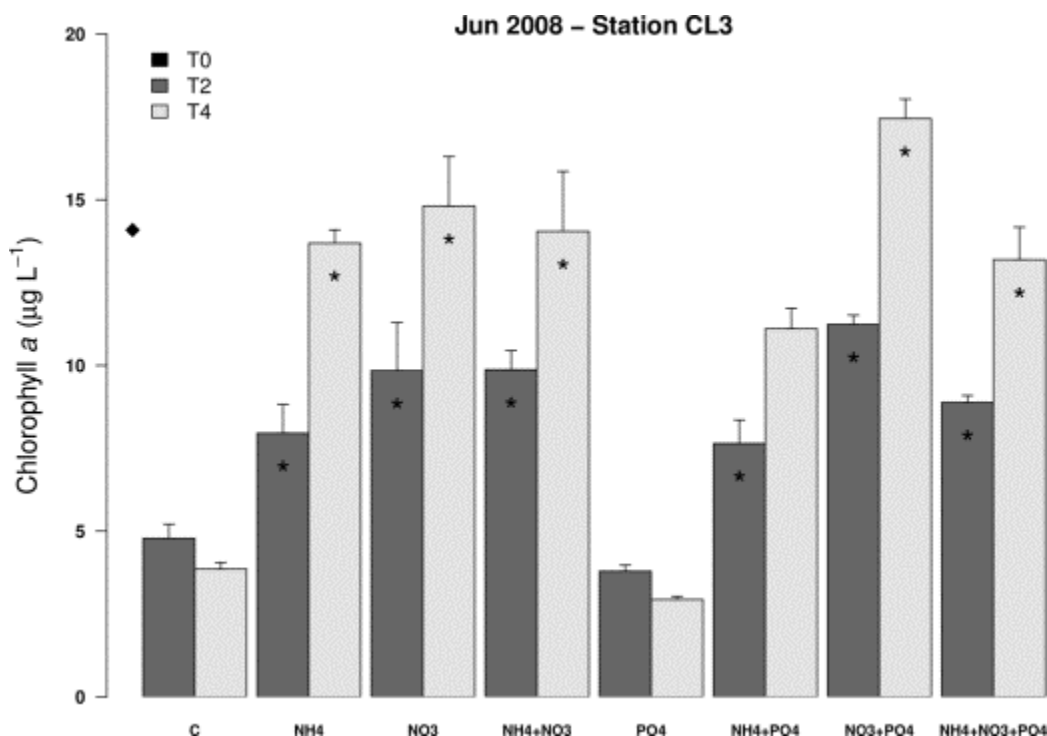
[This page intentionally left blank.]

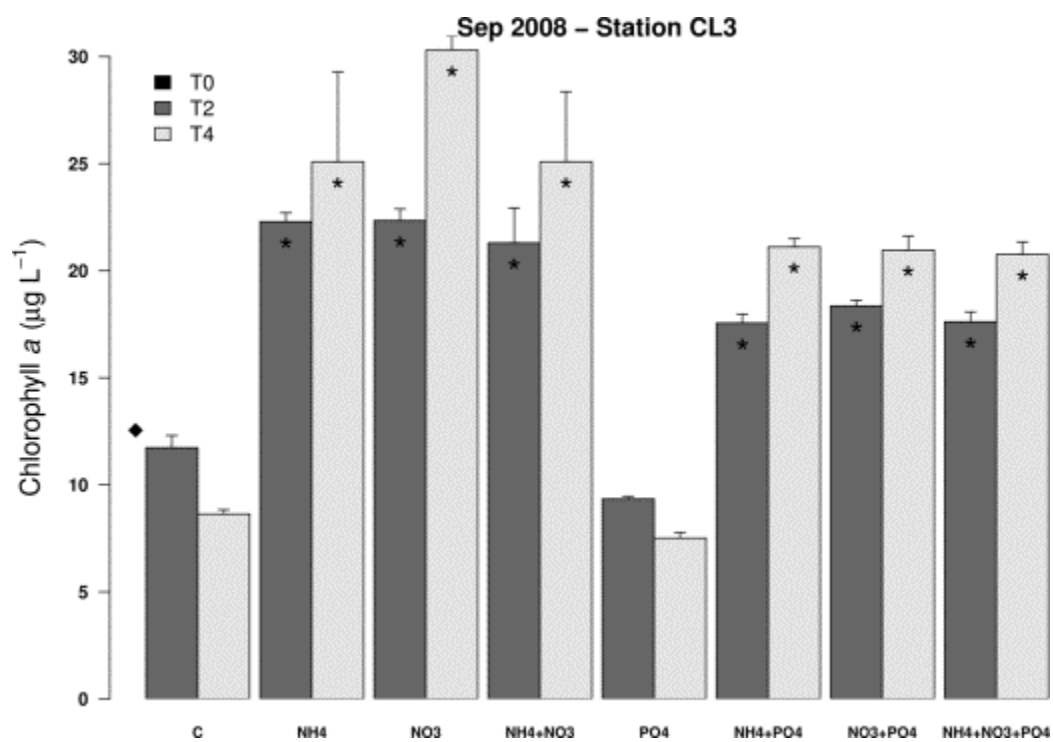
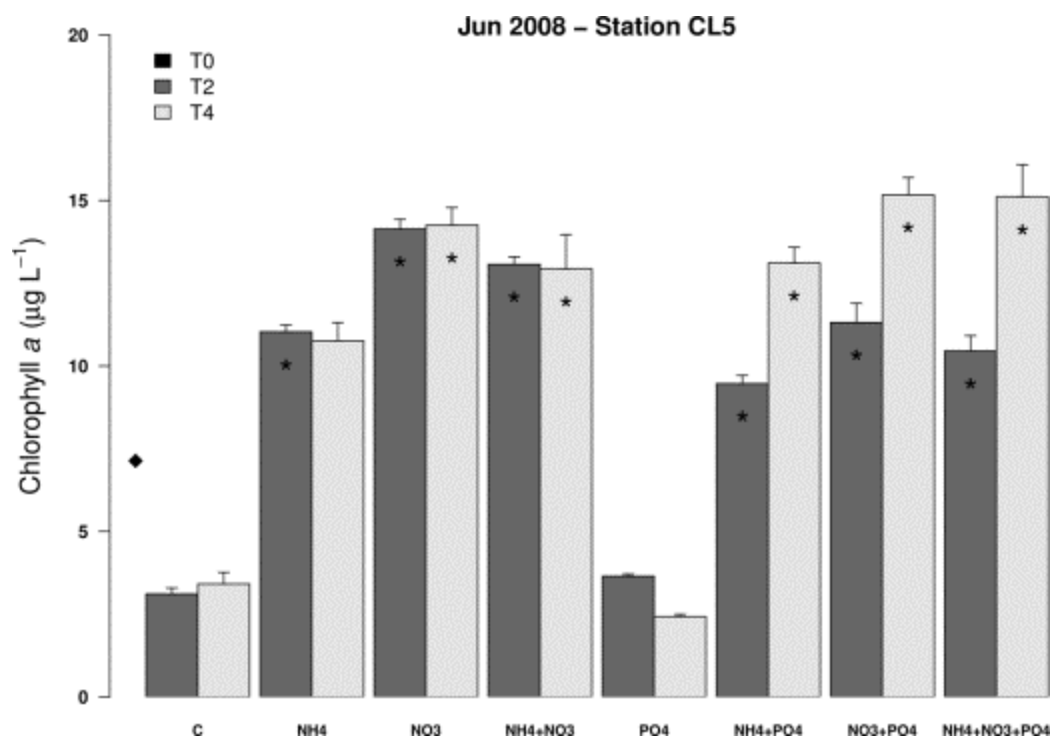
Appendix 3-B

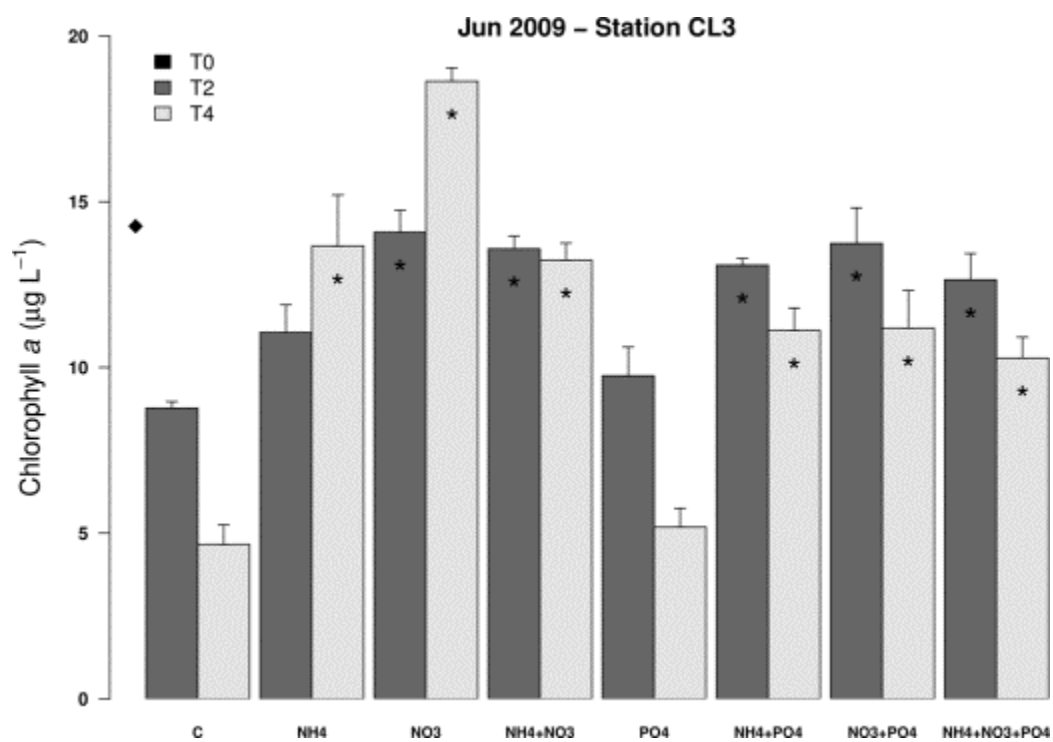
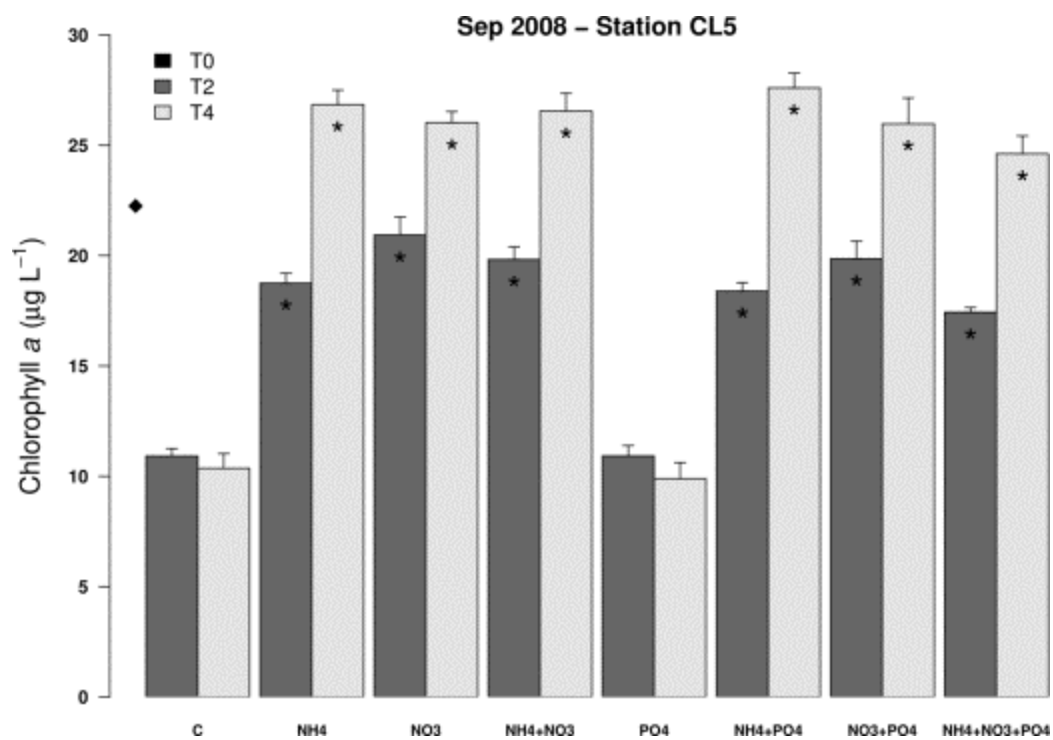
Supporting Data

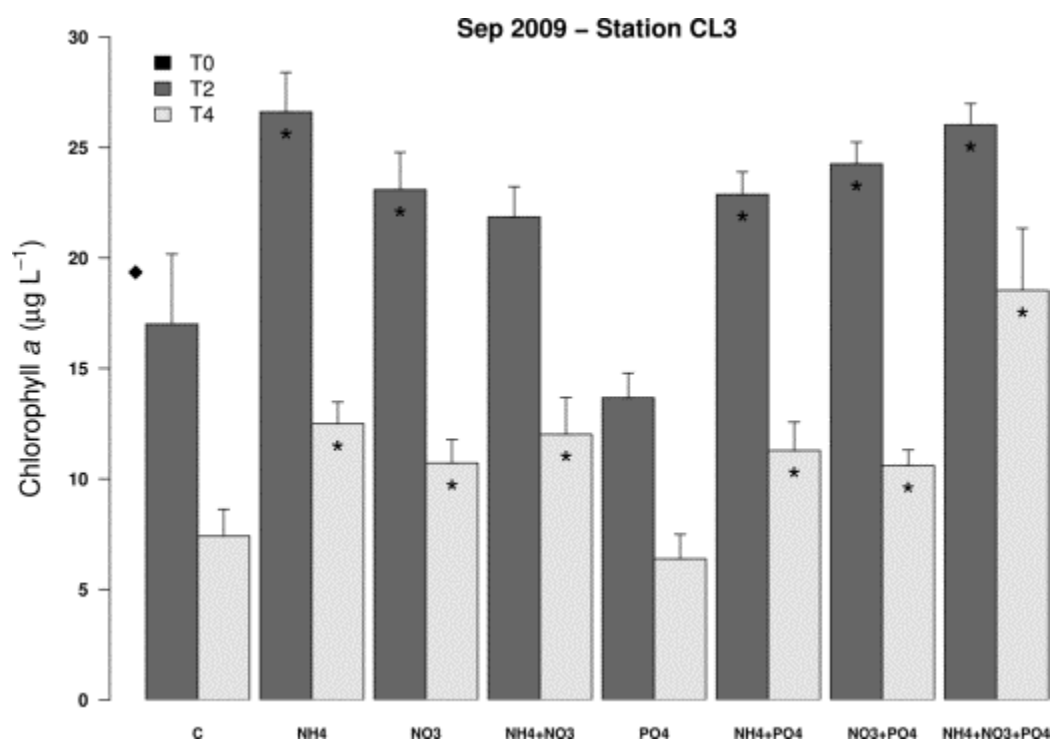
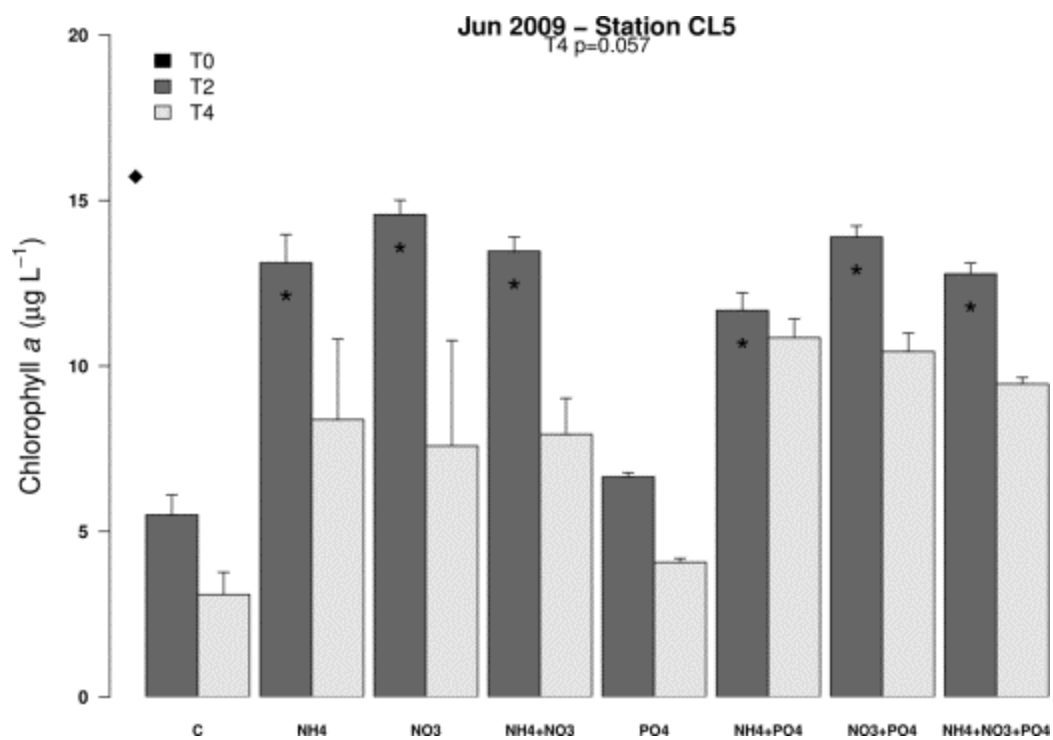
Phytoplankton biomass (chl *a*) responses to nutrient addition bioassays

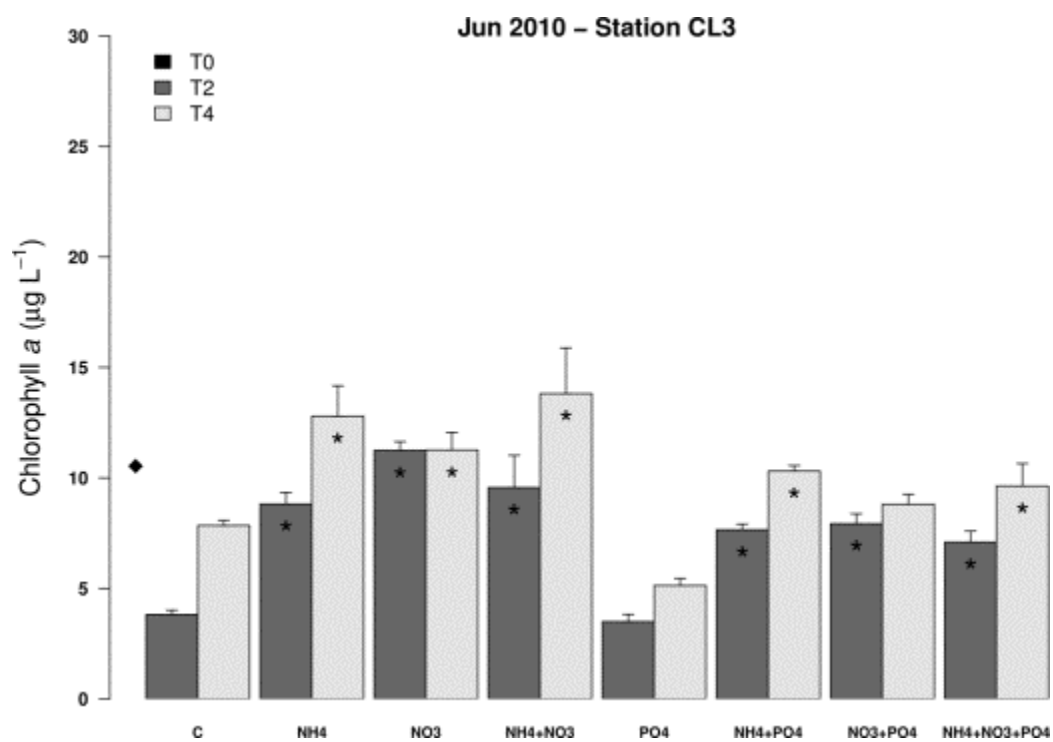
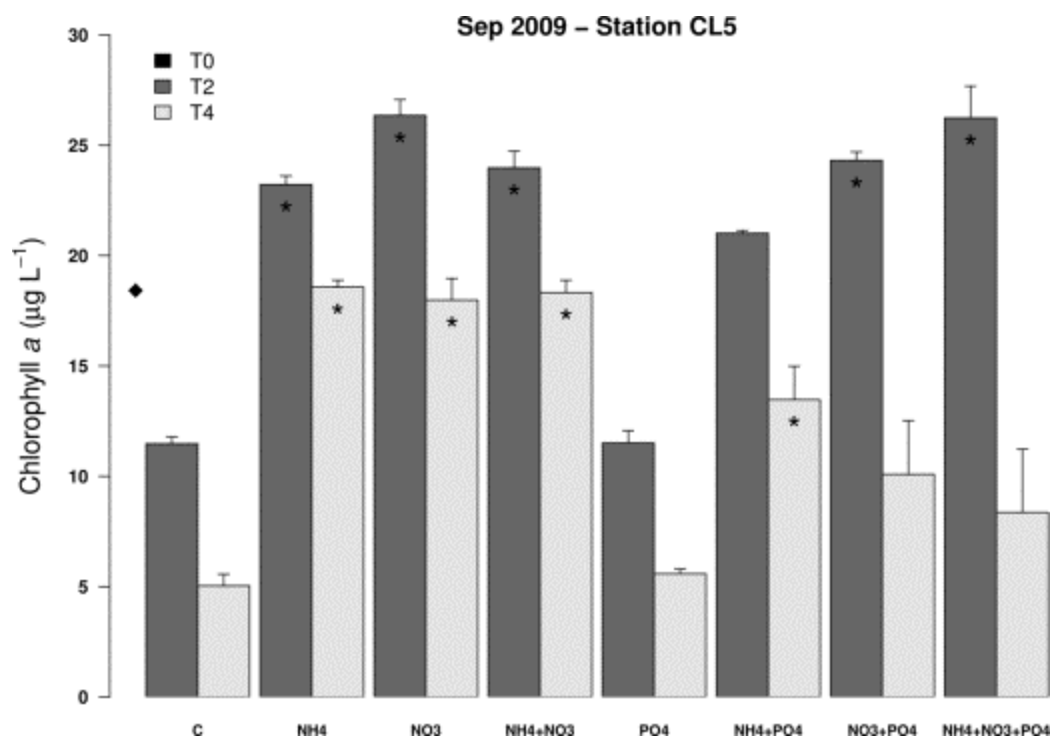
Figures below show the chl *a* response of bioassays performed in June and September of 2008, 2009 and 2010 from surface waters collected at Stations 3 and 5. Filled diamond symbol represents the chl *a* concentration at the time of the beginning of the bioassay (T0). Bars for T2 and T4 represent the mean concentration of the quadruplicated treatments on Days 2 and 4 of the experiment. Error bars are standard error of the mean. Treatments are C= control, NH₄= ammonium addition, NO₃= nitrate addition, NH₄ + NO₃= addition of both ammonium and nitrate, PO₄= phosphate addition, NH₄ + PO₄= addition of both ammonium and phosphate, NO₃+PO₄= addition of both nitrate and phosphate, NH₄+NO₃+PO₄= addition of ammonium, nitrate, and phosphate. All experiments and time points, except one, showed significant treatment effects as determined by the Kruskal-Wallis rank sum test ($p < 0.05$). The exception occurred in the June 2009, CL5, T4 (p value is given below figure title, no multiple comparisons were made for that experimental time-point). Asterisks indicate a significant difference from the Control ($p < 0.05$).

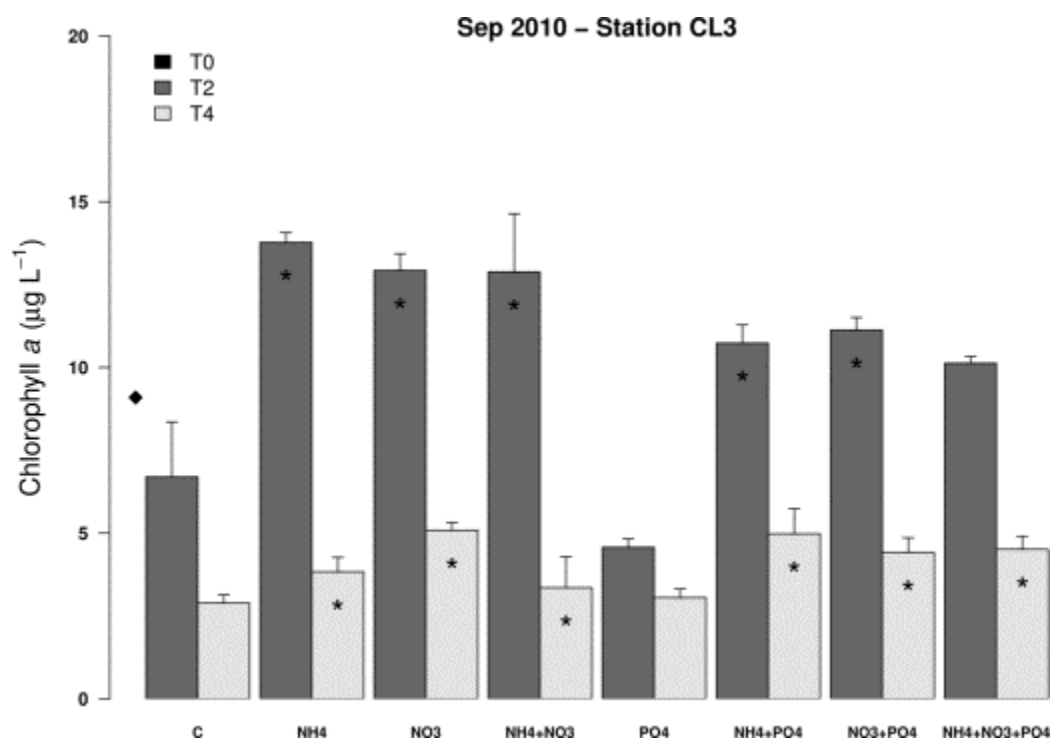
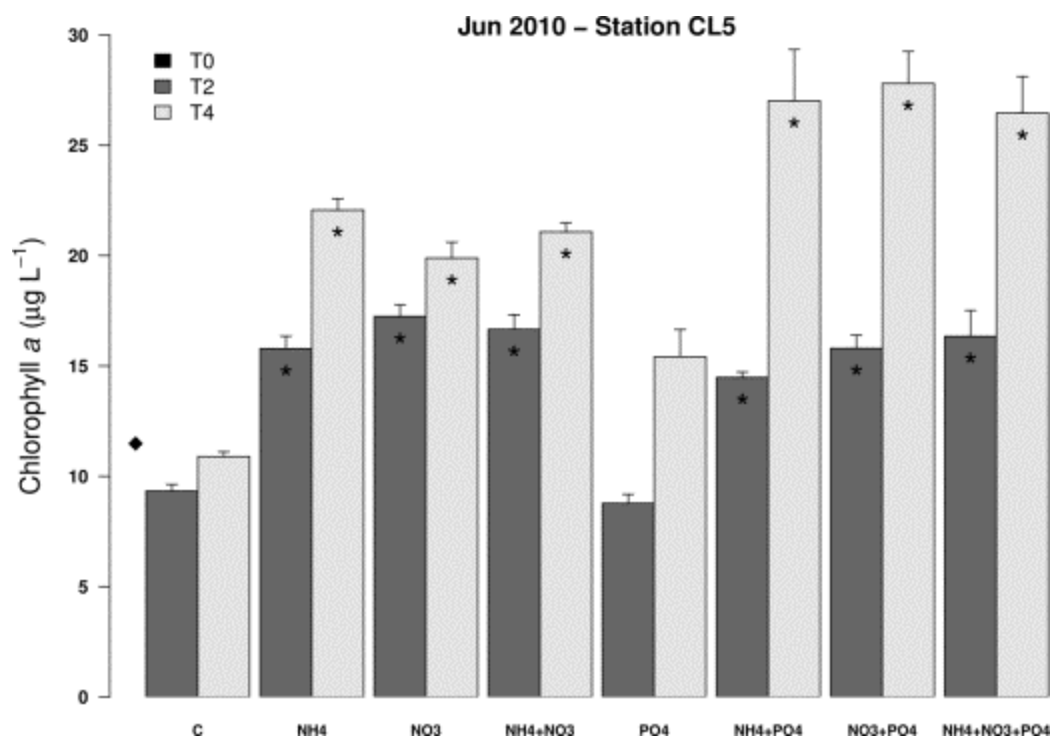


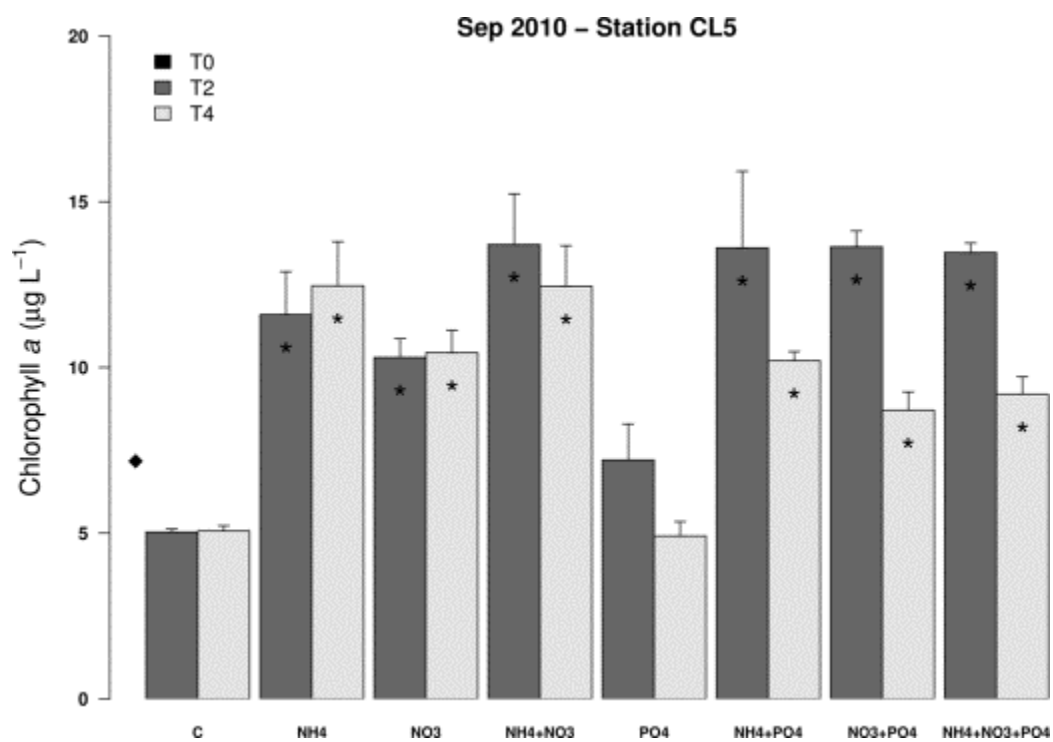












Appendix 3-C

List of Scientific Publications

List of Scientific Publications

- Altman, J., and H.W. Paerl. 2012. The role of organic nitrogen inputs on phytoplankton community composition and activity in the New River Estuary, NC. *Aquatic Ecology* (in revision).
- Hall, N.S., H.W. Paerl, B.L. Peierls, A.C. Whipple, and K.L. Rossignol. 2012. Climatic variability: Its role in determining phytoplankton biomass and community structure in the eutrophic, microtidal, New River Estuary, North Carolina, USA. *Estuarine Coastal Shelf Science* (in revision).
- Kennish, M., and H.W. Paerl. 2010. *Coastal Lagoons: Critical Habitats of Environmental Change*. CRC Marine Science Series. CRC Press: Boca Raton, FL.
- Paerl, H.W. 2009. Controlling eutrophication along the freshwater–marine continuum: Dual nutrient (N and P) reductions are essential. *Estuaries and Coasts* 32:593–601.
- Paerl, H.W., and D. Justic. 2011. Primary producers: Phytoplankton ecology and trophic dynamics in coastal waters. Pp. 23–42 in *Treatise on Estuarine and Coastal Science* (Volume 6). Edited by E. Wolanski, and D.S. McLusky. Waltham: Academic Press.
- Paerl, H., K. Yin, and J. Cloern. 2011. Global patterns of phytoplankton dynamics in coastal ecosystems. *EOS* 92(10):85.
- Peierls, B.L., N.S. Hall, and H.W. Paerl. 2012. Hydrologic control of phytoplankton dynamics: A comparison of two coastal plain North Carolina estuaries. *Estuaries and Coasts* (in revision).

Appendix 3-D

List of Students

- Julia Altman, M.Sc. Ecology (Curriculum in Ecology), University of North Carolina at Chapel Hill, Chapel Hill, NC. 2011.
- Michael Clear, undergraduate independent study, University of North Carolina at Chapel Hill's Institute for the Environment, Chapel Hill NC. Fall 2011.
- Timothy Otten, Ph.D., Environmental Sciences, Department of Environmental Sciences and Engineering, University of North Carolina at Chapel Hill, Chapel Hill, NC. 2012.
- Diana Rypkema, National Science Foundation's Research Experiences for Undergraduates student, Cornell University, Ithaca, NY. Summer 2010.

[This page intentionally left blank.]

Chapter 4

Quantifying and Predicting Watershed Inputs of Nutrients, Sediments, and Pathogens to Tributary Creeks on Marine Corps Base Camp Lejeune

SERDP Project Number: RC-1413

Aquatic-Estuarine Module

Research Project AE-2

Lead Researchers:

Mike Piehler¹, Mark Brush², Craig Tobias³, and Rachel Noble¹

¹ University of North Carolina at Chapel Hill's Institute of Marine Sciences

² Virginia Institute of Marine Science

³ University of Connecticut

May 10, 2013

Final

This report was prepared under contract to the U.S. Department of Defense (DoD) Strategic Environmental Research and Development Program (SERDP). The publication of this report does not indicate endorsement by DoD, nor should the contents be construed as reflecting the official policy or position of DoD. References herein to any specific commercial product, process, or service by trade name, trademark, manufacturer, or otherwise, do not necessarily constitute or imply its endorsement, recommendation, or favoring by DoD.

Table of Contents

List of Acronyms	4-vi
Abstract.....	4-1
Objectives of the Research Project	4-2
Hypotheses	4-2
Technical Goals	4-2
Background	4-2
Section 1: Loading of nutrients, suspended solids, and chlorophyll <i>a</i>	4-4
Materials and Methods.....	4-4
Results and Discussion	4-8
Section 2: Loading of FIB in North Carolina tidal creek headwaters: Hydrographic patterns and terrestrial runoff linkages	4-25
Materials and Methods.....	4-25
Results and Discussion	4-28
Section 3: Quantifying fecal contaminant sources in North Carolina tidal creeks of the NRE system of North Carolina	4-36
Materials and Methods.....	4-36
Results and Discussion	4-39
Conclusions and Implications for Future Research	4-44
Literature Cited	4-46
Appendix 4-A: Stable Isotopic Characterization of Particulate Organic Matter in the New River Estuary	4-A-1
Appendix 4-B: List of Scientific Publications	4-B-1
Appendix 4-C: List of Students	4-C-1

List of Tables

4-1.	Land cover and watershed area of study sites. Percent impervious is indicated in parentheses. (Homer et al., 2007)	4-5
4-2.	Relative model weights (w_i) for the best-fitting regressions for watershed yields of water ($\text{m}^3 \text{ ha}^{-1} \text{ y}^{-1}$) and TSS and PO_4^{3-} ($\text{kg ha}^{-1} \text{ y}^{-1}$) determined by Akaike Information Criterion analysis.	4-12
4-3.	Relative model weights (w_i) for the best-fitting regressions for watershed yields of nitrogen species ($\text{kg ha}^{-1} \text{ y}^{-1}$) determined by Akaike Information Criterion analysis.....	4-13
4-4.	Watershed size, predominant soil and land use types for each tidal creek (from Stumpf et al., 2010).....	4-26
4-5.	Loading differences between storm flow and base flow (times greater), and days required during dry weather to equal total <i>Escherichia coli</i> (<i>E. coli</i>) and <i>Enterococcus</i> spp. (ENT) loading during an average storm for each tidal creek (from Stumpf et al., 2010).....	4-28
4-6.	Spearman rank correlations (R^2) for all creeks combined and individual tidal creeks for loads versus rainfall metrics and <i>t</i> -test results for average EMCs for EC and ENT during both storm and equivalent base-flow periods.	4-34
4-7.	Reaction conditions and standards for all QPCR assays	4-38
4-8.	Description of tidal creek predominant land cover, fecal indicator detection, and percent exceedence of regulatory standards for conventional indicators.	4-41
4-9.	Bivariate correlations among log transformed data from all creeks using two-tailed Spearman rho rank correlation.....	4-43

List of Figures

4-1.	Location of study area in Eastern North Carolina.	4-4
4-2.	(A) Annual freshwater discharge and (B) annual load of TSS from 10 streams draining from MCBCL.	4-14
4-3.	(A) Annual loading of nitrate (as N) and (B) annual load of ammonium (as N) from 10 streams draining from MCBCL.	4-15
4-4.	(A) Annual loading of phosphate (as P) and (B) annual load of TDN (as N) from 10 streams draining from MCBCL.	4-16
4-5.	Annual load of DON (as N) from 10 streams draining from MCBCL.	4-17
4-6.	(A) Scatter points are annual water volume at each site for each of 3 years and (B) load of TSS.	4-18
4-7.	(A) Scatter points are load of nitrate from each site for each of 3 years and (B) load of ammonium.	4-19

4-8.	(A) Scatter points are load of phosphate from each site for each of 3 years and (B) load of TDN.	4-20
4-9.	Scatter points are load of DON from each site for each of 3 years.	4-21
4-10.	Linkages between observed and predicted watershed yields of fresh water for (a) total, (b) base, and (c) storm loads.	4-22
4-11.	Linkages between observed and predicted watershed yields of suspended solids for (a) total, (b) base, and (c) storm loads.	4-23
4-12.	Relationship between observed and predicted watershed yields of total nitrogen for (a) total, (b) base, and (c) storm loads.	4-24
4-13.	Study site including tidal creeks and map of the NRE system on MCBCL.	4-25
4-14.	Stream flow (m ³ /s) versus log FIB concentration (MPN/100 mL) and TSS for creeks (A) Cogdels, (B) French, (C) Gillets, and (D) Freeman during all flow conditions.	4-29
4-15.	Box plots for all four monitored creeks in the NRE system across all storms for (A) <i>Escherichia coli</i> (<i>E. coli</i>), (B) <i>Enterococcus</i> spp., (C) flow, (D) and TSS.	4-30
4-16.	Pollutograph representation of intra-storm variation in log concentrations of <i>E. coli</i> , <i>Enterococcus</i> spp. (MPN/100 mL), and TSS (mg/L) during one representative storm in the four headwater tidal creeks in the NRE system, NC.	4-32
4-17.	Relationship between log concentrations (MPN/100 mL) of <i>E. coli</i> and <i>Enterococcus</i> spp. during wet weather (rainfall >1.27 cm) storm-flow samples, and dry weather (rainfall = 0 cm) base-flow samples in the NRE system, NC.	4-35
4-18.	MCBCL tidal creeks of study.	4-36
4-19.	Regulatory exceedences for <i>E. coli</i> (right half) and <i>Enterococcus</i> spp. (top half) for each creek and bay during all sampling events.	4-40
4-20.	Mean log indicator concentration for each creek.	4-42

List of Acronyms

°C	degrees Celsius
Δ_i	difference of the AIC _c value
μL	microliter
μM	micromoles
μm	micrometer
AIC _c	Akaike Information Criterion corrected for small sample sizes
ANOVA	analysis of variance
BMP	best management practices
cm	centimeter
DEM	Digital Elevation Model
DIN	dissolved inorganic nitrogen
DoD	U.S. Department of Defense
DON	dissolved organic nitrogen
EC	<i>Escherichia coli</i> , <i>E. coli</i>
EMC	event mean concentration
ENT	<i>Enterococcus</i> spp.
FIB	fecal indicator bacteria
ft	feet, foot
GFF	glass fiber filter
ha	hectare
IC	impervious cover
kg ha ⁻¹ y ⁻¹	kilograms per hectare per year
km ²	square kilometer
LIDAR	Light Detection and Ranging
m	meter
M	total pollutant mass
m/m	meter per meter
m/s	meters per second
M/V	total pollutant mass divided by total flow volume
m ²	square meter
m ³	cubic meters
m ³ /s	cubic meters per second
MCBCL	Marine Corps Base Camp Lejeune
mL	milliliter
mm	millimeter
MPN	most probable number
ng	nanogram
NH ₄	ammonium
NH ₄ ⁺	ammonium ion
NH ₄ ⁺ -N	nitrogen as ammonium
NLCD	National Land Cover Dataset
NO _{2/3} ⁻	nitrite/nitrate
NO _x	nitrate (NO ₃ ⁻) plus nitrite (NO ₂ ⁻)

NRE	New River Estuary
OB	optical brightener
PC	polycarbonate
PO ₄	orthophosphate
PO ₄ ³⁺	phosphate ion
PO ₄ ³⁺ -P	phosphorus as phosphate
POM	particulate organic matter
QC	quality control
QPCR	quantitative polymerase chain reaction
r ²	r-squared value
SERDP	Strategic Environmental Research and Development Program
SPC	specimen processing control
SSURGO	Soil Survey Geographic Database
TDN	total dissolved nitrogen
TMDL	Total Maximum Daily Load
TSS	total suspended solids
V	total flow volume
w _i	Akaike weights, relative model weights

[This page intentionally left blank.]

Abstract

Coastal streams are both the receiving waters and transport vectors for landscape-derived materials. This high level of connectivity to surrounding watersheds makes headwater streams sentinels of impacts that may occur due to changing land uses. Determining the impacts of land use and precipitation patterns on material delivery by streams is requisite for quantifying and mitigating degradation resulting from watershed development. Headwater streams in the New River Estuary (NRE), NC, were investigated for 4 years, during which water samples were collected during base flow and throughout storm flow. Samples were analyzed for nutrient and total suspended solids concentrations, and flow was measured continuously. Fecal indicator bacteria (FIB) assessments described below were more focused in both space and time. This research determined that in developed watersheds, loading of most constituents and stream discharge increased, as did the relative importance of storm flow delivery, when compared to less developed watersheds. There was a positive correlation between loads of nutrients and total suspended solids and increasing impervious cover in the watershed. There also was a pattern in nutrient loading that suggested the possibility of a threshold in impervious cover of approximately 15%, above which there were considerably higher nutrient loads. Additionally, comparison of the loading from a drier year (2008–2009) to two wetter years (2009–2010 and 2010–2011) revealed increased loads of most constituents in wetter years. Analysis of the increase in loading from wet to dry years determined that developed watershed had similar proportional increases in loading, as did less developed watersheds. Comparison of the loading of nutrients and suspended solids from watersheds with a range of development, through both dry and wetter years allows us to postulate the impacts of changes in development patterns and climate on loading of materials from coastal streams. Stable isotopes were used to further assess source contributions from the Marine Corps Base Camp Lejeune watershed and adjacent intertidal habitats to the NRE.

Loading patterns of FIB in coastal streams have not received significant attention in the past. FIB (*Escherichia coli* [E. coli (EC)]) and *Enterococcus* spp. [ENT]), which are used as proxies for pathogens of fecal origin, frequently exceeded regulatory standards for fecal contamination in headwater portions of the study streams. Total loads of 10^9 – 10^{12} EC and ENT cells occurred over the course of storm events, and storm loading was as much as 30 to 37 times greater than base-flow loading for EC and ENT, respectively. A “toolbox” approach, including conventional indicators, three alternative fecal indicator *Bacteroides* assays, and optical brighteners, was utilized to make more robust source estimates of fecal contamination in four tidal creeks. Indicators of human contamination were found in all creeks despite relatively undeveloped land surfaces in these watersheds.

Keywords: Coastal creek, watershed, land use, imperviousness, total suspended solids, fecal indicator bacteria, nitrogen, phosphorus, stable isotopes, regression analysis, non-point source pollution, water quality, estuary

Objectives of the Research Project

Hypotheses

1. Land use and environmental conditions (e.g., precipitation patterns, temperature, soil type) interact to control export of nutrients, sediment, and pathogens from coastal watersheds.
2. Predictable patterns of loading of these materials exist for watersheds in different sections of the estuary and with varying land uses.
3. Regression analysis can be used to predict the effects of changes in land-based activities on watershed exports of nutrients, sediments, and pathogens.

Technical Goals

The technical goals included identifying and quantifying tributary creek sources of nutrients, sediments, and pathogens to the New River Estuary (NRE); assessing the impact of Marine Corps Base Camp Lejeune land uses on estuarine water quality, including nutrient, total suspended solids, and FIB loading; and determining the relative amounts of human fecal contamination contributed to the estuarine system, as opposed to non-human fecal contamination. A final goal was to determine the empirical relationships between land use and material export through streams to inform a decision-support tool for predicting watershed inputs of freshwater and pollutants into the NRE for future development scenarios (addressed in Chapter 6, *Synthetic Modeling*).

Background

Changes in watersheds associated with human development affect water quality through impacts on both the hydrology and the sources and composition of materials (e.g., nutrients, sediment, fecal material; Paul and Meyer, 2001). The transition from a natural to a developed landscape results in increases the amount of impervious cover (IC) and decreases in forested area, among other changes. These changes decrease infiltration of precipitation creating periods of increased peak storm flows (Leopold, 1968) of diminished duration (Seaburn, 1969) with the potential for subsequent decreased base flows (Barringer et al., 1994). The net effect is an overall increase in runoff volume, particularly in the storm flow component.

Coastal streams are important conduits for nutrients and contaminants in stormwater runoff to receiving waters (DiDonato et al., 2009; Mallin and Lewitus, 2004). Managing nutrient and sediment loading poses a challenge, as sufficient quantities of each are necessary for proper aquatic ecosystem functioning, but an overabundance can be detrimental. Nutrients are necessary to support primary production to support higher trophic levels. Ecologically valuable saltmarshes that are present downstream in many coastal creeks require sediment to maintain their platform in the face of rising sea levels and wave driven erosion. Sediment delivered in rivers and streams is thought to make an important contribution to saltmarsh accretion (Morris, 2002). However, sediments and nutrients in excess overwhelm ecosystem requirements and can degrade coastal habitats.

Coastal streams in eastern North Carolina are heavily utilized for shellfish harvesting, boating, fishing, swimming, and, in the New River Estuary (NRE), for amphibious military training. Loading of nutrients, sediments and fecal indicator bacteria (FIB) to headwater portions of tidal creeks affects the creek system and will eventually be transported to estuarine receiving waters. Understanding FIB and nutrient and sediment loading characteristics of these tidal creek headwaters are important for overall understanding of estuarine ecosystem function and water quality dynamics.

Because conventional FIB cannot typically be used to differentiate between human or animal fecal contamination (Meays et al., 2004; Noble et al., 2003; Scott et al., 2002), and they may persist and potentially regrow in tropical and sub-tropical water environments (Byappanahalli et al., 2003), in recent years a “toolbox approach” has been lauded for water quality management. This approach combines conventional FIB measurements, with the use of rapid, molecular quantification of alternative source-specific fecal DNA markers. Human specific fecal assays have been widely developed in the past decade, and include *Bacteroides* spp. (Ahmed et al., 2009; Carson et al., 2005; Fiksdal et al., 1985; Layton et al., 2006; Savichtcheva et al., 2007). *Bacteroides* spp. are some of the more promising of the human specific alternative indicators, due to their high concentration in the human gut (Drasar, 2003), potentially limited persistence and regrowth in the environment (Dick and Field, 2004; Kreader, 1998), and evidence for correlation between *Bacteroides* spp. concentrations and risk to human health (Savichtcheva et al., 2007; Wade et al., 2006 and 2008). The assays used in our study, Fecal *Bacteroides* spp. (Converse et al., 2009), human specific (BacHum) *Bacteroides* (Kildare et al., 2007), and human fecal contamination specific (HF183) *Bacteroides* (Bernhard and Field, 2000) have all been developed targeting *Bacteroides* spp.-based genes. Chemical indicator methods have also been used to identify household wastewater in receiving tributary streams. Chemical indicators of anthropogenic inputs into receiving waters include coprostanol (Roser and Ashbolt, 2007), caffeine (Peeler et al., 2006), and optical brighteners (OBs) (Cao et al., 2009). OBs are particularly appealing because their measurement is cost effective and relatively quick (Ahmed et al., 2008; Dickerson et al., 2007; Hartel et al., 2007). Recently, a method for improved OB analysis was developed to deal with natural background fluorescence (Cao et al., 2009), a previous problem for analysis of OBs in environmental water samples.

Coastal streams in the NRE, NC, were instrumented for 4 years, during which water samples were collected during base-flow and throughout storm-flow events. Samples were analyzed for nutrient and total suspended solids (TSS) concentrations, and flow was measured continuously. Stable isotopes were used to further assess source contributions from the Marine Corps Base Camp Lejeune (MCBCL) watershed and adjacent intertidal habitats to the NRE. These analyses were also done in an effort to identify non-conservative behavior of nitrogen and carbon (i.e., processing) on an estuarine scale and infer potential mechanisms behind that behavior. Efforts focused on the particulate organic matter (POM) because it is a large pool of nitrogen and carbon, it serves as the integrator of labile dissolved inorganic nitrogen (DIN) and dissolved organic nitrogen (DON) and carbon pools, and was sufficiently abundant at all times during the year to provide robust isotope analyses (methods and results from the stable isotope research are located in **Appendix 4-A**). FIB assessments were more focused in both space and time. We quantified conventional FIB (*Escherichia coli* [*E. coli* (EC)] and *Enterococcus* spp. [ENT]), three *Bacteroides* spp. based targets, and OBs in four tidal creek headwaters over a range of loading conditions.

Section 1: Loading of nutrients, suspended solids, and chlorophyll *a*

Materials and Methods

Study Sites

The NRE, situated in North Carolina's coastal plain (**Figure 4-1**), is composed of shallow (1-2 m), broad lagoons, with water flow constrained at the mouth by barrier islands (Mallin et al., 2005). Despite improvements to sewage treatment plants in 1998, the NRE has continued to have some phytoplankton blooms and periods of severe bottom water hypoxia (Mallin et al., 2005).



Figure 4-1. Location of study area in Eastern North Carolina.

Ten mixed-cover watersheds of the NRE were investigated to assess impacts of various land uses on stream water quality and patterns of material delivery. The watersheds' characteristics are summarized (**Table 4-1**).

The 10 watersheds drained into headwater streams that were monitored for instream water quality and discharge from 2008 through 2011. The NRE lies within MCBCL, which started expanding in 2008 to accommodate a projected influx of Marines (approximately 5,000) and their families. Land uses on MCBCL are typical of military installations and include residential neighborhoods, barracks, industrial parks, and impact zones for ordnance training. The

characteristic low elevation and shallow slopes of the North Carolina coastal plain have profound implications for mechanisms that deliver material to streams, altering loading patterns as compared to watersheds of a steeper gradient. Coastal North Carolina has a humid, subtropical climate, with average temperatures of 12.8–13.9°C and average precipitation of 142 cm per year. Rainfall is distributed almost evenly throughout the year, with a slight increase from June through September (MCBCL, 2006), minimizing seasonal patterns of material delivery to streams. Watersheds were delineated using 20-ft (6.1-m) elevation Light Detection and Ranging (LIDAR) using ArcGIS (ESRI, Redland, CA). Resulting watersheds were converted to polygons and combined with the National Land Cover Dataset (NLCD) 2001 data to assign areas for each land-use category.

Table 4-1. Land cover and watershed area of study sites. Percent impervious is indicated in parentheses. (Homer et al., 2007)

Site	Forested Land (ha)	Impervious Surface (ha)	Developed Land (ha)	Total Area (ha)
Cogdels Creek	280.53	115.25 (13.8%)	209.16	835.83
French Creek	80.28	8.56 (1.1%)	27.72	807.30
Freeman Creek	151.56	9.32 (1.6%)	21.69	588.24
Gillets Creek	70.74	12.94 (2.9%)	35.28	452.97
Tarawa Terrace	24.48	32.28 (23.2%)	63.90	139.14
Camp Johnson	16.47	0.06 (0.3%)	0.00	22.32
Air Station	14.76	20.96 (26.6%)	39.42	78.93
Southwest Creek	35.55	2.33 (3%)	6.66	77.49
Courthouse Bay	3.06	4.85 (15.5%)	19.62	31.32
Traps Bay	5.76	2.11 (4.1%)	6.39	51.03

Data collection throughout the study period consisted of continuous flow measurements, manual sampling (water grab, water depth measurement, and water velocity using a Sontek Flowtracker Acoustic Doppler Velocimeter) that occurred every other week and after rain events (defined as greater than 2.5 cm of rain). In addition, more frequent automated sampling was conducted to enhance resolution during storm events at some sites equipped with automated samplers (ISCO Models 6700 or 6712). ISCO samplers were located at Cogdels, French, Gillets, and Freeman sites from July 2008 to June 2011, and additional units were deployed at Camp Johnson, Tarawa Terrace, Courthouse Bay, and Traps Bay sites from December 2009 through June 2011.

Samplers were programmed to trigger above a threshold stream velocity set for storms and at flow-paced intervals once enabled. Automated grab samples were collected as soon as possible (usually following day) after a rain event and brought back to the laboratory for processing. Water samples were selected to encompass a period including before, rising, peak and falling limbs of hydrographs for each storm at each site.

All water samples collected were analyzed for TSS and nutrients including nitrate- plus nitrite-nitrogen ($\text{NO}_3^- + \text{NO}_2^-$, referred to as NO_x), ammonium-nitrogen ($\text{NH}_4^+ - \text{N}$, referred to as NH_4), orthophosphate ($\text{PO}_4^{3-} - \text{P}$, referred to as PO_4), and total dissolved nitrogen (TDN). Water samples were filtered through Whatman glass fiber filters (GFFs; 25 mm in diameter, 0.7 μm

nominal pore size) and the filtrate was analyzed with a Lachat Quick-Chem 8000 automated ion analyzer using standard protocols (Lachat Instruments, Milwaukee, WI: NO_x Method 31-107-04-1-A, NH₄ Method 31-107-06-1-A, and PO₄ Method 31-115-01-3-G). DON was calculated as the difference between TDN and the sum of NO_x and NH₄. Additional water was filtered through pre-cleaned and dried Whatman GFF prefilters (47 mm in diameter, 0.7-μm nominal pore size) and residue was dried and weighed for measurement of TSS using standard protocols (Method 2540 D, 2-57 [APHA, 1998]).

Nutrient concentrations that were below the detection limit but above zero were reported as the measured value and concentrations measured as negative were reported as zeros. Detection limits were as follows: NO_x (0.043 μM), NH₄ (0.182 μM), PO₄ (0.059 μM), and TDN (2.529 μM). This was done instead of replacing values with the minimum detection value to avoid overestimating concentration and load calculations.

Flow Computation

ISCO automated samplers were equipped with ISCO model 750 Area Velocity Modules with flow sensors that measured velocity (ultrasonic Doppler) and level (pressure transducer) in culvert pipes. Velocity and level were measured continuously and recorded at 30-minute intervals throughout the study period when the ISCO was present at a particular site, and volumetric flow rates were calculated using velocity and cross-sectional area of water in the pipe. Rainfall data were recorded at Cogdels and Freeman Creeks sites at 30-minute intervals via a tipping gauge connected to the ISCO sampler.

Level gauges (pressure transducers) were placed in sites when ISCO samplers were not available. Water depth was recorded at 30-minute intervals throughout the study period. Discharge was calculated using the Manning equation (Equation 4-1 below) at all sites except at the Air Station and at Southwest Creek.

$$Q=VA$$

or

$$Q=\left(\frac{1}{n}\right)AR^{\frac{2}{3}}S^{\frac{1}{2}} \times A \quad (\text{Eq. 4-1})$$

Where

- A = Area (m²)
- n = Manning “n” constant
- R = Hydraulic radius (m)
- S = Channel slope (m/m)
- V = Velocity (m/s)
- Q = Discharge (m³/s)

Field measurements were made of stream slope and other streambed characteristics to apply as parameters in the Manning equation. Cross-sectional profiles were obtained by measuring channel width and height at three representative locations along the stream reach, and used to

calculate A and R . Water surface slope (S) was measured at three locations along the stream reach via the hydrostatic leveling technique described by Gordon et al. (2004). Adjustments were made to calibrate the Manning equation calculated values to field measurements of water level and water velocity (Flowtracker) made during routine monthly sampling and indexed to ISCO flow sensor data at sites where ISCO's were subsequently deployed

A stage discharge linkage based on water level from pressure transducers and manual velocity measurements was used to calculate discharge at the Air Station. At Southwest Creek, site conditions were different, and pressure transduced water level was adjusted to downstream of pipe, but channel configurations were from conditions upstream of pipe. Mechanical errors resulting in missing level or velocity data were estimated once discharge had been calculated. Base flow was interpolated through periods of missing data. To estimate magnitude of missing storms, nearby storms from 2 to 3 months before and after the missing data time period were used as a model. In each storm, the difference in flow was calculated from base to peak, and from base to inflection point of the falling limb. A second order polynomial curve was fit to a scatter plot of storm precipitation total versus difference to peak discharge, or difference to inflection point on falling limb. These equations were then used to calculate peak and falling inflection point discharges of missing storms based on the total precipitation during that missing storm. Placement of points on the time axis mirrored nearby creeks with similar precipitation patterns, and discharge was interpolated between points.

Load Calculations

A graphical separation technique was utilized to delineate between the base-flow component and total stream flow during storm events (Ward and Robinson, 2000). Groundwater contribution during storms was determined by extending antecedent conditions by interpolating from base flow before the rain event to the point of greatest inflection on the falling limb of the hydrograph. A mass balance equation was used to determine the resultant storm-flow contribution to nutrient and TSS load.

Collection of water samples at sites when ISCOs were deployed was at a fine temporal resolution throughout storms, which enabled development of a continuous record of nutrient and TSS concentrations by interpolating between measured samples. When ISCOs were not present, extrapolating measured data to half hour intervals was accomplished by applying quality control (QC; flow versus concentration) generated polynomials to calculate concentration based on water flow. QC linkages were created using all available data within the study period, but applied only to those times and sites when ISCOs were not present.

Statistical Analysis

We tested a series of linear and nonlinear 1–4 parameter regressions for predicting total, base, and storm watershed yields (m^3 or $\text{kg ha}^{-1} \text{y}^{-1}$) of flow, TSS, and all nutrient species from the eight study watersheds with sufficient data records using an Information Theoretic approach (Burnham and Anderson, 2002). Predictors included the percent of watershed area covered by forest and impervious surfaces, population density (expressed per hectare), percent of well-drained soils, and mean watershed slope, and all possible combinations of percent forest and the latter three parameters. Percent imperviousness was not included in these combinations as it was

highly correlated with percent forested area (impervious surface = -0.40 for $+0.35$; $r^2=0.94$; $p<0.001$). Agricultural lands do not exist within the study watersheds so all land not classified as forested was taken to be developed.

Watersheds were delineated with the ArcGIS 9.3 (ESRI) hydrology toolbox and a LIDAR–derived 6.1 m (20 ft) horizontal resolution surface Digital Elevation Model (DEM) with a vertical root mean squared error of 25 cm or less (MCBCL, 2007). Resulting watershed boundaries were checked against the DEM and high resolution streamlines from the U.S. Geological Survey’s National Hydrography Dataset (available at <http://nhd.usgs.gov>). Land-use data were obtained from the NLCD for 2001 (Homer et al., 2004). Population densities were computed using U.S. Census Bureau data from the 2000 census (TIGER, 2000). Soil drainage type was computed using the Soil Survey Geographic Database (SSURGO, 2009) for Onslow County, NC. The drainage classification for the dominant soil component in each SSURGO polygon was assigned a value of one for excessively, well, and moderately well drained soils and zero for somewhat poorly, poorly, and very poorly drained soils. Polygons without a drainage classification were excluded from the analysis as they typically represent open water or impervious surfaces. Polygons were merged with watershed boundaries to compute the percent of well drained soils within each watershed. Mean watershed slopes were computed from the MCBCL (2007) DEM.

Single and multiple linear regressions were computed using all combinations of parameters listed above. Because watershed yields for some parameters appeared to indicate potential threshold responses, we also computed single parameter power function regressions for each parameter and logistic regressions using all combinations listed above of the form shown in Equation 4-2:

$$y = \frac{1}{1 + \exp^{-(\beta_0 + \beta_1 \cdot x_1 + \beta_2 \cdot x_2 + \dots + \beta_k \cdot x_k)}} \quad (\text{Eq.4- 2})$$

Following the approach of Burnham and Anderson (2002), the Akaike Information Criterion corrected for small sample sizes (AIC_c) was computed from the residual sum of squares of all significant models ($p \leq 0.05$), sample size ($n=8$), and the number of model parameters (k) increased by one when using least squared regression as input to the analysis. The difference (Δ_i) of the AIC_c value for model i from the minimum AIC_c value was computed and used to compute the likelihood of each model given the data (L) for models with $\Delta_i < 10$ and the Akaike weights (w_i) which represent the likelihood of model i being the best model in the set.

Results and Discussion

This study provided data showing that coastal headwater streams are ideal locations to assess impacts of watershed development and environmental variability on stream water quality by quantifying material fluxes that cross the land–water interface. Water quality at the sampling stations was generally a good representation of watershed scale development. Altered water quality was evident in annual material load at very low levels of development. For the most accurate load calculation, water velocity should be measured directly, and frequent sampling of water quality during both base flow and throughout storm flow is necessary to allow for interpolation between concentration measurements.

Base flow and storm flow loading of nutrient and suspended materials

Changes in the relative importance of base-flow and storm-flow material delivery can be a useful index of watershed development because it signifies altered hydrology due to increased imperviousness associated with development. IC, which hinders percolation, can take the form of roads, rooftops, parking lots, and even compacted soil, and ultimately change the fate of rainwater (Arnold and Gibbons, 1996). These minimally porous surfaces simultaneously alter the hydrology of both surface and groundwater by shunting rainwater directly to streams as overland flow, which diverts rainfall away from groundwater recharge via percolation, and reduces evapotranspiration potential (Harbor, 1994). The difference in overland flow between a pristine and developed watershed can be quite dramatic. For example, in a typical pristine watershed with natural groundcover, 50% of rainfall will percolate into soil, 40% will return to the atmosphere via evapotranspiration, leaving only 10% to enter streams directly as overland flow. This relationship begins to shift with watershed development, so that in a typical watershed of 35%–50% IC, percolation drops to 35%, evapotranspiration drops slightly to 35%, but the proportion that would enter the stream directly as overland flow increases 3 times to 30% (see www.coastal.ca.gov/nps/watercyclefacts.pdf).

Loading of nutrients and TSS through 3 years at 10 streams is shown in **Figures 4-2 through 4-5**. Streams are presented from lowest level of development on the left to highest on the right side of each *x*-axis. Percent imperviousness in the watershed is used here as an indicator of development. For all constituents there is a general trend of higher loading at higher levels of development. There were a few notable exceptions to this pattern including Camp Johnson, which had very low imperviousness, but had a gravel road bed proximate to the gaged stream that affected both flow and TSS. Tarawa Terrace was another example of a stream that did not fit in with the trend associated with increasing imperviousness. Tarawa Terrace had TSS loading that exceeded predictions in the second year and then was well below expectations in the third year. Not coincidentally, a stormwater best management practices (BMP) upgrade was being installed during the second year, at the same time significant construction was occurring in the watershed. Our loading data verified the efficacy of the BMP. Because load is the product of water discharge and concentration of specific materials, the relationship of volume of water with degree of development was important and shaped a significant proportion of the linkages between loading and imperviousness (**Figures 4-2 through 4-5**). There were generally higher loads in the second and third years of the study. This was attributed to increased precipitation in these years and is discussed in more detail below.

We were particularly interested in not only the differences in loading of materials from streams with varying degrees of development, but also the distribution of load in base flow and storm flow. This distribution is important for ecosystem function because it determines whether materials delivered to the estuary arrive slowly over a long period (base flow) or quickly in pulses (storm flow). It is important for land managers because it provides information to allow them to manage excessive loads and to understand the consequences of any management activities on the loading of the full suite of materials. To begin to make generalizations about the degree of development and stream storm loading, we calculated the mean percent of each constituent that was delivered in storm flow. As hypothesized, less developed streams generally had lower percent delivered in storm flow (**Figures 4-2 through 4-5**).

Stream loading changes associated with precipitation

Global climate models generally predict more rain for the eastern seaboard of the United States. More precipitation is generally believed to increase runoff and thus loading of nutrients and suspended solids in streams. However, few studies have made measurements at a large enough number of small coastal streams for a long enough period of time to make predictions about loading of nutrients from streams with a range of development in their watersheds with variable climatic conditions. Because we monitored streams through a very dry year and two relatively wet years, our data can be used to test hypotheses related to future impacts of changes in precipitation patterns.

Using each tributary as an individual replicate, a one-way analysis of variance (ANOVA) found there was significantly higher loading of all materials in 2009–2010 and 2010–2011 as compared to 2008–2009. This was attributable to higher precipitation levels in 2009–2010 and 2010–2011. We compared the percent increase in loading between 2008–2009 (dry year) and 2009–2010 (wet year) in more and less developed watersheds (**Figures 4-2 through 4-5**). We hypothesized that more developed streams would have higher increases in loading in the wet year versus the dry year than the less developed sites. TSS loading did increase (dry year versus wet years) significantly more in more developed sites ($p < 0.05$). Nutrient loading increases from the dry year to the wet years were not significantly different at streams with more developed watersheds compared to streams with less developed watersheds ($p > 0.05$). This finding was interesting, but should not be interpreted as conclusive evidence that developed areas do not have disproportionately higher nutrient loading than undeveloped areas in wet years.

Loading and imperviousness

Scatter plots show the linkage between annual load at each stream and imperviousness in the stream watershed (**Figures 4-6 through 4-9**). Loads were generally low for all constituents at low levels of imperviousness. TSS loading at Camp Johnson was again an outlier. There was what appeared to be a threshold at 15% imperviousness at which point loads from those streams increased dramatically. Because our study watersheds had generally low proportions of imperviousness, this conclusion must be tempered. However, as base development continues and the 15% imperviousness level is approached in more of the watersheds, it will be important to remain diligent in assessing potential increases in loading of materials.

Regression analysis of loading and development

Of the 609 regression models fit, 228 were significant at the $\alpha = 0.05$ level; of these, 48 had Akaike weights greater than 0.10 indicating they have at least a 10% likelihood of being the best model (**Tables 4-2 through 4-3**). These best fitting models were either linear or logistic; the single parameter power functions did not successfully predict yields. Similarly, only one and two parameter models provided the best fits for all parameters; more complex models were never significant.

Watershed yields of fresh water and TSS were best described by linear functions based on population density, population combined with percent forest, and watershed slope (**Table 4-2**). However, post-hoc regression of observed yields against those predicted by the regression

equations using slope yielded comparatively weaker fits ($r^2 < 0.75$). Yields of phosphate were better described by logistic regressions, suggesting a threshold response primarily to drainage, slope, and impervious surfaces.

Watershed yields of nitrogen species were best described by a combination of linear and logistic models depending primarily on the parameter but also on the type of load (total, base, storm; **Table 4-3**). As with fresh water and TSS, models based on percent forest and population density were consistently strong, with a variety of the significant models based on other parameters yielding weak ($r^2 < 0.75$) or non-significant ($p > 0.05$) regressions of observed versus predicted yields in post-hoc testing. As with phosphate, the best models for ammonium were logistic and based on the same parameters, suggesting a similarity between these recycled forms of nitrogen.

Given that regressions based on percent forest and population density were often among the best models, we compared predicted watershed yields using these regressions against observed yields for fresh water (**Figure 4-10**), TSS (**Figure 4-11**), and total nitrogen (**Figure 4-12**). The resulting fits were well constrained, highly significant ($p < 0.01$), and explained the majority of the variability in the data in all cases. The models are likely best at predicting base loads given a broader distribution of yields, whereas values for total and storm loads were often dominated by a single high value. Patterns were similar for NO_x , and total, base, and storm yields for phosphate and ammonia were all dominated by a single high value. Total and storm yields of organic nitrogen were also dominated by a high value, and there was no apparent linkage between observed and predicted base yields. Regardless of variability in which parameters and model types best explain the yields (**Tables 4-2 through 4-3**), and the occurrence of some influence points at high yields (**Figures 4-10 through 4-12**), these simple regression models do a good job in reproducing yields of these three key parameters across this low relief, coastal plain setting and have the potential to provide general estimates of likely changes in loads as a function of changes in land use and population density.

Table 4-2. Relative model weights (w_i) for the best-fitting regressions for watershed yields of water ($\text{m}^3 \text{ha}^{-1} \text{y}^{-1}$) and TSS and PO_4^{3-} ($\text{kg ha}^{-1} \text{y}^{-1}$) determined by Akaike Information Criterion analysis.

Linear and logistic models were multiple regressions with independent variables include “for” (% forested), “imp” (% impervious surface); “pop” (population density, person ha^{-1}), “drain” (% well drained soils), and “slope” (mean watershed slope, %).

Parameter	Component	Regression	Variables	w_i
Water	Base	Linear	for pop	1.00
		Linear	slope ^a	0.79
	Storm	Linear	for pop	0.17
		Linear	slope ^a	0.65
		Linear	for pop	0.33
TSS	Base	Linear	for pop	0.85
		Linear	pop	0.15
	Storm	Linear	for pop	0.96
	Total	Linear	for pop	1.00
PO_4^{3-}	Base	Logistic	drain	0.43
		Logistic	for pop	0.31
		Logistic	slope ^a	0.21
	Storm	Logistic	drain	0.57
		Logistic	imp	0.24
		Logistic	slope	0.17
	Total	Logistic	drain	0.58
		Logistic	imp	0.20
		Logistic	slope	0.20

^a Linear regression of predicted and observed watershed yields resulted in fits with adjusted $r^2 < 0.75$.

Table 4-3. Relative model weights (w_i) for the best-fitting regressions for watershed yields of nitrogen species ($\text{kg ha}^{-1} \text{y}^{-1}$) determined by Akaike Information Criterion analysis.

Linear and logistic models were multiple regressions with independent variables include “for” (% forested), “imp” (% impervious surface); “pop” (population density, person ha^{-1}), “drain” (% well drained soils), and “slope” (mean watershed slope, %).

Parameter	Component	Regression	Variables	w_i
TN	Base	Linear	for pop ^a	0.54
		Logistic	imp ^{a, b}	0.14
		Logistic	pop ^{a, b}	0.13
	Storm	Linear	slope ^a	0.81
		Linear	for pop	0.16
	Total	Linear	slope ^a	0.65
		Linear	for pop	0.32
Ammonium (NH_4)	Base	Logistic	drain	0.34
		Logistic	for pop	0.22
		Logistic	slope	0.20
		Logistic	imp	0.20
	Storm	Logistic	imp	0.43
		Logistic	drain	0.36
		Logistic	slope	0.19
	Total	Logistic	drain	0.37
		Logistic	imp	0.32
		Logistic	slope	0.29
Nitrate + nitrite (NO_x)	Base	Logistic	imp	0.89
	Storm	Linear	slope ^a	0.47
		Linear	imp ^a	0.39
		Linear	for pop	0.12
	Total	Linear	slope ^a	0.46
		Linear	imp ^a	0.40
		Linear	for pop	0.11
Organic Nitrogen	Base	Logistic	imp ^{a, b}	0.42
		Logistic	pop ^{a, b}	0.41
	Storm	Linear	slope ^a	0.80
		Linear	for pop	0.16
	Total	Linear	slope ^a	0.62
		Linear	for pop	0.36

^a Linear regression of predicted and observed watershed yields resulted in fits with adjusted $r^2 < 0.75$.

^b Linear regression of predicted and observed watershed yields resulted in fits with $p > 0.05$.

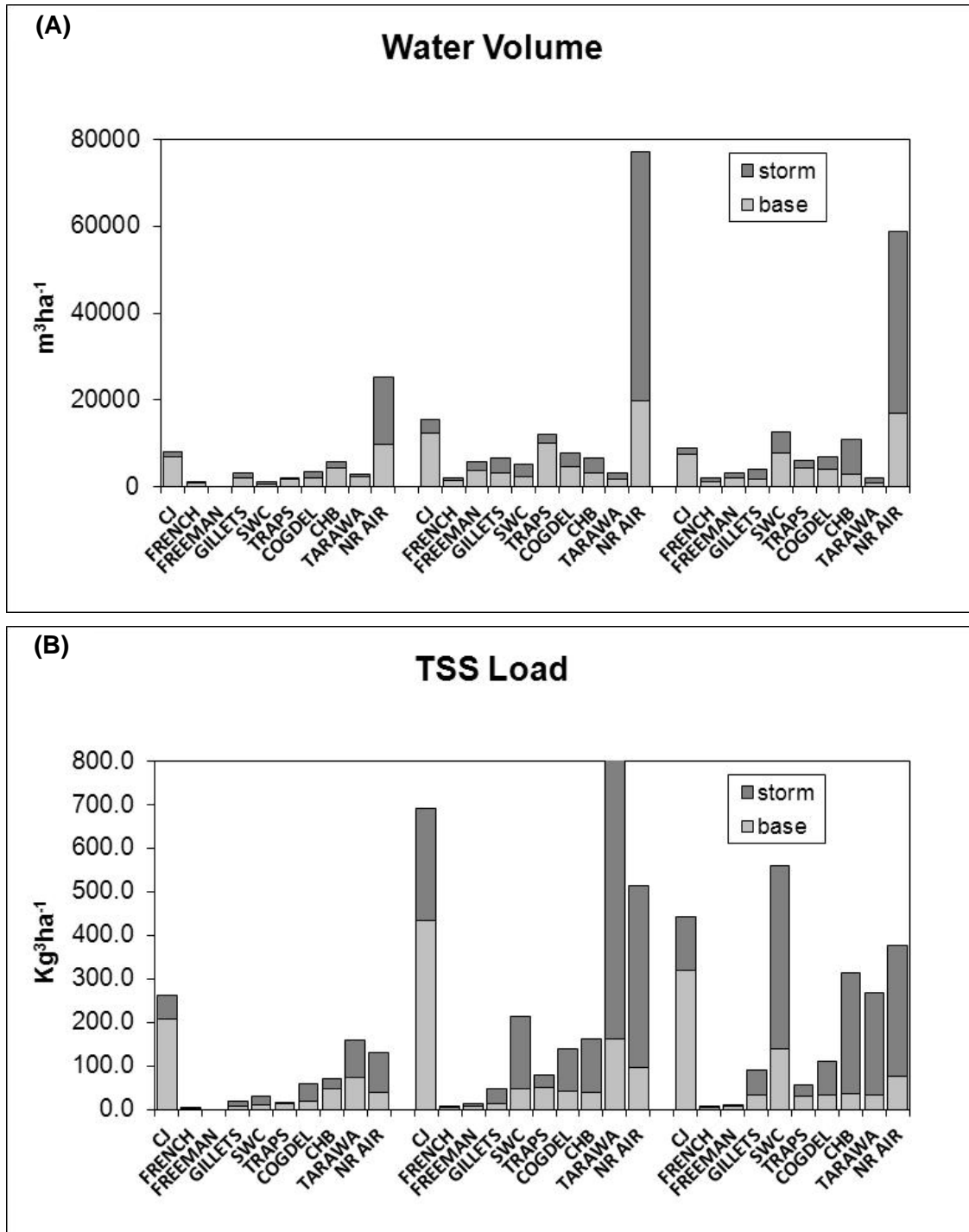


Figure 4-2. (A) Annual freshwater discharge and (B) annual load of TSS from 10 streams draining from MCBCL.

Full bars are the total annual load, the lower lighter portion of the bars are base-flow loading and the darker upper portion of the bars are storm loading. Annual loads are normalized to watershed area. CJ = Camp Johnson, SWC = Southwest Creek, CHB = Courthouse Bay, NR AIR = New River Air Station

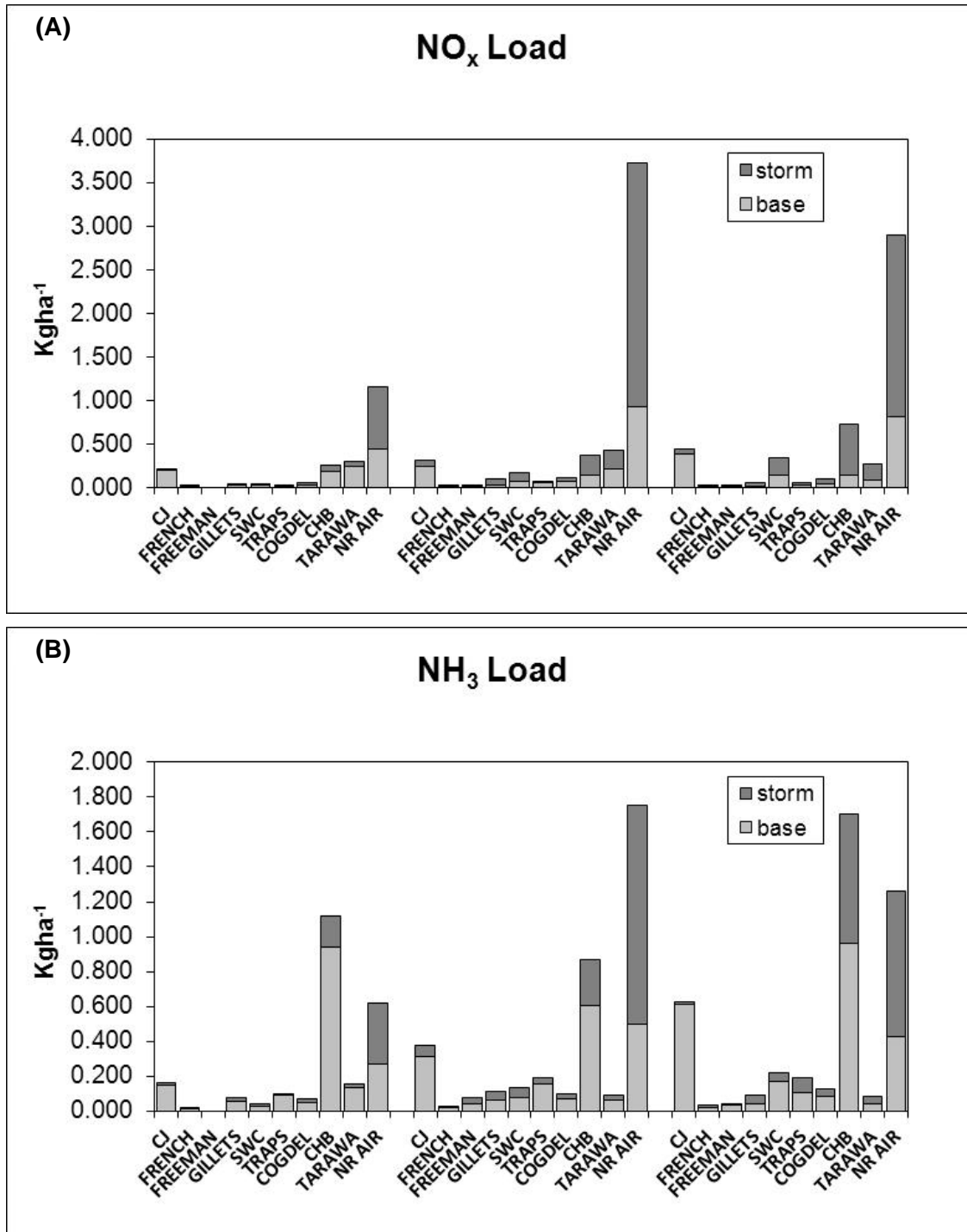


Figure 4-3. (A) Annual loading of nitrate (as N) and (B) annual load of ammonium (as N) from 10 streams draining from MCBCL.

Full bars are the total annual load, the lower lighter portion of the bars are base-flow loading and the darker upper portion of the bars are storm loading. Annual loads are normalized to watershed area. CJ = Camp Johnson, SWC = Southwest Creek, CHB = Courthouse Bay, NR AIR = New River Air Station

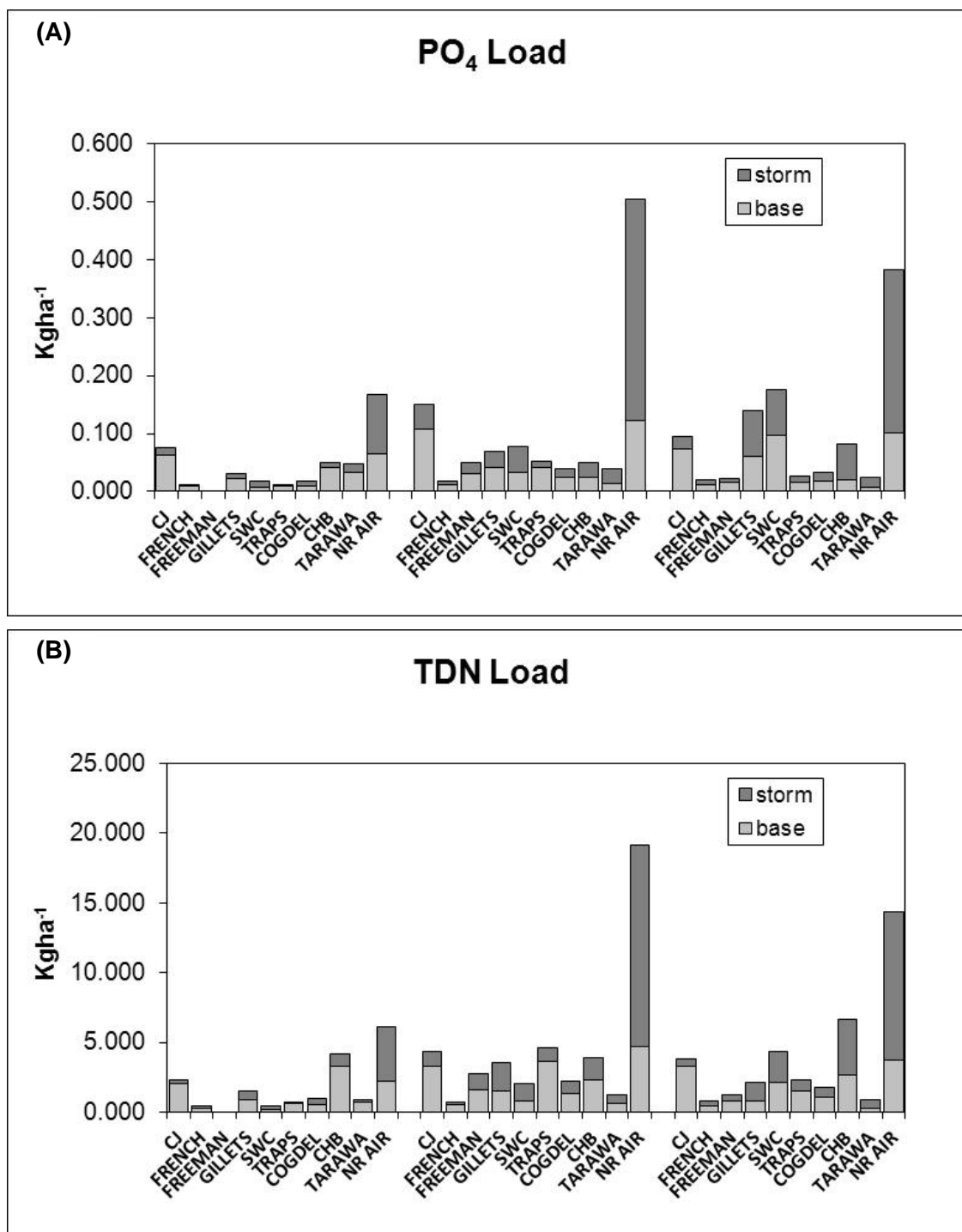


Figure 4-4. (A) Annual loading of phosphate (as P) and (B) annual load of TDN (as N) from 10 streams draining from MCBCL.

Full bars are the total annual load, the lower lighter portion of the bars are base-flow loading and the darker upper portion of the bars are storm loading. Annual loads are normalized to watershed area. CJ = Camp Johnson, SWC = Southwest Creek, CHB = Courthouse Bay, NR AIR = New River Air Station

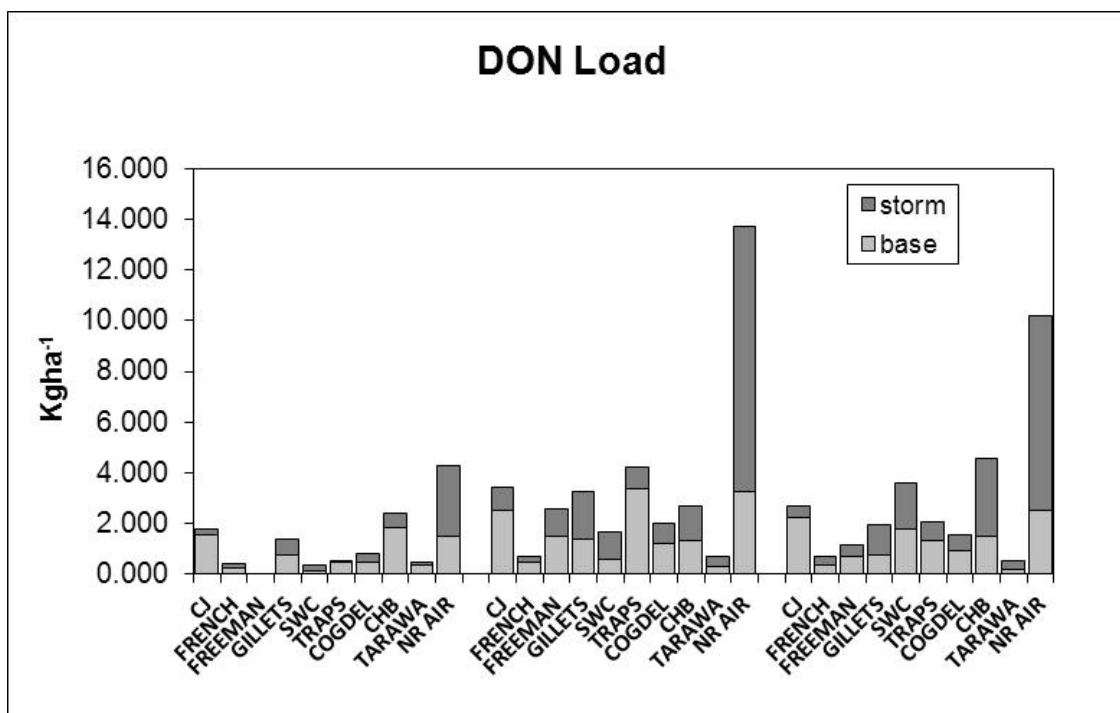


Figure 4-5. Annual load of DON (as N) from 10 streams draining from MCBCL.

Full bars are the total annual load, the lower lighter portion of the bars are base-flow loading and the darker upper portion of the bars are storm loading. Annual loads are normalized to watershed area. CJ = Camp Johnson, SWC = Southwest Creek, CHB = Courthouse Bay, NR AIR = New River Air Station

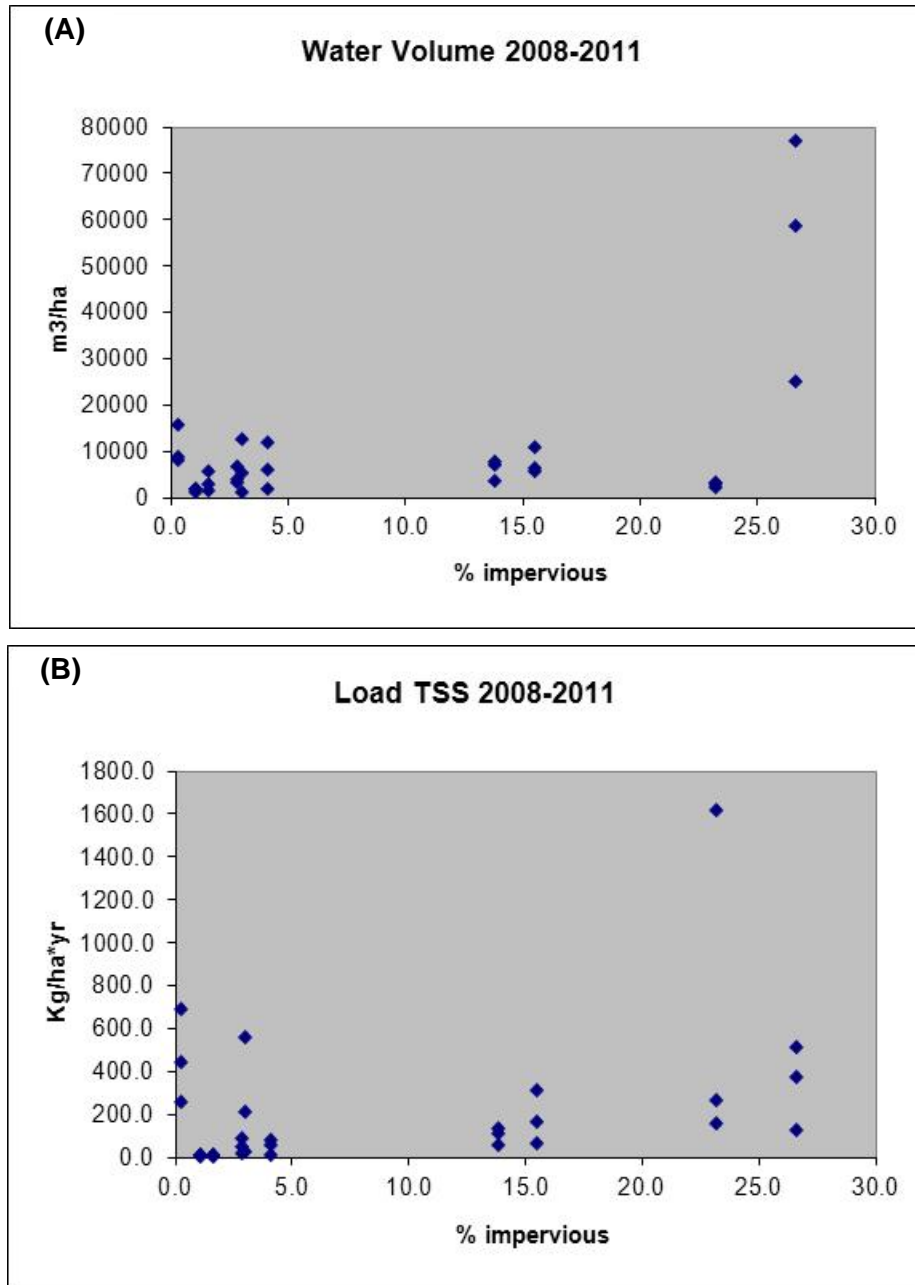


Figure 4-6. (A) Scatter points are annual water volume at each site for each of 3 years and (B) load of TSS.

Plot compares watershed normalized loads are plotted with the proportion of imperviousness in each watershed.

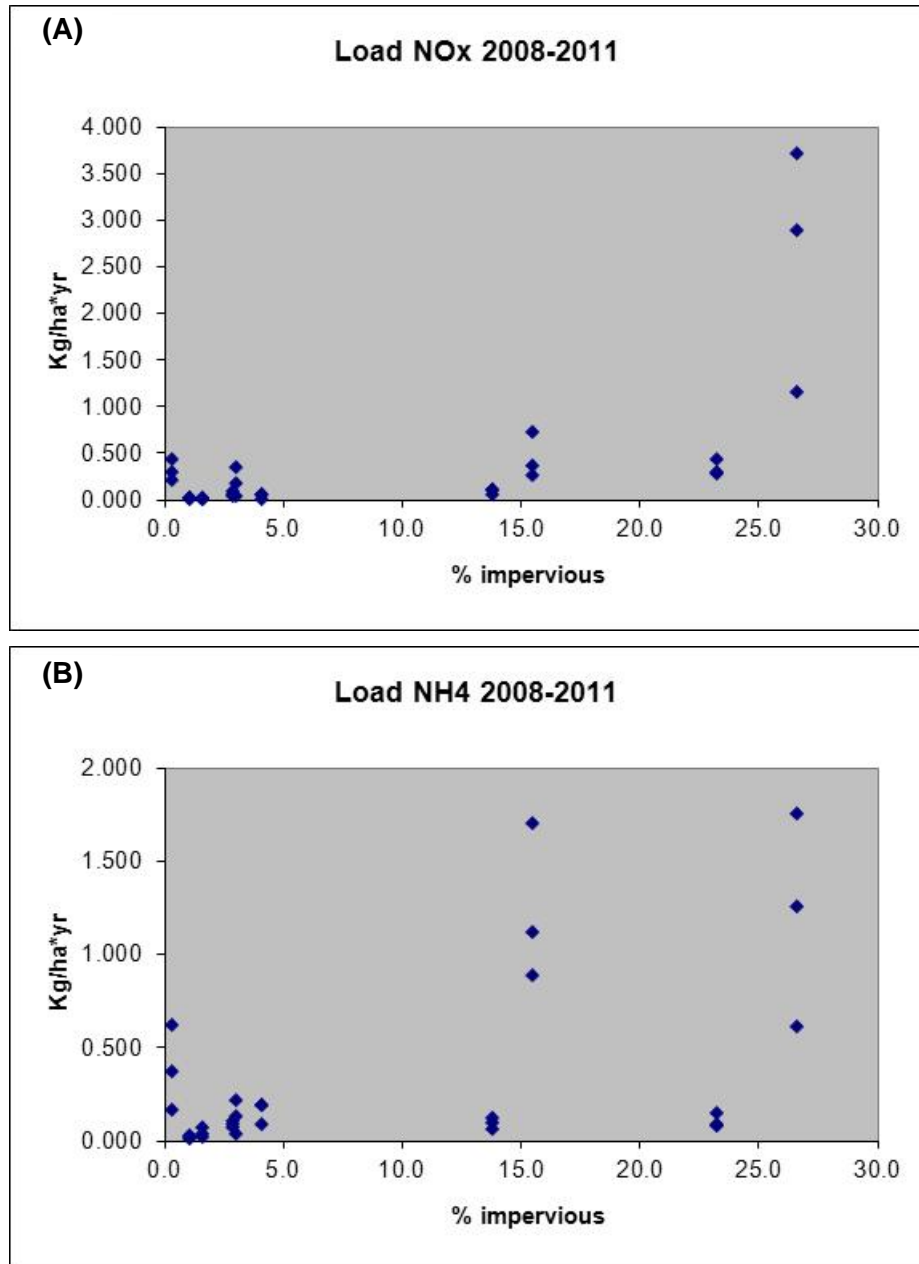


Figure 4-7. (A) Scatter points are load of nitrate from each site for each of 3 years and (B) load of ammonium.

Plot compares watershed normalized loads are plotted with the proportion of imperviousness in each watershed.

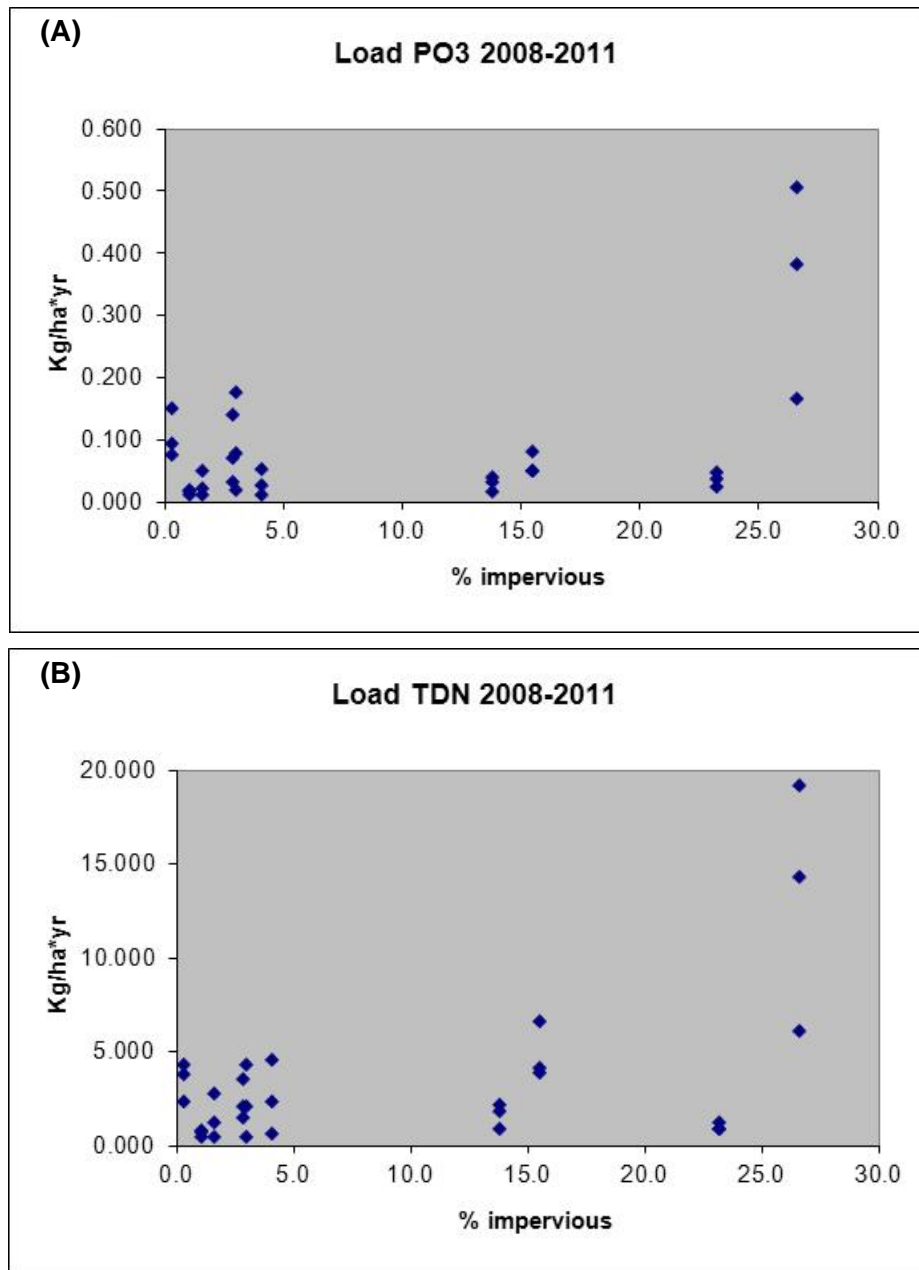


Figure 4-8. (A) Scatter points are load of phosphate from each site for each of 3 years and (B) load of TDN.

Plot compares watershed normalized loads are plotted with the proportion of imperviousness in each watershed.

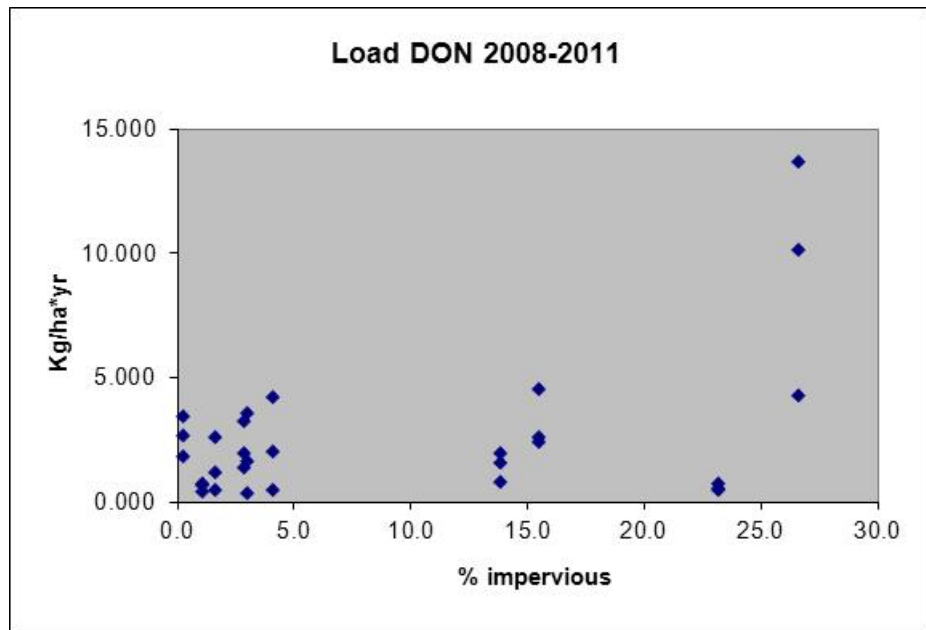


Figure 4-9. Scatter points are load of DON from each site for each of 3 years.
Plot compares watershed normalized loads are plotted with the proportion of imperviousness in each watershed.

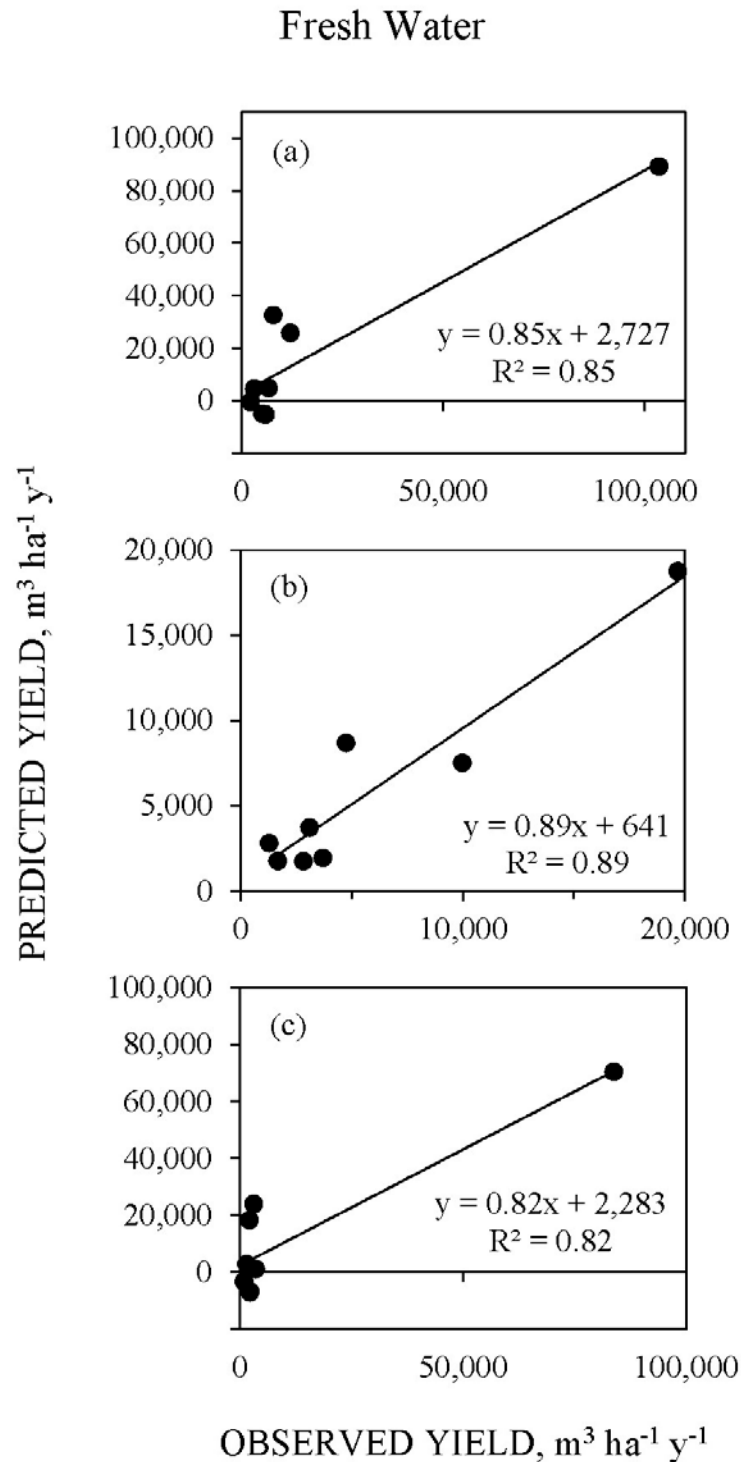


Figure 4-10. Linkages between observed and predicted watershed yields of fresh water for (a) total, (b) base, and (c) storm loads.

Predicted yields are based on the multiple linear regressions as a function of % forest and population density.

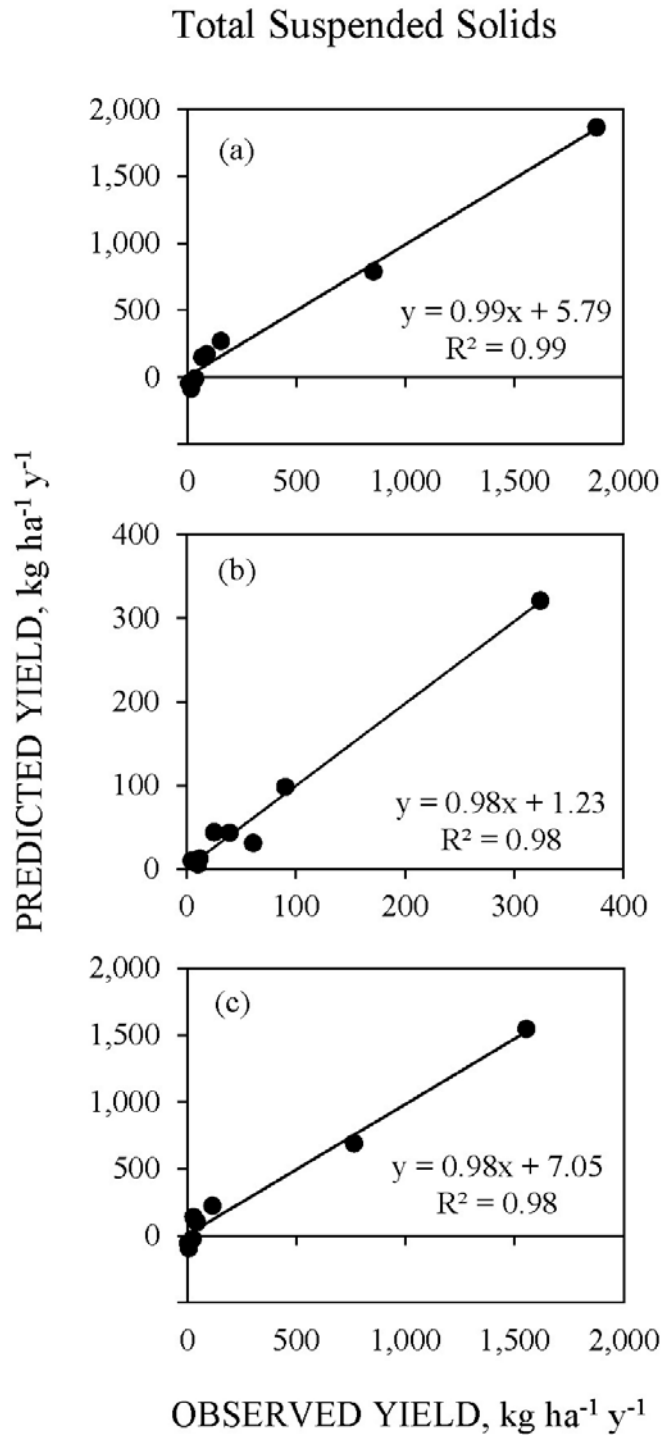


Figure 4-11. Linkages between observed and predicted watershed yields of suspended solids for (a) total, (b) base, and (c) storm loads.

Predicted yields are based on the multiple linear regressions as a function of % forest and population density.

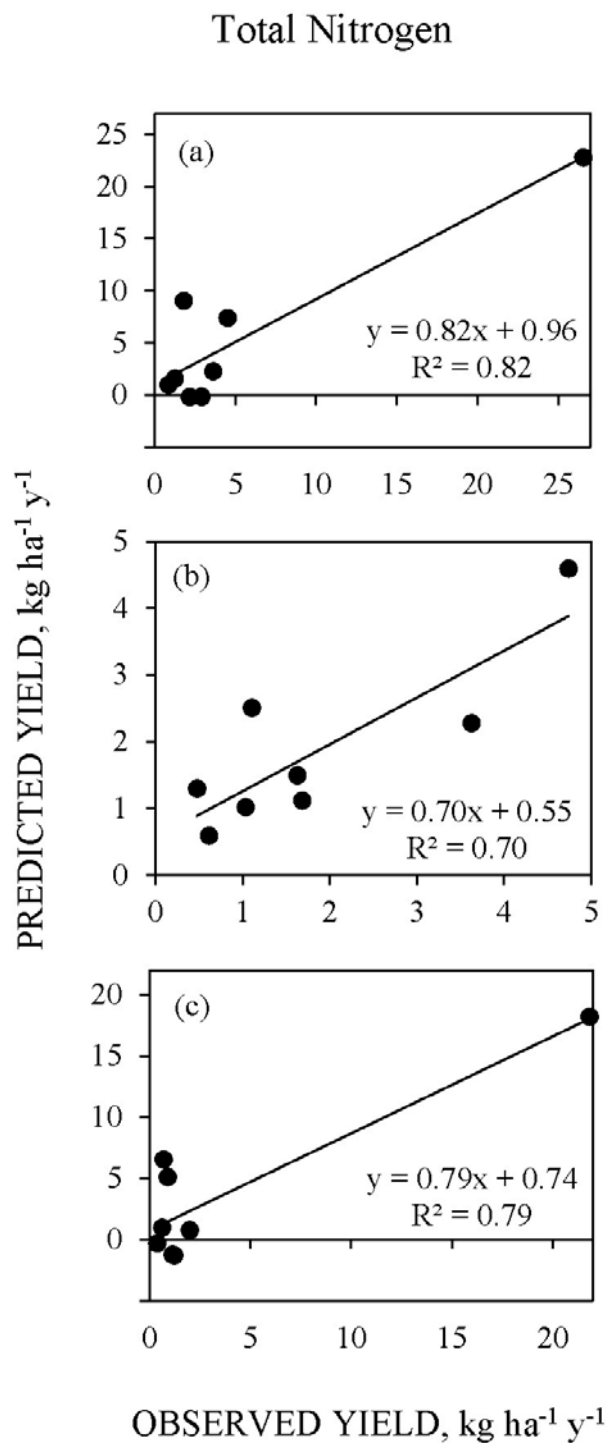


Figure 4-12. Relationship between observed and predicted watershed yields of total nitrogen for (a) total, (b) base, and (c) storm loads.

Predicted yields are based on the multiple linear regressions as a function of % forest and population density.

Section 2: Loading of FIB in North Carolina tidal creek headwaters: Hydrographic patterns and terrestrial runoff linkages

Materials and Methods

Site Description

The study location is described in Section 1 of this document, and includes the New River watershed, located within Onslow County, NC. The watershed encompasses 1,436 km² and contains the NRE, a broad, shallow estuary with a surface area of 88.1 km² (Mallin et al., 2005). MCBCL, the Marine Corp's largest amphibious training base with more than 47,000 Marines, occupies a large portion of the watershed and is located adjacent to Jacksonville, NC. The estuary is used primarily for boating, bathing, and commercial and recreational fishing and shellfish harvesting, but also for military operations. Cogdels, French, Freeman, and Gillets are tributary tidal creeks draining to either the NRE or the Intracoastal Waterway (ICW) (Figure 4-13).

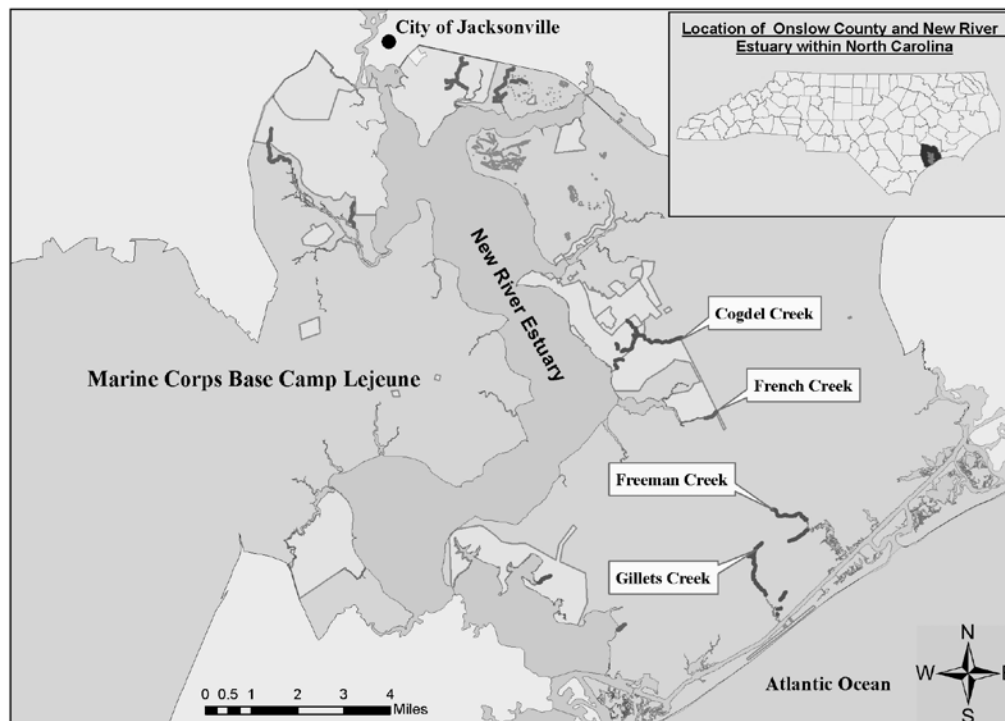


Figure 4-13. Study site including tidal creeks and map of the NRE system on MCBCL.

The four watersheds have similar soils types predominantly comprised of fine sands, have highly vegetated land cover, and little impermeable surfaces and/or development, with the exception of Cogdels Creek (Table 4-4).

**Table 4-4. Watershed size, predominant soil and land use types for each tidal creek
(from Stumpf et al., 2010)**

Watershed	Watershed Size (m²)^a	Predominant Sediment Types^a	Predominant Land Use Types^b	Land-Use Percentage
Cogdels	7,620,939	BaB, Baymeade fine sand	Predominantly pine forest	33.5
		BmB, Baymeade—Urban	Business or commercial area	31.3
		MaC, Marvyn loamy fine sand	Mixed pine and hardwood forest	10.3
		Mk, Muckalee loam	Bottomland hardwood forest	9.3
		On, Onslow loamy fine sand	Forest plantations under 10 years	6.1
		To, Torhunta fine sandy loam	Other	9.7
French	5,872,377	Ln, Leon fine sand	Bare ground	54.3
		KuB, Kureb fine sand	Shrub or scrub	23.7
		Mu, Murville fine sand	Predominantly pine forest	19.5
		BaB, Baymeade fine sand	Other	2.4
Freeman	6251037	BaB, Baymeade fine sand	Mixed pine and hardwood forest	42.5
		Mk, Muckalee loam	Predominantly pine forest	46.4
		KuB, Kureb fine sand	Shrub or scrub	6.7
		AnB, Alpin fine sand	Bare ground	3.7
		Mu, Murville fine sand	Other	0.7
Gillets	4199947	WaB, Wando fine sand	Predominantly pine forest	39.2
		Mk, Muckalee loam	Mixed pine and hardwood forest	32.4
		Ln, Leon fine sand	Bottomland hardwood forest	11.4
		To, Torhunta fine sandy loam	Forest plantations under 10 Years	10.5
		BaB, Baymeade fine sand	Other	6.5

^a USDA, Web Soil Survey, 2010.

^b T. Minter, unpublished data.

Field and Laboratory Methods

Storm- and Base-flow Sampling. Surface water samples were collected during 10 storms from December 2007 to December 2008 using ISCO automated water samplers (Model 6712, ISCO, Lincoln, NE) equipped with flow sensors (Model 750). The ISCO autosamplers were located on the downstream side of road culverts (i.e., drainage pipes) in the four headwater tidal creeks; these autosamplers utilized velocity sensors (pointed upstream) to measure stream velocity by acoustic Doppler and water level by pressure transducer, and collected 1L water samples. The monitored culverts were below the water surface and did not create backwater conditions, cascades, or other changes in normal stream velocity or flow. Flow, rainfall, and water quality data (dissolved oxygen, temperature, and conductivity) were continuously collected and logged at 30-minute intervals using a YSI datasonde, Model 600XL. Base-flow samples (n=102) were collected bi-monthly from September 2007 to December 2008 then placed on ice and processed within 6 hours of collection.

Rainfall. Rainfall was collected via automated rainfall samplers within the Freeman and Cogdels Creeks watersheds. Freeman Creek rainfall data were utilized for Gillets Creek due to the close location, and Cogdels data were used for French Creek. Total storm rainfall was calculated in the time between elevations of hydrograph above baseflow until rainfall ceased. Storm rainfall duration was determined by addition of consecutive 0.5-hour increments when at least 0.025 cm of rainfall was recorded, until storm completion. Seven-day antecedent rainfall was determined by summation of all rainfall during the 7 days previous to an event.

Hydrograph Sample Selection. For each storm event, ISCO water samples were selected based on location within the different stages of the hydrograph, determined using ISCO Flowlink Software (version 4.01) (Stumpf et al., 2010). The four storm stages analyzed were: (1) pre-storm, (2) rising limb, (3) peak, and (4) falling limb, as determined by visual hydrograph analysis. Similar multi-time point sample collection approaches, incorporating pollutograph representations of contaminants, have previously been utilized (Surbeck et al., 2006).

FIB Enumeration and TSS Measurement. Water samples were processed in duplicate using Colilert-18 and Enterolert (IDEXX Laboratories, Westbrook, ME) at a 1:10 dilution to calculate most probable number (MPN) of EC and ENT. TSS concentrations were determined using mass collected on 0.7- μ m filters, after a volume of sample was filtered, according to standard Method 2540D (APHA, 1998).

Data and Statistical Analysis

All statistics were conducted either using SPSS (version 11.0) or Microsoft Excel software. An Excel interpolation function was used to estimate FIB concentrations between sample points, similar to load estimation methods used previously (Ensign et al., 2006). Volumetric flow (m^3/s) was calculated by multiplying velocity (m/s) by wetted cross-sectional area (m^2) of each culvert, which was calculated using the cross sectional geometry and water level (measured using pressure transducers). Total load (cells [MPN]/time) for base-flow and storm-flow conditions were estimated by multiplying FIB concentration (MPN/100 mL) by flow volume (m^3) per 30-minute period.

Relationships among FIB loads, precipitation metrics (total rainfall, storm duration, and antecedent rainfall), stream flow, and TSS were tested using spearman rank correlation coefficient analysis. FIB and TSS concentrations were log transformed due to their non-normal distribution, and log values were used to assess relationships among the indicators and for comparison to stream flow, precipitation metrics, and TSS. Event mean concentrations (EMCs) were log transformed and tested using a *t*-test to measure significant differences between storm and equivalent base-flow periods. Significance was accepted at $\alpha=0.05$.

Results and Discussion

FIB Total Load and EMC

FIB loads during storms exceeded base-flow loads for all creeks. EC loads during storm events were as much as 30 times greater when compared to antecedent base-flow loading over an equivalent time period, whereas ENT loads were as much as 37 times greater than base-flow loads (**Table 4-5**). The smallest difference between base loading and total storm loading for ENT and EC was at Gillets and Cogdels Creek, respectively. The greatest difference between base loading and total storm loading for both EC and ENT was at Freeman Creek. Freeman had the greatest temporal disparity, requiring as many as 110 and 134 base-flow days to achieve similar total loading of EC and ENT, respectively, for one average storm (duration = 1.03 days; **Table 4-5**).

Table 4-5. Loading differences between storm flow and base flow (times greater), and days required during dry weather to equal total *Escherichia coli* (*E. coli*) and *Enterococcus* spp. (ENT) loading during an average storm for each tidal creek (from Stumpf et al., 2010).

Creek	Loading Difference Between Storm Flow and Base Flow		Equivalent Base Flow Days to Equal Average Storm Load	
	EC	ENT	EC	ENT
Cogdels	22	22	121	121
French	25	20	92	73
Gillets	29	14	97	48
Freeman	30	37	110	134

EMCs during storm- and base-flow conditions were examined between creeks and all creeks combined. EMCs are defined as total pollutant mass (M) divided by total flow volume (V), or M/V , and as used as means to compare and correct for different flow volume between creeks and storms (Kayhanian and Stenstrom, 2005). The median storm EMCs were 7.07×10^2 and 1.96×10^2 MPN/100 mL for storm EC and ENT, respectively, and 1.48×10^2 and 4.84×10^1 MPN/100 mL for base flow EC and ENT, respectively, for all creeks combined. Freeman EC EMC and Gillets ENT EMC were the only creeks with no significant differences between storm- and base-flow (**Table 4-6**).

FIB Patterns

Concentrations of FIB were generally strongly correlated with stream flow during both storm- and base-flow conditions. However, Gillets Creek, had no correlation between stream flow and ENT (Figure 4-14), and the creek had unusually high base-flow levels of FIB in relation to other creeks.

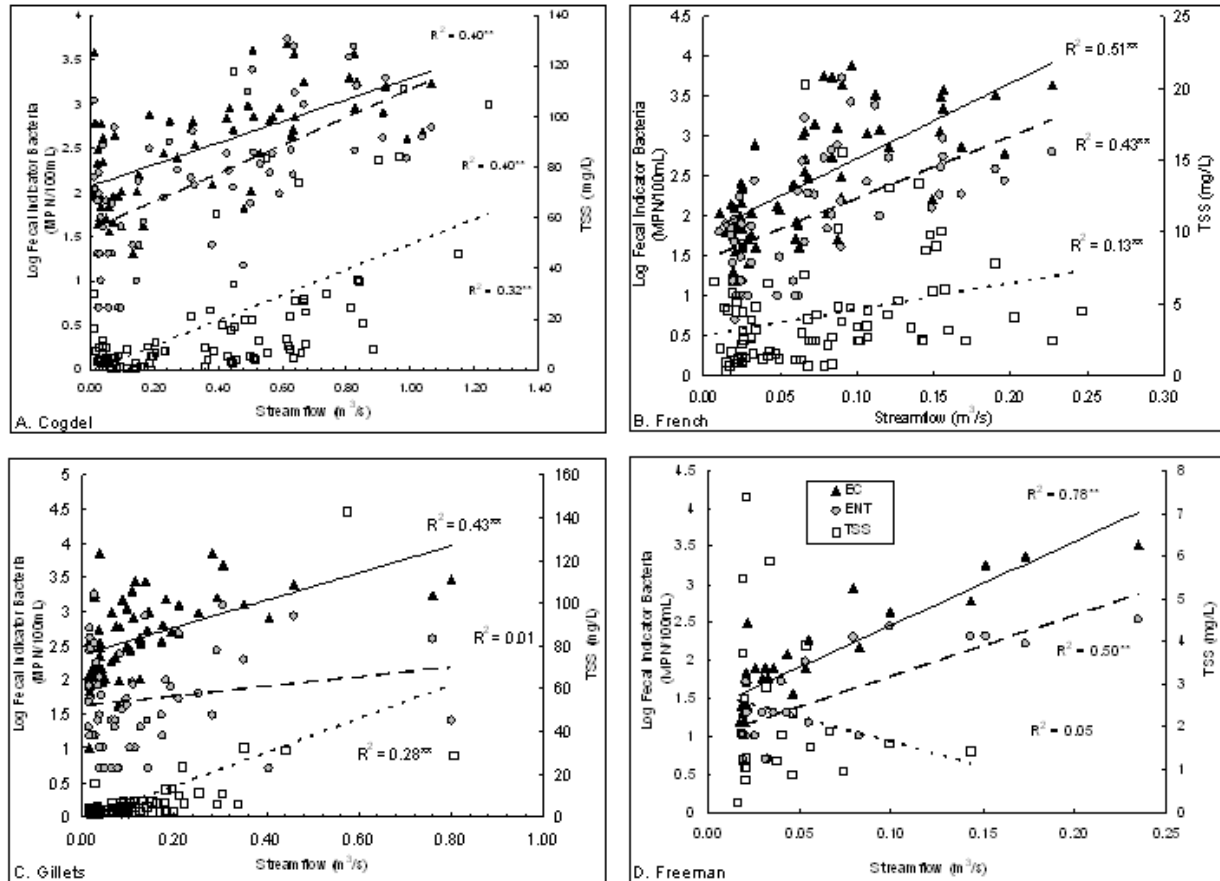


Figure 4-14. Stream flow (m³/s) versus log FIB concentration (MPN/100 mL) and TSS for creeks (A) Cogdels, (B) French, (C) Gillets, and (D) Freeman during all flow conditions.

Significant at $p < 0.01$

When mean creek FIB concentrations from all creeks were examined throughout the four stages of the hydrograph (pre, rising, peak, and falling), bacterial concentrations (EC and ENT) increased during rising and peak stages, and declined with falling hydrograph flow rates (Figure 4-15).

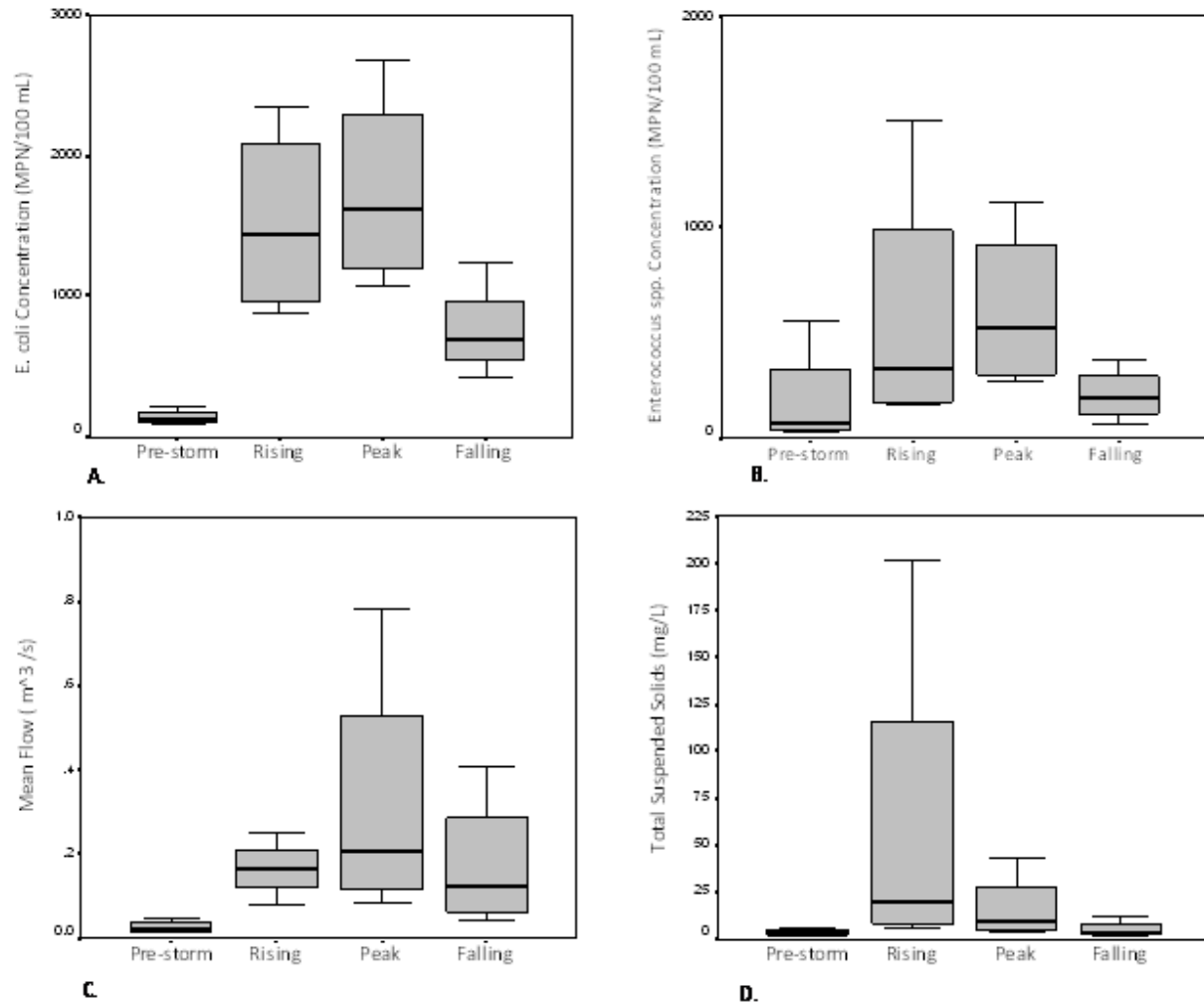


Figure 4-15. Box plots for all four monitored creeks in the NRE system across all storms for (A) *Escherichia coli* (*E. coli*), (B) *Enterococcus* spp., (C) flow, (D) and TSS.

Pollutant mass to discharge volume (M/V) ratios were developed for each creek during each storm event to determine if a “first flush” phenomenon was observed. A first flush is said to exist when the greatest contaminant concentrations, and therefore loads, occur at the onset of a storm (Lee et al., 2002) and decline after the initial contaminant pulse is flushed from the system (Gupta and Saul, 1996). Bertrand-Krajewski et al. (1998) defined a first flush as 80% of total storm pollutant mass occurring in the first 30% of the storm discharge volume. All creeks combined averaged 37 and 44% flushing of EC and ENT loads, respectively, within the first 30% of storm volume. Cogdels, Gillets, and French Creeks had similar average M/V loading ratios, whereas Freeman Creek had the lowest ratio of M/V in the first 30% of discharge volume.

Although the watershed area surrounding MCBCL is generally rural with low density residential and light industrial land use, concentrations and loading rates in these four headwater creeks demonstrate prevalent FIB contamination, and elevated wet weather levels in comparison to base flows. Freeman and Gillets Creek subwatersheds have little to no development and are primarily used for military training exercises, whereas French Creek is used primarily as an artillery impact area. These FIB loads are similar to those reported by Line et al. (2008) in small rural

creeks of eastern North Carolina. However, total loads and EMCs of FIB in our North Carolina tidal creeks were several orders of magnitude lower than those reported in studies of urban watersheds in California (Stein et al., 2007; Surbeck et al., 2006). These results support previous findings of greater concentrations of FIB in developed and more impervious watersheds (Mallin et al., 2000; Schoonover and Lockaby, 2006), but also emphasize the magnitude of these differences between urban versus primarily undeveloped watersheds.

If first flush patterns of FIB delivery to high priority shellfishing waters are observed, with 80% (a mass:volume ratio typically accepted for characterizing stormwater pollutant first flush patterns) of fecal coliforms delivered during the initial 30% of storm runoff volume, then specific types and sizes of BMPs, such as retention basins, may be more appropriate for stormwater treatment. There has been no previous attempt to determine FIB loading characteristics in headwater tidal creeks of North Carolina. Our data do not support a first flush scenario for either EC or ENT concentrations for combined creek loading data.

Pollutographs of EC, ENT, and TSS were developed to determine how contaminant concentrations occurred in comparison to creek discharge (stream flow) over time. Results indicate FIB concentration increase and decrease with similar stream-flow changes. For instance, one representative storm plotted for each creek indicates increases in EC, ENT, and TSS with the rising limb of the hydrograph, higher levels at stream-flow peaks, and a decline with the falling limb (**Figure 4-16**). In addition, variability between sample points emphasizes the need for intensive multi-point sampling throughout storms, to acquire accurate FIB contamination estimates. Current single-grab sample methods for sampling are an insufficient means to accurately characterize FIB during storm events due to this intra-storm variability.

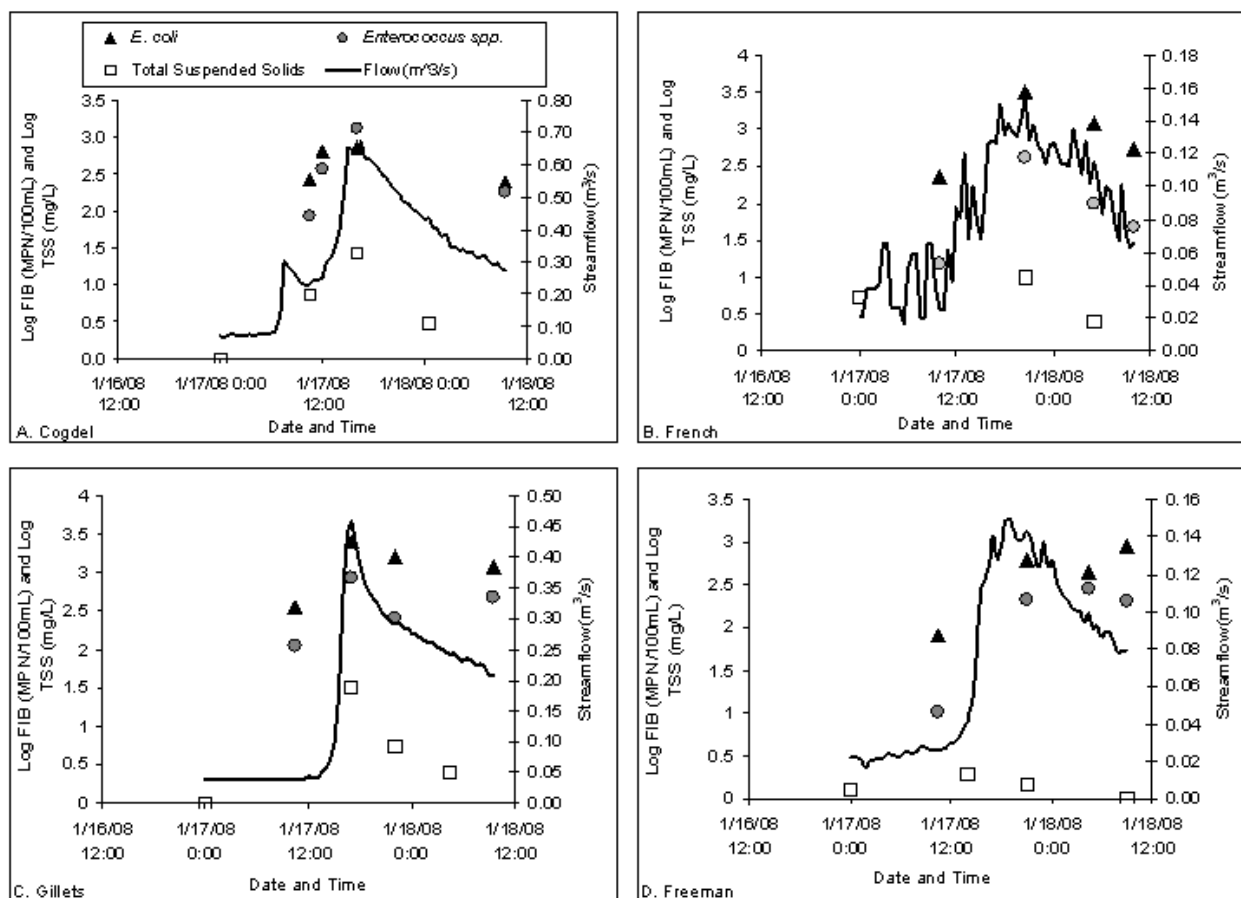


Figure 4-16. Pollutograph representation of intra-storm variation in log concentrations of *E. coli*, *Enterococcus* spp. (MPN/100 mL), and TSS (mg/L) during one representative storm in the four headwater tidal creeks in the NRE system, NC.

Base versus Storm Loading

Load of FIB and EMCs varied among the four sampled creeks; however, total load of FIB and EMCs for all creeks combined during storm events always exceeded base-flow load during equivalent antecedent base-flow periods. Overall, mean storm loads were equivalent to approximately 1.5–4.5 months of base-flow loads. Despite a smaller base-flow loading component, base flows contribute substantial fractions of annual FIB loads and contribute to closures of downstream shellfishing areas, especially in creeks such as Gillets, with high ambient (i.e., non-storm related) FIB concentrations. This would be especially true during years with few rainfall events leading to a greater portion of loading during dry periods. However, in these tidal creeks, and in geographic regions with large scale rainfall events (e.g., tropical storms, nor'easters), storms can contribute concentrations of FIB many orders of magnitude larger than equivalent base-flow periods.

Rainfall Metrics

Variability in total rainfall, rainfall duration, and 7-day antecedent rainfall was high among different storms and creeks. Seven-day antecedent rainfall ranged from 0–5.9 cm, with an

average of 1 cm. Antecedent rainfall was not significantly correlated with FIB load for all creeks combined, or for individual creeks, with the exception of ENT total load at Cogdels (**Table 4-6**). Antecedent rainfall was not significantly correlated with FIB EMC for all creeks combined, or for individual creeks.

Storm load of FIB was most often correlated with the total amount of rainfall, but had a weak relationship to other rainfall metrics. Total rainfall was strongly correlated with both EC and ENT load, and EC and ENT EMCs. Similar FIB concentration increases due to rainfall have been shown in other eastern North Carolina creeks and estuaries (Coulliette and Noble, 2008; Fries et al., 2008; Line et al., 2008; Mallin et al., 2001). However, duration and antecedent rainfall showed varying degrees of correlation with FIB loads with all creek data combined (**Table 4-6**), and little correlation with individual creeks, with the exception of Cogdels (**Table 4-6**). These results demonstrate that rainfall could be a useful predictor, but also highlight the wide range of variability in FIB in relation to rainfall (storm, ambient, and antecedent) rainfall scenarios.

Table 4-6. Spearman rank correlations (R^2) for all creeks combined and individual tidal creeks for loads versus rainfall metrics and *t*-test results for average EMCs for EC and ENT during both storm and equivalent base-flow periods.

Creeks	Loading	Total Rainfall	Rainfall Duration	Antecedent Rainfall			
Creeks	Total Discharge	0.294	0.313	−0.047	Average Storm EMCs		Average Base Flow EMCs
Cogdels	<i>E. coli</i> Total Loading	0.62	−0.134	0.294	<i>E. coli</i>	7.51×10^{2a}	3.58×10^{2a}
French		0.810^a	−0.393	−0.464		1.58×10^{3b}	1.44×10^{2b}
Gillets		0.261	−0.067	−0.506		1.17×10^{3b}	1.92×10^{2b}
Freeman		0.143	0.687	−0.317		5.93×10^2	5.72×10^1
All creeks combined		0.534^b	0.193	−0.145		1.11×10^{3b}	2.03×10^{2b}
Cogdels	<i>Enterococcus</i> spp. Total Loading	0.778^b	0.109	0.657^a	<i>Enterococcus</i> spp.	9.08×10^{2a}	1.24×10^{2a}
French		−0.286	0.071	0.146		5.02×10^{2b}	7.11×10^{1b}
Gillets		0.127	0.128	−0.15		1.18×10^2	8.35×10^1
Freeman		0.429	0.687	−0.049		9.8×10^{1b}	8.25×10^{0b}
All creeks combined		0.537^b	0.393^a	0.118		3.87×10^{2b}	7.91×10^{1b}

^a Significant at $p < 0.5$ (from Stumpf et al., 2010)

^b Significant at $p < 0.01$

EC to ENT Rainfall Relationships

The relationship between EC and ENT changed dramatically depending on rainfall conditions. For all creeks, dry weather resulted in weak EC and ENT correlation, whereas wet weather (rainfall >1.27 cm in 24 hours) resulted in a much stronger correlation (**Figure 4-17**). Wet weather also exhibited a nearly 1:1 ratio of EC to ENT. When streams were examined individually, these relationships were even more strongly correlated. For example, at Cogdels Creek, the EC to ENT correlation was weak during dry weather ($R^2=0.23$, $p<.05$) and strong during wet weather ($R^2=0.80$, $p<.01$).

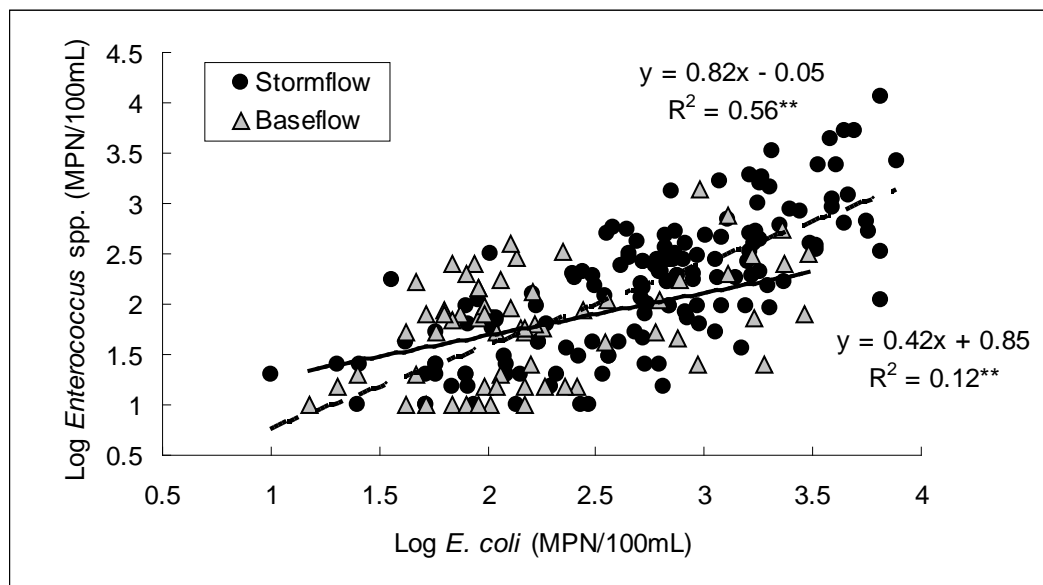


Figure 4-17. Relationship between log concentrations (MPN/100 mL) of *E. coli* and *Enterococcus* spp. during wet weather (rainfall >1.27 cm) storm-flow samples, and dry weather (rainfall = 0 cm) base-flow samples in the NRE system, NC.

Strong coupling of EC and ENT concentrations are observed in fresh fecal material (human and animal), but ENT and EC decay at different rates causing decoupling of the populations over time, especially on terrestrial landscapes (Crane and Moore, 1986; Kibbey et al., 1978). Previous research has examined fecal coliform (*E. coli*) to ENT ratios as a means to assess the likely sources of fecal contamination (Hai and Handao, 1982). Although there are a myriad factors associated with these ratios, the ratio of EC/ENT during storms was consistently close to 1. This could suggest a predominant source of contamination from warm-blooded animals (excluding humans). It is clear that there are strong differences in the stormwater and base flow ENT and EC dynamics in these headwater tidal creeks. It would be useful to use molecular analysis, including source specific targets, and community analysis to further elucidate the meaning of these interesting relationships.

Section 3: Quantifying fecal contaminant sources in North Carolina tidal creeks of the NRE system of North Carolina

Materials and Methods

Study Site and Sample Collection

Tidal creeks were located in the New River watershed, Onslow County, NC, as described in Section 1. Ten total tidal creeks were sampled throughout this study, but for this work, only three creeks (i.e., Freeman, Gillets, and Southwest) and Courthouse Bay were analyzed using quantitative polymerase chain reaction (QPCR) due to the cost and time associated with this analysis (**Figure 4-18**). Tidal creek headwater surface water samples (n=106) were collected from December 2007 to December 2010 using ISCO automated water samplers (Model 6712, ISCO, Lincoln, NE) located on the downstream side of road culverts (i.e., drainage pipes) over a range of sampling conditions (no rain to rainfall events). For details on methodology, see Stumpf et al. (2010).

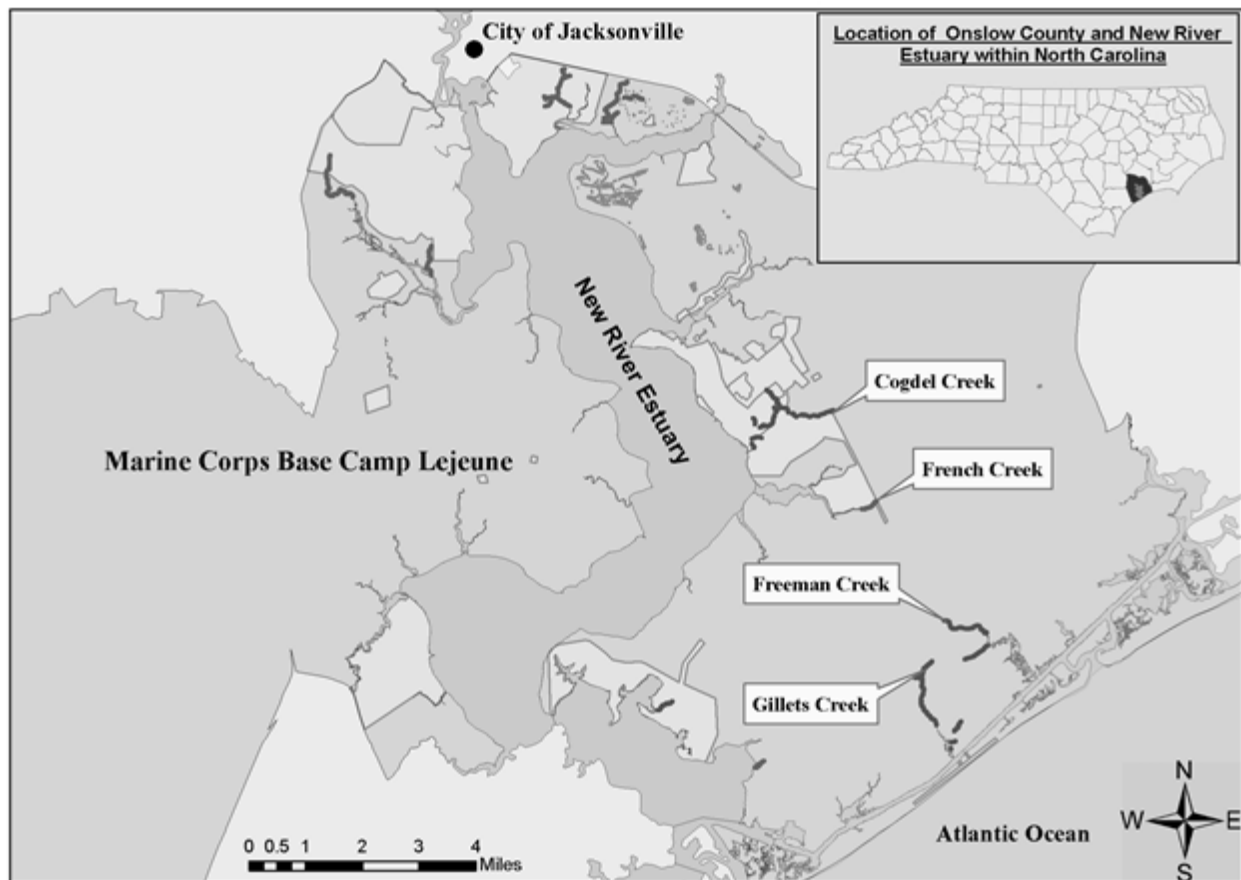


Figure 4-18. MCBCL tidal creeks of study.

Arrows indicate creeks examined for *Bacteroides* spp. using three discrete assays.

Analysis for Chromogenic Substrate Tests

As described in Stumpf et al. (2010), water samples were processed in the laboratory in duplicate using chromogenic substrate tests Colilert-18 and Enterolert (IDEXX Laboratories, Westbrook, ME).

Analysis for Bacteroides spp.

Filtration and DNA Extraction. Duplicate 100-mL volumes were filtered through polycarbonate (PC) filters using sterilized filtration funnels (Pall, East Hills, NY) and the filters were transferred to extraction tubes for processing using aseptic technique.

Samples (n=128) were extracted using a MoBio Power Soil (Carlsbad, CA) DNA extraction kit. MoBio extracted samples were extracted according to manufacturer's instructions with the following exceptions: (1) the sample PC filter was placed into the screw-cap tube and 100 ng of Salmon testes DNA (Sigma, St. Louis, MO) was added per sample as a specimen processing control (SPC); (2) sample was bead beaten for 2 minutes using an 8-place or 45-place bead beater (BioSpec, Bartlesville, OK) instead of vortexing for 10 minutes; and (3) sample was eluted with a final volume of 60 μ L of final elution buffer instead of 100 μ L. Extracted DNA was stored at -20°C until analysis.

Specimen Processing Control. To determine the amount of target DNA loss during extraction and due to environmental matrix inhibition, a known amount of DNA (i.e., SPC) was extracted with each sample. Salmon sperm (*Oncorhynchus keta*) testes DNA was added to the sample before extraction at a final concentration of 100 ng per 500 mL following the techniques of Converse et al. (2009) and based on previous work by Haugland et al. (2005).

Quantitative Polymerase Chain Reaction (QPCR). Calibration standards for the Fecal *Bacteroides* spp. assay were prepared according to the methods of Converse et al. (2009). The SPC (Haugland et al., 2005), Fecal *Bacteroides* spp. (Converse et al., 2009), and BacHum (Kildare et al., 2007) assays were run using TaqMan chemistry primers and probes. Primer and probe sequences can be found in the original studies for each assay. All reactions were performed on a Cepheid Smart-Cycler II (Sunnyvale, CA) with reactions conditions described in **Table 4-7**. Standard curves with either cells or oligonucleotide standards (Table 3.1) with four serial dilutions were completed for each assay. Cycle threshold value was determined automatically by the Cepheid Smart-Cycler II software, after the threshold was manually adjusting to achieve the highest cycling efficiency.

Table 4-7. Reaction conditions and standards for all QPCR assays

General Target	Assay Abbreviation	Study	Reaction Conditions	16S rRNA Fragment Length	Standard
Salmon sperm	SPC	Haugland et al., 2005	95°C for 2 minutes, followed by 45 cycles of 15 seconds at 94°C and 30 seconds at 60°C	Unknown	Cell standard
Fecal <i>Bacteroides</i>	Fecal <i>Bacteroides</i>	Converse et al., 2009	95°C for 2 minutes, followed by 45 cycles of 95°C for 15 seconds and 60°C for 30 seconds	110 Base pair	Cell standard
Human <i>Bacteroides</i>	BacHum	Kildare et al., 2007	50°C for 2 minutes, followed by 95°C for 10 minutes, followed by 40 cycles at 95°C for 15 seconds and 60°C for 1 minute	81 Base pair	Oligonucleotide standard
Sewage <i>Bacteroides</i>	HF183	Bernhard and Field, 2000; Seurinck et al., 2005	50°C for 2 minutes, followed by 95°C for 10 minutes, followed by 40 cycles at 95°C for 30 seconds 53°C for 1 minute and 60°C for 1 minute; follow by a melt curve	82 Base pair	Oligonucleotide standard

A sewage control at four serial 10-fold dilutions was also run with each HF183 assay to confirm the assay's success at determining sewage presence in the sample. A melt curve was run at the conclusion of the HF183 assay, and considered confirmatory for target only when a positive cycle threshold and a melt curve analysis were conducted.

Tidal creek samples were strongly inhibited (the SPC assay run with each set of samples resulted in quantification that was greater than 0.5 log lower than the known concentration of the control), especially during rainfall events. MoBio extraction kits were used to remove inhibitors and further purify DNA. Samples still inhibited after extraction were diluted 1:10 (based on SPC results). No samples required greater than 1:10 dilution after extraction with MoBio Power Soil Extraction Kit. All QPCR assays had high amplification efficiency $\geq 92.7\%$ and linear four-point standard curves ($R^2 \geq 0.993$) were generated for all runs.

Statistics

All statistics were conducted either using SPSS (Chicago, IL) statistical analysis software (version 11.1) or Microsoft Excel software. Data were tested using the Shapiro-Wilk test for normality. Data were not normally distributed and were subsequently analyzed using nonparametric statistical tests. Mean raw data concentrations were log-transformed for graphical purposes. The Spearman rho rank correlation coefficient test was used to determine statistical correlations, the Kruskal-Wallis H test was used to determine significant differences between indicators, and the Mann-Whitney U test was used to determine significant differences between microbial indicators and other watershed fecal indicators in a highly developed watershed (Courthouse Bay). Significance was accepted at $\alpha=0.05$.

Results and Discussion

Conventional FIB concentrations in all tidal creeks were intermittently above single sample regulatory thresholds (104 ENT/100 mL and 320 EC/100 mL), with 39.6% and 49.1% for EC and ENT, respectively, in exceedence (**Figure 4-19**).

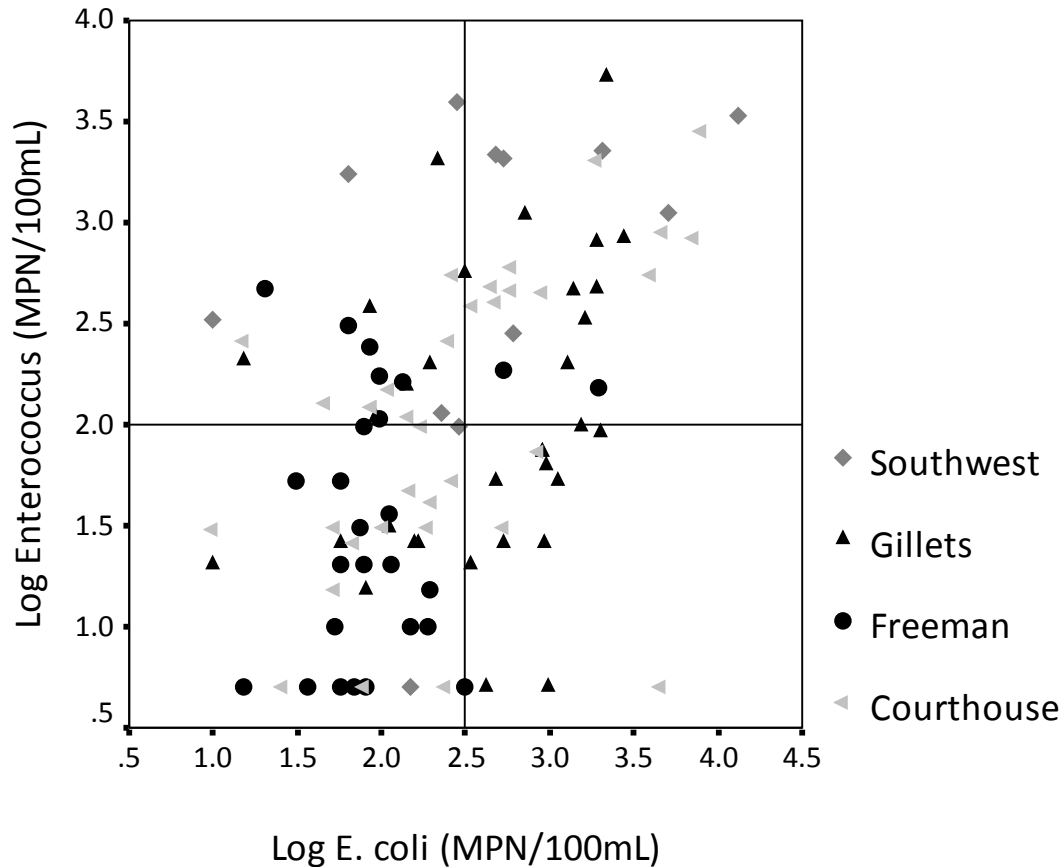


Figure 4-19. Regulatory exceedences for *E. coli* (right half) and *Enterococcus* spp. (top half) for each creek and bay during all sampling events.

E. coli and *Enterococcus* spp. exceedences are based on regulatory standards of 320 and 104 MPN/100 mL, respectively.

Individual creeks varied by percentage of samples that exceeded regulatory standards (**Table 4-8**). Mean EC and ENT levels were highest at Southwest Creek (1.93×10^3 and 1.46×10^3 MPN/100 mL, respectively), whereas the lowest mean concentrations occurred at Freeman Creek (181 and 84.7 MPN/100 mL, respectively). Individual creek correlation between log EC and ENT concentrations varied, with Courthouse Bay ($\rho = 0.364$, $p < .001$) and Gillets Creek ($\rho = 0.149$, $p < .016$) showing significant correlation between indicators, and Southwest ($\rho = 0.176$, $p = 0.175$) and Freeman Creeks ($\rho = 0.0172$, $p = .523$) having no significant correlation.

Table 4-8. Description of tidal creek predominant land cover, fecal indicator detection, and percent exceedence of regulatory standards for conventional indicators.

Tidal Creek Headwater	Predominant Land Cover/ Type	Indicator	Sample #	Log Mean MPN or Cells/100 mL	# Non-Detects	% Exceedence
Courthouse	71.7% Business or Commercial	EC	35	2.43	0	40
		ENT		2.20	0	54
		Fecal <i>Bacteroides</i>		3.33	1	–
		HF183		0.00	35	–
		BacHum		2.97	8	–
Southwest	97.0% Forested	EC	12	2.63	0	92
		ENT		2.95	0	83
		Fecal <i>Bacteroides</i>		2.68	0	–
		HF183		1.81	6	–
		BacHum		3.37	2	–
Gillets	94.5% Forested	EC	33	2.61	0	61
		ENT		2.11	1	50
		Fecal <i>Bacteroides</i>		1.91	2	–
		HF183		0.00	33	–
		BacHum		3.32	5	–
Freeman	96.3% Forested	EC	26	1.97	0	8
		ENT		1.75	0	31
		Fecal <i>Bacteroides</i>		2.16	0	–
		HF183		0.11	25	–
		BacHum		2.83	10	–

– Not applicable because there are no U.S. Environmental Protection Agency regulations for *Bacteroides* spp.

Levels of conventional fecal indicators of water quality in headwater tidal creeks of the NRE are often elevated, especially during wet weather conditions (Stumpf et al., 2010). These levels would, by U.S. Environmental Protection Agency (EPA) regulatory standards, indicate that these waters are unsafe for swimming and shellfish harvesting during certain periods. Based on results from conventional indicators and *Bacteroides* assays, Southwest Creek has convincing evidence of a human source of fecal contamination. Other creeks also have concentrations of indicator bacteria that are representative of human sources of contamination, but results were not consistent between indicators. It is still unclear whether fecal indicators in Courthouse Bay and Gillets and Freeman Creeks are human, animal, or possibly a combination of both.

Bacteroides Assays

Fecal *Bacteroides* spp. Nearly all tidal creek headwater samples tested (95.2%) were positive for the Fecal *Bacteroides* spp. assay with a wide variation in the quantity of target which was dependent on the creek analyzed (**Table 4-9**). Courthouse Bay had the highest mean Fecal *Bacteroides* spp. concentration, whereas Gillets Creek had the lowest mean concentration (**Figure 4-20**, **Table 4-9**).

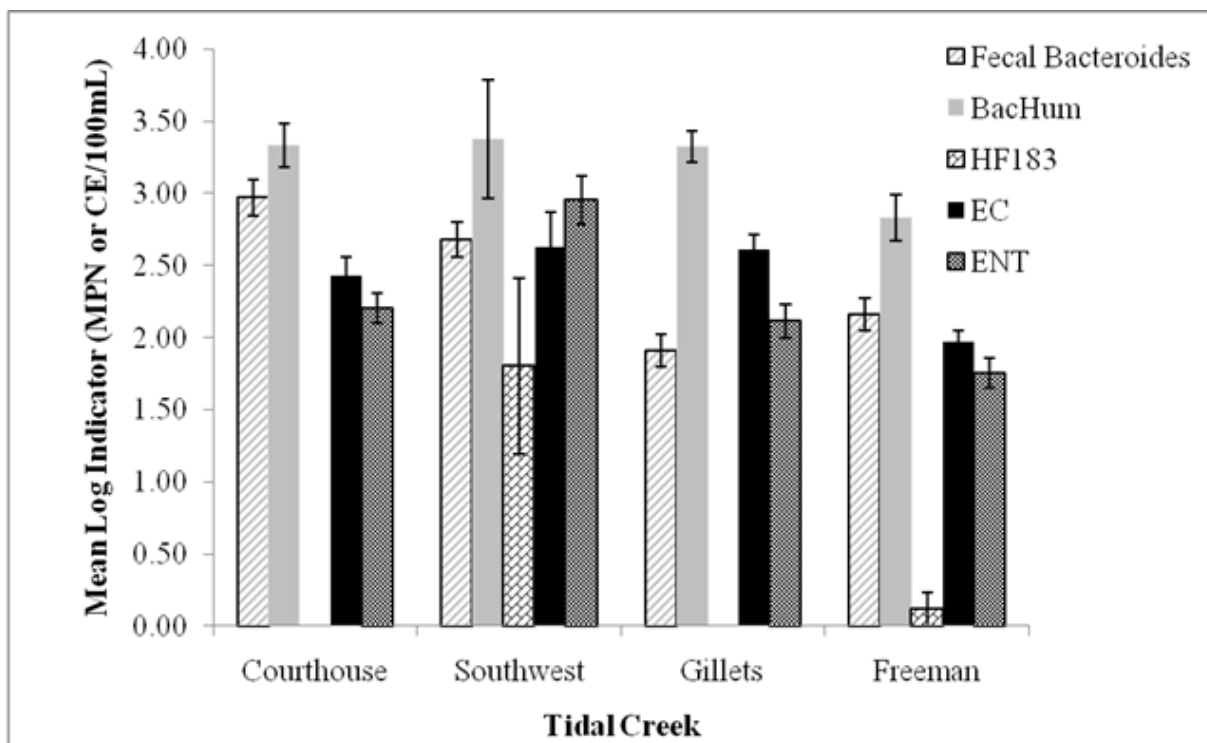


Figure 4-20. Mean log indicator concentration for each creek.

Error bars represent the standard error of the mean.

BacHum. BacHum was less prevalent than Fecal *Bacteroides* spp. and was detected in 81.1% of samples. This is an indicator of human fecal contamination; however, the marker has also been found to cross react with animal fecal contamination such as dog and bird.

HF183. The human-specific HF183 assay rarely had detectable concentrations in headwater creeks. HF183 was found in only 6.60% of samples, with only one sample from Freeman Creek and 6 samples from Southwest Creek positive. However, only twelve samples from Southwest Creek were tested using the HF183 assay, indicating a 50% detection rate (**Figure 4-21**).

Relationship Between Indicators

For all creek data combined there were weak (but statistically significant) positive correlations between Fecal *Bacteroides* spp. and ENT concentrations ($\rho=0.252$, $p<0.009$), between BacHum and EC ($\rho=0.339$, $p<0.001$), and between BacHum and HF183 ($\rho=0.312$, $p<0.001$) (**Table 4-9**).

Table 4-9. Bivariate correlations among log transformed data from all creeks using two-tailed Spearman rho rank correlation.

	Fecal <i>Bacteroides</i>	BacHum	HF183	EC	ENT
Fecal <i>Bacteroides</i>	1.000	0.950	0.159	0.049	0.252 ^a
BacHum	—	1.000	0.312 ^a	0.339 ^a	0.021
HF183	—	—	1.000	0.110	0.120
EC	—	—	—	1.000	0.449 ^a
ENT	—	—	—	—	1.000

^a Indicates $p<0.01$.

Creek Mouth Samples

A small set of samples ($n=23$) collected from each tidal creek mouth during low tide were examined for conventional fecal indicators and the three *Bacteroides* assays. EC and ENT ranged from 5.00 to 1.03×10^3 and 5.00 to 283 MPN/100 mL, respectively, for all creek mouth samples. In all creek samples concentrations were less than 200 MPN/100 mL and less than 63.0 MPN/100 mL for EC and ENT, respectively, with the exception of Gillets EC levels and Southwest ENT levels, which resulted in much larger ranges. For the three *Bacteroides* spp. assays, all samples from Courthouse Bay were negative, Freeman Creek had three samples positive for BacHum, and one sample positive for Fecal *Bacteroides*, whereas Gillets and Southwest Creeks both had more than three samples positive for both Fecal *Bacteroides* spp. and BacHum. The differences observed in the quantification of the BacHum versus the HF183 marker are likely due to cross-reaction of the BacHum assay with canine (Kildare et al., 2007), swine, and horse feces (Ahmed et al., 2009). There is a possibility that many of these detections of BacHum in tidal creeks of MCBCL are the result of fecal contamination from domestic dog populations, or wildlife such as deer, raccoon, beaver, and opossum, which are abundant in these

watersheds (CH2M Hill, 2000). During the few occurrences that the HF183 assay was positive, there was a strong relationship with BacHum.

Conclusions and Implications for Future Research

We found predictable patterns of loading of many materials in coastal streams and were able to relate them to patterns in land cover. We were also able to use regression analyses to model loading of most materials. Thus, we accept our three unifying hypotheses for Research Project AE-2.

Nutrient loads from gaged streams were low compared to the load from the mainstem of the New River; however, many streams drain to ecologically sensitive areas of the estuaries and may still have important effects. In comparing the timing of delivery of loads of suspended solids and nutrients from reference and affected watershed, we found higher proportions of several constituents in storm flow from the affected sites. This finding is important from the management perspective because it supports management of stormwater as a tool to prevent pollution transport from developed watersheds. Regression modeling found linear relationships between metrics of development and loading of nitrogen from tributaries.

Planning for and construction of additional facilities and training areas to fulfill MCBCL's growing military training mission will benefit from information on local land-use impacts on transport of materials from the landscape into the coastal streams and ultimately into the NRE. Tributary creek monitoring data provide information about local and regional water quality resulting from a variety of land-based activities to better inform management actions for compliance with the Clean Water Act. Data that compare sites with and without military training activity and with varying degrees of impervious surfaces determined MCBCL's impacts on creek function and will provide information for decision making about future infrastructure construction sites and training locations. Stream monitoring similar to that conducted during Research Project AE-2 would be valuable for areas slated for significant development. An empirical understanding of the quantity of nutrients and suspended material in coastal streams and some information about their origin are of significant value for making decisions that range from water quality remediation to shoreline stabilization. Suspended materials can impair ecological function through light attenuation and smothering of benthic communities, but they can also enhance the ecological function of coastal wetlands through the provision of organic matter for accretion.

Mitigation of stormwater pollution requires an accurate understanding of the magnitude of pollution in storm flow as compared to base flow. Results of this study showed that the stormwater component of total material load for most materials becomes more important with increased watershed development. Management efforts focusing on site-level stormwater controls could mitigate increased loads associated with this portion of the hydrologic cycle. For example, retention ponds have been shown to decrease the influx of certain materials to streams, and riparian buffers help to dampen peak flows along with associated materials that occur with higher levels of imperviousness. Management efforts to stem large influxes of nutrients and sediments require continued monitoring of affected coastal streams to ensure that implemented techniques are working properly. However, it is theoretically feasible that action taken to reduce

the amount of sediment entering the lotic system would starve downstream wetlands of necessary sediment to offset shoreline erosion and sea level rise.

Overall, the FIB portion of Research Project AE-2 provided approaches for calculating and characterizing FIB loading in headwater tidal creeks, using a multiple indicator approach for robustly determining sources of fecal contamination. This research project also optimized methods for sample processing for downstream application of emerging biosensor technology. Results indicate the need for improved assessment of fecal contamination to inform mitigation strategies for reducing fecal contamination in tidal creeks and marine waters. This research project also identified sites at MCBCL that warrant additional monitoring due to the likelihood of human fecal contamination.

Literature Cited

- Ahmed, W., A. Goonetilleke, D. Powell, and T. Gardner. 2009. Evaluation of multiple sewage-associated *Bacteroides* PCR markers for sewage pollution tracking. *Water Research* 43:4872–4877.
- Ahmed, W., A. Goonetilleke, and T. Gardner. 2008. Alternative indicators for detection and quantification of faecal pollution. *Water*:39–45. February
- APHA (American Public Health Association). 1998. Standard method for the examination of water and wastewater. 20th Edition. Washington, DC.
- Arnold, C.L., and C.J. Gibbons. 1996. Impervious surface coverage: The emergence of a key environmental indicator. *Journal of the American Planning Association* 62(2):243–258.
- Barringer, T.H., R.G. Reiser, and C.V. Price. 1994. Potential effects of development on flow characteristics of two New Jersey streams. *Water Resources Bulletin* 30:283–95.
- Bernhard, A.E., and K.G. Field. 2000. Identification of nonpoint sources of fecal pollution in coastal waters by using host-specific 16S ribosomal DNA genetic markers from fecal anaerobes. *Applied and Environmental Microbiology* 66(4):1587–1594.
- Bertrand-Krajewski, J., G. Chebbo, and A. Saget. 1998. Distribution of pollutant mass vs. volume in stormwater discharges and the first flush phenomenon. *Water Research* 32(8):2341–2356.
- Burnham, K.P., and D.R. Anderson. 2002. *Model Selection and Multimodel Inference: A Practical Information-Theoretic Approach*. 2nd Edition. Springer.
- Byappanahalli, M., M. Fowler, D. Shively, and R. Whitman. 2003. Ubiquity and persistence of *Escherichia coli* in a Midwestern coastal stream. *Applied and Environmental Microbiology* 69(8):4549–4555.
- Cao, Y., J.F. Griffith, and S.B. Weisberg. 2009. Evaluation of optical brightener photodecay for detection of human fecal contamination. *Water Resources* 43(8):2273–2279.
- Carson, C.A., J.M. Christiansen, H. Yampara-Iquise, V.W. Benson, C. Baffaut, J.V. Davis, R.R. Broz, W.B. Kurtz, W.M. Rogers, and W.H. Fales. 2005. Specificity of a *Bacteroides thetaiotaomicron* marker for human feces. *Applied and Environmental Microbiology* 71(8):4945–4949.
- CH2M Hill. 2000. *Freeman Creek Evaluation and Assessment*. C2HM Hill, Inc. Prepared for the U.S. Army Corps of Engineers. Contract number DACA01-96-0028.

- Converse, R.R., A.D. Blackwood, M. Kirs, J.F. Griffith, and R.T. Noble. 2009. Rapid QPCR-based assay for Fecal *Bacteroides* spp. as a tool for assessing fecal contamination in recreational waters. *Water Research* 43(19):4828–4837.
- Coulliette, A.D., and R.T. Noble. 2008. Impacts of rainfall on the water quality of the Newport River Estuary (eastern North Carolina, USA). *Journal of Water and Health* 6(4):473–482.
- Crane, S.R., and J.A. Moore. 1986. Modeling enteric bacterial die-off: A review. *Water, Air, and Soil Pollution* 27:411–439.
- Dick, L.K., and K.G. Field. 2004. Rapid estimation of numbers of fecal *Bacteroidetes* by use of a quantitative PCR assay for 16S rRNA genes. *Applied and Environmental Microbiology* 70(9):5695–5697.
- Dickerson, J.W.J., C. Hagedorn, and A. Hassall. 2007. Detection and remediation of human-origin pollution at two public beaches in Virginia using multiple source tracking methods. *Water Research* 41:3758–3770.
- DiDonato, G.T., J.R. Stewart, D.M. Sanger, B.J. Robinson, B.C. Thompson, A.F. Holland, and R.F. Van Dolah. 2009. Effects of changing land use on the microbial water quality of tidal creeks. *Marine Pollution Bulletin* 58(1):97–106.
- Drasar, B.S. 2003. Microbial flora of the gut. Pp. 99–104 in *Handbook of Water and Wastewater Microbiology*. Edited by D. Mara, and N. Horan. Academic Press: San Diego, CA.
- Ensign, S.H., S.K. McMillan, S.P. Thompson, and M.F. Piehler. 2006. Nitrogen and phosphorus attenuation within the stream network of a coastal, agricultural watershed. *Journal of Environmental Quality* 35(4):1237–1247.
- Fiksdal, L., J.S. Maki, S.J. LaCroix, and J.T. Staley. 1985. Survival and detection of *Bacteroides* spp., prospective indicator bacteria. *Applied and Environmental Microbiology* 49(1):148–150.
- Fries, S.J., G.W. Characklis, and R.T. Noble. 2008. Sediment–water exchange of *Vibrio* sp. and fecal indicator bacteria: Implications for persistence and transport in the Neuse River Estuary, North Carolina, USA. *Water Research* 42(4–5):941–950.
- Gordon, N.D., T.A. McMahon, B.L. Finlayson, C.J. Gippel, and R.J. Nathan. 2004. *Stream Hydrology: An Introduction for Ecologists*. 2nd edition. John Wiley and Sons: Chichester, West Sussex, UK.
- Gupta, K., and A.J. Saul. 1996. Specific relationships for the first flush load in combined sewer flows. *Water Research* 20(5):1244–1252.

- Hai, L., and C. Handao. 1982. Significance of fecal coliform and fecal streptococcus in water pollution monitoring. *Acta Academiae Medicinae Wuhan* 2(4):251–253.
- Harbor, J. 1994. A practical method for estimating the impact of land use change on direct runoff, groundwater recharge, and wetland hydrology. *Journal of American Planning Association* 60(1):91–104.
- Hartel, P.G., J.L. McDonald, L.C. Gentit, S.N.J. Hemmings, K. Rodgers, K. Smith, C.N. Belcher, R.L. Kuntz, Y. Riveria-Torres, and E. Otero. 1997. Improving fluorometry as a source tracking method to detect human fecal contamination. *Estuaries and Coasts* 30(3): 551–561.
- Haugland, R.A., S.C. Sieftring, L.J. Wymer, K.P. Brenner, and A.P. Dufour. 2005. Comparison of *Enterococcus* measurements in freshwater at two recreational beaches by quantitative polymerase chain reaction and membrane filter culture analysis. *Water Research* 39:559–568.
- Homer, C., C. Huang, L. Yang, B. Wylie, and M. Coan. 2004. Development of a 2001 National Landcover Database for the United States. *Photogrammetric Engineering and Remote Sensing* 70(7):829–840.
- Homer, C., J. Dewitz, J. Fry, M. Coan, N. Hossain, C. Larson, N. Herold, A. McKerrow, J.N. VanDriel, and J. Wickham. 2007. Completion of the 2001 National Land Cover Database for the Conterminous United States. *Photogrammetric Engineering and Remote Sensing*, 73(4): 337-341.
- Kayhanian, M., and M.K. Stenstrom. 2005. Mass loading of first flush pollutants with treatment strategy simulations. *Transportation Research Record: Journal of the Transportation Research Board* 1904:133–143.
- Kibbey, H.J., C. Hagedorn, and E.L. McCoy. 1978. Use of fecal streptococci as indicators of pollution in soil. *Applied and Environmental Microbiology* 35(4):711–717.
- Kildare, B.J., C.M. Leutenegger, B.S. McSwain, D.G. Bambic, V.B. Rajal, and S. Wuertz. 2007. 16S rRNA-based assays for quantitative detection of universal, human-, cow-, and dog-specific fecal *Bacteroidales*: A Bayesian approach. *Water Research* 4:3701–3715.
- Kreader, C.A. 1998. Persistence of PCR-detectable *Bacteroides distasonis* from human feces in river water. *Applied and Environmental Microbiology* 64(10):4103–4105.
- Layton, A., L. McKay, D. Williams, V. Garrett, R. Gentry, and G. Sayler. 2006. Development of *Bacteroides* 16S rRNA gene TaqMan-based real-time PCR assays for estimation of total, human, and bovine fecal pollution in water. *Applied and Environmental Microbiology* 72(6):4214–4224.

- Lee, J.H., K.W. Bang, L.H. Ketchum, J.S. Choe, and M.J. Yu. 2002. First flush analysis of urban storm runoff. *Science of the Total Environment* 293(1–3):163–175.
- Leopold, L.B. 1968. *Hydrology for Urban Land Planning—A Guidebook on the Hydrologic Effects of Urban Land Use*. USGS Circular 554. U.S. Department of the Interior, U.S. Geological Survey, Reston, VA.
- Line, D.E., N.M. White, W.W. Kirby-Smith, and J.D. Potts. 2008. Fecal coliform export from four coastal North Carolina Areas. *Journal of American Water Resources Association* 44(3):606–617.
- Mallin, M.A., S.H. Ensign, M.R. McIver, G.C. Shank, and P.K. Fowler. 2001. Demographic, landscape, and meteorological factors controlling the microbial pollution of coastal waters. *Hydrobiologia* 460(1–3):185–193.
- Mallin, M.A., and A.J. Lewitus. 2004. The importance of tidal creek ecosystems. *Journal of Experimental Marine Biology and Ecology* 298(2):145–149.
- Mallin, M.A., M.R. McIver, H.A. Wells, D.C. Parsons, and V.L. Johnson. 2005. Reversal of eutrophication following sewage treatment upgrades in the New River Estuary, NC. *Estuaries* 28(5):750–760.
- Mallin, M.A., K.E. Williams, E.C. Esham, and R.P. Lowe. 2000. Effect of human development on bacteriological water quality in coastal watersheds. *Ecological Applications* 10(4):1047–1056.
- MCBCL (Marine Corps Base Camp Lejeune). 2007. *Integrated Geographic Information Repository*. Data catalog August 2007. Command Geospatial Information System (GIS), Marine Corps Base Camp Lejeune, NC.
- MCBCL (Marine Corps Base Camp Lejeune). 2006. *Integrated Natural Resource Management Plan (INRMP)*. U.S. Marine Corps, Camp Lejeune, NC.
- Meays, C.L., K. Broersma, R. Nordin and A. Mazumder. 2004. Source tracking fecal bacteria in water: a critical review of current methods. *Journal of Environmental Management* 73:71–79.
- Morris, J.T., P.V. Sundareshwar, C.T. Nietch, B. Kjerfve, and D.R. Cahoon. 2002. Responses of coastal wetlands to rising sea level. *Ecology* 83(10):2869–2877.
- Noble, R.T., S.M. Allen, A.D. Blackwood, W. Chu, S.C. Jiang, G.L. Lovelace, M.D. Sobsey, J.R. Stewart, and D.A. Wait. 2003. Use of viral pathogens and indicators to differentiate between human and non-human fecal contamination in a microbial source tracking comparison study. *Journal of Water and Health* 1:195–207.
- Officer, C.B. 1979. Discussion of the behaviour of non-conservative dissolved constituents in estuaries. *Estuarine and Coastal Marine Science* 9:91–94.

- Paul, M.J., and J.L. Meyer, J.L. 2001. Streams in the urban landscape. *Annual Review of Ecology, Evolution, and Systematics* 32:333–365.
- Peeler, K.A., S.P. Opsahl. And J.P. Chanton. 2006. Tracking anthropogenic inputs using caffeine, indicator bacteria, and nutrients in rural freshwater and urban marine systems. *Environmental Science & Technology* 40(24):7616–7622.
- Roser, D.J. and N.J. Ashbolt. 2007. *Source Water Quality Assessment and the Management of Pathogens in Surface Catchments and Aquifers*. Research Report 29. CRC for Water Quality and Treatment, Bolivar.
- Savichtcheva, O., N. Okayama, and S. Okabe. 2007. Relationships between *Bacteroides* 16S rRNA genetic markers and presence of bacterial enteric pathogens and conventional fecal indicators. *Water Research* 41:3615–3628.
- Schoonover, J.E., and B.G. Lockaby. 2006. Land cover impacts on stream nutrients and fecal coliform in the lower piedmont of West Georgia. *Journal of Hydrology* 331(3–4):371–382.
- Scott, T.M., J.B. Rose, T.M. Jenkins, S.R. Farrah, J. Lukasik. 2002. Microbial source tracking: Current methodology and future directions. *Applied and Environmental Microbiology* 68(12):5796–5803.
- Seaburn, G.E. 1969. Effects of Urban Development on Direct Runoff to East Meadow Brook, Nassau County, Long Island, New York. U.S. Geological Survey Professional Paper 627-B. (14 pages).
- Seurinck, S., T. Defoirdt, W. Verstraete, and S.D. Siciliano. 2005. Detection and quantification of the human-specific HF183 *Bacteroides* 16S rRNA genetic marker with real-time PCR for assessment of human faecal pollution in freshwater. *Environmental Microbiology* 7(2):249–259.
- SSURGO. 2009. Soil Survey Geographic (SSURGO) database for Onslow County, North Carolina. U.S. Department of Agriculture, Natural Resources Conservation Service, Fort Worth, TX. Available at <http://soildatamart.nrcs.usda.gov>.
- Stein, E.D., L.L. Tiefenthaler, and K.C. Schiff. 2007. *Sources, Patterns and Mechanisms of Storm Water Pollutant Loading from Watersheds and Land Uses of the Greater Los Angeles Area, California, USA*. Southern California Coastal Water Research Project. Technical Report 510.
- Stumpf, C.H., M.F. Piehler, S. Thompson, and R.T. Noble. 2010. Loading of fecal indicator bacteria in North Carolina tidal creek headwaters: Hydrographic patterns and terrestrial runoff relationships. *Water Research* 44(16):4704–4715.

- Surbeck, C.Q., S.C. Jiang, J.H. Ahn, and S.B. Grant. 2006. Flow fingerprinting fecal pollution and suspended solids in stormwater runoff from an urban coastal watershed. *Environmental Science and Technology* 40(14):4435–4441.
- TIGER. 2000. TIGER line census of population and housing. Topologically Integrated Geographic Encoding and Referencing system. U.S. Census Bureau, Washington, DC. Available at <http://www.census.gov/geo/www/tiger/index.html>.
- USDA (U.S. Department of Agriculture). 2010. *National Resource Conservation Service, Web Soil Survey*. U.S. Department of Agriculture, Natural Resources Conservation Service. Available at <http://websoilsurvey.nrcs.usda.gov/app/WebSoilSurvey.aspx>.
- Wade, T.J., R.L. Calderon, K.P. Brenner, E. Sams, M. Beach, R. Haugland, L. Wymer, and A.P. Dufour. 2008. High sensitivity of children to swimming-associated gastrointestinal illness: Results using a rapid assay of recreational water quality. *Epidemiology* 19(3):375–383.
- Wade, T.J., R.L. Calderon, E. Sams, M. Beach, K.P. Brenner, A.H. Williams, and A.P. Dufour. 2006. Rapidly measured indicators of recreational water quality are predictive of swimming-associated gastrointestinal illness. *Environmental Health Perspectives* 114(1):24–28.
- Ward, R.C. and M. Robinson. 2000. *Principles of Hydrology*. 4th edition Maidenhead: McGraw-Hill.

[This page intentionally left blank.]

Appendix 4-A

Stable Isotopic Characterization of Particulate Organic Matter in the New River Estuary

Stable Isotopic Characterization of Particulate Organic Matter in the NRE

Materials and Methods

Water column particulate nitrogen and carbon concentrations and stable isotopic composition were measured starting in 2009 through 2012. Surface and bottom waters were sampled monthly for POM at the eight mainstem NRE water column monitoring stations identified in Research Project AE-1. In addition, synoptic POM samples from the tributary creeks discharging into the NRE were collected in 2009. All the POM samples (tributaries and mainstem) were collected by pumping 100–500 mL of water through precombusted GFFs. The POM trapped on the filters was freeze-dried and analyzed for $\delta^{15}\text{N}$, $\delta^{13}\text{C}$, and nitrogen and carbon content using a continuous flow isotope ratio mass spectrometer interfaced with an elemental analyzer at the University of Connecticut. The precision of all isotope values reported is better than 0.2‰.

Results and Discussion

The spatial distribution of $\delta^{15}\text{N}$ -POM in the NRE was highly dependent on the season and/or river discharge. The $\delta^{15}\text{N}$ appears to be diagnostic of two modes of operation for the NRE. First when river discharge is higher (e.g., February 2011) and the estuary freshens, the $\delta^{15}\text{N}$ increases to values in excess of 10 per mil (**Figure 4-A-1**). High $\delta^{15}\text{N}$ values in this range (e.g., greater than 7 per mil) carry an inference of either anthropogenic (wastewater) sources of nitrogen or could reflect in-estuary utilization of isotopically heavy DIN delivered to the NRE, which was enriched via denitrification upstream of Jacksonville. Observed drops in the NO_3^- load downstream of Gum Branch, but upstream of Jacksonville support this scenario, but the high $\delta^{15}\text{N}$'s in NRE POM were also coincident with elevated carbon:nitrogen ratios. A more likely explanation is that the river discharge is delivering isotopically heavy watershed derived POM during these periods at magnitudes sufficient to dominate the POM nitrogen pool. This POM appears uniformly distributed through the water column of the NRE. In contrast, when the estuary is seawater dominated in the summer, and the biology is driven by internal recycling, the $\delta^{15}\text{N}$ tended to be depleted; in the range of 4–6 per mil. These summertime values also reflect a difference between surface water and bottom water isotope signatures. This decoupling, with heavier values in the bottom water provides some indication of the relative importance of upper water column versus near-bottom DIN cycling on refueling the POM pool. The lower $\delta^{15}\text{N}$ values are accompanied by lower carbon:nitrogen ratios reflecting in situ production rather than import from the watershed.

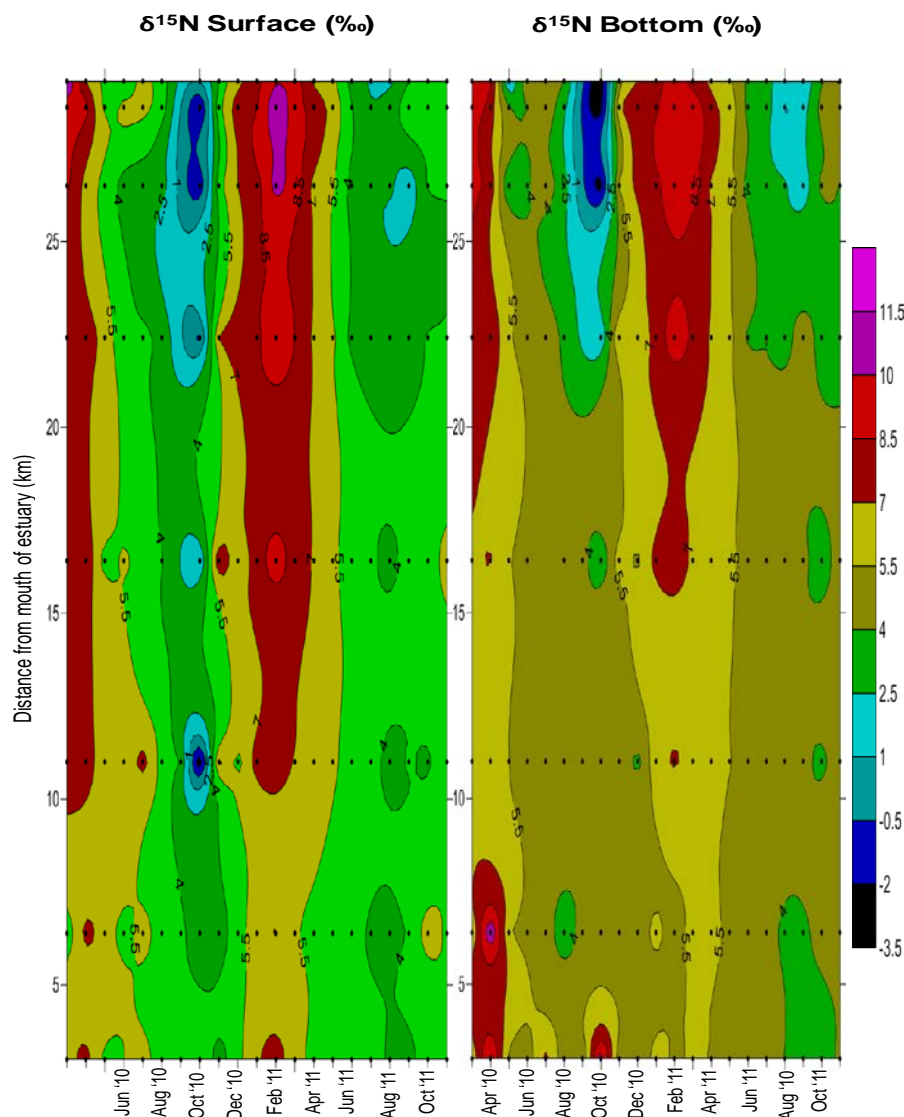


Figure 4-A-1. Spatial and temporal distribution of stable nitrogen isotope signatures in POM in the surface and bottom waters of the NRE. Individual points denote sampling locations and times.

The $\delta^{13}\text{C}$ distribution (**Figure 4-A-2**) showed less sensitivity to seasonal effects than the $\delta^{15}\text{N}$. With the exception of some anomalously low $\delta^{13}\text{C}$ values measured in the surface water in December 2010, the NRE presents the expected isotopic enrichment of $\delta^{13}\text{C}$ from the head to the mouth of the estuary. For the late summer/early fall periods for both 2010 and 2011, the lower portion of the estuary contained POM with $\delta^{13}\text{C}$ values more enriched than -19 per mil. These isotope signatures are typically heavier than phytoplankton or terrestrially derived POM, and are more consistent with resuspended benthic microalgae and/or *Spartina* marsh-derived carbon. These sampling periods coincided with prolonged flooding events in the marshes bordering the downstream stations suggesting a marsh source. But the heavier isotope signatures were also more prevalent in bottom water which would be indicative of benthic microalgal resuspension. This question cannot be resolved currently and requires compound specific analyses to

distinguish these sources. Nevertheless the bulk POM $\delta^{13}\text{C}$ values clearly identify contributions beyond the NRE channel water to the POM dynamics in the lower NRE.

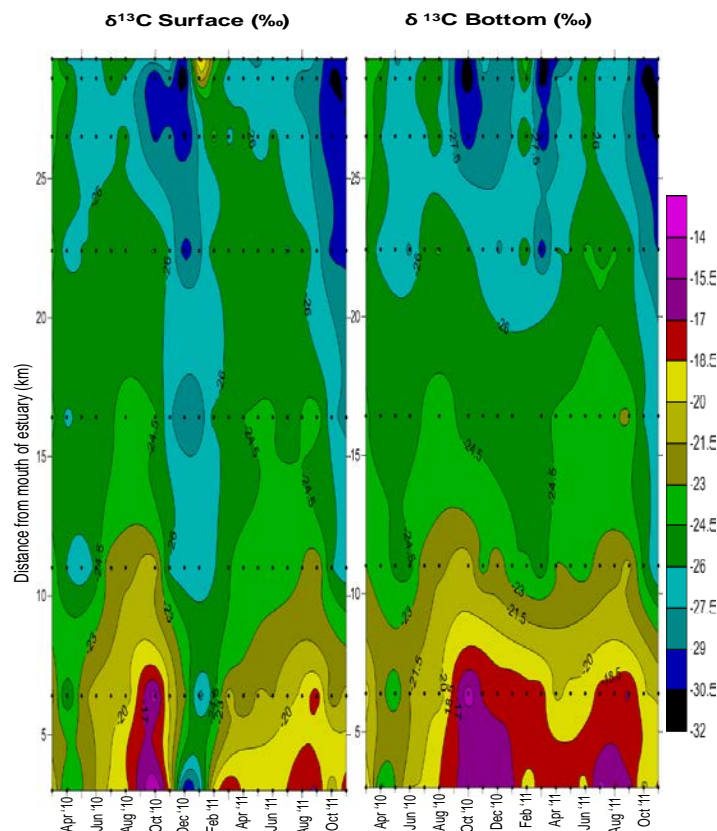


Figure 4-A-2. Spatial and temporal distribution of stable carbon isotope signatures in POM in the surface and bottom waters of the NRE.

Mixing curves for POM carbon and nitrogen (using Stations 7 and 1 as end members) all show that the NRE is a sink for POM (**Figures 4-A-3 and 4-A-4**). Extrapolation of the mixing curves (Officer, 1979) for nitrogen and carbon indicate the magnitude of the estuarine POM sink ranging from 5–75% of the upstream load. Although it is not surprising that the NRE is a particle sink, the magnitudes estimated are highly sensitive to the assignment of the downstream end member POM concentration. An alternative interpretation of the mixing plots is that there may be a reinjection of POM from either marshes or resuspension from the benthic microalgae in the lower NRE (**Figures 4-A-2 and 4-A-4**), which causes downstream end member to be more POM-rich than would be expected. Consequently the mixing curve for the whole NRE would appear to fall below conservative mixing; hence the apparent sink. This issue is being resolved through the analyses of “true” offshore end members to more robustly anchor the downstream portion of the mixing curve. These analyses will either confirm that the POM sink in NRE is as large as currently estimated, or will decrease the magnitude of the that sink but clearly identify a POM source in the lower NRE.

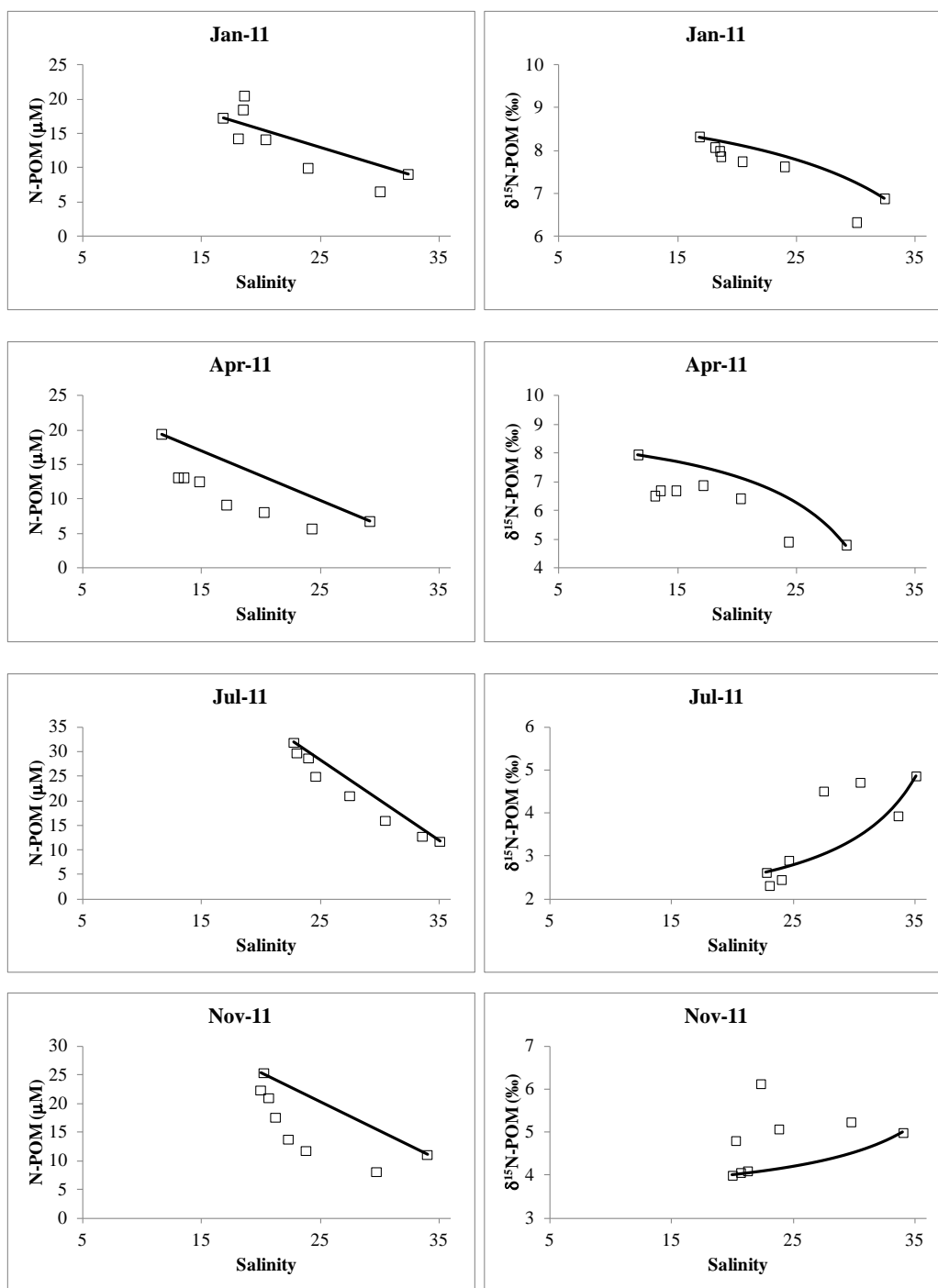


Figure 4-A-3. Seasonal mixing curves of POM–nitrogen and $\delta^{15}\text{N}$ –POM. Solid lines denote predicted values based on conservative mixing of upstream water at Station 7 and saline water from the most downstream station (Station 1). Symbols are measured values.

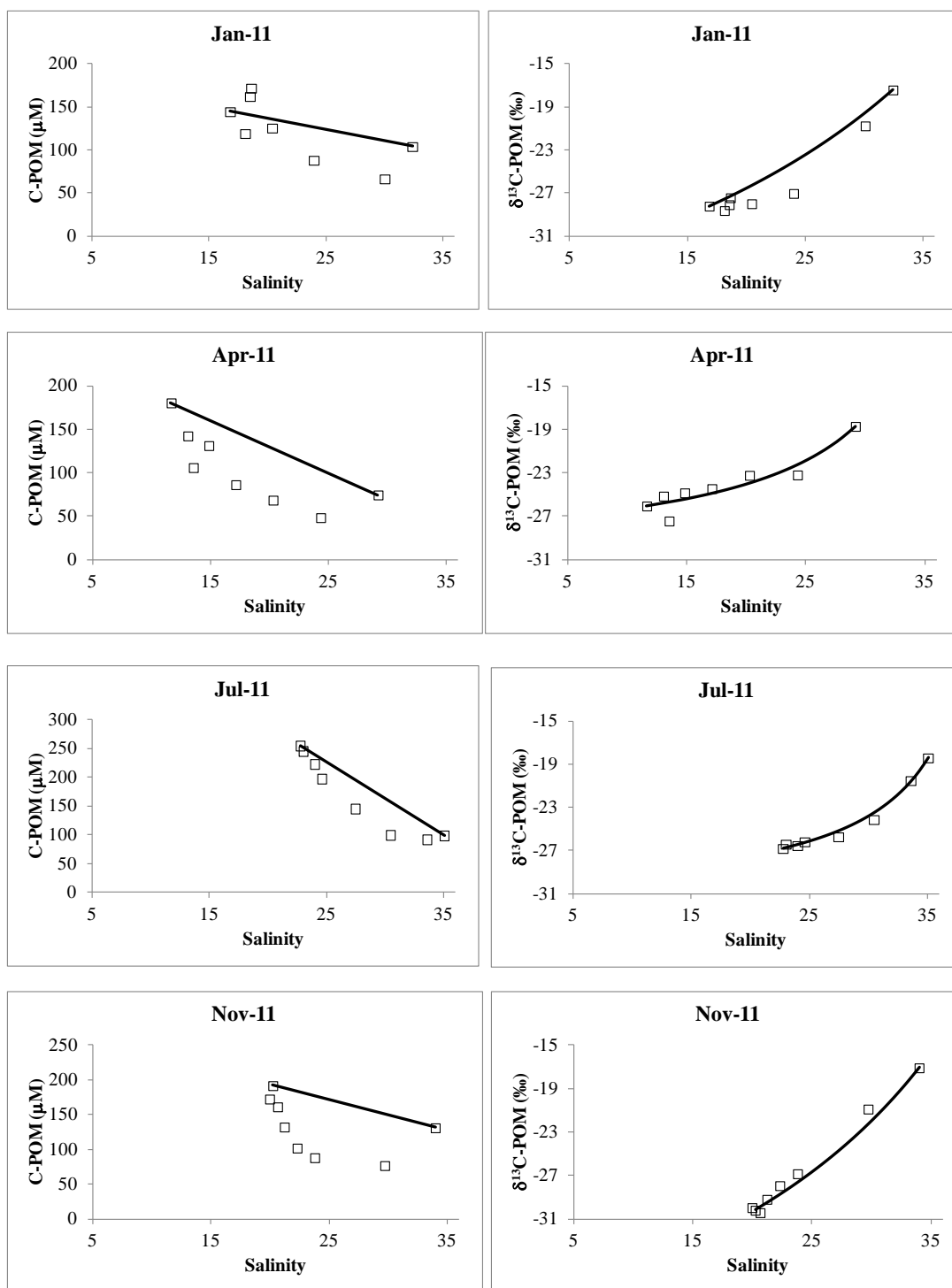


Figure 4-A-4. Seasonal mixing curves of POM-carbon and $\delta^{13}\text{C}$ -POM. Solid lines denote predicted values based on conservative mixing of upstream water at Station 7 and saline water from the most downstream station (Station 1). Symbols are measured values.

Despite the indication of POM carbon and nitrogen loss, the isotope mixing curves for $\delta^{13}\text{C}$ -POM rarely deviated from conservative mixing. Settling/burial on some timescale is consistent

with these two pieces of evidence. Small carbon fractionations during mineralization against a large carbon background may not be detectable in the $\delta^{13}\text{C}$ -POM. However, the $\delta^{15}\text{N}$ -POM periodically diverged from conservative mixing. The most pronounced deviations reflected an enrichment of the $\delta^{15}\text{N}$ -POM. The larger isotope effect of nitrogen mineralization is consistent with the observed enrichment of $\delta^{15}\text{N}$ above conservative mixing during some periods, particularly in the summer and early fall when mineralization rates are high. Collectively the mixing curves for carbon, nitrogen, and $\delta^{13}\text{C}$ and $\delta^{15}\text{N}$ indicate a general estuarine sink for POM that is subject to an unknown degree of mineralization (likely greater for nitrogen) prior to deposition. The relative magnitude of mineralization versus deposition as the agent of the non-conservative POM loss is a necessary metric required for assessing long-term estuarine storage of nitrogen and carbon.

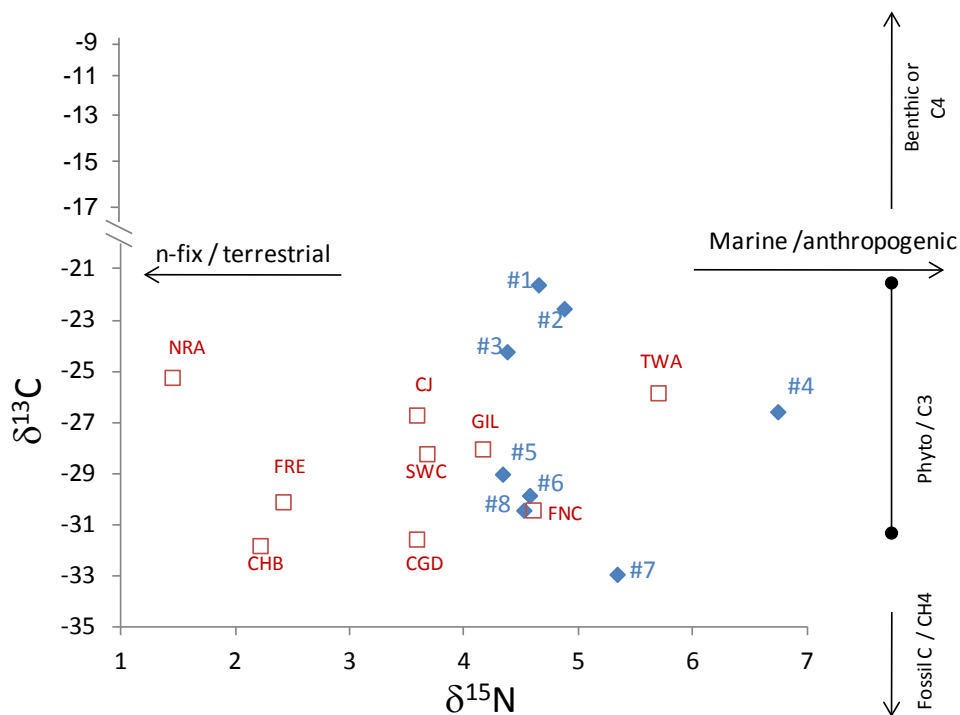


Figure 4-A-5. Isotope space coordinates for POM discharging from tributary creeks (red) and sampled from the NRE (blue).

Note: Diamond symbols represent NRE water column monitoring stations; open square symbols correspond to tributary creek IDs: CHB = Courthouse Bay; CGD = Cogdels Creek; CJ = Camp Johnson; FNC = French Creek; FRE = Freeman Creek; GIL = Gillets Creek; NRA = New River Air Station; SWC = Southwest Creek; and TWA = Tarawa Terrace.

The isotope values of tributary creek POM provide some diagnostic value for identifying potential influence tributary inputs on the NRE (**Figures 4-A-5 and 4-A-6**). The $\delta^{13}\text{C}$ values trended isotopically light and were similar to the $\delta^{13}\text{C}$ values measured in the upper NRE. Because of this overlap, this measurement could not be diagnostic of inputs for tributary creeks that discharged in the upper NRE, but would be useful for creeks that discharged to the lower NRE where higher $\delta^{13}\text{C}$ values were measured. For $\delta^{15}\text{N}$, the creeks tended to be isotopically lighter than $\delta^{15}\text{N}$ measured in anywhere in the NRE, most of the time. The notable exceptions

were Tarawa Terrace (TWA) and French Creek (FHC), two sites whose watersheds are more heavily modified with respect to land-use change than other tributary creeks.

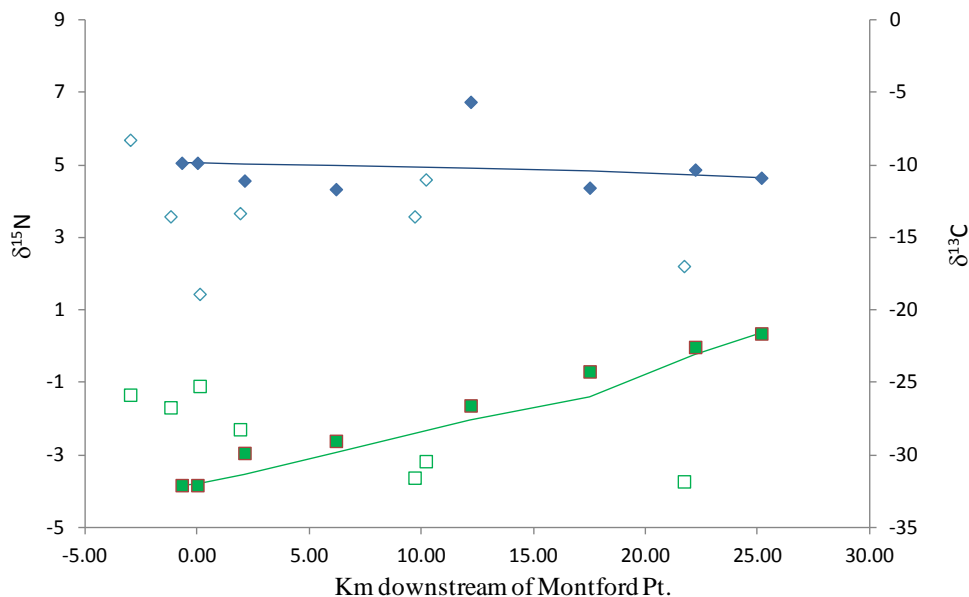


Figure 4-A-6. Observed isotope values for the NRE, creeks, and conservative mixing as a function of downstream estuarine distance.

Blue diamonds = $\delta^{15}\text{N}$, green squares = $\delta^{13}\text{C}$. Open symbols are the creeks placed along the estuarine distance where they discharge. Solid symbols are the NRE monitoring stations. The solid symbols and lines are the conservative mixing lines. Both $\delta^{15}\text{N}$ and $\delta^{13}\text{C}$ are expressed as per mil.

When the isotopic signatures of the creeks and NRE are compared in space (**Figure 4-A-6**), and in the context of conservative isotope mixing in the NRE, some generalizations can be made. The $\delta^{13}\text{C}$ provides no evidence of tributary creek influence on NRE POM composition. The light $\delta^{15}\text{N}$ values measured in the creeks show some spatial correspondence to a lightening of $\delta^{15}\text{N}$ in the upper estuary, but an opposite trend in the lower estuary. Either two independent processes are controlling the $\delta^{15}\text{N}$ and the $\delta^{13}\text{C}$ in the POM pool (lateral inputs for nitrogen and in-estuary processes for carbon, which is unlikely) or both the depletion of $\delta^{15}\text{N}$ and the enrichment of $\delta^{13}\text{C}$ in the NRE results from in-estuarine processes. The $\delta^{13}\text{C}$ values are so close to conservative mixing that again the mechanism might be a nitrogen fractionating process (e.g., mineralization) that has little effect on the large carbon pool.

Conclusions

The $\delta^{15}\text{N}$ can be an indicator of new nitrogen versus recycled nitrogen modes in the NRE. The NRE is a sink for POM and the magnitude of that sink is modified by mineralization in the water column. There is an additional low $\delta^{13}\text{C}$ source of POM in the lower NRE that is likely either from the marsh or resuspended benthic microalgae. There is no isotopic evidence that suggests influence of tributary creeks on NRE POM composition.

Appendix 4-B

List of Scientific Publications

List of Scientific Publications

Papers

Published

Stumpf, C.H., R.T. Noble, M.F. Piehler, and S. Thompson. 2010. Loading of fecal indicator bacteria in tidal creek headwaters: Hydrographic, meteorological, and terrestrial runoff relationships. *Water Research* 44(16):4704–4715.

In Preparation

Piehler, M.F., I.C. Anderson, M.J. Brush, and C.A. Currin. In preparation. Denitrification enhances ecosystem stability through the estuarine gradient. To be submitted to *Estuaries and Coasts*.

Piehler, M.F., N. Poletto, L. Leonard, C.R. Tobias, and C.A. Currin. In preparation. Linking loading of suspended materials to marsh elevation. To be submitted to *Wetlands*.

Schwartz, R., M.F. Piehler, S.P. Thompson, M.J. Brush, and J.C. Poletto. In preparation. Land use affects coastal stream nutrient and total suspended solids loading. To be submitted to *Estuaries and Coasts*.

Stumpf, C.H., M.F. Piehler, S. Thompson, and R.T. Noble. In preparation. Quantifying fecal contaminant sources in North Carolina tidal creeks utilizing a multi-tiered approach. To be submitted to *Journal of Water Research*.

Von Korff, B., and M.F. Piehler. In preparation. Spatial variability of denitrification in tidal freshwater rivers. To be submitted to *Wetlands*.

Walsh, K.E., and M.F. Piehler. In preparation. Differential thermal loading from coastal streams affects estuarine metabolism. To be submitted to *Science of the Total Environment*.

Theses

Ph.D. Dissertation

Stumpf, C.H. 2011. *New Approaches and Technologies for Quantifying Fecal Contamination in Tidal Creek and Coastal Receiving Waters*. Doctoral Dissertation, University of North Carolina at Chapel Hill, Chapel Hill, NC.

Master's Theses

Von Korff, B. 2011. *Spatial Variability of Denitrification in Tidal Freshwater Rivers*. Master of Science in Marine Sciences, University of North Carolina at Chapel Hill, Chapel Hill, NC.

Schwartz, R. 2010. *Land Use Affects the Timing and Magnitude of Material Delivery to Headwater Streams in Coastal North Carolina*. Master of Science in the Curriculum for the Environment and Ecology, University of North Carolina at Chapel Hill, Chapel Hill, NC.

[This page intentionally left blank.]

Appendix 4-C

List of Students

- Curt Stumpf, Ph.D. University of North Carolina at Chapel Hill, Chapel Hill, NC, 2010.
- Rebecca Schwartz, M.S., University of North Carolina at Chapel Hill, Chapel Hill, NC, 2010.
- Ben Von Korff, M.S., University of North Carolina at Chapel Hill, Chapel Hill, NC, 2011.

[This page intentionally left blank.]

Chapter 5

Developing Indicators of Ecosystem Function for Shallow Estuaries: Benthic Functional Responses in the New River Estuary

SERDP Project Number: RC-1413

Aquatic Estuarine Module

Research Project AE-3

Lead Researcher:

Dr. Iris C. Anderson
Virginia Institute of Marine Science
P.O. Box 1346
Route 1208, Greate Road
Gloucester Point, VA 23062

Supporting Researchers:

Dr. Mark J. Brush (VIMS)
Dr. Michael Piehler (UNC-IMS)
Dr. Carolyn Currin (NOAA)

May 10, 2013

Final

This report was prepared under contract to the U.S. Department of Defense (DoD) Strategic Environmental Research and Development Program (SERDP). The publication of this report does not indicate endorsement by DoD, nor should the contents be construed as reflecting the official policy or position of DoD. References herein to any specific commercial product, process, or service by trade name, trademark, manufacturer, or otherwise, do not necessarily constitute or imply its endorsement, recommendation, or favoring by DoD.

Table of Contents

Acronyms	5-ix
Abstract	5-1
Objectives of Research Project	5-2
Technical Goal	5-2
Hypotheses	5-2
Background	5-3
Materials and Methods	5-7
Allochthonous N Loading Estimates	5-7
Sediment and Water Quality Characterizations in the Shallow Photic Zone	5-8
Role of Environmental Variables in Regulating Sediment and Water Quality	5-11
Determinations of Shallow Water Benthic and Pelagic Metabolic and Nutrient- Cycling Rates	5-16
Scaling Up to the Estuary—Determination of Benthic Metabolism, Nutrient Fluxes, and Nitrogen-Cycling Rates at Different Water Depths	5-22
Data Analysis	5-25
Results and Discussion	5-26
Nitrogen Sources to the NRE	5-26
Estuarine Gradients in Sediment and Water Quality	5-28
Effects of Environmental Variables on Water Quality, Light Availability, and Distribution of Benthic Chl <i>a</i>	5-36
Shallow Water Metabolism and Nutrient Flux Studies	5-45
Role of Benthic Processes in Regulating Sediment–Water Nutrient Fluxes in Shallow Water	5-54
Scaling up to the NRE	5-63
Conclusions and Implications for Future Research	5-72
Summary of Key Findings	5-72
Importance of Benthos in the NRE	5-73
Vulnerability of the Benthic Filter to Natural and Anthropogenic Changes and Potential Responses to Climate Change	5-73
Needs for Future Research on Benthic Processes	5-74
Recommended Management Actions to Optimize Water Quality in the NRE	5-74
Literature Cited	5-76
Appendix 5-A: Supporting Data	5-A-1
Appendix 5-B: List of Scientific/Technical Publications	5-B-1
Appendix 5-C: List of Students	5-C-1

List of Figures

5-1. Conceptual model showing the impacts of freshwater discharge on estuarine processes.	5-6
5-2. The NRE is divided into boxes, utilized for the NRE ESM.	5-7
5-3. Map of the NRE, MCBCL, and shallow water research stations (0.5 m water depth).	5-9
5-4. Dataflow surface water mapping cruise track in the NRE.	5-11
5-5. Empirical relationships between the rate of vertical light attenuation (K_d [PAR]) and extracted chl <i>a</i> , turbidity (NTU), and CDOM.	5-12
5-6. Regression of observed K_d (PAR) against values computed using the multiple linear regression in Equation 5-1.	5-13
5-7. Side view of the in situ mesocosm experiment set up.	5-17
5-8. (Left) Small sediment core used for mineralization with magnetic spinner inside core. (Right) Small sediment cores placed around large magnetic spinner in temperature-controlled incubator.	5-20
5-9. NRE bathymetry (meters below MSL; North American Vertical Datum of 1988 [NAV88]) and depth experiment sampling stations in the upper, middle, and lower regions of the estuary.	5-24
5-10. Percent contribution of allocthonous N sources to the NRE on an annual basis.	5-27
5-11. Percent contribution of allocthonous and autocthonous N sources to the NRE for summer and spring.	5-27
5-12. Benthic chl <i>a</i> (0–3 mm depth horizon), sediment OM content, sediment extractable NH_4^+ , and sediment bulk density (0–5 cm depth horizon) (mean \pm standard error) measured at six stations (0.5 m water depth) from July 2007 to December 2011.	5-29
5-13. Sediment C:N ratio (0–5 cm depth horizon) from 2007 to December 2011, porewater sulfide from 2011, and percent sediment grain size type from July 2008 (mean \pm standard error) measured at six stations (0.5 m water depth).	5-30
5-14. Benthic pigment Fuco:chl ratio and Zea:chl ratios (0–3 mm depth horizon) (mean \pm standard error) measured at six stations (0.5 m water depth) from October 2008 to July 2009.	5-30
5-15. Percentage pennate diatoms of total diatoms (pennate and centric) (0–3 mm depth horizon) (mean \pm standard error) measured at six stations (0.5 m water depth) in May and July 2009.	5-31
5-16. Light attenuation, extracted chl <i>a</i> , CDOM absorption, and YSI turbidity (mean \pm standard error) measured at six stations from July 2007 to December 2011.	5-32
5-17. Surface water DIN, DON, DIP, and DOC (mean \pm standard error) measured at six stations from July 2007 to December 2011.	5-32
5-18. Mean (\pm standard error) water column nutrient concentration ratio of DON to TDN, measured at six stations from July 2007 to December 2011.	5-33

5-19. Mean daily freshwater flow at the USGS Gum Branch Station number 02093000.	5-36
5-20. Interpolated maps of surface water quality determined from nearshore Dataflow systems surveys in 2008 and 2009.....	5-38
5-21. Interpolated maps of surface water quality determined from nearshore Dataflow systems surveys in 2010.....	5-39
5-22. Interpolated maps of surface water quality determined from nearshore Dataflow systems surveys in 2011.....	5-40
5-23. Regression of percentage of the NRE area with $\geq 1\%$ surface irradiance (I_0) reaching the bottom versus daily mean freshwater flow at the USGS Gum Branch Station.	5-41
5-24. Regression of mean (\pm standard error) spring (April–June) benthic chl <i>a</i> (0–3 mm depth horizon; 0.5–m water depth) at three upper NRE stations versus mean winter seasonal discharge (January–March) at the USGS Gum Branch Station from 2008–2011.....	5-42
5-25. Linkage between mean (\pm standard error) benthic chl <i>a</i> (0–3 mm depth horizon) and depth grouped by upper, middle, and lower regions of the NRE.	5-42
5-26. Depth gradient of benthic chl <i>a</i> (0–3 mm depth horizon) and RWE from stations located in upper, middle, and lower regions of the NRE.....	5-44
5-27. Mean (\pm standard error) benthic GPP, R, and NCP measured at six stations (0.5 m water depth) from July 2008 to July 2009 and three stations (i.e., SWCR, WALL, and CTBY) in March 2010.	5-46
5-28. Mean (\pm standard error) benthic daily NH_4^+ , NO_x , PO_4^{3-} and DON fluxes measured at six stations (0.5 m water depth) from July 2008 to July 2009 and three stations (i.e., SWCR, WALL, CTBY) in March 2010.....	5-47
5-29. Regression of mean benthic daily NH_4^+ flux versus mean benthic NCP measured at six stations (0.5 m water depth) from July 2008 to July 2009 and three stations (i.e., SWCR, WALL, and CTBY) in March 2010.	5-47
5-30. Regression of daily benthic NH_4^+ fluxes versus daily benthic NO_x fluxes for JACK and SWCR sites (0.5 m water depth) during the May 2009 experiment.	5-48
5-31. P-I curve results and grouping of stations for analysis.....	5-50
5-32. P-I curve results for GPP at 0.5 m and mean depth in the upper, middle, and lower regions of the NRE (see 5-31).	5-51
5-33. Predicted percent change in water column and sediment GPP within each region of the estuary with a 50% reduction in water column concentrations of (a) NTU, (b) chl <i>a</i> , and (c) CDOM.....	5-52
5-34. Multiple regression of mean benthic GPP ($\ln[\text{GPP}+10]$ transformed) versus $K_d(\text{PAR})$ (top left), water temperature (top right), and mean benthic chl <i>a</i> (0–3 mm depth; bottom) measured at six stations (0.5 m water depth) from July 2008 to July 2009 and three stations (i.e., SWCR, WALL, CTBY) in March 2010.....	5-53

5-35. Regression of mean benthic R versus water temperature measured at six stations (0.5 m water depth) from July 2008 to July 2009 and three stations (i.e., SWCR, WALL, CTBY) in March 2010.	5-54
5-36. Mean (\pm standard error) DO and NH_4^+ concentration in overlying water of sediment cores collected from Middle (WALL site) and Lower (CTBY site) regions of NRE (0.5 m water depth) during October 2009.....	5-55
5-37. Mean (\pm standard error) DO concentration in overlying water of sediment cores collected from Middle region (WALL site) of NRE (0.5 m water depth) during August 2009.	5-56
5-38. Mean (\pm standard error) benthic gross N mineralization measured at six stations (0.5 m water depth) from July 2008 to March 2010.	5-56
5-39. Mean (\pm standard error) benthic DNF measured at six stations (0.5 m water depth) from July 2008 to July 2009.	5-57
5-40. Mean benthic daily NFix by sediment depth horizon (0–1 cm, 1–3 cm, 5–7 cm, and 8–10 cm) measured at the six shallow stations (0.5 m water depth) in March and June 2011 and mean (\pm standard error) benthic NFix by site and season measured at six stations (0.5 m water depth) from May 2009 to June 2011.....	5-58
5-41. General bacterial community composition determined by PCR using a 16S primer pair (left) and potential N fixing organisms identified using PCR of the nifH gene (right).	5-59
5-42. Benthic NFix (0–1 cm depth horizon) as a percentage of estimated gross DNF measured at six stations (0.5 m water depth) in May 2009 and July 2009.	5-59
5-43. Mass balance of benthic N sources (positive values; mineralization, benthic NH_4^+ flux into the sediment) and fates (negative values; BMA demand, DNF, and benthic NH_4^+ flux out of the sediment) measured at six stations (0.5 m water depth) from July 2008 to July 2009.	5-60
5-44. Regression of mean benthic gross mineralization (MIN) versus water temperature measured at five stations (i.e., JACK, SWCR, FRCR, CTBY, TRBY; 0.5 m water depth) from July 2008 to March 2011.	5-62
5-45. Regression of mean DNF versus salinity and mean benthic daily NO_x flux measured at six stations (JACK, SWCR, WALL, FRCR, CTBY, and TRBY) (0.5 m water depth) from July 2008 to July 2009.	5-62
5-46. Regression of mean NFix (0–1 cm) versus mean benthic chl <i>a</i> (0–3 mm depth horizon) measured in the July 2010 and April 2011 depth experiments (Left). Regression of mean NFix (0–1 cm) and mean water temperature measured at six stations (i.e., JACK, SWCR, WALL, FRCR, CTBY, and TRBY) (0.5 m water depth) from May 2009 to June 2011 (Right).	5-63
5-47. Regression of mean dark NFix (0–10 cm) versus mean benthic mineralization (MIN) measured in the July 2010 and April 2011 depth experiments (left). Regression of mean dark NFix (0–10 cm) and mean sediment NH_4^+ measured in the April 2011 depth experiments (right).	5-63

5-48. Mean (\pm standard error) benthic chl <i>a</i> (0–3 mm depth) and benthic GPP measured in three regions and at three water depths of the estuary in July 2010 and April 2011.	5-64
5-49. Mean (\pm standard error) benthic R and NCP measured in three regions and at three water depths of the estuary in July 2010 and April 2011.	5-64
5-50. Mean (\pm standard error) benthic daily NH_4^+ , NO_x , PO_4^{3-} , and DON fluxes measured in three regions and at three water depths of the estuary in July 2010 and April 2011.	5-65
5-51. Plot of benthic daily NH_4^+ flux versus benthic NCP for the July 2010 (left) and April 2011 (right) depth experiments.	5-67
5-52. Regressions of benthic NCP (top) and benthic daily NH_4^+ flux (bottom) versus benthic chl <i>a</i> (0–3 mm depth) for the July 2010 (left) and April 2011 (right) depth experiments.	5-68
5-53. Mean (\pm standard error) benthic gross mineralization and net DNF measured in three regions and at three water depths of the estuary (only two depths for DNF) in July 2010 and April 2011.	5-69
5-54. The percent of ammonified N removed by benthic NH_4^+ flux, BMA N demand, and DNF in three regions and at two water depths of the estuary in July 2010 and April 2011.	5-69
5-55. The percent of sediment autochthonous N removed by benthic processes scaled up to the NRE by regions in July 2010 and April 2011.	5-70
5-56. Plot of regional benthic GPP versus pelagic GPP.	5-71

List of Tables

5-1. Summary of Allochthonous N Sources of Data and Timeframes.	5-8
5-2. The NRE Waterbody and Watershed Areas by Box.	5-8
5-3. Summary of Analytical Methods used for Research Project AE-3	5-10
5-4. NRE Stations Sampled for Benthic Chl <i>a</i> Across a Depth Gradient of 0.25–2.0 m.	5-14
5-5. NRE Area by Water Depth Interval for Boxes 1 to 9	5-25
5-6. NRE Area by NRE Region and Depth Treatment	5-25
5-7. Summary of the Two-Way ANOSIMs of Sediment Characterization Data (0.5 m water depth) and Water Column DIP by Site and Season Measured from 2007–2011	5-34
5-8. Summary of the Two-Way ANOVAs of Water Quality Parameters by Site and Season Measured from 2007–2011.	5-35
5-9. Computed Percentages of the NRE Bottom Area Receiving at Least 20%, 10%, and 1% of the Surface Irradiance (I_o) Based on Computed $K_d(\text{PAR})$ from Nearshore Dataflow System Mapping Surveys.	5-41

5-10. Summary of the Two-Way ANOVA of Benthic GPP by Site and Season Measured from July 2008 to July 2009 (0.5 m Water Depth)	5-49
5-11. Summary of the Two-Way ANOSIMs of Benthic R, NCP, and Daily NH_4^+ , NO_x , and PO_4^{3-} Flux by Site and Season Measured from July 2008 to July 2009 (0.5 m Water Depth).....	5-49
5-12. Summary of the Two-Way ANOVAs of Benthic Mineralization from July 2008 to March 2010 and DNF from July 2008 to July 2009 by Site and Season (0.5 m Water Depth)	5-61
5-13. Summary of the Two-Way ANOVA of Benthic NFix from May 2009 to June 2011 by Region and Season (0.5 m Water Depth).....	5-61
5-14. Summary of the Three-Way ANOVAs of Benthic chl <i>a</i> (0–3 mm depth horizon), Benthic GPP, R, NCP, Daily NH_4^+ Flux, MIN, and DNF by Region, Depth, and Season Measured During the July 2010 and April 2011 Depth Experiments.	5-66
5-15. Benthic N Scaled Up to the NRE by Region	5-70
5-16. GPP ($\text{gC m}^{-2} \text{ yr}^{-1}$) Scaled Up to the NRE and by Region	5-71

Acronyms

°C	degrees Celsius
α	photosynthetic efficiency or the initial slope of the photosynthesis-irradiance curve
$\mu\text{E m}^{-2} \text{s}^{-1}$	microEinsteins per second per square meter
μm	micrometer
μmol	micromole
$\mu\text{mol m}^2 \text{d}^{-1}$	micromoles per square meter per day
AC-S	AC-Spectra
AE	Aquatic/Estuarine
AHPT	Across Hospital Point
ANA	Anammox
ANAMMOX	anaerobic ammonium oxidation
ANOSIM	analysis of similarity
ANOVA	analysis of variance
Ar	argon
b_b/b	backscattering to scattering (ratio)
BLAST	Basic Local Alignment Search Tool
BMA	benthic microalgae
BOD	biological oxygen demand
C	carbon
CAFO	confined animal feed operation
CASTNET	Clean Air Status and Trends Network (Program)
CDOM	chromophoric dissolved organic matter
chl <i>a</i>	chlorophyll <i>a</i>
cm	centimeter
CTBY	Courthouse Bay
d^{-1}	per day
DIC	dissolved inorganic carbon
DIN	dissolved inorganic nitrogen
DIP	dissolved inorganic phosphorus
DNF	denitrification
DNRA	dissimilatory nitrate reduction to ammonium
DO	dissolved oxygen
DOC	dissolved organic carbon
DoD	U.S. Department of Defense
DON	dissolved organic nitrogen
$E_d(0)$	downward PAR just below the water surface
$E_d(z)$	downward PAR at <i>z</i> m

EPA	U.S. Environmental Protection Agency
EPS	extracellular polymeric substances
ESM	Estuarine Simulation Model
F	peristaltic pump flow rate (1 hr^{-1})
F_d	hourly flux in the dark
F_l	hourly flux in the light
FRCR	French Creek
FREE	Freeman Creek
g g^{-1}	grams per gram
$\text{gC m}^{-2} \text{ y}^{-1}$	grams of carbon per square meter per year
GFD	glass filter dryer
GFF	glass fiber filter
GLCR	Gillets Creek
GOCR	Goose Creek
GPP	gross primary production
GPS	global positioning system
ha	hectares
h_d	hours of dark
h_l	hours of light
HPPT	Hospital Point
I	irradiance
i.d.	internal diameter
i_{inflow}	concentration (μM) of any dissolved constituent entering the core
I_o	surface irradiance
i_{outflow}	concentration (μM) of any dissolved constituent leaving the core
JACK	Jacksonville
K2IM	K2 Impact Area
KCl	potassium chloride
K_d	vertical attenuation coefficient for downward irradiance
$K_d(\text{PAR})$	diffuse light attenuation coefficient for photosynthetically active radiation
km	kilometer
L	liter
Ln	natural log
m	meter
M	molar
$\text{m}^3 \text{ d}^{-1}$	cubic meters per day
MCBCL	Marine Corps Base Camp Lejeune
mg	milligram
mg l^{-1}	milligrams per liter
mg m^{-2}	milligrams per square meter

MIMS	membrane inlet mass spectrometry
MIN	mineralization
mL	milliliter
MLW	mean low water
mm	millimeter
mM	millimolar
MONT	Montford Point
MSL	mean sea level
N	nitrogen
N ₂	nitrogen gas
Na ₂ MoO ₄	sodium molybdate
NADP	National Atmospheric Deposition Program
NAV88	North American Vertical Datum of 1988
NCP	net community production
NECR	Northeast Creek
NFCR	North French Creek
NFix	nitrogen fixation
NH ₃	ammonia
NH ₄ ⁺	ammonium
nifH	nitrogenase reductase
NIT	nitrification
nm	nanometer
NO ₂ ⁻	nitrite
NO ₃ ⁻	nitrate
NO _x	nitrogen oxides (nitrate plus nitrite)
NRAS	New River Air Station
NRE	New River Estuary
NTU	nephelometric turbidity unit
O ₂	oxygen
OM	organic matter
ON	organic nitrogen
P	phosphorus
P _{max}	maximum rate of photosynthesis
PAR	photosynthetically active radiation
PCR	polymerase chain reaction
P-I	photosynthesis-irradiance
PO ₄ ³⁻	orthophosphate
PRPT	Paradise Point
R	respiration
RGPT	Ragged Point
RHPT	Rhodes Point

RWE	Relative Wave Energy
SERDP	Strategic Environmental Research and Development Program
STBY	Stone Bay
STTR	Stone Bay Tributary
SWCR	Southwest Creek
TDN	total dissolved nitrogen
TKN	total Kjeldahl nitrogen
TN	total nitrogen
T-R	transmittance-reflectance
TRBY	Traps Bay
TRWB	Traps/Wilkins Bluff
TSS	total suspended solids
UNC-IMS	University of North Carolina at Chapel Hill's Institute of Marine Sciences
USGS	U.S. Geological Survey
VIMS	Virginia Institute of Marine Science
WALL	Wallace Creek
WEMo	Wave Energy Model
WWTF	wastewater treatment facility

Abstract

The New River Estuary (NRE) in North Carolina, surrounded by Marine Corps Base Camp Lejeune (MCBCL) and by the city of Jacksonville at its head, is a shallow system with more than half of the estuary at depths less than 2 m at MSL. Shallow photic estuaries such as the NRE are vulnerable to anthropogenic disturbances, including inputs of nutrients, chromophoric dissolved organic matter (CDOM), and sediments, as well as to natural disturbances due to episodic storms and the impacts of climate change, including increased temperature and salinity. To determine the relative importance of off-Base versus on-Base sources of nutrients to the NRE, we compiled information on nitrogen (N) loads from watersheds impacted by the region and by MCBCL, from the atmosphere, coastal ocean, and from measured loads produced within the NRE. On an annual basis, off-Base watersheds contributed 64% of the total allochthonous N load to the NRE. The next largest source of N was exchange with the coastal ocean (15%). MCBCL impacted watersheds and wastewater treatment facility provided 15% of the annual N load. During spring and summer, autochthonous sources internal to the NRE supplied up to 27% of the total nitrogen load. The activity of benthic microorganisms (e.g., the benthic nutrient filter), which play an important role in retention and removal of remineralized nutrients, regulation of benthic–pelagic nutrient exchanges, and stabilization of bottom sediments, provides some protection against nutrient enrichment and accompanying eutrophication of the estuary. To determine the effectiveness of the benthic nutrient filter, we measured seasonal variation along the estuarine gradient of sediment characteristics, benthic chlorophyll *a* biomass, metabolic rates, N cycling rates, and sediment–water nutrient fluxes. Results demonstrated that the NRE is moderately eutrophic with benthic gross primary production (GPP) responsible for approximately 41% of total estuarine productivity. The benthos served as both a source of recycled nutrients supporting pelagic primary production, as well as a benthic filter, sequestering and removing nutrients by benthic microalgal uptake, denitrification, and anaerobic ammonium oxidation (i.e., ANAMMOX). Effectiveness of the benthic filter was dependent on light availability and photic area of the estuary [$\geq 1\%$ surface irradiance (I_0)], which varied as a function of freshwater discharge. Between 2008–2011, the photic area in the NRE varied from 46–97% of total estuarine bottom area. When light availability was low, the benthos switched from net autotrophic (photosynthesizing their food) to heterotrophic (using organic compounds for food) and from a net sink to a source of N to the water column. Estuary-wide benthic processes sequestered from 41–67% of the inorganic nitrogen remineralized from organic matter in sediments in spring and from 27–63% in summer. Whereas uptake of regenerated N by photosynthesizing benthic microalgae (BMA) sequestered more N when sufficient light was available, denitrification proved to be more important for removal of N when light was limiting. Benthic chlorophyll *a* was an excellent indicator of the effectiveness of the BMA N “filter.” During summer 2010 and spring 2011, a threshold for benthic chlorophyll *a*, was observed, ranging from 70–83 mg m⁻², below which the benthos was a source of nutrients supporting primary production by phytoplankton and above which was a sink, sequestering nutrients. In high discharge periods with high nutrient inputs, high pelagic primary production, and low photic area, the BMA “filter” is likely to be less effective due to light limitation and low biomass. CDOM and sediment loads were dominant factors controlling light attenuation, benthic metabolism and nutrient exchange up-estuary; sediment resuspension and phytoplankton abundance were likely more important drivers down-estuary.

Objectives of Research Project

Technical Goal

The overarching objective of Research Project AE-3 was to elucidate the role of benthic processes (e.g., the benthic filter, in modulating the effects of disturbance along gradients of light availability and nutrient enrichment in the New River Estuary [NRE]).

Specific objectives of Research Project AE-3 included field studies and use of historic data to:

- Determine how natural climatic variables (freshwater discharge, temperature, seasonality) and anthropogenic disturbances regulate nutrient sources, photic area, and the effectiveness of the benthic filter in the NRE
- Compare the relative importance of regional versus local (MCBCL) sources of nitrogen (N) to the NRE
- Relate light availability and temperature to benthic metabolic process rates and net benthic–pelagic exchanges of ammonium (NH_4^+)
- Identify dominant benthic processes responsible for sequestering and removing N
- Identify feedbacks between benthic and pelagic primary production
- Determine the effectiveness of the benthic filter on an estuarine-wide basis
- Determine threshold at which benthos switches from net uptake to release of carbon and NH_4^+ to water column
- Identify indicators predictive of the effectiveness of the benthic filter.

Data from these studies were used to calibrate a predictive Estuarine Simulation Model (ESM) to understand system response to natural and anthropogenic stressors and to serve as a decision-support tool for adaptive management and scenario testing of potential restoration strategies (see Chapter 4 for more information on the ESM).

Hypotheses

1. The New River and Southwest and Northeast Creeks are the dominant sources of N to the NRE.
2. Autochthonous N regenerated internally from mineralization of organic matter in the benthos is seasonally important in supporting pelagic primary production.
3. By controlling the extent of photic area in the NRE, freshwater discharge determines the effectiveness of the benthic filter.
4. Sediment–water fluxes of NH_4^+ are modulated by the benthic filter, provided that sufficient light is available.

5. A net autotrophic benthos is a net sink for NH_4^+ , and a net heterotrophic benthos is a net source of NH_4^+ to the water column.
6. The role of the benthic filter in modulating sediment–water NH_4^+ fluxes and the potential for eutrophication in the NRE is determined by the relative importance of benthic nitrogen fixation (NFix), denitrification (DNF), and benthic microalgal N uptake.
7. Estuarine-wide, where sufficient light is available to the benthos, benthic microalgae will take up most of the N regenerated from organic matter and prevent fluxes to the overlying water; where light is insufficient DNF will be the more important process for removal of regenerated N. Overall the benthic filter will prove to be effective in reducing N fluxes to the overlying water.
8. Benthic chlorophyll *a* will serve as an indicator of the effectiveness of the benthic filter.

Background

In deep estuarine systems, primary production and water column concentrations of chlorophyll *a* (chl *a*) a proxy for phytoplankton, exhibit predictable responses to inputs of nutrients. However, in shallow systems in which the benthos is exposed to light the relationship no longer appears to hold and production is far less than predicted (McGlathery et al., 2007; Nixon et al., 2001). One explanation for the behavior of shallow photic systems is that benthic microbial processes can both remove and sequester nitrogen (N), the nutrient, which limits primary production in many coastal systems (Anderson et al., 2003 and 2010; Eyre et al., 2011; Joye and Anderson, 2008; McGlathery et al., 2007; Sundbäck et al., 2004). Benthic processing of N occurs over steep physical and chemical gradients of oxygen (O_2) and nutrients in the top few centimeters of sediment. These gradients are impacted by changes in available light, nutrient, and particulate delivery resuspension events due to winds, tides and currents, temperature, and salinity (Joye and Anderson, 2008). The New River Estuary (NRE; **Figure 5-1**) can serve as a model system for study of the interacting variables that regulate N cycling and benthic–pelagic exchanges of N. Measurements made across the entire system at representative depths allow us to scale measurements made at square meter scale to the entire estuary and thereby determine the estuarine-wide impacts of the benthic filter.

The NRE is a small system of 7,810 ha located in Onslow County, NC. Much of the NRE is surrounded by Marine Corps Base Camp Lejeune (MCBCL; 63,131 ha), with the city of Jacksonville at the head of the estuary and a surrounding community of approximately 180,000 people (<http://www.lejeune.usmc.mil>). Principal tributaries discharging to the NRE include the blackwater New River with a catchment area of approximately 40,483 ha, Southwest Creek with 20,027 ha, and Northeast Creek with 18,612 ha. In addition, numerous small creeks, whose catchment areas lie within MCBCL, also discharge into the NRE. Land use in both the New River and Southwest Creek watersheds is dominated by agriculture and includes numerous swine confined animal feeding operations (CAFOs). Prior to 1998, discharges from CAFOs, a wastewater treatment facility (WWTF) in the City of Jacksonville, and seven WWTFs on MCBCL resulted in massive phytoplankton blooms, widespread hypoxia, and fish kills, such that the estuary was named one of the most eutrophic in the Southeastern United States (Bricker et al., 1999; Mallin et al., 2005b). In 1998, the Jacksonville WWTF was upgraded to secondary

treatment with land spraying of effluent, and the MCBCL facilities were consolidated into one new WWTF with biological nutrient removal located in French Creek. Although the upgrades to the WWTFs have markedly improved water quality (Mallin et al., 2005b), the NRE continues to receive high nutrient loads from allochthonous (external) sources due to inputs from the New River watershed upstream of Jacksonville, episodic WWTF spills, the MCBCL WWTF, remineralization of legacy organic matter (OM) in the upper reaches of the system, atmospheric deposition, and from tidal exchanges with Onslow Bay. Development on MCBCL, with attendant increases in impervious area, forest clear cutting, and development of roads and housing, also has the potential to impact the small tributaries which discharge into the NRE.

Based on a bathymetric study performed in 2009 (McNinch), more than 50% of the NRE is at depths less than 2 m MSL, allowing exposure of much of the benthic surface to light supporting benthic primary production. Previous studies in a wide variety of shallow estuaries and lagoons have shown strong coupling between processes in the benthic and pelagic zones. For example, when sufficient light is available the benthos can behave as a filter, removing and temporarily sequestering nutrients, and thereby reducing the potential for primary production and eutrophication in the water column (Anderson et al., 2003 and 2010; Eyre and Ferguson, 2002 and 2005; Eyre et al., 2011; Hardison et al., 2011; McGlathery et al., 2001, 2004, and 2007; Sundbäck et al., 2000 and 2004). At the head of the estuary, availability of light is reduced by delivery of chromophoric dissolved organic matter (CDOM) and particulates, which vary with freshwater discharge. In addition, primary production in the NRE has been shown to be N limited (Altman and Paerl, 2012; Mallin et al., 2005b); thus, discharge into the estuary proper results in phytoplankton blooms, which further decrease the availability of light to the benthos. As phytoplankton and other particulate and dissolved organic material move down the estuary, the OM may be remineralized (mineralization [MIN]) in either the water column (Lørborg and Søndergaard, 2009; McCallister et al., 2006; Weigner et al., 2006 and 2009) or in the benthos (Anderson et al., 2003 and 2010; Joye and Anderson, 2008; York et al., 2010) serving as an autochthonous (internal) source of N and supporting further primary production down-estuary. Nitrogen fixation (NFix), which converts nitrogen gas (N_2) to ammonia (NH_3), serves as an additional source of autochthonous N to the estuary.

Benthic autotrophs have the capacity to take up nutrients released by microbial remineralization of particulate and dissolved organic matter; thus when light is sufficient the benthos may either take up nutrients from the water column or reduce the flux of nutrients to the water column (Anderson et al., 2003 and 2010; Eyre and Ferguson, 2002; Eyre et al., 2005 and 2011; Hardison et al., 2010 and 2011; Sundbäck and Miles, 2000; Sundbäck et al., 2004; Tyler et al., 2003). In addition, benthic autotrophs can regulate microbial processes such as nitrification (NIT), denitrification (DNF), ANAMMOX (ANA), and dissimilatory nitrate reduction to ammonium (DNRA) by release of O_2 and extracellular polymeric substances (EPS), and by competition for substrates (Joye and Anderson, 2008; Kromkamp et al., 2006; MacIntyre et al., 1996). Whether the benthos is net autotrophic or net heterotrophic is dependent on light, temperature, and nutrients. Whereas an autotrophic benthos is likely to be a net sink, a heterotrophic benthos is likely to be a net source of nutrients to the overlying water. In addition heterotrophic sediments are prone to hypoxia and anoxia, and accumulate sulfide, an end product of OM decomposition by sulfate reduction. Sulfide plays an important role in the fate of sediment N by inhibiting NIT and DNF and enhancing DNRA (Joye and Anderson, 2008).

Microbial N cycling processes (i.e., MIN, NIT, DNF, ANA, DNRA, and NFix), which determine the fate of N in the benthos and exchanges with the water column, are sensitive to sediment oxygenation and the redox gradient (Joye and Anderson, 2008). MIN decomposes OM derived from phytoplankton, detrital material, and legacy organics to mineral products such as ammonium (NH_4^+), which may then be oxidized by NIT (an aerobic process) to nitrite (NO_2^-) and nitrate (NO_3^-). NIT is closely coupled to DNF, ANA, and DNRA because it supplies substrate (NO_x) for those processes. DNF, DNRA, and ANA are all anaerobic processes, which compete with each other and with benthic microalgal uptake for substrate. Whereas benthic microalgal (BMA) photosynthesis can enhance NIT by oxygenating sediment, it can reduce NIT coupled to DNF or DNRA by competing for substrate. NO_3^- produced by NIT may be either removed as N_2 from sediments by DNF and ANA or reduced back to NH_4^+ by DNRA if sulfide is present; thus, DNRA results in retention and accumulation of N as NH_4^+ and potentially increased fluxes of N to the water column. Whereas NO_3^- reduction by DNF and ANA produce N_2 , NFix converts N_2 to NH_4^+ , confounding measurements of DNF or ANA by membrane inlet mass spectrometry (MIMS), which measures net production of N_2 . Benthic NFix, an anaerobic process, which may be performed by a wide variety of archaea and bacteria, including sulfate reducing bacteria and cyanobacteria, is potentially an important source of N to estuarine systems (Cole and McGlathery, 2012; Fulweiler et al., 2007; Joye and Anderson, 2008; Nixon et al., 2009; Steppe and Paerl, 2002). The relative importance of these N cycling processes, all of which are affected by the activity of BMA, determine the effectiveness of the benthic filter in modulating pelagic eutrophication in nutrient enriched estuaries such as the NRE. Although determination of the complex regulation of these various processes in the NRE was beyond the scope of Research Project AE-3, a major objective of the project was to determine the relative importance of benthic MIN and NFix as sources and DNF as a sink for N in the NRE.

The Research Project AE-3 Module was closely integrated with the other aquatic estuarine research and monitoring activities. Although Research Project AE-3 focused on the role of benthic processes in modulating pelagic primary production, it also drew on historic data as well as data from the other Aquatic/Estuarine (AE) Module researchers to determine the relative importance of allochthonous versus autochthonous sources of N to the system and the role of climatic variables (freshwater discharge, wind, and temperature) in regulating distribution of chl *a* and the sources and fates of N in the NRE. As shown in **Figure 5-1**, it was hypothesized that freshwater discharge regulates inputs of allochthonous nutrients, particulates, and CDOM to the NRE impacting light availability, the extent of photic area, and the distribution of benthic chl *a* in the estuary. The effectiveness of the benthic filter depends upon the abundance and distribution of benthic chl *a*. To test the hypotheses and address the objectives for Research Project AE-3, we performed the following tasks:

Hypotheses #1 and 2 (allochthonous versus autochthonous sources of N to the NRE). Data were assembled for off-Base watersheds from the U.S. Geological Survey (USGS) gauging station at Gum Branch, for on-Base watersheds from measurements by Research Project AE-2, from the National Atmospheric Deposition Program (NADP), from the U.S. Environmental Protection Agency's (EPA's) Clean Air Status and Trends Network (CASTNET) program, and from MCBCL Environmental Management WWTF annual reports. The relative importance of autochthonous nutrients compared to total summer loads was based on measurements of fluxes and process rates made down the estuarine gradient at multiple depths during spring 2010 and summer 2009.

Hypothesis #3 (effects of freshwater discharge on photic area). Dataflow surveys were run approximately tri-monthly from 2008 through 2011 for determinations of water column chl *a*, turbidity, and CDOM, all of which were used for calculations of the vertical attenuation coefficient for downward irradiance (K_d) and benthic photic area in the NRE. Along with Dataflow surveys, grab samples were taken at six stations to determine the abundance of benthic chl *a* and water column nutrients. Calibration of a bio-optical model was completed to determine relative roles of phytoplankton, suspended sediment, and CDOM on light attenuation along the estuarine salinity gradient.

Hypotheses #4, 5, and 6 (relative contributions of N cycling processes to the benthic filter and effectiveness of benthic filter in regulating sediment–water nutrient fluxes). Flux and metabolic studies along with measurements of N cycling processes were performed during summer and fall 2008, spring and summer 2009, and winter 2010 at six shallow water stations along the estuarine gradient.

*Hypotheses # 7 and 8 (estuarine-wide effectiveness of the benthic filter; benthic chl *a* as an indicator of effectiveness).* Measurements of benthic chl *a*, metabolism, benthic fluxes, and N cycling process rates were measured along 0.5-, 1.5-, and 3.0-m contours within the upper, middle, and lower estuary during summer 2010 and spring 2011. Additional assessments of the depth distributions of benthic chl *a* in the NRE were made during sampling trips in spring 2008, fall 2009, and spring and fall 2010.

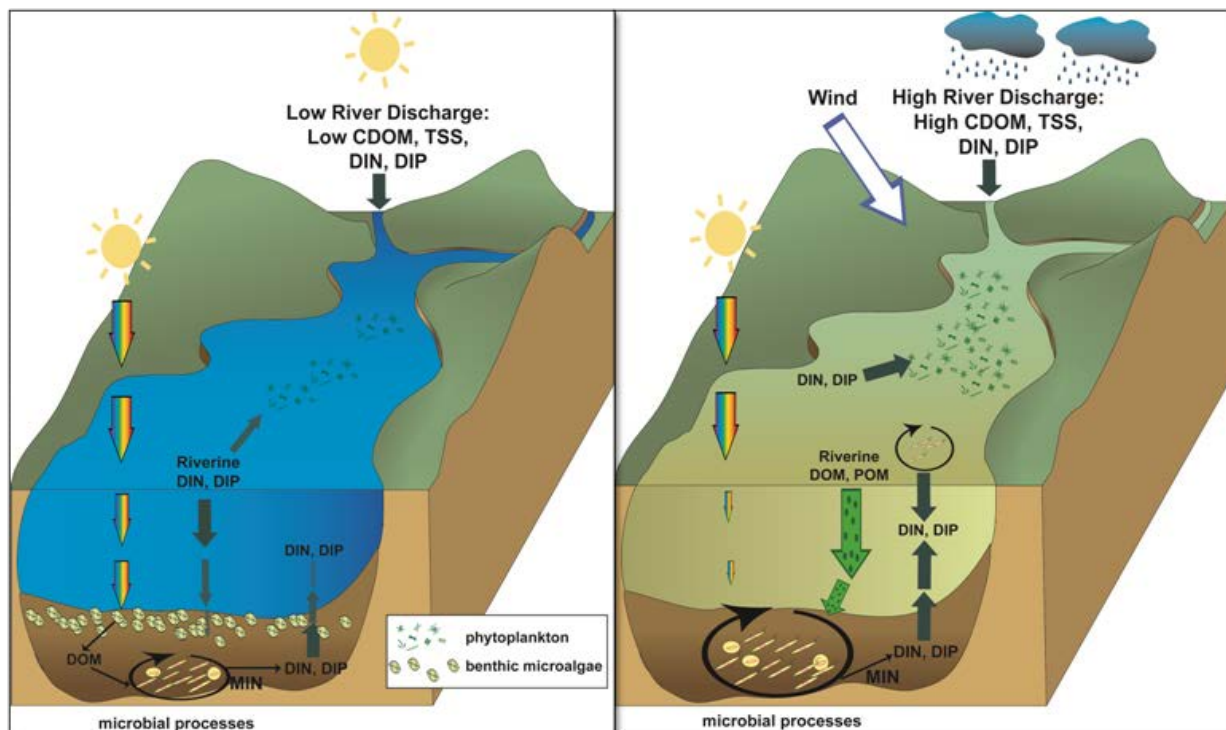


Figure 5-1. Conceptual model showing the impacts of freshwater discharge on estuarine processes.

The left panel shows low freshwater discharge, and the right panel illustrates high freshwater discharge.

Materials and Methods

Allochthonous N Loading Estimates

To determine allochthonous N loads to the NRE, both historic data and stream loading data collected by Research Project AE-2 were compiled. The major sources to the NRE include (1) off-Base watersheds of the New River, Southwest Creek, and Northeast Creek, (2) on-Base watersheds; (3) the MCBCL WWTF; (4) tidal exchange with Onslow Bay; and (5) atmospheric wet and dry deposition to the surface area of the NRE. **Table 5-1** provides a summary of the data sources.

For the NRE Estuarine Simulation Model (ESM), the NRE waterbody was divided into nine areas or “boxes” (**Figure 5-2** and **Table 5-2**). These watershed and waterbody areas were used for estimating off- and on-Base loads and direct atmospheric deposition (**Table 5-1**). Watershed delineations of off-Base versus on-Base areas for each box were performed as part of Research Project AE-2. To calculate the total loadings from off-Base, daily mean total nitrogen (TN) watershed yields from Gum Branch were applied to 98.0% of Box 1, 74.6% of Box 2, and 91.2% of Box 3 watershed areas and then summed for each year. For on-Base loadings, the annual mean TN watershed yields from nine tributaries monitored under Research Project AE-2 (excluding the Camp Johnson site) were applied to the remaining watershed areas of Boxes 1, 2, and 3, and all of Boxes 4 through 9. Annual MCBCL WWTF loads were calculated by multiplying monthly flow rates by TN concentrations and summing them for the year. For each of these sources, an overall annual average loading was calculated from the multiple years of data.

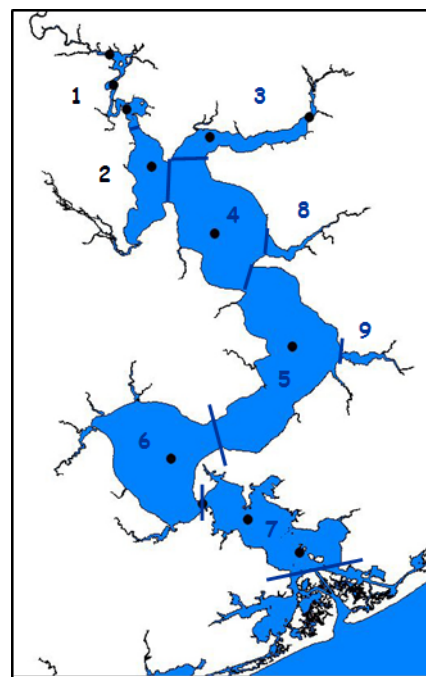


Figure 5-2. The NRE is divided into boxes, utilized for the NRE ESM.

A final N source is the input of TN from Onslow Bay via estuarine circulation, which was estimated from daily volumetric inflows ($\text{m}^3 \text{d}^{-1}$) to the NRE using the physical box model within the ESM combined with estimated mean concentrations of TN in Onslow Bay. Mallin et al. (2005a) reported mean chl *a* and dissolved inorganic nitrogen (DIN) concentrations in Onslow Bay surface water of 0.42 mg l^{-1} and 0.44 mM , respectively, and Dafner et al. (2007) reported a mean ratio of dissolved organic nitrogen (DON) to total dissolved nitrogen (TDN) of 0.90 in Onslow Bay. Chlorophyll values were converted to particulate N assuming Redfield stoichiometry and a typical carbon to chlorophyll ratio of 42 g g^{-1} (Brush et al., 2002; Cloern et al., 1995). TDN was estimated from the mean value of DIN and the DON:TDN ratio, and added to particulate N for an estimate of TN in incoming Onslow Bay water.

TN wet deposition from the NADP is frequently underestimated by 10–20% due to deficient preservation methods and losses of organic nitrogen (ON) and NH_4^+ (Keeney and Nelson, 2002). Therefore, we applied a 15% correction factor to wet inorganic N deposition values to determine

wet TN (including ON) deposition rates, as determined by Meyers et al. (2001). These rates were averaged over the multiple years for each of three sites (Hofmann Forest, Beaufort, and Clinton Crops Research Station). An overall average wet TN deposition was calculated and added to overall annual average dry TN deposition measured at the Beaufort EPA CASTNET site.

Table 5-1. Summary of Allochthonous N Sources of Data and Timeframes

Allochthonous Source	Data Source	Timeframe
Off-Base watersheds	USGS gauging station at New River near Gum Branch, NC, #02093000, discharge and nutrient concentration measurements	1998–2010
MCBCL watersheds	Research Project AE-2 freshwater discharge and nutrient concentration measurements	2008–2011
WWTF	MCBCL waste water treatment facility water flow rate and nutrient concentration measurements	2000–2010
Onslow Bay	Onslow Bay nutrient concentration measurements; ESM	1998–2010
Direct Atmospheric Deposition	Wet deposition: NADP sites NC06 (Beaufort), NC29 (Hofmann Forest), and NC35 (Clinton Crops Research Station); areal N deposition rates	2000–2010
	Dry deposition: EPA CASTNET Site BFT142 (Beaufort); areal N deposition rates	2000–2009

Table 5-2. The NRE Waterbody and Watershed Areas by Box

Box	Area Description	Waterbody Area (ha)	Watershed Area (ha)
1	New River/Wilson Bay	1,939	404,828
2	Southwest Creek and upper NRE	5,931	200,271
3	Northeast Creek	4,180	186,118
4	Morgan Bay	15,268	16,053
5	Farnell Bay	20,973	46,611
6	Stone Bay	16,751	53,252
7	Courthouse Bay, Traps Bay, and lower NRE	12,339	31,553
8	Wallace Creek	718	65,574
9	French Creek	581	19,992
	TOTAL	78,680	1,024,251

Sediment and Water Quality Characterizations in the Shallow Photic Zone

From July 2007 to December 2011, sampling of shallow benthic and pelagic habitats (approximately 0.5 m water depth at MLW) in the NRE was conducted for physical, chemical, and biological characteristics at six sites, including Jacksonville (JACK), French Creek (FRCR), Southwest Creek (SWCR), Wallace Creek (WALL), Courthouse Bay (CTBY), and Traps Bay

(TRBY) (**Figure 5-3**). Parameters measured in sediments included bulk density (0–5 cm depth horizon), organic content (0–5 cm depth horizon), grain size (0–5 cm depth horizon), nutrient concentrations (DIN: NH_4^+ , nitrogen oxides [NO_x ; NO_3^- plus NO_2^-]), distribution and abundance of chl *a* and phaeophytin (0–3 mm depth horizon), porewater sulfide, and major algal taxonomical pigment concentrations. Variables determined in the water column included: temperature, salinity, turbidity, dissolved oxygen (DO), nutrient concentrations (DIN, dissolved inorganic phosphorus [DIP]; orthophosphate [PO_4^{3-}], DON, dissolved organic carbon [DOC]), chl *a*, phaeophytin, photosynthetically active radiation (PAR), vertical light attenuation coefficient ($K_d[\text{PAR}]$), and CDOM. $K_d(\text{PAR})$ determines the quantity (intensity) and quality (wavelength) of light reaching the bottom of the estuary, which in turn control the rate of BMA production (MacIntyre and Cullen, 1996; Pinckney and Zingmark, 1993). **Table 5-3** provides a summary of analytical methods and equipment used for each parameter. Many of these parameters were collected concurrently with shallow benthic and pelagic metabolic and nutrient-cycling rates.



Figure 5-3. Map of the NRE, MCBCL, and shallow water research stations (0.5 m water depth).

Red circles denote shallow water research stations, blue triangles denote shallow water mainstem stations for productivity-irradiance experiments, and purple squares denote Intracoastal Waterway stations.

Table 5-3. Summary of Analytical Methods used for Research Project AE-3

Analyses	Methods/Instrument	References
Sediment characterization		
Sediment organic content	Loss on ignition (500°C)	
Benthic chl <i>a</i> and phaeophytin (microalgae biomass)	chl <i>a</i> –acetone extract/spectrophotometry; Beckman Coulter DU800 spectrophotometer	Lorenzen, 1967; Neubauer et al., 2000
Sediment nutrients	Potassium chloride-extraction	Keeney and Nelson, 1982
Sediment grain size	Sieving method (>63 µ); pipette method (<63 µ)	Plumb, 1981
TN and organic C content	Fision Model EA 1108 elemental analyzer	
Porewater sulfide	Cline’s reagent/methylene blue method; spectrophotometer	Cline, 1969
Porewater nutrients	Push point sampler, peristaltic pump	
Major algal taxonomical pigment concentrations	High performance liquid chromatography (HPLC; Shimadzu model LC-20AB) equipped with a photodiode array spectrophotometric detector (Shimadzu SPD-M20AC) (performed by Hans Paerl’s laboratory)	Pinckney et al., 1996, 1999, and 2001
Water quality		
Temperature, salinity, DO, turbidity, chl <i>a</i> (in vivo) (field measurements)	YSI 6600 multiparameter sonde	
DO (metabolism experiments)	Hach luminescence DO sensor	Hach Method 10360
chl <i>a</i> (extracted; phytoplankton biomass)	chl <i>a</i> –acetone–DMSO extract/fluorometry; Turner Designs Fluorometer, Model 10-AU	Arar and Collins, 1997; Shoaf and Lium, 1976
CDOM	WET Labs CDOM sensor, Beckman Coulter DU800 spectrophotometer (absorption read at wavelength 440 nm)	Gallegos and Neale, 2002; Green and Blough, 1994; Kirk, 1994
PAR	Li-Cor LI-192SA Underwater and LI-190SA quantum sensors	

(continued)

Table 5-3. Summary of Analytical Methods used for Research Project AE-3 (continued)

Analyses	Methods/Instrument	References
Nutrient		
NO ₂ ⁻ , NO ₃ ⁻	Cadmium reduction/diazotization; Lachat ^a	Smith and Bogren, 2001
NH ₄ ⁺	Phenol hypochlorite method; Lachat ^a	Liao, 2001
DIP (phosphate)	Molybdate method; Lachat ^a	Knepel and Bogren, 2001
TDN/DON	Alkaline persulfate digestion; Lachat ^a	Koroleff, 1983
Dissolved inorganic carbon (DIC)	Acidification to carbon dioxide (CO ₂); LI-6252 CO ₂ analyzer	
DOC	680°C catalytically aided combustion oxidation/non-dispersive infrared detection; Shimadzu TOC-V analyzer	Neubauer and Anderson, 2003

^a The Lachat auto analyzer (QuikChem 8000 automated ion analyzer, Lachat Instruments, Loveland, CO) is a continuous flow automated analytical system that complies with EPA standards.

Role of Environmental Variables in Regulating Sediment and Water Quality

Dataflow Surface Water Mapping of Water Quality

From July 2008 to December 2011, Dataflow surface water mapping surveys were conducted seasonally for water quality parameters (e.g., DO, in vivo chl *a*, turbidity, CDOM, salinity, temperature) in shallow habitats and tributary creeks bordering the entire estuary. The Dataflow system was run along the shoreline of the entire estuary, collecting continuous water quality measurements (approximately every 30 m; more than 4,500 datapoints) using a YSI 6600 datasonde, WET Labs's CDOM sensor, Garmin global positioning system (GPS), and data acquisition system (**Figure 5-4**). Calibration samples for CDOM, extracted chl *a*, and dissolved nutrients were collected at 10 stations in triplicate, including the six shallow water sites (**Figure 5-3**). For each survey, regressions were conducted for (1) in situ YSI chl *a* measurements versus laboratory analyzed chl *a* samples and (2) in situ WET Labs CDOM measurements versus CDOM absorption readings (at 440-nm wavelength; m⁻¹). These regression relationships were utilized to predict extracted chl *a* and CDOM absorption values for each datapoint in a specific dataflow survey.

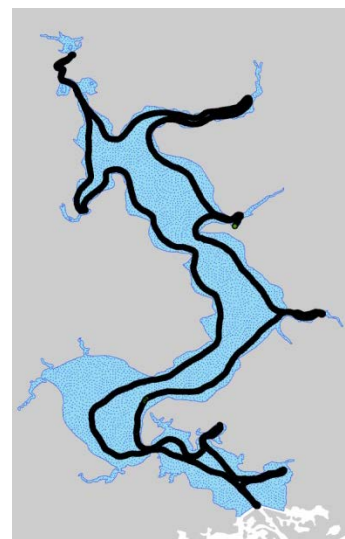


Figure 5-4. Dataflow surface water mapping cruise track in the NRE.

Data from all Research Project AE-3 surveys during 2008 and 2009, including the supplemental mainstem surveys, were combined to develop an empirical model of light attenuation, K_d (PAR). CDOM was the strongest single predictor of attenuation with turbidity playing a weaker role and chl *a* playing almost no role (**Figure 5-5**). The composite multiple linear regression model for

predicting light attenuation [K_d (PAR), m^{-1}] as a function of chl a (extracted), turbidity (NTU), and CDOM (absorption at 440 nm) is shown in Equation 5-1 as follows:

$$K_d \text{ (PAR)} = 0.71 + 0.005*Chl\ a + 0.066*NTU + 0.26*CDOM$$

$$(r^2 = 0.76, p < 0.001) \quad (\text{Eq. 5-1})$$

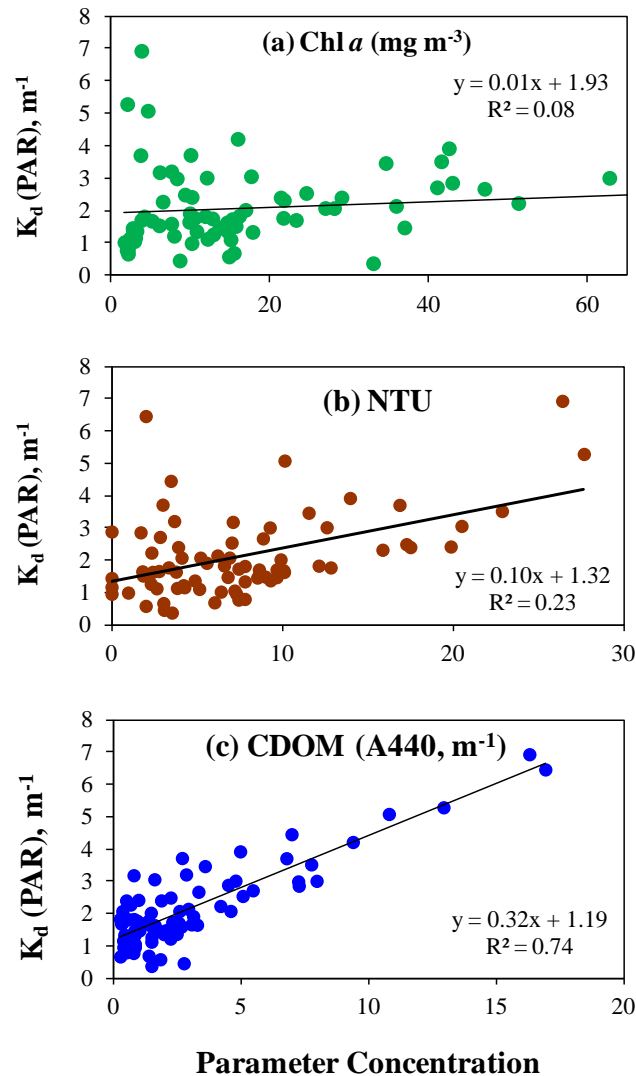


Figure 5-5. Empirical relationships between the rate of vertical light attenuation (K_d [PAR]) and extracted chl a , turbidity (NTU), and CDOM.

Note: (a) chl a , (b) turbidity, and (c) CDOM.

All model terms were highly significant ($p < 0.0093$) with strong correlation between observed and computed K_d (PAR) (**Figure 5-6**). This model was applied to the dataflow surveys to predict K_d (PAR) for each datapoint.

Maps of interpolated surface water quality measurements for the entire NRE were made in ArcGIS 9.3 using Spatial Analyst and an inverse distance weighting technique. Using the interpolated $K_d(\text{PAR})$ values and NRE bathymetry (conducted by McNinch in 2009), the percent of bottom area in the NRE receiving at least 1–20% of surface area was determined.

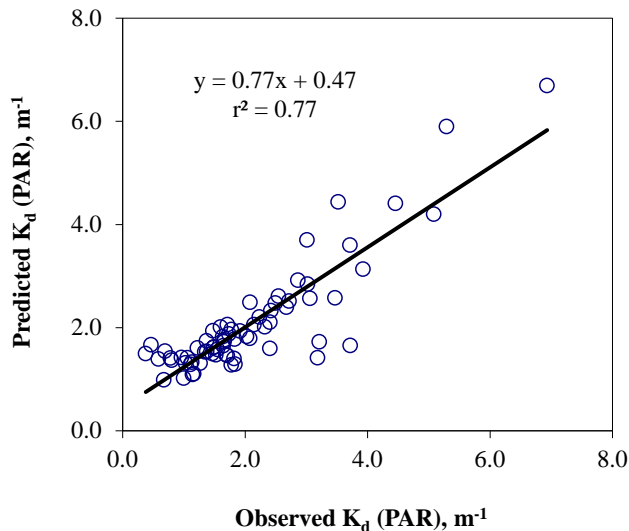


Figure 5-6. Regression of observed K_d (PAR) against values computed using the multiple linear regression in Equation 5-1.

Distribution of Benthic Chl a with Depth: Effects of Wind

Knowledge of the temporal and spatial distribution of chl a , a proxy for BMA biomass, and the environmental controls on microalgal distribution, is key to successfully predicting the impacts of climate change and anthropogenic inputs on NRE productivity. Sediments from each of six Research Project AE-3 sites were sampled in May 2008, October 2009, and October 2010 (excluding JACK because of the difficulty of sampling below 1.0-m depth). Additional sites in the mainstem NRE (**Table 5-4**) were sampled in April 2008, October 2009, and April and October 2010 to provide broader coverage of NRE subtidal sediments. For analysis, sites were divided into three regions (i.e., Upper: sites north of Wallace Creek [corresponding to Boxes 2–4 in **Figure 5-2**]; Mid: sites from Wallace Creek to just north of Stone Bay [Box 5 in **Figure 5-2**]; Low: sites from Stones Bay to Traps Bay [Box 6–7 in **Figure 5-2**; **Table 5-4**]). Subtidal sediments were sampled across a depth gradient from 0.25 m to 2.0 m MLW using a push corer deployed from a small boat. The top 3 mm of sediment was subsampled with a syringe-corer, and stored frozen until analysis. Chl a was measured spectrophotometrically after overnight extraction with a 45:45:10 methanol:acetone:distilled water solution, sonicated for 30 seconds, centrifuged, and determined using the equations of Lorenzen (1967). Wave Energy Analysis was performed to determine how winds impact the distribution of chl a at various water column depths. GPS coordinates were obtained for each sampling point, and Relative Wave Energy (RWE), with units of Joules m^{-1} wave crest, was calculated using the Wave Energy Model (WEMo) described by Malhotra and Fonseca (2007). For this exercise, we used the calculated RWE for the 1.0m depth location to represent overall wave energy at each site. RWE calculations utilized bathymetry, fetch, and wind data from the New River Air Station (top 5% of

wind events between 2006–2008) and represent a long-term characterization of the wave energy experienced by a particular site.

Table 5-4. NRE Stations Sampled for Benthic Chl *a* Across a Depth Gradient of 0.25–2.0 m

Station Name	Station Code	Sampling Dates	Latitude	Longitude
Upper Region				
Montford Point	MONT	May 2008	34.7237	–77.4188
Northeast Creek	NECR	April 2010	34.7197	–77.2984
New River Air Station	NRAS	April 2010	34.7170	–77.431
Paradise Point	PRPT	October 2009, October 2010	34.7057	–77.3855
Ragged Point	RGPT	May 2008	34.6977	–77.4100
Southwest Creek	SWCR	May 2008, October 2009, October 2010	34.6834	–77.4294
Middle Region				
Wallace Creek	WALL	May 2008, October 2009, October 2010	34.6823	–77.3679
Hospital Point	HPPT	April 2010	34.6726	–77.3809
Across Hospital Point	AHPT	April 2010	34.6689	–77.3967
North French Creek	NFCR	May 2008	34.6473	–77.3416
French Creek	FRCR	May 2008, October 2009, October 2010	34.6393	–77.3397
Rhodes Point	RHPT	May 2008, October 2009, October 2010	34.6368	–77.3738
K2 Impact Area	K2IM	April 2010	34.6216	–77.3769
Goose Creek	GOCR	April 2010	34.6201	–77.3591
Lower Region				
Stone Bay	STBY	May 2008	34.5881	–77.4063
Stone Bay Tributary	STTR	October 2009, October 2010	34.585	–77.4328
Courthouse Bay	CTBY	May 2008, October 2009, October 2010	34.5899	–77.3687
Traps/Wilkins Bluff	TRWB	May 2008	34.5672	–77.3548
Traps Bay	TRBY	May 2008	34.5689	–77.3372

Bio-optical Model

A bio-optical model was developed that utilizes calibrated relationships between water quality constituents (chl *a*, total suspended solids [TSS], and CDOM) and their inherent optical properties (absorption and scattering characteristics) to identify water quality conditions that meet specific biological light requirements. This model is an improvement over the linear regression previously described (see Equation 5-1) because it quantifies the direct contribution of water quality constituents to absorption and scattering and uses a measured backscattering to scattering (b_b/b) ratio to correct for forward scattering light, which does not contribute to $K_d(\text{PAR})$. To calibrate the model, chl *a*– and TSS–specific scattering and absorption coefficients were determined at 0.5 m water depth at the six Research Project AE-3 stations plus two

Intracoastal Waterway stations (Gillets Creek [GLCR] and Freeman Creek [FREE]) (**Figure 5-3**). Samples for water quality and optical analysis were collected quarterly from October 2007 to October 2008 (estuarine and intracoastal stations) and monthly from April 2009 to October 2009 and March 2010 (estuarine stations only). Laboratory measurements included algal and non-algal particulate absorption, scattering, as well as absorption by CDOM, chl *a*, TSS, and turbidity. At each sampling period in situ measurements were made of temperature, salinity, chl *a*, and turbidity and $K_d(\text{PAR})$ using a YSI 6600 multimeter probe. Light attenuation data (% underwater PAR irradiance) were collected from simultaneous measurements of two Li-Cor 2 pi sensors. Attenuation data were used to calculate $K_d(\text{PAR})$ using the Lambert-Beer law as shown in Equation 5-2:

$$K_d(\text{PAR})z = \ln E_d(0) - \ln E_d(z) \quad (\text{Eq. 5-2})$$

where $E_d(z)$ and $E_d(0)$ are the values of downward PAR at z m and just below the surface, respectively, and $K_d(\text{PAR})z$ is the vertical attenuation coefficient for downward irradiance.

Water samples for CDOM determinations, prefiltered through glass fiber filters (GFF) followed by a 0.22- μm Poretics polycarbonate filter were measured in a Perkin Elmer Lambda 40 spectrophotometer with 5- or 10-cm pathlength glass cell referenced to distilled water blank. Absorbance units were converted to in situ absorption coefficients, $a_{\text{CDOM}}(\lambda)$, by multiplying 2.303 ($\ln[10]$) and dividing by pathlength. Particulate absorption was measured using the (Tassan and Ferrari, 1995 and 2002) Transmittance-Reflectance (T-R) method modified for an Ocean Optics USB2000 with ISP-30-6-R integrating sphere and HL-2000 tungsten halogen light source. Algal and nonalgal particulate absorption were determined after methanol extraction (Mitchell et al., 2003). The T-R method eliminates the need for a pathlength amplification correction. Water samples for TSS measurements (EPA 2540D), filtered onto GFF and frozen at -80°C , were ground and extracted overnight in 90% methanol at 4°C , centrifuged and measured on a Turner 10AU fluorometer (EPA method 445.0 rev 1.2). TSS on dried filters was determined as weight gain/volume filtered. Turbidity was measured on a Hach 2100P turbidimeter. A WET Labs AC-Spectra (AC-S) was used to measure absorption and beam attenuation coefficients of water samples at 88 wavelengths between 400 nm and 729 nm. The raw absorption and beam attenuation coefficients were corrected for temperature and salinity (WET Labs, 2011) and absorption was corrected for scattering (Gallegos and Neale, 2002). Scattering was calculated as the difference between corrected beam attenuation and absorption coefficients. Radiative transfer modeling was used to predict the apparent optical property $K_d(\text{PAR})$ from spectral characteristics of water samples (Lee et al., 2005) in a modified spreadsheet model from Gallegos (2001). Measured $K_d(\text{PAR})$ was used to evaluate model predictions of $K_d(\text{PAR})$ from the relationship between inherent optical properties (absorption and scattering coefficients) and water quality measurements (Gallegos, 1994 and 2001). In April 2010, in situ b_b/b ratios were measured using WET Labs ECO VSF3 and AC-S instruments along a 30-km transect of 22 stations spaced approximately 2.0 km apart along the mainstem of the NRE from the inlet to Jacksonville bridge.

Determinations of Shallow Water Benthic and Pelagic Metabolic and Nutrient-Cycling Rates

Overall Approach

Seasonal measurements of shallow water (approximately 0.5 m water MLW) benthic and pelagic metabolism were made both in situ and in the laboratory to determine: (1) the role of the benthos in modulating nutrient enrichment of the estuary, and (2) how light limits the ability of the benthos to perform this role. In situ mesocosms (July 2008, October 2008, May 2009, and July 2009) allowed us to determine responses of benthic and water column processes to ambient conditions of temperature and light intensity over diel time scales. To estimate benthic and pelagic primary production rates at water column depths with various levels of irradiance, additional laboratory incubations of water column and sediment cores were performed in light gradient boxes. To understand the mechanisms responsible for modulation of nutrient enrichment in shallow water sites (0.5 m MLW), concurrent measurements were made of water and sediment quality, N-cycling rates (i.e., gross mineralization, DNF, and NFix) and water column optical properties. To obtain winter rates at three of the six Research Project AE-3 sites (i.e., SWCR, WALL, and CTBY), sediment cores were collected for benthic metabolism and nutrient fluxes in March 2010 and incubated in the light and dark in an environmental growth chamber at in situ temperature at the Virginia Institute of Marine Science (VIMS).

Determinations of Shallow Water Benthic Metabolism and Nutrient Fluxes

Sediment mesocosm cores (clear acrylic, 13.3 cm inner diameter \times 40-cm tall, 20-cm depth of sediment), collected at six randomly selected stations within each of Research Project AE-3's six shallow sampling sites (**Figure 5-3**), were used for concurrent determinations of GPP, respiration (R), net community production (NCP), and nutrient fluxes. Additionally, three water blanks were taken from each site (large cores filled with water collected from each site) to distinguish water column from sediment processes. During July and October 2008 and May and July 2009, mesocosms and instrumentation were deployed at three sites within the estuary (i.e., SWCR, FRCR, and CTBY; **Figure 5-3**), representing environments with very different optical properties (**Figure 5-7**). The large sediment mesocosms sampled at JACK and SWCR were incubated at SWCR, cores from WALL and FRCR were incubated at FRCR, and cores from CTBY and TRBY were incubated at CTBY. To determine the net exchange of nutrients, inorganic carbon (C), and DO between the sediment and overlying water, water samples were collected during 24-hour in situ incubations at 4-hour intervals during the day and 12-hour intervals at night (Anderson et al., 2003). The cores were connected to a reservoir system (**Figure 5-7**) so that water removed during sampling was replaced with water from the respective site. DO concentrations in the sampled water were measured using a Hach Luminescence DO sensor. Samples for dissolved inorganic carbon (DIC) were collected in 8-mL hungate tubes (pre-spiked with 15 μ L saturated mercuric chloride) and kept cold under water until analysis. Changes in DIC in the light and dark were used for determination of rates of benthic and pelagic metabolism, including R, GPP, and net NCP. Water samples taken concurrently with the DO and DIC measurements were filtered (Gelman Supor, 0.45 μ m) and frozen until analyzed for DIP, DIN, DOC, and DON (**Table 5-3**). Net uptake or release of nutrients from sediment was determined from changes in nutrient concentrations during the same incubation periods.

For the March 2010 metabolism and nutrient fluxes experiment, rates were calculated based on fluxes of DO, DIC, DIN, DIP, DOC, and DON sampled during a 24-hour incubation in the environmental chamber (at in situ temperature and light). After returning from the field and prior to starting the incubations, cores were uncapped and immersed overnight in the dark in water collected from each site. During this time water within the cores was constantly mixed and aerated. Metabolism and nutrient flux experiments were initiated the next morning by capping the cores with clear acrylic lids under water in large tanks. The sediment mesocosms were sampled as were done for the in situ experiments. At the end of the incubations, sediment mesocosms were sampled for benthic chl *a*, phaeophytin, algal community composition (based on pigment analysis by high performance liquid chromatography conducted at the University of North Carolina at Chapel Hill's Institute of Marine Sciences (UNC-IMS), and porewater nutrient concentrations (**Table 5-3**). Concurrent with the in situ mesocosm studies YSI Model 6600 datasondes and Li-Cor Biosciences' (Li-Cor) sensors were deployed at nearby sites in approximately 1 m water depth (MLW) and set 0.5 m above the bottom (e.g., measuring at a water depth of 0.5 m) for 48-hour periods of continuous measurements of PAR, salinity, turbidity, pH, DO, and temperature recorded at 15-minute intervals.

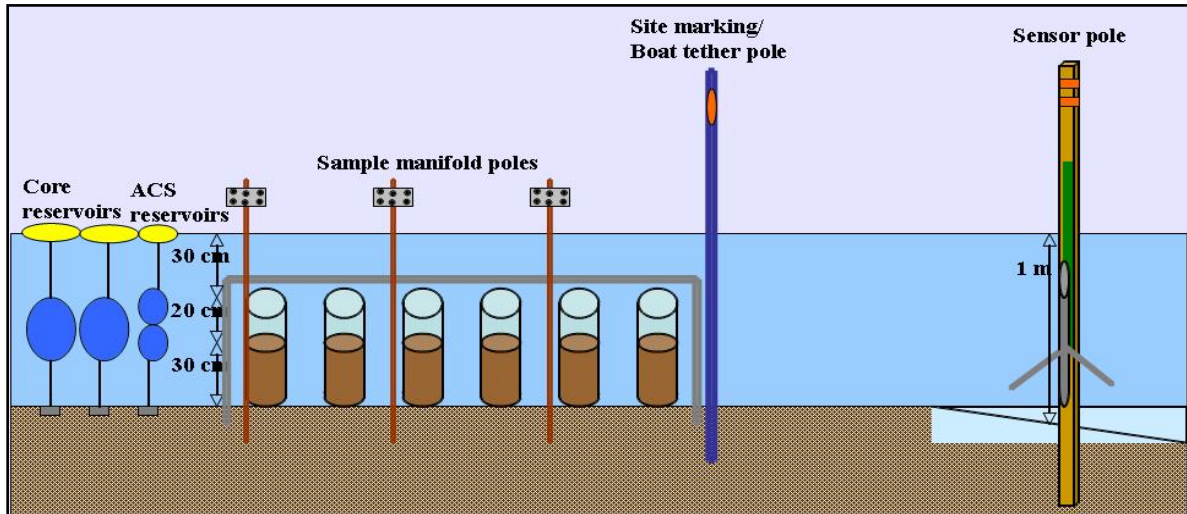


Figure 5-7. Side view of the in situ mesocosm experiment set up.

Benthic DIC, DO, and nutrients fluxes were corrected for DIC, DO, and nutrient uptake or release measured in the water blanks. Benthic metabolism (DIC based) and daily nutrient fluxes were calculated as shown in Equations 5-3 through 5-6 as follows:

$$R = F_d * 24 \text{ hours} \quad (\text{Eq. 5-3})$$

$$GPP = h_l * (F_d - F_l) \quad (\text{Eq. 5-4})$$

$$NCP = - (GPP - R) \quad (\text{Eq. 5-5})$$

$$\text{Daily nutrient flux} = (F_l * h_l) + (F_d * h_d) \quad (\text{Eq. 5-6})$$

F_d = Hourly flux in the dark

F_l = Hourly flux in the light

h_l = Hours of light
h_d = Hours of dark

NCP (Equation 5-5) is represented as a negative number when GPP exceeds R because it was measured as uptake of C. When NCP is negative it represents net autotrophy and net uptake of C; when positive it represents net heterotrophy and net release of C.

BMA N demand was calculated (Equation 5-7) based on 90% of GPP and a C:N of 9:1 (Sundbäck et al., 1991). Because BMA have been shown to exude as much as 70% of the C taken up by photosynthesis as EPSs and colloidal C (Wolfstein et al., 2002), rates of BMA N demand, which may overestimate N assimilation into biomass, were corrected with a conservative assumption that 50% of the C fixed was exuded as EPSs or colloidal C (see Equation 5-7).

$$\text{BMA N-demand} = (0.9 * \text{GPP}) / 18 \quad (\text{Eq. 5-7})$$

Photosynthesis-irradiance experiments

Water column and sediment incubations were conducted to construct photosynthesis-irradiance (P-I) curves concurrent with in situ flux studies at the primary shallow water Research Project AE-3 study sites, as well as at six supplemental stations down the axis of the NRE in March, May, July, and October 2009 (**Figure 5-3**) using the method of Giordano et al. (2012). In this approach, rates of photosynthesis and R are calculated based on DO fluxes measured during light-dark incubations of ambient water and sediments with overlying filtered water (Kemp et al., 1997; Smith and Hollibaugh, 1997). Incubations were conducted in flow-through light gradient boxes maintained at ambient temperatures with PAR ranging from approximately 60 to approximately 2,000 $\mu\text{E m}^{-2} \text{s}^{-1}$. DO concentrations were measured before and after incubations using Hach luminescent DO sensors. On the day of sample collection, 10 water samples per site were incubated in 60 mL biological oxygen demand (BOD) bottles at 10 different light levels for approximately 1 hour, and three per site were incubated in the dark for 24 hours to obtain a measurable change in O₂. Sediment cores (7 cm sediment depth; 3.1-cm internal diameter) were held uncovered overnight in a circulating seawater bath at ambient temperatures and incubated the day following collection in a similar manner to water column incubations. Immediately before incubation, overlying water was siphoned out of each core and replaced with filtered site water (0.45 μm). Cores were incubated unstirred but incubations were kept short (1–2 hours) to minimize build-up of diffusion gradients. Before taking final DO measurements with the Hach probe, we gently mixed the overlying water to obtain a composite sample.

Metabolic rates were expressed as hourly changes in O₂ per unit volume (water column) or surface area (sediments), and per unit biomass of chl *a*. P-I curves were developed from these rates over the range of PAR used in each experiment. The Jassby and Platt (1976) hyperbolic tangent P-I model was fit to hourly metabolic rates from each site on each date as shown in Equation 5-8:

$$\text{Production} = P_{\text{max}} \cdot \tanh\left(\frac{\alpha \cdot I}{P_{\text{max}}}\right) - R \quad (\text{Eq. 5-8})$$

where P_{\max} is the maximum rate of photosynthesis, α is photosynthetic efficiency or the initial slope of the P-I curve, I is irradiance (PAR, $\mu\text{E m}^{-2} \text{s}^{-1}$), and R is respiration. P-I curves were then integrated over depth and 24-hour intervals to obtain system-level, daily estimates of GPP and R for the water column and sediments. This was accomplished by combining estimates of P_{\max} , α , and R at a given station and date with hourly PAR averaged over the month using DCERP monitoring data collected by the Atmospheric Module. Water column GPP was computed in 10-cm depth bins with irradiance attenuated using K_d computed from Equation 5-1; values were summed over station depth (0.5 m) and average depth of the upper, middle, and lower NRE (see below). Sediment GPP was similarly computed in 10-cm depth bins; rates were used from 0.5 m and average depths as for the water column. For both water and sediments, R was assumed to be constant over a 24-hour period. Water column and sediment NCP was computed as the difference between daily GPP and R , and NEM was computed as the sum of water column and sediment NCP.

Determinations of Shallow Water Benthic Gross Mineralization Rates (Autochthonous N Source): To measure autochthonous N sources in the NRE, rates of MIN were determined in sediment cores sampled at the same shallow water six stations (i.e., JACK, SWCR, WALL, FRCR, CTBY, and TRBY, **Figure 5-3**) as for metabolism and nutrient fluxes during July and October 2008, May, July, and October 2009, and March 2010. In June, September, and November 2010 and in March 2011, additional measurements were performed at SWCR, WALL, and CTBY.

Ten small polycarbonate cores (5.7-cm ID \times 20-cm tall, 10-cm depth of sediment) per site were taken for MIN measurements. Following collection, cores were uncapped and immersed in site-specific water and held overnight in the dark with constant mixing and aeration. $^{15}\text{N-NH}_4^+$ (3.6 mL of $[\text{NH}_4]_2\text{SO}_4$ [30 at %, 10 mM]) was injected for determination of MIN using the isotope pool dilution technique as described by Anderson and Collins (1997). After injecting all cores, sediment in five of the cores from each site was extracted with equal volume of 2 M potassium chloride (KCl), representing T-zero measurements; the extractant was filtered (Gelman Supor, 0.45 μm) and the filtrate frozen until analyzed. The remaining five cores per site were capped, stirred, and incubated for 24 hours in the dark in a temperature-controlled incubator (**Figure 5-8**) at in situ temperatures. At the end of the incubation, the sediment in the other five cores were extracted as previously described, representing T-final measurements, giving five replicates per site. NH_4^+ in extracts from the experiment was trapped by diffusion onto acidified filters, as described by Brooks et al. (1989). Previous studies have shown that trapping efficiencies exceed 90%. Samples were analyzed for ^{15}N enrichment at the University of California at Davis's stable isotope facility. Rates of gross MIN were calculated using a model described by Wessel and Tietema (1992).



Figure 5-8. (Left) Small sediment core used for mineralization with magnetic spinner inside core. (Right) Small sediment cores placed around large magnetic spinner in temperature-controlled incubator.

Determinations of Shallow Water Benthic NFix Rates (Autochthonous N Source)

Measurements of NFix were made on sediment cores collected at all six shallow water sites (i.e., JACK, SWCR, WALL, FRCR, CTBY, and TRBY) during May, July, August, and October 2009; March, June, and November 2010; and March and June 2011. Measurements were made using the acetylene reduction method, assuming a ratio of 4 M of acetylene reduced to 1 M of N₂ fixed. In the first three experiments, five sediment cores were subsectioned and treated as follows: 0- to 1-cm sections were incubated aerobically in the light and dark, and 1- to 3-cm sections were incubated anaerobically in the dark. All incubations were conducted in 60-mL serum bottles amended with 15 mL of acetylene for 6 hours at ambient water temperatures in an environmental growth chamber. For the October 2009 experiment, NFix was also measured in an 8–10 cm depth section, and in the 2010 experiments, an additional depth section of 3–5 cm was added. Ethylene was measured by flame ionization gas chromatography.

Characterization of N-Fixing Communities

To determine the relative importance of autotrophic cyanobacteria and heterotrophic sulfate reducing bacteria to the N-fixing process, samples from the six Research Project AE-3 stations were characterized using both molecular techniques and the molybdate inhibition technique. Cores taken in September 2011 were amended with 20 mM sodium molybdate (Na₂MoO₄), an inhibitor of sulfate reduction and compared with non-inhibited samples as described by Oremland and Capone (1988). Polymerase chain reaction (PCR) was conducted on DNA extracted from sediment samples (0–1 cm, 1–3 cm depth horizons) taken in July 2010 at 0.5 m water depth MSL to characterize the microbial communities. Nitrogenase reductase (nifH) sequences were amplified using nested PCR with the internal primer pair of nifH1 and nifH2 (Zehr and McReynolds, 1989) and the external primer pair nifH3 and nifH4 (Zani et al., 2000) to identify NFixing organisms in the sediment. The general bacterial community was identified using a 16S rDNA primer pair. Sequences were aligned in the MacVector 12.0 DNA sequence

analysis software package (Accelrys, San Diego, CA), corrected by manual inspection and analyzed for similarity in BLAST (Basic Local Alignment Search Tool, National Center for Biotechnology Information, Bethesda, MD).

Determinations of Shallow Water Denitrification Rates

In July 2008, October 2008, May 2009, and July 2009 three sediment cores (17-cm sediment \times 7.6-cm diameter, approximately 400 mL water column) and overlying water were collected from all six shallow water benthic sites (i.e., JACK, SWCR, WALL, FRCR, CTBY, and TRBY) for DNF measurements. During each sampling event, TRBY, CTBY, and FRCR were sampled prior to WALL, SWCR, and JACK sites. The two groups were sampled within 4 days of each other (3 days for 2008 and 4 days for 2009). In addition to sediment cores, approximately 75 L of water were collected from each site. Cores and water were transported back to an environmental chamber set to average ambient temperature and submerged in an aerated water bath overnight (8–12 hours) to establish equilibrium prior to the start of the continuous flow incubation.

The following morning, cores were sealed with a gas and water-tight Plexiglas top. The top contained two O-rings and two ports plumbed with Tygon tubing, one for the inflow and one for the outflow. Cores were connected to a 24-channel peristaltic pump (Lavrentyev et al., 2000; Piehler and Smyth, 2011). Site-specific water from the reservoir was continuously pulled over the cores at a flow rate of 1 mL per minute to provide a well-mixed water column. In addition, each site had a line from the reservoir that bypassed the cores and was used to account for the water chemistry entering the cores. All incubations were performed in the dark and at the average ambient temperature of the three sites.

Cores were pre-incubated for no less than 18 hours prior to sampling to ensure that the system was at steady state (Eyre and Ferguson, 2002). 5mL water samples were collected from the outflow port of each core and the site water inflow line at 18, 24, 36 and 48 hours after the start of the incubation for dissolved gas analysis. Upon collection, samples were immediately analyzed using a Balzers Prisma QME 200 quadrupole mass spectrometer (i.e., MIMS) for N₂, O₂, and Ar (Kana et al., 1994). The concentrations of N₂ and O₂ in the water were determined using the ratio with Ar as described by Ensign et al. (2008). Results from successive measurements from each core were averaged to yield core specific values. Additionally, at the 24-hour sampling, 50-mL water samples were collected for nutrient analysis from the inflow and outflow of each core. Water was filtered through Whatman GFF filters (25-mm diameter, 0.7 μ m nominal pore size), and the filtrate was analyzed with a Lachat Quick-Chem 8000 automated ion analyzer for NO₃⁻, NH₄⁺, PO₄³⁻, and TN. At the end of the incubation, the upper 2 cm of each sediment core was sampled for sediment OM determined by loss on ignition.

Flux calculations were based on the assumption of steady-state conditions and a well-mixed water column (Miller-Way and Twilley, 1996). Benthic fluxes were calculated using Equation 5-9 as follows:

$$J = ([i_{\text{outflow}}] - [i_{\text{inflow}}]) * \frac{F}{A} \quad (\text{Eq. 5-9})$$

where $[i_{\text{outflow}}]$ and $[i_{\text{inflow}}]$ is the concentration (μM) of any dissolved constituent leaving and entering the core, respectively; F is the peristaltic pump flow rate (1 hr^{-1}), and A is the surface area of the core (m^2) (Miller-Way and Twilley, 1996). Fluxes calculated using this method are net fluxes. DNF was calculated as the net positive flux of N-N_2 , and sediment oxygen demand (SOD) was calculated as the net negative flux of O_2 (Kana et al., 1994; Smith et al., 2006). For all dissolved nutrients a positive flux indicates net exchange from the sediment to the water column, and a negative flux indicates a net flux from the water column to the sediment.

Determinations of the Role of BMA in Controlling Sediment Water Nutrient Fluxes

Multiple laboratory experiments were performed in 2009 to better understand the roles that BMA play in regulating sediment–water nutrient fluxes in shallow water sediments (0.5 m water depth at MLW). An experiment conducted in June 2009 tested the interactive effects of nutrient enrichment (ambient and two times ambient loading during June at JACK) and light levels (100 and $500 \mu\text{E m}^{-2} \text{ s}^{-1}$) on benthic metabolism and nutrient fluxes in sediment cores collected in FRCR. Cores were exposed to diel conditions for 2 days, and then continuous dark for 14 days in an environmental chamber. A second similar study of the interactive effects of light and nutrients was conducted in October 2009 on cores collected from WALL and CTBY. Samples were taken at timed intervals over 18 days (2 days of diel conditions followed by 16 days of dark) to determine DO, DIN, and DIP concentrations.

Determinations of Nutrient Limitation of Benthic Metabolism

Experiments to determine whether benthic metabolism is limited by water column N were performed in July and August 2009. In the July experiment, cores were collected from FRCR, incubated for 4 hours in the light ($500 \mu\text{E m}^{-2} \text{ s}^{-1}$), and exposed to NO_3^- at concentrations ranging from 1 – $200 \mu\text{M}$ with PO_4^- added at the molar ratio of $16\text{N}:1\text{P}$. In a second nutrient limitation experiment, conducted in August 2009 on samples collected in WALL, sediment cores were exposed to NH_4^+ concentrations ranging from 0 – $100 \mu\text{M}$ with P added in the molar ratio of $16\text{N}:1\text{P}$. To separately determine the effects of nutrient additions on photosynthesis and R, cores were exposed either to a 4-hour light incubation ($500 \mu\text{E m}^{-2} \text{ s}^{-1}$) with nutrient addition, followed by a 4-hour dark incubation or an 8-hour dark exposure with nutrients. In both the July and August experiments DO was measured at timed intervals.

Scaling Up to the Estuary—Determination of Benthic Metabolism, Nutrient Fluxes, and Nitrogen-Cycling Rates at Different Water Depths

To scale measurements made at the square meter scale to the whole estuary it was necessary to measure metabolic and nutrient cycling process rates (NFix, MIN, DNF) as well as nutrient fluxes on sediment cores sampled at representative water depths across the entire estuary. For experiments conducted in July 2010 and April 2011 sediment cores were collected at sites in the upper, middle, and lower regions of the NRE at three different water depths (approximately 0.5 m, 1.5 m, and 3m MSL). Three sampling stations per region and depth were selected randomly using water depth contours determined by the NRE bathymetry study performed in 2009 (McNinch; **Figure 5-9**). The 0.5-m sites were located near or at SWCR, FRCR, and TRBY.

For determinations of benthic metabolism and nutrient fluxes, three sediment mesocosm cores (clear acrylic, 6.5 cm inner diameter x 30-cm tall, 10 cm sediment depth) were collected at each of the nine sites (three depths per each of three regions [27 cores total]). The cores were incubated at UNC-Institute of Marine Science (UNC-IMS) in Morehead City, NC, in July 2010 and at VIMS in Gloucester Point, VA, in April 2011. After returning from the field and prior to starting the incubations, overlying water from the cores was removed and replaced with filtered site-specific water cores to measure benthic processes only. Site water was filtered through a series of 142-mm filters: glass filter dryer(GFD) (2.7 μm), GFF (0.7 μm), and polyethersulfone (0.2 μm). The cores used for the benthic metabolism and nutrient fluxes were incubated in fiberglass chambers filled with water taken from the specific sampling station and held within outdoor flow-through pools at UNC-IMS for more than 24 hours to maintain in situ temperatures. At VIMS, cores were incubated for 24 hours in an environmental growth chamber at in situ temperature and light. Cores collected from the 1.5 m and 3 m water depths were covered with shade cloth to attenuate light to levels that were as similar as possible to in situ conditions. Samples were taken from the benthic flux cores at dawn, dusk, and dawn for determinations of DIC, DIN, DIP, and DON. At the end of the flux experiments, additional samples were taken for benthic chl *a*. Water samples were processed and analyzed and metabolism and nutrient flux rates were calculated as described in the *Determinations of Shallow Water Benthic Metabolism and Nutrient Fluxes* section above.

Additional sediment cores were taken from the 0.5 m and 3.0-m depth contours for determinations of DNF and from the 0.5, 1.5, and 3.0-m depth contours for N gross MIN and NFix. These experiments were conducted in the same manner as described in the previous section for the shallow water MIN, NFix, and DNF experiments, except that NFix was measured in the 0–1 cm, 1–3 cm, and 5–10 cm depth horizons.

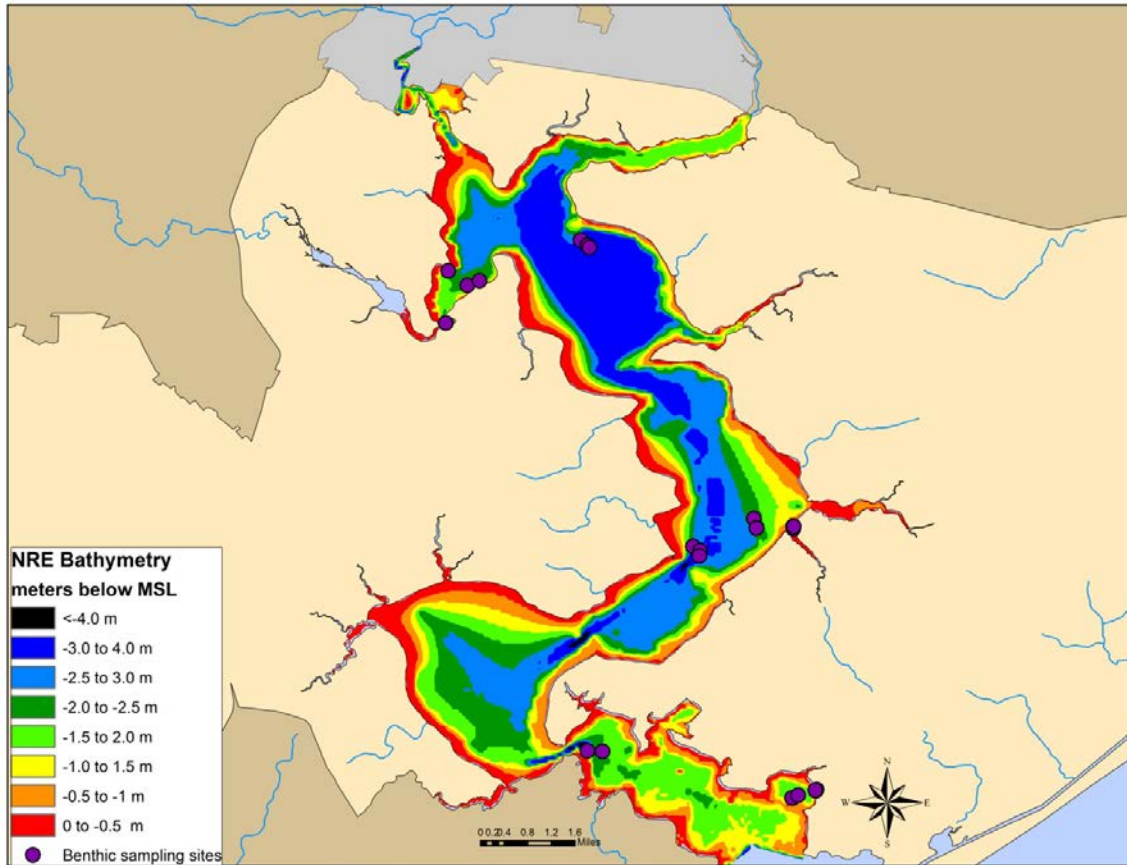


Figure 5-9. NRE bathymetry (meters below MSL; North American Vertical Datum of 1988 [NAV88]) and depth experiment sampling stations in the upper, middle, and lower regions of the estuary.

The areas of the NRE at various depths were determined for each the 9 boxes described in **Table 5-1** and **Figure 5-2** by using ArcGIS 9.3 and the 2009 NRE bathymetric data (**Table 5-5**). For scaling the measurements up to the entire estuary, Boxes 1, 2, 3, 4, and 8 were defined as the Upper region; Boxes 5, 6, and 9 as the Middle region; and Box 7 as the Lower region. Areas of depth intervals from 0.0–1.0 m were combined and applied to the 0.5-m treatment; 1.0- to 2.0-m depth intervals to the 1.5-m treatment, and greater than 2.0-m depth interval to the 3.0-m treatment (**Table 5-6**).

Table 5-5. NRE Area by Water Depth Interval for Boxes 1 to 9(1 ha = 10,000 m²)

Box	Area Description	NRE Area (m ²) by Water Depth (m) Interval				
		≤0.5	0.5–1	1–2	2–4	4–5.5
1	New River/Wilson Bay	142,676	635,006	848,897	312,134	—
2	Southwest Creek and far upper NRE	1,508,587	673,144	1,310,001	2,439,683	—
3	Northeast Creek	450,120	371,747	2,091,756	1,266,680	—
4	Morgan Bay	1,196,576	880,616	1,849,972	11,340,507	—
5	Farnell Bay	2,264,917	2,296,019	4,662,760	11,704,602	44,555
6	Stone Bay	2,912,512	2,226,286	4,689,419	6,884,849	37,767
7	Courthouse Bay, Traps Bay, and lower NRE	2,156,676	2,102,617	7,293,870	763,735	21,846
8	Wallace Creek	245,733	138,233	237,094	97,380	—
9	French Creek	458,760	122,188	—	—	—
Total Area (m²)		11,336,558	9,445,856	22,983,768	34,809,571	104,168
% of total area by depth interval		14.4%	12.0%	29.2%	44.2%	0.1%

Table 5-6. NRE Area by NRE Region and Depth Treatment(1 ha = 10,000 m²)

Region	Water Depth (m)	Total Area (m ²)	% of Total
Upper	0.5	6,242,438	7.9
	1.5	6,337,720	8.1
	3	15,456,384	19.6
Middle	0.5	10,280,682	13.1
	1.5	9,352,179	11.9
	3	18,671,774	23.7
Lower	0.5	4,259,293	5.4
	1.5	7,293,870	9.3
	3	785,581	1.0

Data Analysis

Preliminary analyses of all data (means, standard errors) were completed using Microsoft Excel. Minitab 16 (Minitab, Inc., State College, PA) was used to perform linear and non-linear (e.g., natural log) regressions and analysis of variance (ANOVA) analyses on site characterization and ecosystem process data to determine differences by site and season or region, season, and depth. Interactions between all variables were tested. Levene's test of homogeneity of variance was conducted to determine if means had similar variances. If the test was found to be significant

($p < 0.05$), data were natural log transformed. Tukey's test was used to evaluate pair-wise comparisons after a significant ANOVA; differences were considered significant at $p < 0.05$. When the assumption of homogeneity of variance could not be met, non-parametric two-way analysis of similarity (ANOSIM) was conducted on the data to determine differences by site and season using PRIMER 6 (Primer-E, Inc., Plymouth, UK; Clarke, 1993; Clarke and Warwick, 2001). Euclidean distance matrices on normalized data were used to determine a global R statistic for each main effect (site or season) as well as pairwise comparisons, similar to an F-statistic. ANOSIM then performs a permutation procedure (999 permutations) to provide a p value for the R statistic values. A Bonferroni correction ($0.05/n$; n =number of pairwise comparisons) was applied to adjust the significance level of the multiple pairwise comparisons.

Results and Discussion

Nitrogen Sources to the NRE

For MCBCL environmental management personnel to effectively respond to reductions in water quality within the NRE, it is essential that they be able to distinguish allochthonous nutrient loads derived from on- versus off-Base sources and autochthonous N produced within the NRE. To determine the relative importance of these various sources data were compiled for off-Base watersheds, the New River, Southwest Creek, and Northeast Creek, using the long-term USGS nutrient and freshwater database for the Gum Branch Gauging Station (1998–2011), for on-Base watersheds measured by Research Project AE-2 (2008–2010), for wet atmospheric deposition from the NADP database and dry deposition from the EPA CASTNET database (2000–2010), and for the MCBCL WWTF (2000–2010). Estuarine-wide autochthonous N sources, based on sediment–water fluxes of DIN, were measured by Research Project AE-3 during spring and summer at three sites along the estuarine salinity gradient and at three depth contours (0.5 m, 1.5 m, 3 m MSL). Using these depth measurements, N fluxes were scaled to the entire estuary.

As shown in **Figure 5-10**, on an annual basis off-Base watersheds contributed 64% of the total allochthonous N load to the NRE. The next largest source of N was exchange across the Onslow Bay inlet with the coastal ocean (15%). On-site watersheds provided 8% of the annual N load with smaller contributions from the MCBCL WWTF (7%) and atmospheric deposition (6%). Calculations of these loads assume that there are no losses of N due to processes such as DNF or gains, due to additional baseflow and OM MIN, during transport from the head of tides to the estuary-proper. These losses and gains likely occur both in the New River and in the smaller MCBCL tributaries studied by Research Project AE-2. An attempt to correct for these losses by USGS in 2010–2011 demonstrated the high degree of variability in short-term measurements and the difficulty in accurately correcting for tidal exchanges; thereby demonstrating the importance of using long-term databases to estimate annual N loads. For the purpose of modeling watershed impacts on the NRE, Dr. Brush computed daily freshwater yields ($\text{m}^3 \text{m}^{-2} \text{watershed d}^{-1}$) at Gum Branch from 1998 to 2010 and scaled these values to the entire watershed area draining into the New River at Jacksonville (see Chapter 6, Research Report for Research Projects AE-2 and AE-3 Model Development). Daily DIN and TN concentrations at both sites were estimated using a flow-concentration relationship for NO_x and mean concentrations of NH_4^+ and total Kjeldahl nitrogen (TKN; which were less variable with flow) using USGS data from Gum Branch (primarily 1987–2001). These concentrations were multiplied by flow to estimate daily loads. Comparison of computed DIN and TN concentrations at Gum Branch and Jacksonville using this

approach suggests only 8–9% attenuation between stations, and an overall 1.5-times increase in the load due to an increase in freshwater flow.

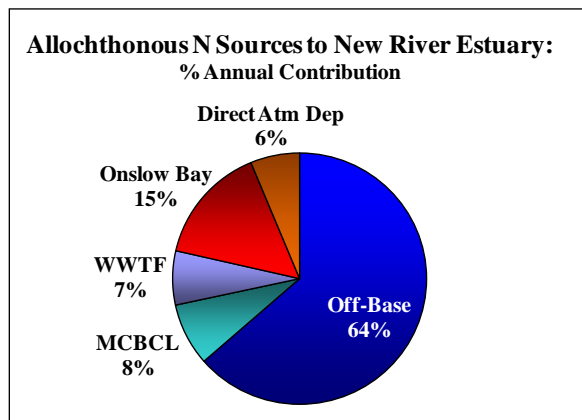


Figure 5-10. Percent contribution of allochthonous N sources to the NRE on an annual basis.

Sources included both off-Base and MCBCL watersheds, MCBCL WWTF, Onslow Bay, and direct atmospheric deposition to the NRE water surface.

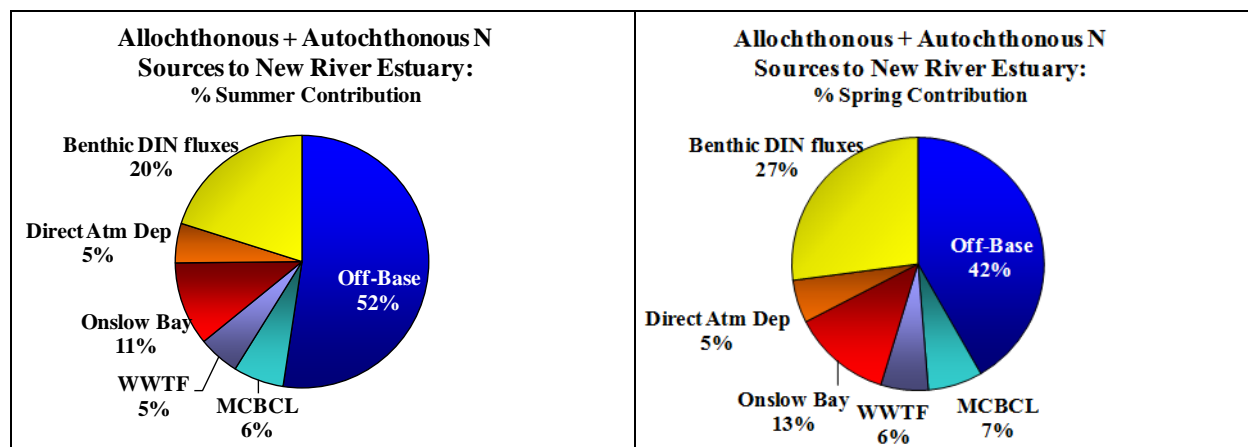


Figure 5-11. Percent contribution of allochthonous and autochthonous N sources to the NRE for summer and spring.

Allochthonous sources included both off-Base and MCBCL watersheds, MCBCL WWTF, Onslow Bay, and direct atmospheric deposition to the NRE water surface. The autochthonous source was based on benthic DIN fluxes from the sediment to the water column.

As temperatures increased during spring and summer autochthonous benthic sources of N, including NFix and MIN, became increasingly important, resulting in increased fluxes of DIN from sediments to the water column, ranging from 20–27% of the TN load to the NRE (**Figure 5-11**). This regenerated DIN may be especially important for support of pelagic primary production resulting in phytoplankton blooms mid-estuary during periods of low freshwater discharge (Hall et al., in revision; Chapter 3, Research Project AE-1 Final Report). However, when light was sufficient, the benthic filter can play an important role in reducing sediment–water fluxes of DIN. These data suggest that steps undertaken to manage water quality to meet state criteria and requirements of the Clean Water Act will be most effective when applied to off-site watersheds. They also demonstrate that the benthos can potentially be an important source of

N supporting pelagic eutrophication and those activities (development or training activities increasing sediment inputs to the water column) that reduce the availability of light to the benthos should be avoided when possible.

Estuarine Gradients in Sediment and Water Quality

Sediment Characteristics

The ability of benthic processes to remove or sequester N varies with sediment type, organic content and composition, nutrient and sulfide content, and composition of the benthic microbial community. Sediments were characterized seasonally throughout the Research Project AE-3 study from 2007–2011. Significant differences in sediment characteristics were observed along the estuarine gradient, with lowest bulk density, low sand content, and high OM content at the head of the estuary near Jacksonville and highest bulk density, high sand content, and low OM content down-estuary (**Figures 5-12 and 5-13; Table 5-7**). Ratios of sediment C:N content averaged 23.4 at JACK and SWCR and 11.6 and 11.1 at mid and down-estuary sites, respectively, suggesting that sources of OM in up-estuary sites were terrestrial and those down-estuary were autochthonous (**Figure 5-13**). Pore water sulfide resulting from OM decomposition was high especially during summer up-estuary at JACK, SWCR, and WALL and low at all other sites (**Figure 5-13**). Benthic chl *a*, a proxy for BMA abundance, extractable NH_4^+ , and pore water NH_4^+ (data not shown) were significantly higher up-estuary; benthic chl *a* was highest in fall and NH_4^+ in summer (**Figures 5-13 and 5-14; Table 5-7**; $p \leq 0.001$). Analysis of benthic pigments performed at UNC-IMS demonstrated increasing ratios of fucoxanthin:chl *a* and decreasing ratios of zeaxanthin:chl *a* along the estuarine gradient from JACK to TRBY suggesting that up-estuary (JACK, SWCR) cyanobacteria potentially played an important role in benthic autotrophy during summer whereas diatoms were increasingly important benthic autotrophs down estuary with little seasonal variation (**Figure 5-14**). Microscopic counts were performed to distinguish the relative importance of benthic versus pelagic diatoms in surface sediments. Whereas benthic diatoms are pennate, pelagic diatoms are usually centric in shape. Pennate diatoms accounted for greater than 90% of the total diatom count during May and July (**Figure 5-15**). Although molecular analysis by PCR, conducted on DNA extracted from sediment samples (0–1 cm, 1–3 cm) taken in July 2010 at 0.5 m water depth to characterize the microbial community demonstrated the presence of cyanobacteria in sediments throughout the estuary (see **Figure 5-41**), they tended to make up a small fraction of the photoautotrophs counted except at JACK.

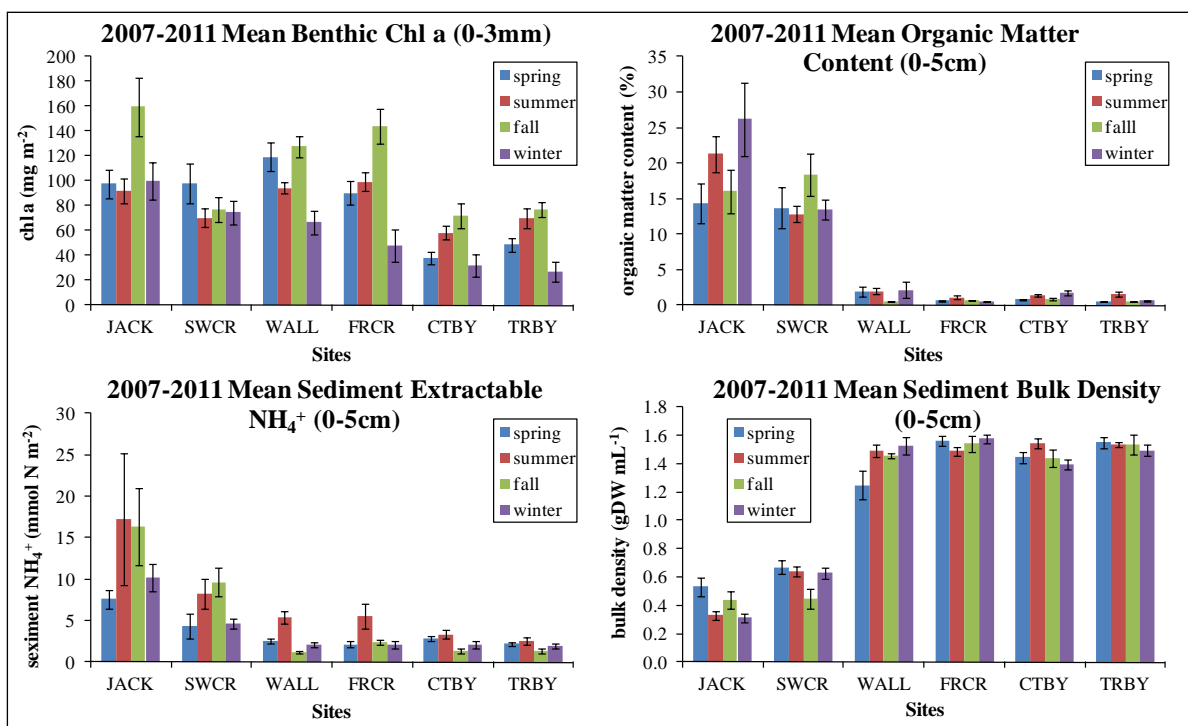


Figure 5-12. Benthic chl *a* (0–3 mm depth horizon), sediment OM content, sediment extractable NH₄⁺, and sediment bulk density (0–5 cm depth horizon) (mean ± standard error) measured at six stations (0.5 m water depth) from July 2007 to December 2011.

Sites are arranged (left to right) from up- to down-estuary.

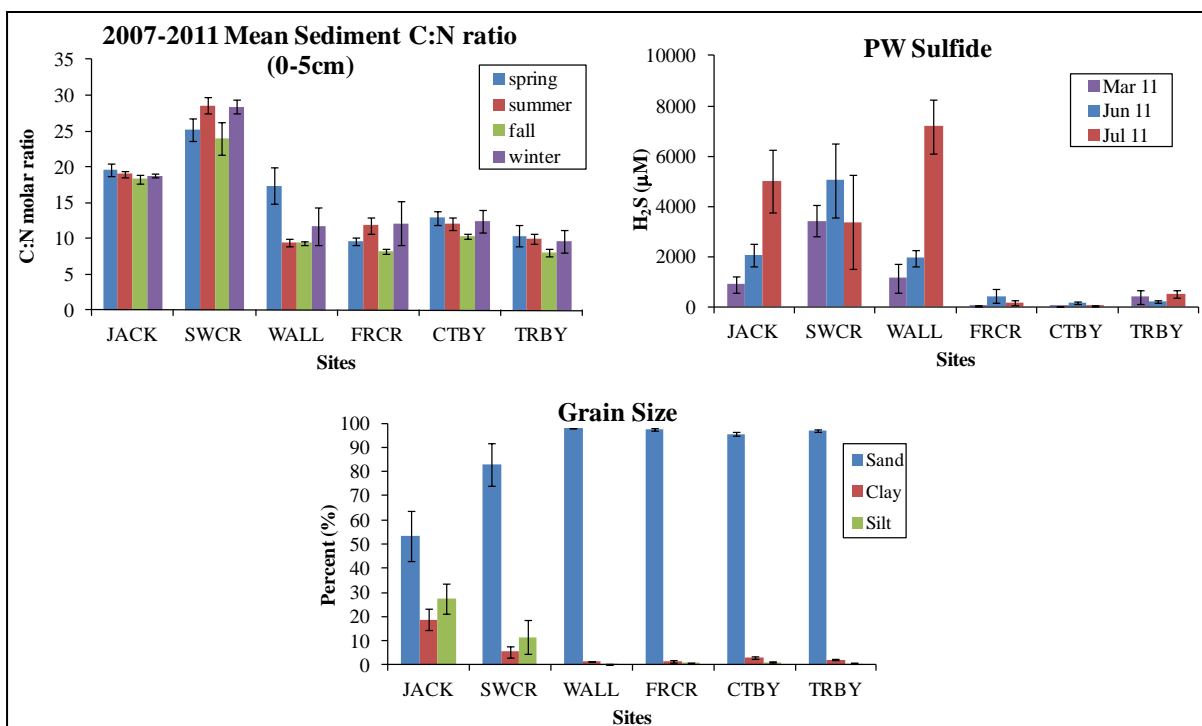


Figure 5-13. Sediment C:N ratio (0–5 cm depth horizon) from 2007 to December 2011, porewater sulfide from 2011, and percent sediment grain size type from July 2008 (mean \pm standard error) measured at six stations (0.5 m water depth).

Sites are arranged (left to right) from up- to down-estuary.

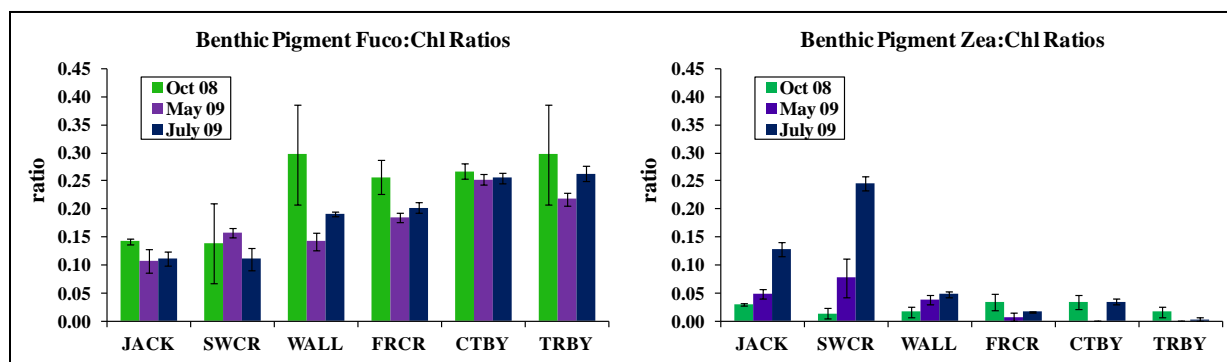


Figure 5-14. Benthic pigment Fuco:chl ratio and Zea:chl ratios (0–3 mm depth horizon) (mean \pm standard error) measured at six stations (0.5 m water depth) from October 2008 to July 2009.

Sites are arranged (left to right) from up- to down-estuary.

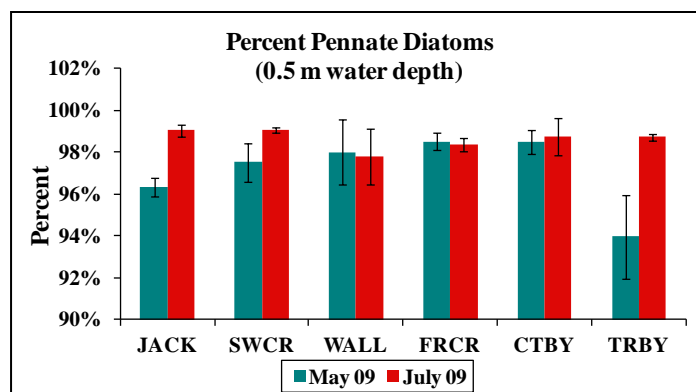


Figure 5-15. Percentage pennate diatoms of total diatoms (pennate and centric) (0–3 mm depth horizon) (mean \pm standard error) measured at six stations (0.5 m water depth) in May and July 2009.

Sites are arranged (left to right) from up- to down-estuary.

Water Quality

Similar to variations in sediment quality, water quality variables likely to impact the benthic filter also demonstrated significant variation down estuary (**Figures 5-16 and 5-17; Table 5-8; $p \leq 0.001$**). In particular K_d and CDOM concentrations were significantly higher in winter at up-estuary stations at sites where most phytoplankton blooms occur (Peierls, et al., in press; Chapter 3, Research Project AE-1 Final Report). Variations in turbidity were not significant although turbidity tended to be highest at both the upper and lower stations in the estuary. Water column chl *a* was highest in summer and fall at up-estuary stations. DIN, DON, and DIP were all highest up-estuary. These sediment and water column results all suggest that the sources of nutrients and particulates affecting light availability and primary production are the New River, Northeast and Southwest Creeks. The dominant dissolved form of N in the NRE was DON, which on average accounted for 87% of the DN (**Figure 5-18**). Tests of lability of the DON by measurement of water column MIN suggest that the DON transported down estuary is recalcitrant and not an important source of N supporting phytoplankton production (Maxey, 2012).

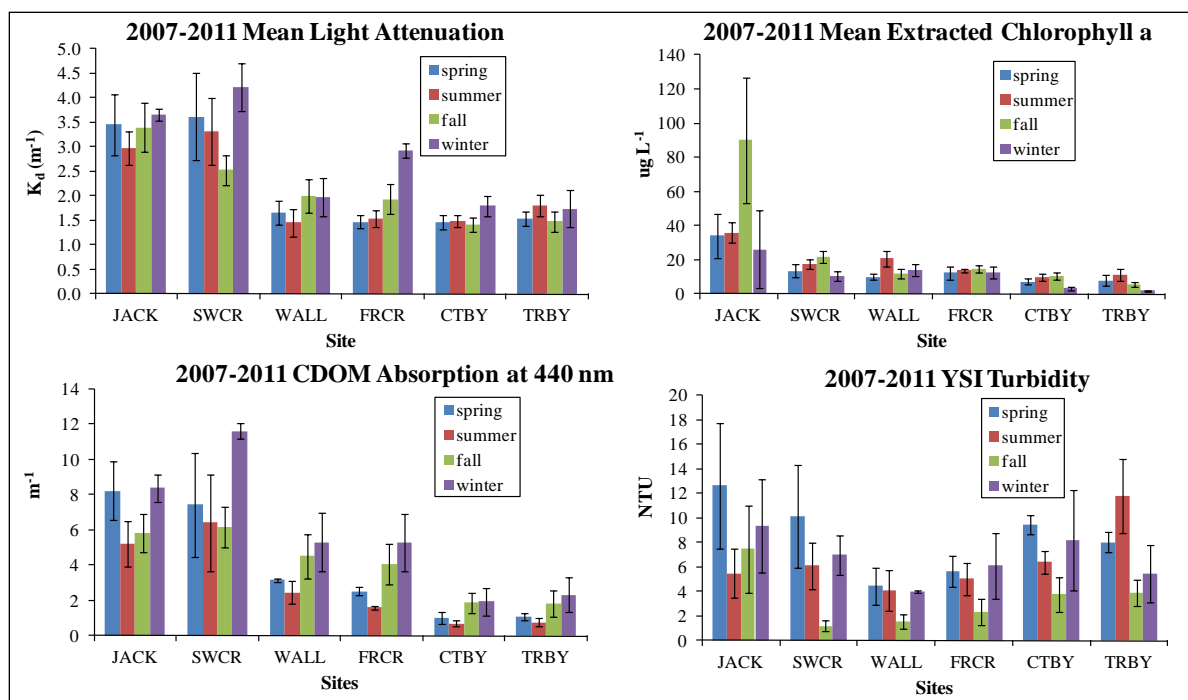


Figure 5-16. Light attenuation, extracted chl *a*, CDOM absorption, and YSI turbidity (mean \pm standard error) measured at six stations from July 2007 to December 2011.

Sites are arranged (left to right) from up- to down-estuary.

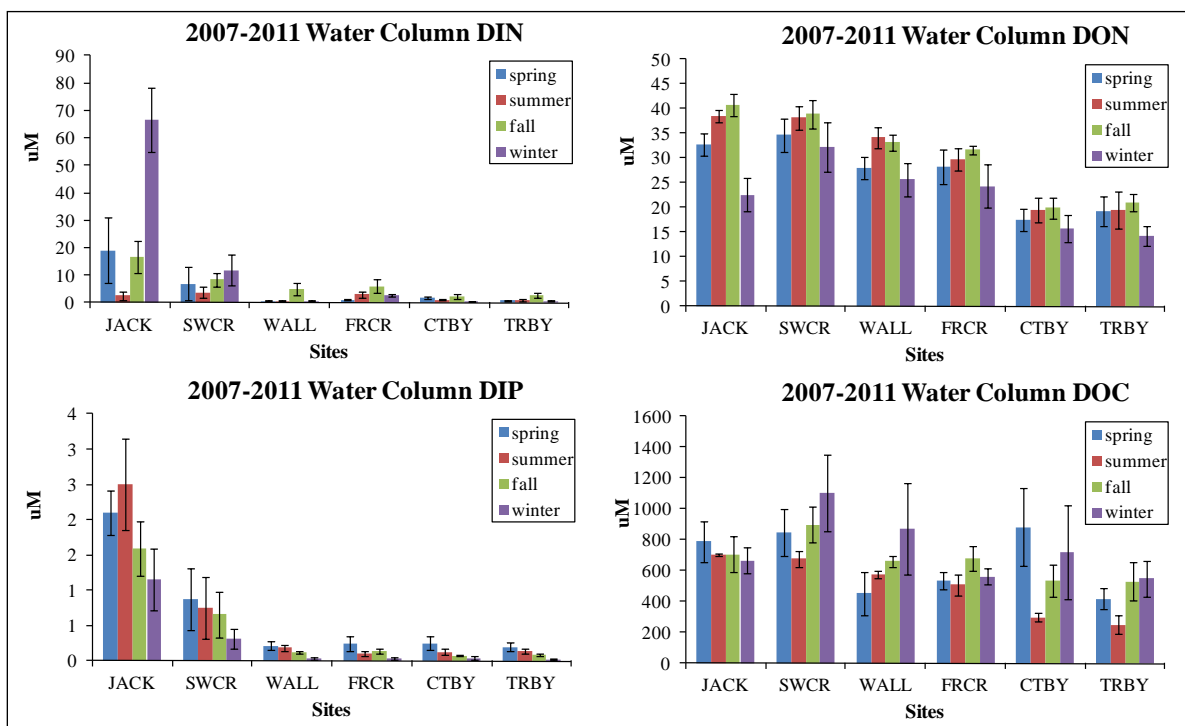


Figure 5-17. Surface water DIN, DON, DIP, and DOC (mean \pm standard error) measured at six stations from July 2007 to December 2011.

Sites are arranged (left to right) from up- to down-estuary.

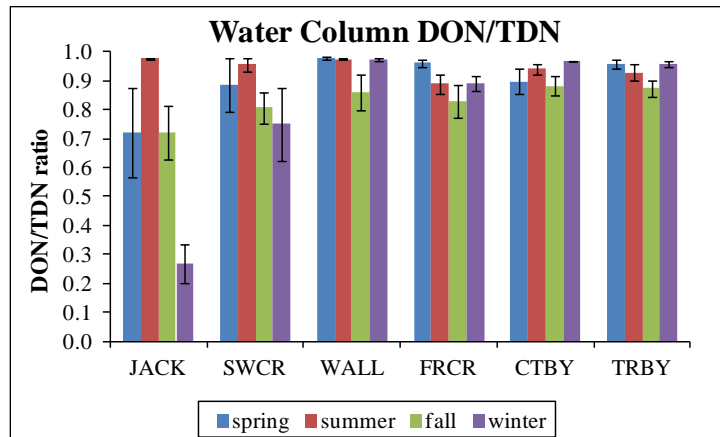


Figure 5-18. Mean (\pm standard error) water column nutrient concentration ratio of DON to TDN, measured at six stations from July 2007 to December 2011.

Sites are arranged (left to right) from up- to down-estuary.

Table 5-7. Summary of the Two-Way ANOSIMs of Sediment Characterization Data (0.5 m water depth) and Water Column DIP by Site and Season Measured from 2007–2011

Parameter	n	Global Test R Values	Site p Value	Season p Value	Site Effect	Season Effect
Benthic chl <i>a</i>	406	0.11, 0.087	0.001	0.001	JACK > (WALL, CTBY, and TRBY)	Fall > (spring, summer, and winter)
					WALL > (SWCR, CTBY, and TRBY)	
					FRCR > (CTBY and TRBY)	
Sediment organic content (%)	236	0.396, 0.02	0.001	0.243	JACK > SWCR > (WALL, FRCR, CTBY, and TRBY)	Not significant
					CTBY > TRBY	
Sediment extractable NH ₄ ⁺	187	0.243, 0.149	0.001	0.001	JACK > (SWCR, WALL, FRCR, CTBY, and TRBY)	Summer > (fall, spring, and winter)
					SWCR > (WALL, CTBY, and TRBY)	Fall > spring
Sediment bulk density	255	0.565, 0.043	0.001	0.022	(WALL, FRCR, CTBY, and TRBY) > (JACK and SWCR)	Not significant
Water column DIP	106	0.209, 0.072	0.001	0.054	JACK > (WALL, FRCR, CTBY, and TRBY)	Not significant

Note: The table provides a summary of the two-way ANOSIMs of the July 2007 to December 2011 benthic chl *a* (0–3mm depth horizon), sediment OM content (0–5 cm depth horizon), sediment extractable NH₄⁺ (0–5 cm depth horizon), sediment bulk density (0–5 cm depth horizon), and water column DIP data with the parameter evaluated, number of samples (n), the global test R values for the main effects (site, season), the probability for each of the main effects (site, season), and the significant ANOSIM pair-wise comparisons for the main effects. The alpha values for the pair-wise comparisons were 0.0033 (0.05/15) and 0.0083 (0.05/6) after application of the Bonferroni correction for site and season, respectively.

Table 5-8. Summary of the Two-Way ANOVAs of Water Quality Parameters by Site and Season Measured from 2007–2011

Parameter	n	F	df	Site p Value	Season p Value	Interaction p Value	Site Effect	Season Effect
Light attenuation (K_d)	112	17.38, 2.96, 0.78	5, 3, 15, 88	<0.0001	0.037	0.701	(JACK and SWCR) > (WALL, FRCR, CTBY, TRBY)	Winter > summer
Water column extracted chl <i>a</i>	101	13.82, 7.93, 1.40	5, 3, 15, 77	<0.0001	<0.0001	0.171	JACK > (WALL and FRCR) > (CTBY and TRBY)	(Summer and fall) > winter
							SWCR > (CTBY and TRBY)	
CDOM (absorption at 440 nm)	106	27.28, 7.78, 0.34	5, 3, 15, 82	<0.0001	<0.0001	0.998	(JACK and SWCR) > (WALL and FRCR) > (CTBY and TRBY)	Winter > (spring and summer)
								fall > summer
Turbidity	112	2.26, 9.97, 1.69	5, 3, 15, 88	0.055	<0.0001	0.785	Not significant	(Spring, winter, and summer) > fall
Water column DIN	106	10.21, 4.48, 1.66	5, 3, 15, 82	<0.0001	0.006	0.077	JACK > (WALL, FRCR, CTBY, TRBY)	Fall > summer
							SWCR > (WALL and TRBY)	
Water column DON	95	32.18, 11.29, 0.69	5, 3, 15, 71	<0.0001	<0.0001	0.781	SWCR > (WALL and FRCR) > (CTBY and TRBY)	Fall > (spring and winter)
							JACK > FRCR > (CTBY and TRBY)	Summer > winter
Water column DOC	89	4.74, 2.15, 0.96	5, 3, 15, 65	0.001	0.103	0.503	SWCR > (CTBY and TRBY)	Not significant
							JACK > TRBY	

Note: Summary of the two-way ANOVAs of the July 2007 to December 2011 light attenuation, water column extracted chl *a*, CDOM, YSI turbidity, and water column DIN, DON, and DOC data with the parameter evaluated, number of samples (n), the F-statistic (site, season, interaction) and degrees of freedom (site, season, interaction, error), the probability for each of the main effects (site, season) and interactions terms, the significant Tukey's pair-wise comparisons ($p < 0.05$) for the main effects. Light attenuation, water column extracted chl *a*, CDOM, and water column DOC were natural log transformed. Turbidity and water column DIN were transformed as $\ln(x+1)$.

Effects of Environmental Variables on Water Quality, Light Availability, and Distribution of Benthic Chl *a*

Freshwater Discharge

Freshwater discharge measured in the New River at Gum Branch varied dramatically during the course of study by Research Project AE-3 (**Figure 5-19**). Annual mean discharge ($\text{m}^3 \text{s}^{-1}$) was well below average in 2008, slightly below average in 2009, average in 2010, and well below average in 2011 affecting delivery of nutrients, CDOM, particulates, and estuarine photic area (see below).

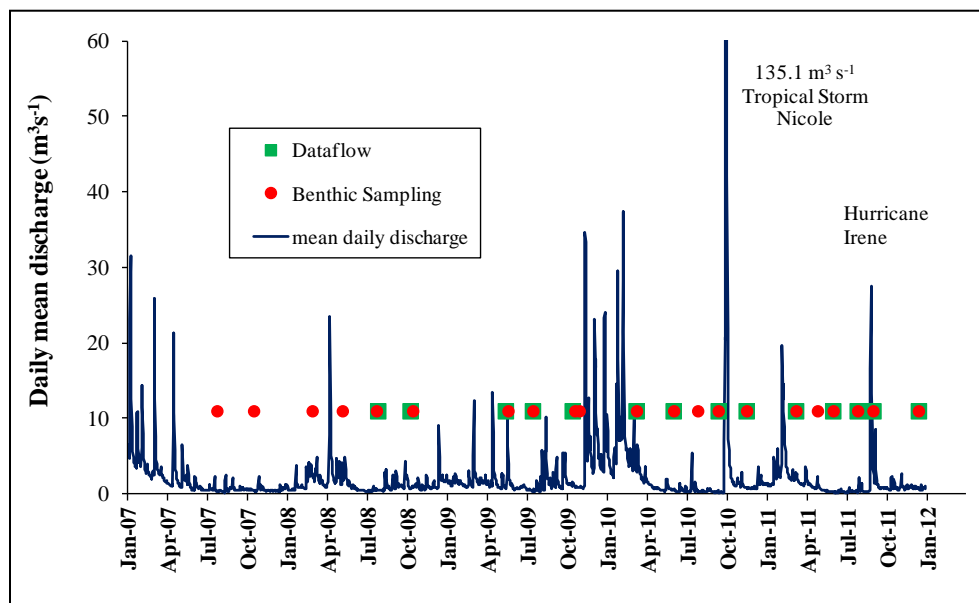


Figure 5-19. Mean daily freshwater flow at the USGS Gum Branch Station number 02093000.

Red circles denote the dates of the benthic sampling and green squares the dates of the 2008–2011 Dataflow system surveys.

Interpolated maps of water quality data collected during Dataflow surveys conducted from 2008–2011 show the expected variations in water quality parameters with freshwater discharge (**Figures 5-20, 5-21, and 5-22**). For example, comparison of parameters during a dry period, July 2011, and a very wet period, 5-days after passage of Hurricane Irene in September 2011 showed high salinity, low CDOM, K_d , and chl *a* during the dry spell and low salinity, high CDOM, K_d , and moderate chl *a* after the wet period. These data suggest nutrient limitation of primary production and an effective benthic filter during July with light limitation of primary production and a less effective benthic filter during September.

Using CDOM, turbidity, and chl *a* data collected from near-shore Dataflow surveys and the 2009 bathymetry data, the percentage of the NRE benthos receiving $\geq 1\%$ surface irradiance (I_0) was calculated according to Equation 5-1. The benthic photic zone was defined as the area of bottom that received $\geq 1\%$ of I_0 . **Table 5-9** demonstrates that the percentage of the benthos in the photic zone was sensitive to freshwater discharge, ranging from a low of 38% in September 2011

following passage of Hurricane Irene to a high of 91% in July 2008, a period of low flow. Regression analysis showed a significant relationship between mean freshwater discharge and benthic photic area, with discharge explaining 69% of the observed variation in photic area ($p \leq 0.001$; **Figure 5-23**). Because a lag is expected before the effects of variation in photic area and production of BMA biomass, measured as benthic chl *a*, we compared winter freshwater discharge with average estuarine benthic chl *a* measured during the following spring. The regression indicated a significant relationship with winter freshwater discharge explaining 63% of the variation in spring benthic chl *a* ($p = 0.002$; **Figure 5-24**).

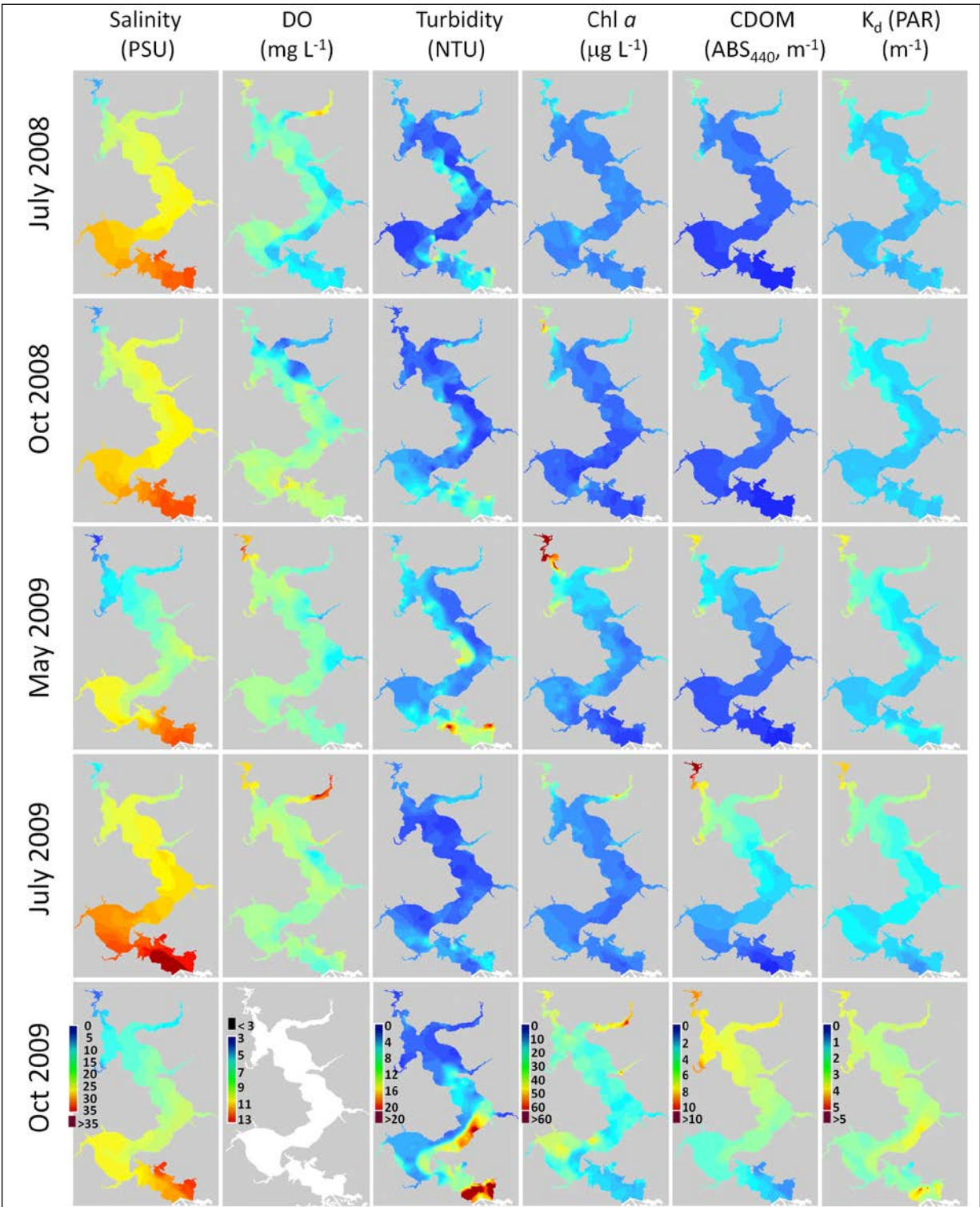


Figure 5-20. Interpolated maps of surface water quality determined from nearshore Dataflow systems surveys in 2008 and 2009.

During the October 2009 survey, the dissolved oxygen probe failed, thus the data were not interpolated. Color bars range from 0 (blue or black) to 35 for salinity, 13 for DO, 20 for NTU, 60 for chl *a* (calibrated to extracted values), 10 for CDOM, and 5 for K_d(PAR) (red). Concentrations that exceeded these upper limits are dark red.

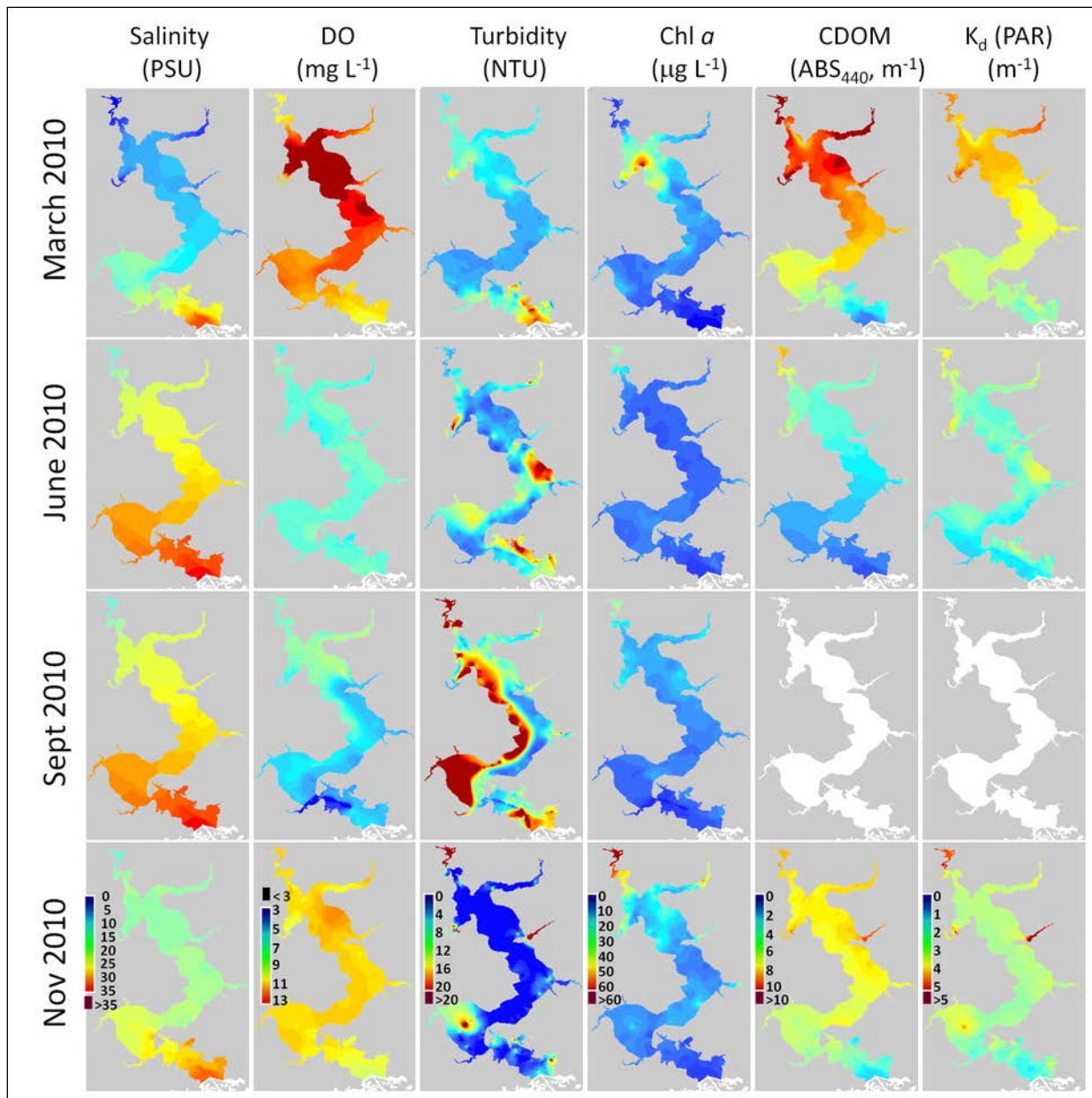


Figure 5-21. Interpolated maps of surface water quality determined from nearshore Dataflow systems surveys in 2010.

Significant portions of the CDOM and K_d (PAR) data were missing from the September 2010 survey, thus the data were not interpolated. Color bars range from 0 (blue or black) to 35 for salinity, 13 for DO, 20 for NTU, 60 for chl *a* (calibrated to extracted values), 10 for CDOM, and 5 for K_d (PAR; red). Concentrations that exceeded these upper limits are dark red.

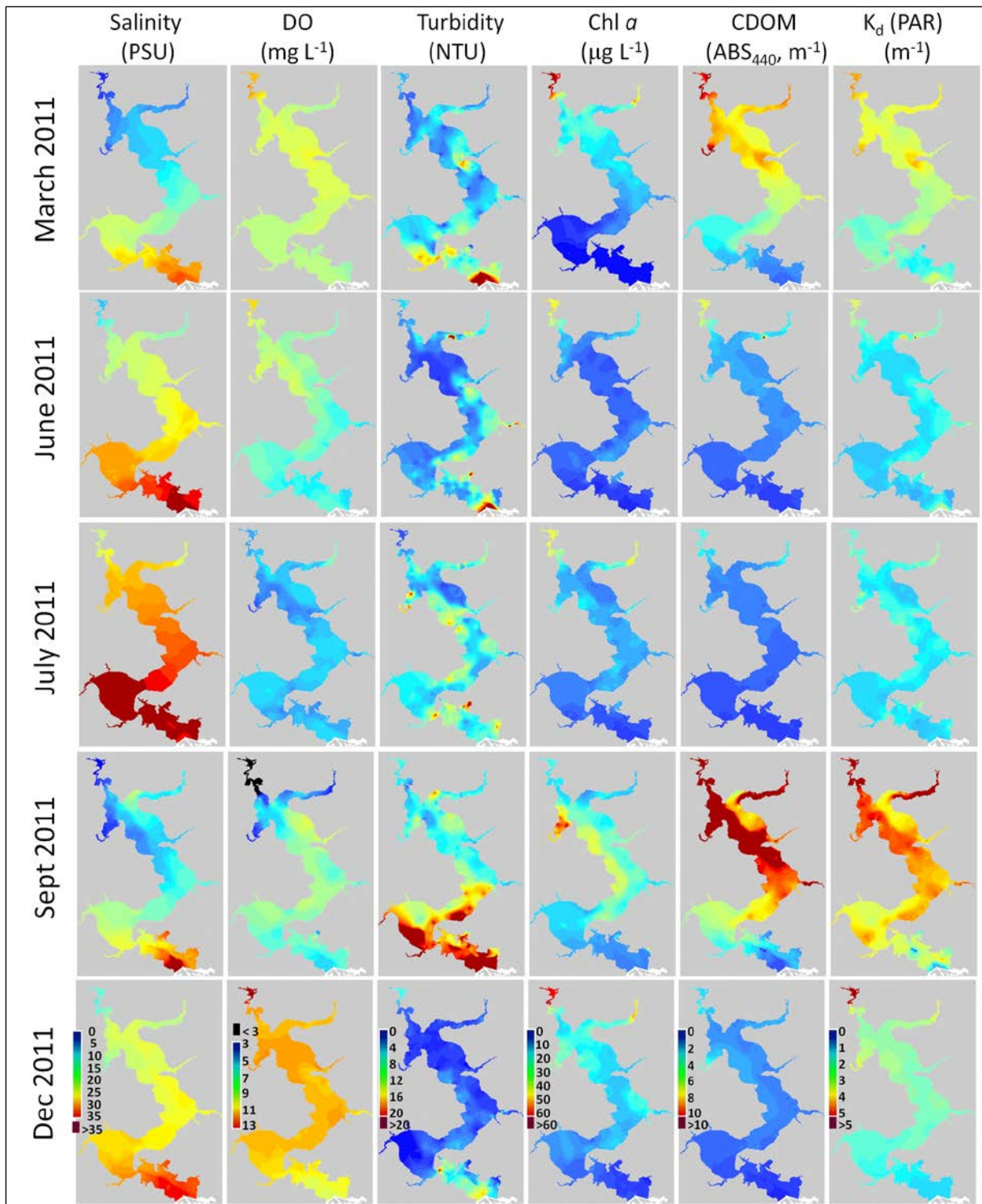


Figure 5-22. Interpolated maps of surface water quality determined from nearshore Dataflow systems surveys in 2011.

Color bars range from 0 (blue or black) to 35 for salinity, 13 for DO, 20 for NTU, 60 for chl *a* (calibrated to extracted values), 10 for CDOM, and 5 for K_d (PAR; red). Concentrations that exceeded these upper limits are dark red.

Table 5-9. Computed Percentages of the NRE Bottom Area Receiving at Least 20%, 10%, and 1% of the Surface Irradiance (I_0) Based on Computed K_d (PAR) from Nearshore Dataflow System Mapping Surveys

Date	$\geq 20\% I_0$	$\geq 10\% I_0$	$\geq 1\% I_0$
7/25/2008	32.3	48.1	91.0
10/7/2008	30.4	43.3	85.6
5/13/2009	28.3	38.8	79.2
7/14/2009	27.5	38.5	73.3
10/13/2009	20.0	26.4	52.4
3/8/2010	19.1	24.9	46.3
6/1/2010	23.4	31.7	65.0
11/15/2010	20.3	26.8	52.3
3/8/2011	20.6	27.4	53.4
6/1/2011	28.5	40.0	81.3
7/27/2011	27.8	39.4	81.2
9/1/2011	16.3	21.2	38.2
12/14/2011	24.0	32.6	61.7

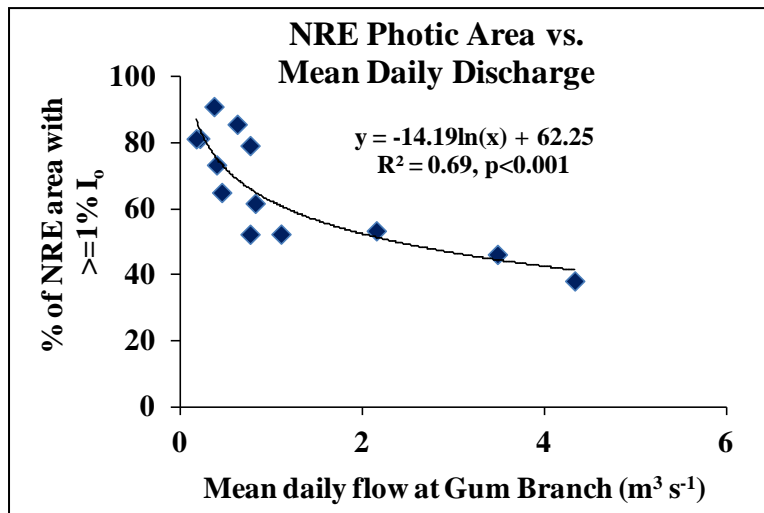


Figure 5-23. Regression of percentage of the NRE area with $\geq 1\%$ surface irradiance (I_0) reaching the bottom versus daily mean freshwater flow at the USGS Gum Branch Station.

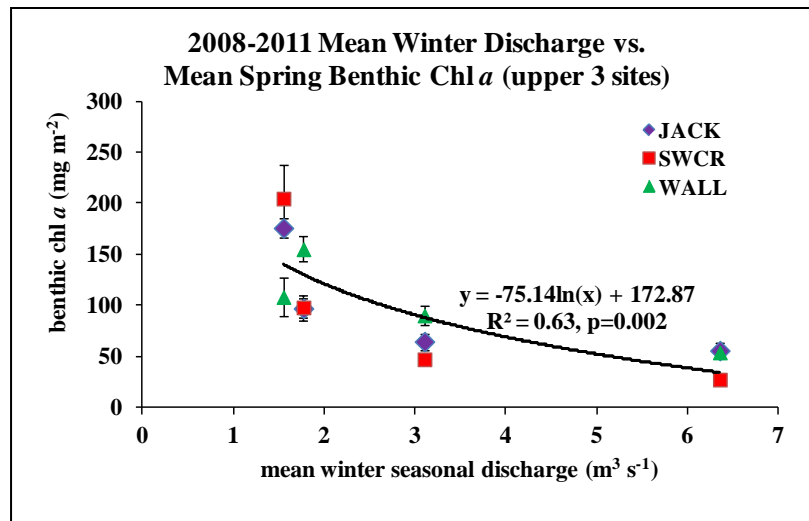


Figure 5-24. Regression of mean (\pm standard error) spring (April–June) benthic chl *a* (0–3 mm depth horizon; 0.5–m water depth) at three upper NRE stations versus mean winter seasonal discharge (January–March) at the USGS Gum Branch Station from 2008–2011.

*Variations in Benthic Chl *a* Distribution with Water Depth: Effects of Wind*

Benthic microalgal biomass, as represented by benthic chl *a*, in subtidal sediments was high throughout the NRE to depths up to 2 m (**Figure 5-25**). Shallow subtidal sediments (0.25 m in depth) averaged at least 100 mg of chl *a* m⁻², whereas deep sediments (2.0 m in depth) maintained an average of at least 30 mg of chl *a* m⁻². The relationship between chl *a* and depth varied along the estuarine salinity gradient (**Figure 5-25**). In the upper NRE, chl *a* was highest at 0.25- and 0.5-m depths, and then sharply declined with depth, whereas at mid-estuary sites, chl *a* abundances were similar at all depths from 0.25 m to 1.5 m. At lower estuary sites, chl *a*, averaged across all stations, also showed a decline with depth. Along the entire NRE sediment chl *a* values generally declined down-estuary across all depths (**Figure 5-25**).

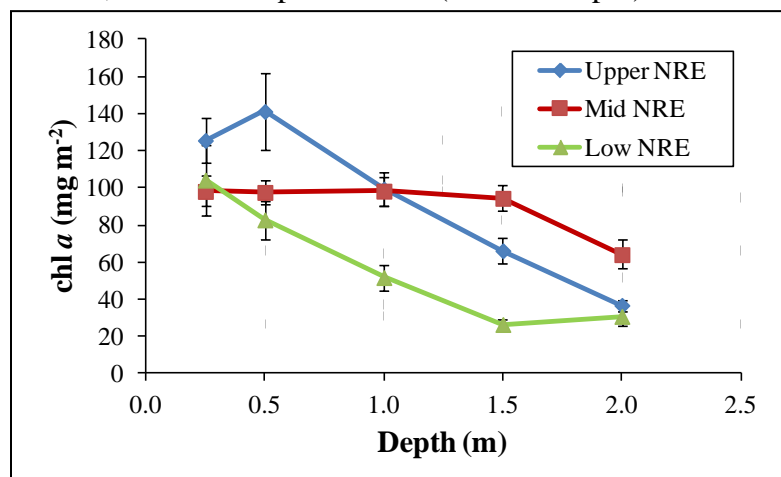


Figure 5-25. Linkage between mean (\pm standard error) benthic chl *a* (0–3 mm depth horizon) and depth grouped by upper, middle, and lower regions of the NRE.

The distribution of chl *a* across the 0.25- to 2.0-m depth gradient varied considerably between stations, as did the depth at which peak biomass was found (**Figure 5-26**). Overall there was a positive relationship between calculated RWE of each station and the depth at which peak biomass was located (**Figure 5-26**), suggesting that at higher energy locations, wave energy

limited microalgal biomass due to resuspension of sediment. Within each portion of the estuary the sites with lowest wave energy values had peak benthic chl *a* values at the shallowest depth sampled (0.25 m); these include NRAS and SWCR in the upper estuary, Across Hospital Point (AHPT) and K2 Impact Area (K2IM) in the mid-estuary, and CTBY and Stone Bay Tributary (STTR) in the lower estuary (**Figure 5-26**). These low-energy stations were the only stations in which the highest BMA biomass was found at the shallowest depth. As RWE increased, the peak in BMA biomass tended to be found at deeper depths. In the upper estuary, higher energy stations (Ragged Point [RGPT], Paradise Point [PRPT], Montford Point [MONT]) had peak biomass at 0.5-m and 1.0-m depths (**Figure 5-26**). In the mid-estuary where stations generally had higher RWE values, peak biomass at high energy stations was found at depths between 1.0 m to 2.0 m (HPPT). In the low-estuary, the two highest energy stations (Traps/Wilkins Bluff [TRWB] and STBY) had peak BMA biomass at depths of 2.0 m and 0.5 m, respectively (**Figure 5-26**).

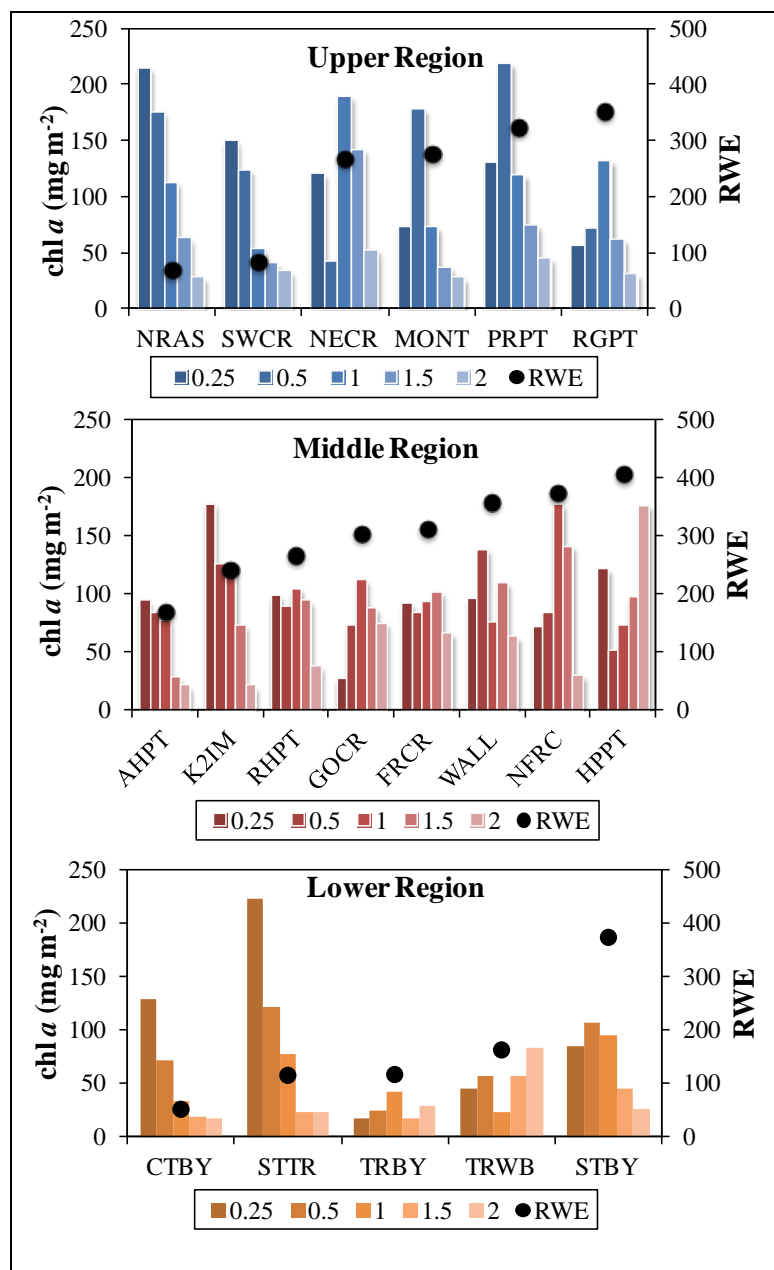


Figure 5-26. Depth gradient of benthic chl *a* (0–3 mm depth horizon) and RWE from stations located in upper, middle, and lower regions of the NRE.

RWE calculated as wave energy at 1-m depth location for each station.

Bio-optical Model

Calibration of the bio-optical model included scaling the absorption and scattering components of light attenuation by regression against measured water quality parameters: TSS for non-algal particulates absorption and particulate scattering, and chl *a* for phytoplankton absorption. A linear relationship was observed between algal particulate absorption and chl *a* concentrations throughout the estuary with approximately a two-fold difference in the absorption and scattering properties of TSS and the b_b/b ratio along the estuary. TSS-specific scattering and absorption coefficients and b_b/b demonstrated a down-estuary gradient, consistent with a downstream decrease in the organic:inorganic composition of particulates and/or a downstream increase in particulate size. The lower b_b/b ratio in the upper estuary reduced the influence of TSS on

$K_d(\text{PAR})$, as only backscattered light reduces the amount of light reaching the bottom. In the lower estuary where b_b/b ratios are higher, similar concentrations of TSS had a greater impact on light availability. The bio-optical model allows us to predict the sensitivity of light availability to the nature of water quality constituents, as well as their concentrations. Percent change in light availability was calculated at specific depths under similar water quality conditions for different sections of the estuary, allowing estimation of downstream effects on benthic primary production associated with changes in particulate composition and size. Small changes in $K_d(\text{PAR})$ associated with b_b/b shifts were more important when light availability was low, for example in deeper waters with reduced clarity. In the more transparent and shallower (approximately 1.5 m water depth) lower estuary, reductions of the relatively high b_b/b lowered $K_d(\text{PAR})$ and increased light at the 1.5 m bottom depth by up to 20%. In the deeper (approximately 1.5 m to 3.0 m) and less transparent upper estuary, increases in b_b/b could potentially reduce light availability at the 2-m depth by more than 30%. The relative impact on production from changes in light availability increases with depth and depends on P-I relationships.

Managers concerned with preserving or enhancing benthic primary production light requirements need to consider all factors affecting light availability: water depth and the spatial and temporal variations of concentration of water quality constituents and their optical properties. The bio-optical model is a decision-support tool that allows managers to evaluate the areal extent of the benthos meeting biological light requirements under a range of prescribed water quality conditions that could be expected with land-use changes or storm events. The bio-optical model also allows managers to assess the relative impacts of erosion, resuspension, and phytoplankton bloom conditions on benthic primary production. Calibrated bio-optical models can also be used to guide seagrass restoration efforts (Kenworthy et al., submitted).

Shallow Water Metabolism and Nutrient Flux Studies

Relationship Between Benthic Metabolism and Nutrient Fluxes

To identify the mechanisms responsible for the functions of the benthic filter and their responses to environmental variables we performed four seasonal studies of benthic metabolism (GPP, R, NCP) and nutrient fluxes at six shallow (0.5 m MLW) stations along the NRE estuarine salinity gradient. **Figure 5-27** shows metabolic results in units of C. Negative bars for NCP, calculated as $-(\text{GPP}-\text{R})$, represent net autotrophy (net C uptake by the benthos) and positive bars net heterotrophy (net C release to the water column). Results of data analysis by two-way ANOVA and by ANOSIM indicated that GPP and R were significantly higher during summer 2008 and 2009 (**Tables 5-10 and 5-11**). NCP was generally net autotrophic at most sites and most seasons except occasionally for up-estuary stations and at mid-estuary station during summer 2008. Daily NH_4^+ and PO_4^{3-} fluxes from sediments to the water column and $\text{NO}_3^- + \text{NO}_2^-$ (NO_x) uptake by sediments were significantly highest at up-estuary stations during spring (May 2009) (**Figure 5-28**). Regression of NH_4^+ fluxes versus benthic NCP showed a highly significant relationship with NCP explaining 59% of the observed NH_4^+ flux (**Figure 5-29**). Net autotrophic stations were sinks and net heterotrophic stations sources of NH_4^+ to the water column; thus, NCP serves as an important indicator of the effectiveness of the benthic filter. During May 2009 at the organic and sulfide-rich JACK and SWCR sites, benthic uptake of NO_3^- explained 92% of the flux of NH_4^+ out of sediments to the water column, suggesting the occurrence of DNRA at that site (**Figure 5-30**).

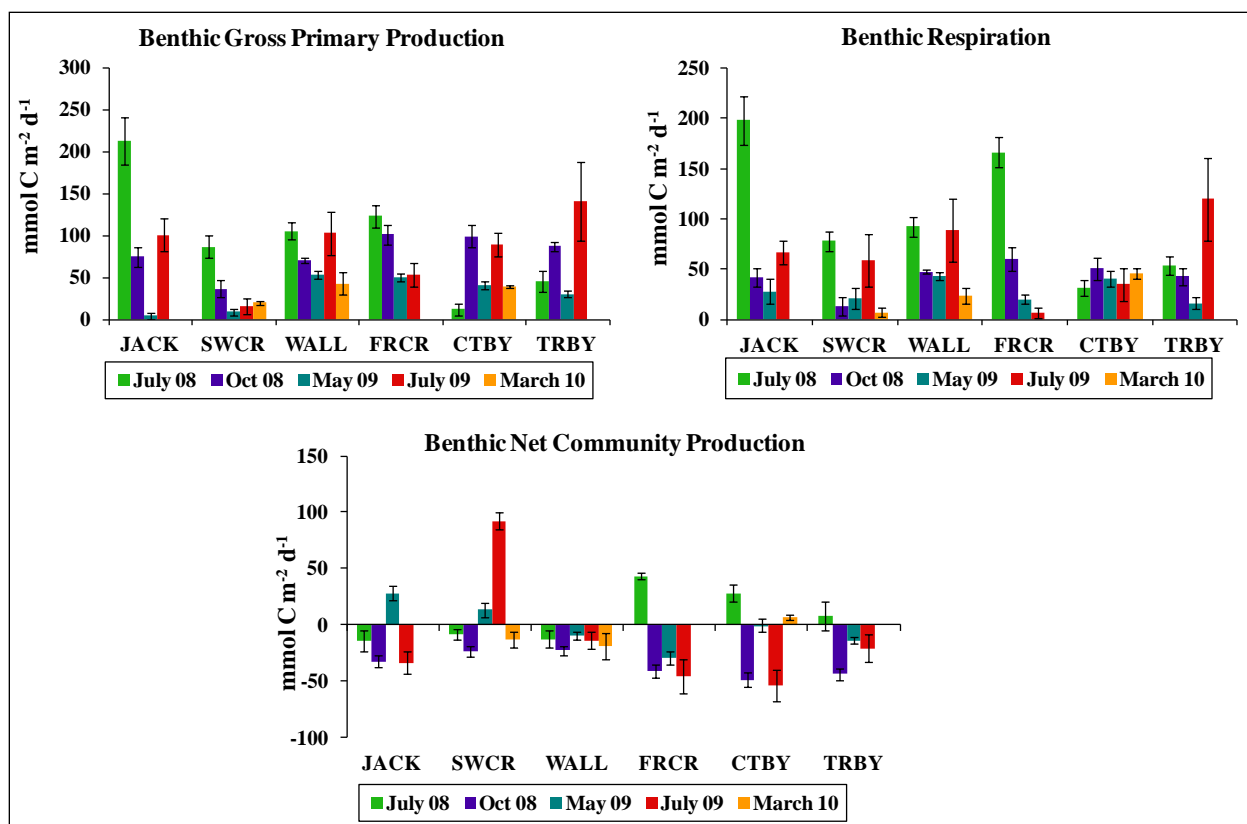


Figure 5-27. Mean (\pm standard error) benthic GPP, R, and NCP measured at six stations (0.5 m water depth) from July 2008 to July 2009 and three stations (i.e., SWCR, WALL, and CTBY) in March 2010.

Sites are arranged (left to right) from up- to down-estuary.

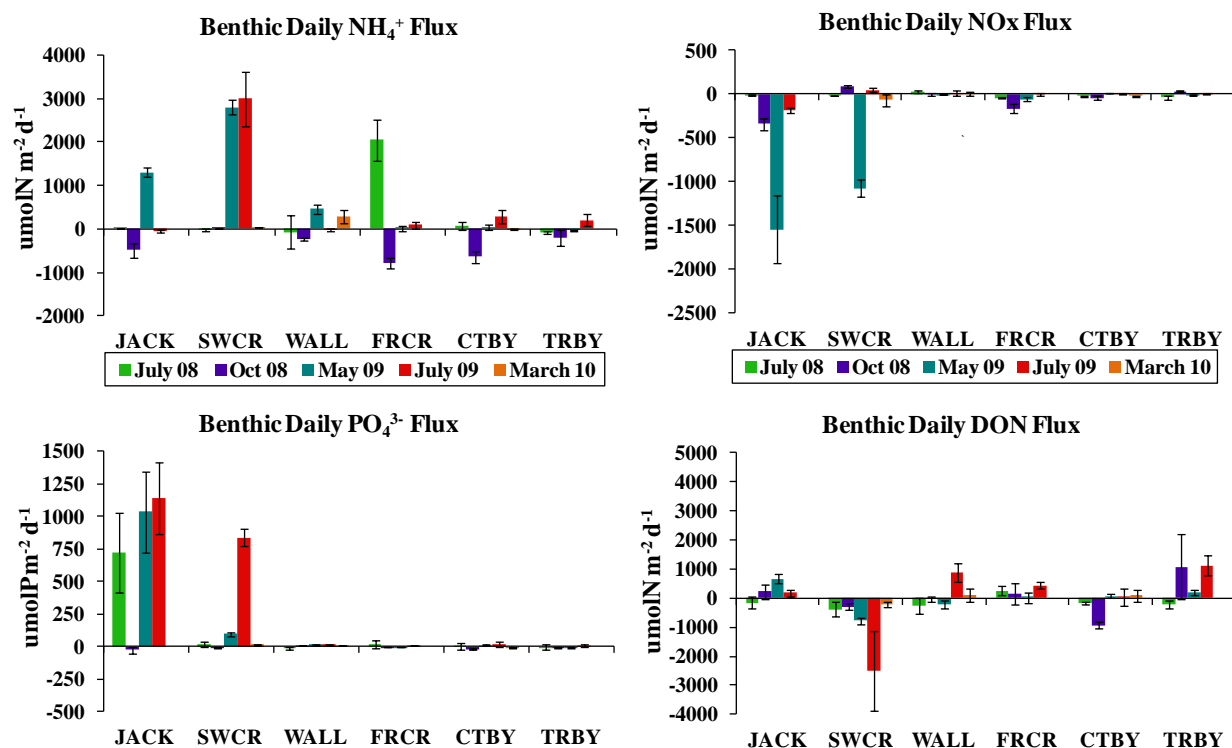


Figure 5-28. Mean (\pm standard error) benthic daily NH_4^+ , NO_x , PO_4^{3-} and DON fluxes measured at six stations (0.5 m water depth) from July 2008 to July 2009 and three stations (i.e., SWCR, WALL, CTBY) in March 2010.

Sites are arranged (left to right) from up- to down-estuary.

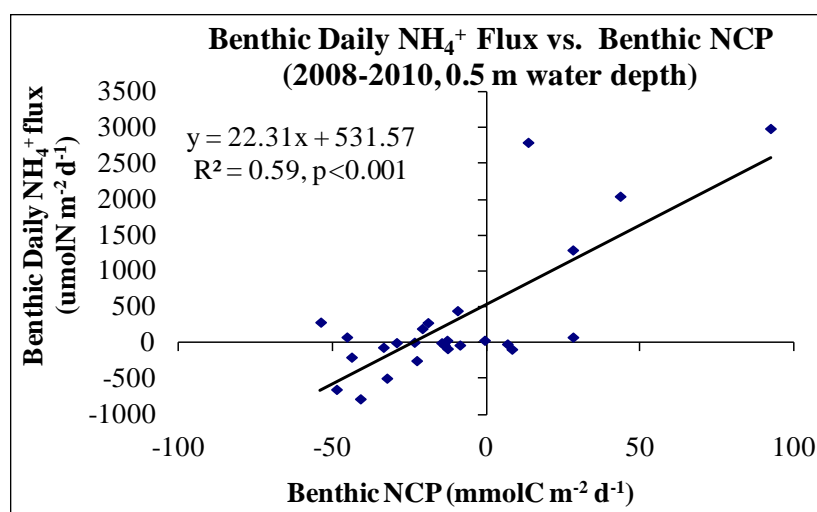


Figure 5-29. Regression of mean benthic daily NH_4^+ flux versus mean benthic NCP measured at six stations (0.5 m water depth) from July 2008 to July 2009 and three stations (i.e., SWCR, WALL, and CTBY) in March 2010.

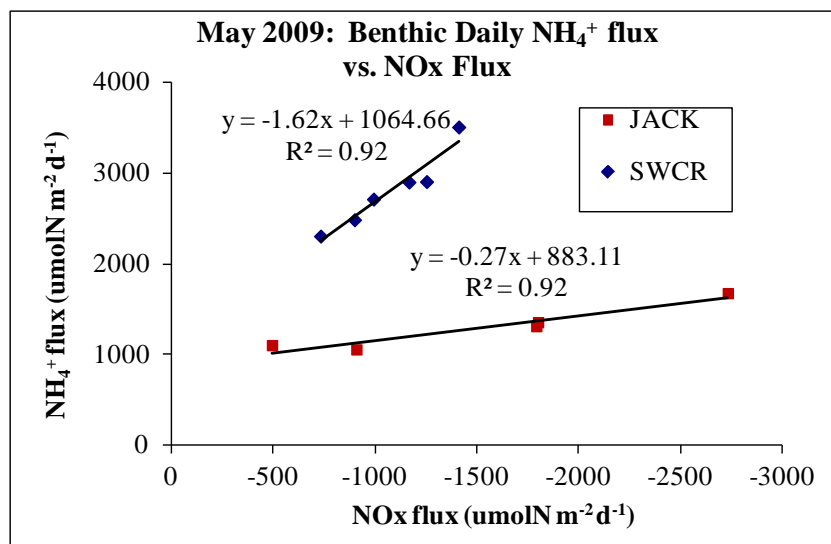


Figure 5-30. Regression of daily benthic NH_4^+ fluxes versus daily benthic NO_x fluxes for JACK and SWCR sites (0.5 m water depth) during the May 2009 experiment.

Table 5-10. Summary of the Two-Way ANOVA of Benthic GPP by Site and Season Measured from July 2008 to July 2009 (0.5 m Water Depth)

Parameter	N	F	df	Site p Value	Season p Value	Interaction p Value	Site Effect	Season Effect
Benthic GPP	139	14.25, 31.01, 13.22	5, 3, 15, 115	<0.0001	<0.0001	<0.0001	(WALL and FRCR) > CTBY > SWCR	(Fall, summer 2008, and summer 2009) > spring
							(JACK and TRBY) > SWCR	Summer 2008 > spring

Note: Summary of the two-way ANOVA of the July 2008 to July 2009 benthic GPP with the parameter evaluated, number of samples (n), the F-statistic (site, season, interaction) and degrees of freedom (site, season, interaction, error), the probability for each of the main effects (site, season) and interaction term, the significant Tukey's pair-wise comparisons ($p < 0.05$) for the main effects. Summer data were separated by year (2008 and 2009). GPP were transformed as $\ln(x+10)$. ^a Higher GPP, more autotrophic.

Table 5-11. Summary of the Two-Way ANOSIMs of Benthic R, NCP, and Daily NH_4^+ , NO_x , and PO_4^{3-} Flux by Site and Season Measured from July 2008 to July 2009 (0.5 m Water Depth)

Parameter	n	Global Test R values	Site p Value	Season p Value	Site Effect	Season Effect
Benthic R	139	0.213, 0.305	0.001	0.001	JACK > WALL > FRCR	Summer 2008 > summer 2009 > (fall and spring)
					FRCR > (SWCR, CTBY, and TRBY)	
Benthic NCP ^a	139	0.301, 0.415	0.001	0.001	SWCR > (JACK, FRCR, CTBY, and TRBY)	Summer 2008 > spring > summer 2009 > fall
					(JACK and WALL) > (FRCR and CTBY)	
Benthic daily NH_4^+ flux ^b	139	0.538, 0.424	0.001	0.001	SWCR > FRCR > JACK > WALL > TRBY	Spring > summer 2009 > summer 2008 > fall
					SWCR > JACK > WALL > TRBY > CTBY	
Benthic daily NO_x flux ^b	139	0.374, 0.326	0.001	0.001	JACK < SWCR < FRCR < CTBY < WALL	Spring < fall < summer 2008
					JACK < SWCR < CTBY < TRBY < WALL	
Benthic daily PO_4^{3-} flux ^b	139	0.291, 0.254	0.001	0.001	JACK > SWCR > (WALL, FRCR, CTBY, and TRBY)	Summer 2009 > spring > Summer 2008 > fall
					WALL > TRBY	

Note: Summary of the two-way ANOSIMs of the July 2008 to July 2009 benthic R, NCP, and daily NH_4^+ flux with the parameter evaluated, number of samples (n), the global test R values for the main effects (site, season), the probability for each of the main effects (site, season), and the significant ANOSIM pair-wise comparisons for the main effects. Summer data were separated by year (2008 and 2009). The alpha values for the pair-wise comparisons were 0.0033 (0.05/15) and 0.0083 (0.05/6) after application of the Bonferroni correction for site and season, respectively. ^a Higher NCP, more heterotrophic. ^b Higher value is flux out.

Variation of Photosynthesis with Irradiance

P-I curves were generally well constrained for most sites (**Figure 5-31a-b**), with some exceptions (primarily at SWC) when R was dominant and rates showed no clear linkage with irradiance; in this case, P_{\max} was set to zero and an average respiratory rate was used in all calculations. For the purposes of analysis, P-I results were averaged across sites in three regions, reflective of the low mesohaline (“upper”), high mesohaline (“middle”), and polyhaline (“lower”) regions of the estuary (**Figure 5-31c**).

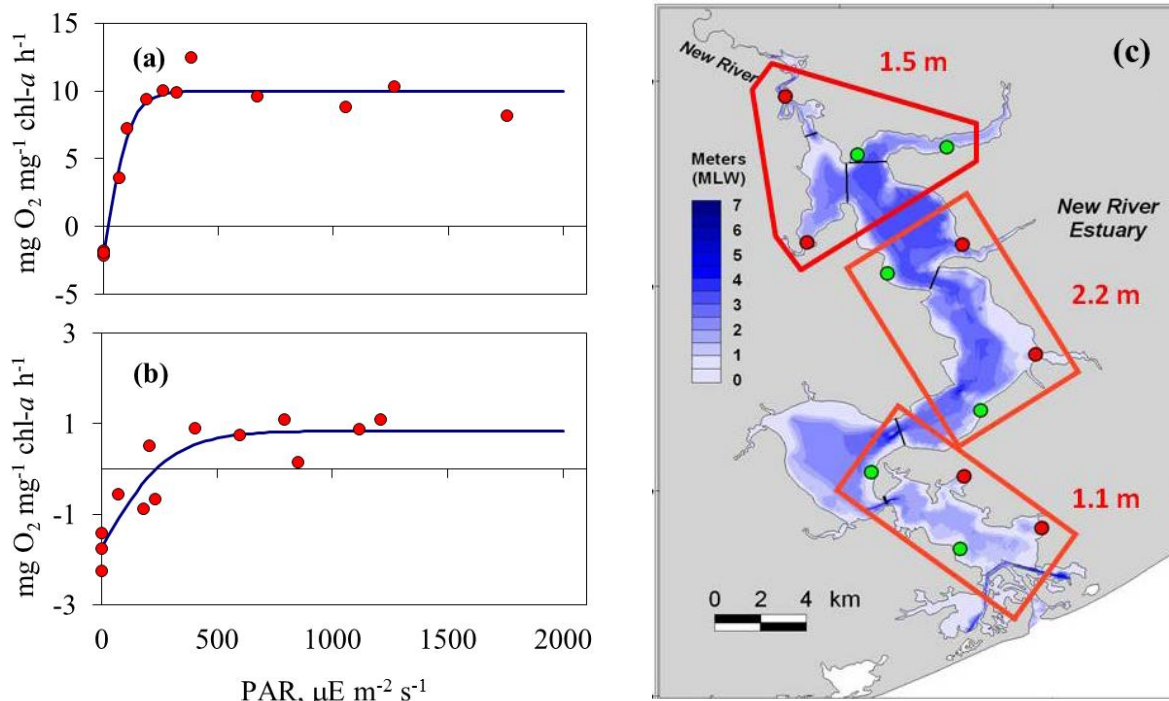


Figure 5-31. P-I curve results and grouping of stations for analysis.

(a) Example water column P-I curve; (b) example sediment P-I curve; (c) Upper, middle, and lower groupings of P-I stations for analysis with mean depths. Red points are the primary Research Project AE-3 experimental sites; green circles are the supplemental mainstem sites.

Rates were computed for both a 0.5 m (MLW) water column, corresponding to the depths where samples were collected and the in situ experiments were conducted, as well as for the mean depth of each NRE segment. Regardless of depth used, water column rates of GPP were generally highest in the upper segment of the estuary and decreased seaward, although rates were highly variable among sites within a region (**Figure 5-32a**). Water column GPP was higher when computed at the mean depth of each region, as more of the water column (and thus the photic zone) was included in the calculations. Rates of sediment GPP were highest in the warmer months (May and July), and there was no clear pattern down estuary (**Figure 5-32b**). Rates were higher when computed at 0.5 m due to greater light availability at shallower depths. The ratio of sediment to water column GPP indicated that microphytobenthic production could often dominate system production or at least equal that by phytoplankton at a depth of 0.5 m, in the zone around the perimeter of the estuary where nutrients first enter the system (**Figure 5-32c**). However, when rates were scaled to the mean depth of each segment, sediment GPP rivaled that

of phytoplankton only in the lower estuary in May. These results suggest that phytoplankton dominate total system production in the NRE; modeling of GPP across a wider range of depths indicates a potential threshold of approximately 0.55-m depth, beyond which water column production exceeds that in the sediments (**Figure 5-32d**).

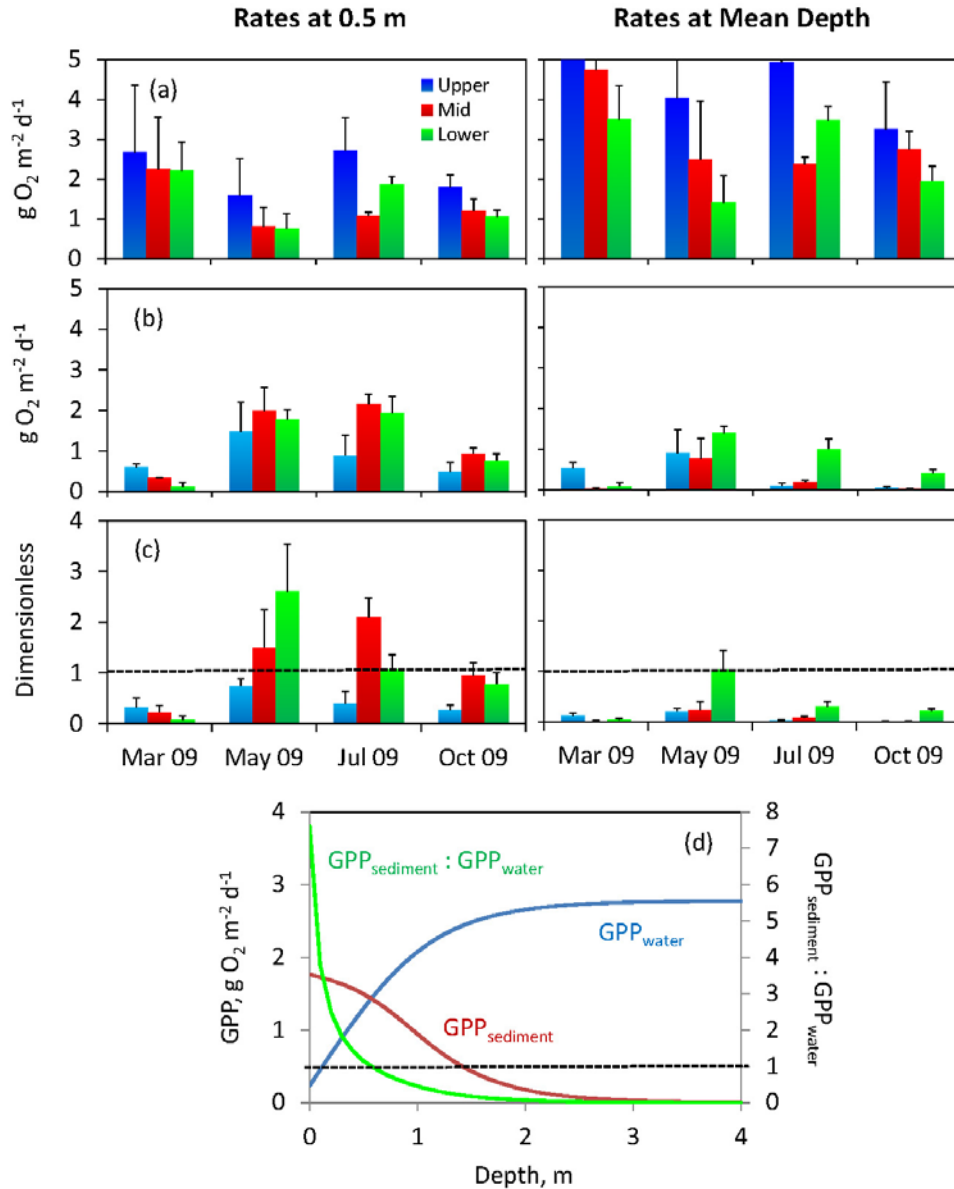


Figure 5-32. P-I curve results for GPP at 0.5 m and mean depth in the upper, middle, and lower regions of the NRE (see Figure 5-31).

Bars represent one standard error based on four stations within each region. (a) Water column GPP; (b) sediment GPP, (c) ratio of sediment to water column GPP, and (d) variation of GPP in the water column ($\text{GPP}_{\text{water}}$) and sediments ($\text{GPP}_{\text{sediment}}$) with depth.

Controls on water column and sediment GPP were assessed by imposing incremental changes in water column chl *a*, turbidity, and CDOM in Equation 5-1, and updating P-I calculations with the

resulting values of K_d . These changes were imposed as a proxy for potential changes in watershed loading of nutrients (chl *a*), sediments (turbidity), and CDOM, and for the effects of resuspension (turbidity) in the lower NRE. Up-estuary concentrations of chl *a* and turbidity have the potential to be controlled through watershed management, and CDOM and down-estuary sediment resuspension are outside of management control.

Changes in turbidity and CDOM had a much greater effect on rates of sediment GPP than on water column GPP (**Figure 5-33**), and changes in chl *a* had a greater effect on water column GPP because changes not only altered K_d but also the biomass of the primary producer. Changes in water column chl *a* had less of an effect on sediment GPP than either turbidity or CDOM. Sediment GPP was typically most strongly controlled by CDOM in the upper estuary and turbidity in the lower estuary. The latter is likely due to resuspension at the shallow depths in the lower estuary segment as opposed to watershed sediment loading. These results suggest that production by BMA in the NRE, and therefore the potential of sediments to mitigate the effects of watershed nutrient loading and resulting eutrophication, may be controlled more by natural processes (i.e., watershed loading of CDOM in the upper estuary and sediment resuspension in the lower estuary) than by anthropogenic stressors (i.e., watershed loading of nutrients and sediments). The absence of a comparable effect of turbidity and CDOM on water column production suggests that phytoplankton are controlled by other factors such as nutrient loading and flushing time, and thus may respond to changes in watershed nutrient loading.

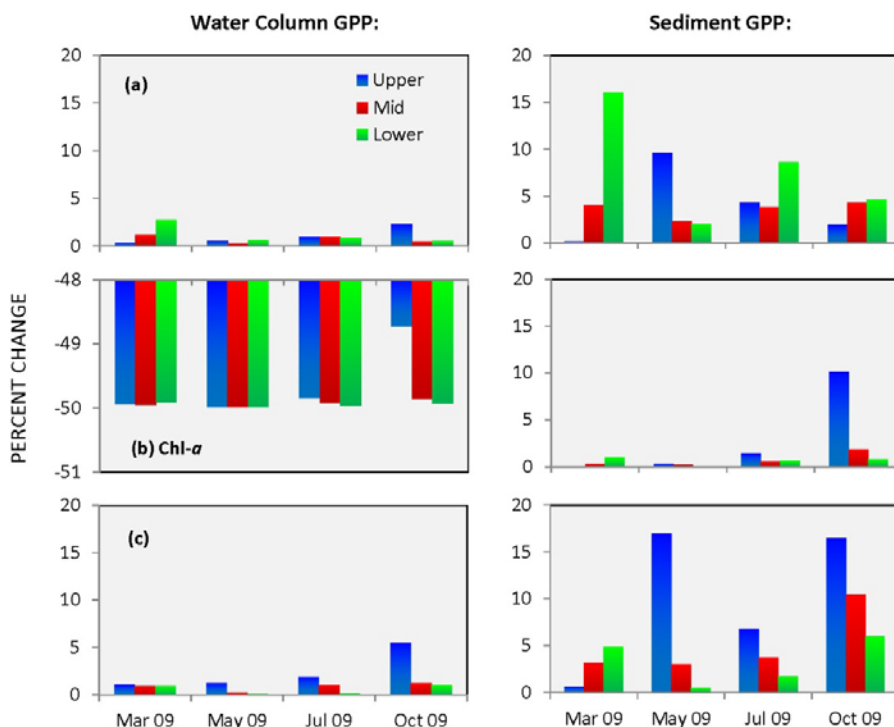


Figure 5-33. Predicted percent change in water column and sediment GPP within each region of the estuary with a 50% reduction in water column concentrations of (a) NTU, (b) chl *a*, and (c) CDOM.

Note the different scale on the water column chl *a* plot.

Environmental Factors Regulating Benthic Metabolism

Multiple regression analyses were performed to identify the environmental parameters, which best predict rates of benthic metabolism in the NRE. As we suspected (see conceptual model, **Figure 5-1**) GPP rates were inversely proportional to K_d and directly proportional to both water temperature and benthic chl a . K_d (PAR). Benthic chl a , and water temperature together explained 52% of the observed variability in GPP (**Figure 5-34**; Equation 5-10).

$$\ln(\text{GPP}+10)=3.24 - 0.206 K_d(\text{PAR}) + 0.0404 \text{ temp} + 0.00479 \text{ benthic chl } a \text{ (Eq. 5-10)}$$

$$(r^2=0.52, p<0.001)$$

As one would expect, benthic R was directly proportional to water temperature, which explained 34% of the variation in R (**Figure 5-35**). Whereas DIC is the measured product of R, NH_4^+ is the product of bacterial MIN. MIN, similar to R, was also directly proportional to water temperature as shown in **Figure 5-44**.

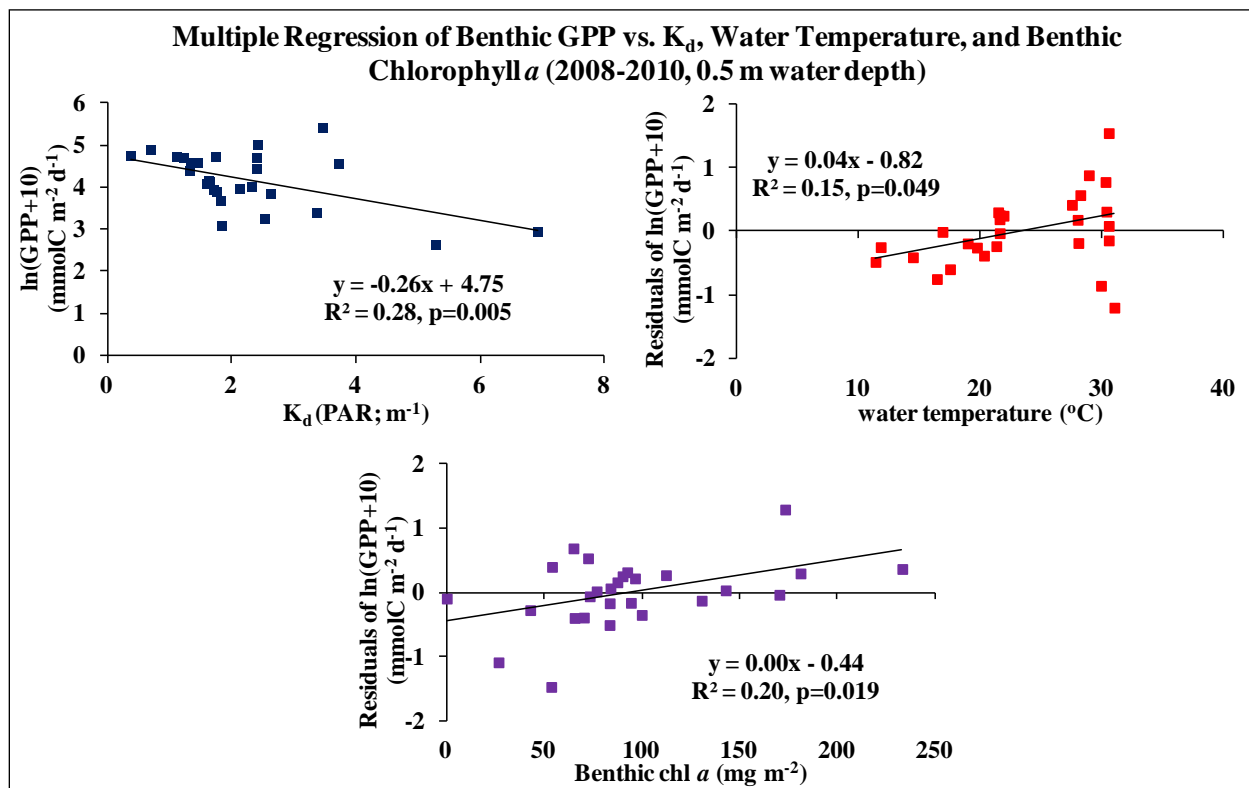


Figure 5-34. Multiple regression of mean benthic GPP ($\ln[\text{GPP}+10]$ transformed) versus K_d (PAR) (top left), water temperature (top right), and mean benthic chl a (0–3 mm depth; bottom) measured at six stations (0.5 m water depth) from July 2008 to July 2009 and three stations (i.e., SWCR, WALL, CTBY) in March 2010.

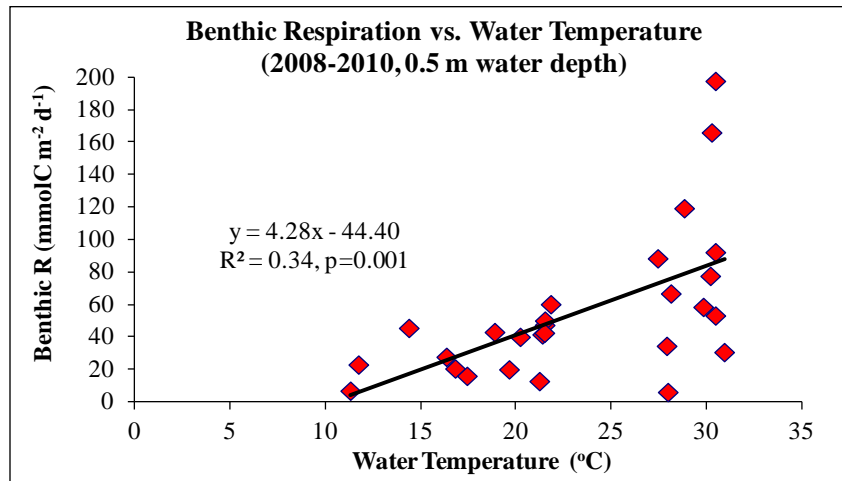


Figure 5-35. Regression of mean benthic R versus water temperature measured at six stations (0.5 m water depth) from July 2008 to July 2009 and three stations (i.e., SWCR, WALL, CTBY) in March 2010.

Role of Benthic Processes in Regulating Sediment–Water Nutrient Fluxes in Shallow Water

The Benthic Cap

The conceptual model shown in **Figure 5-1** predicts that depending on environmental conditions, benthic processes may serve to remove and sequester N and reduce the potential for pelagic primary production. Sources of N to the benthos include remineralization of ON to NH_4^+ , NFix, and uptake of DIN or DON from the water column. NO_3^- taken up by the benthos may be either removed by DNF or reduced to NH_4^+ by DNRA in the presence of sulfide. As observed in **Figure 5-29**, when autotrophic, the benthos serves as a sink for NH_4^+ , preventing its release from the benthos and taking it up from the water column. To further confirm the ability of benthic autotrophs to cap sediment, a laboratory experiment was performed in which sediment cores from the mid-estuary (WALL) and low-estuary (CTBY), amended with NO_3^- , were exposed to diel light conditions for 2 days (two light levels of 550 and 100 $\mu\text{E m}^{-2} \text{s}^{-1}$ at sediment surface), followed by exposure to dark for an additional 16 days. Measurements of water column DO demonstrated the expected variations under diel conditions, with greater production under more light but not with added NO_3^- (**Figure 5-36**). When the lights were turned off the water column became anoxic and remained so for the remainder of the experiment. Under diel conditions there were no releases of NH_4^+ from the benthos for any of the treatments; however, in the dark there was continued release resulting in accumulation of high water column concentrations of NH_4^+ that were not explained by reduction of NO_3^- . This experiment serves to confirm that BMA N uptake is an important mechanism of the benthic filter, provided that sufficient light is available.

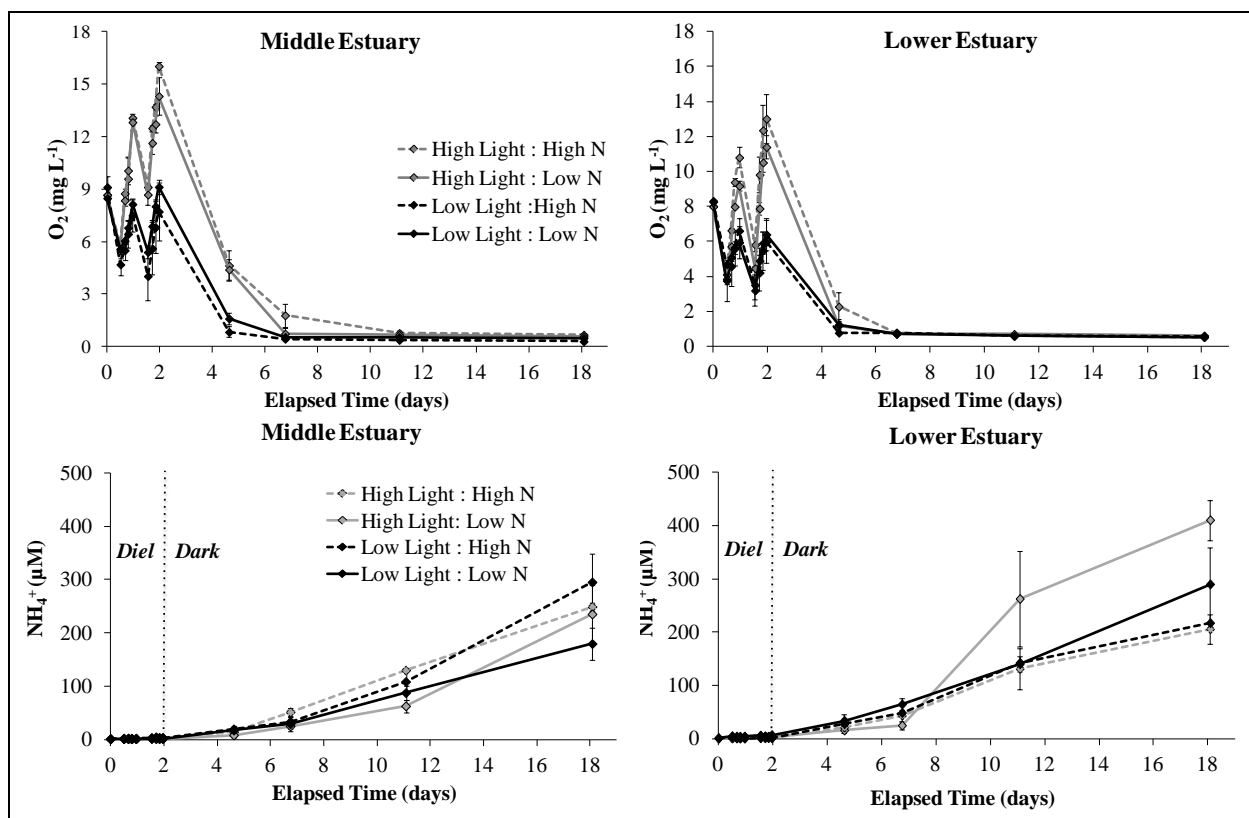


Figure 5-36. Mean (\pm standard error) DO and NH_4^+ concentration in overlying water of sediment cores collected from Middle (WALL site) and Lower (CTBY site) regions of NRE (0.5 m water depth) during October 2009.

The cores were exposed to 2 days of diel conditions, followed by continuous dark for 16 days and four different treatment combinations of high versus low light and high versus low nutrient additions.

N Limitation of Benthic Metabolism

Bioassays conducted in the NRE have shown that primary production in the pelagic zone is N limited (Altman and Paerl, 2012). A laboratory experiment was performed to determine whether benthic autotrophs are similarly limited by the availability of nutrients in the water column. Changes in DO resulting from benthic metabolism in the light and dark were measured in cores from the mid-estuary (WALL) with added NH_4^+ , ranging from 0–100 μM . PO_4^{3-} was added along with N to maintain a 16:1 molar ratio of N:P. There were no differences in rates of either production or R with added nutrients, suggesting that sediment N remineralization supplies sufficient N and P to support benthic production and that water column N and P do not limit benthic autotrophy (**Figure 5-37**).

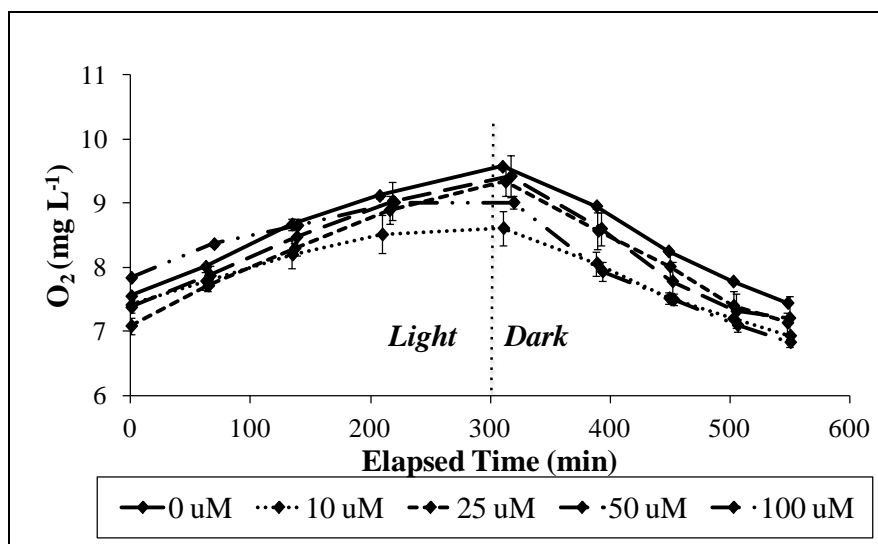


Figure 5-37. Mean (\pm standard error) DO concentration in overlying water of sediment cores collected from Middle region (WALL site) of NRE (0.5 m water depth) during August 2009.

Each core was amended with artificial seawater (PO_4^- added at 16:1 N:P) containing the following concentrations of NH_4^+ : 10, 25, 50, and 100 μM and exposed to 300 minutes of light followed by 240 minutes of dark.

Shallow Water Seasonal N Cycling Rates

The principal processes, which govern production and losses of DIN and the resulting sediment–water fluxes include MIN, a bacterial process which breaks ON to DIN; NFix, a microbial process which converts N_2 to NH_3 ; BMA nutrient uptake, a process by which N is taken up from both sediments and the water column to support production of BMA biomass; DNF, an anoxic microbial process which reduces NO_3^- to N_2 , thereby removing N from the ecosystem.

Competing processes, which were not measured in this study, include ANA, which converts NH_4^+ and NO_2^- to N_2 and may have contributed to the observed production of N_2 , and DNRA, which reduces NO_3^- to NH_4^+ especially in the presence of sulfide and may have contributed to our measured MIN rates.

Results of two-way ANOVA showed that MIN was significantly higher during summer and at WALL (Figure 5-38; Table 5-12).

The high rates observed at WALL were somewhat surprising and may be explained based on the high degree of development within the WALL watershed. Watershed disturbance was particularly intense in 2009 as MCBCL

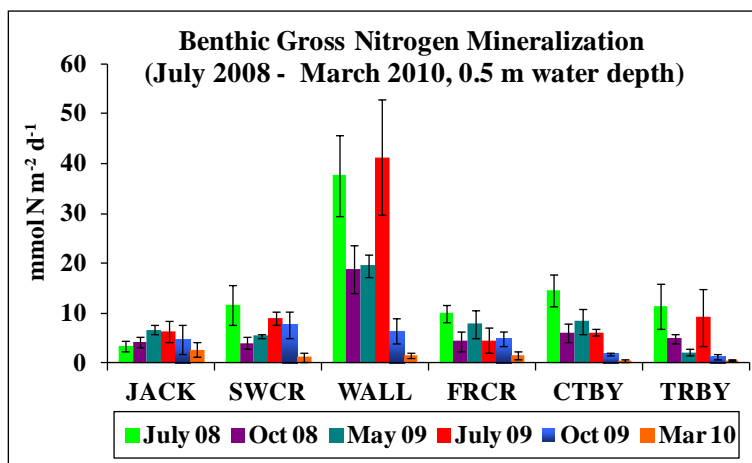


Figure 5-38. Mean (\pm standard error) benthic gross N mineralization measured at six stations (0.5 m water depth) from July 2008 to March 2010.

Sites are arranged (left to right) from up- to down-estuary.

prepared for development of the Wallace Creek Regimental Area. Forest clearcutting was performed in March 2009 with hundreds of acres of forest logged; heavy construction was intense in May–June 2009; slurry dumping from a boring project for the Regimental Area occurred in June 2009 (information from Susan Cohen). The high rates of MIN observed at WALL in 2008 and 2009 were not observed during 2010 (data not shown) perhaps due to a reduction in construction activities.

Net benthic DNF was significantly higher in spring than in summer or fall and at up-estuary sites compared to down-estuary sites (**Figure 5-39, Table 5-12**). The benthic DNF reported represents a net rate, as measured by MIMS. NFix, which can take up N_2 as it is produced by DNF, confounds the determination of gross DNF. Three-way ANOVA showed that NFix was significantly highest in summer at mid- and low-estuary sites (**Figure 5-40; Table 5-13**). Depth profiles of sediment NFix showed that rates decreased with depth, and

were higher in the surface 0–1 cm depth (mean \pm SE $240 \pm 40 \mu\text{mol m}^{-2} \text{d}^{-1}$ over all sites and dates) than the 1–3 cm depth ($112 \pm 13 \mu\text{mol m}^{-2} \text{d}^{-1}$), the 5–7 cm depth ($54 \pm 5 \mu\text{mol m}^{-2} \text{d}^{-1}$), or the 8–10 cm depth ($44 \pm 4 \mu\text{mol m}^{-2} \text{d}^{-1}$) (**Figure 5-40**). Surface sediments incubated in the light and dark showed similar rates, suggesting that heterotrophic NFix may be as important as autotrophic NFix in the sediment (data not shown). The importance of heterotrophic NFix was further supported by results of studies using the inhibitor sodium molybdate (20 mM, Na_2MoO_4) and by molecular analyses. In the presence of molybdate, NFix was decreased by 77–96% in the surface sediment (0–1 cm) incubated in the dark, and 49–83% in the deeper sediments. Surface sediments incubated in the light were inhibited 23% at the mid-estuary site and 49% and 53% at the lower and upper sites respectively. Determination of the general bacterial community composition by PCR, using a 16S primer pair demonstrated the presence of cyanobacteria in shallow sediments from across the entire NRE. However, when nested PCR was used to detect the presence of *nifH* genotypes with the external primer pair *nifH3* and *nifH4* (Zani et al., 2000) and the internal primer pair of *nifH1* and *nifH2* (Zehr and McReynolds, 1989) results showed that Deltaproteobacteria were the dominant NFixers; cyanobacteria carrying the *nifH* genes were rare in the samples analyzed (**Figure 5-41**).

Gross DNF was calculated by adding NFix (0–1 cm depth horizon) to net DNF measured at the same times and sites. **Figure 5-42** shows that during summer and especially in the mid to lower estuary NFix represented as much as 60% of the gross DNF rate, explaining the low net DNF rates measured during summer in the lower estuary. Thus, NFix may offset N removal by DNF;

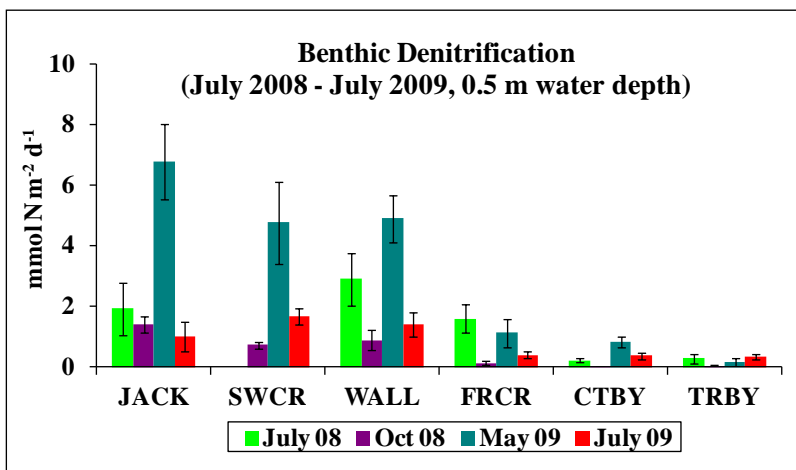


Figure 5-39. Mean (\pm standard error) benthic DNF measured at six stations (0.5 m water depth) from July 2008 to July 2009.

however, an advantage of using MIMS over other methods used to measure DNF is that it more accurately represents net N removal by taking into account the N_2 produced by NFix.

To identify which of the benthic N-cycling processes contribute the most to the benthic filter, a mass balance analysis of sources and sinks of N in the benthos was performed. Sources of N are shown as positive bars and sinks as negative bars in **Figure 5-43**. MIN constituted the largest source of NH_4^+ to the benthos, but included some undetermined contributions from DNRA and NFix. BMA N demand was the major sink at these shallow water (0.5 m MLW) sites in summer; DNF was a more important sink in spring, and the DIN flux out of the sediments was only important at SWCR (**Figure 5-43**).

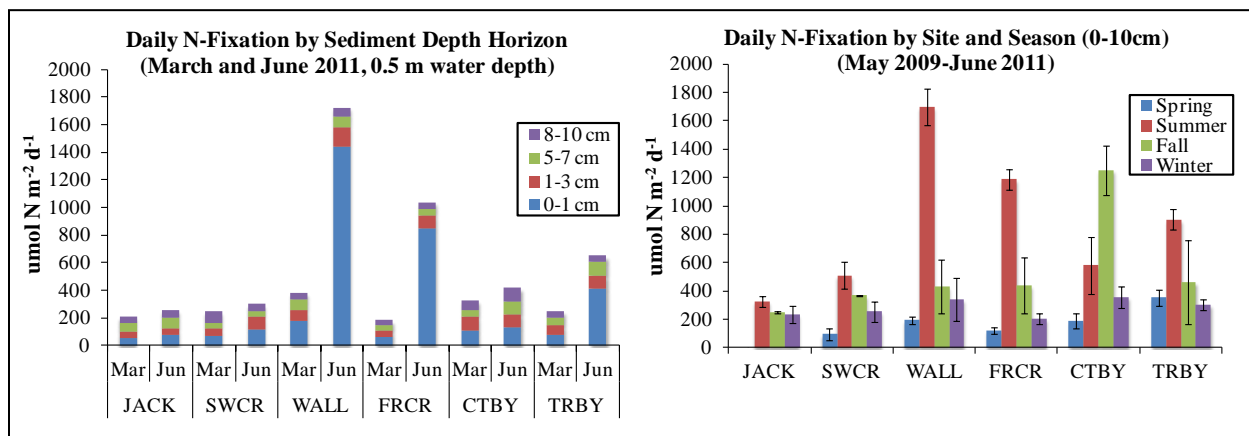


Figure 5-40. Mean benthic daily NFix by sediment depth horizon (0–1 cm, 1–3 cm, 5–7 cm, and 8–10 cm) measured at the six shallow stations (0.5 m water depth) in March and June 2011 and mean (\pm standard error) benthic NFix by site and season measured at six stations (0.5 m water depth) from May 2009 to June 2011.

Sites are arranged (left to right) from up- to down-estuary.

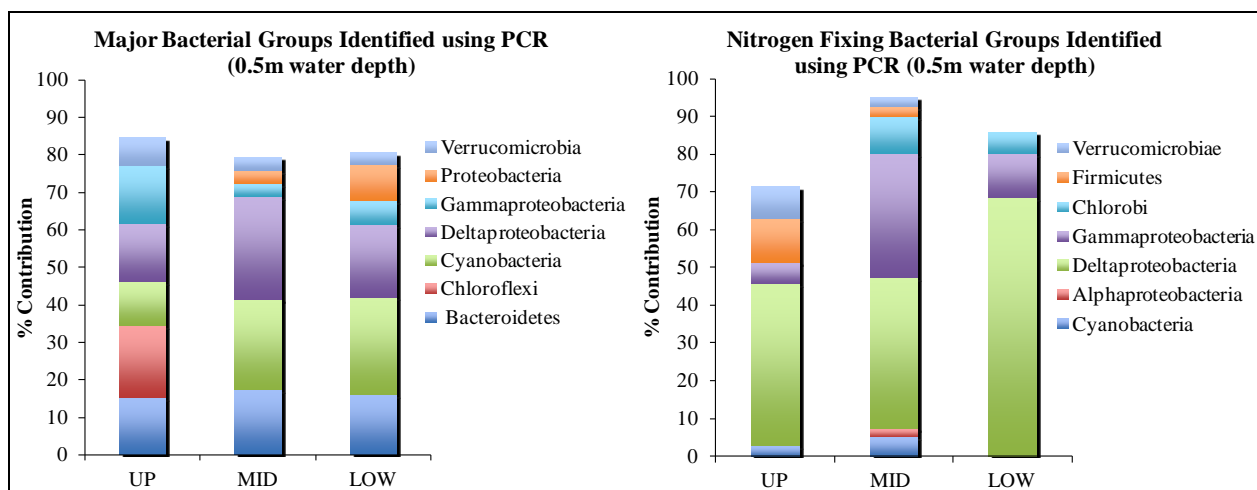


Figure 5-41. General bacterial community composition determined by PCR using a 16S primer pair (left) and potential N fixing organisms identified using PCR of the nifH gene (right).

These results are from samples taken in July 2010 for the 0-1cm and 1-3cm depth horizons in upper, middle, and lower regions of the NRE (0.5m water depth).

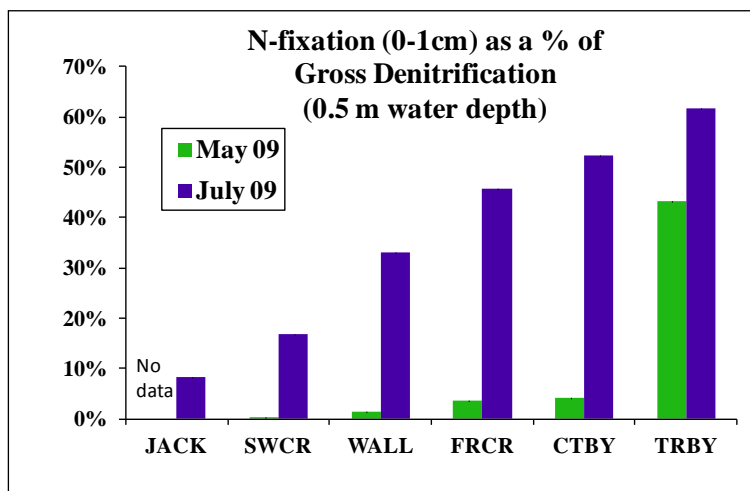


Figure 5-42. Benthic NFix (0–1 cm depth horizon) as a percentage of estimated gross DNF measured at six stations (0.5 m water depth) in May 2009 and July 2009.

Sites are arranged (left to right) from up- to down-estuary.

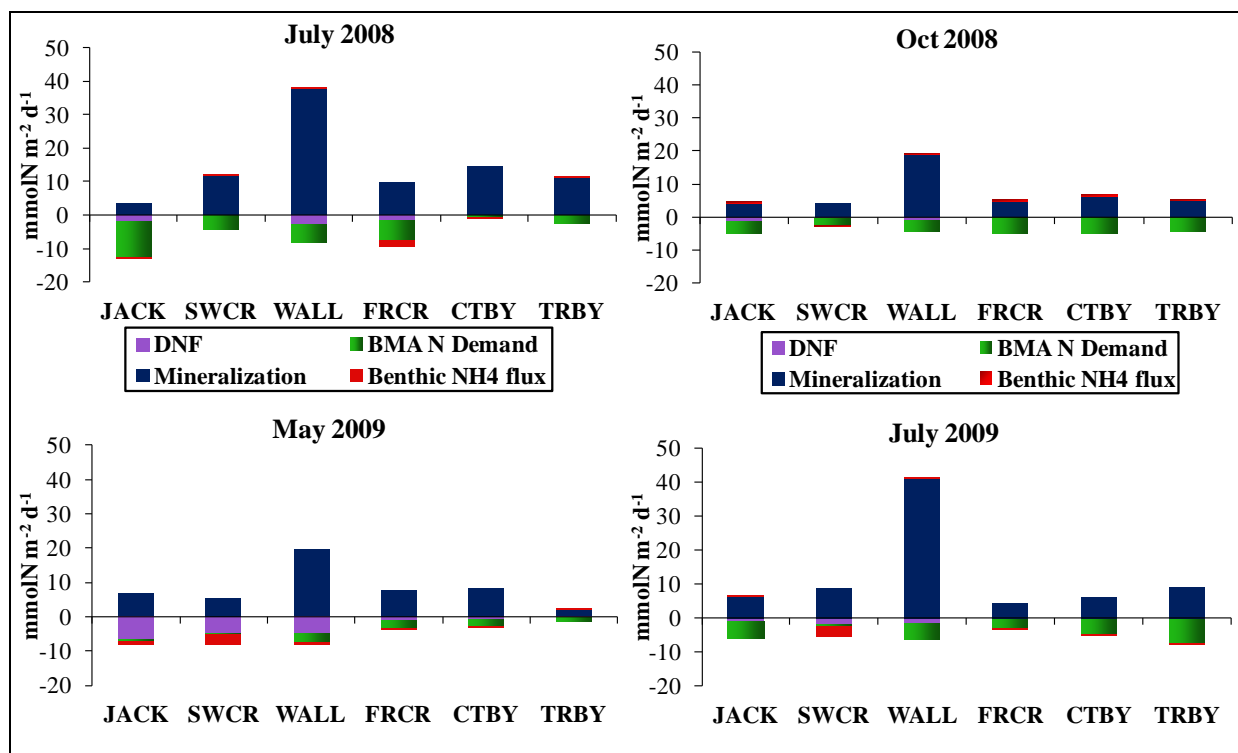


Figure 5-43. Mass balance of benthic N sources (positive values; mineralization, benthic NH_4^+ flux into the sediment) and fates (negative values; BMA demand, DNF, and benthic NH_4^+ flux out of the sediment) measured at six stations (0.5 m water depth) from July 2008 to July 2009.

Sites are arranged (left to right) from up- to down-estuary.

Table 5-12. Summary of the Two-Way ANOVAs of Benthic Mineralization from July 2008 to March 2010 and DNF from July 2008 to July 2009 by Site and Season (0.5 m Water Depth)

Parameter	n	F	df	Site p Value	Season p Value	Interaction p Value	Site Effect	Season Effect
Benthic mineralization	171	8.96, 35.91, 1.51	5, 3, 15, 147	<0.0001	<0.0001	0.11	WALL > (JACK, SWCR, FRCR, CTBY, and TRBY)	Summer > fall > winter
								Spring > fall
Benthic DNF	72	18.81, 37.32, 6.15	5, 2, 15, 54	<0.0001	<0.0001	<0.0001	(JACK, SWCR, and WALL) > (FRCR, CTBY, and TRBY)	Spring > (summer and fall)

Note: Summary of the two-way ANOVAs of benthic mineralization from July 2008 to March 2010 and benthic DNF from July 2008 to July 2009 (no winter measurements) with the parameter evaluated, number of samples (n), the F-statistic (site, season, interaction) and degrees of freedom (site, season, interaction, error), the probability for each of the main effects (site, season) and interactions term, the significant Tukey's pair-wise comparisons ($p < 0.05$) for the main effects. Benthic DNF was natural log transformed. Mineralization was transformed as $\ln(x+1)$.

Table 5-13. Summary of the Two-Way ANOVA of Benthic NFix from May 2009 to June 2011 by Region and Season (0.5 m Water Depth)

Parameter	n	F	df	Region p Value	Season p Value	Interaction p Value	Region Effect	Season Effect
NFix (0 cm to 1 cm)	94	9.254, 2,106, 6.831	3,2, 82	<0.0001	<0.0001	0.0001	Up < (mid and low)	Summer > (winter, fall, and spring)
								Fall > spring

Note: Summary of the two-way ANOVA of the benthic NFix from May 2009 to June 2011 by region and season (0.5 m water depth) with the parameter evaluated, number of samples (n), the F-statistic (season, region, interaction) and degrees of freedom (season, region, interaction, error), the probability for each of the main effects (region, season) and interactions term, the significant Tukey's pair-wise comparisons ($p < 0.05$) for the main effects. NFix was natural log transformed. JACK is excluded from Up region due to the lack of spring data.

Regulation of N-Cycling Rates by Environmental Factors

Just as environmental conditions played an important role affecting benthic metabolism, they similarly impact N cycling rates. Sources of NH_4^+ to sediments, including MIN and NFix, were directly proportional to water temperature; thus as expected the highest concentrations of either extractable or pore water NH_4^+ in sediments were observed in summer (**Figures 5-44 and 5-12; Tables 5-12 and 5-7**). However, BMA N-uptake, the major sink for N in shallow sediments also tended to increase with temperature and could serve to offset production by MIN and NFix, depending on K_d and benthic chl *a* biomass (**Figure 5-34**). DNF was inversely proportional to salinity and was highest, as expected, where NO_x fluxes from the water column into sediments were highest (**Figure 5-45**). The relationship of net DNF with salinity, as mentioned above, may partially result from the increasing NFix down-estuary, resulting in lower observed net DNF.

NFix in surface sediment was directly proportional to benthic chl *a*, suggesting a contribution by cyanobacteria (**Figure 5-46**) although molecular analyses of *nifH* genes and inhibitor studies suggest that heterotrophic bacteria were more abundant N fixers. Although NFix may contribute to the higher sediment NH_4^+ concentrations and sediment MIN observed in summer in the NRE (**Figure 5-47; Table 5-13**), rates were also inversely proportional to both sediment NH_4^+ concentrations and sediment MIN rates; others have similarly observed that NH_4^+ , the product of both MIN and NFix can inhibit NFix (Joye and Anderson, 2008).

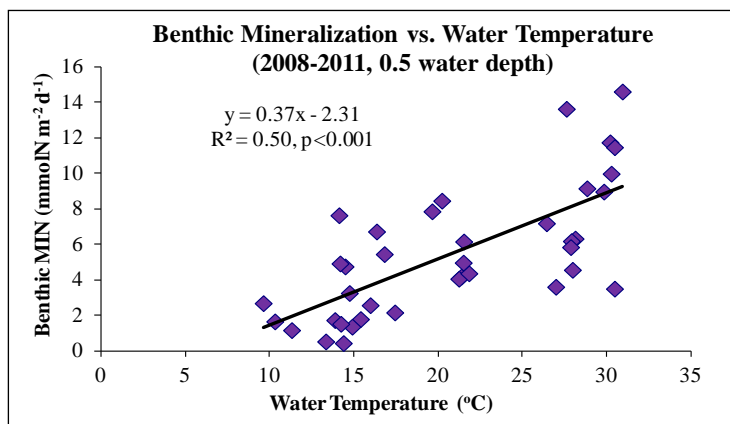


Figure 5-44. Regression of mean benthic gross mineralization (MIN) versus water temperature measured at five stations (i.e., JACK, SWCR, FRCR, CTBY, TRBY; 0.5 m water depth) from July 2008 to March 2011.

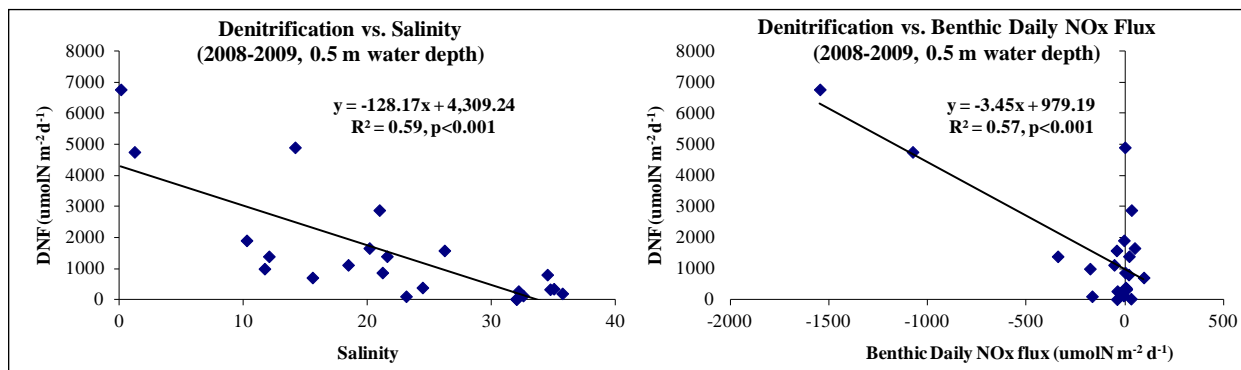


Figure 5-45. Regression of mean DNF versus salinity and mean benthic daily NO_x flux measured at six stations (JACK, SWCR, WALL, FRCR, CTBY, and TRBY) (0.5 m water depth) from July 2008 to July 2009.

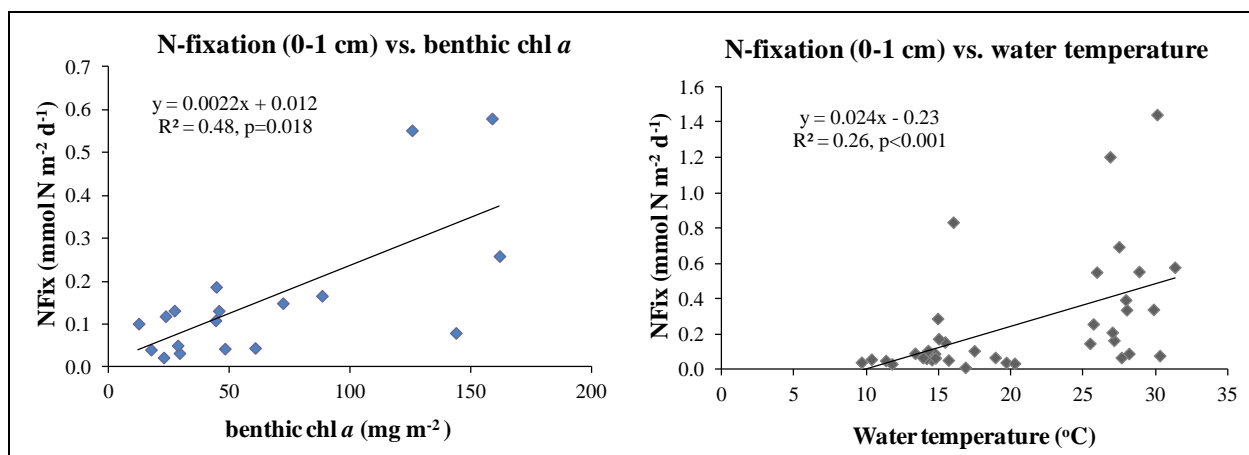


Figure 5-46. Regression of mean NFix (0–1 cm) versus mean benthic chl *a* (0–3 mm depth horizon) measured in the July 2010 and April 2011 depth experiments (Left). Regression of mean NFix (0–1 cm) and mean water temperature measured at six stations (i.e., JACK, SWCR, WALL, FRCR, CTBY, and TRBY) (0.5 m water depth) from May 2009 to June 2011 (Right).

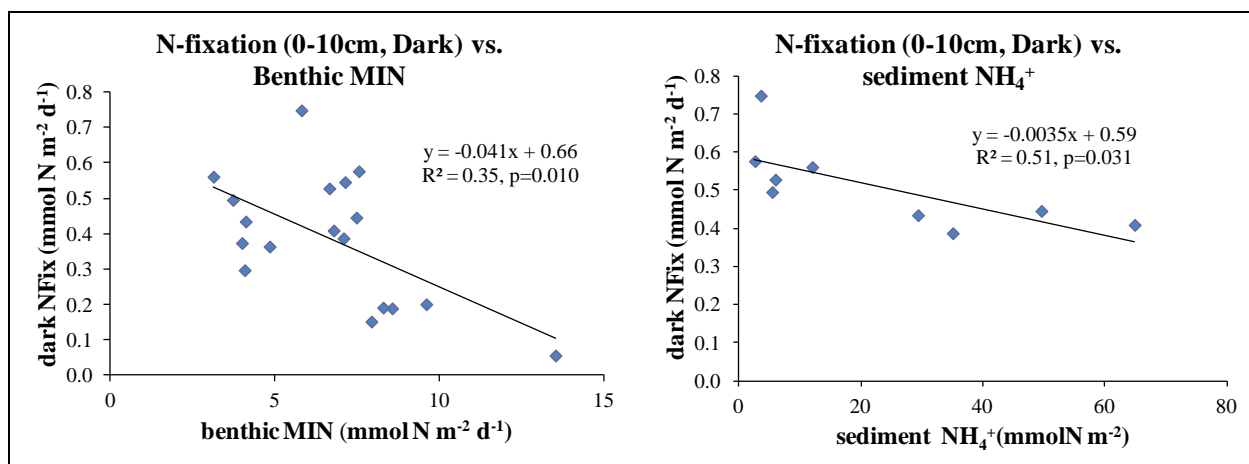


Figure 5-47. Regression of mean dark NFix (0–10 cm) versus mean benthic mineralization (MIN) measured in the July 2010 and April 2011 depth experiments (left). Regression of mean dark NFix (0–10 cm) and mean sediment NH₄⁺ measured in the April 2011 depth experiments (right).

Scaling up to the NRE

To determine the overall impact of the benthic filter at an estuarine-wide scale, it was necessary to make sufficient measurements across the entire estuary at representative water depths and light levels (see Methods). Metabolic, nutrient flux, and N cycling rates measured at the square meter scale at the various depths and locations within the NRE were multiplied by the area within a depth range at each location and summed to provide an estuarine-wide estimate for each of the various process rates.

Variation of Benthic Metabolic and Nutrient Flux Rates with Water Depth

Benthic chl *a* and GPP showed significant declines with water depths from 0.5 to 3m (**Figure 5-48; Table 5-14**). R was significantly higher in the upper estuary and in surface sediment (**Figure 5-49; Table 5-14**). NCP showed a significant shift from net autotrophy in shallow water to net heterotrophy in deep water (**Figure 5-49; Table 5-14**). As NCP shifted from net autotrophy to net heterotrophy, sediment–water fluxes of NH_4^+ switched from net uptake to release (**Figures 5-49, 5-50**). The benthos tended to serve as a sink for NO_x and PO_4^{3-} , except at occasional sites and depths (**Figure 5-50**), and DON uptake was observed mainly at up-estuary sites. These data were used for calibration and/or validation of the ESM and for identification of thresholds and indicators of the effectiveness of the benthic filter (see below)

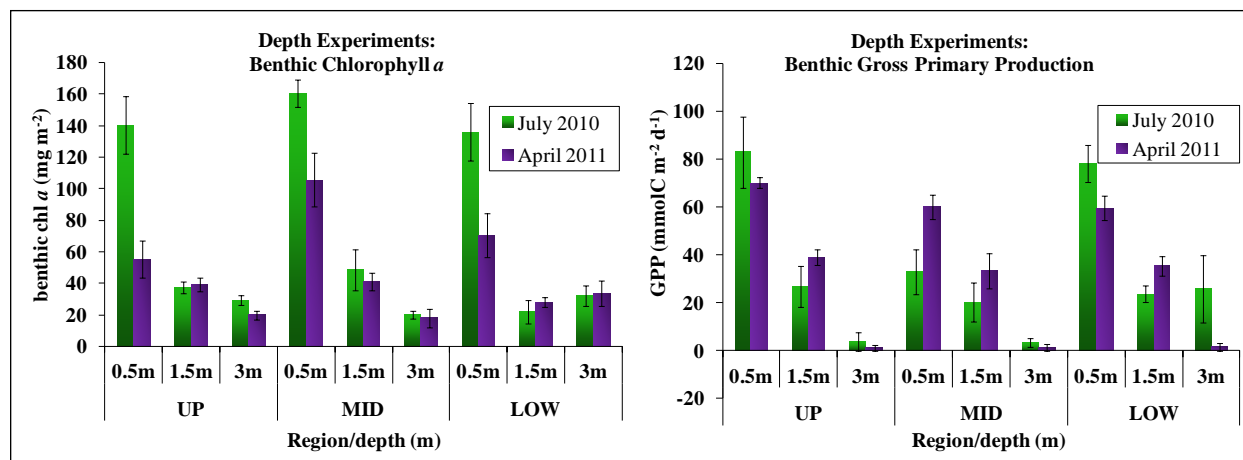


Figure 5-48. Mean (\pm standard error) benthic chl *a* (0–3 mm depth) and benthic GPP measured in three regions and at three water depths of the estuary in July 2010 and April 2011.

UP=upper region; MID= middle region; and LOW= lower region.

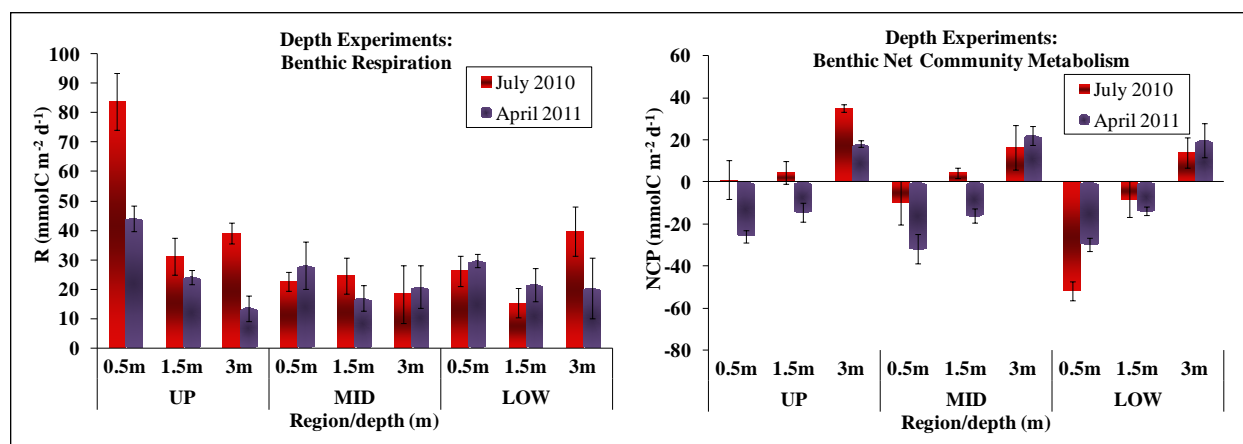


Figure 5-49. Mean (\pm standard error) benthic R and NCP measured in three regions and at three water depths of the estuary in July 2010 and April 2011.

UP=upper region; MID= middle region; and LOW= lower region.

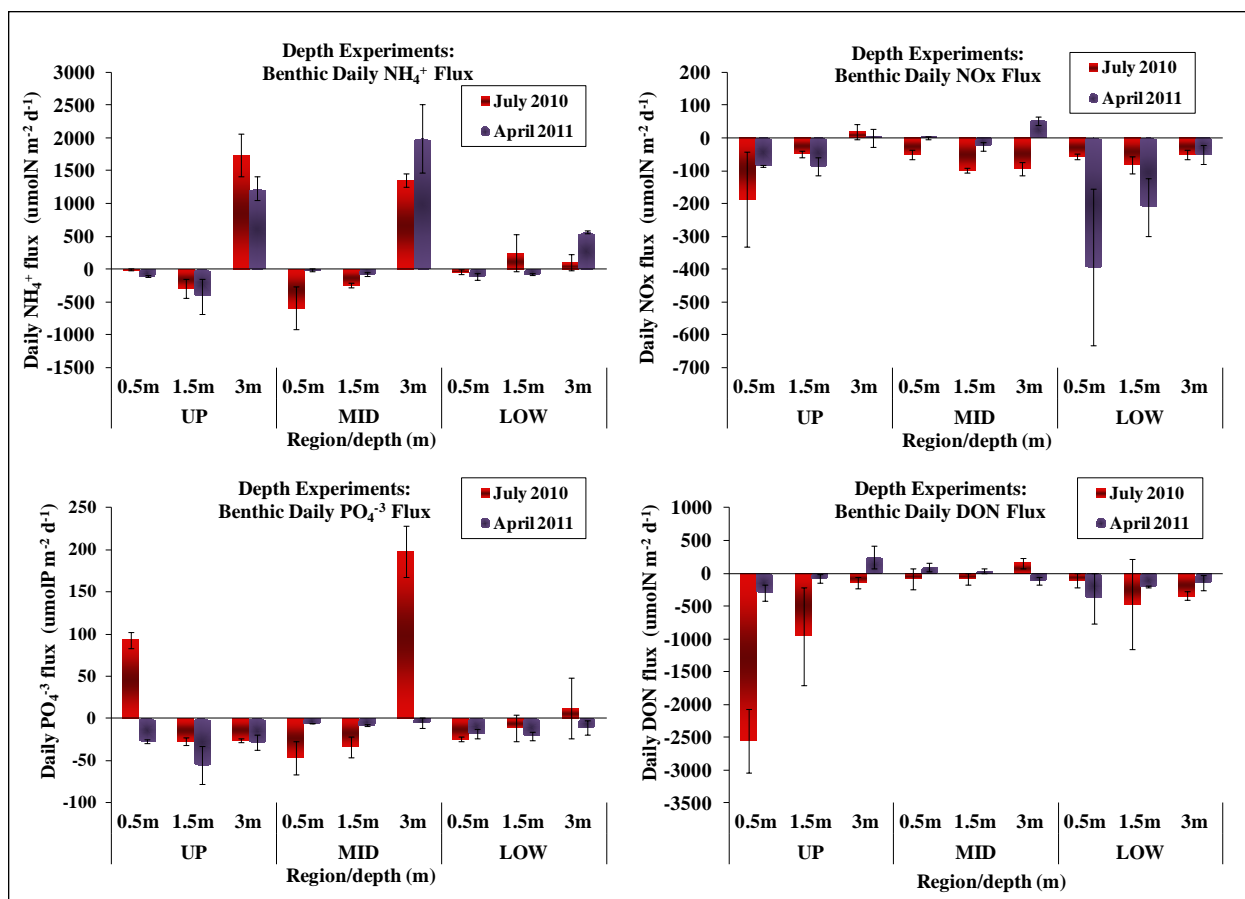


Figure 5-50. Mean (\pm standard error) benthic daily NH_4^+ , NO_x , PO_4^{3-} , and DON fluxes measured in three regions and at three water depths of the estuary in July 2010 and April 2011.

UP=upper region; MID= middle region; and LOW= lower region.

Table 5-14. Summary of the Three-Way ANOVAs of Benthic chl *a* (0–3 mm depth horizon), Benthic GPP, R, NCP, Daily NH₄⁺ Flux, MIN, and DNF by Region, Depth, and Season Measured During the July 2010 and April 2011 Depth Experiments.

Parameter	n	F	df	Region p Value	Depth p Value	Season p Value	Significant Interaction Terms	Region Effect	Depth Effect	Season Effect
Benthic chl <i>a</i>	53	1.00, 64.65, 2.99, 6.32, 0.13, 2.24, 0.75	2, 2, 1, 4, 2, 2, 4, 35	0.377	<0.0001	0.092	Region*depth	Not significant	0.5 m > 1.5 m > 3 m	Not significant
Benthic GPP ^a	53	4.65, 122.76, 0.01, 1.79, 3.67, 7.17, 1.18	2, 2, 1, 4, 2, 2, 4, 35	0.016	<0.0001	0.907	Region*season, depth*season	Low > mid	0.5 m > 1.5 m > 3 m	Not significant
Benthic NCP ^b	53	8.68, 88.56, 8.88, 2.24, 8.43, 1.78, 2.23	2, 2, 1, 4, 2, 2, 4, 35	0.001	<0.0001	0.005	Region*season	(Up and mid) > low	3 m > 1.5 m > 0.5 m	Summer > spring
Benthic R	53	6.33, 6.60, 3.87, 2.15, 2.88, 1.10, 1.53	2, 2, 1, 4, 2, 2, 4, 35	0.005	0.004	0.057	Not significant	Up > mid	0.5 > (1.5 m and 3 m)	Not significant
Benthic daily NH ₄ ⁺ flux ^c	53	5.00, 93.44, 1.40, 12.26, 5.05, 0.39, 1.17	2, 2, 1, 4, 2, 2, 4, 35	0.012	<0.0001	0.245	Region*depth, region*season	(Up and mid) > low	3 m > (0.5 m and 1.5 m)	Not significant
Benthic MIN	82	0.18, 0.43, 0.08, 0.61, 0.19, 0.45, 0.26	2, 2, 1, 4, 2, 2, 4, 64	0.836	0.655	0.783	Not significant	Not significant	Not significant	Not significant
DNF	36	0.10, 34.52, 0.01, 3.28, 3.96, 6.17, 3.18	2, 1, 1, 2, 2, 1, 2, 24	0.909	<0.0001	0.912	Region*season, depth*season	Not significant	3 m > 0.5 m	Not significant

Note: Summary of the three-way ANOVAs with the parameter evaluated, number of samples (n), the F-statistic (region, depth, season, interaction for region*depth, region*season, depth*season, region*season*depth) and degrees of freedom (region, depth, season, interaction for region*depth, region*season, depth*season, region*season*depth, error), the probability for each of the main effects (region, depth, season), significant interaction terms (p<0.05), the significant Tukey's pair-wise comparisons (p<0.05) for the main effects. DNF was only measured at 0.5m and 3m. Benthic chl *a* and DNF were natural log transformed. Respiration was transformed as ln(x+10) and MIN as ln(x+1). ^a Higher GPP, more autotrophic. ^b Higher NCP, more heterotrophic. ^c Higher value is flux out. Low= lower region, Mid=middle region, and Up=upper region.

Thresholds and Indicators of the Effectiveness of the Benthic Filter

Regressions of NCP versus NH_4^+ flux indicated a sharp transition. As NCP became net heterotrophic, NH_4^+ fluxed out of sediments; fluxes were linearly and directly proportional to the degree of benthic heterotrophy (**Figure 5-51**). Benthic chl *a* served as an excellent indicator of both NCP and NH_4^+ flux as demonstrated by the significant and robust relationships between these parameters (**Figure 5-52**). A benthic chl *a* threshold, which predicted NH_4^+ flux, was derived with values ranging from 70–83 mg m^{-2} during spring 2011 and summer 2010, below which the benthos released NH_4^+ to the water column and above which the benthos took up NH_4^+ from the water column. Because benthic chl *a* is an easy and inexpensive measurement to make it could serve MCBCL personnel as an indicator of the effectiveness of the benthic filter.

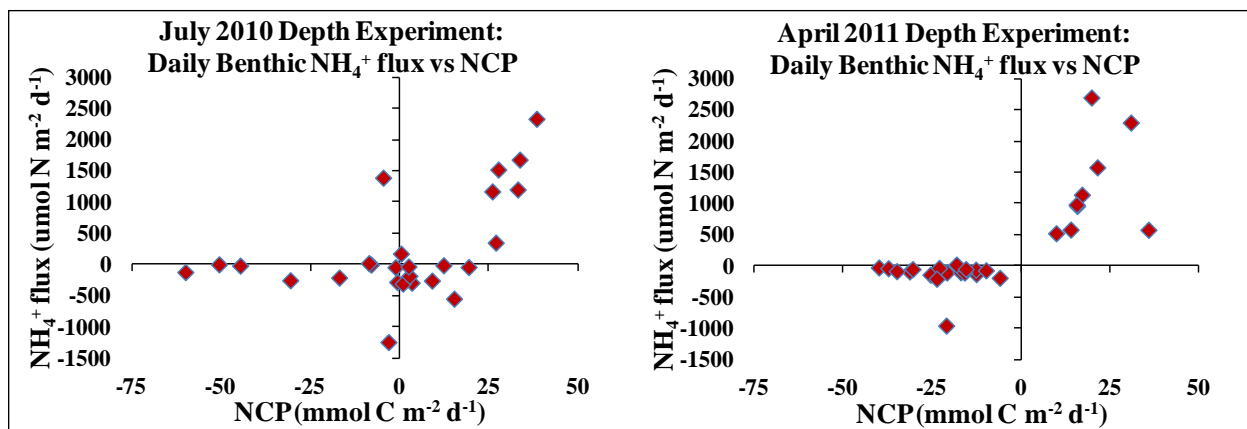


Figure 5-51. Plot of benthic daily NH_4^+ flux versus benthic NCP for the July 2010 (left) and April 2011 (right) depth experiments.

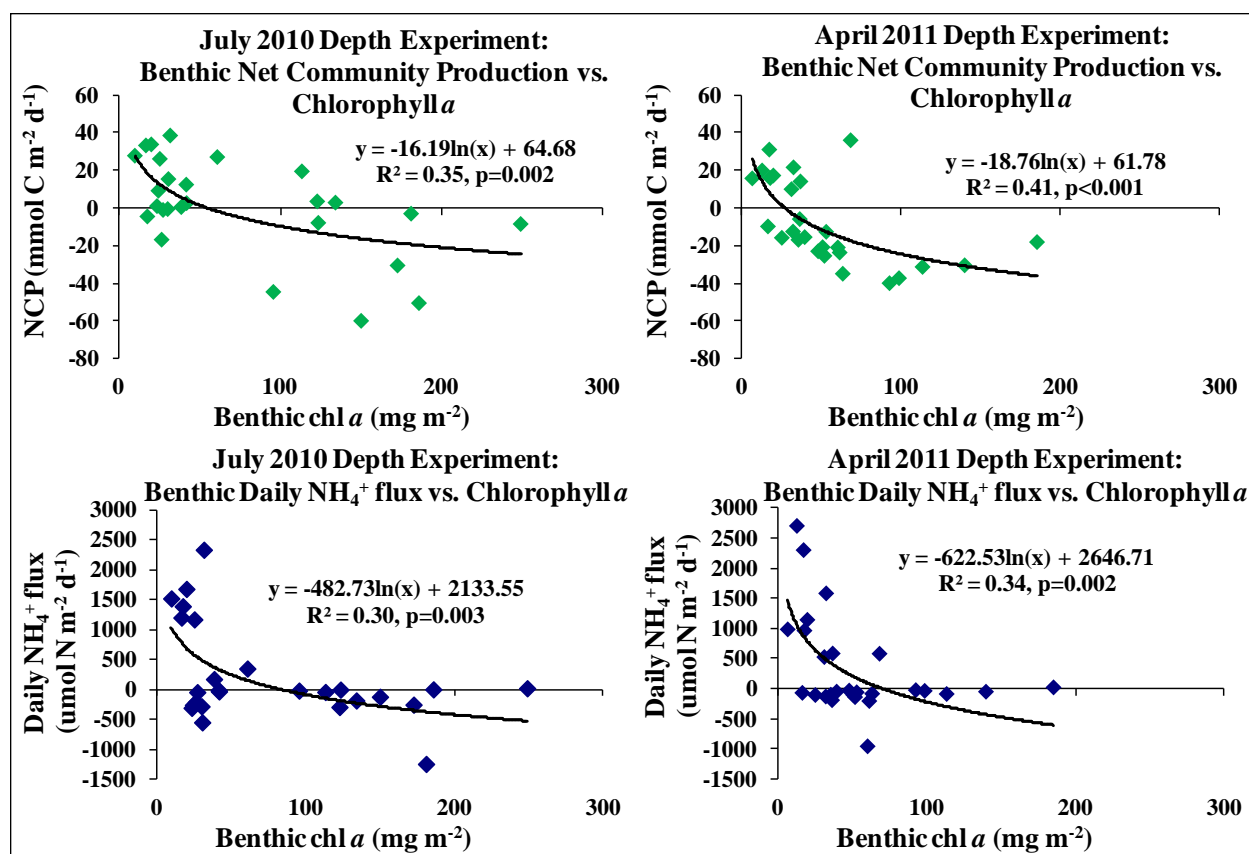


Figure 5-52. Regressions of benthic NCP (top) and benthic daily NH₄⁺ flux (bottom) versus benthic chl *a* (0–3 mm depth) for the July 2010 (left) and April 2011 (right) depth experiments.

Effects of Water Depth on Benthic N Cycling Process Rates

At each location along the estuarine salinity gradient and within each depth contour, rates of N cycling processes were measured concurrently with measurements of benthic metabolism. Rates of MIN tended to increase with depth during summer as did rates of DNF (**Figure 5-53**), whereas rates of BMA N-demand (based on GPP, see **Figure 5-48**) declined with depth. The percentage of mineralized N sequestered by BMA N demand, removed by DNF, or fluxed from sediments to the water column at 0.5-m and 3.0-m depths is shown in **Figure 5-54**. At 0.5-m depth, BMA N-demand sequestered from 23% to 104% of the mineralized N, whereas removal by DNF was a minor component and there was little if any flux of N out of sediments. At 3.0-m depth, DNF was the dominant mechanism for removal, although BMA N-demand was observed in the lower estuary, and fluxes of N out of sediments were large, especially in mid-estuary during spring.

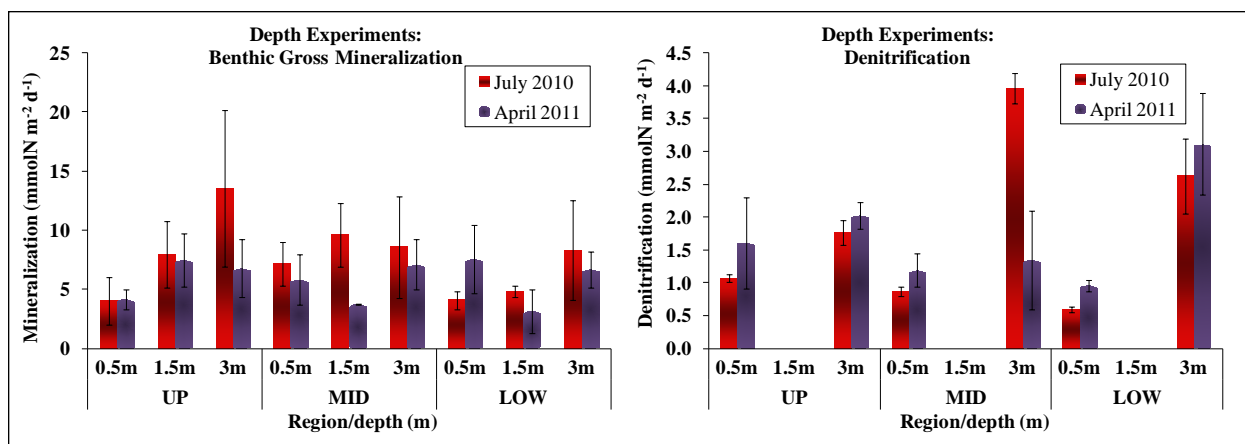


Figure 5-53. Mean (\pm standard error) benthic gross mineralization and net DNF measured in three regions and at three water depths of the estuary (only two depths for DNF) in July 2010 and April 2011.

UP=upper region; MID= middle region; and LOW= lower region.

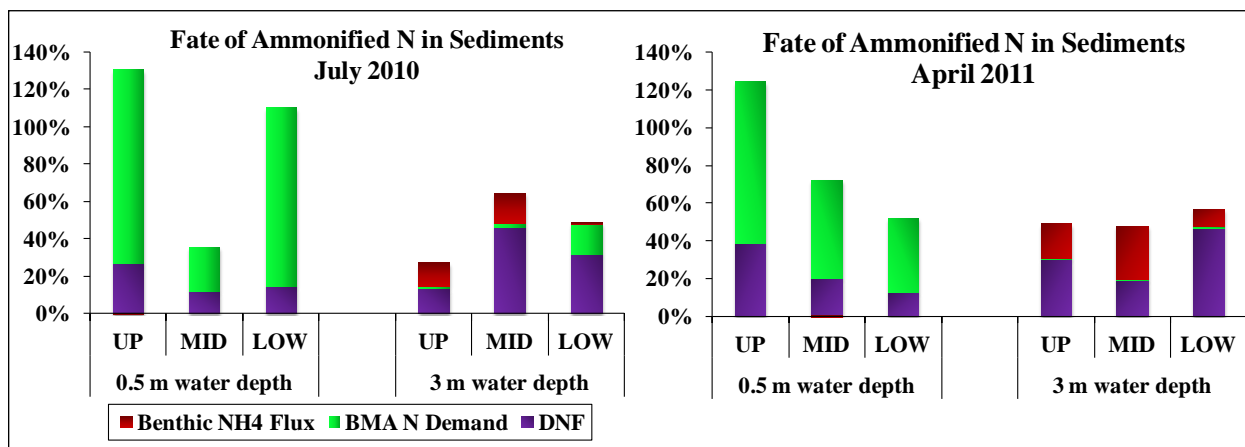


Figure 5-54. The percent of ammonified N removed by benthic NH₄⁺ flux, BMA N demand, and DNF in three regions and at two water depths of the estuary in July 2010 and April 2011.

UP=upper region; MID= middle region; and LOW= lower region.

Estimates of the Estuarine-wide Effectiveness of the Benthic Filter

The overall impact of the benthic filter at the estuarine-wide scale was estimated by scaling rates of benthic MIN, BMA N-demand and DNF, as previously described, to the entire estuary. During spring 2011 and summer 2010 benthic processes were estimated to remove between 28–70% of the TN produced by autochthonous processes, measured as benthic MIN, but including NFix and DNRA (**Figure 5-55**). The percentage removed during spring was somewhat greater than during summer, perhaps due to the higher MIN and NFix rates during summer and reduction in the net DNF rates (**Table 5-15**). Even though this is a preliminary estimate based on limited data, it is clear that the benthic filter plays an important role, at least during spring and summer to reduce fluxes of N from the benthos to the water column and thereby reduces the

potential for pelagic eutrophication. Improvements in this estimate require further measurements during winter and fall.

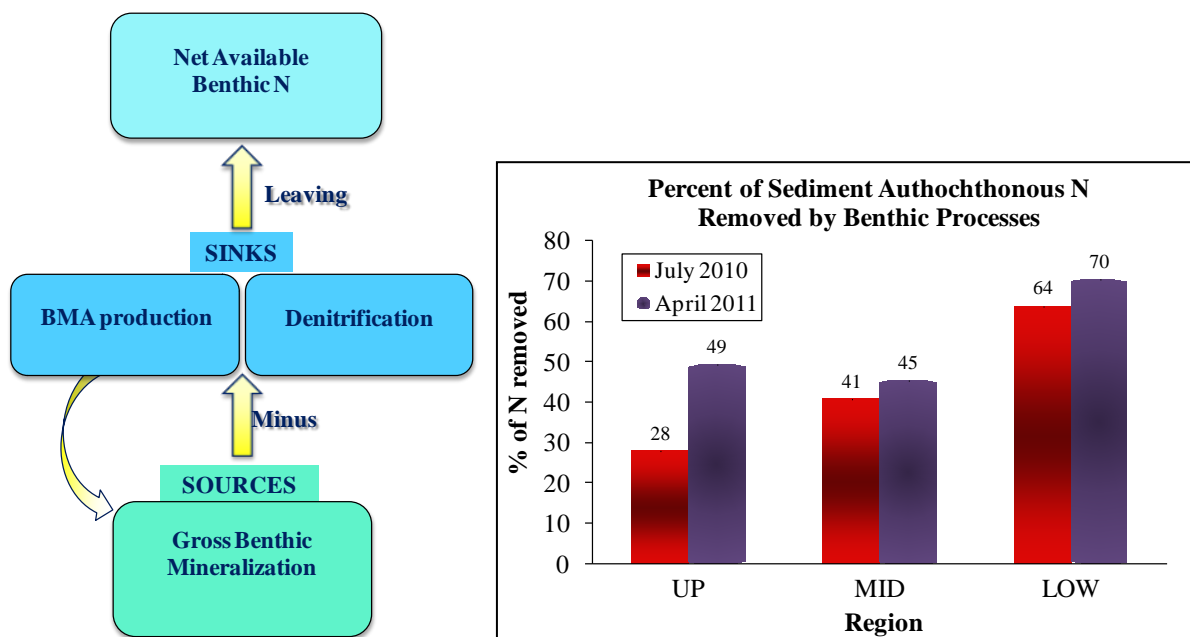


Figure 5-55. The percent of sediment autochthonous N removed by benthic processes scaled up to the NRE by regions in July 2010 and April 2011.

Table 5-15. Benthic N Scaled Up to the NRE by Region

Region	BMA N-Demand (kmol N day ⁻¹)		Gross DNF (kmol N day ⁻¹)		MIN (kmol N day ⁻¹)		Potential Net Available Benthic N (kmol N day ⁻¹)	
	Summer	Spring	Summer	Spring	Summer	Spring	Summer	Spring
UP	-37	-35	-42	-53	284	178	205	90
MID	-30	-48	-102	-55	323	227	192	124
LOW	-26	-26	-12	-17	59	60	21	18

An Estuarine-wide Index of Eutrophication for the NRE

Using data collected across the NRE by Research Project AE-1 for pelagic primary production and by Research Project AE-3 for benthic primary production, a eutrophication index was calculated for the NRE. As shown in **Table 5-16**, total GPP for the entire estuary was 253 g C m⁻² y⁻¹. According to the definition of estuarine eutrophication given in Nixon (1995), the NRE currently is moderately eutrophic. The ratio of water volume to benthic surface area in the NRE varies from 2.1 in the upper estuary to 1.8 in the middle and 1.3 in the lower estuary; thus the percentage of benthic surface in the photic zone is also likely to increase down-estuary. A linear regression of production data from 2007–2011 across the upper, mid, and lower regions of the estuary demonstrates that benthic and pelagic GPP were inversely proportional to each other (**Figure 5-56**), with the highest ratio of benthic:pelagic GPP down-estuary corresponding

to the lowest ratio of water volume to benthic surface area and likely the highest percentage of photic benthos.

Table 5-16. GPP ($\text{gC m}^{-2} \text{yr}^{-1}$) Scaled Up to the NRE and by Region

Section of NRE	Phytoplankton ^a						Benthic Microalgae ^b Average 2008–2010	Salt Marsh ^c Average 2007–2011
	2007 ^d	2008	2009	2010	2011	Average 2007–2011		
Whole estuary	85	102	154	156	186	146	104	1.3
Lower (Stations 1-2)	45	64	74	70	122	80	187	3.4
Middle (Stations 3-4)	74	89	123	132	168	125	95	1.0
Upper (Stations 5-USGS Gage #020903205) ^e	96	123	201	198	217	179	81	1.6

Note: Productivity values of each producer category were divided by the total estuarine surface area of each segment.

^a Phytoplankton data from Research Project AE-1.

^b BMA data from Research Project AE-3.

^c Salt marsh data from the Coastal Wetlands Module.

^d Data from 2007 are the average productivities for the period October 7–December 31, 2007.

^e Productivities at USGS Station number 0209303205 were estimated based on measured chl *a* values and the regression between primary productivity and chl *a*.

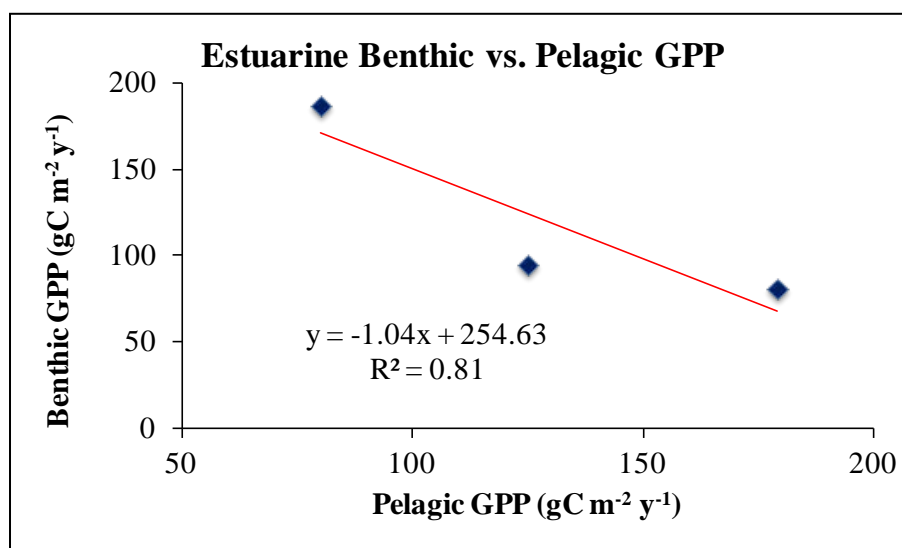


Figure 5-56. Plot of regional benthic GPP versus pelagic GPP.

Conclusions and Implications for Future Research

Summary of Key Findings

1. Allochthonous versus autochthonous sources of N to the NRE
 - On an annual basis, allochthonous off-Base sources, namely the watersheds of the New River and Southwest Creek, supplied 64% of the TN load to the NRE. On-Base sources, which included the WWTF on French Creek and locally impacted watersheds, contributed approximately 15% of the TN load.
 - During spring and summer the influence of regional allochthonous sources of N was reduced as autochthonous sources of N (from benthic fluxes) became more important, contributing up to 26% of the TN load.
2. Effects of freshwater discharge on photic area
 - Between 2008–2011, photic area in the NRE varied from 46–97% of total estuarine bottom area
 - Freshwater discharge was inversely proportional to benthic photic area, accounting for 69% of the observed variability
3. Relative contribution of N cycling processes to the benthic filter
 - In shallow photic sediments (0.5 m average depth at MSL) BMA N-demand sequestered from 23% to 104% of the mineralized N whereas removal by DNF was a minor component, and there was little if any flux of N out of sediments.
 - In deeper aphotic sediments (3.0 m average depth at MSL) DNF was a more important process for removal of regenerated N.
4. Effectiveness of the benthic filter in removing or sequestering inorganic N regenerated from OM in the sediments
 - Effectiveness of the benthic filter was dependent on light availability, temperature, and benthic chl *a*, which accounted for 52% of the observed variability in benthic primary production.
 - Net benthic community production predicted the flux of NH_4^+ to the water column—a net autotrophic benthos took up NH_4^+ ; a net heterotrophic benthos released NH_4^+ .
 - During spring 2011 and summer 2010 benthic processes were estimated to remove between 28–70% of the TN produced by autochthonous processes,
5. Benthic chl *a* as an indicator of the effectiveness of the benthic filter
 - A benthic chl *a* threshold, ranging from 70–83 mg m^{-2} predicted the sediment–water NH_4^+ flux. For values below threshold the benthos released NH_4^+ to the water column; above threshold the benthos took up NH_4^+ from the water column.

Importance of Benthos in the NRE

DCERP1 demonstrated that the NRE is a moderately eutrophic estuary with rates of benthic primary production ($\text{gC m}^{-2} \text{y}^{-1}$) that accounted for 41% of total average annual primary production across the estuary. Although phytoplankton dominated total GPP in the NRE, an active benthic microbial community in the shallow photic zone was highly productive and effective in mitigating watershed nutrient loads, and thereby serving as a benthic filter. The benthos served as both a source of recycled nutrients supporting pelagic primary production as well as a benthic filter, sequestering and removing nutrients by BMA uptake, DNF, and anaerobic NH_4^+ oxidation (i.e., ANA), thereby mitigating eutrophication. The effectiveness of the benthic filter was dependent on light availability and photic area of the estuary ($\geq 1\% I_0$), which varied as a function of freshwater discharge. Between 2008–2011, photic area in the NRE varied from 46–97% of total estuarine bottom area. When light availability was low, the benthos switched from net autotrophic (photosynthesizing their food) to heterotrophic (using organic compounds for food) and from a net sink to a source of N to the water column. Estuary-wide benthic processes sequestered from 41–67% of the IN remineralized from OM in sediments in spring and from 27–63% in summer. Whereas uptake of regenerated N by photosynthesizing BMA sequestered more N when sufficient light was available, DNF proved to be more important for removal of N when light was limiting. Benthic chl *a* was an excellent indicator of the effectiveness of the BMA N “filter.” During summer 2010 and spring 2011, a threshold for benthic chl *a*, was observed that ranged from 70–83 mg m^{-2} , below which the benthos was a source of nutrients supporting primary production by phytoplankton and above which was a sink, sequestering nutrients. In high discharge years with high nutrient inputs, high pelagic primary production, and low photic area, the BMA “filter” is likely to be less effective due to light limitation and low biomass. Wind also affected benthic processes by resuspending particulates in shallow waters, and reducing light availability throughout the water column. Particle-size of suspended particulate matter increased down-estuary. CDOM and sediment loads were dominant factors controlling light attenuation, benthic metabolism and nutrient exchange up-estuary; resuspension and phytoplankton abundance were likely more important drivers down-estuary.

Vulnerability of the Benthic Filter to Natural and Anthropogenic Changes and Potential Responses to Climate Change

The effectiveness of the benthic filter, which is dependent on light availability, is vulnerable to both natural and anthropogenic disturbances. Anthropogenic disturbance due to increased population, accompanied by urban development and other land use changes, will increase delivery of particulates (sediment) and nutrients to the NRE. Climate change, likely to be accompanied by more frequent and intense storm events, will increase inputs of fresh water along with nutrients and both particulate and dissolved forms of OM, including CDOM. Increased inputs of particulates and CDOM will result in decreased light availability especially in the upper NRE. Accompanying winds will increase resuspension and redistribute BMA to greater depths especially in the sandier lower estuary. Increased frequency of phytoplankton blooms, due to higher nutrient loads and reduced effectiveness of the benthic filter, will further decrease light availability. As particulate organic matter inputs and phytoplankton blooms increase in response to disturbance, they will settle out of the water column to the benthos, where the OM will be respired and remineralized to NH_4^+ . Temperatures, also expected to rise over long time scales, increase R and mineralization faster than primary production. As R increases

relative to production, we expect that the benthos will shift toward greater heterotrophy, accompanied by benthic anoxia, sulfide accumulation, and diffusion of C and N back to the water column resulting in increased bloom production down estuary. The intrusion of higher salinity water as sea level rises may also increase fluxes of NH_4^+ out of sediments because of cation exchange and decrease rates of DNF due to sulfide inhibition. Marsh bank erosion due to sea level rise will further increase particulates in the water column and decrease light availability to the benthos. Long-term sequestration of C and nutrients in bottom sediments of both the estuary and marsh is likely to be highest under conditions of high production relative to R (a net autotrophic system); thus, as temperatures increase and the system becomes increasingly net heterotrophic, we would expect decreased storage of C in sediments.

Needs for Future Research on Benthic Processes

1. During DCERP1 we recognized the need to extrapolate from measurements made at the m^2 to the estuarine-wide scale. With help from other DCERP researchers, we were able to perform experiments in April 2011 and July 2010 across depth ranges representative of the whole estuary for determination of the variations in metabolic, N cycling, and flux rates. An additional experiment during fall 2012 would provide a better estimate of annual benthic process rates at the estuarine-wide scale.
2. Results observed during DCERP1 clearly showed strong responses in metabolic and N cycling process rates to freshwater discharge and temperature; however, observations were limited to years 2008–2010, a period exhibiting a shift from drought to more normal precipitation. To more clearly relate process rates to environmental variables, we have proposed during DCERP2 to perform controlled factorial experiments, exposing benthic cores to salinities representing the seasonal range observed in the upper, middle, and lower estuary. Similarly we propose to expose cores to a temperatures ranging from the average ambient for the season to ambient plus 2°C and 5°C .
3. The research emphasis during DCERP1 was on determining the role of natural and anthropogenic disturbances on sources and fates of nutrient, in particular N. During DCERP2 the emphasis will be placed on C and development of a net C budget for the NRE. The AE Module will work together to provide the data necessary to produce a budget.

Recommended Management Actions to Optimize Water Quality in the NRE

The DCERP1 Aquatic/Estuarine Module's study of the NRE was one of the most comprehensive assessments of the effects of both natural and anthropogenic disturbances on an estuarine system thus far performed in the United States. Results demonstrated that effective strategies to regulate water quality must consider anthropogenic disturbance within the context of climatic (hydrologic) variation. Managers must take into account shifting baselines resulting from climate variation when choosing targets for water quality, fisheries resource and other management strategies. The New River watershed is currently the dominant source of nutrients to the NRE, suggesting that nutrient and sediment inputs are currently best managed at the regional level; however, future growth and development on MCBCL should also endeavor to reduce nutrient and sediment loading to streams draining MCBCL watersheds. For example, observations made

in the area of Wallace Creek suggested that forest clearcutting and development in its watershed greatly increased sources of NH_4^+ to the benthos and resulted in water column hypoxia. However, if choices need to be made regarding the geographic focus of remedial actions, those affecting the New River watershed will yield maximum ecosystem benefits. Benthic processes, vulnerable to natural and anthropogenic disturbance, modulate eutrophication. Sustaining the current balance between phytoplankton and BMA primary production can be achieved by limiting excessive N and suspended sediment loads that will favor phytoplankton over BMA primary production. For example, maintaining a vegetated (forest or marsh) buffer zone of approximately 30 m between the water's edge and developed areas would greatly reduce nutrient and sediment inputs to the estuary. Within estuary training activities designed to reduce sediment resuspension would similarly reduce impacts on light availability to the benthos. Current levels of Base activities appear to be sustainable in the context of the function of the NRE. However, DCERP research has shown that estuarine ecosystem function can respond to changing MCBCL activities and that the potential for future impairment does exist.

Literature Cited

- Altman, J.C., and H.W. Paerl. 2012. Composition of inorganic and organic nutrient sources influences phytoplankton community structure in the New River Estuary, North Carolina. *Aquatic Ecology* 46:269–282.
- Anderson, I.C., J.W. Stanhope, A.K. Hardison, and K.J. McGlathery. 2010. Sources and fates of nitrogen in Virginia coastal bays. Pp. 43–72 in *Coastal Lagoons: Critical Habitats of Environmental Change*. Edited by M. Kennish and H. Paerl. CRC Press: Boca Raton, FL.
- Anderson, I.C., K.J. McGlathery, and A.C. Tyler. 2003. Microbial mediation of “reactive” nitrogen in a temperate lagoon. *Marine Ecology Progress Series* 246:73–84.
- Arar, E.J., and G.B. Collins. 1997. In vitro determination of chlorophyll *a* and phaeophytin *a* in marine and freshwater algae by fluorescence. Method 445.0, Revision 1.2. National Exposure Research Laboratory, Office of Research and Development, U.S. Environmental Protection Agency, Cincinnati, OH.
- Bricker, S.B., C.G. Clement, D.E. Pihalla, S.P. Orlano, and D.R.G. Farrow. 1999. *National Estuarine Eutrophication Assessment: Effects of Nutrient Enrichment in the Nation's Estuaries*. National Oceanic and Atmospheric Administration, National Ocean Service, Special Projects Office and the National Centers for Coastal Ocean Science, Silver Spring, MD. (71 pages).
- Brooks, P.D., J.M. Stark, B.B. McInteer, and T. Preston. 1989. Diffusion method to prepare soil extracts for automated nitrogen-15 analysis. *Proceedings—Soil Science Society of America* 53:1707–1711.
- Brush, M.J., J.W. Brawley, S.W. Nixon, and J.N. Kremer. 2002. Modeling phytoplankton production: Problems with the Eppley curve and an empirical alternative. *Marine Ecology Progress Series* 238:31–45.
- Clarke, K.R. 1993. Non-parametric multivariate analyses of changes in community structure. *Australian Journal of Ecology* 18:117–143.
- Clarke, K.R. and R.M. Warwick. 2001. Change in marine communities: An approach to statistical analysis and interpretation (2nd edition). PRIMER-E: Plymouth.
- Cloern, J.E., C. Grenz, and L. Videgar-Lucas. 1995. An empirical model of the phytoplankton chlorophyll:carbon ratio—the conversion factor between productivity and growth rate. *Limnology and Oceanography* 40(7):1313–1321.
- Cline, J.D. 1969. Spectrofluorometric determination of hydrogen sulfide in natural waters. *Limnology and Oceanography* 14:454–458.
- Cole, L.W. and K. J. McGlathery. 2012. Dinitrogen fluxes from restored seagrass meadows. *Marine Ecology Progress Series* 448:235–246.

- Dafner, E.V., M.A. Mallin, J.J. Souza, H.A. Wells, and D.C. Parsons. 2007. Nitrogen and phosphorus species in the coastal and shelf waters of Southeastern North Carolina, Mid-Atlantic U.S. coast. *Marine Chemistry* 103(3–4):289–303.
- Ensign, S., M. Piehler, and M. Doyle. 2008. Riparian zone denitrification affects nitrogen flux through a tidal freshwater river. *Biogeochemistry* 91:133–150.
- Eyre, B.D., and A.J.P. Ferguson. 2005. Benthic metabolism and nitrogen cycling in a subtropical east Australian estuary Brunswick: Temporal variability and controlling factors. *Limnology and Oceanography* 50:81–96.
- Eyre, B.D., and A.J.P. Ferguson. 2002. Comparison of carbon production and decomposition, benthic nutrient fluxes and denitrification in seagrass, phytoplankton, benthic microalgae- and macroalgae-dominated warm-temperate Australian lagoons. *Marine Ecology Progress Series* 229:43–59.
- Eyre, B.D., A.J.P. Ferguson, A. Webb, D. Maher and J.M. Oakes. 2011. Denitrification, N-fixation and nitrogen and phosphorus fluxes in different benthic habitats and their contribution to the nitrogen and phosphorus budgets of a shallow oligotrophic subtropical coastal system (southern Moreton Bay, Australia). *Biogeochemistry* 102:111–133.
- Eyre, B.D., S. Rysgaard, T. Dalsgaard, and P. Christensen. 2002. Comparison of isotope pairing and N₂: Ar methods for measuring sediment denitrification—Assumption, modifications, and implications. *Estuaries and Coasts* 25:1077–1087.
- Fulweiler, R.W., S.W. Nixon, B.A. Buckley, and S.L. Granger. 2007. Reversal of the net dinitrogen gas flux in coastal marine sediments. *Nature* 448:180–182.
- Gallegos, C.L., and P.J. Neale. 2002. Partitioning spectral absorption in Case 2 waters: discrimination of dissolved and particulate components. *Applied Optics* 41(21):4220–4233.
- Gallegos, C.L. 1994. Refining habitat requirements of submersed aquatic vegetation: Role of optic models. *Estuaries* 17:187–199.
- Gallegos, C.L. 2001. Calculating optical water quality targets to restore and protect submersed aquatic vegetation: Overcoming problems in partitioning the diffuse attenuation coefficient for photosynthetically active radiation. *Estuaries* 24(3):381–397.
- Giordano, J.C.P., M.J. Brush, and I.C. Anderson. 2012. Ecosystem metabolism in shallow coastal lagoons: Patterns and partitioning of planktonic, benthic, and integrated community rates. *Marine Ecology Progress Series* 458:21–38.
- Green, S.A., and N.V. Blough. 1994. Optical absorption and fluorescence properties of chromophoric dissolved organic matter in natural waters. *Limnology and Oceanography* 39:1903–1916.

- Hall, N.S., H.W. Paerl, K.L. Rossignol, and B.L. Peierls. In revision. Effects of climatic variability on phytoplankton biomass and community structure in the eutrophic, microtidal, New River Estuary, North Carolina, USA. *Estuarine, Coastal and Shelf Science*.
- Hardison, A., I.C. Anderson, E.A. Canuel, C. Tobias, and B. Veuger. 2011. Carbon and nitrogen dynamics in shallow photic systems: Interactions between macroalgae, microalgae, and bacteria. *Limnology and Oceanography* 56:1489–1503.
- Hardison, A., E. Canuel, I. Anderson, and B. Veuger. 2010. Fate of macroalgae in benthic systems: Carbon and nitrogen cycling within the microbial community. *Marine Ecology Progress Series* 414:41–55.
- Jassby, A.D., and T. Platt. 1976. Mathematical formulation of the relationship between photosynthesis and light for phytoplankton. *Limnology and Oceanography* 21(4):540–547.
- Joye, S.B., and I.C. Anderson, 2008. Nitrogen cycling in coastal sediments. Pp. 867–915 in *Nitrogen in the Marine Environment*. Edited by D.G. Capone, D.A. Bronk, M.R. Mulholland, and E.J. Carpenter. Academic Press.
- Kana, T.M., C. Darkangelo, M. Hunt, J. Oldham, G. Bennett, and J. Cornwell. 1994. Membrane inlet mass-spectrometer for rapid high-precision determination of N₂, O₂, and Ar in environmental water samples. *Analytical Chemistry* 66:4166–4170.
- Keeney, D.R., and D.W. Nelson. 1982. Nitrogen-inorganic forms. Pp. 643–693 in *Methods of Soil Analysis* (2nd edition). Edited by A.L. Page, R.H. Miller, and D.R. Keeney. American Society of Agronomy, Inc. and Soil Science Society of America, Inc.: Madison, WI.
- Kemp, W.M., E.M. Smith, M. Marvin-DiPasquale, and W.R. Boynton. 1997. Organic carbon balance and net ecosystem metabolism in Chesapeake Bay. *Marine Ecology Progress Series* 150:229–248.
- Kenworthy, W.J., C.L. Gallegos, C. Costello, D. Field, and G. di Carlo. Submitted. A calibrated bio-optical water quality model identifies variable eelgrass (*Zostera marina*) light requirements in Massachusetts coastal bays: Implications for environmental remediation and seagrass restoration. To be submitted to *Estuarine Coastal and Shelf Science*.
- Kirk, J.T.O. 1994. *Light and Photosynthesis in Aquatic Ecosystems* (2nd edition). Cambridge University Press: Cambridge, UK. (509 pages).
- Knepel, K., and K. Bogren. 2001. Revised 2002. Determination of orthophosphate by flow injection analysis. QuikChem Method 31-115-01-1-H. Lachat Instruments, Milwaukee, WI.

- Koroleff, F. 1983. Total and organic nitrogen. Pp. 162–169 in *Methods of Seawater Analysis*. Edited by K. Grasshoff, M. Ehrhardt, and K. Kremling. Verlag-Chemie: Weinheim, Germany.
- Kromkamp, J.C., J.F.C. de Brouwer, G.F. Blanchard, R.M. Forster, and V. Créach (Eds). 2006. Functioning of microphytobenthos in estuaries. In *Proceedings of the Colloquium*, Amsterdam, The Netherlands. August 21–23, 2003. Royal Netherlands Academy of Arts and Sciences, Amsterdam, Netherlands.
- Lavrentyev, P., W. Gardner, and L. Yang. 2000. Effects of the zebra mussel on nitrogen dynamics and the microbial community at the sediment-water interface. *Aquatic Microbial Ecology* 21:187–194.
- Liao, N. 2001. Revised 2002. Determination of ammonia in brackish or seawater by flow injection analysis. QuikChem Method 31-107-06-1-B. Lachat Instruments, Milwaukee, WI.
- Lørborg, C., and M. Søndergaard. 2009. Microbial availability and degradation of dissolved organic carbon and nitrogen in two areas. *Estuarine, Coastal and Shelf Science* 81:513–520.
- Lorenzen, C. 1967. Determination of chlorophyll and phaeopigments: Spectrophotometric equations. *Limnology and Oceanography* 12:343–346.
- MacIntyre H.L., R.J. Geider, and D.C. Miller. 1996. Microphytobenthos: The ecological role of the “secret garden” of unvegetated, shallow-water marine habitats. I. Distribution, abundance and primary production. *Estuaries* 19:186–201.
- MacIntyre, H.L. and J.J. Cullen. 1996. Primary production by suspended and benthic microalgae in a turbid estuary: Time-scales of variability in San Antonio Bay, Texas. *Marine Ecology Progress Series* 145:245–268.
- Malhotra, A., and M. S. Fonseca. 2007. Wave Exposure Model (WEMo): Formulation, procedures and validation. National Oceanic and Atmospheric Administration Technical Memorandum. National Ocean Service, National Centers for Coastal Ocean Science, number 65. (28 pages).
- Mallin, M.A., L.B. Cahoon, and M.J. Durako. 2005a. Contrasting food-web support bases for adjoining river-influenced and non-river influenced continental shelf ecosystems. *Estuarine, Coastal and Shelf Science* 62(1–2):55–62.
- Mallin, M.A., M.R. McIver, H.A. Wells, D.C. Parsons, and V.L. Johnson. 2005b. Reversal of eutrophication following sewage treatment upgrades in the New River Estuary, NC. *Estuaries* 28:750–760.
- Maxey, J.D. 2012. Shedding light on the estuarine coastal filter: The relative importance of benthic microalgae in shallow photic systems. M.S. thesis. College of William and Mary, Williamsburg, VA. (154 pages).

- McCallister, S.L., J.E. Bauer, and E.A. Canuel. 2006. Bioreactivity of estuarine dissolved organic matter: A combined geochemical and microbiological approach. *Limnology and Oceanography* 51:94–100.
- McGlathery, K.J., K. Sundbäck, and I.C. Anderson. 2007. Eutrophication in shallow coastal bays and lagoons: The role of plants in the coastal filter. *Marine Ecology Progress Series* 348:1–18.
- McGlathery K.J., K. Sundbäck, and I. Anderson. 2004. The importance of primary producers for benthic nitrogen and phosphorus cycling. Pp. 231–261 in *Estuarine Nutrient Cycling: The Influence of Primary Producers*. Edited by S.L. Nielsen, G.T. Banta, and M. Pedersen. Kluwer Academic Publishers: The Netherlands.
- McGlathery K.J., I.C. Anderson, and A.C. Tyler. 2001. Magnitude and variability of benthic and pelagic metabolism in a temperate coastal lagoon. *Marine Ecology-Progress Series* 216:1–15.
- Meyers, T.P., J. Sickles, R. Dennis, K.M. Russell, J.N. Galloway, and T. Church. 2001. Atmospheric nitrogen deposition to coastal estuaries and their watersheds. P. 254 in *Nitrogen Loading in Coastal Water Bodies: An Atmospheric Perspective*. Edited by R.A. Valigura, R.B. Alexander, M.S. Castro, T.P. Meyers, H.W. Paerl, P.E. Stacey, and R.E. Turner. American Geophysical Union: Washington, DC.
- Miller-Way, T., and R. Twilley. 1996. Theory and operation of continuous flow systems for the study of benthic-pelagic coupling. *Marine Ecology Progress Series* 140:257–269.
- Mitchell, B.G., M. Kahru, J. Wieland, and M. Stramska. 2003. Determination of the spectral absorption coefficients for particles, dissolved material and photoplankton for discrete water samples. Chapter 4 in *Ocean Optics Protocols for Satellite Ocean Color Sensor Validation*. (Revision 4, Volume IV: Special Topics in Ocean Optics Protocols and Appendices, NASA/TM-2003-211621/Rev4-Vol.VI). Edited by J.L. Mueller, G.S. Fargion, and C.R. McClain.
- Neubauer, S.C., and I.C. Anderson. 2003. Transport of dissolved inorganic carbon from a tidal freshwater marsh to the York and Pamunkey river estuary. *Limnology and Oceanography* 48:299–307.
- Neubauer, S.C., W.D. Miller, and I.C. Anderson. 2000. Carbon cycling in a tidal freshwater marsh ecosystem: A gas flux study. *Marine Ecology Progress Series* 199:13–30.
- Nixon, S.W. 1995. Coastal marine eutrophication: A definition, social causes, and future concerns. *Ophelia* 41:199–219.
- Nixon, S.W., R.W. Fulweiler, B.A. Buckley, S.L. Granger, B.L. Nowicki, and K.M. Henry. 2009. The impact of changing climate on phenology, productivity, and benthic-pelagic coupling in Narragansett Bay. *Estuarine, Coastal, and Shelf Science* 82:1–18

- Nixon S.W., B.A. Buckley, S.L. Granger, and J. Bintz. 2001. Responses of very shallow marine ecosystems to nutrient enrichment. *Human and Ecological Risk Assessment* 7:1457–1481.
- Officer, C.B. 1980. Box models revisited. Pp. 65–114 in *Estuarine and Wetland Processes with Emphasis on Modeling*. Edited by P. Hamilton, and K.B. MacDonald.. Plenum Press: New York, NY.
- Oremland, R.S., and D.G. Capone. 1988. Use of “specific” inhibitors in biochemistry and microbial ecology. *Advances in Microbial Ecology* 10:285–383.
- Peierls, B.L., N.S. Hall, and H.W. Paerl. In press. Non-monotonic responses of phytoplankton biomass accumulation to hydrologic variability: a comparison of two coastal plain North Carolina estuaries. *Estuaries and Coasts*.
- Piehlner, M.F., and A. Smyth. 2011. Habitat-specific distinctions in estuarine denitrification affect both ecosystem function and services. *Ecosphere* 2:art12.
- Pinckney, J., and R.G. Zingmark. 1993. Photophysiological responses of intertidal benthic microalgal communities to in situ light environments: Methodological considerations. *Limnology and Oceanography* 38:1373–1383.
- Pinckney, J.L., H.W. Paerl, and M.B. Harrington. 1999. Responses of the phytoplankton community growth rate to nutrient pulses in variable estuarine environments. *Journal of Phycology* 35:1455–1463.
- Pinckney, J.L., D.F. Millie, K.E. Howe, H.W. Paerl, and J. P. Hurley. 1996. Flow scintillation counting of ¹⁴C-labeled microalgal photosynthetic pigments. *Journal of Plankton Research* 18:1867–1880.
- Pinckney, J.L., T.L. Richardson, D.F. Millie, and H.W. Paerl. 2001. Application of photopigment biomarkers for quantifying microalgal community composition and in situ growth rates. *Organic Geochemistry* 32:585–595.
- Plumb, Jr., R.H. 1981. *Procedure for Handling and Chemical Analysis of Sediment and Water Samples*. Technical Report. EPA/CE-81-1. Prepared by Great Lakes Laboratory, State University College at Buffalo, NY, for the U.S. Environmental Protection Agency/U.S. Army Corps of Engineers Technical Committee on Criteria for Dredged and Filled Material: Environmental Laboratory, U.S. Army Waterways Experiment Station, Vicksburg, MS. (403 pages).
- Shoaf, W.T., and B.W. Lium. 1976. Improved extraction of chlorophyll *a* and *b* from algae using dimethylsulfoxide. *Limnology and Oceanography* 21:926–928.
- Smith, L., M. Voytek, J. Bohlke, and J. Harvey. 2006. Denitrification in nitrate-rich streams: Application of N-2: Ar and N-15-tracer methods in intact cores. *Ecological Applications* 16:2191–2207.

- Smith, P., and K. Bogren. 2001. Determination of nitrate and/or nitrite in brackish or seawater by flow injection analysis colorimetry. QuikChem Method 31-107-04-1-E. Lachat Instruments, Milwaukee, WI.
- Smith, S.V., and J.T. Hollibaugh. 1997. Annual cycle and interannual variability of ecosystem metabolism in a temperate climate embayment. *Ecological Monographs* 67(4):509–533.
- Steppe, T.F., and H.W. Paerl. 2002. Potential N₂ fixation by sulfate-reducing bacteria in a marine intertidal microbial mat. *Aquatic Microbial Ecology* 28:1–12.
- Sundbäck, K., F. Linares, F. Larson, A. Wulff, and A. Engelsen. 2004. Benthic nitrogen fluxes along a depth gradient in a microtidal fjord: The role of denitrification and microphytobenthos. *Limnology and Oceanography* 49:1095–1107.
- Sundbäck, K., and A. Miles. 2000. Balance between denitrification and microalgal incorporation of nitrogen in microtidal sediments, NE Kattegat. *Aquatic Microbial Ecology* 22:291–300.
- Sundbäck, K., V. Enoksson, W. Graneli, and K. Pettersson. 1991. Influence of sublittoral microphytobenthos on the oxygen and nutrient flux between sediment and water: A laboratory continuous-flow study. *Marine Ecology Progress Series* 74:263–279.
- Tassan, S., and G.M. Ferrari. 2002. A sensitivity analysis of the “transmittance-reflectance” method for measuring light absorption by aquatic particles. *Journal of Plankton Research* 24(8):757–774.
- Tassan, S., and G.M. Ferrari. 1995. An alternative approach to absorption measurements of aquatic particles retained on filters. *Limnology and Oceanography* 40(8):1358–1368.
- Tyler, A.C., K.J. McGlathery, and I.C. Anderson. 2003. Benthic algae control sediment-water column fluxes of organic and inorganic nitrogen compounds in a temperate lagoon. *Limnology and Oceanography* 48:2125–2137.
- Wessel, W.W. and A. Tietema. 1992. Calculating gross N transformation rates of ¹⁵N pool dilution experiments with acid forest litter: Analytical and numerical approaches. *Soil Biology & Biochemistry* 24:931–942.
- WET Labs, Inc. 2011. *ac Meter Protocol Document*. Revision Q. April 20. Available at <http://www.wetlabs.com/products/pub/ac9/acprotq.pdf>.
- Wiegner, T.N., Tubal, R.L., and R.A. MacKenzie. 2009. Bioavailability and export of dissolved organic matter from a tropical river during base- and storm flow conditions. *Limnology and Oceanography* 54:1233–1242.
- Wiegner, T.N., S.P. Seitzinger, P.M. Glibert, and D.A. Bronk. 2006. Bioavailability of dissolved organic nitrogen and carbon from nine rivers in the eastern United States. *Aquatic Microbial Ecology* 43:277–287.

- Wolfstein, K., J.F.C. de Brouwer, and L.J. Stal. 2002. Biochemical partitioning of photosynthetically fixed carbon by benthic diatoms during short-term incubations at different irradiances. *Marine Ecology Progress Series* 245:21–31
- York, J.K., G. Tomasky, I. Valiela, and A.E. Giblin. 2010. Isotopic approach to determining the fate of ammonium regenerated from sediments in a eutrophic sub-estuary of Waquoit Bay, MA. *Estuaries and Coasts* 33:1069–1079.
- Zani, S., M.T. Mellon, J.L. Collier, and J.P. Zehr. 2000. Expression of nifH genes in natural microbial assemblages in Lake George, New York, detected by reverse transcriptase PCR. *Applied and Environmental Microbiology* 66:3119–3124.
- Zehr, J.P., and L.A. McReynolds. 1989. Use of degenerate oligonucleotides for amplification of the nifH gene from the marine cyanobacterium *Trichodesmium thiebautii*. *Applied and Environmental Microbiology* 55:2522–2526.

[This page intentionally left blank.]

Appendix 5-A

Supporting Data

Supporting Data

**Table 5-A-1. Shallow Water New River Estuary and Intracoastal Waterway Stations
(approximately 0.5 m water depth MLW)**

Station Name	Station Abbreviation	Latitude	Longitude
New River Estuary			
Jacksonville	JACK	34.7512	-77.4354
Southwest Creek	SWCR	34.6839	-77.4271
Wallace Creek	WALL	34.6820	-77.3661
French Creek	FRCR	34.6400	-77.3382
Courthouse Bay	CTBY	34.5901	-77.3684
Traps Bay	TRBY	34.5688	-77.3372
Intracoastal Waterway			
Freeman Creek	FREE	34.5949	-77.2543
Gillets Creek	GLCR	34.5719	-77.2765

Table 5-A-2. NRE July 2010 and April 2011 Depth Experiments Benthic Sampling Stations

Region	Water Depth (m; MSL)	Latitude	Longitude
UPPER	0.5	34.6835	-77.4281
UPPER	1.5	34.6962	-77.4274
UPPER	1.5	34.6927	-77.4228
UPPER	1.5	34.6938	-77.4198
UPPER	3	34.7038	-77.3949
UPPER	3	34.7026	-77.3933
UPPER	3	34.7020	-77.3928
MIDDLE	0.5	34.6329	-77.3428
MIDDLE	0.5	34.6335	-77.3428
MIDDLE	0.5	34.6335	-77.3426
MIDDLE	1.5	34.6354	-77.3524
MIDDLE	1.5	34.3658	-77.3520
MIDDLE	1.5	34.6331	-77.3518
MIDDLE	3	34.6286	-77.3674
MIDDLE	3	34.6275	-77.3656
MIDDLE	3	34.6263	-77.3658
LOWER	0.5	34.5688	-77.3370
LOWER	0.5	34.5686	-77.3372
LOWER	0.5	34.5687	-77.3373
LOWER	1.5	34.5668	-77.3429
LOWER	1.5	34.5668	-77.3430
LOWER	1.5	34.5668	-77.3431
LOWER	3	34.5784	-77.3933
LOWER	3	34.5782	-77.3896
LOWER	3	34.5674	-77.3416

[This page intentionally left blank.]

Appendix 5-B

List of Scientific/Technical Publications

List of Scientific/Technical Publications

Papers

- Anderson, I.C., M.J. Brush, C.A. Currin, M.F. Piehler, and J.W. Stanhope. In preparation. The role of natural and anthropogenic disturbances in regulating the benthic nutrient filter. To be submitted for a special issue of *Estuaries and Coasts* due September 2012.
- Anderson, I.C., M.J. Brush, C.A. Currin, M.F. Piehler, and J.W. Stanhope. In preparation. Benthic indicators of ecosystem function in a shallow photic estuary. To be submitted for the *Marine Ecology Progress Series*.
- Anderson, I.C., M.J. Brush, C.A. Currin, M.F. Piehler, J.D. Maxey, J.W. Stanhope, and M.L. Whitehead. In preparation. Benthic sources and sinks of nitrogen in a shallow photic marine system. To be submitted to *Estuaries and Coasts*.
- Anderson, I.C., J.W. Stanhope, A.K. Hardison, and K.J. McGlathery. 2010. Sources and fates of nitrogen in Virginia coastal bays. Pp. 43–72 in *Coastal Lagoons: Critical Habitats of Environmental Change*. Edited by M. Kennish, and H. Paerl. CRC Press: Boca Raton, FL.
- Brush, M.J., and L.A. Harris (Eds). 2010. Advances in modeling estuarine and coastal ecosystems: Approaches, validation, and applications. Special issue: *Ecological Modelling* 221(7).
- Brush, M.J., and L.A. Harris. 2010. Introduction to the special issue of *Ecological Modelling*: Advances in modeling estuarine and coastal ecosystems: approaches, validation, and applications. *Ecological Modelling* 221(7):965–968.
- Brush, M.J., and H.M. Wiseman. 2011. Modeling the ecosystem role of a suspension and deposit feeding bivalve across hydrologically different years. Submitted to the *Journal of Sea Research*. In review.
- Brush, M.J., I.C. Anderson, C.A. Currin, M.F. Piehler, and J.C.P. Giordano. In preparation. Scaling rates of water column, benthic, and system metabolism as a function of depth and water quality in a shallow, blackwater estuary. To be submitted for the *Marine Ecology Progress Series*.
- Currin, C.A., I.C. Anderson, M.F. Piehler, M. Fonseca, and M.J. Brush. Planned for 2012. Wave energy influence on benthic microalgal distribution and production in a shallow estuary. To be submitted to *Estuaries and Coasts*.
- Hardison, A., I.C. Anderson, E.A. Canuel, C. Tobias, and B. Veuger. 2011. Carbon and nitrogen dynamics in shallow photic systems: Interactions between macroalgae, microalgae, and bacteria. *Limnology & Oceanography* 56:1489–1503.

Hilting, A.K., C.A. Currin, C.L. Gallegos, M.J. Brush, and I.C. Anderson. In preparation. Geospatial predictions of the effects of water quality on benthic microalgal production using a bio-optical model. To be submitted to *Estuaries and Coasts*.

Piehl, M.F., I.C. Anderson, M.J. Brush, and C.A. Currin. In preparation. Denitrification enhances ecosystem stability through the estuarine gradient. To be submitted for a special issue of *Estuaries and Coasts* due September 2012.

Whitehead, M., I.C. Anderson, C.A. Currin, K. Reece, and J. McDowell. In preparation. Structure and function of nitrogen fixing organisms in a shallow coastal ecosystem. To be submitted for the *Marine Ecology Progress Series*.

Presentations

Year	Title/Topic	Publication/Conference^a	Authors
2008	Balancing Precision, Realism, and Generality in Estuarine Ecosystem Models: A Tour from the Practical to the Esoteric and Back Again (invited seminar)	University of North Carolina at Chapel Hill's Institute of Marine Sciences	Brush
2009	Application of Advanced Indicators to Distinguish Military from Other Human and Climatic Impacts on Estuarine Ecosystem Function	SERDP-ESTCP Partners in Environmental Technology Technical Symposium & Workshop (poster)	Pearl, Anderson, Piehler, and Brush
2009	Benthic, Pelagic and System Metabolism in an Optically Diverse Estuary: Results from Measurements and Simulation Modeling	Coastal and Estuarine Research Federation	Brush, Anderson, Currin, and Piehler
2009	Scaling Rates of Water Column, Benthic, and System Metabolism as a Function of Depth and Water Quality in Shallow Photic Estuaries	American Society of Limnology and Oceanography	Brush, Anderson, Currin, and Piehler
2009	Scaling Rates of Water Column, Benthic, and System Metabolism as a Function of Depth and Water Quality in Shallow Photic Estuaries	Atlantic Estuarine Research Society	Brush, Anderson, Currin, and Piehler
2009	Vulnerability and Resilience of Shallow Coastal Systems to Natural and Anthropogenic Disturbances	Coastal and Estuarine Research Federation	Anderson, Currin, Brush, Piehler, and Stanhope
2009	Denitrification and Disturbance: Resilience Through the Estuarine Gradient	Coastal and Estuarine Research Federation	Piehler, Smyth, Schwartz, Brush, Anderson, and Currin
2009	Vulnerability and Resilience of the New River Estuary, North Carolina, to Natural and Anthropogenic Disturbances	SERDP-ESTCP Partners in Environmental Technology Technical Symposium & Workshop (poster)	Anderson and Paerl

Year	Title/Topic	Publication/Conference^a	Authors
2010	Vulnerability and Resilience of the New River Estuary, North Carolina, to Natural and Anthropogenic Disturbances	Atlantic Estuarine Research Society (fall meeting) (poster)	Anderson, Brush, Currin, Paerl, Piehler, and Stanhope
2010	Modeling Through the Macroscope: An Estuarine Potpourri from Watersheds to Water Quality to Fish (invited seminar)	Horn Point Environmental Laboratory, University of Maryland	Brush
2010	Modeling Through the Macroscope: An Estuarine Potpourri from Watersheds to Water Quality to Fish (invited seminar, updated)	Chesapeake Biological Laboratory, University of Maryland	Brush
2010	Application of Microalgal Indicators in the New River Estuary, NC: Quantifying Multiple Stresses to Water Quality	SERDP-ESTCP Partners in Environmental Technology Technical Symposium & Workshop (poster)	Paerl, Anderson, Brush, and Piehler
2010	Light Availability Along a Water Quality Gradient in a Shallow Estuary: Significance of the Backscattering to Scattering Ratio	Ocean Optics XX Conference	Hilting, Currin, Gallegos, Brush, and Anderson
2011	Regional Applications of the Bio-optical Model: Fine Tuning Predictions of Light Availability Along a Water Quality Gradient	Workshop on Bio-optical model and Seagrass Productivity, a European Cooperation in Science and Technology workshop	Hilting, Currin, Gallegos, Brush and Anderson
2011	Investigating the Relative Importance of Allochthonous and Autochthonous Nitrogen Sources in the New River Estuary	Atlantic Estuarine Research Society (spring meeting)	Maxey, Anderson, Brush, Currin, Piehler, and Stanhope
2011	Benthic Nitrogen Fixation in the New River Estuary, NC	Atlantic Estuarine Research Society (spring meeting) (poster)	Whitehead and Anderson
2011	Sources and Sinks of Nitrogen in a Shallow Estuary (invited seminar)	Shallow Water Forum	Anderson, Brush, Currin, Piehler, and Stanhope
2011	The Role of Natural and Anthropogenic Disturbances in Regulating the Benthic Nutrient Filter	Coastal and Estuarine Research Federation	Anderson, Brush, Currin, Piehler, and Stanhope
2011	Modeling Responses to Climatic and Anthropogenic Stressors in a Shallow Coastal Photic System	Coastal and Estuarine Research Federation	Brush, Anderson, Piehler, Currin, and Paerl

Year	Title/Topic	Publication/Conference ^a	Authors
2011	High-Resolution Monitoring of Climatically Driven Variations in Photic Area and Potential Benthic Productivity in a Shallow, Blackwater Estuary	Coastal and Estuarine Research Federation, Shallow Water Monitoring Workshop	Brush, Stanhope, and Anderson
2011	Reduced and Intermediate-Complexity Systems Models for Science and Management: The Macroscopic Estuarine Modeler's Toolbox (invited keynote)	International Estuarine Biogeochemistry Symposium	Brush
2011	Variation in Photic Area with Freshwater Discharge in a Shallow Estuary	Coastal and Estuarine Research Federation (poster)	Stanhope, Anderson, and Brush
2011	Benthic Nitrogen Fixation: An Autochthonous Source of Nitrogen to the New River Estuary, NC	Coastal and Estuarine Research Federation (poster)	Whitehead, Reece, Currin, and Anderson
2011	Estimating System-wide Sources and Sinks of Nitrogen in a Shallow Mid-Atlantic Estuary—The Role of Light Availability	Coastal and Estuarine Research Federation (poster)	Maxey, Anderson, Brush, Currin, Piehler, and Stanhope
2011	The Role of Hydrologic Variability in Determining Microalgal Biomass, Community Structure and Water Quality in the New River Estuary, Marine Corps Base Camp Lejeune, North Carolina	SERDP-ESTCP Partners in Environmental Technology Technical Symposium & Workshop (poster)	Paerl, Hall, Rossignol, Peierls, Joyner, Anderson, Brush, and Stanhope
May 2012	Tracking the Fate of Carbon and Nitrogen in a Shallow Photic Coastal Lagoon (invited speaker)	East China Normal University, Shanghai, China	Anderson
May 2012	The Role of Natural and Anthropogenic Disturbances in Regulating the Benthic Nutrient Filter (invited speaker)	East China Normal University, Shanghai, China	Anderson, Brush, Currin, Piehler, and Stanhope

^a Presentations are oral unless noted as poster.

Masters Theses

Maxey, J.D. June 2012. Shedding Light on the Estuarine Coastal Filter: The Relative Importance of Benthic Microalgae in Shallow Photic Systems. Masters of Marine Science, College of William and Mary, Williamsburg VA.

Whitehead, M. Expected August 2012. Spatial and Temporal Patterns of Benthic Nitrogen Fixation in the New River Estuary, North Carolina. Masters of Marine Science, College of William and Mary, Williamsburg VA.

Wiseman, H. 2010. Quantifying the Ecosystem Role of a Suspension and a Facultative Deposit Feeding Bivalve in the New River Estuary, NC, with Responses to Changes in Nutrient

and Sediment Inputs. Masters of Marine Science, College of William and Mary,
Williamsburg VA.

Appendix 5-C

List of Students

- Wiseman, H., M.S. degree in Marine Science. College of William and Mary, School of Marine Science. December 2010.
- Maxey, J.D., M.S. degree in Marine Science. College of William and Mary, School of Marine Science. June 2012.
- Whitehead, M., M.S. degree in Marine Science. College of William and Mary, School of Marine Science. Expected August 2012.

[This page intentionally left blank.]

Chapter 6

Development and Application of Watershed and Estuarine Simulation Models for the New River Estuary

SERDP Project Number: RC-1413

Aquatic/Estuarine Module

Synthetic Modeling

Lead Researcher:

Dr. Mark J. Brush
Virginia Institute of Marine Science
P.O. Box 1346
Gloucester Point, VA 23062
E-mail: brush@vims.edu

May 10, 2013

Final

This report was prepared under contract to the U.S. Department of Defense (DoD) Strategic Environmental Research and Development Program (SERDP). The publication of this report does not indicate endorsement by DoD, nor should the contents be construed as reflecting the official policy or position of DoD. References herein to any specific commercial product, process, or service by trade name, trademark, manufacturer, or otherwise, do not necessarily constitute or imply its endorsement, recommendation, or favoring by DoD.

Table of Contents

List of Acronyms	6-vii
Abstract.....	6-1
Objectives of the Synthetic Modeling.....	6-2
Technical Goals	6-2
Background.....	6-2
Materials and Methods.....	6-6
Watershed Simulation Modeling	6-6
Estuarine Simulation Model	6-15
Results and Discussion	6-24
Watershed Simulation Models.....	6-24
Estuarine Simulation Model	6-42
Conclusions and Implications for Future Research	6-64
Literature Cited	6-66
Appendix 6-A: List of Scientific Publications.....	6-A-1
Appendix 6-B: List of Students	6-B-1

List of Figures

6-1.	Map of the NRE, its watershed, and MCBCL.	6-4
6-2.	DCERP tributary creek monitoring stations and watershed boundaries.....	6-7
6-3.	Suite of watershed modeling approaches applied to the NRE.....	6-8
6-4.	Schematic of the ESM.	6-16
6-5.	Spatial elements of the ESM and hydrodynamic exchanges.	6-17
6-6.	Stations for 2009 benthic sampling in three salinity zones of the NRE.	6-24
6-7.	Relationship between observed and predicted watershed yields of fresh water for (a) total, (b) base, and (c) storm loads using empirical regression models.....	6-28
6-8.	Relationship between observed and predicted watershed yields of TSS for (a) total, (b) base, and (c) storm loads using empirical regression models.	6-29
6-9.	Relationship between observed and predicted watershed yields of TN for (a) total, (b) base, and (c) storm loads using empirical regression models.	6-30
6-10.	Regressions of annual TN loads from the Research Project AE-2 watersheds during the first year of sampling (July 2008–June 2009) against loads predicted by a variety of watershed models.....	6-32
6-11.	Regressions of annual TN loads from the Research Project AE-2 watersheds during second year of sampling (July 2009–June 2010) against loads predicted by a variety of watershed models.....	6-33
6-12.	Regressions of annual P loads from the Research Project AE-2 watersheds during Year 1 of sampling (July 2008–June 2009) against loads predicted by a variety of watershed models.....	6-34
6-13.	Regressions of annual P loads from the Research Project AE-2 watersheds during Year 2 of sampling (July 2009–June 2010) against loads predicted by a variety of watershed models.....	6-35
6-14.	Regressions of annual TSS loads from the Research Project AE-2 watersheds during Year 1 (July 2008–June 2009) and Year 2 (July 2009–June 2010) of sampling against loads predicted by a variety of watershed models.	6-36
6-15.	Regressions of annual freshwater loads from the Research Project AE-2 watersheds during Year 1 (July 2008–June 2009) and Year 2 (July 2009–June 2010) of sampling against loads predicted by a variety of watershed models.....	6-37
6-16.	Example monthly time series of observed and predicted (ReNuMa) loads for two sub-watersheds in which the correspondence was reasonably close.	6-38
6-17.	Sources of annual allochthonous TN loading to the NRE based on empirical scaling of measured loads and seven different modeling approaches.	6-40
6-18.	Predicted increases in watershed TN yield from MCBCL to the NRE resulting from conversion of forested land to impervious surfaces.	6-41
6-20.	Example ESM calibration results to critical rate process data and BMA biomass.....	6-43

6-21.	Growth and photosynthetic parameters for BMA from Research Project AE-3, two Virginia systems, and a year-long temperature experiment conducted in the York River.	6-44
6-22.	ESM calibration results to eelgrass shoot growth rate, respiratory rate, and biomass in Spatial Element 7 (lower NRE).	6-45
6-23.	Modeled N sources to each NRE spatial element.	6-46
6-24.	ESM estimated sinks for N in the NRE.	6-47
6-25.	ESM computed freshwater flushing time for the NRE as a whole, as a function of mean freshwater flow at Gum Branch (1998–2010).	6-48
6-26.	ESM computed flushing time by NRE spatial element.	6-49
6-27.	ESM predicted phytoplankton biomass as chl <i>a</i> in surface waters of the NRE with (green lines) and without (blue lines) BMA.	6-50
6-28.	ESM predicted phytoplankton biomass as chl <i>a</i> and DIN concentrations in surface waters of Farnell Bay (Box 5) with (blue lines) and without (red lines) denitrification.	6-50
6-29.	Effect of residence and flushing times on the fraction of land- and atmospheric-based N loads denitrified across a range of estuarine systems.	6-51
6-30.	ESM predicted phytoplankton biomass as chl <i>a</i> in surface waters of the NRE with (blue lines) and without (red lines) the presence of CDOM.	6-52
6-31.	<i>M. mercenaria</i> calibration results for individual growth in the (a, b) high mesohaline and (c, d) polyhaline zones in 2009.	6-53
6-32.	<i>M. balthica</i> calibration results for individual growth in the (a, b) low mesohaline and (c, d) high mesohaline zones in 2009.	6-54
6-33.	Daily percentage of available food consumed by <i>M. mercenaria</i> removed by the public fishery harvest in a drought year (2008) and a normal year (2009).	6-56
6-34.	Daily percentage of available food consumed by <i>M. balthica</i> in a drought year (2008) and a normal year (2009) in two salinity zones.	6-57
6-35.	Modeled carrying capacity of <i>M. mercenaria</i> in a drought year (2008) and a normal year (2009) in the hard clam fishing area.	6-58
6-36.	Modeled carrying capacity of <i>M. balthica</i> in a drought year (2008) and a normal year (2009) in the low and high mesohaline zones combined.	6-59
6-37.	Degree of top-down grazing control exerted by benthic filter feeders in a variety of systems.	6-60
6-38.	Effect of the MCBCL WWTF on NRE water quality.	6-61
6-39.	Effect of MCBCL watershed loads on NRE water quality.	6-62
6-40.	Effect of off-Base watershed nutrient loads on surface chl <i>a</i> in the NRE.	6-63
6-41.	Effect of off-Base watershed nutrient loads on the percentage of time the NRE is predicted to be in violation of the state chl <i>a</i> criterion of 40 µg L ⁻¹	6-63

6-42.	Effect of inter-annual hydrologic variability on NRE response to off-Base watershed nutrient loading.	6-64
-------	--	------

List of Tables

6-1.	Re-classification of NLCD 2001 land-cover categories for empirical regression modeling.	6-9
6-2.	Area, land-cover distribution, and physical characteristics of tributary creek watersheds from Research Project AE-2.	6-10
6-3.	Parameters used in linear and logistic watershed regression models.	6-11
6-4.	Information theoretic analysis of regression model fits to measured annual watershed yields of ammonium in baseflow.	6-11
6-5.	Re-classification of NLCD 2001 land-cover categories for the NLM.	6-14
6-7.	Description of the ESM spatial elements.	6-17
6-8.	Parameters and equations for the physical Box Model.	6-18
6-9.	Relative model weights (w_i) for the best-fitting regressions for watershed yields of fresh water ($\text{m}^3 \text{ha}^{-1} \text{y}^{-1}$) and TSS and orthophosphate (PO_4^{3-} ; $\text{kg ha}^{-1} \text{y}^{-1}$) determined by Akaike Information Criterion analysis.	6-25
6-10.	Relative model weights (w_i) for the best-fitting regressions for watershed yields of N species ($\text{kg ha}^{-1} \text{y}^{-1}$) determined by Akaike Information Criterion analysis.	6-26
6-11.	Median percent increases in surface chl <i>a</i> and DIN by ESM spatial element in the absence of denitrification.	6-52
6-12.	Median percentage decreases in surface chl <i>a</i> by ESM spatial element in the absence of CDOM.	6-53
6-13.	Predicted percentage increases in final weight for an individual <i>M. mercenaria</i> and <i>M. balthica</i> in a drought year (2008) and a relatively normal year (2009).	6-55
6-14.	Average daily percentage of available food consumed by <i>M. mercenaria</i> and <i>M. balthica</i> in a drought year (2008) and a normal year (2009).	6-56
6-15.	Annual average number of <i>M. mercenaria</i> and <i>M. balthica</i> supported by the available food supply in a drought year (2008) and a normal year (2009).	6-58
6-16.	Effect of the MCBCL WWTF on NRE water quality.	6-61
6-17.	Effect of MCBCL watershed loads on NRE water quality.	6-62

List of Acronyms

$\mu\text{E m}^{-2} \text{ s}^{-1}$	microEinsteins per square meter per second
$\mu\text{g L}^{-1}$	micrograms per liter
μM	micromole
μm	micrometer
AE	Aquatic/Estuarine Module of DCERP
AFDW	ash-free dry weight
AIC_c	Akaike Information Criterion corrected for small sample sizes
BASINS	Better Assessment Science Integrating point and Non-point Sources (software package)
BMA	benthic microalgae
C	carbon
CAFO	confined animal feeding operation
CASTNET	Clean Air Status and Trends Network
CDOM	chromophoric dissolved organic matter
chl <i>a</i>	chlorophyll <i>a</i>
cm	centimeter
CO_2	carbon dioxide
d	day
DCERP	Defense Coastal/Estuarine Research Program
DEB	Dynamic Energy Budget (model)
DEM	digital elevation model
DIN	dissolved inorganic nitrogen
DIP	dissolved inorganic phosphorus
DO	dissolved oxygen
DoD	U.S. Department of Defense
DON	dissolved organic nitrogen
dw	dry weight
EPA	U.S. Environmental Protection Agency
ESM	Estuarine Simulation Model
ESRI	Environmental Sciences Research Institute
ft	foot, feet
g	gram
g g^{-1}	gram per gram
GIS	geographic information systems
GPP	gross primary production
GWLF	Generalized Watershed Loading Functions
h^{-1}	per hour

ha	hectare
HSPF	Hydrologic Simulation Program–Fortran
kg ha ⁻¹ y ⁻¹	kilograms per hectare per year
km ²	square kilometers
m	meter
m ²	square meters
m ³	cubic meters
m ³ d ⁻¹	cubic meters per day
m ³ ha ⁻¹ y ⁻¹	cubic meters per hectare per year
MCBCL	Marine Corps Base Camp Lejeune
mg	milligram
mg m ⁻²	milligrams per square meter
μm	millimeter
MPB	microphytobenthos
N	nitrogen
NADP	National Atmospheric Deposition Program
NAVD88	North American Vertical Datum of 1988
NH ₄	ammonium
NHD	National Hydrography Dataset
NLCD	National Land Cover Dataset
NLM	Nitrogen Loading Model
NOAA	National Oceanic and Atmospheric Administration
NO _x ⁻	nitrate (NO ₃ ⁻) plus nitrite (NO ₂ ⁻)
NPP	net primary production
NRE	New River Estuary
NTU	nephelometric turbidity units
O ₂	molecular oxygen
P	phosphorus
PAR	photosynthetically active radiation
PC	personal computer
P-I	photosynthesis-irradiance
PLOAD	Pollutant Loading Model
PO ₄ ³⁻	Orthophosphate
POC	particulate organic carbon
ReNuMa	Regional Nutrient Management model
RSS	residual sum of squares
SAV	submerged aquatic vegetation
SERDP	Strategic Environmental Research and Development Program

SSURGO	Soil Survey Geographic database
TDN	total dissolved nitrogen
TIGER	Topologically Integrated Geographic Encoding and Referencing (database)
TMDL	total maximum daily load
TN	total nitrogen
TP	total phosphorus
TSS	total suspended solids
US EPA	U.S. Environmental Protection Agency
USGS	U.S. Geological Survey
VIMS	Virginia Institute of Marine Science
WSM	Watershed Simulation Model
ww	wet weight
WWTF	wastewater treatment facility

[This page intentionally left blank.]

Abstract

Dynamic simulation models provide powerful research and management tools for coastal marine ecosystems, with the potential for integrating diverse data sets, scaling results to the system level, providing insight into ecosystem function, and forecasting changes due to anthropogenic and natural stressors. Application of dynamic models was a key component of the Aquatic/Estuarine Module of the Defense Coastal/Estuarine Research Program (DCERP).

A range of watershed simulation models (WSMs) were applied from simple, annually resolved models with minimal parameterization through complex, daily resolved models with detailed parameterization to predict current material loads to the New River Estuary (NRE), and potential changes in those loads due to Base development. The models differed in their ability to accurately predict annual and monthly loads, and no single model provided the best predictions for all parameters (i.e., fresh water, nitrogen, phosphorus, and sediments). The models universally confirmed results from empirical measurements that the upland, off-Base watershed is the largest source of total nitrogen (TN) to the NRE (48–66%; mean=60%) with a smaller fraction (12–36%; mean=20%) coming from that portion of Marine Corps Base Camp Lejeune [MCBCL] that drains to the NRE (including 5–7% from the MCBCL wastewater treatment facility). When watershed sources alone are considered (excluding inputs from the atmosphere and Onslow Bay), a full 57–85% (mean=76%) of the NRE TN load was predicted to originate from off-Base. Two of the more successful models (i.e., Nitrogen Loading Model [NLM] and Regional Nutrient Management model [ReNuMa]) predicted small increases in watershed TN yields from the Base due to increasing impervious coverage. A comparison of WSMs indicated that models of intermediate complexity are likely the most accurate and useful management tools for the Base.

An Estuarine Simulation Model (ESM) was applied in nine spatial elements down the axis of the NRE, each with a surface and bottom layer separated by the pycnocline, and calibrated initially to MCBCL monitoring data from 1998 through early 2007, and secondly to DCERP monitoring and research data from mid-2007 through 2010. The model reproduced the annual cycles and key events in the data record for concentrations of surface chlorophyll *a*, dissolved inorganic nutrients, and dissolved oxygen, benthic microalgal biomass, and key rate processes, including phytoplankton and benthic microalgae (BMA) primary production, water column and sediment respiration, and sediment denitrification. A series of model simulations indicated that the key controls on NRE response to watershed nutrient loads include flushing time via freshwater loading, nutrient sequestration by BMA, nutrient removal by denitrification, and strong light attenuation in large part due to chromophoric dissolved organic matter. Benthic bivalves do not appear to exert a major top-down control on primary producers in the NRE despite large annual harvests of hard clams, which comprise 28% of annual statewide landings. A series of simulations with varying watershed nutrient inputs indicated minimal effect by the MCBCL wastewater treatment facility and loads originating from MCBCL, but strong effects by loads from the upland, off-Base watershed; this response is modulated by inter-annual hydrologic variability. The intermediate complexity ESM has the potential to be a useful decision-support management tool for MCBCL Natural Resource Managers.

Keywords: watershed simulation model, estuarine simulation model, ecosystem model, mechanistic, watershed, estuary, phytoplankton, microalgae, nutrients, carbon, nitrogen, oxygen, sediments, eelgrass.

Objectives of the Synthetic Modeling

Technical Goals

The overarching objective of the synthetic modeling for the Aquatic/Estuarine Module was to develop and apply simulation models of the New River Estuary (NRE) and watershed to understand controls on ecosystem function and likely responses to natural and anthropogenic stressors.

Specific objectives of the modeling included the following:

- Integrate historic and Defense Coastal/Estuarine Research Program (DCERP) monitoring and research data across the Aquatic/Estuarine Module and from other related modules
- Scale DCERP results to the system level
- Develop models that ultimately can be provided as decision-support tools to inform Base management
- Apply a range of existing watershed models across a continuum of complexity for predicting loads of water, nutrients, and sediments to the NRE from Marine Corps Base Camp Lejeune watersheds
- Use the watershed models to predict the effect of Base development on loads to the estuary, with a focus on expansion of impervious surfaces resulting from land-use change
- Apply an existing, novel estuarine model to the NRE and expand its functionalities to include features specific to the system, including benthic microalgae (BMA), eelgrass, chromophoric dissolved organic matter, and benthic bivalves
- Use the estuarine model to understand NRE structure, function, and response to natural and anthropogenic stressors, with a focus on anthropogenic nitrogen loading.

Background

Estuaries integrate inputs from terrestrial, freshwater, oceanic, and atmospheric systems and are active zones of cycling and transformation of organic matter and nutrients as they transit from land to the sea (Day et al., 1989; Hobbie, 2000; Joye and Anderson, 2008; Paerl and Piehler, 2008). The location of estuaries along coastal margins co-locates them with areas of intense human activity in the form of large urban centers and rapidly increasing population density. Pollution from sewage treatment effluent, residential septic systems, industrial activities, and runoff from impervious surfaces in these more developed areas combined with that from activities in the surrounding watersheds and airsheds, including inputs from agricultural activities and atmospheric deposition all have the potential to reach estuaries (Boesch et al., 2001; Cloern, 2001; Nixon, 1995 and 2009; Paerl, 1997; Valiela et al., 1992).

A number of physical characteristics of estuaries can make them particularly susceptible to inputs of nutrients and organic matter resulting from these anthropogenic activities, including shallow depths, small volumes, a high ratio of watershed to estuarine surface area, stratification from freshwater inputs, restricted exchanges with the ocean, and long flushing times (Bricker et al., 2007; Cloern, 2001). Depending on the combination of these characteristics present in a particular system, anthropogenic loading has the potential to result in cultural eutrophication, or “*an increase in the rate of supply of organic matter to a system*” (Nixon, 1995 and 2009), which can have a variety of negative consequences including excessive and sometimes harmful (i.e., toxic) algal blooms, proliferation of nuisance macroalgae, decline of submerged aquatic vegetation (SAV), depletion of water column dissolved oxygen (DO) concentrations (hypoxia/anoxia), and fish kills (Bricker et al., 2007). In response to the eutrophication problem, the United States has implemented a Total Maximum Daily Load (TMDL) program through the Clean Water Act, which attempts to set limits on the amount of pollutants that can be discharged to a system to maintain or restore ecosystem health (U.S. EPA, 1999).

The New River Estuary (NRE) is a moderately eutrophic, semi-lagoonal estuary in southeastern North Carolina (**Figure 6-1**; Bricker et al., 2007; Mallin et al., 2005a). The NRE is relatively small (approximately 64 km²) with a ratio of watershed to estuarine surface area of approximately 16.1. The system is shallow (mean depth approximately 1.8 m North American Vertical Datum of 1988 [NAVD88]) with more than 50% of the bottom less than 2-m deep and more than 25% less than 1 m (2009 bathymetry data collected by Dr. Jesse McNinch for Defense Coastal/Estuarine Research Program [DCERP]). The NRE has a restricted connection with the ocean via the New River Inlet, which results in mean and median freshwater flushing times as defined by Monsen et al. (2002) of 70 and 64 days, respectively, which vary from 8 to 187 days depending on freshwater inputs (Ensign et al., 2004). The estuary is primarily surrounded by Marine Corps Base Camp Lejeune (MCBCL), which is a mixture of forested, open, and impervious land cover, with the City of Jacksonville, NC, at the head and an upper, off-Base watershed dominated by forested and agricultural land cover, the latter being dominated by row crops and intensive confined animal feeding operations (CAFOs), primarily for hogs and turkeys (Mallin et al., 2005a).

Historically, the NRE received partially treated sewage effluent from both Jacksonville and MCBCL and was characterized by extensive phytoplankton blooms, including toxic species, frequent hypoxia/anoxia, fecal contamination, low water clarity, and fish kills (Mallin et al., 2005a). In 1998, both treatment plants were upgraded and Jacksonville effluent was diverted to spray operations in the upper watershed, resulting in markedly reduced nutrient loads to the estuary and documented improvements in water quality, although phytoplankton blooms and hypoxia/anoxia continue to be a problem (Mallin et al., 2005a; Paerl et al., 2012). Continued high rates of nutrient loading from the upper watershed together with recent decisions to increase the population of Marines on MCBCL remain a threat to NRE water quality. In the context of water quality, the Clean Water Act, and potential need for a TMDL for the NRE, the most immediate issue for the estuary is the need to maintain compliance with the State of North Carolina’s “acceptable” chlorophyll *a* (chl *a*) concentration of 40 µg L⁻¹ (NCDENR, 2001).

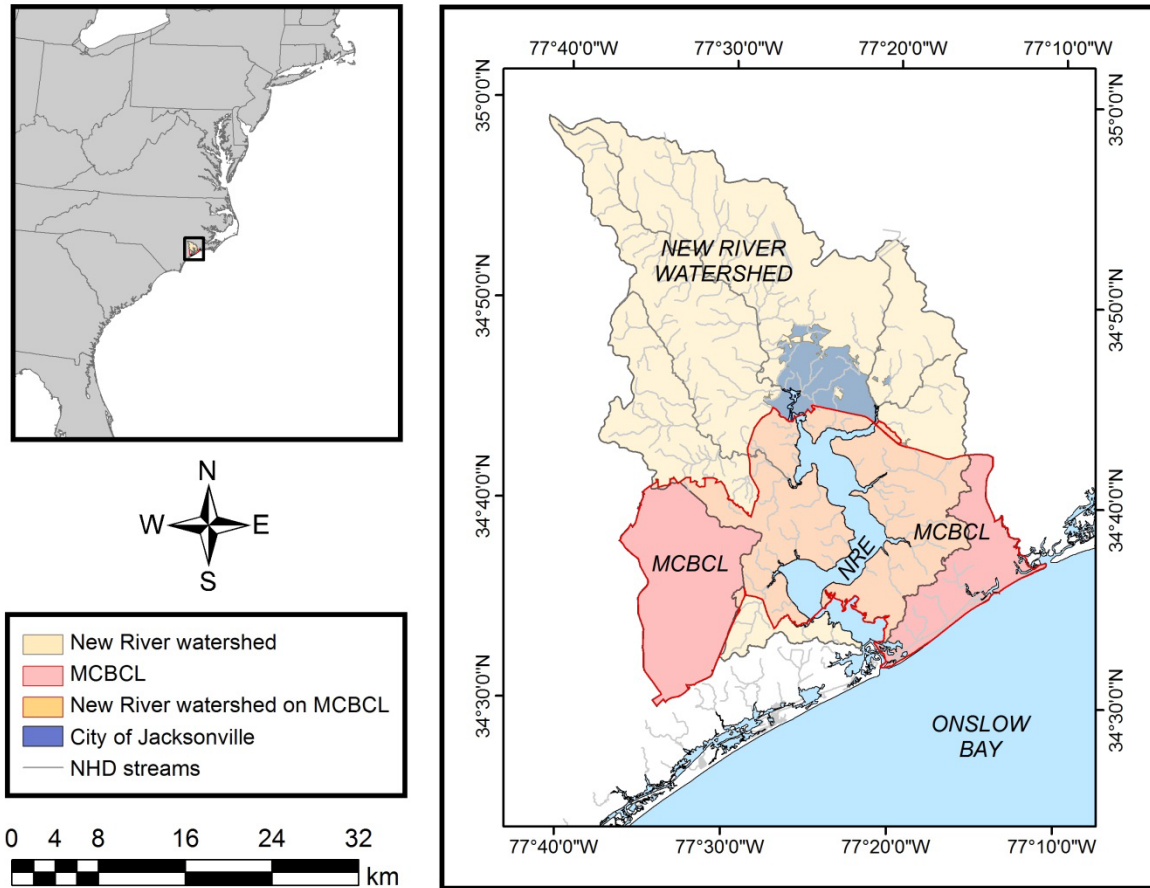


Figure 6-1. Map of the NRE, its watershed, and MCBCL.

NHD = the U.S. Geological Survey's National Hydrography Dataset.

Given the combination of legacy and ongoing stressors to the NRE, the Aquatic/Estuarine Module of DCERP has been conducting cross-disciplinary research and monitoring in the NRE since 2007. The overarching goal of this module has been to understand NRE structure, ecosystem function, and its response to both natural (e.g., climatic, hydrologic) and anthropogenic (e.g., nutrient and sediment loading) stressors. As part of this research, simulation models have been developed for both loading of water and materials (nutrients, sediment) from the surrounding watershed (Watershed Simulation Models [WSMs]) and response of the estuary to these loads (Estuarine Simulation Model [ESM]). The purposes of these models were to: (1) provide a focal point for the integration of historic monitoring and process-level data across the Aquatic/Estuarine Module of DCERP and from related projects in other modules; (2) provide tools to predict likely changes in nutrient loads from MCBCL due to ongoing land development and to understand NRE structure, function, and response to natural and anthropogenic stressors; (3) serve as a tool for guiding future iterations of the monitoring program (e.g., de Jonge and DeGroodt, 1989); and (4) provide ultimate development of useful management models and decision-support tools for MCBCL.

Models have a long history as heuristic and synthetic research tools in the study of coastal marine ecosystems and nutrient-rich estuaries in particular (Brush and Harris, 2010; Canham et al., 2003; Kremer and Nixon, 1978; Riley et al., 1949; Steele, 1974). In recent decades, these

models have been increasingly applied to guide management, particularly related to the effects of nutrient loading on cultural eutrophication and development of TMDLs (Giblin and Vallino, 2003; Harris et al., 2003; NRC, 2000; U.S. EPA, 1999). In the United States, large investments over many years have been made in development of high resolution, biogeochemically complex ecosystem models of major estuarine and coastal systems, including the Chesapeake Bay (Cercio and Noel, 2004), the Long Island Sound (HydroQual, 1991), and the Massachusetts Bay/Boston Harbor (Chen et al., 2010; Jiang and Zhou, 2008). Similarly, a wide variety of watershed models have been developed over the past several decades for predicting loads of fresh water, nutrients, and sediments to receiving waterbodies, ranging from spatially averaged, bulk empirical approaches to spatially resolved, highly complex mechanistic models (e.g., Alexander et al., 2002).

A growing body of work has been developing over the past two decades examining the role of complexity and spatial resolution in these models (Baird et al., 2003; Denman, 2003; Friedrichs et al., 2006; Fulton et al., 2003 and 2004; Ménesguen et al., 2007; Raick et al., 2006). Multiple calls have been made for development of simpler, “intermediate complexity,” and more generally applicable models particularly for application to management and ready transfer to other systems (Duarte et al., 2003; NRC, 2000; Pace, 2001; Rigler and Peters, 1995). Additional calls have been made to evaluate multiple models for the same problem and to use multiple modeling approaches (or “ensembles”) to inform coastal management (Scavia et al., 2004; Stow et al., 2003; Van Nes and Scheffer, 2005).

Given these recent directions in aquatic modeling, the focus of the modeling activities in the Aquatic/Estuarine Module was to develop reduced complexity, management-relevant models that could ultimately be provided to the Base as decision-support tools. The focus of the DCERP WSMs was to take advantage of the large number of closely located, but contrasting, small watersheds across MCBCL in which loads were monitored for 3 years through Research Project AE-2 (see Chapter 4 of this report). This data set provided a unique opportunity to compare a wide range of existing watershed models across a continuum from simple to complex for evaluation of their ability to simulate loads from these small watersheds and their utility as management tools. Although such a comparison has been conducted by Alexander et al. (2002) for large northeastern and mid-Atlantic U.S. watersheds, it has yet to be performed on small, relatively flat coastal plain watersheds. Following calibration to tributary creek loading data, selected models were used to quantify the likely changes in watershed loads to the NRE due to future Base development.

The focus of the DCERP ESM was to apply a previously developed, reduced complexity model that captures the key aspects of estuarine eutrophication while reducing uncertainty due to error propagation from poorly constrained parameters (Brush and Nixon, in review; Reckhow 1994). The reduced complexity approach makes possible fast run times on desktop personal computers (PCs), which therefore will ultimately enable transition to an online decision-support tool that can be provided to the Base. Following calibration to historic monitoring data and data from DCERP Research Projects AE-1 and AE-3, the ESM was used for two major applications. First, a series of simulation analyses were conducted to understand the factors that control NRE response to anthropogenic nutrient loading. These factors are processes that “filter” estuarine response to nutrient loading (Cloern, 2001) and include the physical processes previously discussed (e.g., flushing time, depth, volume) and the biological and biogeochemical processes

such as sequestration of nutrients by benthic microalgae (BMA), denitrification, and filtration by benthic bivalves, which can play important roles in mitigating against the deleterious effects of nutrient loading, particularly in shallow systems (Anderson et al., 2003; Cloern, 1982; Grall and Chauvaud, 2002; McGlathery et al., 2007; Nixon et al., 2001 and 2006; Piehler and Smyth, 2011). The second main application of the model was in a series of scenario analyses in which nutrient loading from the off-Base watershed, on-Base watershed, and the MCBCL wastewater treatment facility (WWTF) was altered and the model used to quantify NRE response, particularly with respect to the $40 \mu\text{g L}^{-1}$ state chl *a* criterion (NCDENR, 2007).

Materials and Methods

Watershed Simulation Modeling

Watershed Delineation

Watersheds for the 10 tributary creek stations from Research Project AE-2 were delineated in ArcMap 9.3 (ESRI ArcGIS 9) using the hydrology toolbox and the MCBCL 20-ft surface digital elevation model (DEM) for Onslow County, NC. All sinks were filled using the fill sink function to remove natural and artificial depressions in the DEM which can complicate calculations of flow paths in subsequent steps. The direction of flow in each cell of the DEM was determined using the flow direction tool. We then used the non-weighted cell flow accumulation function to determine flow amounts entering each cell from surrounding cells. Pour points were created and snapped to the flow accumulation raster. We experimented with numerous snap distances to search for high flow cells around the pour points; a distance of 30 m was ultimately determined to produce the best watershed boundaries based on visual inspection of the MCBCL DEM and high-resolution flowlines (e.g., streams, rivers) from the National Hydrography Dataset (NHD; for more information, see <http://nhd.usgs.gov>). Finally, the watershed tool was used to delineate the resulting watersheds (**Figure 6-2**).

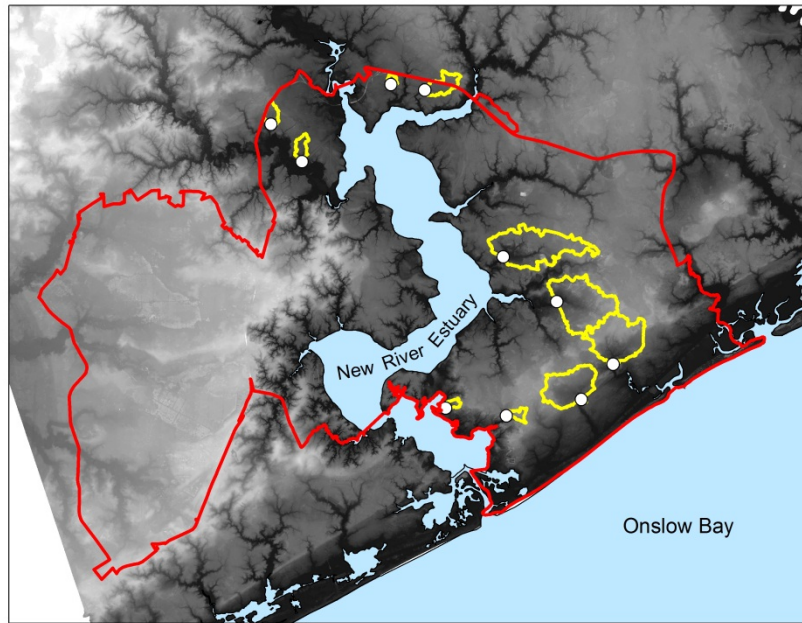


Figure 6-2. DCERP tributary creek monitoring stations and watershed boundaries.

The red line denotes the MCBCL boundary; the gray-scale image is the MCBCL 20-ft DEM; and yellow line denotes the boundaries of the MCBCL watersheds studied by Research Project AE-2.

For the purpose of scaling modeled watershed loads to the entire NRE watershed, the New River sub-basin boundary from the NHD was modified to the exact NRE watershed boundary using the MCBCL 20-ft Onslow County DEM and NHD flowlines. This watershed was combined with the MCBCL installation area to obtain the portion of the NRE watershed originating on- and off-Base (**Figure 6-1**).

Watershed Simulation Models

The relatively large number of small watersheds with varying land use monitored as part of DCERP provided an ideal opportunity to evaluate a range of existing watershed models for their ability to reproduce observed loads in this low relief, coastal plain setting, similar to the comparison performed by Alexander et al. (2002) in large, northeastern watersheds. A series of modeling approaches from simple to complex were evaluated for their ability to reproduce observed loads, and include those commonly in use by the U.S. Environmental Protection Agency (EPA) and multiple states for TMDL development, along with a series of simpler, more empirical approaches (**Figure 6-3**). All of the models tend to be lumped-parameter in nature, although the more complex models include an increasing amount of detail on watershed processing and distinction between groundwater processes and overland flow. With the exception of the scaling and regression approaches, all of the models compute loads by land-use category. The simpler approaches predict annual loads, the more complex models predict monthly loads, and the most complex model (e.g., Hydrologic Simulation Program–Fortran [HSPF]) predicts daily loads.

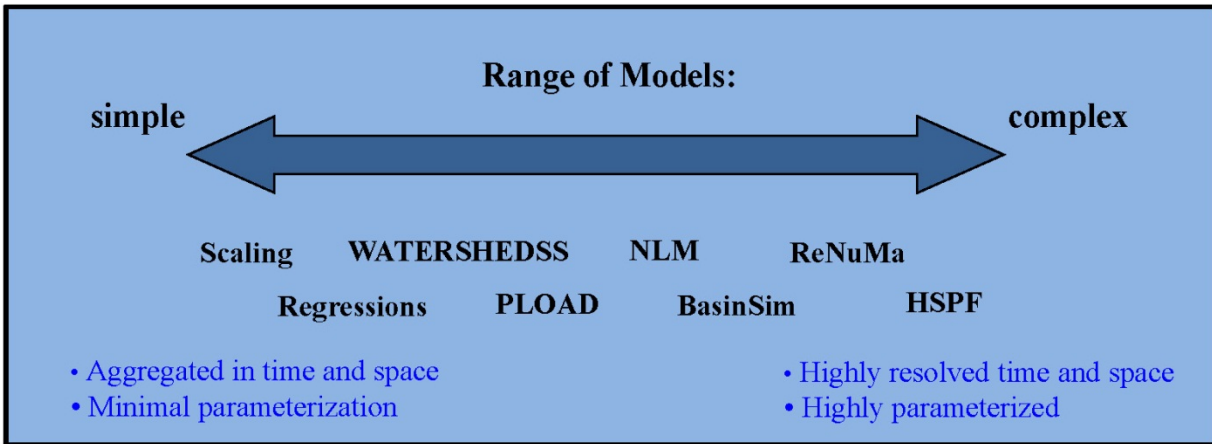


Figure 6-3. Suite of watershed modeling approaches applied to the NRE.

GWLF = Generalized Watershed Loading Functions; HSPF = Hydrologic Simulation Program–Fortran; NLM = Nitrogen Loading Model; PLOAD = Pollutant Loading Model; ReNuMa = Regional Nutrient Management model.

(1) *Empirical Scaling of Observations*: Our first “model” for computing loads to the entire NRE was simply to scale observed annual loads from the U.S. Geological Survey (USGS) Gaging Station #020903205 in the upper New River watershed at Gum Branch and tributary creek stations (Research Project AE-2) to account for the ungaged portion of the watershed. The average annual watershed yield (load per hectare of watershed area) at Gum Branch was computed for the period for which sufficient nutrient data were available at the gage for computing loads (1988–2000). The average annual watershed yields across the 10 tributary creek stations were similarly computed. The Gum Branch yield was applied across the area of the New River, Southwest Creek, and Northeast Creek watersheds lying outside the MCBCL boundaries given their similar land-use distributions and the presence of CAFOs in these watersheds. The mean yield from the tributary creek stations from Research Project AE-2 was applied across all other watershed areas given the similar land-use distributions across those MCBCL watersheds.

(2) *Empirical Regression Modeling*: Our second approach for modeling annual loads was to fit a series of candidate 1–4 parameter single and multiple regression models to observed base, storm, and total loads of each watershed constituent from Research Project AE-2. Response variables included the fraction of forested land cover and impervious surfaces within each watershed (based on the 2001 National Land Cover Dataset [NLCD; see http://www.mrlc.gov/nlcd01_data.php; Homer et al., 2004]), mean watershed slope (%) estimated from the MCBCL 20-foot DEM for Onslow County, 2000 population density estimated from the U.S. Census Bureau TIGER (Topologically Integrated Geographic Encoding and Referencing) database (see <http://www.esri.com/data/download/census2000-tigerline>), and the fraction of well-drained soils computed from the U.S. Department of Agriculture’s Soil Survey Geographic database (SSURGO; see <http://soils.usda.gov/survey/geography/ssurgo>) database for Onslow County. The latter was computed by selecting the dominant soil component for each map unit in the SSURGO “comp” table, assigning a value of 1 to those soils labeled as “excessively drained,” “well drained,” and “moderately well drained,” assigning a value of 0 to soils labeled as “somewhat poorly drained,” “poorly drained,” and “very poorly drained,” and computing the fraction of area within each soil polygon with a value of 1.

NLCD 2001 land cover was reclassified into major categories, including forested (i.e., natural vegetation), developed, and agricultural (**Table 6-1**). Impervious areas were computed directly from the NLCD 2001 impervious coverage. Classification of Base land as agricultural is erroneous; areas identified as agricultural in each sub-watershed were inspected in Google Earth and determined to be developed (primarily residential lawns), with the exception of Cogdels Creek watershed, where approximately 90% of the land identified as agricultural was a cut forest tract (assigned to forested land) and the other 10% is now a building (assigned to developed). Given this re-classification scheme, percent forested and percent developed were perfectly correlated, so only percent forest was included in the regression models. Percent forest and percent impervious were strongly correlated ($\% \text{ impervious} = -0.40 * [\% \text{ forested}] + 0.35$; $r^2 = 0.95$) so they were not run in the same model; instead, both parameters were used to fit single-parameter models, but only percent forest was used in all multiple parameter models.

The NLCD 2001 land cover database was used as it was the most recent database available at the beginning of DCERP that covered all of Onslow County and the NRE watershed. Recently, the NLCD 2006 database became available which reflects land cover closer to the time period of load sampling by Research Project AE-2. To determine the degree to which land use changed on the Base between 2001 and 2006, and the potential effect this may have on modeled loads, areas of land in major land-use categories were regressed between the two data sets. Distribution of impervious land area in categories from 2–100% (in 1% increments) was strongly correlated between the two data sets ($2006 \text{ \% impervious} = 1.06 * [2001 \text{ \% impervious}] + 0.48$; $r^2 = 0.99$), with an overall 0.26% increase in impervious area on the Base over the 5-year period. Similarly, area of land in the 15 NLCD cover classes (see **Table 6-1**) was highly correlated between the 2 years ($2006 \text{ area} = 1.04 * [2001 \text{ area}] - 762$; $r^2 = 0.91$), with a 5.7% increase and 1.3% decrease in developed and forested land area over the 5 years, respectively. Land-use distributions and regression model input values are summarized in **Table 6-2**.

Table 6-1. Re-classification of NLCD 2001 land-cover categories for empirical regression modeling.

NLCD 2001 Code	NLCD 2001 Categories	Empirical Regression Model Categories
21 22 23 24 31	Developed, open space Developed, low intensity Developed, medium intensity Developed, high intensity Barren land	Developed
41 42 43 52 71 90 95	Deciduous forest Evergreen forest Mixed forest Shrub/scrub Herbaceous Woody wetlands Emergent herbaceous wetlands	Forested (i.e., natural vegetation)
81 82	Hay/pasture Cultivated crops	Agricultural

Note: Pixels with NLCD Code 11 (open water) were excluded from the analysis.

Table 6-2. Area, land-cover distribution, and physical characteristics of tributary creek watersheds from Research Project AE-2.

Site	Area (ha)	% Forested	% Developed	% Impervious	Population Density (# of people per ha ⁻¹)	% Well-Drained Soils	Mean Slope (%)
Air Station	78.9	25.9	74.1	26.6	0.13	100	10.4
Camp Johnson	22.3	95.2	4.8	0.3	0.36	77.1	9.8
Cogdels Creek	836	62.4	37.6	13.8	0.080	76.2	9.4
Courthouse Bay	31.3	29.6	70.4	15.5	0.00007	100	7.5
Freeman Creek	588	87.1	12.9	1.6	0.034	36.9	6.7
French Creek	807	84.1	15.9	1.1	0.031	40.0	7.4
Gillets Creek	453	81.1	18.9	2.9	0.0087	38.6	6.7
Southwest Creek	77.5	79.9	20.1	3.0	0.50	96.8	8.0
Tarawa Terrace	139	24.4	75.6	23.2	3.8	90.7	7.3
Traps Bay	51.0	67.9	32.1	4.1	0.0034	55.3	7.2

Three types of regression models were fit, including single and multiple linear models, as shown in Equation 6-1:

$$y = \beta_0 + \beta_1 x_1 + \cdots \beta_k x_k \quad (\text{Eq. 6-1})$$

single parameter power functions, as shown in Equation 6-2:

$$y = \beta_0 \cdot x_1^{\beta_1} \quad (\text{Eq. 6-2})$$

and single and multiple parameter logistic models, as shown in Equation 6-3:

$$y = \frac{1}{1 + \exp^{-(\beta_0 + \beta_1 x_1 + \cdots \beta_k x_k)}} \quad (\text{Eq. 6-3})$$

where β_{0-k} are the regression parameters and x_{1-k} are the predictors (% forest or % impervious, slope, population density, and fraction of drained soils). Although power functions were run for single parameters only, a range of predictor combinations were run for linear and logistic models (**Table 6-3**).

Table 6-3. Parameters used in linear and logistic watershed regression models.

Predictors include “for” (% forested area), “imp” (% impervious surfaces), “pop” (population density, persons ha⁻¹), “drain” (% well-drained soils), and “slope” (mean slope, %).

One Parameter Models	Two Parameter Models	Three Parameter Models	Four Parameter Models
For	for pop	for pop drain	for pop drain slope
Imp	for drain	for pop slope	
Pop	for slope	for drain slope	
drain			
slope			

Following the approach of Burnham and Anderson (2002), the Akaike Information Criterion corrected for small sample sizes (AIC_c) was computed from the residual sum of squares (RSS) of all significant models ($p \leq 0.05$), sample size (n), and the number of model parameters (k) increased by one when using least squared regression as input to the analysis (see Equation 6-4):

$$AIC_c = 2(k + 1) + n \cdot \ln\left(\frac{RSS}{n}\right) + \frac{2(k+1)(k+2)}{(n-k)} \quad (\text{Eq. 6-4})$$

The difference (Δ_i) of the AIC_c value for model i from the minimum AIC_c value for each constituent was then used to calculate the likelihood (L) of each model given the data among all models with $\Delta_i < 10$, as well as the Akaike weights (w_i) which represent the likelihood of model i being the best model in the set (see Equations 6-5 and 6-6):

$$L = e^{-\Delta_i/2} \quad (\text{Eq. 6-5})$$

$$w_i = \frac{L_i}{\sum_1^i L_i} \quad (\text{Eq. 6-6})$$

An example of these calculations is given in **Table 6-4** below for baseflow yields (kg ha⁻¹ y⁻¹) of ammonium.

Table 6-4. Information theoretic analysis of regression model fits to measured annual watershed yields of ammonium in baseflow.

Terms are defined in the text. Shaded region identify those models with $\Delta_i > 10$ which were subsequently excluded from the analysis based on convention (Burnam and Anderson, 2002).

Regression	Predictors	RSS	k+1	AIC_c	Δ_i	L	w_i
Logistic	drain	0.0467	3	-29.1	0.0	1.00	0.34
Logistic	for pop	0.0161	4	-28.3	0.8	0.67	0.22
Logistic	slope	0.0531	3	-28.1	1.0	0.60	0.20
Logistic	imp	0.0532	3	-28.1	1.0	0.59	0.20
Linear	slope	0.10182	3	-22.9	6.2	0.04	0.01
Linear	for pop	0.03432	4	-22.3	6.9	0.03	0.01
Logistic	for slope	0.042	4	-20.7	8.5	0.01	0.00
Logistic	for drain	0.0429	4	-20.5	8.7	0.01	0.00

(continued)

Table 6-4. Information theoretic analysis of regression model fits to measured annual watershed yields of ammonium in baseflow. (continued)

Regression	Predictors	RSS	k+1	AIC _c	Δi	L	w _i
Logistic	for pop slope	0.00742	5	-15.9	13.3	0.00	0.00
Power	imp	0.314	3	-13.9	15.2	0.00	0.00
Power	slope	0.3144	3	-13.9	15.3	0.00	0.00
Power	drain	0.3208	3	-13.7	15.4	0.00	0.00
Logistic	for pop drain	0.0144	5	-10.6	18.6	0.00	0.00
Linear	for pop drain	0.03168	5	-4.3	24.9	0.00	0.00
Linear	for pop slope	0.03187	5	-4.2	24.9	0.00	0.00
Logistic	for drain slope	0.038	5	-2.8	26.4	0.00	0.00
Logistic	for pop drain slope	0.000279	6	13.9	43.0	0.00	0.00
Linear	for pop drain slope	0.01486	6	45.7	74.8	0.00	0.00

(3) *WATERSHEDSS (export coefficient approach)*: A related approach to the empirical scale up and regression exercises is to use published estimates of annual nutrient yields (both nitrogen [N] and phosphorus [P]) from various land uses. This is the approach used by North Carolina State University's WATERSHEDSS decision-support tool (see www.water.ncsu.edu/watershedss), which uses published export coefficients from Athayde et al. (1983) and Reckhow et al. (1980). These coefficients were combined with NLCD 2001 land-cover distributions to compute loads.

(4) *Pollutant Loading Model (PLOAD) (export coefficient approach)*: PLOAD is a simple model for computing annual loads within EPA's BASINS (Better Assessment Science Integrating point and Non-point Sources; see <http://water.epa.gov/scitech/datait/models/basins/index.cfm>) software package. The model can be run using two separate methods, the "export coefficient" or "simple" method. The former uses export coefficient tables similar to the approach in the WATERSHEDSS model, and the latter—chosen in the current study—allows for the specification of annual precipitation and event mean constituent concentrations, and computes pollutant loads from runoff coefficients for each land-use category (U.S. EPA, 2001). Standard runoff coefficients provided with PLOAD were used for all model runs given the lack of site-specific data. Land-cover distributions were obtained from the NLCD 2001 database.

(5) *Nitrogen Loading Model (NLM)*: The NLM is a spreadsheet model for computing annual TN loads, originally developed by Valiela et al. (1997) and adapted to the mid-Atlantic region by Cole (2005) and Giordano et al. (2011). The NLM begins with estimates of N inputs from atmospheric deposition onto natural vegetation, turf (i.e., lawns), agricultural fields (none on MCBCL), and impervious surfaces, plus fertilizer inputs (to residential lawns) and septic leaching. These inputs are then attenuated to account for vegetative uptake and net losses in the vadose zone and aquifer. The resulting loads are combined with point source discharges to compute total annual loads.

Atmospheric deposition was estimated using data for wet deposition from the National Atmospheric Deposition Program (NADP; see <http://nadp.sws.uiuc.edu>) and dry deposition from EPA's Clean Air Status and Trends Network (CASTNET; <http://www.epa.gov/castnet>). NLCD

2001 land cover was re-classified as in **Table 6-5**, with agricultural land divided between natural vegetation and developed categories (as previously described) and impervious areas computed directly from the NLCD 2001 impervious coverage. Population and housing densities were obtained from the U.S. Census Bureau's TIGER database (as previously described) and the fraction of the population using septic systems was estimated from a geographic information systems (GIS) shapefile of the sewered population in 2004 (NCCGIA, 2007). Point source discharges were computed using EPA's Water Discharge Permits Web site (see http://www.epa.gov/enviro/html/pcs/pcs_query_java.html), which provides permit data for regulated facilities. Two discharges were identified within that fraction of MCBCL draining to the NRE with an estimated annual load of TN and total phosphorus (TP) of 900.6 and 93.6 kg y⁻¹, respectively; these values do not include the MCBCL WWTF, which discharges directly to the open NRE in Farnell Bay and was addressed separately (see below). All other calculations in the NLM were as described in Cole (2005), Giordano et al. (2011), and Valiela et al. (1997).

(6) *BasinSim (Generalized Watershed Loading Functions [GWLF])*: BasinSim 1.0 (Dai et al., 2000) is a watershed modeling software based on the GWLF, a widely used watershed model developed by Haith and Shoemaker (1987) and Haith et al. (1992). The BasinSim model, similar to the GWLF, estimates monthly and annual watershed nutrient and sediment loads in stream flow. BasinSim models the hydrologic cycle and uses watershed specific loading functions to arrive at stream-flow nutrient and sediment loads. The hydrologic model relies on a lumped parameter water balance based on precipitation, evapotranspiration, soil characteristics, and land use. The model simulates pollutants in both groundwater discharge and runoff to arrive at stream-flow loads, also accounting for point sources including septic systems. Model inputs were previously described, with monthly meteorological data obtained from the National Oceanic and Atmospheric Administration's (NOAA's) National Climatic Data Center (see <http://www.ncdc.noaa.gov/oa/ncdc.html>) for the Marine Corps Air Field (station #723096) at the head of the NRE.

Table 6-5. Re-classification of NLCD 2001 land-cover categories for the NLM.

Pixels with NLCD Code 11 (open water) were excluded from the analysis.

NLCD 2001 Code	NLCD 2001 Categories	NLM Model Categories
21	Developed, open space + ½ (developed ^a – impervious ^b)	Turf (i.e., lawns)
22	Developed, low intensity	Developed
23	Developed, medium intensity	
24	Developed, high intensity	
31	Barren land	Barren
41	Deciduous forest	Natural vegetation
42	Evergreen forest	
43	Mixed forest	
52	Shrub/scrub	
71	Herbaceous	
90	Woody wetlands	
95	Emergent herbaceous wetlands	
81	Hay/pasture	Agricultural
82	Cultivated crops	

^a Sum of area in NLCD Categories 22, 23, and 24.

^b Area determined directly from the NLCD 2001 impervious coverage.

(7) *Regional Nutrient Management Model (ReNuMa; GWLF)*: ReNuMa (see <http://www.eeb.cornell.edu/bigeo/nanc/usda/renuma.htm>) is a more recent version of the GWLF approach with improved representations of watershed N biogeochemistry. The model also features an automated calibration routine to obtain the best possible fit to observed data. All inputs were as previously described.

(8) *Hydrologic Simulation Program–Fortran (HSPF)*: HSPF is a highly parameterized model that predicts fresh water, nutrient, and sediment loads with daily or sub-daily resolution, and results can be integrated to monthly and annual values (Bicknell et al., 2005; Donigian and Imhoff, 2002 and 2006). The model is widely used to set TMDLs and is the primary watershed model used by EPA’s Chesapeake Bay Program (see www.chesapeakebay.net). The HSPF model was run through EPA’s BASINS software; complete details can be found in a Virginia Institute of Marine Science (VIMS) master’s degree thesis (Koroknay, 2012). Model inputs were as previously described. Hourly, daily, and monthly meteorological data were obtained from NOAA’s National Climatic Data Center (see <http://www.ncdc.noaa.gov/oa/ncdc.html>) for the Marine Corps Air Station at the head of the NRE, and solar radiation data were obtained from the nearest long-term NOAA monitoring station #312517 in Kinston, NC.

Calibration and Scale-Up of the WSMs

Model predictions of annual loads were compared to observed loads calculated in Research Project AE-2 (see Chapter 4) over the first 2 years of data collection (i.e., July 2008–June 2009

and July 2009–June 2010). Monthly output from BasinSim, ReNuMa, and HSPF were similarly compared to the observations. Each model was then used to compute the total load entering the NRE from that portion of its watershed lying on MCBCL for comparison with estimates of loads from the off-Base watershed, direct atmospheric deposition, the MCBCL WWTF, and exchange with Onslow Bay. A summary of these data is presented in **Table 6-6**. Finally, two of the best fitting models (i.e., NLM and ReNuMa) were used to predict changes in the MCBCL TN loads to the NRE as forested lands are converted to developed, impervious surfaces.

Table 6-6. Summary of data sources and timeframes for estimating allochthonous N sources to the NRE.

Table adapted from Anderson et al. (2012).

Source	Data Source	Timeframe
Off-Base watersheds	USGS Gaging Station #02093000 at New River near Gum Branch, NC; discharge and nutrient concentration measurements	Data from 1988–2000 used to project loads during 1998–2010
MCBCL watersheds	Research Project AE-2 freshwater discharge and nutrient concentration measurements; WSM load estimates	2008–2011 (2008–2010 used in WSM calibration)
WWTF	MCBCL WWTF water flow rate and nutrient concentration measurements	2000–2010
Onslow Bay	Onslow Bay nutrient concentration measurements combined with advective exchanges computed using the ESM	1998–2010
Direct atmospheric deposition	Wet deposition: NADP sites NC06 (Beaufort), NC29 (Hofmann Forest), and NC35 (Clinton Crops Research Station); areal N deposition rates	2000–2010
	Dry deposition: EPA CASTNET Site BFT142 (Beaufort); areal N deposition rates	2000–2009

Estuarine Simulation Model

Ecosystem Kinetics

A previously developed, intermediate complexity estuarine ecosystem model was applied to the NRE (**Figure 6-4**). The ecosystem model includes only those state variables, rate processes, and parameters of primary importance to eutrophication in shallow coastal marine ecosystems. State variables include the pools of organic carbon, N, and P in phytoplankton (PHYTO), BMA, and eelgrass (*Zostera marina*), phytoplankton and BMA chl *a*, water column pools of dissolved inorganic nitrogen (DIN), dissolved inorganic phosphorus (DIP), DO (shown as O₂ in **Figure 6-4**), total suspended solids (TSS), and water column and sediment pools of labile organic carbon (C_{WC} and C_{SED}, respectively) and their associated N and P. Several state variables and rate processes are aggregated into bulk terms to reduce the number of parameters, and key processes are formulated with cross-system empirical formulations to reduce parameterization, root model

predictions in cross-system observations, and enable direct comparison of model predictions to observations (Brush et al., 2002; Brush and Nixon, 2010). The approach is in line with recent calls for management-relevant models of intermediate complexity as an alternative to more complex, highly parameterized models (e.g., Duarte et al., 2003; NRC, 2000). Full documentation of ecosystem model kinetics can be found in Brush (2002) and Brush and Nixon (in review).

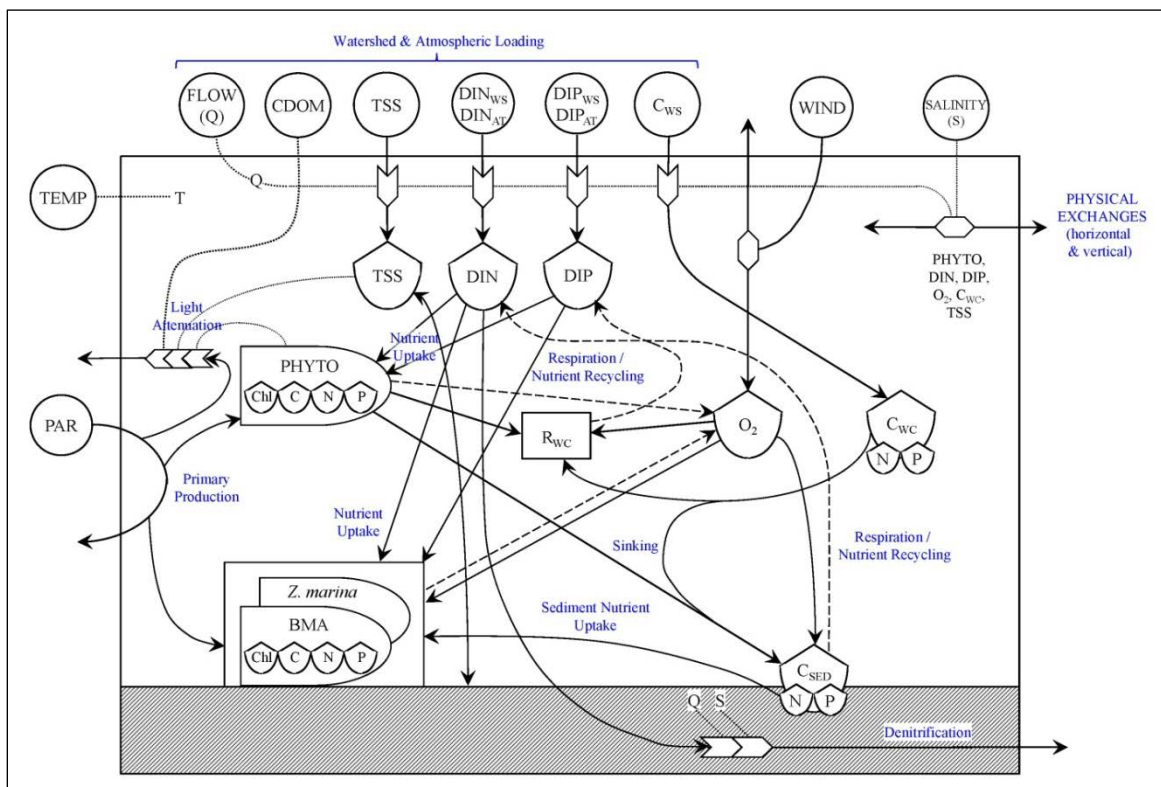


Figure 6-4. Schematic of the ESM.

PAR = photosynthetically active radiation; CDOM = chromophoric dissolved organic matter; subscript WS = watershed; subscript AT = atmospheric deposition; R_{wc} = integrated water column respiration. All other terms are defined in the text.

Physical Box Model

The ESM was implemented in a series of nine relatively coarse boxes arranged primarily along the axis of the NRE, each with a surface and bottom layer separated by the approximate long-term average position of the pycnocline determined from NRE water column monitoring data (**Figure 6-5; Table 6-7**). Hydrodynamic exchanges across all box faces are computed with an Officer-type Box Model based on forced freshwater inputs and salinity distributions (**Table 6-8**) (Officer, 1980; Swanson and Jayko, 1988). Although boxed schemes are relatively coarse, the purpose of the current work was to produce a fast-running model with utility for use by management personnel on PCs. Recent work has confirmed the utility of boxed approaches (Kremer et al., 2010; Ménesguen et al., 2007; Testa and Kemp, 2008). Area, volume, mean depth, and the fraction of sediment area in the surface and bottom layers were determined by Dr. Jesse McNinch from interpolated bathymetric data generated as part of DCERP (**Table 6-9**).

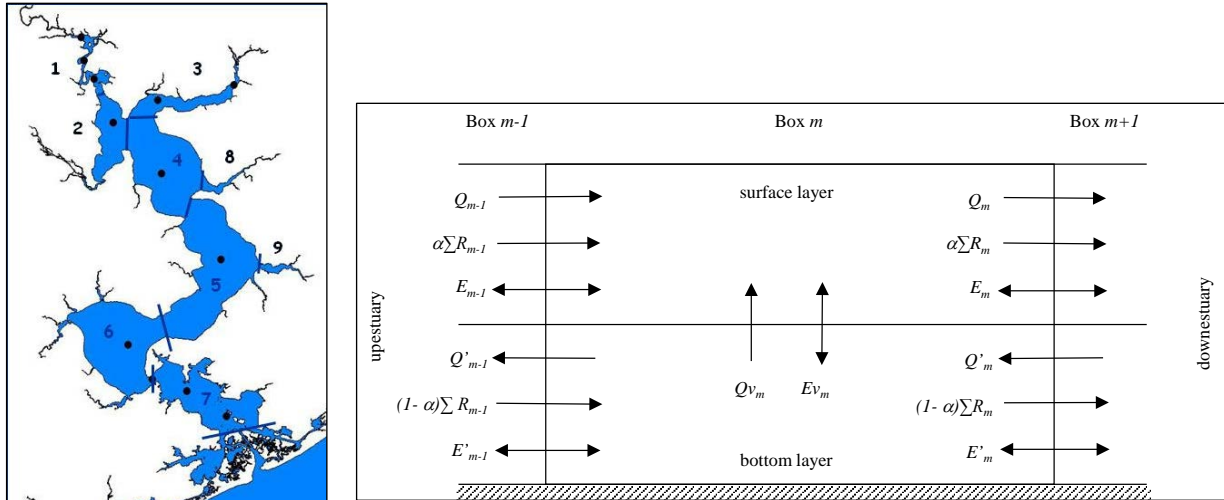


Figure 6-5. Spatial elements of the ESM and hydrodynamic exchanges.

(Left) Plan-view of Spatial Elements 1–9. Each element has a surface and bottom layer separated by the pycnocline. Locations of the Research Project AE-1 monitoring stations are denoted with points. (Right) Schematic of exchange flows computed by the Box Model. Terms are defined in Table 6-8.

Table 6-7. Description of the ESM spatial elements.

Values in parentheses for Boxes 1–3 are the percentages of watershed area lying on MCBCL for use in computing loads for the ESM.

Box	Area Description	Waterbody Area (ha)	Watershed Area (ha)	Watershed: Waterbody Ratio
1	New River/Wilson Bay (2.0)	157	40,483	258
2	Southwest Creek and upper NRE (25.4)	481	20,027	41.7
3	Northeast Creek (8.8)	339	18,612	55.0
4	Morgan Bay	1,237	1,605	1.3
5	Farnell Bay	1,699	5,325	3.1
6	Stone Bay	1,357	6,557	4.8
7	Courthouse Bay, Traps Bay, lower NRE	1,000	1,999	2.0
8	Wallace Creek	58	4,661	80.1
9	French Creek	47	3,155	67.0
TOTAL		6,375	102,425	16.1

Table 6-8. Parameters and equations for the physical Box Model.

Subscript m denotes the spatial element. Prime (') denotes the lower layer. ΣR_m indicates the sum of all freshwater flows into box m and all boxes upstream from box m. v is the Hansen-Rattray parameter and was estimated following the approach of Officer and Kester (1991).

Parameter	Definition	Units
V	Volume	m ³
S	Salinity	—
R	Freshwater input	m ³ d ⁻¹
Vfw _{surf}	Volume of freshwater in the surface layer	m ³
Vfw _{bott}	Volume of freshwater in the bottom layer	m ³
α	Fraction of freshwater input in the surface layer	—
Q _m	Advective horizontal flow from box m	m ³ d ⁻¹
Qv _m	Advective vertical flow from box m	m ³ d ⁻¹
E _m	Non-advective horizontal flow from box m	m ³ d ⁻¹
Ev _m	Non-advective vertical flow from box m	m ³ d ⁻¹
v	Fraction of the exchange due to non-advective flows	—
τ	Residence time	D
S _i	Volume-weighted salinity inside box m	—
S _o	Volume-weighted salinity downstream of box m	—
S _u	Volume-weighted salinity upstream of box m	—
Equations		
$Vfw_{surf} = V_{surf} \frac{S_{bott} - S_{surf}}{S_{bott}} \quad Vfw_{bott} = V_{bott} \frac{S_{bott} - S_{surf}}{S_{surf}} \quad \alpha = \frac{Vfw_{surf}}{Vfw_{surf} + Vfw_{bott}}$ $Q_m = Q'_m = \frac{(1 - v_m) \alpha_m \Sigma R_m S_m + (1 - v_m) (1 - \alpha_m) \Sigma R_m S'_m}{S'_{m+1} - S_m}$ $Qv_m = -(\alpha_{m-1} \Sigma R_{m-1} + Q_{m-1}) + (\alpha_m \Sigma R_m + Q_m)$ $E_m = \frac{v_m \alpha_m \Sigma R_m S_m}{S_{m+1} - S_m} \quad E'_m = \frac{v_m (1 - \alpha_m) \Sigma R_m S'_m}{S'_{m+1} - S'_m}$ $Ev_m = \frac{((1 - v_{m-1}) \alpha_{m-1} \Sigma R_{m-1} + Q_{m-1}) S_{m-1} - ((1 - v_m) \alpha_m \Sigma R_m + Q_m) S_m + (Qv_m S'_m)}{S_m - S'_m}$ $\tau_{1,2,3,5} = \frac{V_m}{R_m} \left(\frac{S_o - S_i}{S_o} \right) \quad \tau_{4,6,7} = \frac{V_m}{\Sigma R_m} \left(\frac{(S_i - S_u)(S_o - S_i)}{S_i(S_o - S_u)} \right)$		

Table 6-9. Physical characteristics of the ESM spatial elements.

Box	Area (m²)	Volume, m³	Mean Depth (m)	Pycnocline Depth (m)	Mean Depth in Surface Layer (m)	Mean Depth in Bottom Layer (m)	Maximum Depth (m)	Percent of Area in Surface Layer	Percent of Volume in Surface Layer
1	1,570,800	1,999,662	1.3	2	1.2	2.5	3.9	83.9	93.6
2	4,805,800	7,340,884	1.5	2	1.3	2.5	3.4	58.9	86.0
3	3,387,000	5,665,676	1.7	2	1.5	2.6	3.4	69.7	89.1
4	12,370,300	32,464,976	2.6	2	1.7	3.2	3.7	25.7	66.0
5	16,992,800	33,428,167	2.0	2	1.6	2.7	4.8	44.0	79.6
6	13,572,000	21,613,721	1.6	2	1.4	2.4	4.8	58.7	88.6
7	9,997,200	12,543,240	1.3	2	1.2	2.4	5.0	93.6	98.1
8	582,100	606,304	1.0	1	0.7	1.7	2.8	53.4	67.0
9	470,700	152,881	0.32	0.2	0.2	0.4	0.8	21.7	57.7

Input Data and Calibration

The ESM is driven with daily freshwater inputs (including rivers/groundwater and precipitation less evaporation), water temperature, and salinity in each spatial element, and daily meteorology (air temperature, dew point temperature, mean wind speed) and photosynthetically active radiation (PAR). Meteorological and PAR data were obtained from the NOAA National Climatic Data Center as previously described. Daily records of surface and bottom temperature and salinity were developed by interpolating the approximately monthly NRE monitoring data at each station since 1998 (MCBCL for 1998 through June 2007 and DCERP for July 2007 through 2010). Daily freshwater inputs from that portion of the watershed of Boxes 1–3 lying off-Base were estimated from daily flows at the USGS Gum Branch Gaging Station #0209303205 on the New River (see <http://waterdata.usgs.gov/nwis>), linearly scaled to account for watershed area below the station. Daily freshwater inputs from the remainder of the watershed were computed from mean flow rates from the 10 tributary creek stations determined by Research Project AE-2. Nutrient loads (N and P) from the off-Base watershed were computed from long-term nutrient monitoring data at Gum Branch, and loads from on-Base were computed with mean concentrations collected during Research Project AE-2. Atmospheric N deposition was estimated as previously described; deposition of P was assumed to be negligible. Daily flows and nutrient loads to Box 5 from the MCBCL WWTF were forced from plant data. Daily values of chromophoric dissolved organic matter (CDOM) in each box were estimated from a regression with salinity using Research Project AE-3 data, and daily interpolated values of turbidity (NTU) were forced based on monitoring data since 1998. The model was initially calibrated to historical (1998 to mid-2007) MCBCL monitoring data at eight to 10 stations down the axis of the NRE (Mallin et al., 2005a), and subsequently calibrated to DCERP data (mid-2007 to 2010). Calibration was conducted on both concentrations and key rate processes given the importance of adequately calibrating both (Brush et al., 2002; Grangere et al., 2009).

Benthic Bivalve Models

Benthic bivalves (e.g., clams and oysters) have been shown to exert a significant top-down control on estuarine phytoplankton biomass in some systems (Cloern, 1982; Dame, 1996; Grall and Chauvaud, 2002; Smaal and Prins, 1993). The NRE contributes approximately 28% of statewide landings of the hard clam (*Mercenaria mercenaria*), which suggests a large abundance of these key filter-feeding organisms (NCDMF, 2008). Additionally, the shallow nature of the NRE and high productivity of BMA suggest that a large community of deposit-feeding benthic organisms may also occur in the system; it is unknown if they are also able to exert a top-down control on benthic productivity.

To address these questions, two target species of benthic bivalves were selected for modeling, one a suspension feeder (*M. mercenaria*) and one a facultative deposit feeder (*Macoma balthica*, the Baltic clam or Baltic macoma). Bivalves are ideal target species because they are easily sampled and have contrasting feeding modes (suspension versus deposit) and life histories (long versus short lived) depending on the species. The suspension feeding hard clam (*M. mercenaria*) was selected because it supports an active public fishery across the lower half of the estuary, with annual landings ranging from 3.9 to 10 million individuals, contributing 28% of all hard clam landings in North Carolina (NCDMF, 2008). *M. mercenaria* is a large suspension feeding bivalve ranging in length from a few millimeters to almost 70 mm, and surviving up to 40 years

or more (Harding, 2007; Jones et al., 1989). The facultative deposit feeding clam (*M. balthica*) was selected, given its abundance and widespread distribution in oligohaline to polyhaline regions of estuarine systems in the eastern United States and Europe (Holland et al., 1987; Ysebaert et al., 2002). *M. balthica* in the Neuse River and Pamlico Sound, just north of the NRE, have been reported to live up to 8 years and range in maximum length from 25 to 35 mm (Kamermans et al., 1999). The high abundance and biomass of *M. balthica* in many estuaries make it a key link from primary producers to commercially and recreationally important species of fish and crabs (Powers et al., 2005; Seitz et al., 2003 and 2006).

Individual-based energetics models were developed for both species; the hard clam bioenergetics model of Hofmann et al. (2006) was adapted for *M. mercenaria* and the Dynamic Energy Budget of Cardoso et al. (2006) and van der Veer et al. (2001 and 2006) was adapted for *M. balthica*. Once calibrated to individual growth, the models were used to quantify the effects of inter-annual hydrologic variability (2008 versus 2009) on individual growth, total consumption of carbon (C) over the 2 years, and the total carrying capacity for both species within the system. The models were developed independently from the ESM, so clam food sources (phytoplankton, particulate, BMA, and sediment carbon) were forced directly from DCERP monitoring data. Full details of the models can be found in Wiseman (2010).

Data Collection in Support of ESM Calibration

BMA Photosynthesis-Temperature Formulation: Although much of the ESM had been previously developed at the start of DCERP, BMA were a new addition. BMA models are generally less well-developed than more traditional phytoplankton models, and key parameters are poorly constrained. The most critical parameters for construction of a new BMA model were those that govern growth. Aquatic plant models typically assign a temperature-dependent maximum growth rate that is reduced to account for light and nutrient limitation. Although a series of photosynthesis-irradiance (P-I) curves were collected as part of Research Project AE-3 for determining the light effect (see Chapter 5), and the presence of BMA on the sediment surface implies a lack of nutrient limitation, limited data were available to determine the linkage between temperature and maximum growth rate.

A series of auxiliary P-I incubations were performed on cores collected approximately monthly over an annual cycle (February 2010–May 2011) in the lower York River Estuary, VA, thereby covering a full cycle of annual temperature fluctuations. To develop a widely transferable temperature function for BMA, results were combined with those collected as part of Research Project AE-3 in the NRE (2009), over an annual cycle (2007–2008) in four lagoons on the Delmarva Peninsula (MD–VA; Giordano et al., 2012), and during summer 2008 in the lower York River, VA (S. Lake, personal communication).

Incubations were conducted using the method of Giordano et al. (2012). This method rates of photosynthesis and respiration are calculated based on DO fluxes measured during light-dark incubations of sediments with overlying filtered site water. Incubations were conducted in flow-through light gradient boxes maintained at ambient temperatures with PAR ranging from 60 to 2,000 $\mu\text{E m}^{-2} \text{ s}^{-1}$. DO concentrations were measured before and after incubations using Hach luminescent DO sensors. Following collection, sediment cores (7-cm sediment depth; 3.1 cm inner diameter) were held uncovered overnight in a circulating seawater bath at ambient

temperatures and incubated the following day. Immediately before incubation, overlying water was siphoned out of each core and replaced with filtered site water (0.45 µm). Two replicate P-I curves were incubated on each date, with 10 cores per replicate incubated at 10 different light levels, and three cores per replicate incubated in the dark. Cores were incubated unstirred, but incubations were kept short (1–2 hours) to minimize build-up of diffusion gradients. Before taking final DO measurements with the Hach probe, overlying water was gently mixed to obtain a composite sample.

Metabolic rates were expressed as hourly changes in oxygen per unit biomass of chl *a* in the top 3 mm of each core (mg m⁻²), measured spectrophotometrically after acetone extraction (Lorenzen, 1967; Neubauer et al., 2000). P-I curves were developed from these rates over the range of PAR used in each experiment. The Jassby and Platt (1976) hyperbolic tangent function was fit to hourly metabolic rates on each date as shown in Equation 6-7:

$$P = P_{max} \cdot \tanh\left(\frac{\alpha \cdot I}{P_{max}}\right) - R \quad (\text{Eq. 6-7})$$

where P is the hourly rate of photosynthesis and P_{max} is the maximum rate of photosynthesis (mg of molecular oxygen [O₂] mg⁻¹ chl *a* h⁻¹), α is photosynthetic efficiency or the initial slope of the P-I curve (mg of O₂ mg⁻¹ of chl *a* h⁻¹ [µE m⁻² s⁻¹]⁻¹), I is irradiance (PAR, µE m⁻² s⁻¹), and R is respiration (mg of O₂ mg⁻¹ chl *a* h⁻¹). Regression parameters from replicate cores were averaged, and values of P_{max} were converted to 24-hour, light-saturated growth rates (G_{max} , d⁻¹) assuming a BMA C to chl *a* ratio typical of nutrient replete, light limited cultures of 42 g g⁻¹ (Brush et al., 2002; Cloern et al., 1995) and a photosynthetic quotient (mol O₂ produced: mol carbon dioxide [CO₂] fixed) of 1 (see Equation 6-8):

$$G_{max} = \frac{1}{\Delta t} \ln\left(\frac{B_0 + P_d}{B_0}\right) \quad (\text{Eq. 6-8})$$

where Δt is the interval of the calculation (1 day), B_0 is the initial chl *a* biomass (0–3 mm, averaged over all cores), and P_d is an estimate of 24-hour production assuming maximal rates (= P_{max} chl *a* 24 hours). Resulting values of G_{max} along with values computed in the same way from the other studies previously listed were plotted against incubation temperature, as were values of α and the light saturation parameter, I_k (µE m⁻² s⁻¹), which represents the value of PAR at which production becomes saturated with light (see Equation 6-9):

$$I_k = \frac{P_{max}}{\alpha} \quad (\text{Eq. 6-9})$$

Eelgrass P-I Curves: Given the presence of SAV in the lower NRE, a sub-model for one of the dominant species, eelgrass (*Zostera marina*) was also added to the ESM. To obtain data on photosynthetic and respiratory rates for model calibration, P-I curve incubations were conducted on eelgrass in June, July, September, and November 2010, and in March and May 2011, using the same approach as for BMA. Whole eelgrass plants were collected from one to three sites in the lower NRE on each date and incubated at field temperatures in light gradient boxes as for BMA. Three P-I curves were incubated on each date, either from three separate sites or by replicating within sites. For each replicate P-I curve, small sections of shoots were scraped free of epiphytes and incubated at 10 light levels and in the dark (n=3); pieces of roots and rhizomes

were incubated in the dark only (n=3). Plants were rinsed free of salts and dried for normalization of metabolic rates to biomass (g dry weight). Hourly rates were fit to the Jassby and Platt (1976) hyperbolic tangent function, and fitted values of P_{max} and R were converted to instantaneous rates (d^{-1}) for comparison to modeled rates as for BMA, assuming a C to dry weight ratio of 0.45 g g^{-1} and a photosynthetic quotient of 1.

Benthic Bivalve Monitoring: Although total population size is not available for *M. mercenaria* in the NRE, detailed landings and size class data are available from the statewide fishery (NCDMF, 2008) for use in scaling modeled estimates of growth and consumption to the ecosystem level. To obtain abundance and size class data for *M. balthica*, we conducted targeted bivalve sampling on four dates from March to October of 2009 in the low mesohaline, high mesohaline, and polyhaline regions of the NRE (**Figure 6-6**), defined from long-term (1998–2006) salinity measurements (Mallin et al., 2005a). Samples were taken at 0.5-m water depth at six randomly selected stations within each region (**Figure 6-6**). At each site, all benthic infauna were collected in a 37-cm diameter cylinder to a depth of approximately 32 cm via suction core and passed through a 1-mm mesh (Brylawski, 2008). This sampling depth is in keeping with Hines and Comtois (1985), who found the majority of *M. balthica* in 30 cm of sediment or less in both sandy and muddy substrates. A persistent shallow clay layer in the NRE often prevents sampling up to 30 cm, but animals are not expected to burrow far into this layer. Samples were frozen for subsequent sorting of bivalves, identification to species, and measurement of individual length, wet weight (ww), dry weight (dw), and ash-free dry weight (AFDW). Suction sampling is known to restrict the maximum possible size collected for hard clams and is best used to characterize the abundance of smaller bivalves; however some *M. mercenaria* were collected in samples and measured for length and weight (shell and flesh measured separately). Data were used to derive weight-length relationships for both species, in situ densities for *M. balthica*, and seasonal growth trajectories for *M. balthica* for use in model calibration.

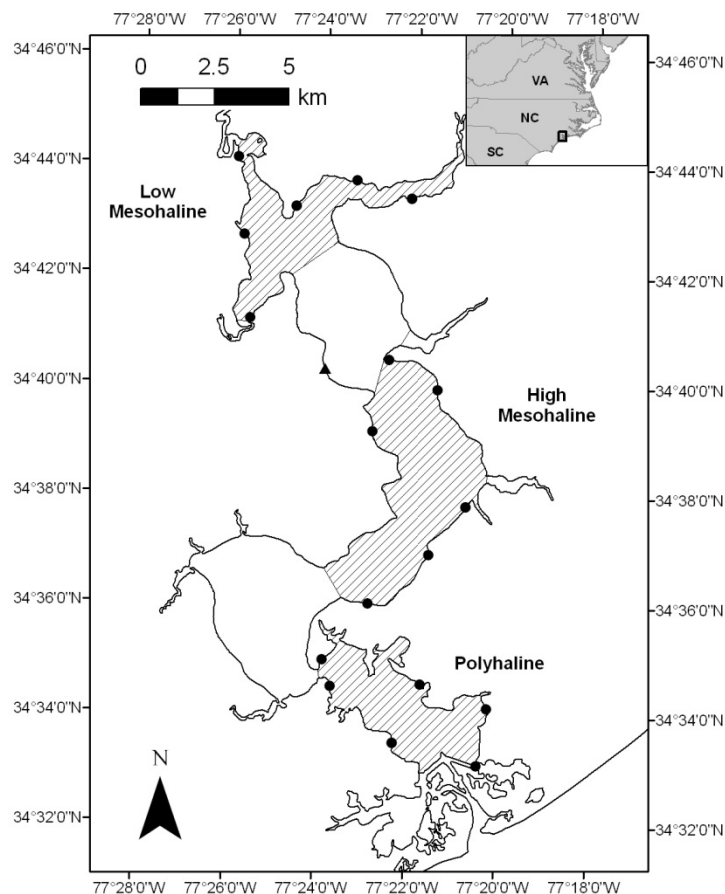


Figure 6-6. Stations for 2009 benthic sampling in three salinity zones of the NRE.

The site denoted by a triangle was sampled in March 2009, but was replaced with a site in the high mesohaline polygon for all subsequent sampling. The harvest zone for the public fishery runs from the high mesohaline zone to the mouth of the estuary.

Results and Discussion

Watershed Simulation Models

Empirical Regression Models

Of the 609 regression models fit, 228 were significant at the $p=0.05$ level; of these, 48 had Akaike weights greater than 0.10, indicating they have at least a 10% likelihood of being the best model (**Tables 6-9 and 6-10**). These best fitting models were either linear or logistic; the single parameter power functions did not successfully predict yields. Similarly, only one and two parameter models provided the best fits for all parameters; more complex models were never significant. Watershed yields of fresh water and TSS were best described by linear functions based on population density, population combined with percent forest, and watershed slope (**Table 6-9**). However, post-hoc regression of observed yields against those predicted by the regression equations using slope yielded comparatively weaker fits ($r^2 < 0.75$). Yields of phosphate were better described by logistic regressions, suggesting a threshold response primarily to drainage, slope, and impervious surfaces.

Table 6-9. Relative model weights (w_i) for the best-fitting regressions for watershed yields of fresh water ($\text{m}^3 \text{ ha}^{-1} \text{ y}^{-1}$) and TSS and orthophosphate (PO_4^{3-} ; $\text{kg ha}^{-1} \text{ y}^{-1}$) determined by Akaike Information Criterion analysis.

Predictors include “for” (% forested area), “imp” (% impervious surfaces), “pop” (population density, persons ha^{-1}), “drain” (% well-drained soils), and “slope” (mean slope, %).

Parameter	Component	Regression	Predictors	w_i
Water	Base	Linear	for pop	1.00
	Storm	Linear	slope ^a	0.79
		Linear	for pop	0.17
	Total	Linear	slope ^a	0.65
		Linear	for pop	0.33
TSS	Base	Linear	for pop	0.85
		Linear	pop	0.15
	Storm	Linear	for pop	0.96
	Total	Linear	for pop	1.00
PO_4^{3-}	Base	Logistic	drain	0.43
		Logistic	for pop	0.31
		Logistic	slope ^a	0.21
	Storm	Logistic	drain	0.57
		Logistic	imp	0.24
		Logistic	slope	0.17
	Total	Logistic	drain	0.58
		Logistic	imp	0.20
		Logistic	slope	0.20

^a Linear regression of predicted and observed watershed yields resulted in fits with adjusted $r^2 < 0.75$.

Table 6-10. Relative model weights (w_i) for the best-fitting regressions for watershed yields of N species ($\text{kg ha}^{-1} \text{ y}^{-1}$) determined by Akaike Information Criterion analysis.

Predictors include “for” (% forested area), “imp” (% impervious surfaces), “pop” (population density, persons ha^{-1}), “drain” (% well-drained soils), and “slope” (mean slope, %).

Parameter	Component	Regression	Predictors	w_i
TN	Base	Linear	for, pop ^a	0.54
		Logistic	imp ^{a, b}	0.14
		Logistic	pop ^{a, b}	0.13
	Storm	Linear	slope ^a	0.81
		Linear	for pop	0.16
	Total	Linear	slope ^a	0.65
		Linear	for pop	0.32
Ammonium (NH_4^+)	Base	Logistic	drain	0.34
		Logistic	for pop	0.22
		Logistic	slope	0.20
		Logistic	imp	0.20
	Storm	Logistic	imp	0.43
		Logistic	drain	0.36
		Logistic	slope	0.19
	Total	Logistic	drain	0.37
		Logistic	imp	0.32
		Logistic	slope	0.29
Nitrate + nitrite (NO_x)	Base	Logistic	imp	0.89
	Storm	Linear	slope ^a	0.47
		Linear	imp ^a	0.39
		Linear	for pop	0.12
	Total	Linear	slope ^a	0.46
		Linear	imp ^a	0.40
		Linear	for pop	0.11
Organic Nitrogen	Base	Logistic	imp ^{a, b}	0.42
		Logistic	pop ^{a, b}	0.41
	Storm	Linear	slope ^a	0.80
		Linear	for pop	0.16
	Total	Linear	slope ^a	0.62
		Linear	for pop	0.36

^a Linear regression of predicted and observed watershed yields resulted in fits with adjusted $r^2 < 0.75$.

^b Linear regression of predicted and observed watershed yields resulted in fits with $p > 0.05$.

Watershed yields of N species were best described by a combination of linear and logistic models depending primarily on the parameter, but also on the type of load (total, base, storm;

Table 6-10). As with water and TSS, models based on percent forest and population density were consistently strong, with a variety of the significant models based on other parameters yielding weak ($r^2 < 0.75$) or non-significant ($p > 0.05$) regressions of observed versus predicted yields in post-hoc testing. As with phosphate, the best models for ammonium were logistic and based on the same parameters, suggesting a similarity between these recycled forms of nutrients.

Given that regressions based on percent forest and population density were often among the best models, predicted watershed yields using these regressions were compared to observed yields of fresh water (**Figure 6-7**), TSS (**Figure 6-8**), and TN (**Figure 6-9**). The resulting fits were well-constrained, highly significant ($p < 0.01$), and explained the majority of the variability in the data in all cases. The models are likely best at predicting base loads given a broader distribution of yields, and values for total and storm loads were often dominated by a single high value. Patterns were similar for nitrate plus nitrite (NO_x), whereas total, base, and storm yields for phosphate and ammonium were all dominated by a single high value. Total and storm yields of organic nitrogen were also dominated by a high value, and there was no apparent linkage between observed and predicted base yields. Regardless of variability in which parameters and model types best explain the yields (**Tables 6-9 and 6-10**), and the occurrence of some influence points at high yields (**Figures 6-7 through 6-9**), these simple regression models do a good job in reproducing yields of these three key parameters across this low relief, coastal plain setting and have the potential to provide general estimates of likely changes in loads as a function of changes in land use and population density.

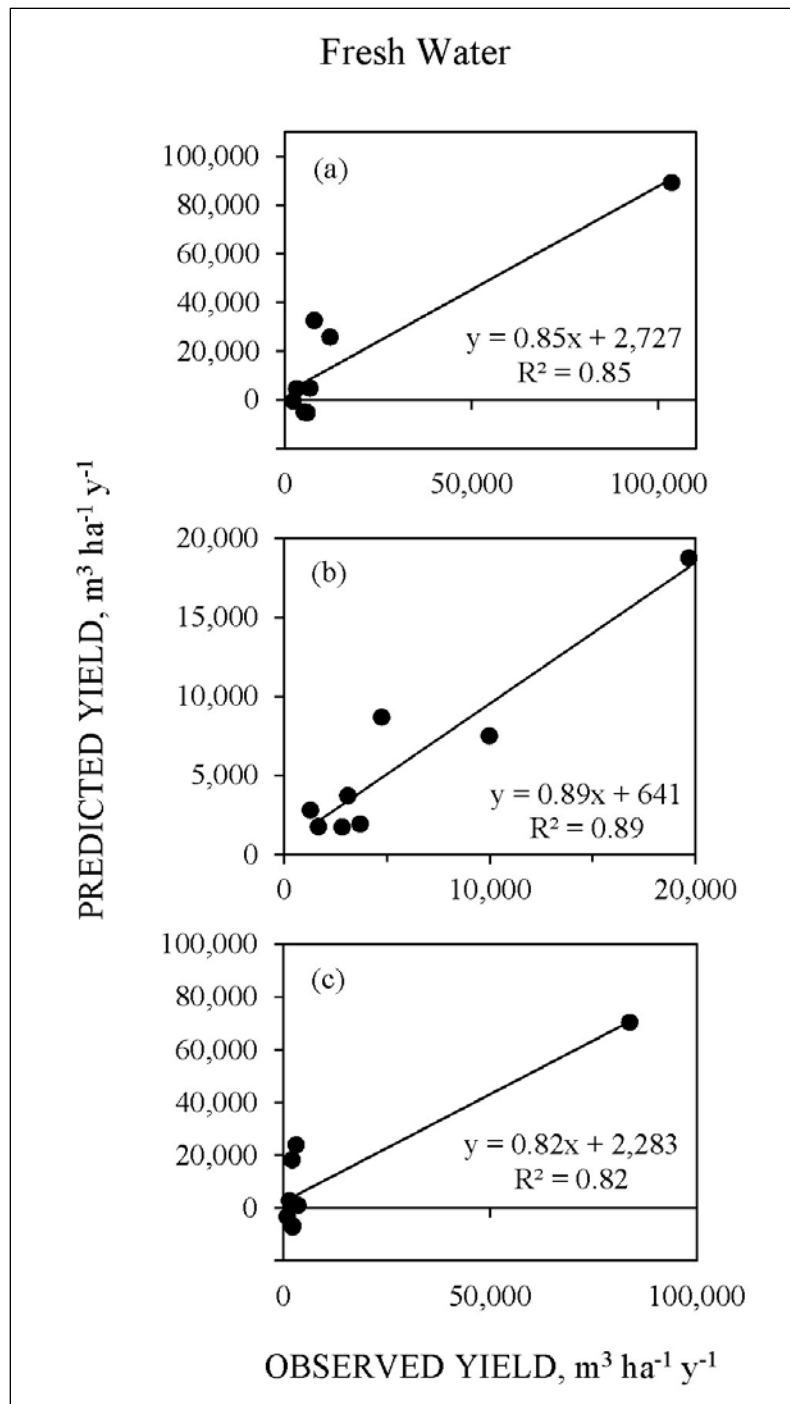


Figure 6-7. Relationship between observed and predicted watershed yields of fresh water for (a) total, (b) base, and (c) storm loads using empirical regression models.

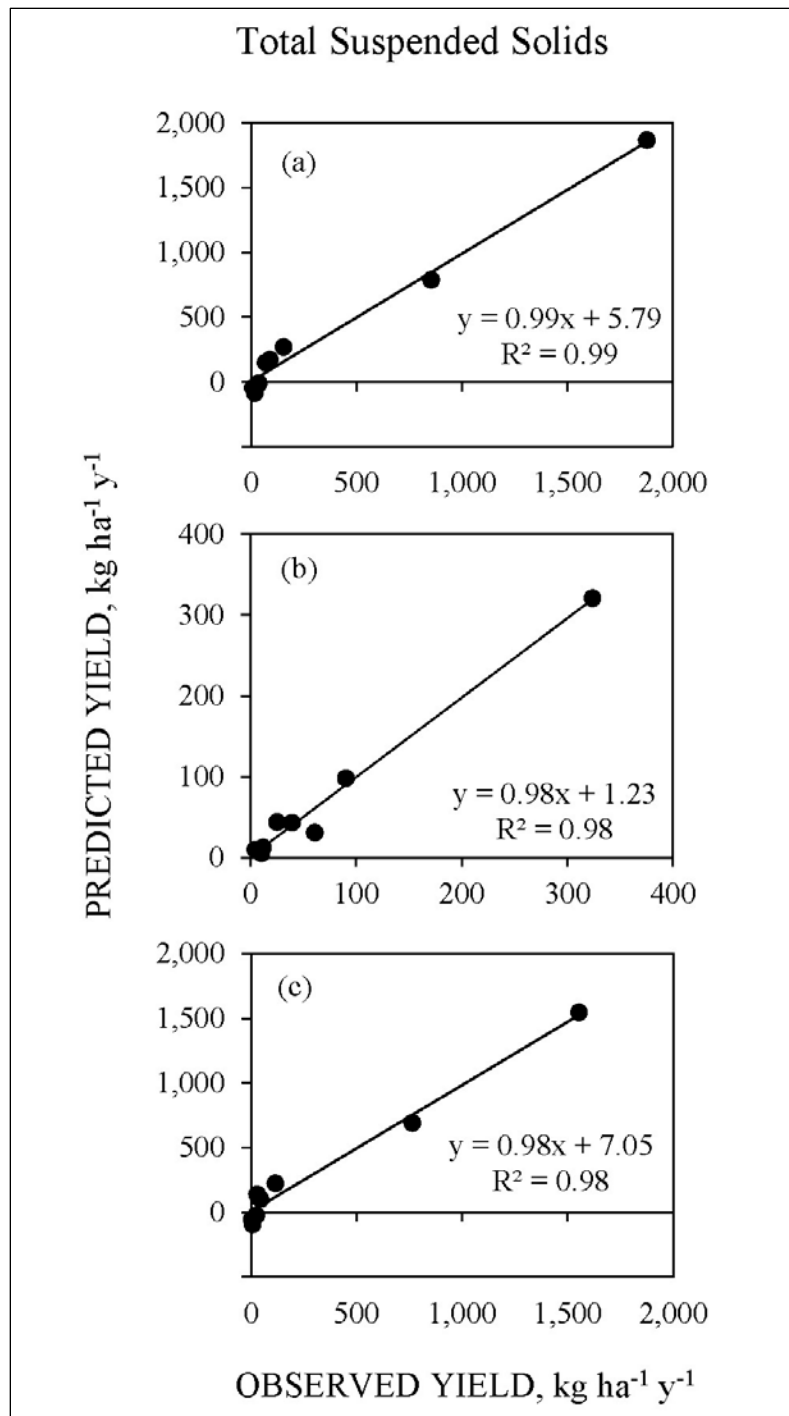


Figure 6-8. Relationship between observed and predicted watershed yields of TSS for (a) total, (b) base, and (c) storm loads using empirical regression models.

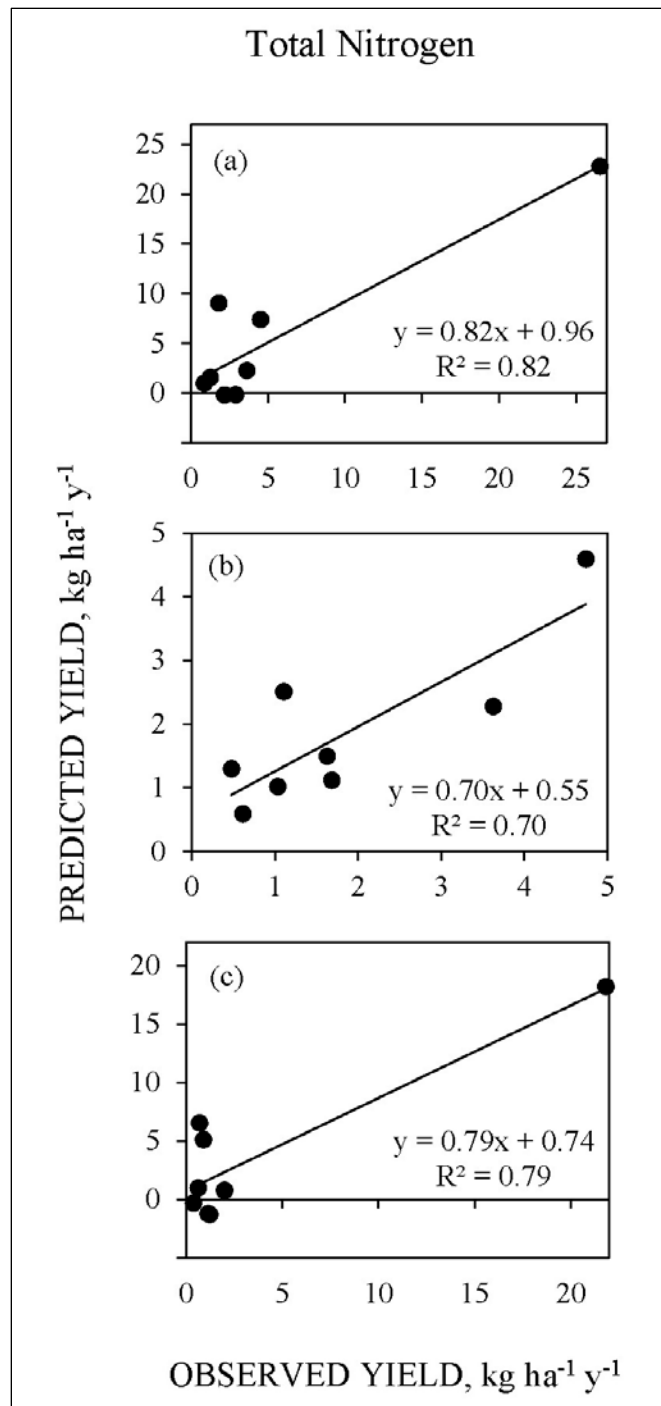


Figure 6-9. Relationship between observed and predicted watershed yields of TN for (a) total, (b) base, and (c) storm loads using empirical regression models.

Other Watershed Models

The other watershed models developed for the NRE generally predicted annual TN loads that were directly proportional to observed loads from the first year of sampling (Year 1 from 2008–2009, **Figure 6-10**), but the models were less successful for the second year (Year 2 from 2009–2010, **Figure 6-11**). The 2 years differed markedly in annual rainfall, which may account for the differing model success, with 105.5 and 131.5 cm of precipitation in Years 1 and 2, respectively. Year 1 was relatively dry, with the precipitation in Year 2 closely matching the long-term (1995–2010) annual mean rainfall of 134 cm.

Although most models in Year 1 predicted TN loads in proportion to observed loads, the regression slopes between observed and predicted loads varied markedly, with WATERSHEDSS, PLOAD, and BasinSim greatly overestimating the observations. Overestimation in the first two models is likely due to their use of relatively old export coefficients. Overestimation by BasinSim is likely due to the lack of an automated calibration procedure, a feature that is available in the ReNuMa model which is based on the same underlying approach (GWLF). Regression slopes for ReNuMa and the NLM were much closer to unity; the latter model performed particularly well when two outlying watersheds, Airport and Gillets Creeks, were removed from the analysis. It is unclear why the NLM underestimated loads in Gillets Creek watershed, but the Airport Creek watershed is characterized by high impervious cover and multiple drainage ditches, which complicated the determination of its watershed boundary. Moreover, the observed loads at Airport Creek in Year 1 were extrapolated from only 6 months of monitoring data.

The models tended to underpredict TN loads in the second, wetter year. The best fitting model was again ReNuMa. When the single outlier (Gillets) was removed from the regression, the slope decreased to 0.60 and the r^2 increased to 0.46. Unlike Year 1, the NLM performed poorly in Year 2. It is unclear why this was the case, although the NLM is intended to predict long-term average annual TN loads and is therefore not generally used to predict inter-annual variations in loads; the current configuration of the NLM as applied to the NRE watershed may work best in drier years.

The most complex, highly parameterized model (i.e., HSPF) performed poorly during both years for TN loads. HSPF is typically applied in larger, higher relief watersheds, and the NRE is characterized by a low relief, wetland-dominated landscape; HSPF tends not to perform as well in wetland-dominated systems. Additionally, prediction of loads with such a highly resolved model in terms of both rate processes and temporal simulation (hourly) may be complicated by the small, intermittent nature of some streams on MCBCL; these issues may not be as important in less resolved models that simulate over longer time periods (months to years). Note, we were not able to use the automated calibration procedure within BASINS to constrain HSPF output.

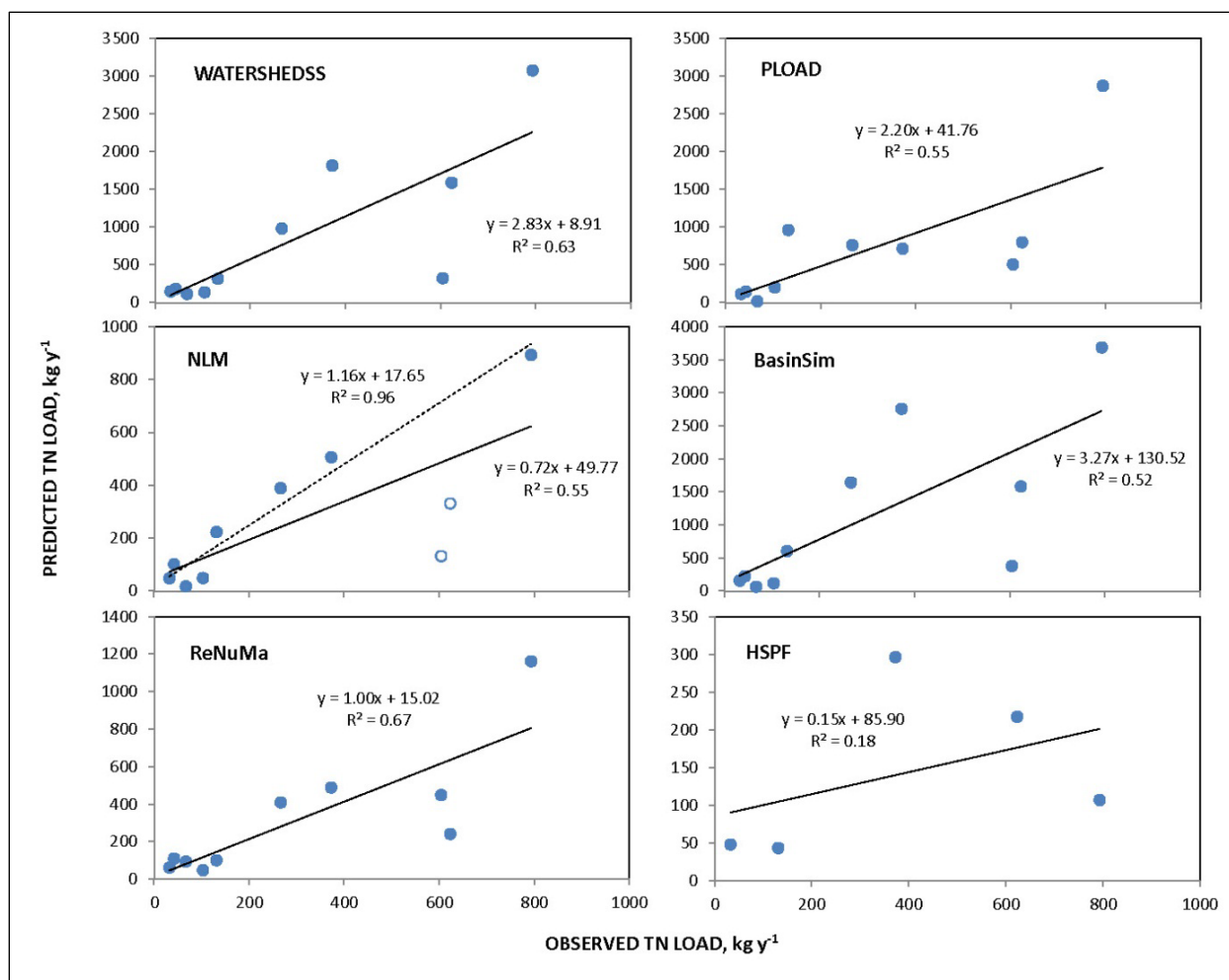


Figure 6-10. Regressions of annual TN loads from the Research Project AE-2 watersheds during the first year of sampling (July 2008–June 2009) against loads predicted by a variety of watershed models.

The solid trend line on the NLM panel is a regression fit to the entire data set; a dashed line is a regression with the two open symbols omitted.

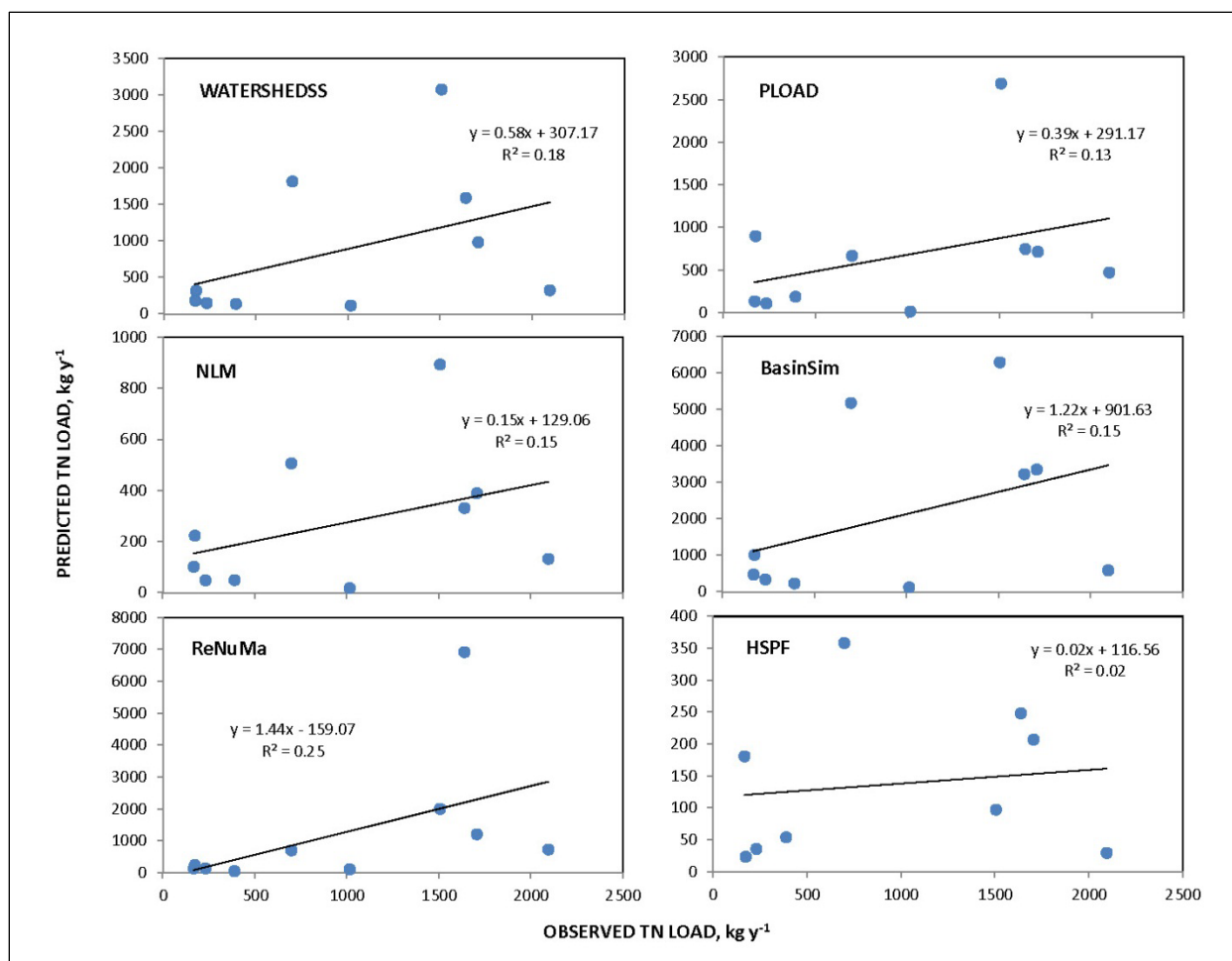


Figure 6-11. Regressions of annual TN loads from the Research Project AE-2 watersheds during second year of sampling (July 2009–June 2010) against loads predicted by a variety of watershed models.

Modeled P loads are complicated by the forms of P simulated. Although observed loads are for orthophosphate (PO_4^{3-}) only, some models simulate PO_4^{3-} , some simulate dissolved phosphorus, and others simulate TP. In general, most models predicted loads that were correlated to observed loads in both years (**Figures 6-12 and 6-13**). Again, WATERSHEDSS, PLOAD, and BasinSim tended to greatly overestimate loads; the degree of overestimation was much greater in the drier year (i.e., Year 1). ReNuMa again emerged as the best fitting model, with regression slopes closest to unity across both years. However, HSPF also performed well, with a slope of almost exactly 1 in Year 2 when two outliers were removed. For both ReNuMa and HSPF, the Airport Creek watershed was again an outlier; the second outlier for HSPF in Year 2 was French Creek, which is heavily dominated by wetlands which again pose a problem for HSPF.

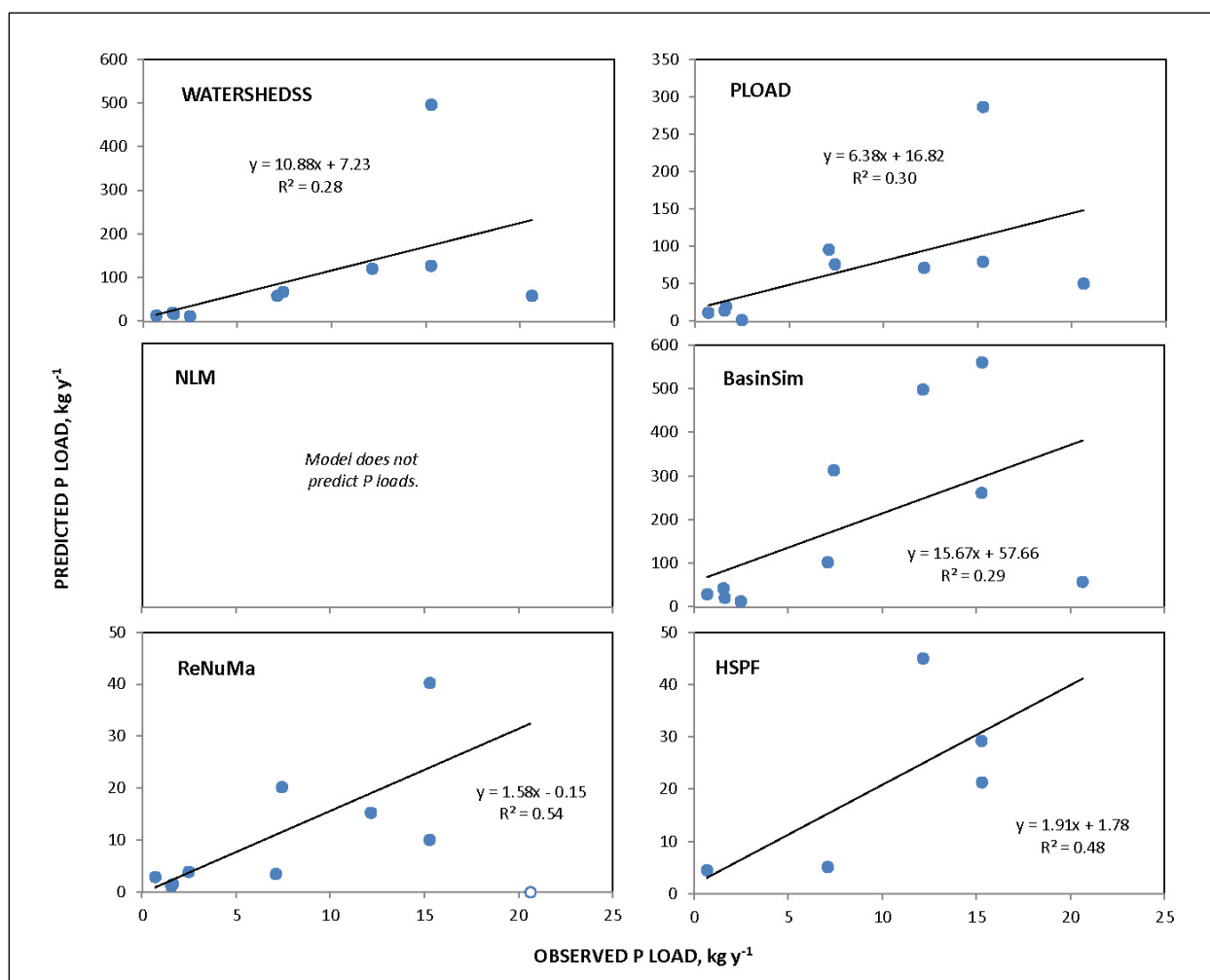


Figure 6-12. Regressions of annual P loads from the Research Project AE-2 watersheds during Year 1 of sampling (July 2008–June 2009) against loads predicted by a variety of watershed models.

Observed, PLOAD, and HSPF loads represent PO_4^{3-} , BasinSim, and ReNuMa loads represent dissolved phosphorus, and WATERSHEDSS loads are TP. Open symbols represent data that were omitted from the regressions.

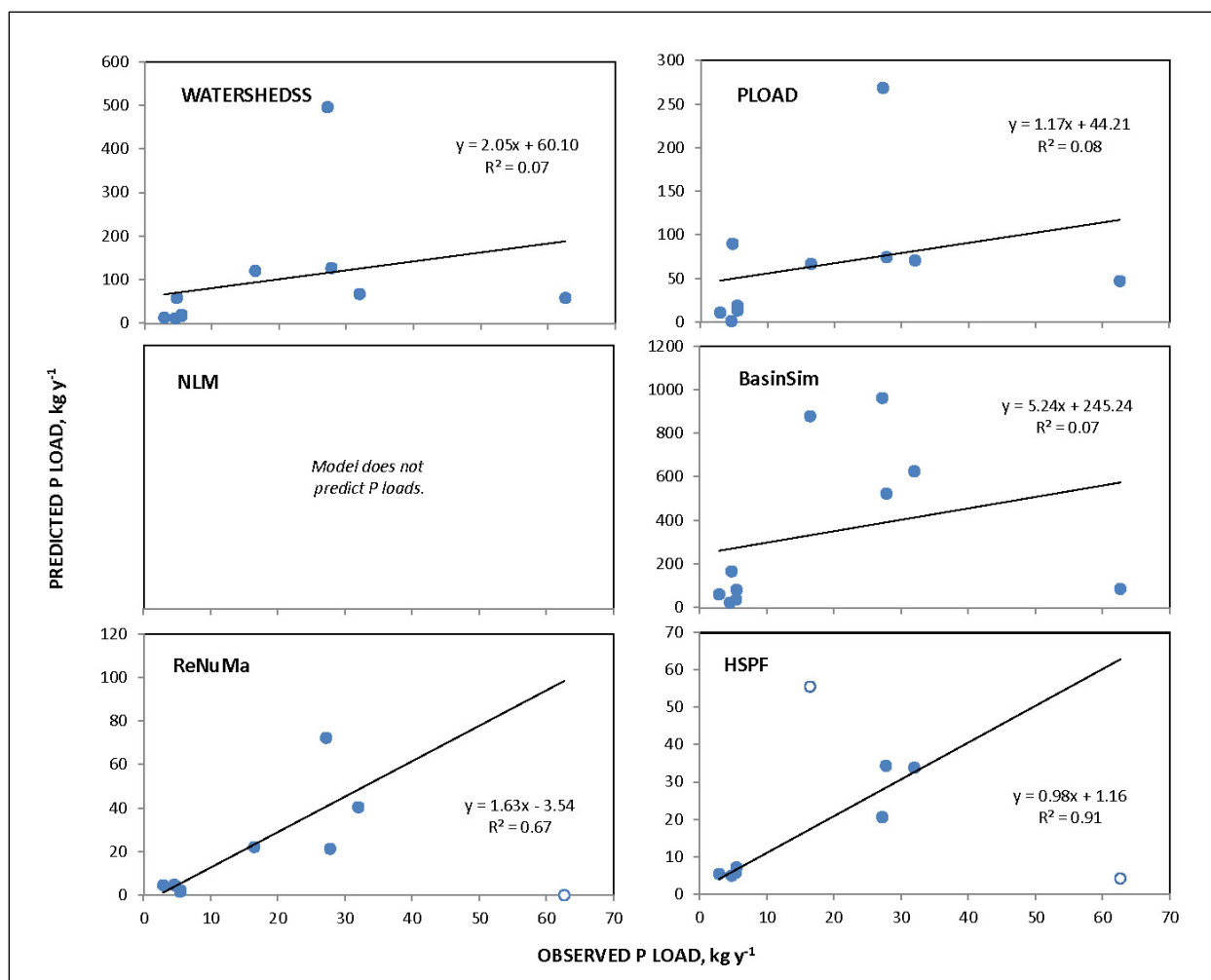


Figure 6-13. Regressions of annual P loads from the Research Project AE-2 watersheds during Year 2 of sampling (July 2009–June 2010) against loads predicted by a variety of watershed models.

Observed, PLOAD, and HSPF loads represent PO_4^{3-} , BasinSim and ReNuMa loads represent dissolved phosphorus, and WATERSHEDSS loads are TP. Open symbols represent data that were omitted from the regressions.

The only models that predicted TSS and freshwater loads were BasinSim, ReNuMa, and HSPF. The models did not tend to perform well for TSS in this low relief setting, with a tendency to greatly underestimate the observed loads (**Figure 6-14**). The exception was the HSPF model in Year 1. Freshwater loads were predicted well in both years by the models based on the GWLF approach (i.e., BasinSim and ReNuMa), with slopes close to 1 in all cases, whereas the HSPF did not perform well (**Figure 6-15**). The outlier in both years for BasinSim was again the Airport Creek watershed.

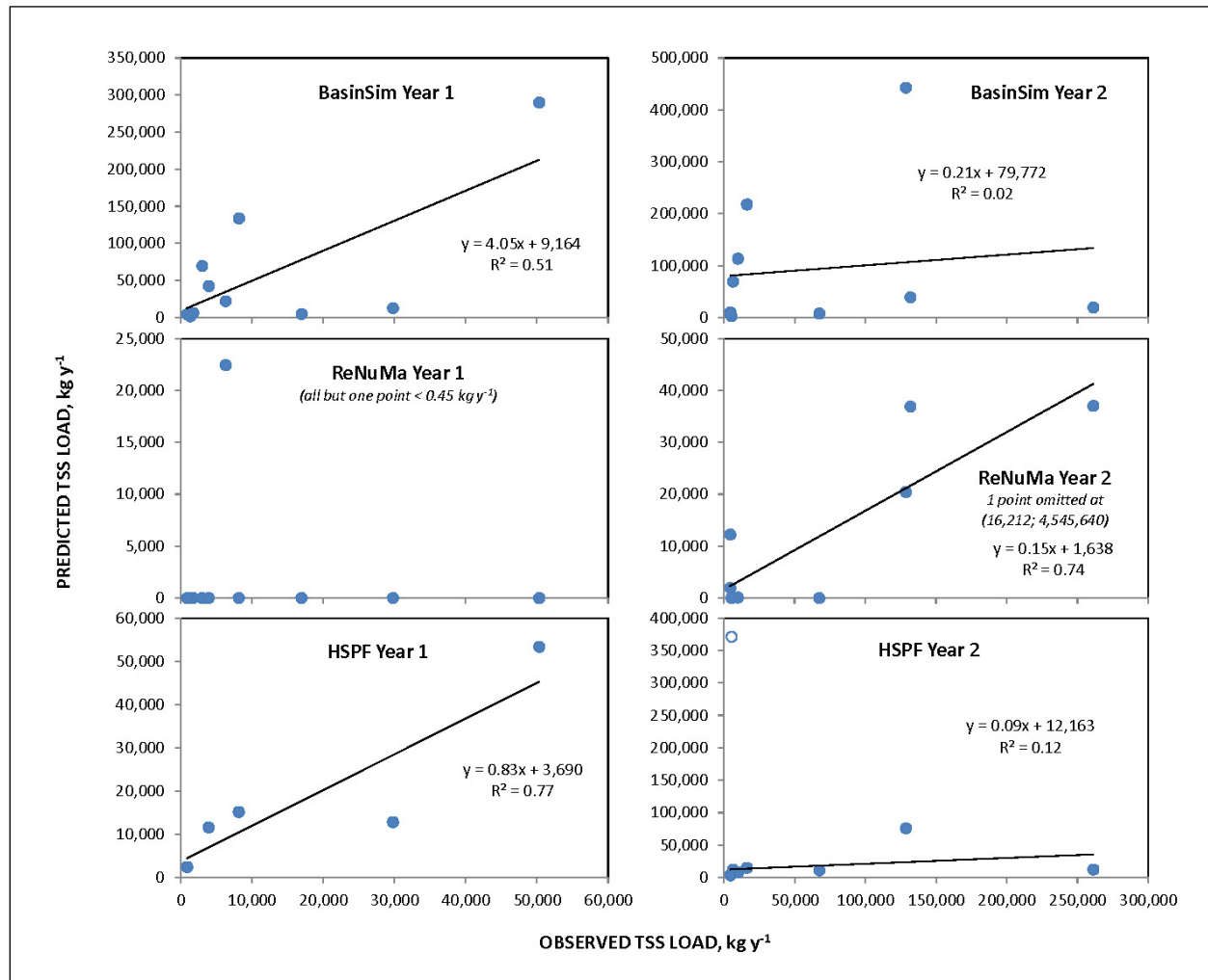


Figure 6-14. Regressions of annual TSS loads from the Research Project AE-2 watersheds during Year 1 (July 2008–June 2009) and Year 2 (July 2009–June 2010) of sampling against loads predicted by a variety of watershed models.

Open symbols represent data that were omitted from the regressions.

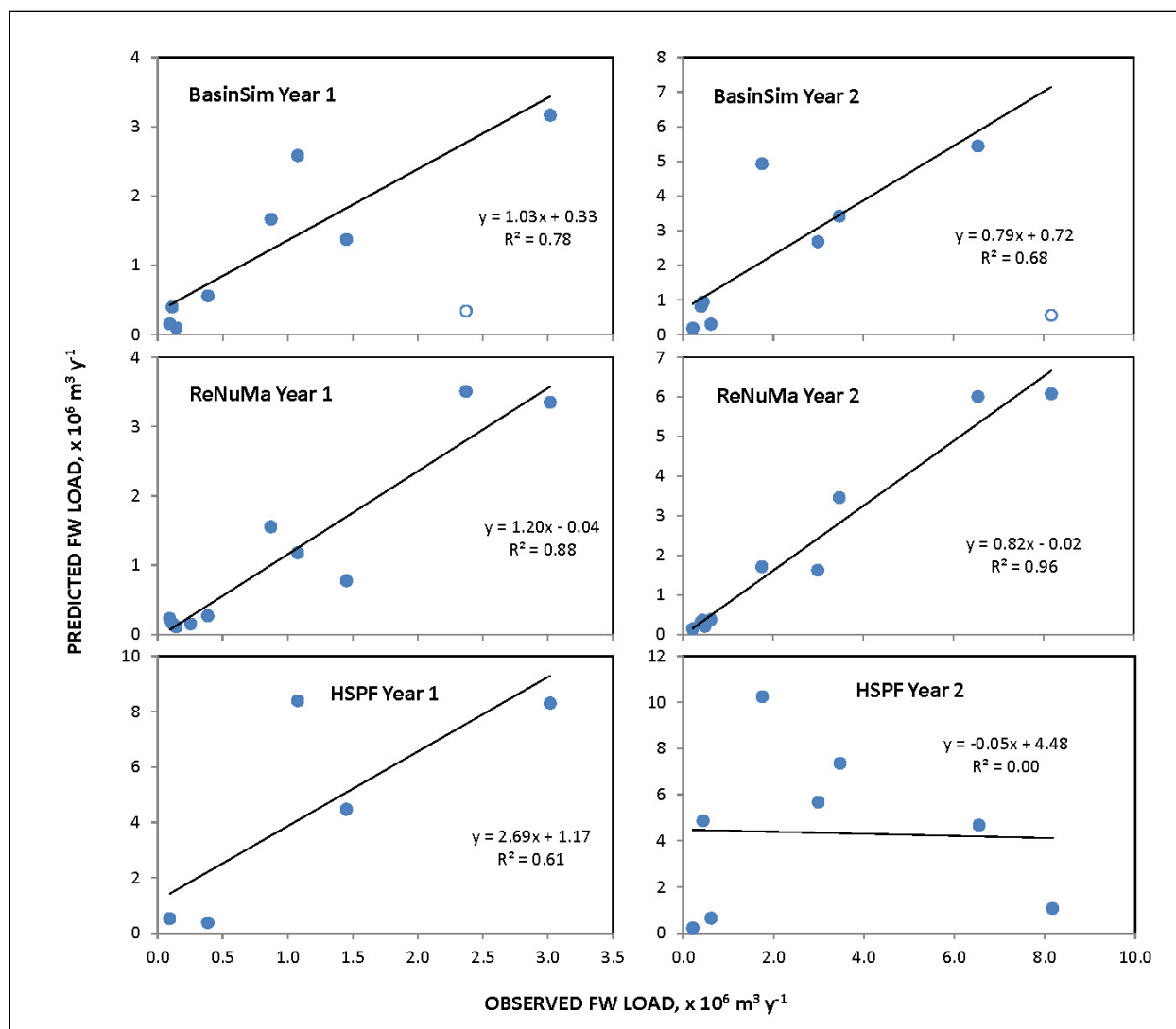


Figure 6-15. Regressions of annual freshwater loads from the Research Project AE-2 watersheds during Year 1 (July 2008–June 2009) and Year 2 (July 2009–June 2010) of sampling against loads predicted by a variety of watershed models.

Open symbols represent data that were omitted from the regressions.

BasinSim, ReNuMa, and HSPF also predict loads at the monthly time scale, and HSPF predicts loads at the monthly, daily, and hourly scales. The focus of the current research was on prediction of annual loads, but an example of monthly output is presented in **Figure 6-16**. The models were sometimes quite successful at reproducing the observed trends in the monthly observations, particularly for ReNuMa, but in other cases the correspondence was not good and fits were not as good as at the annual scale. Daily estimates of loads from HSPF were similarly poorly matched to the data (Koroknay, 2012).

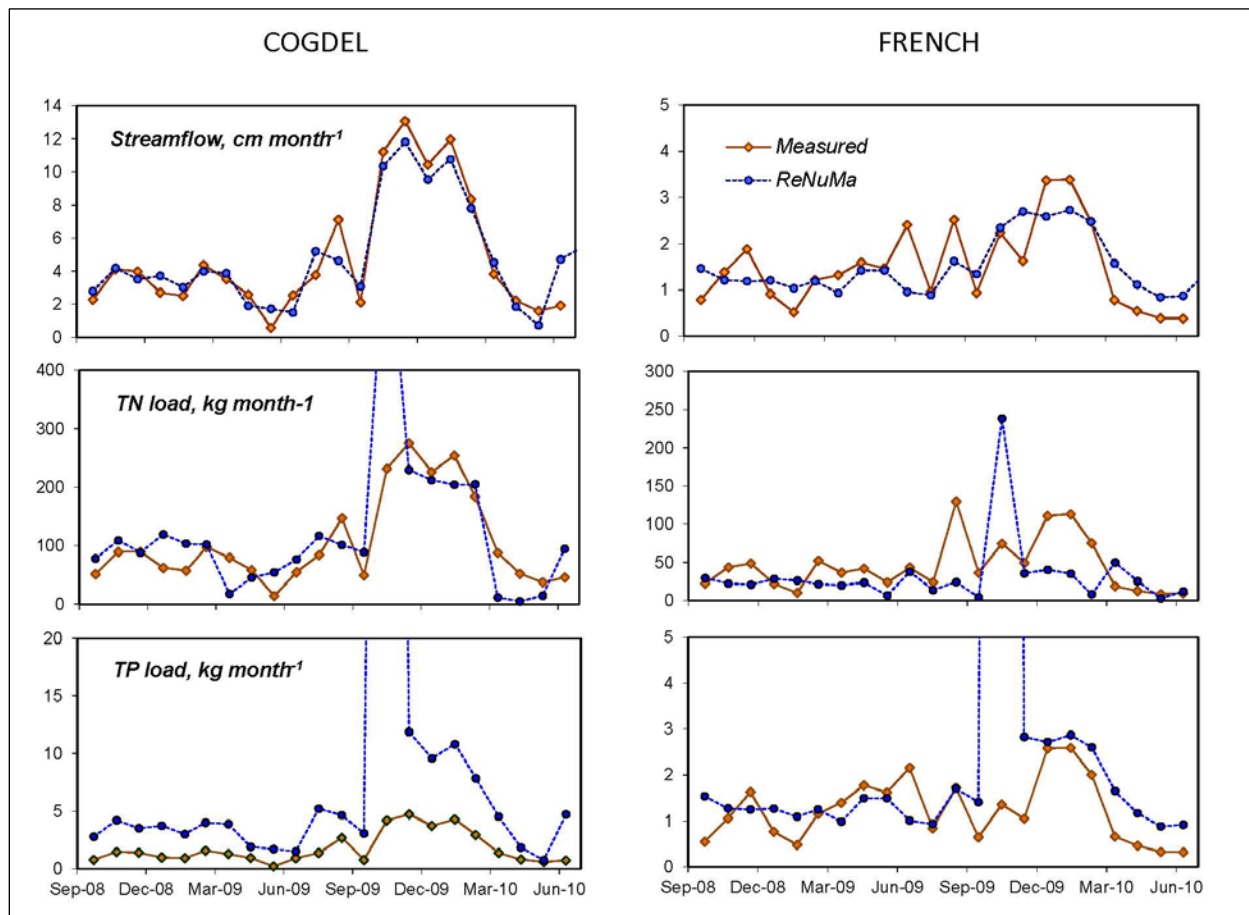


Figure 6-16. Example monthly time series of observed and predicted (ReNuMa) loads for two sub-watersheds in which the correspondence was reasonably close.

Scale Up to MCBCL

All watershed models were scaled across that portion of MCBCL lying within the NRE watershed to estimate the total load to the estuary from on-Base sources. These loads were combined with estimates of the load from the upper (off-Base) watershed, atmospheric deposition, and discharge from the MCBCL WWTF using data sources previously described (see **Table 6-6** for a summary). A final N source is the input of TN from Onslow Bay via estuarine circulation, which was estimated from daily volumetric inflows ($\text{m}^3 \text{d}^{-1}$) to the NRE using the physical Box Model within the ESM combined with estimated mean concentrations of TN in Onslow Bay. Mallin et al. (2005b) reported mean chl *a* and DIN concentrations in Onslow Bay

surface water of $0.42 \mu\text{g L}^{-1}$ and $0.44 \mu\text{M}$, respectively, and Dafner et al. (2007) reported a mean ratio of dissolved organic nitrogen (DON) to total dissolved nitrogen (TDN) of 0.90 in Onslow Bay. Chlorophyll values were converted to particulate N assuming Redfield stoichiometry and a typical C to chlorophyll ratio of 42 g g^{-1} (Brush et al., 2002; Cloern et al., 1995). TDN was estimated from the mean value of DIN and the DON:TDN ratio, and added to particulate N for an estimate of TN in incoming Onslow Bay water.

Results were consistent across all models and supported results from the field sampling (i.e., empirical scaling) and other Aquatic/Estuarine Module researchers, indicating that the dominant source of TN to the NRE is from the off-Base, upper watershed (**Figure 6-17**). The models predicted from 48% to 66% (mean=60%) of the annual allochthonous (i.e., external) TN load to the estuary originating from off-Base sources, with loads from the Base contributing only 12% to 36% of the load (mean=20%), including 5–7% from the MCBCL WWTF. When only watershed sources are considered (i.e., excluding direct atmospheric deposition and the input from Onslow Bay), a full 57% to 85% (mean=76%) of the allochthonous TN load was predicted to originate from the off-Base watershed.

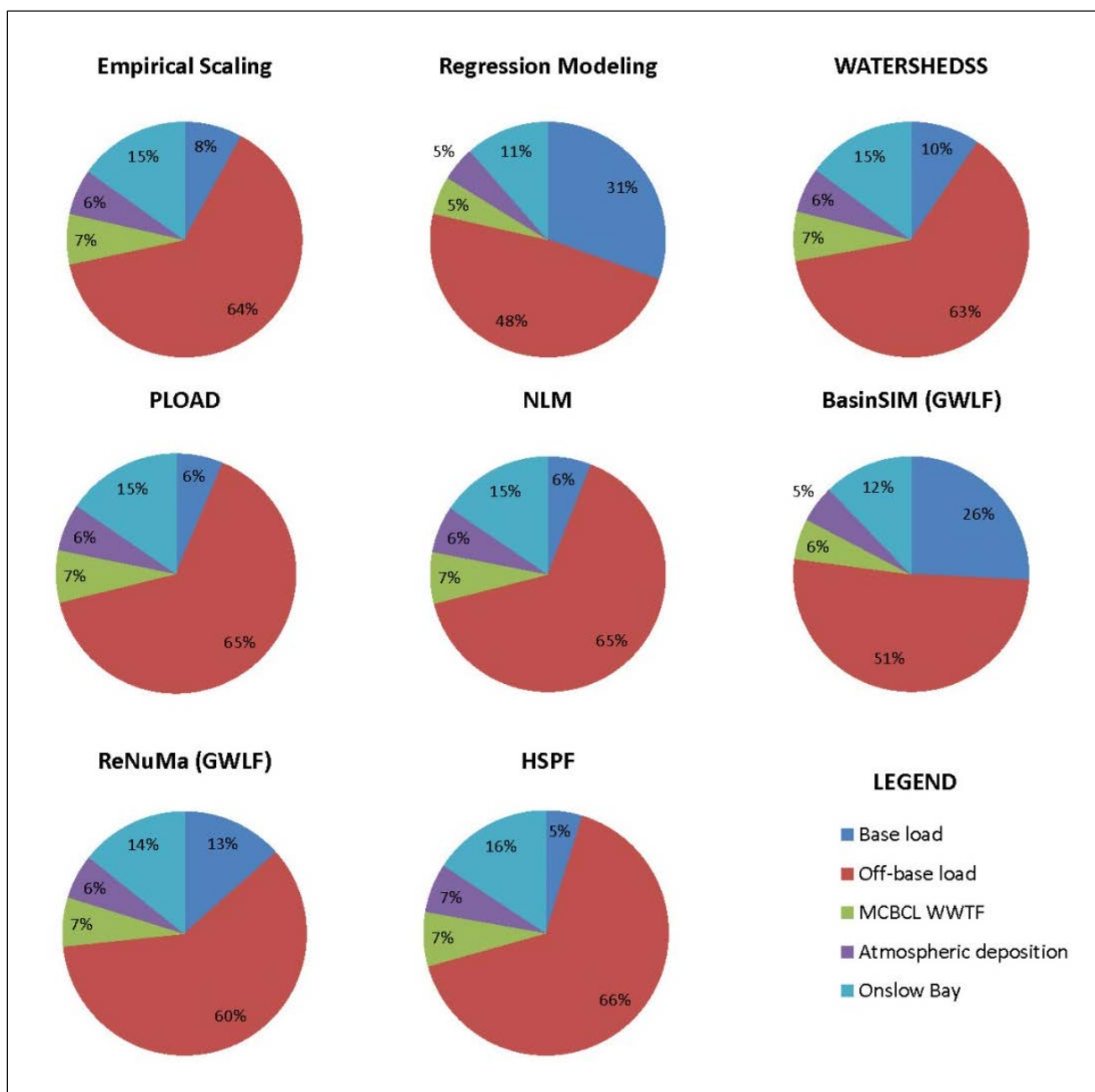


Figure 6-17. Sources of annual allochthonous TN loading to the NRE based on empirical scaling of measured loads and seven different modeling approaches.

Finally, the two most successful models for predicting TN loads (i.e., NLM and ReNuMa) were used to predict the potential changes in watershed TN yields from MCBCL due to continuing land development, as reflected in an increase in impervious surfaces on the Base. Models were run with 1, 5, 10, 15, 20, 25, and 30% impervious MCBCL cover by taking existing lands out of forested/natural vegetation (current MCBCL imperviousness is approximately 13%). The models predicted TN yields in the same range as those based on the observations in the individual Research Project AE-2 sub-watersheds (**Figure 6-18**). The NLM predicted small (not apparent in the **Figure 6-18**) increases in TN yields with increasing impervious cover, with a 0.50% increase in total Base loads for every 1% increase in impervious cover. ReNuMa predicted larger increases in TN yields, with an average 3.2% increase in the MCBCL load for every 1% increase in impervious cover over the range modeled. An important caveat, however, is that the models did not reproduce the apparent 15% threshold in impervious cover above which loads appear to rapidly increase, as documented by Research Project AE-2 (see Chapter 4) and apparent in **Figure 6-18**.

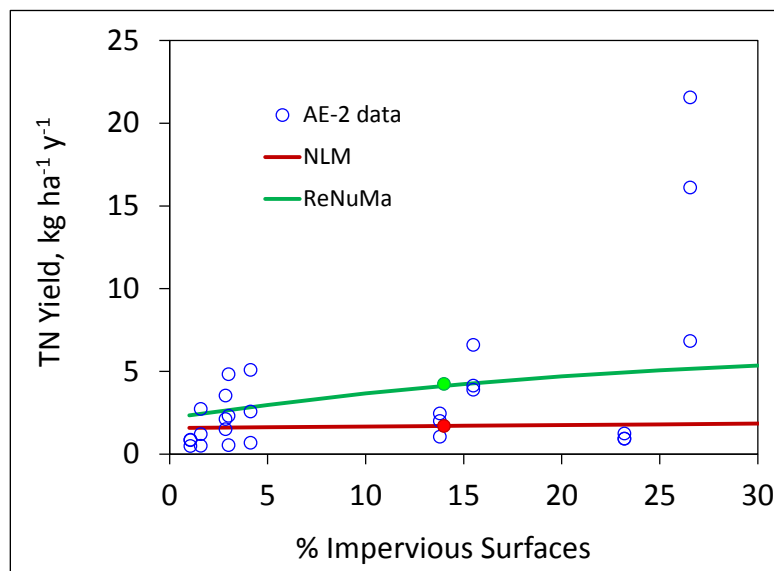


Figure 6-18. Predicted increases in watershed TN yield from MCBCL to the NRE resulting from conversion of forested land to impervious surfaces.

Points represent annual observations during 3 years (July 2008–June 2011) across the Research Project AE-2 watersheds. The colored points on the modeled lines represent the current impervious coverage on the Base.

Estuarine Simulation Model

Model calibration

The ESM was initially calibrated to MCBCL monitoring data available prior to the start of DCERP (1998–2006) and was subsequently calibrated to DCERP data from 2007 to 2010 (**Figure 6-19**). The model reproduced observed concentrations of surface chl *a*, DIN, and DO, capturing both seasonal cycling and key events in the record (e.g., blooms, inputs of nutrients). The model also reproduced key ecosystem rate processes including phytoplankton and benthic microalgal primary production, water column and sediment respiration, and sediment denitrification (**Figure 6-20**).

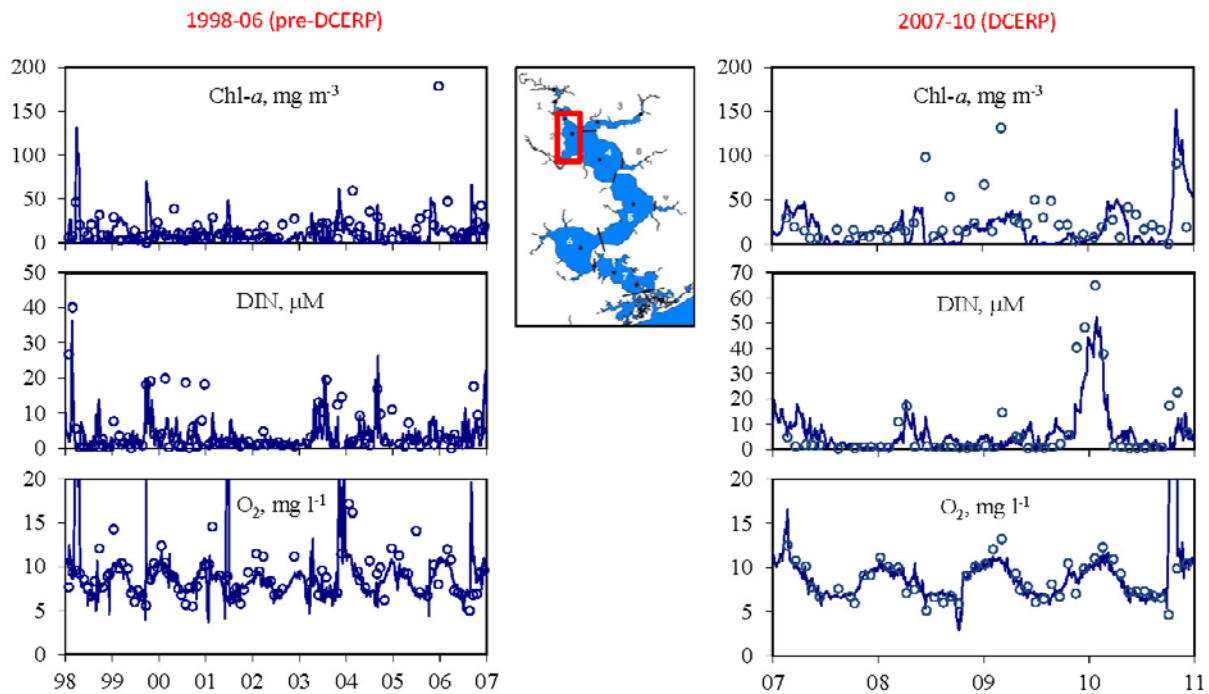


Figure 6-19. Example ESM calibration results (lines) compared to observations (circles) in the surface of the upper NRE (Spatial Element 2) for chl-*a*, DIN, and DO.

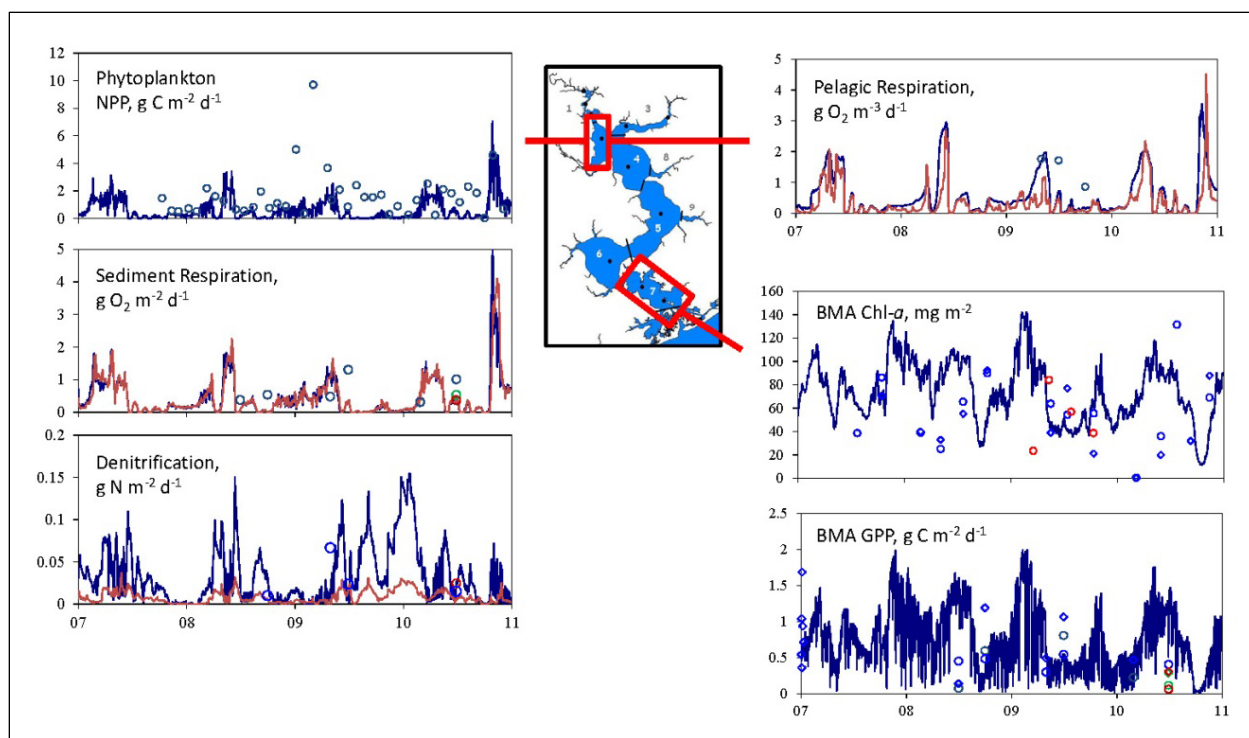


Figure 6-20. Example ESM calibration results to critical rate process data and BMA biomass.

NPP = net primary production; GPP = gross primary production. BMA plots are from ESM Box 7; all other plots are from ESM Box 2. Blue and red lines are from the surface and bottom layers of each box, respectively. Blue, green, and red points are from 0.5-, 1.5-, and 3-m depth, respectively. Blue diamonds and circles on the BMA chl *a* panel are observations at 0.5 m at the Research Project AE-3 Courthouse and Traps Bays sites, respectively. Red circles are observations at 0.5 m at a mainstem NRE site collected as part of supplemental P-I curve measurements in 2009 (see Chapter 5, Research Project AE-3)

Simulation of BMA biomass and production (**Figure 6-20**) was enhanced by the auxiliary P-I curve determinations in the York River, VA. These were conducted to constrain the relationship between BMA production (and therefore growth rate) and water temperature (**Figure 6-21**). Growth rates measured in this experiment were insensitive to temperature, and fell within the range of measurements in the NRE (see Chapter 5, Research Project AE-3) and additional measurements in the York River. Rates also fell within the lower range of values measured in shallow lagoons on the Delmarva Peninsula, although the higher rates in the latter study may be artifacts of curve fitting rather than actual growth rates. As reported for estuarine phytoplankton by Brush et al. (2002), BMA growth appears fairly insensitive to temperature, and the linear fit to the observations is markedly different from the formulations for maximum growth rate used in existing BMA models (e.g., Buzzelli et al., 1999) which caused simulated BMA biomass in the initial version of the ESM to display strong seasonality not supported by the data. Application of the new, linear function in Figure 6-20 resulted in a much improved simulation of BMA biomass. The data also indicate decreasing photosynthetic efficiency at low light (α) and increasing light saturation points (I_k) with increasing temperature.

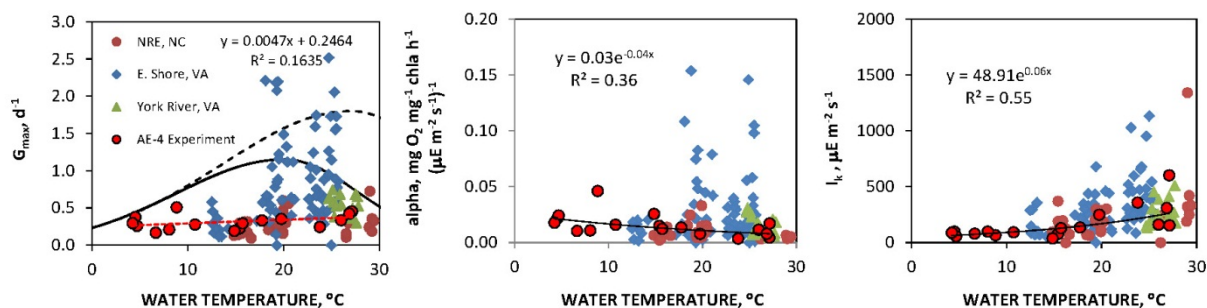


Figure 6-21. Growth and photosynthetic parameters for BMA from Research Project AE-3, two Virginia systems, and a year-long temperature experiment conducted in the York River.

(Left) Maximum daily growth rate (G_{max}) under light saturation. Solid line is the formulation reported in Buzzelli et al. (1999), dashed black line is an elevated version to capture the upper envelope of the Virginia data, and red dashed line is a regression fit to the data from the temperature experiment ($y=0.0025x+0.3131$) and currently used in the ESM. (Middle) Initial slope of the P-I curve (α) and regression fit to the temperature experiment data. (Right) Light saturation parameter (I_k) and regression fit to the temperature experiment data.

The model also reproduced typical growth and respiratory rates for eelgrass (*Zostera marina*). Predicted maximum and actual daily growth rates of *Zostera* shoots (G_{max} and G , respectively) were in the range of light-saturated growth rates measured in supplemental P-I incubations of *Zostera* (**Figure 6-22a-b**), as were predicted rates of shoot respiration (**Figure 6-22c**). The model predicted substantial biomass of *Zostera* only in the lowermost spatial element of the ESM (Box 7), the shallowest portion of the mainstem NRE with the clearest water (**Figure 6-22d**). Although no data are available on *Zostera* biomass in the NRE, this prediction matches our field observations that *Zostera* is only found in Box 7 and the lowermost portions of Box 6. While some aspects of habitat suitability for *Zostera* are excluded from the ESM such as sediment type, organic content, and wave exposure, these model results suggest that based on water quality and light availability, efforts to restore *Zostera* to the NRE should be focused in Boxes 6 and 7 as conditions up-estuary are not likely to be favorable.

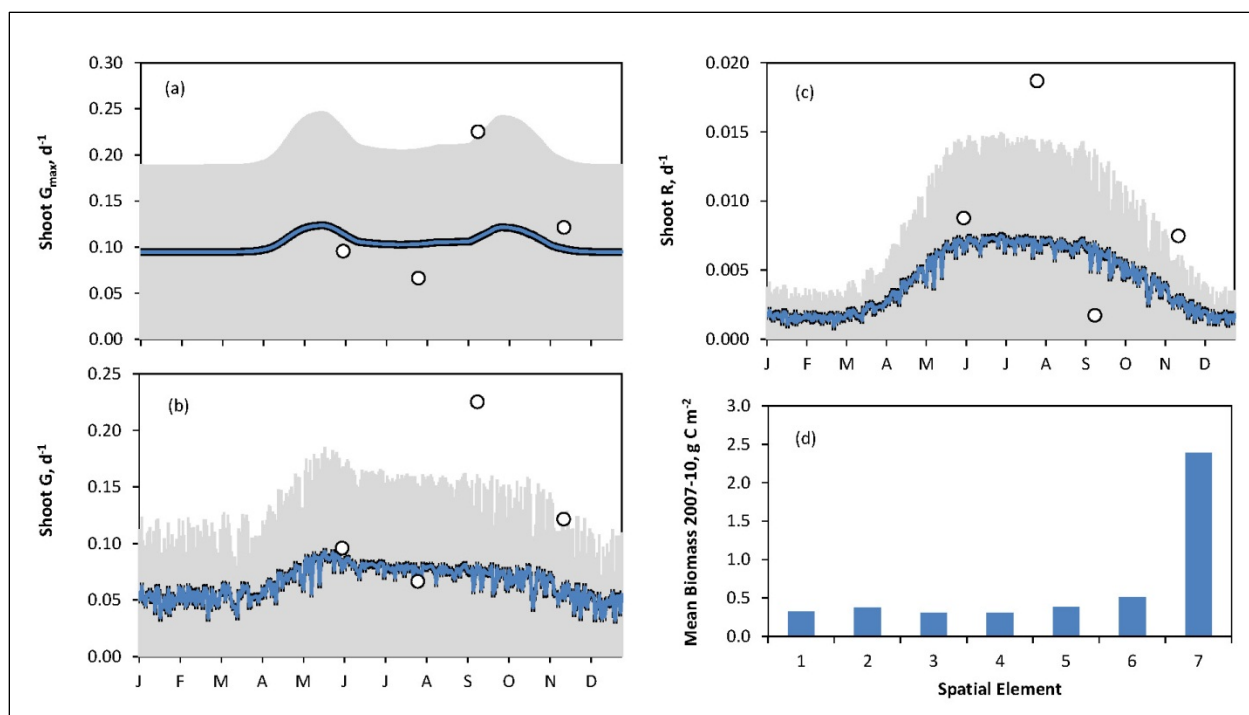


Figure 6-22. ESM calibration results to eelgrass shoot growth rate, respiratory rate, and biomass in Spatial Element 7 (lower NRE).

(a) Maximum daily growth rate, (b) actual daily growth rate, (c) daily respiratory rate, and (d) mean modeled shoot biomass by spatial element. Lines in panels (a) through (c) represent mean daily values across four modeled years (2007–2010), gray bars denote one standard deviation around these means, and points are from the supplemental eelgrass P-I curve experiments in 2010.

ESM Simulation Analysis

Following calibration of the ESM, the model was used to conduct a series of simulations to understand NRE structure and function. The model was initially used to compute the external sources of N to each spatial element as had previously been done for the estuary as a whole (**Figure 6-23**). The model indicated that as for the entire system, the major source of external N to the uppermost spatial elements (Boxes 1–3) is the upland, off-Base watershed, with Box 2 receiving the greatest fraction of its N input from advection of N down-estuary from Box 1. In the middle of the estuary (Boxes 4–6), the major source of N is also that advecting down-estuary, which was originally derived from the upper, off-Base watershed. An important fraction of the load in Farnell Bay (Box 5) originates from the MCBCL WWTF. Downstream of the Route 172 constriction (Box 7), the major source of N originates from advection up-estuary (i.e., Onslow Bay). In all of these mainstem boxes, loads from the Base are minor. Wallace and French Creeks (Boxes 8 and 9, respectively) provide interesting contrasts, with a major input of N coming from the mainstem of the NRE; this is the dominant source to Wallace Creek. In these small, fringing creek systems, inputs from the Base also appear relatively important.

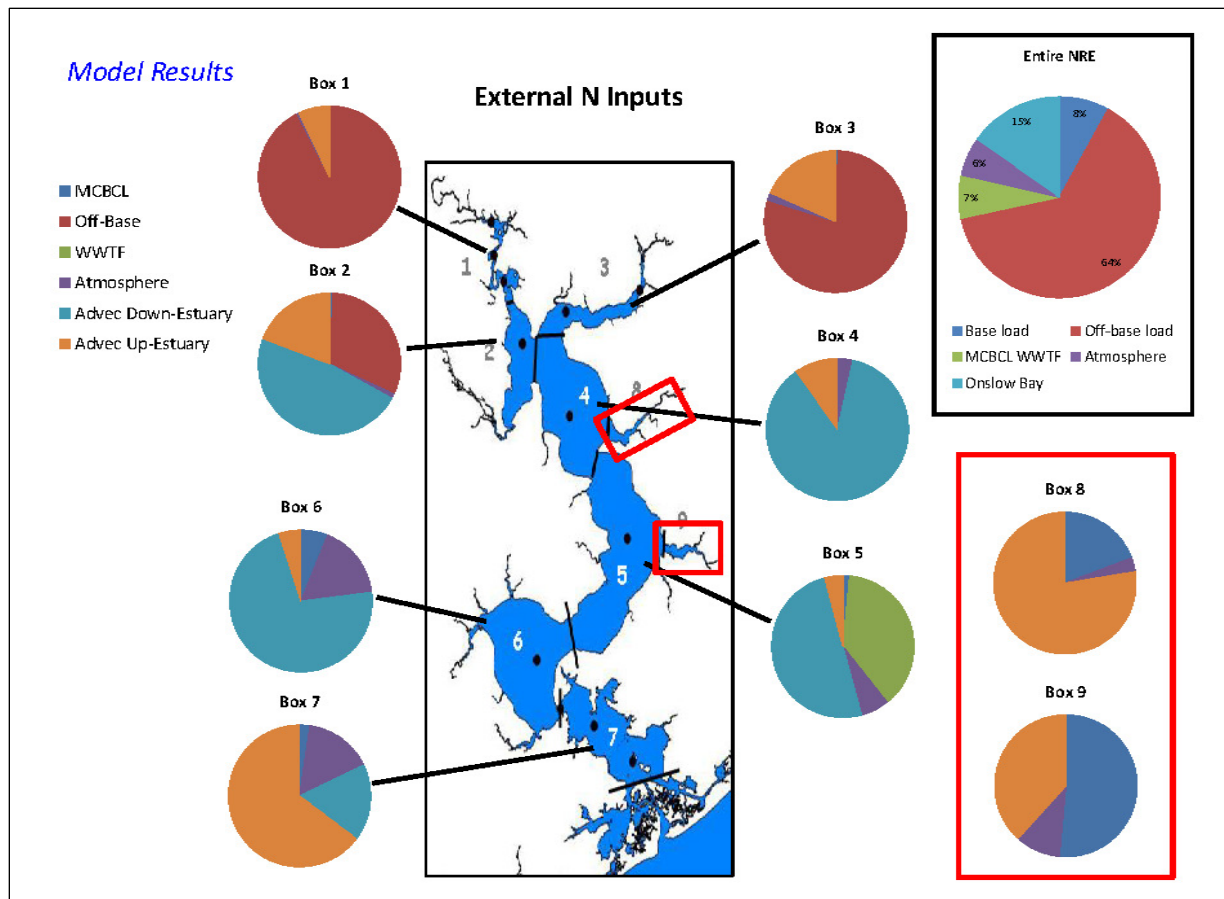


Figure 6-23. Modeled N sources to each NRE spatial element.

“Advect Down-Estuary” refers to input of N in water moving from an upstream box into a given spatial element.
 “Advect Up-Estuary” refers to input of N in water moving from a downstream box into a given spatial element.

The only sinks for N in the ESM are denitrification and export to Onslow Bay because burial in sediments is not explicitly considered; however, this is generally a small loss term. Annual losses due to removals in the hard clam fishery were estimated from reported landings (NCDMF, 2008) and literature-based estimates of N content of hard clam tissues. The major sink for N over the annual cycle in the NRE appears to be denitrification, with a smaller loss due to export (**Figure 6-24**), as with other systems, removals in the fishery were estimated to be small. The NRE is estimated to export 31.5% of the annual N load from land-based and atmospheric sources, which falls somewhat below that expected based on residence times from a synthesis of a wide variety of estuarine systems (Nixon et al., 1996; **Figure 6-24**).

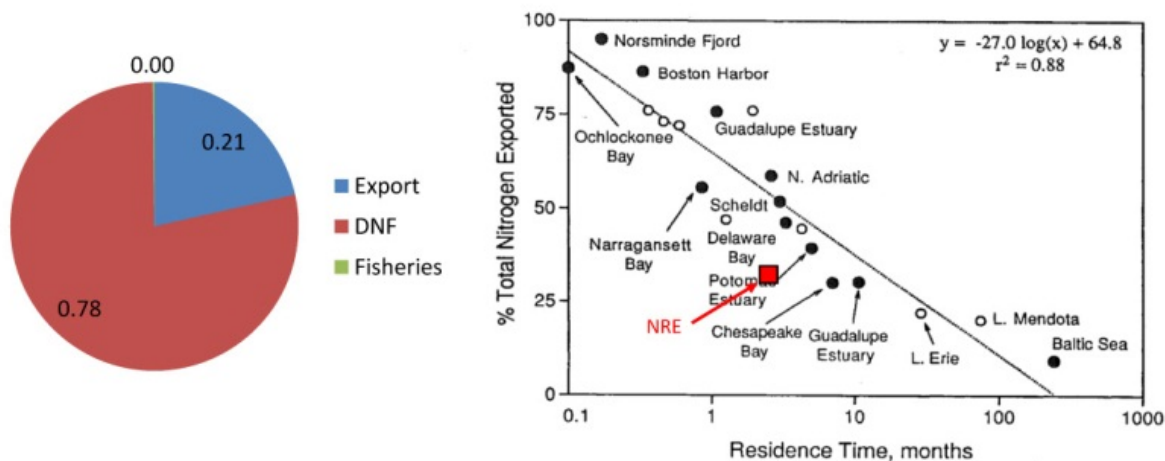


Figure 6-24. ESM estimated sinks for N in the NRE.

(Left) Long-term (1998–2010) mean distribution of sinks between export across the mouth of the estuary, denitrification (DNF), and fisheries harvests (<1%). Right: figure reproduced from Nixon et al. (1996) showing the effect of estuarine residence time (in this case equivalent with flushing time as defined by Monsen et al. [2002] and as computed by the ESM) on the fraction of land- and atmospheric-based N loads that get exported.

A primary goal for the ESM was to determine the features of the NRE ecosystem that make it particularly susceptible or resistant to anthropogenic nutrient loading. These features have been identified as “filters” in that they modify or filter an estuary’s response to nutrient inputs (Cloern, 2001). The first main filter in the NRE appears to be flushing time. Following the definition in Monsen et al. (2002), flushing time is the “freshwater replacement time” (i.e., the time it takes to fully replace the volume of freshwater in the system at any point in time). Flushing times computed for the NRE as a whole by the physical box model were highly variable and a function of freshwater inputs (**Figure 6-25**); values ranged from 100 or more days at low freshwater inputs to a month or less at the highest flows. The median flushing time of the NRE was estimated to be 69 days (mean=87 days) over the period 1998–2010; this value closely matches a median of 64 days determined by Ensign et al. (2004).

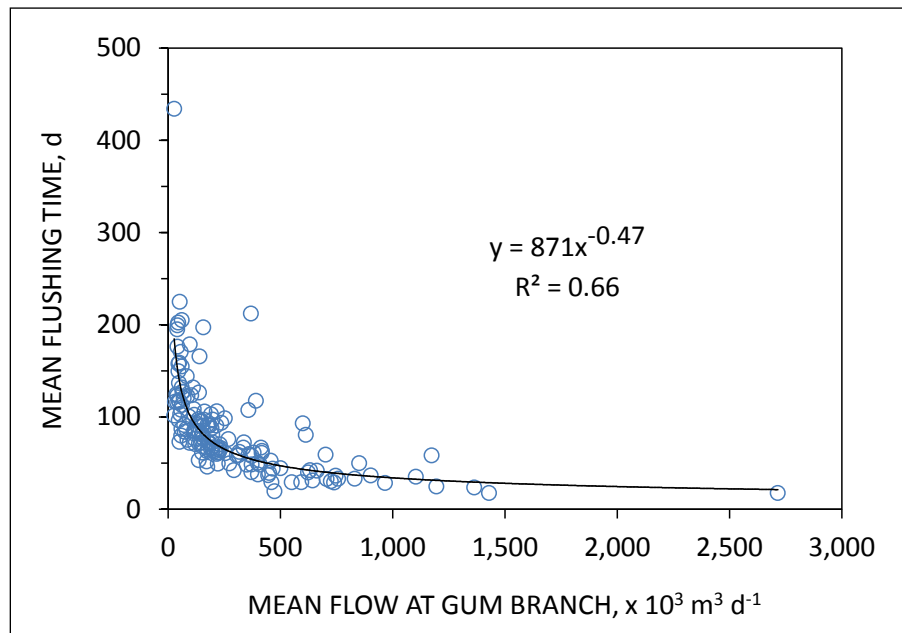


Figure 6-25. ESM computed freshwater flushing time for the NRE as a whole, as a function of mean freshwater flow at Gum Branch (1998–2010).

Flushing time varies markedly, however, down the axis of the NRE (**Figure 6-26**). Flushing is rapid out of the upper boxes (1–3), with typical flushing times of 3–10 days. Rates slow substantially in mid-estuary, however, with median flushing times reaching 24 and 18 days in Boxes 4 and 5, respectively. Flushing again speeds up in the lower estuary with median times of 9 and 1.5 days in Boxes 6 and 7, respectively. This pattern has strong implications for material processing in the NRE; watershed-derived nutrients are quickly flushed out the tributaries, but are held for much longer in mid-estuary where blooms and hypoxia can occur, before they are quickly flushed from the lower estuary. Although this overall pattern exists from year to year, the magnitude of flushing is dependent on inter-annual variability in freshwater inputs (**Figure 6-26**).

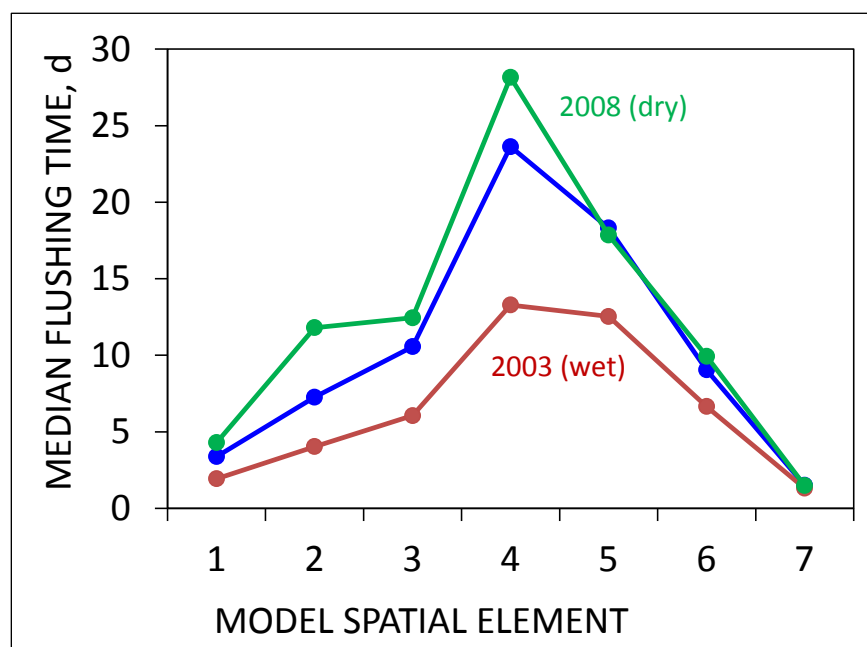


Figure 6-26. ESM computed flushing time by NRE spatial element.

The blue line represents the long-term mean (1998–2010), and the red and green lines depict major wet and dry years, respectively.

As described in Anderson et al. (2003), BMA can exert a strong influence on coastal systems and serve as a filter by sequestering watershed-derived nutrients and mitigating against the effects of anthropogenic nutrient loading (see also Chapter 5). The ESM was run with and without BMA to determine the strength of this effect in the NRE; results for 1998–2006 are shown in **Figure 6-27**. BMA appear to exert a strong role on NRE ecosystem dynamics. In the absence of BMA, phytoplankton concentrations in the lower estuary where BMA production is especially active were approximately 50% greater than when BMA were included in the model. This effect is still noticeable, although somewhat suppressed, in the upper estuary where increased light attenuation reduces BMA photosynthesis.

Another key filter in the NRE is the high rate of denitrification. The ESM predicted much higher concentrations of water column chl *a* and N in the absence of denitrification (**Figure 6-28**). Median concentrations of chl *a* and DIN were predicted to increase by 32–85% and 120–820% in the absence of this key rate, respectively (**Table 6-11**). Based on flushing times of each box

(from **Figure 6-26**) and a synthesis of a wide range of temperate estuaries (Nixon et al., 1996), the model estimates suggest that the NRE is highly efficient at removing N via denitrification relative to other temperate estuaries (**Figure 6-29**).

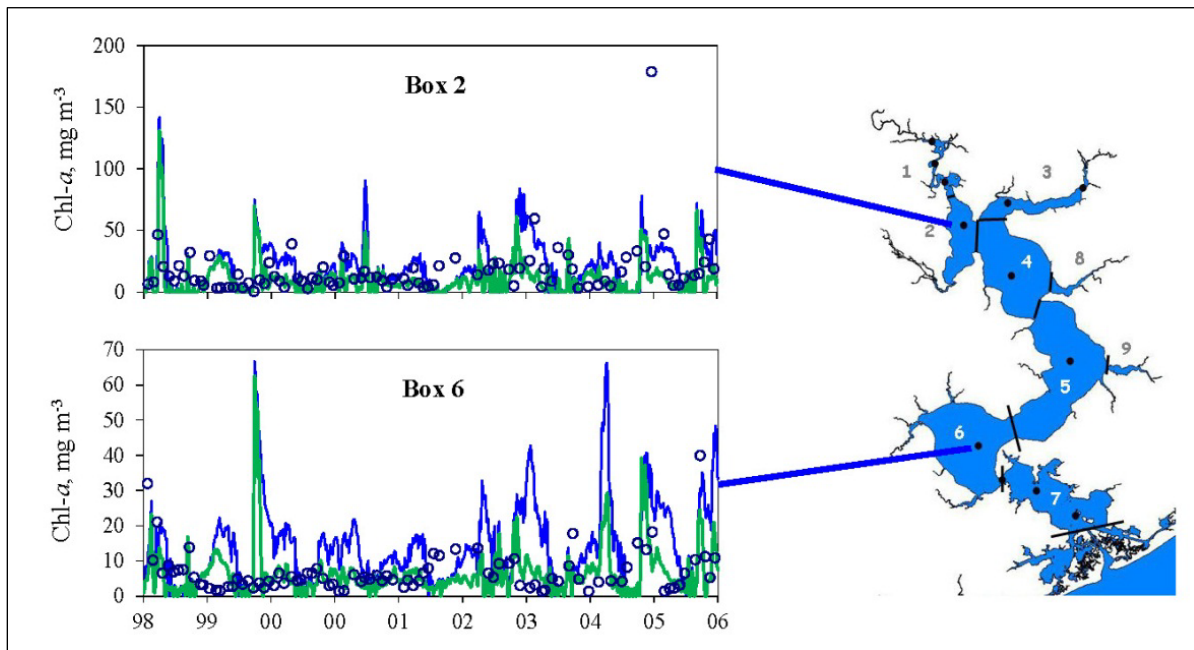


Figure 6-27. ESM predicted phytoplankton biomass as chl *a* in surface waters of the NRE with (green lines) and without (blue lines) BMA.

Circles depict monitoring data from the corresponding spatial element.

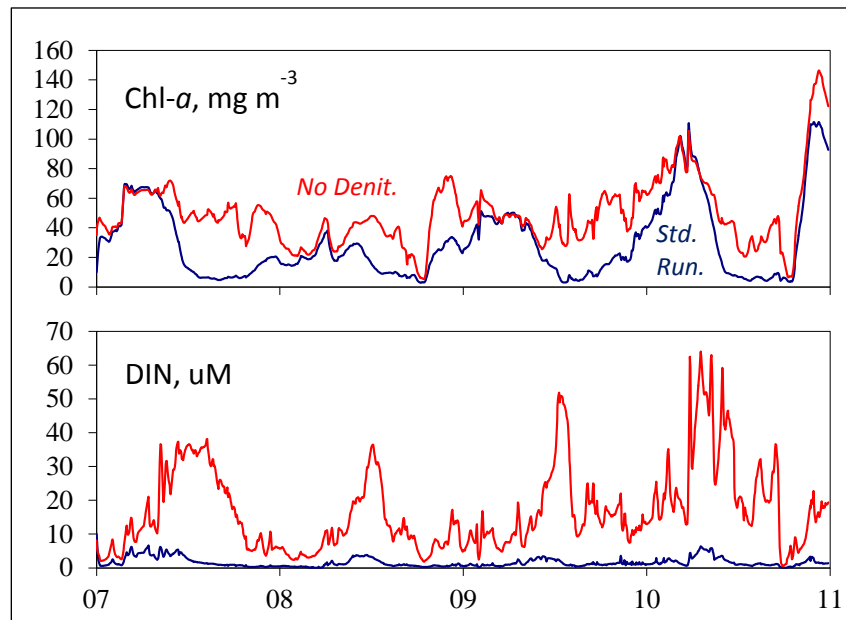


Figure 6-28. ESM predicted phytoplankton biomass as chl *a* and DIN concentrations in surface waters of Farnell Bay (Box 5) with (blue lines) and without (red lines) denitrification.

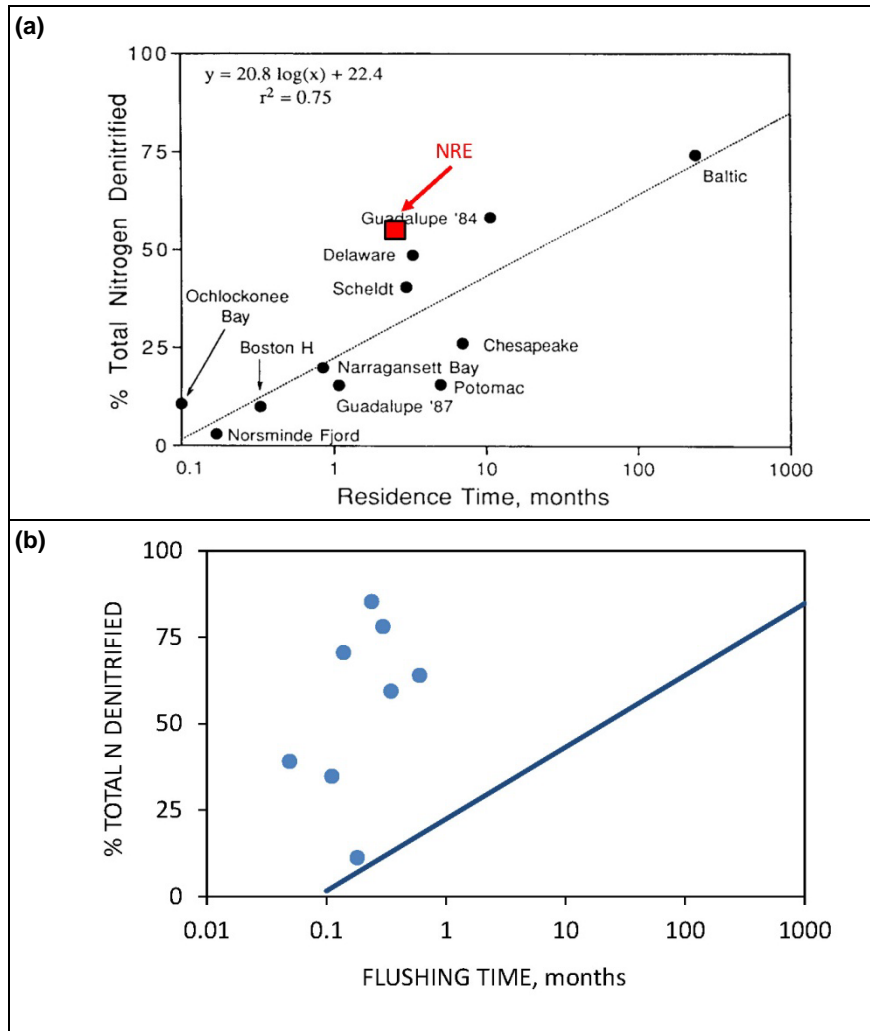


Figure 6-29. Effect of residence and flushing times on the fraction of land- and atmospheric-based N loads denitrified across a range of estuarine systems.

(a) Figure reproduced from Nixon et al. (1996). Residence times on this figure are equivalent with flushing times as defined by Monsen et al. (2002) and as computed by the ESM. (b) ESM results by spatial element averaged across the period 1998–2010 plotted along with Nixon et al.'s regression from the upper panel.

Table 6-11. Median percent increases in surface chl *a* and DIN by ESM spatial element in the absence of denitrification.

Element	chl <i>a</i>	DIN
1	32.4	124
2	51.1	489
3	60.4	433
4	68.3	706
5	85.3	821
6	80.9	703
7	58.3	190

Light attenuation is another key filter that affects NRE response to nutrient loads. Attenuation in the NRE is the combined result of that due to water, chl *a*, suspended sediments, and CDOM (Chapter 5, Research Project AE-3). The ESM was run with and without CDOM to assess its effect on limiting photosynthesis via reducing light penetration. In the absence of CDOM, phytoplankton biomass was predicted to be lower, with overall decreases of 10–27% (**Figure 6-30 and Table 6-12**), due to resultant increases in BMA productivity which removed nutrients from the water column.

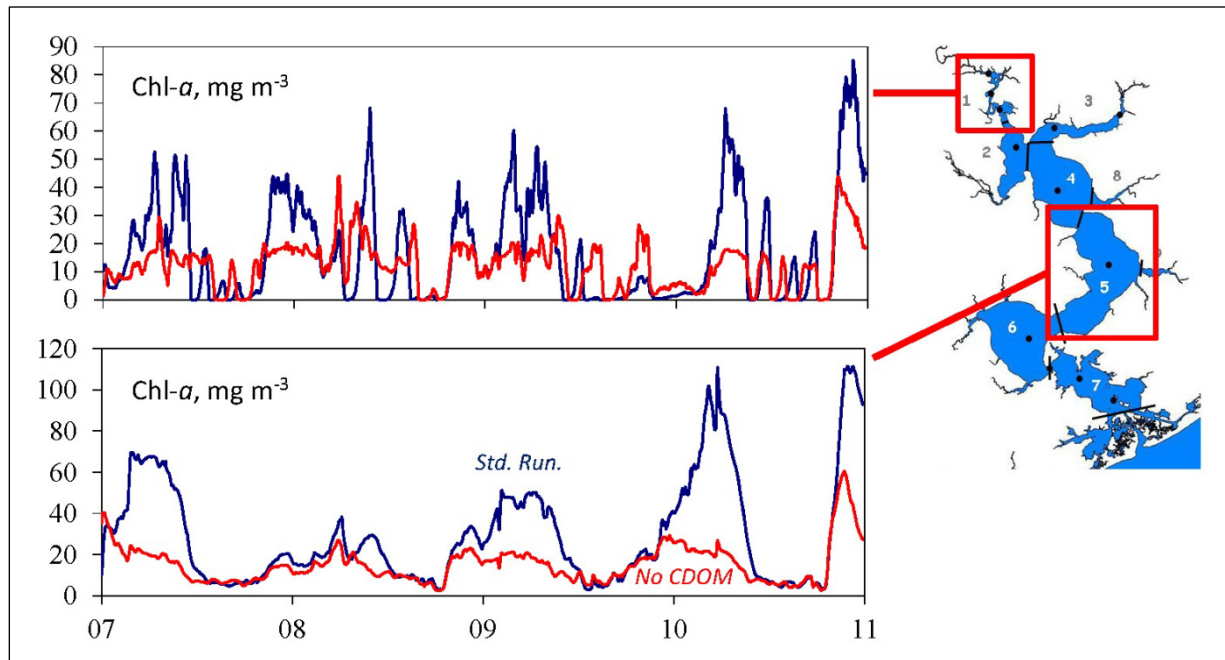


Figure 6-30. ESM predicted phytoplankton biomass as chl *a* in surface waters of the NRE with (blue lines) and without (red lines) the presence of CDOM.

Table 6-12. Median percentage decreases in surface chl *a* by ESM spatial element in the absence of CDOM.

Element	chl <i>a</i>
1	-11.3
2	-25.6
3	-22.2
4	-25.4
5	-26.6
6	-20.5
7	-9.7

Benthic Bivalve Modeling

The *M. mercenaria* model closely matched expected final clam lengths and weights (**Figure 6-31**), with highly significant regressions between expected (x) and modeled (y) values (for length: $y=0.99x+0.077$, $r^2=0.98$, $F<0.001$; for weight: $y=0.93x+100$, $r^2=0.99$, $F<0.001$) and low root mean squared errors (2.3 mm and 0.18 g dw). Modeled clams began rapid growth around Day 105, which later slowed due to allocation of net production to reproductive tissue and subsequent spawning (**Figure 6-31**). Weight was predicted to decrease early and late in the year due to simulated respiration exceeding assimilation; this was a consequence of our temperature limitation function for filtration in which rates below 15°C were negligible. However, without this new function clams were predicted to grow far beyond reasonable sizes. Modeled length followed the same pattern as weight because they were empirically related; decreases are artificial and highlight the advantage of simulating length independently as discussed by Hofmann et al. (2006).

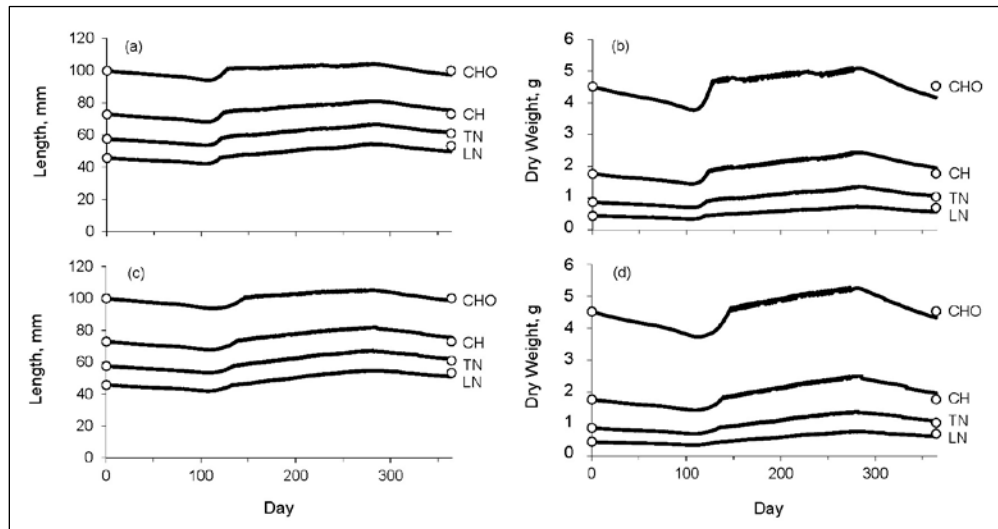


Figure 6-31. *M. mercenaria* calibration results for individual growth in the (a, b) high mesohaline and (c, d) polyhaline zones in 2009.

Initial and expected final values are shown as open circles; runs were conducted for little neck (LN), top neck (TN), cherry (CH), and chowder (CHO) size classes.

The *M. balthica* model also closely matched the growth trajectories from field sampling (**Figure 6-32**), with highly significant regressions between observed (x) and modeled (y) values (for length: $y=0.87x+2.81$, $r^2=0.96$, $F<0.001$; $y=0.74x+0.015$, $r^2=0.78$, $F=0.0037$) and low root mean squared errors (1.6 mm and 0.026 g dw). The model predicted continuous growth until late in the year when a decrease in weight resulted from spawning. Modeled length generally matched the observations better than modeled weight. The initial value for length in the high mesohaline zone was set so the model fit the final three measured values (**Figure 6-32c**); setting the initial length at a lower value allowed the model to pass through the first length measurement, but with subsequent under-prediction of lengths. Without this point, the fit between the model and observations improved with a slope near 1:1 ($y=1.07x-1.53$, $r^2=0.99$, $F<0.001$). Although the model over-predicted AFDW in the high mesohaline zone, it nevertheless reproduces the correct seasonal pattern (**Figure 6-32d**); the model-data fit for this region is stronger than the composite fit ($y=1.58x+0.0006$, $r^2=0.98$, $F=0.010$). Observed AFDW in the low mesohaline region did not follow a clear seasonal pattern, but the model produced the expected growth trajectory and fell within the same range as the measurements (**Figure 6-32b**).

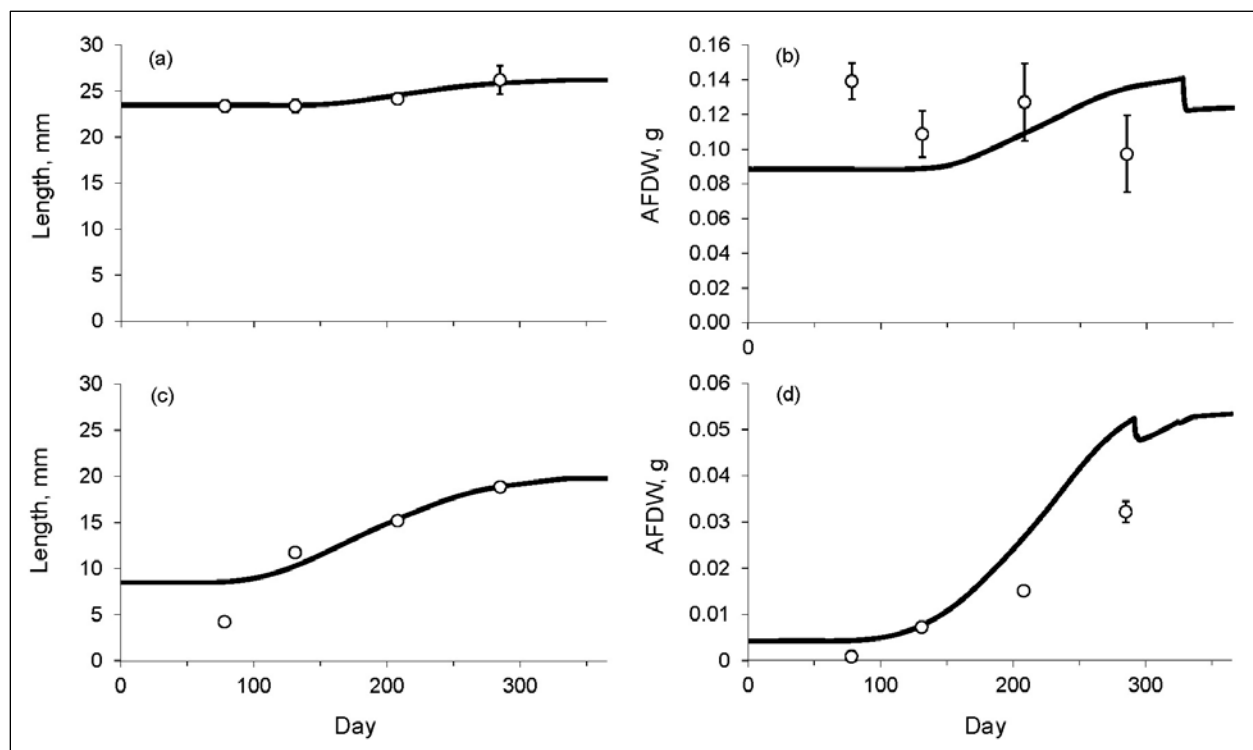


Figure 6-32. *M. balthica* calibration results for individual growth in the (a, b) low mesohaline and (c, d) high mesohaline zones in 2009.

Symbols are the means from field samples; error bars are one standard error.

The models predicted a larger percentage increase in weight for hard clams during a normal hydrologic year (2009) than in a drought year (2008, **Table 6-13**). Despite lower salinities in 2009, the greater availability of food as phytoplankton biomass and total particulate organic carbon (POC) resulted in greater growth. Conversely, growth of *M. balthica* changed very little between years (**Table 6-13**), which was expected because biomass of BMA carbon and sediment POC were held constant as not enough data were available to resolve seasonal or inter-annual

differences. This limited inter-annual difference in growth was also the result of having to force *M. balthica* to be food saturated to obtain reasonable growth, and the absence of any effect of salinity on clam physiology in the Dynamic Energy Budget (DEB) model (for details, see Wiseman, 2010).

Table 6-13. Predicted percentage increases in final weight for an individual *M. mercenaria* and *M. balthica* in a drought year (2008) and a relatively normal year (2009).

Values for *M. mercenaria* are those for the entire harvest zone.

Species	Size Class or Location	2008	2009
<i>M. mercenaria</i>	Little Neck	73.6	97.0
	Top Neck	52.7	72.2
	Cherry	32.8	43.5
	Chowder	7.1	10.3
<i>M. balthica</i>	Low mesohaline	40.5	40.0
	High mesohaline	1,146	1,164

Consumption scaled to the total number of hard clams removed annually by the fishery indicated removals of less than 1.6% of total phytoplankton biomass on a daily basis, and less than 0.6% of available water column POC, with highest rates in summer when water temperatures were highest (**Figure 6-33**). Given lower overall food concentrations, a larger percentage was consumed in the drought year (2008) compared to 2009. On an annual basis, the number of hard clams removed by the fishery consumed from 0.15% to 0.60% of the food supply depending on food source and year (**Table 6-14**). Based on individual filtration rates and estimated densities, the little neck size class was predicted to consume the largest proportion of available food and chowder clams the smallest (data not shown).

Assuming our measured *M. balthica* densities at 0.5 m apply across the entire system, consumption scaled to the population level indicated removals of less than 1% of the sediment food supply on both a daily and annual basis (**Figure 6-34 and Table 6-14**). Although *M. balthica* are predominantly deposit feeders, they are able to suspension feed, so we also computed their population level impact on water column food sources. In this case, the population was predicted to remove up to 8% of phytoplankton biomass on a daily basis and up to 1.5% annually; removal of water column POC was lower with a maximum of 2% removed daily. As with hard clams, consumption was highest during the summer months. Consumption of sediment food sources was identical between years, but greater for water column sources in 2008, given the lower concentrations of phytoplankton and water column POC in the drought year.

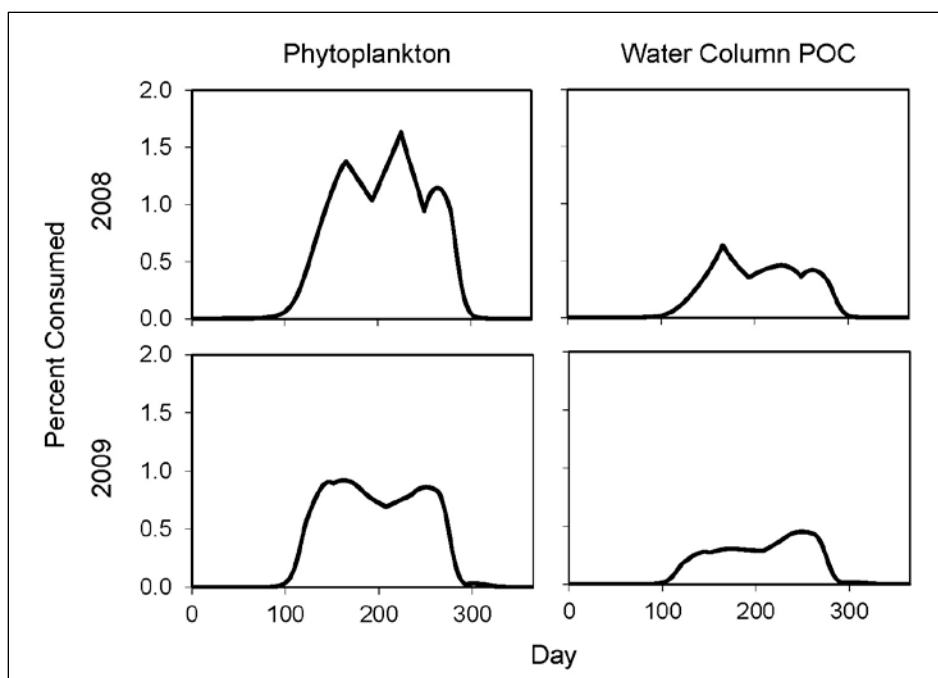


Figure 6-33. Daily percentage of available food consumed by *M. mercenaria* removed by the public fishery harvest in a drought year (2008) and a normal year (2009).

Consumption was computed using both phytoplankton C and water column POC as food sources.

Table 6-14. Average daily percentage of available food consumed by *M. mercenaria* and *M. balthica* in a drought year (2008) and a normal year (2009).

Values were computed based on phytoplankton and microphytobenthic carbon (Phyto and MPB, respectively) and water column and sediment POC (POC_{WC} and POC_{SED}, respectively). Values for *M. mercenaria* represent the impact of clams harvested by the public fishery throughout the harvest zone. Values for *M. balthica* represent averages for the low and high mesohaline regions of the system after scaling measured densities to the entire system.

Species	Year	Food Source	% Consumed
<i>M. mercenaria</i>	2008	Phyto	0.60
		POC _{WC}	0.20
	2009	Phyto	0.37
		POC _{WC}	0.15
<i>M. balthica</i>	2008	MPB	0.42
		POC _{SED}	0.08
		Phyto	1.51
		POC _{WC}	0.78
	2009	MPB	0.42
		POC _{SED}	0.09
		Phyto	0.87
		POC _{WC}	0.50

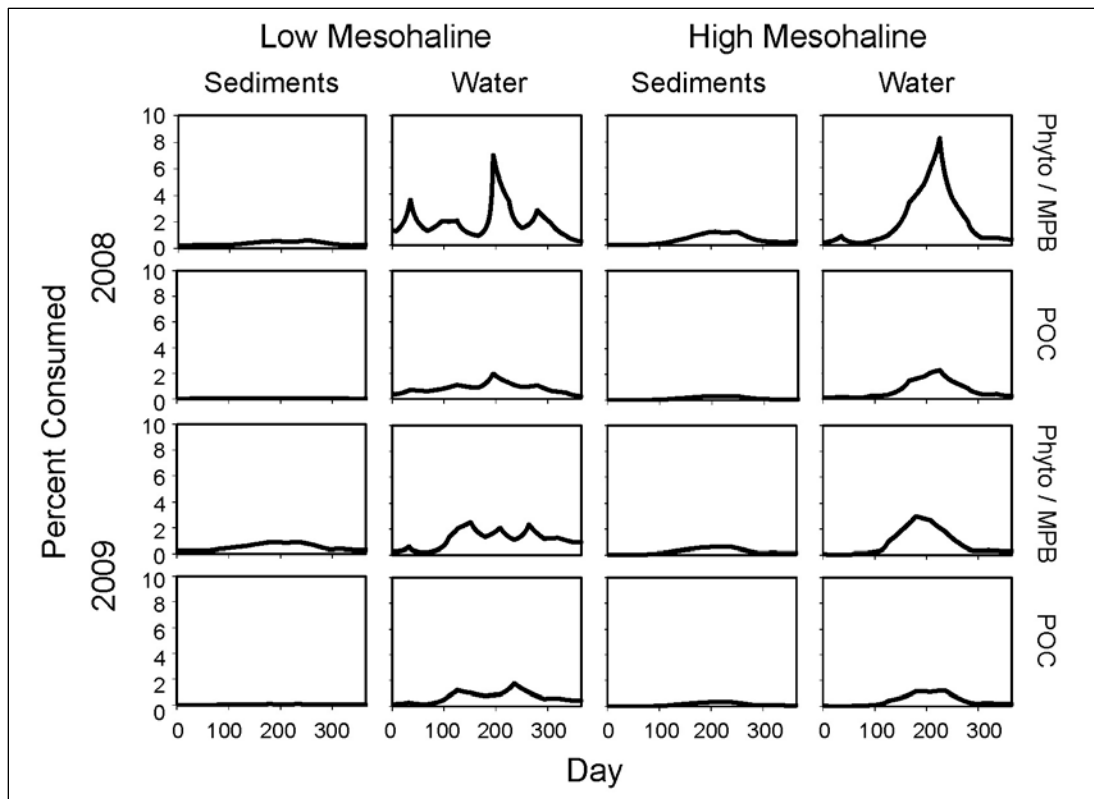


Figure 6-34. Daily percentage of available food consumed by *M. balthica* in a drought year (2008) and a normal year (2009) in two salinity zones.

Calculations assume measured *M. balthica* densities at 0.5 m apply over the entire system. Consumption was computed based on available phytoplankton (Phyto) carbon, microphytobenthic (MPB) carbon, water column POC, and sediment POC as potential food sources.

Predicted carrying capacity for hard clams in the NRE was seasonal with highest values in the colder months (**Figure 6-35**). The mean annual carrying capacity for the system was estimated to be 1 to 3 orders of magnitude greater than mean annual landings (7.2×10^6 clams), depending on the year and food source (**Table 6-15**). Predicted carrying capacity was approximately an order of magnitude greater in 2009 than in 2008.

Measured *M. balthica* densities (3.1×10^9 clams) were between 2 and 3 orders of magnitude lower than the calculated annual carrying capacity (**Table 6-15**), which was again seasonal with highest values in the winter–spring period (**Figure 6-36**). A greater number of clams could be supported on sediment carbon compared to water column sources, given the higher concentrations in the sediments. Although carrying capacity based on sediment sources was similar across years, estimates based on water column sources were higher in the normal hydrologic year (2009), given the higher water column concentrations.

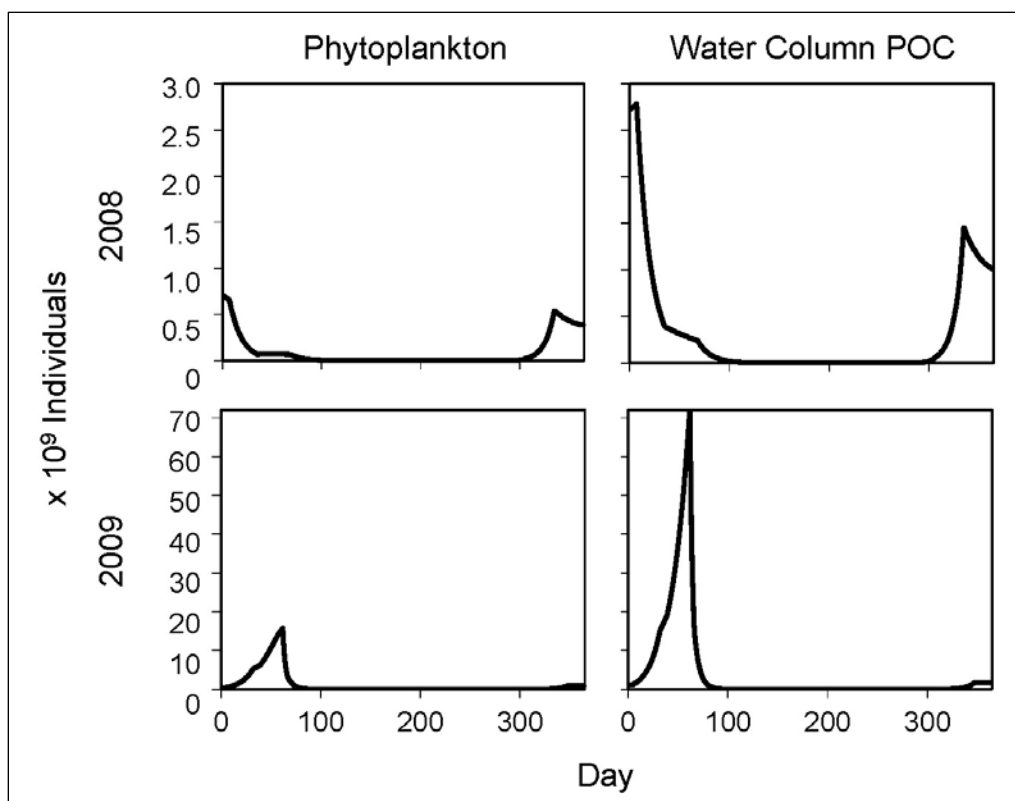


Figure 6-35. Modeled carrying capacity of *M. mercenaria* in a drought year (2008) and a normal year (2009) in the hard clam fishing area.

Values are based on available phytoplankton C and water column POC.

Table 6-15. Annual average number of *M. mercenaria* and *M. balthica* supported by the available food supply in a drought year (2008) and a normal year (2009).

Food sources are defined in Table 6-15. Values for *M. mercenaria* are those for the entire harvest zone; values for *M. balthica* are those for the low and high mesohaline regions combined.

Species	Food Source	2008	2009
<i>M. mercenaria</i>	Phyto	$9.2 \cdot 10^7$	$1.2 \cdot 10^9$
	POC _{WC}	$3.1 \cdot 10^8$	$4.1 \cdot 10^9$
<i>M. balthica</i>	MPB	$1.2 \cdot 10^{12}$	$1.4 \cdot 10^{12}$
	POC _{SED}	$5.9 \cdot 10^{12}$	$6.7 \cdot 10^{12}$
	Phyto	$3.0 \cdot 10^{11}$	$9.9 \cdot 10^{11}$
	POC _{WC}	$6.5 \cdot 10^{11}$	$2.2 \cdot 10^{12}$

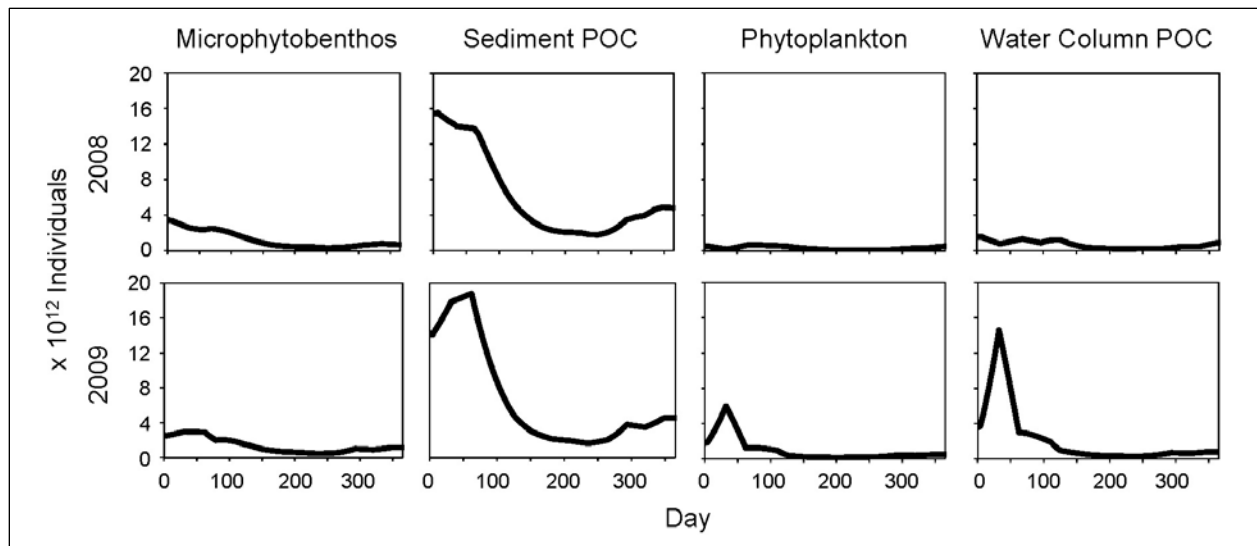


Figure 6-36. Modeled carrying capacity of *M. balthica* in a drought year (2008) and a normal year (2009) in the low and high mesohaline zones combined.

Values are based on available microphytobenthic carbon, sediment POC, phytoplankton C, and water column POC.

Although various studies in the ecological literature have shown the potential for top-down control of phytoplankton biomass by benthic filter feeders (e.g., Cloern, 1982; Dame, 1996; Grall and Chauvaud, 2002), our simulations suggest this is not the case for the NRE despite its relatively long residence time of approximately 2 months (Ensign et al., 2004; ESM simulations; **Figure 6-37**). Hard clams and *M. balthica* were predicted to consume less than 2% of their primary food source (water column and sediment carbon, respectively) on a daily and annual basis. If *M. balthica* were to feed on water column sources, it could exert a greater impact, but this species predominantly relies on deposit feeding on the bottom. However, it should be noted that these calculations are based on the number of hard clams removed by the fishery as a minimum estimate of abundance; it is impossible to determine their actual abundance throughout the NRE. Estimates of clearance rates have been provided on **Figure 6-37** if the population was 10 times and 100 times greater than landings; the population would have to be 100 times higher than current landings for hard clams to begin to exert top-down control on phytoplankton populations in the NRE. Calculations for *M. balthica* assume that densities measured along the shore in depths less than 1 m apply throughout the estuary. Again, it is impossible to know the true NRE-wide population size. Finally, only two bivalve species were considered in this exercise while our sampling found some other abundant bivalve species that add an additional filtration capacity (see Wiseman, 2010). Other abundant species included gem clam (*Gemma gemma*), Matagorda macoma (*Macoma mitchelli*), and dwarf surf clam or coot clam (*Mulinia lateralis*).

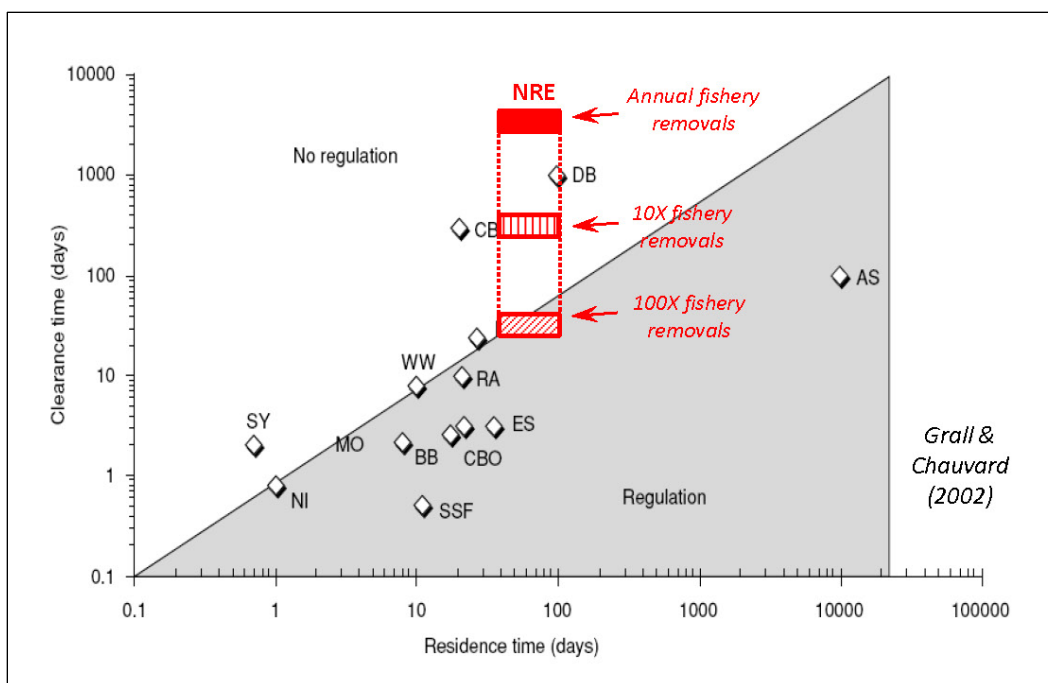


Figure 6-37. Degree of top-down grazing control exerted by benthic filter feeders in a variety of systems.

The ability to exert top-down control on estuarine phytoplankton biomass is dependent on the balance between water residence time and the time it takes for the filter feeder population to clear the volume of water in the system (clearance time). Reproduced from Grall and Chauvard (2002).

NRE estimates are derived from the benthic bivalve modeling.

Nitrogen Loading Scenarios

Finally, a series of nutrient loading scenarios were run in the ESM to determine the role of three key nutrient sources (both N and P) in controlling water quality in the system. These sources included the MCBCL WWTF, loads from MCBCL, and loads from the upland, off-Base watershed. Current loads from the MCBCL were predicted to have minimal impacts on current water quality in the NRE (**Figure 6-38**). In the absence of the WWTF, modeled chl *a* and DIN concentrations decreased by 8–17% and 0.6–5.6% in most of the estuary, respectively, with the exception of that portion of the estuary that receives the effluent directly (Box 5) or is immediately downstream (Box 6), where changes were greater (**Table 6-16**). Removal of the WWTF was predicted to result in a small decrease in the amount of time the estuary exceeds the current state water quality criterion of $40 \mu\text{g L}^{-1}$ of chl *a* (NCDENR, 2007; **Table 6-16**).

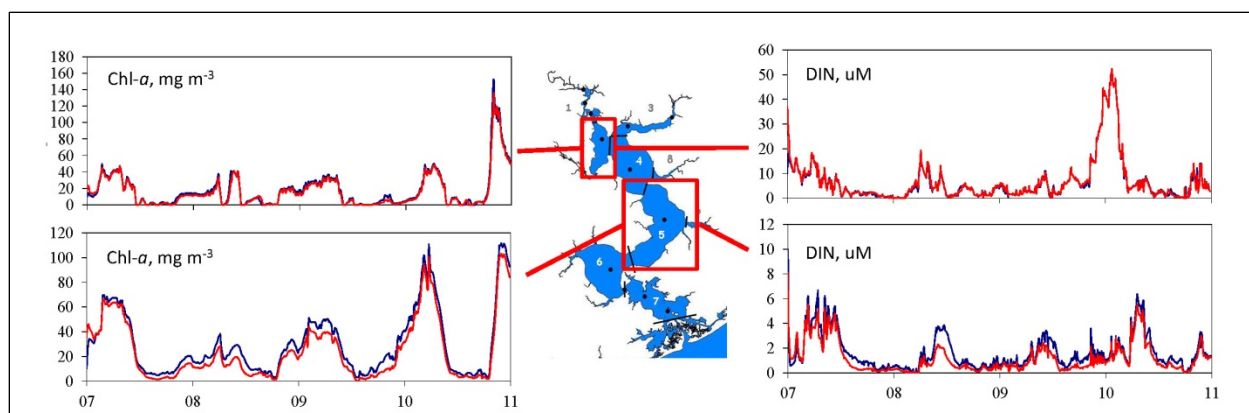


Figure 6-38. Effect of the MCBCL WWTF on NRE water quality.

ESM predicted surface chl *a* and DIN concentrations under current conditions (blue line) and a run in which the WWTF was removed (red line).

Table 6-16. Effect of the MCBCL WWTF on NRE water quality.

Columns 2 and 3 indicate the median percentage change in surface chl *a* and DIN in the ESM run with the WWTF removed. Columns 4 through 6 indicate the percentages of time when modeled chl *a* concentrations exceeded the state criterion of 40 $\mu\text{g L}^{-1}$ with and without the WWTF, and the difference between the two runs.

Element	chl <i>a</i>	DIN	% Violations, Standard Run	% Violations, No WWTF	Change
1	-8.3	0.7	13.4	11.4	-2.0
2	-10.0	-0.6	11.5	9.3	-2.2
3	-10.0	-1.9	9.0	8.2	-0.8
4	-13.3	-5.6	5.2	4.9	-0.3
5	-28.1	-25.4	27.9	21.2	-6.7
6	-24.5	-5.0	20.4	14.7	-5.8
7	-16.7	2.0	6.8	4.5	-2.3

Changes in water quality in the absence of loads from that portion of MCBCL that drains to the NRE were similarly predicted to be small (**Figure 6-39**). Predicted decreases in chl *a* and DIN concentrations were only 2–4.5% and 0–2.9%, respectively, with only small predicted changes in the amount of time the state chl-*a* criterion is exceeded (**Table 6-17**).

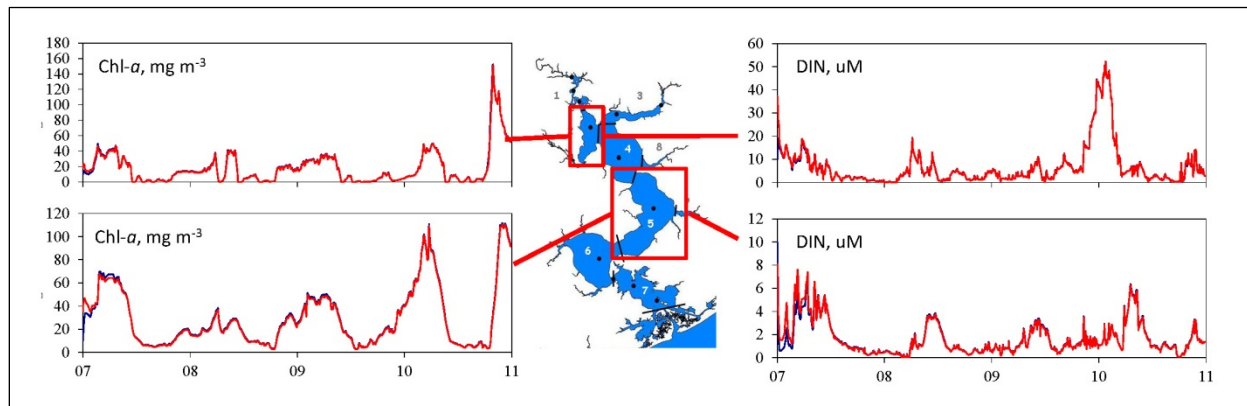


Figure 6-39. Effect of MCBCL watershed loads on NRE water quality.

ESM predicted surface chl *a* and DIN concentrations under current conditions (blue line) and a run in which nutrient loads from the MCBCL watershed were removed (red line).

Table 6-17. Effect of MCBCL watershed loads on NRE water quality.

Columns 2 and 3 indicate the median percentage change in surface chl *a* and DIN in the ESM run with MCBCL watershed loads removed. Columns 4 through 6 indicate the percentages of time when modeled chl *a* concentrations exceeded the state criterion of 40 $\mu\text{g L}^{-1}$ with and without the MCBCL loads, and the difference between the two runs.

Element	chl <i>a</i>	DIN	% Violations, Standard Run	% Violations, No WWTF	Change
1	–2.0	–0.1	13.4	12.9	–0.5
2	–2.8	–1.4	11.5	10.1	–1.4
3	–2.4	–1.3	9.0	8.8	–0.2
4	–3.3	–2.0	5.2	5.1	–0.1
5	–4.1	–2.9	27.9	29.0	1.1
6	–4.5	–1.0	20.4	19.8	–0.6
7	–3.0	0.0	6.8	6.5	–0.3

The simulated effects of nutrient loads from the upland, off-Base watershed were much greater than that for the MCBCL WWTF and watershed (**Figure 6-40**). Annual mean chl *a* displayed marked increases for the estuary as a whole and within each spatial element as loads were varied from 0 times to 10 times the current loads. The middle estuary was most susceptible to these loads, with the greatest effects in Boxes 5 and 6, just downstream of where flushing time reaches its minimum (**Figure 6-26**). Predicted increases in chlorophyll translated to rapid increases in exceedance of the state chl *a* criterion (**Figure 6-41**). Finally, the position of these load–response relationships is highly dependent on inter-annual variability in freshwater loading, given its influence on both loads and flushing time (**Figure 6-42**).

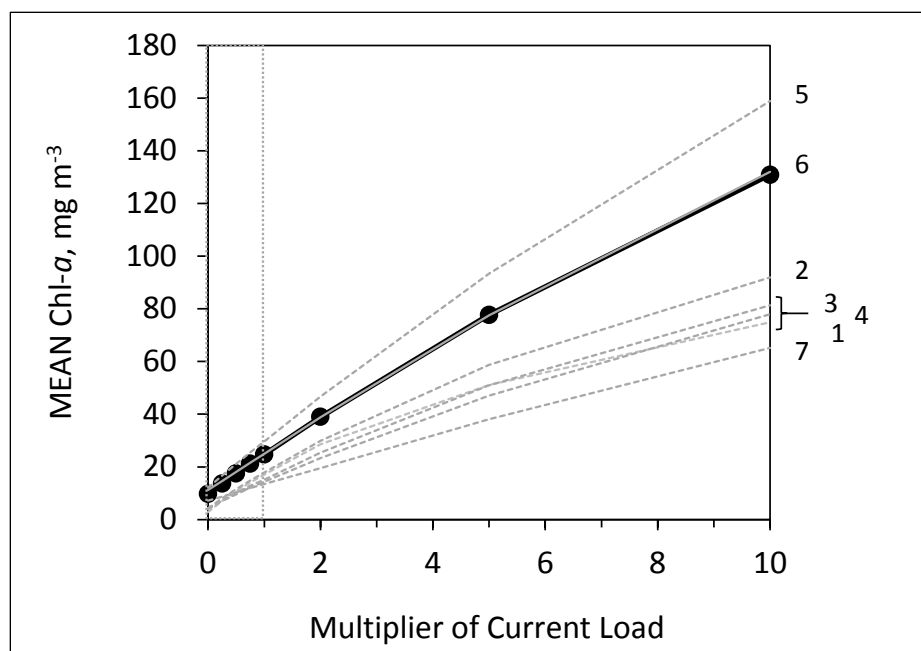


Figure 6-40. Effect of off-Base watershed nutrient loads on surface chl *a* in the NRE.

Thick black line gives the system-average response; dashed lines show the responses for ESM Spatial Elements 1–7 (labeled to the right; line for Spatial Element 6 overlaps that for the system-average response). Vertical line denotes current conditions. Results are averaged over the period from 1998–2010.

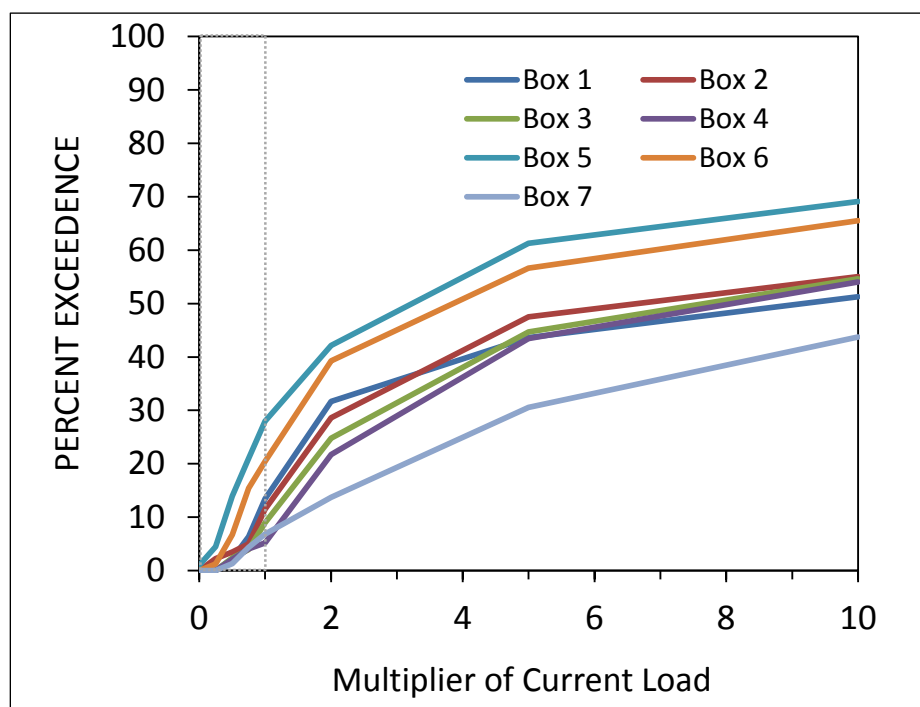


Figure 6-41. Effect of off-Base watershed nutrient loads on the percentage of time the NRE is predicted to be in violation of the state chl *a* criterion of 40 µg L⁻¹.

Vertical line denotes current conditions. Results are averaged over the period from 1998–2010.

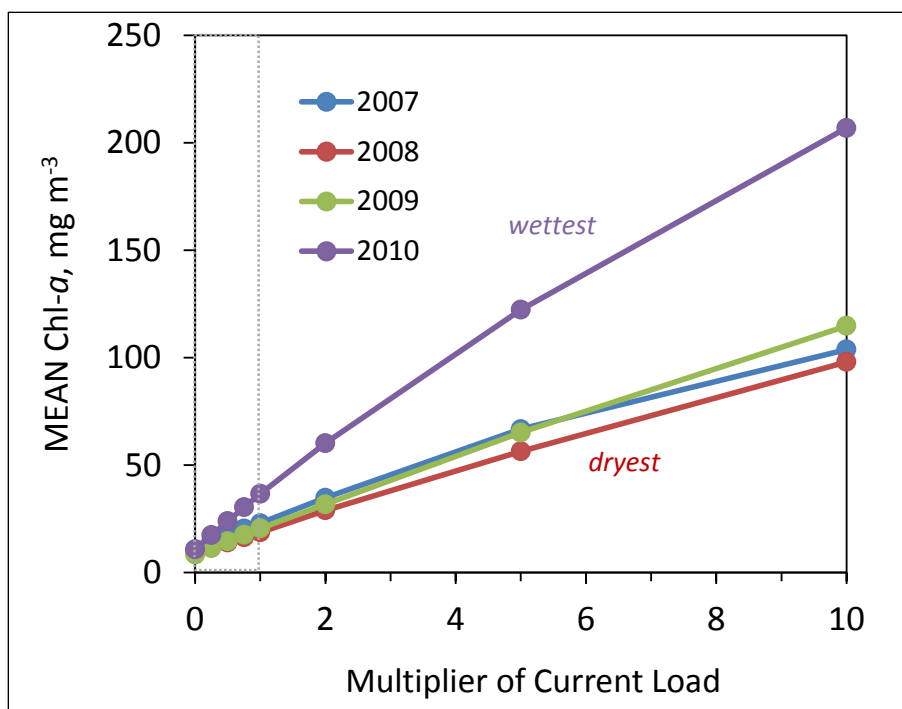


Figure 6-42. Effect of inter-annual hydrologic variability on NRE response to off-Base watershed nutrient loading.

Vertical line denotes current conditions.

Conclusions and Implications for Future Research

Watershed and estuarine simulation models successfully served as integrative tools for synthesizing many of the diverse data sets collected as part of both DCERP research and monitoring projects, along with historical monitoring and meteorological data. The models were successfully applied to understand system responses to natural and anthropogenic stressors. In the case of the WSM, the primary stressor analyzed was anthropogenic conversion of forested land to impervious surfaces through ongoing Base development. In the case of the ESM, the primary model application was to understand the factors that modulate NRE response to watershed nutrient loading; in this case, natural hydrologic variability and natural properties of the system (high BMA productivity, high rates of denitrification, and high CDOM concentrations) appear to play a critical role in shaping system response to nutrient loads.

This project provided a unique opportunity for simultaneous development and comparison of a range of watershed modeling approaches in a small, low relief, coastal plain setting. Models were most successful when predicting loads at an annual scale, and models of intermediate complexity (i.e., NLM and ReNuMa) tended to produce the most accurate predictions. All models provided a similar conclusion on a key research question for DCERP and a critical management issue for MCBCL: the large majority of external N loading to the NRE originates from off-Base. However, loads that do enter the estuary from the Base do so in a region of the estuary likely to be nutrient-limited, and ongoing conversion of forested to developed landscapes is predicted to produce small, but quantifiable, increases in TN loads from MCBCL watersheds with corresponding increases in chl *a* concentrations.

Application of the ESM demonstrated the further wide applicability of this intermediate complexity tool in temperate estuaries. The model successfully identified key features of the NRE that modulate its response to anthropogenic nutrient loading, and answered another key question for DCERP and management issue for MCBCL: water quality in the NRE is primarily responsive to loads from the upper, off-Base watershed, with minimal current impacts from Base watersheds or the Base WWTF. Nutrient load-response curves developed with the model take into account inter-annual hydrologic variability and can serve as useful tools for predicting NRE water quality.

A key feature of Aquatic/Estuarine Module's model development during DCERP has been the focus on reduced and intermediate complexity models, which have the potential for rapid deployment, fast run times on PCs, and potential for direct use by management personnel. The successful application of both watershed and estuarine models as part of DCERP has resulted in tools that can be readily adapted for use by Base personnel on MCBCL, and which can be readily transferred to other installations and coastal systems.

Literature Cited

- Alexander, R.B., P.J. Johnes, E.W. Boyer, and R.A. Smith. 2002. A comparison of models for estimating the riverine export of nitrogen from large watersheds. *Biogeochemistry* 57/58:295–339.
- Anderson, I.C., M.J. Brush, M.F. Piehler, and C.A. Currin. 2012. *Developing Indicators of Ecosystem Function for Shallow Estuaries: Benthic Functional Responses in the New River Estuary*. Final report to the Strategic Environmental Research and Development Program, U.S. Department of Defense, Washington, DC.
- Anderson, I.C., K.J. McGlathery, and A.C. Tyler. 2003. Microbial mediation of “reactive” nitrogen in a temperate lagoon. *Marine Ecology Progress Series* 246:73–84.
- Athayde, D.N., P.E. Shelley, E.D. Driscoll, D. Gaboury, and G.B. Boyd. 1983. *Results of the Nationwide Urban Runoff Program: Final Report*. U.S. Environmental Protection Agency Water Planning Division, Washington, DC.
- Baird, M.E., S.J. Walker, B.B. Wallace, I.T. Webster, and J.S. Parslow. 2003. The use of mechanistic descriptions of algal growth and zooplankton grazing in an estuarine eutrophication model. *Estuarine, Coastal and Shelf Science* 56(3–4):685–695.
- Bicknell, B.R., J.C. Imhoff, J.L. Kittle Jr., T.H. Jobes, and A.S. Donigian Jr. 2005. *Hydrological Simulation Program–Fortran (HSPF): User’s Manual for Release 12.2*. National Exposure Research Laboratory, U.S. Environmental Protection Agency, Athens, GA, in cooperation with the Water Resources Division, U.S. Geological Survey, Reston, VA. Available at <http://water.epa.gov/scitech/datait/models/basins/bsnsdocs.cfm#hspf>.
- Boesch, D.F., E. Burreson, W. Dennison, E. Houde, M. Kemp, V. Kennedy, R. Newell, K. Paynter, R. Orth, and W. Ulanowicz. 2001. Factors in the decline of coastal ecosystems. *Science* 293:629–638.
- Bricker, S., B. Longstaff, W. Dennison, A. Jones, K. Boicourt, C. Wicks, and J. Woerner. 2007. *Effects of Nutrient Enrichment in the Nation’s Estuaries: A Decade of Change*. NOAA Coastal Ocean Program Decision Analysis Series No. 26, National Centers for Coastal Ocean Science, Silver Spring, MD.
- Brush, M.J. 2002. *Development of a Numerical Model for Shallow Marine Ecosystems with Application to Greenwich Bay, RI*. Ph.D. dissertation, University of Rhode Island, Kingston, RI.
- Brush, M.J., and S.W. Nixon. In review. An intermediate complexity, hybrid empirical-mechanistic eutrophication model for shallow marine ecosystems. Submitted to *Ecological Modelling*.
- Brush, M.J., and S.W. Nixon. 2010. Modeling the role of macroalgae in a shallow sub-estuary of Narragansett Bay, RI (USA). *Ecological Modelling* 221:1065–1079.
- Brush, M.J., and L.A. Harris. 2010. Introduction to the special issue of *Ecological Modelling*: “Advances in modeling estuarine and coastal ecosystems: approaches, validation, and applications.” *Ecological Modelling* 221:965–968.

- Brush, M.J., J.W. Brawley, S.W. Nixon, and J.N. Kremer. 2002. Modeling phytoplankton production: Problems with the Eppley curve and an empirical alternative. *Marine Ecology Progress Series* 238:31–45.
- Brylawski, B. 2008. Cultural eutrophication and the clam *Macoma balthica*: Evidence for trophic disruption and effects on blue crabs. Ph.D. dissertation, College of William and Mary, Gloucester Point, VA.
- Burnham, K.P., and D.R. Anderson. 2002. Model Selection and Multimodel Inference: A Practical Information-Theoretic Approach. Second edition. Springer, New York, NY.
- Buzzelli, C.P., R.L. Wetzel, and M.B. Meyers. 1999. A linked physical and biological framework to assess biogeochemical dynamics in a shallow estuarine ecosystem. *Estuarine, Coastal and Shelf Science* 49:829–851.
- Canham, C.D., J.J. Cole, and W.K. Lauenroth (Eds). 2003. *Models in Ecosystem Science*. Princeton University Press: Princeton, NJ.
- Cardoso, J.F.M.F., H.W. van der Veer, and S.A.L.M. Kooijman. 2006. Body-size scaling relationships in bivalve species: A comparison of field data with predictions by the Dynamic Energy Budget (DEB) theory. *Journal of Sea Research* 56:125–139.
- Cerco, C.F., and M.R. Noel. 2004. *The 2002 Chesapeake Bay Eutrophication Model*. Report 903-R-04-004, Chesapeake Bay Program Office, U.S. Environmental Protection Agency, Annapolis, MD.
- Chen, C., R. Tian, R.C. Beardsley, J. Qi, and Q. Xu. 2010. *Modeling 2008 in Massachusetts Bay Using an Upgraded Unstructured-Grid Bays Eutrophication Model*. Report 2010-15, Massachusetts Water Resources Authority, Boston, MA.
- Cloern, J.E. 2001. Our evolving conceptual model of the coastal eutrophication problem. *Marine Ecology Progress Series* 210:223–253.
- Cloern, J.E. 1982. Does the benthos control phytoplankton biomass in south San Francisco Bay? *Marine Ecology Progress Series* 9:191–202.
- Cloern, J.E., C. Grenz, and L. Vidregar-Lucas. 1995. An empirical model of the phytoplankton chlorophyll:carbon ratio—The conversion factor between productivity and growth rate. *Limnology and Oceanography* 40(7):1313–1321.
- Cole, L.W. 2005. *Nitrogen Loading to Chincoteague Bay (MD, VA): A Reassessment*. M.S. thesis, University of Rhode Island, Kingston, RI.
- Dafner, E.V., M.A. Mallin, J.J. Souza, H.A. Wells, and D.C. Parsons. 2007. Nitrogen and phosphorus species in the coastal and shelf waters of southeastern North Carolina, mid-Atlantic U.S. coast. *Marine Chemistry* 103(3–4):289–303.
- Dai, T., R.L. Wetzel, T.R.L. Christensen, and E.A. Lewis. 2000. BasinSim 1.0: A Windows-Based Watershed Modeling Package User's Guide. Special Report in Applied Marine Science and Ocean Engineering #362, Virginia Institute of Marine Science, School of Marine Science, College of William and Mary, Gloucester Point, VA.

- Dame, R.F. 1996. *Ecology of Marine Bivalves: An Ecosystem Approach*. CRC Marine Science Series: Boca Raton, FL.
- Day, J.W., C.A.S. Hall, W.M. Kemp, and A. Yañez-Arancibia (Eds.). 1989. *Estuarine Ecology*. Wiley Interscience: New York, NY.
- de Jonge, V.N., and E.G. DeGroot. 1989. The mutual relationship between the monitoring and modelling of estuarine ecosystems. *Helgoland Marine Research* 43(3–4):537–548.
- Denman, K.L. 2003. Modelling planktonic ecosystems: Parameterizing complexity. *Progress in Oceanography* 57(3–4):429–452.
- Donigian Jr., A.S., and J.C. Imhoff. 2006. History and evolution of watershed modeling derived from the Stanford Watershed Model (SWM). Pp. 21–45 in *Watershed Models*. Edited by V.P. Singh, and D.K. Frevert. CRC Press: Boca Raton, FL.
- Donigian Jr., A.S., and J.C. Imhoff. 2002. *From the Stanford Model to BASINS: 40 years of Watershed Modeling*. ASCE Task Committee on Evolution of Hydrologic Methods Through Computers, ASCE 150th Anniversary Celebration, Washington, DC. November 3–7.
- Duarte, C.M., J.S. Amthor, D.L. DeAngelis, L.A. Joyce, R.J. Maranger, M.L. Pace, J. Pastor, and S.W. Running. 2003. The limits to models in ecology. Pp. 437–451 in *Models in Ecosystem Science*. Edited by C.D. Canham, J.J. Cole, and W.K. Lauenroth. Princeton University Press: Princeton, NJ.
- Ensign, S.H., J.N. Halls, and M.A. Mallin. 2004. Application of digital bathymetry data in an analysis of flushing times of two North Carolina Estuaries. *Computers and Geosciences* 30:501–511.
- Friedrichs, M.A.M., R.R. Hood, and J.D. Wiggert. 2006. Ecosystem model complexity versus physical forcing: Quantification of their relative impact with assimilated Arabian Sea data. *Deep-Sea Research Part II* 53:576–600.
- Fulton, E.A., A.D.M. Smith, and C.R. Johnson. 2004. Effects of spatial resolution on the performance and interpretation of marine ecosystem models. *Ecological Modelling* 176(1–2):27–42.
- Fulton, E.A., A.D.M. Smith, and C.R. Johnson. 2003. Effect of complexity on marine ecosystem models. *Marine Ecology Progress Series* 253:1–16.
- Giblin, A.E., and J.J. Vallino. 2003. The role of models in addressing coastal eutrophication. Pp. 327–343 in *Models in Ecosystem Science*. Edited by C.D. Canham, J.J. Cole, and W.K. Lauenroth. Princeton University Press: Princeton, NJ.
- Giordano, J.C.P., M.J. Brush, and I.C. Anderson. 2012. Ecosystem metabolism in shallow coastal lagoons: Patterns and partitioning of planktonic, benthic, and integrated community rates. *Marine Ecology Progress Series* 458:21–38.

- Giordano, J.C.P., M.J. Brush, and I.C. Anderson. 2011. Quantifying annual nitrogen loads to Virginia's coastal lagoons: Sources and water quality response. *Estuaries and Coasts* 34:297–309.
- Grall, J., and L. Chauvaud. 2002. Marine eutrophication and benthos: the need for new approaches and concepts. *Global Change Biology* 8:813–830.
- Grangere, K., S. Lefebvre, A. Menesguen, and F. Jouenne. 2009. On the interest of using field primary production data to calibrate phytoplankton rate processes in ecosystem models. *Estuarine, Coastal and Shelf Science* 81(2):169–178.
- Haith, D.A., and L.L. Shoemaker. 1987. Generalized watershed loading functions for stream flow nutrients. *Journal of the American Water Resources Association* 23(3):471–478.
- Haith, D.A., R. Mandel, and R.S. Wu. 1992. *Generalized Watershed Loading Functions Version 2.0 User Manual*. Department of Agricultural and Biological Engineering, Cornell University, Ithaca, NY.
- Harding, J.M. 2007. Northern quahog (= hard clam) *Mercenaria mercenaria* age at length relationships and growth patterns in the York River, Virginia, 1954 to 1970. *Journal of Shellfish Research* 26(1):101–107.
- Harris, G.P., S.W. Bigelow, J.J. Cole, H. Cyr, L.L. Janus, A.P. Kinzig, J.F. Kitchell, G.E. Likens, K.H. Reckhow, D. Scavia, D. Soto, L.M. Talbot, and P.H. Templer. 2003. The role of models in ecosystem management. Pp. 299–307 in *Models in Ecosystem Science*. Edited by C.D. Canham, J.J. Cole, and W.K. Lauenroth. Princeton University Press: Princeton, NJ.
- Hines, A.H., and K.L. Comtois. 1985. Vertical distribution of infauna in sediments of a subestuary of central Chesapeake Bay. *Estuaries* 8(3):296–304.
- Hobbie, J.E. (Ed.). 2000. *Estuarine Science: A Synthetic Approach to Research and Practice*. Island Press: Washington, DC.
- Hofmann, E., J.M. Klinck, J.N. Kraeuter, E. Powell, R.E. Grizzle, S.C. Buckner, and V.M. Brice. 2006. A population dynamics model of the hard clam *Mercenaria mercenaria*: Development of the age- and length-frequency structure of the population. *Journal of Shellfish Research* 25(2):417–444.
- Holland, A.F., A.T. Shaughnessy, and M.H. Hiegel. 1987. Long-term variation in mesohaline Chesapeake Bay macrobenthos: Spatial and temporal patterns. *Estuaries* 10(3):227–245.
- Homer, C., C. Huang, L. Yang, B. Wylie, and M. Coan. 2004. Development of a 2001 National Landcover Database for the United States. *Photogrammetric Engineering and Remote Sensing* 70(7):829–840.
- HydroQual. 1991. *Water Quality Modeling Analysis of Hypoxia in Long Island Sound*. Report to the Management Committee of the Long Island Sound Estuary Study and the New England Interstate Water Pollution Control Commission, HydroQual, Inc., Mahwah, NJ.
- Jassby, A.D., and T. Platt. 1976. Mathematical formulation of the relationship between photosynthesis and light for phytoplankton. *Limnology and Oceanography* 21(4):540–547.

- Jiang, M.S., and M. Zhou. 2008. *Massachusetts Bay Eutrophication Model: 2005 Simulation*. Report 2008-13. Massachusetts Water Resources Authority, Boston, MA.
- Jones, D.S., M.A. Arthur, and D.J. Allard. 1989. Sclerochronological records of temperature and growth from shells of *Mercenaria mercenaria* from Narragansett Bay, Rhode Island. *Marine Biology* 102:225–234.
- Joye, S.B., and I.C. Anderson. 2008. Nitrogen cycling in coastal sediments. Pp. 867–915 in *Nitrogen in the Marine Environment* (second edition). Edited by D.G. Capone, D.A. Bronk, M.R. Mulholland, and E.J. Carpenter. Elsevier: Burlington, MA.
- Kamermans, P., H.W. van der Veer, J.I.J. Witte, and E.J. Adriaans. 1999. Morphological differences in *Macoma balthica* (Bivalvia, Tellinacea) from a Dutch and three southeastern United States estuaries. *Journal of Sea Research* 41:213–224.
- Koroknay, B.J. 2012. *Quantifying Watershed Loads to a Low Relief, Coastal Plain Estuary: The New River Estuary, NC*. M.S. thesis, College of William and Mary, Gloucester Point, VA.
- Kremer, J.N., and S.W. Nixon. 1978. *A Coastal Marine Ecosystem: Simulation and Analysis*. Springer-Verlag: New York, NY.
- Kremer, J.N., J. Vaudrey, D. Ullman, D. Bergondo, N. LaSota, C. Kincaid, D. Codiga, and M.J. Brush. 2010. Simulating property exchange in estuarine ecosystem models at ecologically appropriate scales. *Ecological Modelling* 221:1080–1088.
- Lorenzen, C. 1967. Determination of chlorophyll and phaeopigments: Spectrophotometric equations. *Limnology and Oceanography* 12:343–346.
- Mallin, M.A., M.R. McIver, H.A. Wells, D.C. Parsons and V.L. Johnson. 2005a. Reversal of eutrophication following sewage treatment upgrades in the New River Estuary, North Carolina. *Estuaries* 28:750–760.
- Mallin, M.A., L.B. Cahoon, and M.J. Durako. 2005b. Contrasting food-web support bases for adjoining river-influenced and non-river influenced continental shelf ecosystems. *Estuarine, Coastal and Shelf Science* 62(1–2):55–62.
- McGlathery, K.J., K. Sundbäck, and I.C. Anderson. 2007. Eutrophication in shallow coastal bays and lagoons: The role of plants in the coastal filter. *Marine Ecology Progress Series* 348:1–18.
- Ménesguen, A., P. Cugier, S. Loyer, A. Vanhoute-Brunier, T. Hoch, J-F. Guillaud, and F. Gohin. 2007. Two- or three-layered box-models versus fine 3-D models for coastal ecological modelling? A comparative study in the English Channel (Western Europe). *Journal of Marine Systems* 64(1–4):47–65.
- Monsen, N.E., J.E. Cloern, L.V. Lucas, and S.G. Monismith. 2002. A comment on the use of flushing time, residence time, and age as transport time scales. *Limnology and Oceanography* 47:1545–1553.
- NCCGIA (North Carolina Center for Geographic Information and Analysis). 2007. *Type A Current Public Sewer Systems (GIS Shapefile)*. Raleigh, NC. Available at <http://www.lib.ncsu.edu/gis>.

- NCDENR (North Carolina Department of Environment and Natural Resources). 2007. "Redbook" *Surface Water and Wetland Standards*. NCDENR, Division of Water Quality. May 1. Available at <http://portal.ncdenr.org/web/wq/ps/csu>.
- NCDENR (North Carolina Department of Environment and Natural Resources). 2001. *Phase II of the Total Maximum Daily Load for Total Nitrogen to the Neuse River Estuary, North Carolina*. NCDENR, Division of Water Quality, Raleigh, NC. Available at http://portal.ncdenr.org/c/document_library/get_file?uuid=48bc46d8-c344-4f07-a656-7a211157c985&groupId=38364.
- NCDMF (North Carolina Division of Marine Fisheries). 2008. North Carolina Hard Clam Fishery Management Plan. North Carolina Department of Environment and Natural Resources, Division of Marine Fisheries, Morehead City, NC. Available at http://portal.ncdenr.org/c/document_library/get_file?uuid=d26254b4-ae68-4c3a-bdd8-ac03e190a9c7&groupId=38337.
- Neubauer, S.C., W.D. Miller, and I.C. Anderson. 2000. Carbon cycling in a tidal freshwater marsh ecosystem: A gas flux study. *Marine Ecology Progress Series* 199:13–30.
- Nixon, S.W. 2009. Eutrophication and the macroscope. *Hydrobiologia* 207:5–19.
- Nixon, S.W. 1995. Coastal marine eutrophication: A definition, social causes, and future concerns. *Ophelia* 41:199–219.
- Nixon, S.W., J.W. Ammerman, L.P. Atkinson, V.M. Berounsky, G. Billen, W.C. Boicourt, W.R. Boynton, T.M. Church, D.M. DiToro, R. Elmgren, J.H. Garber, A.E. Giblin, R.A. Jahnke, N.J.P. Owens, M.E.Q. Pilson, and S.P. Seitzinger. 1996. The fate of nitrogen and phosphorus at the land-sea margin of the North Atlantic Ocean. *Biogeochemistry* 35:141–180.
- Nixon, S., B. Buckley, S. Granger, and J. Bintz. 2001. Response of very shallow marine ecosystems to nutrient enrichment. *Human and Ecological Risk Assessment* 7:1457–1481.
- Nixon, S.W., J.W. Ammerman, L.P. Atkinson, V.M. Berounsky, G. Billen, W.C. Boicourt, W.R. Boynton, T.M. Church, D.M. DiToro, R. Elmgren, J.H. Garber, A.E. Giblin, R.A. Jahnke, N.J.P. Owens, M.E.Q. Pilson, and S.P. Seitzinger. 1996. The fate of nitrogen and phosphorus at the land-sea margin of the North Atlantic Ocean. *Biogeochemistry* 35:141–180.
- NRC (National Research Council). 2000. *Clean Coastal Waters: Understanding and Reducing the Effects of Nutrient Pollution*. National Academy Press: Washington, DC.
- Officer, C.B. 1980. Box models revisited. Pp. 65–114 in *Estuarine and Wetland Processes with Emphasis on Modeling*. Edited by P. Hamilton, and K.B. MacDonald. Plenum Press: New York, NY.
- Officer, C.B., and D.R. Kester. 1991. On estimating the non-advective tidal exchanges and advective gravitational circulation exchanges in an estuary. *Estuarine, Coastal and Shelf Science* 32:99–103.
- Pace, M.L. 2001. Prediction and the aquatic sciences. *Canadian Journal of Fisheries and Aquatic Science* 58(1):63–72.

- Paerl, H.W. 1997. Coastal eutrophication and harmful algal blooms: Importance of atmospheric deposition and groundwaters as “new” nitrogen and other nutrient sources. *Limnology and Oceanography* 42:1154–1165.
- Paerl, H.W., and M.F. Piehler. 2008. Nitrogen and marine eutrophication. Pp. 529–567 in *Nitrogen in the Marine Environment* (second edition). Edited by D.G. Capone, D.A. Bronk, M.R. Mulholland, and E.J. Carpenter. Elsevier: Burlington, MA.
- Paerl, H.W., N.S. Hall, B.L. Peierls, K.L. Rossignol, A.R. Joyner, T. Ottenand, K.H. Reckhow, and F. Nojavan. 2012. *Develop and Deploy Microalgal Indicators as Measures of Water Quality, Harmful Algal Bloom Dynamics, and Ecosystem Condition*. Final report to the Strategic Environmental Research and Development Program, U.S. Department of Defense, Washington, DC.
- Piehler, M.F., and A.R. Smyth. 2011. Habitat-specific distinctions in estuarine denitrification affect both ecosystem function and services. *Ecosphere* 2(1), Part 12.
- Powers, S.P., C.H. Peterson, R.R. Christian, E. Sullivan, M.J. Powers, M.J. Bishop, and C.P. Buzzelli. 2005. Effects of eutrophication on bottoms habitat and prey resources of demersal fishes. *Marine Ecology Progress Series* 302:233–243.
- Raick, C., K. Soetaert, and M. Gregoire. 2006. Model complexity and performance: How far can we simplify? *Progress in Oceanography* 70(1):27–57.
- Reckhow, K.H. 1994. Water quality simulation modeling and uncertainty analysis for risk assessment and decision making. *Ecological Modelling* 72(1–2):1–20.
- Reckhow, K.H., M.N. Beaulac, and J.T. Simpson. 1980. *Modeling Phosphorus Loading and Lake Response Under Uncertainty: A Manual and Compilation of Export Coefficients*. Report 440/5-80-011. U.S. Environmental Protection Agency, Washington, DC.
- Rigler, F.H., and R.H. Peters. 1995. Science and limnology. Book 6 in *Excellence in Ecology*. Edited by O. Kinne. International Ecology Institute: Oldendorf/Luhe.
- Riley, G.A., H. Stommel, and D.F. Bumpus. 1949. Quantitative ecology of the plankton of the Western North Atlantic. *Bulletin of the Bingham Oceanographic Collection* 12:1–169.
- Scavia, D., D. Justic, and V.J. Bierman Jr. 2004. Reducing hypoxia in the Gulf of Mexico: Advice from three models. *Estuaries* 27(3):419–425.
- Seitz, R.D., R.N. Lipcius, N.H. Olmstead, M.S. Seebo, and D.M. Lambert. 2006. Influence of shallow-water habitats and shoreline development on abundance, biomass, and diversity of benthic prey and predators in Chesapeake Bay. *Marine Ecology Progress Series* 326:11–27.
- Seitz, R.D., R.N. Lipcius, W.T. Stockhausen, K.A. Delano, M.S. Seebo, and P.D. Gerdes. 2003. Potential bottom-up control of blue crab distribution at various spatial scales. *Bulletin of Marine Science* 72(2):471–490.
- Smaal, A.C., and T.C. Prins. 1993. The uptake of organic matter and the release of inorganic nutrients by bivalve suspension feeder beds. Pp. 273–298 in *Bivalve Filter Feeders in Estuarine and Coastal Ecosystem Processes*. Edited by R.F. Dame. Springer-Verlag: Heidelberg, Germany.

- Steele, J.H. 1974. *The Structure of Marine Ecosystems*. Harvard University Press: Cambridge, MA.
- Stow, C.A., C. Roessler, M.E. Borsuk, J.D. Bowen, and K.H. Reckhow. 2003. Comparison of estuarine water quality models for total maximum daily load development in Neuse River Estuary. *Journal of Water Resources Planning and Management* 129(4):307–314.
- Swanson, J.C., and K. Jayko. 1988. *A Simplified Estuarine Box Model of Narragansett Bay*. Final report to the Narragansett Bay Project and U.S. Environmental Protection Agency, Applied Science Associates, Narragansett, RI.
- Testa, J.M., and W.M. Kemp. 2008. Regional, seasonal, and inter-annual variability of biogeochemical processes and physical transport in a partially stratified estuary: A box-modeling analysis. *Marine Ecology Progress Series* 356:63–79.
- U.S. EPA (Environmental Protection Agency). 2001. *PLOAD Version 3.0: An ArcView GIS Tool to Calculate Nonpoint Sources of Pollution in Watershed and Stormwater Projects (User's Manual)*. U.S. Environmental Protection Agency, Office of Water, Washington, DC. Available at http://water.epa.gov/scitech/datait/models/basins/upload/2002_05_10_BASINS_b3docs_PLOAD_v3.pdf.
- U.S. EPA (Environmental Protection Agency). 1999. *Protocol for Developing Nutrient TMDLs*. U.S. Environmental Protection Agency report 841-B-99-007. EPA Office of Water, Washington, DC.
- Valiela, I., G. Collins, J. Kremer, K. Lajtha, M. Geist, B. Seely, J. Brawley, and C.H. Sham. 1997. Nitrogen loading from coastal watersheds to receiving estuaries: New method and application. *Ecological Applications* 7(2):358–380.
- Valiela, I., K. Foreman, M. LaMontagne, D. Hersh, J. Costa, P. Peckol, B. DeMeo-Andreson, C. D'Avanzo, M. Babione, C-H. Sham, J. Brawley, and K. Lajtha, K. 1992. Couplings of watersheds and coastal waters: Sources and consequences of nutrient enrichment in Waquoit Bay, Massachusetts. *Estuaries* 15(4):443–457.
- van der Veer, H.W., J.F.M.F. Cardoso, and J. van der Meer. 2006. The estimation of DEB parameters for various Northeast Atlantic bivalve species. *Journal of Sea Research* 56:107–124.
- van der Veer, H.W., S.A.L.M. Kooijman, and J. van der Meer. 2001. Intra- and interspecies comparison of energy flow in North Atlantic flatfish species by means of dynamic energy budgets. *Journal of Sea Research* 45:303–320.
- Van Nes, E.H. and M. Scheffer. 2005. A strategy to improve the contribution of complex simulation models to ecological theory. *Ecological Modelling* 185:153–164.
- Wiseman, H.M. 2010. *Quantifying the Ecosystem Role of a Suspension and a Facultative Deposit Feeding Bivalve in the New River Estuary, NC, with Responses to Changes in Nutrient and Sediment Inputs*. M.S. thesis, College of William and Mary, Gloucester Point, VA.

Ysebaert, T., P. Meire, P.M.J. Herman, and H. Verbeek. 2002. Macrobenthic species response surfaces along estuarine gradients: Prediction by logistic regression. *Marine Ecology Progress Series* 225:79–95.

Appendix 6-A
List of Scientific Publications

List of Scientific Publications

Edited Volumes

Brush, M.J., and L.A. Harris (Eds). 2010. Advances in modeling estuarine and coastal ecosystems: Approaches, validation, and applications. Special issue, *Ecological Modelling* 221(7):965–1088.

Papers

Brush, M.J., and H.M. Wiseman. Submitted. Modeling the ecosystem role of a suspension and deposit feeding bivalve across hydrologically different years. *Journal of Sea Research*.

Brush, M.J., and L.A. Harris. 2010. Introduction to the special issue of *Ecological Modelling*: Advances in modeling estuarine and coastal ecosystems: Approaches, validation, and applications. *Ecological Modelling* 221(7):965–968.

Thesis

Koroknay, B.J. 2012. Quantifying watershed loads to a low relief, coastal plain estuary: The New River Estuary, NC. M.S. thesis, College of William and Mary, Gloucester Point, VA. (134 pages).

Wiseman, H.M. 2010. Quantifying the ecosystem role of a suspension and a facultative deposit feeding bivalve in the New River Estuary, NC, with responses to changes in nutrient and sediment inputs. M.S. thesis, College of William and Mary, Gloucester Point, VA. (151 pages).

Presentations

Brush, M.J. 2012. *A Reduced Complexity, Hybrid Empirical Mechanistic, Management-Relevant Model for Shallow, Fringing Embayments*. Presented at the Chesapeake Community Modeling Program symposium, Annapolis, MD.

Brush, M.J. 2012. *A Rapidly Deployable, Reduced Complexity Model for Estuarine Management: Case Studies and Development of an Online Decision-Support Interface*. Presented at the Chesapeake Community Modeling Program symposium, Annapolis, MD.

Brush, M.J. 2011. *Reduced and Intermediate-Complexity Systems Models for Science and Management: The Macroscopic Estuarine Modeler's Toolbox*. Invited keynote presentation at the 11th International Estuarine Biogeochemistry Symposium, Atlantic Beach, NC.

Brush, M.J., I.C. Anderson, M.F. Piehler, C.A. Currin, and H.W. Paerl. 2011. *Modeling Response to Climatic and Anthropogenic Stressors in a Shallow, Photoc Coastal System*.

Presented at the 21st biennial conference of the Coastal and Estuarine Research Federation, Daytona Beach, FL.

- Brush, M.J. 2010. *Modeling Through the Macroscopic: An Estuarine Potpourri from Watersheds to Water Quality to Fish*. Invited seminar presented at the Chesapeake Biological Laboratory, University of Maryland Center for Environmental Science, Solomons, MD (updated from May seminar at HPL). Invited seminar also presented at the Horn Point Environmental Laboratory, University of Maryland Center for Environmental Science, Cambridge, MD. Also a seminar presented to the VIMS Biological Sciences Department, Gloucester Point, VA.
- Brush, M.J. and M.F. Piehler. 2009. *DCERP Watershed Simulation Model*. Presented at the Strategic Environmental Research and Development Program-Environmental Security Technology Certification Program Partners in Environmental Technology Technical Symposium and Workshop, Washington, DC.
- Brush, M.J. 2008. *Balancing Precision, Realism, and Generality in Estuarine Ecosystem Models: A Tour from the Practical to the Esoteric and Back Again*. Invited seminar presented at University of North Carolina at Chapel Hill's Institute of Marine Sciences, Morehead City, NC.
- Brush, M.J. 2008. *Modeling in the Dark: Simulating the Blackwater New River Estuary*. Seminar presented to the VIMS Biological Sciences Department, Gloucester Point, VA.

[This page intentionally left blank.]

Appendix 6-B

List of Students

- Giordano, Juliette C.P., M.S., College of William and Mary, May 2009; partial support. Following graduation from VIMS, Ms. Giordano joined the staff to participate in DCERP field work (part of Research Project AE-3) and developed the NLM, BasinSim, and ReNuMa models.
- Koroknay, Brittani J., M.S., College of William and Mary, December 2012; independently supported student, but thesis topic focused on DCERP (application of PLOAD and HSPF).
- Lake, Samuel J., Ph.D. candidate, College of William and Mary; partial support.
- Wiseman, Heather M., M.S., College of William and Mary, December 2010; full support with thesis topic focused on DCERP (development of benthic bivalve models).

[This page intentionally left blank.]

Chapter 7

**Drivers and Forecasts of the Responses
of Tidal Salt Marshes to Sea Level Rise**

SERDP Project Number: RC-1413

Coastal Wetlands Module

Research Project CW-1

Lead Researchers:

James T. Morris
University of South Carolina
Columbia, SC
E-mail: morris@inlet.geol.sc.edu

and

Carolyn Currin
National Oceanic and Atmospheric Administration
Beaufort, NC

May 10, 2013

Final

This report was prepared under contract to the U.S. Department of Defense (DoD) Strategic Environmental Research and Development Program (SERDP). The publication of this report does not indicate endorsement by DoD, nor should the contents be construed as reflecting the official policy or position of DoD. References herein to any specific commercial product, process, or service by trade name, trademark, manufacturer, or otherwise, do not necessarily constitute or imply its endorsement, recommendation, or favoring by DoD.

Table of Contents

List of Acronyms	7-v
Abstract.....	7-1
Objectives of the Research Program.....	7-2
Background.....	7-2
Materials and Methods.....	7-4
Marsh Elevation	7-4
Fertilization Study.....	7-5
Marsh Bioassay (Marsh Organ) Experiment	7-6
Environmental Data	7-8
Marsh Digital Elevation Model	7-10
The Marsh Equilibrium Model (MEM)	7-11
Results and Discussion	7-13
Marsh Elevation: Current Status	7-13
Fertilization Study.....	7-14
Marsh Bioassay (Marsh Organ) Experiment	7-15
Marsh Elevation: Rates of Change	7-17
Marsh Elevation: 100-Year Forecasts.....	7-19
Conclusions and Implications for Future Research	7-21
Literature Cited	7-25
Appendix 7-A: List of Scientific Publications.....	7-A-1
Appendix 7-B: List of Students	7-B-1

List of Figures

7-1. Monitoring and research stations for the Coastal Wetlands Module and Research Project CW-1 showing the locations of surface elevation table (SET) sites and water-level sensor.	7-4
7-2. The SET device is in place over a marsh plot and leveled with pins touching the surface.	7-5
7-3. Schematic of the three sites established to support the marsh surface elevation monitoring and Research Project CW-1.	7-6
7-4. Intact sediment core pulled from one of the marsh organ pipes prior to washing, dissecting, drying, and weighing.	7-7
7-5. Fertilized (left) and control (right) marsh organs at FC in July 2009.	7-8

7-6.	Comparison of tides at two locations in the ICW including MHB (the location of the NOAA tide gage) and FC (the location of the marsh organ experiment and an SET site).....	7-9
7-7.	National Wetland Inventory delineation of intertidal salt marsh landscapes on the east and west sides of the ICW.	7-10
7-8.	Frequency distributions of elevations of salt marsh habitat (top) east of the ICW and (bottom) west of the ICW (see 7-7 for a map of these areas classified by the National Wetland Inventory as salt marsh).....	7-14
7-9.	Total above-ground biomass of <i>S. alterniflora</i> as a function of elevation in controls (left) and fertilized treatments (right).....	7-16
7-10.	Total below-ground biomass of <i>S. alterniflora</i> as a function of elevation in controls (left) and fertilized treatments (right).....	7-16
7-11.	Measured surface elevations of marshes at FC, MHB, and OB over 4 years beginning in February 2008.	7-18
7-12.	MEM forecasts of marsh elevation and standing biomass for different SLR scenarios.....	7-20
7-13.	MEM-forecasted survival times of MCBCL marshes for different SLR scenarios ranging from a constant rate, equivalent to 25 cm/y, to a rapidly accelerating rate that raised mean sea level to 200 cm by the end of a century.....	7-21
7-14.	Demonstrated here are alternative frequency distributions of hypothetical marsh elevations (LIDAR) from different estuaries (from Morris et al., 2005).....	7-22
7-15.	Conceptual “dredge and slump” model explaining how marshes west of the ICW could be presently far below the equilibrium elevation.....	7-23

List of Tables

7-1.	Arithmetic TSS mean (± 1 standard deviation [SD], n) and maximum TSS sampled at stations in tidal creeks adjacent to the ICW (FC, Gillets Creek) and elsewhere within the NRE.	7-8
7-2.	Parameter and variable inputs used for simulations of current and forecasted rates of change of marsh elevation in MCBCL salt marshes	7-12
7-3.	Mean (± 1 standard deviation [SD]) standing biomass (live plus dead) of <i>Spartina alterniflora</i> by site [†] and treatment ^{††}	7-15
7-4.	Observed rates of change of marsh elevation (mm/y) at the study sites, lower and upper 95% confidence limits (L95 and U96), and MEM predicted rates.....	7-18

List of Acronyms

°C	degrees Celsius
ϕ	root:shoot quotient
v	constant that depends on the value chosen for L
μm	Micrometer
3-D	three dimensional
B_r	production of roots and rhizomes
B_s	standing biomass density
cm	Centimeter
cm/y	centimeter per year
D	depth of marsh surface below MHW
DCERP	Defense Coastal/Estuarine Research Project
DEM	Digital Elevation Model
DoD	U.S. Department of Defense
E	Elevation
EOS	end of season
FC	Freeman Creek
$\text{g cm}^{-3} \text{ y}^{-1}$	grams per cubic centimeters per year
g/g	grams per gram
g/m^2	grams per square meters
GPS	global positioning system
ICW	Intracoastal Waterway
kg/m^2	kilograms per square meter
km	Kilometer
k_r	refractory fraction of annual root and rhizome production
k_s	trapping coefficient
$L(t)$	eustatic sea level rise
LIDAR	Light Detection and Ranging
m	Meter
m	concentration of suspended solids
m^2	square meter
MCBCL	Marine Corps Base Camp Lejeune
MEM	Marsh Equilibrium Model
mg/L	milligrams per liter
MHB	Mile Hammock Bay
MHHW	mean higher high water
MHW	mean high water

MLLW	mean lower low water
MLW	mean low water
mm	Millimeter
mm/y	millimeters per year
$\text{mol m}^{-2} \text{y}^{-1}$	moles per square meter per year
MSPE	mean square percentage error
NAVD88	North American Vertical Datum of 1988
$(\text{NH}_4)_2\text{SO}_4$	ammonium sulfate
N	Nitrogen
NOAA	National Oceanic and Atmospheric Administration
NRE	New River Estuary
OB	Onslow Beach
O_i	observed rate of change of marsh elevations in the i^{th} SET site out of n sites
OPUS	Online Positioning User Service
P	Phosphorus
P_2O_5	phosphorus oxide
P_i	predicted rate of change of marsh elevations in the i^{th} SET site out of n sites
PVC	polyvinyl chloride
q	settling velocity
SD	standard deviation
SERDP	Strategic Environmental Research and Development Program
SET	surface elevation table
SLR	sea level rise
T	tide range
t	number of years from present
TSS	total suspended solids
W_A	average tidal amplitude
W_a	total above-ground biomass
W_b	total below-ground biomass

Abstract

Sediment accretion in Freeman Creek (FC), Mile Hammock Bay (MHB), and Onslow Beach (OB) salt marshes (≥ 2.3 mm/y) is keeping pace with or exceeding the current rate of sea level rise (SLR). The accretion rate was greatest at FC (9 mm/y) and exceeds the current rate of SLR by at least 6 mm/y. However, the elevation of the FC marsh in 2008 (-6 cm North American Vertical Datum of 1988 [NAVD88]) was significantly lower than study sites at MHB and OB ($\geq +14$ cm, NAVD88) east of the Intracoastal Waterway (ICW). In contrast, FC is west of the ICW, which acts as a sediment trap, cutting off western shore marshes from a sediment subsidy derived from overwash and aeolian transport from the dunes on Onslow Island. In addition, the marshes may be slumping into the ICW following each dredging of the ICW. We refer to this conceptual model as the “dredge and slump model,” and it describes a cycle consisting of the episodic lowering of marsh elevation, coincident with dredging, followed by a rapid recovery, which is occurring now at FC. As predicted by the Marsh Equilibrium Model (MEM), the speed of recovery should be directly proportional to the depth of the marsh surface below the mean high water level.

Fertilization of marshes with nitrogen increased above-ground biomass and, as predicted by MEM, sediment accretion rates. Treatment with nutrients raised the accretion rate (the incremental increase above the control rate) by an average of 4.6 ± 0.5 mm/y (± 1 standard deviation). The increased rate ranged from 4 mm/y at FC to 5.1 mm/y at OB (Table 7-4). These increases were sustained over the course of the 4-year study and showed no evidence of abating. The mean percentage error of the MEM predicted rates of change of marsh elevation, inclusive of all sites and treatments was 15%. Moreover, the predicted trends among sites and treatments were consistent with observations. In the absence of fertilization and dredging, the MEM forecasts a 95-year survival time of area marshes, given a sea level rise scenario of 100 cm in a century.

Analysis of classified Light Detection and Ranging (LIDAR) data indicates that Marine Corps Base Camp Lejeune (MCBCL) salt marshes tend to be relatively low in elevation. Their elevations differed depending on their position east or west of the ICW. Marshes west of the ICW have positive skewness (1.08) and a modal elevation of 8.2 cm. East of the ICW, marshes have a modal elevation of 21.6 cm and positive skewness (1.26). These elevations leave only a small buffer for loss of relative vertical elevation in the event of an acceleration in the rate of SLR.

Two strategies for increasing the likelihood of marsh survival were envisioned. Fertilization of the MCBCL salt marshes is predicted to increase their sediment accretion and survival time. However, should fertilization be considered as a viable strategy to mitigate SLR, the effects on the water quality in adjacent waterways would need to be investigated. A second option is to use thin-layer disposal of dredge material to nourish the marshes. This would have short-term, negative consequences for marsh infauna, but the consequences to infauna and ecosystem services of the loss of marsh due to SLR would be permanent.

Keywords: Sediment, accretion, salt marsh, coastal, *Spartina alterniflora*, cordgrass, ICW, sea level rise, dredging, Marsh Elevation Model (MEM), marsh mesocosms, marsh fertilization

Objectives of the Research Program

Hypothesis 1: Intertidal salt marshes will equilibrate at an elevation within the tidal frame that is inversely proportional to the rate of sea level rise (SLR).

Goals and Objectives:

- a. Calibrate the Marsh Equilibrium Model (MEM) of Morris et al. (2002) to Marine Corps Base Camp Lejeune salt marshes.
- b. Forecast changes in marsh elevation and vegetation to different SLR scenarios.

Hypothesis 2: The equilibrium elevation of salt marshes can be increased by raising biomass density by fertilization of the marsh

Goals and Objectives:

- a. Measure the current rate of sediment accretion in salt marshes at control sites, and at sites treated with nitrogen (N) and phosphorus (P) nutrients
- b. Identify the primary nutrient (e.g., N or P) that limits primary production in local salt marshes and the response of primary production to N and P fertilization
- c. Measure the responses of above-ground and below-ground primary production to changes in the relative elevation of the marsh surface.

Hypothesis 3: The relative elevation of the marsh platform within the tidal frame is a diagnostic of its vulnerability to SLR or disturbance.

Goals and Objectives:

- a. Map the current elevations of intertidal salt marshes of the NRE and the Intracoastal Waterway relative to mean sea level
- b. Identify areas of salt marsh that are low in the tidal frame and, therefore, are vulnerable to SLR.

Background

Global climate change is predicted to cause extensive changes in Earth's ecosystems, which face increases in temperature and rates of sea level rise (SLR), changes in precipitation regimes, and increased frequency of extreme weather events (Meehl et al., 2007). Perhaps some of the most sensitive systems to climate change will be those that exist at the interface between land and sea, tidal wetlands. Tidal wetlands have existed in a state of equilibrium with sea level over the past 4,000 years by adding elevation via the accumulation of mineral and organic sediments and via in situ production of organic matter by marsh macrophytes (Craft, 2007; Friedrichs and Perry, 2001; McCaffrey, and Thomson, 1980; Morris et al., 2002; Redfield, 1972), but the future of these ecosystems and their responses to accelerating SLR are uncertain.

Sea level and sediment supply are the governing factors in the persistence of tidal wetlands. The marsh surface elevation relative to sea level together with the availability of suspended sediment determines wetland area and productivity (Kirwan and Murray, 2007; Kirwan et al., 2010; Morris, 2005; Morris et al., 2002). SLR increased from 1–2 mm/y early in the twentieth century to current rates of approximately 3 mm/y (Church et al., 2008; Fitzgerald et al., 2008), and the bulk of scientific evidence suggests that SLR will further accelerate (Bindoff et al., 2007; Rahmstorf, 2007). Sea level may rise by as much as 1 m by the end of the current century (Richardson et al., 2009; Vermeer and Rahmstorf, 2010) leading to concerns that tidal wetlands will become increasingly vulnerable as they are unable to maintain elevation against rising water levels (Craft et al., 2009; Day and Templet, 1989; Donnelly and Bertness, 2001; Kirwan et al., 2010).

There is great interest in the response of coastal wetlands to rising sea level due to the high value of ecosystem services that they provide, including their value to Marine Corps Base Camp Lejeune (MCBCL) as an important habitat upon which to conduct training exercises. Coastal wetlands provide a range of supporting, regulating, provisioning, and cultural services that include maintenance of soil and sediment (shoreline stabilization), nutrient regulation and water quality, provisioning of food, recreational opportunities, and hazard moderation (Barbier et al., 2011; Jordan et al., 1983; Kneib, 1997; Knutson, 1988; Möller et al., 1999; Morris, 1991; Shepard et al., 2011; Valiela and Teal, 1979). Coastal wetlands provide habitat and food to species of commercial importance, which in turn support a community of commercial fishers that depends on these species for their livelihoods, as well as a robust recreational fishing industry. Also, coastal wetlands protect against the damaging effects of storms, provide filtration services that improve water quality, and mitigate the consequences of SLR.

There are now a variety of models that were designed to forecast the responses of coastal wetlands to SLR. The first generation of these models predict that intertidal marshes approach an equilibrium elevation that approximates that of mean high water (MHW; Krone, 1985), but they failed to address important feedbacks with marsh vegetation and limits to sediment accretion. The model by Krone (1985) assumes that the rate of sedimentation is proportional to the depth of water overlying the marsh at high tide, as this is related to inundation time. As inundation time increases, the settling of sediment particles suspended in the overlying water increases, and as inundation time and depth approach zero, at mean high tide, net sedimentation rate also approaches zero. However, recent work in a North Inlet, SC, marsh has shown that, in addition to depth, the effect of relative marsh elevation on the vegetation, and subsequently the effect of vegetation on sedimentation rate, is a critically important variable that ultimately controls the productivity of the saltmarsh plant community and has a powerful effect the rate of accretion of the marsh surface (Morris et al., 2002). This type of feedback has been termed ecogeomorphology (Fagherazzi et al., 2004) or ecogeomorphic feedback (Kirwan et al., 2010).

These processes were investigated in salt marshes on the MCBCL in the New River Estuary (NRE), NC, to assess the current state of MCBCL marshes and to extend the model of Morris et al. (2002) to marshes within the study area. The research combined field studies and modeling. The design and rationale of the field studies were informed by the conceptual model, and the outcome of the field experiments were, in turn, used to parameterize the numerical model. Once parameterized, the model was used to simulate changes in marsh elevation during the past 4

years corresponding to known conditions and to forecast changes in elevation and productivity to the end of the century.

Materials and Methods

Research Project CW-1 was conducted on three salt marsh sites, all dominated by the salt marsh grass *Spartina alterniflora*. Two sites were located south and east of the ICW at Onslow Beach (OB), and Mile Hammock Bay (MHB), and one site (i.e., Freeman Creek [FC]) was located west of the ICW (**Figure 7-1**). These sites were used to study marsh elevation and the effects of nutrients on marsh growth, to conduct in situ bioassay (marsh organ) experiments, and to conduct a field survey of standing biomass and marsh elevation.

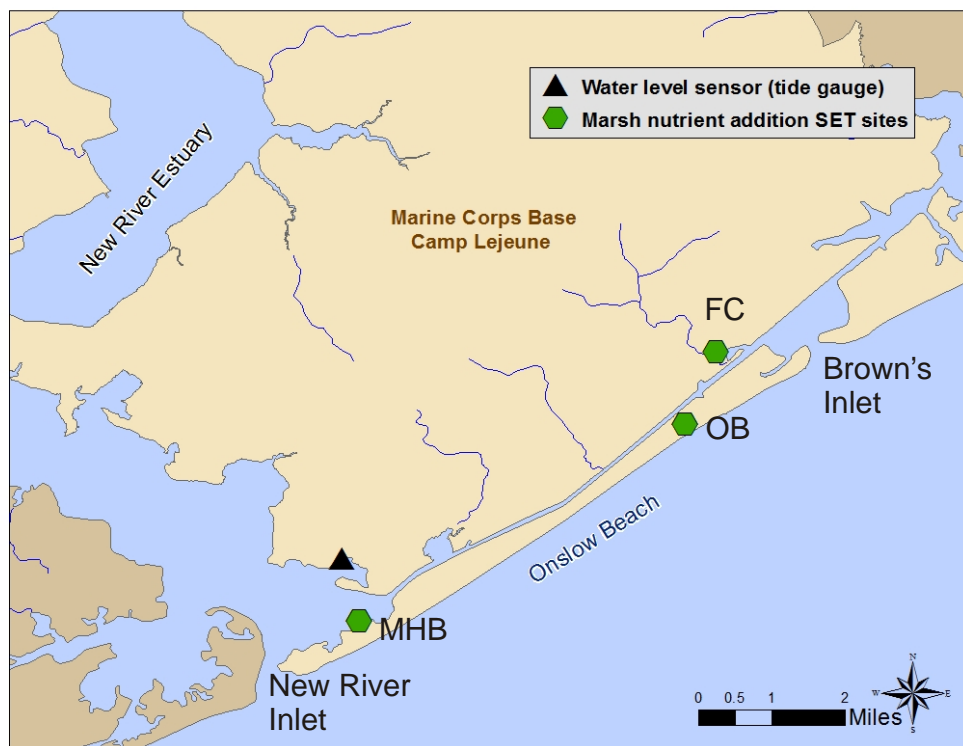


Figure 7-1. Monitoring and research stations for the Coastal Wetlands Module and Research Project CW-1 showing the locations of surface elevation table (SET) sites and water-level sensor.

Marsh Elevation

Commencing in February 2008 and continuing until February 2012, changes in marsh elevation were measured using surface elevation tables (SETs). SET installation followed the procedures for a Deep Rod SET described by Cahoon et al. (2002). Marker horizons and estimates of marsh surface elevation were obtained as described in Cahoon (1999). Additional details on protocols are available on the U.S. Geological Survey's Web site at <http://www.pwrc.usgs.gov/set>. To minimize disturbance to the research study sites, we installed boardwalks of pressure-treated lumber leading from an access point to the SET site and used fiberglass grating to provide access and a research staging area inside each of the SET sites (**Figure 7-2**). At FC, six SET sites were

installed (**Figure 7-3**), and three of these were fertilized and three served as controls. At the MHB and OB sites, two SETs were installed; one served as a control and the other was fertilized. The objective of fertilizing half of the SET sites was to increase the standing biomass and to observe the effect on sediment accretion. The addition of fertilizer increased the biomass of the vegetation and allows us to assess the influence of biomass density on sedimentation rate and provides an additional calibration point to the MEM. Fertilized plots received granular salts of N and P applied to the marsh surface quarterly as phosphorus oxide (P_2O_5) and ammonium sulfate ($(NH_4)_2SO_4$) at a rate of $15 \text{ mol m}^{-2} \text{ y}^{-1}$ of P and $30 \text{ mol m}^{-2} \text{ y}^{-1}$ of N. The physical layout and orientation of the SET sites is shown in **Figure 7-3**.

Fertilization Study

Independent of the SET plots, we established 12, $1.5\text{-m} \times 1.5\text{-m}$ plots along a boardwalk at the FC site (**Figure 7-3**) to support a factorial design to determine the limiting nutrient (N or P) for marsh primary production. Three replicates of four treatments (i.e., control, +N, +P, and N+P) were delineated and were fertilized three times during the growing season at 2-month intervals from February 2008 through August 2010. Fertilizer was applied to the marsh surface as granular salts at rates equivalent to $30 \text{ mol m}^{-2} \text{ y}^{-1}$ of N as $(NH_4)_2SO_4$ and $15 \text{ mol m}^{-2} \text{ y}^{-1}$ of P as P_2O_5 either alone or in combination, depending on the treatment. At the OB and MHB sites N+P and control plots were established. On all plots, two replicates of above-ground, end-of-season (EOS) standing biomass were harvested. The harvest consisted of live and dead biomass taken from 0.0625 m^2 quadrats. Samples were dried in an oven at 100°C , and weighed on a balance in the laboratory. The average ratio of fertilized (N+P) to control biomass from this study was used to scale the biomass response curve in MEM for simulations of the fertilized SET treatments.



Figure 7-2. The SET device is in place over a marsh plot and leveled with pins touching the surface.

The operator deployed the SET several times annually and measured the length of these pins.

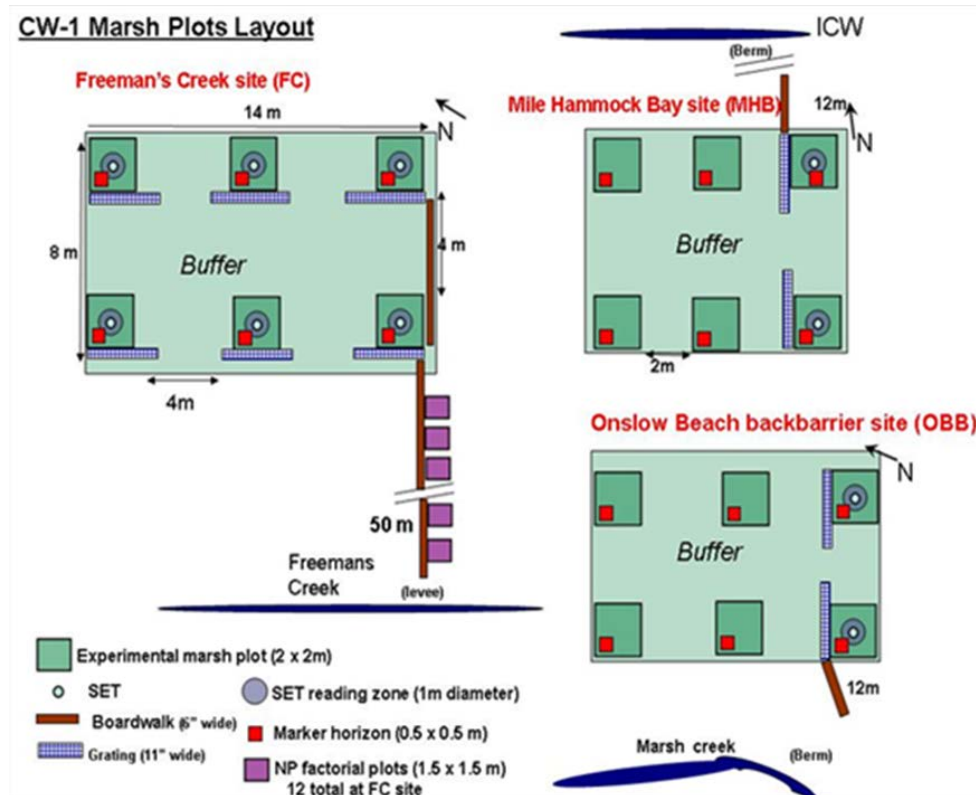


Figure 7-3. Schematic of the three sites established to support the marsh surface elevation monitoring and Research Project CW-1.

Each SET provided a means to measure changes in marsh surface elevation with a ± 2 -mm resolution.

Marsh Bioassay (Marsh Organ) Experiment

We conducted a bioassay experiment to determine the vertical growth range and optimum elevation for growth of *Spartina alterniflora*. *S. alterniflora* is the dominant salt marsh species in MCBCL salt marshes, and its response to relative elevation is a critical input for the MEM (Morris et al., 2002). The bioassay was carried out using a type of planter known as a “marsh organ” that consists of standing polyvinyl chloride (PVC) pipes cut to different lengths to simulate different marsh surface elevations (Morris, 2007). The device was planted with sprigs of *S. alterniflora* taken from the neighboring marsh that we subsequently harvested after a season of growth. The bioassay experiment yielded data that included EOS above and below-ground biomass (**Figure 7-4**) made in 2008 through 2010, inclusive, from two planters that were located in the FC marsh. A third marsh organ was established and harvested at Onslow Bay in 2010.

The organs were positioned vertically such that the rows corresponded with an elevation range between approximately -25 cm to $+55$ cm with respect to the North American Vertical Datum of 1988 (NAVD88). The elevation of each row of pipes was measured with respect to NAVD88, which at this location was approximately 7 cm above mean sea level (unpublished data NOAA, 2011). Measurements were taken by DCERP researchers from the National Oceanic and Atmospheric Administration’s (NOAA’s) Laboratory in Beaufort, NC, using an Online Positioning User Service (OPUS) global positioning system (GPS), referenced to a nearby control point, and a laser level.



Figure 7-4. Intact sediment core pulled from one of the marsh organ pipes prior to washing, dissecting, drying, and weighing.

Photo courtesy of
Siobhan Scott.

To determine if the range and optimum elevation for growth was altered by the nutrient status of the plants, we fertilized one of the marsh organs at FC with a combination of granular salts of N and P at rates equivalent to $30 \text{ mol m}^{-2} \text{ y}^{-1}$ of N as $(\text{NH}_4)_2\text{SO}_4$ and $15 \text{ mol m}^{-2} \text{ y}^{-1}$ of P as P_2O_5 . Fertilizer was applied to each of the pipes three times during the growing season at 2-month intervals. The first treatment in March was made below the sediment surface before planting, while subsequent treatments in May and July were accomplished by adding the fertilizer to holes punched around the periphery of each pipe with a 1-inch dowel to a depth of approximately 10 cm. The other two marsh organs served as controls. In 2010, the below-ground biomass from the FC marsh organs was cleaned and separated into roots and rhizomes, and the parts dried and weighed separately. In earlier years, below-ground biomass was washed and weighed in bulk. After drying the samples at 100°C in an oven and weighing the dried samples on a balance, above-ground and below-ground biomass were analyzed by elevation, year, and treatment.

The marsh organs were constructed from 6-inch diameter and 1/8-inch wall green PVC pipe cut to form six rows of six pipes each, with the first row being approximately 12-inches in length and each subsequent row being 6-inches taller than the previous (**Figure 7-5**). The tubes were fastened together using stainless steel nuts and bolts creating a structure loosely resembling a pipe organ. The organs were assembled on site and anchored to the marsh using wooden 2- × 4-inch wooden pilings. The marsh organs were placed in a location at the study site that provided protection from waves, as well as a south facing orientation to eliminate any self-shading from the pipes. Early in the spring of each growing season, individual *S. alterniflora* culms with intact roots and rhizomes were transplanted to the pipes from the adjacent marsh. Transplants were checked after 1 month for mortality and dead plants were replaced with new plugs taken from the adjacent marsh. Mortality within the first month was assumed to be due to transplant stress, and subsequent mortality was considered to be the result of suboptimal growing conditions.

The pipes were open-ended to allow vertical drainage through sediment that was taken from the surrounding marsh. Planter sediment was allowed to settle for at least 1 week before planting. Because there is no possibility of lateral drainage, we regard the marsh organ as a suitable model of the interior marsh platform, but not a good model of a creek bank. Creek banks are often riddled with the burrows of infauna and have steep hydraulic gradients that allow for greater drainage than occurs in the marsh interior.



Figure 7-5. Fertilized (left) and control (right) marsh organs at FC in July 2009.

Environmental Data

In addition to sedimentological and biological measurements previously described, measurements of total suspended solids (TSS) and water level were made to provide necessary inputs for MEM.

Table 7-1. Arithmetic TSS mean (± 1 standard deviation [SD], n) and maximum TSS sampled at stations in tidal creeks adjacent to the ICW (FC, Gillets Creek) and elsewhere within the NRE.

Site	Distance from Inlet (km)	Sampling Period	Mean TSS (± 1 SD, n) (mg/L)	Maximum TSS (mg/L)
Freeman Creek (FC)	1.0	2007–2008	15.5 (3.6, 4)	17.5
Gillets Creek	4.1	2007–2008	16.4 (3.5, 4)	18.9
Traps Bay	3.7	2007–2010	18.0 (7.9, 14)	31.9
Courthouse Bay	6.7	2007–2010	17.7 (10.7, 12)	46.3
French Creek	20.7	2007–2010	11.5 (3.6, 13)	25.3
Wallace Creek	25.7	2007–2010	10.6 (7.8, 13)	11.2

The distance from inlet is calculated from Browns Inlet for Freeman Creek and Gillets Creek and from the New River Inlet for the other stations.

Total Suspended Solids (TSS): Research Project AE-3 collected water samples from shallow embayments around our study sites. The mean TSS ($>0.7 \mu\text{m}$) concentrations at the FC and Gillets Creek stations, sampled four times from 2007 to 2008, were 15 ± 4 and 16 ± 4 mg/L, respectively (**Table 7-1**). These values were consistent with TSS measures made at other stations in the NRE (**Table 7-1**). These data represent the total TSS concentration. They were converted

to inorganic TSS concentrations, needed for the model, using the percentage of organic matter in TSS samples collected on October 19, 2009 from Courthouse, Traps, and Stone Bays, which averaged $22.1 \pm 8\%$ (± 1 SD, $n=12$). Applying this percentage to total TSS at FC gave 12 mg/L for suspended, inorganic solids, which compares favorably to data from North Inlet, SC (Oyster Landing 1996–2008), where the concentration averaged 26 ± 16 mg/L (± 1 SD, $n=3280$). For the purpose of making model forecasts, we selected 12 mg/L as being representative of the inorganic suspended solids. More than 90% of salt marsh habitat on MCBCL lies along the ICW between Browns and New River inlets, which is where these samples were collected.

Tides: Tide range, MWH level, and mean higher high water level (MHHW) are important model parameters and to establish their values it is necessary to measure a time series of local water-level (tides) in the vicinity of study sites within the model domain. A YSI 600LS sonde was established as a secondary tide gauge in the MHB basin (**Figure 7-1**) and has been maintained since November 2009, collecting water level, temperature and salinity data every 6 minutes. In addition, pressure transducers to measure water level were placed in FC from September 2008 to March 2010 and surveyed into the local SET benchmarks. (Further details are available in the *Final DCERP1 Monitoring Report* and in Chapter 9 of this report).

An analysis of the MHB tide data placed MHHW and MHW at 0.193 m and 0.15 m (NAVD88), and mean lower low water level (MLLW) and mean low water level (MLW) at -0.309 m and -0.278 m, respectively. The NOAA datums were determined by harmonic analysis and, therefore, did not account for the wind tides, which can have a significant effect on sedimentation and plant growth.

The sedimentological data used to test the model were collected in and around the FC marsh, and it is important to characterize the water level at that site. We found significant differences in water levels between FC and MHB. The tide range at FC, where we have less water level data, is significantly greater than at MHB (**Figure 7-6**). The data from FC show that MHHW during September 2009 was between 0.6 m and 0.8 m, and we used a value of 0.7 m in the model.

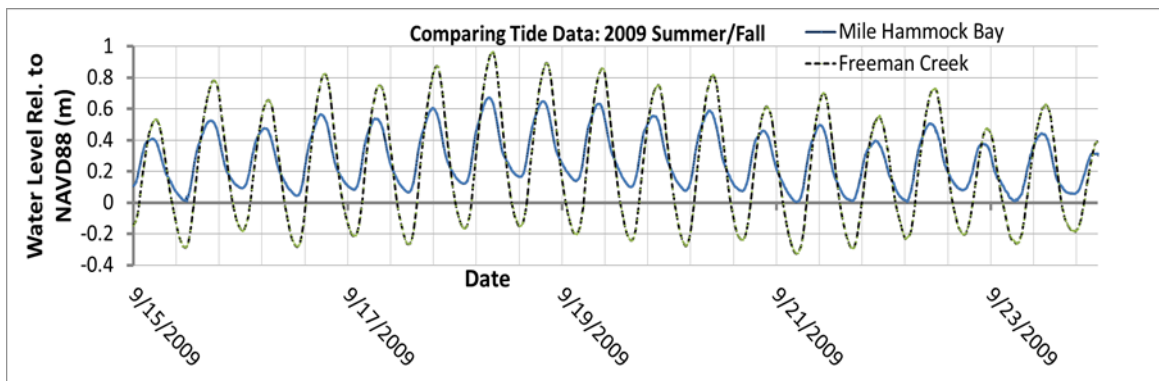


Figure 7-6. Comparison of tides at two locations in the ICW including MHB (the location of the NOAA tide gage) and FC (the location of the marsh organ experiment and an SET site).

The comparisons are available for September 2009 and March 2010. Note that the tidal amplitude is highest for FC marshes which are closer to Browns Inlet as compared to MHB that is closer to the New River Inlet. New River Inlet has a smaller tidal amplitude than Browns Inlet.

Marsh Digital Elevation Model

The elevations of salt marsh areas within the region between New River Inlet and Browns Inlet were analyzed by classifying a Digital Elevation Model (DEM) by overlaying polygons obtained from the National Wetland Inventory database using polygons classified as E2M2, or estuarine intertidal and marine intertidal wetland (**Figure 7-7**). The DEM was created from a Light Detection and Ranging (LIDAR) dataset obtained from a survey of MCBCL and produced for the National Geospatial-Intelligence Agency. The MCBCL LIDAR survey project area consisted of approximately 235 square miles. The LIDAR point cloud was flown at a density sufficient to support a maximum final post spacing of 1 m. Approximately 205 flight lines were acquired by 3001, Inc., using an ALS50 (Leica) system between February 16–24, 2007. All ground-control processing and adjustment was performed using published coordinate horizontal and vertical datums (e.g., National Geodetic Survey Continuously Operating Reference Stations [NGS CORS]). An accuracy assessment was performed using a standard method to compute the root mean square error (RMSE) based on a comparison of ground control points and filtered LIDAR data points. The bare Earth DEM was extracted from the raw LIDAR products. Bare Earth DEMs do not include buildings, vegetation, or bridges or overpass structures. The resulting marsh DEM was analyzed using PROC UNIVARIATE in the SAS 9.2 software package.

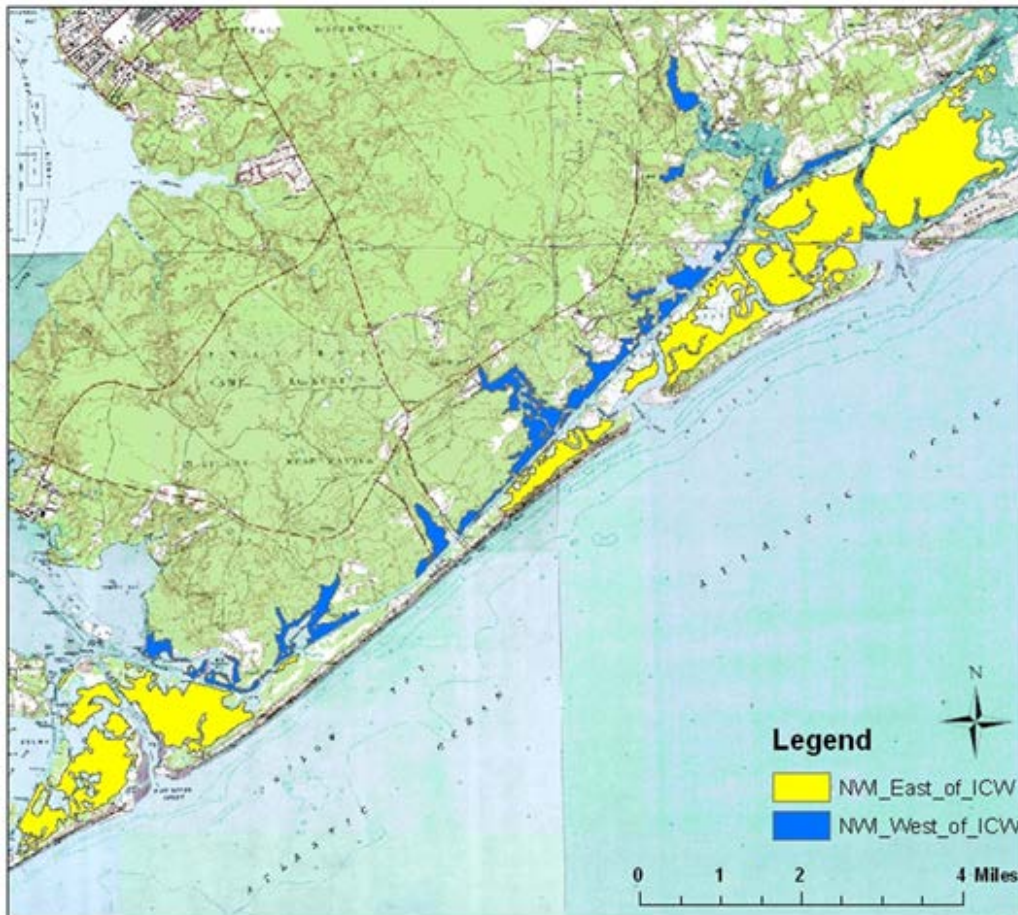


Figure 7-7. National Wetland Inventory delineation of intertidal salt marsh landscapes on the east and west sides of the ICW.

The Marsh Equilibrium Model (MEM)

Fundamental to Research Project CW-1 was the application of a model that describes feedbacks among plants, sediments, and tides in marshes that keep the marsh surface in equilibrium with sea level, provided the rate of SLR does not exceed a threshold (Morris, 2006; Morris et al., 2002 and 2012). The MEM is an ordinary differential equation with the general form as shown in Equation 7-1:

$$E' = f(D, T, m, B_s) \quad (\text{Eq. 7-1})$$

where time-varying independent variables are marsh depth below MHW (D), tide range (T), concentration of suspended solids (m), and standing biomass (B_s). The variable m represents the concentration of suspended inorganic solids, as opposed to TSS, because we assume that organic fraction is labile and does not contribute appreciably to marsh sediment volume. For purposes of fitting and/or solving the model, dependent variable B_s can be input explicitly using a time-series of biomass measurements or B_s can be input implicitly by substitution of $B_s = f(D)$, because biomass is a function of the depth of the marsh below MHW level. Equation 7-1 is integrated numerically to obtain the time series of marsh elevations as shown in Equation 7-2:

$$E(t+1) = E(t) + E'(t) \quad (\text{Eq. 7-2})$$

The MEM computes plant productivity and sediment accretion in marshes. The MEM also forecasts changes in marsh elevation as a function of primary productivity, suspended sediments, and flooding, and primary production as a function of relative elevation. The model assumes that the sedimentation of suspended solids carried by tides over the marsh surface increases with the concentration of suspended solids (m), also referred to as TSS, duration of flooding (Friedrichs and Perry, 2001; Krone 1985), and standing biomass density (B_s) (Morris et al., 2002). Flood duration is proportional to the depth (D) of the marsh surface below MHW divided by the tide range (T). In addition to surface deposition, production of organic matter, primarily of roots and rhizomes, contributes to the total accumulation rate (Reed, 1995; Turner et al., 2001). These surface and subsurface processes can be expressed as shown in Equation 7-3:

$$dS/dt = m(q + k_s B_s) D^2 / T + k_r B_r \quad (\text{Eq. 7-3})$$

Parameter q is the settling velocity, k_s is a trapping coefficient, and k_r is the refractory fraction of annual root and rhizome production (B_r). The production of roots and rhizomes (B_r) is proportional to the EOS standing biomass density (B_s) by virtue of a below-ground turnover rate and a root:shoot quotient (ϕ). B_s is a function of the depth of the marsh surface below MHW (Morris et al., 2002) as shown in Equation 7-4 as follows:

$$B_s = aD + bD^2 + c \quad (\text{Eq. 7-4})$$

Coefficients a , b , and c determine the growth range and optimum depth below MHW. Substituting for B_s into Equation 7-3 results in the following calculation (Equation 7-5):

$$dS/dt = c\phi k_r + aD\phi k_r + D^2(c k_s m + m q + b\phi k_r T) / T + aD^3 k_s m / T + bD^4 k_s m / T \quad (\text{Eq. 7-5})$$

Dividing by bulk density (Harrison and Bocock, 1981; Jeffrey, 1970) gives the change in sediment volume and, hence, surface elevation. The settling velocity (q), trapping coefficient (k_s), and refractory fraction (k_r) were derived by fitting MEM to data from North Inlet, SC, using the dynamic solution option of PROC MODEL in SAS. These parameter values are appropriate to use at other locations, particularly those with similar vegetation, tides, and sediments. The simulations of marsh dynamics at the three study sites (i.e., FC, OB, and MHB) were made using variables measured on site, namely elevation, depth (D), tide range (T), suspended sediment (m), standing biomass (B_s) and root:shoot quotient (ϕ). An interactive version of this model that can be found on at <http://jellyfish.geol.sc.edu/model/marsh/mem.asp>.

The MEM was used to calculate the current changes in marsh elevation at the three study sites, for both controls and fertilized plots using parameter values obtained from the biological experiments and environmental data previously described (**Table 7-2**). The mean square percentage error (MSPE) of the predicted rates of change was computed as $MSPE = 1/n \sum ((P_i - O_i)/O_i)^2$ where P_i and O_i are the predicted and observed rates of change of marsh elevations in the i^{th} SET site out of n sites. The model was also used to forecast the changes in marsh elevation and standing biomass over the next century using different forecasted rates of SLR.

Sea level was simulated using the function recommend by the NRC (1987) to simulate an acceleration in sea level (see Equation 7-6):

$$L(t) = 0.17t + vt^2 \quad (\text{Eq. 7-6})$$

where $L(t)$ is the eustatic SLR (cm) at a number of years from present (t) and v is a constant that depends on the value chosen for $L(100)$. The constant 0.17 was used by the IPCC (2007) to represent the present eustatic rate of SLR in cm/y, but for the present MCBCL study we used a value of 0.21, which was the current, local relative rate of SLR. Mean high water was computed as shown in Equation 7-7:

$$W_H(t) = W_A + L(t) + 3.1 * \sin(2\pi t / 18.6 - 0.512) \quad (\text{Eq. 7-7})$$

where W_A is the average tidal amplitude (cm), 3.1 is the amplitude (cm) of the solar annual cycle having a period of 18.6 years, and 0.512 is a phase shift.

Table 7-2. Parameter and variable inputs used for simulations of current and forecasted rates of change of marsh elevation in MCBCL salt marshes

Physical Inputs	Value	Unit
Century SLR	Variable ^a	Cm
Mean high water	70	cm NAVD88
Mean sea level	-2	cm NAVD88
Initial rate SLR	0.21	cm/y
Suspended sediment concentration	12	mg/L
Marsh elevation	Variable ^a	cm NAVD88

(continued)

Table 7-2. Parameter and variable inputs used for simulations of current and forecasted rates of change of marsh elevation in MCBCL salt marshes (continued)

Biological Inputs	Value	Unit
Maximum elevation	100	Cm
Minimum elevation	-30	Cm
Maximum peak biomass ^b	800	g/m ²
Organic matter decay rate	-0.6	1/y
BG Biomass ^c to shoot ratio	3	g/g
Refractory fraction (<i>kr</i>)	0.1	g/g
BG turnover rate	0.5	1/y
Maximum (95%) root depth	20	Cm
Trapping Coefficient and Settling Velocity Unit		
<i>Ks</i>	3.30E-02	cm ⁻¹ y ⁻¹
<i>Q</i>	1.36E-03	g cm ⁻³ y ⁻¹

^a SLR and initial marsh elevation were varied depending on scenario and site.

^b Maximum above-ground biomass of control and fertilized sites were 800 and 2,240 g/m², respectively.

^c BG Biomass is below-ground biomass, which includes roots and rhizomes.

Results and Discussion

Marsh Elevation: Current Status

Salt marshes of the MCBCL tend to be relatively low in elevation. Moreover, their elevations differed depending on their position east or west of the ICW. An analysis of LIDAR data showed that marshes west of the ICW have positive skewness (1.08) and a modal elevation of 8.2 cm. East of the ICW, marshes have a modal elevation of 21.6 cm and positive skewness (1.26, **Figure 7-8**).

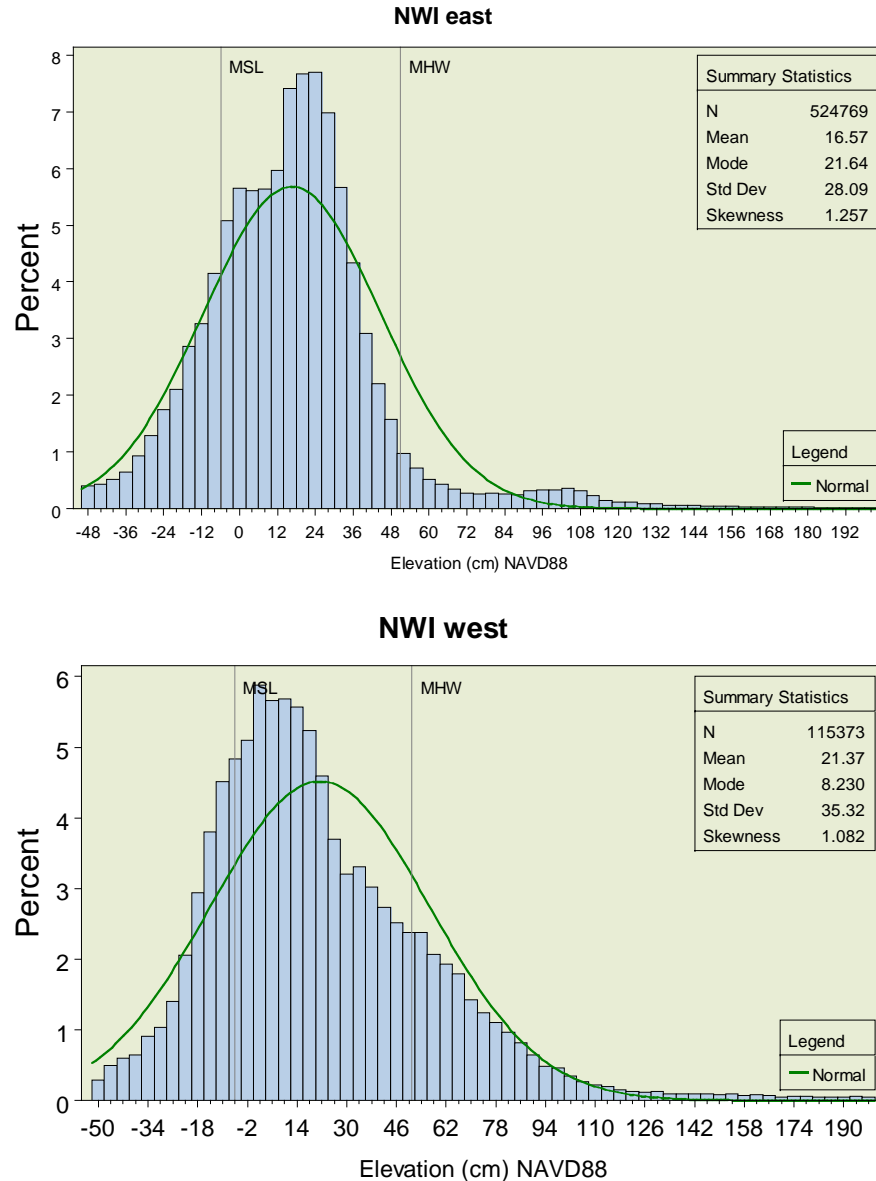


Figure 7-8. Frequency distributions of elevations of salt marsh habitat (top) east of the ICW and (bottom) west of the ICW (see Figure 7-7 for a map of these areas classified by the National Wetland Inventory as salt marsh).

Fertilization Study

Total standing biomass of *S. alterniflora* did not differ significantly among sites (FC, MB, or OB) (**Table 7-3**), and the treatment by site interaction was not significant. The mean EOS standing biomass derived from 2 years of harvest data (2008 and 2009) at the three study sites was $1,093 \pm 522 \text{ g/m}^2$ and $381 \pm 166 \text{ g/m}^2$ in sites fertilized with N+P and control sites, respectively, giving an N:P fertilized:control biomass ratio of 2.8. At the FC site where there was a factorial design, the mean responses to N fertilization and P fertilization were greater than the control, but these increases in biomass were not significant at the 5% level.

Table 7-3. Mean (± 1 standard deviation [SD]) standing biomass (live plus dead) of *Spartina alterniflora* by site[†] and treatment^{††}.

Site [†]	Treatment ^{††}	Biomass (g/m ²)
FC	C ^a	396 \pm 81
FC	N ^a	789 \pm 285
FC	P ^a	588 \pm 250
FC	N+P ^b	1542 \pm 320
MHB	C ^a	204 \pm 4
MHB	N+P ^b	824 \pm 550
OB	C ^a	543 \pm 124
OB	N+P ^b	912 \pm 585

Notes: Treatment codes with the same superscript letter are not significantly different. Otherwise, treatments differed significantly at the 5% level according to Scheffe's multiple comparison test.

[†] FC = Freeman Creek, MHB = Mile Hammock Bay, OB = Onslow Beach

^{††} C = control, N = nitrogen-fertilized, P = phosphorus-fertilized, N+P = fertilized with nitrogen and phosphorus

Marsh Bioassay (Marsh Organ) Experiment

Total EOS above-ground biomass of *S. alterniflora* was found to vary with marsh organ pipe elevation and by treatment (**Figures 7-9 and 7-10**). Nonlinear polynomial regressions on these data gave the following best fits:

$$\text{Control weights: } W_a = 15.7E - 0.2E^2 + 596, r^2 = 0.22$$

$$\text{Fertilized weights: } W_a = 8.8E - 0.35E^2 + 1144, r^2 = 0.07$$

where W_a is the total above-ground biomass (g/m²) and E is the elevation (cm). Elevation had a statistically significant effect on above-ground biomass in the controls ($p=0.039$), but not in the fertilized samples ($p=0.525$).

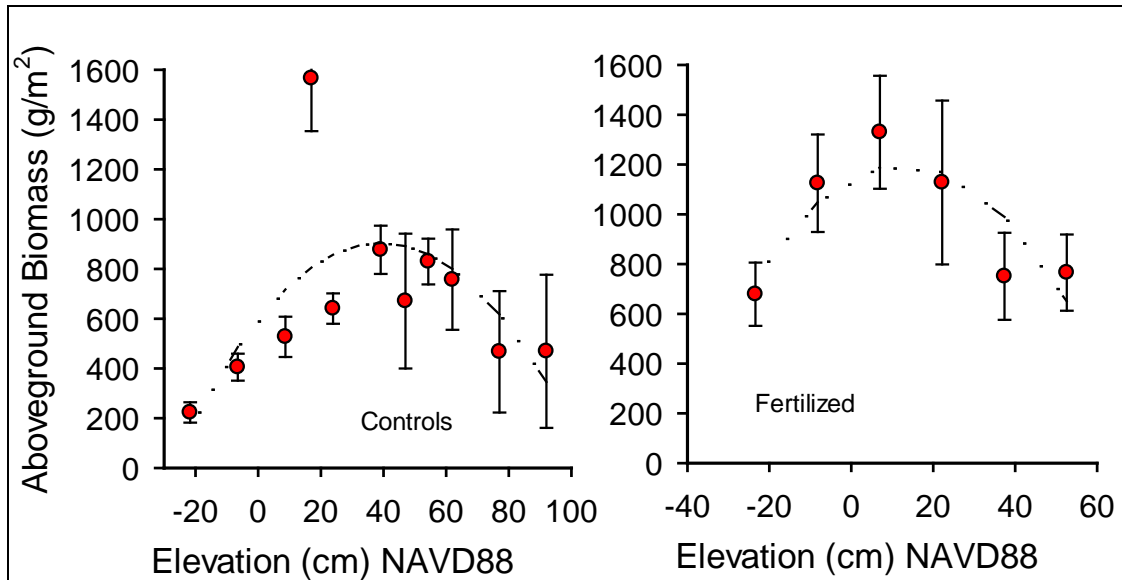


Figure 7-9. Total above-ground biomass of *S. alterniflora* as a function of elevation in controls (left) and fertilized treatments (right).

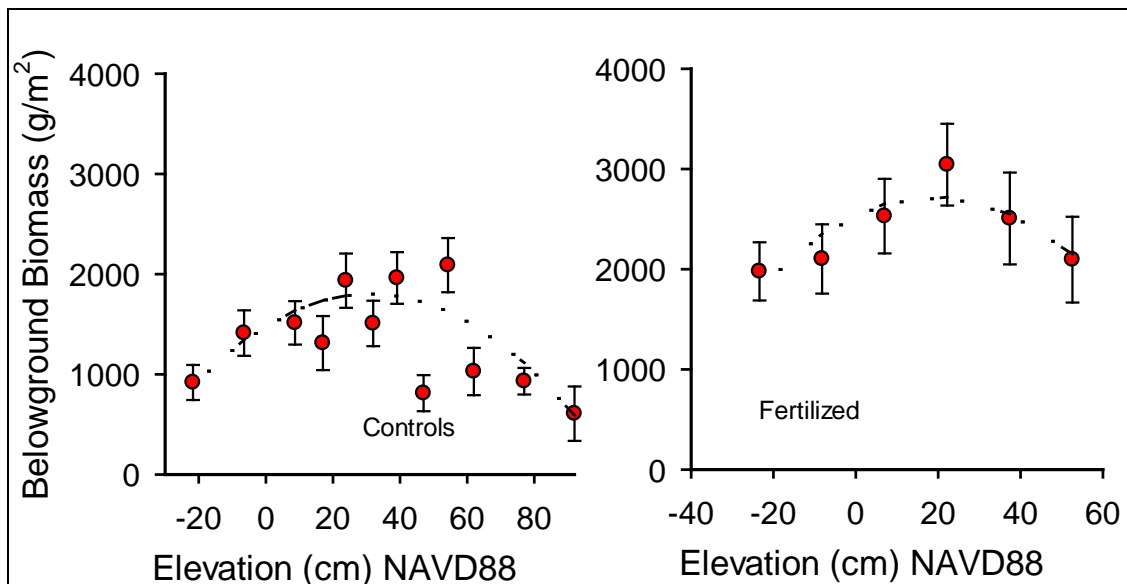


Figure 7-10. Total below-ground biomass of *S. alterniflora* as a function of elevation in controls (left) and fertilized treatments (right).

Total EOS below-ground biomass of *S. alterniflora* also was observed to vary with marsh organ pipe elevation and by treatment (**Figure 7-10**). Nonlinear polynomial regressions on these data gave the following best fits:

$$\text{Control weights: } W_b = 20E - 0.326E^2 + 1489, r^2 = 0.12$$

$$\text{Fertilized weights: } W_b = 19E - 0.505E^2 + 2545, r^2 = 0.03$$

where W_b is the total below-ground biomass (g/m^2) and E is the elevation (cm).

The fertilized treatment had significantly ($p < 0.0001$) greater above- and below-ground biomass than the controls (**Figures 7-9 and 7-10**). Averaged over all elevations, years, and sites, EOS above-ground biomass in the controls was $678 \pm 532 \text{ g/m}^2$ (± 1 standard deviation [SD]) and $936 \pm 750 \text{ g/m}^2$ in the fertilized treatment. Below-ground biomass in the controls was $1,487 \pm 1,006 \text{ g/m}^2$ and $2,376 \pm 1,643 \text{ g/m}^2$ in the fertilized treatment. Estimates of the optimum elevations, calculated from the first derivative of the polynomial ($dW/dE = 0 = a + bE$), were 39 cm and 31 cm for the above-ground biomass and 13 cm and 19 cm for below-ground biomass in control and fertilized treatments, respectively.

The mean ratio of total below-ground to above-ground biomass in the fertilized and control treatments, 1.1 and 1.4 respectively, did not differ significantly according to Tukey's multiple comparison test at $\alpha = 0.05$. However, the ratios of root:shoot (rhizomes excluded), 0.3 in fertilized and 0.6 in control treatments, differed significantly and in a direction that is entirely consistent with numerous studies (Asher and Ozanne, 1967; Caloin et al., 1980; Davidson, 1969; Hunt, 1975; Loneragan and Asher, 1967; McCain and Davies, 1983; Schlossberg and Karnok, 2011; Yeager and Wright, 1981) of effects of nutrients on root:shoot ratios. Furthermore, although the root:shoot ratio was lower in the fertilized treatment, the mean total below-ground biomass was significantly greater in the fertilized treatment (2.4 versus 1.5 kg/m^2).

Marsh Elevation: Rates of Change

The FC salt marsh site west of the ICW had the greatest rate of elevation gain, 9 mm/y (**Figure 7-11 and Table 7-4**) in spite of having a lower elevation than study areas east of the ICW. MHB and OB salt marshes had rates of elevation gain amounting to 2.3 mm/y and 2.6 mm/y, respectively. All three sites had rates of elevation gain that were approximately equal to or, in the case of FC, greater than the current rate of SLR.

Fertilization with a combination of N and P had a positive effect on elevation gain irrespective of site, and the stimulation was sustained throughout the 4 years of the study (**Figure 7-11**). The average increase in rate (the delta increase above the control rate) was $4.6 \pm 0.5 \text{ mm/y}$ (± 1 SD). Treatment with nutrients raised the rate of elevation gain from 4 mm/y to 5.1 mm/y at FC and OB, respectively.

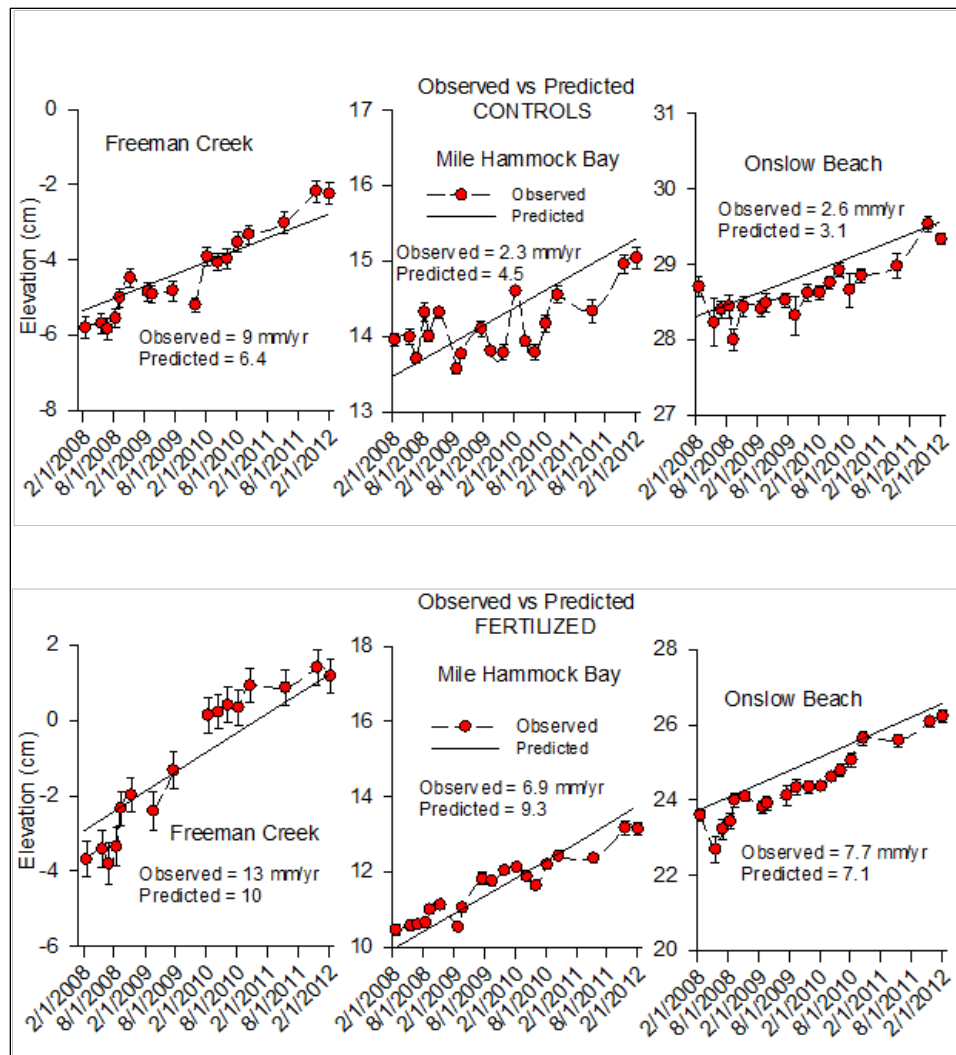


Figure 7-11. Measured surface elevations of marshes at FC, MHB, and OB over 4 years beginning in February 2008.

In general, fertilized sites had higher rates of elevation gain. This generality applies equally well to model predictions and observations.

Table 7-4. Observed rates of change of marsh elevation (mm/y) at the study sites, lower and upper 95% confidence limits (L95 and U96), and MEM predicted rates.

Study Site		Observed	L95	U95	Predicted
FC	Control	9	8	10	6.4
	Fertilized	13	11.1	15.2	10
MHB	Control	2.3	1.9	2.7	4.5
	Fertilized	6.9	6.4	7.4	9.3
OB	Control	2.6	2	3.2	3.1
	Fertilized	7.7	7	8.5	7.1

The MSPE of model predictions of the change in marsh elevation over the 4 year study, inclusive of all sites and treatments was 15%. Moreover, the predicted trends among sites and treatments were consistent with the observed rates. The predicted changes in marsh elevation at FC are greater than at sites east of the ICW because its elevation was significantly lower (depth greater) and from Equation 7-5 it can be seen that $dS/dt \propto D$. Predicted changes in elevation at fertilized sites are greater because their biomass was greater and from Equation 7-3 it can be seen that $dS/dt \propto B_s$.

Marsh Elevation: 100-Year Forecasts

MEM simulations of marsh elevation and biomass were made for different SLR scenarios (**Figure 7-12**). Simulations of control or ambient marsh sites showed that the vegetation survived 100 years only when sea level was assumed to rise either 24 cm or 60 cm by the end of a century, and in the case of the 60 cm rise the biomass was beginning to decline rapidly. The 24-cm scenario is essentially the current rate of relative SLR held constant. It was predicted to gain approximately 55 cm in elevation from a starting elevation of 0 cm, which indicates that at that rate of SLR, the starting elevation was less than the equilibrium elevation. By the end of the 100-year simulation, this marsh had reached its equilibrium, which is approximately 31 cm (55 cm final marsh elevation minus 24 cm increase in sea level). This is approximately the optimum elevation for the vegetation (**Figure 7-9**) and evidence that the current marsh landscape here is below its equilibrium elevation at current rates of SLR. Perhaps counter intuitively, predicted marsh elevation at the end of the century increased as the rate of SLR was increased (**Figure 7-12**). However, although the marsh elevation rises more quickly when sea level is raised, it cannot rise as quickly as sea level and its relative elevation declines.

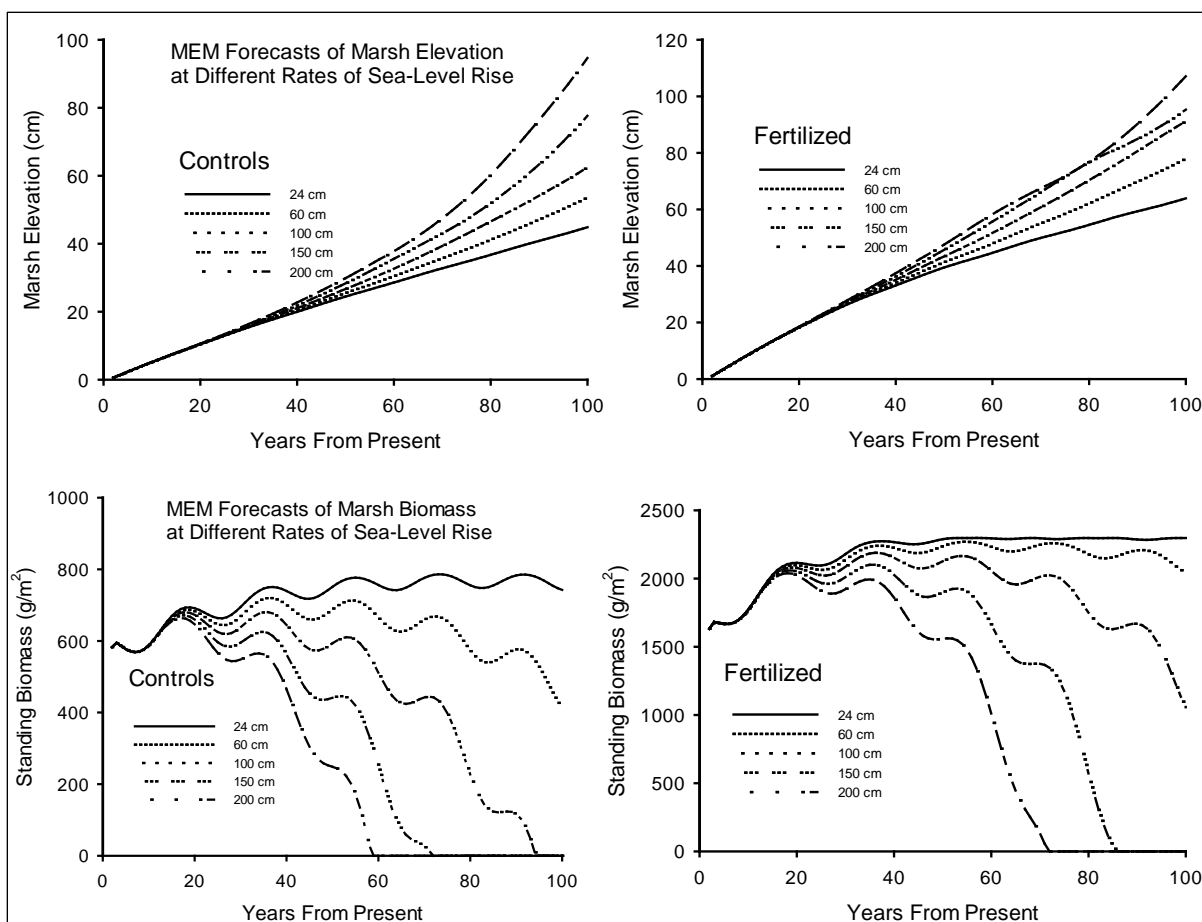


Figure 7-12. MEM forecasts of marsh elevation and standing biomass for different SLR scenarios.

Forecasts were made for ambient (controls) and fertilized marshes. The SLR scenarios ranged from a constant rate equivalent to 25 cm/y to a rapidly accelerating rate that raised mean sea level to 200 cm by the end of a century.

In simulations, fertilized sites fared better than controls (**Figure 7-12**). In the case of the constant, current rate of SLR, marsh elevation reached approximately 65 cm by the end of the century and its standing biomass approached the maximum. The 60 cm sea level simulation resulted in a biomass and elevation by the end of the century that also were nearly in equilibrium. Fertilized sites were also predicted to survive a 100-cm rise in sea level, although biomass was beginning to decline rapidly by the end of the century (**Figure 7-12**).

The survival times for the various simulations ranged from less than 60 years for ambient marshes that experience a 200 cm rate of SLR to greater than 100 years, depending on the sea level scenario and nutrient treatment (**Figure 7-13**). Extrapolating the curve (**Figure 7-13**) for ambient marsh or controls, it is predicted that control sites would survive no more than a century if sea level were to rise 80 cm in the next century. Fertilized marshes tolerate a higher rate of SLR; only at the highest rates of SLR, 150 and 200 cm, did the marshes succumb before the end of the century (**Figure 7-13**).

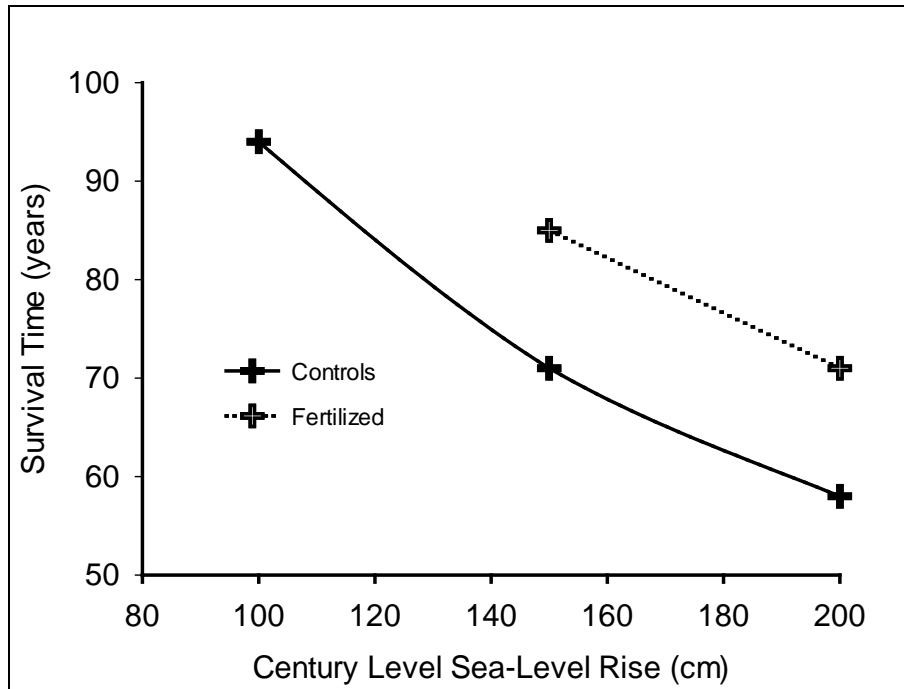


Figure 7-13. MEM-forecasted survival times of MCBCL marshes for different SLR scenarios ranging from a constant rate, equivalent to 25 cm/y, to a rapidly accelerating rate that raised mean sea level to 200 cm by the end of a century.

Conclusions and Implications for Future Research

Intertidal salt marshes typically occupy the upper half of the tidal frame (McKee and Patrick, 1988). The lower end of the vertical distribution is set by physiological tolerance of the vegetation to hypoxia, the upper limit is set by tolerance to osmotic stress (salinity and drought) (Mendelssohn and Morris, 2000). The absolute range is directly proportional to the tidal amplitude. Morris et al. (2005) hypothesized that the frequency distribution of marsh elevations from any specific marsh or estuary would (1) lie within the growth range of the vegetation, and (2) have a statistical distribution (skewness) that was diagnostic of resilience to SLR. The researchers argued that stable marshes that were most resilient would have elevations concentrated near the upper end of the vertical range and have a negative skew (**Figure 7-14A**), whereas the most vulnerable marshes would have elevations that were right skewed and concentrated near the lower end of the range (**Figure 7-14**).

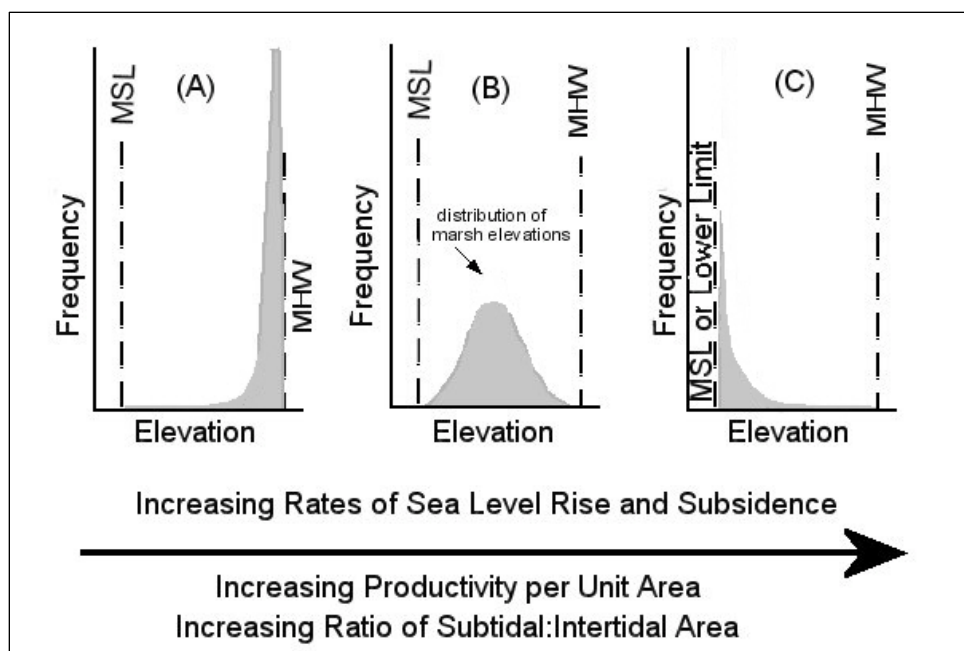


Figure 7-14. Demonstrated here are alternative frequency distributions of hypothetical marsh elevations (LIDAR) from different estuaries (from Morris et al., 2005).

The salt marshes of MCBCL provide some evidence in support of the concept that the relative elevations of marsh landscapes vary and demonstrate skewness in a direction that is diagnostic of their position. All of the marshes along the ICW between the New River and Browns Inlets have positive skew and are relatively low in elevation, and marshes west of the ICW are lower than marshes east of the ICW. Marshes west of the ICW have positive skew and a modal elevation of 8.2 cm in an estuary with MHW of approximately 50 cm. East of the ICW, marshes have a modal elevation of 21.6 cm and positive skewness (**Figure 7-7**).

The empirical results of the SET experiments and the MEM predictions indicate that the FC marsh is far from equilibrium with sea level. Its elevation is significantly lower than marshes east of the ICW, yet it had the highest rate of sediment accretion (**Figure 7-11** and **Table 7-4**). Model results (**Figure 7-12**) suggest that the equilibrium elevation of this marsh should be about 31 cm, and at the observed rate of 9 mm/y accretion (**Table 7-4**) and a -5 cm elevation (**Figure 7-11**) it should take this marsh no more than approximately 45 years to equilibrate with sea level rising at a rate of 0.25 cm/y.

The FC marsh is evidently much older than 45 years, so how can we explain the apparent contradiction that its elevation is low when its accretion rate is high? Predicting the response of the Freeman Creek marsh to SLR is complicated by the history and effects of dredging the ICW. The ICW is repeatedly dredged to a box cut-shaped channel on a 5-year cycle. We hypothesize that when this happens, the vertical walls of the channel begin to collapse and the adjacent marsh slumps into the channel (**Figure 7-15**). The same process likely occurs on both sides of the ICW, but over time the sediments on the east side have become sandier and less prone to collapse due to nourishment from the barrier island. The channel acts as a trap for sand and sediment eroded from the barrier island and this dune-derived sand and sediment never reaches the western shore. This is consistent with the analysis of frequency distributions made of LIDAR (**Figure 7-8**), and

suggests that marshes west of the ICW are more vulnerable to a rise in sea level than marshes east of the ICW. We refer to this as the “dredge and slump” model.

The dredge and slump model (**Figure 7-15**) has significant management implications. Firstly, the model predicts that the presence of the ICW, which was dredged originally through the backbarrier marshes, threatens the existence of the marshes. We foresee two possible outcomes: (1) the marshes, particularly those west of the ICW slump following a dredging event and rebuild, and exist on the edge of extinction in a state of dynamic equilibrium; and (2) the marshes rebuild, but never recover completely before the next dredging event, which would lead to eventual collapse. The ICW also threatens the survival of the coastal barrier because it is migrating to the west and toward the channel.

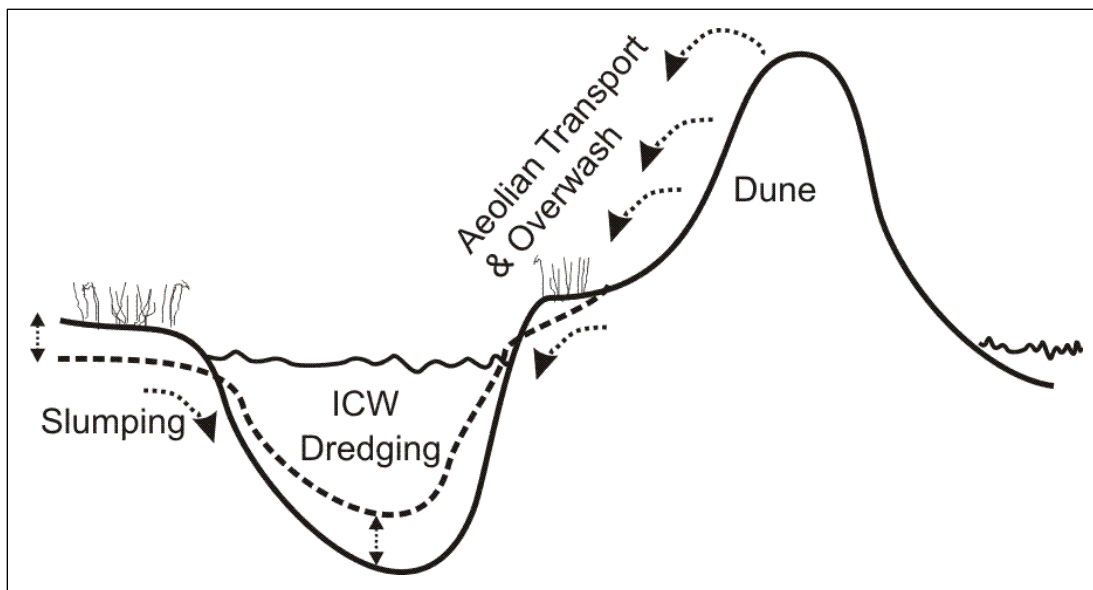


Figure 7-15. Conceptual “dredge and slump” model explaining how marshes west of the ICW could be presently far below the equilibrium elevation.

There are two management strategies that could mitigate the effect of the ICW on the surrounding marshes. These would be nutrient enrichment to enhance biomass production and sediment accretion and thin layer disposal of dredge spoil. Thin layer disposal is an alternative to the current practice of removing the dredged sediment from the system. The dredge would essentially spray a thin layer of sediment onto the marsh surface. This practice has been tested experimentally and has been shown to promote growth of healthy marshes for applications of as much as 17 cm of material (USACE, 1993). The marsh grass *S. alterniflora* appears to be adapted to burial with sediment and thrives (Deng et al. 2008; Fragoso and Spencer, 2008). There likely would be negative consequences for the infauna, but so would the loss of the marsh, and probably the negative effects would be temporary. Any solution will have costs and benefits.

The factorial fertilization study indicates that the salt marsh vegetation *S. alterniflora* at MCBCL is co-limited by N and P, and it is the increase in biomass on fertilized plots that raised the elevation of the marsh plots so significantly (**Figure 7-11**). Singular additions of N or P did not elicit a statistically significant increase in production, but the combined effect of N and P raised

the end-of-year standing biomass by a factor of 2.8 above the controls and raised the average rate of sediment accretion by 4.6 mm/y. Considering the options for nutrient sources for nutrient enrichment as a management strategy, the effluent from a waste water treatment facility is typically enriched with both macronutrients, N and P. Having a wetland treatment site with vegetation that is co-limited by both nutrients is desirable from the standpoint of nutrient removal. However, the possibility of collateral damage needs to be investigated before nutrient enrichment for marsh survival is put into practice. For example, there could be negative consequences for water quality.

Results from the harvest of vegetation in the marsh organ support the concept of an optimum elevation for growth of marsh vegetation (**Figures 7-9 and 7-10**). However, there are several important variables that are constant across elevations in the bioassay experiment, but uncontrolled in situ. These variables include drainage, tide range, nutrient availability, and interspecific competition. For example, significant variation among sites in tide range were documented (**Figure 7-5**). In addition, the bioassay experiment measures the fundamental niche (response to elevation in the absence of competition), while the actual distribution and growth response of species in the field is a manifestation of the realized niche. Consequently, results of a bioassay like those obtained from the marsh organ experiment should be used with caution and preferably in combination with field data.

Finally, the growth response (Equation 7-1) is depicted as being simply a function of depth below MHW. However, the growth response of the vegetation (Equation 7-1 and **Figures 7-9 and 7-10**) is species-specific and will vary with tide range and with variables such as salinity. In reality, the growth response is n-dimensional. For example, one can imagine a simple three-dimensional (3-D) response surface with salinity on one axis and elevation or depth on another. Tide range will add a fourth dimension because the shape of that 3-D surface will vary between micro- and macro-tidal estuaries, and so on. In conclusion, the model can be applied to other marsh ecosystems, but not without adjusting the parameter values (**Table 7-2**) to each specific marsh landscape. That can be as simple as adjusting the tide range and suspended sediment concentration for salt marshes dominated by *S. alterniflora*, or it can be much more complex.

Literature Cited

- Asher, C.J., and P.G. Ozanne. 1967. Growth and potassium content of plants in solution cultures maintained at constant potassium concentrations. *Soil Science* 103:155–156.
- Barbier, E.B., S.D. Hacker, C. Kennedy, E.W. Koch, A.C. Stier, and B.R. Silliman. 2011. The value of estuarine and coastal ecosystem services. *Ecological Monographs* 81:169–193.
- Bindoff, N.L., J. Willebrand, V. Artale, A. Cazenave, J. Gregory, S. Gulev, K. Hanawa, C. Le Quéré, S. Levitus, Y. Nojiri, C.K. Shum, L.D. Talley, and A. Unnikrishnan. 2007. Observations: Oceanic climatic change and sea level. In *Climate Change 2007: The Physical Science Basis—Contribution of Working Group I to the Fourth Assessment Report of the Intergovernmental Panel on Climate Change*. Edited by S. Solomon, D. Qin, M. Manning, Z. Chen, M. Marquis, K.B. Averyt, M. Tignor, and H.L. Miller. Cambridge University Press: Cambridge, United Kingdom and New York, NY.
- Cahoon, D.R., J.C. Lynch, P. Hensel, R. Boumans, B.C. Perez, B. Segura, and J.W. Day Jr. 2002. A device for high precision measurement of wetland sediment elevation: I. Recent improvements to the sedimentation-erosion table. *Journal of Sedimentary Research* 72(5):730–733.
- Cahoon, L.B. 1999. The role of benthic microalgae in neritic ecosystems. *Oceanography and Marine Biology: An Annual Review* 37:47–86.
- Caloin, M., A. El Khodre, and M. Atry. 1980. Analysis of the time course of change in nitrogen content in *Dactylis glomerata* L. using a model of plant growth. *Annals of Botany* 54:69–76.
- Church, J.A., N.J. White, T. Aarup, W.S. Wilson, P.L. Woodworth, C.M. Domingues, J.R. Hunter, and K. Lambeck. 2008. Understanding global sea levels: Past, present, and future. *Sustainability Science, Special Feature* 3(1):9–22.
- Craft, C., J. Clough, J. Ehman, S. Joye, R. Park, S. Pennings, H. Guo, and M. Machmuller. 2009. Forecasting the effects of accelerated sea-level rise on tidal marsh ecosystem services. *Frontiers in Ecology* 7:73–78.
- Craft, C.B. 2007. Freshwater input structures soil properties, vertical accretion, and nutrient accumulation of Georgia and U.S. tidal marshes. *Limnology and Oceanography* 52(3):1220–1230.
- Davidson, R.L. 1969. Effects of soil nutrients and moisture on root/shoot ratios in *Lolium perenne* L. and *Trifolium repens* L. *Annals of Botany* 33:571–577.
- Day, Jr., J.W., and P.H. Templet. 1989. Consequences of sea level rise: Implications from the Mississippi delta. *Coastal Management* 17:241–257.

- Deng Z., S. An, C. Zhao, L. Chen, C. Zhou, and Y. Zhi. 2008. Sediment burial stimulates the growth and propagule production of *Spartina alterniflora* Loisel. *Estuarine Coastal and Shelf Science* 76:818–826.
- Donnelly, J.P., and M.D. Bertness. 2001. Rapid shoreward encroachment of salt marsh cordgrass in response to accelerated sea-level rise. *Proceedings of the National Academy of Sciences of the United States of America* 98:14218–14223.
- Fagherazzi, S., M. Marani, and L. Blum (Eds). 2004. The ecogeomorphology of tidal marshes. *Coastal and Estuarine Studies* 59. (268 pages).
- Fitzgerald, D.M., M.S. Fenster, B.A. Argow, and I.V. Buynevich. 2008. Coastal impacts due to sea-level rise. *Annual Review of Earth and Planetary Sciences* 36:601–647.
- Fragoso, G., and T. Spencer. 2008. Physiographic control on the development of *Spartina* marshes. *Science* 322:1064.
- Friedrichs, C.T., and J.E. Perry. 2001. Tidal salt marsh morphodynamics: A synthesis. *Journal of Coastal Research* 27:7–37.
- Harrison, A.F., and K.L. Bocock. 1981. Estimation of soil bulk-density from loss-on-ignition values. *Journal of Applied Ecology* 8:919–927.
- Hunt, R. 1975. Further observations on root-shoot equilibria in perennial ryegrass (*Lolium perenne* L.). *Annals of Botany* 39:745–755.
- IPCC (Intergovernmental Panel on Climate Change). 2007. *Climate Change 2007: The Physical Science Basis: Contribution of Working Group I to the Fourth Assessment Report of the Intergovernmental Panel on Climate Change*. Cambridge University Press. Available at http://www.ipcc.ch/publications_and_data/publications_and_data_reports.shtml.
- Jeffrey, D.W. 1970. A note on the use of ignition loss as a means for the approximate estimation of soil bulk density. *Journal of Ecology* 58:297–299.
- Jordan, T.E., D.L. Correll, and D.F. Whigham. 1983. Nutrient flux in the Rhode River: Tidal exchange of nutrients by brackish marshes. *Estuarine Coastal and Shelf Science* 17:651–667.
- Kirwan, M.L., and A.B. Murray. 2007. A coupled geomorphic and ecological model of tidal marsh evolution. *Proceedings of the National Academy of Sciences of the United States of America* 104:6118–6122.
- Kirwan, M.L., G.R. Guntenspergen, A. D’Alpaos, J.T. Morris, S.M. Mudd, and S. Temmerman. 2010. Limits on the adaptability of coastal marshes to rising sea level. *Geophysical Research Letters* 37, L23401 (5 pages).

- Kneib, R.T. 1997. The role of tidal marshes in the ecology of estuarine nekton. Pp. 163–220 in *Oceanography and Marine Biology: An Annual Review*. Edited by A.D. Ansell, R.N. Gibson, and M. Barnes. Kluwer Academic Publishers.
- Knutson, P.L. 1988. Role of coastal marshes in energy dissipation and shore protection. Pp. 161–175 in *The Ecology and Management of Wetlands*. Edited by D.D. Hook, W.H. McKee, Jr., H.K. Smith, J. Gregory, V.G. Burrell, Jr., M.R. DeVoe, R.E. Sojka, S. Gilbert, R. Banks, L.H. Stolzy, C. Brooks, T.D. Matthews, and T.H. Shear. Timber Press: Portland, OR.
- Krone, R.B. 1985. Simulation of marsh growth under rising sea levels. Pp. 106–115 in *Hydraulics and Hydrology in the Small Computer Age*. Edited by W.R. Waldrop. Hydraulics Division of the American Society of Civil Engineers.
- Loneragan, J.F., and C.J. Asher. 1967. Response of plants to phosphate concentration in solution culture. II. Rate of phosphate absorption and its relation to growth. *Soil Science* 103:311–318.
- McCaffrey, R.J., and J. Thomson. 1980. A record of the accumulation of sediment and trace metals in a Connecticut salt marsh. Pp. 165–236 in *Advances in Geophysics Estuarine Physics and Chemistry: Studies in Long Island Sound*. Edited by S. Barry. Elsevier.
- McCain, S., and M.S. Davies. 1983. Effects of pretreatment with phosphate in natural populations of *Agrostis capillaries* L. 1. Influences on the subsequent long-term yield of, and accumulation of phosphorus in plants grown from tillers. *New Phytologist* 94:367–379.
- McKee, K.L., and W.L. Patrick. 1988. The relationship of smooth cordgrass (*Spartina alterniflora*) to tidal datums: A review. *Estuaries* 11:143–151.
- Meehl, G.A., J.M. Arblaster, and C. Tebaldi. 2007. Contributions of natural and anthropogenic forcings to changes in temperature extremes over the United States. *Geophysical Research Letters* 34, L19709. (5 pages).
- Mendelssohn, I.A., and J.T. Morris. 2000. Ecophysiological controls on the growth of *Spartina alterniflora*. Pp. 59–80 in *Concepts and Controversies in Tidal Marsh Ecology*. Edited by N.P. Weinstein, and D.A. Kreeger. Kluwer Academic Publishers.
- Möller, I., T. Spencer, J.R. French, D. Leggett, and M. Dixon. 1999. Wave transformation over salt marshes: A field and numerical modelling study from North Norfolk, England. *Estuarine Coastal and Shelf Science* 49:411–426.
- Morris, J.T. 2007. Ecological engineering in intertidal saltmarshes. *Hydrobiologia* 577:161–168.
- Morris, J.T. 2006. Competition among marsh macrophytes by means of geomorphological displacement in the intertidal zone. *Estuarine and Coastal Shelf Science* 69:395–402.

- Morris, J.T. 2005. Effects of changes in sea level and productivity on the stability of intertidal marshes. Pp. 121–127 in *Lagoons and Coastal Wetlands in the Global Change Context: Impacts and Management Issues*. Proceedings of the International Conference, ICAM Dossier N3, United Nations Educational, Scientific, and Cultural Organization. Edited by P. Lasserre, P. Viaroli, and P. Campostrini.
- Morris, J.T. 1991. Effects of nitrogen loading on wetland ecosystems with particular reference to atmospheric deposition. *Annual Review of Ecology and Systematics* 22:257–279.
- Morris, J.T., J. Edwards, S. Crooks, and E. Reyes. 2012. Assessment of carbon sequestration potential in coastal wetlands. Pp. 517–531 in *Recarbonization of the Biosphere: Ecosystem and Global Carbon Cycle*. Edited by R. Lal, K. Lorenz, R. Hüttl, B.U. Schneider, and J. von Braun. Springer.
- Morris, J.T., D. Porter, M. Neet, P.A. Noble, L. Schmidt, L.A. Lapine, and J. Jensen. 2005. Integrating LIDAR elevation data, multispectral imagery and neural network modeling for marsh classification. *International Journal of Remote Sensing* 26:5221–5234.
- Morris, J.T., P.V. Sundareshwar, C.T. Nietch, B. Kjerfve, and D.R. Cahoon. 2002. Responses of coastal wetlands to rising sea level. *Ecology* 83:2869–2877.
- NRC (National Research Council). 1987. *Responding to Changes in Sea Level: Engineering Implications*. National Academy of Sciences, Washington, DC. (160 pages).
- Rahmstorf, S. 2007. A semi-empirical approach to projecting future sea-level rise. *Science* 315:368–370.
- Redfield, A.C. 1972. Development of a New England salt marsh. *Ecological Monographs* 42:201–237.
- Reed, D.J. 1995. The response of coastal marshes to sea-level rise: Survival or submergence? *Earth Surface Processes and Landforms* 20:39–48.
- Richardson, K., W. Steffen, H.J. Schellnhuber, J. Alcamo, T. Barker, D.M. Kammen, R. Leemans, D. Liverman, M. Munasinghe, B. Osman-Elasha, N. Stern, and O. Waever. 2009. *Climate Change: Global Risks, Challenges and Decisions. Synthesis Report*. International Alliance of Research Universities. Available at <http://climatecongress.ku.dk/pdf/synthesisreport>.
- Schlossberg, M.J., and K.J. Karnok. 2011. Root and shoot performance of three creeping bentgrass cultivars as affected by nitrogen fertility. *Journal of Plant Nutrition* 24:535–548.
- Shepard, C.C., C.M. Crain, and M.W. Beck. 2011. The protective role of coastal marshes: A systematic review and meta-analysis. *PLoS ONE* 6:e27374.

- Turner, R.E., E.M. Swenson, and C. S. Milan. 2001. Organic and inorganic contributions to vertical accretion in salt marsh sediment. Pp. 583–595 in *Concepts and Controversies in Tidal Marsh Ecology*. Edited by M. Weinstein, and D. Kreeger.
- USACE (U.S. Army Corps of Engineers). 1993. *Environmental Effects of Dredging Technical Notes: Managing Dredged Material Via Thin-Layer Disposal in Coastal Marshes*. Technical Report EEDP-01-32. U.S. Army Engineer Waterways Experiment Station.
- Valiela, I., and J.M. Teal. 1979. The nitrogen budget of a salt marsh ecosystem. *Nature* 280:652–656.
- Vermeer, M., and S. Rahmstorf. 2010. Global sea level linked to global temperature. *Proceedings of the National Academy of Sciences of the United States of America* 106:21527–21532.
- Yeager, T.H., and R.D. Wright. 1981. Influence of nitrogen and phosphorus on shoot:root ratio of *Ilex crenata* Thunb. “Helleri.” *HortScience* 16:564–565.

[This page intentionally left blank.]

Appendix 7-A

List of Scientific Publications

List of Scientific Publications

Papers

Morris, J.T., J. Edwards, S. Crooks, and E. Reyes. 2012. Assessment of carbon sequestration potential in coastal wetlands. Pp. 517–531 in *Recarbonization of the Biosphere: Ecosystem and Global Carbon Cycle*. Edited by R. Lal, K. Lorenz, R. Hüttel, B.U. Schneider, and J. von Braun. Springer.

Master's Thesis

Priest, B. 2011. Effects of elevation and nutrient availability on the primary production of *Spartina alterniflora* and the stability of southeastern coastal salt marshes relative to sea level rise. M.S. Thesis. University of South Carolina, Columbia, SC. (73 pages).

Appendix 7-B

List of Students

- Brant Priest. Master of Science. Marine Science Program, University of South Carolina, Columbia, SC. 2011.

[This page intentionally left blank.]

Chapter 8

Forecasting Influence of Natural and Anthropogenic Factors on Estuarine Shoreline Erosion Rates

SERDP Project Number: RC-1413

Coastal Wetlands Module

Research Project CW-2

Lead Researchers:

Drs. Mark Fonseca* and Carolyn Currin
National Oceanic and Atmospheric Administration
National Ocean Service
National Centers for Coastal Ocean Science—Beaufort

* Current address:
Continental Shelf Associates
8502 SW Kansas Avenue
Stuart, FL 34997

E-mails: fonseca.mark@gmail.com and carolyn.currin@noaa.gov

Amit Malhotra
JHT
National Oceanic and Atmospheric Administration
National Ocean Service
National Centers for Coastal Ocean Science—Beaufort

May 10, 2013

Final

This report was prepared under contract to the U.S. Department of Defense (DoD) Strategic Environmental Research and Development Program (SERDP). The publication of this report does not indicate endorsement by DoD, nor should the contents be construed as reflecting the official policy or position of DoD. References herein to any specific commercial product, process, or service by trade name, trademark, manufacturer, or otherwise, do not necessarily constitute or imply its endorsement, recommendation, or favoring by DoD.

Table of Contents

List of Acronyms	8-vii
Abstract.....	8-1
Objectives of the Research Project	8-2
Objectives	8-2
Alternate Hypotheses	8-2
Background	8-2
Section 1: NRE Shoreline Types, Erosion Rate, and Sediment Input	8-4
Materials and Methods.....	8-4
Results and Discussion	8-13
Section 2: ICW Erosion Rates and Boating Impacts	8-34
Materials and Methods.....	8-34
Results and Discussion	8-45
Conclusions and Implications for Future Research	8-58
Section 1: NRE Shoreline Types, Erosion Rate, and Sediment Input	8-58
Section 2: ICW Waterway Erosion Rates and Boating Impacts.....	8-60
Literature Cited	8-62
Appendix 8-A: List of Scientific Publications.....	8-A-1

List of Figures

8-1. Number of hurricanes affecting eastern North Carolina, by decade.....	8-11
8-2. Surface wave height (m) chart of NRE for the top 5% of wind events (2007–2010).	8-15
8-3. Cumulative frequency plot of top 5% of wind events for the NRE (2007–2010).	8-16
8-4. Surface wave energy (J m^{-1} wave crest) chart of the NRE for the top 5% of wind events (2007–2010).....	8-17
8-5. Seafloor shear stress (pascals) for the NRE with some sediment resuspension “hot spots” indicated.	8-18
8-6. Distribution of NRE shoreline types by RWE class, as determined using WEMO.	8-19
8-7. Number of hardened shoreline segments in the NRE, NC, by wave energy class.	8-21
8-8. Shoreline erosion (m y^{-1}) by shoreline type and four wave energy classes for the “Early” period (1956–1989) in the NRE, NC.	8-25
8-9. Shoreline erosion (m y^{-1}) by shoreline type and four wave energy classes for the “Recent” period (1989–2004) in the NRE, NC.	8-25

8-10.	Location of modified shorelines in the NRE, and illustration of overlap with low-energy shoreline sections.	8-28
8-11.	Location of modified shorelines in the NRE, and illustration of overlap with medium-energy shoreline sections.....	8-29
8-12.	Location of modified shorelines in the NRE, and illustration of overlap with high-energy shoreline sections.	8-30
8-13.	Location of modified shorelines in the NRE, and illustration of overlap with highest-energy shoreline sections.	8-31
8-14.	Topographic map of MCBCL showing existing saltmarsh (light green), some of the primary shore side facilities (beige) and the +1-m isobath (red) for SLR.	8-32
8-15.	Map of MCBCL showing existing saltmarsh (yellow), overlaying a map of surface slopes as a guide to where saltmarsh may transgress landward with SLR.....	8-33
8-16.	Water surface elevation data from ICW site illustrating boat wake and tidal signals (data shown here are from April 12, 2010).....	8-36
8-17.	Boat wake signatures extracted after running high pass filter (data shown here are from April 12, 2010).	8-37
8-18.	Boat wake signatures extracted after removing the tidal signal and data within the range of ± 5 cm of the threshold value (data shown here are from April 12, 2010).....	8-37
8-19.	Boat wake signatures extracted (blue diamonds) overlaid with boat wake wave heights (red squares; data shown here are from April 12, 2010).	8-38
8-20.	Boat wake signatures extracted (blue diamonds) overlaid with boat wake wave heights (red squares) for zoomed in for a 1-hour window as shown in 8-18 inside the red rectangular box.....	8-39
8-21.	Test bed area at MCBCL in the lower NRE and ICW for assessment of boat wake effects in comparison to wind waves (n=290).	8-41
8-22.	The location of splash points; military vehicle ingress and egress points for crossing the ICW.....	8-42
8-23.	The MHB marsh showing location of vegetation plots (dark green rectangles), elevation benchmarks (green and yellow triangles), and digitized LCAC tracks.....	8-44
8-24.	Cumulative frequency of V-hull boats by size and speed transiting MCBCL during April and May 2008.....	8-46
8-25.	Cumulative frequency distributions comparing both ICW boat wakes and NRE wind wave heights.....	8-47
8-26.	Frequency count of locations where boat wakes exceed the background, 95 th percentile wind waves in the test bed.	8-49
8-27.	Forecast showing areas where observed boat wakes in the ICW over a 16-month period exceed wind waves of the 95 th percentile.	8-50
8-28.	Maps of the SCR within the ICW from New River Inlet to Browns Inlet, NC.	8-53

8-29.	Maps showing the calculated width (m) of the ICW in 1938, 1956, 1989, and 2009.....	8-54
8-30.	Map of ICW splash point locations (A) and SCRs (B-G).	8-55
8-31.	Bar graph showing salt marsh and open water area (ha) in the MHB LCAC operation area as determined from aerial photography.....	8-56
8-32.	Maps of the MHB area displaying the 1956 shoreline (yellow) on the (A) 1956 imagery and (B) 2004 imagery, where LCAC tracks are visible.....	8-57

List of Tables

8-1.	Flow diagram of the shoreline characterization scheme used in ground-truthing fieldwork.	8-9
8-2.	Listing of the horizontal precision, distance to corresponding points within each time period, and the mean distance of each time periods for the 16 GCPs collected in the field.	8-10
8-3.	RWE ($j \text{ m}^{-1}$ wave crest) classes created by binning percentiles from cumulative frequency distribution of shoreline wave climates in the NRE, NC.....	8-12
8-4.	Summary of shoreline length for each shoreline type as classified through aerial and field ground-truthing methods.....	8-19
8-5.	Shoreline change rate (m y^{-1}) as determined using aerial photography in NRE. SCR given as mean and standard error; n=number of segments used in analysis per shoreline type.	8-20
8-6.	Two-way ANOVA comparing erosion rates by shoreline type and wave energy class in the NRE 1956-1989(Early period).....	8-21
8-7.	Two -way ANOVA comparing erosion rates by shoreline type and wave energy class in the NRE 1989–2004 (Recent period).....	8-22
8-8.	ANOVA comparing erosion rates by wave class type irrespective of shoreline type in the NRE 1956–1989 (Early period).	8-22
8-9.	ANOVA comparing erosion rates by wave class type irrespective of shoreline type in the NRE 1989–2004 (Recent period).....	8-22
8-10.	ANOVA comparing erosion rates by shoreline type irrespective of wave class in the NRE 1956–1989 (Early period).	8-22
8-11.	ANOVA comparing erosion rates by shoreline type irrespective of wave class in the NRE 1989–2004 (Recent period).....	8-23
8-12.	Estimated volume of sediment liberated via Sediment Bank erosion in the NRE.....	8-26
8-13.	Mean SCR (m y^{-1}) calculated from aerial photography for ICW shorelines within MCBCL. Shoreline type determined from field survey conducted in 2009 (n=number of points per shoreline type).....	8-51

8-14. Mean SCR (m y^{-1}) calculated from aerial photography of the shoreline area surrounding military splash points 1989 to 2009 (mean, standard error).	8-52
8-15. Mean percent particle size and organic matter (OM) content of sediment collected offshore from Marsh and Splash Point (SP) shorelines at three water depths. VF = very fine; M = medium.	8-53

List of Acronyms

μm	Micrometer
$^{\circ}\text{C}$	degrees Celsius
ANOVA	analysis of variance
CCFHR	Center for Coastal Fisheries and Habitat Research
chl <i>a</i>	chlorophyll <i>a</i>
cm	Centimeter
CW	Coastal Wetlands (Module)
DCERP	Defense Coastal/Estuarine Research Program
DGPS	differential global positioning systems
DoD	U.S. Department of Defense
DSAS	Digital Shoreline Analysis System
ESA	Estimated Spectral Analysis
ESTCP	Environmental Security Technology Certification Program
ft	Feet
GB	Gigabyte
GCP	ground control point
GEODAS	Geophysical Data System
GIS	geographic information systems
GPS	global positioning system
ha	Hectare
ha y^{-1}	hectares per year
H_s	significant wave height
Hz	Hertz
ICW	Intracoastal Waterway
J m^{-1}	joules per meter
JONSWAP	Joint North Sea Wave Project
kg/m^3	kilograms per cubic meter
km^2	Square kilometer
LCAC	Landing Craft Air Cushion
LIDAR	Light Detection and Ranging
LWT	Linear Wave Theory
m	Meter
m y^{-1}	meters per year
m^2	square meter
MARDIS	Monitoring and Research Data Information System
m^3	cubic meter
$\text{m}^3 \text{ y}^{-1}$	cubic meters per year

MARDIS	Monitoring and Research Data and Information System
MB	Megabyte
MCBCL	Marine Corps Base Camp Lejeune
MHB	Mile Hammock Bay
MHBC	Mile Hammock Bay Creek
MHBL	Mile Hammock Bay LCAC
mm	Millimeter
mm y ⁻¹	millimeters per year
NAVD88	North American Vertical Datum of 1988
NDBC	National Data Buoy Center
NGDC	National Geophysical Data Center
NOAA	National Oceanic and Atmospheric Administration
NRE	New River Estuary
OM	organic matter
RWE	Representative Wave Energy
SCR	shoreline change rate
SERDP	Strategic Environmental Research and Development Program
SLR	sea level rise
USACE	U.S. Army Corps of Engineers
UTM	Universal Transverse Mercator
WEMo	Wave Exposure Model

Abstract

The Coastal Wetlands (CW) Team investigated factors affecting the sustainability of coastal salt marshes on Marine Corps Base Camp Lejeune (MCBCL), and the role of salt marsh habitats within the coastal ecosystem. The Research Project CW-2 Module assessed shoreline erosion rates on MCBCL, and the relative impacts of military training, wind wave and boat wake energy, and shoreline type on erosion rates. We also examined the impact of specific military training activities on coastal wetlands habitats, calculated the contribution of eroding sediment banks to the New River Estuary (NRE) sediment budget, and provide recommendations for management of MCBCL shorelines.

The NRE shoreline is primarily Sediment Bank (55%), and a substantial amount has been Modified, or hardened (22%). Shoreline erosion rates along the mainstem of the NRE for the period 1956–2004 ranged from -0.08 m y^{-1} for Swamp Forest shorelines to -0.38 m y^{-1} for Sediment Bank shorelines. Overall, shoreline erosion rates were higher during the period 1989–2004 than the 1956–2004 period. High and medium relief Sediment Banks, defined as greater than 3 m and 1–3 m in height respectively, exhibited mean erosion rates of approximately -0.5 m y^{-1} . Generally, Saltmarsh shorelines exhibited lower erosion rates than Sediment Bank shorelines across all wave energy environments, and Saltmarsh shorelines were found in all wave energy classes. A subset of Sediment Bank shorelines included a narrow fringing marsh (less than 5 m in width), and these shorelines had significantly lower shoreline erosion rates than Sediment Banks without fringing marsh. Wave energy along the NRE is primarily from wind waves, whereas wave energy on Intracoastal Waterway (ICW) shorelines is primarily from boat wakes. The ICW shoreline is primarily Saltmarsh (greater than 75%), and only a small portion (less than 5%) has been hardened. In contrast to results along the NRE, ICW shoreline erosion rates were higher in the period 1956–1989 than the 1989–2009 period. This difference is likely due to an initial erosive period after establishment of the ICW in 1938 as a narrow channel, and the lower impact of storms and wind waves on ICW erosion rates. Analysis of aerial photographs revealed that the average width of the ICW increased from approximately 70 m in 1938 to more than 145-m wide in 2009.

We found that the current rate of military training exercises, including Landing Craft Air Cushion (LCAC) operations at Mile Hammock Bay, have a relatively minor impact on MCBCL marshes. Several splash points along the ICW do exhibit slightly higher erosion rates and may be candidates for shoreline stabilization. We identified areas in both the NRE and ICW where shoreline hardening may be replaced by marsh restoration efforts, based on site-specific wave energy characteristics.

We estimated the annual input of sediment into the NRE via sediment bank erosion to be approximately $17,500 \text{ m}^3 \text{ y}^{-1}$. This volume of sediment is approximately half of that required for salt marshes to keep up with current rates of sea level rise (2.7 mm y^{-1}). This estimate also demonstrates the potential importance of coastal marshes in trapping sediments and maintaining water quality in the NRE.

Keywords: Marine Corps Base Camp Lejeune, New River Estuary, shorelines, erosion, waves, wave energy, wave height, Wave Exposure Model (WEMo), military, boats, vessels, Intracoastal Waterway (ICW), wetlands, saltmarsh, Defense Coastal/Estuarine Research Program (DCERP), Strategic Environmental Research and Development Program (SERDP).

Objectives of the Research Project

Objectives

Research Project CW-2 objectives were to

1. Classify shorelines by wind wave energy using the National Oceanic and Atmospheric Administration's Wave Exposure Model (WEMo)
2. Identify shorelines where boat wake energy significantly increases total wave energy
3. Quantify effect of military training on shoreline erosion
4. Evaluate vegetation and ecosystem services of shoreline habitats along estuarine physico-chemical gradients
5. Integrate shoreline habitat classification and erosion rate with wave energy assessments to inform shoreline management practices
6. Provide data to estimate the contribution of sediment loading to the estuary via shoreline erosion
7. Develop a spatially registered predictive model of estuarine shoreline erosion and resuspension
8. Develop a Base-wide shoreline erosion protection plan

Alternate Hypotheses

1. Exposure to wind wave energy is not a significant factor in shoreline erosion on MCBCL.
2. Military activities and recreational boating do not contribute significantly to shoreline erosion in MCBCL.
3. Shoreline does not affect shoreline erosion rates on MCBCL.
4. Storm events do not alter shoreline sediment accretion or erosion rates.

Background

Our studies were part of the Coastal Wetlands (CW) Module of the Defense Coastal/Estuarine Research Program (DCERP). The efforts of the CW Module were designed to support the long-term sustainability of important coastal resources necessary for training at Marine Corps Base Camp Lejeune (MCBCL), and the U.S. Department of Defense's (DoD's) military mission.

Coastal wetlands are a vital component of the estuarine landscape that link terrestrial and freshwater habitats with the sea (Levin et al., 2001). Marshes improve water quality by serving as nutrient transformers and trapping sediment, attenuating wind wave and boat wake energy,

providing critical habitat area for a diverse group of estuarine organisms, serving as nursery habitat for commercially important fishery species, helping stabilize the coastal barriers, accreting sediments and building land, and providing recreational opportunities for people (Jordan et al., 1983; Kneib, 1997; Knutson, 1988; Moller et al., 1999; Morris, 1991; Valiela and Teal, 1979).

The coastal wetlands of this module are defined as the vegetated and non-vegetated intertidal habitat in salt and brackish waters and include marshes and adjacent mudflats, sandflats, and tidal creeks. Marshes within the MCBCL region are typically dominated by smooth cordgrass (*Spartina alterniflora*) and black needle rush (*Juncus roemerianus*). Although these marshes represent less than half of the designated wetlands on MCBCL, they are the only wetlands that directly adjoin (or sometimes intersect) amphibious military training exercises and they are also the only wetlands that play a role in coastal barrier island stabilization.

The area of marsh in the New River Basin represents approximately 10% of the surface area of open water and, given the ability of marshes to trap sediments and transform nutrients (Morris et al., 2002; Tobias et al., 2001) have an impact on water quality. Marshes also provide a platform over which the barrier dune system can migrate, and the dunes protect the marshes from erosive wave energy that would otherwise degrade them. Likewise, the marsh can migrate over the terrestrial landscape in response to rising sea level.

The CW Module's monitoring activities and research projects have been designed as an integrated program. The monitoring activities included measuring surface elevation of marshes, tracking changes in spatial extent over time, measuring shoreline position, and monitoring nutrients in shallow groundwater within the marsh zone. The stations established for the monitoring activities were used directly by the research projects of this module to determine the response of the coastal marsh to added nutrients, to model the impacts from wind and boat wakes on shoreline erosion vulnerability, and to evaluate the impacts of hydraulic and nutrient exchange in coastal wetlands. This report focuses on shoreline erosion, wave regimes and vessel wake effects.

Given the importance of the estuarine shoreline for military training activities, as well as its role in protecting MCBCL infrastructure, it is crucial that research be conducted to address estuarine shoreline erosion within the New River Estuary (NRE). A previous study by the U.S. Army Corps of Engineers (USACE, 2001) estimated recession rates in the NRE ranging from 0.1 (0.03 m) to 1.7 ft (0.52 m) per year, though these estimates do not include effects of the hurricanes that impacted MCBCL post-1988. The study also noted that many of the shoreline stabilization efforts, including revetments, were unstable and had failed (USACE, 2001). The study recommended that a shoreline management plan be developed to protect upland areas (which are being lost at a rate of 0.81 ha y^{-1}), man-made structures and training areas, and fishery and wetlands habitat (USACE, 2001). Shoreline stabilization of the land-water interface on the high wave energy oceanfront has been studied extensively (USACE, 1977), but shoreline erosion on estuarine coasts is less well understood (NRC, 2000). Wave energy is the putative, primary force driving estuarine shoreline erosion, and models have been developed to predict marsh vegetation and community composition based on wave energy (Keddy, 1982; Roland and Douglass, 2005). Our ability to predict and mitigate estuarine shoreline erosion is complicated by the fact that the wave environment in estuarine waters is also changing as a result of more and

larger-sized boats and their wakes (Crawford et al., 1998; Kennish, 2002). This is particularly an issue in the NRE, which is traversed by the Intracoastal Waterway (ICW) and supports a variety of military vessels and landing craft, as well as commercial and recreational watercraft.

The importance of salt marshes in attenuating wave energy and protecting estuarine shorelines from erosion has been documented in numerous field studies (e.g., Knutson, Broome et al., 1992), and more recently, the protective role of coastal wetlands in reducing hurricane impacts has been demonstrated (Fitzgerald et al., 2008; Gedan et al., 2011). This ability of salt marshes has led to efforts to incorporate marsh vegetation into shoreline stabilization efforts (Currin et al., 2010), although additional research is needed to determine the physical settings in which vegetated shoreline can be effective (Roland and Douglass, 2005)

Section 1: NRE Shoreline Types, Erosion Rate, and Sediment Input

Materials and Methods

Study site—NRE: We defined our study area as having two parts, the NRE and the ICW. We separate these areas largely because of their fundamentally different geomorphology and genesis. The NRE is a natural-formed, broad waterbody with many tributaries and shoreline types. In contrast much of the ICW is a narrow, ditch-like structure created by dredging. Here we describe the work that took place in the NRE and reserve a separate section for work on the ICW (**Section 2, ICW Erosion Rates and Boating Impacts**).

The NRE is a fifth-order, black water stream located entirely within Onslow County in North Carolina (Mallin et al., 2005). The NRE drains a catchment area of approximately 1,436 km² and consists of a series of shallow (1–2 m), broad lagoons of varying salinities, from full oceanic salinity at the mouth of the estuary and tidal freshwater components anastomosing off of the main body of the estuary. The mouth of the estuary is constrained by barrier islands and a series of natural upland peninsulas that together, restrict flushing, and result in the typical net migration of sand into the mouth of the estuary and the ICW, which traverses the NRE and MCBCL just landward of the barrier islands; much of the area adjacent to the estuary proper consists of the MCBCL which was chosen as the DCERP site for a variety of reasons, including the following:

- NRE watershed, which borders the site, is relatively small and, therefore, manageable
- MCBCL occupies a substantial portion (approximately 80%) of the NRE shoreline
- A barrier island and coastal dune system occurs within MCBCL's boundary that provides a unique and mission critical amphibious assault training environment
- The variety of ongoing military operations at MCBCL enables researchers to examine training impacts on a broad range of coastal habitat types the results of which may be applicable to other DoD installations.

Wind wave energy assessment: We used the National Oceanic and Atmospheric Administration's (NOAA's) Wave Exposure Model (WEMo¹) to conduct shore-to-shore wave

¹ NOAA Coastal Services Center. Wave Exposure Model. Available at <http://www.csc.noaa.gov/digitalcoast/tools/wemo/index.html>.

height, wave energy, and seafloor shear stress chart products to guide identification of erosion “hot spots.” The wave forecasting component of WEMo returned the following values for each point selected within the waterbody:

- XYZ coordinates in UTM (Universal Transverse Mercator)
- Wave energy (J m^{-1} wave crest)
- Maximum wave height
- Significant wave height
- Significant direction of waves
- Average wave period
- Maximum wave period.

We used WEMo to create wave energy (J m^{-1}) and wave height chart products over a spatially registered structured geographic information systems (GIS) grid (200 m on center) based on NOAA shoreline shapefiles, local bathymetry (NOAA Coastal Relief Model² augmented by additional local surveys; see below) and wind data covering the 3 years (2008–2010) from National Data Buoy Center (NDBC) Buoy 41035. Although innumerable combinations of wind data may be used, convention calls for use of exceedance events (top 5% of wind speed events; Keddy, 1982; Kelly et al., 2001) because these are the most likely to produce changes in habitat organization and distribution.

Unfortunately preliminary WEMo runs and calibration exercises revealed substantial problems with the quality of the previously existing NRE bathymetric data. Thus, a bathymetric survey of shallow near-shore areas was conducted by the Center for Coastal Fisheries and Habitat Research (CCFHR), NOAA in the NRE during October and November 2008 and was fused with the bathymetric survey conducted by DCERP in 2009. The NOAA survey was conducted on three separate dates (i.e., October 27, November 5, and November 24) and covered the western shore along with the head of the estuary and French Creek on the eastern shore. The area surveyed was selected based on the existing gaps in the GEODAS (Geophysical Data System) data collected by NOAA and USACE. The extent of the survey stretched from the shore until a lateral distance of 1 km in the river, this was accomplished by surveying a series of transects to include all the shallow waters. A flat-bottom boat fitted with Lowrance depth sounder LCX135 and connected to Trimble Pro XT global positioning system (GPS) unit was used for the purpose. Bathymetry data were collected at an interval of 2 seconds, and a total of 30,000 pings were collected each having a GPS X, Y coordinates. Filtering the data to remove the false readings produced approximately 25,000 georeferenced soundings that were converted to an ArcGIS shapefile. The tidal corrections obtained from a DCERP-maintained the tide gauge installed in Gottschalk Marina were added to the bathymetry soundings. Additional and more extensive bathymetric surveys were conducted by other DCERP-funded researchers, including the ICW. We fused these three bathymetric data sources and produced both a wave energy and seafloor erosion chart products to assist in identifying “hot spots” of wave energy and sediment

² National Geophysical Data Center (NGDC). NGDC Coastal Relief Model. Available at <http://www.ngdc.noaa.gov/mgg/coastal/starterm.htm>.

movement that could then be linked with shoreline change rate (SCR). From this bathymetry and the aforementioned buoy data, a complete NRE wave height and benthic shear (sediment movement) map set was created to help forecast locations of potential erosion and sediment resuspension sources.

As the DCERP evolved it became clear that we needed to not only forecast wave energy at the water surface, but to provide a seafloor shear stress computation. Although there may be high wave energy at the water surface, if the water is sufficiently deep then no tractive force will be transferred to the seafloor and sediments will not be moved or resuspended. Because surface wave energy and sediment movement may be uncoupled through bathymetric effects the presence of high waves and wave energy are not adequate to predict areas of suspected erosion; therefore, we developed a new component of WEMo that returned the following values at the seafloor along with the previously described (significant) wave height, wave power and wave energy:

- Horizontal velocity
- Shear stress
- Critical shear stress (sediment particle size specific)
- Sediment motion test (Yes/No) based on Equation 8-1.

Two different methods were made available in a new version (4.0) of WEMo for calculating the bottom orbital velocities and shear stress. The first method used Linear Wave Theory (LWT). According to linear wave theory bottom orbital velocities are proportional to wave height and water depth. For small amplitude and monochromatic waves, horizontal orbital velocity was calculated using Equation 8-1.

$$u_b = \frac{H_s \pi}{T \sinh(kh)} \quad (\text{Eq. 8-1})$$

where, u_b is orbital velocity, H_s is wave height (m), T is wave period (s), h is water depth (m), and k is wave number (m^{-1}). Velocities calculated using LWT are in good agreement with observed flow under monochromatic waves except very near the bottom where friction plays a significant part because linear theory assumes frictionless bottom. Shear stress was calculated using the velocity profile method and Karman-Prandtl equations for boundary layers Equation 8-2 (Bowden, 1962):

$$\tau_b = \frac{\rho f_w}{2} u_b^2 \quad (\text{Eq.8-2})$$

where, u_b was orbital velocity, f_w was friction factor and ρ was water density (kg/m^3).

Alternatively, WEMo can also utilize the Estimated Spectral Analysis (ESA) method to calculate bottom orbital velocities from estimated wave spectra as compared to the LWT method that uses a monochromatic wave for calculation. Under natural conditions the wave climate is typically represented by a spectrum of waves of different frequencies, amplitudes and directions. Because

WEMo only outputs significant wave height H_s and peak wave period T_s , a potentially more robust way to obtain orbital velocities was to fit a realistic surface elevation spectrum to these two parameters (Soulsby, 1987). The full wave spectra was then estimated from different general forms of wind-generated wave spectra, including Pierson and Moskowitz (1964) spectrum, the Joint North Sea Wave Project (JONSWAP) spectrum (Hasselmann et al., 1973), and modifications of each (Donelan et al., 1985; Mitsuyasu et al., 1980). WEMo used JONSWAP spectra for the estimating the wave conditions because of its wider acceptability and ease of use (Wiberg and Shorewood, 2008). The JONSWAP general spectrum rescaled in terms of H_s was calculated as shown in Equation 8-3:

$$S_{\eta}(f) = \frac{\chi H_s^2 f_p^4}{16 f^5} \left(\frac{f}{f_p} \right)^{\xi} \exp \left[-\beta \left(\frac{f}{f_p} \right)^{-4} \right] \gamma e^{\exp[-(f-f_p)^2/(2\sigma^2 f_p^2)]} \quad (\text{Eq. 8-3})$$

where, f is frequency, f_p is peak frequency and $\beta, \xi, \gamma, \sigma$ are parameters that adjust the magnitude and shape of the spectrum and χ was the function of dimensionless peak frequency f_p ; typical values for the JONSWAP parameters are as follows:

JONSWAP parameters	β	ξ	γ	σ
	0.33	0	3.3	0.7 for $f/f_p \leq 1$ or 0.9 for $f/f_p > 1$

The calculated surface-wave spectra S_{η} allowed the calculation of spectrum of wave induced bottom orbital velocity S_u using Equation 8-4.

$$S_{u,i} = \frac{4\pi^2}{T_i^2 \sinh^2(k_i h)} S_{\eta,i} \quad (\text{Eq. 8-4})$$

From this, bottom orbital velocity was calculated by summing $S_{u,i}$ at each frequency as in Equation 8-5.

$$u_{br} = \left(2 \sum S_{u,i} \Delta f_i \right)^{1/2} \quad (\text{Eq. 8-5})$$

The ESA method often estimates orbital velocities which are closer to actual conditions due to the random nature of sea waves and the presence of more than one wave frequency although in many areas with simple geomorphology and the 6-hour minimum time recommended for using WEMo, both methods often return similar results (not shown).

From these computations of bottom velocities, we then added predictions of sediment motion at the seafloor depending on the user-provided sediment characteristics: mean sediment particle diameter and sediment particle density. Default values in the model were set for siliceous medium sand (200- μm diameter and 2,650 kg/m^3 particle density). With these additional data, WEMo calculated critical shear stress for movement of that sediment size and density and then

compared it to the calculated wave induced shear stress for each sample point selected by the user. Equations 8-6 through 8-10 calculate the critical shear stress for given sediment characteristics.

$$\nu = (1.14 - 0.031(T_s - 15) + 0.00068(T_s - 15)^2) 10^{-6} \quad (\text{Eq. 8-6})$$

$$S_* = \frac{\phi_{sed}}{4\nu} \left[\left(\frac{\rho_{sed}}{\rho_{sea}} - 1 \right) g \phi_{sed} \right]^{1/2} \quad (\text{Eq. 8-7})$$

$$SS_c = 0.095 S_*^{(-2/3)} + 0.056 (1 - \exp\left(\frac{-S_*^{(3/4)}}{20}\right)) \text{ if } S_* \geq 0.8$$

$$\text{and} \quad (\text{Eq. 8-8})$$

$$SS_c = 0.1 S_*^{(-2/7)} \text{ if } S_* < 0.8$$

$$u_* = \left[\left(\frac{\rho_{sed}}{\rho_{sea}} - 1 \right) g \phi_{sed} \right]^{1/2} S_*^{(-2/7)} \quad (\text{Eq. 8-9})$$

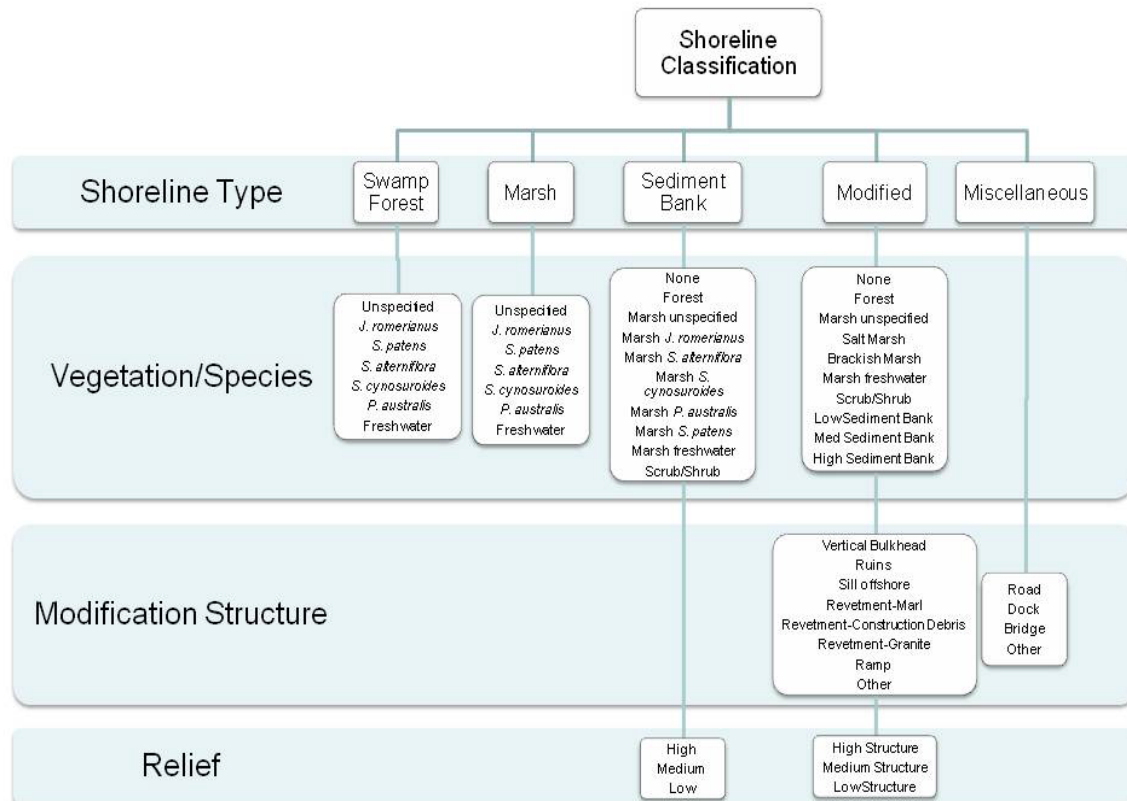
$$\tau_c = u_*^2 \rho_{sea} \quad (\text{Eq. 8-10})$$

where, ν is kinematic viscosity, T_s is sea temperature in Celsius, ϕ_{sed} is sediment diameter (m), ρ_{sed} is particle density (kg/m^3), ρ_{sea} is sea water density (kg/m^3), u_* is shear velocity (m/s), τ_c is shear stress (Pa).

Shoreline survey and classification: Shoreline habitat type was initially characterized using aerial photography. We evaluated available imagery and selected the 2004 true color imagery, which had a scale of 1:12500, a 0.61 m horizontal accuracy, and resolution of $0.30 \text{ m pixel}^{-1}$. We developed a shoreline type classification scheme, in consultation with MCBCL and N.C. Division of Coastal Management staff, which was consistent with other shoreline mapping efforts (Cowart et al., 2010). Shoreline sections were assigned to one of five shoreline types (i.e., Swamp Forest, Saltmarsh, Sediment Bank, Modified, or Miscellaneous), and a shapefile of shoreline types was created using ArcGIS. In 2009, preliminary ground-truthing of the assigned shoreline types revealed that the imagery did not provide accurate shoreline characterization and the decision was made to ground-truth the entire shoreline of the NRE. The shoreline characterization was conducted by small boat using Trimble differential global positioning systems (DGPS) equipment and a laptop with ArcGIS software. A Trimble Pro XH DGPS was used to collect points along the shoreline at modification structures such as dock corners. ArcGIS software was used to edit the data layer of shoreline habitat types that had been created using the 2004 aerial photography. We supplemented the original designation of five shoreline types by creating a matrix of additional GIS attributes that could be determined in the field, including

information on vegetation type or species, modification type, and relief of sediment banks and shoreline structures (**Table 8-1**). The matrix provided a unique four-digit identifying code for each possible combination of attributes.

Table 8-1. Flow diagram of the shoreline characterization scheme used in ground-truthing fieldwork.



GCPs collected to determine error of NRE imagery datasets: Ground control points (GCPs) were collected to determine the rectification error associated with each imagery dataset. The GCPs were usually located at road intersections, building corners, or other infrastructure that was identifiable in all three time periods used in the analysis (i.e., 1956, 1989, and 2004; **Table 8-2**). Twenty GCPs were identified within the three imagery datasets; however, due to changes that have occurred since 2004 and access issues, only 16 GCPs were collected (**Table 8-2**). GCP's were collected using a Trimble ProXH receiver with Zephyr antenna and stored in a Ranger hand-held computer running Trimble Terrasync v.2.61. Data were post-processed and transferred to ArcGIS using Trimble Pathfinder Office v3.10.

Table 8-2. Listing of the horizontal precision, distance to corresponding points within each time period, and the mean distance of each time periods for the 16 GCPs collected in the field.

Unique GCP Point ID	Horizontal Precision	Distance (m)		
		2004	1989	1956
3	0.6	4.49	6.84	3.04
6	0.7	1.23	3.17	7.35
9	1.1	3.36	5.15	6.46
15	0.9	3.17	2.13	3.17
18	1.0	0.34	6.63	5.18
21	0.6	3.37	3.75	0.95
27	1.0	0.94	5.42	4.36
30	0.7	2.38	5.74	3.04
33	0.6	2.95	7.91	5.36
36	0.4	1.53	0.77	4.04
45	1.0	4.63	2.76	7.23
48	0.6	3.92	3.97	4.66
51	0.6	1.78	4.77	10.76
54	0.6	6.42	8.11	6.31
60	0.6	2.42	1.78	3.63
63	0.4	5.56	7.57	6.93
Mean		3.03	4.77	5.15

Shoreline change rates: Aerial photography from 1956, 1989 and 2004 was used to digitize the NRE shoreline edge. The wet-dry line was delineated on sediment shorelines, and the vegetation boundary was used on vegetated shorelines (Boak and Turner, 2005; Cowart et al., 2010). The point-based method (Cowart et al., 2010) was used to measure the SCR at 50 m intervals for the intervals 1956–1989 (Early period), 1989–2004 (Recent period), and 1956–2004 (Total period). To test the effect of shoreline type and wave energy on observed erosion rates we conducted two-way analyses of variances (ANOVAs) for both the Early and Recent periods.

Wave energy regime versus shoreline erosion: To understand the potential influence of waves impacting the shoreline, shoreline-type specific SCRs were compared with Representative Wave Energy (RWE; J m^{-1} wave crest) values determined using WEMo³. For this exercise, we used WEMo to calculate wave energy at the shoreline considering both local bathymetry and wind data along the entire NRE shoreline using points every 50 m. Wind data were not available with the precision needed to run WEMo before 1985; therefore, we used hourly wind data from nearby Cape Lookout as a representative wind field for all analyses, which assumes wind events during these time periods have had inter-annual consistency of extreme events.

³ WEMo was developed at CCFHR. For more information about WEMo, see the NOAA Coastal Services Center's Web site at <http://www.csc.noaa.gov/digitalcoast/tools/wemo/index.html>.

To examine the assumption of consistent extreme wind events, we examined historical records with respect to extreme events, from 1950 through 2008, the average number of hurricanes per decade⁴ has been 31 (1950s = 24; 1960s = 23; 1970s = 32; 1980s = 32; 1990s = 36; 2000–2008: 39; decadal std. dev. 6.4), but have increased linearly over the decades (**Figure 8-1**) indicating that extreme events could be contributing disproportionately to erosion among what we term the Recent period (1989–2004; 15 years). Moreover, from 1956 to 1989 sea level has risen approximately 90 mm, which could have exacerbated erosion and instigated modification of NRE shorelines.

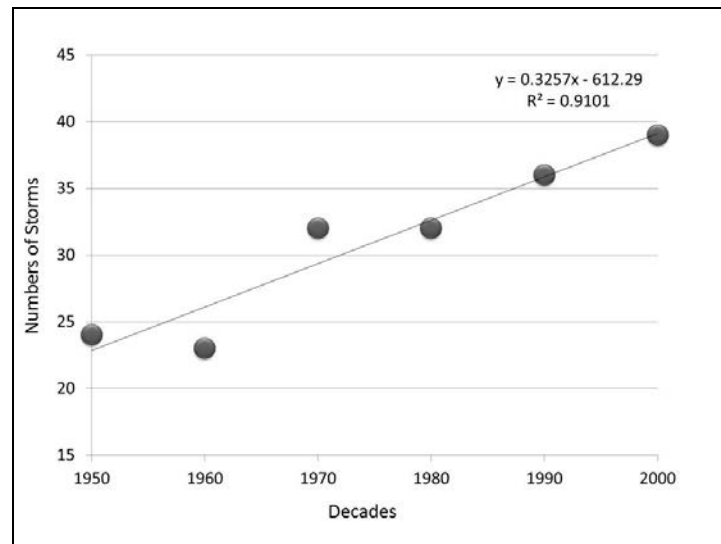


Figure 8-1. Number of hurricanes affecting eastern North Carolina, by decade.

A cumulative frequency plot was developed for the RWE values for all the shoreline points. Because of the typical, highly skewed distribution of wind events, we created binned wave categories (**Table 8-3**). Having only three useful imagery sets spanning decades inherently limited our ability to detect year to year influence of shoreline armoring on erosion. This is because we could only classify shoreline type based on the 2009 field-based survey given that shoreline type could not be readily defined from the aerial photography (some shorelines were overgrown, and, based on field survey, even shorelines with an unobstructed aerial view often were found to have revetment hardening that was not obvious even in the best, recent imagery available). Thus, we applied the 2009 shoreline-type categories to each 50-m point in the 1956, 1989, and 2004 photography, even though we could not know when in the past a particular shoreline point may have been modified.

⁴ http://en.wikipedia.org/wiki/List_of_North_Carolina_hurricanes

Table 8-3. RWE (J m^{-1} wave crest) classes created by binning percentiles from cumulative frequency distribution of shoreline wave climates in the NRE, NC.

RWE Class	RWE	Percentiles
3	≥ 583	Top 5 th
2	< 583 and ≥ 337	75 th –95 th
1	< 337 and ≥ 184	50 th –75 th
0	< 184	Bottom 50 th

Projecting the present-day condition of the shoreline back onto the erosion levels from 1956–1989 provided insight as to what erosion levels were present that likely provoked later modification. One other source of error in associating shoreline erosion with the modification status (or lack of modification) is when a shoreline was modified late in the period of time between images; this would cause us to associate erosion observed during that time with the “modified” category when in fact it was un-modified most of that time period; thus timing of hardening among imagery dates has the potential to cause the wave energy–shoreline erosion relationship in terms of SCR to be conservative from the standpoint of hardening effectiveness. However, keeping these potentially confounding issues in mind, analysis of the two time periods still provided interesting comparisons regarding shoreline vulnerability and stabilization choices. Because the bathymetry data did not align with the most recent, available digital shoreline (2004) the nearest bathymetric cell for each shoreline point was determined using the ArcInfo Near tool. A point was created at the nearest bathymetry cell and WEMo was then run from each of the nearest bathymetric points. The RWE values calculated within WEMo were then paired with their associated shoreline point. The shoreline points SCRs and RWE values were then plotted according to shoreline type (2009) for all points along the NRE shoreline (here we report on the following categories: Saltmarsh, Sediment Bank with and without Saltmarsh fringe, Swamp Forest, and Modified [subgroups of which included revetments, vertical bulkheads, and stone sills]).

In 2009, we completed evaluation of shoreline erosion as a function of both shoreline type (Modified, Saltmarsh, Sediment Bank, and Swamp Forest) and wave energy. In addition, to understanding how the shoreline management of the NRE over the past 50 years has influenced erosion, we calculated shoreline erosion rates for 50-m sections of the entire NRE shoreline between each of the imagery sets available (i.e., 1956, 1989, and 2004).

Based on past analysis of wind data over much longer time periods using the wind data from Cape Lookout, NC (not shown), we determined that a 3-year dataset is highly representative for estimated wind wave development for any other time period as well. Therefore, we used our recent wave energy maps to provide a basis for comparing the change in shoreline type among imagery sets with the corresponding shoreline erosion that occurred among imagery dates. We used these results to develop detailed shoreline management recommendations for MCBCL.

Sediment loading: We combined the shoreline characterization mapping results (collected the summer of 2009) with SCR measures (based on aerial photography from 1956, 1989, and 2004) to estimate the annual volume of sediment liberated to the NRE via sediment bank erosion. In the shoreline characterization scheme, Sediment Bank shorelines were placed into three categories

based on visual estimation during field surveys; high (greater than 3-m bank height), medium (1- to 3-m bank height), and low (less than 1-m bank height). Assuming a height of 3 m for high relief banks, 2 m for medium relief banks, and 0.5 m for low relief banks, we estimated annual sediment volume using Equation 8-11 as follows:

$$V = R \ R_{scr} \ L \quad (\text{Eq. 8-11})$$

where,

V = Annual sediment volume ($\text{m}^3 \text{ y}^{-1}$)

R = Relief height (m)

R_{scr} = Relief SCR (m y^{-1})

L = Length of sediment bank shoreline (m)

Restoration and Sea Level Rise Planning: As part of our commitment to MCBCL, we evaluated the information derived from this study in the context of restoration and mitigation options. First, we utilized information regarding the distribution of natural Saltmarsh across wave energy regimes and compared that to where shoreline hardening had taken place. From this, we created chart products of locations where conversion of modified shorelines to living shorelines would be feasible. We also created chart products where “hot spots” of erosion were most likely to be found and therefore should receive special scrutiny for performance of existing hardening and potential erosion of living shorelines. We make recommendations of shoreline management options based on the shoreline community and wave regime. Additionally, we created initial assessments of where MCBCL facilities would be affected by a +1-m rise in sea level.⁵

Results and Discussion

Wind wave energy: The wave height map product revealed the strong northern component of the top 5% wind events, making south-facing shores comparatively protected (**Figure 8-2**). Maximum wave heights approach 0.4 m for the most exposed shorelines; the ICW had comparatively low wind wave energy conditions. The cumulative frequency distribution of wave heights (**Figure 8-3**) indicates that the median wave height was 0.22 m, and the 95th percentile wave height was approximately 0.38 m. However, in the most exposed areas of the NRE, maximum wave heights were forecast to slightly, but rarely, exceed 0.5 m (not shown).

Wave energy distribution closely resembles the wave height distribution (**Figure 8-4**) with differences being driven by the non-linear relationship of wave energy to wave height (wave energy proceeding as the square of wave height). However, the distribution of sediment (benthic) shear stress (the driver for sediment movement and sediment resuspension events; **Figure 8-5**) revealed a very different pattern only loosely coupled to the water surface-based wave height and energy because of the exponential decay of surface wind wave effects to the seafloor as a function of water depth. The entrance to Wallace Creek emerged as an area of very high shear stress as did Duck Creek and the entire north side of the peninsula at the south gate of the Base. The entrance to French Creek also has a moderately elevated zone of resuspension at its mouth.

⁵ We have also provided a preliminary storm surge and wave energy assessment for MCBCL that may be found on the DCERP Web site.

This suggests that any discharge from these creeks in particular could often be passing an area of high resuspension capacity, which could enhance the liberation of any water column sediments or nutrients emerging from these creeks' watersheds into the rest of the estuary. Thus, sediment and nutrient loading into these creeks in particular should receive special attention from managers.

In addition to the creek mouths, many zones and "hot spots" of potential sediment resuspension were identified (**Figure 8-5**). The isolated nature of these locations (as compared to the geographically broad surface wave energy classifications) can help guide water quality sample stratification (e.g., suspended solids, chlorophyll *a* [chl *a*], turbidity overall) and reveal where additional military training activities (such as splash points) should potentially be limited given the potential for sediment resuspension and downstream water quality effects.

Shoreline survey and classification: An initial ground-truth survey comparing shoreline classifications made from the 2004 aerial imagery with field observation revealed frequent errors of classification. By conducting a field survey of the entire shoreline in 2009, we reduced the unclassifiable shoreline to zero and found substantial changes in all other shoreline classes (**Table 8-4**). In particular, what was previously classified as Sediment Bank was frequently found to be Saltmarsh, Modified, or Swamp Forest. Unlike the natural shoreline habitat classes, we suspect that the increase in modified shoreline percentage was in part due to real increases in shoreline hardening between 2004 and 2009. Over half of the NRE shoreline, approximately 63 km, is Sediment Bank. Most of this is low-relief (less than 1-m height), with approximately 5 km of medium relief (1- to 3-m height) and 15 km-high relief (greater than 3-m height). Field surveys noted that a narrow marsh fringe was associated with a small percentage (8%) of Sediment Bank shorelines. Approximately one-fifth of the NRE shoreline has been modified, or hardened. Revetments (loose rubble or rip-rap composed of granite, marl or construction material) accounted for 18% of the NRE shoreline, 3% of the vertical bulkhead, and 0.005% of the stone sills. Vegetated shoreline, including Saltmarsh and Swamp Forest, constitute 21% and 6%, respectively (**Table 8-4**).

Sediment Banks and Modified shorelines are found more often in higher wave energy settings, but all shoreline types occur in all wave energy classes, with the exception that Swamp Forest was not found in the highest wave energy class. The cumulative frequency distribution of wave energy on NRE shorelines shows that overall, half of NRE shorelines have a RWE less than 184 j m^{-1} . The large majority of Saltmarsh shorelines (88%) are found in RWE wave Classes 0 and 1 (**Table 8-4**), as are 73% of Sediment Bank shorelines and 72% of Modified shorelines (**Figure 8-6**). Revetments occurred in all wave classes but comparatively fewer were found in the highest wave class (**Figure 8-6**). Similarly, stone sills were located only in the lower wave classes and vertical bulkheads showed a generally inverse relationship of numbers with increasing wave class. This is due to the fact that most vertical bulkheads on MCBCL are located in boat basins, which are low wave energy areas.

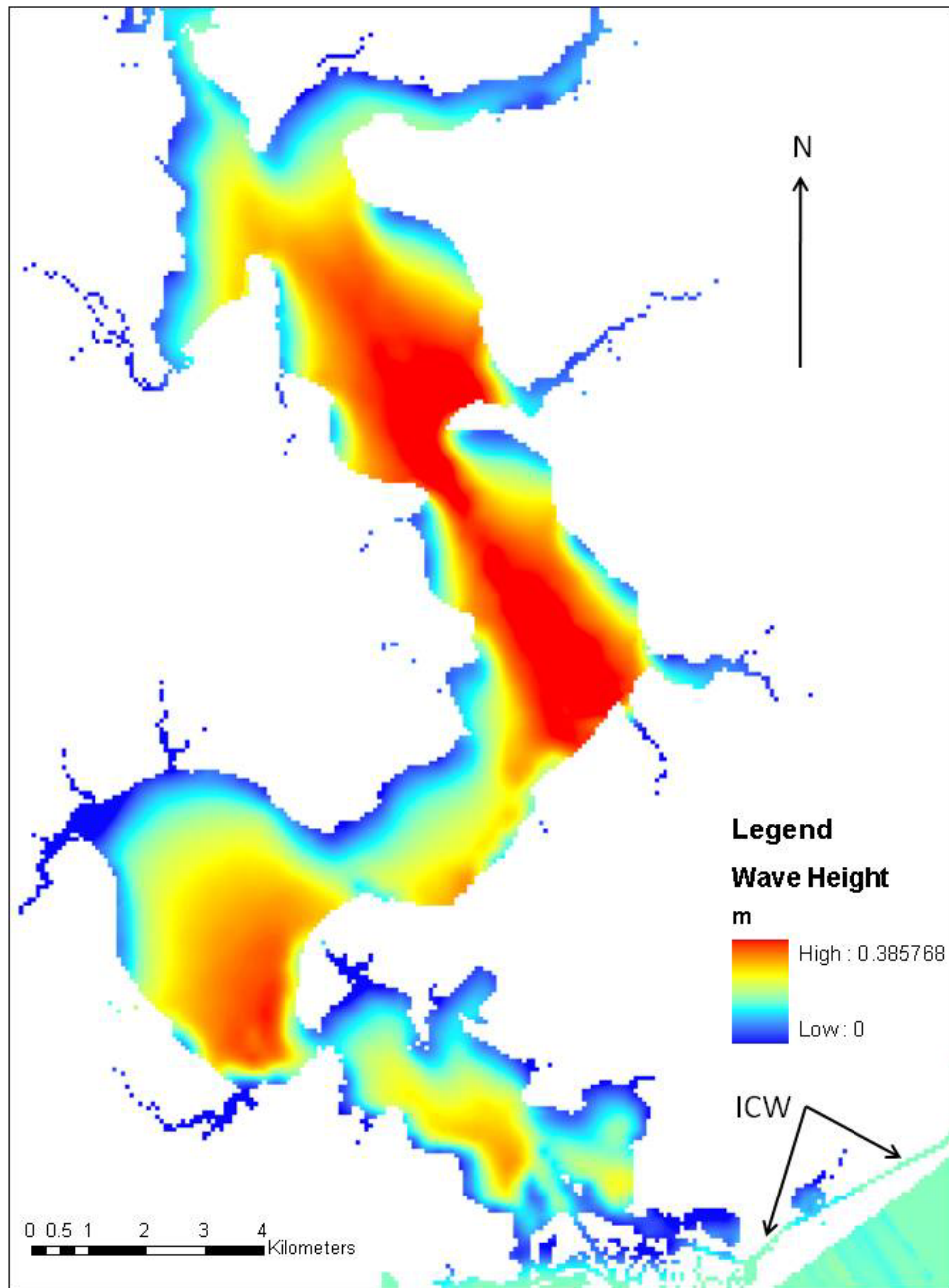


Figure 8-2. Surface wave height (m) chart of NRE for the top 5% of wind events (2007–2010).

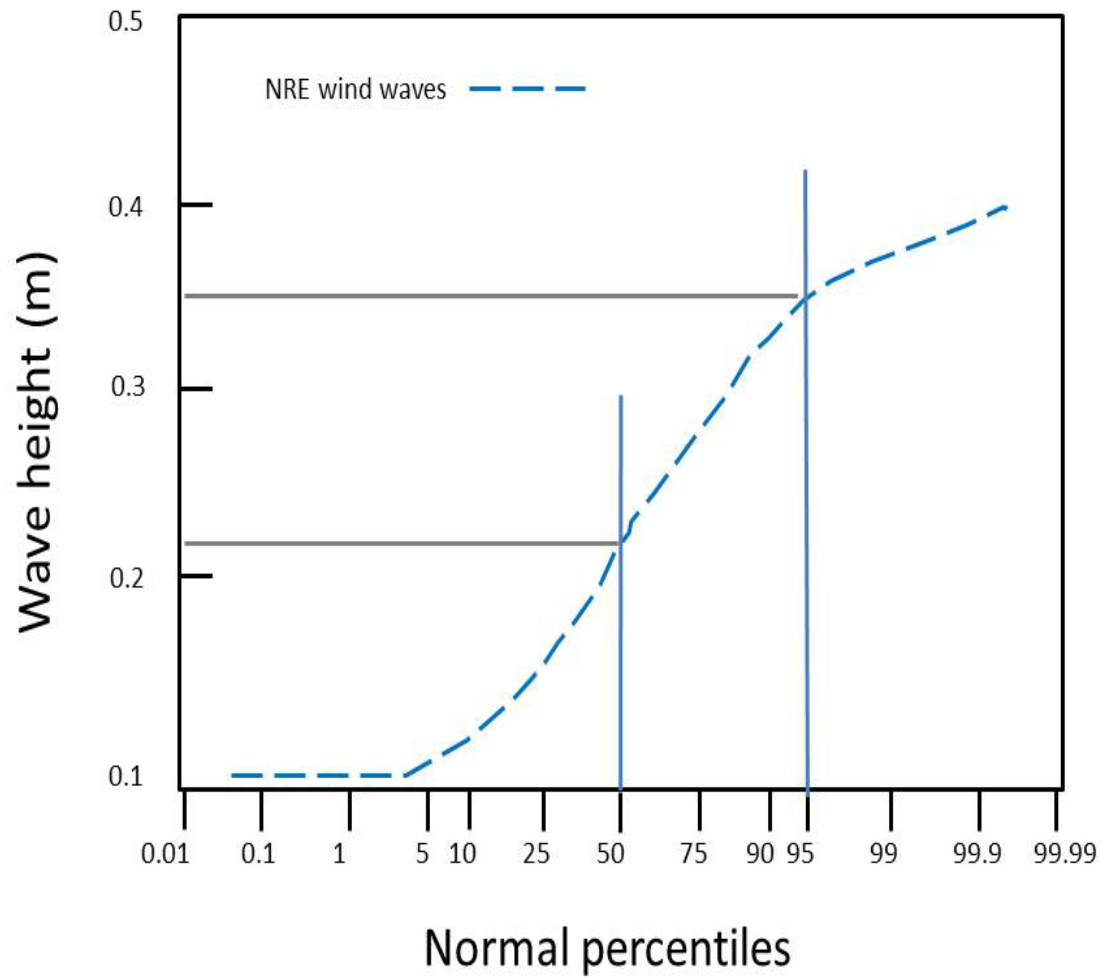


Figure 8-3. Cumulative frequency plot of top 5% of wind events for the NRE (2007–2010).

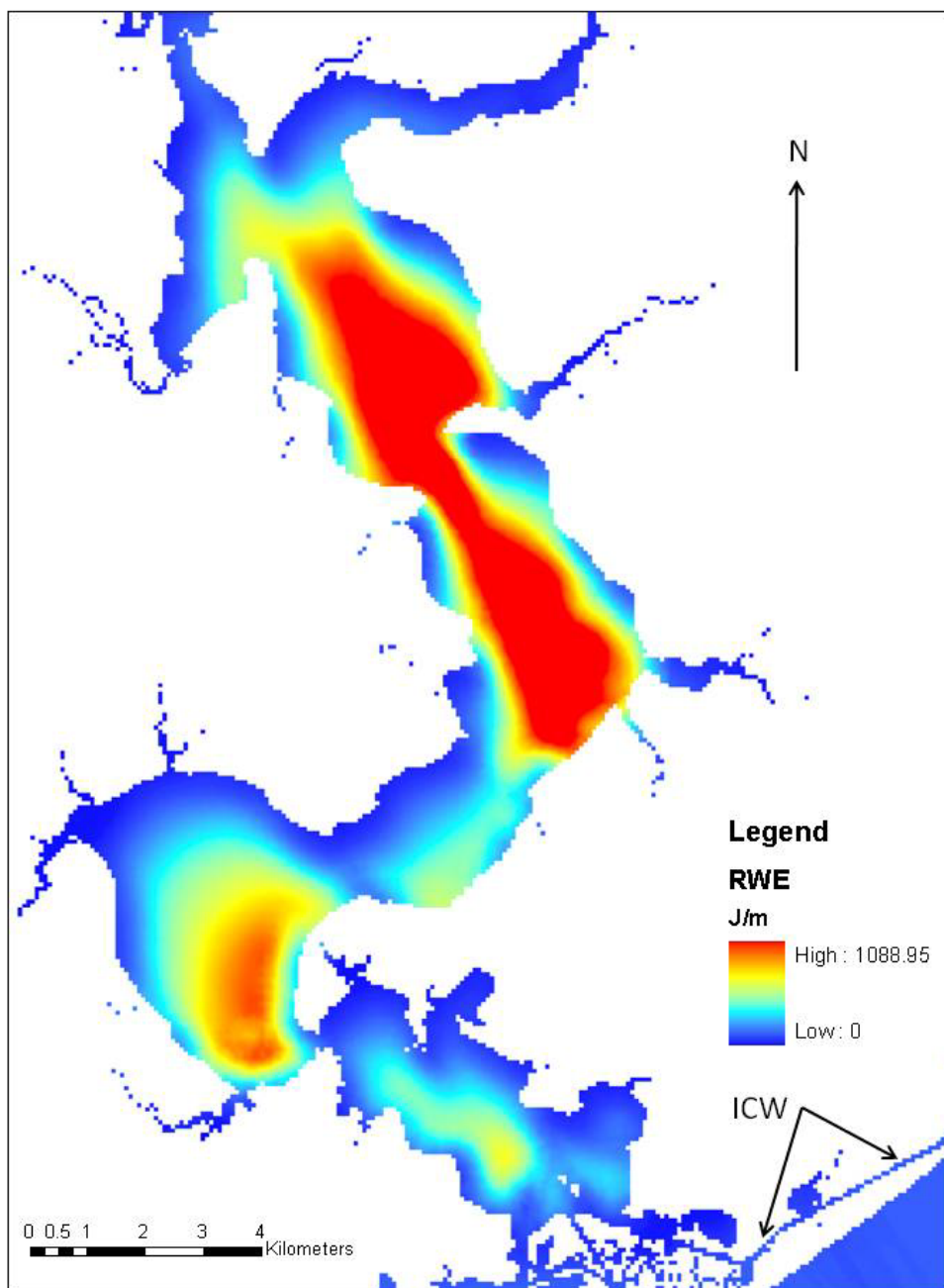


Figure 8-4. Surface wave energy (j m^{-1} wave crest) chart of the NRE for the top 5% of wind events (2007–2010).

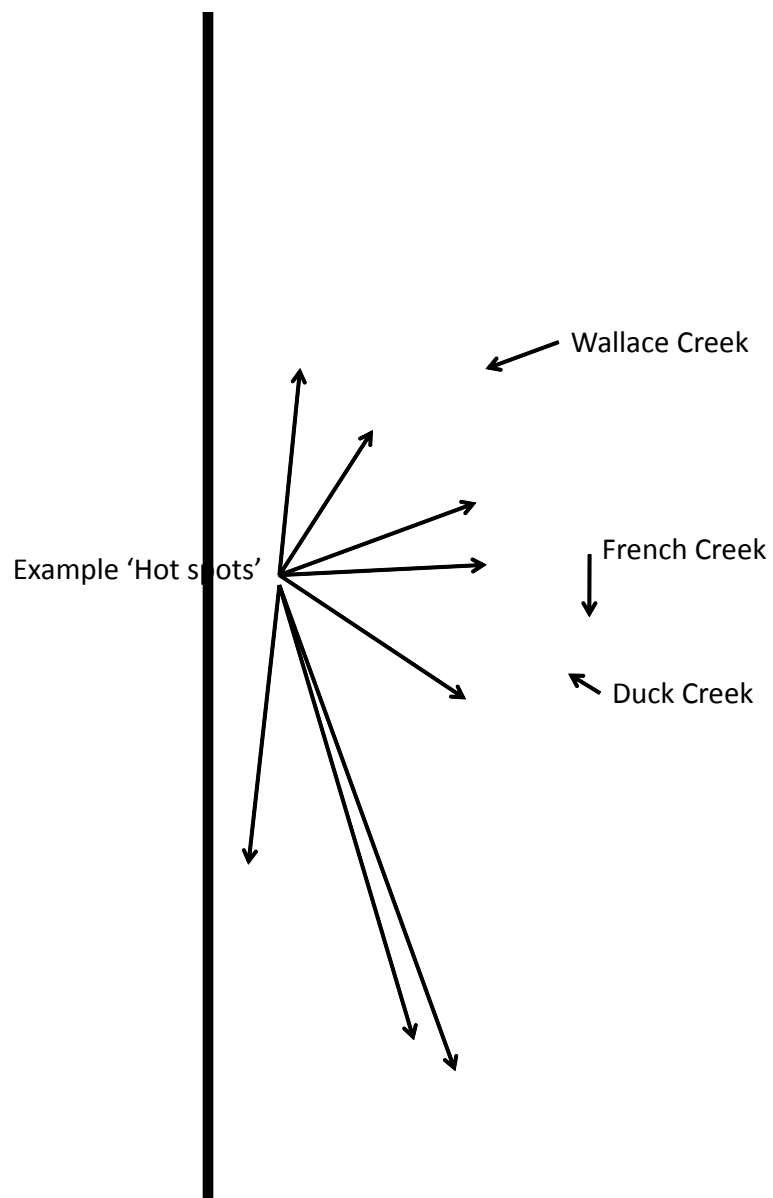


Figure 8-5. Seafloor shear stress (pascals) for the NRE with some sediment resuspension "hot spots" indicated.

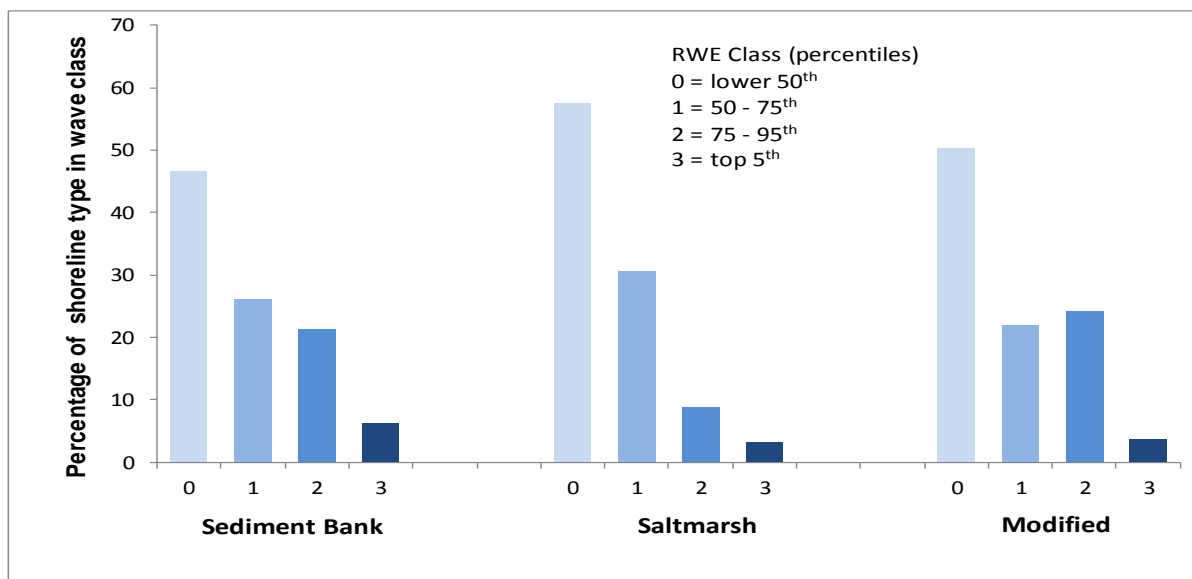


Figure 8-6. Distribution of NRE shoreline types by RWE class, as determined using WEMO.

Table 8-4. Summary table of shoreline length for each shoreline type as classified through aerial and field ground-truthing methods.

Description	Aerial (2004)		Field (2009)	
	Length (km)	%	Length (km)	%
Unclassified	3.6	3	0.0	0
Swamp Forest	0.0	0	7.3	6
Marsh	15.9	13	26.5	21
Sediment Bank	91.6	73	66.3	53
Modified	13.1	10	24.3	19

Error associated with estimation of shoreline position in aerial photography: The rectification error as determined with 16 GCPs was 5.15, 4.77, and 3.03 m for the 1956, 1989, and 2004 imagery, respectively (**Table 8-2**). Digitization error was not measured directly, but similarities in photography, landscape features and personnel suggest that a digitization error of 0.55 m as reported in Cowart et al. (2010) is a reasonable estimate. Tidal fluctuation may have added some additional error, but the relatively low tidal range in the NRE (0.1–0.4 m) and steep topography of sediment bank-dominated shorelines suggest this error is small.

Shoreline change rate: Over the time period of 1956–2004, the NRE Sediment Bank SCR averaged -0.30 m y^{-1} (**Table 8-5**). High and medium relief Sediment Banks (greater than 1 m) exhibited greater erosion rates than banks less than 1 m in height. The SCR for low and medium relief banks was higher during the period 1989–2004 than from 1956–1989, coinciding with an active hurricane period.

Table 8-5. Shoreline change rate (m y^{-1}) as determined using aerial photography in NRE. SCR given as mean and standard error; n=number of segments used in analysis per shoreline type.

Shoreline Type (n)	SCR m y^{-1} 1956–2004	SCR m y^{-1} 1956–1989	SCR m y^{-1} 1989–2004
Swamp Forest (140)	−0.08 (0.01)	−0.05 (0.04)	−0.27 (0.05)
Saltmarsh (532)	−0.18 (0.01)	−0.16 (0.02)	−0.26 (0.02)
Sediment Bank (301) (low relief, <1 m)	−0.51 (0.03)	−0.52 (0.04)	−0.51 (0.04)
Sediment Bank (99) (medium relief, 1–3 m)	−0.52 (0.0□)	−0.49 (0.08)	−0.59 (0.05)
Sediment Bank (867) (high relief, >3 m)	−0.32 (0.01)	−0.28 (0.01)	−0.42 (0.02)
Modified (482)	−0.23 (0.01)	−0.27 (0.02)	−0.13 (0.02)
Miscellaneous (16)	−0.09 (0.12)	−0.08 (0.21)	−0.12 (0.03)

SCR in both the Early and Recent time periods exhibited significant differences in erosion rates among both shoreline types and wave energy categories with a significant interaction term in all cases (**Tables 8-6 and 8-7**). This meant that there were significant differences in erosion rates among shoreline types but that the distribution of erosion by wave category among shoreline types was different.

Because these data are the results of a survey and not a balanced experimental design, we may discuss the behavior of shoreline erosion under the individual main effects (here, with one-way ANOVA) the ordering of erosion rates among shoreline types and among wave energy classes. For both time periods, irrespective of shoreline type, erosion was not significantly different among the three lowest categories but was significantly greater in the highest category (**Tables 8-8 and 8-9**).

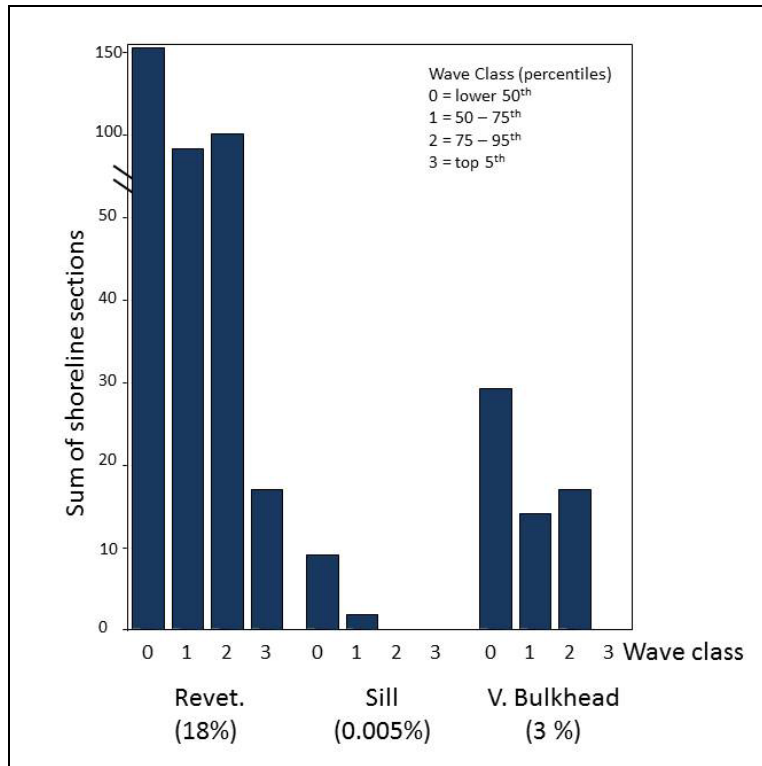


Figure 8-7. Number of hardened shoreline segments in the NRE, NC, by wave energy class.

Percentages are for the entire NRE shoreline. Revet. = revetments; V. Bulkhead = vertical bulkhead

In the Early (1956–1989) period, erosion was statistically highest along Sediment Bank shorelines without Saltmarsh, irrespective of wave class (**Table 8-10**). Shorelines that were classified as Modified in 2009, and Sediment banks with Saltmarsh were next highest during this period. Swamp Forest shorelines had the lowest erosion rate.

Calculated SCR from the Recent (1989–2004) period show that erosion was again statistically highest along shorelines with Sediment Banks without Saltmarsh, whereas Sediment Bank shorelines with Saltmarsh had the next highest, though significantly lower, SCR, irrespective of wave class (**Table 8-11**). Swamp Forest and Saltmarsh shorelines had the next lowest erosion rates and were statistically similar, and the Modified shorelines had the lowest erosion rates.

Table 8-6. Two-way ANOVA comparing erosion rates by shoreline type and wave energy class in the NRE 1956-1989(Early period).

DF	Type I SS	F Value	Pr >F	Variable
4	19.90	32.63	<0.0001	Shoreline type
3	5.85	12.80	<0.0001	Wave category
11	5.57	−0.27206	<0.0001	Type X Class

Table 8-7. Two -way ANOVA comparing erosion rates by shoreline type and wave energy class in the NRE 1989–2004 (Recent period).

DF	Type I SS	F Value	Pr >F	Variable
4	42.73	10.68	<0.0001	Shoreline type
3	1.66	0.55	0.0378	Wave category
11	8.35	0.76	<0.0001	Type X Class

Table 8-8. ANOVA comparing erosion rates by wave class type irrespective of shoreline type in the NRE 1956–1989 (Early period).

N	Duncan Grouping	Erosion	Wave Class
436	A	−0.267	2
1,058	A	−0.271	0
579	A	−0.306	1
110	B	−0.524	3

Table 8-9. ANOVA comparing erosion rates by wave class type irrespective of shoreline type in the NRE 1989–2004 (Recent period).

N	Duncan Grouping	Erosion	Wave Class
579	A	−0.330	1
1058	A	−0.347	0
436	A	−0.355	2
110	B	−0.494	3

Table 8-10. ANOVA comparing erosion rates by shoreline type irrespective of wave class in the NRE 1956–1989 (Early period).

N	Duncan Grouping	Erosion	Shoreline Type
34	A	−0.055	Swamp Forest
458	B	−0.159	Saltmarsh
261	B C	−0.254	Sandbank with marsh
470	C	−0.271	Hardened
960	D	−0.391	Sandbank without marsh

Table 8-11. ANOVA comparing erosion rates by shoreline type irrespective of wave class in the NRE 1989–2004 (Recent period).

N	Duncan Grouping	Erosion	Shoreline Type
34	A	−0.135	Hardened
458	B	−0.271	Saltmarsh
261	B C	−0.272	Swamp Forest
470	C	−0.406	Sediment Bank with marsh
960	D	−0.484	Sediment Bank no marsh

The relationship between wave energy class and erosion rates across wave classes varied among shoreline types and time period, driving the significant interaction term. However, shoreline erosion was highest in the highest wave class for most shorelines. Saltmarsh shorelines exhibited net erosion although a small set of the shoreline in the 75th–95th percentile wave class drove a net accretion for this wave energy class. Sediment Banks without a salt marsh fringe had more erosion in every wave class as compared to Sediment Banks with fringing marsh. Swamp Forest shorelines were few, did not exist in the highest wave classes, and showed some accretion in some cases. Shorelines that were modified by 2009 had similar overall erosion rates as Saltmarsh shorelines. However, recall that the Modified shoreline type category includes shoreline sections that would become modified later in time. Our general observation is that these putative modified areas were usually in proximity to MCBCL infrastructure, thus, the moderately negative SCR could have driven shoreline stabilization efforts.

Interestingly, SCR for most of the putative Modified shorelines (except the lowest wave energy class) were not unlike that of the Saltmarsh shorelines (**Table 8-5**), suggesting that some Modified shorelines might not have been as effective as expected and that there may have been a significant increase in the hardening of shorelines from 2004–2009 (and thus, any mitigation of SCR would be undetected). There is some suggestion in all these analyses that portions of the shoreline experiencing the highest wave energy category, representing the top 5% of the wind events experienced in the NRE, may be “hot spots” for erosion and may be areas of special attention for shoreline management plans. However, the existence of Saltmarsh across all wave classes and their mitigative effect on Sediment Bank erosion (see highest wave class; **Figure 8-4**) suggests that Saltmarshes are providing important stabilization services and that “hot spots” in this category should receive highest priority for shoreline erosion protection to preserve key fishery habitat, and Sediment Banks should be considered for stabilization to reduce sediment loading and potential water quality impacts from elevated suspended sediment loads.

Of the natural habitats, Swamp Forest only occur in the lowest wave energy climates (0, 1, and 2), suggesting that these will not require substantial artificial protection from chronic wave events. The pattern of high frequency of Saltmarsh in lower wave energy regimes mirrors that of other nearby surveys⁶. The evaluation of shoreline erosion based on the time series of imagery suggests that some Saltmarsh habitats will require additional protection to maintain their

⁶ NOAA Coastal Services Center. In Action: Digital Coast resources. Available at <http://www.csc.noaa.gov/digitalcoast/action/windwave.html>. Accessed February 29, 2012.

integrity. Similarly, Sediment Bank habitats, the most frequently encountered natural habitat in the NRE exist across the widest range of wave energy regimes and exhibit some of the consistently highest shoreline erosion.

Comparison of our estimates of SCR in the NRE with other estimates made in North Carolina estuarine waters provide additional insight into the relationship between wave energy setting, shoreline type, and erosion processes. Riggs and Ames (2003) summarized shoreline type and erosion rates for the estuarine shorelines in northeastern North Carolina, including those bordering the Albemarle-Pamlico Sound. The estimates were obtained using a variety of methods, including analysis of aerial photography, and encompass dates from the 1960s to the early 2000s. Across the entire study area, 55% of the shoreline was marsh and 33% was low Sediment Banks (less than 1.5-m height); reflecting the lower topography of this part of the state in comparison to the NRE, where over half the shoreline is Sediment Bank, and sediment banks greater than 3 m in height represent greater than 10% of the shoreline. Riggs and Ames (2003) report an overall average erosion rate of -0.82 m y^{-1} , which is greater than the average 1956–2004 NRE erosion rates reported here, and likely reflects the much greater fetches and wind wave energy experienced by shorelines in the northeastern part of the state. Riggs and Ames (2003) estimate a slightly lower erosion rate (-0.42 m y^{-1}) for backbarrier island marshes, and also estimate a slightly higher erosion rate for low Sediment Banks than high Sediment Banks; an opposite pattern than we found in the NRE (**Table 8-12**). A study of shoreline erosion rates using techniques similar to those used in this study was completed for the lower Neuse River Estuary for the time period from 1958 to 1998 (Coward et al., 2010). The majority of that shoreline was low-lying Saltmarsh or Sediment Bank, and the average SCR was -0.24 m y^{-1} , which is very similar to the value reported here for marsh and low Sediment Bank shorelines.

Variability in estimated shoreline erosion rates is considerable and a number of factors which influence erosion rates, including fetch, sediment bank height, presence of fringing vegetation, boat wakes, and storm events, have been identified in these and other studies (Coward et al., 2010; Gedan et al., 2011; Riggs and Ames, 2003). Wave energy, often represented by fetch, is an obvious factor affecting shoreline erosion, and previous studies have sometimes (Schwimmer, 2001), but not always (Brinson et al., 1991; Coward et al., 2010) found a robust positive relationship between wave energy and shoreline erosion rates. We found a significant interaction between shoreline type, wave energy setting, and erosion rate, although there was a general trend of increasing erosion with increasing wave energy (**Figures 8-8 and 8-9**). Our data also provide clear evidence of the role of vegetation in mitigating erosion on a landscape-scale. Sediment Bank without marsh vegetation exhibited the highest erosion rate regardless of wave energy setting, with the single exception of Swamp Forest located in high energy environments (**Figures 8-8 and 8-9**). The degree to which wetlands vegetation can minimize shoreline erosion has important management implications as coastal states develop strategies to deal with sea level rise (SLR) and the loss of coastal wetlands (Gedan et al., 2011).

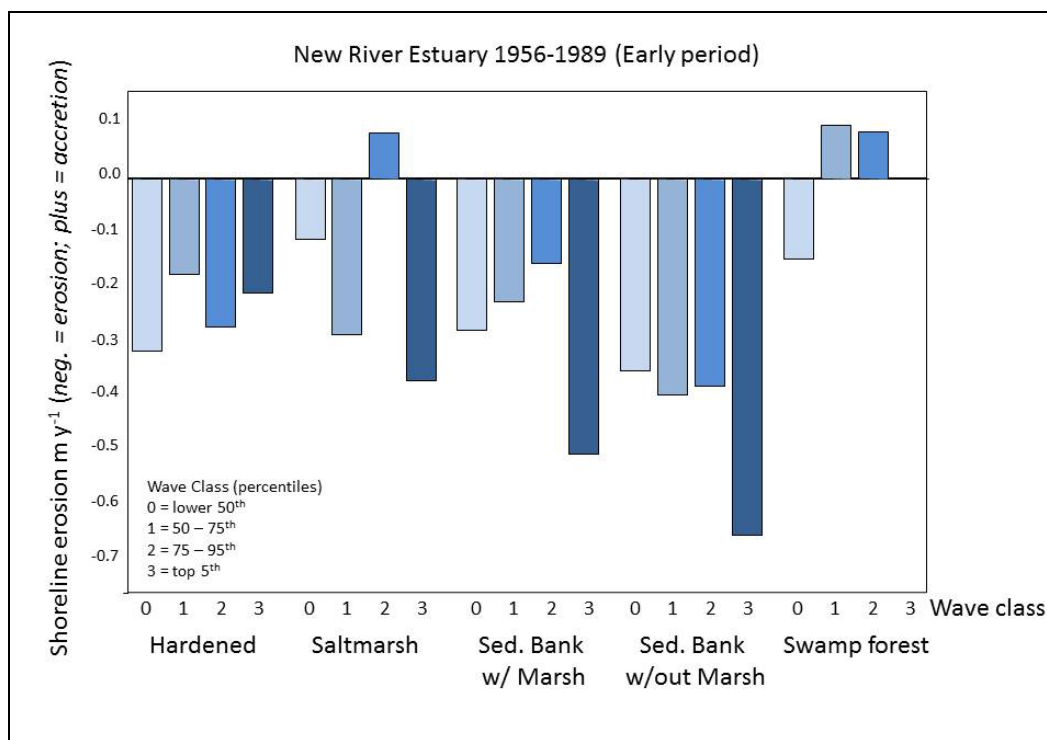


Figure 8-8. Shoreline erosion (m y^{-1}) by shoreline type and four wave energy classes for the “Early” period (1956–1989) in the NRE, NC.

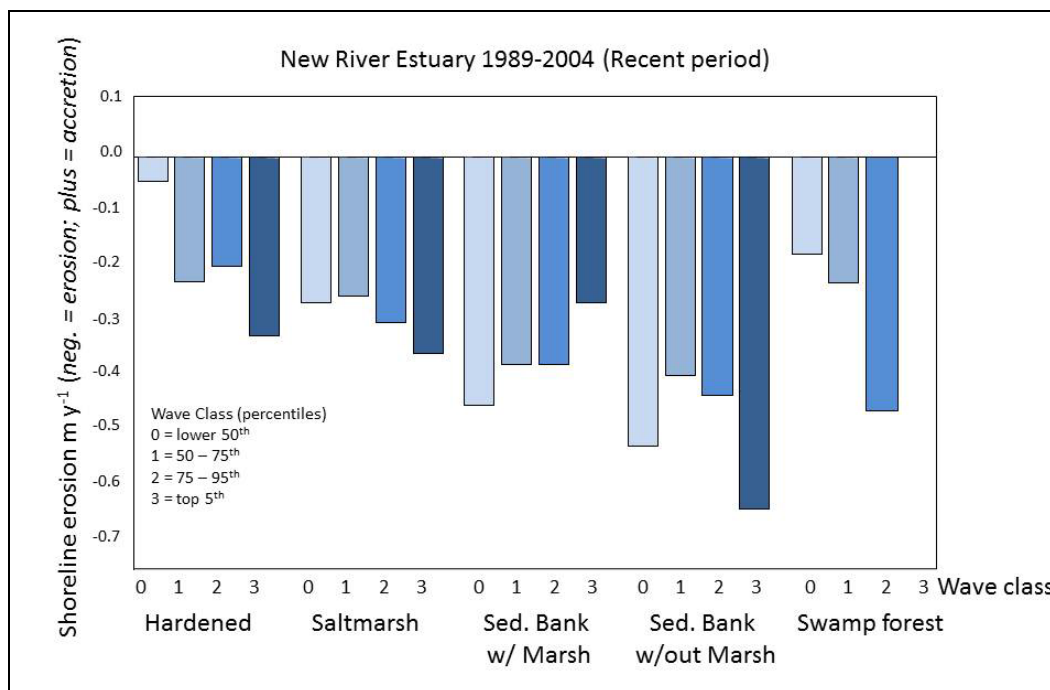


Figure 8-9. Shoreline erosion (m y^{-1}) by shoreline type and four wave energy classes for the “Recent” period (1989–2004) in the NRE, NC.

Sediment loading: The average annual volume of sediment eroded from NRE Sediment Banks was 35,328 m³ y⁻¹ (**Table 8-12**), assuming a vertical shore face. A more conservative estimate, assuming a 45-degree angle, would be half that amount, or approximately 17,500 m³ y⁻¹. Sediment released from bank erosion is transported into the water column, where it may remain in suspension, be deposited to the estuarine bottom, deposited within salt marshes with tidal waters, or carried out of the inlet. Resuspended sediments are a significant cause of light attenuation in the upper and middle estuary and can contribute to reduced benthic and aquatic primary production (see Chapter 5 of this report for more details). Salt marshes, however, rely on the influx of sediments with tidal waters to maintain their elevation relative to SLR (Morris et al., 2002). There are approximately 130 ha of salt marsh within the main stem of the NRE, and another 940 ha on either side of the ICW (see the *DCERP1 Baseline Monitoring Report*). The current average rate of SLR along the North Carolina coast is 2.7 mm y⁻¹ (Zervas, 2004) and is expected to accelerate (IPCC, 2007). For the approximately 11 million m² of salt marsh on MCBCL to keep up with SLR, 32,100 m³ of sediment must be accreted annually, an amount that falls close to the estimate of annual sediment volume released by bank erosion. These estimates demonstrate the potential importance of NRE bank erosion in supplying sediment to sustain the coastal wetlands on MCBCL.

Table 8-12. Estimated volume of sediment liberated via Sediment Bank erosion in the NRE.

1956–2004 (Whole Study Period)				
Relief	Bank Height (m)*	Length (m)**	Mean Shoreline Change Rate (m y ⁻¹)	Volume (m ³ y ⁻¹) ***
High	3	15,050	–0.51	–23,027
Med	2	4,950	–0.52	–5,148
Low	0.5	43,350	–0.32	–7,153
Sum				–35,328
1956–1989 (Early Period)				
Relief	Bank Height (m)*	Length (m)**	Mean Shoreline Change Rate (m y ⁻¹)	Volume (m ³ y ⁻¹) ***
High	3	15,050	–0.52	–23,478
Med	2	4,950	–0.49	–4,851
Low	0.5	43,350	–0.28	–6,069
Sum				–34,398
1989–2004 (Recent Period)				
Relief	Bank Height (m)*	Length (m)**	Mean Shoreline Change Rate (m y ⁻¹)	Volume (m ³ y ⁻¹) ***
High	3	15,050	–0.51	–23,027
Med	2	4,950	–0.59	–5,841
Low	0.5	43,350	–0.42	–9,104
Sum				–37,972

* For Low and Medium Banks, the median bank height value of the class was used for volume calculations; for High Banks, the minimum bank height was used for volume calculations.

** Length = Count*50 m.

*** Volume = Height*Length*SCR. Note: negative volume is volume lost due to erosion (negative SCR)

Restoration and Sea Level Rise Planning: There exist a large number of Modified shoreline segments that have potential to be converted to living, or vegetated, shorelines based on their existence in low wave energy regimes. Based on our surveys here and elsewhere in North Carolina (author's unpublished data), we conclude that from the perspective of wave energy, Saltmarsh can readily persist on shorelines where WEMo forecasts values $\leq 300 \text{ j m}^{-1}$. In **Figure 8-10**, we show the intersection of existing Modified shorelines with low wave energy settings (less than approximately 185 j m^{-1}). We suggest that these shoreline segments are strong candidates for ecological restoration by removal of the modified structures and transplanting. If there is any remaining vegetation after removal of the modified structures, this may supplement the revegetation process significantly.

Shorelines shown in **Figure 8-11** (wave regimes up to approximately 340 j m^{-1}) represent a transition condition from strong candidates (**Figure 8-12**) to where conversion of modified to living shoreline through removal of hardening and vegetative restoration would be more slightly more experimental, although saltmarsh in coastal North Carolina occurs on shorelines with RWE values well above the 583 j m^{-1} of this wave energy class. Conversely, there are a number of locations where high wave energy can be expected at the shoreline and special attention should be given to maintaining the status of shoreline structures (**Figure 8-13**). We posit that much of the modified shoreline was created for conditions not arising from wind waves (e.g., aesthetic choices) or may have been in response to shoreline erosion that was associated with unusually high water levels, which would in part explain the ongoing erosion of Modified shorelines because such events might overtop the Modified structures and cause landward erosion. In such a case, reformulating structures to account for storm surge might be warranted (a preliminary analysis of extra tropical storm surge forecasting and applications to protecting MCBCL shoreline facilities was presented to the Base in a report titled *Hurricane Emergency Drill, MCBCL*).

There exists one caveat that arises with stabilization of eroding Sediment Banks. As we point out under the **Sediment Loading** section, the Sediment Bank shorelines may be liberating a portion of the sediment that Saltmarshes need to cope with SLR. Thus, any large-scale actions that would limit that sediment source to the estuary should be accompanied by careful assessment of nearby saltmarsh systems to determine if there has been a negative impact on their ability to accrete sediment. We also observed that many of the eroding Sediment Bank shorelines are not in close proximity to any military infrastructure or assets, thus the need to curb erosion on these shoreline segments may be low.

Restoration options for living shorelines in North Carolina are well-established, arising from decades of experimentation. Saltmarsh restoration techniques were pioneered in North Carolina (see review: Craft et al., 1993) and many documents are available from USACE demonstration projects where restoration techniques were successfully tested (Knutson et al., 1990). These documents provide a ready source of user-friendly protocols and techniques that would guide the shoreline restoration projects such as we have outlined here.

For long-term planning besides that of storm surge and wave, rise in sea level should also be considered. This planning would affect not only construction of facilities, but would require planning space for landward migration of existing marsh to sustain ecosystem services such as shoreline stabilization and wildlife habitat. In **Figure 8-14**, we have placed the present day

saltmarsh distribution and overlaid that with a +1-m isobaths to show in a rudimentary manner the direction and extent of shoreline migration in the future. The location of the +1-m isobath would be the baseline from which to add space for saltmarsh. For a starting point, allowing space to accommodate the area of the present-day saltmarsh above the isobath would be a prudent starting point. A more detailed examination of the topography for the low slope areas (**Figure 8-15**) will suggest areas where the present-day saltmarsh might expand above the +1-m isobath.

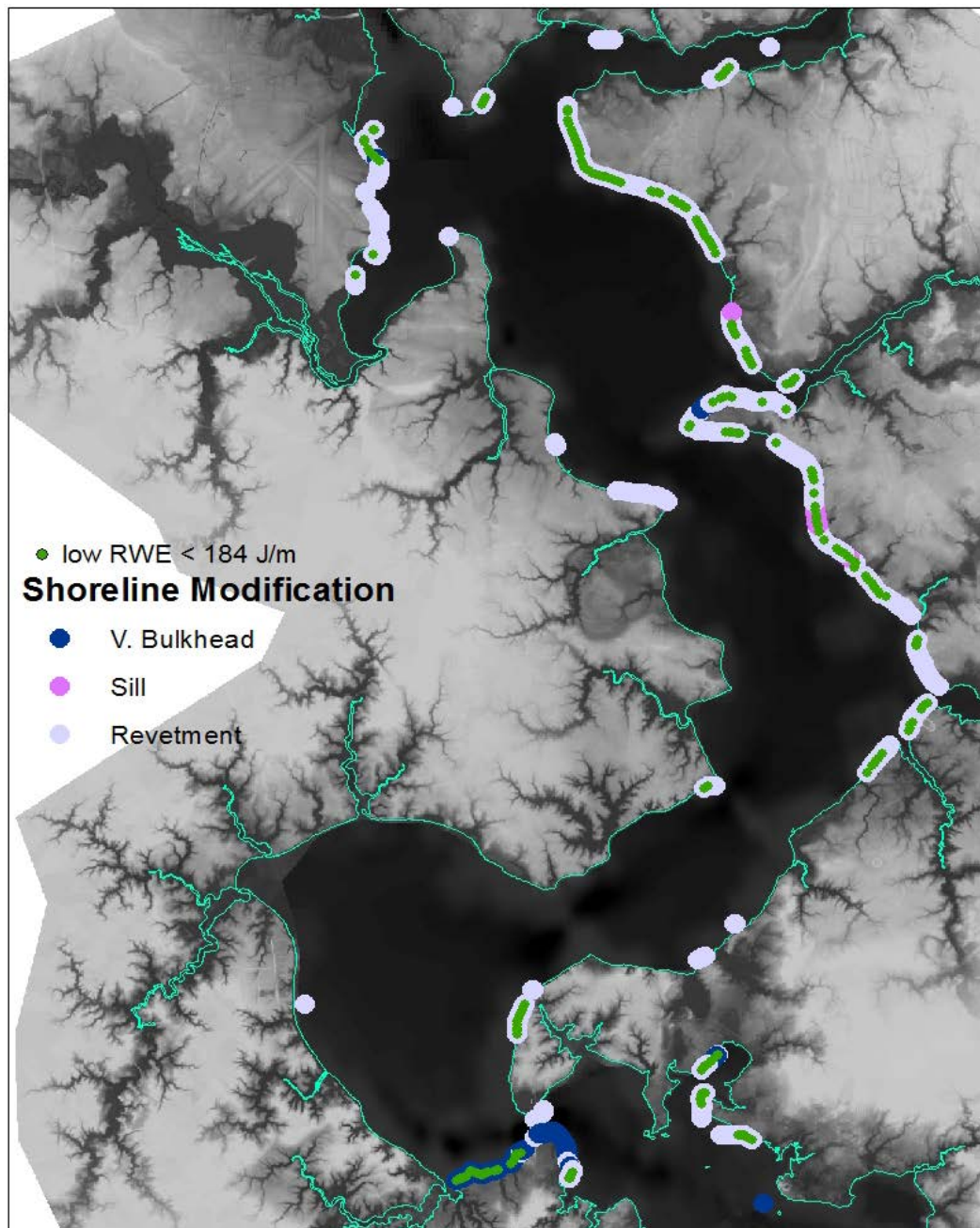


Figure 8-10. Location of modified shorelines in the NRE, and illustration of overlap with low-energy shoreline sections.

Modified shorelines determined by ground-truthing and include vertical bulkheads (blue), stone sills (purple) and revetments (gray). Green dots indicate areas where RWE is in the lowest class (less than 184 j m^{-1}).

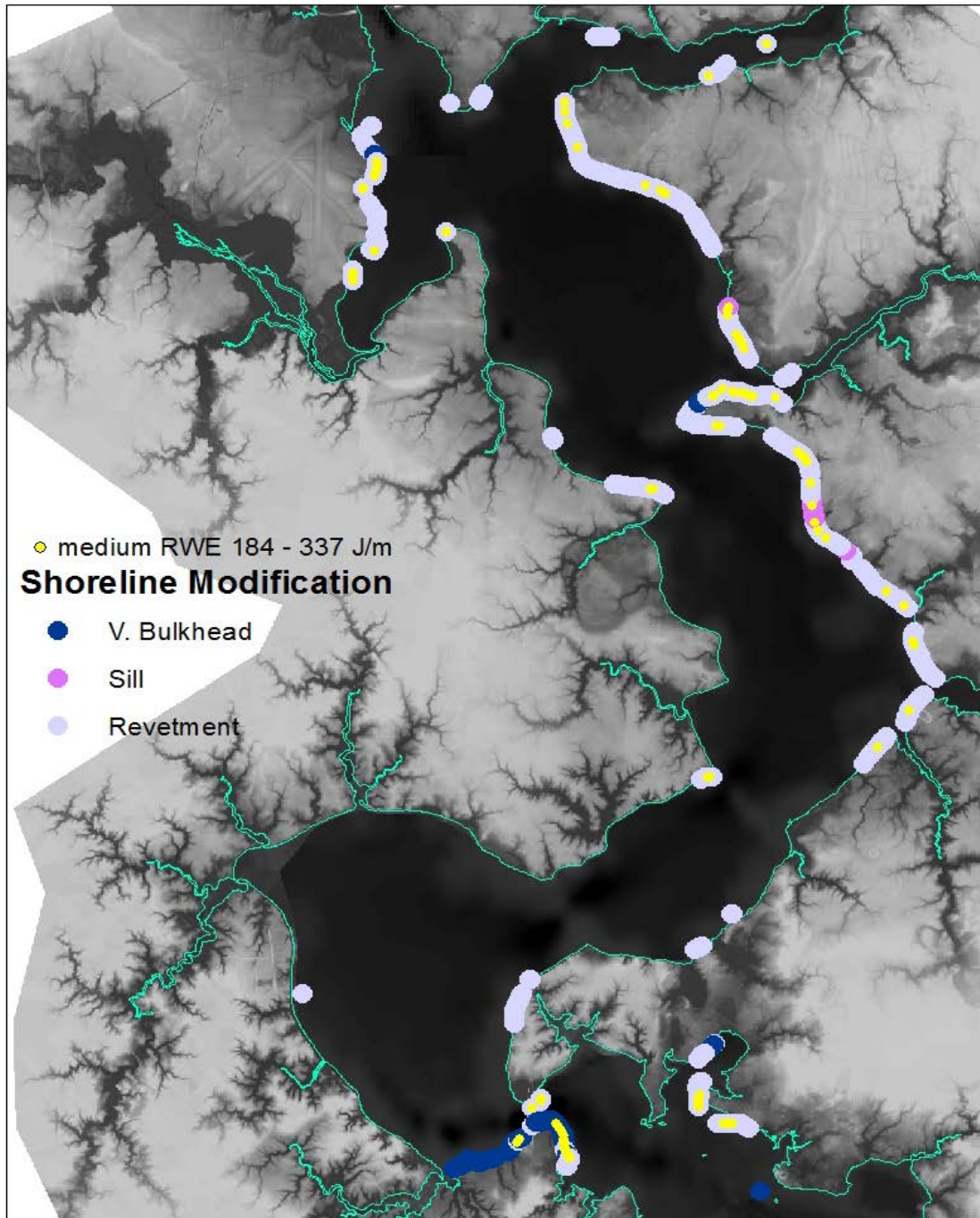


Figure 8-11. Location of modified shorelines in the NRE, and illustration of overlap with medium-energy shoreline sections.

Modified shorelines determined by ground-truthing and include vertical bulkheads (blue), stone sills (purple) and revetments (gray). Yellow dots indicate areas where RWE is in the medium class (184–337 j m⁻¹).

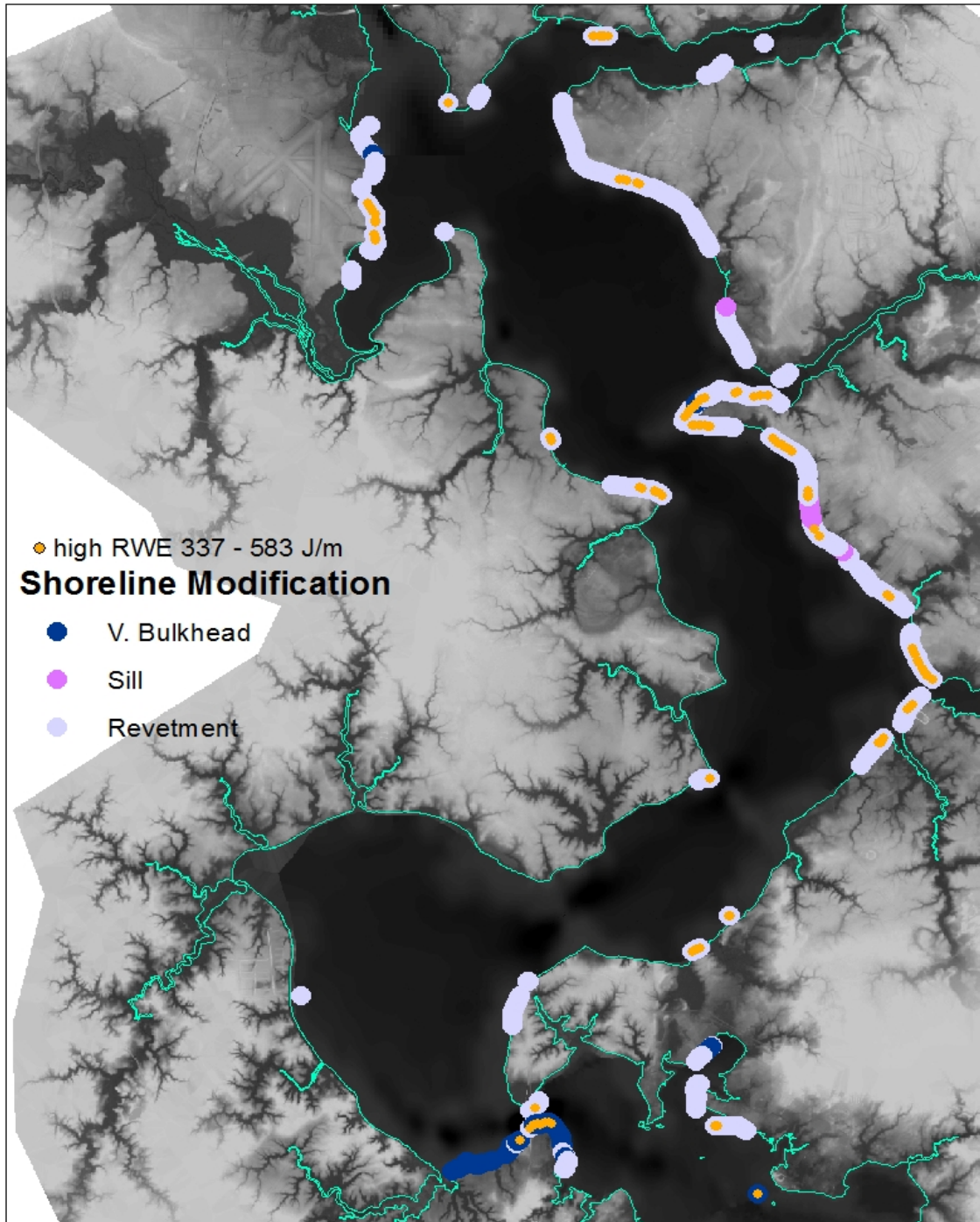


Figure 8-12. Location of modified shorelines in the NRE, and illustration of overlap with high-energy shoreline sections.

Modified shorelines determined by ground-truthing and include vertical bulkheads (blue), stone sills (purple) and revetments (gray). Orange dots indicate areas where RWE is in the high class ($337\text{--}582 \text{ j m}^{-1}$).

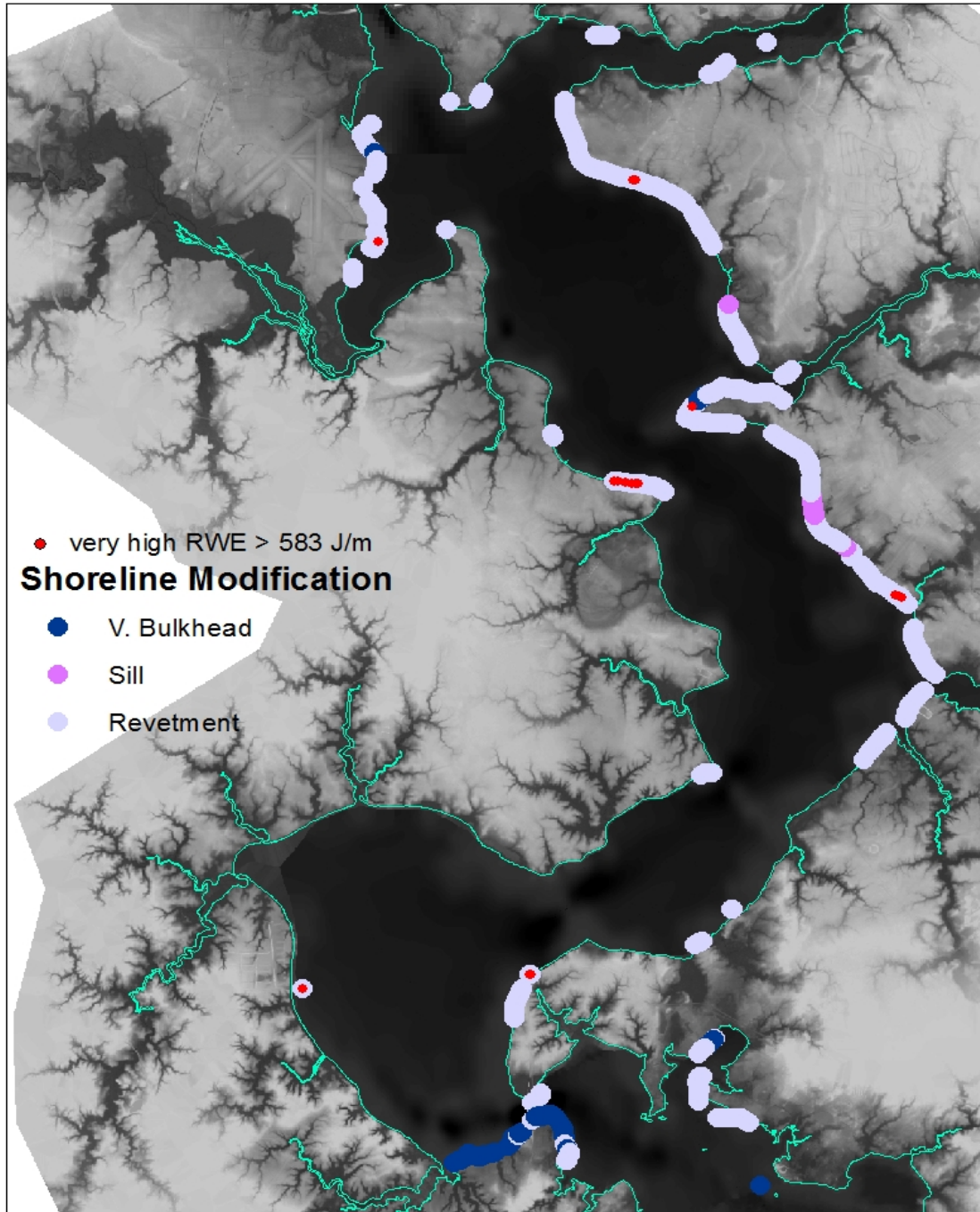


Figure 8-13. Location of modified shorelines in the NRE, and illustration of overlap with highest-energy shoreline sections.

Modified shorelines determined by ground-truthing and include vertical bulkheads (blue), stone sills (purple) and revetments (gray). Red dots indicate areas where RWE is in the highest class (greater than 583 j m^{-1}).

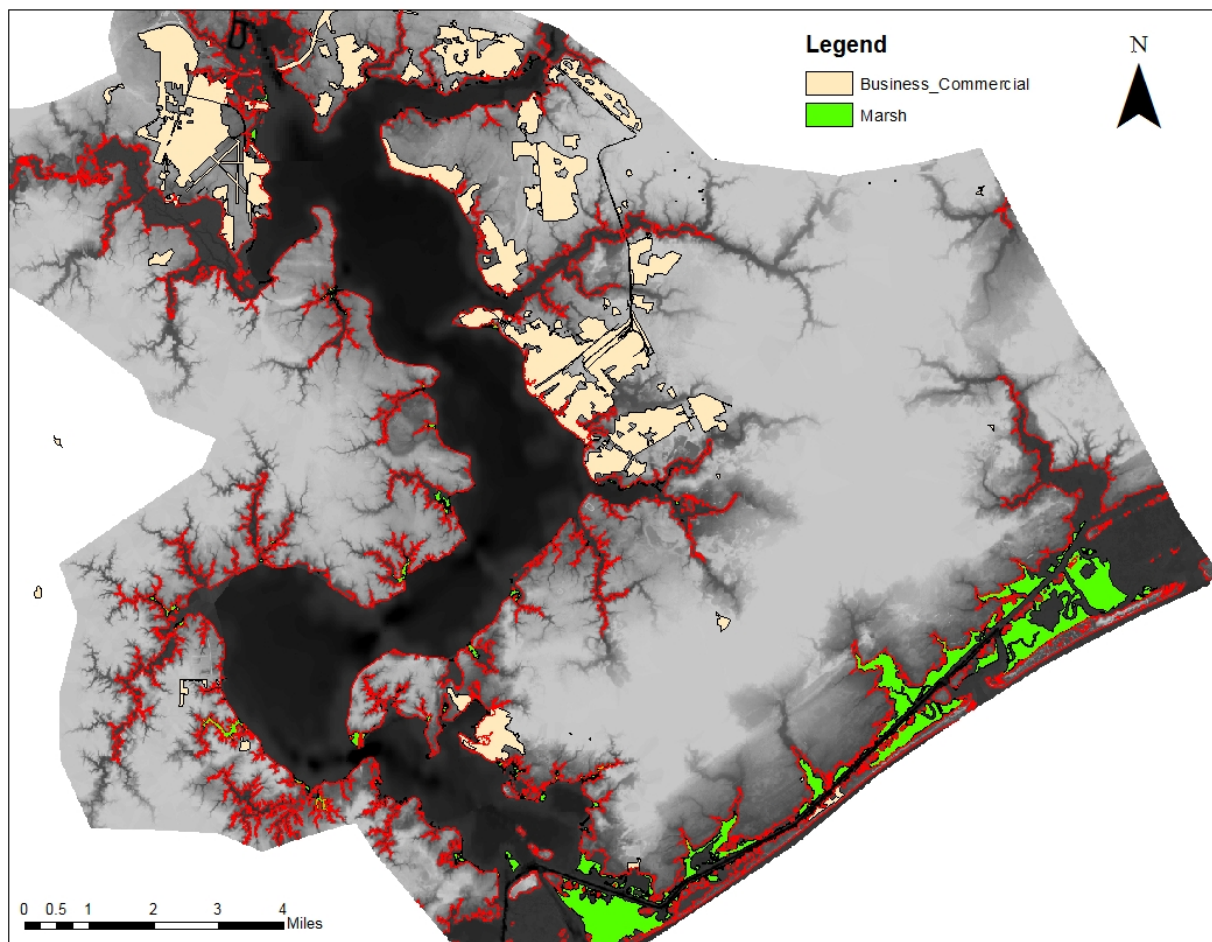


Figure 8-14. Topographic map of MCBCL showing existing saltmarsh (light green), some of the primary shore side facilities (beige) and the +1-m isobath (red) for SLR.

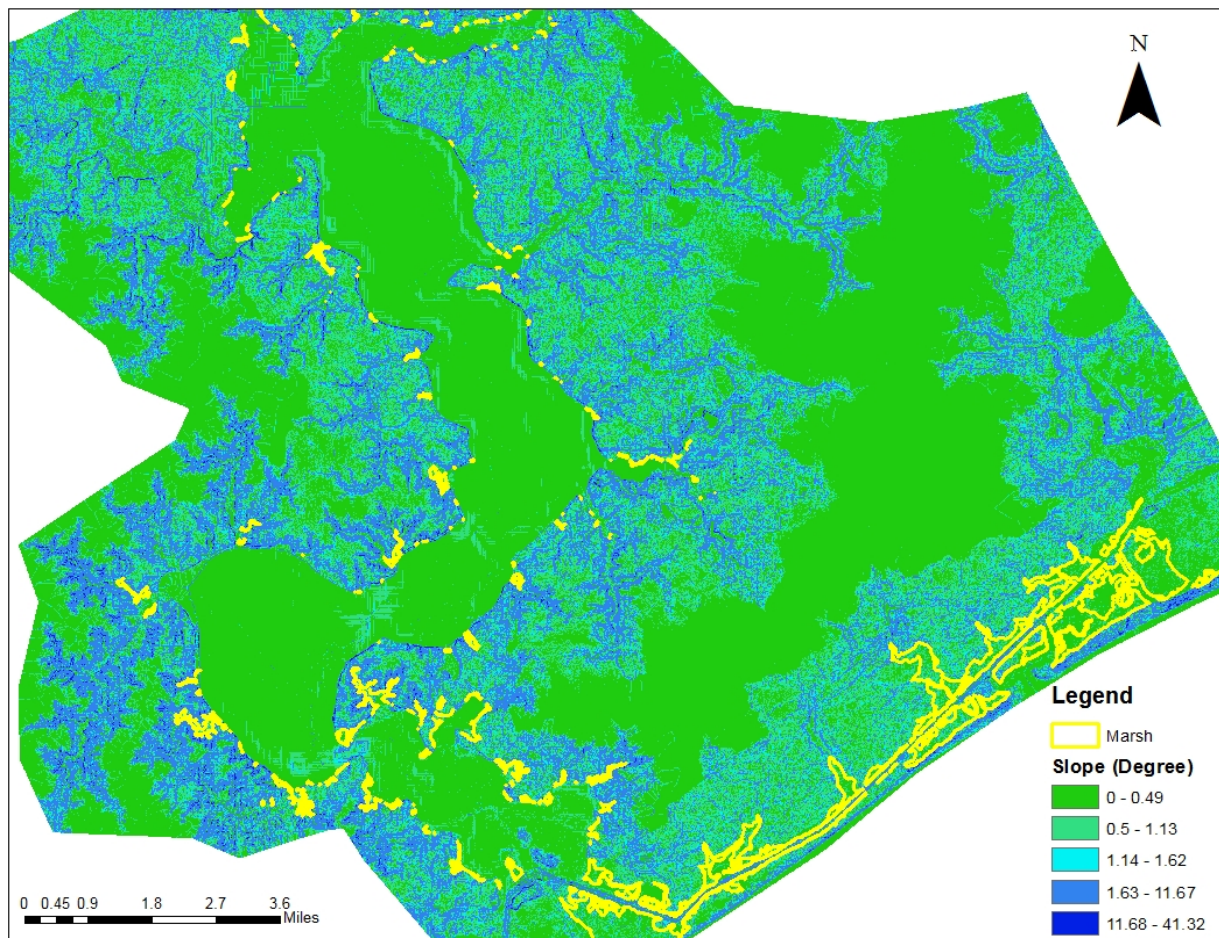


Figure 8-15. Map of MCBCL showing existing saltmarsh (yellow), overlaying a map of surface slopes as a guide to where saltmarsh may transgress landward with SLR.

Section 2: ICW Erosion Rates and Boating Impacts

Materials and Methods

Study site—ICW: Vessel or boat wakes have been recognized as a significant management issue in the coastal waters of the United States (NRC, 2000). However, the absence of a geographically accurate means of predicting boat wakes has limited manager's abilities to evaluate their effect on coastal shorelines, property, maritime safety and maintenance dredging frequency. Boat wakes are generally, but non-specifically, associated with shoreline erosion and boating safety yet we lack a quantitative basis for determining to what level boat wakes should be managed to constitute effective mitigation of impacts.

The ICW is an integrated economic and ecological system. Originally conceived as a safe route for marine cargo, the ICW is now used for both commerce and probably more extensively for recreation. The ICW traverses approximately 17 km of the lower boundary of MCBCL, intersecting with the lower reaches of the NRE and physically dividing the barrier islands and their back-island saltmarsh habitats from the mainland. Much of the ICW was dredged as a near-linear, ditch-like channel through shallow, anastomosing saltmarsh tidal creek environments. These historically quiescent creek systems are now joined much more directly with oceanic influence through inlets that connect through the barrier island to the ICW. Although wind waves are minimal in much of the dredged areas of the ICW given its location among saltmarsh habitats, tidal currents can sometimes be quite strong in proximity to inlets, creating migrating sand shoals and contributing to shoreline erosion and saltmarsh collapse.

This work in the portion of the ICW that passes through MCBCL is, to our knowledge, the first quantitative assessment of boat wakes in the ICW that evaluates historical shoreline erosion and additionally, conducts a comparative analysis among wind waves and boat wakes to define the potential tipping point where boat wake impacts would be eclipsed by the natural, wind wave environment for effects on shoreline stability.

ICW Boat wakes: We conducted surveys of boats and their wakes by simultaneously videotaping boat passage and recording their wake signature in April–May 2008 to understand the distribution of boat traffic in ICW section. These surveys were conducted at an unregulated speed portion of the ICW through MCBCL lands and near the point where the ICW has eroded to create the shortest distance between it and the ocean (Camera: 77° 18' 42.43"W, 34° 33' 4.66"N; Sensor: 77° 18' 37.98"W, 34° 33' 3.26"N). We placed a motion-activated, automated camera (model Advance Integrations HPS1000DVR-C) that recorded the passage of vessels. From these video clips we obtained vessel size, speed and hull type (V-hull, displacement hull). Simultaneously we deployed a pressure sensor that recorded vessel-generated wakes (RBR sensor XR 620) continuously at a frequency of 6 Hz. We conducted surveys when boating activity was expected to be high (e.g., seasonal migration periods and weekends). These data were used to provide an assessment of peak boat activity and users (e.g., public use versus military).

In addition to the coordinated boat type (camera) and wave sensor measures work, wave sensors were placed to record continuously at the aforementioned boat survey location for 17 months (February 2010–June 2011). This continual record of the low natural wave environment provided

an unprecedented evaluation of boat wake magnitude and frequency within the ICW. The array consisted of four RBR loggers XR 620D and one RBR logger XR 620 attached to a piling installed in the ICW. Each logger collected pressure data continuously over the year at 6 Hz) to overcome any uncertainty in identifying the transient (short duration, high frequency) of boat wakes. This continuous collection of data at 6 Hz resulted in each logger being able to record for approximately 5 days before meeting battery and data storage limits. The loggers were programmed to start and stop sequentially with minimum time overlap thereby providing a continuous record for approximately 3 weeks. At this interval, the loggers were downloaded, cleaned, serviced (including checks for drift and data quality) and redeployed. During these 3-week periods, the five loggers collected approximately 500 MB of pressure data making it a very large dataset for a whole year with more than 5 million records.

The processing of the dataset was accomplished using SAS[®]. The data processing was divided into three phases: transformation, extraction and loading. The *Transformation phase* involved taking raw data from the logger and converting into the SAS dataset. The converted SAS dataset was created in a standard SAS format and all outlier and unwanted data were removed. Unwanted data were temperature time series data and header statements collected by the loggers as well as very small (less than 5 cm) wind ripple waves. Outliers were introduced while retrieving and installing the loggers (which artificially changed water pressure) as well as rare, extremely low, wind-driven tides; these were removed during visual inspection of each retrieved data file.

The *Extraction phase* involved using algorithms to extract boat wakes from the raw pressure data. The first step involved converting pressure data to depth (summing the water level and the elevation of the sensor above the seafloor) using standard equations from linear wave theory that incorporate both static pressure and kinematic velocity of the propagating wave. These depth data include signals of boat wakes, tide, a wide range of wind generated waves and minor tidal current-induced changes in pressure at the sensor surface (**Figure 8-16**).

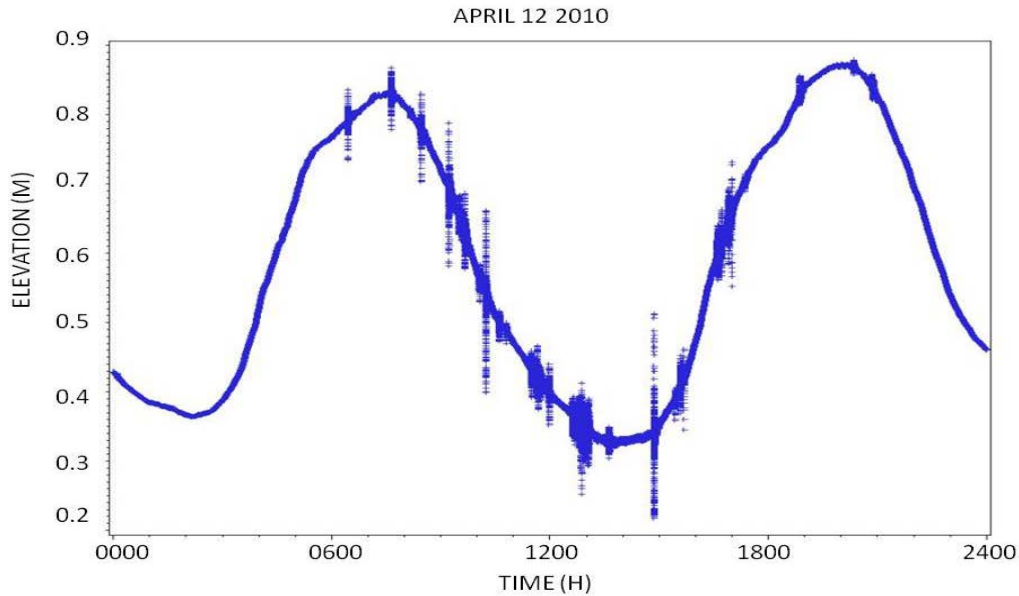


Figure 8-16. Water surface elevation data from ICW site illustrating boat wake and tidal signals (data shown here are from April 12, 2010).

Because a boat wake has a characteristic, transient wave signature (i.e., the wave signature does not have the duration of a wind-generated wave train), it can be distinguished from the background noise or other wave signals by running the loggers at these high frequencies. This characteristic was exploited to design a high pass filter for extracting boat wakes from the background noise. The high pass filter was designed and built using SAS. These boat wake signatures extracted using the high pass filter (**Figure 8-17**) consisted of series of elevation data recorded by the loggers but still contained external noise (i.e., the tidal cycle signal over which the boat wakes are superimposed). To isolate the boat wakes, tidal effects were removed by applying a 10-second moving average window (boat wakes have wave periods less than 10 seconds), thus normalizing all the remaining signals to a common elevation basis. In addition, the signal noise from very small waves (± 5 cm) were also removed (**Figure 8-18**).

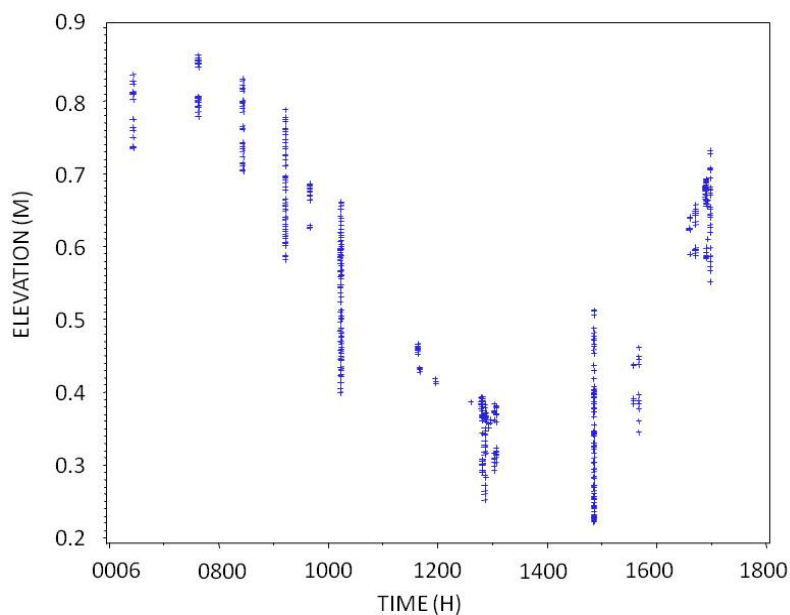


Figure 8-17. Boat wake signatures extracted after running high pass filter (data shown here are from April 12, 2010).

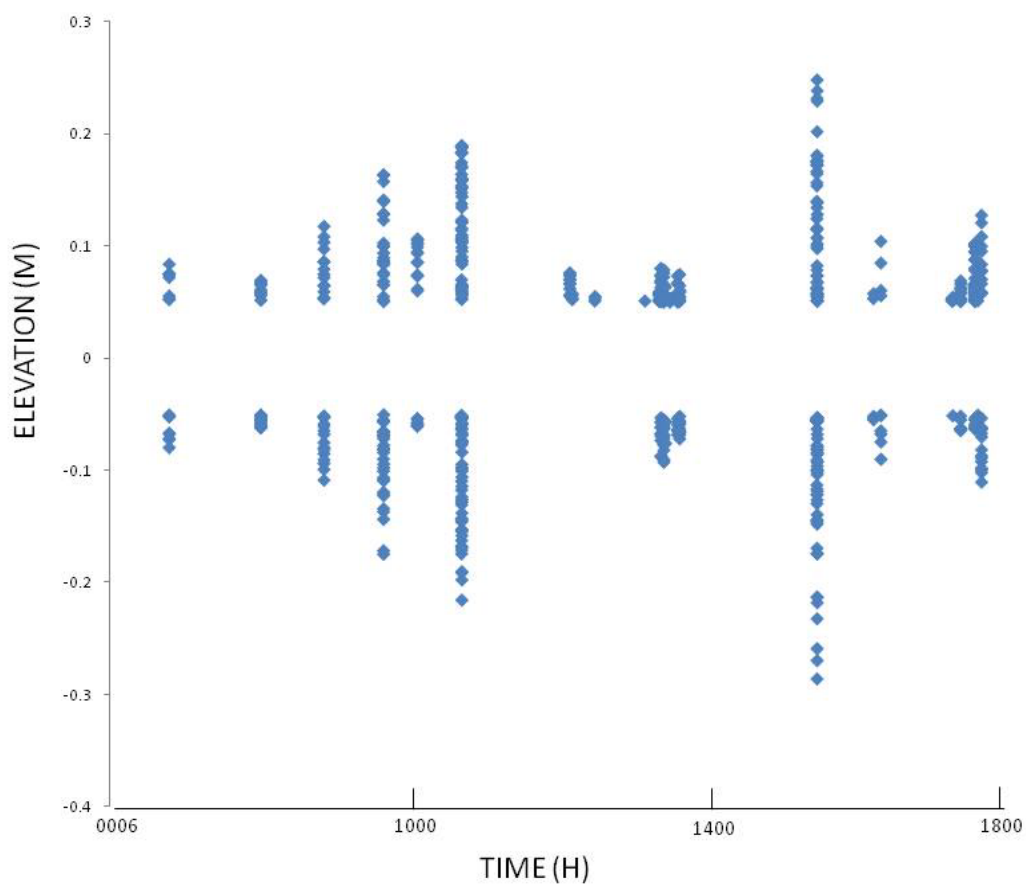


Figure 8-18. Boat wake signatures extracted after removing the tidal signal and data within the range of ± 5 cm of the threshold value (data shown here are from April 12, 2010).

The final step of the extraction process was to calculate the maximum wave height of individual boat wakes. An algorithm was written in SAS to isolate individual boat wakes by comparing the difference in wave height among sequential records and applying a Boolean test that changed the value in a companion data field if the time between a 5-cm change in water level among sequential records exceeded 10 seconds. Once the water level records were thus uniquely named as individual waves, we computed the minimum and maximum of each individual wave signature; the difference of maximum and minimum provided the boat wake height (**Figure 8-19**). For illustration purposes, the time scale represented by red box in **Figure 8-18** was expanded in **Figure 8-20**. The red box represented series of three individual boat wakes that occurred at 16:00 hours on April 12, 2010.

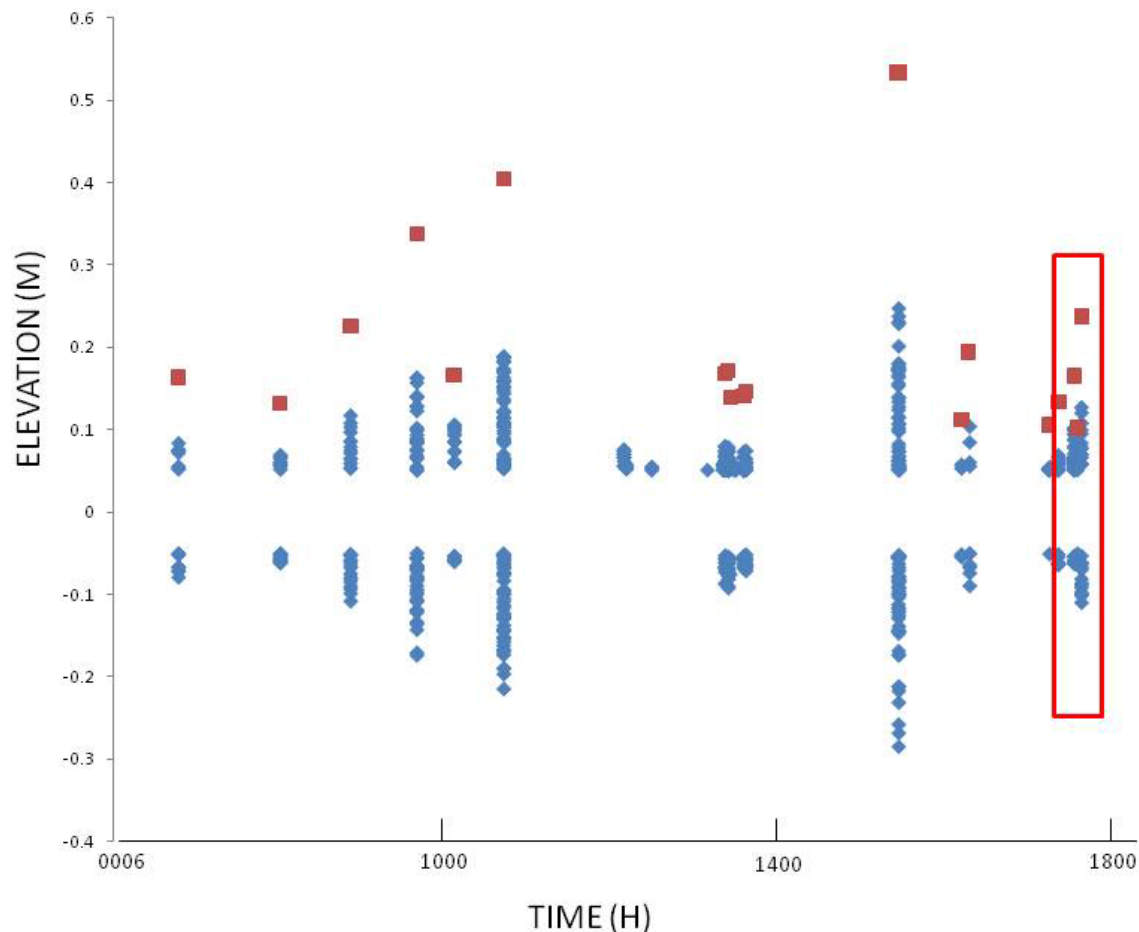


Figure 8-19. Boat wake signatures extracted (blue diamonds) overlaid with boat wake wave heights (red squares; data shown here are from April 12, 2010).

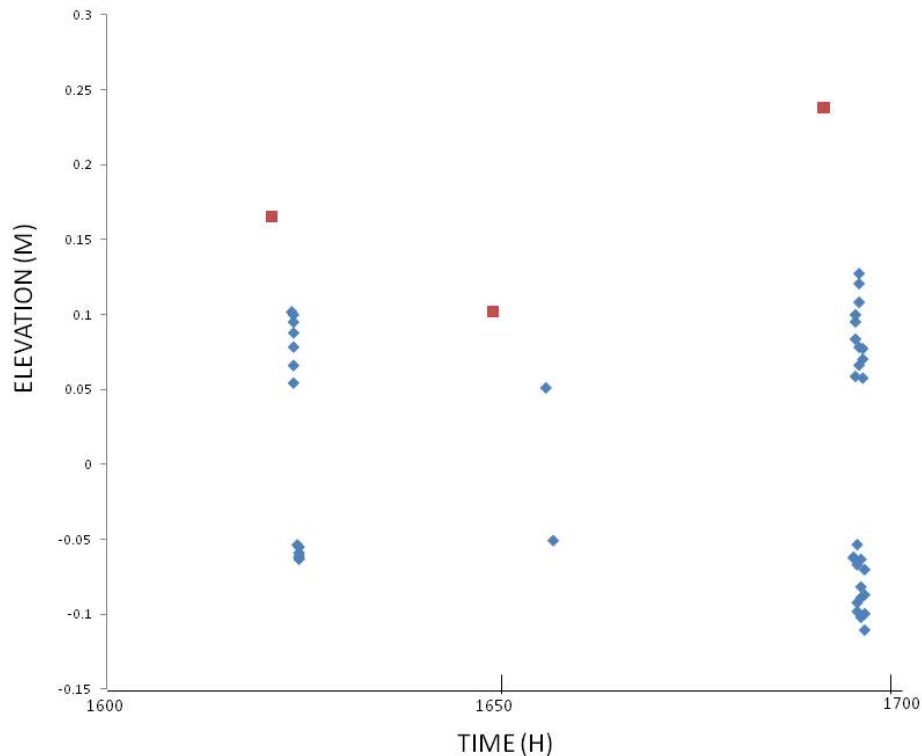


Figure 8-20. Boat wake signatures extracted (blue diamonds) overlaid with boat wake wave heights (red squares) for zoomed in for a 1-hour window as shown in Figure 8-18 inside the red rectangular box.

The *Loading phase* included putting the raw and processed data into a database. An open-source database (i.e., the PostgreSQL Database Management System) was chosen for ease and cost effectiveness after approval by NOAA Information Technology. All data were transferred from SAS to PostgreSQL using SAS scripts. Ten GB of data were loaded into the database for efficient access in this standard format. After final processing and checking, these data were archived into the DCERP Monitoring and Research Data and Information System (MARDIS).

Wind waves versus boat wake comparison: We attempted to determine at what locations in the NRE the effects of wind waves on shoreline erosion would eclipse that created by boat wakes. Wind waves interact with the estuarine shoreline almost continuously, ranging from small ripples to large storm-induced wave events. From the previous section (**Section 1: NRE Shoreline Types, Erosion Rate, and Sediment Input**) we saw that those waves rarely exceeded 0.4 m in the most exposed portion of the NRE. The challenge in this analysis was to determine the relative effect on shorelines of (1) the near-continual, but wide range of wind wave heights and energy versus (2) the comparatively aperiodic, but on average, larger and thus more energetic boat wakes especially in areas with little wind wave development.

It is very difficult to directly compare wind waves and boat wakes. As mentioned, wind waves can be virtually continuous as long as the wind is blowing; thus, simply summing the energy of all the waves that could impinge on a shoreline over hours or days would yield a tremendous amount of energy. In contrast, boat wakes are comparatively rare and episodic but for many boat

passages, wakes may be quite large. Yet, even with highly trafficked waterways simply summing boat wake wave energy would yield only a small fraction of the wave energy produced by wind reaching an exposed shoreline (e.g., a typical wind wave period for the estuary would be approximately 0.6 seconds meaning that in a 24-hour period, more than 140×10^3 waves could reach a shoreline). If we assume that most shorelines are in some dynamic equilibrium with wind waves, highly exposed shorelines may be little affected by boat wakes. However, large boat wake waves that exceeds the typical wind wave range not only introduces additional wave energy, but may occur over portions of the shoreline that are seldom exposed to wind wave energy. Here we are especially concerned with the situation where boat wakes are introduced into areas of very low wind wave development. To identify potential boat wake exceedance (over wind waves) events, we hypothesized that sites where a boat wake's maximum wave height (H_{bw}) exceeded significant wind wave height (H_s) would be an appropriate starting point to structure future studies directed at detecting the additive effect of boat wakes over wind waves. We chose to determine the "exceedance boat wakes" by comparing the frequency and magnitude for which H_{bw} would exceed the 95th percentile H_s for a range of sites near the ICW.

For this comparative analysis, we chose a test bed extent to include the portion of the NRE south of the Highway 172 bridge to the Onslow Beach Road bridge over the ICW (**Figure 8-21**). The extent was chosen due to the proximity of the sites to the ICW and thus included both the most probable areas that would be affected by boat wakes and would be near to our observation location for boat passage and wake measurement. We do not claim that this test bed area is the full extent of the boat wake impact on NRE and ICW shorelines but was arbitrarily selected to provide some manageable context for this preliminary comparative analysis. In fact, by applying the ICW boat wake information to all the test bed points equally, we overestimate the reach and effect of boat wakes propagating out of the ICW, making our analysis a likely maximum for potential boat wake effects.

Our grid points were assembled to emphasize potential shoreline impacts. The grid spacing was arbitrarily selected at 100 m near the shore and 300 m further offshore making a grid of 290 grid points (Figure 8-21). We used WEMo⁷ to generate wind waves as done previously. In this test bed area, the time period for WEMo runs was from February 2010 to June 2011 (482 days; the time frame of the continuous boat wake recording). For the WEMo calculations we imported wind datasets for each day during this period (NDBC Buoy 41035 LLNR 735) and ran WEMo in batch mode for 482 wind files using all (100%) of wind data yielding the average H_s per day. For each grid point, the cumulative frequency of daily average wind wave heights (n=482) was used to compute the 95th percentile average significant wave height. Boat wake wave heights were then compared to these 95th percentile wind wave heights to determine the number of times boat wakes could have exceeded this wind wave envelope and then were normalized by the number of boat wakes observed during the whole period. We then plotted where in the landscape this level of boat wake energy would match or exceed that of wind wave energy.

⁷ NOAA Coastal Services Center. Wave Exposure Model. Available at <http://www.csc.noaa.gov/digitalcoast/tools/wemo/index.html>. Accessed March 9, 2012.

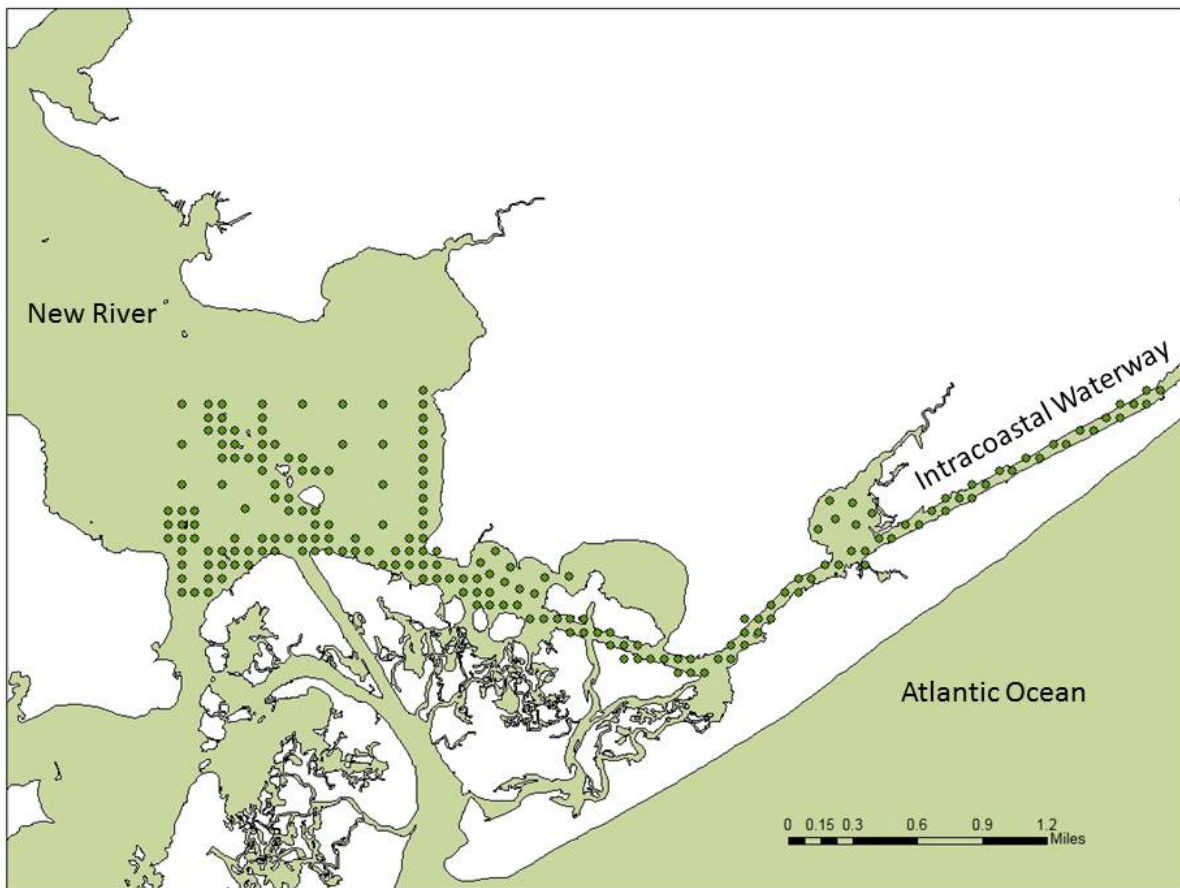


Figure 8-21. Test bed area at MCBCL in the lower NRE and ICW for assessment of boat wake effects in comparison to wind waves (n=290).

Shoreline change and erosion analysis: Shoreline change was analyzed using aerial photography from 1956, 1989, and 2009. The shoreline was digitized as the apparent shoreline on vegetated shorelines (Ellis, 1978) and the wet/dry line on Sediment Bank shorelines (Boak and Turner, 2005). Once the shorelines were digitized, SCRs were calculated using a point-based approach (Cowart et al., 2010). Briefly, points were created along the most recent shoreline at intervals of 50 m, and SCR calculated as described in the previous section (**Section 1: NRE Shoreline Types, Erosion Rate, and Sediment Input**).

We also computed the change in width of the ICW channel over a longer time frame. We used the Digital Shoreline Analysis System (DSAS; Theiler et al., 2009) and imagery from 1938, 1956, 1989, and 2009. DSAS uses a transect-based approach to determine change where transects are created from a baseline. Transects which intersect the east and west shorelines of the ICW were created at a 10-m interval and width was calculated within DSAS. The shorelines used to determine change in width were also used to calculate SCRs. Additionally, we characterized ICW shoreline habitat type by small boat in April and June 2010 using GPS equipment and ArcGIS software, as described previously. The previously digitized 2009 shoreline was edited within ArcGIS, using GPS equipment to obtain the position of the boat relative to the shoreline. Four fields were created for the shoreline shapefile, including shoreline

type, vegetation/species, modification type, and relief. A unique identifying code was created by concatenating the field values of the four fields.

Special attention was given to military “splash points” (locations where mechanized military vehicles enter and exit from a waterbody). Shoreline change was calculated at a denser scale at nine military splash point locations bordering the ICW (**Figure 8-22**). Splash point locations were obtained from MCBCL, and include locations currently used as well as some that have been largely abandoned (personal communication). Shoreline sections ranging from 150 m to 180 m in length were selected surrounding the splash point locations. Points were created every 5 m in the sections, and SCR calculated as previously described.



Figure 8-22. The location of splash points; military vehicle ingress and egress points for crossing the ICW.

We characterized sediments along transects perpendicular to the ICW shoreline at three marsh and three splash point sites. Duplicate sediment cores were collected from three depths (i.e., 0.5, 1.0, and 1.5 m) and the top 2 cm were retained for analysis. Organic matter content was determined by difference on combustion at 500°C, and particle-size was determined by wet-sieving.

Landing Craft Air Cushion marsh margin impact assessment: The Mile Hammock Bay (MHB) boat basin on MCBCL is a landing area for Landing Craft Air Cushion (LCAC) exercises. The LCAC is a light assault hovercraft which has been used on MCBCL since the mid-1990s. During this time, training exercises took the LCACs directly over a salt marsh which lay between the barrier island-inlet system and the MHB boat platform. However, because of concerns about the impact of the LCACs on the salt marsh, and the perception that fragmentation of the marsh may have resulted from LCAC passage over the marsh, the LCAC approach to the MHB boat basin was rerouted to minimize LCAC passages over the salt marsh. Instead, LCACs approached the boat basin using the navigation channel and ICW between the New River Inlet and the MHB boat basin. This alternative pathway, however, is much longer than the direct path over the marsh, and the wakes created by the LCAC contribute to shoreline erosion in the navigation

channels. We evaluated the evidence that past LCAC passages over the MHB marshes has contributed to marsh fragmentation to make recommendations on the utilization of large hovercraft in this and other coastal environments.

We used three approaches to evaluate the impact of LCAC passage over salt marsh: (1) assessment of the marsh:open water ratio from aerial photography taken before and after LCAC utilization of the marsh, (2) examination of aerial photographs of the study area for visual evidence of marsh damage and recovery, (3) examination of digital elevation models obtained for the current MHB marsh surface for evidence of elevation changes that could be linked to LCAC passage. We examined the available imagery for the area and selected four sets that provided adequate spatial coverage, image quality and resolution, and rectification (i.e., 1989, 1996, 1998, and 2004).

The marsh edge/water interface was digitized within the MHB area using tools within the ArcGIS EDITOR toolbar. Once the marsh edge/water interface was digitized, a polygon shapefile was created that included the land area and surrounding water area. The polygons were designated as “marsh” or “water” within the polygon attribute table, and the total marsh and open water was calculated for each time sequence (**Figure 8-23**). LCAC tracks were visible in aerial photographs taken in 2002 and 2004. Polygons were created in ArcGIS to document the boundaries of visible LCAC tracks in the marsh. The polygons were overlaid on 2007 aerial imagery and visually examined to see if evidence of LCAC passage was still apparent.

We established two 50 m × 100 m plots in the MHB marsh to aid in the evaluation of LCAC impact on the salt marsh (**Figure 8-23**). One plot was established between the two tidal creeks that bounded the area utilized by LCACs, according to MCBCL staff, and is designated as MHL. The other plot lay outside the tidal creek boundary, and designated as Mile Hammock Bay Creek (MHBC). Unfortunately, after the plots were established in 2008 we found evidence from aerial photography that one LCAC, at least, had traversed the MHBC plot, outside the area bounded by the tidal creeks in 1998 (6C), and in fact went directly over our “control” plot. The path of this event from 1998 is shown in (**Figure 8-23**).

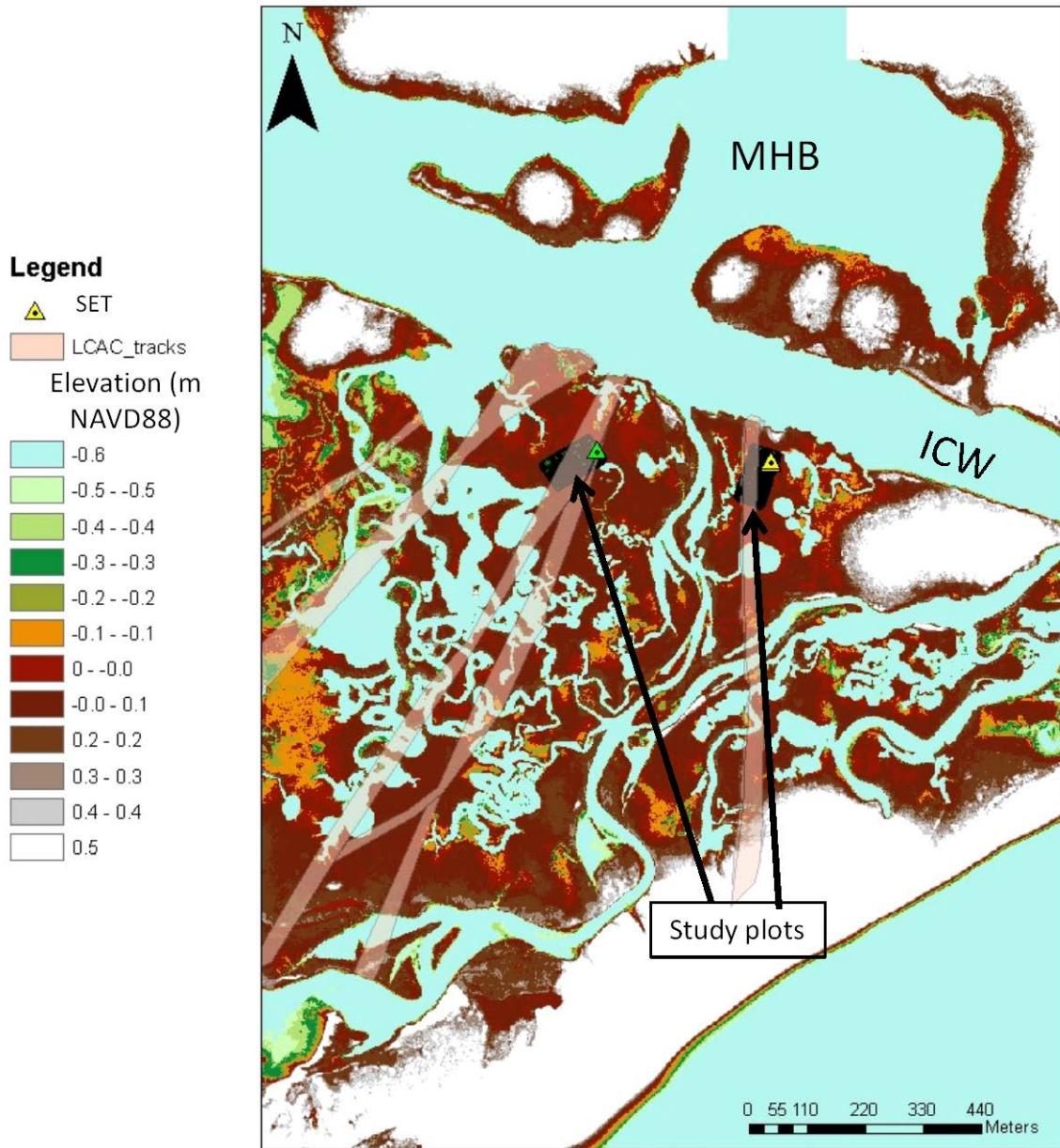


Figure 8-23. The MHB marsh showing location of vegetation plots (dark green rectangles), elevation benchmarks (green and yellow triangles), and digitized LCAC tracks.

Underlying imagery is Light Detection and Ranging (LIDAR) data from 2007. The prescribed area for LCAC utilization is to the west of the tidal creek system bisecting the marsh to the east of the green triangle. The LCAC path from 1998 which intersects the vegetation plot marked by the yellow triangle is outside the prescribed area.

Vegetation Plot MHB1 is marked with a green triangle, and the MHB2 plot is marked with a yellow triangle.

We compared marsh surface elevation, vegetation biomass, and the linkage between marsh elevation and biomass at the two MHB marshes, as well as at other marsh sites located along the ICW on MCBCL, in an attempt to discern any impacts from historic LCAC passage over the MBH marsh. We were not able to arrange an experimental LCAC passage over the marsh during the study period.

Results and Discussion

ICW boat wakes: Using an automated video surveillance system, we captured the passage of several hundred vessels on video tape many of which were of sufficient video quality to obtain data for each of the following categories:

- Hull type: V = “V” hull; D = displacement hull; C = cathedral hull; T = tunnel (catamaran) hull; S = sailboat
- Military: Yes = 1; no =0
- Hull length in meters from freeze frame
- Wetted water line length in meters from freeze frame
- Start time to nearest second from frames
- Stop time to nearest second from frames
- Column “Stop”–column “Start”
- Percent of frame traveled (in the event camera did not start until vessel was already in the frame)
- Direction = N (north; from right to left) or S (south; from left to right)
- Velocity (#5–#6/time).

Using these categories we were able to record and measure 528 V-hull vessels, or approximately 14 per day. Because these vessels were the ones that dominated wake development, we have focused on analysis solely on this hull type (sailboats and larger displacement hull vessels were traveling almost exclusively at very low speeds and generated little detectable wake; very large displacement vessels such as tugs or barges create unique effects on the shoreline, but for this portion of the waterway were very rare events and were not included in our current analysis).

Figure 8-24 shows the percent frequency distribution of V-hull boats and their speeds captured by the surveillance camera. This survey was performed during a period of time that coincides with a substantial northward, seasonal migration of private recreational vessels (April–May 2008). The average hull length was 13m and 95% of the vessels were less than approximately 22 m in length. Approximately 30% were approximately 7.5 m or less, and are likely locally operated vessels. Overall during the 17-month period (February 2010–June 2011) that included the video surveillance period we detected a total of 4,823 boat wakes.

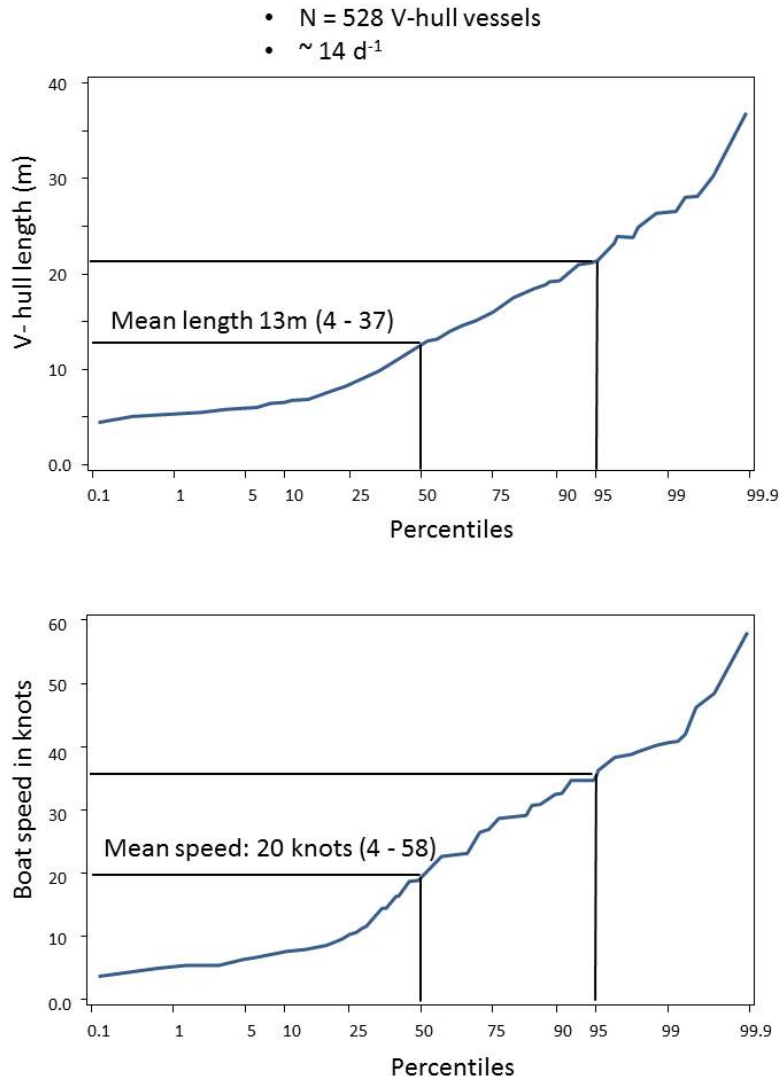


Figure 8-24. Cumulative frequency of V-hull boats by size and speed transiting MCBCL during April and May 2008.

Wind waves versus boat wake comparison: Figure 8-25 compares the frequency distribution of wave heights for both the 95th percentile wind waves in the entire NRE and the ICW boat wake data during the 17 months starting from February 2010–June 2011. Wind waves have a stronger central tendency and have a slightly greater average wave height. However, V-hulled boat wakes also have a number (albeit a few) of comparatively large wave height events and thus a broader range of wave heights. Both the median and 95th percentile of wind waves are larger than those of the boat wakes sampled, but the top 1% of wave events are much larger for boat wakes. However, the relative distribution of wind waves versus boat wakes in the estuary will determine impacts; areas subjected to frequent large wind waves will likely prove resilient to most boat wakes. Here, boat wakes were measured in a portion of the ICW where fetches are limited and wind wave heights rarely exceed 0.15 m (not shown), meaning that for the sheltered reaches of the ICW we expected that over half of the boat wakes would be exceedance events. We have observed large marsh peat fragments tossed onto the marsh surface during the passage of large

boat wakes, and suspect that the frequency of these extreme event boat wakes is sufficient to cause substantial shoreline erosion. Given that un-modified shorelines in the NRE exposed to wind wave heights of approximately 0.35 m exhibit net erosion, it is not surprising that larger waves from vessels would be responsible for similar levels of shoreline erosion that we have documented along the ICW.

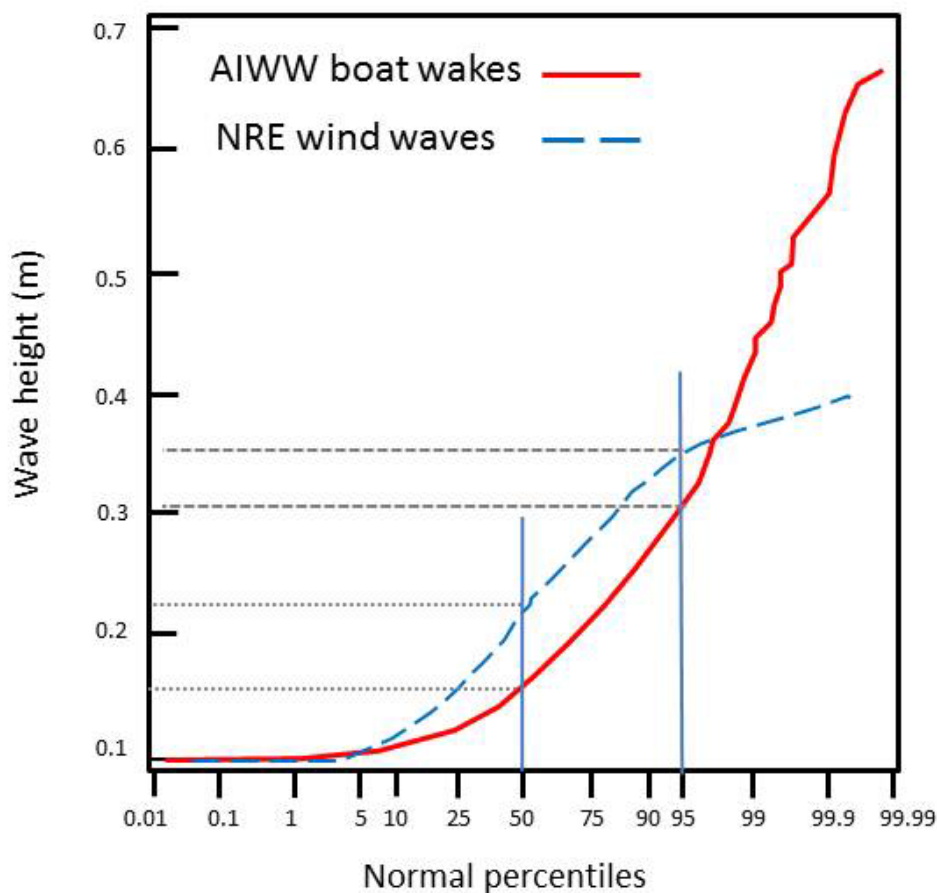


Figure 8-25. Cumulative frequency distributions comparing both ICW boat wakes and NRE wind wave heights.

Tidal currents and the impact of large displacement vessels were not included in our assessment. One of the principal roles that tidal currents could play would be to increase or decrease the wave energy at which sediment motion initiates. Thus, aside from re-distributing sediment in the waterway and contributing to the formation of shoal features, tidal currents could contribute to near-shore liberation of sediment. A comprehensive energy budget of the waterway that examines the comparative contribution of the comparatively few, but extreme wake waves generated by the largest V-hulled vessels should be considered; extreme events are well-known agents in exceeding living habitat and shoreline stability limits. Additionally, the influence of other large, but slow-moving, vessels such as barges that have substantial displacement as compared with the volume of the waterway should be studied; these vessels generate what is effectively a very long period wave with high erosive capacity and fast moving currents along the edges of the shore. Their rare appearance in the waterway may also constitute an extreme

event. Based on these observations and comparisons with boat wakes elsewhere in the ICW (Fonseca and Malhotra, 2012) we posit that the larger size vessels transiting the ICW frequently generate wakes of heights that result in sediment movement in nearshore area that are substantially in exceedance of natural wind wave events.

For any given vessel, its speed determines the size of its wake. If the speed, particularly of large V-hulled vessels, were reduced to pre-plowing levels (approximately 7 knots from 20 knots) vessel wakes will be sufficiently small so as to not transform into sediment-eroding waves as they encounter shallow water at the margins of the waterway (Fonseca and Malhotra, 2012). No wake zones in the ICW will increase transit time, but only marginally if properly constructed. Fonseca and Malhotra (2012) point out that a 2-mile slow speed zone in the ICW study area would increase transit time by only 10 minutes. These longer transit times (and smaller wakes) would likely substantially reduce the creation of erosion-generating boat wakes in both the ICW and small bays adjacent to the ICW.

To begin to understand where the tipping point between wind and boat wake wave effects may occur in an estuary, we compared the relative contribution of wind wave versus potential boat wake wave energies at 290 locations in a test section of the NRE. For this analysis, we assumed the same boat wakes, collected at a single site in ICW, hitting all the 290 test bed sites. From our simulation, we forecast that approximately 39% of the test sites would not experience boat wakes greater than that of the background (95th percentile) wind wave conditions (i.e., exceedance ≤ 0 ; **Figure 8-26**). The majority of the boat wakes that exceeded wind waves (31.7%) were approximately 0.45 m larger than wind waves; this difference is larger than the top 5% of wind waves normally observed throughout the entire NRE. The top 5% of boat wake waves exceeded wind waves by greater than 0.75 m with a few percent exceeding ambient wind conditions by almost 0.9 m. The vast majority of the sites that were dominated by boat wakes were located in or near to the mainstem of the ICW (**Figure 8-27**). This preliminary comparison of wind wave and boat wake wave regimes shows that boat wake effects will diminish rapidly with distance away from the ICW in the mainstem NRE, where the embayment is expanding to larger fetches. In contrast, small bays that communicate exclusively with the ICW (note the boxes in **Figure 8-27**) are forecast to experience substantial boat wake waves which may drive shifts in shoreline composition and stability.

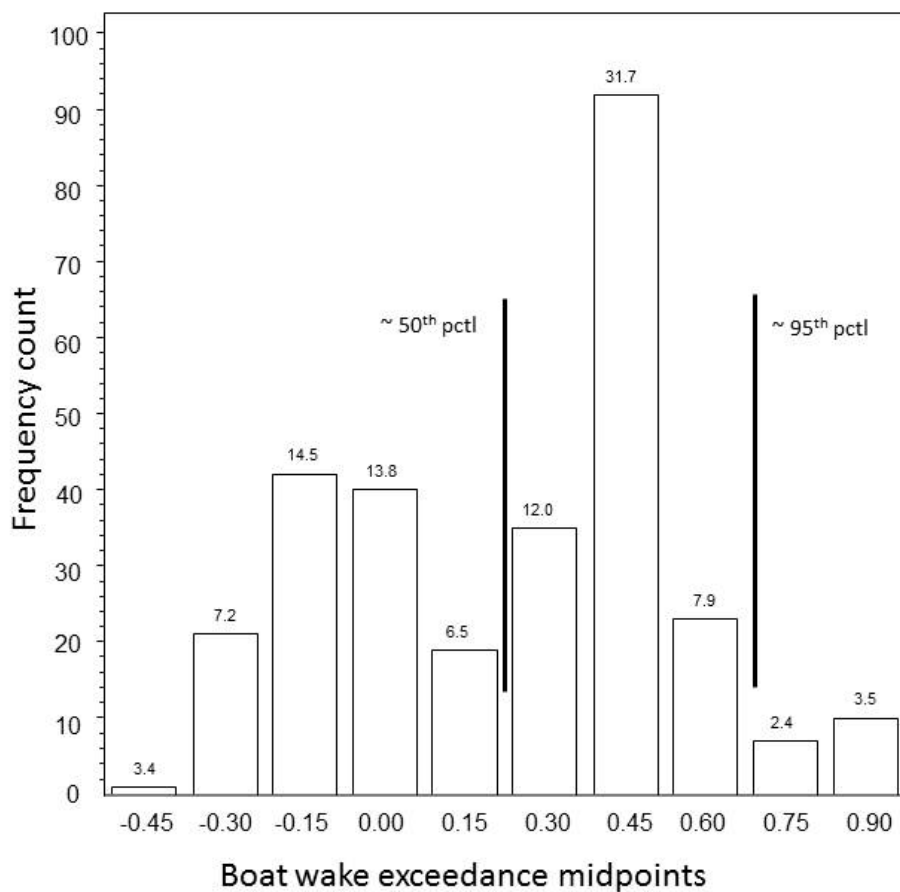


Figure 8-26. Frequency count of locations where boat wakes exceed the background, 95th percentile wind waves in the test bed.

The x -axis values less than zero represent locations where wind wave heights were larger than boat wakes; values greater than zero are locations where boat wake heights were larger than wind waves. Column labels are percentages.

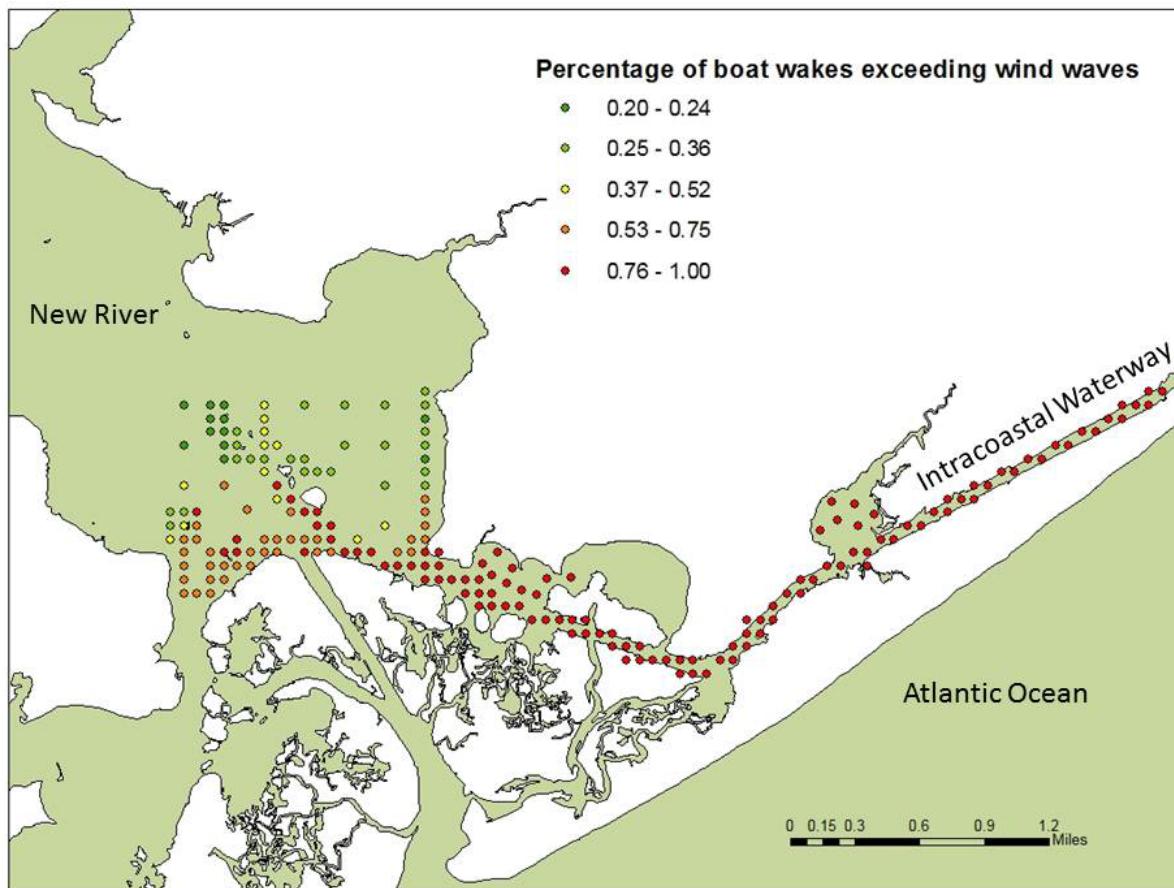


Figure 8-27. Forecast showing areas where observed boat wakes in the ICW over a 16-month period exceed wind waves of the 95th percentile.

Inset boxes contrast constrained embayments where boat wake effects do not diminish versus the comparatively rapid decline of percentage exceedance away from the ICW in more open areas (green dots).

Shoreline change and erosion analysis: In 2009, the ICW shoreline was predominantly marsh (80%), with sediment bank (19%) and modified (1%) shorelines providing the remainder. More than 90% of sediment banks were low relief (less than 1-m high). Marsh shorelines were predominantly vegetated with *Spartina alterniflora*, often found in association with *Spartina patens* and *Juncus roemerianus*.

Between 1956 and 2009, the majority of the shoreline within the study area exhibited net erosion (**Figure 8-28, Table 8-13**). The mean SCR from 1956 to 1989 was -0.44 m y^{-1} with a minimum of -4.07 m y^{-1} and a maximum of 5.27 m y^{-1} . The 1989 to 2009 time period was less erosive, with a mean SCR of -0.21 m y^{-1} , with a minimum of -4.28 m y^{-1} , and maximum of 2.70 m y^{-1} . Most importantly, the width of the ICW almost doubled between 1938 and 2009 (**Figure 8-29**), from an average of 65 m in 1938 to an average width of 149 m in 2009. There was little difference between the SCR of different shoreline types between 1956 and 1989, and it should be noted that shoreline types identified in 2009 may not have been present during the earlier time periods, particularly shoreline modifications. Between 1989 and 2009, there were clear, though statistically non-significant, differences in SCR between the three shoreline types, with sediment banks exhibiting highest erosion rates, followed by marsh and modified shorelines. The ICW

shorelines are a contrast both in terms of wave exposure and shoreline type to the mainstem NRE shorelines. The ICW was dredged through existing marsh habitat in the 1930s and the shoreline is relatively low-relief and still primarily composed of marsh habitat. Less than 1% of the ICW shoreline has been hardened, in comparison to the NRE, which has more than 20% of the shoreline modified. The narrow (less than 150-m wide) diameter of the ICW means that wind wave energy is limited, although tidal currents may be substantial in places. Despite the low relief, vegetated shoreline and low fetch exposure to wind waves, rates of SCR in the ICW are substantial, ranging from over -0.4 m y^{-1} prior to 1989 and to -0.2 m y^{-1} over the past few decades (**Table 8-13**). A separate, longer term estimate of shoreline erosion rate was made using the width of the ICW from aerial photographs dating back to 1938. The lack of fixed points in the oldest set of photographs prevented geo-rectification and thus inclusion in the point-based estimate of SCR, but we were able to measure the width of the channel in these and later photographs. This analysis demonstrated that the ICW has essentially doubled in width since construction, from approximately 70 m in 1938 to over 145 m in 2009. The SCR needed to provide this rate of channel widening is approximately -0.5 m y^{-1} . Together, these data suggest that as the channel has widened since construction, shoreline erosion rates were initially quite substantial, but have subsequently been reduced.

The ICW adjacent to Browns Inlet was particularly dynamic. High erosion was located on the eastern side of Browns Island for both time periods; however, the western side of the island eroded from 1956 to 1989, but accreted between 1989 to 2009 (**Figure 8-29**). Between 1956 and 1989, the only areas of net accretion in the study area were located in the MHB area and the northern side of Browns Inlet (**Figure 8-29**). Less erosion and more accretion occurred from 1989 to 2009 compared to the previous time period (**Figure 8-29**). The widest (150-m) portions of the ICW in 2009 include the Browns Inlet area, an area before a large creek opening on the western side of the ICW where it turns sharply west, and the MHB area). Inlet dynamics are the system drivers in these locations, and these areas may be expected to remain dynamic sites of erosion and accretion. It should be noted that the New River Inlet receives regular maintenance dredging by the USACE, but Browns Inlet is not maintained.

Table 8-13. Mean SCR (m y^{-1}) calculated from aerial photography for ICW shorelines within MCBCL. Shoreline type determined from field survey conducted in 2009 (n=number of points per shoreline type)

Shoreline Type (n)	Shoreline Change Rate (m y^{-1})	
	1956–1989	1989–2009
All Shorelines (803)	–0.44	–0.20
Marsh (716)	–0.43	–0.19
Sediment Bank (77)	–0.46	–0.31
Modified (10)	–0.44	–0.09

Shorelines adjacent to military splash points eroded more from 1956–1989 than from 1989–2009 (**Table 8-14**). Compared to the mean SCR for the ICW dataset from 1956–1989 (-0.44 m y^{-1}), seven of the nine splash point areas had a higher mean SCR. In comparison, only four of the nine mean SCRs at the 1989–2009 splash point areas were higher than the mean SCR of the ICW dataset (-0.20 m y^{-1} ; **Table 8-4**). The use frequency of the splash point areas could not be

obtained; however, it was determined that Splash Points 4, 5, and 7 have not been used in the past decade. MCBCL utilizes the barrier island beach on the south side of the ICW for landing exercise and other training operations. A variety of amphibious vessels enters and exits the ICW at a number of designated splash points. Observations and discussions with Base personnel suggest that several of these are particularly active; including Splash Points 9, 10, 11, and 12 (**Figure 8-30**). None of these splash points are hardened (paved or with concrete ramps leading into the water), and three of them exhibit higher erosion rates between 1989 and 2009 than the average ICW SCR. We recommend that Splash Points 10, 11, and 12 be considered for modification, reinforcement, or relocation.

Table 8-14. Mean SCR (m y^{-1}) calculated from aerial photography of the shoreline area surrounding military splash points 1989 to 2009 (mean, standard error).

The locations of the splash points were supplied by MCBCL.

Splash Point ID Number	1956–1989 SCR	1989–2009 SCR	2009 Shoreline Type
3 ^a	−0.34 (0.06)	0.00 (0.12)	Modified
4 ^b	−0.59 (0.13)	−0.19 (0.13)	Marsh
5 ^b	−0.50 (0.13)	−0.35 (0.10)	Marsh
6	−0.08 (0.30)	−0.34 (0.23)	Modified
7 ^b	−0.56 (0.13)	−0.13 (0.26)	Marsh
9	−1.16 (0.18)	−0.15 (0.11)	Sediment Bank
10	−1.00 (0.05)	−0.30 (0.37)	Sediment Bank
11	−0.92 (0.25)	0.33 (0.28)	Sediment Bank
12	−0.79 (0.18)	−0.49 (0.37)	Sediment Bank

^a Not located directly on ICW.

^b Not in current use (MCBCL personal communication).

The mean organic matter (OM) content of ICW sediments offshore of marsh and splash point shorelines ranged from 1.55% to 3.38%, with a trend of increasing OM content with depth. Sediments off-shore of splash points had significantly lower OM content than those adjacent to marsh shorelines (*t*-test, $p=0.0048$). Sediment adjacent to both splash point and marsh shorelines were predominantly sand-sized particles (74–86%, **Table 8-15**). However, in general it appears that splash points are localized sources of sediment resuspension and movement, although given their small size and low numbers, they do not appear to be a substantial threat to shoreline integrity.

Table 8-15. Mean percent particle size and organic matter (OM) content of sediment collected offshore from Marsh and Splash Point (SP) shorelines at three water depths.
VF = very fine; M = medium.

Water Depth		0.5 m		1.0 m		1.5 m	
Site		Marsh	SP	Marsh	SP	Marsh	SP
Percent	OM	2.6	1.6	3.0	2.1	3.2	3.4
	Coarse sand/gravel	1.2	1.2	1.1	1.7	0.9	1.1
	VF/M Sand	80.9	86.6	79.8	85.1	74.0	79.6
	Silt	8.8	12.3	19.2	13.7	25.0	19.4

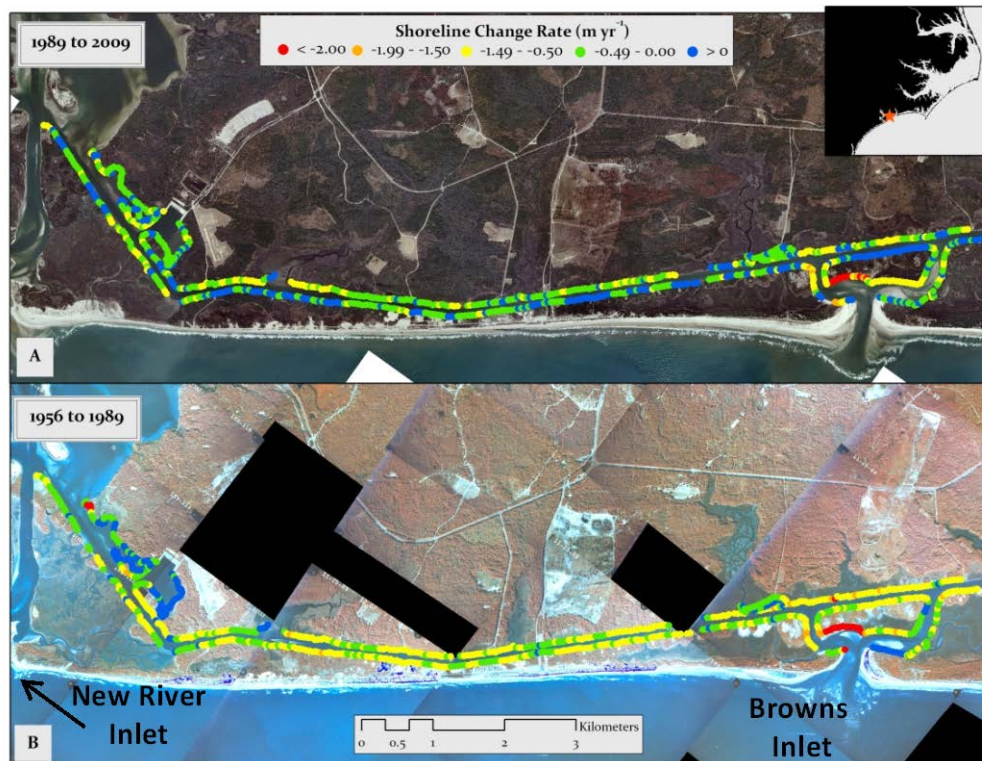


Figure 8-28. Maps of the SCR within the ICW from New River Inlet to Browns Inlet, NC. Shoreline change was determined for two time periods, from 1956 to 1989 (A) and 1989 to 2009 (B). Warmer colors denote higher erosion and cooler colors represent less erosion. Accretion is shown in blue. Shoreline-change rates are in meters per year.

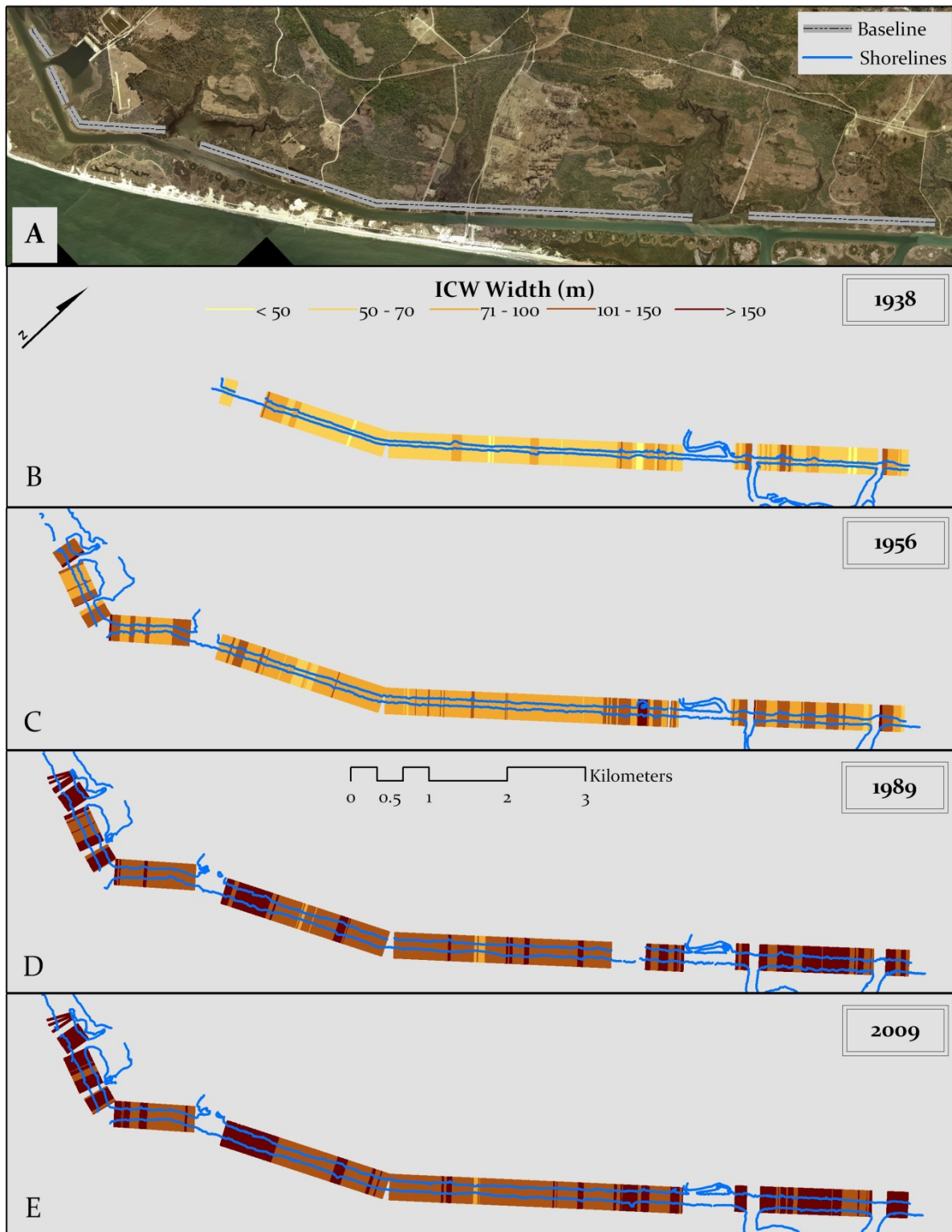


Figure 8-29. Maps showing the calculated width (m) of the ICW in 1938, 1956, 1989, and 2009.

Lighter colors represent narrower width and darker colors denote wider width.

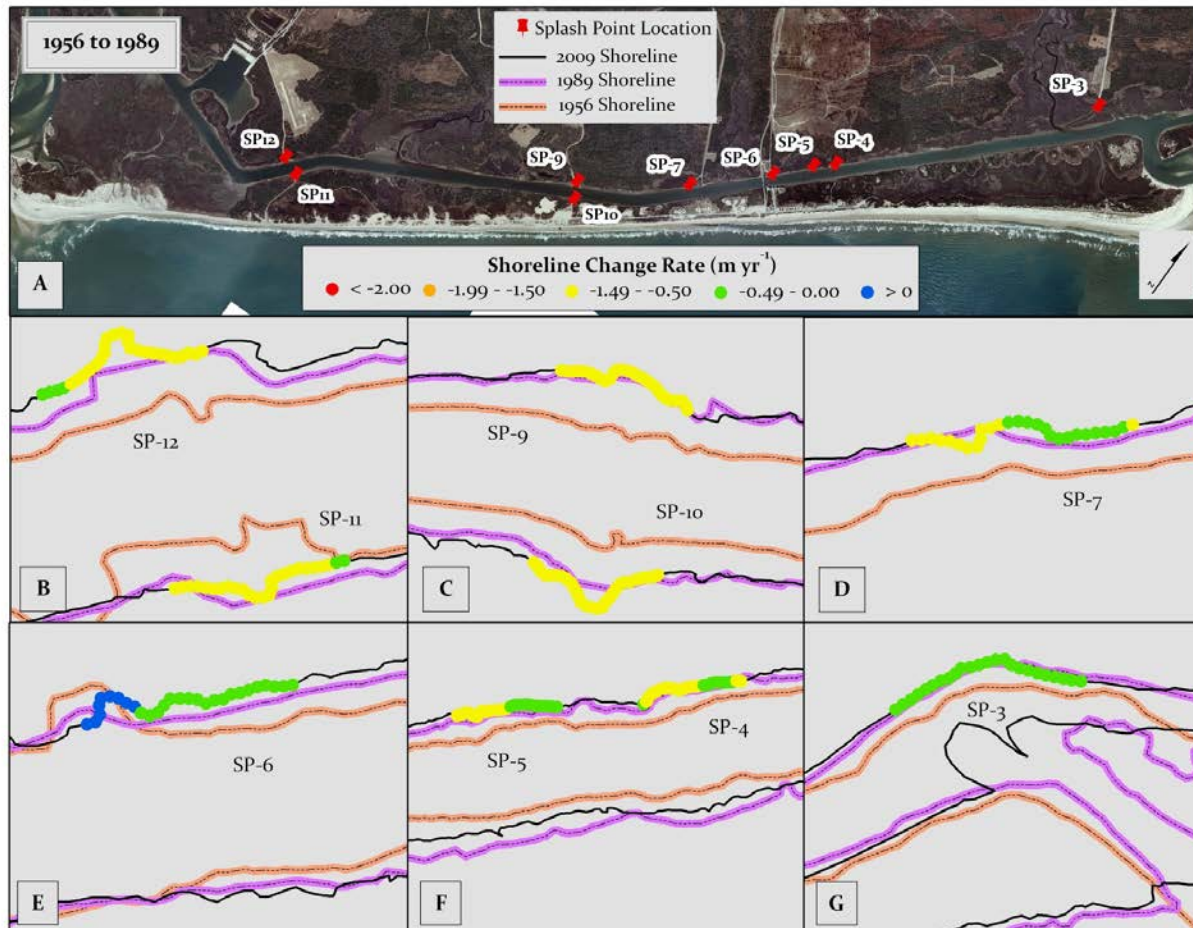


Figure 8-30. Map of ICW splash point locations (A) and SCR rates (B-G).

Shoreline-change rates from 1989 to 2009 are shown at each of the splash point areas w/ high erosion represented by red and orange and lower erosion shown as blue and green. Accretion is shown as purple. The 1956 (brown), 1989 (purple), and 2009 (black) shorelines are shown.

LCAC marsh margin impact assessment: The area of the polygons was calculated and summarized according to “water” and “marsh” for each time sequence (**Figure 8-31**). The area of marsh and water does not change significantly through the time series analyzed. The amount of marsh area is highest in 1989 and does decrease slightly over time. Therefore the water area increases from 1989 to 2004. However, these increases and decreases in area are not significantly different.

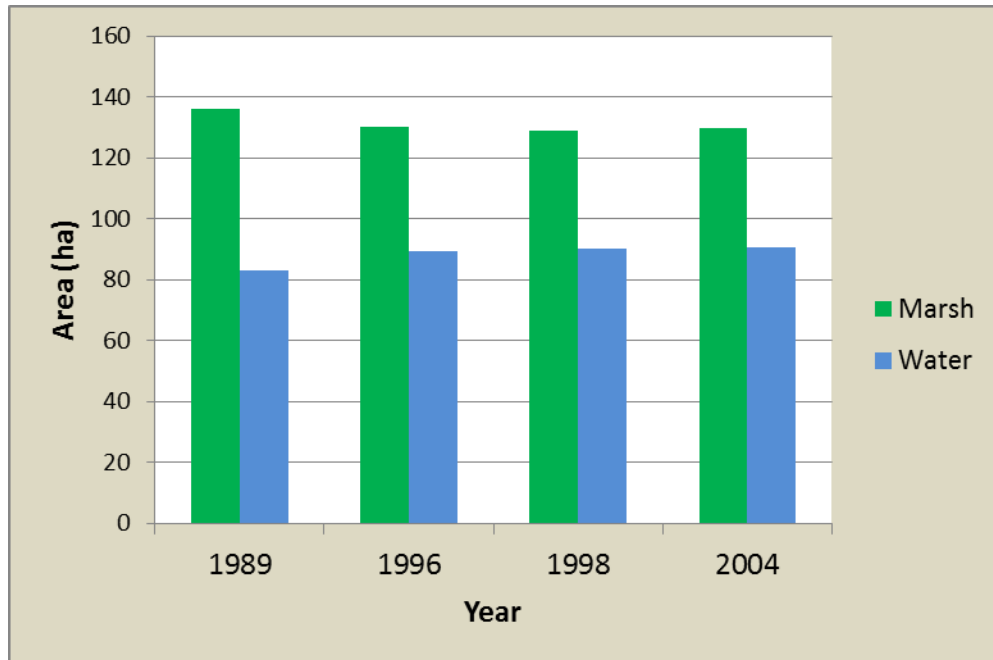


Figure 8-31. Bar graph showing salt marsh and open water area (ha) in the MHB LCAC operation area as determined from aerial photography.

Although the 1956 imagery was too coarse to perform an area analysis, the shoreline was digitized to show the amount of marsh loss that has occurred from 1956 to 2004 (**Figure 8-29A** and **32B**). Clearly the most significant marsh loss is associated with migration of the inlet channel (**Figure 8-32B**). Additionally, the LCAC tracks that were visible in the available imagery were digitized. One LCAC track was present in the 2002 imagery and five LCAC tracks were present in the 2004 imagery (**Figure 8-32C**). However, in the most recent imagery (from 2007), there are no visible remnants of the LCAC tracks (**Figure 8-32D**).

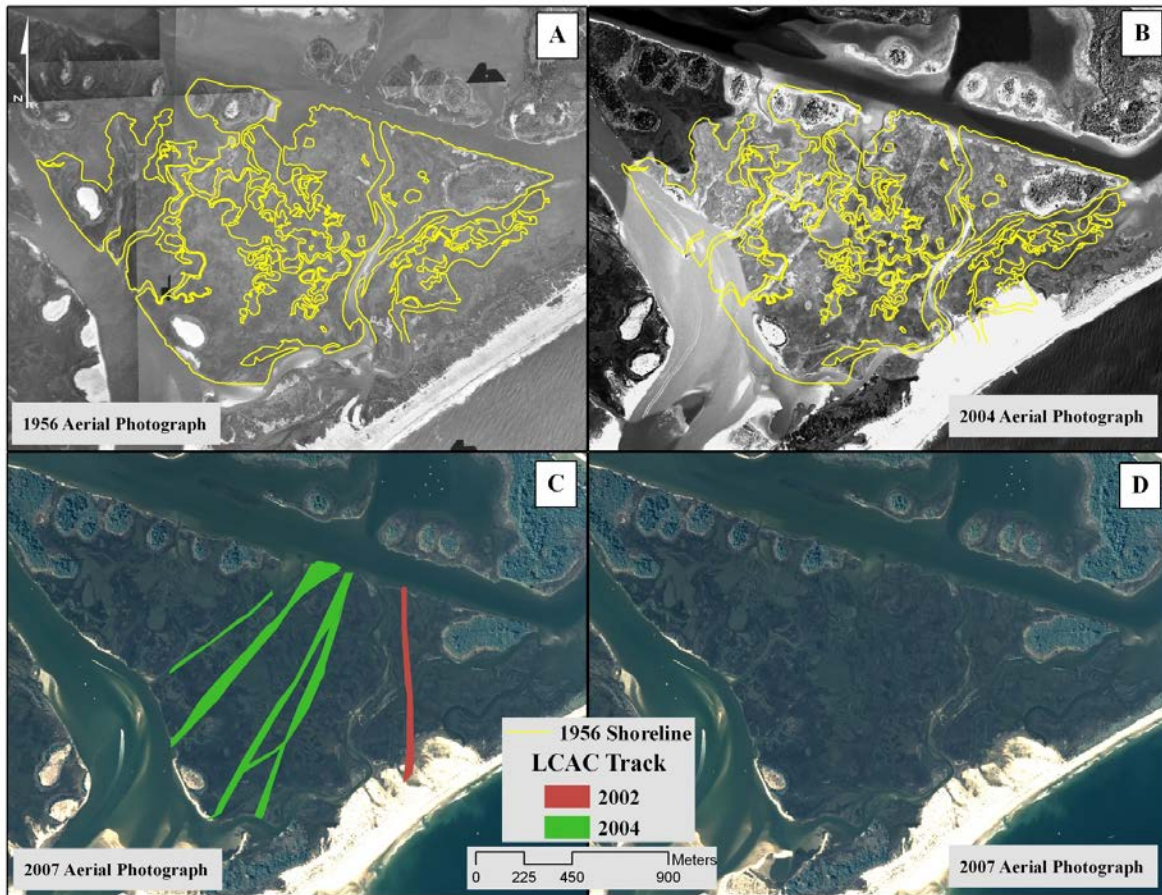


Figure 8-32. Maps of the MHB area displaying the 1956 shoreline (yellow) on the (A) 1956 imagery and (B) 2004 imagery, where LCAC tracks are visible.

2007 imagery is displayed with (C) the location of LCAC tracks digitized from 2002 and 2004 imagery; and (D) without overlying tracks demonstrating no visible LCAC tracks in the 2007 imagery.

Data obtained from the MHB-area study plots showed that the average elevation was similar in the MHBC (0.103 m North American Vertical Datum of 1988 [NAVD88]) and MHCL (0.097 m NAVD88) plots. This elevation is intermediate between the two other major marsh vegetation study sites established along the ICW, and in fact is near the optimum elevation for aboveground marsh biomass as determined from data collected for the Coastal Wetlands research program. Within each plot, we also compared marsh elevations in areas where there was evidence from aerial photographs of direct LCAC impact, and areas that lay outside of the LCAC impacts as recorded in aerial photographs. In the MHL plot, there were only six elevation points obtained in areas outside the observed impact, compared to 19 points which coincided with LCAC impact, and the difference in average elevation was only 3 mm, and was not statistically significant. There was a statistically significant difference ($p=0.027$, t -test) between elevation points taken in the MHBC plot which coincided with the recorded LCAC impact ($\bar{x}=0.064$ m, $n=12$) and areas which had not been observed to be directly impacted by LCAC passage ($\bar{x}=0.101$ m, $n=13$).

Although, experimental passages of an LCAC over the marsh would be required to test the hypothesis that LCAC utilization lowers the marsh elevation, based on the analysis of

marsh:water area over time and the aerial record of LCAC track visible disturbance, we conclude that at the historic rate of usage, LCACs do not have a lasting impact (greater than 3 years) on the marsh, either in terms of elevation, production or fragmentation. There is a large amount of marsh loss when the historical 1956 imagery is included. The largest area of marsh loss is located on the marsh edge adjacent to the New River Inlet main channel. We note that although the impacts of LCACs may not be present through aerial analysis after a few years, there may be smaller scale physical impacts that are not apparent through aerial analysis. This will be addressed further in the *DCERP1 Final Monitoring Report*.

Conclusions and Implications for Future Research

Section 1: NRE Shoreline Types, Erosion Rate, and Sediment Input

We utilized a customized WEMo to evaluate the wind wave and sediment erosion potential of the NRE. The median wind wave height was 0.22 m, and the 95th percentile wave height was approximately 0.38 m. However, in the most exposed areas of the NRE, maximum wave heights were forecast to slightly exceed 0.5 m. Several creek mouths were found to be points of high wave energy, suggesting that any discharge from these creeks in particular could often be passing an area of high resuspension capacity, which could enhance the liberation of any water column sediments or nutrients emerging from these creeks' watersheds into the rest of the estuary. Thus, sediment and nutrient loading into these creeks in particular should receive special attention from managers.

In addition to the creek mouths, many zones and "hot spots" of potential sediment resuspension were identified. The isolated nature of these locations (as compared to the geographically broad surface wave energy classifications) can help guide water quality sample stratification (e.g., suspended solids, chl *a*, turbidity overall) and reveal where additional military training activities (such as splash points) should potentially be limited given the potential for sediment resuspension and downstream water quality effects.

We conducted a detailed survey of the NRE shoreline. As of our survey in 2009, approximately 21% of the shoreline of the NRE had been modified. Revetments (loose rubble along the shoreline composed of granite, marl or construction material) accounted for 18% of the shoreline, 3% of the vertical bulkhead, and 0.005% of stone sills. Revetments occurred in all wave classes but comparatively fewer were found in the highest wave class. Similarly, stone sills were located only in the lower wave classes and vertical bulkheads showed a generally inverse relationship of numbers with increasing wave class, possibly the result of boat basins (in low wave energy areas) to preferentially utilize these structures.

An initial ground-truthing survey comparing shoreline classifications made from the 2004 aerial imagery with field observation revealed frequent errors of classification. By conducting a field survey of the entire shoreline in 2009, we reduced the unclassifiable shoreline to zero and found substantial changes in all other shoreline classes. In particular, what was previously classified as Sediment Bank was frequently found to be either Saltmarsh, Modified, or Swamp Forest. The amount of hardened shoreline also increased substantially after the ground-truthing, which may be a result of both real increases in shoreline hardening between 2004 and 2009, and the fact that

many revetments are obscured by overlying trees and vegetation, and thus missed in aerial imagery assessments.

SCR was determined from analysis of historical aerial imagery and based on the survey dates, divided into an Early (1956–1989) and Recent period (1989–2004). Over the time period of 1956–2004, the NRE Sediment Bank SCR averaged -0.45 m y^{-1} . High and medium relief Sediment Banks (greater than 1 m) exhibited greater erosion rates than banks less than 1 m in height. The SCR for low and medium relief banks was higher during the Recent period than from the Early period, coinciding with an active hurricane period. With the exception of the Sediment Bank with Saltmarsh fringe, all shorelines demonstrated increased erosion with increased wave energy. For the Sediment Bank with Saltmarsh shoreline type, SCR decreased with increasing wave energy, suggesting that these sites were depleted in remaining sediment to be eroded. Swamp Forest shorelines had the most substantial change with strongly negative SCR values in the Recent period of increased hurricane activity. SCR for most of the putative modified shorelines (except the lowest wave class) were not unlike that of the saltmarsh shorelines, and unlike other shoreline types, rates decreased in the Recent period (Table 8-5). We suspect that this is in part due to modifications that occurred post-1989, so that Early period erosion rates include what were then unmodified shorelines. Shorelines experiencing the highest wave energy category, representing the top 5% of the wind events experienced in the NRE, may be “hot spots” for erosion and may be areas of special attention for shoreline management plans (**Figure 8-13**).

The existence of Saltmarsh across all wave classes and their mitigative effect on Sediment Bank erosion suggests that saltmarshes are providing important stabilization services and should receive high priority for shoreline erosion protection. We have identified several erosion “hot spots” where salt marsh restoration may provide erosion protection, in addition to the other ecosystem services marshes are noted for, including fishery and nursery habitat, filtration of pollutants and sediment, and reduction of nutrients. Marshes may also be used to stabilize sediment banks to reduce sediment loading and potential water quality impacts from elevated suspended sediment loads.

Through SCR analysis we determined that the average annual volume of sediment eroded from NRE Sediment Banks was approximately $35,300 \text{ m}^3 \text{ y}^{-1}$, assuming a vertical shore face. A more conservative estimate, assuming a 45-degree angle, would be half that amount, or approximately $17,500 \text{ m}^3 \text{ y}^{-1}$. Given that the current average rate of SLR along the North Carolina coast is 2.7 mm y^{-1} , and is expected to accelerate, for the approximately 1,100 ha of salt marsh on MCBCL to keep up with SLR, approximately $32,100 \text{ m}^3$ of sediment must be accreted annually, an amount which falls close to the higher estimates of annual sediment volume released by bank erosion, but only about half the amount assuming a less steep shore face. These estimates demonstrate the potential importance of NRE bank erosion in supplying sediment to sustain the coastal wetlands on MCBCL, as well as the important role of marshes in maintaining water quality.

We found that there were many hardened shoreline segments in areas of low forecast wind wave energy. We suggest that these locations are strong candidates for evaluation of ecological restoration by removal of the modified structures and transplanting. Moreover, if there was any remaining vegetation after removal of the modified structures, this may supplement the

revegetation process significantly. Shorelines with wave regimes up to approximately 340 j m^{-1} represent a transition condition from good potential for restoration candidates to where conversion of modified to living shoreline through removal of hardening and vegetative restoration would be more slightly more experimental, although saltmarsh in coastal North Carolina occurs on shorelines with RWE values well above the 583 j m^{-1} of this wave energy class. Conversely, we documented a number of locations where high wave energy can be expected at the shoreline and special attention should be given to maintaining the status of shoreline structures.

These results provide evidence to reject the null hypotheses that exposure to wind wave energy, marsh vegetation, and storm events do not affect sediment erosion rates. In addition, we were able to characterize the distribution of shoreline types in different wave energy settings, provide the first evidence of narrow marsh fringe protecting estuarine sediment banks from erosion in high energy settings, and provide historic shoreline erosion rates during periods of both high and low hurricane activity for a number of shoreline types.

Section 2: ICW Waterway Erosion Rates and Boating Impacts

Using an automated video surveillance system, we captured the passage of several hundred vessels on video tape; from this sampling we detected 528 V-hull vessels. Because these vessels were the ones that dominated wake development, we have focused analysis solely on this hull type (sailboats and larger displacement hull vessels were traveling almost exclusively at very low speeds and generated little detectable wake; very large displacement vessels such as tugs or barges create unique effects on the shoreline but for this portion of the waterway were very rare events). During peak migration time, April–May, we detected an average of approximately 14 V-hull vessels per day. The average hull length was 13 m, and 95% of the vessels were less than approximately 22 m in length. Approximately 30% were approximately 7.5 m or less and are typically locally operated vessels. Overall during the 16-month period, we detected 4,824 boat wakes. Both the median and 95th percentile of wind waves are larger than those of the boat wakes sampled but the top few percent of boat wake wave events exceed the top few percent of wind waves. However, the relative distribution of wind wave versus boat wakes in the estuary will determine impacts; areas subjected to frequent large wind waves will likely prove resilient to most boat wakes. Given that un-modified shorelines in the NRE exposed to wind wave heights of approximately 0.35 m are eroding from year to year, it is not surprising that larger waves from vessels would be responsible for similar levels of shoreline erosion that we have documented along the ICW.

To begin to understand where the tipping point between wind and boat wake wave effects may occur in the estuary, we computed the relative contribution of wind wave versus potential boat wake wave energies in a test section of the lower NRE. Of the 290 test bed locations, approximately 43% would not experience boat wakes greater than that of the background (95th percentile) wind wave conditions. Based on this preliminary approach of comparing wind wave and boat wake wave regimes, it appears that boat wake effects will diminish rapidly with distance away from the ICW in situations where the embayment is expanding to larger fetches. In contrast, small bays that communicate exclusively with the ICW are forecast to experience substantial boat wake waves and thus, potential ecological shifts in shoreline composition and stability.

ICW SCR was determined from analysis of historical aerial imagery. This analysis demonstrated that the ICW has essentially doubled in width since construction, from approximately 70 m in 1938 to more than 145 m in 2009. The SCR needed to provide this rate of channel widening is approximately -0.5 m y^{-1} . Analysis of SCR in the ICW between 1989 and 1999 revealed a reduction in SCR of -0.21 m y^{-1} . Together, these data suggest that although the channel has widened substantially since construction, shoreline erosion rates have been reduced in more recent years.

We also considered the potential impacts associated with military access to the NRE and ICW. A variety of amphibious vessels enters and exits the ICW at a number of designated “splash points.” Observations and discussions with Base personnel suggest that several of these are particularly active, including Splash Points 9, 10, 11, and 12. None of these splash points are hardened, and three of them exhibited higher erosion rates between 1989 and 2009 than the average ICW SCR. We recommend that Splash Points 10, 11, and 12 be considered for modification, reinforcement, or relocation. However, in general it appears that splash points are localized sources of sediment resuspension and movement, although given their small size and low numbers, do not appear to be forming a substantial threat to shoreline integrity.

Finally, although experimental passages of an LCAC vehicle over the marsh would be required to test the hypothesis that LCAC utilization lowers the marsh elevation, based on the analysis of marsh:water area over time and the aerial record of LCAC track visible disturbance we conclude that the historic rate of LCAC training events does not have a lasting impact (greater than 3 years) on saltmarsh production, elevation or fragmentation, under historical usage.

In contrast to the NRE, in most sections of the ICW on MCBCL, wind wave energy is not a significant factor affecting shoreline erosion, but recreational boating traffic has the potential to be a significant factor. Because the ICW had doubled in width since its creation, the effect of boat wakes may have lessened over time, even as their frequency has increased. Military activities, including exercises utilizing splash points and LCAC passage over salt marsh, have a minimum to moderate impact on shoreline erosion rates. Several splash points demonstrated increased erosion rates and would be good candidates for modification or revegetation. Historic rates of LCAC training appear to have had temporary adverse impact to MHB-area marshes.

Literature Cited

- Boak, E.H., and I.L. Turner. 2005. Shoreline definition and detection: A review. *Journal of Coastal Research* 12:688–703.
- Bowden, K.F. 1962. Measurements of turbulence near the sea bed in a tidal current. *Journal of Geophysical Research* 67:3181–3186.
- Brinson, M.M., W.L. Bryant, and M.N. Jones. 1991. Pp. 23–46 in *Composition, Distribution and Dynamics of Organic Sediments: Ecology of a Nontidal Brackish Marsh in Coastal North Carolina*. Edited by M.M. Brinson. U.S. Fish and Wildlife Service and East Carolina University.
- Broome, S.W., S.M. Rogers Jr., and E.D. Seneca. 1992. *Shoreline Erosion Control Using Marsh Vegetation and Low-Cost Structures*. UNC-SG-92-12. University of North Carolina Sea Grant College, Kure Beach, NC.
- Cowart, L., J.P. Walsh, and D.R. Corbett. 2010. Analyzing estuarine shoreline change: A case study of Cedar Island, NC. *Journal of Coastal Research* 26(5):817–830.
- Craft, C.B., J.M. Reader, J.N. Sacco, and S.W. Broome. 1999. Twenty five years of ecosystem development on constructed *Spartina alterniflora* (Loisel) marshes. *Ecological Applications* 9:1405–1419.
- Craft, C.B., E.D. Seneca, and S.W. Broome. 1993. Vertical accretion in microtidal regularly and irregularly flooded estuarine marshes. *Estuarine, Coastal and Shelf Science* 37:371–386.
- Crawford, R. 1998. Measuring Boating Effects of Turbidity in a Shallow Coastal Lagoon. In *The Environmental Impacts of Boating: Workshop Proceedings*, Woods Hole Oceanographic Institution, Woods Hole, MA. December 7–9, 1994. Technical Report: WHOI-98-03. Edited by R. Crawford, N. Stolpe, and M. Moore.
- Curran, C.A., W.S. Chappell, and A. Deaton. 2010. Developing Alternative Shoreline Armoring Strategies: The Living Shoreline Approach in North Carolina. Edited by H. Shipman, M. Dethier, G. Gelfanbaum, K.L. Fresh, and R.S. Dinicola. Pp. 91–102 *Proceedings of Puget Sound Shorelines and the Impacts of Armoring*. USGS Scientific Investigations Report 2010-5254.
- Donelan, M.A., J. Hamilton, and W.H. Hui. 1985. Directional spectra for wind-generated waves. *Philosophical Transactions of the Royal Society of London A* 315L:509–562.
- Ellis, M.Y. 1978. *Coastal Mapping Handbook*. U.S. Department of the Interior, U.S. Geological Survey, and U.S. Department of Commerce, National Ocean Service and Office of Coastal Zone Management, U.S. Government Printing Office, Washington, DC.

- FitzGerald, D.M., S.F. Michael, A.A. Britt, and V.B. Ilya, 2008. Coastal Impacts Due to Sea-Level Rise. *Annual Review of Earth and Planetary Sciences* 36: 601-647.
- Fonseca, M.S., and A. Malhotra. 2012. Boat Wakes and Their Influence on Erosion in the Atlantic Intracoastal Waterway, North Carolina. NOAA Technical Memorandum NOS NCCOS #143. U.S. Department of Commerce, National Oceanic and Atmospheric Administration, National Ocean Service, Beaufort, NC. (24 pages).
- Gedan, K.B., M.L. Kirwan, E. Wolanski, E.B. Barbier, and B.R. Silliman. 2011. The present and future role of coastal wetland vegetation in protecting shorelines: Answering recent challenges to the paradigm. *Climatic Change* 106:7–29.
- Hasselmann, K., T.P. Barnett, E. Bouws, H. Carlson, D.E. Cartwright, K. Enke, and J.A. Ewing. 1973. Measurements of wind-wave growth and swell decay during the Joint North Sea Wave Project (JONSWAP). Deutsche Hydrographisches Institute, Hamburg, Germany *Supplement. A 12*. (95 pages).
- IPCC (Intergovernmental Panel on Climate Change). 2007. *Climate Change 2007: The Physical Science Basis: Contribution of Working Group I to the Fourth Assessment Report of the Intergovernmental Panel on Climate Change*. Cambridge University Press. Available at http://www.ipcc.ch/publications_and_data/publications_and_data_reports.shtml.
- Jordan, T.E., D.L. Correll, and D.F. Whigham. 1983. Nutrient flux in the Rhode River and tidal exchange by brackish marshes. *Estuarine, Coastal and Shelf Science* 17:651–667.
- Keddy, P.A. 1982. Quantifying within-lake gradients of wave energy: Interrelationships of wave energy, substrate particle size and shoreline plants in Axe Lake, Ontario. *Aquatic Botany* 14:41–58.
- Kelly, N.M., M. Fonseca, and P. Whitfield. 2001. Predictive mapping for management and conservation of seagrass beds in North Carolina. *Aquatic Conservation. Marine and Freshwater Ecosystems* 11:437–451.
- Kennish, M.J. (Ed.). 2002. Impacts of motorized watercraft on shallow estuarine and coastal marine environments. *Journal of Coastal Research, Special Issue 37*. (202 pages).
- Kneib, R.T. 1997. The role of tidal marshes in the ecology of estuarine nekton. Pp. 163–220 in *Oceanography and Marine Biology: An Annual Review* 35. Edited by A.D. Ansell, R.N. Gibson, and M. Barnes.
- Knutson, P.L. 1988. Role of coastal marshes in energy dissipation and shore protection. Pp. 161–175 in *The Ecology and Management of Wetlands, Volume 1: Ecology of Wetlands*. Edited by D.D. Hook, W.H. McKee Jr., H.K. Smith, J. Gregory, V.G. Burrell Jr., M.R. DeVoe, R.E. Sojka, S. Gilbert, R. Banks, L.H. Stolzy, C. Brooks, T.D. Matthews, and T.H. Shear. Timber Press: Portland, OR.

- Knutson, R.A., C.R. Taylor, J.B. Penson, and E.G. Smith. 1990. *Economic Impacts of Reduced Chemical Use*. Knutson and Associates: College Station, TX.
- Levin, L.A., D.F. Boesch, A. Covich, C. Dahm, C. Erséus, K.C. Ewel, R.T. Kneib, A. Moldenke, M.A. Palmer, P. Snelgrove, D. Strayer, and J.M. Weslawski. 2001. The function of marine critical transition zones and the importance of sediment biodiversity. *Ecosystems* 4:430–451.
- Mallin, M.A., M.R. McIver, H.A. Wells, D.C. Parsons, and V.A. Johnson. 2005. Reversal of eutrophication following sewage treatment upgrades in the New River Estuary, North Carolina. *Estuaries* 28:750–760.
- Mitsuyasu, H., F. Tasai, T. Suhara, and S. Mizuno. 1980. Observations of the power spectrum of ocean waves using a cloverleaf buoy. *Journal of Physical Oceanography* 10:286–296.
- Moller, I., T. Spencer, and J.R. French. 1999. Wave transformation over salt marshes: A field and numerical modeling study from North Norfolk, England. *Estuarine Coastal Shelf Science* 49:411–426.
- Morris, J.T. 1991. Effects of nitrogen loading on wetland ecosystems with particular reference to atmospheric deposition. *Annual Review of Ecology and Systematics* 22:257–279.
- Morris, J.T., P.V. Sundareshwar, C.T. Nietch, B. Kjerfve, and D.R. Cahoon. 2002. Responses of coastal wetlands to rising sea level. *Ecology* 83:2869–2877.
- NRC (National Research Council). 2007. *Mitigating Shore Erosion Along Sheltered Coasts*. National Academy Press: Washington, DC.
- NRC (National Research Council). 2000. *Clean Coastal Waters: Understanding and Reducing the Effects of Nutrient Pollution*. National Academy Press: Washington, DC.
- Pierson, W.J., and L. Moskowitz. 1964. A proposed spectral form for fully developed wind seas based on the similarity theory of S.A. Kitaigorodskii. *Journal of Geophysical Research* 69:5181–5190.
- Riggs, S.R., and D.V. Ames. 2003. *Drowning the North Carolina coast: Sea Level Rise and Estuarine Dynamics*. North Carolina Department of Environment and Natural Resources and the North Carolina Sea Grant, Raleigh, NC. UNC-SG-03-04. (152 pages). Available at <http://core.ecu.edu/geology/riggs/DROWNING%20The%20NC%20Coast.pdf>.
- Roland, R.M., and S.L. Douglass. 2005. Estimating wave tolerance of *Spartina alterniflora* in coastal Alabama. *Journal of Coastal Research* 21(3):453–463.
- Schwimmer, R.A. 2001. Rates and processes of marsh shoreline erosion in Rehoboth Bay, Delaware, USA. *Journal of Coastal Research* 17:672–683.

- Soulsby, R.L. 1987. Calculating bottom orbital velocity beneath waves. *Journal of Coastal Engineering* 11:371–380.
- Thieler, E.R., E.A. Himmelstoss, J.L. Zichichi, and A. Ergul. 2009. Digital Shoreline Analysis System (DSAS) Version 4.0—An ArcGIS Extension for Calculating Shoreline Change: U.S. Geological Survey Open-File Report 2008-1278. Tobias, C.R., S.A. Macko, I.C. Anderson, E.C. Canuel, and J.W. Harvey. 2001. Tracking the fate of a high concentration groundwater nitrate plume through a fringing marsh: A combined groundwater tracer and in situ isotope enrichment study. *Limnology Oceanography* 46:1977–1989.
- USACE (U.S. Army Corps of Engineers). 2001. *U.S. Army Corps of Engineers, Coastal Engineering Manual*. EM 1110-2-1100 (6 volumes). Washington, DC.
- USACE (U.S. Army Corps of Engineers). 1977. *Shore Protection Manual, Volume 1*. U.S. Army Corps of Engineers, Coastal Engineering Research Center, Ft. Belvoir, VA.
- Valiela, I., and J.M. Teal. 1979. The nitrogen budget of a salt marsh. *Nature* 280:652–656.
- Wiberg, P.L., and C.R. Sherwood. 2008. Calculating wave-generated bottom velocities from surface-wave parameters. *Computers and Geosciences* 34:1243–1262.
- Zervas, C. 2004. *North Carolina Bathymetry/Topography Sea Level Rise Project: Determination of Sea Level Trends*. U.S. Department of Commerce, National Ocean Service, Center for Operational Oceanographic Products and Services. NOAA Technical Report NOS CO-OPS 041. Available at <http://tidesandcurrents.noaa.gov/publications/techrpt41.pdf>.

[This page intentionally left blank.]

Appendix 8-A

List of Scientific Publications

List of Scientific Publications

Papers

- Currin, C.A., M.F. Fonseca, A. Malhotra, and L. Cowart. In preparation. Role of wave energy and shoreline type on erosion rates in the New River Estuary, NC. To be submitted to the *Journal of Coastal Research*.
- Malhotra, A., M.F. Fonseca, C.A. Currin, G. Fisher, and L. Cowart. In preparation. Quantifying the effects of boat wake and wind energy on shoreline erosion in Intracoastal Waterways, North Carolina. To be submitted to the *Journal of Ocean and Coastal Management*.

Technical Reports

- Currin, C.A., W.S. Chappell, and A. Deaton. 2010. Developing alternative shoreline armoring strategies: The living shoreline approach in North Carolina. Pp. 91–102 in *Puget Sound Shorelines and the Impacts of Armoring. In Proceedings of a State of the Science Workshop. May 2009*. Edited by H. Shipman, M.N. Dethier, G. Gelfenbaum, K.L. Fresh and R.S. Dinicola. U.S. Department of the Interior, U.S. Geologic Survey, Reston, VA. Scientific investigations report 2010-5254.
- Fonseca, M.S., and A. Malhotra. 2009. *Hurricane Emergency Drill, Marine Corps Base Lejeune*. A report to MCBCL. NOAA, National Ocean Service, Center for Coastal Fisheries and Habitat Research.

Presentations

- Cowart, L., C. Currin, M. Fonseca, and A. Malhotra. 2010. *Analyzing Shoreline Change in the New River Estuary, North Carolina*. Presented at the Coastal Society's 22nd International Conference, Wilmington, NC. June 13–16.
- Currin, C.A. et al. 2012. *Guidance for Estuarine Shoreline Stabilization Policy: Shoreline Erosion Rates and Impact of Stabilization Structures*. Presented at the Southeastern Estuarine Research Society Biannual Meeting, Beaufort, NC. April 11–13.
- Currin, C.A., M. Greene, P. Delano, and L. Cowart. 2011. *Measuring Marsh Surface Elevation and Shoreline Changes at Multiple Spatial and Temporal Scales in the New River Estuary, NC*. Presented at the Coastal and Estuarine Research Federation Annual Conference, Daytona Beach, FL. November 6–10.
- Currin, C.A. 2009. *Wave Energy Alters Patterns and Rates of Marsh Sediment Accretion and Primary Production*. Presented at Society of Wetland Scientists Annual Meeting, Madison, WI. June 22–24.
- Currin, C. 2009. *Analyzing Shoreline Change in the New River Estuary*. Presented at the SERDP/Environmental Security Technology Certification Program (ESTCP) Symposium, Washington, DC. December 2.

Curran, C.A., M.S. Fonseca, A. Malhotra, and D. Field. 2009. *The Influence of Wave Energy on Plant Communities and Sedimentary Processes in Salt Marsh and Shallow Subtidal Estuarine Habitats*. Presented at the American Society of Limnology and Oceanography Meeting, Nice, France. January 25–30.

Fonseca, M.S., A. Malhotra, and C.A. Currin. 2011. *Wind Waves and Boat Wakes—A Challenge for Sustainable Shorelines at Marine Corps Base Camp Lejeune*. Presented at the SERDP/ESTCP Partners in Environmental Technology Technical Symposium & Workshop, Washington, DC. November 29–December 1.

[This page intentionally left blank.]

Chapter 9

**Hydraulic Exchange and Nutrient Reactivity
in the New River Estuary Wetlands**

SERDP Project Number: RC-1413

Coastal Wetlands Module

Research Project CW-3

Lead Researcher:
Dr. Craig Tobias
University of Connecticut
Groton, CT
E-mail: craig.tobias@uconn.edu

May 10, 2013

Final

This report was prepared under contract to the U.S. Department of Defense (DoD) Strategic Environmental Research and Development Program (SERDP). The publication of this report does not indicate endorsement by DoD, nor should the contents be construed as reflecting the official policy or position of DoD. References herein to any specific commercial product, process, or service by trade name, trademark, manufacturer, or otherwise, do not necessarily constitute or imply its endorsement, recommendation, or favoring by DoD.

Table of Contents

List of Acronyms	9-vi
Abstract.....	9-1
Objectives of the Research Project	9-3
Objectives	9-3
Hypotheses	9-3
Background	9-4
Section 1: Assessment of Groundwater Nitrogen Delivery to MCBCL Marshes	9-6
Materials and Methods.....	9-6
Results and Discussion	9-8
Summary Points	9-18
Section 2: Advective Marsh-Estuary Exchange—Hydrologic and Dissolved Nitrogen	
Fluxes	9-19
Materials and Methods.....	9-19
Results and Discussion	9-20
Summary Points	9-31
Section 3: Marsh–Estuary Exchange—Attenuation of Dissolved Inorganic Nitrogen	
Fluxes by Denitrification	9-32
Methods and Materials.....	9-32
Results and Discussion	9-35
Summary Points	9-44
Section 4: Summary and Synthesis—Marsh Nitrogen Source/Sink Budget	9-46
Methods and Materials.....	9-46
Results and Discussion	9-46
Summary Points	9-48
Literature Cited	9-49
Appendix 9-A: List of Scientific Publications.....	9-A-1
Appendix 9-B: List of Students	9-B-1

List of Figures

9-1.	Conceptual model of salt marsh nitrogen linkages.	5
9-2.	Site locations and piezometer transect orientations.	6
9-3.	Salt balance estimation of groundwater flux based on monthly mean values.	7
9-4.	Box and whisker plots of fresh groundwater discharge to the French Creek marsh; March 2009–March 2010.	8
9-5.	Box and whisker plots of fresh groundwater discharge to the Traps Bay marsh; March 2009–March 2010.	10
9-6.	Box and whisker plots of fresh groundwater discharge to the Freeman Creek marsh; March 2009–March 2010.	11
9-7.	Upland water table elevations for French Creek (a), Traps Bay (b), and Freeman Creek (c).	13
9-8.	Short duration fluctuations in upland water table elevation (grey uppermost line), tidal elevation (black), and precipitation (bar) for French Creek (a), Traps Bay (b), and Freeman Creek (c).	14
9-9.	Contribution of groundwater to the total marsh water budget as a function of evapotranspiration.	15
9-10.	Groundwater inorganic nitrogen flux to the study marshes.	17
9-11.	Representative daily fluctuation of tidal elevation (solid), creekbank gradient (triangle), and interior gradient (circle) for French Creek (a), Traps Bay(b), and Freeman Creek (c).	23
9-12.	Creekbank drainage versus tidal elevation for French Creek transect 3 (a), transect 5 (b), and transect 7 (c).	24
9-13.	Creekbank drainage versus tidal elevation for Traps Bay transect 1 (most upstream) (a), transect 3 (b), transect 5 (c), and transect 7 (most downstream) (d).	25
9-14.	Creekbank drainage versus tidal elevation for Freeman Creek transect 1 (a), transect 3 (b), and transect 5 (c).	26
9-15.	All sites daily maximum drainage versus daily tidal amplitude.	27
9-16.	Mean monthly drainage corrected for cross sectional drainage area for French Creek (solid triangles), Traps Bay (open boxes), and Freeman Creek (solid diamonds).	28
9-17.	Monthly average Darcy-derived nitrogen flux for French Creek, Traps Bay, and Freeman Creek.	29
9-18.	Daily maximum observed high tide (black) and low tide (grey) for French Creek (a), Traps Bay (b), and Freeman Creek (c).	30
9-19.	Predicting marsh N flux based on tidal amplitude.	31
9-20.	Mean direct denitrification rates from 4-hour incubations for French Creek (a, b), Traps Bay (c, d), and Freeman Creek (e, f).	35

9-21.	Comparison of direct denitrification rates of May versus February (a) and marsh interior versus creekbank (b).	36
9-22.	Mean coupled denitrification rates from 4-hour incubations for French Creek (a–d), Traps Bay (e–h), and Freeman Creek (i–l).	38
9-23.	Comparison of coupled denitrification rates of marsh May versus February (a,b) and interior versus creekbank (c,d).	39
9-24.	Direct denitrification versus coupled denitrification for all samplings.	40
9-25.	Coastal marine denitrification rates compiled by Fennel et al. (2008).	42
9-26.	Denitrification and ANAMMOX capacity for French Creek creekbank (a) and interior (b), Traps Bay creekbank (c) and interior (d), and Freeman Creek creekbank (e) and interior (f).	43
9-27.	Nitrogen source/sink summary with respect to adjacent surface waters.	47

List of Tables

9-1.	Water Balance Summary for the French Creek Marsh. Monthly means \pm (standard deviation [SD]) of all piezometers.	9
9-2.	Water Balance Summary for the Traps Bay Marsh.	11
9-3.	Water Balance Summary for the Freeman Creek Marsh.	15
9-4.	Quarterly dissolved nitrogen concentrations.	16
9-5.	Hydraulic Conductivity (K_h) of Traps Bay and French and Freeman Creeks.	21
9-6.	Quarterly Porewater Concentrations of Total Dissolved Nitrogen (TDN) Based on Location Within Each Marsh.	29
9-7.	Per area marsh N burial rates.	46

List of Acronyms

%N	percent nitrogen content
μL	microliter
μM	micromolar
Mmole	micromole
$^{15}\text{KNO}_3$	potassium nitrate enriched with ^{15}N
^{15}N	nitrogen with a mass of 15 (labeled)
$^{15}\text{N}_2$	heavy nitrogen (nitrogen gas composed of two ^{15}N molecules)
$^{15}\text{NH}_4^+$	ammonium enriched with ^{15}N
$^{15}\text{NO}_3^-$	nitrate enriched with ^{15}N
$^{29}\text{N}_2$	paired nitrogen isotopes $^{15}\text{N} + ^{14}\text{N}$
$^{30}\text{N}_2$	paired nitrogen isotopes $^{15}\text{N} + ^{15}\text{N}$
A	area of the control volume
A_C	core area (square meters [m^2])
A_{total}	total ANAMMOX
ANAMMOX	anaerobic ammonium oxidation (reaction) in which ammonium and nitrite are converted to nitrogen (N_2) gas
cm	centimeter
cm^{-3}	per cubic centimeter
cm s^{-1}	centimeters per second
C_{N_2}	concentration of N_2 resulting from air equilibration in μM and V
C_{Post}	NH_4^+ concentration in μM after tracer addition
C_{Pre}	background concentration of NH_4 before tracer addition in μM
C_T	tidal salinity
C_W	porewater salinity
d	day
D	barometric pressure corrected depth
D	coupled denitrification rate
D_{14}	denitrification rate of $^{14}\text{NO}_3^-$
D_{15}	denitrification rate of $^{15}\text{NO}_3^-$
DCERP	Defense Coastal/Estuarine Research Program
D_{col}	total water column denitrification
D_{coupled}	coupled denitrification
D_{direct}	direct denitrification
dh	hydraulic head
dh/dx	hydraulic gradient
DIN	dissolved inorganic nitrogen
DIP	dissolved inorganic phosphate

DOC	dissolved organic carbon
DoD	U.S. Department of Defense
DON	dissolved organic nitrogen
dS/dt	change in salt inventory over time
D_{Tot}	total denitrification is the reduction of nitrates into nitrogen (N_2) gas
DTT	depth to transducer
DTW	depth to water
dV/dt	monthly change in volume storage in the subsurface
dx	horizontal distance between water porewater elevation measurements
E_E	effective isotopic enrichment
F_N	the fraction of ^{15}N in NO_3^-
g	gram
GPS	global positioning system
GW	groundwater
H	a plot of the ratio of water level
h_0	maximum water level
H_3PO_4	phosphoric acid
h_{PW}	porewater elevation
hr	hour
HM	horizon marker
HS^-	hydrogen sulfide ion
H_{TOC}	elevation of the top of casing
ICW	Intracoastal Waterway
IPT	isotope pairing technique
IRMS	isotope ratio mass spectrometer
K	hydraulic conductivity in Darcy's Law
KCl	potassium chloride
kg	kilogram
$kg\ N\ y^{-1}$	kilograms of nitrogen per year
K_h	horizontal hydraulic conductivity
km	kilometer
KOH	potassium hydroxide
L	liter
L_e	length of well screen
$L\ m^{-2}\ d^{-1}$	liters per square meter per day
m	meter
M	molar
m^2	square meter

$\text{m}^{-2} \text{d}^{-1}$	per meter squared per day
$\text{m}^{-2} \text{hr}^{-1}$	per meter squared per hour
m^3	cubic meter
$\text{m}^3 \text{yr}^{-1}$	cubic meters per year
MCBCL	Marine Corps Base Camp Lejeune
MF	mole fraction
mL	milliliter
mm	millimeter
mM	millimolar
MSL	mean sea level
N	nitrogen
N	frequency of tidal inundation
$\text{N mass m}^{-2} \text{y}^{-1}$	mass of nitrogen per square meter per year
N_2	nitrogen gas
n.a	not applicable
NAVD88	North American Vertical Datum of 1988
N_E	amount of excess ^{15}N
NH_4^+	ammonium
NH_4Cl	ammonium chloride
nmol	nanomole
NO_2	nitrite
NO_3^-	nitrate
NO_x	nitrate plus nitrite
NRE	New River Estuary
O_2	oxygen gas
P	porosity of the sediment
P_{29}	$^{29}\text{N}_2$ production
P_{30}	$^{30}\text{N}_2$ production
PN	particulate nitrogen
PON	particulate organic nitrogen
Q	drainage flux in Darcy's Law
Q_D	drainage flux
Q_{ET}	evapotranspiration flux
Q_{GW}	groundwater flux
Q_P	precipitation flux
Q_T	tidal infiltration flux
r	radius of well casing
R	radius of well screen

r_{29}	rate of $^{29}\text{N}_2$ production
r_{30}	rate of $^{30}\text{N}_2$ production
rhizosphere	the zone of soil surrounding a plant's roots
rpm	revolutions per minute
S	sediment volume in liters
SD	standard deviation
SET	sediment elevation table
SERDP	Strategic Environmental Research and Development Program
SLR	sea level rise
S_y	measured specific yield
T	temperature
T	incubation time in hours
$T_{0\ 29}$	initial concentration of $^{29}\text{N}_2$ in μM
$T_{0\ 30}$	initial concentration of $^{30}\text{N}_2$ in μM
t_{37}	time required for the water level to fall to 37% of the initial rise
TDIN	total dissolved inorganic nitrogen
TDN	total dissolved nitrogen
$T_{F\ 29}$	final concentration of $^{29}\text{N}_2$ in μM
$T_{F\ 30}$	final concentration of $^{30}\text{N}_2$ in μM
TOC	top of the casing
V	the overlying water volume in liters
y	year
ZnCl_2	zinc chloride
$(z_{\text{sed}}-h_{\text{min}})$	thickness of unsaturated zone at low tide

[This page intentionally left blank.]

Abstract

Our study assessed nitrogen (N) exchanges among intertidal marshes and adjacent watersheds and marine/estuarine waters within the Marine Corps Base Camp Lejeune (MCBCL). The work was performed in three marshes (i.e., French Creek, Traps Bay, and Freeman Creek) that represent a gradient in tidal amplitude, and marsh ecotypes common to the Base. Routes of N exchange focused on the following: groundwater discharge to marshes, marsh drainage to the New River Estuary (NRE) and Intracoastal Waterway (ICW), denitrification, and burial. The magnitude of the net N source or sink of the marshes was quantified.

Groundwater inputs to MCBCL were found to be an important source of fresh water to the rhizosphere (root zone of the marsh plants), but not an important source of N to the marshes of MCBCL principally because groundwater dissolved inorganic nitrogen (DIN) concentrations are low. The marshes of MCBCL do not function to remove large groundwater-derived N fluxes from the watershed because there are none. We estimated that there is a factor of 5–10 buffer for rising groundwater DIN concentrations before the groundwater N flux to the marshes could be deemed significant.

The N inputs from marsh drainage to open water are trivial, relative to other sources, from the marshes to the NRE, but are not trivial from the marshes to the ICW. Dissolved N inputs from marsh drainage can be estimated for a specific site given tidal amplitude, and estimates have a higher certainty at higher tidal amplitudes. Higher tidal amplitudes found in marshes along the southern margin of MCBCL translated into a factor of 10–50 higher rates of N delivery to adjacent surface waters through marsh porewater drainage. The higher tidal amplitude and greater marsh perimeter-to-area ratio in these southern marshes resulted in these systems being a local source of N to the mouth of the NRE and ICW.

Ambient denitrification rates in marshes of MCBCL are low and dominated by coupled denitrification because tidal nitrate (NO_3^-) concentrations are low and there is no groundwater source of NO_3^- . The NRE marshes remove N through denitrification that is equivalent to 1% of inputs from the New River mainstem. MCBCL marshes have a huge denitrification capacity and show linear increases in rates up to NO_3^- concentrations 2 orders of magnitude larger than current concentrations. With respect to the N source/sink budget of the marsh, denitrification is 1 to 2 orders of magnitude larger than marsh N export through drainage and inputs of groundwater N via groundwater.

When all exchange routes for N were considered, the intertidal marshes of MCBCL should be considered overwhelmingly large sinks for N. The N sink strength is dominated by sediment N burial during accretion (80–90%), and denitrification (10–20%). Scaling rates from each of the marshes to estimates of total marsh area across the Base, we estimated that 9,660 kg N y^{-1} is buried into the marshes bordering the NRE and 23,460 kg N y^{-1} is buried in the marshes bordering the ICW. The magnitude of the N sinks within the marshes would have to decrease on the order of 20-fold before the marshes would switch from being a net sink to a net source of N. Barring any extreme changes in marsh geomorphology (e.g., marsh edge to area ratio) or severe increases in tidal amplitude, if the existing marshes continue to accrete at rates keeping pace with sea level rise they will remain as a net N sink.

Keywords: Nitrogen, marsh, estuary, groundwater, drainage, denitrification, accretion, sediment, New River

Objectives of the Research Project

Objectives

1. Determine water exchange of groundwater and tidal water through the coastal marshes along the New River Estuary (NRE)
2. Couple water fluxes with nitrogen (N) chemistry to estimate dissolved N exchanges between marsh-estuary and marsh-upland boundaries.
3. Quantify marsh reactivity with respect to N (e.g., denitrification)
4. Couple reactivity measurements with solute fluxes and sediment deposition rates to determine the source/sink nature of marshes with respect to N.

Hypotheses

1. The marshes of the NRE attenuate watershed inputs of N by intercepting and processing shallow groundwater arriving from adjacent watersheds.
2. These marshes also modify the water quality of the NRE directly by processing organic and inorganic N delivered by tidal water.
3. NRE marshes are a net sink for N.

Background

Rates of nutrient loading and turnover affect water quality, recreational uses of coastal waters, and coastal ecosystem sustainability in the long term (Cloern, 2001; Valiela et al., 1990). Each of these factors is of concern to Marine Corps Base Camp Lejeune (MCBCL) with respect to sustainability of the military mission, and compliance with state and federal regulatory statutes. Nitrogen (N) is the principal nutrient limiting estuarine primary production in the New River Estuary (NRE). The availability of N is controlled by external rates of loading from the watershed and rates of N recycling/removal within and between ecosystem components within the estuarine landscape. Specific habitats that can modify both incoming loads of N from the watershed and also affect turnover of N once it enters the estuary play a central role in regulating overall N availability on an estuarine scale. Intertidal marshes represent such a habitat. They are situated between the N-rich upland and the N-limited estuary; well-positioned to impact the N budget through marsh-upland interactions and through marsh-estuary interactions.

Much effort has been exerted over the past 35 years to generally characterize the source and sink nature of intertidal marshes with respect to N (Childers, 1994; Correll, 1981; Valiela and Teal, 1979). No clear unifying consensus has emerged over whether marshes uniformly behave in all locations at all times as a source or sink. Groundwater, tidal exchange, burial, and denitrification represent significant pathways through which marshes may regulate N speciation and availability in adjacent estuarine waters (**Figure 9-1**; Tobias and Neubauer, 2009).

Groundwater at the coast is focused in the intertidal zone, areas commonly inhabited by emergent marshes (Bokuniewicz, 1992; Reilly and Goodman, 1985). Nitrate tends to be the dominant form of N delivered from the shallow aquifer to the marshes, and organic-rich wetland sediments are highly efficient at attenuating that nitrate load through denitrification (Tobias et al., 2001a). For groundwater to be considered a significant source of N to the marsh, the following two criteria must be met: (1) groundwater discharge into the marsh must be a large component of the marsh water budget; (2) groundwater N concentrations must be significant. If those two criteria are met, and the denitrification capacity of marsh sediments is high, the marsh can be considered as a buffer for direct watershed N inputs that would otherwise discharge to the estuary.

In combination with groundwater inputs, tidal flooding drives the hydrology of the marsh. During tidal infiltration and subsequent advection through the marsh subsurface, porewaters accumulate dissolved organic nitrogen (DON) and ammonium (NH_4^+) liberated from the decomposition of organic matter. The dissolved inorganic nitrogen (DIN) and DON drains from the marsh to adjacent surface waters at low tide (Harvey et al., 1987). The drainage flux of porewater integrates contributions from groundwater, tidal infiltration, and precipitation, with water loss from macrophyte evapotranspiration. Coupling the porewater drainage “water” flux with measurements of the N chemical composition of the porewater permits calculation of the source strength of marsh N to adjacent open water. The magnitude of both the drainage water and N fluxes varies temporally from hours to months as the magnitude of the components of the water budget changes in response to tidal cycles, precipitation patterns, and temperature, and mineralization rates change with growing season. As such, its characterization requires a high degree of temporal resolution.

The N delivered to the marsh via groundwater, tidal infiltration, and produced by organic matter decomposition may have alternate fates other than draining into the estuary. Some fraction of N

is converted to nitrogen gas (N_2) via denitrification, and some is used by macrophytes to, in concert with particle settling, yield vertical accretion of the marsh surface. Both of these fates can be considered N sinks in the coastal landscape. Denitrification can constitute a large N sink on par with rates of plant uptake. Unlike plant uptake or accretion that stores N in the marsh on varying timescales, denitrification converts N into N_2 and facilitates its complete removal from the coastal landscape to the atmosphere. Unlike the drainage N flux, denitrification is uncoupled from advective water transport. Although denitrification can be affected by patterns of tidal infiltration and drainage, rates of denitrification can be calculated independently of water movement. Marsh denitrification operates either directly on nitrate supplied by flooding water, precipitation, and groundwater (Seitzinger et al., 2006) or “indirectly” on nitrate produced from the nitrification of NH_4^+ produced during mineralization of organic matter in marsh sediments (“coupled denitrification”; Hamersley and Howes, 2005; Seitzinger et al., 2006). It therefore has the potential to attenuate N availability by acting on allochthonous (external) N loads and by decreasing the amount of N internally recycled within the marsh that would otherwise be available for drainage. Vertical accretion of the marsh surface represents burial of N on the decadal scale. Long-term sustainability of this N sink depends upon the ability of marsh accretion to keep pace with local sea level rise (2–3 mm for southeastern North Carolina).

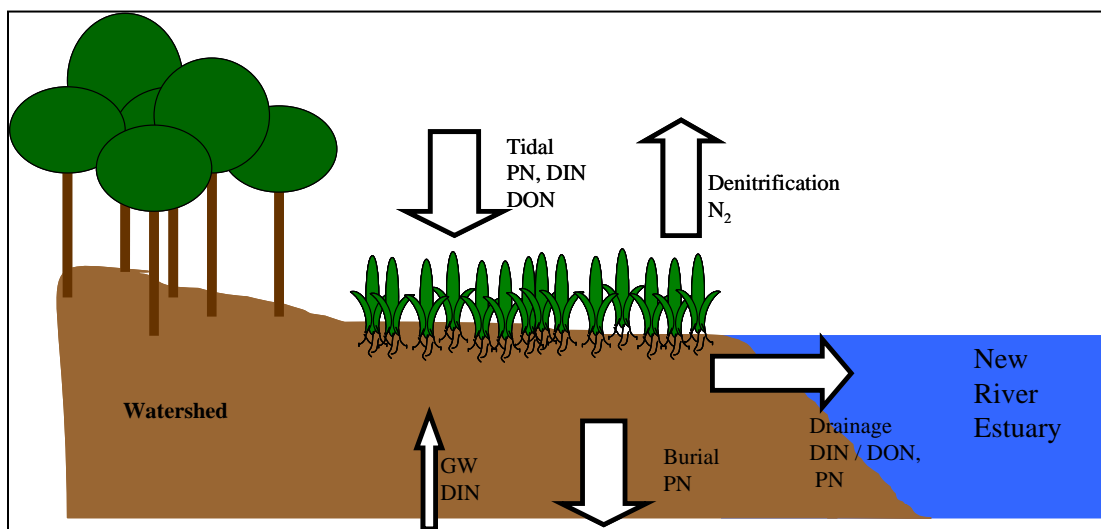


Figure 9-1. Conceptual model of salt marsh nitrogen linkages.

Tidal recharge supplies particulate nitrogen (PN), dissolved inorganic nitrogen (DIN), and dissolved organic nitrogen (DON). Groundwater (GW) inputs supply DIN. Burial removes PN. Denitrification results in gaseous loss of nitrogen gas (N_2). Porewaters drain to the adjacent estuary resulting in export of DIN, DON, and PN from the salt marsh system.

The net effect of the groundwater N inputs, tidal infiltration and drainage, and denitrification ultimately modify the availability of N to the adjacent estuary and resultant water quality (**Figure 9-1**). The overall balance of these processes determines the role and magnitude of intertidal marshes within the landscape as a source or sink for N.

Section 1: Assessment of Groundwater Nitrogen Delivery to MCBCL Marshes

Materials and Methods

Study Sites

The following three intertidal wetlands used for this study are located on MCBCL in Jacksonville, NC (**Figure 9-2**): Traps Bay, French Creek, and Freeman Creek. Each of the three sites contains shallow piezometers at 1 m below the marsh surface. Tide gauges were installed at each of the three study sites that recorded tidal elevation at 15-minute intervals. French Creek (**Figure 9-2**) is a fringing marsh dominated by needlerush (*Juncus* spp). It drains a high density area of woodland, industries, training areas, and the wastewater treatment plant. The site contains five piezometer transects.

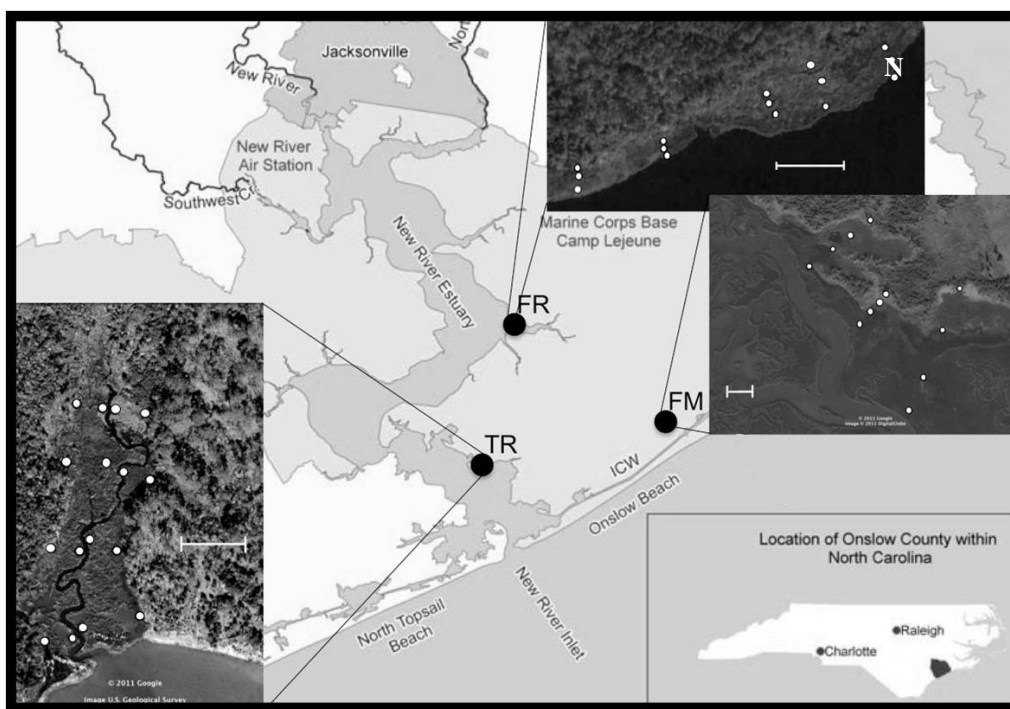


Figure 9-2. Site locations and piezometer transect orientations.

FR = French Creek, FM = Freeman Creek, and TR = Traps Bay. White dots denote piezometer locations.

Traps Bay (**Figure 9-2**) is a filled stream valley characterized by a wide distribution of *Juncus*, *Spartina*, and *Typha* spp. Traps Bay drains live fire and demolition ranges. Traps Bay contains four transects with four piezometer clusters. The Freeman Creek marsh (**Figure**) is the largest site with the largest tidal range. It is dominated by *Spartina* spp. exchanges with the Intracoastal Waterway (ICW) via a single channel. The site contains three parallel transects with four piezometer clusters along each and a tide gauge.

Salt Balance Estimation of Groundwater Flux

To determine the fresh groundwater discharge through each of these three salt-marshes, the water and salt mass balance method (salt balance) was used. This model calculates the groundwater

flux into a controlled volume of marsh subsurface, necessary to produce an observed monthly change in porewater storage and salinity (Tobias et al., 2001b, see **Figure 9-3**). A control volume of 1 m³ was used for the model in this study.

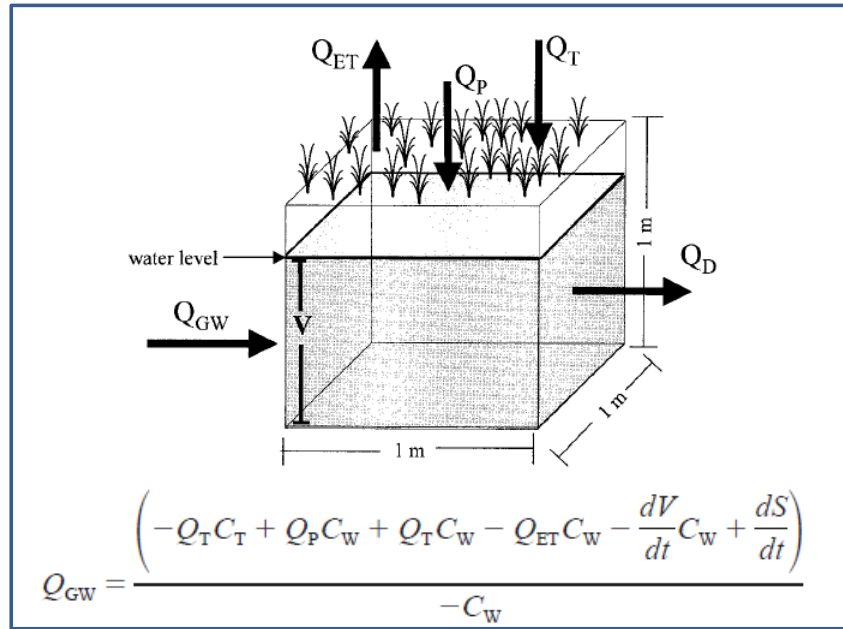


Figure 9-3. Salt balance estimation of groundwater flux based on monthly mean values.

Q_{GW} , Q_T , and Q_P are the monthly mean input fluxes of fresh groundwater, tidal infiltration, and precipitation, respectively. Q_{ET} and Q_D are the monthly output fluxes for evapotranspiration and drainage. C_W and C_T are the salinities of marsh porewater and flooding tidal water. V and S denote the water and salt inventories in the control volume. The equation is solved as a finite difference using biweekly data.

Each variable in the groundwater mass balance equation was determined monthly and normalized to a per day rate ($L\ m^{-2}\ d^{-1}$) for input into the model for calculating the groundwater discharge for each of the three wetlands. Evapotranspiration (Q_{ET}) and precipitation (Q_P) flux were derived from temperature and rainfall data collected at Defense Coastal/Estuarine Research Program (DCERP) Atmospheric Module's stations on the Base and the North Carolina climate network's station at Sneads Ferry. Q_{ET} was assumed to be equivalent to the temperature-derived potential evapotranspiration as defined by Bosen (1960) and Hamon (1961). The Q_P flux was equivalent to 14% of the rainfall deposited during periods of marsh emersion (i.e., not flooded), where 14% was defined by the measured specific yield (S_y) of the marsh sediments. Tidal infiltration (Q_T) was calculated from Equation 9-1 using the frequency of tidal inundation (N), the thickness of the unsaturated zone at low tide ($z_{sed}-h_{min}$), the S_y , and the area of the control volume (A). The average S_y was determined by triplicate cores at each of the sites according to a modification of an equation from Prathapar and Sides (1993).

$$Q_T = N (z_{sed} - h_{min}) S_y \times A \quad (\text{Eq. 9-1})$$

The thickness of the unsaturated zone and the flooding frequency per month was determined from surveyed marsh elevation, tidal and piezometer water levels measured with pressure transducers at 15-minute intervals. Piezometer water levels and porosity were used to calculate the monthly change in volume storage in the subsurface (dV/dt). Changes in salt inventory over

time (dS/dt) were calculated from biweekly porewater salinity (C_w) measurements conducted in all piezometers, and tidal salinity (C_T) was monitored at 15-minute intervals on each site specific tide gauge with the combined temperature-conductivity-pressure sensors (Aqua TROLL 2000, In-Situ Inc.).

Nitrogen Characterization of Groundwater and Calculation of Groundwater N flux

Quarterly measurement of shallow upland groundwater dissolved N chemistry were made in wells installed into the shallow water table upgradient from each marsh. Two wells each were installed at French Creek and Traps Bay, and three wells at the Freeman Creek site. Nitrate, NH_4^+ , and total dissolved N were measured. Dissolved N concentrations in these fresh groundwater endmembers were multiplied time the fresh volumetric groundwater fluxes calculated by the salt balance to yield N mass fluxes of groundwater derived N to each marsh. Quarterly N concentrations were interpolated to monthly values prior to matching the temporal interval of the fresh groundwater flux measurements. Total marsh scale groundwater N input and groundwater N input normalized to marsh/upland boundary distance were calculated.

Results and Discussion

Groundwater Input

The daily groundwater input rates into the French Creek marsh over the course of the year (2009) (**Figure 9-4**) ranged from 0 to more than $100 \text{ L m}^{-2} \text{ d}^{-1}$ with a marsh-wide average of $3.6 \pm 1.5 \text{ L m}^{-2} \text{ d}^{-1}$ through the year. The largest and most variable fluxes occurred along the marsh-upland edge. During periods of high discharge the upland border received 1 to 2 orders of magnitude more groundwater input than creekside locations. But these larger fluxes reflect the influence of a few transient hotspots for discharge and otherwise a relatively narrow range of discharge was measured across the marsh on the order of 1 to $15 \text{ L m}^{-2} \text{ d}^{-1}$ (**Table**).

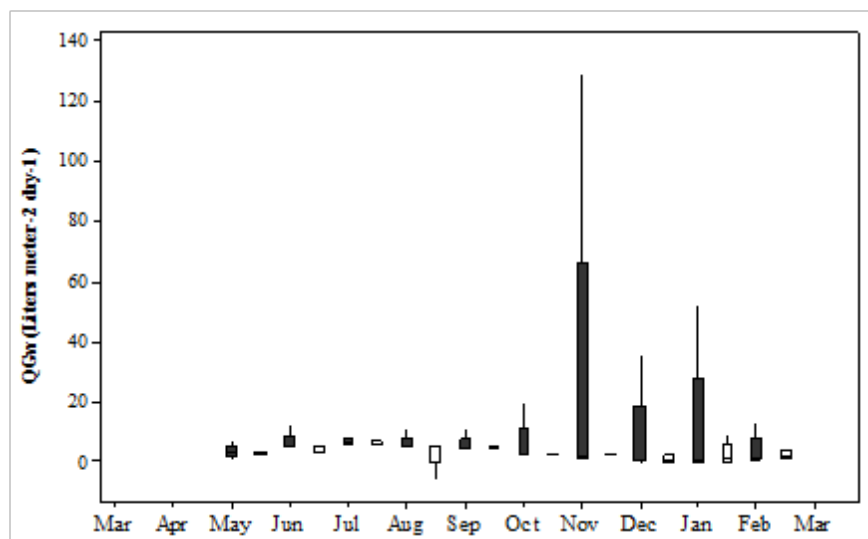


Figure 9-4. Box and whisker plots of fresh groundwater discharge to the French Creek marsh; March 2009–March 2010.

Solid bars are marsh-upland edge discharges. Open bars denote creekside discharges.

Table 9-1. Water Balance Summary for the French Creek Marsh. Monthly means \pm (standard deviation [SD]) of all piezometers.

	Qgw	Qt	Qp	Qet	%Gw
May-09	3.4 (1.5)	0.6 (0.4)	0.6 (0.1)	4.4 (n.a)	71.3 (11.3)
Jun-09	14.9 (2.1)	1.0 (0.7)	0.2 (0.1)	5.5 (n.a)	80.6 (9.4)
Jul-09	6.5 (0.7)	0.6 (0.7)	0.3 (0.1)	5.9 (n.a)	87.8 (8.8)
Aug-09	4.7 (3.3)	1.5 (0.4)	0.7 (0.1)	5.6 (n.a)	76.5 (25.1)
Sep-09	4.7 (1.7)	0.9 (1.1)	0.1 (0.1)	4.0 (n.a)	84.0 (16.3)
Oct-09	3.7 (4.6)	1.1 (0.4)	0.1 (0.0)	2.8 (n.a)	71.8 (12.0)
Nov-09	2.0 (0.8)	3.7 (1.1)	0.3 (0.1)	2.1 (n.a)	37.7 (19.9)
Dec-09	3.2 (9.2)	2.7 (0.8)	0.4 (0.2)	1.4 (n.a)	22.2 (31.8)
Jan-10	1.4 (3.0)	3.7 (1.1)	0.4 (0.0)	1.1 (n.a)	18.5 (38.2)
Feb-10	2.3 (2.8)	0.9 (0.3)	0.3 (0.1)	1.1 (n.a)	57.2 (16.6)

Note: n.a = not applicable; a single calculated value from a common temperature measurement.

The daily groundwater fluxes into the Traps Bay marsh (**Figure 9-5**) ranged from 0 to 50 L m⁻² d⁻¹ with a marsh wide average of 8.8 \pm 3.8 L m⁻² d⁻¹ through the year (**Table 9-2**). As observed in French Creek, the largest and most variable fluxes occurred along the marsh-upland edge. The observed factor of 2 decrease in discharge from the upper to lower portion of the marsh parallels at the whole site scale the general trend of decreasing discharge with distance from the upland to creek on the individual transect scale. Higher overall discharge rates at all locations relative to French Creek reflect the geomorphology of this site. This relatively small pocket-type marsh cuts into the watershed with short distances between the upland edge and creek edge. The same pattern of higher discharge along the upland edge was repeated at Traps Bay, particularly for the lower portion of the site that is less incised into the watershed.

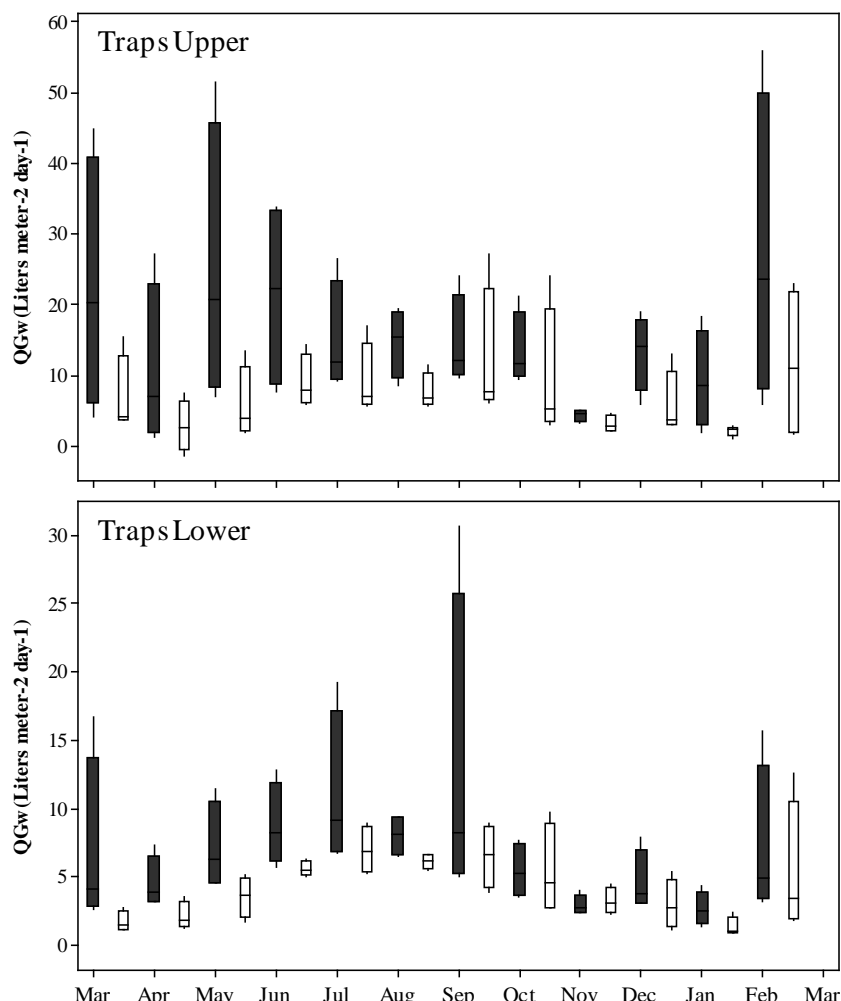


Figure 9-5. Box and whisker plots of fresh groundwater discharge to the Traps Bay marsh; March 2009–March 2010.

Solid bars are marsh-upland edge discharges. Open bars denote creekside discharges.

Freeman Creek marsh showed the most heterogeneity in discharge (**Figure 9-6**) with values ranging from less than $1 \text{ L m}^{-2} \text{ d}^{-1}$ at some creekside locations to over $200 \text{ L m}^{-2} \text{ d}^{-1}$ at one upland edge piezometer in March 2010. Mean monthly marsh-wide average discharge was between 5 and $31 \text{ L m}^{-2} \text{ d}^{-1}$ with an annual average of $16.9 \pm 8.8 \text{ L m}^{-2} \text{ d}^{-1}$ (**Table 9-3**). The very high variance in the high discharge values at the upland interface may be in part due to the evolutionary history of this marsh. During piezometer installation, relict fluvial gravel deposits were found to underlay some portions of the marsh. This paleochannel may have provided a subsurface high conductivity zone through which groundwater could flow and enter the marsh. These locations were coincident with zones of higher and more variable discharge, but were not characteristic of the majority of the piezometers installed at any of the sites.

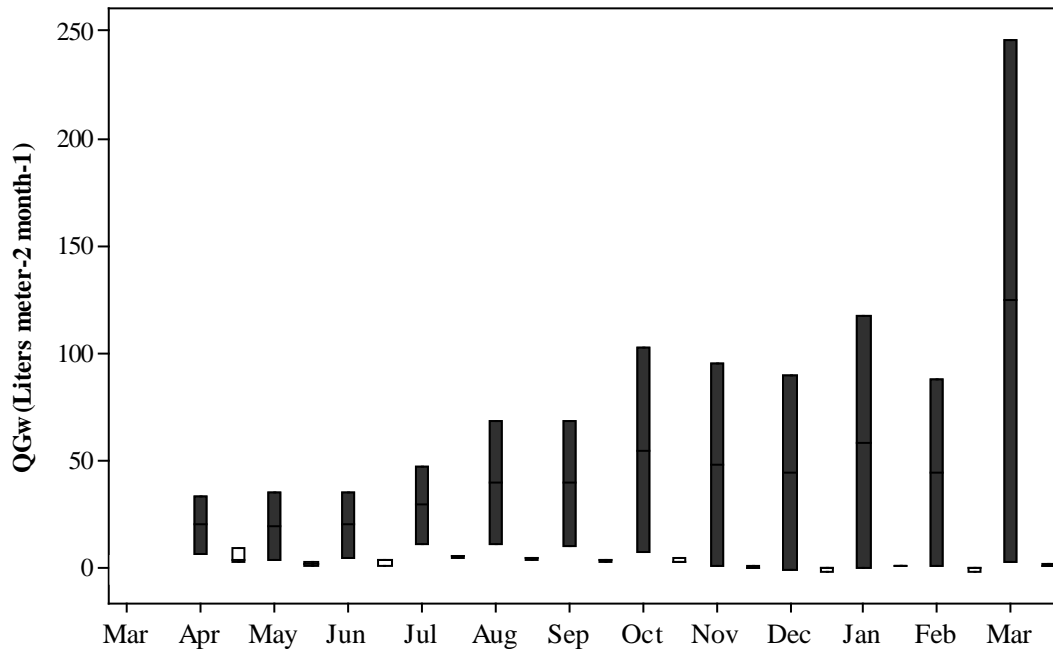


Figure 9-6. Box and whisker plots of fresh groundwater discharge to the Freeman Creek marsh; March 2009–March 2010.

Solid bars are marsh-upland edge discharges. Open bars denote creekside discharges.

Table 9-2. Water Balance Summary for the Traps Bay Marsh.

	Qgw	Qt	Qp	Qet	%Gw
Mar-09	9.8 (12.5)	1.5 (0.7)	0.3 (0.0)	2.0 (n.a)	72.8 (14.7)
Apr-09	5.0 (6.5)	0.7 (0.3)	0.2 (0.0)	3.1 (n.a)	81.0 (14.2)
May-09	10.7 (13.3)	2.4 (1.4)	0.6 (0.0)	4.4 (n.a)	70.5 (12.9)
Jun-09	11.1 (9.0)	2.5 (1.1)	0.2 (0.0)	5.3 (n.a)	75.0 (9.1)
Jul-09	10.9 (6.1)	2.6 (2.1)	0.3 (0.0)	5.9 (n.a)	79.2 (10.3)
Aug-09	9.4 (4.4)	2.4 (1.7)	0.6 (0.0)	5.6 (n.a)	76.3 (10.2)
Sep-09	11.6 (8.3)	5.7 (5.1)	0.0 (0.0)	4.0 (n.a)	65.2 (12.5)
Oct-09	8.7 (6.5)	3.6 (1.3)	0.1 (0.0)	2.8 (n.a)	65.1 (15.0)
Nov-09	3.4 (1.0)	0.5 (0.2)	0.1 (0.0)	2.1 (n.a)	86.0 (5.3)
Dec-09	6.9 (5.5)	2.4 (1.4)	0.4 (0.0)	1.4 (n.a)	66.1 (16.8)
Jan-10	4.0 (4.7)	0.7 (0.6)	0.3 (0.0)	1.1 (n.a)	76.1 (12.3)
Feb-10	12.0 (13.5)	3.1 (1.1)	0.3 (0.0)	1.1 (n.a)	65.7 (18.2)

Monthly means \pm (standard deviation [SD]) of all piezometers.

Note: n.a = not applicable.

The pattern of higher discharge along the upland edge was a consistent feature of all sites. Regardless of location in the marsh the upland edge discharge was “flashy” in response to discrete recharge events within a month and also showed more spatial heterogeneity. Both of these factors contributed to the higher variance in discharge. When all sites were considered collectively, no clear unifying seasonal pattern was observed for the highest discharge zone along the upland edge. This lack of strong seasonal pattern stands in contrast to observations in more temperate marshes (Tobias et al., 2001b) where the water table exhibits highs in the spring and lows in the late fall. This lack of high spring discharge is largely due to the coincidence of high evapotranspiration and high precipitation during the year at MCBCL, rather than a clear wet/dry season or a period dominated by snowmelt followed by increased recharge and water table response. As such there is little seasonal pattern to the rise and fall of the upland water table which provides the hydraulic head that helps drive groundwater input (**Figure 9-7**). The lack of a strong seasonal component to water table dynamics is compounded by the overall low slope of the water table from the watershed to the marsh which permits propagation of tidal signal well into the shallow water table. Watershed recharge events frequently coincided with tidal set-ups driven by low atmospheric pressure and/or Eckman-driven tidal flooding of the NRE and ICW. In these instances, the rise in hydraulic gradient normally associated with large precipitation events was dampened because of tidal flooding and this confounds the correlation of groundwater flux (Q_{GW}) directly to changes in water table height (**Figure 9-8**). These events still initiated the discrete increases in groundwater discharge locally, but served primarily as noise when trying to identify a seasonal pattern in groundwater discharge along the upland edge. In contrast, once away from the upland edge, the discharge rates dropped significantly, became less variable, and demonstrate a more seasonal dynamic with higher mean groundwater inputs in the summer when evapotranspiration was high. The observation of a groundwater discharge response to evapotranspiration (**Figure 9-4** through **Figure 9-6**, and **Figure 9-9**) is wholly consistent with evapotranspiration pulling fresh groundwater into the rhizosphere (Harvey and Nuttle, 1995). The data indicate two separate mechanisms driving groundwater input depending on the marsh size or geomorphology. Small (short distance from upland to open water) pocket-type marshes that are deeply incised into the watershed show discharge patterns controlled largely by discrete responses of the watertable to individual recharge events. Larger marshes (ratio of higher area:upland edge) show discharge patterns largely responding to evapotranspiration. The upshot of these two different controls is that discharge to the smaller, narrower marshes (i.e., those more common in the NRE) are most susceptible to MCBCL activities that might draw down level water table. Larger marshes (i.e., those bordering the ICW), with the exception of the upland edge, would be less susceptible to local hydrologic alterations but more sensitive to factors that control evapotranspiration; like rising temperatures. It is not clear at this juncture whether evapotranspiration-driven groundwater inputs are likely to keep pace with increases in evapotranspiration.

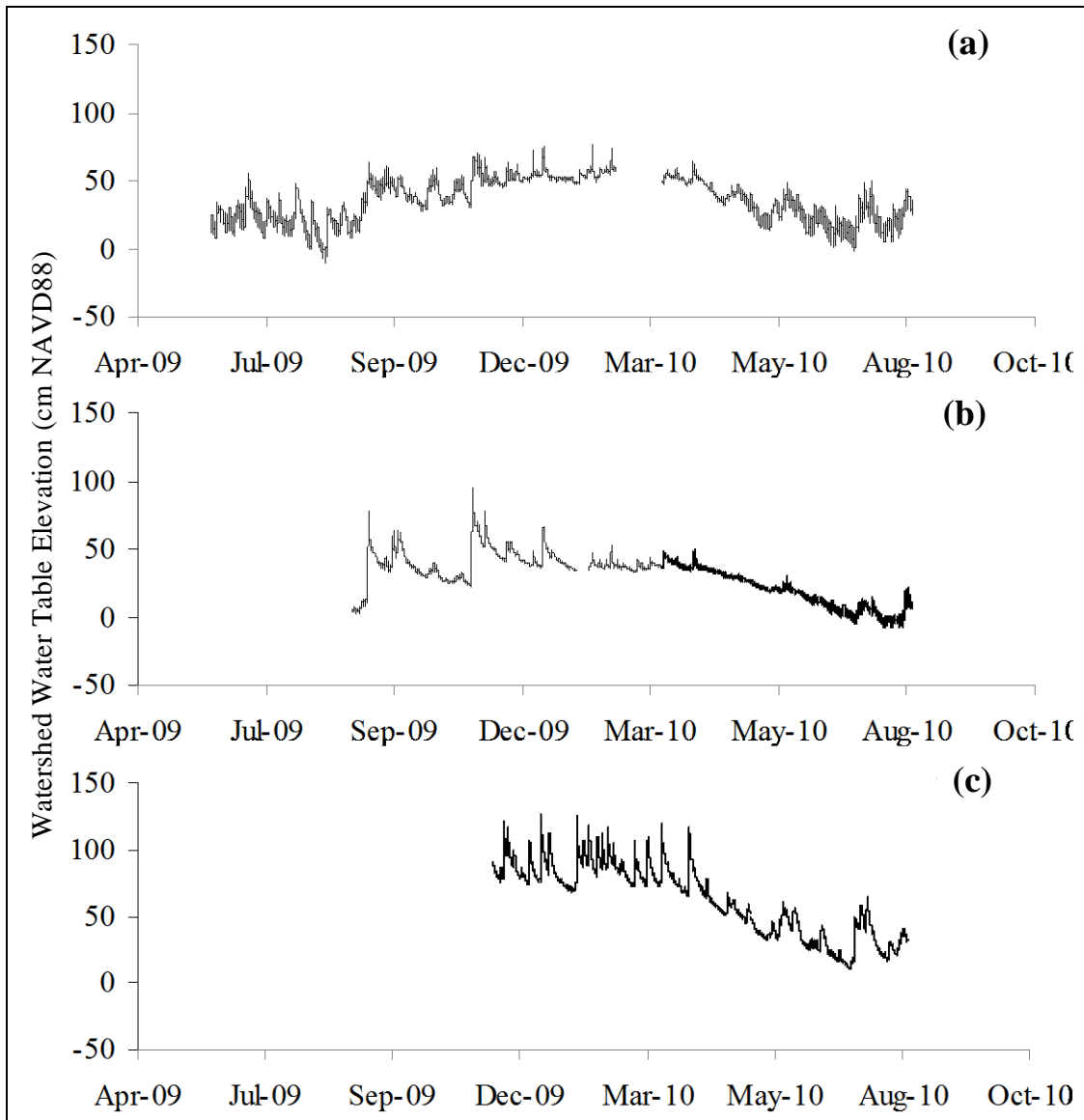


Figure 9-7. Upland water table elevations for French Creek (a), Traps Bay (b), and Freeman Creek (c).

Freeman Creek and Traps Bay showed responses to precipitation events, whereas French Creek predominantly responded to tidal elevation.

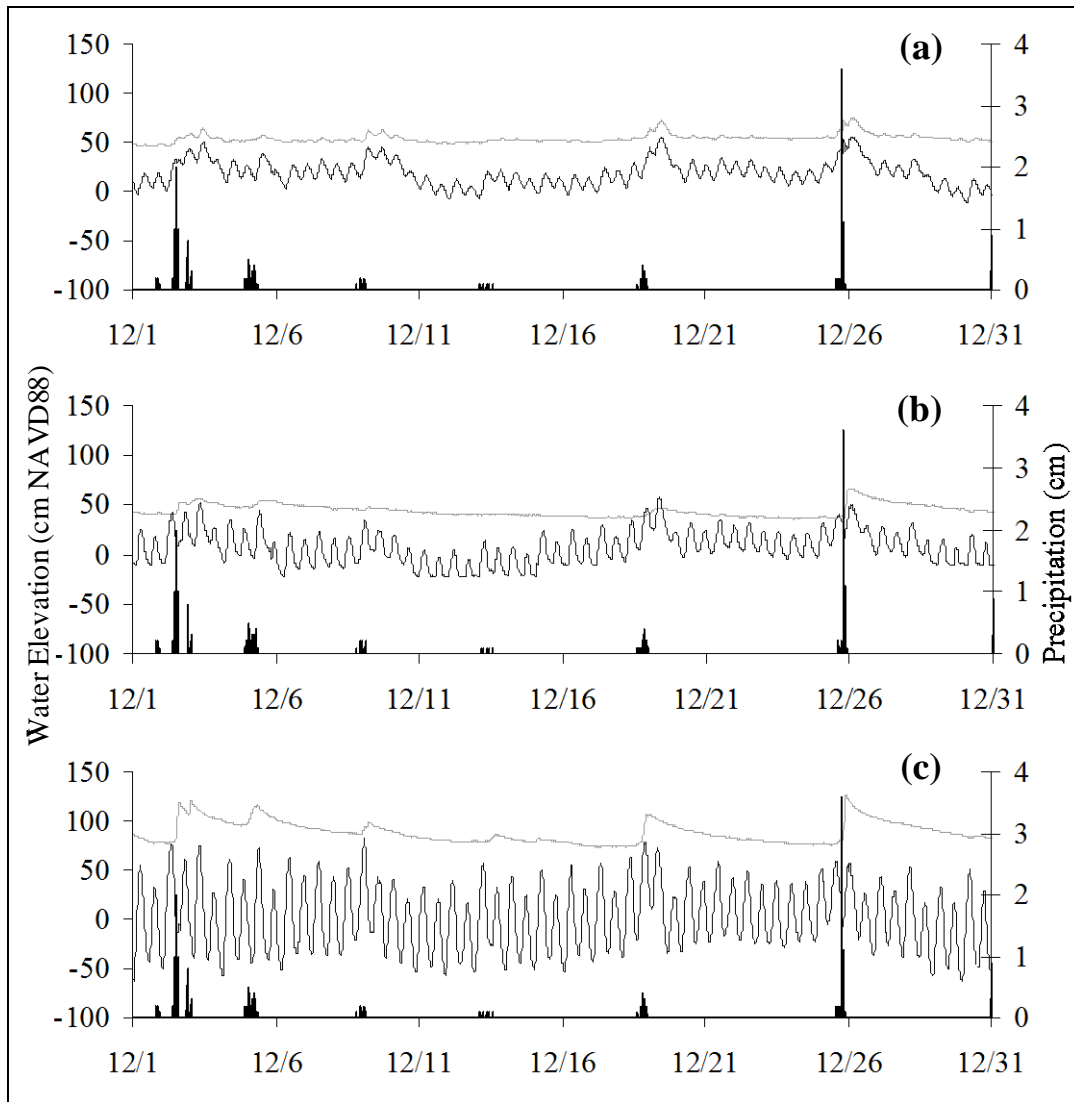


Figure 9-8. Short duration fluctuations in upland water table elevation (grey uppermost line), tidal elevation (black), and precipitation (bar) for French Creek (a), Traps Bay (b), and Freeman Creek (c).

The magnitude of decrease in discharge between the upland edge and creekside piezometers is analogous to the observed exponential decrease in discharge with distance from the shoreline observed in non-vegetated subtidal habitats. Consequently the total marsh-scale discharge can be calculated as the geometric mean of the upland edge and creekside discharges applied to the total area of each marsh. Marsh areas of 9,712 m², 13,354 m², and 100,000 m² for French Creek, Traps Bay, and Freeman Creek marshes, respectively, were used to scale discharge to the entirety of each marsh. The total annual fresh groundwater input to the French, Traps, and Freeman Creek marshes were 13,000, 43,000, and 617,000 m³ y⁻¹ respectively. The breakdown of the water budgets for all marshes (**Tables 9-1 through 9-3**) clearly indicates the importance of groundwater as a freshwater source to the subsurface. The large contribution of Q_{GW} to the overall water budget is due largely to the constraint imposed on Q_T and Q_P that an unsaturated zone be present to recharge water into the subsurface.

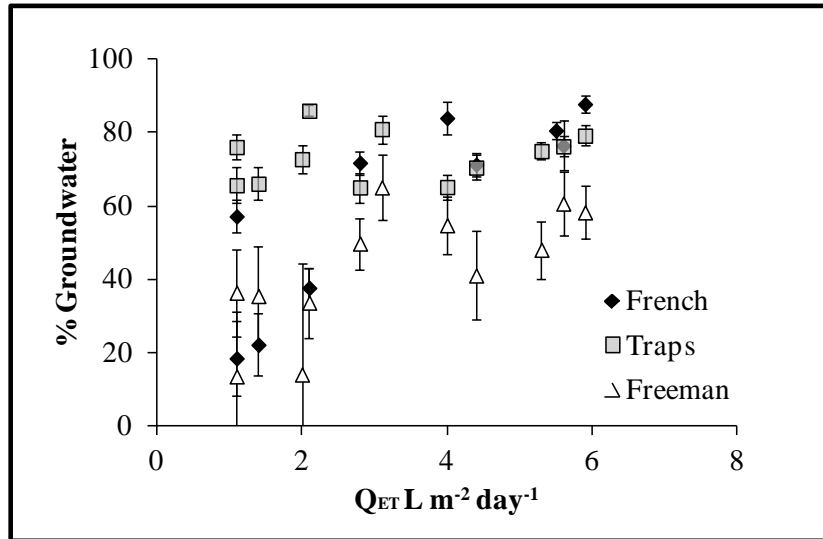


Figure 9-9. Contribution of groundwater to the total marsh water budget as a function of evapotranspiration.

Table 9-3. Water Balance Summary for the Freeman Creek Marsh.

	Q _{gw}	Q _t	Q _p	Q _{et}	%G _w
Apr-09	7.9 (10.2)	2.8 (2.6)	0.2 (0.0)	3.1 (n.a)	65.1 (33.1)
May-09	5.2 (10.4)	6.0 (5.7)	0.4 (0.0)	4.4 (n.a)	41.1 (45.3)
Jun-09	7.1 (9.7)	6.8 (5.3)	0.2 (0.0)	5.3 (n.a)	48.1 (29.6)
Jul-09	11.3 (13.5)	6.7 (5.3)	0.3 (0.0)	5.9 (n.a)	58.3 (26.6)
Aug-09	15.2 (21.8)	7.1 (6.0)	0.5 (0.0)	5.6 (n.a)	60.7 (33.1)
Sep-09	26.5 (31.7)	9.1 (6.5)	0.4 (0.0)	3.9 (n.a)	54.8 (29.3)
Oct-09	30.5 (44.6)	9.1 (6.1)	0.1 (0.0)	2.7 (n.a)	49.8 (26.1)
Nov-09	17.2 (34.1)	8.6 (6.0)	0.3 (0.0)	2.1 (n.a)	33.7 (35.6)
Dec-09	19.6 (42.0)	8.0 (5.8)	0.4 (0.0)	1.4 (n.a)	35.5 (51.3)
Jan-10	17.9 (39.0)	7.2 (5.8)	0.2 (0.0)	1.1 (n.a)	13.6 (65.5)
Feb-10	13.2 (27.2)	6.9 (5.0)	0.3 (0.0)	1.1 (n.a)	36.4 (44.7)
Mar-10	31.4 (75.5)	6.2 (5.8)	0.2 (0.0)	2.0 (n.a)	14.1 (112.9)

Monthly means \pm (standard deviation [SD]) of all piezometers.

No such constraint exists for Q_{GW} . The groundwater input plays a role in regulating plant species composition and distribution along the upland edge. More importantly it suppresses the onset of hypersaline conditions and modifies the concentrations of hydrogen sulfide released during sulfate reduction. Porewater hypersalinity was rarely encountered despite high rates of

evapotranspiration. Both and hydrogen sulfide (HS^-) negatively impact the macrophytes production which figures prominently into the balance among production, respiration and net accretion (e.g., Bradley and Morris, 1991; Morris, 1995). But is groundwater a significant source of N to the marshes of MCBCL?

Concentrations of DIN in the shallow groundwater collected from watershed wells adjacent to the sites were generally low (**Table 9-4**). Annual total dissolved inorganic nitrogen (TDIN; NH_4^+ + nitrate [NO_3^-]) at French Creek and Traps Bay ranged from 5–8 μM of N. The Freeman site had elevated NH_4^+ concentrations (14–36 μM) owing to the top of the water table residing in relict hydric soils. For all sites, the TDIN was dominated by NH_4^+ , with NO_3^- concentrations often below the detection limit of 1 μM for NO_3^- . With respect to NO_3^- , the most mobile of the total dissolved nitrogen (TDN) constituents, and considering the NO_3^- drinking water standard of 714 μM , these groundwaters are at near pristine concentrations. The DON fraction was the dominant or co-dominant N species. However the biological lability of groundwater DON is typically believed to be low and was not used in subsequent N flux calculations. The relatively low overall N concentrations coupled with the dominance of the dissolved pool by NH_4^+ and DON (TDN–TDIN), indicated little anthropogenic influence on the shallow groundwater discharging to these marshes.

Table 9-4. Quarterly dissolved nitrogen concentrations.

	French Creek				Traps Bay				Freeman Creek			
	NO_3^-	NH_4^+	TDIN	TDN	NO_3^-	NH_4^+	TDIN	TDN	NO_3^-	NH_4^+	TDIN	TDN
Feb 09	2	7	9	nd	1	12	13	nd	nd	nd	nd	nd
May 09	2	11	13	22	0	4	4	21	0	36	36	79
Aug 09	0	9	9	45	0	3	3	16	1	47	48	68
Nov 09	0	5	5	24	2	6	8	52	4	14	28	88
Feb 10	0	5	5	90	0	3	3	75	2	14	16	124
May 10	0	1	1	38	nd	nd	nd	46	0	26	0	25

Mean micromolar concentrations collected from watershed wells installed 1 m into the shallow water table.
French Creek and Traps Bay, n=2 wells; Freeman Creek: n=3 wells.

For the purpose of calculating the groundwater N flux to the marshes, the TDIN groundwater concentrations were used (i.e., NO_3^- + NH_4^+ only). For French Creek and Traps Bay, the input ranged from 0.01 to 0.07 g TDIN per meter of upland edge per day. Freeman exceeded that range by up to a factor of 10 in the summer due to both increased discharge and elevated TDIN concentrations in the watershed.

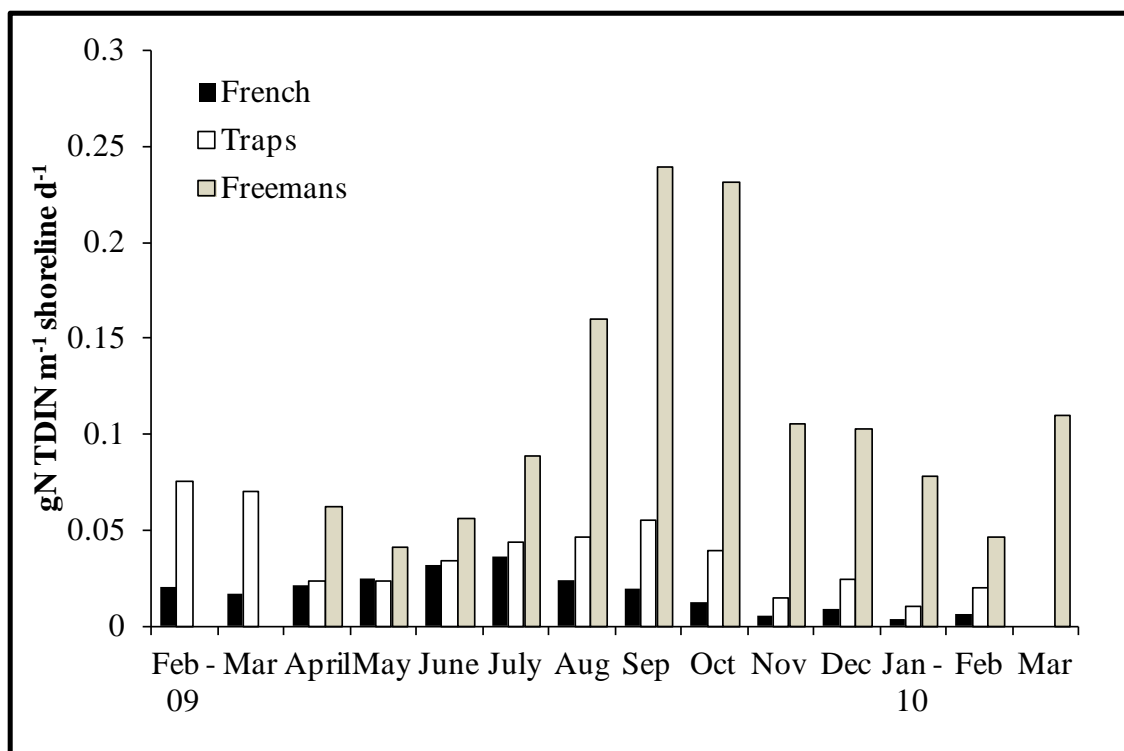


Figure 9-10. Groundwater inorganic nitrogen flux to the study marshes.

When scaled to the entire marsh(es), the annual groundwater derived inorganic N input for French Creek, Traps Bay, and Freeman Creek sites were 1, 8, and 215 kg N y⁻¹, respectively. These estimates, as will be shown, in subsequent pages of this report, are a small portion of the total N budget for each of the marshes. The N input estimate should be considered generous because it included NH₄⁺ whose transport through porous media is strongly attenuated by sorption within the aquifer matrix. If only NO₃⁻ was considered in the flux calculation, the groundwater N input estimates would drop by a factor of 3 to 4 for French Creek and Traps Bay, and by a factor of 10 for Freeman Creek. Nevertheless the total mass flux of groundwater N, including the NH₄⁺, is small. If values calculated for Traps and French are indicative of NRE marshes, and given an estimated NRE marsh total upland edge of 17 km, we estimate that on the order of 150–200 kg N y⁻¹ are delivered via groundwater to all NRE marshes. For the 15 km of upland edge bordering ICW marshes, the total groundwater N input estimate is approximately 600 kg N y⁻¹. The groundwater N delivery to all marshes totals about 1% of the total N flux delivered via the New River mainstem annually. It is unlikely that large wholesale increases in groundwater discharge would happen in the near future, so the only way for groundwater N fluxes to become a prominent component of the marsh N budget would require degradation of shallow groundwater quality to increase DIN concentrations by a factor of 5 to 10. Intense changes in land-use practices in recharge areas (e.g., wastewater spray irrigation or infiltration beds) could elicit such an impact, but it is unlikely that the current management schemes would result in such an increase. The conclusions of this work should be placed within the context that they do not constitute a base-wide characterization of shallow groundwater N, but we have no reason to believe that they ill-represent the state of the shallow aquifer with respect to N loading.

Summary Points

- Groundwater inputs to MCBCL marshes are important sources of fresh water to the rhizosphere
- The magnitude of groundwater inputs are driven more by evapotranspiration and less by large seasonal changes in the upland water table.
- Groundwater is not an important source of N to the marshes of MCBCL principally because groundwater DIN concentrations are low.
- The marshes of MCBCL do not function to remove large groundwater derived N fluxes from the watershed; there are none.
- Currently there is a factor of 5 to 10 buffer for rising groundwater DIN concentrations before the groundwater N flux to the marshes could be deemed significant.

Section 2: Advective Marsh-Estuary Exchange—Hydrologic and Dissolved Nitrogen Fluxes

Materials and Methods

General Approach

Two approaches were used to quantify marsh export of dissolved N. First, porewater drainage from the marsh to adjacent open water was estimated by using a hydraulic gradient approach (i.e., Darcy's Law). These measurements occurred on the tens of meters spatial scales, but with high temporal resolution. Because these fluxes could be related to easily measured (and remotely measured) water levels, they are scalable spatially, and can be applied to any type of marsh geomorphology. The drawback to this hydraulic gradient approach is that it includes only advective fluxes from the marsh subsurface (drainage) and not necessarily any diffusive exchanges between the marsh surface and flooding tidal water. The hydraulic gradient approach was conducted at French Creek, Traps Bay, and Freeman Creek marshes. The second approach consisted of whole-creek tidal flood and ebb flux studies. This approach integrates advective and diffusive exchanges and provides a large spatially integrated estimate (marsh-wide). The tidal flux approach has the following three considerable drawbacks: (1) it is limited to single snapshots in time and cannot be scaled temporally; (2) it is limited to marsh geomorphologies that have a centralized drainage artery and thus cannot be used for fringing marshes; and (3) for large systems, any tidal asymmetry in the flood and ebb water fluxes will nullify the ability to calculate robust mass fluxes. The tidal flux approach was applied only in Traps Bay and Freeman Creek marshes, and problems with this tidal asymmetry were deemed to be insurmountable. The approach was abandoned and its description and results are not contained within this final report.

The Hydraulic Gradient Approach

Piezometer arrays and tide gauges previously described in Section 1 for French Creek, Traps Bay, and Freeman Creek marshes were used for hydraulic and chemical sampling. Hydraulic parameters and water levels were measured in piezometers to determine the water flux in each marsh. This water flux was coupled with quarterly measurements of porewater dissolved N to yield a N mass flux from the marsh to open water associated with drainage. Horizontal porewater drainage between any two given piezometers or a piezometer and the tidal creek was calculated (see Equation 9-2) using measured hydraulic head and hydraulic conductivity values according to Darcy's Law:

$$Q = -K \frac{dh}{dx} \quad (\text{Eq. 9-2})$$

where Q is the drainage flux, K is the hydraulic conductivity, and $\frac{dh}{dx}$ is the hydraulic gradient, and Q is either expressed as $\text{L m}^{-2} \text{d}^{-1}$ assuming a cross sectional discharge area of 1 m^2 normal to flow, or Q is converted to $\text{L m}^{-1} \text{shoreline d}^{-1}$ by using the specific cross sectional discharge area (per meter of shoreline) at each site (i.e., the marsh bank at low tide). Porewater drainage was then brought to the marsh-scale by multiply the marsh shoreline length by the per meter shoreline drainage.

Piezometers used for the hydraulic gradient calculations and determination of K , were equipped with pressure transducers (i.e., Level TROLL 100 [In-Situ Inc.]). All water levels were corrected

for barometric pressure as measured at each site by a BaroTROLL (In-Situ Inc.), and normalized to the North American Vertical Datum of 1988 (NAVD88).

The hydraulic conductivity (K) was measured using slug tests (Hvorslev, 1951). The initial depth to water (DTW) from the top of the casing (TOC) was taken using a hand-held water-level meter. A pressure transducer recording depth at 1-second intervals was then placed in the well at a known depth from the TOC. Immediately, a volume of water (the slug) was added to the well. After approximately 5 minutes, the terminal DTW was read using a hand-held water-level meter and the transducer was removed. The data were downloaded and a plot of the ratio of water level (h) to maximum water level (h_0) versus time was generated with the y-axis on a log scale. Hydraulic conductivity was calculated according to Equation 9-3:

$$K = [r^2 \ln(L_e/R)] / [2L_e t_{37}] \quad (\text{Eq. 9-3})$$

where K is hydraulic conductivity, r is the radius of the well casing, R is the radius of the well screen, L_e is the length of the well screen, and t_{37} is the time required for the water level to fall to 37% of the initial rise.

Hydraulic head, dh , in selected piezometers was monitored with a Level TROLL 100 pressure transducer (In-Situ Inc.) recording water level at 15-minute intervals. A separate transducer was left exposed solely to the atmosphere to record barometric pressure at 15-minute intervals. The data from the pressure transducers in the wells was corrected for barometric effects.

A global positioning system (GPS) survey was used to determine the coordinates of each well and elevation with regard to NAVD88 at the TOC for each well. Porewater elevations were calculated as shown in Equation 9-4:

$$h_{PW} = H_{TOC} - DTT + D \quad (\text{Eq. 9-4})$$

where h_{PW} is the porewater elevation, H_{TOC} is the elevation of the TOC, DTT is the depth to the transducer, and D is the barometric pressure corrected depth of water recorded by the transducer. Horizontal distance between water porewater elevation measurements, dx , was determined using GPS coordinates.

Chemical Sampling

Porewater chemistry was sampled seasonally to be combined with porewater drainage to calculate solute export fluxes. Porewaters were sampled from all piezometers at all sites for a range of inorganic and organic analytes. Sampling occurred seasonally, taking place in February, May, August, and November in 2009 and February, May, and August 2010. All collections were made at low tide. At each piezometer, water level was recorded using a handheld water level meter and the piezometer was pumped dry with a peristaltic pump and then given approximately 2 minutes to recharge. The porewater was then pumped with a peristaltic pump through an in-line glass fiber filter and a 0.45- μm filter for subsequent analysis of nitrate, nitrite, NH_4^+ , and TDN. The TDN samples were preserved with phosphoric acid (H_3PO_4) and refrigerated prior to analysis. DIN and dissolved inorganic phosphate (DIP) were frozen and stored until analysis.

Results and Discussion

Horizontal hydraulic conductivity (K_h) of the rhizosphere (0- to 50-cm depth) determined by in situ slug tests were on the order of that typically found in fine sands (**Table 9-5**). K_h averaged

$2.3 \pm 0.5 \times 10^{-3} \text{ cm s}^{-1}$ for French Creek, $4.1 \pm 0.7 \times 10^{-3} \text{ cm s}^{-1}$ for Traps Bay, and $1.7 \pm 0.4 \times 10^{-3} \text{ cm s}^{-1}$ for Freeman Creek. Mean K_h for the interior of French Creek was twice that of mean creekside K_h . With the exception of the most upstream transects at Traps Bay dominated by *Typha spp*, mean interior K_h was 2–3 times greater in the interior of the marshes than in the creekbanks for all sites (**Table 9-5**). There were no significant inter-marsh differences between interior K_h or creekbank K_h values.

Table 9-5. Hydraulic Conductivity (K_h) of Traps Bay and French and Freeman Creeks.

Transect	$K_h \times 10^{-3} \text{ cm s}^{-1}$	
	Well location	
	Creekside	Interior
Traps 1 East	6.32	3.72
Traps 1 West	9.03	9.03
Traps 3 East	7.90	1.86
Traps 3 West	-	4.10
Traps 5 East	1.44	7.90
Traps 5 West	2.60	1.58
Traps 7 East	0.84	1.34
Traps 7 West	1.41	2.04
French 1	0.93	5.26
French 3	0.67	0.79
French 7	0.73	3.72
French 9	1.32	4.20
Freeman 1	1.47	1.19
Freeman 3	0.97	0.63
Freeman 5	1.40	5.50

The horizontal hydraulic gradient was considered separately for the creekbank and interior zones of the marsh. The creekbank gradients were calculated from the difference in hydraulic head between the creekbank piezometer and tidal stage, and the marsh interior gradient was calculated from the difference in hydraulic head measured at the upland-marsh border and the creekbank piezometers. The daily maximum hydraulic gradient towards open water (i.e., drainage) in the creekbank exceeded the interior gradient by a factor of between 10 and 100. The creekbank gradient was dynamic and exhibited hourly variation throughout the tidal cycle, whereas fluctuations on hourly to daily scales in the interior gradient were barely detectable at all sites (**Figure 9-11**). The gradient from the creekbank to open water was maximized at low tide for all sites. Consistent with the different marsh elevations relative to mean high water and the different tidal amplitudes, the low tide creekbank hydraulic gradients among sites differed by a factor of 10 (**Figure 9-11**) with a maximum and minimum occurring at Freeman and French creeks, respectively. For all marshes, as the tide rose the creekbank gradient decreased until the tidal elevation matched or exceeded the porewater elevation (**Figure 9-11**). When tidal elevation was greater than porewater elevation, either no gradient existed, or a negative gradient was created (**Figure 9-11a,b**), indicating periods of horizontal recharge. The subsurface was principally recharged vertically during flooding events that topped the marsh platform (vertical gradients not

shown; Harvey et al., 1987; Harvey and Odum, 1990). The mean positive creekbank gradient increased with distance down-estuary from French Creek (0.021) and Traps Bay (0.025) to Freeman Creek (0.103). This is the gradient that drives drainage and advective delivery of N-rich porewater to the NRE or ICW.

Interior drainage gradients were on the order of 20% of the creekbank gradient in French Creek, to less than 2% of the creekbank gradient in Freeman Creek. Mean positive interior drainage gradient decreased with distance down-estuary from 0.004 in French Creek to 0.003 in Traps Bay and 0.001 in Freeman Creek. Because the gradient through the interior of the marsh is small relative to the hydraulic gradient between open water and the creekbank extending a few meters into the marsh, the source of N that is exported from the marsh by drainage is not derived from the interior of the marsh. It is principally generated from mineralization locally within the creekbank zone. This first conclusion is consistent with the observation in Section 1 of this report that the water budget has a strong evapotranspiration component to it. Dissolved N generated in the marsh interior does not advect to any great extent (a maximum of 20% at French Creek) all the way to the creekbank where it can drain into open water. Much of that water flux is intercepted by evapotranspiration, and much of the associated N flux is likely re-assimilated into macrophytes (Tobias and Neubauer, 2007) or immobilization (Anderson et al., 1997). Secondly, any effect exerted on drainage from changes in the watershed must be propagated through the marsh interior, and because the interior water flux is small, the watershed hydrology must act independently from the creekbank hydrology that controls the delivery of dissolved N to open water via drainage. The magnitude of the drainage flux is controlled almost exclusively by the tidal stage relative to the marsh elevation.

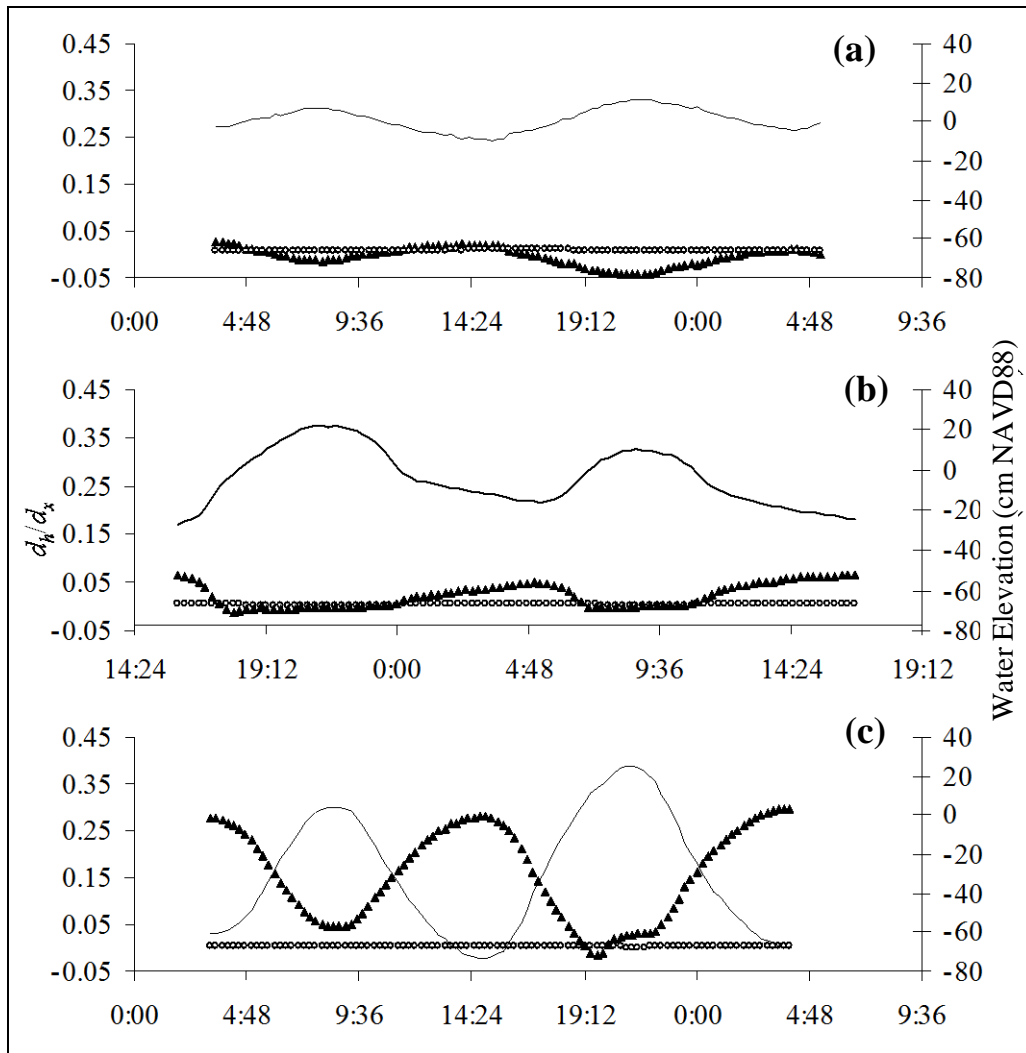


Figure 9-11. Representative daily fluctuation of tidal elevation (solid), creekbank gradient (triangle), and interior gradient (circle) for French Creek (a), Traps Bay(b), and Freeman Creek (c).

d_h represents the difference in hydraulic head between either the tide gauge and creekbank piezometer (creekbank gradient), or the upland-marsh border piezometer and the creekbank piezometer (interior gradient). d_x represents the distance between the points where hydraulic head (d_h) is determined. A positive gradient indicates a slope from the marsh towards open water.

Although porewater drainage through the creekbank within a site was related most strongly to tidal elevation (**Figures 9-12 through 9-14**), marsh drainage trended with daily tidal amplitude at the estuarine scale (**Figure 9-15**). Greater tidal amplitude yielded greater maximum creekbank drainage.

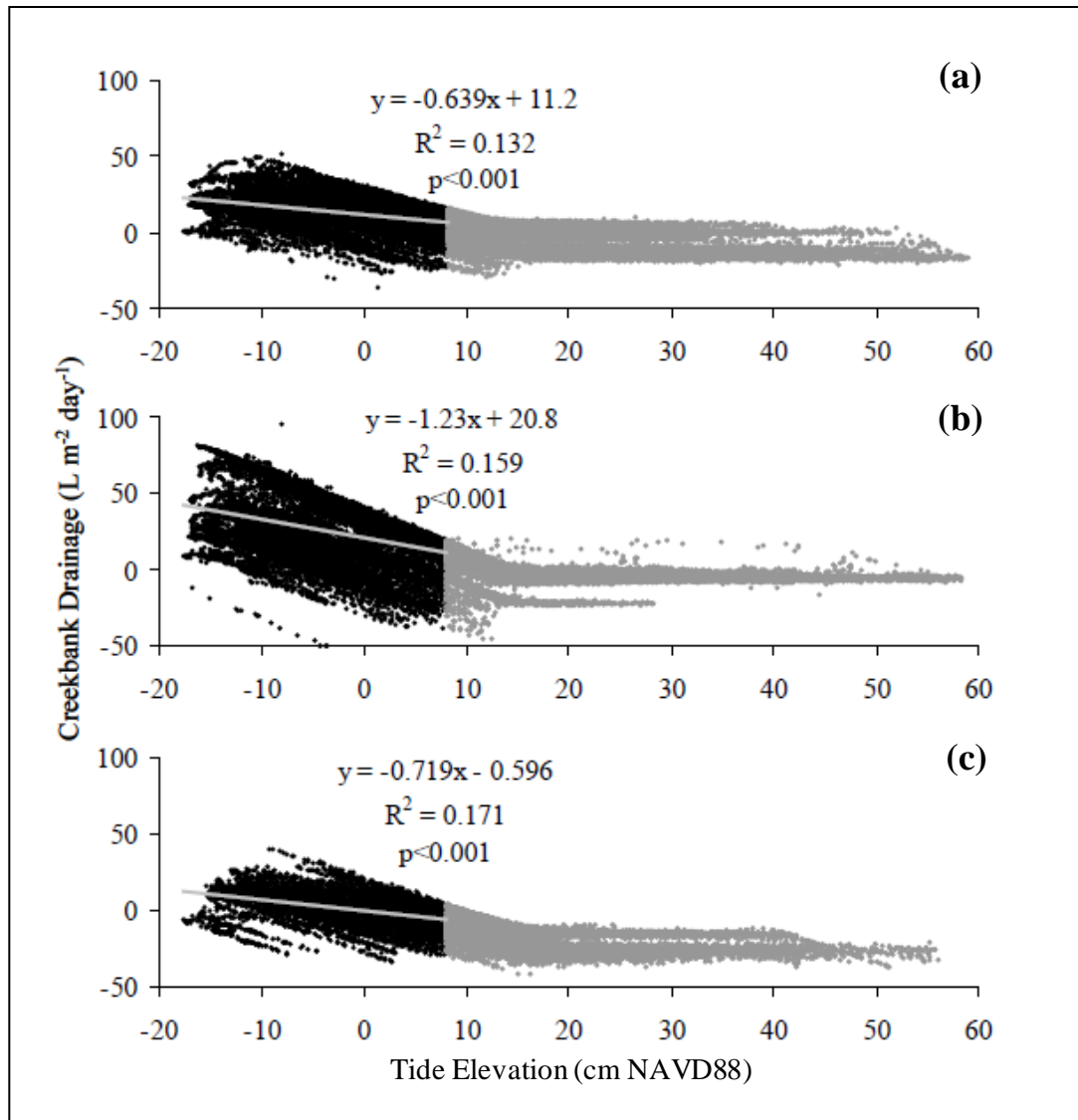


Figure 9-12. Creekbank drainage versus tidal elevation for French Creek transect 3 (a), transect 5 (b), and transect 7 (c).

A two-phase response was observed with increased drainage at elevations below the marsh surface (black) and recharge for tidal elevations greater than the marsh surface (grey). Grey points greater than zero occur as the marsh is draining on the falling tide and grey values less than zero occur as the marsh is flooding on the rising tide.

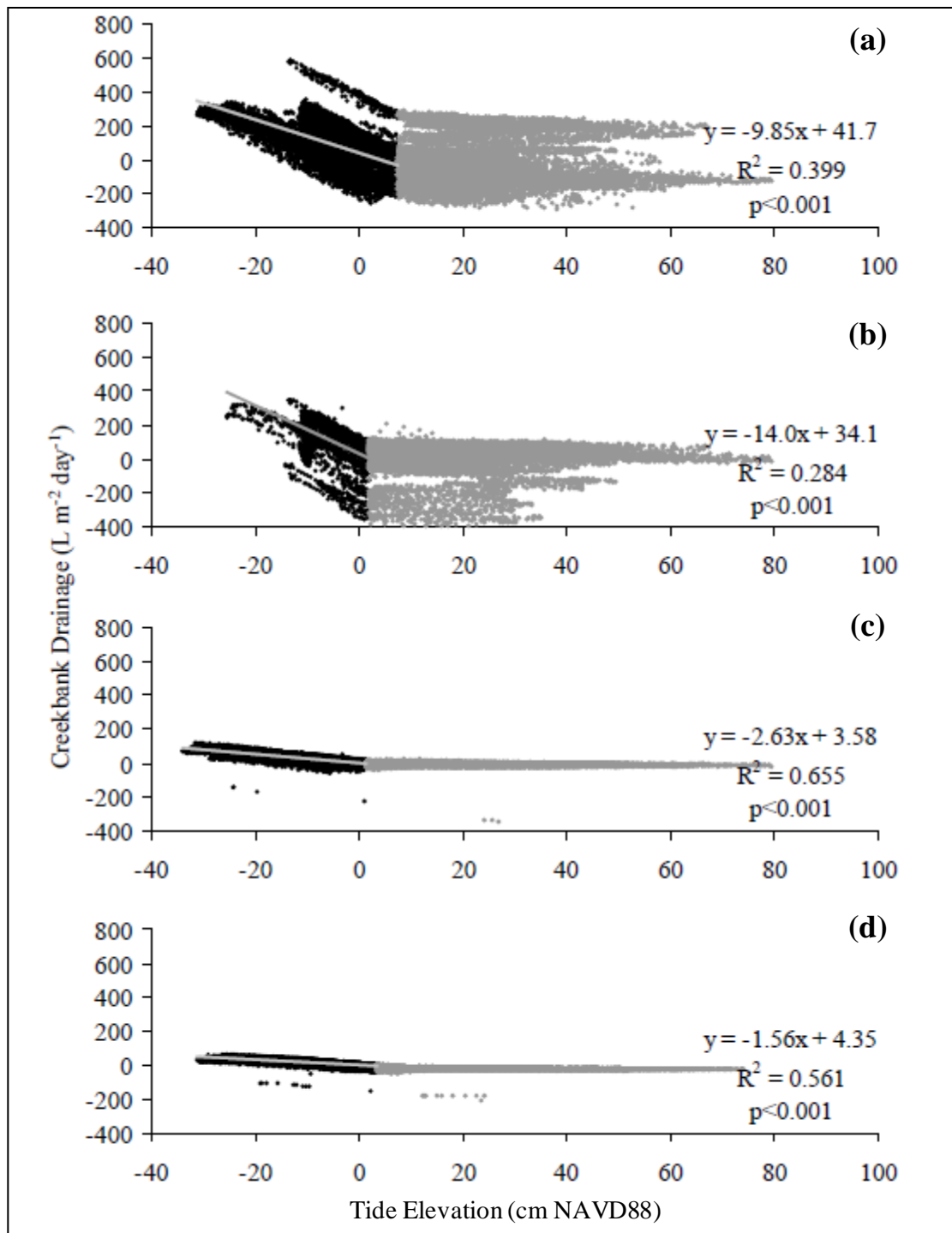


Figure 9-13. Creekbank drainage versus tidal elevation for Traps Bay transect 1 (most upstream) (a), transect 3 (b), transect 5 (c), and transect 7 (most downstream) (d).

A two-phase response was seen with increased drainage at elevations below the marsh surface (black) and recharge for tidal elevations greater than the marsh surface (grey). Grey points greater than zero occur as the marsh is draining on the falling tide and grey values less than zero occur as the marsh is flooding on the rising tide.

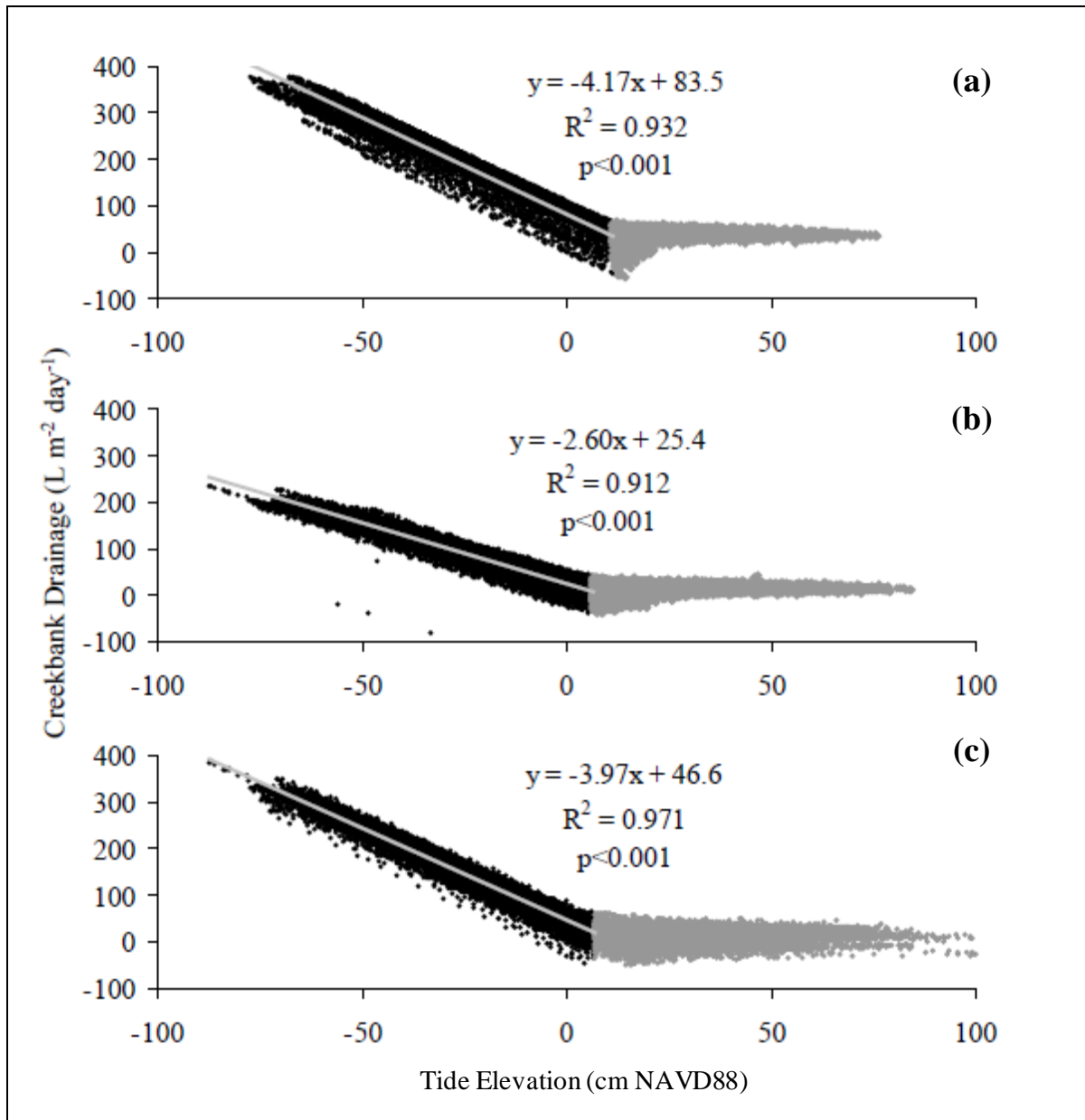


Figure 9-14. Creekbank drainage versus tidal elevation for Freeman Creek transect 1 (a), transect 3 (b), and transect 5 (c).

A two-phase response was seen with increased drainage at elevations below the marsh surface (black) and recharge for tidal elevations greater than the marsh surface (grey). Grey points greater than zero occur as the marsh is draining on the falling tide and grey values less than zero occur as the marsh is flooding on the rising tide.

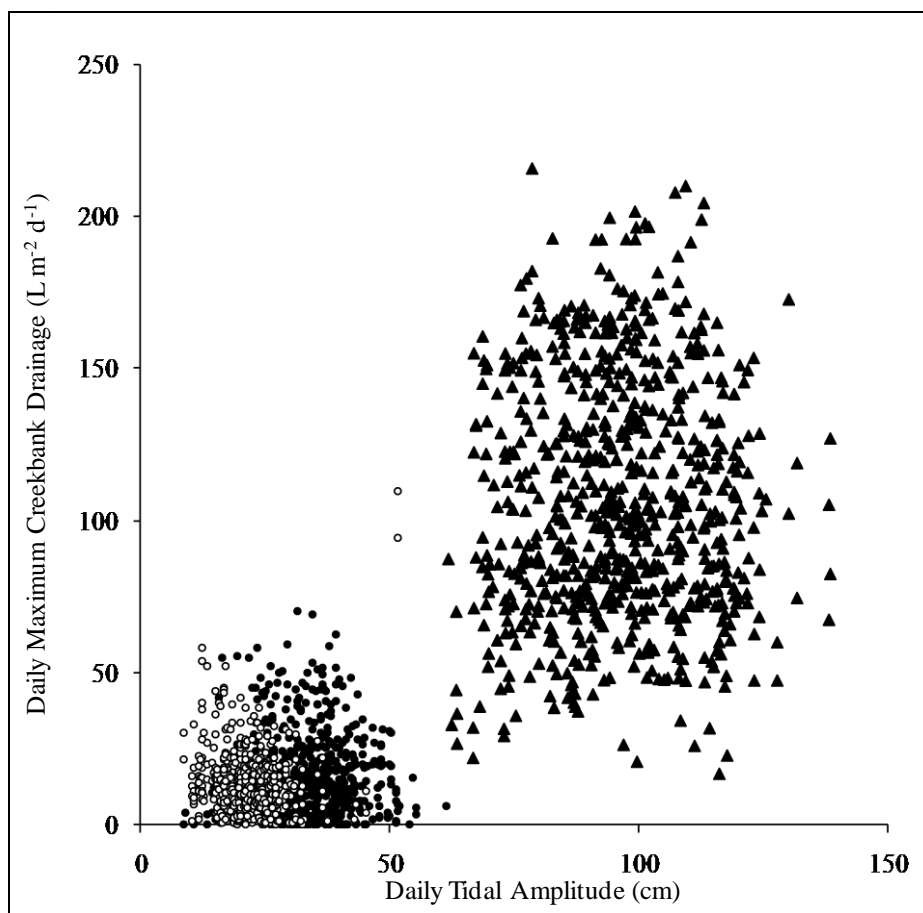


Figure 9-15. All sites daily maximum drainage versus daily tidal amplitude.

French Creek (open circles), Traps Bay (black circles), and Freeman Creek (triangles).

Monthly averaged, Darcy-derived estimates of creekbank drainage were used to scale up time series drainage fluxes to the marsh-scale. Per-square meter fluxes ($\text{L m}^{-2} \text{d}^{-1}$) were scaled to the cross-sectional face of the creekbank for each marsh based upon the height of the creekbank relative to mean low water and mean tidal amplitude at the site such that the resultant flux was given units of $\text{L m shoreline}^{-1} \text{d}^{-1}$. The monthly estimates of drainage at each site varied several-fold over an annual period, but showed no seasonal patterns. Monthly average porewater drainage in Freeman Creek (**Figure 9-14c**, $44.4\text{--}123.6 \text{ L m shoreline}^{-1} \text{d}^{-1}$) was 20 times greater than in Traps Bay (**Figure 9-14**, $0.5\text{--}5.9 \text{ L m shoreline}^{-1} \text{d}^{-1}$) and Traps Bay was 5 times greater than in French Creek (**Figure 9-14**, $0.01\text{--}0.9 \text{ L m shoreline}^{-1} \text{d}^{-1}$) each month. Greater drainage generally occurred during periods of lower mean tidal elevation for all sites, such that longer periods of tidal inundation, such as those associated with wind-driven flooding, equated with little to no drainage. Traps Bay monthly mean drainage per day differed by 1 order of magnitude between upstream (groundwater influenced) and downstream transects, whereas drainage was more consistent between transects at the other sites.

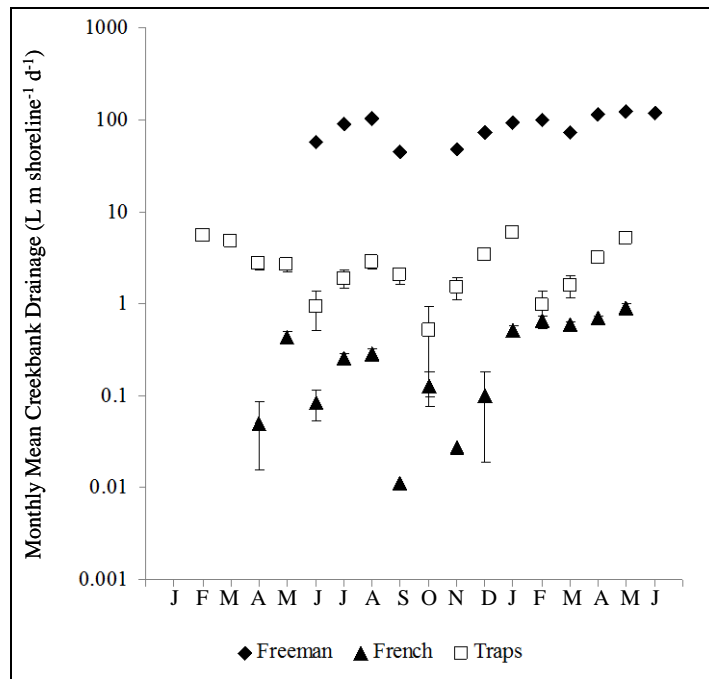


Figure 9-16. Mean monthly drainage corrected for cross sectional drainage area for French Creek (solid triangles), Traps Bay (open boxes), and Freeman Creek (solid diamonds).

Error bars represent standard error.

Porewater Nitrogen Flux from Marsh to Open Water

The TDN (DIN + DON) flux attributable to porewater drainage was derived from the monthly aggregated porewater drainage fluxes and seasonally measured porewater TDN values. TDN varied within the marsh and the highest concentrations were found between the creekbank and the interior. Mean creekbank TDN concentrations were greatest during the winter (**Table 9-6**). Mean TDN concentrations were greatest in the marshes that had the least drainage with annual mean TDN concentration greatest in French Creek ($158 \pm 15 \mu\text{M}$), followed by Traps Bay ($103 \pm 8 \mu\text{M}$), and lowest in Freeman Creek ($85 \pm 9 \mu\text{M}$). For all porewaters, nitrite (NO_2)+ NO_3^- was negligible (generally $<1 \mu\text{M}$) and TDN was comprised of approximately 50–70% DON and 30–50% NH_4^+ . When coupled with the creekbank porewater drainage estimates (**Figure 9-16**), the advective fluxes of N showed a seasonal pattern in all three sites with a peak at the end of summer and a second more prolonged peak at the beginning of winter (**Figure 9-17**). French Creek showed the least seasonal variation ($.02\text{--}1.7 \text{ g N-TDN d}^{-1}$) and the least drainage, followed by Traps ($0.7\text{--}9.2 \text{ g N-TDN d}^{-1}$), and Freeman Creek showed the greatest temporal variation in N flux ($44\text{--}120 \text{ g N-TDN d}^{-1}$) accompanied by the greatest drainage (**Figure 9-18**). Despite higher TDN concentrations in the up-estuary marshes, the inter-marsh differences in N flux was almost solely attributable to differences in porewater drainage rates.

Table 9-6. Quarterly Porewater Concentrations of Total Dissolved Nitrogen (TDN) Based on Location Within Each Marsh

	Mean porewater TDN concentration (μM)					
	French Creekside	French Interior	Traps Creekside	Traps Interior	Freeman Creekside	Freeman Interior
Feb. 2009	71 ± 11	43 ± 17	68 ± 12	55 ± 16	40 ± 11	57 ± 20
May 2009	155 ± 41	151 ± 99	65 ± 12	95 ± 41	28 ± 4	32 ± 9
Aug. 2009	210 ± 60	126 ± 44	106 ± 23	86 ± 28	69 ± 9	44 ± 25
Nov. 2009	218 ± 69	130 ± 51	175 ± 40	110 ± 24	144 ± 46	59 ± 28
Feb. 2010	243 ± 87	204 ± 77	122 ± 19	99 ± 15	128 ± 38	108 ± 9
May 2010	184 ± 54	186 ± 86	124 ± 20	107 ± 19	58 ± 14	53 ± 17

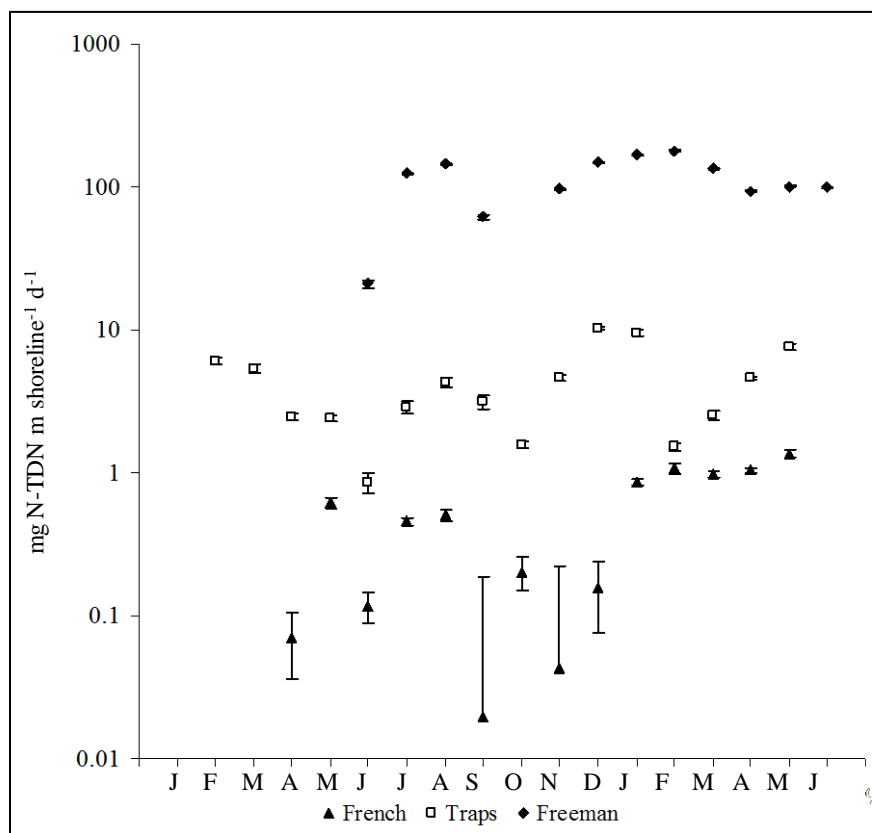


Figure 9-17. Monthly average Darcy-derived nitrogen flux for French Creek, Traps Bay, and Freeman Creek.

Freeman Creek drains 2 orders of magnitude more N per day than Traps Bay and French Creek. Rates were scale up to the whole marsh using shoreline length estimates of 1300m for French Creek, 900 m for Traps Bay, and 9,600 m for Freeman Creek. Open diamonds represent Freeman Creek tidal flux estimates out of the marsh.

The higher contribution of drainage N to adjacent waters found in Freeman Creek relative to Traps Bay and French Creek is likely a pattern characteristic of the ICW bordering marshes relative to the NRE bordering marshes. We make this generalization based upon the interpretation that the higher N drainage flux is driven by a higher water flux and the higher water flux is a function of the higher tidal amplitude in the ICW relative to the NRE. More specifically the larger difference between the marsh elevation (situated near MSL) and the low tide elevation. This difference is maximized at higher tidal amplitudes found in the lower NRE and ICW.

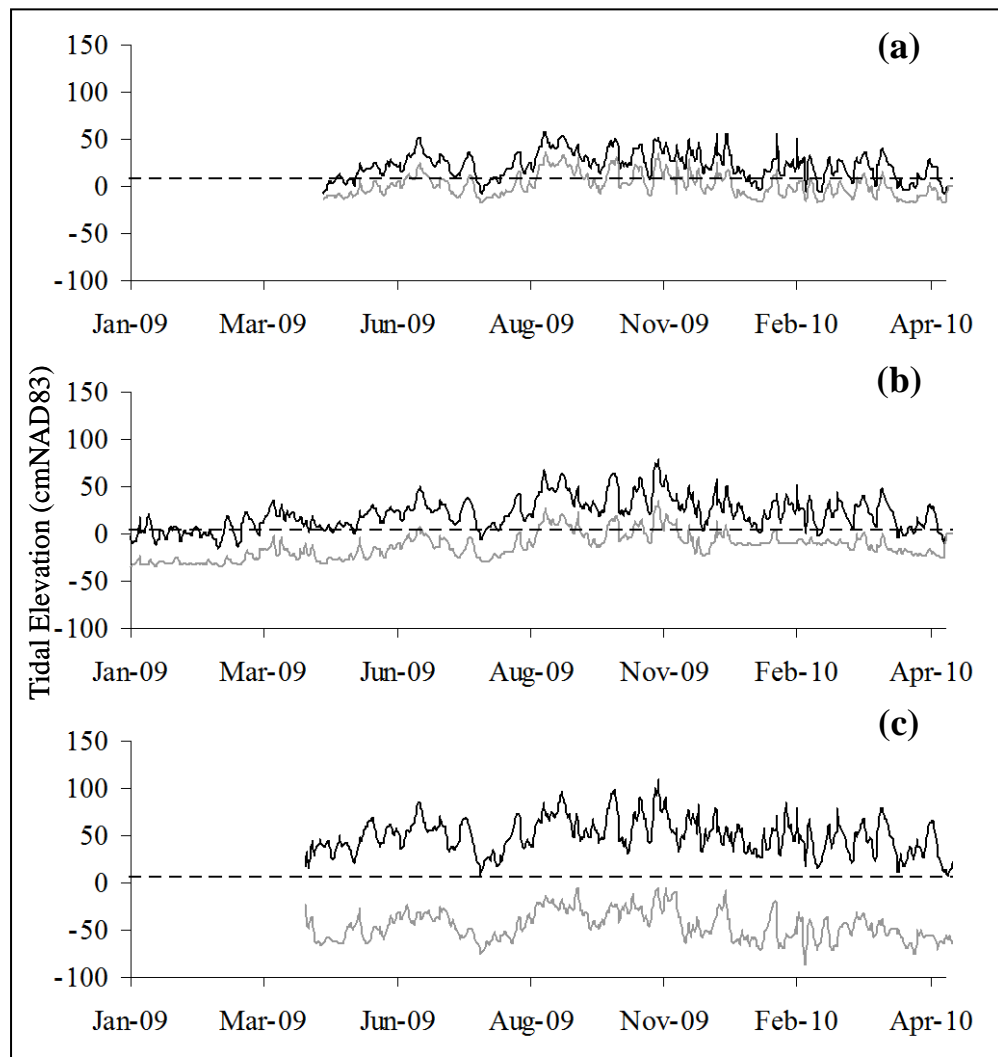


Figure 9-18. Daily maximum observed high tide (black) and low tide (grey) for French Creek (a), Traps Bay (b), and Freeman Creek (c).

Creekbank marsh surface elevation is indicated by the dashed line.

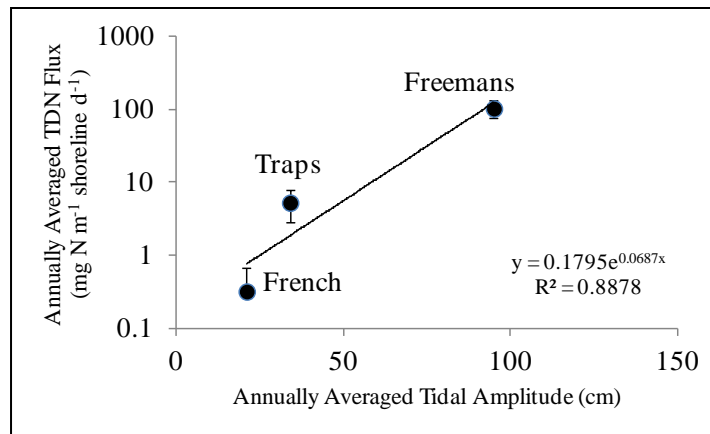


Figure 9-19. Predicting marsh N flux based on tidal amplitude.

The more efficient delivery of N from marshes to adjacent waters along the ICW spatially coincides locally with a lack of external N sources in that region. Small drainage fluxes of N from French Creek and Traps Bay marshes to the NRE are dwarfed by the inputs from the New River mainstem. But the larger inputs from Freeman Creek enter waters that are nearly always N deplete; affected only by New River mainstem at the extreme discharges and modest atmospheric deposition rates. Some supporting evidence of marsh inputs to the lower NRE can be found in the Research Project AE-2 stable isotope surveys.

Annually, N loads derived from drainage from the marshes were estimated at: French Creek=0.1–0.5 kg N y⁻¹; Traps Bay= 0.4–4.0 kg N y⁻¹; and Freeman Creek= 175–350 kg N y⁻¹. Using estimates of 26 km of marsh shoreline for the marshes of the NRE, and 20 km for the ICW (mainland side) total marsh N drainage rates for NRE marshes and ICW marshes are approximately 10 kg N y⁻¹ and 550 kg N y⁻¹, respectively.

In addition to higher water drainage rates and larger marsh at Freeman Creek, the 4 order of magnitude difference in N flux between sites is due to shoreline geomorphology of Freeman Creek. Specifically, the highly sinuous shoreline provides a large drainage face through which the N flux occurs. This sinuosity, or high shoreline frontage to area ratio, is a defining feature of the ICW marshes relative to their NRE counterparts. The net result is that drainage of N is an inconsequential component of the marsh N budgets for French Creek and Traps Bay, but it is not inconsequential for Freeman Creek; and arguably the ICW marshes in general.

Summary Points

- N inputs from marsh drainage can be estimated for a specific site given tidal amplitude, and estimates have a higher certainty at higher tidal amplitudes.
- N inputs from marsh drainage to open water are trivial for the NRE, but not trivial for the ICW
- Higher tidal amplitude and higher shoreline frontage to marsh area ratio in the lower NRE and ICW result in marshes being a local source of N.

Section 3: Marsh–Estuary Exchange—Attenuation of Dissolved Inorganic Nitrogen Fluxes by Denitrification

Methods and Materials

Coupled denitrification, direct denitrification, denitrification capacity, and anaerobic ammonium oxidation (ANAMMOX) reaction capacity were assessed in all three marshes seasonally in 2010. Three methods (all using nitrogen with a mass of 15 [labeled] ^{15}N) were used to quantify rates and capacities.

Labeled Ammonium-based Estimates of Coupled Denitrification

First, sediment incubations were performed to estimate coupled denitrification using a labeled ammonium ($^{15}\text{NH}_4^+$) spike. Sediment cores (2-cm diameter, 3-cm deep) were collected at six locations (three creekside and three upland fringe) in each marsh. Cores were collected using cut-off 30-mL syringes and transferred immediately to 40-mL amber I-CHEM vials and placed on ice. Four liters of site water was collected from the adjacent waterbody at each site and sealed with no headspace.

Ambient extractable NH_4^+ was measured on a subset of vials which were not spiked with isotope (“pre-spike”). These NH_4^+ concentrations (along with post-incubation NH_4^+ measurements) were used to calculate the effective isotopic enrichment (E_E) of the $^{15}\text{NH}_4^+$ substrate. Each of the vials was loaded with 30 mL 2 M of potassium chloride (KCl). These were placed on a shaker table for 2 hours, filtered, and frozen for DIN analysis.

The I-CHEM vials used in the incubations were loaded with 300 μL 10 mM $^{15}\text{NH}_4^+$ (99 at %), filled with corresponding site water, and sealed with no headspace. Prior to sealing, each I-CHEM top was equipped with a glass bead strung from monofilament that hung halfway down the water column to serve as a stirring apparatus. The samples were then placed on an orbital shaker table at 60 rpm. Samples were killed using 1 mL of saturated zinc chloride (ZnCl_2) at time intervals of 4, 8, and 18 hours. At the time of the ZnCl_2 addition, sediment was stirred to ensure a complete kill and then recapped with zero headspace.

Following termination of the incubation, a 2-mL aliquot was transferred using a peristaltic pump to a helium-flushed 12-mL exetainer loaded with 50 μL of potassium hydroxide (KOH). Samples were vortexed and then analyzed for dissolved heavy nitrogen ($^{15}\text{N}_2$) using an isotope ratio mass spectrometer (IRMS) following an equilibration period of 1 hour. The remainder of the incubation volume was shaken into solution (in the I-CHEM vial), combined with equal parts 2M of KCl, and placed on a shaker table for 2 hours. The samples were then spun down on a centrifuge at 2,000 rpm for 10 minutes, filtered, and frozen for NH_4^+ analysis.

The effective $^{15}\text{NH}_4^+$ enrichment (E_E) of the sample was calculated as shown in Equation 9-5:

$$E_E = ([C_{\text{Post}} - C_{\text{Pre}}] / C_{\text{Post}}) * 0.99 \quad (\text{Eq. 9-5})$$

where C_{Post} is the NH_4^+ concentration in μM after addition of tracer and C_{Pre} is the background concentration of NH_4^+ in μM before the addition of tracer.

Coupled denitrification rates were calculated using the $\delta^{15}\text{N}_2$ measured according the following steps: first, the $\delta^{15}\text{N}_2$ was converted to mole fraction ^{15}N (MF) using Equation 9-6 as shown below:

$$MF = ([(\delta^{15}\text{N}/1000) + 1] * 0.0036765) / (1 + ([(\delta^{15}\text{N}/1000) + 1] * 0.0036765)) \quad (\text{Eq. 9-6})$$

The excess ^{15}N (N_E) in the N_2 pool was determined from the MF using Equation 9-7 as shown below:

$$N_E = (MF - 0.0036630329) * (C_{\text{N}_2} * V * 2) \quad (\text{Eq. 9-7})$$

where C_{N_2} is the concentration of N_2 resulting from air equilibration in μM and V is the overlying water volume in liters.

Finally, the coupled denitrification rate (D) was calculated (as shown in Equation 9-8) from the excess $^{15}\text{N}_2$ and effective NH_4^+ ammonium isotope enrichment calculated from Equation 9-5.

$$D = ([N_E * (1/E_E)]/T) * (1/A_C) \quad (\text{Eq. 9-8})$$

T is the incubation time in hours and A_C is the core area (m^2).

Isotope Pairing Labeled Nitrate-based Coupled and Direct Denitrification

A second set of sediment incubations were performed to estimate coupled and direct denitrification. Sediment cores were collected as described. In the laboratory, three I-CHEM vials from each marsh were loaded with 225 μL 10 mM of labeled nitrate ($^{15}\text{NO}_3^-$) and filled to the top with corresponding site water. The overlying water was filtered and frozen for DIN analysis. The remaining I-CHEM vials were loaded with 225 μL 10 mM of $^{15}\text{NO}_3^-$ and filled to the top with corresponding site water. Samples were handled, killed, transferred, and extracted for DIN as previously described.

Isotope analysis was performed using a gas bench on an IRMS to determine N_2 volumes and paired isotope ($^{29}\text{N}_2$ and $^{30}\text{N}_2$) production. Denitrification rates were calculated according to Equations 9-9 through 16. The rate of $^{29}\text{N}_2$ production (r_{29}) was calculated as shown in Equation 9-9:

$$r_{29} = ([T_{F\ 29} - T_{0\ 29}] * [V + (P * S)]) / (A_C * T) \quad (\text{Eq. 9-9})$$

where $T_{F\ 29}$ is the final concentration of $^{29}\text{N}_2$ in μM , $T_{0\ 29}$ is the initial concentration of $^{29}\text{N}_2$ in μM , V is the overlying water volume in liters, P is the porosity of the sediment, S is the sediment volume in liters, A_C is the core area in m^2 , and T is the incubation time in hours.

The rate of $^{30}\text{N}_2$ production (r_{30}) was calculated as shown in Equation 9-10:

$$r_{30} = ([T_{F\ 30} - T_{0\ 30}] * [V + (P * S)]) / (A_C * T) \quad (\text{Eq. 9-10})$$

where $T_{F\ 30}$ is the final concentration of $^{30}\text{N}_2$ in μM and $T_{0\ 30}$ is the initial concentration of $^{30}\text{N}_2$ in μM .

The denitrification rate of $^{15}\text{NO}_3^-$ (D_{15}) was calculated as shown in Equation 9-11:

$$D_{15} = r_{29} + 2 * r_{30} \quad (\text{Eq. 9-11})$$

The denitrification rate of $^{14}\text{NO}_3^-$ (D_{14}) was calculated as shown in Equation 9-12:

$$D_{14} = D_{15} * (r_{29} / [2 * r_{30}]) \quad (\text{Eq. 9-12})$$

Total denitrification (D_{Tot}) was calculated as shown in Equation 9-13:

$$D_{\text{Tot}}=D_{14}+D_{15} \quad (\text{Eq. 9-13})$$

Total water column denitrification (D_{col}) was calculated as shown in Equation 9-14:

$$D_{\text{col}}=D_{15}/E_E \quad (\text{Eq. 9-14})$$

where E_E is the effective isotopic enrichment of the sample.

Coupled denitrification (D_{coupled}) was calculated as shown in Equation 9-15:

$$D_{\text{coupled}}=(D_{\text{Tot}}-D_{\text{col}}) * 2 \quad (\text{Eq. 9-15})$$

Direct denitrification (D_{direct}) was calculated as shown in Equation 9-16:

$$D_{\text{direct}}=(D_{\text{col}} * [1-E_E]) * 2 \quad (\text{Eq. 9-16})$$

Direct Denitrification and Anaerobic Ammonium Oxidation Capacity

These were assessed using a sealed tube anaerobic slurry incubation. The top 3 cm of sediment was collected from a creekside location and an upland fringe location in each marsh. In the laboratory, each sample was homogenized using a mortar and pestle. Two grams of sediment and a glass bead were added to 12-mL exetainers. The exetainers were capped and incubated overnight in the dark. The exetainers were then flushed with helium. Two exetainers from each sampling location were frozen to later have porewater extracted and analyzed for NO_x (nitrate+nitrite) using vanadium reduction/chemiluminescence.

The exetainers were separated into four groups to be loaded with 0.1 mL of different concentrations (i.e., 0.11 mM, 0.275 mM, 0.825 mM, and 1.1 mM) of labeled potassium nitrate ($^{15}\text{KNO}_3$) to meet target porewater NO_3^- concentrations of 10 μM , 25 μM , 75 μM , and 100 μM , respectively. All exetainers were then loaded with 0.1 mL 0.55 mM of ammonium chloride (NH_4Cl) and vortexed. The reactions were killed at 0-, 1-, 2-, and 3-hour time points using 0.3 mL of 4M KOH, vortexed, and then ready to run on the IRMS after 2 hours.

Isotope analysis was performed using a gas bench on an IRMS to determine $^{29}\text{N}_2$ and $^{30}\text{N}_2$ production. Denitrification and ANAMMOX rates were calculated as shown in Equation 9-17 (Thamdrup and Dalsgaard, 2002):

$$D_{\text{total}}=P_{30} * F_N^{-2} \quad (\text{Eq. 9-17})$$

where P_{30} is $^{30}\text{N}_2$ production attributed to denitrification and F_N is the fraction of ^{15}N in NO_3^- . Total ANAMMOX (A_{total}) was calculated as shown in Equation 9-18:

$$A_{\text{total}}=F_N^{-1} * (P_{29}+2 * [1-F_N^{-1}] * P_{30}) \quad (\text{Eq. 9-18})$$

where P_{29} is $^{29}\text{N}_2$ production attributed to ANAMMOX.

Results and Discussion

Direct Denitrification

In French Creek, mean creekbank direct denitrification was $1.25 \mu\text{moles m}^{-2} \text{hr}^{-1}$ in February and $1.14 \mu\text{moles m}^{-2} \text{hr}^{-1}$ in May. French Creek mean interior direct denitrification was $1.02 \mu\text{moles m}^{-2} \text{hr}^{-1}$ in February and $1.31 \mu\text{moles m}^{-2} \text{hr}^{-1}$ in May (**Figure 9-20a,b**). In Traps Bay, mean creekbank direct denitrification was $1.42 \mu\text{moles m}^{-2} \text{hr}^{-1}$ in February and $2.89 \mu\text{moles m}^{-2} \text{hr}^{-1}$ in May. Traps Bay mean interior direct denitrification was $1.22 \mu\text{moles m}^{-2} \text{hr}^{-1}$ in February and $1.45 \mu\text{moles m}^{-2} \text{hr}^{-1}$ in May (**Figure 9-20c,d**). In Freeman Creek, mean creekbank direct denitrification was $0.16 \mu\text{moles m}^{-2} \text{hr}^{-1}$ in February and $2.11 \mu\text{moles m}^{-2} \text{hr}^{-1}$ in May. Freeman Creek mean interior direct denitrification was $0.20 \mu\text{moles m}^{-2} \text{hr}^{-1}$ in February and $0.96 \mu\text{moles m}^{-2} \text{hr}^{-1}$ in May (**Figure 9-20e,f**).

Direct denitrification rate was greater in May than in February for all locations at all sites except French Creek creekbank, which had greater direct denitrification rate in February than May (**Figure 9-21a**). Direct denitrification was greater in the creekbank than the interior for all locations in February and May except for French Creek in May (**Figure 9-21b**).

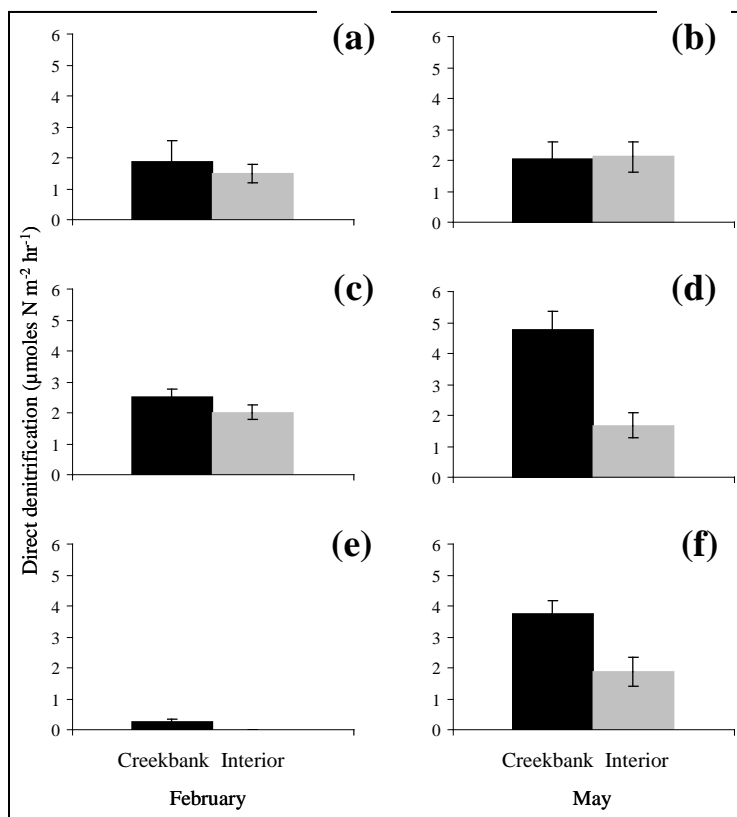


Figure 9-20. Mean direct denitrification rates from 4-hour incubations for French Creek (a, b), Traps Bay (c, d), and Freeman Creek (e, f).

Black represents creekbank, grey represents interior.

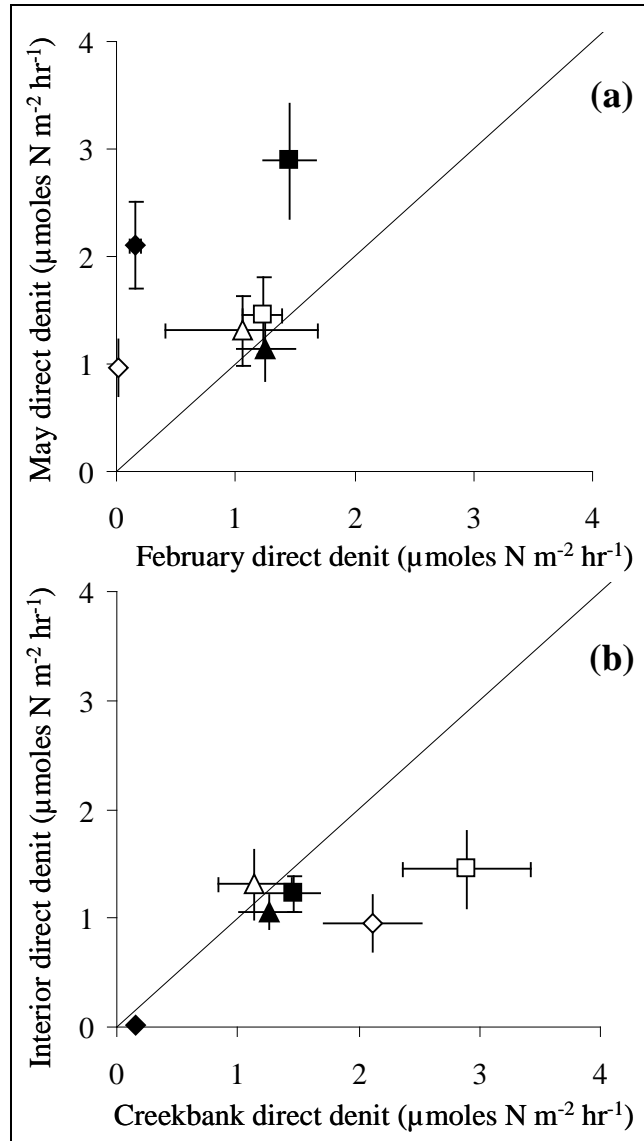


Figure 9-21. Comparison of direct denitrification rates of May versus February (a) and marsh interior versus creekbank (b).

Triangles represent French Creek, boxes represent Traps Bay, and diamonds represent Freeman Creek. For May versus February (a), solid symbols represent creekbank and open symbols represent interior. For interior versus creekbank (b), solid symbols represent February, and open symbols represent May.

Coupled denitrification was measured two ways: isotope pairing technique (IPT)— $^{15}\text{NO}_3^-$ labeling (Nielsen, 1992; Steingruber et al., 2001) and through the addition of $^{15}\text{NH}_4^+$ tracer.

From the IPT $^{15}\text{NO}_3^-$ addition experiments: In French Creek, mean creekbank coupled denitrification was $6.72 \mu\text{moles m}^{-2} \text{ hr}^{-1}$ in February and $4.34 \mu\text{moles m}^{-2} \text{ hr}^{-1}$ in May. French Creek mean interior coupled denitrification was $4.08 \mu\text{moles m}^{-2} \text{ hr}^{-1}$ in February and $9.74 \mu\text{moles m}^{-2} \text{ hr}^{-1}$ in May (Figure 9-22 b,d). In Traps Bay, mean creekbank coupled denitrification was $14.63 \mu\text{moles m}^{-2} \text{ hr}^{-1}$ in February and $23.42 \mu\text{moles m}^{-2} \text{ hr}^{-1}$ in May. Traps Bay mean interior coupled denitrification was $11.15 \mu\text{moles m}^{-2} \text{ hr}^{-1}$ in February and $4.97 \mu\text{moles m}^{-2} \text{ hr}^{-1}$ in

May (**Figure 9-22f,h**). In Freeman Creek, mean creekbank coupled denitrification was $3.11 \mu\text{moles m}^{-2} \text{hr}^{-1}$ in February and $8.00 \mu\text{moles m}^{-2} \text{hr}^{-1}$ in May. Freeman Creek mean interior coupled denitrification was undetectable in February and $3.90 \mu\text{moles m}^{-2} \text{hr}^{-1}$ in May (**Figure 9-22j,l**). Coupled denitrification rate was greater in May than in February for all locations at all sites (**Figure 9-23**). Coupled denitrification was greater in the creekbank than the interior for all locations in February and May except for French Creek in May (**Figure 9-23d**).

From the $^{15}\text{NH}_4^+$ addition experiments: In French Creek, mean creekbank coupled denitrification was $9.01 \mu\text{moles m}^{-2} \text{hr}^{-1}$ in February and $0.90 \mu\text{moles m}^{-2} \text{hr}^{-1}$ in May. French Creek mean interior coupled denitrification was $9.41 \mu\text{moles m}^{-2} \text{hr}^{-1}$ in February and $5.30 \mu\text{moles m}^{-2} \text{hr}^{-1}$ in May (**Figure 9-22a,c**). In Traps Bay, mean creekbank coupled denitrification was $5.82 \mu\text{moles m}^{-2} \text{hr}^{-1}$ in February and $8.90 \mu\text{moles m}^{-2} \text{hr}^{-1}$ in May. Traps Bay mean interior coupled denitrification was $6.93 \mu\text{moles m}^{-2} \text{hr}^{-1}$ in February and $3.09 \mu\text{moles m}^{-2} \text{hr}^{-1}$ in May (**Figure 9-22e,g**). In Freeman Creek, mean creekbank coupled denitrification was $0.64 \mu\text{moles m}^{-2} \text{hr}^{-1}$ in February and $4.95 \mu\text{moles m}^{-2} \text{hr}^{-1}$ in May. Freeman Creek mean interior coupled denitrification was $0.15 \mu\text{moles m}^{-2} \text{hr}^{-1}$ in February and $1.24 \mu\text{moles m}^{-2} \text{hr}^{-1}$ in May (**Figure 9-22i,k**). The $^{15}\text{NH}_4^+$ based coupled denitrification rates were greater in the interior than in the creekbank for both February and May in French Creek and February in Traps Bay. Coupled denitrification rates in the creekbank exceeded those in the interior for both February and May in Freeman Creek and in May at Traps Bay (**Figure 9-23a**). Coupled denitrification was greater in May for all locations at all sites except for the French Creek creekbank, where the rates were approximately equivalent (**Figure 9-23c**). The $^{15}\text{NH}_4^+$ approach and IPT-based calculations produced similar coupled denitrification rates that, although mean rates differed by a factor of 1.5, were effectively equivalent within the observed variance.

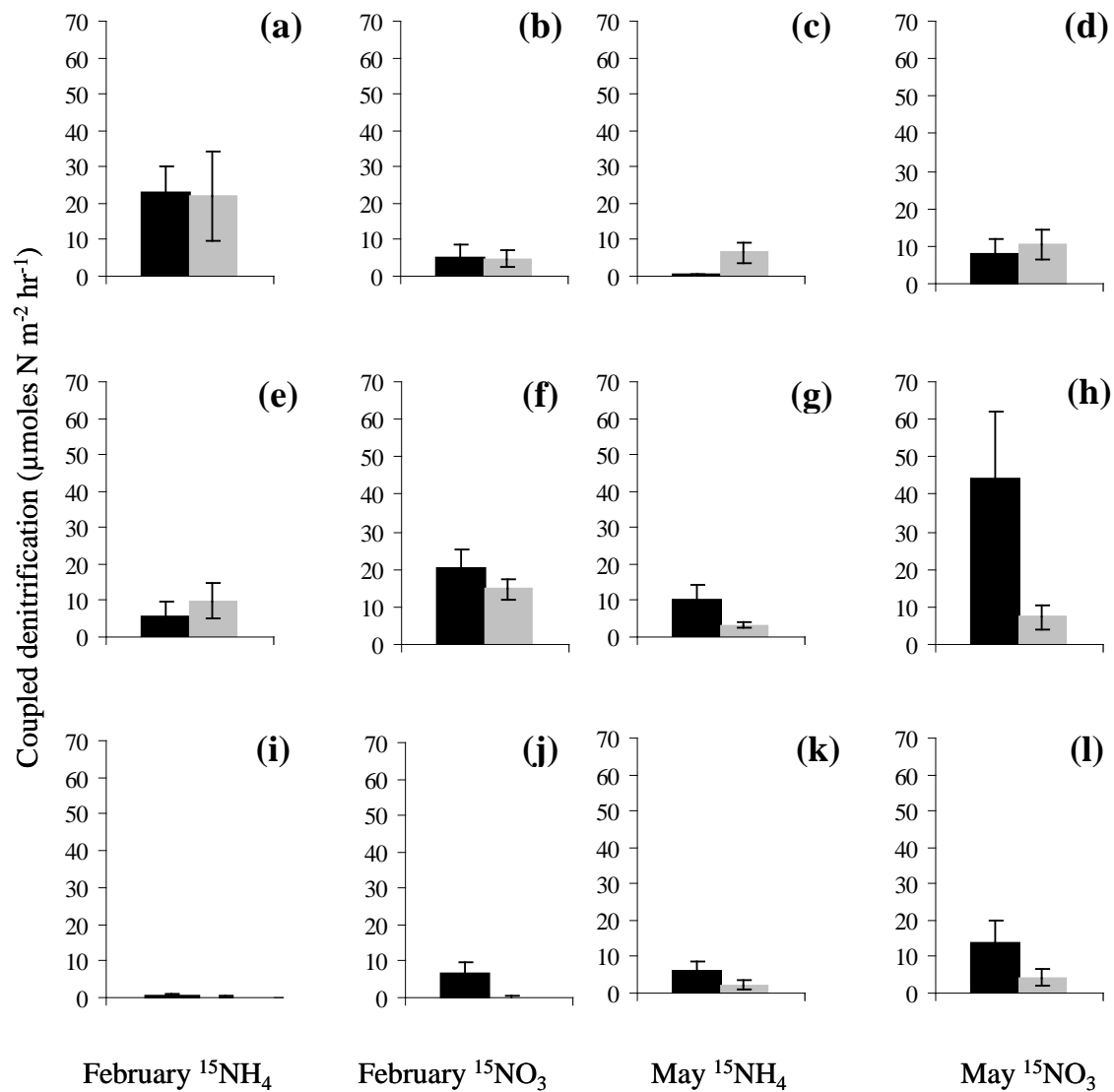


Figure 9-22. Mean coupled denitrification rates from 4-hour incubations for French Creek (a–d), Traps Bay (e–h), and Freeman Creek (i–l).

Black represents creekbank sediment incubations, grey represents interior sediment incubations.

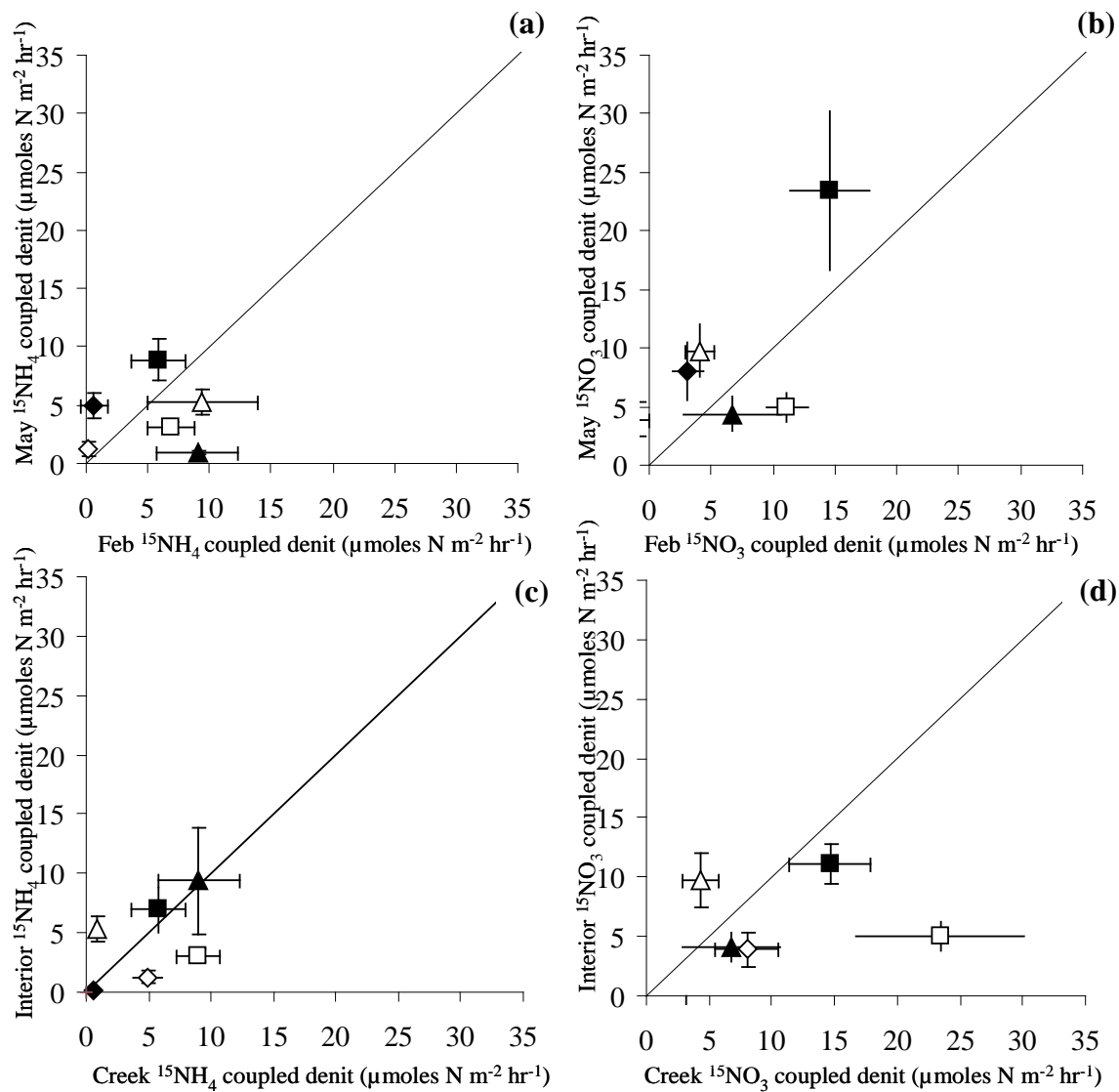


Figure 9-23. Comparison of coupled denitrification rates of marsh May versus February (a,b) and interior versus creekbank (c,d).

Triangles represent French Creek, boxes represent Traps Bay, and diamonds represent Freeman Creek. For May versus February (a,b), solid symbols represent creekbank and open symbols represent interior. For interior versus creekbank (c,d), solid symbols represent February and open symbols represent May.

Comparison of direct denitrification rates versus coupled denitrification rates ($^{15}\text{NH}_4^+$ -based and IPT) showed that the coupled denitrification rate was greater than direct denitrification rate for almost all of the sampled locations and times with the exception of the interior of Freeman Creek in February (Figure 9-24). Coupled denitrification typically exceeded direct denitrification by a factor of 2 or greater.

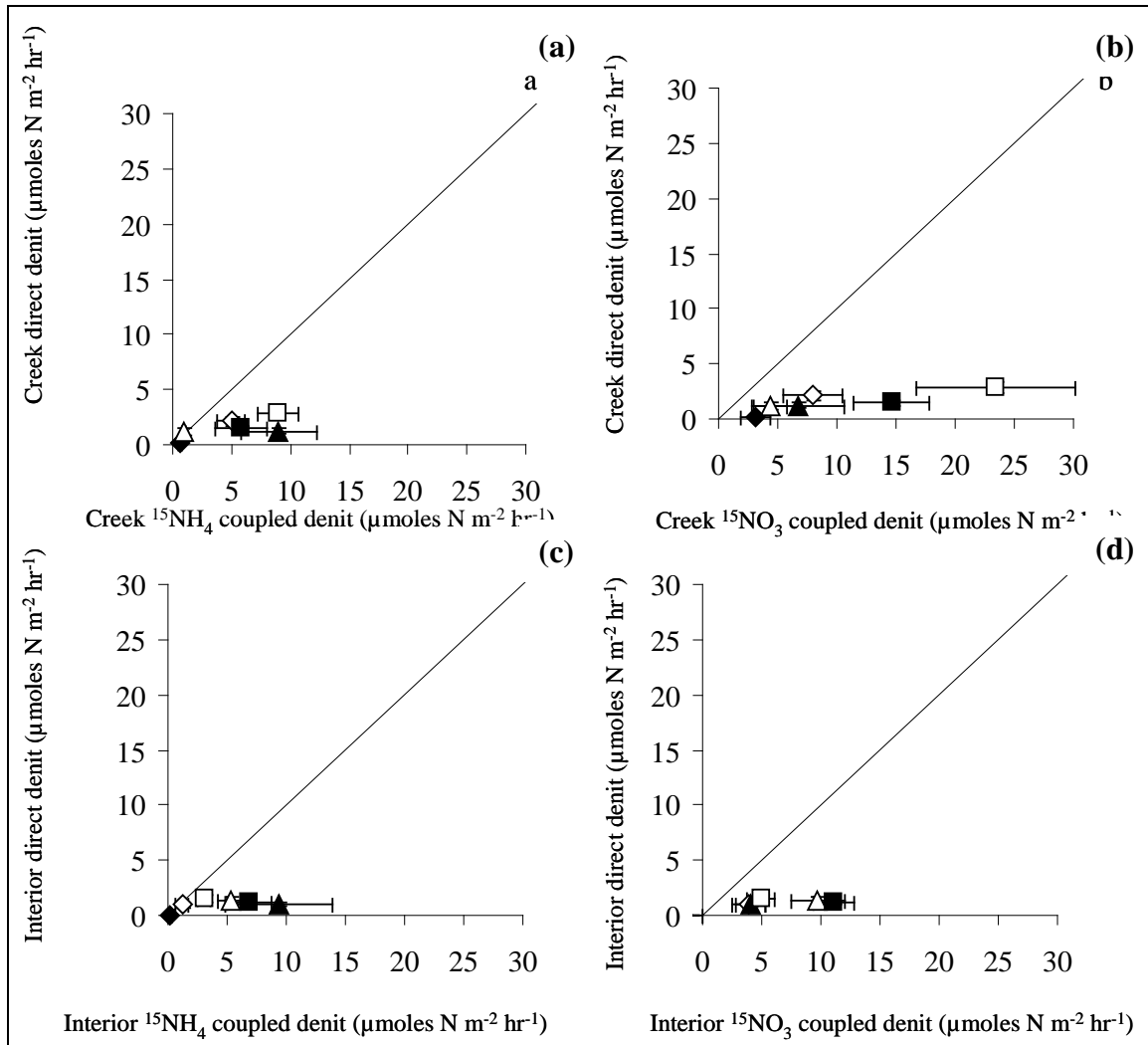


Figure 9-24. Direct denitrification versus coupled denitrification for all samplings.

Triangles represent French Creek, boxes represent Traps Bay, and diamonds represent Freeman Creek. Closed symbols represent February samples and open symbols represent May samples.

Total denitrification (coupled + direct) measured in this study ranged from 1–27 $\mu\text{moles N m}^{-2} \text{ hr}^{-1}$ and was overwhelmingly dominated at nearly all times and locations by coupled denitrification. An increase in total denitrification was observed from February to May in Traps Bay and Freeman Creek samples, and a decrease in total denitrification was seen from February to May for French Creek samples. This lack of a consistent seasonal pattern between marshes is not surprising considering variable seasonal results from other studies (Anderson et al., 1997, Eriksson et al., 2003). Kaplan et al. (1979) found that temperature is the primary control on

denitrification, whereas other studies have found that nitrate concentration is the primary control on denitrification (Eriksson et al., 2003). An increase in ambient NO_3^- and an increase in temperature were concurrent in this study and the effects of both could not be isolated. Covariance between temperature and NO_3^- , as well as other factors that help control coupled denitrification (e.g., variable mineralization rates in wetlands [Seitzinger, 1994]) yielded an incomplete picture of whether denitrification was seasonally different in the NRE marshes.

Likewise there was no clear dominance of denitrification in the creekbank versus the interior. Higher direct denitrification in the creekbank was observed (with one exception; French Creek in May). Higher rates in the creekbank might be expected where high NO_3^- in flooding water is the norm and because a greater volume of tidal water is recharged in the creekbank relative to the interior. However, high NO_3^- is not characteristic of the NRE or ICW. It is possible that higher amounts of plant production in the creekbank might supply a higher concentration of or more labile dissolved organic carbon (DOC). However the results from the denitrification capacity experiments indicate plenty of useable carbon to drive denitrification at all sites and locations. So it remains unclear why direct denitrification in the creekbank seems to be generally higher relative to the interior. Regardless, the contribution of direct denitrification relative to coupled denitrification is small and there was no spatial pattern in coupled denitrification and, by extension, no spatial pattern in total denitrification. Because coupled denitrification in marshes is limited by the nitrification rate (Tobias and Neubauer, 2009), and nitrification is limited by oxygen (O_2) availability in the subsurface, the increased recharge of oxygenated tidal water into the creekbank might be expected to enhance coupled denitrification, or at the least contribute to a larger denitrifying microbial community in the creekbank. Although the comparison of the creekbank versus interior coupled denitrification rates observed within a site does not indicate that these O_2 delivery mechanisms are contributing to spatial differences in coupled denitrification rates within a site, coupled denitrification rates at Traps Bay were 1.5 to 4 times greater than both French Creek and Freeman Creek (with the exception of the $^{15}\text{NH}_4^+$ experiment in February at French Creek that was higher than both), indicating that O_2 delivery mechanisms differ between sites.

Comparisons to Other Systems

The range of rates measured in the NRE marshes is comparatively low relative to other denitrification rates compiled for coastal systems (**Figure 9-25**). Some of the disparity in rate measurements between the NRE marshes and other systems may be attributable to differences in methods used to measure denitrification (Groffman et al., 2006). More likely however, the lower total denitrification rates in the NRE can be explained primarily by the very small contribution of direct denitrification that resulted from low ambient NO_3^- conditions in the NRE. In comparison, many past studies (Anderson et al., 1997; Tobias et al., 2001a and c) were conducted in systems with high NO_3^- or under non- NO_3^- -limiting conditions where direct denitrification rates were high.

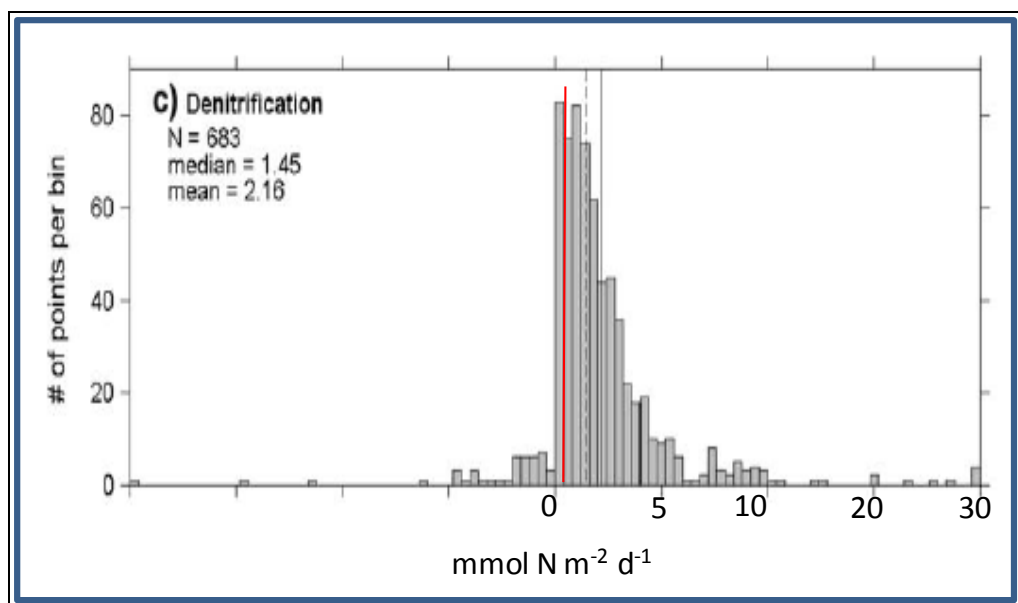


Figure 9-25. Coastal marine denitrification rates compiled by Fennel et al. (2008).

Red line denotes the mean total denitrification rate measured in the study marshes.

Direct Versus Coupled Denitrification

In the marshes of the NRE, direct denitrification rate was 10–50% that of coupled denitrification for more than 85% of the measurements and less than 25% for 50% of the measurements. These ratios are consistent with the observed low NO_3^- in flooding waters (approximately 1 μM in February, approximately 3 μM in May). Seitzinger et al. (2006) presented a compilation of coupled versus direct denitrification ratios across aquatic and marine systems reported as a function of NO_3^- concentrations. Coupled- and direct- denitrification were equivalent at ambient NO_3^- concentration of 10 μM . Coupled denitrification was favored at lower NO_3^- and direct favored at NO_3^- concentrations above 10 μM . The observed greater than 80% dominance of coupled, predicted by Seitzinger et al. (2006) for these NO_3^- concentrations is consistent with the ratio of coupled denitrification to direct denitrification of 7:1 measured in the NRE marshes.

Low DIN in the NRE (particularly NO_3^-) is the dominant low-flow condition in the NRE because wastewater treatment improvements were made in the late 1990s (Mallin et al., 2005). These conditions were prevalent during the February and May experiments. However, pulses of high NO_3^- to the NRE accompany high watershed discharge events and a disproportionately enhanced, but transient, direct denitrification rate would be expected under those conditions.

Direct Denitrification Capacity

The strong linear response of direct denitrification rates in sediment slurries to increasing NO_3^- concentration indicates high denitrification capacity at the creekbank and marsh interior of all three sites. The increase in denitrification per μM NO_3^- increase ranged from 0.02 in the Freeman Creek creekbank to 0.12 in the Traps Bay creekbank. The increase in denitrification per μM NO_3^- increase was more than double in the French Creek creekbank than in the French Creek interior (**Figure 9-26a,b**). The response in the creekbank was 1.25 times that of the response in the interior in Traps Bay (**Figure 9-26c,d**). The Freeman Creek creekbank showed the weakest

linear response of all sites, being 25% of the French Creek creekbank response and 20% of the Traps Bay creekbank response. The Freeman Creek creekbank denitrification response to increasing NO_3^- was one-fifth that of the Freeman Creek interior (Figure 9-26e,f).

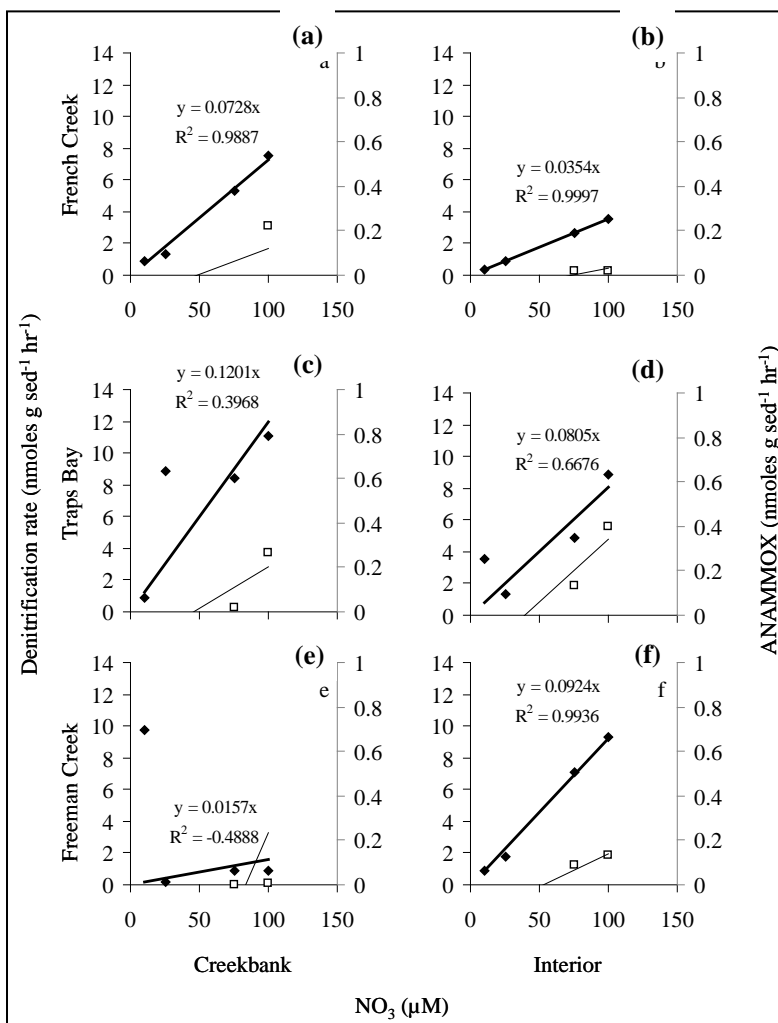


Figure 9-26. Denitrification and ANAMMOX capacity for French Creek creekbank (a) and interior (b), Traps Bay creekbank (c) and interior (d), and Freeman Creek creekbank (e) and interior (f).

Solid symbols denote denitrification, open symbols denote that ANAMMOX was undetectable at ambient concentrations and ranged from 0 to less than 2% of the denitrification at ambient concentrations and at higher NO_3^- treatments, respectively.

For all treatments, increasing direct denitrification rate occurred up to the highest NO_3^- concentration (100 μM), indicating that there was no saturation of denitrification kinetics or evidence of co-limiting substrate in the 10- to 100- μM range. ANAMMOX rates were low in all locations at all sites at rates of less than 0.5 nmol $\text{g}^{-1} \text{hr}^{-1}$ measured at higher NO_3^- concentrations ANAMMOX in the marshes of the NRE was negligible, contributing approximately 1% of the N loss from denitrification. This low contribution of ANAMMOX is consistent with the findings of Koop-Jakobsen and Giblin (2009), who found ANAMMOX to

account for less than 3% of total N_2 production. Additionally, the findings from the increasing NO_3^- incubations using NRE marsh sediments support the assertions of Koop-Jakobsen and Giblin (2009) that increased N loading does not yield a greater proportional contribution of ANAMMOX to gaseous N losses. ANAMMOX is not expected to play a role in marsh N removal at MCBCL.

Considering ambient NO_3^- concentration in the flooding waters is currently around 1 μM , the relative response of denitrification to rising NO_3^- is indicative of the marshes' ability to denitrify increasing environmental NO_3^- loads. Increased NO_3^- concentration resulted in a linear increase in denitrification rate attributable to enhanced direct denitrification. Rates did not plateau even at the higher NO_3^- concentration (100 μM) because NO_3^- and labile organic matter are the limiting factors regarding denitrification rates. The surface of marshes are organic carbon rich, with availability well beyond even higher NO_3^- loads (Tobias et al., 2001a). The relationship between the increased denitrification rate and the increased concentration shows that given a 100-fold increase in NO_3^- load, the marshes would respond with 85–90 fold increase in denitrification for French Creek, and equivalent 100-fold rise in denitrification for Traps Bay, and an enhanced 125- to 160-fold increase in denitrification for Freeman Creek. Development of the watershed, an increased population and wastewater generation, and additional agriculture up-estuary could all increase NO_3^- loads, but even at 100-fold increase in current NO_3^- concentration, it appears that the marshes of the NRE will accelerate removal of N on an almost 1:1 basis on average. This is not to say that marshes can remove all of the new N through denitrification, merely that the proportional amount of removal via denitrification will stay roughly constant relative to the new load. This response may continue until the large NO_3^- loads impact the marsh geomorphology as presented by Drake et al. (2009).

On the whole marsh scale, denitrification is heavily weighted to the interior rate measurements (most of the marsh area is interior). The net result is that per area rates appropriate for scaling total denitrification to the whole of each marsh are: French Creek: 11 $\mu mol\ N\ m^{-2}\ hr^{-1}$, Traps Bay: 12 $\mu mol\ N\ m^{-2}\ hr^{-1}$, Freeman Creek: 3 $\mu mol\ N\ m^{-2}\ hr^{-1}$. Given area estimates of each marsh at 13,354 m^2 ; 9712 m^2 ; and 100,000 m^2 for French Creek, Traps Bay, and Freeman Creek, the total annual removal of N via denitrification for each marsh are as follows: French: 18 kg $N\ y^{-1}$; Traps: 14 kg $N\ y^{-1}$; and Freeman: 36 kg $N\ y^{-1}$. Assuming that the French Creek and Traps Bay sites are representative of the NRE marshes, and Freeman of the ICW bordering marshes, and estimated total NRE marsh area of 700,000 m^2 and ICW marsh area of 1,700,000 m^2 , the NRE and ICW marshes denitrify on the order of 944 kg $N\ y^{-1}$ and 6,254 kg $N\ y^{-1}$. The magnitude of this removal in the NRE is on the order of 1% of inputs from the New River mainstem. The impact of ICW marsh denitrification, given the lack of large watershed inputs in the lower part of MCBCL for comparison, is more difficult to assess but should be considered non-trivial, as was observed with the marsh drainage of N into the ICW. Relative to the rate of marsh N supply to adjacent waters through drainage, denitrification-driven removal of N, even at the low ambient rates, is 1 to 2 orders of magnitude larger than the N drainage flux for both the NRE and the ICW marshes.

Summary Points

- Ambient denitrification rates in marshes of MCBCL are low, and dominated by coupled denitrification because tidal NO_3^- concentrations are low and there is no groundwater source of NO_3^- .

- The NRE marshes remove N through denitrification that is equivalent to 1% of inputs from the mainstem New River.
- MCBCL marshes have a huge denitrification capacity and show linear increases in rates up to NO_3^- concentrations 2 orders of magnitude larger than current levels.
- With respect the N source/sink budget of the marsh, denitrification is 1 to 2 orders of magnitude larger than marsh N export through drainage and inputs of groundwater N via groundwater.

Section 4: Summary and Synthesis—Marsh Nitrogen Source/Sink Budget

Methods and Materials

To characterize the net source and sink strengths of MCBCL marshes with respect to N, groundwater N inputs, marsh supply of N to adjacent water via drainage, denitrification, and accretion of sediment N were compared. Approaches for estimating groundwater, drainage, and denitrification are described in Sections 1 through 3 of this chapter. Burial of sediment N was calculated from sediment accretion rate estimates derived from sediment elevation tables (SETs) and horizon markers described in final report for Research Project CW-2 (Chapter 8). Because the SET and sediment horizon marker measurements provide a short-term accretion rate, we used a secondary constraining accretion rate that sets the marsh accretion rate equal to a conservatively estimated local sea level rise rate of 2 mm y^{-1} . Sediment accretion rates were converted to N mass burial rates ($\text{N mass m}^{-2} \text{ y}^{-1}$) using the measured sediment bulk densities and N content (%N) as measured using elemental analysis.

Results and Discussion

The mean bulk density and %N of all surface marsh sediments analyzed were 2.3 g cm^{-3} and 0.3% N. When combined with sediment accretion estimates (short-term and based on SLR), N burial magnitudes for the three marshes ranged from 13–66 $\text{g N m}^{-2} \text{ y}^{-1}$ (**Table 9-7**)

Table 9-7. Per area marsh N burial rates.

Marsh	<u>SET / HM</u>	<u>SLR</u>
	$\text{gN m}^{-2} \text{ y}^{-1}$	$\text{gN m}^{-2} \text{ y}^{-1}$
French Creek	12.6 - 41.3	13.8
Traps Bay	29.8 - 55.2	13.8
Freeman	13.0 - 66.4	13.8

The range of burial rates derived from sediment elevation tables (SETs) or horizon markers (HMs) is compared to N burial minimums for marshes accreting at a rate that keeps pace with sea level rise (SLR).

The high accretion/N burial rates well in excess of SLR are not sustainable. The more conservative N burial rates that were derived from SLR were used to scale N burial to the whole marsh and extrapolate to rates for all NRE and ICW marshes. French Creek, Traps Bay, and Freeman Creek marshes are burying 184, 134, and 1,380 kg N y^{-1} . The NRE marshes ($700,000 \text{ m}^2$) bury 9,660 kg N y^{-1} from the NRE, and the ICW marshes ($1,700,000 \text{ m}^2$) bury 23,460 kg N y^{-1} . These burial numbers dominate the marsh N mass balance and tip the overall function of the marsh strongly towards being a net sink for N (**Figure 9-27**) for both the NRE and ICW marshes.

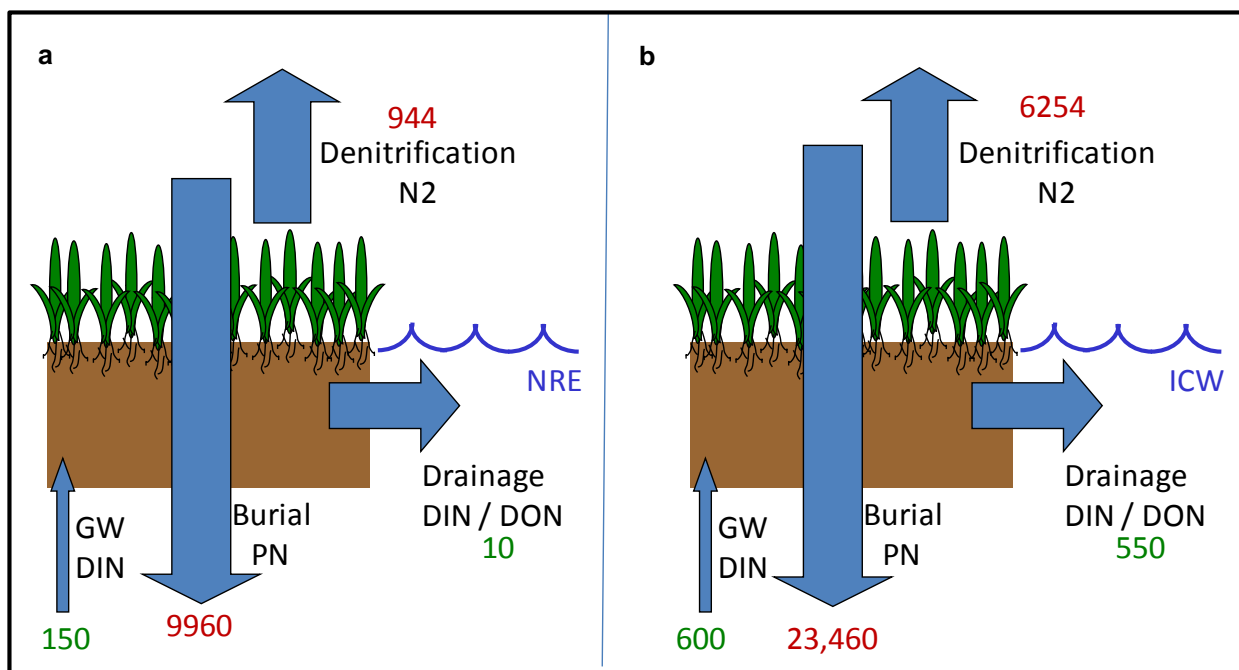


Figure 9-27. Nitrogen source/sink summary with respect to adjacent surface waters.

(a) NRE marshes, and (b) ICW marshes. All fluxes in kg N y⁻¹.

Denitrification comprises 10–20% of the source strength of the N removal in the marshes. Denitrification is important although it is not the largest flux. However, denitrification represents the only pathway whereby N is truly lost from the system because “buried” N remains available for remobilization during periods of erosion. In total, the rate at which marshes are either burying or denitrifying N within the NRE is on the order of 10% of the DIN flux supplied by the New River mainstem. If one includes the contribution from the ICW marshes, the N removal is on the scale of one quarter of the watershed DIN load. The extent to which the incoming DIN is converted to particulate organic nitrogen (PON) within the estuary and subsequently trapped is currently unresolved. In other words the sources of sediment, N, and carbon to marsh accretion/burial is not presently known. However provided the marshes of MCBCL keep pace with sea level rise, the net sink nature of the marshes with respect to N appears robust. There is greater than a factor of twenty between marsh burial + denitrification and export of N from marsh to open water. Granted there is the potential for a diffusive N flux from the marsh surface during flood tide but that would have to be easily measurable as a large change in N concentration in ebbing tides. We measured no such changes in concentration during tidal flux studies, and in contrast detected very little change in N concentration between flood and ebb tides. So such an unaccounted for diffusive flux large enough to tip the balance from sink to source seems highly unlikely. Changing geomorphology remains one additional consideration for changing the source strength of the marsh. Drainage (source) scales with marsh edge, and burial and denitrification scale with marsh area. Any substantial fragmentation of the marsh would result in increasing the edge:area ratio, presumably impacting the source:sink ratio. However this ratio would have to increase by more than a factor of twenty to substantially affect the sink dominance of the marshes. Currently the N removal efficiency of the marshes is large. Provided they keep pace with sea level, this function is likely to remain intact. A clearer picture

of sediment source supplying accretion, would yield a better understanding of how much N (or carbon) that is buried is external to the NRE and MCBCL versus that recycled internally within the system.

Summary Points

- Intertidal marshes of MCBCL are overwhelmingly sinks for N.
- The N sink strength is dominated by sediment N burial during accretion (80–90%), and denitrification (10–20%).
- N sinks within the marshes would have to decrease on the order of 20-fold before the marshes switch from a net sink to a net source of N.

Literature Cited

- Anderson, I.C., C.R. Tobias, B.B. Neikirk, and R.L. Wetzel. 1997. Development of a process-based nitrogen mass balance model for a Virginia (USA) *Spartina alterniflora* salt marsh: Implications for net DIN flux. *Marine Ecology-Progress Series* 159:13–27.
- Bokuniewicz, H.J. 1992. Analytical descriptions of subaqueous groundwater seepage. *Estuaries* 15:458–464.
- Bosen, J.F. 1960. A formula for approximation of saturation vapor pressure over water. *Monthly Weather Review* 88:275–276.
- Bradley, P.M., and J.T. Morris. 1991. Relative importance of ion exclusions, secretion, and accumulation in *Spartina alterniflora* Loisel. *Journal of Experimental Botany* 42:1525–1532.
- Childers, D.L. 1994. Fifteen years of marsh flumes: a review of marsh-water column interactions in Southeastern USA estuaries. Pp. 277–293 in *Global Wetlands: Old World and New*. Edited by M.J. Mitsch. Elsevier Science: New York.
- Cloern, J.E. 2001. Our evolving conceptual model of the coastal eutrophication problem. *Marine Ecology-Progress Series* 210:223–253.
- Correll, D.L. 1981. Nutrient mass balances for the watershed, headwaters inter-tidal zone, and basin of the Rhode River Estuary. *Limnology and Oceanography* 26:1142–1149.
- Dalsgaard, T., and B. Thamdrup. 2002. Factors controlling anaerobic ammonium oxidation with nitrite in marine sediments. *Applied and Environmental Microbiology* 68:3802–3808.
- Drake, D. C., B. J. Peterson, L. A. Deegan, L. A. Harris, E. E. Miller, and R. S. Warren. 2008. Plant N dynamics in fertilized and natural New England salt marshes: a paired ¹⁵N tracer study. *Marine Ecology Progress Series* 354:35–46.
- Eriksson, P.G., J.M. Svensson, and G.M. Carrer. 2003. Temporal changes and spatial variation of soil oxygen consumption, nitrification and denitrification rates in a tidal salt marsh of the Lagoon of Venice, Italy. *Estuarine, Coastal, and Shelf Science* 58:861–871.
- Fennel, K., D. Brady, D. DiToro, W. Fulweiler, W.S. Gardner, A. Giblin, M.J. McCarthy, A. Rao, S. Seitzinger, M. Thouvenot-Korppoo, and C. Tobias. 2008. Modeling denitrification in aquatic sediments. *Biogeochemistry* 93:159–178.
- Groffman, P.M., M.A. Altabet, J.K. Böhlke, K. Butterbach-Bahl, M.B. David, M.K. Firestone, A.E. Giblin, T.M. Kana, L.P. Nielsen, and M.A. Voytek. 2006. Methods for measuring denitrification: Diverse approaches to a difficult problem. *Ecological Applications* 16(6):2091–2122.

- Hamersley, M.R., and B.L. Howes. 2005. Coupled nitrification-denitrification measured in situ in a *Spartina alterniflora* marsh with a (NH_4^+) -N-15 tracer. *Marine Ecology-Progress Series* 299:123–135.
- Hamon, W.R. 1961. Estimating potential evapotranspiration. *Proceedings of the American Society of Civil Engineering, Journal of the Hydraulic Division* 87(HY3):107–120.
- Harvey, J.W., and W.K. Nuttle. 1995. Fluxes of water and solute in a coastal wetland sediment 2: Effect of macropores on solute exchange with surface water. *Journal of Hydrology* 164:109–125.
- Harvey, J.W., and W.E. Odum. 1990. The influence of tidal marshes on upland groundwater discharge to estuaries. *Biogeochemistry* 10:217–236.
- Harvey, J.W., P.F. Germann, and W.E. Odum. 1987. Geomorphological control of subsurface hydrology in the creek-bank zone of tidal marshes. *Estuarine Coastal and Shelf Science* 25:677–691.
- Hvorslev, M.J. 1951. Time lag and soil permeability in groundwater observations. Bulletin number 36. U.S. Army Corps of Engineers. Waterways Experiment Station, Vicksburg, MS.
- Kaplan, W., I. Valiela, and J.M. Teal. 1979. Denitrification in a salt marsh ecosystem. *Limnology and Oceanography* 24(4):726–734.
- Koop-Jakobsen, K., and A. Giblin. 2009. Anammox in tidal marsh sediments: The role of salinity, nitrogen loading, and marsh vegetation. *Estuaries and Coasts* 32:238–245.
- Mallin, M.A., M.R. McIver, H.A. Wells, D.C. Parsons, and V.L. Johnson. 2005. Reversal of eutrophication following sewage treatment upgrades in the New River Estuary, North Carolina. *Estuaries* 28:750–760.
- Morris, J.T. 1995. The mass balance of salt and water in intertidal sediments: Results from North Inlet, South Carolina. *Estuaries* 18(4):556–567.
- Nielsen, L.P. 1992. Denitrification in sediment determined from nitrogen isotope pairing. *FEMS Microbiology Letters* 86(4):357–362.
- Prathapar, S.A., and R.D. Sides. 1993. A practical guide for estimating recharge from water table hydrographs. Technical Memorandum 93/15. CSIRO, Institute of Natural Resources and Environment, Division of Water Resources. Available at <http://www.clw.csiro.au/publications/divisionofwaterresources/techmemos/wr-tm-93-15.pdf>.

- Reilly, T.E., and A. S. Goodman. 1985. Quantitative analysis of saltwater–freshwater relationships in groundwater systems—a historical perspective. *Journal of Hydrology* 80: 125–160.
- Seitzinger, S.P. 1994. Linkages between organic matter mineralization and denitrification in 8 riparian wetlands. *Biogeochemistry* 25(1):19–39.
- Seitzinger, S., J.A. Harrison, J.K. Bohlke, A.F. Bouwman, R. Lowrance, B. Peterson, C. Tobias, and G. Van Drecht. 2006. Denitrification across landscapes and waterscapes: A synthesis. *Ecological Applications* 16:2064–2090.
- Steingruber, S.M., J. Friedrich, R. Gatcher, and B. Wehrli. 2001. Measurement of denitrification in sediments with the ^{15}N isotope pairing technique. *Applied and Environmental Microbiology* 67:3771–3778.
- Thamdrup, B., and T. Dalsgaard. 2002. Production of N_2 through anaerobic ammonium oxidation coupled to nitrate reduction in marine sediments. *Applied and Environmental Microbiology* 68, 1312–1318.
- Tobias, C.R., and S.C. Neubauer. 2009. Salt marsh biogeochemistry—an overview. Pp. 535–562 in *Coastal Wetlands: An Integrated Ecosystem Approach*. Edited by G. Perillo, E. Wolanski, D. Cahoon, and M. Brinson. Elsevier.
- Tobias, C.R., I.C. Anderson, E.A. Canuel, and S.A. Macko. 2001a. Nitrogen cycling through a fringing marsh-aquifer ecotone. *Marine Ecology-Progress Series* 210:25–39.
- Tobias, C.R., J.W. Harvey, and I.C. Anderson. 2001b. Quantifying groundwater discharge through fringing wetlands to estuaries: Seasonal variability, methods comparison, and implications for wetland-estuary exchange. *Limnology and Oceanography* 46:604–615.
- Tobias, C.R., Macko, S.A., Anderson, I.C., Canuel, E.A., and J.W. Harvey. 2001c. Tracking the fate of a high concentration groundwater nitrate plume through a fringing marsh: A combined groundwater tracer and in situ isotope enrichment study. *Limnology and Oceanography* 46:1977–1989.
- Valiela, I., J. Costa, K. Foreman, J.M. Teal, B. Howes, and D. Aubrey. 1990. Transport of groundwater-borne nutrients from watersheds and their effects on coastal waters. *Biogeochemistry* 10:177–197.
- Valiela, I., and J.M. Teal. 1979. Nitrogen budget of a salt-marsh ecosystem. *Nature* 280:652–656.

[This page intentionally left blank.]

Appendix 9-A

List of Scientific Publications

List of Scientific Publications

Papers in Preparation

Lettrich, M., and C.R. Tobias. In preparation. Tidal forcing of hydraulic exchanges in estuarine marshes. Journal to be determined.

Planned Papers

Tobias, C.R., and R. Young. Planned for 2012. Groundwater supplies freshwater but little dissolved nitrogen to New River, NC, tidal marshes. Journal to be determined.

Tobias, C.R., and M. Lettrich. Planned for 2012. Marsh denitrification measured by IPT and $^{15}\text{NH}_4$ tracer approaches. Journal to be determined.

Appendix 9-B

List of Students

- Kerri Allen, B.S., University of North Carolina at Wilmington, Wilmington, NC, May 2010.
- Matthew Lettrich, M.S., University of North Carolina at Wilmington, Wilmington, NC, January 2011.
- Yvonne Marsan, M.S., University of North Carolina at Wilmington, Wilmington, NC, December 2012.
- Ryan Young, M.S., University of North Carolina at Wilmington, Wilmington, NC, December 2012.

[This page intentionally left blank.]

Chapter 10

Short-Term Barrier Evolution: Overwash at Onslow Beach Through Assessment of Training Activities and Model Predictions

SERDP Project Number: RC-1413

Coastal Barrier Module

Research Project CB-1

Lead Researcher:

Jesse E. McNinch
U.S. Army Corps of Engineers
Engineer Research and Development Center
Field Research Facility
Duck, NC
E-mail: Jesse.McNinch@usace.army.mil

Supporting Researchers:

Heidi M. Wadman
Katherine L. Brodie
Amy C. Foxgrover

May 10, 2013

Final

This report was prepared under contract to the U.S. Department of Defense (DoD) Strategic Environmental Research and Development Program (SERDP). The publication of this report does not indicate endorsement by DoD, nor should the contents be construed as reflecting the official policy or position of DoD. References herein to any specific commercial product, process, or service by trade name, trademark, manufacturer, or otherwise, do not necessarily constitute or imply its endorsement, recommendation, or favoring by DoD.

Table of Contents

List of Acronyms	10-v
Abstract.....	10-1
Objectives	10-1
Hypotheses.....	10-2
Background.....	10-2
Overwash	10-2
Predicting wave runup and dune overwash	10-3
Study area.....	10-4
Methods and Methods.....	10-5
Mapping overwash deposits.....	10-5
Nearshore bathymetry	10-7
Beach and dune topography: Coastal Lidar and Radar Imaging System (CLARIS).....	10-8
Modeling nearshore waves	10-9
Results and Discussion	10-11
Overwash	10-11
Predicting Overwash.....	10-12
Conclusions and Implications.....	10-15
Literature Cited	10-16
Appendix 10-A: Supporting Data	10-A-1
Appendix 10-B: List of Scientific Publications	10-B-1
Appendix 10-C: List of Students	10-C-1

List of Figures

10-1.	Overwash and washover.....	10-2
10-2.	Runup overwash.	10-3
10-3.	Location map.	10-5
10-4.	Mapping spatial extent of washover deposits.....	10-7
10-5.	Nearshore bathymetry.	10-8
10-6.	CLARIS measures beach and dune topography and surf zone.	10-8
10-7.	Beach and dune topography.	10-9
10-8.	Topographic and bathymetric model grid.	10-10
10-9.	Spatial extent of washover deposits.	10-12
10-10.	Modeled water level and overwash prediction.....	10-13
10-11.	Washover deposit from Hurricane Irene.	10-14

List of Acronyms

ADCIRC	Advanced Circulation (model)
CLARIS	Coastal Lidar and Radar Imaging System
Cm	centimeter
d _c	primary dune
DoD	U.S. Department of Defense
FRF	Field Research Facility
GHz	gigahertz
GIS	geographic information systems
HWL	high water line
ICW	Intracoastal Waterway
kHz	kilohertz
km	kilometer
km/hr	kilometer per hour
km ²	square kilometer
kW	kilowatt
LIDAR	Light Detection and Ranging
m	meter
m/y	meters per year
m ²	square meter
MCBCL	Marine Corps Base Camp Lejeune
MHz	megahertz
NAD83	North American Datum of 1983
NAVD88	North American Vertical Datum of 1988
NOAA	National Oceanic and Atmospheric Administration
POS-LV	Position and Orientation System for Land Vehicles
R	wave-driven runup
ROM	Runup and Overwash Model
RTK-GPS	real-time kinematic global positioning system
S	regional surge water level
SERDP	Strategic Environmental Research and Development Program
STWAVE-FP	steady-state spectral WAVE model full plane
USACE	U.S. Army Corps of Engineers

[This page intentionally left blank.]

Abstract

Research Project CB-1 investigated overwash processes, defined here as ocean breaching of the primary dune, along the southern half of Onslow Beach, NC. Overwash processes and the resulting transport of sand from the beach to the backbarrier environments can dramatically change the topography of barrier islands, create and destroy habitat for birds and sea turtles, and change the geotechnical properties (i.e. vehicle use) of the beach. Amphibious training at Marine Corps Base Camp Lejeune (MCBCL) has been active on the southern half of Onslow Beach since the late 1940s, and sustaining this environment for continued expeditionary training is of high importance. Our objectives were two-fold: (1) to assess whether training activities on Onslow Beach have measurably changed the occurrence of overwash, and (2) to develop an analytical model that can accurately predict the location of overwash during storm events at Onslow Beach. Changes in the spatial extent of washover deposits created by overwash since 1938, prior to MCBCL use, were measured for each decade (1930–2010) from aerial photographs and field mapping. Results suggest a relationship between the amount of overwash and the number of tropical cyclones that impacted the region in a given decade. Neither an increase nor a decrease in washover deposits were discernable as a linear trend, suggesting that MCBCL training activities did not measurably influence overwash processes. Observed boundary conditions required for overwash modeling included high-resolution beach and dune topography, nearshore bathymetry, and surf-zone waves and water level. New observational techniques, namely Coastal Lidar and Radar Imaging System (CLARIS), were developed to measure these conditions and refine model equations. Modeled wave runup, defined as the elevation reached by the upper 2% of wave swash on the beach foreshore, and projected locations of overwash (where runup exceeded the elevation of the primary dune crest) demonstrated strong skill during Hurricane Irene. Our Runup and Overwash Model (ROM) simulations correctly predicted all four overwash locations along Onslow Beach. Model results imply that runup elevations vary along Onslow Beach as a function of beach slope and nearshore bathymetry such that overwash and inundation predictions based solely on regional tides and surge would likely have poor skill except for the most extreme storm events. Furthermore, outcropping hardbottom in the surf zone in the central portion of the region (near the old Riseley Pier) will likely continue to induce higher elevations of runup. Best management practices designed to minimize lowering of the primary dune crest and anticipating likely inundation of sea turtle nest in this region should be considered.

Keywords: Onslow Beach, overwash, washover, barrier island, Light Detection and Ranging (LIDAR), X-band radar, runup, Hurricane Irene, steady-state spectral WAVE model full plane (STWAVE-FP), real-time kinematic global positioning system (RTK-GPS), MCBCL

Objectives

1. Assess whether amphibious training activities have influenced overwash processes on Onslow Beach.
2. Develop a numerical model that predicts the location of overwash during storms at Onslow Beach. Model skill was assessed during a severe storm event (i.e., Hurricane Irene) in August 2011.

Hypotheses

1. The number and spatial area of washover deposits did not change significantly prior to or after training operations began at Marine Corps Base Camp Lejeune (MCBCL).
2. The location of overwash can be predicted using high-resolution bathymetry and wave runup simulations at Onslow Beach.

Background

Overwash

Barrier islands are dynamic features that migrate in response to both natural forcings (e.g., storms, sea level rise) and anthropogenic activities through a combination of mechanisms including aeolian transport and overwash. Overwash occurs when either wave runup or storm surge exceeds dune height, generating a unidirectional flow of sediment-laden water from the nearshore over the beach crest and towards the back of the island (e.g., Davis, 1994; Donnelly et al., 2006; Leatherman, 1979; Schwartz, 1975), resulting in permanent changes to island morphology (**Figure 10-1**). This transport of sand onto and/or behind the barrier surface supports backbarrier marsh habitats while also providing a mechanism for barrier island stability in regions with rising sea level (e.g., Godfrey, 1970; Kochel and Dolan, 1986 and 1989; Leatherman, 1983). Overwash processes may also result in a thin veneer of sand on the beach which could impact training exercises with respect to geotechnical (e.g. beach stability, etc.) requirements for military vehicles, as well as potentially influencing suitable habitat for nesting sea turtles. The likelihood of overwash penetration and potential island breaching is significantly higher where dune fields are lower than the relevant storm tide elevation (or are absent altogether) compared to regions of the beach characterized by higher and/or broader dune fields (Houser et al., 2007 and 2008; Morton, 2002; Sallenger, 2000; Thieler and Young, 1991).

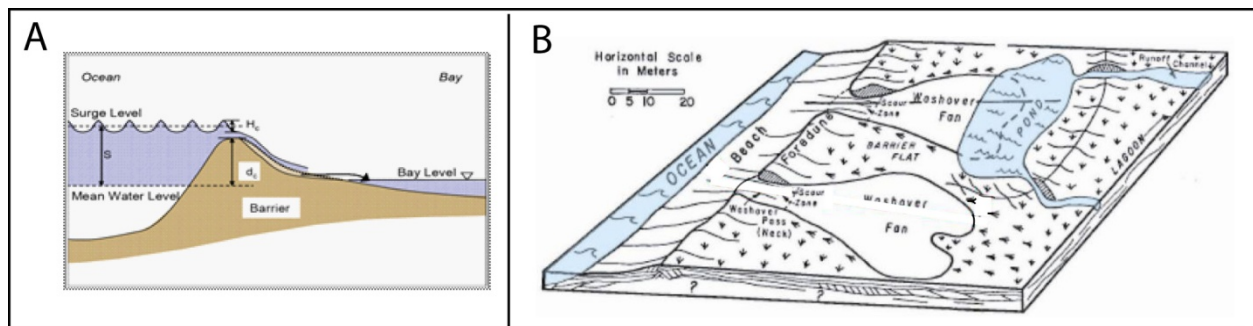


Figure 10-1. Overwash and washover.

Panel A: The process of dune overtopping from the sea causing overwash; Panel B: Overwash leaving a fan-shaped deposit of beach sediment, known as washover (after Donnell et al., 2004; and Schwartz, 1975).

Recent work (Donnelly et al., 2006; Morton et al., 2000; Sallenger, 2000) has refined the definition of overwash into the following two regimes: (1) runup overwash, and (2) inundation overwash. Runup overwash occurs under conditions of excess wave runup, usually associated with lower magnitude storm events and/or barrier islands with high, well-developed dune fields

(**Figure 10-2**). During runup overshoot, water and sediment are funneled through existing lows of the dune crest and spread laterally on the backbarrier. In contrast, inundation overshoot occurs when the mean water level exceeds the dune crest, usually during extreme storms and/or on low-lying barrier islands with poorly developed dune fields (**Figure 10-1**; Panel B). In addition, although the terms “overshoot and washover” are occasionally used interchangeably, “overshoot” is the mass of water or the physical process by which water and sediment are carried over a dune crest, and “washover” refers to the actual geologic deposit of sediment created by the action of overshoot (Donnelly et al., 2006).

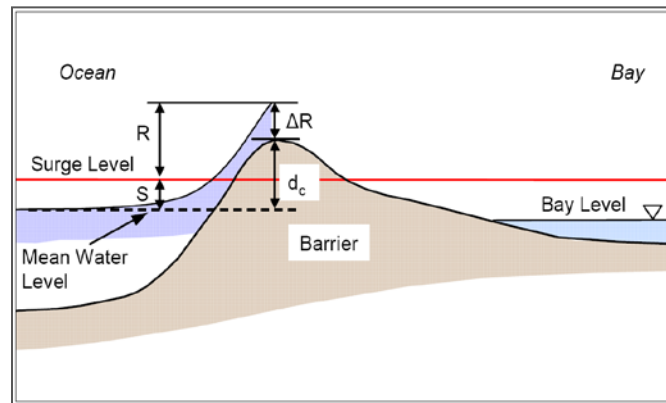


Figure 10-2. Runup overshoot.

Breaching the crest of the primary dune (d_c) by wave-driven runup (R) well above the regional surge water level (S) (after Donnelly et al., 2004).

Washover can extend landward from the shoreline up to hundreds of meters and ranges in thickness from a few tens of centimeters (Davis, 1994) up to a meter (McCubbin, 1982). Washover is distinguished from other barrier deposits by specific sedimentological characteristics such as grain size and mineralogy (Buynevich et al., 2004; Davis, 1994; Donnelly et al., 2004; Heron et al., 1984; Hippensteel and Martin, 1999). Multiple overshoot episodes may result in a composite fan that is meters thick (Davis, 1994) and, in undeveloped settings, washover sequences are likely superimposed upon vegetated backbarrier surfaces, dunes, or previously deposited washover deposits.

Predicting wave runup and dune overshoot

Accurate model predictions of overshoot during storms necessitate a correct parameterization of wave runup, a principal driver of elevated water levels on beaches. Observations at the Field Research Facility (FRF) in Duck, NC, for example, revealed that wave runup accounted for 78% of the elevated water level whereas astronomical tides and surge were responsible for 9% and 13%, respectively, during Hurricane Irene. Wave runup certainly does not always dwarf storm surge or tidal forcing, but it can be an important driver in settings such as Onslow Beach and cannot be ignored when predicting overshoot.

Measuring wave runup, however, is challenging because the interface between water and beach is spatially dynamic and extremely energetic. Previous studies aimed at measuring wave runup, defined here as the time-varying motion of wave swash on the beach foreshore, have been

restricted to analyzing water-elevation time series of the shoreward-most swash excursion using video imaging or near-bed resistance wires (e.g., Aagard and Holm, 1989; Holland et al., 1995; Holman and Guza, 1984), or measurement of water elevation at a particular location using pressure sensors (e.g., Guza and Thornton, 1982). These data are then compared with wave forcing parameters in deeper water, as well as with beach topography observed at finite intervals throughout the time series (e.g., Holland and Puleo, 2001). These approaches have led to numerous parameterizations and empirical equations for wave runup (e.g., Stockdon et al., 2006), but have so far been ineffective at providing data that are spatially and temporally dense enough to accurately understand the complex physical processes that govern wave runup during both storm and quiescent times. As a result, model skill (a measure of a physical model's ability to accurately reproduce observations) is often poor with respect to beach response and overwash during storms.

Study area

Onslow Beach, located on the North Carolina coast midway between Cape Lookout to the north and Cape Fear to the south, is a 12-km long barrier island with a nearshore region (shoreline to approximately 10-m depth) that spans 20 km² (**Figure 10-3**). The southern portion of the island is characterized by a low-gradient beach that varies greatly in width and contains numerous washover fans (**Figure 10-3A**). With increasing distance to the north, beach width stabilizes and is characterized by a high primary dune field with little to no evidence of overwash (**Figure 10-3B**). Onslow Beach is bordered on the northeast by Browns Inlet, on the southwest by the New River Inlet, and on the landward side by the linear channel of the Intracoastal Waterway (ICW), which was dredged in 1932 through a marshy habitat previously characterized by numerous, sinuous channels (Cleary and Riggs, 1999). The ICW currently averages 130 m in width and is maintained to a depth of approximately 4 m by the U.S. Army Corps of Engineers (USACE; available at <http://www.saw.usace.army.mil/nav/aiww.htm>). The island and surrounding lands were purchased by the U.S. Department of the Navy in 1941, and are part of Marine Corps Base Camp Lejeune (MCBCL), serving as the largest U.S. Marine Corps amphibious training facility in the world.

Onslow Beach is microtidal, with a mean tidal range of approximately 1 m (Cleary and Riggs, 1999). Both a 20-year hindcast model generated by the USACE (available at http://www.frf.usace.army.mil/cgi-bin/wis/atl/atl_main.html) and hourly wave data from an offshore National Oceanic and Atmospheric Administration (NOAA) buoy indicate the region experiences mean significant wave heights of approximately 1 m, with an average wave period of 4.6 seconds. Dominant wave direction is from the southeast in the summer and northeast during the winter, but the sheltering effects of northern Cape Lookout shadow the beach from much of the winter wave energy, thus minimizing the effect of winter storms (nor'easters) on the shoreline and beach morphology (Cleary and Riggs, 1999). Tropical cyclones (hurricanes) are episodic in North Carolina, with a predicted recurrence interval of about once in a 4-year period (Barnes, 2001). Although during-storm tropical storm wave heights have not historically been measured on Onslow Beach, predicted tropical storm wave heights for adjacent Topsail Island range from 3.3 m for a 50-year storm to 3.8 m for a 100-year storm (Cleary and Riggs, 1999) and provide an accurate representation of general tropical conditions for the overall region.

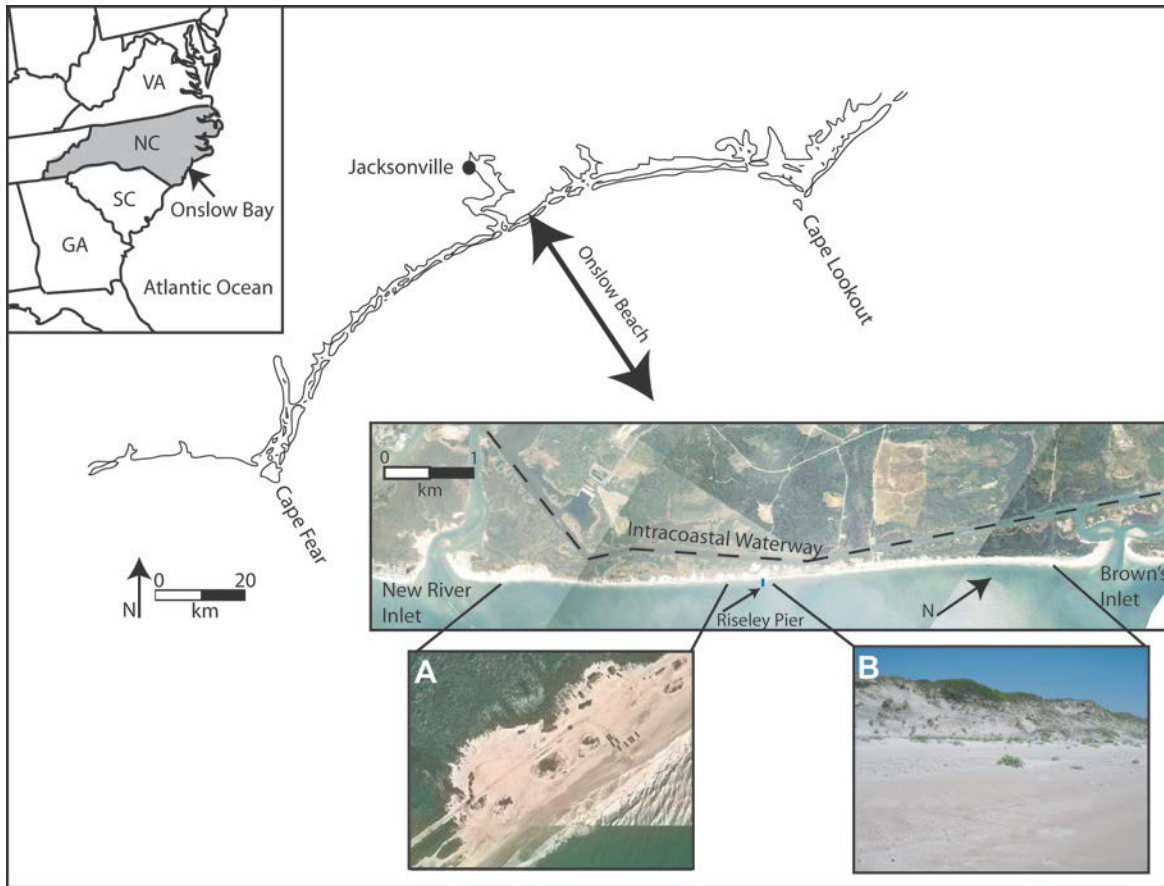


Figure 10-3. Location map.

Onslow Beach, NC, is a microtidal barrier island that experiences frequent overwash events in the southern half of the island. A = Numerous washover fans on the south portion of the island (aerial view), and B = high primary dune field on the northern end of the island with no evidence of overwash.

Methods and Methods

Mapping overwash deposits

Changes in overwash processes along the southern half of Onslow Beach, a portion of which includes the amphibious training zone, were evaluated by mapping the spatial extent of washover deposits through time. A series of aerial photographs and satellite images depicting six time periods between 1938 and 2008 were used to track how the shoreline and vegetation line, which marked the landward extent of recent overwash events, has changed along Onslow Beach before and after amphibious exercises commenced (Foxgrover, 2009). An IKONOS satellite image collected in September 2006 was used as the basis by which all other imagery was georeferenced to a common projection and horizontal datum (UTM Zone 18, North American Datum of 1983 [NAD83]). The 2006 imagery has a resolution error of 80 cm and a reported horizontal circular error of 2.2 m at the 90% confidence interval. We used a National Map Accuracy Standards application factor of 2.146, which equates to a horizontal positioning root-mean squared error (RMSE) of 1 m (FGDC, 1998).

Additional aerial imagery was georeferenced to the 2006 image using a minimum of four secondary, or supplemental, control points (Thieler and Danforth, 1994). A first-degree polynomial transformation was performed on each image to estimate the best fit between all control points. Unfortunately, in the absence of primary control points providing accurate coordinate and elevation data, and without camera calibration reports, it was not possible to assess errors introduced through the distortion of the camera lens and/or film or any tilt in the aircraft at the time of exposure. The majority of images used, however, did have adjacent overlap of approximately 30% and, whenever possible, data from the center of the photo were used to limit the effects of radial or tilt distortion (Foxgrover, 2009).

A geographic information systems (GIS)–based tool (i.e., Beach Tools), developed by USACE for the purpose of delineating features on aerial imagery, was used to automate digitization of features. Software details and a description are available at the following link: <http://oai.dtic.mil/oai/oai?verb=getRecord&metadataPrefix=html&identifier=ADA490237>. The wet/dry line was used as a proxy for the high water line (HWL). Potential errors associated with shoreline change assessment based upon aerial imagery include the following: (1) seasonal and tidal fluctuation of the wet/dry line, (2) errors in delineating features, and (3) errors in the original source data. The excursion of the HWL ranges from 1 m to 2 m over a tidal cycle on medium-sized, sandy North Carolina and Virginia beaches (Dolan et al., 1980; Moore, 2000). Larger variations on the order of ± 10 m are estimated for seasonal fluctuations of HWL (Smith and Zarillo, 1990), but offset of the wet/dry line due to seasonal variability was minimized by selecting imagery collected between January and May (with the exception of the November 1989 digital orthophoto quadrangles), and that did not immediately proceed or follow large storm events (Foxgrover, 2009). User error associated with pixel identification and digitization of features from aerial imagery was assessed by performing a repetitive measurement of the wet/dry line three times over a 600-m long stretch of beach, as well as comparisons to field mapping of recent washovers using a real-time kinematic global positioning system (RTK-GPS; **Figure 10-4**). A different set of pixels was highlighted in each repetition to perform the classification analyses, and the difference in positioning between the three lines suggests a potential digitization error of ± 5.6 m.

Due to the fragmentation of the dunes in all post-1938 imagery, the vegetation line cannot be accurately represented by a single line in all of the images. Rather, the vegetation line was augmented by a number of “vegetation islands” that occur landward of a shore-parallel beach access road. Because the aim of this research is to evaluate naturally forced vegetation change, the vegetation line that coincides with the landward side of the road was not traced. The pockets of dune vegetation seaward of the road were considered a better representation of a natural vegetation line and, despite occasionally being difficult to distinguish due to their limited size, vegetation clusters with an area of 20 m² or more were encircled using BeachTools.

The position of both the shoreline and the vegetation line was extracted at a 50-m alongshore interval from each aerial photograph using the Digital Shoreline Analysis System (Thieler et al., 2005), yielding a time-series of shoreline and vegetation line positions. The average and standard deviation of the shoreline and vegetation line positions at each transect were then derived using MATLAB.



Figure 10-4. Mapping spatial extent of washover deposits.

The spatial area of recent washover deposits was digitized from aerial photographs spanning six decades using vegetation and open sandy areas as a delineation of washover deposits. Digitizing error was assessed through RTK-GPS field mapping of the digitized features.

Nearshore bathymetry

Accurate nearshore and surf zone bathymetry is a critical boundary condition for correctly modeling wave dissipation, runup and, ultimately, overwash. These data are often very sparse and questionable in quality when derived from traditional sources such as NOAA bathymetric charts because depths are infrequently measured in the shallow nearshore. Accordingly, high-resolution, interferometric swath bathymetry (Sea SwathPlus, 234 kHz) was collected over approximately 18 km² of the Onslow Beach nearshore (**Figure 10-5**). Line spacing ranged from 25–75 m, depending upon water depth, and the position of each data point was related to NAD83 using RTK-GPS. Vessel heave, pitch, and roll were corrected in real-time using an IXSEA Octans motion sensor. Seafloor depths were corrected for tides by using the real-time, motion-corrected vertical movement of the vessel throughout the survey as recorded with Hypack Oceanographics software. Similar studies using identical methodology in other nearshore regions indicate an average horizontal and vertical elevation error of ± 10 cm and ± 12 cm, respectively. Data were initially gridded using line averaging at a 1m resolution and subsequently despiked, filtered, and smoothed. Cleaned data were re-gridded at 5-m resolution in IVS Fledermaus Professional (version 7.0d), using a weighted moving average interpolation algorithm at a spacing of 5 m and a search diameter of 7 m.

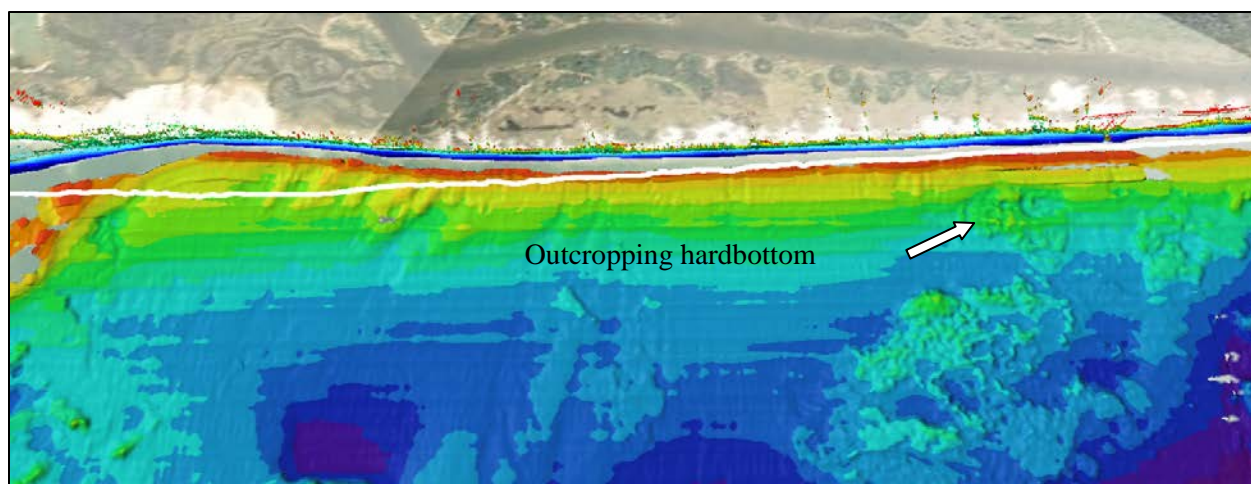


Figure 10-5. Nearshore bathymetry.

Multibeam (interferometric) bathymetry of the nearshore, southern half of Onslow Beach, shown with 5-m grid spacing. Note presence of outcropping hardbottom in the surf zone in the central region of the nearshore.

Beach and dune topography: Coastal Lidar and Radar Imaging System (CLARIS)

High-resolution topography of the upper beach, primary dune face, and dune crest are critical boundary conditions for modeling wave runup and overwash. Traditional topographic data sources, such as U.S. Geological Survey topographic maps and airborne Light Detection and Ranging (LIDAR), are often limited for predicting overwash because the data are typically dated (rarely more frequent than annual), and the resolution of the dune crest and shape of the dune face are reduced by data density and vegetation. The Coastal Lidar and Radar Imaging System (CLARIS) is a fully mobile mapping system that integrates two state of the art remote sensing technologies, a terrestrial laser scanner (Riegl LMS-z390i; vz1000) and X-Band radar (4 kW, X-band 9.4 GHz), with precise motion (Position and Orientation System for Land Vehicles [POS-LV]) and location (RTK-GPS) information (**Figure 10-6**).



Figure 10-6. CLARIS measures beach and dune topography and surf zone.

CLARIS, developed in-house at the FRF (Brodie and McNinch, 2011), is a robust system capable of rapidly (10 km/hr) and quantitatively measuring beach and dune topography (accuracy of 10 cm) with terrestrial LIDAR, and nearshore bathymetry from radar-derived wave velocity measurements (to within 10% of the actual depth). Vehicle motion is removed from both radar and laser data using the POS-LV observations in real-time and post-processed using Applanix PosPAC software for increased accuracy. The heading angle of each radar pulse is recorded using an Applanix POS-LV motion system with a less than 0.05 degree accuracy, and the location of

the center of each radar collection is recorded using RTK-GPS to 10 cm to 15 cm accuracy. The radar range is 1.2 km and at 10 km/hr, every location across the surf zone has at least a 10-minute time series of radar observations. Range resolution is 3 m, a function of analog to digital sampling using a 50-MHz card, and temporal resolution is 1.2 seconds. Radar observations are rectified through a polar transformation from azimuth-range space using heading and position information, to Cartesian coordinates (e.g., North Carolina State Plane Easting and Northing, Horizontal Datum: NAD83). The laser scanner simultaneously scans the topography starboard of the vehicle during transit along the beach. Terrestrial laser scanner survey precision is on the order of 1.3 cm and accuracy is ± 5 –10 cm. Point-cloud density averages 30 to 40 points per m^2 , with higher density in the near range. Mobile, ground-based LIDAR provides complete spatial coverage and high data density, enabling three-dimensional features such as the beach cusps, primary dunes, and the berm (exemplified in **Figure 10-7**) to be robustly mapped without the data aliasing errors common in traditional survey methods (Plant et al., 2002). Once the LIDAR data are edited, they are typically gridded at 0.25- to 0.5-m spacing, and pertinent elevations such as dune crest are contoured.

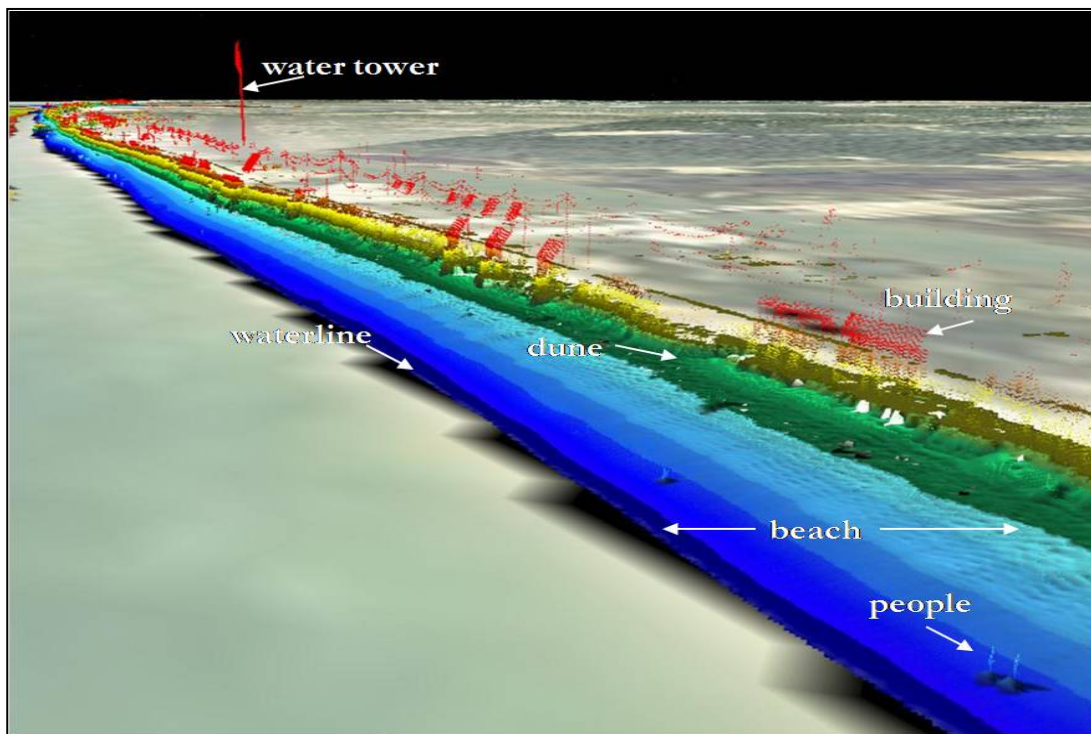


Figure 10-7. Beach and dune topography.

CLARIS-measured beach and dune topography at Onslow Beach showing the high resolution of geomorphic features that are critical to improving model skill (perspective view looking south).

Modeling nearshore waves

CLARIS provides a quasi-instantaneous measure of waves in the surf zone providing a powerful tool for inferring bathymetry and showing the complexity of breaking wave parameters in the shallow surf zone. These data are useful for establishing boundary conditions and assessing the skill of wave model results but a continuous time series of wave conditions near the beach

throughout storm events are needed to force the Runup and Overwash (ROM) model. The STeady-state spectral WAVE model Full Plane (STWAVE-FP) version was used to model wave transformation over nearshore bathymetry during the storm event to assess spatial variations in wave height and direction (and subsequently radiation stress), the dominant hydrodynamic forcing mechanisms in the surf zone. STWAVE-FP solves the steady-state conservation of spectral wave action along wave rays enabling the modeling of wave transformation (refraction, shoaling, and breaking) and wind-wave generation in the nearshore (Smith and Sherlock, 2007; Smith et al., 2001). STWAVE-FP assumes a mild bottom slope with no wave reflection, a spatially homogeneous offshore wave field, steady-state waves and winds (i.e., wave-generation from winds assumes fetch-limited or fully developed conditions), and linear refraction and shoaling. STWAVE-FP is used in this study because it was recently calibrated for an optimal bottom friction coefficient using the cross-shore wave array at the FRF in Duck, NC (Hanson et al., 2009). Though STWAVE-FP attempts to improve wave modeling within the surf zone through the use of a wave-steepness breaking criterion, as opposed to a simple depth-dependence breaking criterion, the non-linear nature of breaking waves in the surf zone makes them difficult to model using linear wave theory, and thus wave heights predicted by STWAVE-FP within the surf zone are neglected in this study.

Nearshore bathymetric survey data were used to generate an inner nested bathymetric grid (15-m \times 15-m resolution) from the shoreline to 10-m depths, and a courser (25 m \times 25 m) grid was used to characterize the region from 10- to 17-m depth. The model was forced hourly at the offshore boundary with spectral wave and wind data from a suite of NOAA nearshore wave buoys and run for 10 directional sweeps to ensure maximum accuracy. Water level data may be input from either local tide stations or water level surge models such as the Advanced Circulation (ADCIRC) model (Luettich et al., 1992). Bottom friction is also held spatially constant, with Manning's coefficient set to 0.073, as calibrated by Hanson et al. (2009). Given the heterogeneity in sediment found at Onslow Beach (e.g., hardbottom, peat, gravel), the assumption of spatially constant bottom friction may be a source of error in the model results; however, defining spatially variable bottom friction coefficients given gross sediment parameters is beyond the scope of this study.

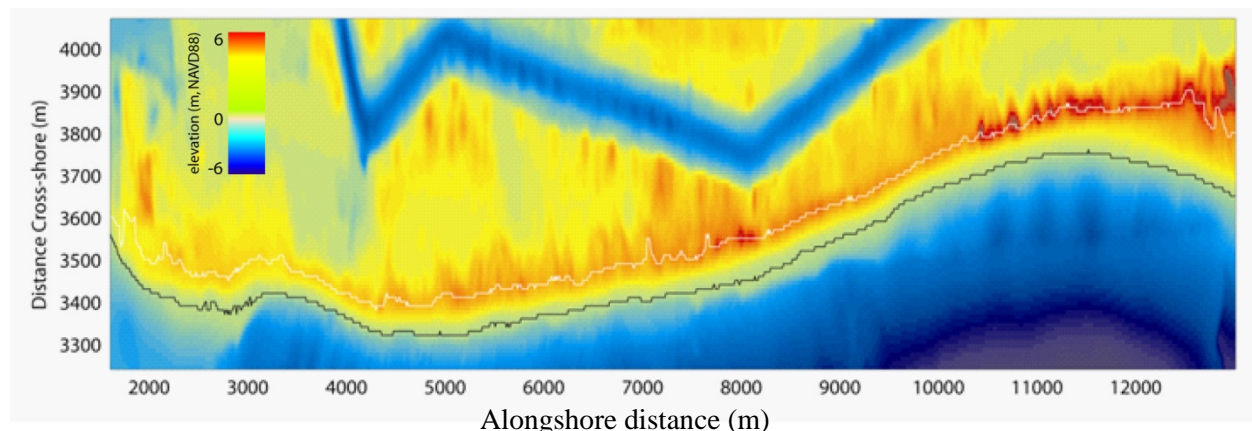


Figure 10-8. Topographic and bathymetric model grid.

A portion of the model grid showing nearshore bathymetry and island topography with the shoreline (0 m, North American Vertical Datum of 1988 [NAVD88]), black line, and the crest of the primary dune defined by the white line.

Significant wave height and peak period is extracted along the 5- and 10-m contours (approximate edge of the surf zone) hourly, every 10 m alongshore and input to the Stockdon et al. (2006) overwash equation (Equation 10-1).

$$R_2 = 1.1 \left\{ 0.35 \beta_f (H_0 L_0)^{\frac{1}{2}} + \frac{[H_0 L_0 (0.563 \beta_f^2 + 0.004)]^{\frac{1}{2}}}{2} \right\} \quad \text{Eq. 10-1}$$

Stockdon et al. (2006) defines the 2% exceedence elevation of runup (R_2) and foreshore beach slope (β_f), local wave height (e.g., 10-m water depth) reverse-shoaled to its deep-water equivalent (H_0), and deep-water wavelength (L_0). Peak wave period (T_p) is converted to deep-water wavelength (L_∞) in Eq. 10-1 using the deep water approximation of the linear dispersion equation. Wave parameters are available at every 15 m alongshore throughout the study site and every hour during the modeled events. Beach foreshore slope was extracted from CLARIS LIDAR topographic data by fitting an average linear trend of the topography between the dune toe and the water line every 15 m alongshore. Runup elevations were added to observed and modeled tide and surge water level to determine a total dune cresting potential. If dune crest elevations were exceeded by modeled dune cresting potential (total water level height), overwash is predicted to occur.

Results and Discussion

Overwash

To test the hypothesis that the number and spatial extent of washover deposits did not change significantly prior to and after training operations began at MCBCL, an estimate of washover area per decade was determined starting in 1938. We compared decadal-scale changes in washover area due to tropical storm activity since the mid-1930s. Changes in washover area per decade were quantified using aerial photographs. On each image, both the wet/dry line and the farthest landward vegetation line were digitized, and the distance between the two lines was calculated every 50 m along Onslow Beach. The wet/dry line is a standard estimate of shoreline position in aerial photography and the location of an island's vegetation line reflects the extent of the sandy washover deposit extending from the beach to the backbarrier. A large distance between the shoreline and vegetation lines on any one image indicates a large washover deposit and thus represents significant overwash breaching the barrier and dune during that period of time. The overall extent of washover deposits, based on the average distance between the shoreline and vegetation lines, was averaged from aerial photographs for each of the six decades (1930–2010) and is plotted on the left y-axis on **Figure 10-9** as a proxy for washover extent. From these data, it is evident that the highest extent of washover deposits occurred in 1950, and again in 1990. The lowest extent of washover deposits, as reflected by the smallest average distance between shoreline and vegetation lines, was found in 1980. Overwash processes thus peaked both in 1950 and again in 1990, but a clear linear trend (either increase or decrease) was not evident suggesting that MCBCL amphibious training activities did not have a measurable effect on overwash processes at Onslow Beach.

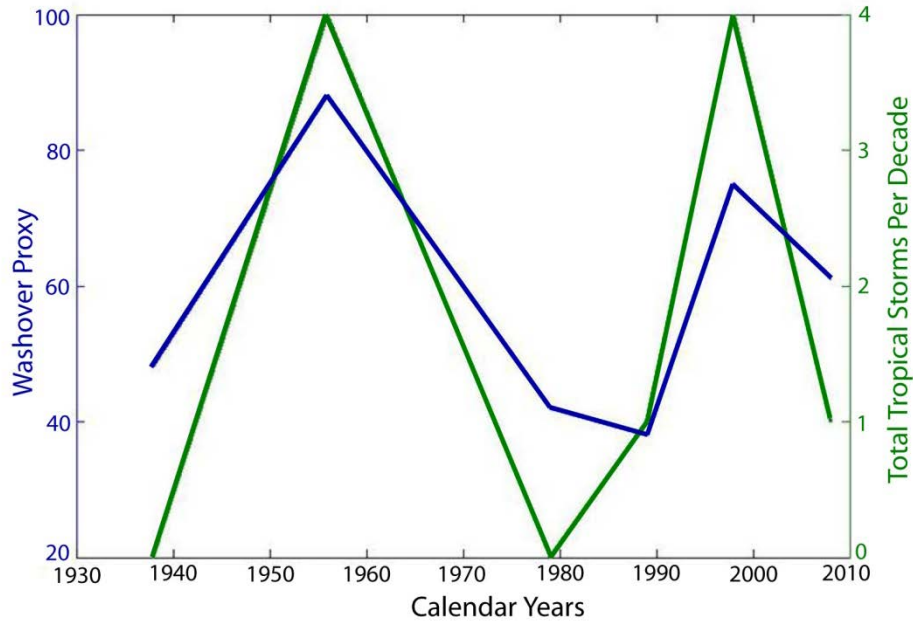


Figure 10-9. Spatial extent of washover deposits.

A proxy for the spatial extent of washover deposits from 1938 to 2010 (blue line; left y-axis) and the number of tropical cyclones per decade (green line; right y-axis).

Overwash is a result of inundation from wave runup or storm surge, or both, exceeding dune height during storms. The orientation of Onslow Beach protects it from the worst of the energy from winter nor'easters due to the partial sheltering provided by Cape Lookout, but not from storm systems approaching from the southeast. Along the North Carolina coast, most southeastern storms are tropical in nature and impact some portion of the coastline on average once every 4 years, with the result that most of the significant, overwash-generating storms impacting Onslow Beach are tropical in origin (Barnes, 2001; Cleary and Riggs, 1999). Tropical cyclone data for the region of Onslow Beach was obtained from NOAA's Atlantic basin hurricane database called HURDAT (available on NOAA's Web site at <http://www.csc.noaa.gov/hurricanes>) and included all hurricanes or tropical storms passing near Onslow Beach and the southern North Carolina Outer Banks. Storms were summed per decade (1930–2010) and plotted on the right y-axis of **Figure 10-9**. The highest numbers of tropical storms impacting the greater Onslow Beach region were found both in 1950 and 1990, mirroring the greatest extent of washover deposits. The lowest number of storms was noted in 1980, comparable to the lowest digitized extent of washover deposits.

Predicting Overwash

Overwash was modeled at Onslow Beach during Hurricane Irene using a combination of observational data (i.e., CLARIS topography, nearshore bathymetry, regional surge, and offshore wave spectra) and modeled nearshore waves (i.e., STWAVE-FP). Model and observational techniques were developed at both Onslow Beach and at the FRF over several years but Hurricane Irene was the only severe storm (with respect to wind and wave energy) to impact the study site during the DCERP1. **Figure 10-10**, top panel, shows primary dune crest elevation (purple) and predicted water level along the ocean beach which includes runup, surge, and

astronomical tides. The bottom two panels of **Figure 10-10** present before and after aerial photographs of the study site and exhibit clear evidence of washover deposits at the predicted locations. Locations where the ROM model predicted water levels to exceed dune crest elevations (highlighted by vertical red bars) and thus overwash to occur were consistent with aerial photographs and visual observations (Rodriguez, personal communication) as exemplified in **Figure 10-11**. The two most substantial washover deposits generated by Hurricane Irene (two located farthest west; highlighted red bars) had not been overwashed, at least since 1938, and thus are not just a reoccurrence of overwash at a previously breached dune (as occurred at the two eastern locations).

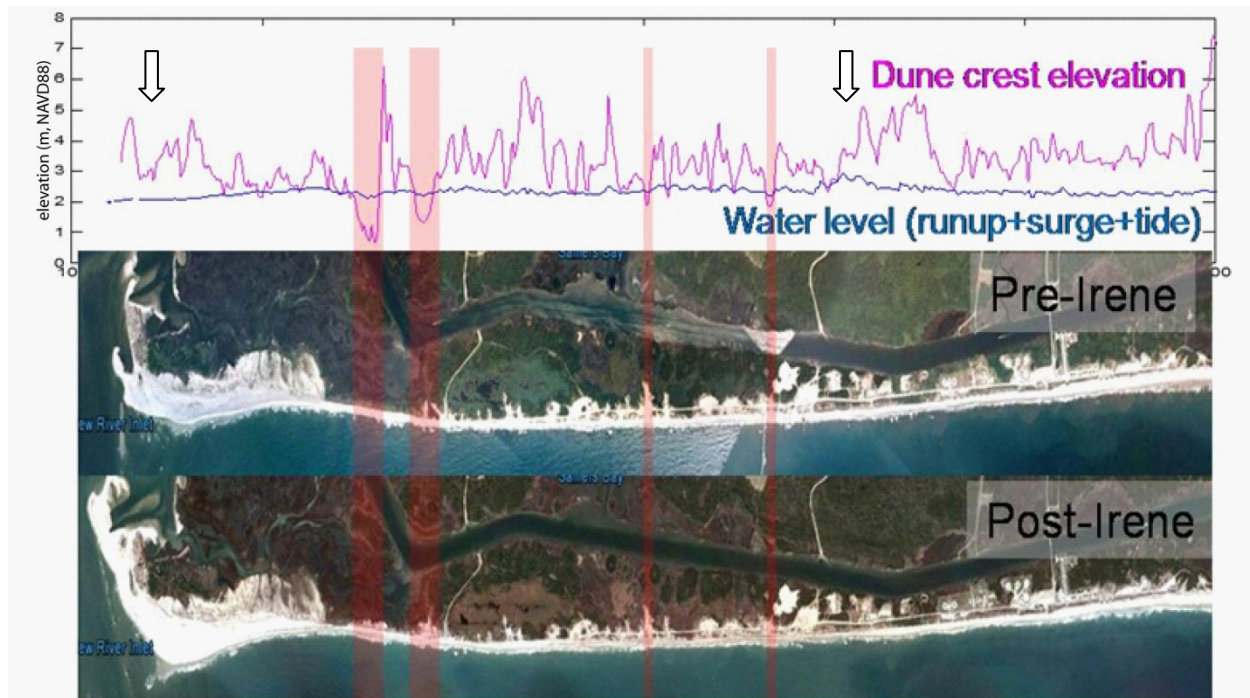


Figure 10-10. Modeled water level and overwash prediction.

Dune crest elevation (purple line; top panel) and predicted water level (runup+surge+tide) along Onslow Beach during Hurricane Irene. Bottom two panels show washover deposits before and after Hurricane Irene.



Figure 10-11. Washover deposit from Hurricane Irene.

A photograph showing the same region (similar camera orientation) before (top panel) and after (bottom panel) Hurricane Irene passage where the overwash model predicted substantial breaching of the dune.

ROM results also indicate the importance of spatial variations in nearshore bathymetry and wave runup. In particular, these varying runup elevations highlight the disadvantages and poor skill of simply flooding a beach with predicted tide and surge, except for the most extreme storms when surge levels completely inundate the primary dune. The differences in water level elevation reached across Onslow Beach during Hurricane Irene varied by almost 1 m, exemplified by the arrows in top panel of **Figure 10-10**, and can only be explained by differences in wave runup. Recent experiments at the FRF (Brodie and McNinch, 2011) reveal the sensitivity of wave runup to the amount of wave dissipation (breaking) across the surf zone which, in turn, is partly controlled by surf zone sand bars and foreshore slope. Simply put, spatial differences in the nearshore bathymetry of Onslow Beach due to sandbars and outcropping hard-bottom (**Figure 10-5**) drives differences in runup and may ultimately dictate the location of overwash. The region marked by the arrow (eastern; farthest to the right in top panel of **Figure 10-10**) shows the highest runup elevations, almost 3 m (North American Vertical Datum of 1988 [NAVD88]),

during Hurricane Irene. The nearshore bathymetry in that region has pronounced outcrops of hardbottom (**Figure 10-5**) elevated above the surrounding sandy seabed that likely leads to greater wave dissipation and steeper beach slopes which, in turn, force higher runup. Fortunately, the crest of the primary dune is relatively high in that region and did not overwash extensively during Hurricane Irene. Over longer time periods, however, this region will likely continue to experience elevated runup during storm events and remain prone to overwash should the primary dune become further degraded by repeated dune scarping during storms or anthropogenic activities.

Conclusions and Implications

- Overwash and its resulting washover deposits provides a means to accumulate sediment on and behind Onslow Beach, and thus is an important mechanism by which island morphology changes in response to changes in storm frequency and sea level rise over seasonal to decadal timescales. Overwash, however, may also reduce sand thickness on the beach, possibly affecting vehicle-related training exercises, and destroy habitat for nesting sea turtles.
- A comparison of washover extent, as obtained from aerial photographs from 1938–2010, suggest that the primary forcing mechanism generating overwash processes on Onslow Beach was tropical storm activity. Despite MCBCL using Onslow Beach as a training area since the late 1940s, no significant increases or decreases in overwash extent were observed post-MCBCL that were not also directly comparable to changes in tropical storm frequency. In short, MCBCL training activities on Onslow Beach have not measurably influenced the number of overwash events.
- Wave runup is an important component of elevated water levels during storm events at Onslow Beach. Maximum runup elevations vary spatially along Onslow Beach depending on the surf zone geology and bathymetry, which influences wave height, wave dissipation, and beach slope. In all but the most severe storm events, when storm surge far exceeds the elevation of the primary dune crest, runup may determine the location of overwash. Overwash predictions during Hurricane Irene demonstrated strong skill, correctly predicting all four overwash locations.
- The more central region of Onslow Beach, where outcropping rock in the surf zone influences wave energy and creates steeper beach slopes, will likely continue to experience increased runup elevations during storm events as compared to surrounding areas. Management strategies that help maintain dune crest elevations and care for sea turtle nest, with respect to minimizing inundation, should be closely followed in this region.

Literature Cited

- Aagaard, T., and J. Holm. 1989. Digitization of wave run-up using video records. *Journal of Coastal Research* 5(3):547–551.
- Barnes, J. 2001. *North Carolina's Hurricane History* (3rd edition). The University of North Carolina Press: Chapel Hill, NC. (319 pages).
- Brodie, K.L., and J.E. McNinch. 2011. Beach change during a nor'easter: Relationships to wave steepness and inner surf zone dissipation. Pp. 1360–1374 in *Proceedings of the Coastal Sediments I*. Edited by J.D. Rosati, P. Wang, and T.M. Roberts.
- Buynevich, I.V., D.M. FitzGerald, and S. Van Heteren. 2004. Sedimentary records of intense storms in Holocene barrier sequences, Maine, USA. Storms and their significance in coastal morpho-sedimentary dynamics, *Marine Geology* 210(1–4):135–148.
- Cleary, W.J., and S.R. Riggs. 1999. Beach Erosion and Hurricane Protection Plan for Onslow Beach, Camp Lejeune: Comprehensive Geologic Characteristics Report. U.S. Marine Corps Base Camp Lejeune.
- Buynevich, I.V., D.M. FitzGerald, and S. Van Heteren. 2004. Sedimentary records of intense storms in Holocene barrier sequences, Maine, USA. Storms and their significance in coastal morpho-sedimentary dynamics. *Marine Geology* 210(1–4):135–148.
- Davis, R.A. 1994. Barrier island systems: A geologic overview. *Geology of Holocene Barrier Island Systems*. Edited by R.A. Davis. Springer-Verlag: Berlin, Germany.
- Dolan, R., B.P. Hayden, P. May, and S. May. 1980. The reliability of shoreline change measurements from aerial photographs. *Shore Beach* 48(4):22–29.
- Donnelly, J.P., N. Kraus, and M. Larson. 2006. State of knowledge on measurement and modeling of coastal overwash. *Journal of Coastal Research* 22(4):965–991.
- Donnelly, J.P., J. Butler, S. Roll, M. Wengren, and T. Webb III. 2004. A backbarrier overwash record of intense storms from Brigantine, New Jersey: Storms and their significance in coastal morpho-sedimentary dynamics. *Marine Geology* 210(1–4):107–121.
- FGDC (Federal Geographic Data Committee). 1998. Geospatial Positioning Accuracy Standards Part 3: National Standard for Spatial Data Accuracy FGDC-STD-007.3-1998.
- Foxgrover, A.C. 2009. *Quantifying the Overwash Component of Barrier Island Morphodynamics: Onslow Beach, NC*. Master's thesis: Virginia Institute of Marine Science, College of William and Mary, Williamsburg, VA. (145 pages).
- Godfrey, P.J. 1970. Oceanic overwash and its ecological implications on the outer banks of North Carolina. Pp. 321–333 in *Overwash Processes, Benchmark Papers in Geology*. Edited by S.P. Leatherman. Hutchinson Ross Publishing Company: Stroudsburg, PA.

- Guza, R.T., and E.B. Thornton. 1982. Swash oscillations on a natural beach. *Journal of Geophysical Research* 87(C1):483–492.
- Hanson, J.L., H.C. Friebel, and K.K. Hathaway. 2009. Coastal wave energy dissipation: Observations and STWAVE-FP performance. *11th International Workshop on Wave Hindcasting and Forecasting*, Halifax, NS. October 18–23.
- Heron Jr., S.D., T.F. Moslow, W.M. Berelson, J.R. Herbert, G.A. Steele III, and K.R. Susman. 1984. Holocene sedimentation of a wave-dominated barrier island shoreline: Cape Lookout, North Carolina. *Marine Geology* 60(1–4):413–434.
- Hippensteel, S.P., and R.E. Martin. 1999. Foraminifera as an indicator of overwash deposits, barrier island sediment supply, and barrier island evolution; Folly Island, South Carolina: Taphonomy as a tool in paleoenvironmental reconstruction and environmental assessment. *Palaeogeography, Palaeoclimatology, Palaeoecology* 149(1–4):115–125.
- Holland, K.T., B. Raubenheimer, R.T. Guza, and R.A. Holman. 1995. Run-up kinematics on a natural beach. *Journal of Geophysical Research* 100(C3):4985–4993.
- Holland, K.T., and J.A. Puleo. 2001. Variable swash motions associated with foreshore profile change. *Journal of Geophysical Research* 106(C3):4613–4623.
- Holman, R.A., and R.T. Guza. 1984. Measuring run-up on a natural beach. *Coastal Engineering* 8(2):129–140.
- Houser, C., C. Hapke, and S. Hamilton. 2008. Controls on coastal dune morphology, shoreline erosion and barrier island response to extreme storm. *Geomorphology* 100:223–240.
- Houser, C., S. Hamilton, K. Meyer-Arendt, and J. Oravetz. 2007. EOF analysis of morphological change during Hurricane Ivan. *Coastal Sediments '07*:986–995.
- Kochel, R.C., and L.A. Wampfler. 1989. Relative role of overwash and aeolian processes on washover fans, Assateague Island, Virginia–Maryland. *Journal of Coastal Research* 5(3):453–475.
- Kochel, R.C., and R. Dolan. 1986. The role of overwash on a Mid-Atlantic coast barrier island. *Journal of Geology* 94(6):902–906.
- Leatherman, S.P. 1983. Barrier dynamics and landward migration with Holocene sea level rise. *Nature* 301(5899):415–417.
- Leatherman, S.P. 1979. *Barrier Island Handbook: National Park Service Cooperative Research Unit, Amherst, MA*. The Environmental Institute, University of Massachusetts at Amherst.
- Luetich, Jr., R.A., J.J. Westerink, and N.W. Scheffner, 1992. ADCIRC: An Advanced Three-Dimensional Circulation Model for Shelves, Coasts, and Estuaries, Report 1: Theory and Methodology of ADCIRC-2DDI and ADCIRC-3DL. Dredging Research Program

- Technical Report DRP-92-6. U.S. Army Corps of Engineers Waterways Experiment Station, Vicksburg, MS. (137 pages).
- McCubbin, D.G. 1982. Barrier-island and strand-plain facies: Sandstone depositional environments. *Memoir—American Association of Petroleum Geologists* 31:247–279.
- McNinch, J.E. 2004. Geologic control in the nearshore: Shore-oblique sandbars and shoreline erosional hotspots, Mid-Atlantic Bight, USA. *Marine Geology* 211(1–2):121–141.
- Miselis, J.L., and J.E. McNinch. 2006. Calculating shoreline erosion potential using nearshore stratigraphy and sediment volume: Outer Banks, North Carolina. *Journal of Geophysical Research* 111(F2). (15 pages).
- Moore, L.J. 2000. Shoreline mapping techniques. *Journal of Coastal Research* 16(1):111–124.
- Morton, R.A. 2002. Factors controlling storm impacts on coastal barriers and beaches—A preliminary basis for near real-time forecasting. *Journal of Coastal Research* 18:486–501.
- Morton, R.A., J.L. Gonzalez, G.I. Lopez, and I.D. Correa. 2000. Frequent non-storm washover of barrier islands, Pacific Coast of Colombia. *Journal of Coastal Research* 16(1):82–87.
- Plant, N.G., K.T. Holland, and J.A. Puleo. 2002. Analysis of the scale of errors in nearshore bathymetric data. *Marine Geology* 1910:71–86.
- Sallenger, A.H. 2000. Storm impact scale for barrier islands. *Journal of Coastal Research* 16(3):890–895.
- Schwartz, R.K. 1975. Nature and genesis of some storm washover deposits. Technical memorandum. U.S. Army Corps of Engineers, Coastal Engineering Research Center, Fort Belvoir, VA.
- Smith, J. M., A. R. Sherlock, and D. T. Resio. 2001. STWAVE: STeady-state spectral WAVE model: User’s manual for STWAVE Version 3.0. *Supplemental Report ERDC/CHL SR-01-1*, US Army Engineer Research and Development Center, Vicksburg, MS.
- Smith, J.M., and A.R. Sherlock. 2007. Full-plane STWAVE with bottom friction: II. Model overview. *System-Wide Water Resources Program Technical Note*. U.S. Army Engineer Research and Development Center, Vicksburg, MS.
- Smith, G.L., and G.A. Zarillo. 1990. Calculating long-term shoreline recession rates using aerial photographic and beach profiling techniques. *Journal of Coastal Research* 6(1):111–120.
- Stockdon, H.F., R.A. Holman, P.A. Howd, J. Sallenger, and H. Asbury. 2006. Empirical parameterization of setup, swash and run-up. *Coastal Engineering* 53(7):573–588.

- Thieler, E.R., E.A. Himmelstoss, J.L. Zichichi, and T.L. Miller. 2005. *Digital Shoreline Analysis System (DSAS) Version 3.0: An ArcGIS Extension for Calculating Shoreline Change*. U.S. Geological Survey Open-File Report 2005-1304.
- Thieler, E.R., and W.W. Danforth. 1994. Historical shoreline mapping: (I): Improving techniques and reducing positioning errors. *Journal of Coastal Research* 10(3):549–563.
- Thieler, E.R., and R.S. Young. 1991. Quantitative evaluation of coastal geomorphological changes in South Carolina after Hurricane Hugo. *Journal of Coastal Research* 8:187–200.

[This page intentionally left blank.]

Appendix 10-A

Supporting Data

Supporting Data

- (1) Foxgrover, A.C. 2006. Quantifying the overwash component of barrier island morphodynamics: Onslow Beach, NC (Master's Thesis). Virginia Institute of Marine Science, College of William and Mary, Williamsburg, VA. (145 pages).

Summary: In addition to the nearshore interferometric bathymetry data presented in this report, greater than 330 km of co-registered side-scan sonar reflection data (234 kHz), greater than 120 km of high-resolution seismic reflection data, and detailed sedimentological analysis (wet-pipette grain-size analysis) performed on nine marine vibracores (4–6 m in length) were used to characterize the bottom geology and nearshore sediment volume at Onslow Beach. These data were coupled with the aerial photography and shorelines change data presented in this report, as well as the data collected for Ms. Foxgrover's master's thesis, to: (1) test the skill of previously developed metrics for predicting shoreline change along Onslow Beach, and (2) develop metrics to reliably predict potential amphibious coastal landing and staging hazards (i.e., littoral penetration points).

1. Specific results pertinent to predicting shoreline change include the following:

- The northern region of Onslow Beach is characterized by stable to accreting short- and long-term erosion rates. In contrast, erosion rates increase with increasing distance south along the study site.
- The previously described spatial relationship of high alongshore steepness values with regions of elevated shoreline erosion (McNinch, 2004) held true for only the portion of varying nearshore gradients controlled by sedimentary features, suggesting that bottom type has an unquantified influence on the alongshore steepness metric.
- The previously described spatial relationship of low nearshore sediment volumes with regions of elevated shoreline erosion (Miselis and McNinch, 2006) held true only when transport-relevant (i.e., unconsolidated sand) sediment was considered.
- Combining both nearshore and subaerial volumes of transport-relevant sediment improved the sediment volume metric's skill at predicting regions of elevated shoreline erosion.

2. Specific results pertinent to predicting amphibious coastal landing and staging hazards include the following:

- Even up-to-date topographic maps and bathymetric charts are often insufficient for predicting hazards relevant to transporting and/or staging personnel and equipment in the dynamic coastal zone (i.e., identifying littoral penetration points) because most maps and charts are based on sparse and static datasets.
- Several easily measurable environmental metrics can be identified, including gradients in nearshore bathymetry and nearshore sediment volume, and variation in shoreline and vegetation line positions as derived from aerial photograph, that allow for rapid and accurate evaluation of the suitability of various coastal regions for potential military applications.

- These metrics were integrated with high-resolution bathymetric and isopach maps, and adjacent aerial photography, to generate a map of suggested littoral penetration points as well as coastal hazards for Onslow Beach.
- (2) Heidi Wadman, Postdoctoral Research Associate, Virginia Institute of Marine Science, College of William and Mary, Williamsburg, VA. May 2008.

Summary: Geophysical, geospatial, and sedimentological data indicate that: (1) the relevant-sand prism of Onslow Beach is severely limited; (2) approximately 11% of the prism is comprised of sedimentologically distinct washover deposits; (3) the southern portion of Onslow Beach is actively undergoing barrier-island rollover; and (4) natural forcings have predominately shaped the evolution of Onslow Beach over the past 80 years. These conclusions are based not only on the overwash and aerial imagery data presented in this final report, but also on data from the collection of RTK-GPS transects of modern overwash fans, nine short (less than 2 m) and 12 long (up to 4 m) vibracores from the beach and backbarrier of Onslow Beach, and the collection of approximately 80 km of ground-penetrating radar (GPR) data collected throughout southern Onslow Beach. Sediment analysis included full Rapid-Sediment-Analyzer (sand-size, fractional-phi, grain-size analysis) of hundreds of core samples to distinguish overwash-transported sediment from aeolian-transported sediment. Overwash locations and beach volumes were compared to a multitude of previously defined proxies for predicting shoreline erosional hotspots, including long- and short-term shoreline change rates, and cross-island sediment volume (normalized to transect area). Specific findings include:

- The volume of the relevant-sand prism south of the former Riseley Pier is $1.8 \pm 1.1 \times 10^6 \text{ m}^3$ and averages approximately 90 cm in thickness.
- Sedimentologically distinct washover deposits make up approximately $199 \pm 88 \times 10^3 \text{ m}^3$ of sediment, which equals 29% of the active overwash complex or 11% of the entire study area's relevant sand-prism.
- Large overwash events are a mechanism by which sediments can accumulate on and behind the island, thereby increasing the relevant-sand prism and decreasing susceptibility to future erosion.
- Although a simple linear relationship between spatial and temporal variability in shoreline behavior and volume of the relevant-sand prism did not exist, a positive correlation does exist between both rates of change and net movement of the shorelines and vegetation lines.
- The region of Onslow Beach experiencing the highest rate of erosion from 1938–2008 (3.85 m/y) is not the region used for military amphibious training activities.

[This page intentionally left blank.]

Appendix 10-B

List of Scientific Publications

List of Scientific Publications

Peer-Reviewed Publications

- Brodie, K.L., and J.E. McNinch. 2011. Beach change during a nor'easter: Relationships to wave steepness and inner surf zone dissipation. Pp. 1360–1374, Volume 1 in *Proceedings of the Coastal Sediments 2011*. Edited by J.D. Rosati, P. Wang, and T.M. Roberts.
- Wadman, H.M., and J.E. McNinch. 2011. Evaluating subaerial and nearshore geologic metrics for prediction shoreline change: Onslow Beach, NC. Pp.1946–1961 in *Proceedings of the Coastal Sediments 3*. Edited by J.D. Rosati, P. Wang, and T.M. Roberts.
- Wadman, H.M., J.E. McNinch, and A.C. Foxgrover. In press. Environmental metrics for assessing optimal littoral penetration points and beach staging locations: MCBCL amphibious training grounds, Onslow Beach, NC. In *Reviews in Engineering Geology Volume XX: Military Geoscience in the 21st Century*. Edited by R.S. Harmon, and E.V. McDonald. Geological Society of America: Denver, CO.
- Brodie, K.L., and J.E. McNinch. Accepted 2010. Coastal Lidar and Radar Imaging System (CLARIS): A mobile, integrated system for measuring nearshore wave parameters, bathymetry, and beach topography during storms. *Coastal Engineering*. In review.
- Brodie, K.L., and J.E. McNinch. 2009. Erosional hotspot storm morphodynamics: Coastal Lidar and Radar Imaging System, CLARIS, reveals persistent three-dimensional morphologies and alongshore variable water levels. *Journal of Geophysical Research—Earth Sciences*. In review.
- McNinch, J.E., K.L. Brodie, H.M. Wadman, and A.C. Foxgrover. In preparation. The influence of geological framework on predicting event-scale, overwash: Onslow Beach, NC. To be submitted to *Marine Geology* in 2012.

Thesis

- Foxgrover, A.C. 2006. Quantifying the overwash component of barrier island morphodynamics: Onslow Beach, NC. Virginia Institute of Marine Science, College of William and Mary, Williamsburg, VA. (145 pages).

Presentations

- Brodie, K.L., J.E. McNinch, and R.K. Slocum. 2012. Hourly Measurement of Beach Topography, Wave Runup and Surf-Zone Wave Heights During Hurricane Irene from a Terrestrial Laser Scanner at Duck, NC. Presented at the Ocean Sciences Meeting, Salt Lake City, UT. February 24. [Abstract ID 11399].
- McNinch, J.E., and R.K. Slocum. 2012. *Methods for Extracting Beach Evolution, Runup and Wave Bore Heights from an Automated Terrestrial Laser Scanner*. Poster presented at the 2012 Ocean Sciences Meeting, Salt Lake City, UT. February 22. [Abstract ID 11414].

- Brodie, K.L., and J.E. McNinch. 2011. *Beach Change During a Nor'easter: Relationships to Wave Steepness and Inner Surf Zone Dissipation*. Presented at the 7th International Symposium on Coastal Engineering and Science of Coastal Sediment Processes, Miami, FL. May 2–6.
- Wadman, H.M., and J.E. McNinch. 2011. *Evaluating Subaerial and Nearshore Geologic Metrics for Predicting Shoreline Change: Onslow Beach, NC*. Presented at the 7th International Symposium on Coastal Engineering and Science of Coastal Sediment Processes, Miami, FL. May 2–6.
- Theuerkauf, E.J., A.B. Rodriguez, S.R. Fegley, J.V. Flemming, J.E. McNinch, and H.M. Wadman. 2010. Extreme Along-Beach Variations in Morphodynamics Attributed to Nearshore Bathymetry and Underlying Geology over the Short-Term, Onslow Beach, North Carolina. American Geophysical Union Fall Meeting. [Abstract number EP43A-0639].
- McNinch, J.E., and K.L. Brodie. 2009. Shallow-Water Bathymetry Measurements During Storm Events Using Bar and Swash Imaging Radar (BASIR), A Mobile X-Band Radar. Presented at the U.S. Hydrographic Conference, Norfolk, VA. May 11–14.
- Theuerkauf, E.J., K.L. Brodie, H.M. Wadman, and J.E. McNinch. 2009. Beach erosion and geomorphology: Assessing correlations between beach and nearshore morphodynamics. *Geological Society of America Abstracts with Programs* 41(1):42.
- McNinch, J.E., K. Brodie, H.M. Wadman, and J.L. Miselis. 2008. A Possible Explanation for Elevated Shoreline Change at Erosional Hotspots: Observations of Waves, Surf-Zone Bathymetry and Shoreline Morphology During a Storm Event. Presented at the American Geophysical Union, Fall Meeting 2008, San Francisco, CA. December 15–19. [Abstract number OS53F-05].
- Foxgrover, A.C., J. McNinch, H. Wadman, and A.B. Rodriguez. 2008. *Quantifying Barrier-Island Overwash Through Sedimentological, Geophysical, and Geospatial Analyses: Onslow Beach, NC*. American Geophysical Union Fall Meeting. [Abstract number OS23A-1235].
- Rodriguez, A.B., S.R. Fegley, C.R. Mattheus, E.A. Timmons, J. McNinch, and H. Wadman. 2008. Spatial Variation of Shoreline Change Along an Important Marine Corps Amphibious Training Ground, Onslow Beach, North Carolina; Part 2: Beach Morphology. Presented at the Joint Meeting of The Geological Society of America, Soil Science Society of America, American Society of Agronomy, Crop Science Society of America, Gulf Coast Association of Geologic Societies with the Gulf Coast Section of SEPM 40(6).
- Wadman, H., J. McNinch, A.C. Foxgrover, and A.B. Rodriguez. 2008. Spatial Variation of Shoreline Change Along an Important Marine Corps Amphibious Training Ground, Onslow Beach, NC: Part 1: Nearshore Geology and Morphology. Presented at the Joint Meeting of The Geological Society of America, Soil Science Society of America, American Society of Agronomy, Crop Science Society of America, Gulf Coast

Association of Geological Societies with the Gulf Coast Section of the Society for Sedimentary Geology (SEPM) 40(6).

Appendix 10-C

List of Students

- Heidi Wadman, Postdoctoral Research Associate, Virginia Institute of Marine Science, College of William and Mary, Williamsburg, VA. May 2008.
- Amy Foxgrover, M.S., Virginia Institute of Marine Science, College of William and Mary, Williamsburg, VA. May 2010.

[This page intentionally left blank.]

Chapter 11

**Long-Term Barrier Evolution Related to Variations
in Underlying Geology and Land Use**

SERDP Project Number: RC-1413

Coastal Barrier Module

Research Project CB-2

Lead Researcher:

Antonio B. Rodriguez

Supporting Researchers:

Stephen R. Fegley, Winnie Yu, Ethan Theuerkauf

University of North Carolina at Chapel Hill

Morehead City, NC

E-mail: abrodrig@email.unc.edu

May 10, 2013

Final

This report was prepared under contract to the U.S. Department of Defense (DoD) Strategic Environmental Research and Development Program (SERDP). The publication of this report does not indicate endorsement by DoD, nor should the contents be construed as reflecting the official policy or position of DoD. References herein to any specific commercial product, process, or service by trade name, trademark, manufacturer, or otherwise, do not necessarily constitute or imply its endorsement, recommendation, or favoring by DoD.

Table of Contents

List of Acronyms	11-v
Abstract.....	11-1
Objectives	11-2
Background.....	11-2
Study Area	11-4
Materials and Methods.....	11-7
Seismic and side-scan sonar data.....	11-7
Coring	11-8
Radiocarbon Dating	11-9
Mapping Shoreline Changes	11-9
Results and Discussion	11-12
Nearshore Framework Geology	11-12
Depositional Environments and Lithologic Facies	11-14
Stratigraphy	11-20
Timing of Washover Fan Emplacement	11-23
Shoreline Movement at Decadal to Yearly Time Scales	11-24
Along-shore variability in rates of shoreline movement.....	11-24
Impacts of Changes in Storminess and the Rate of SLR on Island Evolution.....	11-27
Conclusions and Implications for Future Research	11-30
Literature Cited	11-32
Appendix 11-A: Onslow Beach Cross Sections	11-A-1
Appendix 11-B: List of Scientific Publications	11-B-1
Appendix 11-C: List of Students	11-C-1

List of Figures

11-1. Regional Study Area Map.....	11-5
11-2. Decadal-Scale Trends in Shoreline Position.....	11-6
11-3. The bathymetry map of the nearshore area of Onslow Beach shows high-relief features located offshore of the headland at the same location where Riggs et al. (1995) recognized outcropping rock limestone.	11-6
11-4. MCBCL use zones on Onslow Beach, NC.	11-7
11-5. Seismic and side-scan sonar trackline map of area offshore Onslow Beach, NC.	11-8
11-6. Core-transect locations.....	11-9
11-7. Mapping shoreline movement.....	11-11
11-8. Sea-floor bottom types.....	11-13
11-9. Sand-thickness map.	11-14
11-10. Lithofacies of depositional environments on Onslow Beach, NC.....	11-16
11-11. Proximal washover fan facies.	11-18
11-12. Distal washover fan facies.	11-18
11-13. Fence diagram.....	11-21
11-14. Decadal and annual rates of shoreline movement along the various zones on Onslow Beach, NC.....	11-25
11-15. Record of washover fans along Onslow Beach, NC.....	11-28

List of Tables

11-1. Radiocarbon data and sample information	11-10
---	-------

List of Acronyms

°C	degrees Celsius
μm	micrometer
Φ	phi
3-D	three dimensional
A.D.	Anno Domini
AMS	Accelerator Mass Spectrometry
BP	Before present (1950)
cal yr BP	calibrated years before present
cm	centimeter
DEM	Digital Elevation Model
DoD	U.S. Department of Defense
ICW	Intracoastal Waterway
kHz	kilohertz
km	kilometer
km/h	kilometers per hour
LiDAR	light detection and ranging
m	meter
m ²	square meter
m/s	meters per second
m/yr	meters per year
mm/yr	millimeters per year
MCBCL	Marine Corps Base Camp Lejeune
MWP	Medieval Warm Period
NAVD88	North American Vertical Datum of 1988
NCDCM	North Carolina Division of Coastal Management
NOAA	National Oceanic and Atmospheric Administration
RTK-GPS	real-time kinematic global positioning system
SEGSA	Southeastern Section of the Geological Society of America
SERDP	Strategic Environmental Research and Development Program
SLR	sea level rise

[This page intentionally left blank.]

Abstract

Onslow Beach is an important asset to Marine Corps Base Camp Lejeune (MCBCL) being the primary Atlantic Ocean location where amphibious military training takes place and also a popular spot for military-staff and -family recreation. The future sustainability and effective management of that resource depends on a better understanding of the evolution of the barrier in terms of shoreline movement and landscape changes. The main objective of this study is to examine the evolution of Onslow Beach over millennial to yearly time scales to help better manage future landscape changes that may occur in response to changes in storminess and sea level rise (SLR). Shoreline displacements at decadal and yearly time scales were measured from aerial photography and terrestrial laser scanning, respectively and the evolution of the barrier at millennial to centennial time scales was reconstructed from sediment cores and radiocarbon data. Those data show that Onslow Beach is a transgressive barrier island that moved from approximately 300 m seaward of its present location approximately 200 Anno Domini (A.D.) to its present position during the late Holocene principally through overwash processes and washover fan formation. The oldest washover fan deposits preserved in the stratigraphy of the island are approximately 200 A.D. and at that time an open-water lagoon separated Onslow Beach from the mainland. At approximately 1850 A.D., the number and landward extent of washover fans increased sharply along the entire island. This corresponds to an increase in the rate of SLR to 3.2 mm/yr and a low number of annual tropical cyclones in the Atlantic Ocean. The increase in number and landward extent of washover fans at 1850 A.D. also implies that the rate of island transgression increased. The increase in the rate of SLR likely lowered the elevation of the island principally through erosion of the dunes, and made the island more vulnerable to overwash. These data suggest that Onslow Beach is extremely sensitive to increases in the rate of SLR, which cause an immediate decrease in the elevation of the island and its resistance to overwash. This sensitivity is likely the result of the island being sediment starved, a product of its framework geology (limestone outcropping near the shoreface) and its location at the center of a coastal embayment. Military training activities have little impact on island evolution because the decadal record of shoreline movement and the geological record of island evolution show that the military training zone has been vulnerable to overwash and experienced high rates of shoreline retreat since at least 1850 A.D., long before MCBCL existed. High rates of shoreline retreat at the military training zone are due to the low sediment supply there as compared to the northeastern part of the island where nearshore sand thicknesses are greater. Yearly rates of shoreline retreat at the military training zone, measured November 2007–September 2011, are up to four times higher than the decadal rates, but some of that difference is likely due to different measurement methodology (aerial photos versus laser scanning). The yearly and decadal rates of shoreline movement documented in this study should be used by MCBCL for making management decisions at those respective time scales; however, some of those rates include high variability indicating that the long-term trend should not be projected into the future.

Keywords: Barrier island, transgression, washover fan, sea level rise, beach, overwash, Medieval Warm Period, Little Ice Age, beach erosion, salt marsh, peat

Objectives

The North Carolina Division of Coastal Management's long-term average erosion rates for Onslow Beach (1938–1992) show significant along-beach variability. Erosion of Onslow Beach impacts Marine Corps Base Camp Lejeune (MCBCL) amphibious training and recreation and habitat distribution and quality making management challenging. The main objectives of this research are to

1. Determine the principle drivers of along-beach variations in erosion rates by comparing the historical rates of shoreline erosion with anthropogenic activities and the underlying geology.
2. Place the short-term (yearly) geomorphic evolution of the island, derived from the monitoring data, in context with the historical (100 years) and geological (thousands of years) geomorphic evolution.
3. To provide a model that can be used to predict short-term (yearly to decadal) morphologic changes (shoreline migration).
4. To test **H1**: Erosional “hot spots”, identified as localized areas with higher than average coastal retreat rates, are not a result of anthropogenic activities and **H2**: Onslow Beach is sediment starved due to a lack of unconsolidated material located seaward of the shoreface and insufficient amount of sediment transported to the area by longshore drift and a low rate of production of new sediment through bioerosion of limestone outcrops.

Background

Sustaining the value of environmental and mission-related assets while conducting shoreline management requires a better understanding of the short- and long-term rates of coastal change, which will help differentiate between geologic, hydrodynamic, and anthropogenic forcing mechanisms. The coastal barrier ecosystem is organized directly and indirectly by the physical dynamics of ocean forcing and sediment transport. Physical processes operating in the nearshore vary in magnitude on time scales ranging from hours (coastal storms) and months (seasonal weather patterns) to decades (climate and associated sea level change). The morphological response of the coastal barrier ecosystem to these perturbations is poorly understood, but is critically needed for better shoreline management.

Ocean shorelines retreat at different rates in response to rising sea level due to many factors, including variations in framework geology (antecedent topography and lithology), sediment supply, shoreface hydrodynamics, and storminess. The significant variability in shoreline position and morphology that exists along many coasts at spatial scales of 10–100 km is a reflection of their different rates of retreat and implies differences in coastal evolution at centennial to millennial time scales. The Carolina Capes, including Cape Fear, Cape Lookout, and Cape Hatteras (**Figure 11-1**), likely transgressed landward at a slower rate than the adjacent embayments (Onslow Bay, Raleigh Bay) in response to sea level rise (SLR) from the last glacial maximum (approximately 20,000 years ago) to present. This is because the continental shelf break, which is where the shoreline was located during the early deglaciation, does not mimic the cape-embayment-morphology of the modern shoreline. Understanding the regional controls on coastal evolution and the responses of coastal environments to changing processes at geological

time scales is important due to imminent accelerated SLR and predicted increased storminess and their associated impacts on coastal systems (Donnelly et al., 2004; Scott et al., 2003).

As sea level rises over geologic time scales, waves are generally assumed to erode headlands and straighten a coastline; however, the Carolina Capes are still prominent features along the southeastern U.S. coastline. Ashton et al. (2001) challenged that notion using a numerical model to demonstrate that waves with large angles between their crests and the coast (high-angle waves) can develop coastal perturbations that resemble the Carolina Capes (Cape Fear, Cape Lookout, Cape Hatteras; **Figure 11-1**). The high-angle wave energy makes the cape flanks more stable than the central embayments (e.g., Cape Lookout and Onslow Bay; Ashton and Murray, 2006). Model predictions compared well with the wave-climate variability that exists along the Carolina Capes (Ashton and Murray, 2006) and with field data that show the slow (approximately 5,000 years) degradation (capture) of a former Carolina Cape in Raleigh Bay (Thieler and Ashton, 2011). It takes approximately 50,000 years to produce perturbations of a similar scale as the Carolina Capes from high-angle waves impacting a straight coastline, which is much longer than the less than 9,000 years that the continental shelf was flooded after the last glacial maximum (Ashton et al., 2001; Thieler and Ashton, 2011). This discrepancy implies coastal modification over multiple sea-level cycles and likely influence of pre-existing capes on coastal evolution during the last episode of SLR on the continental shelf (approximately 9,000 years ago; Ashton and Murray, 2006). Many researchers have demonstrated the strong influence of variations in the elevation and lithology of the pre-Holocene antecedent topography that formed during previous sea-level cycles on the evolution of coastal systems (Belknap and Kraft, 1985; Kraft 1971; Pierce and Colquhoun, 1970; Rodriguez et al., 2004; Wilkinson and Basse, 1978).

Storms can produce profound morphologic changes to a barrier island over a short period. Changes in storm climate (i.e., storminess; storm frequency and magnitude) over decadal time scales also strongly affect barrier morphology, which is compounded with SLR. Storms accelerate longshore transport, remove sediment from the shoreface, and deposit sediment in backbarrier environments by producing washover fans and/or flood-tidal deltas, which create rapid changes to the morphology of a coastline. Although individual storms occur on short time-scales (days to weeks) and are not commonly integrated into long-term shoreline-change models (Valvo et al., 2006), changes in the storm climate occurs across centennial to millennial time scales and should be considered. Mann et al. (2009) showed an increase in hurricane landfall along the U.S. Atlantic Coast during the Medieval Warm Period (MWP) at approximately 1,000 cal yr BP. During the Little Ice Age at approximately 400 cal yr BP there is also evidence of increased storminess (nor'easters) impacting the U.S. Atlantic coastline (Mallinson et al., 2011). Slott et al. (2006) simulated coastline changes over 200 years of evolution of the Carolina Capes with a wave climate that is similar to increased tropical and extra-tropical storm conditions. Those scenarios of increased storminess show accretion near the capes and erosion at the embayments occurring at rates several times higher than rates simulated without the change in storm climate (Slott et al., 2006). Although that model's output corresponds with historic rates of shoreline movement when input parameters match the recent wave climate (Slott et al., 2006), results from increased storminess have not been empirically tested.

Barrier islands located at the maximum curvature of a coastal embayment, similar to Onslow Beach, are predicted to have transgressed more rapidly during the Holocene and experienced

increased rates of erosion during stormy periods than barrier islands located along cape flanks, similar to Bogue Banks (Ashton and Murray, 2006; Slott et al., 2006). Both of these predictions can be tested along Onslow Bay, which experienced variations in storminess during the Holocene (Mallinson et al., 2011; Mann et al., 2009). Anthropogenic stressors such as dredging, construction, landing craft deployment, amphibious training, and munitions practice further impact the morphology of the coastal barrier at yearly to decadal time scales and play a large role in regulating rates of change. It is necessary to place short-term morphologic changes, measured directly, in context with the long-term evolution, derived from the geologic record, to differentiate between background and anthropogenic stressors. Additionally, it has been demonstrated that shorelines can exhibit non-linear rates of retreat in response to variations in underlying geology at century and decadal time scales (Browder and McNinch, 2006; Rodriguez et al., 2004).

Study Area

Onslow Beach is a northeast-southwest trending barrier island located at Marine Corps Base Camp Lejeune (MCBCL) in southeast North Carolina (**Figure 11-1**). It is a wave-dominated barrier with a mean wave height of 0.91 m and tidal range of 1.2 m based on National Oceanic and Atmospheric Administration's (NOAA's) tide gauge at Wrightsville Beach, NC (Station ID 8658163, located 60 km southwest of Onslow Beach). This 12 km-long barrier fronts saltmarsh with sinuous tidal channels and is bounded by the New River Inlet to the southwest and Browns Inlet to the northeast. The Intracoastal Waterway (ICW) extends through the backbarrier marsh. The shoreline of Onslow Beach is sinusoidal with a central headland separating two embayments (**Figure 11-1**). The morphology of the island also varies along its length. The northeastern arcuate section has a wide beach (approximately 80-m wide) with multiple well-developed dune ridges (7–9 m in height). Landward of the dune ridges a narrow (less than 100-m wide) maritime forest abuts the backbarrier saltmarsh. This northeastern section of the barrier has low net decadal rates of accretion of approximately 0.25 m/yr (**Figure 11-2**; Rodriguez et al., 2012). The central headland area has a narrow beach (approximately 20-m wide) with a single discontinuous dune ridge less than 4 m in height. Numerous washover fans extend less than 100 m across the dunes and the vegetation is dominated by shrub thickets, but dead standing and fallen trees are frequently observed. The beach widens significantly along the southwestern embayment from 20 m in the northeast to 80 m in the southwest. The discontinuous dunes are less than 2 m in height and washover fans can be extensive (250-m wide) and extend across backbarrier marshes. This southwestern part of Onslow Beach has a net erosion rate of approximately 2 m/yr and erosion rates decrease toward the headland where shoreline position is highly variable through time (**Figure 11-2**; Rodriguez et al., 2012). The variable morphology of Onslow Beach reflects its central location within Onslow Bay because it defines the border between the high-elevation regressive islands with multiple beach ridges to the north and the low-elevation, narrow transgressive islands to the south (Cleary et al., 1996).

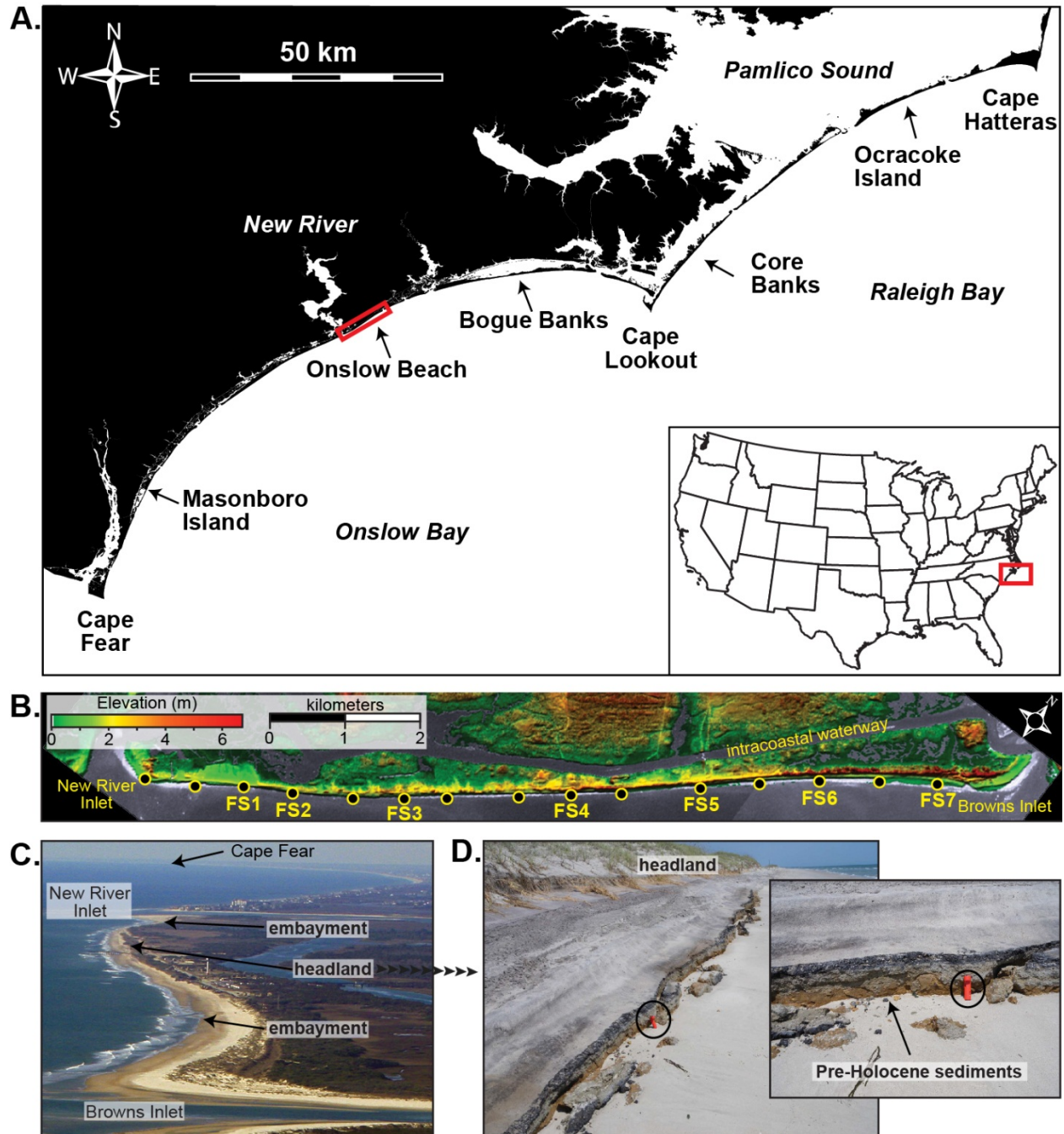


Figure 11-1. Regional Study Area Map.

(A) Onslow Beach is located in the center of Onslow Bay, NC. (B) Map showing changes in elevation along the island and the locations of the 15 focus sites. (C) Oblique aerial photo looking towards the southwest shows the sinusoidal morphology of the island. (D) At the headland, consolidated and oxidized gravelly sand is outcropping on the beachface.

The central headland is produced by a submarine rock ridge that intersects Onslow Beach (**Figure 11-3**; Riggs et al., 1995). The rock ridge is composed of the Oligocene Silverdale Formation, a sandy, molluscan-mold limestone unit (Harris et al., 2000). The Quaternary sediment layer is thin and patchy offshore of southern and central Onslow Beach, where more

than 50% of the inner shelf is exposed limestone (Johnston, 1998) and Riggs et al. (1995) labeled the Onslow Beach as being “sediment starved.”

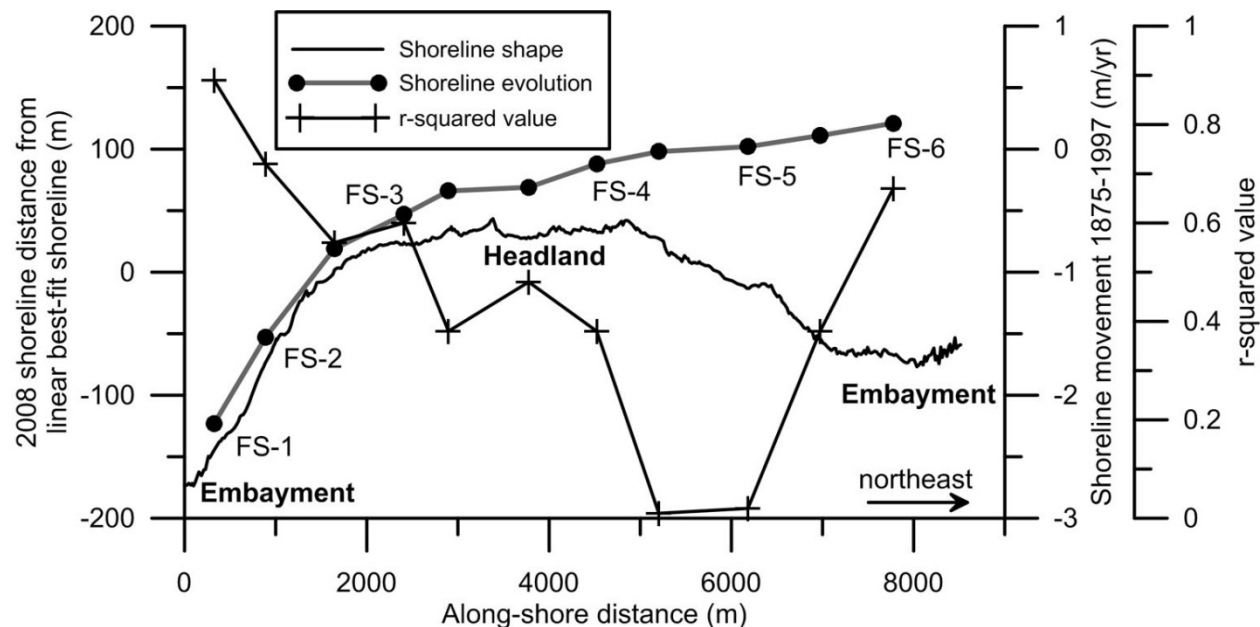


Figure 11-2. Decadal-Scale Trends in Shoreline Position.

The shoreline shape curve was derived from measuring the maximum distance between the 2008 digitized shoreline and the best-fit line through the points that define the shoreline positions in 1938, 1956, 1979, 1989, 1998, 2006, and 2008. Positive values are where the 2008 shoreline is seaward of the best-fit line. Rates of shoreline movement and r-squared values are based on Benton et al. (2004). Notice that the along-shore distance of 0 m is very close to Focus Site 1.

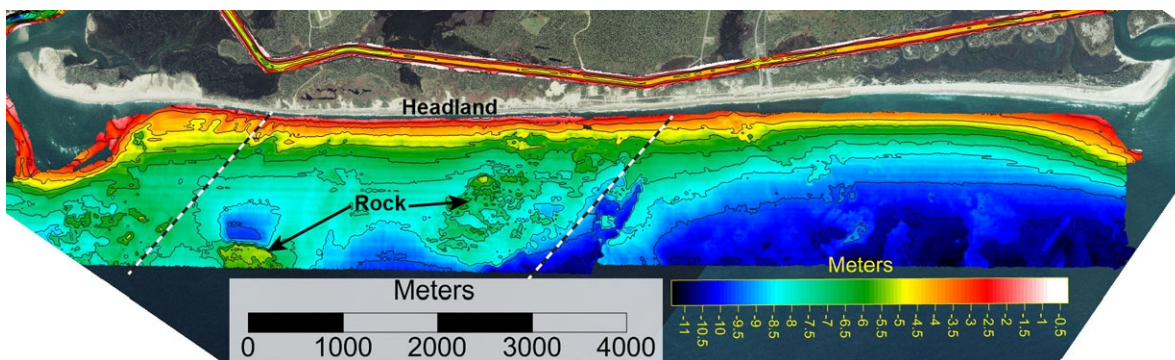


Figure 11-3. The bathymetry map of the nearshore area of Onslow Beach shows high-relief features located offshore of the headland at the same location where Riggs et al. (1995) recognized outcropping rock limestone.

The washover fans in the central and southwestern parts of Onslow Beach indicate storms are an important driver of geomorphologic change on the island. Historical records show 35 hurricanes passed within 120 km of Onslow Beach from 1857 A.D. to 2011, six of which were Category 3 or higher (wind speeds ≤ 178 km/h; csc.noaa.gov/hurricanes [NOAA, 2012]). Hurricane Fran (Category 3) made landfall in September 1996 and transported $199 \pm 88 \times 10^3 \text{ m}^3$ of sand across the backbarrier environments forming an extensive washover fan at the southwestern end of

Onslow Beach (Foxgrover, 2009). Hurricane Bertha (Category 3) made landfall 2 months prior and likely contributed to the significant overwash of the island during Hurricane Fran by eroding the dunes. After Hurricane Fran, Hurricane Irene (Category 1, wind speeds ≤ 119 km/h) was the next large storm to cause significant overwash at Onslow Beach. That storm made landfall in August 2011 at Cape Lookout, NC, 70 km northeast of the study area (**Figure 11-1**), and formed washover terraces and fans along the southwestern and central parts of Onslow Beach.

The MCBCL created four spatially explicit use zones along Onslow Beach (**Figure 11-4**). The southwestern part of the island is used primarily by off-road recreation vehicles. People drive to this end of the island mainly to access fishing spots near the inlet. The central part of the island is used for military training and the main disturbance is large vehicles and equipment creating ruts in the beach. An access road (unpaved) behind the dune line is maintained. Egress points connect the road to the beach and are situated at natural breaks in the dune line that were formed by storms. Northeast of the training zone is the recreational part of the beach where the main impact is from foot traffic. The northeastern end of the island serves as a buffer zone between Onslow Beach and adjacent Browns Island, which is an impact area that is used in ordnance testing and is restricted from foot and vehicular traffic.



Figure 11-4. MCBCL use zones on Onslow Beach, NC.

Materials and Methods

The broad time-scales included in this study require using a variety of diverse methods. The geologic history of the island was reconstructed based on identifying depositional environments and mapping their distribution from sediment cores and geophysical data. Depositional environments were placed in a chronostratigraphic framework by radiocarbon dating shells and wood subsampled from the cores. Shoreline movements at decadal and yearly time scales were measured from aerial photos and laser scanning, respectively.

Seismic and side-scan sonar data

Seismic and side-scan sonar data (approximately 50 km) were collected at the same time along the shoreface of Onslow Beach to map the sand thickness and the sea floor bottom type (sand, peat, or rock), respectively (**Figure 11-5**). These data were collected at high-tide so that acoustic facies interpretations of the intertidal and shallow subtidal areas could be verified with observations made at low tide from the shore. Seismic data were collected using an EdgeTech

SB-216S chirper set at 2–12 kHz and triggered every 0.25 seconds. Side-scan sonar data were collected using an EdgeTech 4200-Full Spectrum system set at 410 kHz, which has an across-track resolution of 2 cm. Side-scan sonar data are displayed with areas of high acoustic backscatter as dark to black-colored and low acoustic backscatter as light to white colored. All marine seismic data sets were interpreted using Chesapeake Technology, Inc. SonarWiz software and maps were generated using Surfer 9.0. A velocity of 1,500 m/s was used to convert the two-way travel time to depth.

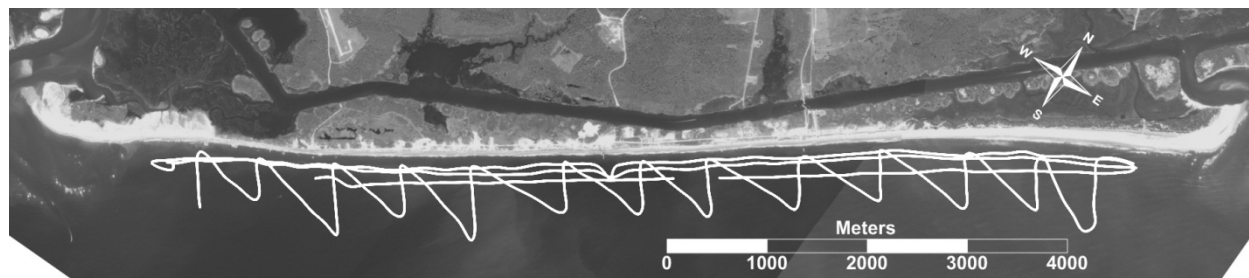


Figure 11-5. Seismic and side-scan sonar trackline map of area offshore Onslow Beach, NC.

Coring

To determine the stratigraphy of Onslow Beach, we collected 43 cores from 11 transects in the barrier and adjacent environments. The cores make up one shore-parallel, two backbarrier and eight cross-island transects separated by an average of 1.2 km (**Figure 11-6**). Transect locations were selected based on accessibility, spacing, and presence of relevant geomorphic features like the locations of embayments, the headland and washover fans. Many transects were sampled near sandy paths leading to the ICW from the main paved road that runs along the central part of the island. The northeastern end of Onslow Beach has restricted access because it acts as a buffer between the recreational part of the beach and an area that receives live fire and may contain unexploded ordnance; therefore, we could not collect cores from this portion of the island.

Most of the cores were obtained using the standard vibracoring method (Lanesky et al., 1979), which retrieved cores 0.62 m to 3.94 m in length. The vibracorer had difficulty penetrating through the upper dry sediment, requiring hand auguring to the water table (the upper ~100 cm) at most of the sites. The augured sediment was logged in the field and the depth of the hole was recorded before vibracoring. The washover fan that formed during Hurricane Irene was sampled on September 1, 2011, 5 days after the storm, with four cores ranging 43–65 cm in length (F2wash). These short cores were collected by pounding aluminum pipe into the ground with a sledgehammer. The locations and elevations of the cores, as well as topographic profiles crossing the barrier at the eleven transects, were surveyed with a Trimble R8/5800 real-time kinematic global positioning system (RTK-GPS) unit. Average horizontal and vertical precisions were 0.015 m and 0.020 m, respectively.

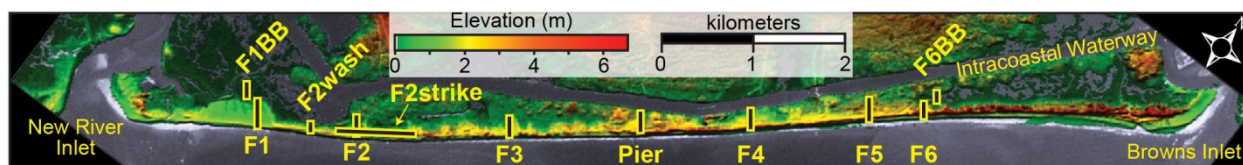


Figure 11-6. Core-transect locations.

The cores were split length-wise, photographed, described (color descriptions based on the Munsell color chart), and subsampled. Interpretations of depositional environments relied on constraining lithologies, sedimentary structures, and macrofossil assemblages. Approximately 370 subsamples were taken from the cores for grain size analyses. A 2,000- μm sieve was used to determine the greater than 2,000- μm fraction and a Cilas laser particle-size analyzer for the 2,000- μm to 0.04- μm component (see manufacturer's specifications).

The organic matter content of approximately 300 subsamples from the cores was measured using the loss on ignition method (Heiri et al., 2001). Subsamples were collected at 15-cm intervals or at 1- or 2-cm intervals for high-resolution analyses of the modern marsh sediment. After drying the samples overnight at 110°C, they were burned at 550°C in a muffle furnace for 5 hours. Percent organic matter was calculated from the measured dry masses before and after the burning stage.

Radiocarbon Dating

Shell and organic material from the cores were selected for accelerator mass spectrometry radiocarbon dating. Articulated bivalves, large pieces of wood, and plant seeds were preferentially chosen over bulk organic samples, small wood fragments and unpaired valves to minimize the adverse effects of reworking on developing an accurate chronostratigraphy. Radiocarbon analysis of 18 samples was performed by Woods Hole Oceanographic Institution and Beta Analytic (for details on methodology used, see www.whoi.edu/nosams). Ages in this study are reported as calibrated years before present (1950) or A.D. at two standard deviations obtained by using the CALIB 6.0 program (Stuiver and Reimer, 1993; **Table 11-1**).

Mapping Shoreline Changes

Shoreline changes were measured at 15 focus sites selected to represent the diverse morphologies along Onslow Beach (**Figure 11-1**). Topographic data were collected using a Riegl three-dimensional (3-D) LMSZ210ii Terrestrial Laser Scanner. The scanner was mounted onto a truck and rotated 360 degrees while collecting approximately 2 million spatial (x, y, and z) data points from laser returns. RTK-GPS surveyed reflectors, positioned within the scan area, were used to reference the data points to a global coordinate system Universal Transverse Mercator (Theuerkauf and Rodriguez, 2012). Two scan positions were occupied at each focus site, resulting in approximately 200 m of coverage along the beach (approximately 4-million points per site per survey). Beach surveying was restricted to 2 hours before and after low tide to maximize subaerial beach coverage. Error in the 3-D topographic data is estimated to be ± 3.0 cm, which includes a ± 1.5 cm factory-estimated maximum instrument error and an average ± 1.5 cm RTK-GPS error. The RTK-GPS error is reported from the instrument as horizontal and vertical error and varies based on factors such as number of satellites, position of satellites and

cloud cover. Each focus site along the island was scanned biannually in association with the beach monitoring program (May 2008 to September 2011).

Table 11-1. Radiocarbon data and sample information

Laboratory Identification	Core Location	Core Name	Sample Depth (cm)	Material Dated	Conventional ¹⁴ C Age: Yr BP; 2σ	Calibrated ^a ¹⁴ C Age: Yr BP; 2σ	Depositional Environment
OS-90480	F1	F1_7	193	Plant material	>Modern		Marsh
OS-82867	F1	F1_4	177–179	<i>Macoma constricta</i>	1,390 ±20	885–1003	Lagoon
OS-82889	F2	F2_5	164–167	Wood	115 ±20	55–145	Marsh
OS-90478	F2strike	F2strike_4	184–186	Plant material	250 ±25	280–318	Marsh
OS-90479	F2strike	F2strike_4	226–228	Plant material	660 ±25	560–598	Marsh
OS-82890	Pier	Pier_5	177–179	Wood	105 ±15	55–140	Marsh
OS-82891	Pier	Pier_5	202–204	organic sediment	115 ±15	55–145	Marsh
Beta-283047	Pier	Pier_5	302–304	Wood	2,270 ±40	2,156–2,268	Fringe marsh
Beta-283048	Pier	Pier_5	420–422	Wood	3,400 ±40	3,556–3,728	Fringe marsh
OS-90490	Pier	Pier_1	63–66	Plant material	715 ±35	644–724	Marsh
OS-90484	Pier	Pier_1	115–117	Wood/plant	1,850 ±25	1,715–1,832	Marsh
OS-90492	F4	F4_4	144	Wood	520 ±35	505–559	Marsh
OS-90548	F4	F4_4	198–200	Plant material	1,430 ±30	1,293–1,376	Marsh
OS-82892	F5	F5_5	218–220	Wood	100 ±15	53–138	Marsh
OS-82894	F5	F5_5	258–260	Wood	605 ±15	583–649	Marsh
OS-82895	F5	F5_5	322–324	Wood	975 ±15	902–931	Lagoon
OS-90602	F6	F6_10	130–133	<i>Tagelus plebeius</i>	1,000 ±30	525–641	Lagoon

^a Using the CALIB 6.0 program (Stuiver and Reimer, 1993).

Macoma constricta = Constricted macoma; *Tagelus plebeius* = Stout tagelus.

Ground points (x, y, and z data points) were isolated from the raw data using an algorithm included in the Terrasolid LTD software package and by manual editing. Surface-grid models were created from approximately 125,000 ground points for sites with narrow cross-shore widths (e.g., F4) and approximately 500,000 ground points for sites with wide cross-shore widths (e.g., F7) using Delaunay triangulation (Guibas and Stolfi, 1985; Lawson, 1977; Lee and Schachter, 1980; **Figure 11-7**). Woolard (1999) and Woolard and Colby (2002) suggest that Digital Elevation Models (DEMs) derived from airborne light detection and ranging (LiDAR) most accurately represent coastal topography with a spatial resolution of 1–2 m. Given the high density of points derived from the laser scans at each site in this study, a 0.5-m grid spacing was used. This 0.5-m grid spacing is generally much larger than the spacing of the laser returns, thus each grid node is based on an average of several topographic measurements. Areas of the focus sites greater than 5 m² with no laser returns, which only occurs in the dunes, were not included in the surface model (i.e., the areas were defined with blanked grid nodes; **Figure 11-7**) because the

limited data would not depict the ground surface accurately at the desired resolution. Surface-grid files were imported into Golden Software's Surfer 10.0 to generate contour maps and DEMs.

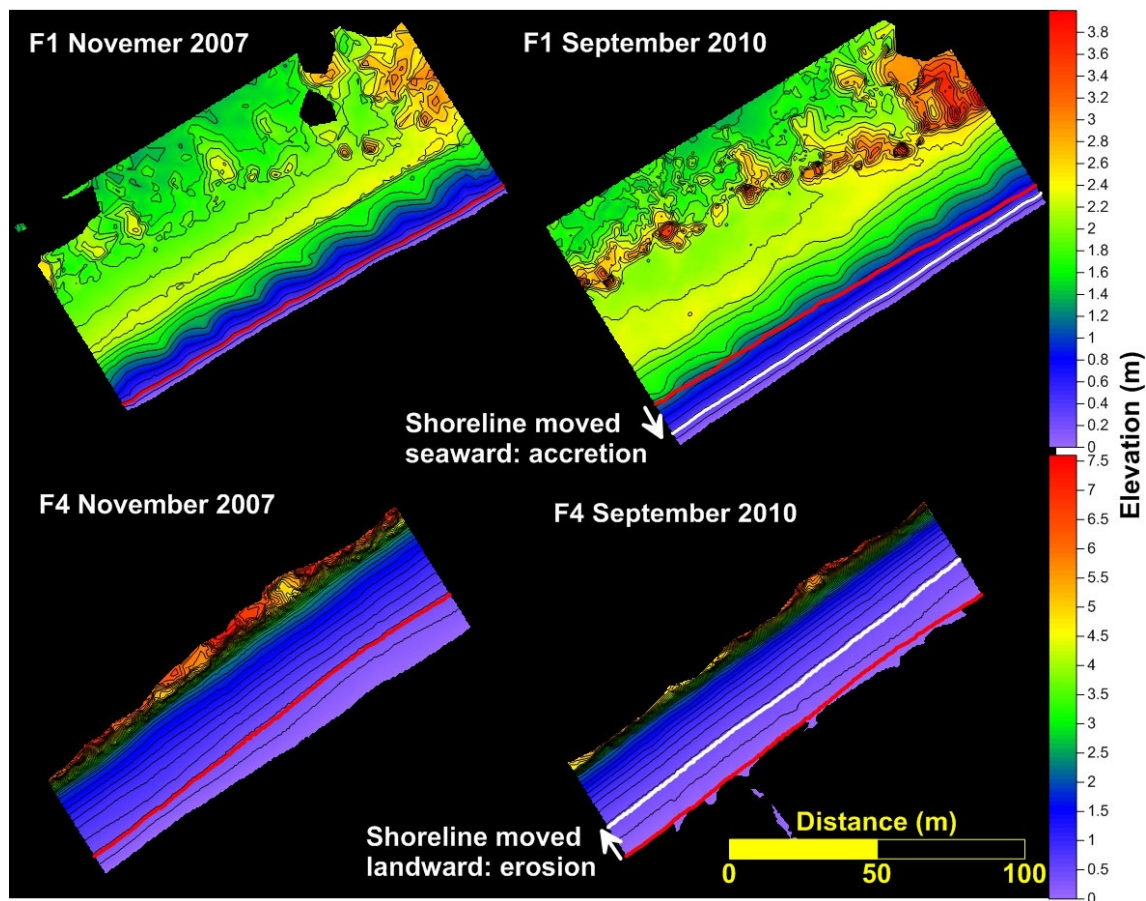


Figure 11-7. Mapping shoreline movement.

DEMs of Focus Sites 1 and 4 on Onslow Beach, NC, with the shoreline position (mean high water) highlighted in red for November 2007 and white for September 2010. The along-beach extent of each map is the same across time steps (see Figure 11-1 for locations).

The position of the laser scanner was not the same for each re-occupation of the focus sites due to changes in barrier morphology and unavoidable circumstances (e.g., beachgoers, MCBCL training activities). This caused the mapped area of a site to be slightly different for each survey. To account for this, DEMs were cropped to reflect only areas of overlapping survey coverage; resulting in an along-beach extent of approximately 150 m for each focus site. The data points also extend further landward at sites with low-elevation dunes and overwash fans (e.g., F3), but these data are patchy landward of the foredune crest because of shadowing. Portions of the dune landward of the foredune crest were cropped out of the maps to normalize coverage across the beach between surveys. The seaward boundaries were cropped at zero meters North America Vertical Datum of 1988 (NAVD88) on the maps to normalize coverage across the beach caused by differences in tidal height (the laser does not penetrate the surface of the water) between surveys.

Shoreline change was measured from the monitoring data using the mean high water (MHW) line, which is located 0.36 m above NAVD88 at Onslow Beach (Weber et al., 2005). The MHW line was contoured from the DEMs and exported as a shapefile into ArcGIS. Shoreline change at the decadal time scale was measured using shorelines digitized from aerial photos by the North Carolina Division of Coastal Management (NCDCM) since 1935. Shoreline change at the yearly (monitoring data) and decadal (NCDCM) time scales was measured using the Digital Shoreline Analysis System, an extension in ArcGIS that computes shoreline change by calculating the distance each shoreline is away from a known baseline (Thieler et al., 2009). Rates of shoreline movement were calculated using linear regression.

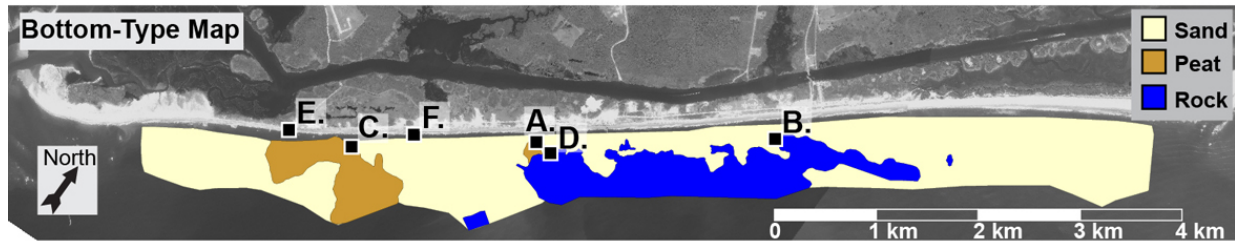
Results and Discussion

The facies concept is used in the description and interpretation of the sedimentological and geophysical data and this descriptive methodology has been in use for almost 200 years (since Gressly, 1838). Readers of this report who are unfamiliar with Geology can find an introductory overview of the facies concept in Boggs (2001) and Reading (2000).

Nearshore Framework Geology

A mosaic of the side-scan sonar data set shows that the sea floor is composed of three acoustic facies (i.e., Facies 1 through 3; **Figure 11-8**), identified on the basis of their backscatter characteristics. Facies 1 is located throughout the nearshore and is characterized by a smooth, uniform low-reflectivity, with localized bedforms, including subaqueous sand dunes and ripples. Where this facies exists in the intertidal and shallow subtidal, it is observed from the beach as sand. Facies 2 is located in the southwest in intertidal and shallow subtidal areas and is characterized by moderate to high backscatter with locally developed shadows as linear features and decimeter-scale spots. Facies 2 is interpreted as outcropping peat which forms terraces in the intertidal and shallow subtidal with exposed tree stumps (**Figure 11-8E**). Facies 3 is primarily located along the center of the island and is characterized by an acoustically patchy sea floor associated with rugged bathymetric relief. Facies 3 is interpreted as outcropping rock of the Oligocene Silverdale Formation, and clasts of this material are commonly found on the beach in areas where this facies exists offshore (**Figure 11-8F**).

An acoustically transparent seismic unit, which thins across the shoreface in a seaward direction, was imaged below the sea floor along Onslow Beach (**Figure 11-9**). At the toe of the shoreface, the unit thickens towards the northeast from approximately 0.5–2.5 m (**Figure 11-9**). The unit pinches out in areas where peat or rock is exposed at the sea floor and is interpreted as sand. As the island transgressed in response to SLR over the past ~9000 years, erosional processes at the shoreface and the shallow elevation of old rock formations have resulted in a the sand-starved coast line (Riggs et al., 1995).



Side-scan sonar images of peat exposed on the shoreface during high tide.

Side-scan sonar images of rock exposed on the shoreface during high tide.

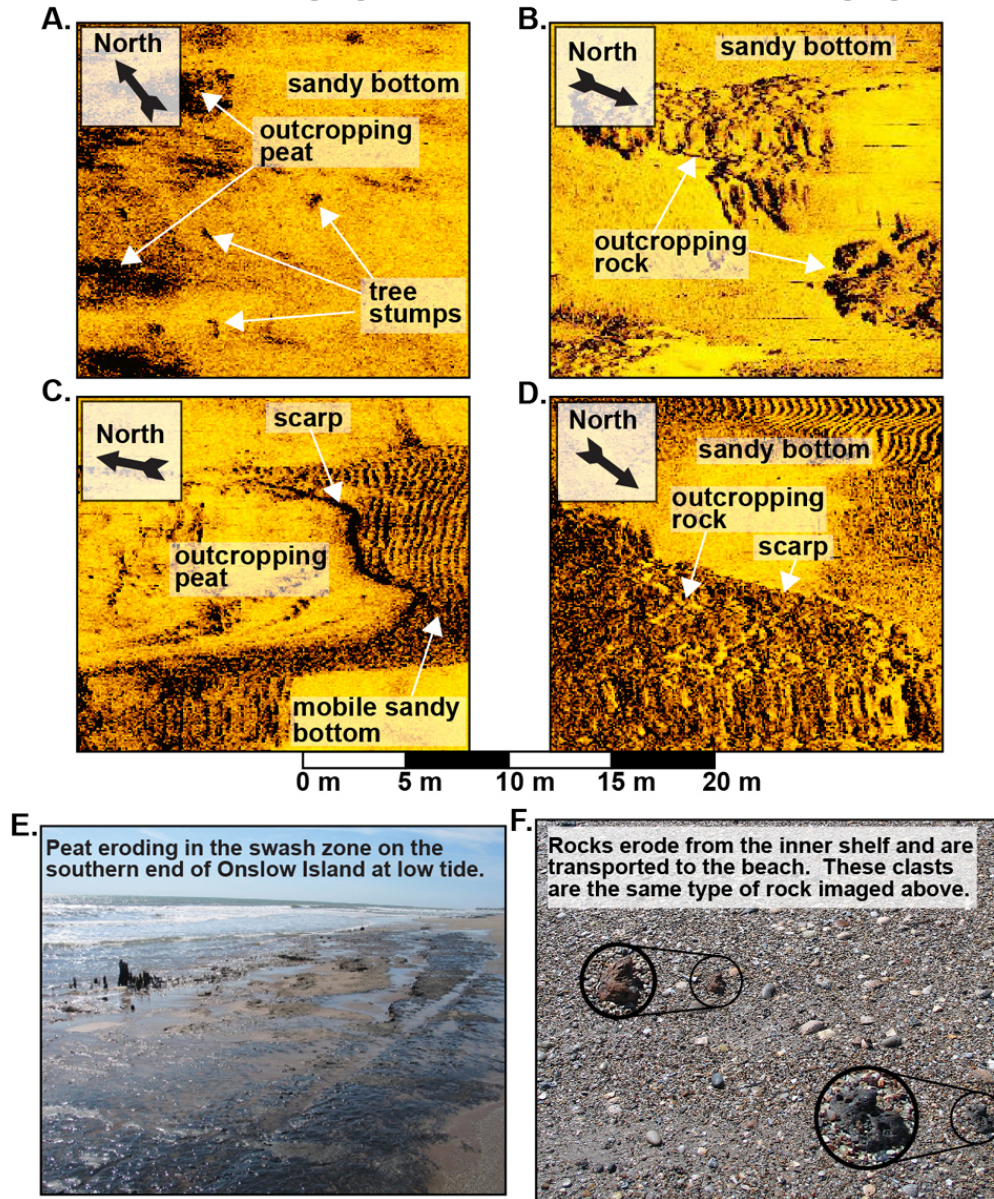


Figure 11-8. Sea-floor bottom types.

The distribution of acoustic facies along the nearshore of Onslow Beach shows that peat (Facies 2) is exposed at the sea-floor in the southwest (A and C), rock (Facies 3) is exposed at the sea floor in the center of the island (B and D) and sand (Facies 1) is exposed at the seafloor in the northeast. These interpretations are supported with observations made from the beach (E and F).

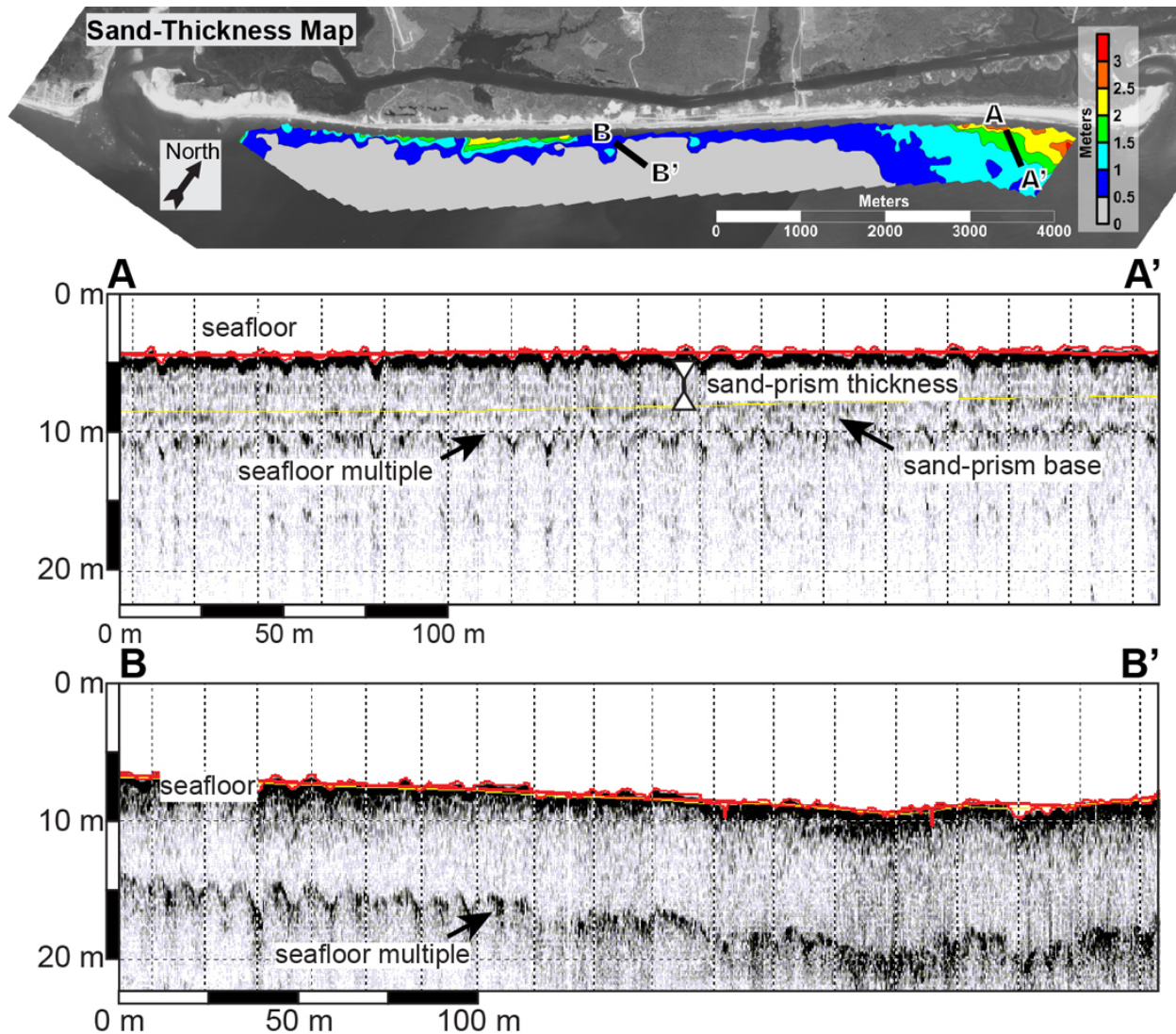


Figure 11-9. Sand-thickness map.

The thickness of shoreface and inner shelf sand decreases towards the southwest and in an offshore direction at Onslow Beach, NC (A and B).

Depositional Environments and Lithologic Facies

The depositional environments along Onslow Beach, including beach (foreshore and backshore), dune, marsh, and washover fan, were sampled in the tops of the 43 vibracores. Lithologic-facies descriptions of these modern environments were used as benchmarks to help interpret the older sedimentary units. Two lithologic facies, A and B, were sampled at depth and were not similar to any of the modern depositional environments that exist across Onslow Beach.

Beach Facies

The beach facies is characterized by fine to medium quartz sand (0.91-2.38 Φ ; for details on the phi scale for grain size, see Krumbein and Sloss, 1963) with gently dipping heavy-mineral laminae and beds and gravelly sand beds (**Figure 11-10A**). Swash processes in the foreshore

produce the gently dipping to parallel heavy mineral laminae and beds (Davis, 1978), and the weathered shells and gravelly sand beds are the result of reworking and transport in the high-energy surf zone (Komar, 1976). The average gravel content is 6.75%, but can be as high as 41.72% within those coarse-grained beds, which were predominantly sampled in the foreshore and contain abraded *Mercenaria* sp., *Crassostrea virginica*, and *Oliva sayana* shells and well-rounded oblate lithoclasts. The backshore is predominantly influenced by aeolian processes, which results in finer grained and better sorted sands there than in the foreshore. The shell beds that exist in the backshore were likely emplaced during storms and subsequently winnowed by aeolian processes (**Figure 11-10A**).

The beach facies ranges in thickness from 32 cm to greater than 204 cm (in places where the core was not long enough to sample the entire thickness). Cores from the southwest end of the island commonly sampled pieces of peat where this facies is thin, corresponding to the seismic and side-scan sonar data that imaged peat at shallow depths. Overall, the thickness of the beach facies decreases, and the percent gravel and the mean grain size of the sand fraction increases towards the southwest and from the toe of the foredune seaward. Rodriguez et al. (2012) also recognized those trends in sediment texture at Onslow Island from surface-sediment samples.

Dune Facies

The dune facies is a well-sorted, pale orange (10YR 8/2) fine-grained siliciclastic sand with highly spherical and rounded grains (**Figure 11-10B**). Sand-sized fragmented shell beds may be present but are generally only a few centimeters thick. These beds were likely emplaced during storm events and represent thin localized washover fans. Plant roots and organic detritus were sampled particularly near the top of the unit where dune grasses are present (**Figure 11-10B**). Steeply dipping heavy mineral cross laminae and bedding are common sedimentary structures preserved in the cores (**Figure 11-10B**) and are typical of coastal dunes (Davis, 1978). The mean grain size of the dune sand decreases slightly towards the northeast from 1.81 Φ at cross-section F1 to 2.30 Φ at cross-section F6. The thickness of this unit ranges from 83 cm to >274 cm and generally increases towards the northeast. Anthropogenically disturbed material was found at the top of three of the cores collected near roads that were constructed on the dunes.

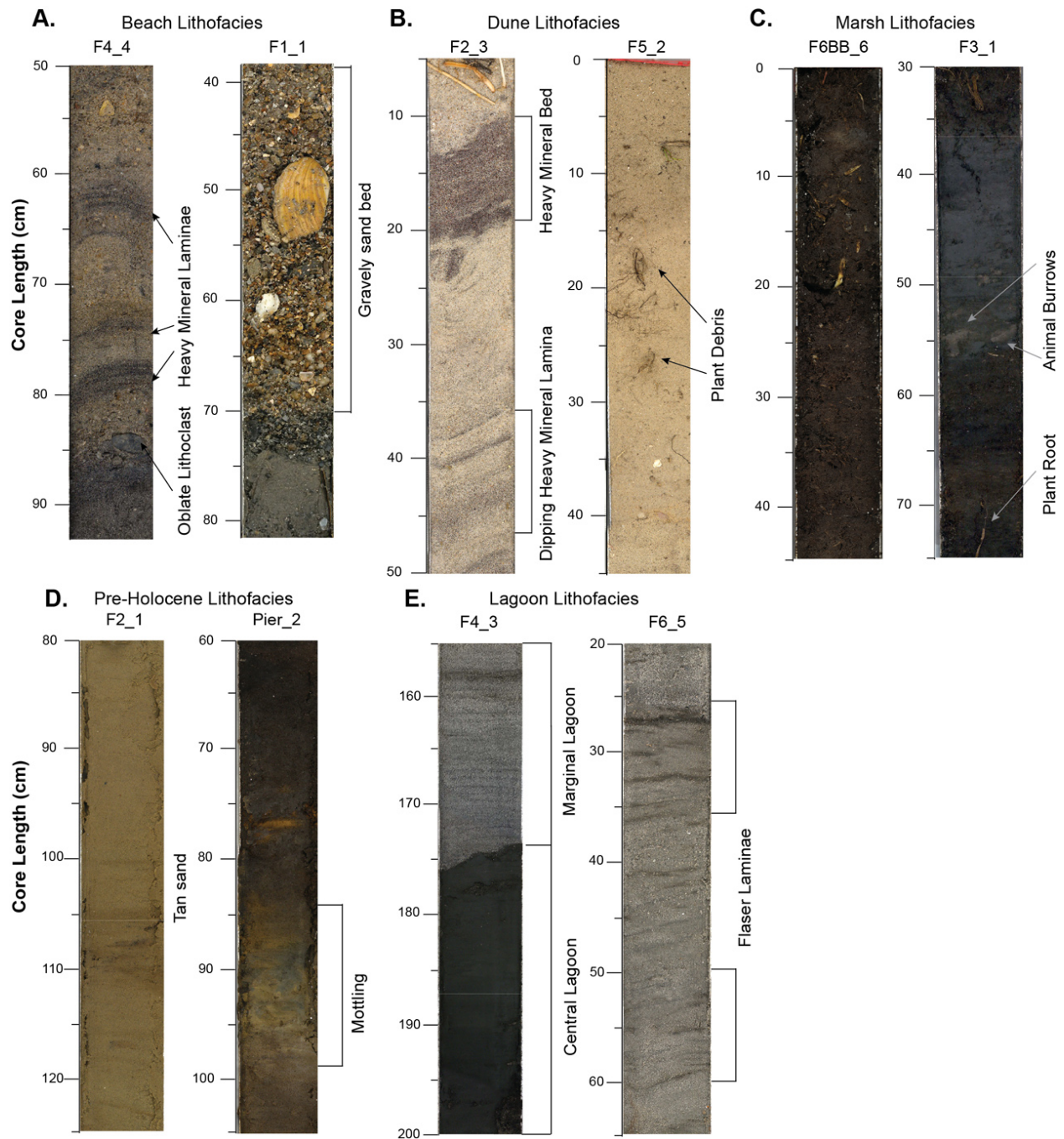


Figure 11-10. Lithofacies of depositional environments on Onslow Beach, NC.

Photographs of vibracores showing beach (A), dune (B), marsh, (C), pre-Holocene (D), and lagoon (E) lithofacies. Notice scale is in cm.

Marsh Facies

The marsh facies is an olive gray (5Y 3/2) to brownish gray (5YR 4/1) bioturbated (mixed by burrowing animals) carbonaceous muddy sand (**Figure 11-10C**). The fine sediment fraction is mainly produced by biogenic pelletization and settlement from suspension (Davis, 1978). Dense mats of *Spartina alterniflora* and *Juncus roemerianus* plant, roots and woody material contribute

to the organic carbon sediment fraction within the marsh facies, which can be as high as 74%. Marsh sediments have a mean grain size of 3.58 Φ and contain a sand component that is transported from the dunes by aeolian processes. The wind-blown sediment has a similar texture as the adjacent dunes and is recognized as discrete sand beds (3–15 cm thick) or is integrated with the organic-rich muddy sediment through heavy bioturbation. Active burrowing from backbarrier species such as fiddler crabs and mud crabs frequently destroy primary sedimentary structures that may be present, resulting in intermixed clay and fine sand (Staub and Cohen, 1979).

Washover Fan Facies

The washover fans that formed at the southwestern end of the island from Hurricanes Fran (September 1996) and Irene (August 2011) were each sampled by four cores in July 2010 (vibracores) and August 2011 (push cores), respectively. Cores were collected along a transect at each fan oriented from the landward edge of the backshore to the distal margin of the fan in the marsh. The proximal fan is closer to the beach and at a higher elevation than the distal fan. Although the cores displayed predominantly fine sand in sharp contact with the underlying marsh sediment, diverse hydraulic conditions and post-storm modifications resulted in lateral heterogeneity within the washover fan.

Proximal washover fan. This unit is pale yellowish brown (10YR 6/2), medium sand that has a fining-upward trend and is dominated by heavy-mineral laminae (**Figure 11-11**). Core F2wash_3, from the Irene washover fan, sampled this unit in its entirety and shows that the sand grain size increases from 1.87 Φ to 1.03 Φ and that the gravel content increases towards the base (Figure 11-11C). The basal gravelly sand beds are 15-17 cm thick, predominately composed of shell fragments and contain up to 7.18% gravel. Those beds are likely scour-lag deposits emplaced during high-energy conditions in the channel throat or mid-fan area (Leatherman and Williams, 1983). The heavy-mineral laminae were likely deposited as the result of swash and backwash of waves that followed the initial high-energy scouring. This facies is similar to the “stratified sand” and “normal-graded sand” subfacies identified by (Sedgwick and Davis, 2003).

Distal washover fan. This unit is light olive gray (5Y 6/1) to brownish gray (5YR 4/1) medium sand containing abundant sand-sized shell fragments (**Figure 11-12**). Heavy mineral sand laminae are present throughout causing grain-size measurements, obtained at 2-cm intervals, to alternate between approximately 1.5 and 2.0 Φ . This unit was likely deposited at intertidal to subtidal elevations and has a finer grain size than the proximal washover fan, which is likely due to reworking of backbarrier sediments during the overwash event and/or lower energy distal flow conditions. Sedgwick and Davis (2003) identified this subfacies as a “bioturbated muddy sand” unit. The lack of fine sand laminae or grading within the “bioturbated muddy sand” unit was related to intense bioturbation by backbarrier species (Sedgwick and Davis, 2003) that has yet to occur within the relatively young Irene and Fran fans (**Figure 11-12**). Over time, rapid marsh colonization may also take place, which would increase the fine sediment content, bioturbation, and organic matter content.

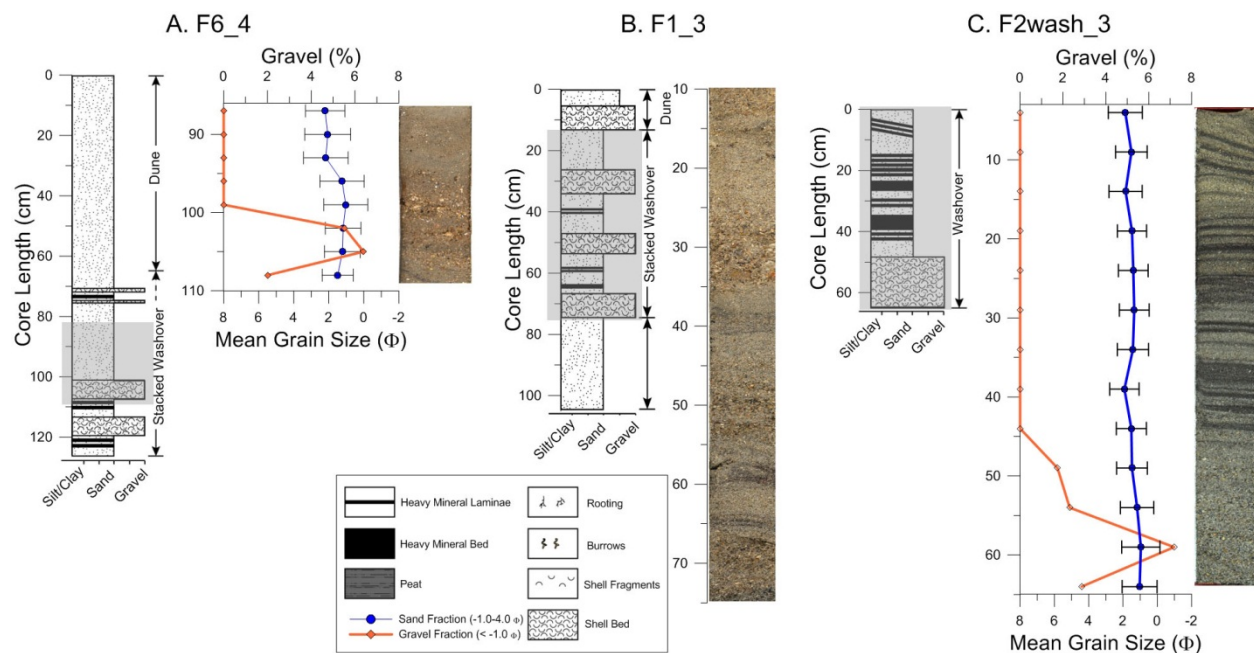


Figure 11-11. Proximal washover fan facies.

Facies examples from the northeastern transect (A), the Hurricane Fran washover fan (B), and the Hurricane Irene washover fan (C) on Onslow Beach, NC.

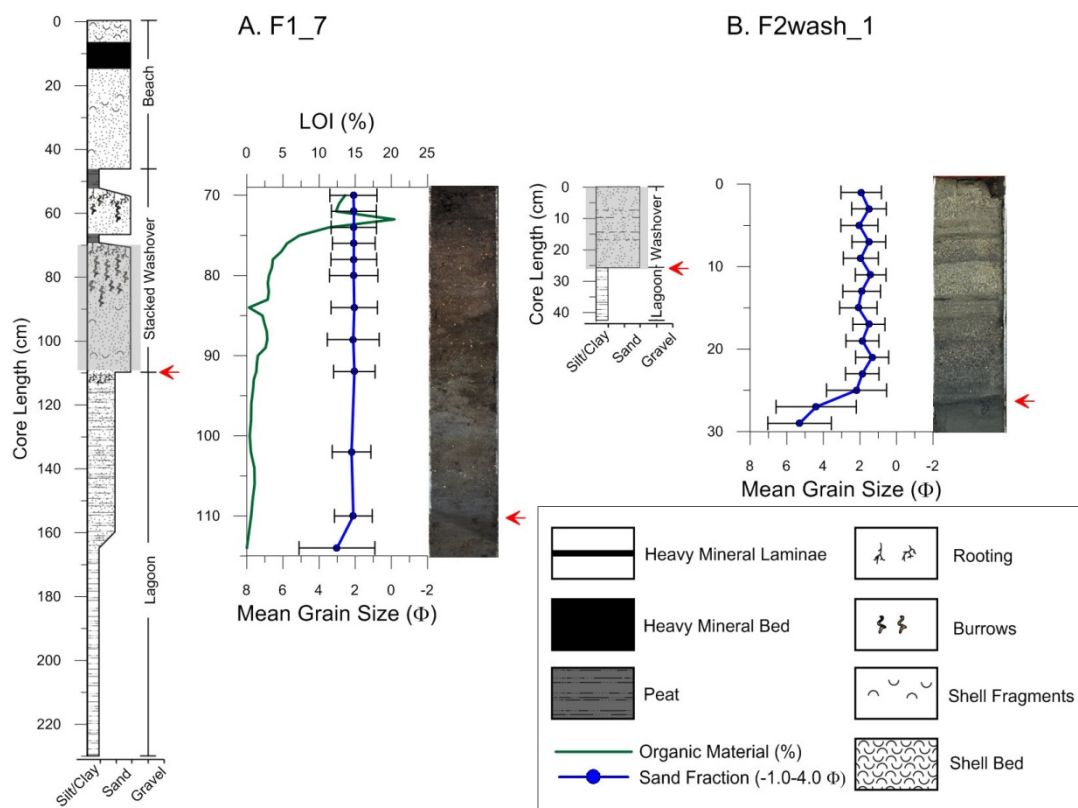


Figure 11-12. Distal washover fan facies.

Facies examples from the Hurricane Fran washover fan (A) and the Hurricane Irene washover fan (B) along Onslow Beach, NC.

Facies A (Lagoonal Depositional Environment)

Facies A was sampled below the previously described four facies in all transects except F2 and F2strike on Onslow Beach. This facies typically thickens seaward and in places is greater than 231-cm thick (some cores were not long enough to sample its entire thickness). The whole shells sampled in this unit were always backbarrier fauna such as stout tagelus (*Tagelus plebeius*), Eastern mudsnail (*Ilyanassa obsoleta*), Eastern oyster (*Crassostrea virginica*), and Baltic macoma clam (*Macoma balthica*). Facies A is composed of two lithologically distinct subfacies (i.e., A1 and A2).

Subfacies A1. This unit is medium light gray (N6) to olive gray (5Y 4/1) sand with silty laminae and was sampled by 17 cores (**Figure 11-10E**). The sediment is 97% sand with a mean grain size of 1.77 Φ . Flaser bedding (the clay-sand labeled on **Figure 11-10E**, Core F6_5) is common in this subfacies. Sand-sized shell fragments are common throughout the unit while gravel-sized shell fragments are only present as individual beds and can be up to 10-cm thick. These gravel beds are uncommon and were only found in three cores.

Based on the macrofauna and the flaser and gravel beds interpreted as tidal-bedding structures and tidal-channel lag deposits, respectively, this subfacies is interpreted as a marginal lagoon environment. The high sand fraction indicates bed-load transport by tidal currents and waves that can dominate the tidal flat zone (Davis, 1978). Sections of mud interbedded with sand are common within this subfacies and denote alternating bedload and suspension transport and deposition on the sand flats. Shell lag deposits imply scouring that is typically associated with tidal channels or storm deposits (Davis, 1978). This facies is currently being deposited adjacent to the barrier island in Bogue Sound, a shallow lagoon located approximately 40 km northeast of Onslow Beach (Timmons et al., 2010).

Subfacies A2. This unit is a light gray (N7) to grayish black (N2) mud with abundant articulated shells and sand burrows (**Figure 11-10E**, Core F3_3, bottom). Subfacies A2 has a greater mud fraction (61% mud) and is finer grained (mean grain size of 4.0 Φ) than A1. Lenticular (lens-shaped) sand beds up to 5-cm thick are occasionally present.

The high mud content, excellent preservation of estuarine fauna, and bioturbation indicates a low-energy, central lagoon environment. Molluscs commonly colonize in reefs within low-energy areas and an oyster reef was sampled in Core F1_5. Silt and fine sands accumulate from suspension while periodic high-energy tidal processes and/or storm events may deposit coarser-grained sand lenses (Davis, 1978). Sedimentary bedding is often disturbed in the central lagoon due to extensive bioturbation and reworking, resulting in a homogenous sandy mud (Reading, 2000). A silty clay unit with abundant *C. virginica*, similar to subfacies A2, was also sampled at the bottom of central Bogue Sound (Timmons et al., 2010).

Facies B (pre Holocene fluvial)

Facies B was sampled at the base of 14 cores and displays a wide range of textural characteristics that are distinct from those observed in the two lagoonal subfacies or in the modern depositional units. The cores did not penetrate the entire unit and facies B sediments were sampled at variable depths that generally decrease landward and towards the southwestern end of the island. This

facies is primarily composed of a massive moderate yellowish brown (10 YR 5/4) sand (**Figure 11-10D**) and is easily distinguished from beach facies by its distinct color, finer-grained texture (mean grain size of 2.19 Φ versus 1.75 Φ for the beach facies), and poorer sorting, which is caused by a minor silt component. Thin beds of well-rounded quartz pebbles within greenish gray (5 G 6/1) to medium gray (N5) or moderate brown (5 YR 3/4) sand were sampled underlying the massive yellowish brown fine sand. These beds could represent scour lag deposits of river channels when sea level was lower. Stiff light gray (N7) clay with yellow mottling is also indicative of oxidation and subaerial exposure. Sedimentary structures and organic material were absent within this basal unit. Although no material from Facies B was appropriate for radiocarbon dating, the homogenous, indurated, and oxidized nature of the upper part of the facies suggests subaerial exposure and the unit is interpreted to be pre Holocene (greater than 10,000 years) in age.

Stratigraphy

The stratigraphic cross-sections through Onslow Beach show a typical transgressive facies succession (**Figure 11-13**). The contact between the basal pre-Holocene unit (Facies B) and the overlying lagoonal mud (Facies A) is sharp and shows evidence of subaerial exposure and pedogenesis indicating that it is associated with a significant hiatus. This unconformity was sampled at variable depths and generally slopes seaward with high relief in the along-beach direction. It is interpreted to have formed during the last glacial maximum when sea level was approximately -120 m. The elevation of the sequence boundary strongly controls the thickness of overlaying Holocene coastal deposits (e.g., modern depositional facies). The sequence boundary is shallow (greater than 0 m NAVD88) in the middle of transect F2 where pre-Holocene strata outcrops in the foreshore but further to the southwest and northeast, the sequence boundary is at deeper elevations and overlain by thick (greater than 5 m) coastal deposits.

At transects F2strike, F2, and Pier, carbonaceous sand to sandy mud (20–90 cm thick) overlies the sequence boundary at depths shallower than approximately -1.50 m NAVD88 (**Figure 11-13**). That unit is interpreted as fringing marsh and/or maritime forest based on its similar lithology to the modern marsh facies sampled in transects F1BB and F6BB, the presence of wood, and its superposition above the upland pre-Holocene unit. It represents the leading edge of the Holocene marine incursion. Roots extend into the pre-Holocene strata and radiocarbon dates of wood found at the bottom and top of this marsh/maritime forest in the Pier transect are 3556–3728 cal years BP and 2156–2268 cal years BP, respectively (**Table 11-1**).

Where the sequence boundary is at a depth greater than -1.25 m NAVD88, it is overlain by lagoonal sands and mud. The sequence boundary is at a depth deeper than the cores reached in cross-sections F3 and F6 (**Figure 11-13**). The lagoonal unit is wedge-shaped and pinches out landward towards the modern backbarrier marsh, which is dictated by the paleotopography of the seaward-dipping sequence boundary. In addition to sea level changes, accommodation controlled by the antecedent topography (the sequence boundary) plays a large role in the timing of flooding along the island and the type of environment that is deposited above the sequence boundary.

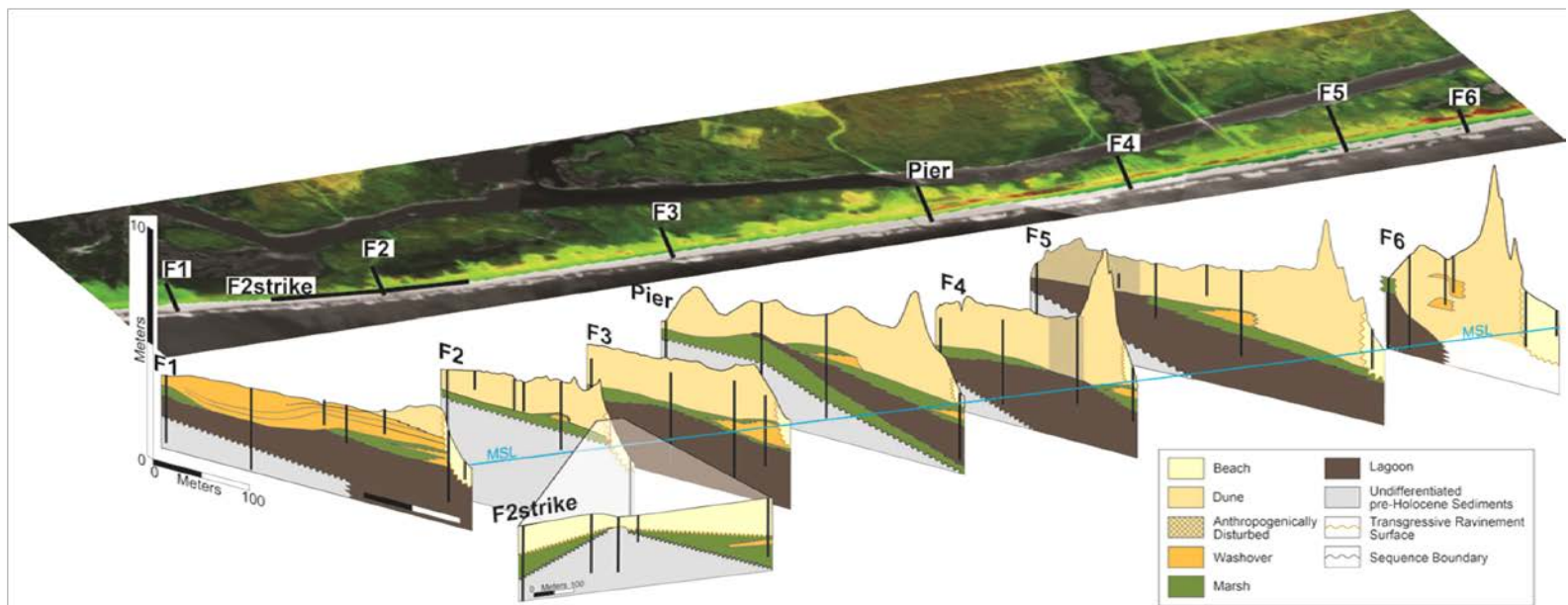


Figure 11-13. Fence diagram.

Cross-sections from the backbarrier marsh to the beach show along-beach variations in facies architecture on Onslow Beach, NC. Notice the large number of washover fans preserved in the stratigraphy (for more information, see Figure 11-6 and Appendix 11-A).

A natural lagoon does not exist behind Onslow Beach today because of the relatively steep topographic relief on the sequence boundary. At transect F2 and at the landward margin of the Pier transect, the pre-existing topographic highs prevented inundation during Holocene SLR, which resulted in the absence of a lagoon facies and only the presence of a thin fringing marsh and/or maritime forest facies preserved in the subsurface. Overall, the sequence boundary deepens towards the northeastern end of the island which increases local accommodation and permits thick lagoon sediments to accumulate and be preserved beneath the beach facies. Transects F1, F4, F5, and F6 show a sharp contact between pre-Holocene and lagoonal strata indicating that any fringing marsh and/or maritime forest that may have existed, was likely eroded away by bay-ravinement processes (waves and tidal currents). Lagoonal facies thicknesses of 224 cm or greater are common for the northern core transects (F5 and F6), but is also observed at F3, where there is a paleotopographic low (Figure 11-13). The high accommodation at transect F3 could be due to a low stand fluvial channel intersecting the island, which is imaged in seismic data offshore in that area and along adjacent barriers like Bogue Banks to the north (Timmons et al., 2010) and Wrightsville Beach to the south (Thieler et al., 2001).

Radiocarbon dating from the basal Holocene coastal deposits suggests a lagoon formed earlier in the southwest than the northeast part of the barrier system. An *M. constricta* valve, which is a common open-bay species (Andrews, 1981), sampled at the base of the lagoon facies at F1 was dated as 885–1003 cal yr BP. A date obtained from the middle of the lagoon at transect F5 was 902–931 cal yr BP and suggests a deep lagoon was already present at F5 when shallow-water sedimentation initiated at F1. Radiocarbon dates from the middle of the lagoon unit at F6 are 525–641 cal yr BP indicating that a lagoon existed landward of the barrier until at least approximately 600 years ago. Radiocarbon ages from the lagoon facies all fall below the estimated relative sea level for those time periods within error margins (Kemp et al., 2009).

Above the lagoon unit, a discontinuous organic-rich clay and peat unit, interpreted as a backbarrier marsh, was sampled. This marsh correlates with the present-day backbarrier marsh sampled at the landward margin of the transects. Due to compaction and decaying organic matter following burial, marsh sediments are preserved in the subsurface as dusky brown (5 YR 2/2) to black (N1) stiff carbonaceous mud with fine-grained organic matter. The marsh unit is absent where lagoonal sediments are directly overlain by the extensive washover fan at F1 and the aeolian dune at F6 and the unit was likely exhumed at those locations by storm and/or tidal ravinement processes. In addition, the marsh unit is missing at F5 and F4 where anthropogenic activities associated with road construction likely removed it.

Sharp-based fine sand beds ranging from 12–80 cm thick that pinch out in a landward direction are intercalated with the marsh unit at the seaward and middle parts of the transects. Based on textural and compositional similarities between these beds and the modern washover facies, the beds are interpreted to be the distal portions of relict washover fans; however, they have experienced some post-depositional modifications. These paleo-washover fans have a mean grain size 2.17Φ and have greater mud content (approximately 6%) than modern fans. Based on the fine-grained texture of these beds and association with salt marsh sediment they were likely emplaced in the intertidal zone and are interpreted as distal washover fan deposits. These sand beds were re-colonized by marsh vegetation, which was preserved as an overlaying carbonaceous mud bed. Heavily bioturbated sediments dominate the upper portion of the

washover deposit resulting in a mixed sediment of fine sand and organics which increases in organic carbon content from 3% 10-cm below the marsh unit to 20% at the contact in the marsh unit. Primary sedimentary structures, like the heavy mineral laminae observed in the distal portion of the modern Irene fan are rarely preserved in ancient distal washover units due to intensive bioturbation (Sedgwick and Davis, 2003).

The dune facies thickens towards the northeast from 83 cm at F2 to greater than 700 cm at F6 and overlies the backbarrier and lagoon sediments. Sharp-based medium-grained sand beds were sampled across 3 cores in the F1 transect overlying the Hurricane Fran washover fan and two cores behind the high-elevation dunes in the transect at F6. These beds have a mean grain size of 1.57Φ and become more fine-grained upward, with lower portions (5- to 10-cm thick) that contain up to 6.39% gravel and upper portions with heavy-mineral laminae and beds (**Figure 11-8**). Based on their similarity to modern washover facies, these beds are interpreted as proximal washover deposits that have experienced some post-depositional modification. Reworking by aeolian processes following deposition likely removed some upper heavy-mineral laminae and also transported dune sand that overlays those washover beds (**Figure 11-8**). At F1, the two washover beds merge at the distal end of the fan. At F6 the beds could not be traced laterally because they were only sampled with single cores. Washover fans are absent in cores collected from the modern backbarrier marsh. The leading edge of the shoreface ravinement surface located seaward of the dune is defined by the erosional truncation of the older units that extend beneath the beach and are exposed and eroding in the surf zone.

Timing of Washover Fan Emplacement

In addition to overwash, tidal currents, and aeolian processes are other major mechanisms for transporting sand to the backbarrier environment during transgression, but the sand layers sampled in the marsh preserved below the island are not interpreted as such. These sand beds could not have been generated within a flood-tidal delta due to the absence of deep scours and channels filled with gravel, representative of past inlets, as found along other barrier islands (Heron et al., 1984; Mallinson et al., 2011). Wind-blown sand beds, which were sampled below the present marsh surface, are distinguishable from washover sediments due to their finer grain size, massive bedding and overall thinness (less than 12 cm). Thus the sand beds preserved within the ancient marsh deposit beneath the island could only have been generated by episodic overwash sand deposition in a previous backbarrier marsh environment located seaward of the present-day backbarrier marsh. This microtidal, wave-dominated barrier island system migrated landward mainly by overwash processes.

Nine distinct distal washover fans were identified along the island (Appendix 11-A). Marsh sediments above and below the washover units were radiocarbon dated to determine the timing of overwash events. The age of the marsh below the fan is assumed to better constrain the timing of overwash than the age of marsh above the fan because of the possible long time lag between washover fan deposition and peat formation. The ages of the washover fans are all maximum ages. Along the Pier transect at the seaward margin of the island, marsh sediments above and below the washover fan are 644–724 and 1715–1833 cal yr BP, respectively. The two shoreward cores in the adjacent transect, F3, sampled a thick landward-thinning washover fan with its basal contact at a similar elevation as the washover fan sampled at the Pier transect, which suggests deposition during the same event, or close to the same time.

Ages of the marsh sediments below and above the washover fan sampled in Core F4_4 were 1293–1376 and 505–559 cal yr BP, respectively, and the washover fan sampled in Core F2strike_4 were 560–598 and 280–318 cal years BP, respectively (Table 11-1). At the seaward margin of F1, two distinct washover fans were sampled in the same core. The base of the lower washover fan is at a similar elevation as the base of the washover fan sampled in transect F5 and the base of the marsh unit sampled in transect F2, which are both within the 53–145 cal yr BP time frame (Table 11-1). It is assumed that the lower washover fan in transect F1 was also emplaced at that time. The age of the top washover fan in transect F1 was constrained from plant material in the underlying marsh layer, which was deposited within the past 77 years (post-bomb radiocarbon age). Washover fans were also sampled towards the middle of the island at transects F5, Pier, and F2. Our ^{14}C data of the marsh sediments directly underlying the fans sampled in Cores Pier_5 and F5_5 show that they were deposited by storm events within the nineteenth century. The washover fan sampled in Core F2_7 was likely deposited in the twentieth century based on a radiocarbon date of 55–145 cal yr BP from wood sampled at the base of the marsh and maritime forest unit sampled in Core F2_5 that is approximately 50 cm below the base of the washover fan.

Shoreline Movement at Decadal to Yearly Time Scales

At the decadal time scale (1935–2004), the southwestern part of Onslow beach has the highest shoreline retreat rates and these rates decrease towards the northeast where the beach is accreting (**Figure 11-14**). Although the rates of shoreline retreat at the decadal scale correspond overall with the measured annual rates (2007–2011), there are some differences. At the annual time scale, the central Onslow beach shoreline (military training zone) has the highest shoreline retreat rates (2–6 m of landward movement/year), but that area experienced much lower rates of shoreline retreat at the decadal time scale. Seaward movement (accretion) of the shoreline at yearly time scales in the southeast contrasts with the decadal record that shows high rates of erosion (2–4 m/yr; Figure 11-14).

Along-shore variability in rates of shoreline movement

Shoreline movement at millennial-centennial time scales

The internal facies architecture of Onslow Beach (**Figure 11-13**) varies along its 12-km length, similar to its geomorphology (**Figure 11-8**), suggesting that its landward retreat history was not uniform along the island. Deposition at the southwestern end of Onslow Beach was influenced by a pre-Holocene topographic high that correlates with the submarine limestone headland exposed on the inner shelf (shown on Figure 11-8). The Holocene record at this portion of the island is generally thin due to low accommodation, except at F3 in which a more complete sedimentary record is preserved in a paleochannel (Figure 11-10, Appendix 11-A). Basal lagoon sediments at the southwestern end of the island at transect F1 were deposited at the same time (~1000 cal yr BP) as sediment at the northeastern end of the island sampled in transect F5 from the middle of the lagoon facies. This indicates that the initial flooding of the southwestern end of the island occurred as the lagoon was already well established on the northeastern end.

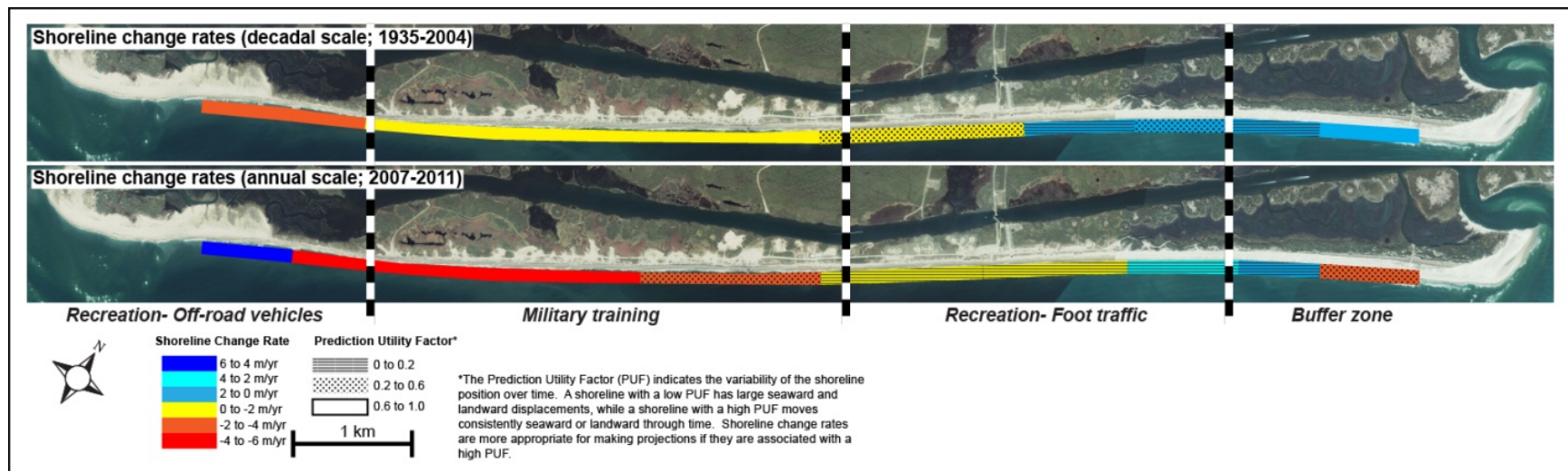


Figure 11-14. Decadal and annual rates of shoreline movement along the various zones on Onslow Beach, NC.

In addition, marsh sediment that was radiocarbon dated as 1292–1376 cal yr BP and 1715–1832 cal yr BP was sampled above the lagoon facies in transects F4 and Pier, respectively, indicating that a lagoon existed at the northern part of the study area for greater than 1,000 years before the southern area of Onslow Beach was inundated. The variable timing of backbarrier lagoon emplacement along the island is a consequence of the greater accommodation (lower elevation pre Holocene surface) at the northern end of the region. Variations may also be due to the variable preservation of lagoon deposits along the island, which is related to rates of island transgression. The lagoonal deposits being younger in the south than the north could be due to the rates of shoreline transgression being higher in the south than the north over 1,000 years ago. Higher rates of transgression in the south would have eroded those older lagoon deposits situated in an offshore location. Alongshore variability in shoreline migration rates may be linked to local offshore sand sources at the northeastern end of the island, but the lack of preservation of paleo ocean-shoreline indicators limits our ability to quantify shoreline-retreat rates at long time scales (millennial).

The oldest washover fan was emplaced approximately 1,800 cal yr BP at Onslow Beach, indicating the island was close to its present position at that time and was separated from the mainland by an open-water lagoon. Onslow Beach exhibited landward retreat via recurring overwash events along the entire length of the island during the late Holocene. More regionally, the overwash-dominated barrier islands of southwestern Onslow Bay that comprise the high-energy flank of the Cape Fear foreland (east facing; Cleary and Hosier, 1979) have a similar transgressive history as Onslow Beach. Radiocarbon ages of peat sampled beneath Masonboro Island, southwest of Onslow Beach, are 902–1066 and 545–797 cal yr BP. These ages are similar to the dates from the peat underlying Onslow Beach revealing a rapid transgressive history of Masonboro Island. The inner shelf of southwestern Onslow Bay is sediment-starved and dominated by rock outcrops (Thieler et al., 2001), similar to the southwestern end of Onslow Beach.

Onslow Beach and Masonboro Island reached their present positions within the past approximately 1,000 years and are considerably younger than the barriers in northeast Onslow Bay. The barrier islands on the lower energy limb south of Cape Lookout such as Bogue Banks, have a history of progradation as evidenced by a higher, wider profile with multiple beach ridges which are younger in a seaward direction (Cleary and Hosier, 1979; Heron et al., 1984; Timmons et al., 2010). The oldest beach ridge on Bogue Banks formed approximately 3,300 years ago, and lagoon sediments sampled in the center of Bogue Sound are approximately 5,500 cal yr BP. During the Holocene, the northeastern barriers along Onslow Bay retreated at a slower rate, a shorter distance and reached their current positions approximately 1,300 years before the central-southeastern barriers, including Onslow Beach. The young radiocarbon ages and resultant rapid retreat rates in central Onslow Bay, from our stratigraphic data, supports the Ashton et al. (2001) prediction that the highest shoreline retreat rates should occur in the central embayment areas between capes at centennial to millennial time scales.

Shoreline Movement at Decadal to Yearly Time Scales

The geologic record (based on the vibracores) suggests that the southwestern part of Onslow Island moved landward more rapidly than the northeastern part of the island over the past 1,000–2,000 years, which generally corresponds to the pattern of shoreline movement along Onslow

Beach at the decadal and yearly time scales. Along-beach variations in shoreline-change rates at sub-centennial time scales are principally controlled by variations in the underlying framework geology. A rock ridge intersecting the shore where military training occurs forms a headland resulting in a steeper beachface there than in the adjacent embayments. The military training zone has the highest annual shoreline retreat rates (2–6 m of landward movement per year), but high shoreline change rates existed prior to Base operations (pre-1940s) and are likely related to the sediment supply and storage of this island compartment being low, as evidenced by the thin sand veneer that exists at the beach and nearshore above older less erosive sedimentary units. The region of highest decadal shoreline retreat extends southwest of the training zone and the geological record shows that this erosional hotspot existed long before the Base was established. The shoreline in the recreational zone where foot traffic is the main anthropogenic impact is moving seaward (accretion) at less than 1 to 4 m/yr (**Figure 11-14**). Unlike the military training zone, this northeastern third of the island shows high variability in the direction and magnitude of shoreline movement at annual and decadal time scales, but overall displays long-term accretion. The southwestern third of Onslow Beach, conversely, has exhibited sustained landward migration (beach erosion) over both short and long time periods (**Figure 11-14**).

Impacts of Changes in Storminess and the Rate of SLR on Island Evolution

Storms have played an important role in the evolution of Onslow Beach over at least the past approximately 1,800 years. Island overwash principally occurs during storms and deposits a washover fan. The landward extent of the washover fan is dependent upon the size of the storm and the morphology of the island. Generally, larger storms produce larger washover fans and low-elevation barriers are more vulnerable to overwash than high-elevation barriers. The landward pinch out of the relict and modern washover fans that impacted the backbarrier marsh at Onslow Beach was measured against a baseline, which is the best-fit linear regression through the 2006 shoreline, digitized from a rectified aerial photograph (**Figure 11-15**). Older washover fans are positioned closer to the baseline than younger washover fans, which correspond with the open-ocean and backbarrier shorelines continually moving landward throughout the late Holocene. All of the paleo-washover fans addressed here impacted the backbarrier marsh and became colonized with new marsh suggesting that emplacement was the result of large events like recent hurricanes Fran and Irene. Smaller events can overwash the island, but typically only impact the dune or older washover fans as sampled in the dune and washover facies in transects F6 and F1, respectively (**Appendix 11-A**). Those smaller washover fans are not included in Figure 11-15 because those events did not displace the backbarrier shoreline landward. Although the morphology of the barrier varies significantly from the southwest to the northeast today, paleo-washover fans were sampled along the entire island, even from areas where the modern dunes are high and continuous (transect F5), supporting the fact that tall dunes can accrete or erode over sub-millennial time scales.

At millennial time scales, SLR is another important factor that determines the landward extent of washover fans. If sea level rose at a constant rate during the late Holocene, all else being equal (island morphology, storminess and preservation), then a plot of the landward pinch out of washover fans through time would also be linear and would match the rate of island transgression. Figure 11-15 shows that the landward pinch-out distance of washover fans increases sharply at around 1850 A.D. More washover fans that moved the backbarrier shoreline landward formed along Onslow Beach over the past approximately 150 years (seven washover

fans) than the preceding approximately 1650 years (four washover fans) and the more recent fans extend two to four times farther landward than the older fans (**Figure 11-15**). This trend could be explained by an increase in storminess or acceleration in the rate of SLR.

The earliest washover fans preserved in our sedimentary record were emplaced approximately 200 A.D. (transects F3 and Pier; Appendix 11-A) indicating that the island was near its current position at that time. Four washover fans were sampled that formed between 200 A.D. and 1375 A.D. and indicate that the island was likely migrating landward at a relatively slow rate because the landward extent of those fans did not increase more than 60 m over that 1175-year time period. Correspondingly, sea level was rising at a very low rate at that time (1–1.4 mm/yr; Kemp et al., 2011). The MWP (approximately 800–1300 A.D.) was a time of increased tropical storm landfall along the U.S. Atlantic Coast (Mann et al., 2009) that resulted in increased erosion along the lagoon side of Bogue Banks, NC (Timmons et al., 2010) and island “collapse” and inlet formation along the northern Outer Banks (Culver et al., 2007; Mallinson et al., 2011). No evidence exists along Onslow Beach for increased erosion or washover fan formation during that time period; however, it is possible that washover fans were emplaced between our sampling sites during the MWP.

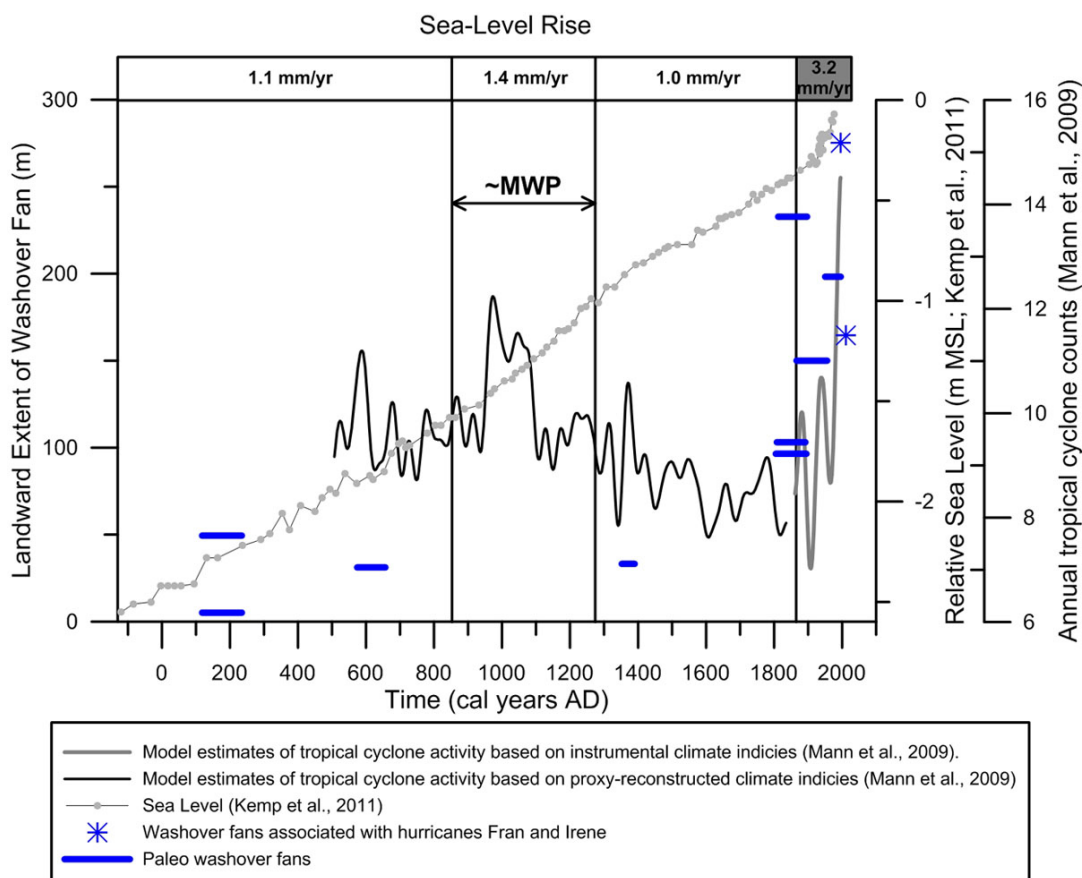


Figure 11-15. Record of washover fans along Onslow Beach, NC.

The number and landward extent of washover fans increases sharply along the island at approximately 1850 A.D. The width of the blue line indicates the uncertainty in the age of the paleo washover fan.

The Slott et al. (2006) numerical model simulation of the cumulative effects of increased tropical and extra-tropical storms predicts that cusate bays will erode at increased rates while the cape tips will accrete at centennial time scales. In response to the increase in storminess during the MWP at Onslow Beach, neither the number of washover fans nor the rate of island transgression increased; however, we cannot discount that some washover fans from that time period were not preserved and/or sampled along the island. Bogue Banks, located on the southern flank of Cape Lookout, experienced rapid erosion of the backbarrier shoreline during the MWP that caused the island to narrow at its center (Timmons et al., 2010); however, it is unclear if the ocean shoreline experienced accretion as predicted by the numerical model. An obvious increase in shoreline transgression at Onslow Beach and regression at Bogue Banks was not associated with the increase in storminess during the MWP as predicted by the Slott et al. (2006) model.

Possible discrepancies between model predictions and coastal impacts from increased storminess during the MWP along Onslow Bay could lie in the model assumptions that wave-driven alongshore forcing is the dominant mechanism for sediment transport and the sea floor is composed of unconsolidated sand. In the barrier-lagoon complexes that dominate the North Carolina coast, the significant role of cross-shore sediment transport is evident in the abundant relict washover fans and tidal inlets that this study and many others have mapped (Mallinson et al., 2011; Moslow and Heron, 1978). Overwash and inlet processes are two primary mechanisms that control island widening and the removal of sediment from the active littoral zone and deposition into the backbarrier environment. These processes were not factored into the Slott et al. (2006) model and are driven by rising sea level and storms. During periods of increased storm activity, sediment lost from the active system cannot be delivered to the cusate foreland region in its entirety. In addition, the entire shoreface is not composed of unconsolidated sandy sediment and the inherited geologic framework, in part controls sediment supply and accommodation in Onslow Bay due to the shallow limestone rock outcrops on the shelf near Onslow Beach and sandy paleochannels offshore of Bogue Banks (Timmons et al., 2010).

The past approximately 150 years, when the number and landward extent of washover fans increased along Onslow Beach does fall within the Little Ice Age (approximately 1400 A.D.–1900 A.D.), a time when tropical storm activity was at a low (Mann et al., 2009; **Figure 11-15**), but nor'easters along the US Atlantic coast may have been more intense (Mallinson et al., 2011). Intense nor'easters during the Little Ice Age are thought to have caused the formation of large inlet complexes along the northern Outer Banks but most of those inlets formed around 1400 A.D.–1700 AD., at least 150 years earlier than the washover fans preserved along Onslow Beach. In addition, Onslow Beach is southeast facing and thought to be impacted less from nor'easters than the Outer Banks north of Cape Hatteras, which are east-northeast facing (Mallinson et al., 2011). It is unlikely that more intense nor'easters played a role in the increased number and landward extent of washover fans emplaced along Onslow Beach over the past approximately 150 years than the previous 1,700 years.

The rate of relative SLR increased at 1865–1892 A.D. from 1 mm/yr to 3.2 mm/yr (Kemp et al., 2011), the same time as the number and landward extent of washover fans increased along Onslow Beach. This sharp increase in the rate of SLR likely had an immediate effect on the vulnerability of Onslow Beach to overwash. Higher sea level causes increased dune erosion lowering the elevation of an island and increasing its potential to overwash. Because overwash is the mechanism for island transgression, the rate that the open-ocean and backbarrier shorelines

were moving landward also increased approximately 1850 A.D. This increased rate of island transgression also decreased the preservation of older washover fans, including those that may have been associated with the MWP, especially along the southwest part of the island where shoreline retreat rates were most rapid.

Conclusions and Implications for Future Research

Onslow Beach is a transgressive barrier island that moved landward during the late Holocene principally through overwash processes and washover fan formation. The oldest washover fan deposits preserved in the stratigraphy of the island are approximately 200 A.D. indicating that the island has been close to its present position since that time. Around 200 A.D. an open-water lagoon separated Onslow Beach from the mainland, as opposed to marshes and tidal channels that have characterized the backbarrier landscape since at least 1850 A.D. Assuming that the oldest washover fans were similar in size to the largest modern washover fan, which was emplaced during Hurricane Fran, then the coeval ocean shoreline would be located approximately 300 m seaward of its present location at approximately 200 A.D. Because the landward extent of washover fans was fairly constant 200 A.D.–1850 A.D., the rate of island transgression was also likely low during that period (0.2 m/yr), which corresponds to the low rates of SLR that the North Carolina coastline was experiencing (1–1.4 mm/yr; Kemp et al., 2011).

At around 1850 AD, the number and landward extent of washover fans increased sharply along the entire island. This corresponds to an increase in the rate of SLR to 3.2 mm/yr and a low number of annual tropical cyclones in the Atlantic (Kemp et al., 2011; Mann et al., 2009). The increase in number and landward extent of washover fans at 1850 A.D. also implies that the rate of island transgression increased. The increase in the rate of SLR likely lowered the elevation of the island principally through erosion of the dunes, and made the island more vulnerable to overwash. These data suggest that Onslow Beach is extremely sensitive to increases in the rate of SLR, which cause an immediate decrease in the elevation of the island and its resistance to overwash. This sensitivity is likely the result of the island being sediment starved, a product of its framework geology (limestone outcropping near the shoreface) and its location at the center of a coastal embayment (Ashton et al., 2001).

Given that the rate of SLR is predicted to increase in the next 100 years, it is appropriate to use our data across the most recent increase in the rate of SLR at 1850 A.D. as an analog to future changes. Our recommendation is that the Base needs to plan for an increase in the frequency and magnitude of overwash events, regardless of future changes in storminess, which will occur as higher sea levels increase dune erosion and lower the elevation of the island making it more vulnerable to overwash. Currently, the island is most vulnerable to overwash in the southwest where elevation is lowest, annual erosion rates are high, sediment supply is low, and accommodation is low. Differences between the northeastern and southwestern parts of the island are principally due to the high elevation of pre-Holocene rock and sediment that is erosion resistant in the southwest. The distance between the ocean and the ICW is also smallest in the southwest, indicating the waterway may be impacted by overwash in the near future (see results of Research Project CB-1). Given the high rates of landward shoreline movement at the center of the island and the narrow dunes, soon (1–20 years) the island will overwash there again, as it did in approximately 1850 A.D. We recommend that if MCBCL has plans to build additional

permanent structures or modify existing structures located on the dunes, they recognize that the vulnerability of these sites to inundation will increase in the near future (within the next 10–20 years). Depending on the construction project, it might be more prudent to place additional infrastructure further landward than the existing bathhouses and cottages are located today. In addition, the Base should plan to increase expenditure for post-storm clean up on the island.

Military training activities have little impact on island evolution because the decadal record of shoreline movement and the geological record of island evolution show that the military training zone has been vulnerable to overwash and experienced high rates of shoreline retreat since at least 1850 A.D., long before MCBCL existed. High rates of shoreline retreat at the military training zone (the “erosional hot spot”) is due to the low sediment supply there as compared to the northeastern part of the island where nearshore sand thicknesses are greater. The limestone outcrops located seaward of the military training zone are not producing enough new sediment through bioerosion to compensate for the erosion there. Yearly rates of shoreline retreat at the military training zone, based on November 2007–September 2011 measurements and the resulting model (**Figure 11-14**), are up to four times higher than the decadal rates. The magnitude of the difference between the yearly and decadal retreat rates is too large to be explained by error differences between the methods (aerial photography for the decadal record and terrestrial laser scanning for the yearly record). The increase is also difficult to explain because the time period 2007–2011 was not stormier than previous time periods and island management did not change. However, there was an anomalous increase in water level in 2009 when sea level was approximately 20 cm higher than predicted (Sweet and Zervas, 2011; Sweet et al., 2009). Future work needs to focus on that event because if that brief sea level anomaly is the cause for the high rates of shoreline retreat recorded between 2007 and 2011, then the island could be even more sensitive to SLR than the geological record indicates.

Literature Cited

- Andrews, J. 1981. *A Field Guide to Shells of the Texas Coast*. Gulf Publishing Company, Houston.
- Ashton, A., A.B. Murray, and O. Arnault. 2001. Formation of coastline features by large-scale instabilities induced by high-angle waves. *Nature* 414:269–300.
- Ashton, A.D., and A.B. Murray. 2006. High-angle wave instability and emergent shoreline shapes: 1. Modeling of sand waves, flying spits, and capes. *Journal of Geophysical Research: Earth Surface* 111, F04011. (19 pages).
- Belknap, D.F., and J.C. Kraft. 1985. Influence of antecedent geology on stratigraphic preservation potential and evolution of Delaware's barrier systems. *Marine Geology* 63:235–262.
- Benton, S.B., C.J. Bellis, J.M. Knisel, M.F. Overton, and J.S. Fisher. 2004. *1998 Long-Term Average Annual Erosion Rate Update: Methods Report*. (23 pages). North Carolina Division of Coastal Management, North Carolina Coastal Resources Commission.
- Boggs, S. 2001. *Principles of Sedimentology and Stratigraphy*. Prentice Hall: Upper Saddle River.
- Browder, A.G., and J.E. McNinch. 2006. Linking framework geology and nearshore morphology: Correlation of paleo-channels with shore-oblique sandbars and gravel outcrops. *Marine Geology* 231:141–162.
- Cleary, W.J., and P.E. Hosier. 1979. Geomorphology, washover history and inlet zonation: Cape Lookout to Bird Island, North Carolina. Pp. 237–271 in *Barrier Islands Gulf of St. Lawrence to the Gulf of Mexico*. Edited by S.P. Leatherman. Academic Press: New York, NY.
- Cleary, W.J., and O.H. Pilkey. 1996. Environmental coastal geology: Cape Lookout to Cape Fear, North Carolina regional overview. Pp. 87–128 in *Environmental Coastal Geology: Cape Lookout to Cape Fear, NC*. Edited by W.J. Cleary. Carolina Geological Society Fieldtrip Guidebook.
- Culver, S.J., C.A. Grand Pre, D.J. Mallinson, S.R. Riggs, D.R. Corbett, J. Foley, M. Hale, L. Metger, J. Ricardo, J. Rosenberger, C.G. Smith, C.W. Smith, S.W. Snyder, and D. Twamley. 2007. Late Holocene barrier island collapse: Outer Banks, North Carolina, USA. *The Sedimentary Record* 5:4–8.
- Davis, R.A. 1978. *Coastal Sedimentary Environments*. Springer-Verlag: Berlin, Germany.
- Donnelly, J.P., P. Cleary, P. Newby, and R. Ettinger. 2004. Coupling instrumental and geological records of sea-level change: Evidence from southern New England of an increase in the

- rate of sea-level rise in the late 19th century. *Geophysical Research Letters* 31, GL018933.
- Foxgrover, A.C. 2009. Quantifying the overwash component of barrier island morphodynamics: Onslow Beach, NC. Unpublished Master's thesis. The College of William and Mary, Williamsburg, VA.
- Gressly, A. 1838. Observations géologiques sur le Jura Soleurois. *Bulletin de la Société neucheloise des sciences naturelles* 2:1–112.
- Guibas, L., and J. Stolfi. 1985. Primitives for the manipulation of general subdivisions and the computation of Voronoi diagrams. *ACM Transactions on Graphics* 4:74–123.
- Harris, W.B., S. Mendrick, and P.D. Fullagar. 2000. Correlation of onshore-offshore Oligocene through lower Miocene strata using $^{87}\text{Sr}/^{86}\text{Sr}$ isotopic ratios, north flank of Cape Fear Arch, North Carolina, USA. *Sedimentary Geology* 134:49–63.
- Heiri, O., A.F. Lotter, and G. Lemcke. 2001. Loss on ignition as a method for estimating organic and carbonate content in sediments: Reproducibility and comparability of results. *Journal of Paleolimnology* 25:101–110.
- Heron, D.S., T.F. Moslow, W.M. Berelson, J.R. Herbert, G.A.I. Steel, and K.R. Susman. 1984. Holocene sedimentation of a wave-dominated barrier island shoreline: Cape Lookout, North Carolina. *Marine Geology* 60:413–434.
- Johnston, M.K. 1998. *The Inherited Geologic Framework of the New River Submarine Headland Complex, North Carolina, and Its Influence on Modern Sedimentation*. University of North Carolina, Wilmington, NC. (166 pages).
- Kemp, A.C., B.P. Horton, J.P. Donnelly, M.E. Mann, M. Vermeer, and S. Rahmstorf. 2011. Climate related sea-level variations over the past two millennia. In *Proceedings of the National Academy of Sciences*.
- Kemp, A.C., B.P. Horton, D. Reide Corbett, S.J. Culver, R.J. Edwards, and O. van de Plassche. 2009. The relative utility of foraminifera and diatoms for reconstructing late Holocene sea-level change in North Carolina, USA. *Quaternary Research* 71:9–21.
- Komar, P.D. 1976. *Beach Processes and Sedimentation*. Prentice-Hall: Englewood Cliffs.
- Kraft, J.C. 1971. Sedimentary facies patterns and geologic history of a Holocene marine transgression. *Geological Society of America Bulletin* 82:2131–2158.
- Krumbein, W.C., and L.L. Sloss. 1963. *Stratigraphy and Sedimentation*. Freeman: San Francisco, CA.

- Lanesky, D.E., B.W. Logan, R.G. Brown, and A.C. Hine. 1979. A new approach to portable vibracoring underwater and on land. *Journal of Sedimentary Research* 49:654–657.
- Lawson, C.L. 1977. Software for C1 surface interpolation. Pp. 161–193 in *Mathematical Software III*. Edited by J. Rice. Academic Press: New York, NY.
- Leatherman, S.P., and A.T. Williams. 1983. Vertical sedimentation units in a barrier island washover fan. *Earth Surface Processes and Landforms* 8:141–150.
- Lee, D.T., and B.J. Schachter. 1980. Two algorithms for constructing a Delaunay triangulation. *International Journal of Computer and Information Sciences* 9:219–242.
- Mallinson, D.J., C.W. Smith, S. Mahan, S.J. Culver, and K. McDowell. 2011. Barrier island response to late Holocene climate events, North Carolina, USA. *Quaternary Research* 76:46–57.
- Mann, M.E., J.D. Woodruff, J.P. Donnelly, and Z. Zhang. 2009. Atlantic hurricanes and climate over the past 1,500 years. *Nature* 460:880–883.
- Moslow, T.F., and D.S. Heron. 1978. Relict inlets: preservation and occurrence in the Holocene stratigraphy of southern Core Banks, North Carolina. *Journal of Sedimentary Petrology* 48:1275–1286.
- NOAA (National Oceanic and Atmospheric Administration). 2012. Historical Hurricane Tracks. Available at csc.noaa.gov/hurricanes. Accessed August 27, 2012.
- Pierce, J.W., and D.J. Colquhoun. 1970. Holocene evolution of a portion of the North Carolina Coast. *Geological Society of America Bulletin* 81:3697–3714.
- Reading, H.G. 2000. *Sedimentary Environments: Processes, Facies and Stratigraphy*. Blackwell Science: Oxford.
- Riggs, S.R., W.J. Cleary, and S.W. Snyder. 1995. Influence of inherited geologic framework on barrier shoreface morphology and dynamics. *Marine Geology* 126:213–234.
- Rodriguez, A.B., J.B. Anderson, F.P. Siringan, and M. Taviani. 2004. Holocene evolution of the east Texas coast and inner continental shelf: Along-strike variability in coastal retreat rates. *Journal of Sedimentary Research* 74:406–422.
- Rodriguez, A.B., P.L. Rodriguez, and S.R. Fegley. 2012. One-year along-beach variation in the maximum depth of erosion resulting from irregular shoreline morphology. *Marine Geology* 291:12–23.
- Scott, D.B., E.S. Collins, P.T. Gayes, and E. Wright. 2003. Records of prehistoric hurricanes on the South Carolina coast based on micropaleontological and sedimentological evidence,

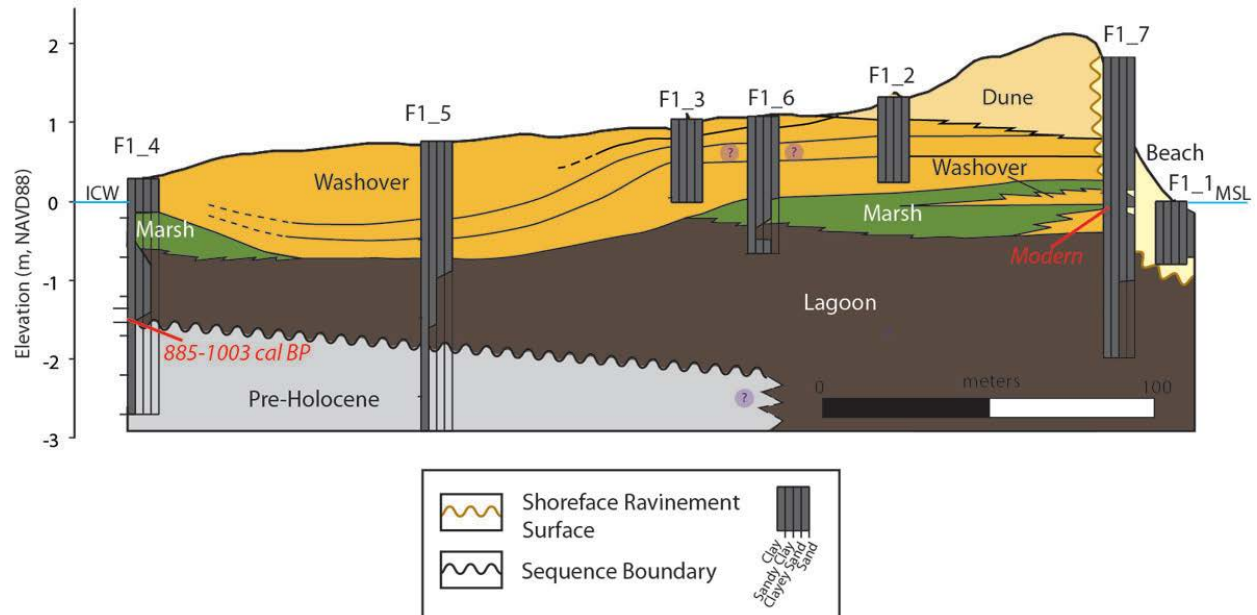
- with comparison to other Atlantic Coast records. *Geological Society of America Bulletin* 115:1027–1039.
- Sedgwick, P.E., and R.A. Davis Jr. 2003. Stratigraphy of washover deposits in Florida: Implications for recognition in the stratigraphic record. *Marine Geology* 200:31–48.
- Slott, J.M., A.B. Murray, A.D. Ashton, and T.J. Crowley. 2006. Coastline responses to changing storm patterns. *Geophysical Research Letters* 33, L18404. (6 pages).
- Staub, J.R., and A.D. Cohen. 1979. The Snuggedy Swamp of South Carolina, a back-barrier coal forming environment. *Journal of Sedimentary Petrology* 49:133–144.
- Stuiver, M., and P.J. Reimer. 1993. Extended ^{14}C database and revised CALIB radiocarbon calibration program. *Radiocarbon* 35:215–230.
- Sweet, W.V., and C. Zervas. 2011. Cool-season sea level anomalies and storm surges along the U.S. East Coast: Climatology and comparison with the 2009/10 El Niño. *Monthly Weather Review* 139:2290–2299.
- Sweet, W.V., C. Zervas, and S. Gill. 2009. *Elevated East Coast Sea Level Anomaly: July–July 2009*. (30 pages). National Oceanic and Atmospheric Administration Technical Report National Ocean Service, Center for Operational Oceanographic Products and Services, Silver Spring, MD. Available at http://tidesandcurrents.noaa.gov/publications/EastCoastSeaLevelAnomaly_2009.pdf.
- Theuerkauf, E.J., and A.B. Rodriguez. 2012. Impacts of transect location and variations in along-beach morphology on measuring volume change. *Journal of Coastal Research* 28(3):707–718.
- Thieler, E.R., and A.D. Ashton. 2011. Cape capture: Geologic data and modeling results suggest the Holocene loss of a Carolina Cape. *Geology* 39:339–342.
- Thieler, E.R., E.A. Himmelstoss, J.L. Zichichi, and A. Ergul. 2009. Digital Shoreline Analysis System (DSAS) version 4.0—An ArcGIS extension for calculating shoreline change. In *U.S. Geological Survey Open-File Report 2008-1278*.
- Thieler, E.R., O.H. Pilkey Jr., W.J. Cleary, and W.C. Schwab. 2001. Modern sedimentation on the shoreface and inner continental shelf at Wrightsville Beach, North Carolina, USA. *Journal of Sedimentary Research* 71:958–970.
- Timmons, E.A., A.B. Rodriguez, C.R. Mattheus, and R. DeWitt. 2010. Transition of a regressive to a transgressive barrier island as a function of back-barrier erosion, climate change, and low sediment supply, Bogue Banks, North Carolina, USA. *Marine Geology* 278:100–114.

- Valvo, L., A.B. Murray, and A. Ashton. 2006. How does underlying geology affect coastline change? An initial modeling investigation. *Journal of Geophysical Research* 111, F02025. (18 pages).
- Weber, K.M., J.H. List, and K.L.M. Morgan. 2005. An operational mean high water datum for determination of shoreline position from topographic LiDAR data. In *U.S. Geological Survey Open-File Report 2005-1027*. U.S. Geological Survey.
- Wilkinson, B.H., and R.A. Basse. 1978. Late Holocene history of the central Texas coast from Galveston Island to Pass Cavallo. *Geological Society of America Bulletin* 89:1592–1600.
- Woolard, J.W. 1999. *Volumetric change of coastal dunes using airborne LiDAR, Cape Hatteras National Seashore, North Carolina*. East Carolina University, Greenville, NC. (218 pages)
- Woolard, J.W., and J.D. Colby. 2002. Spatial characterization, resolution, and volumetric change of coastal dunes using airborne LiDAR: Cape Hatteras, North Carolina. *Geomorphology* 48:269–287.

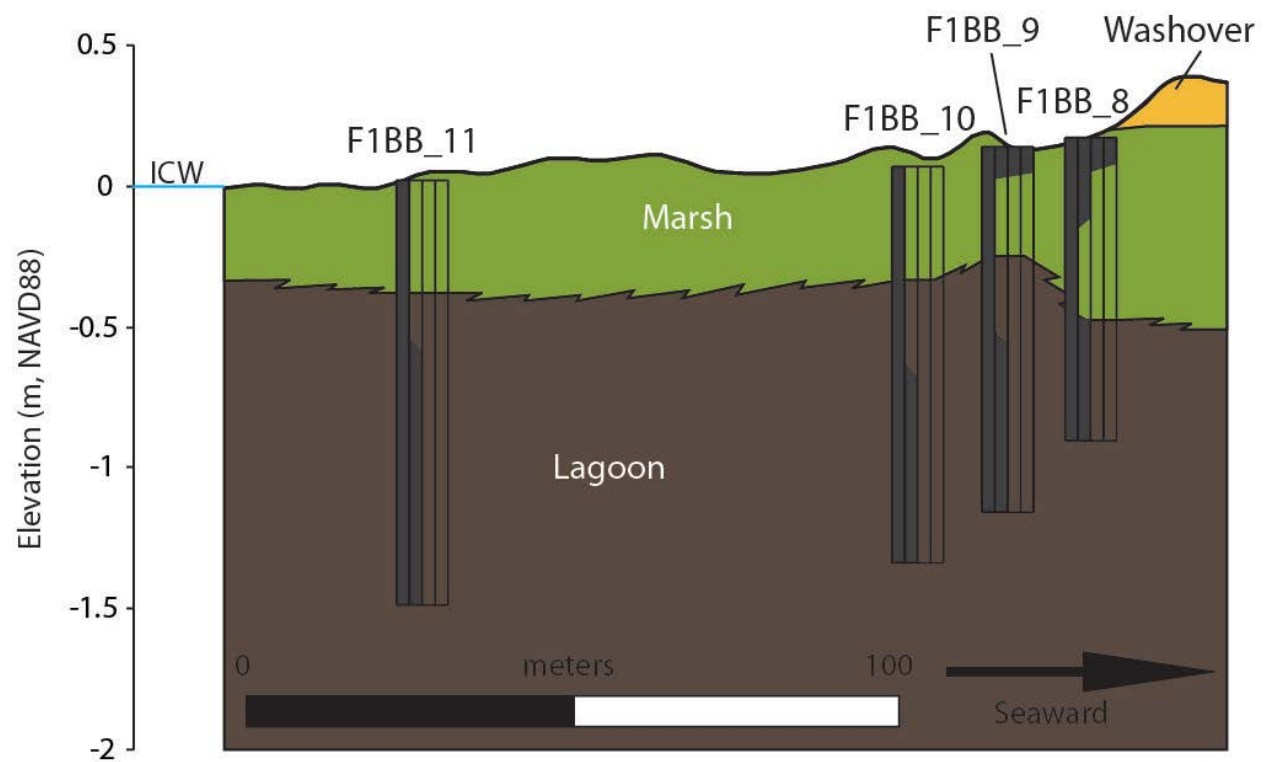
Appendix 11-A

Onslow Beach Cross Sections

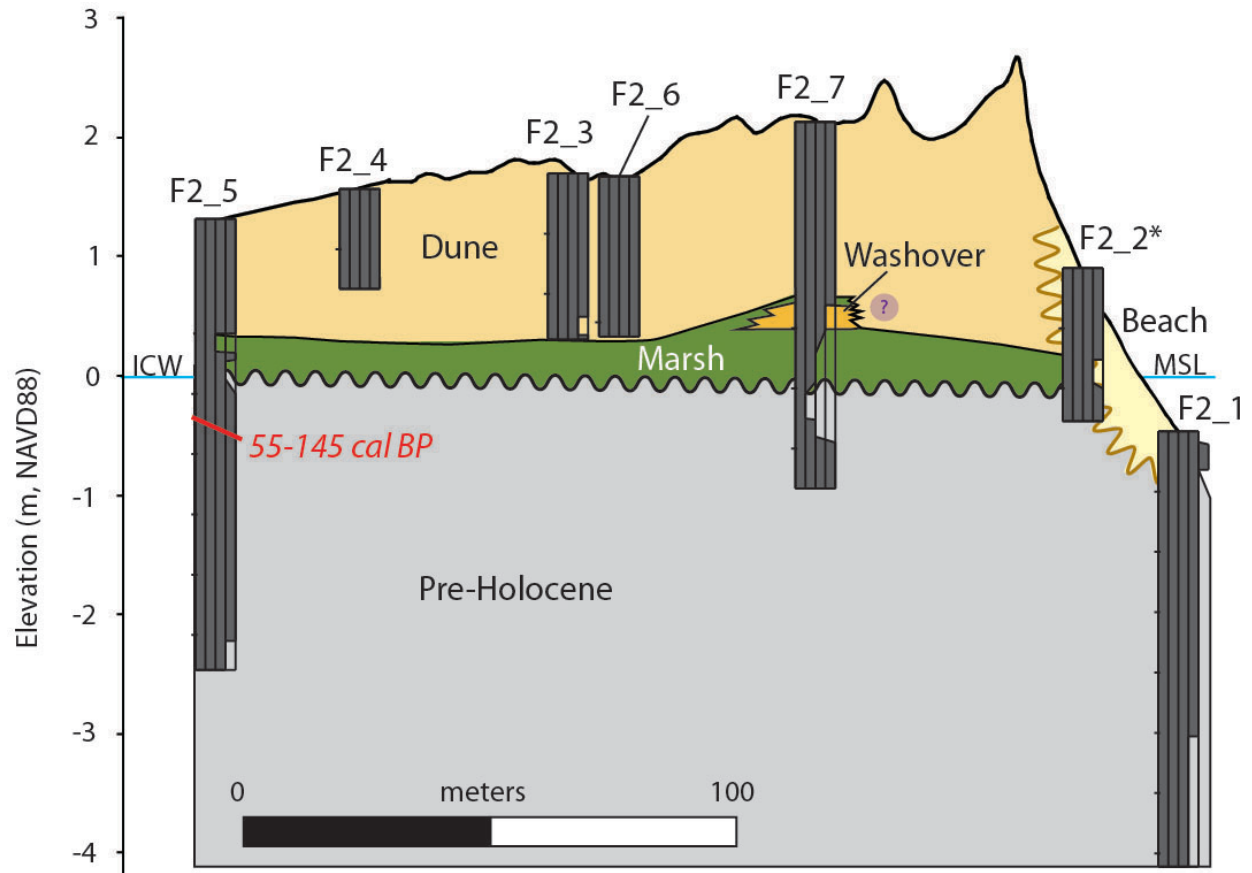
Cross-section F1



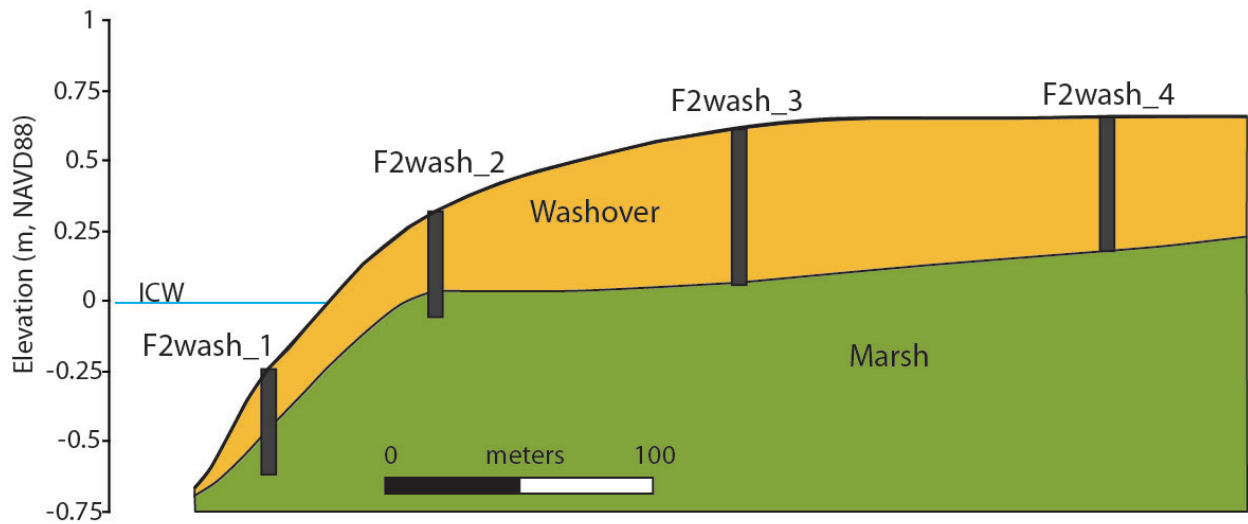
Cross-section F1BB



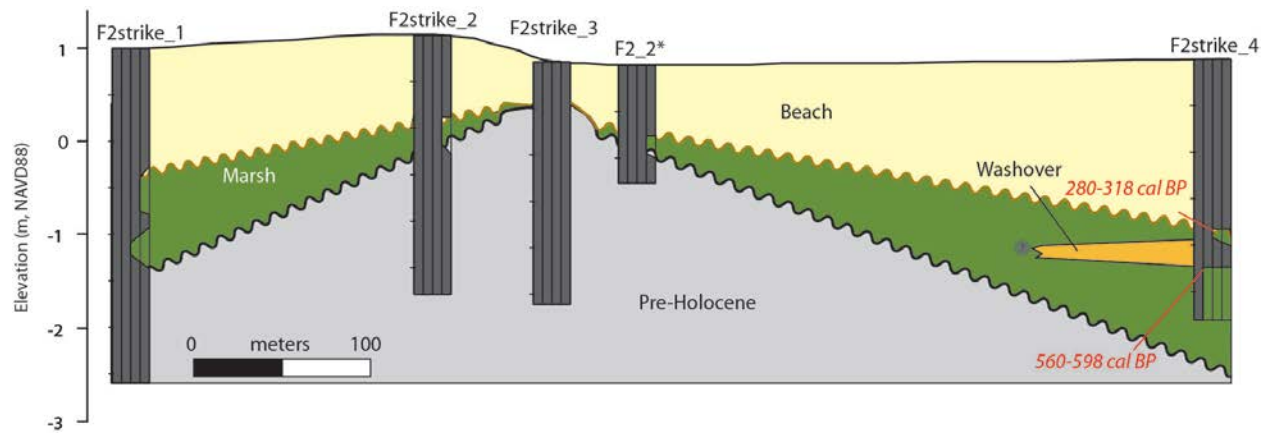
Cross-section F2



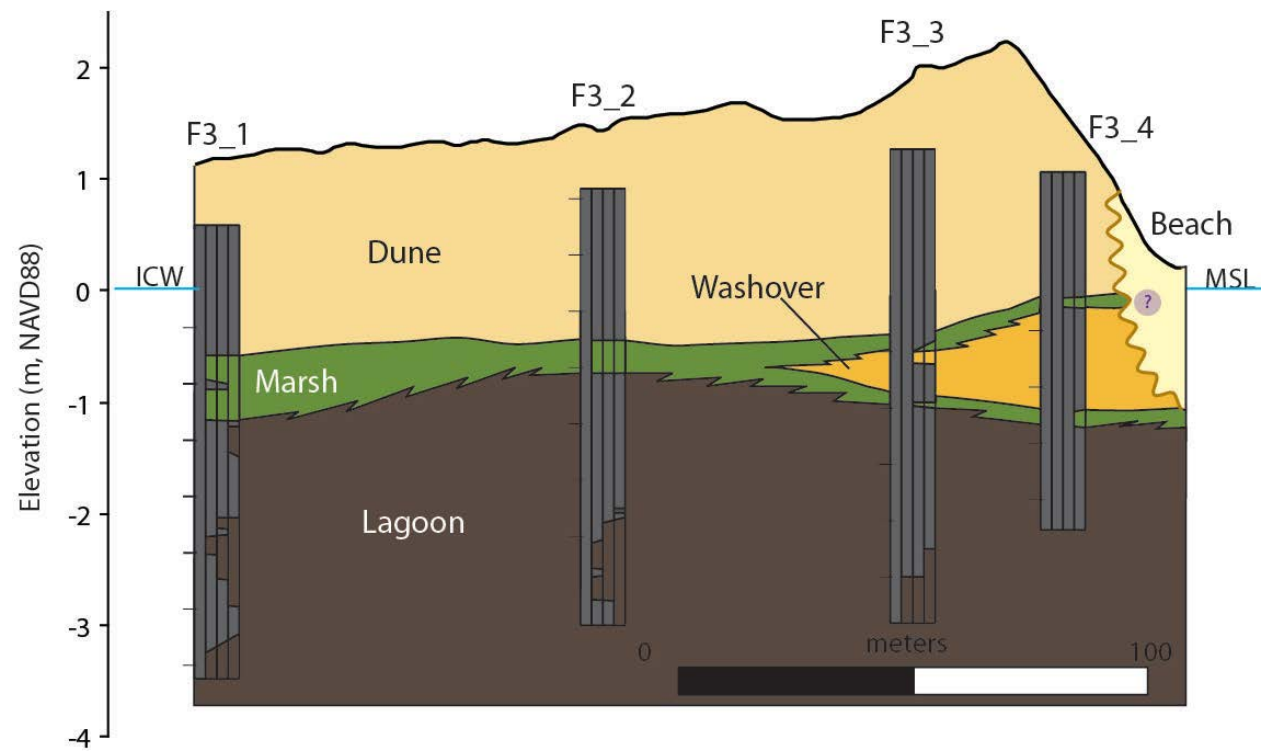
Cross-section F2wash



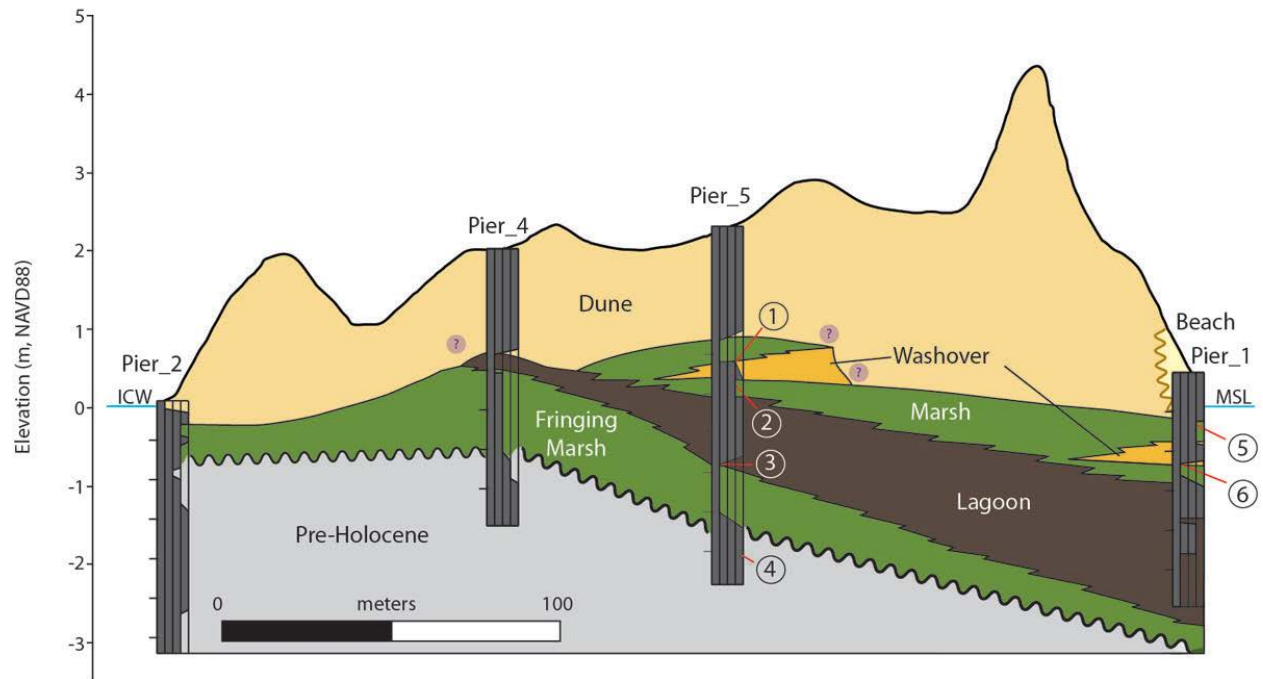
Cross-section F2strike



Cross-section F3



Cross-section Pier

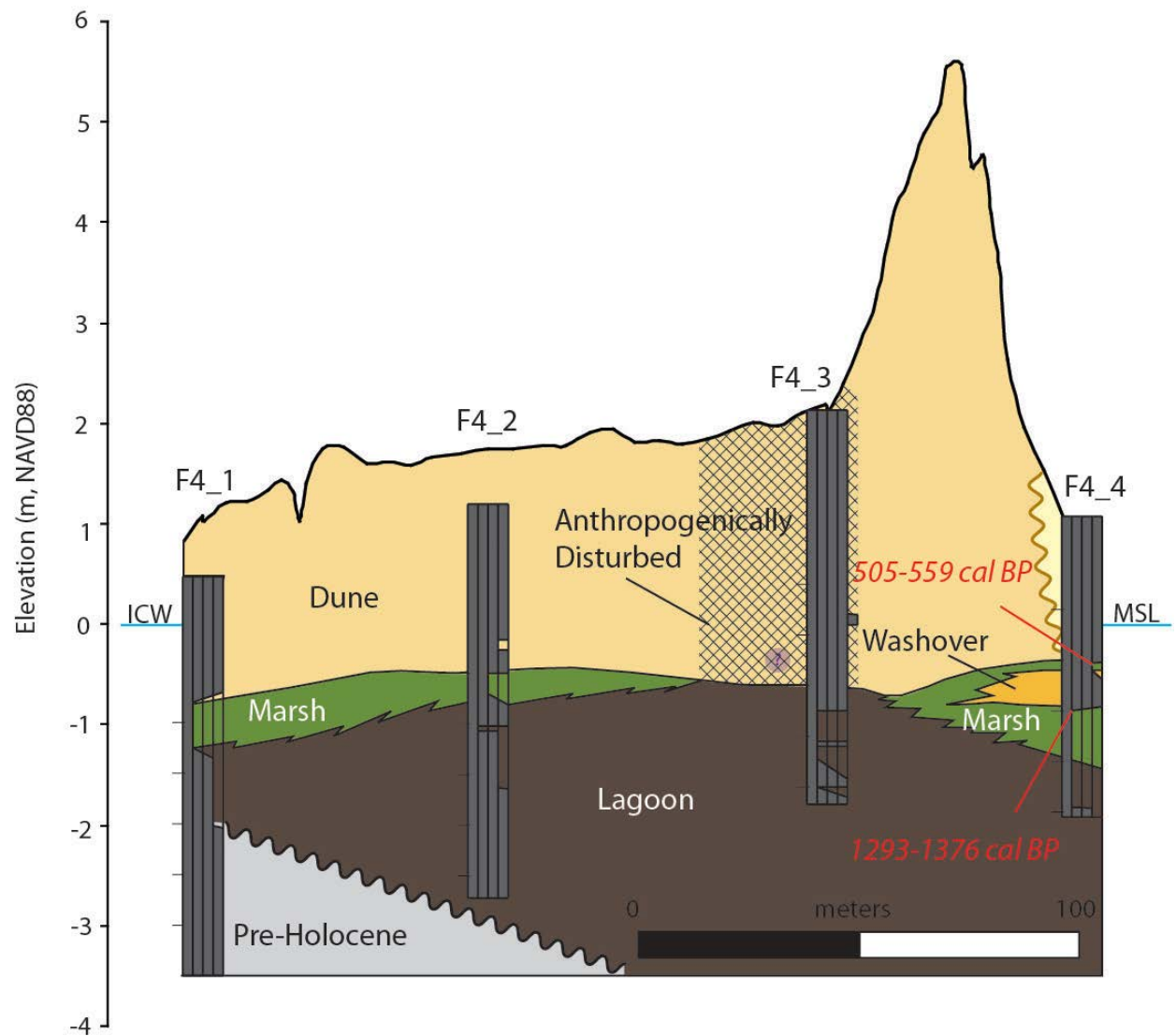


RADIOCARBON DATES

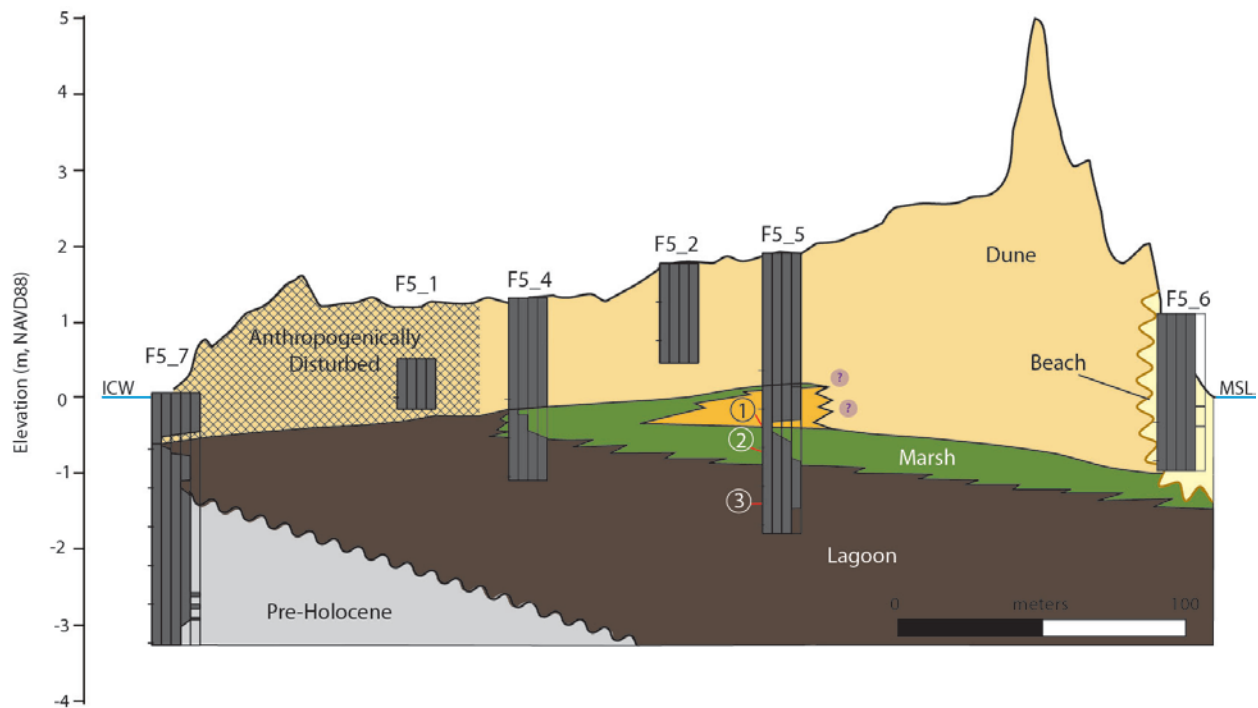
AGE IN CALIBRATED YEARS BEFORE PRESENT

DEPTH	MATERIAL DATED	AGE
Core Pier_5		
① 177-179 cm	Wood	55-140
② 202-204 cm	Wood/Plant	55-145
③ 302-304 cm	Wood	2156-2268
④ 420-422 cm	Wood	3556-3728
Core Pier_1		
⑤ 63-66 cm	Wood/Plant	644-724
⑥ 115-117 cm	Wood/Plant	1715-1832

Cross-section F4

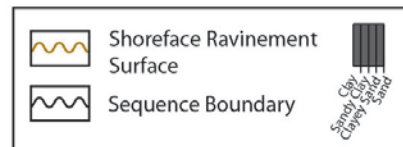


Cross-section F5

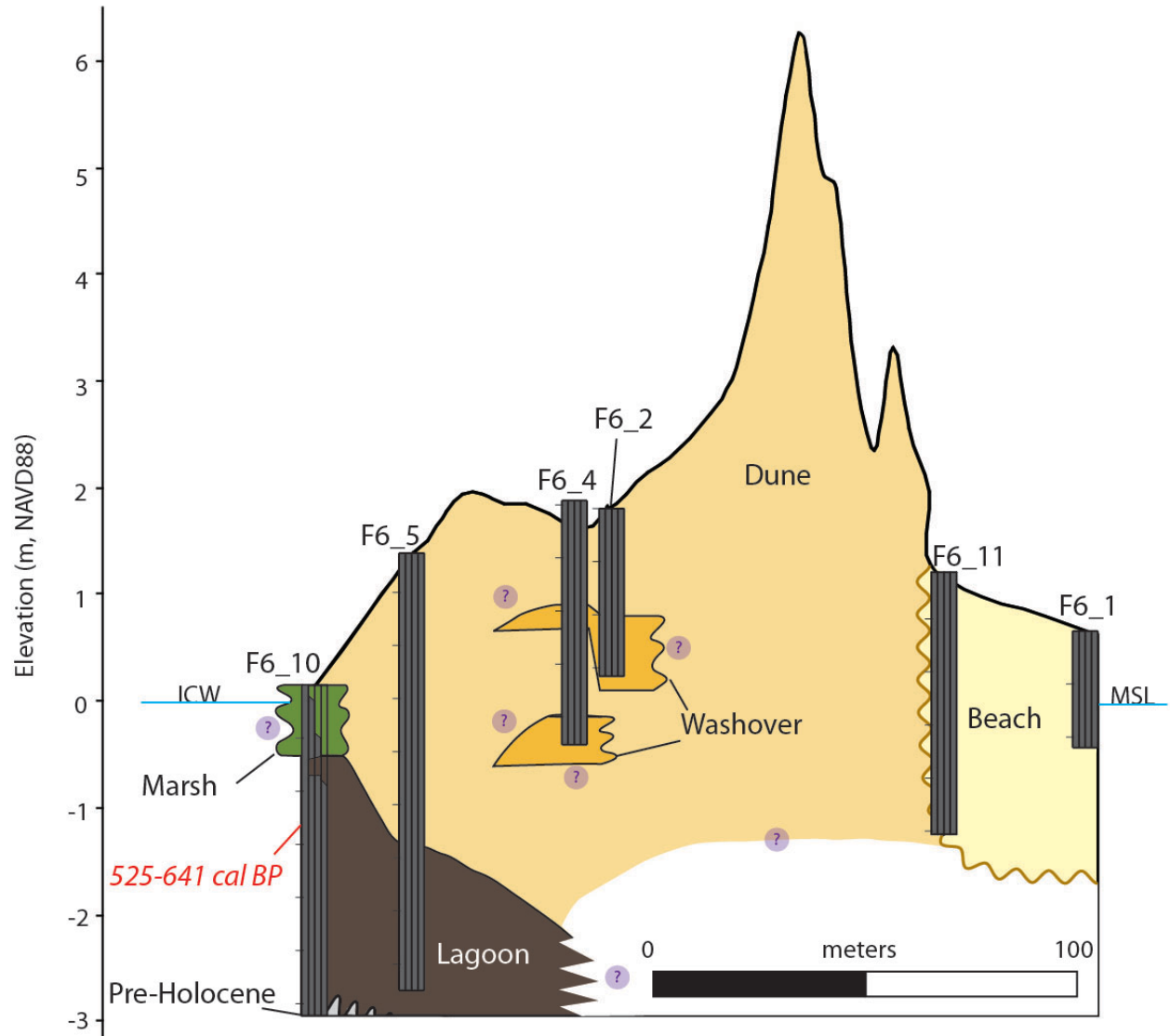


RADIOCARBON DATES AGE IN CALIBRATED YEARS BEFORE PRESENT

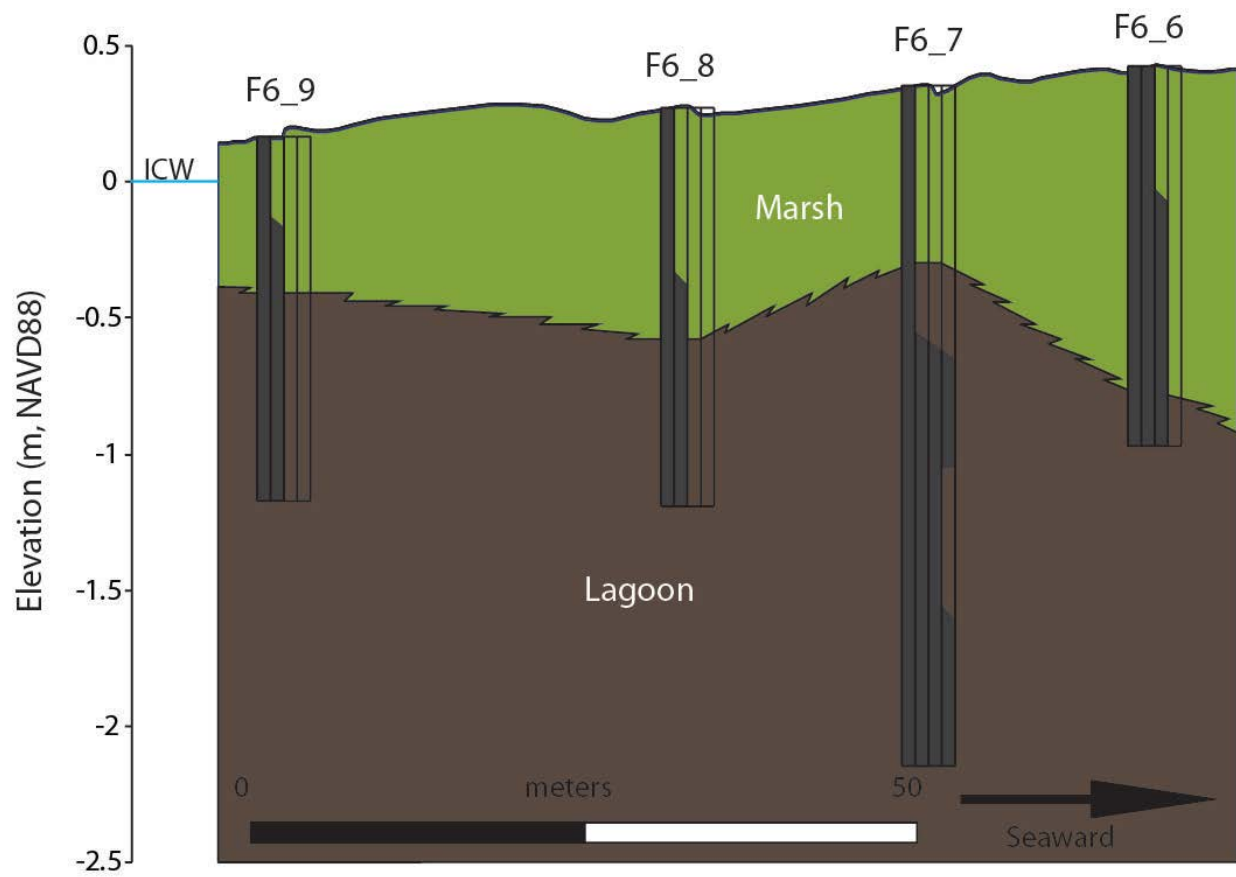
	DEPTH	MATERIAL DATED	AGE
①	218-220 cm	Wood	53-138
②	258-260 cm	Wood	583-649
③	322-324 cm	Wood	902-931



Cross-section F6



Cross-section F6BB



[This page intentionally left blank.]

Appendix 11-B

List of Scientific Publications

List of Scientific Publications

Papers

- Rodriguez, A.B., J.T. Ridge, S.R. Fegley, and N. Anderson. In preparation for a 2012 submission. Contribution of aeolian sand to backbarrier marsh sedimentation. To be submitted to *Estuarine Coastal and Shelf Science*.
- Theuerkauf, E.J., and A.B. Rodriguez. In preparation for a 2012 submission. Evaluating proxies of subaerial beach volume change across various short time scales and morphodynamics. To be submitted to the *Journal of Coastal Research*.
- Theuerkauf, E.J., and A.B. Rodriguez. 2012. Impacts of transect location and variations in along-beach morphology on measuring volume change. *Journal of Coastal Research* 28(3):707–718.
- Rodriguez, A.B., P.L. Rodriguez, and S.R. Fegley. 2012. One-year along-beach variation in the maximum depth of erosion resulting from irregular shoreline morphology. *Marine Geology* 291:12–23.
- Ridge, J.T., A.B. Rodriguez, S.R. Fegley, R. Browne, and D. Hood. 2011. A new “pressure” sensitive method of measuring aeolian sediment transport using a Gauged Sediment Trap (GaST). *Geomorphology* 134:426–430.
- Mattheus, C.R., and A.B. Rodriguez. 2011. Controls on late Quaternary incised-valley dimension along passive margins evaluated using empirical data: *Sedimentology* 58:1113–1137.

Thesis

- Theuerkauf, E.J. 2012. Evaluating proxies of subaerial beach volume change using terrestrial LiDAR data from Onslow Beach, NC, USA. Department of Marine Sciences, University of North Carolina at Chapel Hill, Chapel Hill, NC.
- Yu, W. In preparation, expected in 2012. Impacts of storms and sea-level rise on coastal evolution between two capes: Onslow Bay, NC, USA. Department of Marine Sciences, University of North Carolina at Chapel Hill, Chapel Hill, NC.

Presentations

- Theuerkauf, E.J., W. Yu, and A.B. Rodriguez. 2011. *The Influence of Framework Geology on the Evolution of Onslow Beach, NC, at Multiple Time Scales*. Presented at the Southeastern Section of the Geological Society of America (SEGSA) 60th Annual Meeting, Wilmington, NC. March 23–25. 43(1).
- Ridge, J.T., A.B. Rodriguez, and S.R. Fegley. 2011. *Shifting Sands: Quantifying Landscape Effects on the Contribution of Aeolian Sand to Back-Barrier Accretion*. Presented at the SEGSA 60th Annual Meeting, Wilmington, NC. March 23–25. 43(1).

- Theuerkauf, E.J., and A.B. Rodriguez. 2010. *Quantifying Differences in Beach Volume Change Between 2-D and 3-D Survey Methods*. Presented at the American Geophysical Union's (AGU's) Fall Meeting, San Francisco, CA. December 13–17.
- Yu, W., D. Hood, R. Browne, and A.B. Rodriguez. 2010. *Variations in Barrier-Island Evolution at Millennial and Decadal Time Scales Related to Underlying Geology, Onslow Beach, NC, USA*. Presented at AGU's Fall Meeting, San Francisco, CA. December 13–17.
- Rodriguez, A.B., S.R. Fegley, and P.L. Rodriguez. 2010. *A Novel Method for Quantifying the Maximum Depth of Beach Erosion over a One-Year Period at Onslow Beach, North Carolina Resolves Along- and Across-Beach Variability*, Presented at AGU's Fall Meeting, San Francisco, CA. December 13–17.
- Fegley, S.R., C.H. Peterson, A.B. Rodriguez, J.V. Reynolds-Fleming, R.A. Luettich, B.M. VanDusen, and C.M. Voss. 2010. *Perturbation in a Dynamic System: Variable Consequences of Coastal Storms on Habitat Structure and Faunal Composition in an Exposed Beach*. Presented at the 39th Benthic Ecology Meeting, Wilmington, NC. March 10–13.
- Theuerkauf, E.J., A.B. Rodriguez, S.R. Fegley, J.V. Fleming, J.E. McNinch, and H.M. Wadman. 2009. *Extreme Along-Beach Variations in Morphodynamics Attributed to Nearshore Bathymetry and Underlying Geology over the Short-Term, Onslow Beach, North Carolina*. Presented at AGU's Fall Meeting, San Francisco, CA. December 14–18.
- Reynolds-Fleming, J., R. Luettich, and A.B. Rodriguez. 2009. *Sequential Storm Effects on Barrier Island Morphology*. Presented at the Coastal Estuarine Research Federation's 20th Biennial Conference, Portland, OR. November 1–5.
- Foxgrover, A.C., J. McNinch, H. Wadman, and A.B. Rodriguez. 2008. *Quantifying Barrier-Island Overwash Through Sedimentological, Geophysical, and Geospatial Analyses: Onslow Beach, NC*. Presented at AGU's Fall Meeting, San Francisco, CA. December 15–19.
- Wadman, H., J. McNinch, A.C. Foxgrover, and A.B. Rodriguez. 2008. *Spatial Variation of Shoreline Change Along an Important Marine Corps Amphibious Training Ground, Onslow Beach, NC; Part 1: Nearshore Geology and Morphology*. Presented at the Joint Meeting of the Geological Society of America, Soil Science Society of America, American Society of Agronomy, Crop Science Society of America, Gulf Coast Association of Geological Societies with the Gulf Coast Section of the Society for Sedimentary Geology, Houston, TX. October 5–9. 40(6).
- Rodriguez, A.B., S.R. Fegley, C.R. Mattheus, E.A. Timmons, J. McNinch, and H. Wadman. 2008. *Spatial Variation of Shoreline Change Along An Important Marine Corps Amphibious Training Ground, Onslow Beach, North Carolina; Part 2: Beach Morphology*. Presented at the Joint Meeting of the Geological Society of America, Soil Science Society of America, American Society of Agronomy, Crop Science Society of

America, Gulf Coast Association of Geological Societies with the Gulf Coast Section of the Society for Sedimentary Geology, Houston, TX. October 5–9. 40(6).

Appendix 11-C

List of Students

- Ethan Theuerkauf, M.S., University of North Carolina at Chapel Hill, Chapel Hill, NC. Graduated May 2012.
- Winnie Yu, M.S., University of North Carolina at Chapel Hill, Chapel Hill, NC. Expected graduation in December 2012.

[This page intentionally left blank.]

Chapter 12

Understanding the Top-Down and Bottom-Up Drivers of Shorebird Nest Success and Habitat Use in Relation to Beach Management Practices on Marine Corps Base Camp Lejeune

SERDP Project Number: RC-1413

Coastal Barrier Module

Research Project CB-3

Lead Researchers:

Drs. Sarah Karpanty and Jim Fraser

Virginia Tech

Blacksburg, VA

E-mails: karpanty@vt.edu and fraser@vt.edu

December 26, 2011

Final

This report was prepared under contract to the U.S. Department of Defense (DoD) Strategic Environmental Research and Development Program (SERDP). The publication of this report does not indicate endorsement by DoD, nor should the contents be construed as reflecting the official policy or position of DoD. References herein to any specific commercial product, process, or service by trade name, trademark, manufacturer, or otherwise, do not necessarily constitute or imply its endorsement, recommendation, or favoring by DoD.

Table of Contents

List of Acronyms	12-ix
Abstract.....	12-1
Objectives of the Research Project	12-2
Objectives	12-2
Alternate Hypotheses	12-2
Background	12-3
Section 1: Wilson’s Plover Population Demographics	12-5
Materials and Methods.....	12-5
Results and Discussion	12-8
Section 2: Wilson’s Plover Habitat Selection	12-14
Materials and Methods.....	12-14
Results and Discussion	12-18
Section 3: Distribution and Abundance by Shorebirds and Predators at MCBCL	12-33
Materials and Methods.....	12-33
Results and Discussion	12-39
Conclusions and Implications for Future Research	12-60
Factors Affecting the Demography of Wilson’s Plovers	12-60
Factors Affecting Wilson’s Plover Nesting and Foraging Habitat Use	12-61
Future Challenges for Shorebird Conservation at MCBCL.....	12-63
Literature Cited	12-66
Appendix 12-A: List of Scientific Publications.....	12-A-1
Appendix 12-B: List of Students	12-B-1

List of Figures

12-1.	Study area at Onslow Beach on MCBCL, North Carolina, 2008–2009.	12-5
12-2.	Predicted survival of Wilson’s Plover chicks based on the top-ranked model containing actual covariate values predicting survival as a function of hatch date and distance (km) from nest to final foraging territory at MCBCL, North Carolina, 2008–2009.....	12-10
12-3.	Daily proportion of known Wilson’s Plover (<i>Charadrius wilsonia</i>) broods observed on fiddler crab (<i>Uca</i> spp.) mud flats in 2008 and 2009 at Onslow Beach, MCBCL, North Carolina, during the date range in 2009 (19 – 26 June) when near-complete inundation of flats were observed on Onslow Beach.	12-27
12-4.	Count per survey effort (2-yr average) of American Oystercatchers (<i>Haematopus palliatus</i>) per land use area (Developed Recreation, Amphibious Training, and Low Impact Wildlife) on beach and marsh transects at Onslow Beach on MCBCL, North Carolina, 2008–2009.	12-39
12-5.	Count per survey effort (2-yr average) of Piping Plovers (<i>Charadrius melodus</i>) per land use area (Developed Recreation, Amphibious Training, and Low Impact Wildlife) on beach and marsh transects at Onslow Beach on MCBCL, North Carolina, 2008–2009.....	12-40
12-6.	Count per survey effort of Red Knots (<i>Calidris canutus</i>) per land use area (Developed Recreation, Amphibious Training, and Low Impact Wildlife) on beach transects at Onslow Beach on MCBCL, North Carolina, 2008 and 2009.	12-40
12-7.	Count per survey effort (2-yr average) of Sanderlings (<i>Calidris alba</i>) per land use area (Developed Recreation, Amphibious Training, and Low Impact Wildlife) on beach and marsh transects at Onslow Beach on MCBCL, North Carolina, 2008–2009.....	12-41
12-8.	Count per survey effort (2-yr average) of Willets (<i>Catoptrophorus semipalmatus</i>) per land use area (Developed Recreation, Amphibious Training, and Low Impact Wildlife) on beach and marsh transects at Onslow Beach on MCBCL, North Carolina, 2008–2009.....	12-41
12-9.	Count per survey effort (2-yr average) of Wilson’s Plovers (<i>Charadrius wilsonia</i>) per land use area (Developed Recreation, Amphibious Training, and Low Impact Wildlife) on beach and marsh transects at Onslow Beach on MCBCL, North Carolina, 2008–2009.....	12-42
12-10.	Count per survey effort (2-yr average) of breeding plovers (<i>Charadrius spp.</i>) observed beachfront by land use area (Developed Recreation, Amphibious Training, and Low Impact Wildlife) at Onslow Beach on MCBCL, North Carolina, 2008–2009.....	12-42
12-11.	Count per survey effort (2-yr average) of breeding plovers (<i>Charadrius spp.</i>) observed marshside by land use area (Developed Recreation, Amphibious Training, and Low Impact Wildlife) at Onslow Beach on MCBCL, North Carolina, 2008–2009.....	12-43

12-12. Count per survey effort (2-yr average) of wintering, non-breeding or migrating plovers observed beachfront by land use area (Developed Recreation, Amphibious Training, and Low Impact Wildlife) at Onslow Beach on MCBCL, North Carolina, 2008–2009.....	12-44
12-13. Count per survey effort (2-yr average) of wintering, non-breeding or migrating plovers observed marshside by land use area (Developed Recreation, Amphibious Training, and Low Impact Wildlife) at Onslow Beach on MCBCL, North Carolina, 2008–2009.....	12-44
12-14. Count per survey effort (2-yr average) of breeding terns (<i>Sterna</i> spp.) observed beachfront by land use area (Developed Recreation, Amphibious Training, and Low Impact Wildlife) at Onslow Beach on MCBCL, North Carolina, 2008–2009. ...	12-45
12-15. Count per survey effort (2-yr average) of breeding terns (<i>Sterna</i> spp.) observed marshside by land use area (Developed Recreation, Amphibious Training, and Low Impact Wildlife) at Onslow Beach on MCBCL, North Carolina, 2008–2009. ...	12-45
12-16. Beach predator trap success metrics (2-yr mean number of capture events per 100 trap nights) by land use area (Developed Recreation and Low Impact/Wildlife Area) and monitoring period (month and year) for bobcat (<i>Lynx rufus</i>), gray fox (<i>Urocyon cinereoargenteus</i>), red fox (<i>Vulpes vulpes</i>), and feral cat (<i>Felis domesticus</i>) at Onslow Beach on MCBCL, North Carolina, 2008–2009.	12-47
12-17. Marsh predator trap success metrics (2-yr mean number of capture events per 100 trap nights) by land use area (Developed Recreation and Low Impact Wildlife) and monitoring period (month and year) for bobcat (<i>Lynx rufus</i>), gray fox (<i>Urocyon cinereoargenteus</i>), red fox (<i>Vulpes vulpes</i>), and feral cat (<i>Felis domesticus</i>) at Onslow Beach on MCBCL, North Carolina, 2008–2009.	12-48
12-18. Beach predator trap success metrics (2-yr mean number of capture events per 100 trap nights) by land use area (Developed Recreation and Low Impact Wildlife) and monitoring period (month and year) for domestic dogs (<i>Canis familiaris</i>) at Onslow Beach on MCBCL, North Carolina, 2008–2009.	12-49
12-19. Beach predator trap success metrics (2-yr mean number of capture events per 100 trap nights) by land use area (Developed Recreation and Low Impact Wildlife) and monitoring period (month and year) for raccoon (<i>Procyon lotor</i>), Virginia opossum (<i>Didelphis virginiana</i>), and ghost crab (<i>Ocypode quadrata</i>) at Onslow Beach on MCBCL, North Carolina, 2008–2009.	12-51
12-20. Marsh predator trap success metrics (2-yr mean number of capture events per 100 trap nights) by land use area (Developed Recreation and Low Impact Wildlife) and monitoring period (month and year) for raccoon (<i>Procyon lotor</i>), Virginia opossum (<i>Didelphis virginiana</i>), and ghost crab (<i>Ocypode quadrata</i>) at Onslow Beach on MCBCL, North Carolina, 2008–2009.	12-52
12-21. Average 2-year trap success metrics (mean number of capture events per 100 trap nights) by land use area (Developed Recreation, Amphibious Training, and Low Impact Wildlife) by monitoring period (month) for vehicles detected on Onslow Beach at MCBCL, North Carolina, 2008–2009.....	12-53

12-22. Average 2-year trap success metrics (mean number of capture events per 100 trap nights) by land use area (Developed Recreation, Amphibious Training, and Low Impact Wildlife) by monitoring period (month) for domestic dogs (<i>Canis familiaris</i>) on- and off-leash detected on Onslow Beach at MCBCL, North Carolina, 2008–2009.....	12-54
12-23. Average 2-year trap success metrics (mean number of capture events per 100 trap nights) in the Developed Recreation Area by monitoring period (month) for human activities occurring at Onslow Beach on MCBCL, North Carolina, 2008–2009.....	12-55
12-24. Average 2-year trap success metrics (mean number of capture events per 100 trap nights) in the Amphibious Training Zone by monitoring period (month) for human activities occurring at Onslow Beach on MCBCL, North Carolina, 2008–2009.....	12-56
12-25. Average 2-year trap success metrics (mean number of capture events per 100 trap nights) in the Low Impact Wildlife area by monitoring period (month) for human activities occurring at Onslow Beach on MCBCL, North Carolina, 2008–2009.	12-57

List of Tables

12-1.	Demographic estimates (\pm standard error [SE]) for Wilson's Plovers (<i>Charadrius wilsonia</i>) on Onslow Beach, MCBCL, North Carolina, 2008–2009.	12-9
12-2.	Causes of failure for Wilson's Plover (<i>Charadrius wilsonia</i>) nests on Onslow Beach, MCBCL, North Carolina, 2008–2009.	12-9
12-3.	Model-selected parameter estimates (βx), standard errors (\pm SE), and 95% lower confidence limit (LCL) and upper confidence limit (UCL) for the best-fitting model a ($AIC_c < 2.00$ or model likelihood ≥ 0.125) predicting Wilson's Plover (<i>Charadrius wilsonia</i>) chick survival ($N = 20$ broods) on Onslow Beach, MCBCL, North Carolina, 2008–2009.	12-10
12-4.	Top-ranked models ($\Delta AIC_c \leq 2.00$ or model likelihood ≥ 0.125) from 36 single- and multi-variable logistic regressions of habitat characteristics at Wilson's Plover (<i>Charadrius wilsonia</i>) nest sites and paired non-used locations ($n = 42$ nests) at Onslow Beach, MCBCL, North Carolina, 2008–2009.	12-19
12-5.	Model-averaged parameter estimates, unconditional SE, LCL and UCL, and relative importance (R_i) from 36 single- and multi-variable logistic regression models of habitat characteristics at Wilson's Plover (<i>Charadrius wilsonia</i>) nest sites and paired non-used locations ($n = 42$ nests) on Onslow Beach, MCBCL, North Carolina, 2008–2009.	12-19
12-6.	Top-ranked models ($\Delta AIC_c \leq 2.00$ or model likelihood ≥ 0.125) from 37 single- and multi-variable logistic regressions of habitat characteristics influencing nest ($n = 42$ nests) hatching success of Wilson's Plovers (<i>Charadrius wilsonia</i>) at Onslow Beach, MCBCL, North Carolina, 2008–2009.	12-20
12-7.	Model-averaged parameter estimates, unconditional standard errors (SE) and confidence limits (CL), and relative importance (R_i) from 37 single- and multi-variable logistic regression models of habitat characteristics influencing nest hatching success ($n = 42$ nests) of Wilson's Plovers (<i>Charadrius wilsonia</i>) on Onslow Beach, MCBCL, North Carolina, 2008–2009.	12-21
12-8.	Top-ranked models ($\Delta AIC_c \leq 2.00$ or Model Likelihood ≥ 0.125 out of 16 models) predicting Wilson's Plover (<i>Charadrius wilsonia</i>) brood foraging territory establishment on fiddler crab (<i>Uca</i> spp.) mud flats ($n = 9$) at Onslow Beach, MCBCL, North Carolina, 2009.	12-22
12-9.	Model-averaged parameter estimates, unconditional standard errors (SE), upper confidence limit (UCL), lower confidence limit (LCL), and relative importance (R_i) from multi-variable logistic regression models predicting Wilson's Plover (<i>Charadrius wilsonia</i>) brood foraging territory establishment on fiddler crab (<i>Uca</i> spp.) mud flats ($n = 9$) on Onslow Beach, MCBCL, North Carolina, 2009.	12-22
12-10.	Top single- and multi-variable logistic regression models ($\Delta AIC_c \leq 2.00$ or model likelihood ≥ 0.125 , 28 models) of habitat characteristics at foraging sites used by Wilson's Plover (<i>Charadrius wilsonia</i>) broods and random non-use sampling points on fiddler crab (<i>Uca</i> spp.) mud flats ($n = 25$ paired samples), beach front ($n = 25$ paired samples), interdune sand flats ($n = 10$ paired samples), and all habitats	

($n = 60$ paired samples) combined at Onslow Beach, MCBCL, North Carolina in 2009.....	12-24
12-11. Model-averaged parameter estimates, unconditional standard errors (SE) and confidence limits (CL), and relative importance (R_i) from single- and multi-variable logistic regression models examining habitat characteristics at foraging sites used by Wilson’s Plover (<i>Chardrius wilsonia</i>) broods and random non-use sampling points on fiddler crab (<i>Uca</i> spp.) mud flats ($n = 25$ paired samples), beach front ($n = 25$ paired samples), interdune sand flats ($n = 10$ paired samples), and all habitats ($n = 60$ paired samples) combined on Onslow Beach, MCBCL, North Carolina in 2009.	12-25
12-12. Fiddler crab (<i>Uca</i> spp.) burrow counts and individual counts at focal Wilson’s Plover (<i>Charadrius wilsonia</i>) foraging locations (i.e., use sites) and paired, non-use samples on fiddler flats at Onslow Beach, MCBCL, North Carolina, 2008–2009.....	12-26
12-13. Total mean insect counts (insects collected per min^{-1}) at focal Wilson’s Plover (<i>Charadrius wilsonia</i>) foraging locations (i.e., use sites) and paired, non-use samples at Onslow Beach, MCBCL, North Carolina, 2008–2009.	12-26
12-14. Wilson’s Plover (<i>Chardrius wilsonia</i>) chick ($n = 10$ broods) pecking rates (pecks per min^{-1}) on fiddler crab (<i>Uca</i> spp.) mud flats, beach front, and interdune sand flats at Onslow Beach, MCBCL, North Carolina, 2008–2009.	12-28
12-15. Wilson’s Plover (<i>Chardrius wilsonia</i>) adult ($n = 10$ pairs) and chick ($n = 10$ broods) “run and grab” rates (run and grab per min^{-1}) on fiddler crab (<i>Uca</i> spp.) mud flats at Onslow Beach, MCBCL, North Carolina, 2008–2009.	12-28
12-16. Shorebird and tern species included in this study’s summary analyses, along with each species’ federal and state listing status, the US Shorebird Conservation Plan’s prioritization designation, and temporal occurrence on Onslow Beach at MCBCL, North Carolina, 2008–2009.	12-34
12-17. Predator monitoring periods, dates monitored, total days monitored, mean days monitored, and calculated camera trap nights (16 camera stations (n) * total days monitored; $n =$ eight camera stations per land use area (Developed Recreation and Low Impact Wildlife)) at Onslow Beach on MCBCL, North Carolina, 2008–2009...	12-36
12-18. Human activity monitoring periods by weekday (Sun/Mon – Thurs) or weekend (Thurs/Fri – Sun) occurrences, dates monitored, total days monitored (1 day = 24 hrs), and calculated camera trap nights (6 camera stations (n) * total days monitored; $n =$ two camera stations per land use area (Developed Recreation, Amphibious Training, and Low Impact Wildlife)) at Onslow Beach on MCBCL, North Carolina, 2008–2009.	12-38

List of Acronyms

ΔAIC_c	difference between any given model's AIC_c and the best-fit model
P	detection probabilities
Φ	apparent survival
°C	degrees Celsius
AAV	amphibious assault vehicle
AIC	Akaike's Information Criterion
AIC_c	Akaike's Information Criterion adjusted for sample size
ATV	all-terrain vehicle
BurrCount	mean burrow count
cm	centimeter
cm ²	square centimeter
DCERP	Defense Coastal/Estuarine Research Program
DistFidd	distance to nearest fiddler crab (<i>Uca</i> spp.) flat from the nest site
DistFTerr	final foraging territory
DistNrNest	distance to nearest nest site (meter)
DoD	U.S. Department of Defense
DSR	daily survival rate
EIS	Environmental Impact Statement
EMD	Environmental Management Division
EPA	U.S. Environmental Protection Agency
GPS	global positioning system
ha	hectare
HMMWV	high-mobility multipurpose wheeled vehicle
ICW	Intracoastal Waterway
km	kilometer
LCAC	Landing Craft Air Cushion
LCL	lower confidence limit
m	meter
m ²	square meter

MARDIS	Monitoring and Research Data Information System
MCBCL	Marine Corps Base Camp Lejeune
MLShell	percent cover of medium (2-64 mm) and large (> 64 mm) shells
mm	millimeter
MOU	Memorandum of Understanding
MTVR	medium tactical vehicle replacement
NCWRC	North Carolina Wildlife Resources Commission
NOAA	National Oceanic and Atmospheric Administration
PVC	polyvinyl chloride
R_i	relative importance
SE	standard error
SERDP	Strategic Environmental Research and Development Program
Sshell	percent coverage of small (<2 mm) shells
TallVeg5	height of tall vegetation (≥ 1.0 m) within a 5-m radius of sample sites
UCL	upper confidence limit
USACE	U.S. Army Corps of Engineers
VegCover	percent cover of dead and live vegetation
VegForm	vegetation growth form within 15 cm of the nest site
VegTrnDist	length (m) of vegetated path from interdune sand flat to fiddler crab mud flat
VegVO	index depicting visual obstruction (density) of vegetation around the fiddler crab mud flat
w_i	weight of each model as compared to all candidate models
WSR	weekly survival rate

Abstract

Our studies were part of the Coastal Barrier module of the Defense Coastal/Estuarine Research Program (DCERP). The efforts of the Coastal Barrier Module were designed to support the long-term sustainability of important coastal resources necessary for amphibious military training. We focused our studies at two levels. First, we studied the breeding ecology of Wilson's Plovers (*Charadrius wilsonia*) at Onslow Beach from March–August 2008 and 2009. We also resighted plovers banded in the first two seasons in 2010 in order to calculate adult survival. Second, we surveyed all shorebirds, terns, and predators at Onslow Beach during 2008–2009 while the breeding studies were taking place. We selected Wilson's Plover as the focal species for this study because it is a Species of Concern in this region, and Onslow Beach appeared to be an important breeding location for this species in North Carolina. Despite its conservation status, Wilson's Plover population trends are poorly understood and little research has been conducted on the habitat factors affecting this species' breeding and foraging ecology. We collected Wilson's Plover demographic data and explored which habitat characteristics influenced breeding success and foraging site selection among three coastal habitat types (i.e., fiddler crab (*Uca* spp.) mud flats, beach front, and interdune sand flats). We observed little difference between years in nest success (≥ 1 egg hatched), failure, and overall nest survival. The majority of nest failures were caused by mammalian predators. For those nests that hatched successfully, greater proportions were located in clumped vegetation than on bare ground or sparsely vegetated areas. In-season chick survival for both years was higher for nests that hatched earlier in the season, and for nests farthest from the broods' final foraging territory. Productivity estimates (chicks fledged per breeding pair) were not significantly different between years (0.88 ± 0.26 fledged/pair in 2008, 1.00 ± 0.25 fledged/pair in 2009) despite a shift in foraging behavior, possibly related to habitat alterations caused by a sea level anomaly and availability in 2009. Adult Wilson's Plover apparent survival was high (82%) and consistent with studies of other plover species on the Atlantic Coast. Our findings indicate that Wilson's Plover adults and broods were flexible in establishing final foraging territories; in 2008 all final brood foraging territories were on fiddler flats while in 2009, final foraging territories were sometimes split between fiddler flats, beach front, and interdune sand flats. For those Wilson's Plovers establishing territories on fiddler flats, area of the flat was the most important feature explaining use versus non-use of a particular flat; area $\geq 1,250 \text{ m}^2$ was preferred. Close proximity to water and vegetative cover were also important habitat features in foraging site selection on fiddler crab mud flats, and in all habitat types combined. Our findings will directly contribute to population and habitat research goals outlined in the U.S. Shorebird Plan and will supplement limited data about foraging and habitat use related to Wilson's Plover breeding ecology. Further, these studies provide Marine Corps Base Camp Lejeune with guidance as to which bottom-up (i.e., prey and habitat characteristics) and top-down (i.e., predator characteristics) factors are important to manage for ground-nesting shorebirds, such as the Wilson's Plover as both processes are important in this, and many other, systems.

Keywords: beach accretion, bottom-up, prey characteristics, *Charadrius wilsonia*, fiddler crab, *Uca*, foraging territory, hatching success, nest success, predation, productivity, reproduction, sea level anomaly, survival, top-down, predator characteristics, Wilson's Plover, shorebirds

Objectives of the Research Project

Objectives

1. To understand the biotic and abiotic variables that drive shorebird reproductive output and breeding-season distribution on Marine Corps Base Camp Lejeune (MCBCL; see Sections 1 and 2)
2. To relate trends in shorebird foraging and nesting distributions, abundance and reproductive output to variations in land use and management practices (see Section 3)
3. To understand those elements of predator ecology on coastal barrier islands needed to enhance shorebird conservation and the most efficient control of predators. (see Sections 1, 2 and 3)
4. To quantify apparent survival rates for Wilson's plovers. (see Section 1)

Alternate Hypotheses

1. Shorebird breeding-season distribution, abundance, nest success, and survival are driven by bottom-up processes, such as physical sedimentary structure, prey abundance, prey diversity, and prey distribution, which vary in relation to beach management practices.
2. Shorebird breeding-season distribution, abundance, nest success, and survival are driven by top-down processes, such as predation by natural or feral predators, which vary in relation to beach management practices.

Background

Our studies were part of the Coastal Barrier module of the Defense Coastal/Estuarine Research Program (DCERP). The efforts of the Coastal Barrier module were designed to support the long-term sustainability of important coastal resources necessary for amphibious training at Marine Corps Base Camp Lejeune (MCBCL), and the U.S. Department of Defense's (DoD's) military mission. On Onslow Beach at MCBCL, amphibious military training along a portion of the beach has introduced a novel type of disturbance into its coastal barrier habitat. The Landing Craft Air Cushion (LCAC) is a vehicle that can traverse both land and water at speeds exceeding 40 knots, and is used to transport equipment, supplies, and troops with a load capacity of 60 to 75 tons (FAS 2000). Other military vehicles used in beach training include amphibious assault vehicles (AAVs, amphibious tracked vehicle with landing capabilities), high-mobility multipurpose wheeled vehicles (HMMWVs, also referred to as Humvees), and medium tactical vehicle replacements (MTVRs, 7-ton six-wheel drive all-terrain transport trucks). As the largest amphibious assault marine training base in the United States (MCBCL, 2007), Onslow Beach plays a critical role in the Marine Corps' training efforts, as LCACs, AAVs, 4- and 6-wheeled military vehicles, and troops regularly use the beach throughout the year. Training exercises have impacts on the beach which may include erosion, sand compaction, disturbance, and the potential for direct mortality to migratory and breeding shorebirds. This study is also relevant to a Memorandum of Understanding (MOU, Federal Register 51580-51585) between MCBCL and the U.S. Fish and Wildlife Service which outlines efforts to protect and promote the conservation of migratory birds on its lands, including breeding shorebirds.

We focused our studies at two levels to address the objectives and hypotheses outlined above. First, to address objectives 1, 3 and 4, we studied the breeding ecology of Wilson's Plovers (*Charadrius wilsonia*) at Onslow Beach (34°32' N, 77°21' W), MCBCL, North Carolina from March–August 2008 and 2009. We also resighted plovers banded in the first two seasons in 2010 in order to calculate adult survival. To address objectives 2 and 3, we surveyed all shorebirds, terns, and predators at Onslow Beach during 2008–2009 while the breeding surveys were being conducted.

We chose Wilson's Plover as the focal species for this study because it is a Species of Concern in this region, and Onslow Beach appeared to be an important breeding location for this species in North Carolina. While we had originally hoped to use multiple focal shorebird species to address these objectives, the funds available during the implementation stage did not allow for detailed studies of demographics and habitat ecology for multiple species. We found and studied 20 nests of Wilson's Plovers in 2008 and 26 in 2009. The North Carolina Wildlife Resources Commission (NCWRC) considers a coastal habitat containing ≥ 25 Wilson's Plover pairs to be an important breeding location for sustaining and increasing regional and range-wide populations (Susan Cameron, NCWRC, personal communication).

Ground-nesting coastal shorebirds, like the Wilson's Plover, American Oystercatcher (*Haematopus palliatus*), Piping Plover (*Charadrius melodius*), and Least Tern (*Sterna antillarum*), among others, depend on a variety of dynamic and ephemeral habitats for breeding and rearing young (Brown et al. 2001). Intertidal habitats provide foraging resources and resting sites (Brown et al. 2000, Corbat and Bergstrom 2000, Elias et al. 2000, Lowther et al. 2001, Fraser et al. 2005, Cohen et al. 2008). Habitats less susceptible to inundation (e.g. dunes, beach backshore, and interdune sand flats) provide nesting habitat (Corbat 1990, Nol and Humphrey

1994, Elliot-Smith and Haig 2004), and foraging opportunities (Corbat 1990, Hubbard and Dugan 2003, Defeo et al. 2009). Widespread coastal development and human recreation have resulted in degradation of such habitats (Burger 1989, Nol and Humphrey 1994, Loegering and Fraser 1995, Corbat and Bergstrom 2000, Page et al. 2009, Cohen et al. 2009). Emerging threats, such as climate change-related sea level rise (IPCC 2007), present additional challenges. Increased sea level may decrease the availability of shorebird foraging resources, as current intertidal zones are converted to sub-tidal habitats and sound side marshes become subject to increased periods of inundation that alter the benthic prey community (Galbraith et al. 2002). Population declines have been linked to the decline and deterioration of both nesting and foraging habitat used by shorebirds (Burger 1994, Corbat and Bergstrom 2000, Brown et al. 2001, Galbraith et al. 2002, Hunter 2002). Understanding the key features that make habitat suitable for breeding shorebirds is an essential precursor to developing effective conservation and management plans.

There have been few studies about the breeding and foraging habitat ecology of Wilson's Plovers, which is another reason that this species was chosen as our focal species; most of the available studies have focused on nesting ecology and life history traits (Tomkins 1944, 1959; Bergstrom 1982, 1988; Bergstrom and Terwillinger 1987; Corbat 1990; Hood 2006; Dikun 2008). Those studies examining nest hatching success (Bergstrom 1982, 1988; Corbat 1990; Hood 2006) found higher success for nests placed in or adjacent to vegetation. These studies also documented the primary causes of nest failure as mammalian predation [bobcat (*Lynx rufus*), coyote (*Canis latrans*), raccoon (*Procyon lotor*)], cattle (Bergstrom 1982, 1988) and feral hog (Corbat 1990) trampling, and heavy rain and tidal flooding (Bergstrom 1982, 1988; Hood 2006). Of all studies, only three (Tomkins 1944, 1959; Bergstrom and Terwillinger 1987; Corbat 1990) were conducted on the Atlantic coast, and Corbat's was the only one to examine habitat characteristics influencing nest site selection and hatching success.

Fiddler crabs (*Uca* spp.) have been identified as a key component of Wilson's Plover diets in both their wintering and breeding seasons (Tomkins 1944, Strauch and Abele 1979, Bergstrom 1982; Morrier and McNeil 1991; Thibault and McNeil 1994, 1995; Corbat and Bergstrom 2000; Leary 2009), suggesting that the presence or density of these prey may play an important role in Wilson's Plover foraging habitat selection. We are unaware of other studies addressing the effect of habitat or prey distribution on selection of brood foraging sites and territory establishment for Wilson's Plovers except for another study ongoing by Virginia Tech at Cape Lookout National Seashore (Derose-Wilson, Virginia Tech, personal communication).

In order to test our hypotheses as to the relative importance of top-down and bottom-up processes on the distribution, abundance, nest success, and survival of shorebirds at Onslow Beach, Camp Lejeune, we took a dual approach as noted above. Below, we report first on how predation impacted Wilson's plover nest and chick survival as well as adult apparent survival (Section 1) and then more generally on how predator relative abundance varied by beach habitat and management practices (Section 3). In Section 2, we discuss how both top-down (i.e., predation) and bottom-up (i.e., fiddler crab availability) processes affected Wilson's Plover distribution, nest success and survival. In Section 3 we also report on the general distribution and abundance of shorebirds by beach management zone and season, but we were unable to test detailed hypotheses for what was driving this distribution for waterbird species other than the Wilson's Plover.

Section 1: Wilson's Plover Population Demographics

Materials and Methods

Study Site: We conducted this study on Onslow Beach (34°32' N, 77°21'W), a 12.9-kilometer (km) barrier island in southeastern North Carolina. It is bounded by New River Inlet and Brown's Inlet (**Figure 12-1**). Human impacts vary across the island. The south end of the island is managed for low impact recreation and wildlife (Wildlife Area), and is closed to recreational vehicles from 1 April to 31 August, annually (**Figure 12-1**). The Amphibious Training Zone is designated for military training and the Developed Recreation Area provides recreational opportunities for Marine Corps personnel and their families (**Figure 12-1**); surveys in 2008–2010 found no Wilson's Plovers nesting in these two areas, so we do not discuss them further in this section. Access to the Military Buffer Zone was restricted and sporadic; we include data from these areas only when they are comparable to the data reported from the more intensely studied Wildlife Area.

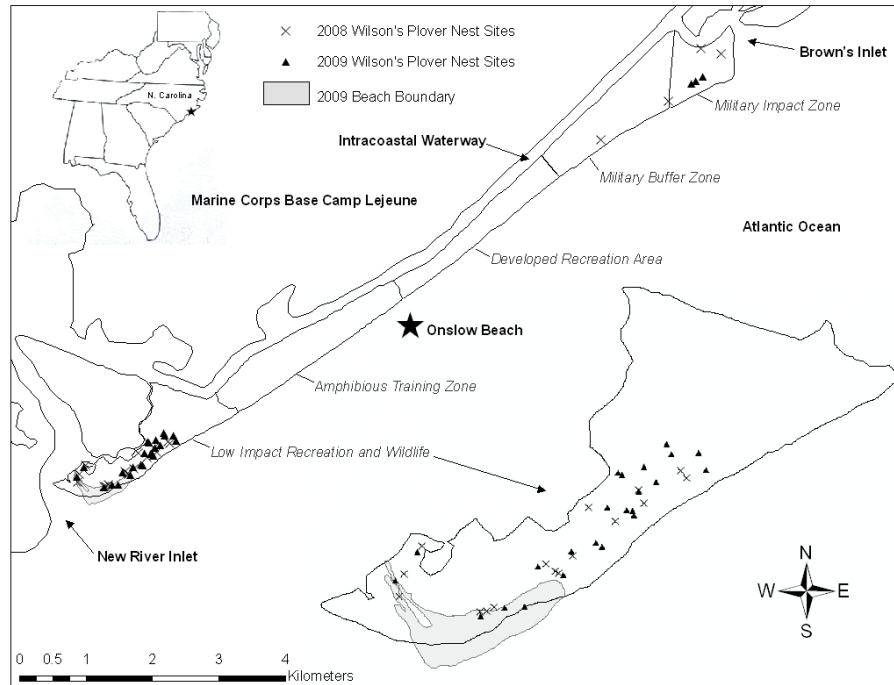


Figure 12-1. Study area at Onslow Beach on MCBCL, North Carolina, 2008–2009.

The low impact recreation and wildlife area is enlarged to clearly depict Wilson's Plover (*Charadrius wilsonia*) nest site locations, and changes in the beach boundary between years.

Habitats were typical of barrier islands in this region, and included, from the ocean to the marsh: ocean intertidal zone, backshore, primary dunes, interdune sand flats, maritime shrub and forest, and bay-side intertidal flats and marshes. An overwash fan formed during Hurricanes Bertha and Fran in 1996 removed woody vegetation and created an approximately 200 m wide by 1 km long interdune sand flat that included about 400-m of direct interface with marsh and bay-side intertidal flats. Since 1996, sparse low-growing vegetation and clumped grasses have grown in

the interdune sand flats (i.e., overwash), including primarily sea rocket (*Cakile harperi*), seashore elder (*Iva imbricate*), seaside pennywort (*Hydrocotyle bonariensis*), dotted horsemint (*Monarda punctata*), saltmeadow cordgrass (*Spartina patens*), sea oats (*Uniola paniculata*), American beach grass (*Ammophila breviligulata*), and smartweed (*Polygonum* spp.).

Field Methods and Analyses: We searched for nests in the Wildlife Area, primarily from 06:00–10:00 hours, from the end of March through mid-July in 2008 and 2009. In 2008, we searched for nests by walking daily along the primary dunes and through interdune sand flats. In 2009, we established three transects through the interdune sand flats (0.75 km, 0.77 km, and 1.61 km long, respectively, 45–190 meters (m) apart depending on patches of forest and large dunes) and three through the beach front habitat (0.53 km, 0.83 km, and 0.98 km long, respectively, 35–60 m apart). We searched for nests on these transects 2–3 days per week during the egg-laying period. We used behavioral cues such as territory defense, mock brooding, broken-wing displays, and incubation to locate nesting areas and nest sites.

We used a global positioning system (GPS; Garmin 76, Garmin International, Olathe, KS) to mark nest locations. We checked nests every 1–3 days, standing 2–5 m away to avoid attracting predators. In 2009, we wore rubber boots and sprayed them with Scent-A-Way™ (Hunter's Specialties, Cedar Rapids, IA) to minimize human scent around the nest site. We placed motion-triggered cameras (Reconyx Rapidfire ICR-Color RC55 digital cameras; Reconyx, Inc., Holmen, WI) inside secured wooden boxes to deter theft, at randomly selected nest sites to monitor causes of nest failure. In 2008, we placed cameras 5–8 m from the nest. In 2009, we moved the cameras to within 1.5–2.0 m of the nest (as in Sabine et al. 2005, 2006) to increase the probability of detection and to improve picture clarity. To deter avian predators from perching on the box, we placed a convex chicken-wire perch deterrent on top of each camera box.

We considered nests successful if at least one egg hatched. When we discovered a nest during initiation (i.e., < 3 eggs in nest and the male primarily incubating during daylight hours; Bergstrom 1986) we predicted hatch date to be 25 days from clutch completion. We considered clutch completion as a nest typically containing three eggs with the female primarily incubating during daylight hours (Bergstrom 1988, this study). We deemed a nest abandoned if the eggs did not hatch 5 days after the predicted hatch date or if adults were not observed defending a nest containing eggs for ≥ 72 hours. When nests failed, we examined the nest site for signs of the cause; including avian or mammalian tracks, shell fragments, or wrack deposition (due to tidal flooding). We investigated such signs at nest sites with and without cameras.

We trapped adult plovers within 48 hours of nest detection using drop box (Wilcox 1959, Graul 1979) and oblong funnel traps (Lessells 1984, Paton 1994), and banded them with three unique color bands on the left tarsometatarsus. We captured chicks by hand in or near the nest bowl usually 3–8 hours post-hatch ($N = 29$), or opportunistically at a later date ($N = 7$), and banded them using the same scheme as we did for adults. After adults and chicks were banded, we attempted to re-sight them every 1–2 days through the end of the season. We used the same searching techniques for re-sighting that were used for nest searching in 2008 and 2009 (i.e., we searched by walking the dune line and interdune sand flats in 2008 and along established transects in 2009).

In 2009, we used radio-telemetry to assist in locating broods during the first 5–10 days after hatch, when chicks were difficult to detect (see Ray 2011 thesis for details). We targeted adult males for transmitter attachment since they are the primary incubators approximately 48 hours prior to hatch and attend chicks more frequently than females (Bergstrom 1986, this study); however, females were tagged when males could not be trapped. We used 1.6-g BD-2 transmitters (Holohil Systems Ltd., Ontario, Canada) weighing $< 3\%$ of the average adult Wilson's Plover weight (average adult weight = approximately 68 g; this study, Corbat and Bergstrom 2000). We plucked dorsal contour feathers between the bird's scapulae in an approximately 1 square centimeter (cm^2) patch to fit the dimensions (18x10x3.5 millimeters [mm]) of the transmitters. We glued the devices to the exposed skin using cyanoacrylate gel (Loctite®, Westlake, Ohio). We used 3-element Yagi antennae and handheld receivers to locate the birds (Communication Specialists, Inc., Orange, California). We searched for radio-tagged Wilson's Plovers and broods every 2–4 days after tag attachment along the same transects established for nest searching and brood re-sighting until the tags were dropped or the birds migrated from the site.

We used Mayfield's method (1961, 1975) to calculate daily survival rate (DSR) and overall nest survival (DSR^d ; d = incubation days). For survival estimates, we adapted terminology and symbols for our models from Lebreton et al. (1992). We estimated chick survival for 2008 and 2009 using a Cormack-Jolly-Seber recapture model in program MARK (White and Burnham 1999) to generate apparent survival (Φ) and detection probabilities (ρ) based on weekly re-sightings. We estimated weekly survival rates (WSR) using four seven-day encounter periods (chicks fledge in 28 days; this study) with a fifth week accounting for post-fledge survival. We executed all model combinations including the effects of year (i.e., 2008 and 2009 re-sightings), time (i.e., weekly encounter), and additive and multiplicative interactions of year and time on apparent survival (Φ) and detection rate (ρ). We used the resultant top model as a basis for building additional biologically plausible models that included habitat covariates. We included the covariates hatch date, distance (km) from nest site to final brood foraging territory, distance (km) to nearest fiddler crab mud flat, and distance (km) to nearest vegetated edge (vegetation continuously ≥ 1 m tall for at least ≥ 10 m at a habitat type boundary) in the additional modeling efforts. Our chick re-sighting data was not overdispersed ($\hat{c} = 0.99$), therefore no model adjustments were necessary.

We used Akaike's Information Criterion (AIC, Akaike 1973) adjusted for small sample size (AIC_c) to determine the best fitting model for apparent chick survival (Anderson et al. 2001, Burnham and Anderson 2002). We considered models with ΔAIC_c values < 2.0 and model likelihoods ≥ 0.125 as equally competitive in estimating apparent survival (Burnham and Anderson 2002). Model covariates whose 95% confidence limits did not include zero were considered to be statistically significant in our results.

Since the single best-fit model was based on mean values of each covariate of interest, we executed individual models with user-specified covariate values (i.e., the actual covariate value for each brood) in program MARK to attain a WSR for each brood. Apparent survival for each brood was determined by raising the WSR to the number of weeks (w) to fledging ($w = 4$, WSR^w). Overall apparent survival for chicks in 2008 and 2009 was determined by averaging the brood WSR estimates and raising the mean to the number of weeks to fledging (i.e., 4 weeks).

Minimum-known-alive adult survival rate was calculated as the proportion of birds banded in 2008 that returned to Onslow Beach in 2009. In 2010, we resighted Wilson's Plovers banded in 2008–2009 in all habitats on Onslow Beach, on the northern-most end of Topsail Island adjacent to MCBCL, and along the ocean and back-side beach at Hammocks Beach State Park on Bear Island. We used these 2010 resightings to calculate apparent survival of birds that were banded as both adults and chicks in 2008–2009. Apparent survival is an estimate of the probability that an animal will remain in the population between periods of the study. Animals can leave the population through mortality or permanent emigration from the study area. We used Program MARK to calculate apparent survival (Φ) and recapture rate (p).

Results and Discussion

We found 20 nests in 2008 and 26 in 2009. These totals included three re-nests in 2008 and four in 2009. We typically observed a clutch size of three eggs (three nests in two years with two eggs) and an incubation period of 25–26 days (**Table 12-1**). Raw nest hatching success and Mayfield nest survival estimates were similar between years (**Table 12-1**). Predation was the leading cause of nest loss (**Table 12-2**). We were able to confirm more depredations in 2009 due to improved camera placement at nests; however, we continued to examine physical signs at the nest site as we did in 2008 (**Table 12-2**). For both years, predators included Virginia opossums (*Didelphis virginiana*, seven nests), raccoons (*Procyon lotor*, three nests), ghost crab (*Ocypode quadrate*, one nest), and unidentified rodents (Rodentia, two nests). In two cases, opossums were the first of two sequential nest predators; consuming two eggs before a raccoon consumed the last one the next day, and eating two eggs from another nest prior to a ghost crab taking the last one two days later.

Mean chicks hatched per pair and fledged per pair were 1.56 and 0.94, respectively, for both years combined (**Table 12-1**). Ninety percent (18 out of 20) of adult Wilson's Plovers banded in 2008 were observed on the study area in 2009, but only 9.5% (two out of 21) of the 2008-banded chicks were observed in 2009.

Table 12-1. Demographic estimates (\pm standard error [SE]) for Wilson's Plovers (*Charadrius wilsonia*) on Onslow Beach, MCBCL, North Carolina, 2008–2009.

Year	Mean clutch size	Incubation days	Hatching success (≥ 1 egg)	Mayfield nest survival	Chicks hatched per pair	Chicks fledged per pair	Days to fledging
2008	2.80 \pm 0.12 (20)	25 (9)	45% (17)	46% (17)	1.47 \pm 0.36 (17)	0.88 \pm 0.26 (17)	28 (9)
2009	2.96 \pm 0.04 (26)	25–26 (11)	50% (22)	44% (20)	1.64 \pm 0.31 (22)	1.00 \pm 0.25 (20)	28–29 (11)

Note: Sample size of nests/pairs/broods used in calculating each estimate is in parentheses after value.

Table 12-2. Causes of failure for Wilson's Plover (*Charadrius wilsonia*) nests on Onslow Beach, MCBCL, North Carolina, 2008–2009.

	Depredated <i>N</i> ^a (%)	Abandoned <i>N</i> (%)	Washed out <i>N</i> (%)	Unknown <i>N</i> (%)	Physical signs	Camera confirmation	Both
2008	3 (15)	1 (5)	1 (5)	6 (30)	3	0	0
2009	8 (31)	1 (4)	0 (0)	4 (15)	3	6	3
Total	11 (24)	2 (4)	1 (2)	10 (22)	6	6	4

^a *N* = number of nests failed by given cause; total nests observed were 20 (2008) and 26 (2009)

Note: Confirmed depredations via physical signs, camera confirmation, or both techniques are reported.

Only hatch date and distance from nest site to final brood territory (km) were used in building biologically plausible models, and both appeared in the resultant single top model (**Table 12-3**). We excluded the other two covariates because often times the fiddler crab mud flat was the brood's final foraging territory, and vegetated edges (as previously defined) were almost always next to sound-side mud flats (i.e., fiddler crab mud flats). The top model including covariates estimated the maximum possible chick survival based on mean values (\bar{x} distance to final foraging territory = 0.54 km; \bar{x} hatch date = 20th day of the breeding season – approximately 5 Jun at MCBCL) used in our analyses. Wilson's Plover chick survival was best predicted by a model including the distance a brood traveled from its nest site to its final foraging territory (km), and the date the brood hatched (**Table 12-3**). We identified a positive relationship between chick survival and distance to final foraging territory, while hatch date was negatively related to chick survival (i.e., confidence limits do not encompass zero, **Table 12-3**, **Figure 12-2**).

Table 12-3. Model-selected parameter estimates (β_x), standard errors (\pm SE), and 95% lower confidence limit (LCL) and upper confidence limit (UCL) for the best-fitting model a ($AIC_c < 2.00$ or model likelihood ≥ 0.125) predicting Wilson's Plover (*Charadrius wilsonia*) chick survival (N = 20 broods) on Onslow Beach, MCBCL, North Carolina, 2008–2009.

Model Covariates	β_x	\pm SE	95% LCL	95% UCL
Hatch Date	-0.23	0.10	-0.44	-0.03
Distance to Final Foraging Territory (km)	2.73	1.16	0.46	4.99

^a $\{\Phi(\text{HatchDate DistFTerr}) \rho(\text{year} \times \text{week})\}$ was the best-fitting model predicting chick survival (Φ) as a function of hatch date (HatchDate), and the distance (km) a brood traveled from its nest site to its final foraging territory (DistFTerr), $AIC_c = 222.25$, ΔAIC_c (difference between candidate model's score and the top model score) = 0.00, K (number of model parameters) = 11, w_i (weight of each model as compared to all candidate models) = 0.87, model likelihood = 1.00.

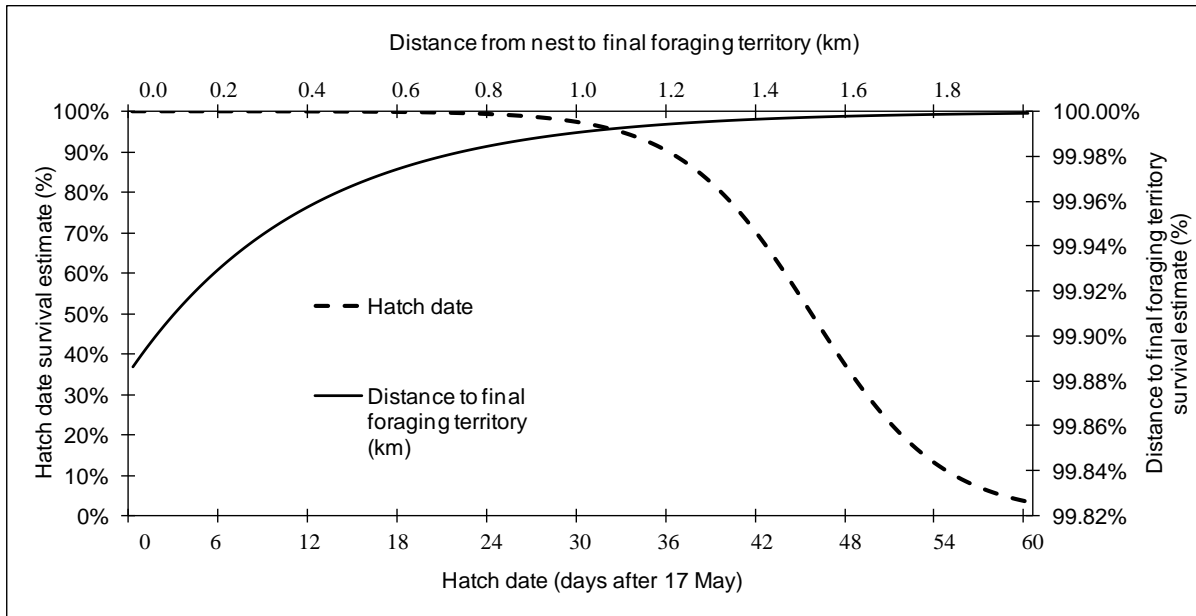


Figure 12-2. Predicted survival of Wilson's Plover chicks based on the top-ranked model containing actual covariate values predicting survival as a function of hatch date and distance (km) from nest to final foraging territory at MCBCL, North Carolina, 2008–2009.

Weekly survival rate and overall apparent survival from our top model, which predicted chick survival based on average apparent survival estimates from the user-specified covariate models for all broods, was 93% and 75% respectively (**Table 12-1**). In 2009, we observed 20 of 30 chicks (0.67 ± 0.08) at age 28 days or older, and 15 of 25 chicks (0.60 ± 0.13) fledged in 2008. Detection probabilities of chicks (ρ) differed by week within each year (2008 = 0.21 – 1.00, 2009 = 0.59 – 0.77).

The apparent survival of Wilson's Plovers banded as adults was $82 \pm 0.09\%$ from 2008–2010, while the apparent survival of Wilson's Plovers banded as chicks was only $13 \pm 0.08\%$ during this same time period.

Clutch sizes and incubation periods in this study were similar to those observed in Georgia and Texas (2.90–2.92 eggs, 25–27 days; Bergstrom 1988, Corbat 1990; **Table 12-2**). However, nest survival at Camp Lejeune was higher than what was documented in those studies (means of 23% and 27% respectively; Bergstrom 1988, Corbat 1990; **Table 12-2**), but similar to Hood's (2006) findings in south Texas (58%, **Table 12-2**). Nest predators identified in those studies included raccoons, coyotes (*Canis latrans*), bobcats (*Lynx rufus*), feral hogs, unidentified rodents, and unidentified birds. In addition, some nests in Texas were trampled by cattle. We identified raccoons and opossums as the primary nest predators in our North Carolina study. Bobcats were present at Camp Lejeune, but we found no evidence that they depredated Wilson's Plover nests. In 2009, one motion-triggered camera recorded a bobcat walking within 1–2 m of a nest at night; this nest hatched successfully.

We identified the cause of failure for a higher percentage of nests in 2009 than in 2008, likely because we put cameras closer to nests in 2009. In 2008, some nests were lost, but the predators did not trigger the cameras and we could not easily confirm the suspected cause of failure from physical signs (tracks and egg shell fragments) alone. We moved our cameras closer (i.e., within 1.5–2.0 m) to nest sites in 2009, and increased confirmed depredation events by approximately 15%, subsequently reducing unknown nest fates from 30% to 15% in 2008. In our study and others (Bergstrom 1988, Corbat 1990), nests with unknown fates had no physical signs of depredation or wash out (e.g. flooding, high tides), and there were no adults or pairs defending the nest as if the eggs hatched and the chicks were nearby. It is likely that nests with unknown fates were depredated; however, blowing sand may have concealed indicative signs and some predators, such as birds, may not leave tracks (Bergstrom 1988, Corbat 1990).

We found few cases of nest abandonment related to direct human disturbance, similar to studies in Texas (Bergstrom 1988) and Georgia (Corbat 1990). We observed only one nest abandonment each year; both cases occurred over Memorial Day weekend when an influx of boats and people were observed picnicking and walking near nest sites that were not located within protected areas marked with symbolic fencing and signs. Roche et al. (2010) found that the disappearance of an attending adult was the primary reason behind nest abandonment in the Great Lakes Piping Plover population. It is plausible this happened in 2008 on Onslow Beach, as we never observed the male with the female or incubating the nest. We did not observe any abandonment due to camera placement or regular monitoring of nest sites (i.e., nest checks every 2–3 days). Similarly, Sabine et al. (2005, 2006) did not find that the close proximity of their cameras (1.5–2.0 m) to American Oystercatcher (*Haematopus palliatus*) nests caused nest abandonment.

Nest failure due to flooding or high tides was also minimal during our study (only one nest in 2008) despite anomalous sea level heights (+ 0.20 m residual (observed –predicted) water height) reported by the National Oceanic and Atmospheric Administration (NOAA) for June and July 2009 (Sweet et al. 2009). Most of the Wilson's Plover nests in this study were located in interdunal habitat (i.e., overwash) or immediately adjacent to it along primary dunes. The mean elevation of the overwash in the southern end of the island was 1.52 m above mean sea level (A. Rodriguez, University of North Carolina at Chapel Hill Institute of Marine Sciences, personal communication), and no major storm events (i.e., Nor'easters, tropical storms, or hurricanes) occurred during the breeding seasons of this study.

Hood's (2006) overall nest survival estimate (58%) as calculated from a recently developed generalized linear modeling approach (Dinsmore et al. 2002, Rotella et al. 2004) was higher than our nest survival estimates (46%, 44% in 2008, 2009) and those of Bergstrom (1988) and Corbat (1990), both of which used Mayfield's method for calculating nest success (1961, 1975). The Mayfield method assumes that nest survival is constant throughout the incubation period, while the generalized linear modeling approach (i.e., a likelihood-based model) is more flexible and able to account for spatial- and temporal-specific covariates influencing variation in daily nest survival (Rotella et al. 2004). Nest survival estimates using Mayfield's method may result in underestimated survival rates since day-to-day variation is not accounted for, and nests are not commonly monitored from the onset of incubation (Mayfield 1975), as was the case in this study. Hood (2006) did not find evidence that seasonal or annual variation or nest age influenced Wilson's Plover nest survival, but rather discovered that an assumption of constant survival best fit the data. Given her findings (and our raw calculations), it is plausible that we attained a reasonably precise overall nest survival estimate using Mayfield's method.

We are unaware of previous published estimates of Wilson's Plover chick survival. In this study, chick survival was negatively related to hatch date such that later hatching nests had lower chick survival, similar to findings for other shorebirds (Nisbet et al. 1978, Moreno 1998, Arnold et al. 2004, Arnold et al. 2006, Catlin 2009). As in previous studies, we hypothesize that this negative relationship between hatch date and chick survival is due to fact that experienced breeders arrive to breeding grounds first (Møller 2001, Møller et al. 2004) and establish higher quality nesting and foraging territories (Aebischer et al. 1996). This mechanism remains to be tested for Wilson's Plovers. Those broods hatching later in the breeding season may also experience reduced survival due to heat stress associated with higher temperatures (Burger 1982, Safina and Burger 1983), an influx in juvenile avian and mammalian predators at this time of year, or a reduction in food availability (Loefering and Fraser 1995, Elias et al. 2000).

We included distance from the nest to the final foraging area in our candidate models expecting that greater distances traveled to reach foraging sites would increase the chances of chick predation. In contrast to our expectation, we found a positive relationship between survival and the distance to the final foraging territory. This may be explained by the foraging patterns in the first days after hatching. In 2008, the final foraging territory was always a fiddler crab (*Uca* spp.) mud flat. In 2009, birds often established two-fold foraging territories encompassing fiddler crab mud flats and another habitat type (e.g. interdune sand flat or beach front containing ephemeral pools). When nests hatched on Onslow Beach, broods foraged near the nest site on insects among sparse clumps of vegetation on interdune sand flats or along dune toes. Chicks easily camouflaged themselves during foraging by remaining motionless in vegetation and using litter

and debris as protective cover (e.g. driftwood, shells, dead vegetation, peat deposits). After ≤ 10 days, broods typically moved toward sound-side mud flats where final foraging territories were established, and where chicks fed primarily on fiddler crabs until fledging. Of the nine flats in the study area, six were surrounded by vegetation ≥ 1 m tall in ≥ 10 m increments which might offer cover and concealment for mammalian predators (Dijack and Thompson 2000, Erwin et al. 2001, Mazzocchi and Forsys 2005), such as raccoons and opossums observed on Onslow Beach during both years of the study. We hypothesize that the farther the nest site (i.e., the initial foraging territory) was from the densely vegetated edges (≥ 1 m tall) of sound-side mud flats, the higher the probability that chicks escaped potential predators in their first days of life when their motor skills were relatively undeveloped (i.e., hiding versus running). Kotliar and Burger (1986) suggested that dense vegetation may inhibit maneuverability of Least Tern (*Sterna antillarum*) chicks evading predators. As Wilson's Plover chicks progress in development (≥ 7 days observed in this study), their motor skills improved, and they began to run as a mechanism to escape perceived threats, less often sitting motionlessly under clumped vegetation to evade potential danger. Increased chick mobility and independence may allow adults and broods begin to establish final foraging territories on fiddler crab mud flats (that may or may not be obstructed by vegetation ≥ 1 m tall) at this stage of chick growth.

This research contributes valuable information towards evaluating the validity of the population goals for Wilson's Plovers as identified in the U.S. Shorebird Plan for the southeastern coastal plains region (Hunter 2002). The plan set a regional goal to double the Wilson's Plover population over the next 50 years (Hunter 2002), and suggested a 5-yr mean productivity of 1.5 fledglings per breeding pair based on estimates from Piping Plovers (*Charadrius melodus*) and Snowy Plovers (*Charadrius alexandrinus*, Page et al. 2009). We observed a mean fledging rate over a 2-yr period of only 0.94 fledglings per pair. It may be plausible that 1.5 fledglings per breeding Wilson's Plover pair are unnecessary to maintain a viable population. An increased understanding of Wilson's Plover population demography in this region is needed before setting target productivity values necessary to sustain or increase this population. For instance, target productivity rates for sustaining the Threatened Atlantic coast Piping Plover population were determined by analyzing 10 years of pooled demographic data collected from areas that accounted for 90% of the breeding coastal population (USFWS 1996); thus, at this stage in our knowledge of Wilson's Plover demography, it is premature to estimate sustainable productivity levels.

Peer reviewed research efforts pertaining to all life history aspects of the Wilson's Plover to date are modest. Considering the 1) dynamic nature of coastal barrier ecosystems that Wilson's Plovers depend on for breeding, 2) documented anthropogenic impacts that have reduced the quality, quantity, and availability of shorebird nesting and foraging habitat over the past 50 years on barrier islands (Brown et al. 2001, Peterson and Bishop 2005, Peterson et al. 2006, Schlacher et al. 2008, Defeo et al. 2009), and 3) current predictions of sea level rise which may reduce the availability of breeding habitat (Galbraith et al. 2002, IPCC 2007, Defeo et al. 2009), ongoing demographic research and monitoring of this species is critical in sustaining and growing regional populations while simultaneously conserving Wilson's Plovers across their entire range.

Section 2: Wilson's Plover Habitat Selection

Materials and Methods

Study Site: We studied breeding Wilson's Plovers at Onslow Beach, MCBCL, North Carolina from March–August 2008 and 2009. Onslow Beach (77°20'9.751"W 34°31'52.911"N) is a 12.9-km coastal barrier island bounded by the New River Inlet and Brown's Inlet (**Figure 12-1**). The south end of the island (Wildlife Area) is designated and managed for Low Impact Recreation and Wildlife and is closed to recreational vehicles from 1 April–31 August, annually. The Amphibious Training Zone is designated for military training and the Developed Recreation Area provides recreational opportunities for Marine Corps personnel and their families; no nesting Wilson's Plovers were found in these two areas, so we do not discuss them further. Access to the Military Buffer Zone was restricted and sporadic; we include data from these areas only when they are comparable to the data reported from the more intensely studied Wildlife Area (**Figure 12-1**).

For purposes of this study, we described three habitat types found in both the Wildlife Area and Military Buffer zones: 1) sound-side intertidal mud flats colonized by fiddler crabs (fiddler flats); 2) sparsely vegetated sand flats behind the primary dunes, and adjacent to sound-side mud flats (interdune sand flats), and 3) ocean beach front consisting of the ocean intertidal zone, the backshore (open sand between the intertidal zone and foredune), and primary dunes (beach front). Vegetation on the fiddler flats included smooth cordgrass (*Spartina alterniflora*) and glasswort (*Salicornia* spp.). An overwash fan formed in the interdune sand flats of the Wildlife Area when Hurricanes Fran and Bertha in 1996 removed woody vegetation and created an approximately 200 m wide by 1 km long interdune sand flat that included about 400 m of direct interface with marsh and bay-side intertidal flats. Since 1996, sparse low-growing vegetation, such as sea rocket (*Cakile harperi*), seashore-elder (*Iva imbricate*), seaside pennywort (*Hydrocotyle bonariensis*), and dotted horsemint (*Monarda punctata*); and clumped grasses and forbs including saltmeadow cordgrass (*Spartina patens*), sea oats (*Uniola paniculata*), American beach grass (*Ammophila breviligulata*), and smartweed (*Polygonum* spp.) have grown in these interdune sand flats. Beach front habitat included those plants adapted to the coastal dynamics of tidal fluctuations, wind, and sand movement; specifically, clumped grasses growing on primary dunes (e.g. sea rocket, new growth seashore-elder, dune spurge (*Euphorbia polygonifolia*), sea oats, and American beach grass). While the Military Buffer zone also contained these habitat types, they also had a complex dune system unlike the rest of the island. Primary and secondary dune heights in the Military Buffer Zone were more than double the height (~3-5 m) of the dunes in the Wildlife Area (~0-2 m). Further, the interdune sand flats in the Military Buffer Zone were more commonly adjacent to maritime forest than those in the Wildlife Area, which were adjacent to sound-side inter-tidal flats.

Typical of barrier islands, Onslow Beach differed in size and shape during the two years of the study. In 2009, Onslow Beach experienced unusually high water levels from 18 – 26 June 2009 (Sweet et al. 2009), which covered most fiddler flats across all tidal states. Further, there was substantial sand accretion at the south end of the island between 2008 and 2009 that resulted in the addition of approximately 15 hectares (ha) of beach front in 2009 (**Figure 12-1**). The newly accreted area was largely vegetation-free and contained several ephemeral pools.

Nest searching and habitat measurements: In 2008, we walked the study area to search for Wilson's Plover nests and used behavioral cues (e.g. territorial defense, broken-wing displays, incubation posture) to locate nest sites. In 2009, we established two paths through fiddler flats (0.78 km and 1.36 km, respectively; 1.1 km apart separated by maritime forest), and three paths each on beach front (0.53 km, 0.83 km, and 0.98 km, respectively; 35–60 m apart separated by dunes), and interdune sand flats (0.75 km, 0.77 km, and 1.61 km, respectively; 45–190 m apart separated by dunes and woody shrubs) in the Wildlife Area. We walked these paths 2–3 times weekly in 2009 searching for nests. We monitored located nests in the Wildlife Area every 1–3 days in both years and nests in the Military Buffer zone opportunistically. We considered nests successful if ≥ 1 egg(s) hatched.

We sampled substrate at the nest site within 3 days after hatching or failure using a 1 square meter (m^2) polyvinyl chloride (PVC) pipe quadrat containing 5 x 5 centimeter (cm) cells made of plastic string (Cook and Bonham 1977). We centered the quadrat over the nest and performed ocular estimates of the percent composition of pebbles (2–64 mm), cobble (> 64 mm), small shells (< 2 mm), medium shells (2–64 mm), and large shells (> 64 mm). We determined percent composition by counting the number of cells containing the substrate variable and dividing by the total cells in the quadrat.

We recorded vegetation characteristics at the nest site that included 1) an ocular estimate of percent composition of vegetation cover within a 1 m^2 quadrat, 2) height of tallest vegetation (i.e., vegetation ≥ 1 m tall) within a 5-m radius of the nest bowl, and 3) vegetation growth form within 15 cm of the nest bowl. We defined vegetation growth form as either 1) bare ground and low-growing sparse vegetation (e.g. sea rocket, seaside pennywort, new-growth seashore-elder, and dune spurge) or 2) clumped grasses (e.g. sea oats, American beach grass, saltmeadow cordgrass, smartweed), or any combination of clumped vegetation and low-growing sparse vegetation. Finally, we recorded distance (m) to nearest nest (any species), and distance (m) to fiddler flat from each nest site.

We sampled the same characteristics at a paired, randomly-selected point 1–18 m from the nest within the same habitat type to examine differences between used and non-used sites within the same locale. We chose the upper sampling limit (18 m) as half of the shortest inter-nest distance documented for Wilson's Plovers in Bergstrom's (1982) Texas study.

Brood identification and territory establishment: We trapped adult plovers on nests within 48 hours of nest detection using drop box (Wilcox 1959, Graul 1979) and oblong funnel traps (Paton 1994, Lessells 1984), and banded them with three unique color bands on the left tarsometatarsus. We captured chicks by hand in or near the nest bowl usually 3–8 hrs post-hatch ($n = 29$), or opportunistically at a later date ($n = 7$), and banded them using the same scheme as we did for adults described in Section 1. We attempted to capture and band all adults and chicks from each nest. We searched for banded, foraging adults and chicks in the same manner as we searched for nests in 2008 and 2009. We recorded locations of banded individuals observed in all habitat types using a handheld GPS (Garmin 76, Garmin International, Olathe, KS).

We sampled all known fiddler flats in the study area to determine which habitat features influenced flat selection in establishing a brood foraging territory. We sampled each fiddler flat

within 2 hours of low tide (to ensure flats were not inundated) once in each of three periods in 2009 (21 May–25 May, 5 June–9 June, and 30 June– 6 July).

We characterized vegetation along a path of least obstruction from the interdune sand flat (where most Wilson's Plovers nested in this study) to each fiddler flat (where most broods established final foraging territories) during each sampling period to determine if dense vegetation prevented use of certain flats. Starting points on the interdune sand flats and sampling paths were established using a combination of criteria. First, the interdune sand flat edge at the start of each transect was identified as the point where vegetation cover was $\leq 30\%$ within a 0.5 m^2 plot. Second, sampling paths between the interdune sand flat and fiddler flat were selected after having met one or both of the following criteria: 1) a continuous path approximately 0.5 m wide where $>50\%$ bare ground was visible between the sand flat and fiddler flat (e.g. a predator trail or path with less vegetation compared to its immediate surroundings), and/or 2) the shortest distance between the sand and fiddler flats. Lastly, we defined the fiddler flat edge when a plot contained $\leq 50\%$ *Spartina* spp. or glasswort cover, and its location was $\leq 5 \text{ m}$ from the bare exposed flat. We recorded path locations using a handheld GPS and collected data along the same path in each of the sampling periods.

We used a modified vegetation density board (Higgins et al. 2005) to obtain an index of vegetation obstruction along each path. The density board contained three rows (11.3 cm high) and 11 columns (8.3 cm wide) with each grid row containing the numbers 3 (top row), 2 (middle row), or 1 (ground row). We performed density board readings every 10 m along the path until the edge of the fiddler flat was reached. Observers placed their heads as close to the ground as possible 5 m from the density board and summed the numbered squares obstructed by $\geq 70\%$ by vegetation. We used the average of the density board readings taken along the path to calculate the obstruction index for each fiddler flat during each sampling period. We recorded a boundary along the defined edge of each fiddler flat with a GPS, and uploaded the track into ArcMap 9.3 (ESRI, Redlands, CA) as a polygon shape file to calculate flat area (m^2). Finally, we measured the shortest distance (m) from the fiddler flat to water, and categorized the flat as 1) frequently subject to tidal inundation or 2) infrequently subject to tidal inundation.

For each fiddler flat in each period, we used Hawth's Tools in ArcMap 9.3 to generate 1) five random points within a 5-m buffer extending inward from the vegetated fiddler flat edge, and 2) five points in the area extending from the 5-m buffer towards the bare or nearly-bare center of the flat. We counted fiddler crab burrows and individual crabs (males, females/juveniles, or unknown) within a 1 m^2 quadrat centered on each point. Depending on vegetation density and line of sight distance, we stood 1–3 m from the plot to count crabs for 5 min using 8 x 40 mm binoculars. We counted all individuals 3–4 times throughout the 5-min observation and recorded the greatest count in each age class as a single value for the sample. At the end of the observation, we approached the quadrat and counted the burrows (Macia et al. 2001). We calculated separate averages for fiddler crab and burrow counts on each flat. For each 1-m^2 plot, we recorded an ocular estimate of the percentage of bare ground, smooth cordgrass, and glasswort.

Foraging site selection and behavioral observations: We gathered information about Wilson's Plover foraging site selection and behavior by conducting focal observations of banded adults and chicks across all tidal stages on fiddler flats, interdune sand flats, and beach front habitat.

We concealed ourselves 10–80 m away from the brood in blinds or behind natural barriers, such as vegetated dunes, for each observation. We continuously recorded 5-min focal samples of foraging attempts that included pecks, which are indicative of insect consumption, and “run and grabs,” which is a behavior used by Wilson’s Plovers to hunt fiddler crabs (Altmann 1974, Lehner 1979, Tyler 1979). Each focal observation included a single chick or adult. After we obtained one focal observation for each visible chick in a brood, we sampled the adult male or female (or both, if present). We repeated observations of individuals when possible. Our sampling took 30 min – 2 hrs per brood, during which 1-8 focal bird samples were collected. We included samples in analyses if the bird was visible for ≥ 2.5 min. We calculated foraging rates (attempts per min) for adults and chicks and categorized them by habitat type (Elias et al. 2000, Fraser et al. 2005). Mean foraging rates were calculated for adults and chicks within each brood.

After the observation period ended, we conducted prey sampling within 5 m of each location most used by each focal bird. At each focal bird foraging location, we sampled insects using wooden paint stirrers covered in Tree Tanglefoot® Insect Barrier (The Tanglefoot Company, Grand Rapids, Michigan; Loegering and Fraser 1995, Elias et al. 2000). Sticks were positioned with one inserted vertically into the substrate and the other placed horizontally on the ground. We exposed “sticky sticks” for approximately 40 min, leaving an observer nearby (≥ 40 m) to prevent plovers from coming into contact with the sticks. Insects were counted and identified to order at the end of the sampling period. We accounted for exposure time by dividing our prey counts by the number of minutes each set of sticks was collecting insects, and report the results as insects collected per min. We measured vegetation characteristics at each focal bird sampling location (within a 1-m² plot) by visually estimating 1) percent cover of vegetation and species composition, 2) distance (m) to vegetative cover beyond the plot, and 3) distance (m) to water from the center of the sampling plot.

We sampled prey abundance (insects, fiddler crabs, and fiddler crab burrows) and vegetation in the same manner described above at paired, randomly-selected non-use points within the same habitat ≤ 40 m from the used, focal bird sampling points. The upper limit (40 m) between used and non-used points was selected as it is the mean of the lengths and widths of all fiddler flats in the Wildlife Area. Distance and direction from the used point to the paired non-use point was selected randomly. If the habitat edge was reached before the selected distance was reached, the researcher would reverse direction and continue until the selected distance was traversed.

Inter-annual variation in fiddler flat use and foraging behavior: We compared inter-annual observations of broods, and analyzed differences in foraging behavior potentially related to anomalous water heights (Sweet et al. 2009) in 2009 and beach front sand accretion that occurred between the 2008 and 2009 breeding seasons on Onslow Beach. We plotted the daily proportion of Wilson’s Plover broods observed using fiddler flats in both years during the time frame corresponding with near-complete fiddler flat inundation in 2009 against the daily mean residual water height (m, observed height – predicted height) within 2 hours of the lowest tide (i.e., daily average based on five hourly water heights) to determine if a higher proportion of broods used this habitat at low tide in 2008 than in 2009. We used predicted and observed water heights reported at the NOAA tidal station in Beaufort, North Carolina (the closest tidal station to Onslow Beach) to calculate daily mean residual water heights. We compared mean adult and chick foraging rates for each brood by year and habitat type.

Statistical analyses: We used SAS 9.2 (SAS Institute Inc., Cary, NC) for all analyses. We used logistic regressions to assess which habitat features distinguished 1) nest sites from paired, unused locations, 2) successfully hatched nests from failed nests, 3) fiddler flats containing brood foraging territories from those that did not, and 4) foraging sites from paired, non-used areas. To identify candidate variables used in modeling efforts, we computed Pearson correlation coefficients (r) for all habitat variables collected. We considered variables with $r \geq 0.60$ highly correlated, and chose the variable best representing the habitat characteristic of interest or combined correlated variables into one composite variable. We executed biologically plausible single- and multi-variable logistic regressions, and ascertained model fit using Hosmer and Lemeshow's (2000) goodness-of-fit test. We used AIC (Akaike 1973) adjusted for small sample size (AIC_c) to rank the logistic models (Burnham and Anderson 2002, Anderson et al. 2001). We considered models with ΔAIC_c values ≤ 2.0 as top models, but also reported models with likelihoods ≥ 0.125 (Burnham and Anderson 2002) as being competitive. When our analyses resulted in ≥ 1 competitive model(s), we used model-averaging to estimate model parameters and confidence limits to determine the relative importance (R_i) of each covariate from all model results (Burnham and Anderson 2002). Relative importance (R_i) was calculated by summing the AIC_c weight of each variable for all model results (Burnham and Anderson 2002). Post-hoc, we used Pearson's chi-squared analyses (χ^2_{df}) to compare the proportions of successful and failed nests placed in each of the two vegetation growth form categories examined in logistic regressions.

We used Wilcoxon signed-rank tests to examine 1) differences in prey abundance between used foraging sites and paired, non-used sampling points, and 2) inter-annual variation in the proportion of habitat use and mean adult and chick foraging rates across all habitat types. We report means \pm standard errors (SE), medians, and 25–75% inter-quartile ranges (Q1-Q3) in the results; we consider $P \leq 0.05$ to be significant.

Results and Discussion

Correlates of nest site selection and hatching success: We found 20 Wilson's Plover nests in 2008 and 26 in 2009. Accounting for both years, most nests were in the interdunal area, 19 on sand in vegetation and 12 on dunes in clumped grasses. Eleven nests were on the beach front berm (150–200 m wide); nine of these were in sparsely distributed clumped grasses, and two were placed in vegetation-free areas.

Shells 2 to ≥ 64 mm, appeared in both top models differentiating used nest sites from paired unused locations (**Table 12-4**); this variable had a high relative importance ($R_i = 0.87$), but its confidence limits encompassed zero, and thus its effect on nest site selection was unclear (**Table 12-5**). While distance to the nearest nest of any species and tall vegetation within 5 m were in the top models, the relative importance values of these variables were low and their coefficients were not different than zero (**Table 12-5**).

Table 12-4. Top-ranked models ($\Delta AIC_c \leq 2.00$ or model likelihood ≥ 0.125) from 36 single- and multi-variable logistic regressions of habitat characteristics at Wilson's Plover (*Chardrius wilsonia*) nest sites and paired non-used locations ($n = 42$ nests) at Onslow Beach, MCBCL, North Carolina, 2008–2009.

Variables in Model ^a		K^b	Prob $> \chi^2$ ^c	AIC_c ^d	ΔAIC_c ^e	w_i ^f	Model Likelihood
MLShell	TallVeg5	3	0.64	46.81	0.00	0.35	1.00
MLShell	DistNrNest	3	0.53	48.79	1.97	0.13	0.37

^a DistNrNest = distance to nearest nest site (m) of any species; MLShell = percent cover of medium (2-64 mm) and large (> 64 mm) shells within 1-m² plot; TallVeg5 = height of tall vegetation (≥ 1.0 m) within a 5-m radius of sample sites.

^b K = Number of model parameters.

^c Prob $> \chi^2$ = Hosmer and Lemeshow goodness-of-fit test for binary logistic regression models.

^d AIC_c = Akaike's Information Criterion corrected for sample size.

^e ΔAIC_c = Difference between any given model's AIC_c and the best-fit model.

^f w_i = Weight of each model as compared to all candidate models.

Table 12-5. Model-averaged parameter estimates, unconditional SE, LCL and UCL, and relative importance (R_i) from 36 single- and multi-variable logistic regression models of habitat characteristics at Wilson's Plover (*Chardrius wilsonia*) nest sites and paired non-used locations ($n = 42$ nests) on Onslow Beach, MCBCL, North Carolina, 2008–2009.

Variable ^a	Parameter Estimate	SE	95% LCL	95% UCL	R_i ^b
Intercept	0.00	0.00	0.00	0.00	—
MLShell	-0.08	0.05	-0.17	0.02	0.87
TallVeg5	0.38	0.51	-0.62	1.38	0.44
DistNrNest	0.01	0.01	-0.02	0.03	0.15

^a MLShell = percent cover of medium (2-64 mm) and large (> 64 mm) shells within 1-m² plot; TallVeg5 = height of tall vegetation (≥ 1.0 m) within a 5-m radius of sample site; DistNrNest = distance (m) to nearest nest site of any species.

^b R_i = Relative importance.

Vegetation growth form (**Table 12-6**) within 15 cm of the nest bowl was in all top models explaining the success or failure of a Wilson's Plover's nest (**Table 12-7**). Despite its high importance ($R_i = 0.75$), the confidence interval for vegetation growth form overlapped zero (**Table 12-7**). Sixteen of 20 (80%) nests placed in clumped grasses or mixed vegetation were successful, compared to 9 of 22 (41%) nests in low-growing sparse vegetation or open sand ($\chi^2_1 = 6.66$, $P = 0.01$, $n = 42$). Mean percent vegetation cover at nest sites was 15.33 ± 2.33 for both years (**Table 12-4**); successfully hatched nests had an average $18.85 \pm 3.57\%$ vegetation cover within 1 m² of the nest bowl.

Table 12-6. Top-ranked models ($\Delta AIC_c \leq 2.00$ or model likelihood ≥ 0.125) from 37 single- and multi-variable logistic regressions of habitat characteristics influencing nest ($n = 42$ nests) hatching success of Wilson's Plovers (*Chardrius wilsonia*) at Onslow Beach, MCBCL, North Carolina, 2008–2009.

Variable(s) in Model ^a		K^b	Prob $> \chi^2^c$	AIC_c^d	ΔAIC_c^e	w_i^f	Model Likelihood
VegForm	—	2	.	53.07	0.00	0.14	1.00
VegForm	MLShell	3	0.16	53.08	0.01	0.14	1.00
VegForm	VegCover	3	0.83	53.53	0.46	0.11	0.79
VegForm	TallVeg5	3	0.09	53.86	0.79	0.10	0.68
VegForm	Sshell	3	0.10	53.96	0.89	0.09	0.64
VegForm	DistFidd	3	0.46	54.02	0.96	0.09	0.62
VegForm	DistNrNest	3	0.59	54.03	0.96	0.09	0.62

^a VegForm = vegetation growth form within 15 cm of the nest site defined as (1) bare ground or low-growing sparse vegetation or (2) clumped grasses or a combination of clumped grasses and low-growing sparse vegetation; MLShell = percent cover of medium (2-64 mm) and large (> 64 mm) shells within a 1-m² quadrat placed over the nest site; VegCover = percent cover of dead and live vegetation; TallVeg5 = height of tall vegetation (≥ 1.0 m) within a 5 m radius of the nest site; Sshell = percent coverage of small (< 2 mm) shells within a 1-m² quadrat placed over the nest site; DistFidd = distance to nearest fiddler crab (*Uca* spp.) flat from the nest site; DistNrNest = distance to nearest nest site (m, any species) from the nest site.

^b K = Number of model parameters.

^c Prob $> \chi^2$ = Hosmer and Lemeshow goodness-of-fit test for binary logistic regression models.

^d AIC_c = Akaike's Information Criterion corrected for sample size.

^e ΔAIC_c = Difference between any given model's AIC_c and the best-fit model.

^f w_i = Weight of each model as compared to all candidate models.

Table 12-7. Model-averaged parameter estimates, unconditional standard errors (SE) and confidence limits (CL), and relative importance (R_i) from 37 single- and multi-variable logistic regression models of habitat characteristics influencing nest hatching success ($n = 42$ nests) of Wilson's Plovers (*Chardrius wilsonia*) on Onslow Beach, MCBCL, North Carolina, 2008–2009.

Variable ^a	Parameter Estimate	SE	Lower 95% CL	Upper 95% CL	R_i ^b
Intercept	-2.42	1.74	-5.82	0.98	—
VegForm	1.29	0.99	-0.66	3.24	0.75
MLShell	0.004	0.01	-0.01	0.02	0.21
VegCover	0.003	0.01	-0.01	0.01	0.21
TallVeg5	0.03	0.08	-0.13	0.20	0.17
DistFidd	-1.13	0.76	-2.62	0.36	0.15
Sshell	0.000	0.002	-0.003	0.003	0.14
DistNrNest	0.000	0.001	-0.001	0.001	0.13

^a VegForm = vegetation growth form within 15 cm of the nest site defined as (1) bare ground or low-growing sparse vegetation, or (2) clumped grasses or a combination of clumped grasses and low-growing sparse vegetation; MLShell = percent cover of medium (2-64 mm) and large (> 64 mm) shells within a 1-m² quadrat placed over the nest site; VegCover = percent cover of dead and live vegetation within a 1-m² quadrat placed over the nest site; TallVeg5 = height of tall vegetation (≥ 1.0 m) within a 5-m radius of the nest site; DistFidd = distance to nearest fiddler crab (*Uca* spp.) mud flat from the nest site; Sshell = percent coverage of small (< 2 mm) shells within a 1-m² quadrat placed over the nest site. DistNrNest = distance to nearest nest site (m) of any species from the nest site.

^b R_i = Relative importance.

Brood territory establishment: Wilson's Plovers selected the largest fiddler flats to rear their broods and only one brood occupied a flat at any given time, with the exception of one long flat divided by *Spartina* spp. exceeding 1 m tall. Fiddler flat area was in all top models predicting whether or not Wilson's Plover broods used a given fiddler flat (**Table 12-8**). The probability of a brood establishing a territory on a fiddler flat increased with the area of the flat, and area was the most important variable in predicting establishment of a brood foraging territory on a fiddler flat ($R_i = 0.97$, **Table 12-9**). Burrow count had slightly more predictive power than crab count in our initial AIC_c analyses, and neither variable was significant in model averaging results. A subsequent analysis omitting crab count did not demonstrate marked differences from our initial analyses. All other habitat variables appeared in at least one of the top selected models, but the relative importances of each of these other variables were low ($R_i < 0.30$; **Tables 12-8 and 9**).

Table 12-8. Top-ranked models ($\Delta AIC_c \leq 2.00$ or Model Likelihood ≥ 0.125 out of 16 models) predicting Wilson's Plover (*Charadrius wilsonia*) brood foraging territory establishment on fiddler crab (*Uca* spp.) mud flats ($n = 9$) at Onslow Beach, MCBCL, North Carolina, 2009.

Variable(s) in Model ^a		K^b	Prob $> \chi^2^c$	AIC_c^d	ΔAIC_c^e	w_i^f	Model Likelihood
Area	—	2	0.11	27.86	0.00	0.26	1.00
Area	BurrCount	3	0.23	28.14	0.28	0.22	0.87
Area	VegTrnDist	3	0.11	28.78	0.92	0.16	0.63
Area	VegVO	3	0.13	28.79	0.93	0.16	0.63
Area	VegCover	3	0.11	28.79	0.93	0.16	0.63

^a Area = area of fiddler crab mud flat (m^2); BurrCount = mean burrow count in 1- m^2 sampling quadrat; VegTrnDist = length (m) of vegetated path from interdune sand flat to fiddler crab mud flat; VegVO = index depicting visual obstruction (density) of vegetation around the fiddler crab mud flat; VegCover = mean percent of vegetation cover in 1- m^2 sampling quadrat.

^b K = Number of model parameters.

^c Prob $> \chi^2$ = Hosmer and Lemeshow goodness-of-fit test for binary logistic regression models.

^d AIC_c = Akaike's Information Criterion corrected for sample size.

^e ΔAIC_c = Difference between any given model's AIC_c and the best-fit model.

^f w_i = Weight of each model as compared to all candidate models.

Table 12-9. Model-averaged parameter estimates, unconditional standard errors (SE), upper confidence limit (UCL), lower confidence limit (LCL), and relative importance (R_i) from multi-variable logistic regression models predicting Wilson's Plover (*Charadrius wilsonia*) brood foraging territory establishment on fiddler crab (*Uca* spp.) mud flats ($n = 9$) on Onslow Beach, MCBCL, North Carolina, 2009.

Variable ^a	Parameter				R_i^b
	Estimate	SE	95% LCL	95% UCL	
Intercept	-1.07	1.52	-4.06	1.92	—
Area	0.002	0.001	0.000	0.003	0.97
BurrCount	-0.007	0.02	-0.04	0.02	0.23
VegCover	-0.002	0.008	-0.02	0.01	0.18
VegTrnDist	0.001	0.005	-0.01	0.01	0.18
VegVO	-0.002	0.009	-0.02	0.02	0.18

^a Area = area of fiddler crab mud flat (m^2); BurrCount = mean burrow count in 1- m^2 sampling quadrat; VegTrnDist = length (m) of vegetated path from interdune sand flat to fiddler crab mud flat; VegVO = index depicting visual obstruction (density) of vegetation around the fiddler crab mud flat; VegCover = mean percent of vegetation cover in 1- m^2 sampling quadrat.

^b R_i = Relative importance.

Fiddler flats ranged in size from approximately 44–14,029 m^2 (Table 12-5). In both years, ≥ 1 brood established foraging territories concurrently or sequentially on three of the largest fiddler

flats ($> 1,250 \text{ m}^2$), two of which had no vegetation obstruction around their borders (**Table 12-5**). Fiddler flats $\geq 1,250 \text{ m}^2$ had less cover (mean cover based on 1 m^2 quadrats) per flat (9.43–35.15% for 3 flats) compared to those $\leq 1,250 \text{ m}^2$ (36.03–55.83% for 6 flats). Most flats were within 10 m of water; however, not all were subject to regular tidal inundation (**Table 12-5**).

Foraging site selection: Wilson's Plovers foraged closer to water and vegetation cover than expected at random. Distance to water and to vegetative cover from the foraging bird's location were in all top models distinguishing used from unused points at foraging sites on fiddler flats, interdune sand flats, beach front, and all habitat types combined (**Table 12-10**). Within each habitat type, the probability of foraging site selection by Wilson's Plovers increased as distance to water decreased, although the confidence interval overlapped zero, except when all habitats were combined (**Table 12-11**). Mean percent vegetation cover at focal bird foraging locations in all habitat types ranged from 12.50 ± 4.17 to 14.44 ± 3.47 . On average, Wilson's Plover broods foraged closer to water on fiddler flats than in beach front habitat or on interdune sand flats (**Table 12-6**).

When on fiddler flats, Wilson's Plovers foraged in areas with the highest individual crab densities. The number of crab burrows and individual crabs in sampling plots were similar between years (**Table 12-12**). For both years of the study (i.e., 2-yr mean), burrow counts were higher at used ($\bar{x} = 53.64 \pm 3.60$, median = 45, Q1-Q3 = 35-78) than unused sites (42.40 ± 4.04 , $n = 81$, median = 36, Q1-Q3 = 9-48, $z = 601$, $P = 0.004$). Likewise, crab counts were higher at used ($\bar{x} = 25.55 \pm 2.34$, median = 25.5, Q1-Q3 = 3-42) than unused points over the 2-yr study period (12.17 ± 1.38 , $n = 82$, median = 9, Q1-Q3 = 1-19, $z = 1131$, $P = <0.0001$).

We exposed "sticky sticks" for an average of 41 min to collect insects in 2008 and 2009. The average number of insects caught in sticky traps on the beach front increased between 2008 and 2009 (**Table 12-13**). For both years combined (i.e., 2-yr mean), we collected more insects at beach front focal bird foraging locations ($n = 84$; $\bar{x} = 0.08 \pm 0.01 \text{ insects min}^{-1}$, median = 0.03, Q1-Q3 = 0.00–0.09) than at random non-use sites ($\bar{x} = 0.06 \pm 0.02 \text{ insects min}^{-1}$, median = 0.02, Q1-Q3 = 0.00–0.06; $z = 387$, $P = 0.01$). We found no differences in 2-yr mean insect counts at used and paired non-use sampling points on fiddler and interdune sand flats.

Inter-annual variation of fiddler crab flat use and foraging behavior: From 20–25 June 2009, tidal heights were $> 20 \text{ cm}$ higher than predicted, and many fiddler flats were continually inundated, even during low tide (**Figure 12-3**). From 20–26 June 2009, we observed only one of nine (11%) known Wilson's Plover broods using fiddler flats, on one day only, 23 June. For the same time period in 2008, we re-sighted 12.5–25% of known broods using fiddler flats on 3 different days (22, 24, and 26 June). We did not conduct surveys of fiddler flats 19–20 June 2008, but we did conduct brood surveys on all other days in 2008 and 2009.

Chick pecking rates on interdune sand flats were higher in 2009 than in 2008 (**Table 12-14**); however, there were no differences in Wilson's Plover adult ($n = 10$ pairs) and chick ($n = 10$ broods) foraging behavior between years (**Tables 12-14 and 15**) in other habitats.

Table 12-10. Top single- and multi-variable logistic regression models ($\Delta AIC_c \leq 2.00$ or model likelihood ≥ 0.125 , 28 models) of habitat characteristics at foraging sites used by Wilson's Plover (*Chardrius wilsonia*) broods and random non-use sampling points on fiddler crab (*Uca* spp.) mud flats ($n = 25$ paired samples), beach front ($n = 25$ paired samples), interdune sand flats ($n = 10$ paired samples), and all habitats ($n = 60$ paired samples) combined at Onslow Beach, MCBCL, North Carolina in 2009.

Habitat Type	Variables in Model		K^a	AIC_c^b	ΔAIC_c^c	w_i^d	Model Likelihood
All Habitats:	Distance to Water (m)	Distance to Vegetative Cover (m)	3	89.45	0.00	0.595	1.000
Fiddler Crab Mud Flats:	Distance to Water (m)	Distance to Vegetative Cover (m)	3	31.14	0.00	0.348	1.000
	Distance to Water (m)	—	2	31.24	0.10	0.332	0.953
	Distance to Water (m)	Mean Percent Vegetation Cover (1 m ²)	3	32.22	1.08	0.203	0.582
Beach Front:	Distance to Water (m)	Distance to Vegetative Cover (m)	3	31.14	0.00	0.348	1.000
	Distance to Water (m)	—	2	31.24	0.10	0.332	0.953
	Distance to Water (m)	Mean Percent Vegetation Cover (1 m ²)	3	32.22	1.08	0.203	0.582
Interdune Sand Flats:	Distance to Water (m)	Distance to Vegetative Cover (m)	3	7.02	0.00	0.614	1.000

^a K = Number of model parameters.

^b $\text{Prob} > \chi^2$ = Hosmer and Lemeshow goodness-of-fit test for binary logistic regression models.

^c AIC_c = Akaike's Information Criterion corrected for sample size.

^d ΔAIC_c = Difference between any given model's AIC_c and the best-fit model.

^e w_i = Weight of each model as compared to all candidate models.

Table 12-11. Model-averaged parameter estimates, unconditional standard errors (SE) and confidence limits (CL), and relative importance (R_i) from single- and multi-variable logistic regression models examining habitat characteristics at foraging sites used by Wilson's Plover (*Chardrius wilsonia*) broods and random non-use sampling points on fiddler crab (*Uca* spp.) mud flats ($n = 25$ paired samples), beach front ($n = 25$ paired samples), interdune sand flats ($n = 10$ paired samples), and all habitats ($n = 60$ paired samples) combined on Onslow Beach, MCBCL, North Carolina in 2009.

Habitat Type	Variables by Habitat	Parameter Estimate	SE	Lower 95% CL	Upper 95% CL	R_i^a
All Habitats:	Distance to Water (m) ^b	-0.02	0.01	-0.05	-0.001	0.79
	Distance to Vegetative Cover beyond 1 m ² (m) ^b	-0.05	0.02	-0.10	-0.001	0.77
Fiddler Crab Mud Flats:	Distance to Water (m)	-0.06	0.04	-0.15	0.02	0.88
	Distance to Vegetative Cover beyond 1 m ² (m) ^b	-0.07	0.02	-0.11	-0.02	0.43
	Mean Percent Vegetation Cover (1 m ²)	0.001	0.01	-0.01	0.01	0.27
Beach Front:	Distance to Water (m)	-0.001	0.003	-0.01	0.01	0.22
	Distance to Vegetative Cover beyond 1 m ² (m)	-0.003	0.02	-0.04	0.03	0.55
	Mean Percent Vegetation Cover (1 m ²) ^a	0.04	0.02	-0.01	0.08	0.89
Interdune Sand Flats:	Distance to Water (m)	-0.16	0.11	-0.37	0.06	0.87
	Distance to Vegetative Cover beyond 1 m ² (m)	-0.67	0.44	-1.53	0.18	0.69

^a R_i = Relative importance.

^b Significant variable (confidence limits do not include zero)

Table 12-12. Fiddler crab (*Uca* spp.) burrow counts and individual counts at focal Wilson's Plover (*Charadrius wilsonia*) foraging locations (i.e., use sites) and paired, non-use samples on fiddler flats at Onslow Beach, MCBCL, North Carolina, 2008–2009.

Prey Item (Use/non-use)	2008						2009					
	<i>n</i>	\bar{x} (\pm SE)	Median	Q1–Q3	<i>Z</i>	$P \geq z$	<i>n</i>	\bar{x} (\pm SE)	Median	Q1–Q3	<i>Z</i>	$P \geq z$
Burrows (use)	66 ^a	53.09 (4.09)	44	37–78	379.	0.01	15	56.07 (7.63)	53	31–81	29.5	0.10
Burrows (non-use)	67 ^a	44.27 (4.61)	44	13–98	5		15	34.07 (7.93)	30	7–54		
Crabs (use)	69 ^b	24.45 (2.66)	17	2–45	694	<0.001	15	30.60 (4.62)	33	15–38	52.5	0.001
Crabs (non-use)	68 ^b	12.47 (1.56)	9	2–20			15	10.80 (2.92)	10	0–17		

^a sample size (*n*) for Wilcoxon results = 66 paired samples

^b sample size (*n*) for Wilcoxon results = 67 paired samples

Note: Wilcoxon signed-rank test ($P \geq z$) results comparing yearly means (\bar{x}) and standard errors (SE), medians, and 25-75% (Q1-Q3) inter-quartile ranges for fiddler crab (*Uca* spp.) counts.

Table 12-13. Total mean insect counts (insects collected per min⁻¹) at focal Wilson's Plover (*Charadrius wilsonia*) foraging locations (i.e., use sites) and paired, non-use samples at Onslow Beach, MCBCL, North Carolina, 2008–2009.

Prey Item (Use/non-use)	2008						2009					
	<i>N</i>	\bar{x} (\pm SE)	Median	Q1–Q3	<i>z</i>	$P \geq z$	<i>n</i>	\bar{x} (\pm SE)	Median	Q1–Q3	<i>Z</i>	$P \geq z$
Total Insects (use)	6	0.02 (0.01)	0.02	0.00–0.05	-10.5	0.03	78	0.09 (0.02)	0.03	0.00–0.10	367.5	0.003
Total Insects (non-use)	6	0.04 (0.01)	0.04	0.02–0.07			78	0.07 (0.02)	0.02	0.00–0.04		

Note: Wilcoxon signed-rank test ($P \geq z$) results comparing yearly means (\bar{x}) and standard errors (SE), medians, and 25-75% (Q1-Q3) inter-quartile ranges for beach front insect counts.

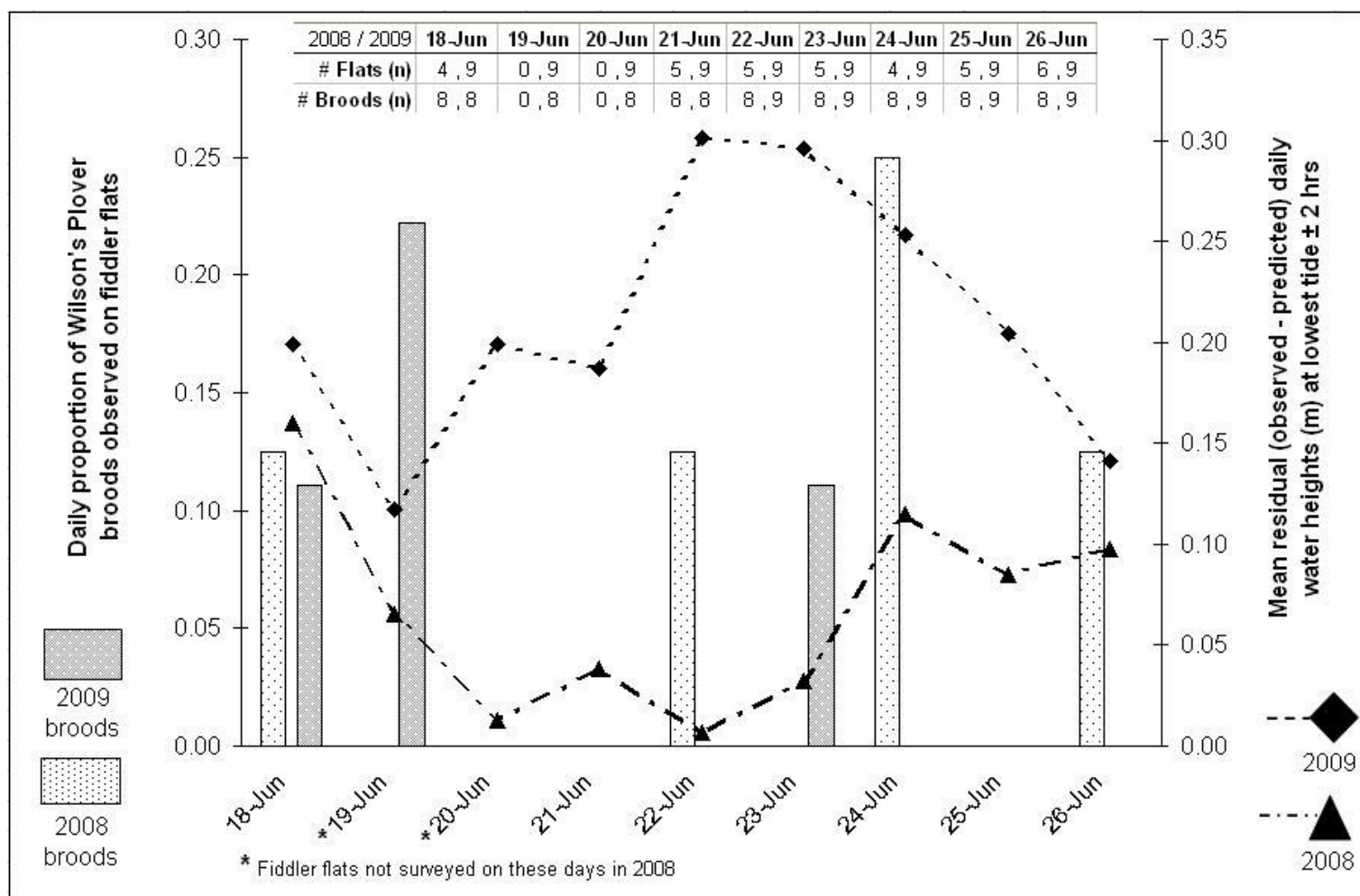


Figure 12-3. Daily proportion of known Wilson's Plover (*Charadrius wilsonia*) broods observed on fiddler crab (*Uca* spp.) mud flats in 2008 and 2009 at Onslow Beach, MCBCL, North Carolina, during the date range in 2009 (19 – 26 June) when near-complete inundation of flats were observed on Onslow Beach.

The number of fiddler crab mud flats surveyed (out of nine) and broods followed each day in 2008 and 2009 appear at the top of the figure. Mean residual water heights (m, observed - predicted height) \pm 2 hrs of the lowest daily tide are based on tidal station data collected by National Oceanic and Atmospheric Administration in Beaufort, North Carolina.

Table 12-14. Wilson’s Plover (*Chardrius wilsonia*) chick ($n = 10$ broods) pecking rates (pecks per min⁻¹) on fiddler crab (*Uca* spp.) mud flats, beach front, and interdune sand flats at Onslow Beach, MCBCL, North Carolina, 2008–2009.

Habitat	2008			2009			Results	
	\bar{x} (\pm SE)	Median	Q1–Q3	\bar{x} (\pm SE)	Median	Q1–Q3	z	$P \geq z$
Fiddler flat	2.41 (0.63)	2.13	1.23–2.99	3.53 (0.87)	2.97	1.48–5.57	6.5	0.56
Beach front	0.43 (0.42)	0.00	0.00–0.03	2.66 (1.23)	0.70	0.00–4.01	9	0.23
Interdune sand flat	0.73 (0.23)	0.00	0.00–0.00	2.50 (1.04)	1.16	0.00–3.63	10.5	0.03

Note: Wilcoxon signed-rank test ($P \geq z$) results comparing yearly means (\bar{x}) and standard errors (SE), medians, and 25-75% (Q1-Q3) inter-quartile ranges for chick pecking rates.

Table 12-15. Wilson’s Plover (*Chardrius wilsonia*) adult ($n = 10$ pairs) and chick ($n = 10$ broods) “run and grab” rates (run and grab per min⁻¹) on fiddler crab (*Uca* spp.) mud flats at Onslow Beach, MCBCL, North Carolina, 2008–2009.

	2008			2009			Results	
	\bar{x} (\pm SE)	Median	Q1–Q3	\bar{x} (\pm SE)	Median	Q1–Q3	z	$P \geq z$
Age								
Adults	0.15 (0.08)	0.04	0.00–0.14	0.11 (0.04)	0.09	0.00–0.12	1	0.95
Chicks	0.12 (0.04)	0.08	0.04–0.18	0.06 (0.03)	0.00	0.00–0.11	-16	0.06

Note: Wilcoxon signed-rank ($P \geq z$) test results comparing yearly means (\bar{x}) and standard errors (SE), medians, and 25-75% (Q1-Q3) inter-quartile ranges for “run and grab” rates.

Wilson's Plovers have been observed placing their nests at the toe of dunes, in overwash areas, or in newly accreted beach where vegetation is sparse (Corbat and Bergstrom 2000, Dikun 2008). In this study, we observed most Wilson's Plovers placing nests on interdune sand flats and dunes adjacent to or within vegetation. In our study, a greater proportion of nests placed in clumped grasses and mixed vegetation were successful than those placed on bare ground or in low-growing sparse vegetation. Our findings are similar to those of Corbat (1990) who found higher hatching success rates for nests placed within 0.5 m² of vegetation on Georgia barrier islands, and Bergstrom (1982) who observed 83% of known nests ($n = 29$) located adjacent to clumped vegetation in Texas. Dikun (2008) found an average $12.9 \pm 1.9\%$ vegetation cover within 1 m² of nest sites in her South Carolina study examining habitat features influencing nest placement, which is similar to our findings of $15.33 \pm 2.33\%$ vegetation cover within 1 m² of successful nests. In contrast, Hood (2006) identified a decrease in nest survival for those nests placed within 0.5 m² of dense clumps of vegetation compared to nest bowls located in sparse, diffuse vegetation in south Texas. The average density of vegetation surrounding our nest sites was higher than the density in Hood's (2006) study (7.9% within 0.5 m²). These differences may be attributable to the fact that Onslow Beach has not experienced a significant overwash event since Hurricanes Fran and Bertha in 1996, while lower elevation nesting habitat in Hood's (2006) study included coastal bays and sound-side sand flats on barrier islands prone to frequent inundation. Accordingly, Hood commonly observed washouts as a cause of nest failure, while we identified only 2 losses in 2 years attributed to tidal fluctuations or storm-increased water levels. In the absence of overwash, the sand flats on Onslow Beach have become increasingly vegetated, but are suitable for Wilson's Plover nesting success.

Area of a fiddler flat was the most important factor in Wilson's Plover brood territory establishment. Similarly, wintering Ruddy Turnstone (*Arenaria interpres*) and Sooty Oystercatcher (*Haematopus fuliginosus*) densities in northwest Tasmania were higher in larger habitat patches, but in that study increased prey densities and the absence of a non-preferred food resource were equally important to area in foraging site selection (Spruzen et al. 2008). We did not find evidence that prey abundance (e.g. crab burrows or individual crabs) was an influential factor in Wilson's Plover brood territory establishment on fiddler flats. However, within used flats, Wilson's Plovers foraged in areas with higher prey abundance than found at random on the same flat. Thus, broods may select a fiddler flat based on its size, and then select a specific foraging location on that flat according to prey abundance, as would be consistent with other studies showing that shorebirds select foraging sites based on the availability, distribution, and abundance of food resources (Thibault and McNeil 1995, Backwell et al. 1998, Elias et al. 2000, Placyk and Harrington 2004, Ribeiro et al. 2004, Karpanty et al. 2006, Spruzen et al. 2008). Spatial distribution of conspecifics in an area (e.g. on a selected fiddler flat) may also be influenced by competition with other species (Folmer et al. 2010), but we did not address interspecific resource competition in this study.

In our study, three of the largest mud flats ($> 1,250 \text{ m}^2$) also lacked dense vegetation around their borders, making these foraging locations both the most accessible and large enough for ≥ 1 brood to establish concurrent or sequential territories. While we hypothesized that accessibility of fiddler flats might be an important characteristic influencing Wilson's Plover brood territory establishment, we did not find that any of our metrics of accessibility (i.e., vegetation density measures) were important in predicting territory establishment. These large flats had lower mean percentages of vegetation cover per 1 m² than the smaller flats, likely because the large flats

were adjacent to or within 10 m of a fluctuating body of water (i.e., tidal creek or ponds fed by creeks) and therefore experienced more inundation than other flats.

Foraging broods were closer to vegetation and water on fiddler flats (and in all habitats combined) than at paired random sampling locations within a foraging site. Vegetation likely provided chicks the necessary cover to evade predators, rest, and regulate their body temperature while proximity to water may have increased foraging success rates if fiddler crab or insect densities increase with close proximity to water or inundation frequencies (Elias et al. 2000, Cohen et al. 2009); however, this remains to be tested. Wilson Plover chicks in Texas similarly fed in low-lying wet areas where young could conceal themselves in vegetation (Bergstrom 1982). These findings suggest that an ideal fiddler flat for Wilson's Plover brood territory establishment at Onslow Beach, and possibly other areas, would be one that is $\geq 1250 \text{ m}^2$, within 10 m of water, subject to regular tidal inundation, and within approximately 4 m of vegetation adapted to water fluctuations (i.e., glasswort).

Wilson's Plovers have also been observed foraging along the beach front intertidal zone, above the high tide line on the beach backshore, and along the toes of primary dunes (Corbat 1990, Leary 2009, this study). We found that an increased density of vegetation and number of insects around beach front foraging sites were important characteristics for Wilson's Plovers foraging in this habitat. Our results suggest an optimal range of 11–18% vegetation cover per 1 m^2 of beach front habitat for foraging broods at Onslow Beach. There is likely a vegetation cover threshold at which foraging site selection on beach front habitat will begin to decline. Habitat containing coverage $< 11\%$ may be unattractive to Wilson's Plover chicks which require some vegetation cover to thermoregulate and avoid predation, especially by avian-predators as has been shown to be important for Least Terns (Burger 1989).

We did not find nesting Wilson's Plovers in the Developed Recreation Area or the Amphibious Training Zone. This may be partly attributed to topographical differences between these use areas and the Wildlife Area. Sound-side intertidal flats colonized by fiddler crabs do not exist in the Developed Recreation Area, and while present in the Amphibious Training Zone, were not accessible to broods. The road behind the primary dunes in the Amphibious Training Zone, combined with dense vegetation (primarily *Phragmites* spp.) surrounding any present mud flats, present a barrier to Wilson's Plover broods. In both of these use zones, the landward side of the island is adjacent to Intracoastal Waterway (ICW), where boats frequently travel. In the Wildlife Area and the Military Buffer Zone, marsh and inter-tidal mud flats act as a buffer between the island and the ICW, providing habitat and shelter for Wilson's Plover broods.

We observed a lower proportion of Wilson's Plover broods using fiddler flats from 18 – 26 June 2009 (i.e., the time period we observed near complete inundation of fiddler flats regardless of tidal state on Onslow Beach) compared to the same time frame in 2008. NOAA reported (Sweet et al. 2009) an average 0.2 m residual water level height (i.e., observed – predicted water height) extending along the Atlantic coast from North Carolina to New Jersey during this time period in 2009 only. By establishing a systematic survey scheme in 2009, we increased our visits to fiddler flats in 2009 compared to 2008. As a result, we expected to observe more brood use of fiddler flats during the second year of the study, but we actually identified fewer broods than in the first year. The decrease in broods observed using fiddler flats from 18-26 June 2009 in comparison to this same time period in 2008 may be related to two environmental changes: 1) the sea level

anomaly that began mid-June 2009, and 2) beach front sand accretion that occurred on the southwestern end of Onslow Beach from 2008 to 2009 which created habitat that was not available in 2008. Tidal height fluctuations and sand accumulation influence the area, availability, and micro-fauna abundance on beach fronts (Hubbard and Dugan 2003) and can create important foraging habitat for shorebirds (Burger et al. 1977, Connors et al. 1981, Warnock and Takekawa 1995, Long and Ralph 2001). The atypically high water heights in 2009 may have reduced the availability of fiddler flats on Onslow Beach, but also contributed to the formation of ephemeral pools on newly accreted beach front sand that served as important foraging habitat for Wilson's Plover broods. In 2009, we observed six brood foraging territories encompassing > 1 habitat type (e.g. fiddler flat and beach front or interdune sand flat). Two of these multi-habitat final brood foraging territories did not include fiddler flats, but rather a combination of beach front ephemeral pools and sparsely vegetated interdune sand flats. In 2008, we observed Wilson's Plover broods establishing final foraging territories only on fiddler flats.

Our inter-annual findings related to foraging behavior do not indicate strong differences in feeding strategies from one year to the next despite these habitat changes; however, chick pecking was higher across all habitats in 2009 than in 2008, and adult and chick behavior associated with hunting fiddler crabs decreased in 2009, suggesting an opportunistic response to decreased accessibility to preferred habitat (i.e., fiddler flats) and prey items (i.e., fiddler crabs). In Florida, Leary (2009) observed a Wilson's Plover chick capture and consume a small finfish, which is an uncommon prey item, trapped in a shallow beach front tidal slough; he attributed this unusual behavior to the presence of an ephemeral pool in the beach front habitat. In 2009, we occasionally watched adults and young probe for and consume benthic worms and unidentifiable aquatic invertebrates on inter-tidal mud flats and around the edges of ephemeral pools in beach front and sound-side habitats, an observation analogous to Leary's (2009). We did not observe Wilson's Plovers consuming benthic invertebrates in 2008; however, we observed one female eating *Donax* spp. in the inter-tidal zone.

Management and conservation implications: The U.S. Shorebird Conservation Plan (Brown et al. 2001, Hunter 2002) states that efforts are needed to determine key habitat characteristics supporting nesting, foraging, and roosting of Wilson's Plovers to support the goal to double the breeding Wilson's Plover population in the southeastern coastal plains-Caribbean region over the next 50 years. Currently, it is estimated that there are approximately 1500 breeding pairs along the Gulf and Atlantic coasts (Hunter 2002), but there is low confidence in this estimate due to a lack of regionally coordinated, systematic surveys for this species (Brown et al. 2001). Protection and maintenance of sparsely vegetated interdune sand flats may be an important contributor in maintaining and increasing Wilson's Plover nest numbers. Our work, combined with other studies in the southeastern U.S. and Gulf Coasts, suggest that there may be a threshold density of sparse vegetation after which a site becomes unsuitable for nesting Wilson's Plovers, but that threshold may vary by region and/or preferred nesting habitat within a region. Protecting the integrity of, and access to, large fiddler flats (< 1,250 m²) is crucial for foraging Wilson's Plover broods; specifically, broods in our study preferred to forage in habitat with close proximity (≤ 10 m) to water and sparse vegetation (≤ 4 m), which is presumably used as protective cover from predators, and provides opportunity for body temperature regulation. We found no evidence of differences in chick survival between years (Ray et al. unpublished data), and our data suggest that Wilson's Plovers exhibit some behavioral plasticity and are able to successfully fledge

broods that forage not only on fiddler flats, but also on interdune sand flats, beach front, or a combination of multiple habitats.

Management that focuses on providing a matrix of potential foraging sites from the beach front to sound-side fiddler flats will provide multiple opportunities for foraging Wilson's Plover broods that may be prevented from accessing a certain habitat type due to stochastic environmental factors (e.g. storms that result in beach erosion), variations in land management, or longer-term changes such as sea-level rise that may alter intertidal areas or render them inaccessible.

Section 3: Distribution and Abundance by Shorebirds and Predators at MCBCL

Materials and Methods

Study Area: We conducted this study on Onslow Beach (34°32' N, 77°21'W), a 12.9-km barrier island in southeastern North Carolina. It is bounded by New River Inlet and Brown's Inlet (**Figure 12-1**). Human impacts vary across the island. The south end of the island is managed for low impact recreation and wildlife (Low Impact Wildlife), and is closed to recreational vehicles from 1 Apr to 31 Aug, annually (**Figure 12-1**). The Amphibious Training zone is designated for military training and the Developed Recreation area provides recreational opportunities for Marine Corps personnel and their families.

Habitats were typical of barrier islands in this region, and included, from the ocean to the marsh: ocean intertidal zone, backshore, primary dunes, interdune sand flats, maritime shrub and forest, and bay-side intertidal flats and marshes. An overwash fan formed during Hurricanes Bertha and Fran in 1996 removed woody vegetation and created an approximately 200 m wide by 1 km long interdune sand flat that included about 400-m of direct interface with marsh and bay-side intertidal flats. Since 1996, sparse low-growing vegetation and clumped grasses have grown in the interdune sand flats (i.e., overwash), including primarily sea rocket (*Cakile harperi*), seashore elder (*Iva imbricate*), seaside pennywort (*Hydrocotyle bonariensis*), dotted horsemint (*Monarda punctata*), saltmeadow cordgrass (*Spartina patens*), sea oats (*Uniola paniculata*), American beach grass (*Ammophila breviligulata*), and smartweed (*Polygonum* spp).

Shorebird Surveys: We conducted shorebird surveys along established transects on the beach and in the marsh (**Figure 12-1**) ≥ 1 times per 7-10 days in 2008 and 2009. We walked along the beach and boated or kayaked through the marsh to conduct surveys from 0630 – 1030 hours. We counted all focal shorebird and tern species (**Table 12-16**) seen and heard within approximately 100 m of our location on the transect (ocular and auditory estimations) beachfront and marshside, and recorded our geographic coordinates at the time of identification using a handheld Garmin 76 GPS unit (Garmin International, Olathe, KS). We recorded environmental variables at the beginning of each survey, which included temperature (C), wind speed (knots) and cardinal direction, tidal stage (low, low-rising, mid-rising, high, high-falling, mid-falling), time of first high and low tides, and an ocular estimate of cloud cover (%).

Table 12-16. Shorebird and tern species included in this study’s summary analyses, along with each species’ federal and state listing status, the US Shorebird Conservation Plan’s prioritization designation, and temporal occurrence on Onslow Beach at MCBCL, North Carolina, 2008–2009.

Common Name	Scientific Name	Federal Status	State Status	US Shorebird Conservation Plan Status	Temporal Occurrence
American Oystercatcher	<i>Haematopus palliates</i>	None	Special Concern	Species of High Concern (4)	breeding resident
Black-bellied Plover*	<i>Pluvialis squatarola</i>	None	None	Species of Moderate Concern (3)	wintering, migratory
Killdeer	<i>Charadrius vociferus</i>	None	None	Species of Moderate Concern (3)	breeding resident
Piping Plover	<i>Charadrius melodus</i>	Threatened	Endangered	Highly Imperiled (5)	breeding
Semipalmated Plover	<i>Charadrius semipalmatus</i>	None	None	Species of Low Concern (2)	wintering, migratory
Wilson’s Plover	<i>Charadrius wilsonia</i>	None	Special Concern	Species of High Concern (4)	breeding
Red Knot	<i>Calidris canutus</i>	Candidate Species	None	Species of High Concern (4)	resident, migratory
Sanderling*	<i>Calidris alba</i>	None	None	Species of High Concern (4)	wintering, migratory
Willet	<i>Catoptrophorus semipalmatus</i>	None	None	Species of Moderate Concern (3)	breeding resident
Common Tern	<i>Sterna hirundo</i>	None	Special Concern	Not applicable	breeding
Gull-billed Tern	<i>Sterna nilotica</i>	None	Threatened	Not applicable	breeding
Forster’s Tern	<i>Sterna forsteri</i>	None	None	Not applicable	wintering
Least Tern	<i>Sterna antillarum</i>	None along Atlantic coast	Special Concern	Not applicable	breeding

Common Name	Scientific Name	Federal Status	State Status	US Shorebird Conservation Plan Status	Temporal Occurrence
Royal Tern	<i>Sterna maxima</i>	None	None	Not applicable	breeding resident
Sandwich Tern	<i>Sterna sandvicensis</i>	None	None	Not applicable	breeding

* potentially non-breeding birds observed during breeding season

While we temporally standardized our surveying efforts, tidal stages fluctuated daily and throughout each breeding season and thus, accounted for tidal variation. We alternated the starting point on all transects for each survey to minimize detection bias potentially influenced by tidal state. We did not conduct surveys when ocular estimates of cloud cover were $\geq 95\%$, precipitation (e.g. rain, fog, storms) was persistent for ≥ 3 hrs, and/or winds ≥ 17 knots during the designated morning survey period (i.e., 0630 – 1030 hours).

We minimized double counting birds through careful observation that included noting the direction birds or flocks flew, and counting only birds observed on the leading portion of the transect. In cases of large aggregations of birds (e.g. colonial nesting terns, birds resting and foraging on sandbars) observed in the same micro-habitat, we tallied individuals by species within boundaries of physical landmarks (e.g. fence posts or signs, dunes, vegetation, pylons, buoys, or landmark on an adjacent visible island) and summed the total of each species for the given geographic location.

Predator Monitoring: We conducted predator monitoring in the Developed Recreation and Low Impact Wildlife areas four times a year (Jan, Apr, Jul, and Oct) for 11–15 day intervals during 2008 and 2009 to examine patterns of predator relative abundance during shorebird wintering, migratory, and breeding seasons (**Table 12-17**). We used infrared, heat- and motion-triggered Reconyx RapidFire RC55 Color digital cameras (Reconyx, Inc, Holmen, WI) at 16 semi-permanent (i.e., some stations were washed out by high tides or storms, and were re-established as close to the original site as possible) camera stations distributed along the beach and in the marsh. We did not conduct predator monitoring in the Amphibious Training zone to minimize risk of camera damage from military training and operations.

Table 12-17. Predator monitoring periods, dates monitored, total days monitored, mean days monitored, and calculated camera trap nights (16 camera stations (n) * total days monitored; n = eight camera stations per land use area (Developed Recreation and Low Impact Wildlife)) at Onslow Beach on MCBCL, North Carolina, 2008–2009.

Monitoring Period	Dates Monitored	Total Days Monitored	Mean Days Monitored	Trap Nights
Jan 2008	10–23	14	14	224
Apr 2008	11–25	14–15	14.5	232
Jul 2008	8–19	12	12	192
Oct 2008	6–18	11–14	12.8	205
Jan 2009	11–25	14	14	224
Apr 2009	6–21	14–15	14.5	232
Jul 2009	8–23	15	15	240
Oct 2009	7–21	13–14	13.8	214

We placed stations in the Developed Recreation and Low Impact Wildlife areas – in each area, four cameras were positioned beachfront and four along the marsh (**Figure 12-1**). In the Developed Recreation area ocean-side, we placed camera stations cameras approximately 800–900 m apart beginning approximately 500 m south of the North Tower. In the marshes behind

the Developed Recreation area, cameras were placed approximately 450 m apart, and included a 750-m stretch that was not monitored due to access constraints that included the ICW traffic, recreational use, island topography, and tidal fluctuations. We placed stations approximately 750 m apart beach front, beginning at the southern-most end of the Low Impact Wildlife area. On the marsh side, cameras were placed approximately 500 m apart with the exception of the northern-most station that was located 700 m from the southern border of the Amphibious Training zone. Woody vegetation and topography prevented us from installing the last camera station within a 500-m range of the previous one.

We encased all cameras in wood housings (26.4 cm x 28.6 cm x 12.7 cm) and anchored each one into the sand attached to a 1.52-m steel t-bar or elevated the unit on 2 t-stakes in the marsh where tidal fluctuations presented threats of immersion. We attached insulated wire cables (4.0 cm diameter) to the t-bars to secure the camera unit and deter potential theft. We fed the crimped cable ends (ferrule and lock) through holes drilled on the back of the wooden boxes, through the camera unit handles, and locked the ends with a Master Lock®. We spray painted each wooden camera box in beach- or marsh-appropriate camouflage.

We tested daytime trigger distance of all cameras prior to each monitoring effort. Cameras were set to three RapidFire images (series of three images captured at 1 image per sec), “Very High” trigger sensitivity (the most sensitive trigger setting), and a 30-sec “Quiet Time” (i.e., if an animal remained in the camera’s detection range 30 sec after the initial trigger, the camera was not triggered during this time). We did not bait any of the camera stations and checked the units for maintenance and functionality every 3–4 days during the monitoring period (more frequent checks occurred following storms or high winds).

Human Activity Monitoring: We implemented camera monitoring across all land use areas to build indices of human activity and distribution Mar – Aug in 2008 and 2009. We used the same cameras (i.e., infrared, heat- and motion-triggered Reconyx RapidFire RC55 Color digital cameras), wooden housing units, and theft-deterrent mounting systems that we designed and utilized for predator monitoring. We deployed eight camera units (two per land use zone) adjacent to beach access points in the Developed Recreation area, Amphibious Training egress points, and used established beach front predator monitoring stations in the Low Impact Wildlife area to count human activities twice a month for 48 hrs. We geographically and temporally randomized our anthropogenic data collection by drawing camera station identifiers (i.e., an alphanumeric station identifier by land use area) from a hat, and using a random number generator to determine start dates for weekday (Sunday/Monday – Thursday) and weekend (Thursday/Friday – Sunday) monitoring events each month (**Table 12-18**). If two randomly determined start dates occurred on a weekday or on the weekend, we continued to generate numbers until we met the requirements of our temporal randomization design.

We categorized monthly human activities and impacts into the following classifications by land use area for our analyses: active people (Active); military personnel (Marines); recreational fishermen (Fishing); horseback riding (Horses), dogs on- and off-leash; personal vehicles (Private); Environmental Management Division (EMD) or Base personnel vehicles; all-terrain vehicles (ATVs) and Gators; civilian boats and kayaks (Civilian Boat/Kayak); 4- and 6-wheeled military vehicles (Military 4WD); LCAC and AAVs; military watercraft (Military Boat); and military aircraft (Aircraft).

Table 12-18. Human activity monitoring periods by weekday (Sun/Mon – Thurs) or weekend (Thurs/Fri – Sun) occurrences, dates monitored, total days monitored (1 day = 24 hrs), and calculated camera trap nights (6 camera stations (*n*) * total days monitored; *n* = two camera stations per land use area (Developed Recreation, Amphibious Training, and Low Impact Wildlife)) at Onslow Beach on MCBCL, North Carolina, 2008–2009.

Monitoring Period	Weekdays/ Weekend	Dates Monitored	Total Days Monitored	Trap Nights
Apr 2008	Weekdays	Not monitored	0	0
	Weekend	4–6	2	12
May 2008	Weekdays	11–13	2	12
	Weekend	29–31	2	12
Jun 2008	Weekdays	26–29	3	18
	Weekend	3–5	2	12
Jul 2008	Weekdays	29–31	2	12
	Weekend	Not monitored	0	0
Aug 2008	Weekdays	7–9	2	12
	Weekend	8–9	2	12
Apr 2009*	Weekdays	22–24	2	8
	Weekend	3–5	2	8
May 2009	Weekdays	13–15	2	12
	Weekend	23–25	2	12
Jun 2009	Weekdays	3–5	2	12
	Weekend	19–22	3	18
Jul 2009	Weekdays	29–31	2	12
	Weekend	3–5	2	12
Aug 2009	Weekdays	Not monitored	0	0
	Weekend	7–10	3	18

* Camera stations not set up in Amphibious Training Zone due to training exercises (*n* = 4)

Analyses: We report 2-year mean counts of shorebird and tern species per survey effort by land use area (i.e., Developed Recreation, Amphibious Training, and Low Impact Wildlife areas) in the marsh and beachfront, and group data into two time categories (e.g., 15 Mar – 31 May, 1 Jun – 15 Aug) to separate out spring migration and breeding season birds. We calculated survey effort based on the number of beach and marsh surveys conducted both years in each land use area.

We report a 2-year mean camera trap success (i.e., an index of relative abundance) for potential shorebird predators each season on the beach and in the marsh by land use area. Similarly, we summarize monthly human activity and impacts trap success beachfront by land use zone.

We calculated camera trap success at each station for each predator species and human impact as the number of capture events per number of trap nights. We considered a single capture event to be all photographs of a given species or human activity within a 30-min period (Di Bitetti et al., 2006). We determined trap nights per monitoring period based on the number of complete 24-hr cycles all camera stations were functioning (i.e., number of days functioning multiplied by total number of camera stations).

Results and Discussion

Shorebird Surveys: We identified the highest diversity of breeding shorebird species (i.e., 2-year mean count per survey effort) in the Low Impact Wildlife area beachfront and marsh side (**Figures 12-4 to 11**), with the exception of Sanderlings and Willets. American Oystercatchers, Piping Plovers, Wilson’s Plovers, and Killdeer were observed primarily in the Low Impact Wildlife area beachfront and marsh side throughout the study (**Figures 12-4, 5, 9, 10, 11**). Sanderlings were more abundant on the beachfront in the Amphibious Training Zone from 1 Jun – 15 Aug both years (**Figure 12-7**). We counted more Willets in the Developed Recreation area beachfront in the latter part (1 Jun – 15 Aug) of the season both years (**Figure 12-8**).

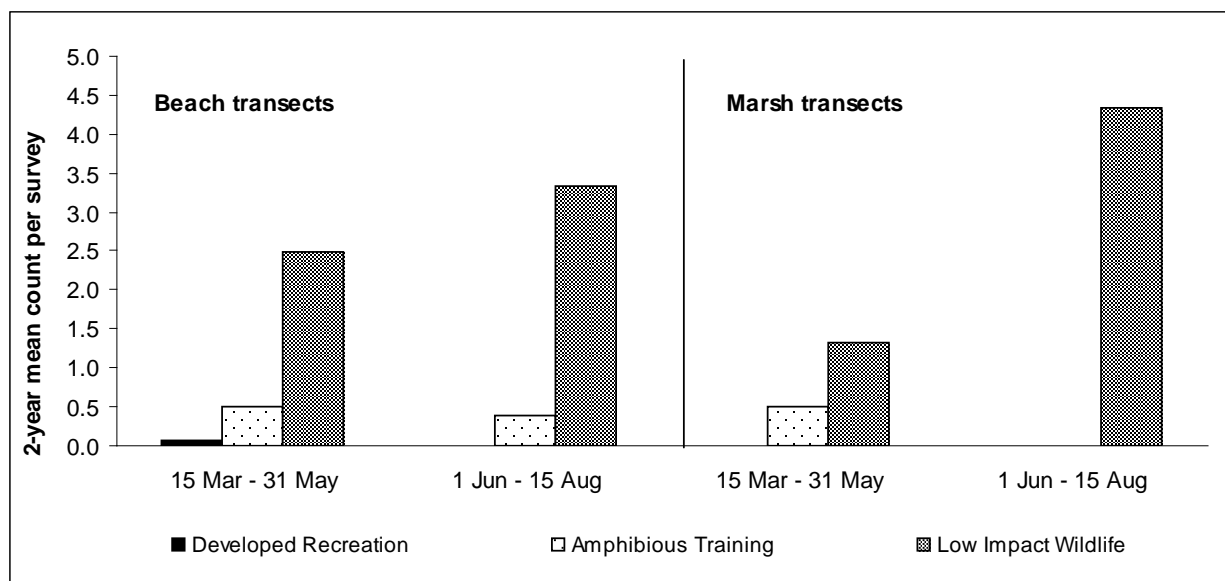


Figure 12-4. Count per survey effort (2-yr average) of American Oystercatchers (*Haematopus palliatus*) per land use area (Developed Recreation, Amphibious Training, and Low Impact Wildlife) on beach and marsh transects at Onslow Beach on MCBCL, North Carolina, 2008–2009.

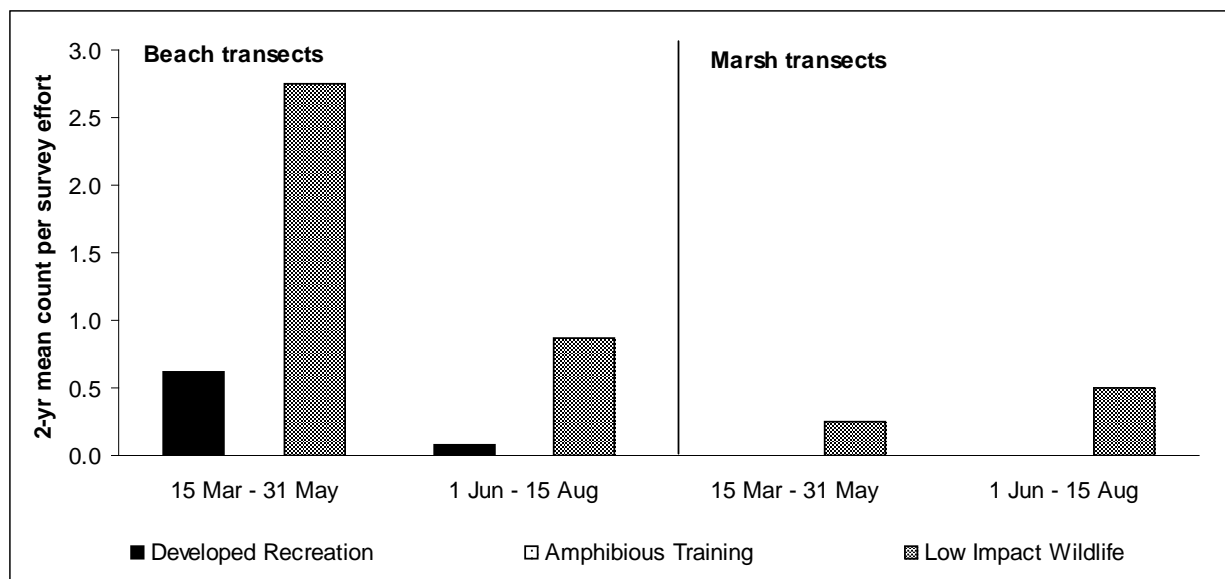


Figure 12-5. Count per survey effort (2-yr average) of Piping Plovers (*Charadrius melodus*) per land use area (Developed Recreation, Amphibious Training, and Low Impact Wildlife) on beach and marsh transects at Onslow Beach on MCBCL, North Carolina, 2008–2009.

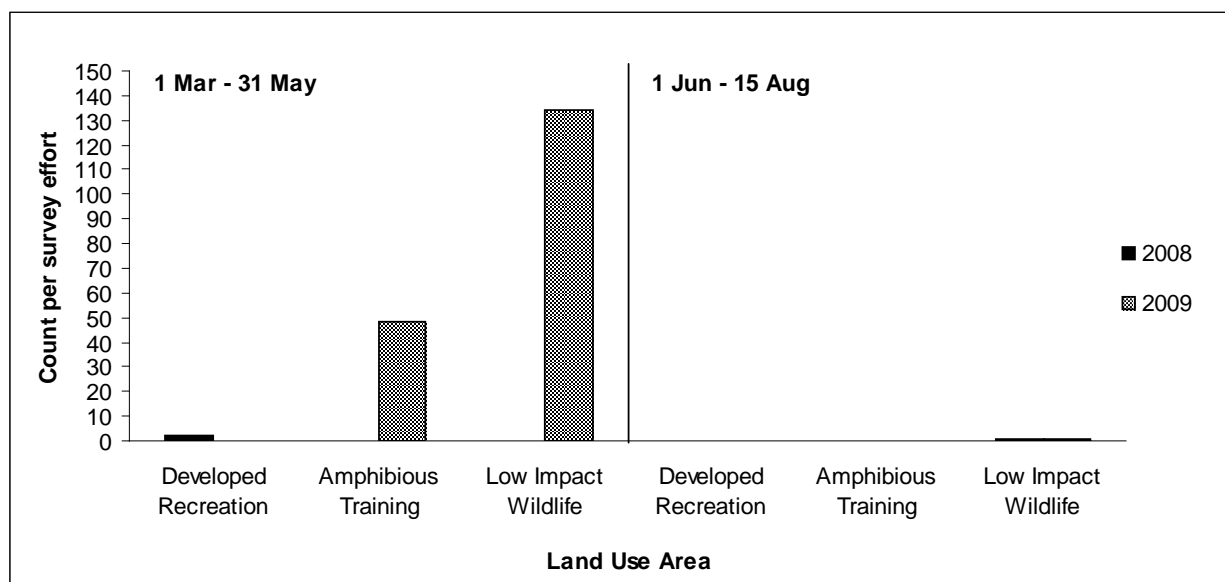


Figure 12-6. Count per survey effort of Red Knots (*Calidris canutus*) per land use area (Developed Recreation, Amphibious Training, and Low Impact Wildlife) on beach transects at Onslow Beach on MCBCL, North Carolina, 2008 and 2009.

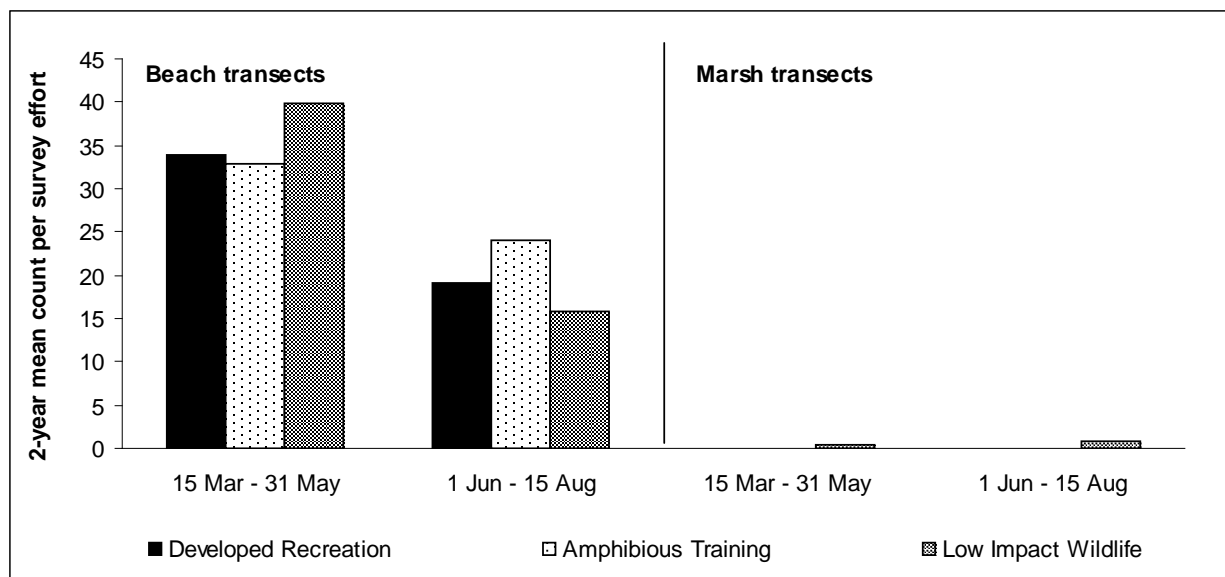


Figure 12-7. Count per survey effort (2-yr average) of Sanderlings (*Calidris alba*) per land use area (Developed Recreation, Amphibious Training, and Low Impact Wildlife) on beach and marsh transects at Onslow Beach on MCBCL, North Carolina, 2008–2009.

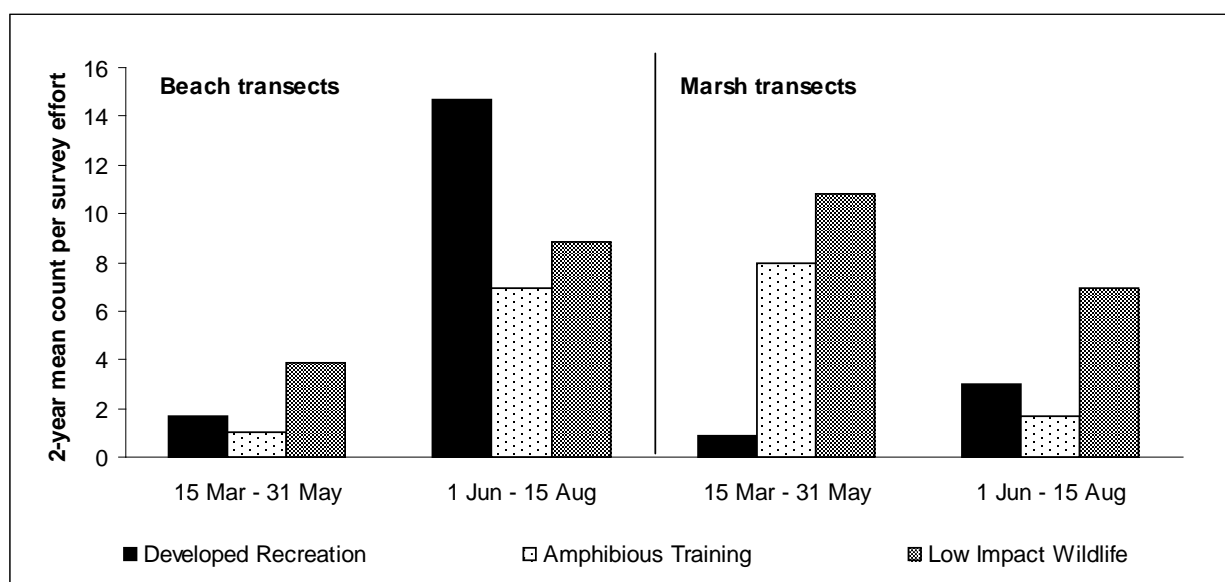


Figure 12-8. Count per survey effort (2-yr average) of Willets (*Catoptrophorus semipalmatus*) per land use area (Developed Recreation, Amphibious Training, and Low Impact Wildlife) on beach and marsh transects at Onslow Beach on MCBCL, North Carolina, 2008–2009.

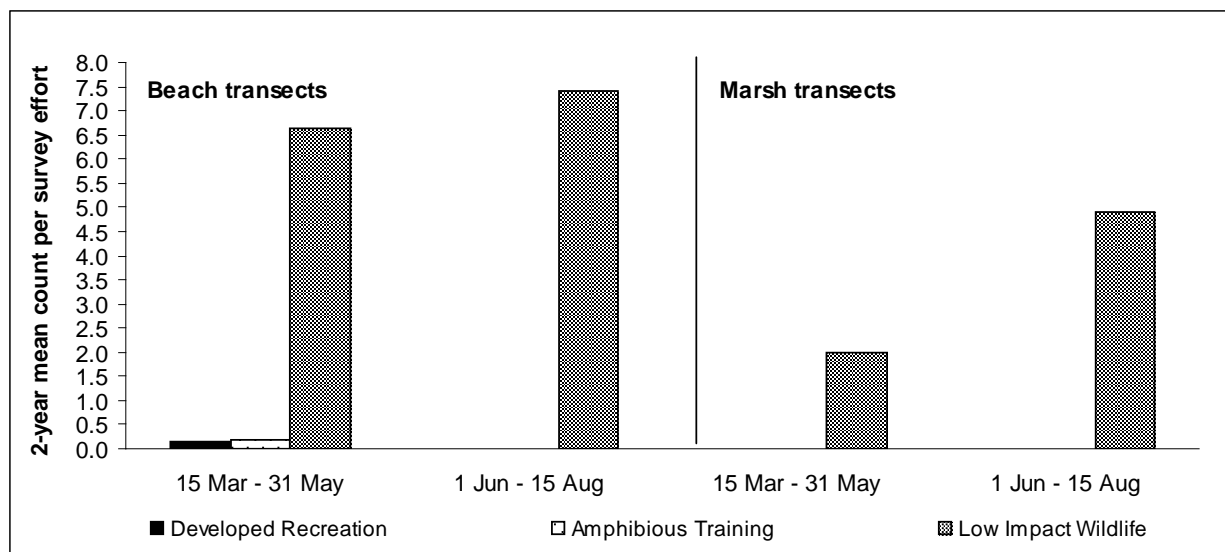


Figure 12-9. Count per survey effort (2-yr average) of Wilson's Plovers (*Charadrius wilsonia*) per land use area (Developed Recreation, Amphibious Training, and Low Impact Wildlife) on beach and marsh transects at Onslow Beach on MCBCL, North Carolina, 2008–2009.

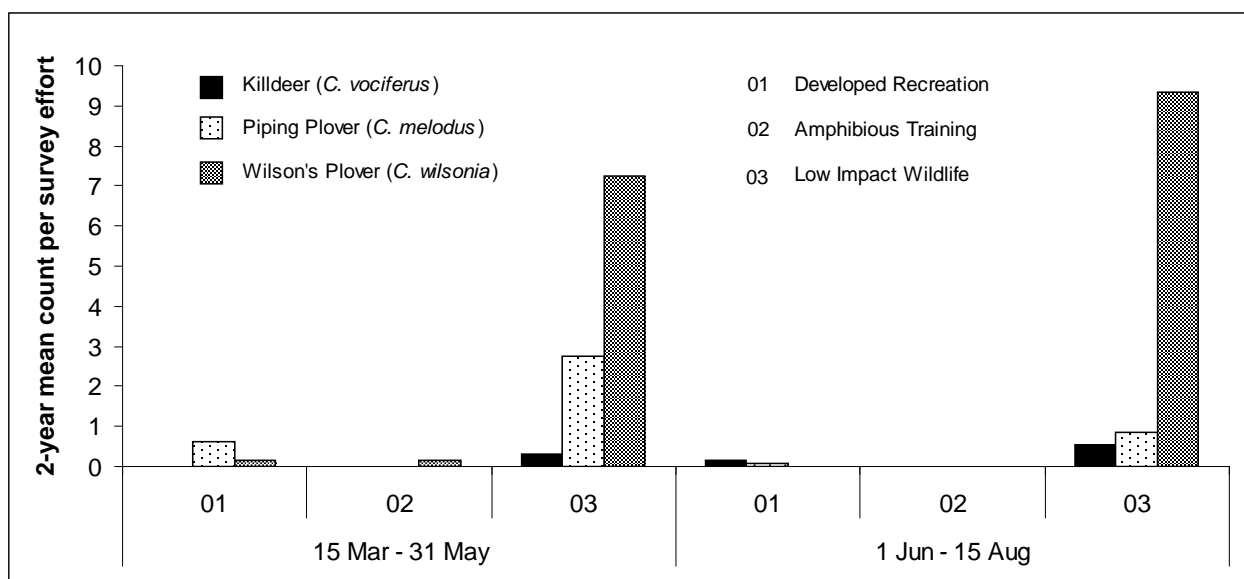


Figure 12-10. Count per survey effort (2-yr average) of breeding plovers (*Charadrius spp.*) observed beachfront by land use area (Developed Recreation, Amphibious Training, and Low Impact Wildlife) at Onslow Beach on MCBCL, North Carolina, 2008–2009.

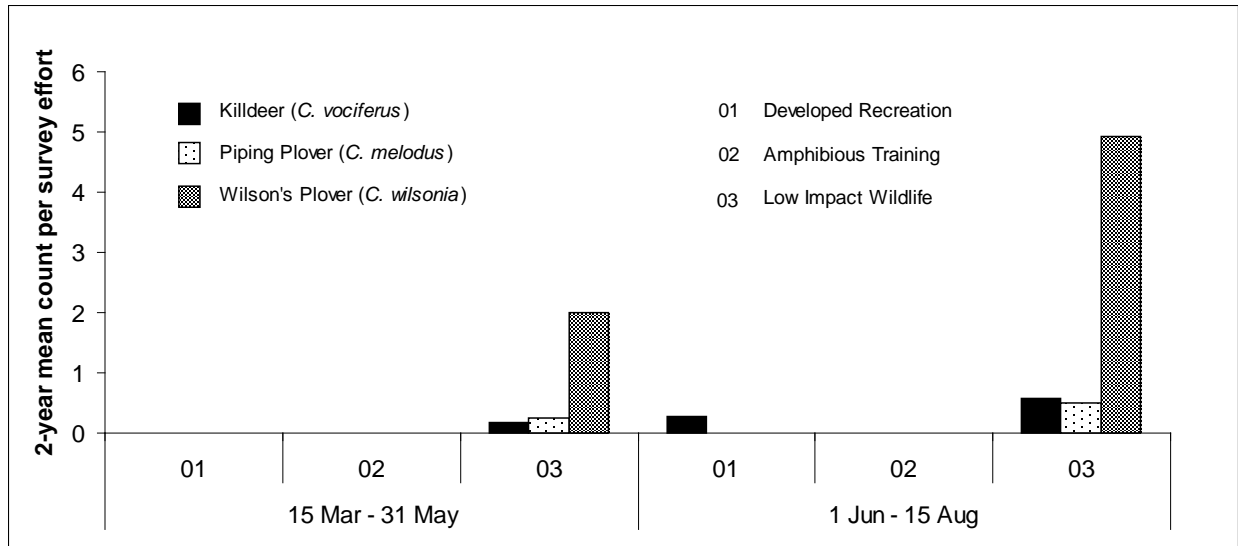


Figure 12-11. Count per survey effort (2-yr average) of breeding plovers (*Charadrius spp.*) observed marshside by land use area (Developed Recreation, Amphibious Training, and Low Impact Wildlife) at Onslow Beach on MCBCL, North Carolina, 2008–2009.

We detected more Black-bellied and Semipalmated Plovers during the first part (15 Mar – 31 May) of the season beachfront in the Low Impact Wildlife area (**Figure 12-12**), and observed a relatively equal proportion of the same species in the same land use area and the Amphibious Training zone during the end of the season. We observed Black-bellied Plovers more often marshside in the Amphibious Training and Low Impact Wildlife areas during the first part of the season (**Figure 12-13**) but detected them late season only in the Low Impact Wildlife zone. We counted Semipalmated Plovers marshside in the beginning of each year in the Developed Recreation and Low Impact Wildlife areas (**Figure 12-13**), but only detected this species in the latter part of the year in the Low Impact Wildlife area.

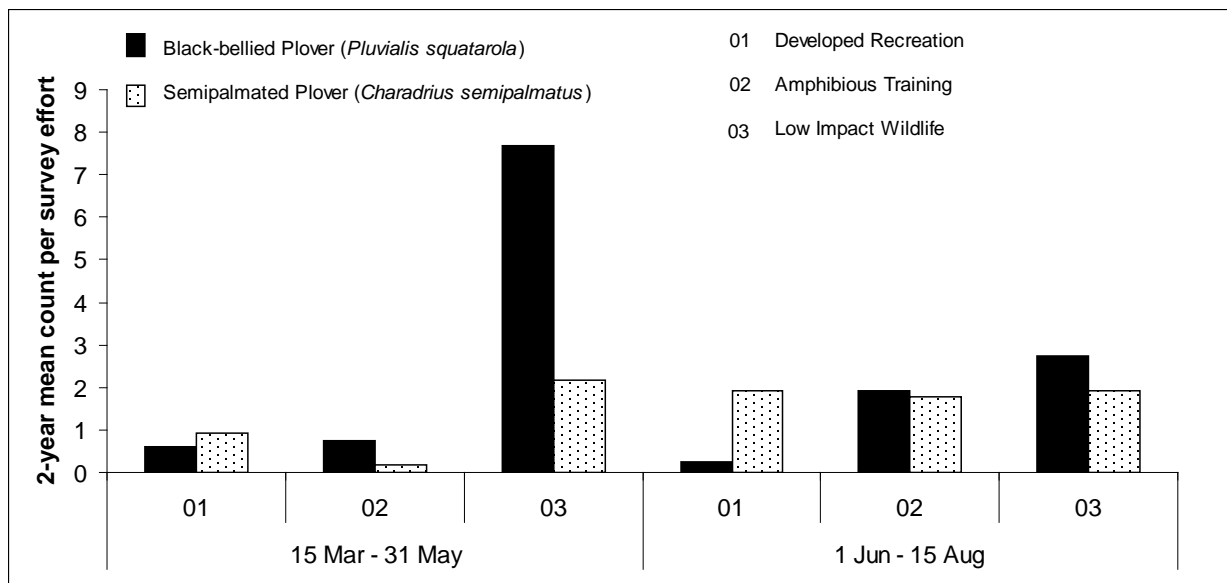


Figure 12-12. Count per survey effort (2-yr average) of wintering, non-breeding or migrating plovers observed beachfront by land use area (Developed Recreation, Amphibious Training, and Low Impact Wildlife) at Onslow Beach on MCBCL, North Carolina, 2008–2009.

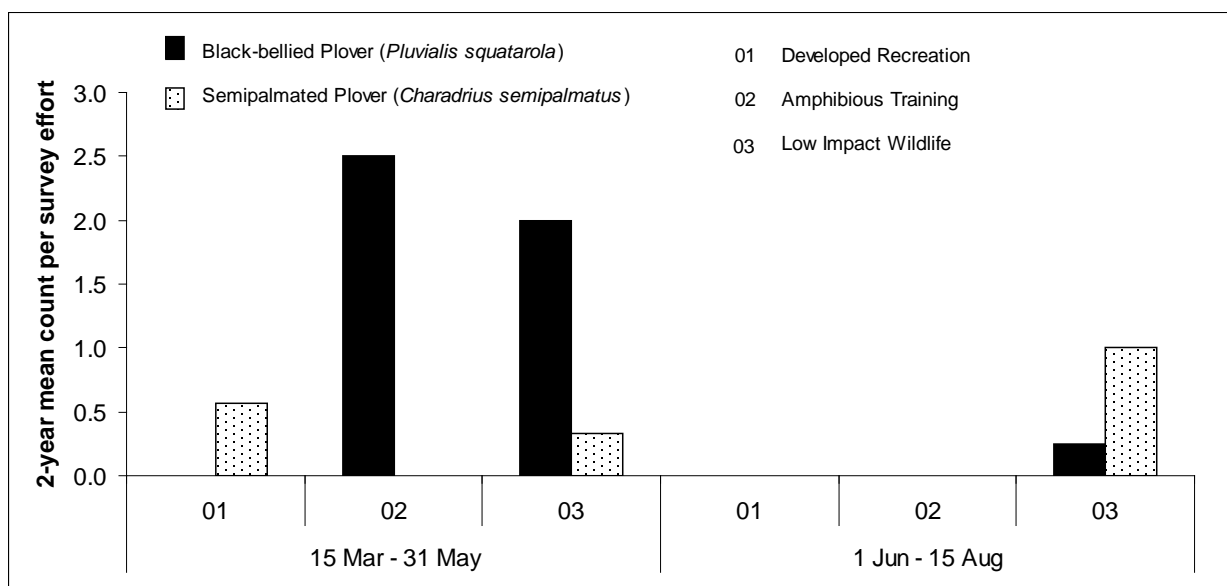


Figure 12-13. Count per survey effort (2-yr average) of wintering, non-breeding or migrating plovers observed marshside by land use area (Developed Recreation, Amphibious Training, and Low Impact Wildlife) at Onslow Beach on MCBCL, North Carolina, 2008–2009.

At the beginning and end of both seasons, we observed increased numbers of breeding terns beachfront in the Low Impact Wildlife area (**Figure 12-14**). We counted more Royal Terns

beachfront, but Least Terns were the only terns to establish colonies in the Low Impact Wildlife area both years. Diversity of breeding terns varied marsh side across land use areas and between the beginning and end of both seasons (**Figure 12-15**). Least Terns were the most commonly detected tern marsh side in the Low Impact Wildlife area during the study. We observed a relatively higher number of Common Terns compared to other tern species during the first part of each season in the Amphibious Training zone.

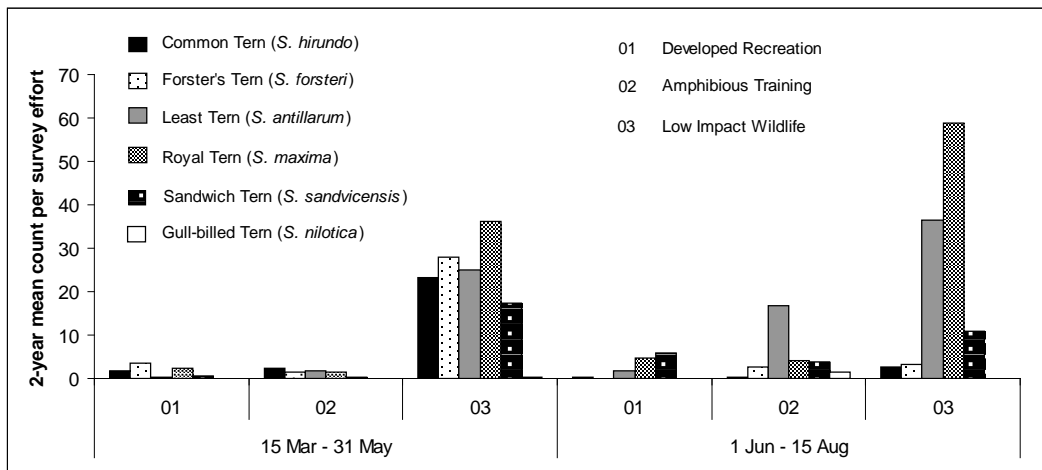


Figure 12-14. Count per survey effort (2-yr average) of breeding terns (*Sterna* spp.) observed beachfront by land use area (Developed Recreation, Amphibious Training, and Low Impact Wildlife) at Onslow Beach on MCBCL, North Carolina, 2008–2009.

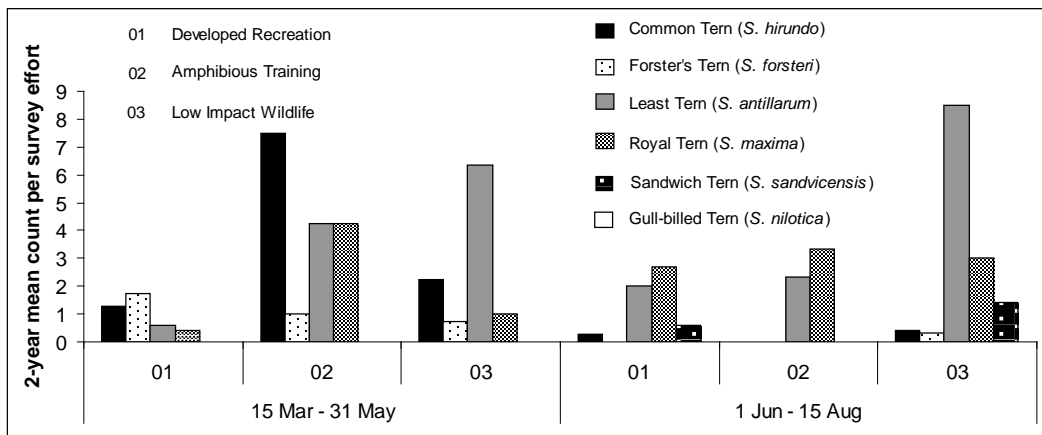


Figure 12-15. Count per survey effort (2-yr average) of breeding terns (*Sterna* spp.) observed marshside by land use area (Developed Recreation, Amphibious Training, and Low Impact Wildlife) at Onslow Beach on MCBCL, North Carolina, 2008–2009.

Predator Monitoring: In 2008, we detected gray fox (*Urocyon cinereoargenteus*) more than other potential shorebird and tern predators in the Developed Recreation area beachfront, observing peak trap success in October 2008 followed by continued decrease throughout 2009 (**Figure 12-16**). Gray fox were rarely recorded in the Low Impact Wildlife area at beachfront camera stations. Bobcat (*Lynx rufus*) were detected most frequently in the Low Impact Wildlife area beachfront both years with the exception of red fox in January 2009 (**Figure 12-16**). We

observed few red fox (*Vulpes vulpes*) in both land use areas on the beach, only occurring in October 2008 and January 2009. Bobcat were rarely detected in the Developed Recreation area occurring beachfront and marsh side only in January 2009. Feral cats using beachfront were primarily detected in the Developed Recreation area both years, and we observed very few occurrences during the study in the Low Impact Wildlife area (**Figure 12-16**). We observed similar trap success of gray fox in the Developed Recreation area and bobcat in the Low Impact Wildlife area marsh side both years (**Figure 12-17**). However, gray fox were more abundant in the Developed Recreation area beachfront than marsh side in the same land use area. We observed bobcat more frequently marsh side in the Low Impact Wildlife area compared to beachfront detections both years (**Figure 12-17**). Gray fox were more commonly recorded using marsh side habitat in the Low Impact Wildlife area than beachfront in the same land use zone. Feral cats were not detected using marsh habitat in either land use area during the study (**Figure 12-17**). Most occurrences of dogs were in the Developed Recreation area both years (**Figure 12-18**) with trap success peaking in April 2009 and decreasing again by July. We observed higher trap success of domestic dogs during fall seasons in the Low Impact Wildlife area, and during winter and spring in 2009.

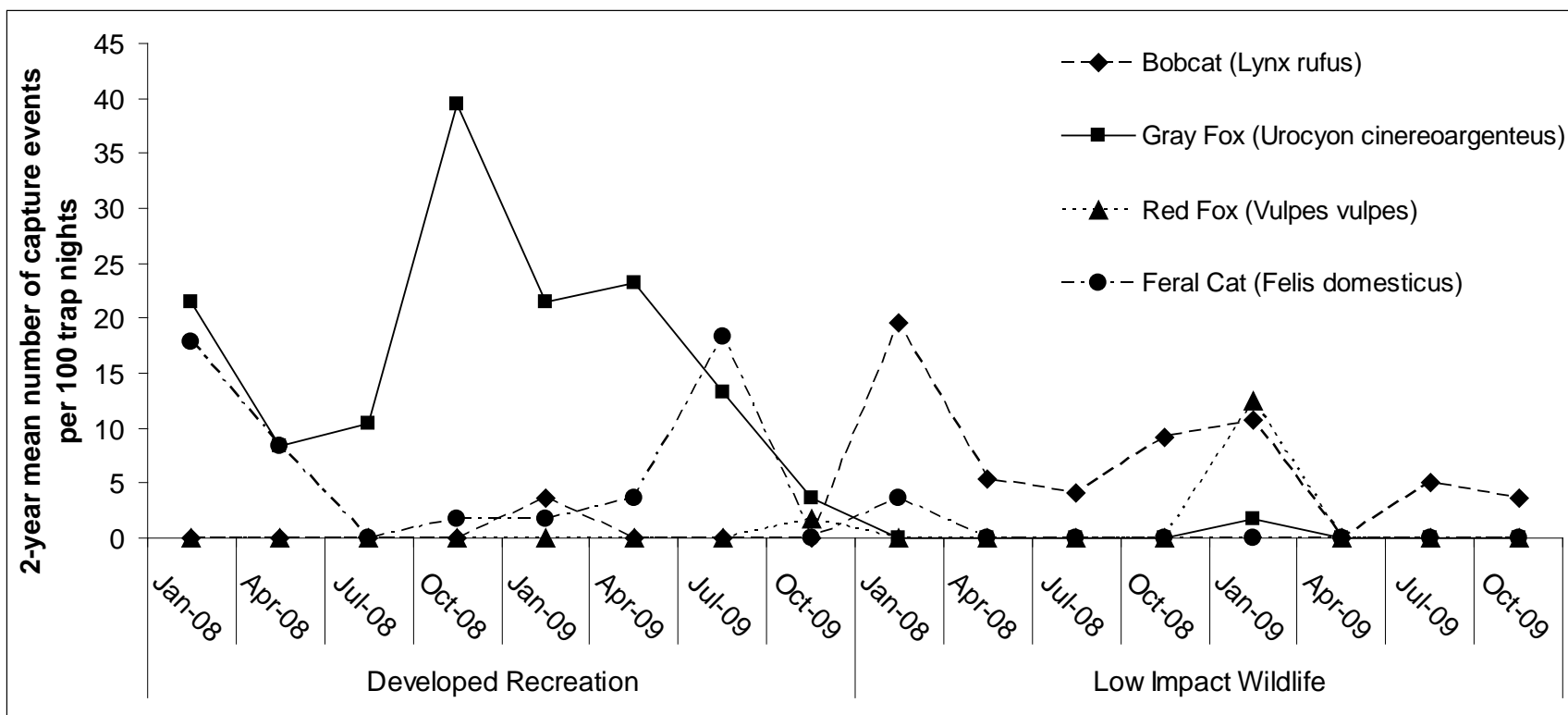


Figure 12-16. Beach predator trap success metrics (2-yr mean number of capture events per 100 trap nights) by land use area (Developed Recreation and Low Impact/Wildlife Area) and monitoring period (month and year) for bobcat (*Lynx rufus*), gray fox (*Urocyon cinereoargenteus*), red fox (*Vulpes vulpes*), and feral cat (*Felis domesticus*) at Onslow Beach on MCBCL, North Carolina, 2008–2009.

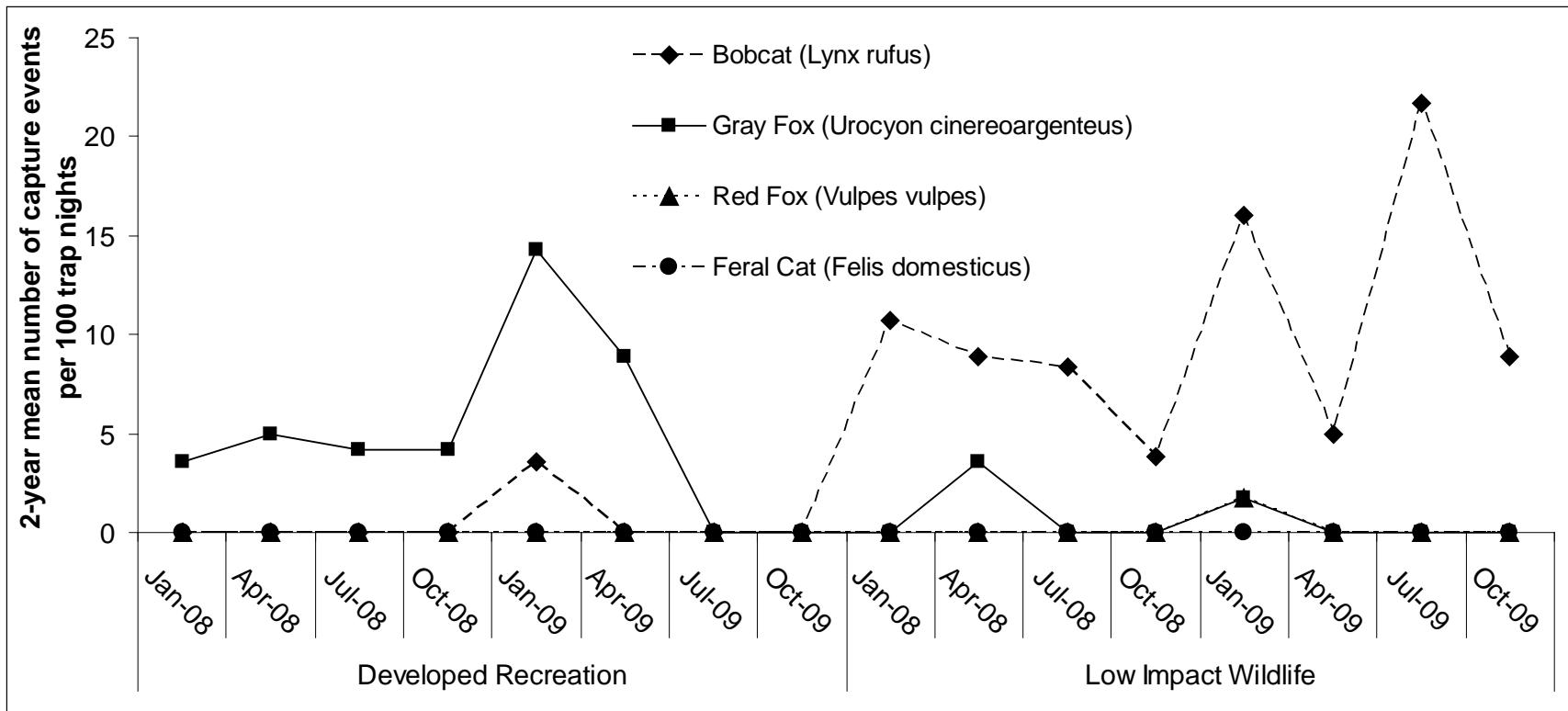


Figure 12-17. Marsh predator trap success metrics (2-yr mean number of capture events per 100 trap nights) by land use area (Developed Recreation and Low Impact Wildlife) and monitoring period (month and year) for bobcat (*Lynx rufus*), gray fox (*Urocyon cinereoargenteus*), red fox (*Vulpes vulpes*), and feral cat (*Felis domesticus*) at Onslow Beach on MCBCL, North Carolina, 2008–2009.

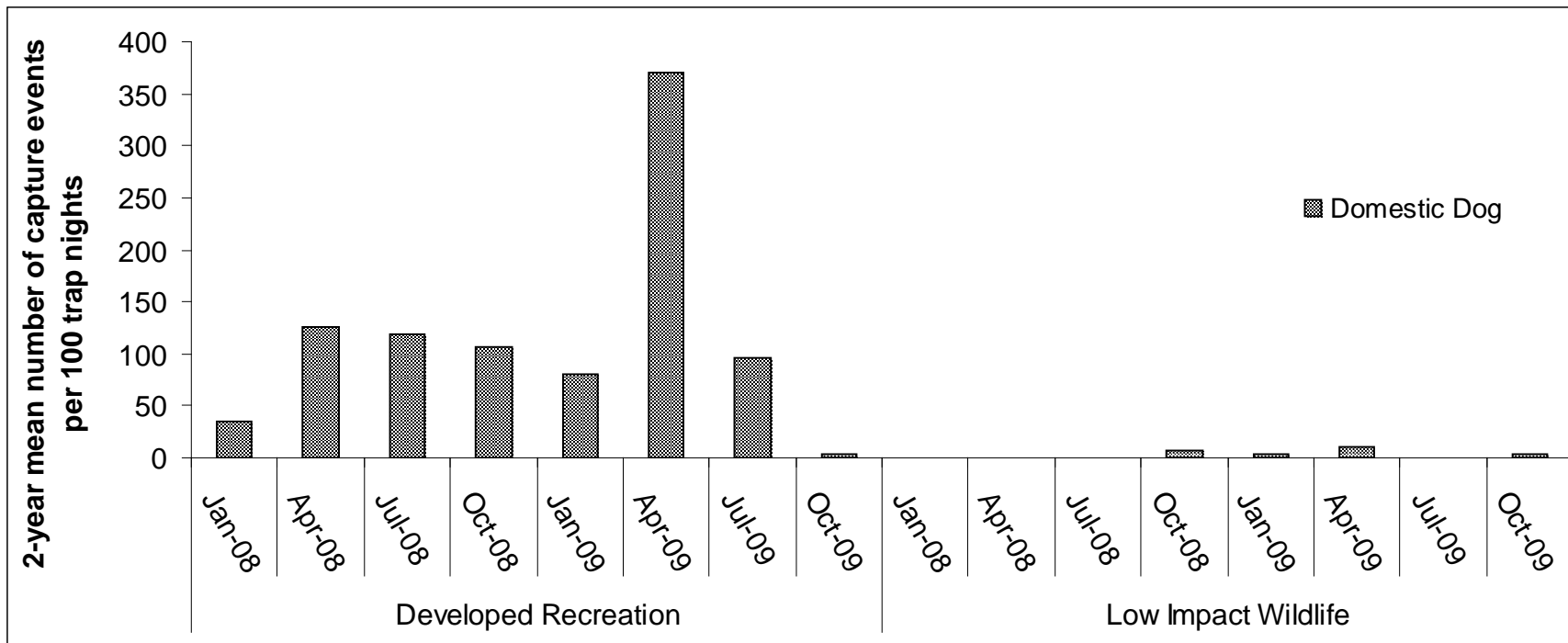


Figure 12-18. Beach predator trap success metrics (2-yr mean number of capture events per 100 trap nights) by land use area (Developed Recreation and Low Impact Wildlife) and monitoring period (month and year) for domestic dogs (*Canis familiaris*) at Onslow Beach on MCBCL, North Carolina, 2008–2009.

Ghost crabs were the most commonly detected beachfront potential predator in the Developed Recreation area both years (Fig 19). Raccoon (*Procyon lotor*) and Virginia opossum (*Didelphis virginiana*) were detected < 5 capture events per 100 camera trap nights beachfront in the Developed Recreation area during the study, but increased in the Low Impact Wildlife area to 10 – 15 capture events (**Figure 12-19**). We detected raccoons more than Virginia opossums and ghost crabs marsh side in both land use areas during the study (**Figure 12-20**). We generally observed more Virginia opossum marsh side in the Low Impact Wildlife area than in the Developed Recreation area. We observed more raccoon marsh side both years in the Low Impact Wildlife area than beachfront in the same land use zone (**Figures 12-19 and 20**).

Human Activity Monitoring: We detected the highest vehicle use and variation in vehicle types in the Amphibious Training zone for both years (**Figure 12-21**). Interestingly, privately owned vehicles were the most commonly detected in the Amphibious Training area, not military vehicles. We identified private vehicles and ATVs (i.e., Gators or 4-wheelers) as the most abundant types used in the Developed Recreation area as well (**Figure 12-21**). In the Low Impact Wildlife area, we observed very few vehicles of any type from May through August of both years, except Base Environmental Management Division trucks and other approved research vehicles as this area is closed to private vehicles during this time period for shorebird and turtle conservation efforts (**Figure 12-21**). April had the highest personal vehicle use compared to subsequent months, where there was little to no detection of privately owned vehicles in the Low Impact Wildlife area.

Our results indicate that most dogs are kept on leashes in the Developed Recreation area through the spring and summer seasons (**Figure 12-22**). Off-leash detection of dogs was low compared to on-leash trap success metrics in this land use area. We observed approximately equal proportions of domestic dogs on- and off-leash in the Amphibious Training zone for both years (**Figure 12-22**), but more were on leashes than not. Our human activity monitoring efforts did not detect domestic dogs in the Low Impact Wildlife area on Onslow Beach; however our predator monitoring did (**Figures 12-18 and 22**).

We observed people engaged in physical activity (i.e., walking, running, volleyball, biking) in all land use areas and report a 2-year mean trap success in the category, Active (**Figures 12-23 to 25**). We observed the highest number of Active people using the Developed Recreation area (**Figure 12-23**) and the lowest number were detected in the Low Impact Wildlife area (**Figure 12-25**). The greatest number of all human activities occurred in the Developed Recreation area (**Figure 12-23**), although we observed recreational use in the Amphibious Training zone that not only included Active people, but families and individuals sitting, fishing, and horseback riding (**Figure 12-24**). The only category of use we observed in the Low Impact Wildlife area was Active people, with the highest mean trap success occurring in April (**Figure 12-25**). Marines were observed using the Amphibious Training zone in April and July of both years (**Figure 12-24**), and were detected in the Developed Recreation area only in July (**Figure 12-23**).

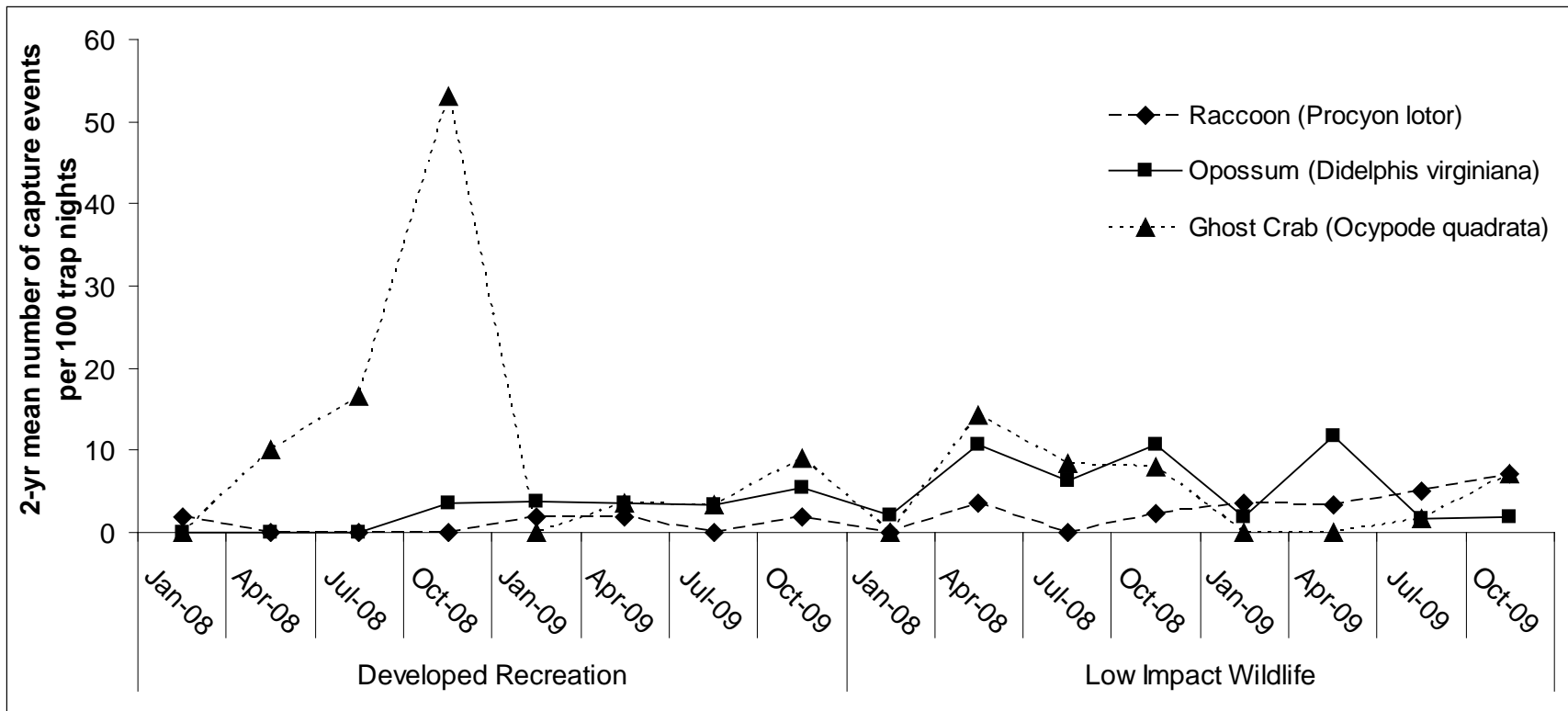


Figure 12-19. Beach predator trap success metrics (2-yr mean number of capture events per 100 trap nights) by land use area (Developed Recreation and Low Impact Wildlife) and monitoring period (month and year) for raccoon (*Procyon lotor*), Virginia opossum (*Didelphis virginiana*), and ghost crab (*Ocypode quadrata*) at Onslow Beach on MCBCL, North Carolina, 2008–2009.

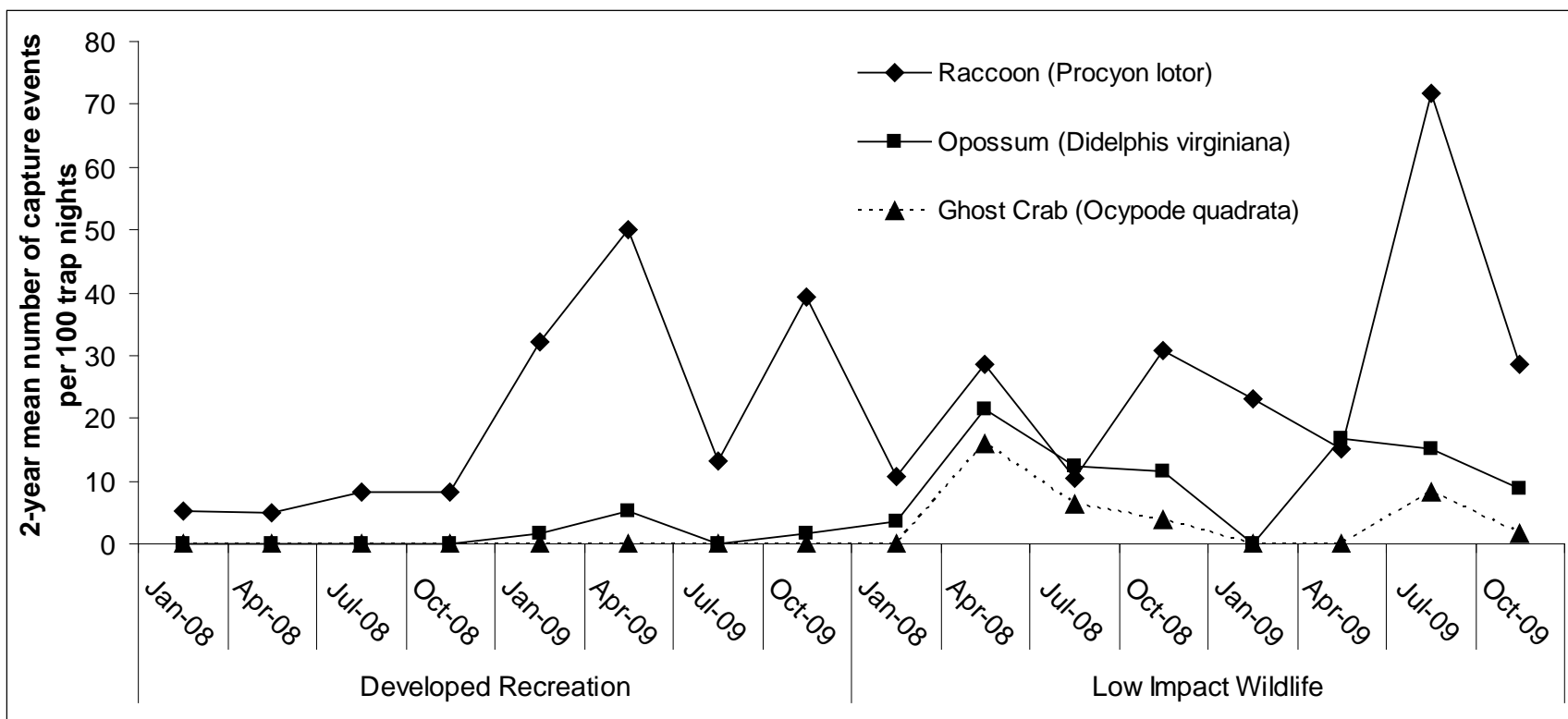


Figure 12-20. Marsh predator trap success metrics (2-yr mean number of capture events per 100 trap nights) by land use area (Developed Recreation and Low Impact Wildlife) and monitoring period (month and year) for raccoon (*Procyon lotor*), Virginia opossum (*Didelphis virginiana*), and ghost crab (*Ocypode quadrata*) at Onslow Beach on MCBCL, North Carolina, 2008–2009.

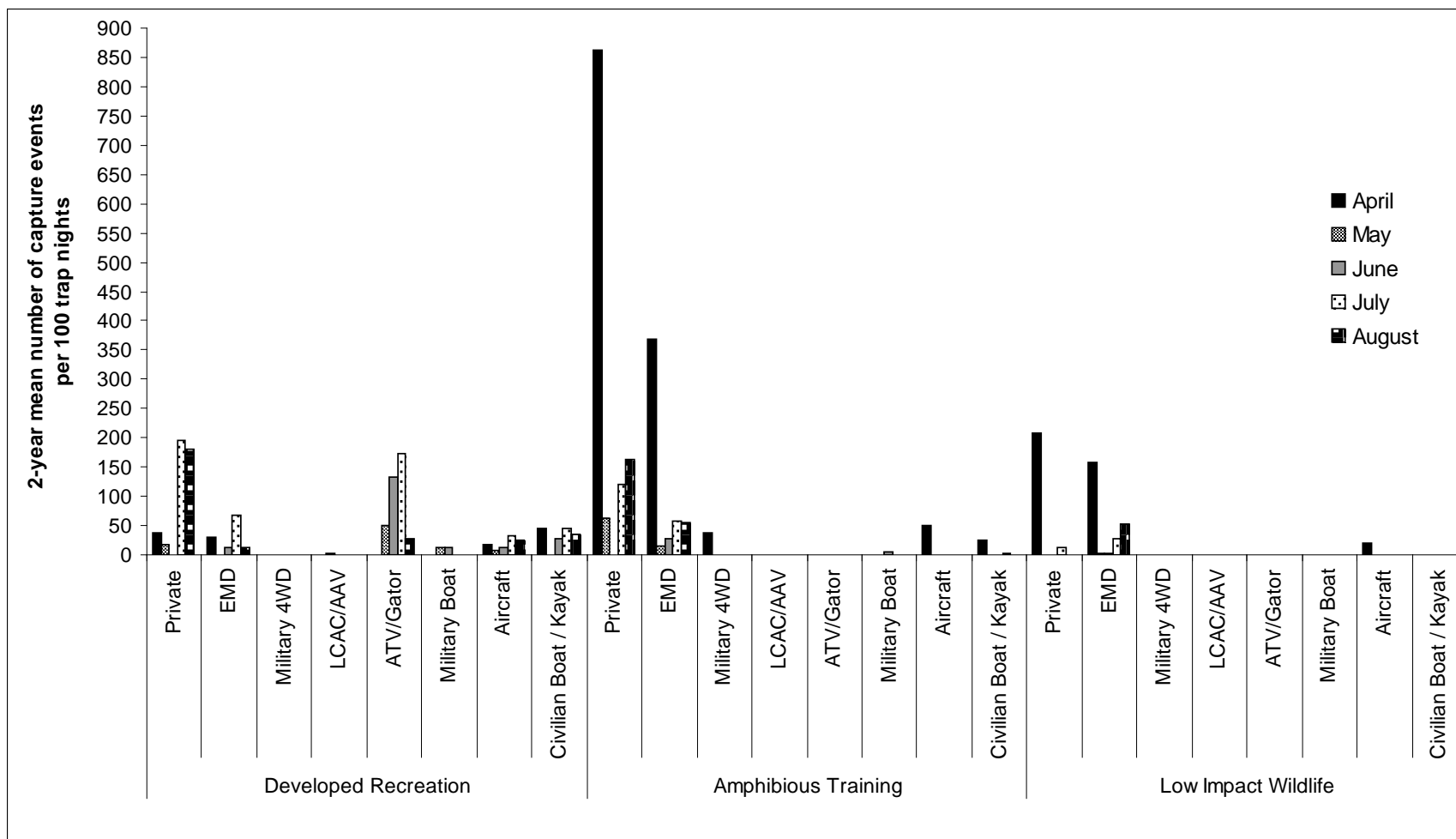


Figure 12-21. Average 2-year trap success metrics (mean number of capture events per 100 trap nights) by land use area (Developed Recreation, Amphibious Training, and Low Impact Wildlife) by monitoring period (month) for vehicles detected on Onslow Beach at MCBCL, North Carolina, 2008–2009.

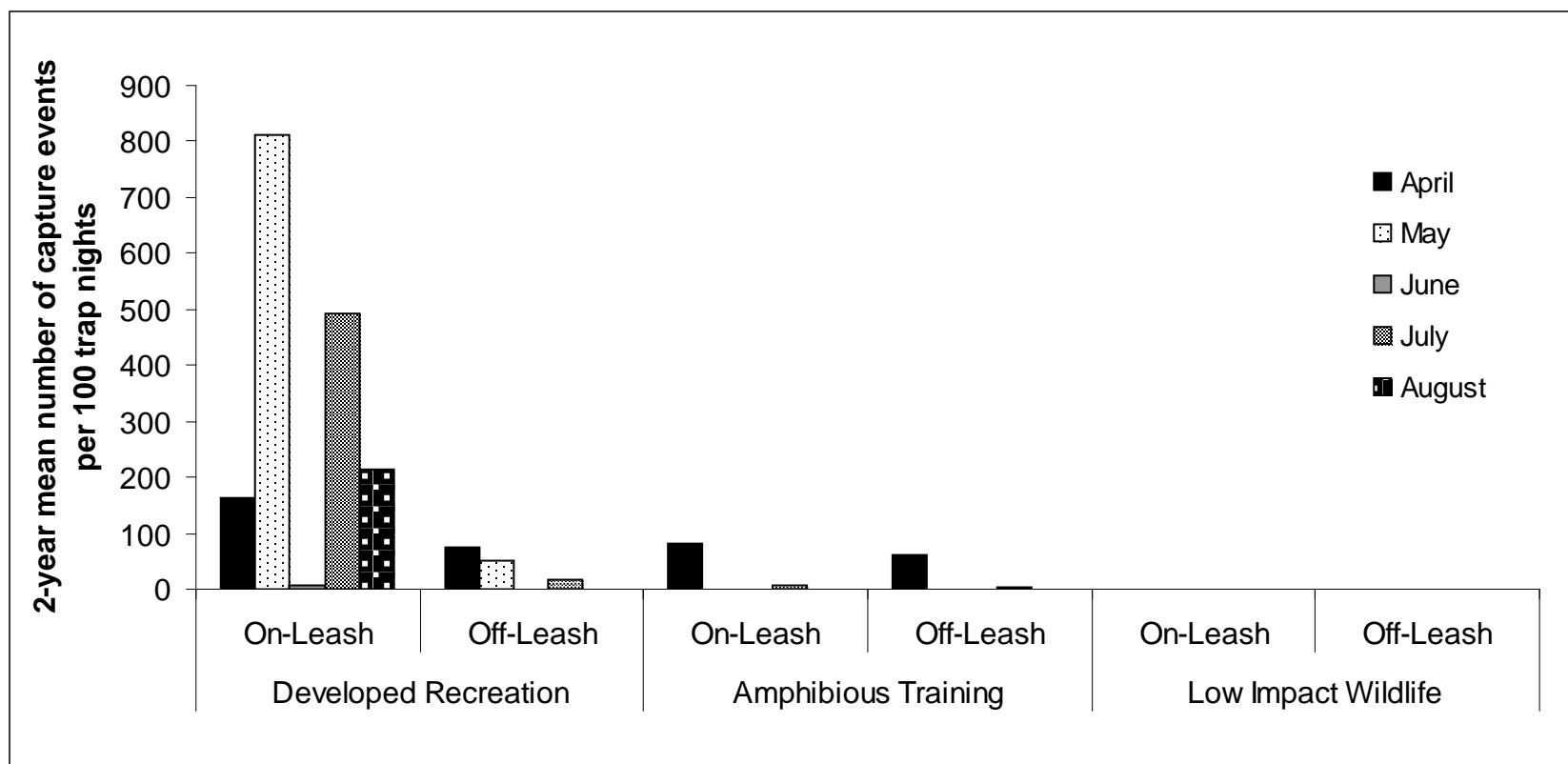


Figure 12-22. Average 2-year trap success metrics (mean number of capture events per 100 trap nights) by land use area (Developed Recreation, Amphibious Training, and Low Impact Wildlife) by monitoring period (month) for domestic dogs (*Canis familiaris*) on- and off-leash detected on Onslow Beach at MCBCL, North Carolina, 2008–2009.

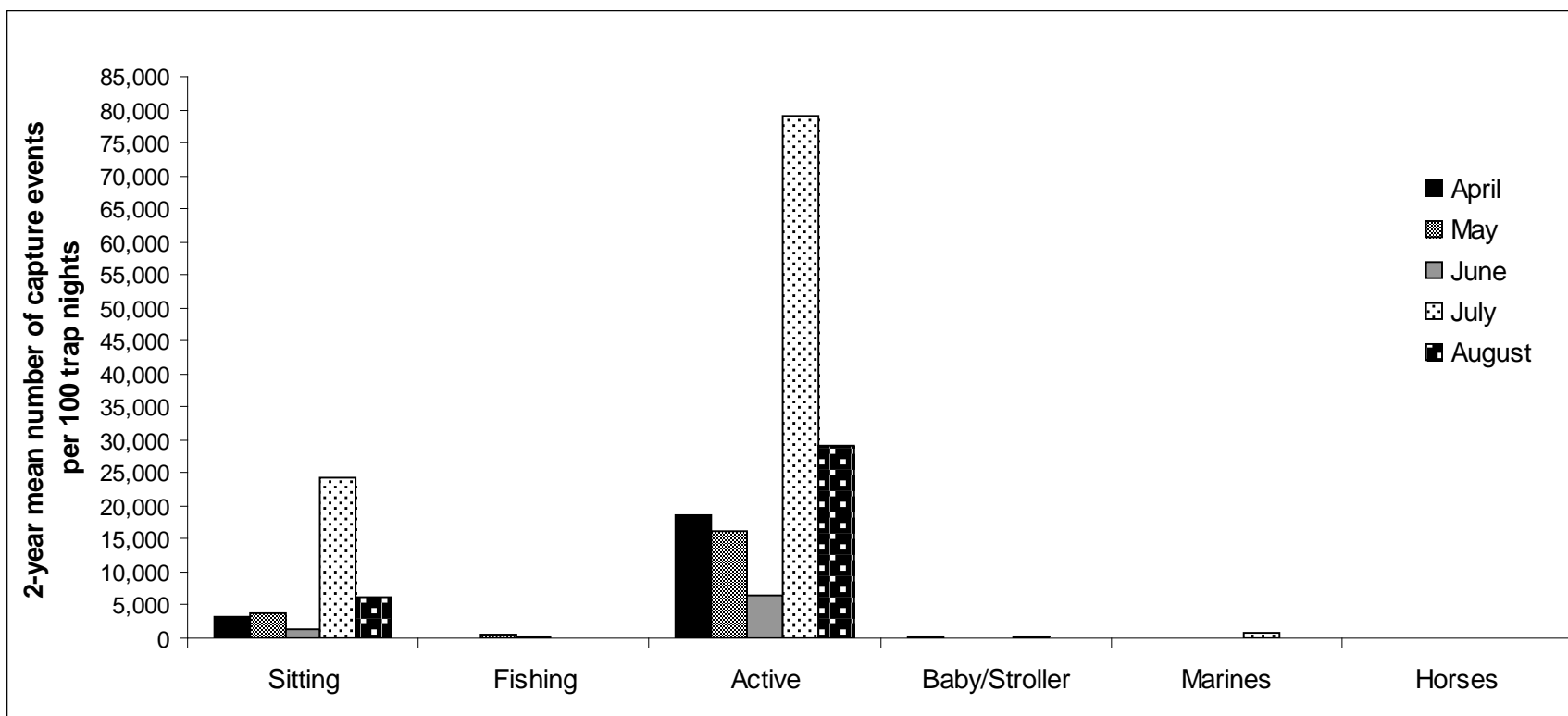


Figure 12-23. Average 2-year trap success metrics (mean number of capture events per 100 trap nights) in the Developed Recreation Area by monitoring period (month) for human activities occurring at Onslow Beach on MCBCL, North Carolina, 2008–2009.

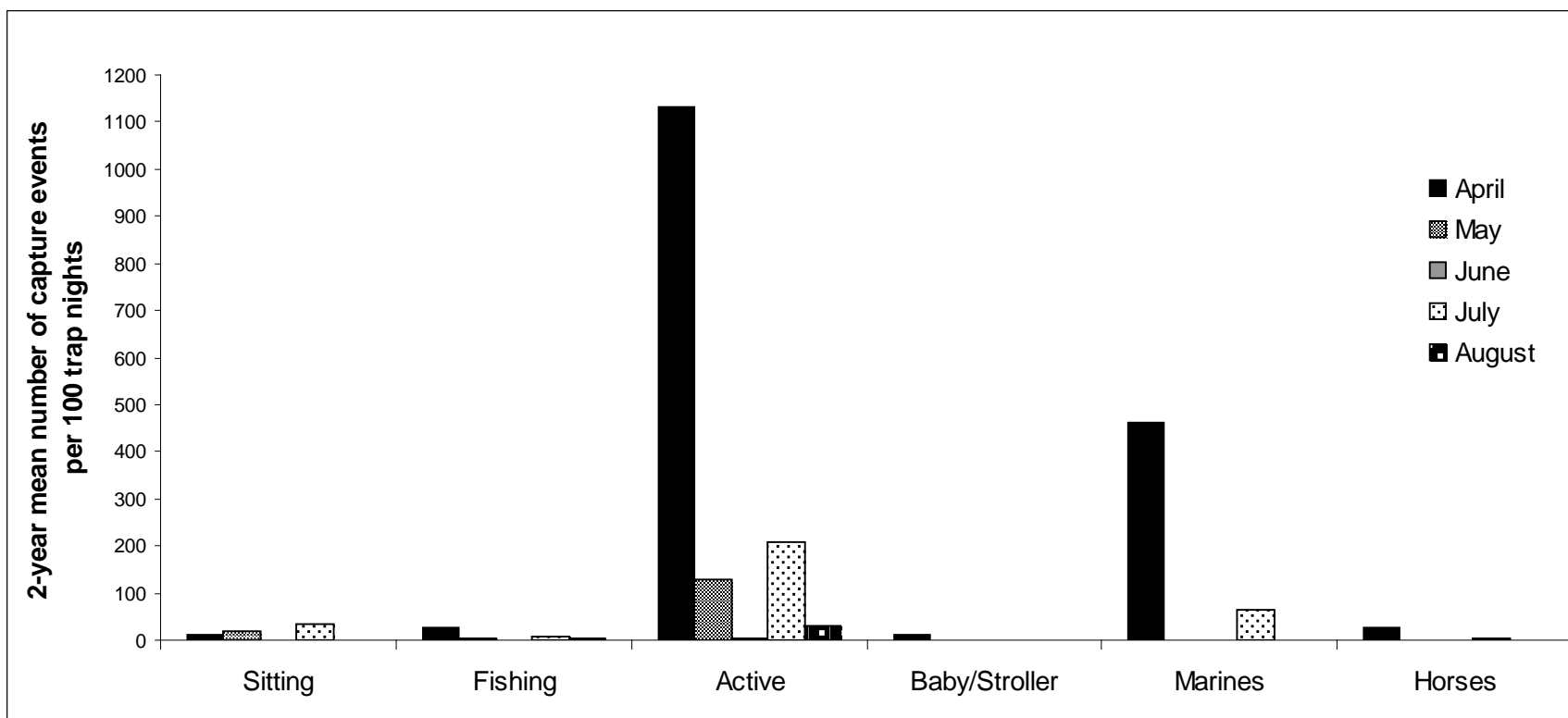


Figure 12-24. Average 2-year trap success metrics (mean number of capture events per 100 trap nights) in the Amphibious Training Zone by monitoring period (month) for human activities occurring at Onslow Beach on MCBCL, North Carolina, 2008–2009.

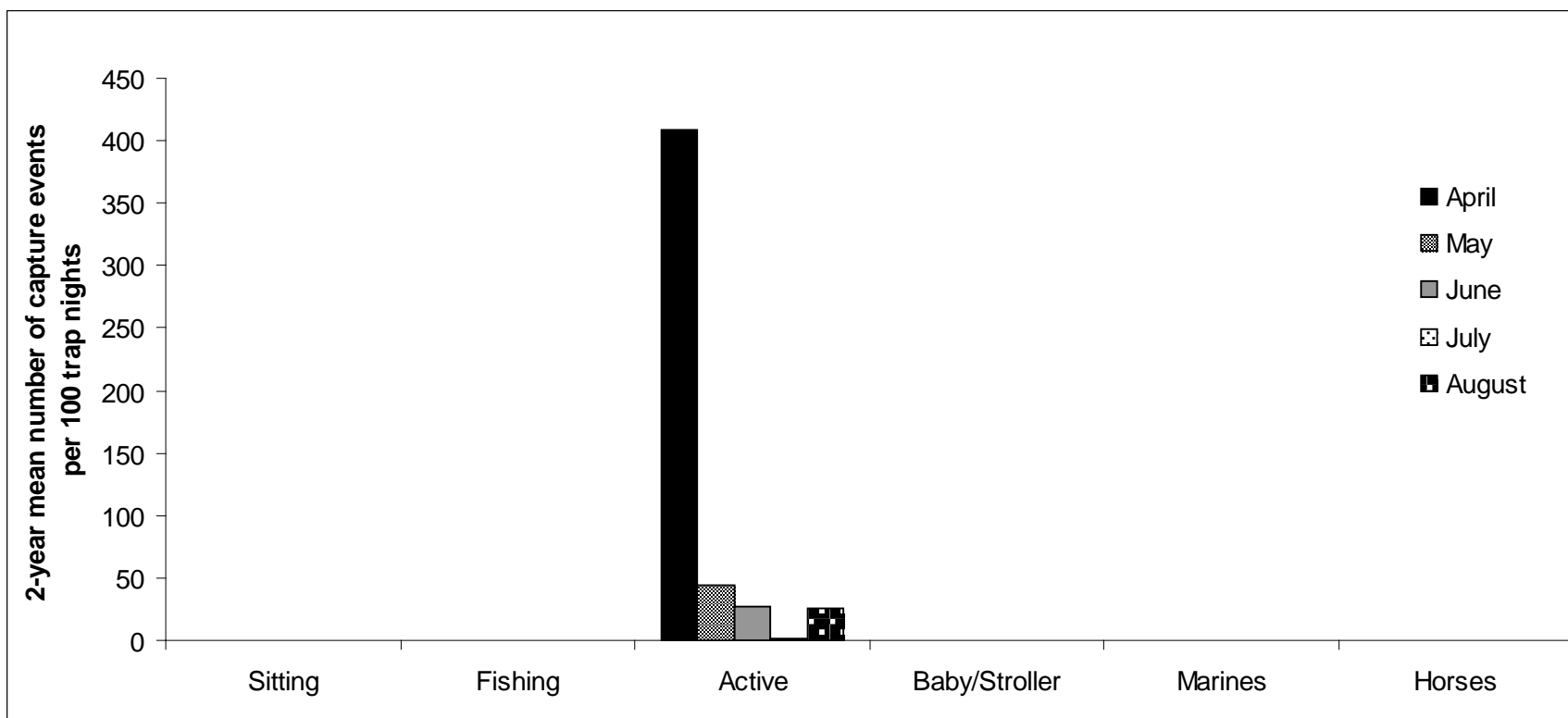


Figure 12-25. Average 2-year trap success metrics (mean number of capture events per 100 trap nights) in the Low Impact Wildlife area by monitoring period (month) for human activities occurring at Onslow Beach on MCBCL, North Carolina, 2008–2009.

Our results demonstrate the greatest diversity and abundances of shorebird and tern species occurring in the Low Impact Wildlife area where indices of human use are less than in other land use areas. We observed the least number and diversity of shorebirds and terns in the Developed Recreation area where human impacts were the greatest. Shorebirds and terns used the Amphibious Training zone more than the developed area, where vehicles were the greatest anthropogenic impact. We detected relatively comparable proportions of Sanderlings and Willets beachfront in all land use areas in the beginning and end of each season. These shorebird species demonstrated a higher human tolerance (e.g. recreational inter-tidal walkers and runners) than others in all land use zones. Gulls were also common and human-tolerant, especially in the Developed Recreation area, but are not discussed or reported in this paper.

Studies have addressed the effects of anthropogenic disturbances on foraging, breeding, wintering, and migrating shorebirds and terns (Collazo et al. 1994, Burger 1998, Lafferty 2001, Burger et al. 2004, Botto et al. 2008), and findings demonstrate that human activity can flush birds from feeding and roosting sites and adversely affect fitness levels due to decreased habitat availability. Coastal flora and fauna are sensitive to low levels of foot traffic (Davenport and Davenport 2006). Biodiversity of inter-tidal algae has been shown to decrease with increased occurrences of people walking through the surf (Brosnan and Crumrine 1994, Schiel and Taylor 1999). Similarly, vegetation species growing in coastal dunes and their associated insect communities are altered when people use this habitat for recreation (Hylgaard and Liddle 1981). Shorebirds depend on inter-tidal and dune resources for foraging, nesting, and roosting.

Domestic dogs have been documented in other studies to harass and kill coastal birds and their young (Burger 1986, Burger et al. 2004). At Camp Lejeune, we recorded more dogs on-leash than off-leash in designated and non-designated pet areas; thus, it appears that ongoing dog management activities are highly effective. Our results indicate that personal vehicles were detected in all land use areas during the study; however, detection of privately owned vehicles was minimal in the Low Impact Wildlife and Developed Recreation area compared to the Amphibious Training zone that remained open to daytime beach driving from May to August.

Increasing levels of human activity and development in coastal habitats are often accompanied by the introduction of non-native predators (NCWRC 2005) such as feral cats, raccoons, and red fox, whether intentional or accidental. These animals are attracted to garbage, fish remains, and other food associated with human activities in beach habitats. Often, shorebirds (adults, chicks, and eggs) and other coastal wildlife fall victim to these predators. The effects of predation on a particular shorebird species may depend on the activity cycle of the predators (diurnal vs. nocturnal vs. crepuscular), their hunting style, and their home range. Gray fox, feral cats, and ghost crabs were most prevalent beachfront in the Developed Recreation area, while bobcat was commonly identified in the Low Impact Wildlife use zone. We found greater numbers of raccoons and Virginia opossums marsh side in both land use areas, which may be partly attributable to increased trapping efforts by MCBCL in beachfront habitat over the course of this study. The removal of raccoons and opossums may have opened foraging niches for gray fox in the Developed Recreation area; however this species is commonly associated with human presence. The bobcat in the Low Impact Wildlife area may have suppressed gray fox from establishing territories in that use zone, but further research is needed to explore this possibility. Occurrences of feral cats are commonly attributed to pet dumping at Onslow Beach in the Developed Recreation area, where island accessibility is the greatest. We observed few red fox

on Onslow Beach, with the first occurring in October 2008. It is unknown whether this canid previously occupied the area or if it is just establishing territories on the island.

The level of human disturbance as documented in our studies in 2008–2009 (**Table 12-18**) may affect the distribution, abundance and diversity of shorebird and tern species in all land use areas on Onslow Beach, but other factors (i.e., vegetation structure, predator community, topography) also influence the coastal avian community. For example, in the Low Impact Wildlife area, shorebirds and terns have access to inter-tidal mud flats at the southwestern end of the island and in the marshes. The same accessibility is limited in other land use areas by physical barriers, such as paved and unpaved roads, encroaching *Phragmites* spp. in the marsh, maritime shrub-scrub habitat separating the beach from the marsh, and the Intra-coastal Waterway. It is unclear how the distribution and diversity of predators influence the coastal avian community at Onslow Beach, but we did not find breeding shorebirds or terns in the Amphibious Training and Developed Recreation areas during our study. It is plausible that a combination of human impacts, topography, and habitat availability are the primary drivers of shorebird and tern distribution, abundance, and diversity on Onslow Beach. Our detailed study of Wilson's Plovers as part of this DCERP project provides an in-depth exploration of the importance of these different factors for one species of special concern at MCBCL; other species also likely experience a variety of physical and biological influences on their abundance and distribution. This report is intended to serve as a starting point for future research and management decisions and its authors are willing to engage in such discussions as desired by MCBCL EMD personnel.

Conclusions and Implications for Future Research

Our study showed that the distribution, abundance, nest success, and survival of our focal species of shorebird, the Wilson's Plover, was affected by both bottom-up (i.e., area of the fiddler crab flat, sea-level, and vegetation density and type) and top-down (i.e., predation by native and non-native predators) at all points in its life history (e.g. from nest site selection to brood foraging site selection). Most importantly, our research provides detailed information on the particular factors affecting Wilson's Plovers nesting at MCBCL which will be of assistance to base staff seeking to manage to best protect habitats for this Species of Special Concern, which also shares its nesting habitat with other protected species, including the federally-threatened Piping Plover.

To date, peer reviewed research on Wilson's Plovers has been limited. However, studies addressing population declines in other shorebird species suggest that human impacts and coastal development have been primary contributors to pervasive degradation of nesting and foraging habitat necessary to support viable populations (Brown et al. 2000, Hunter 2002, Peterson and Bishop 2005, Peterson et al. 2006, Schlacher et al. 2008, Cohen et al. 2009, Defeo et al. 2009). More recently, climate change-related sea level rise (Galbraith et al. 2002, IPCC 2007, Defeo et al. 2009) has arisen as a factor that may alter the availability of foraging resources by modifying prey communities in intertidal feeding areas or resulting in the permanent loss of important habitat (Galbraith et al. 2002). Developing an increased understanding of how shorebirds respond to short- and long-term changes in habitat availability, quantity, and quality is necessary to most effectively develop conservation and management plans. In this conclusion section, we summarize the main findings of our work and their relevance to conservation and management of Wilson's Plovers and other shorebirds at MCBCL and other Atlantic Coast military installations.

Factors Affecting the Demography of Wilson's Plovers

1. In both years, Wilson's Plover's nests at Onslow Beach were depredated most commonly by Virginia opossums and raccoons. We confirmed 15% of nests were lost to predators in 2008 and 31% in 2009 using only physical signs around the nest bowl in 2008, and camera data combined with physical signs in 2009. There were minimal differences between yearly overall nest survival calculated using Mayfield's (1961, 1975) method (46% nest survival in 2008 and 44% in 2009) and actual observations of successfully hatched nests (45% nest success in 2008 and 50% in 2009).
2. Mean chicks hatched per pair and fledged per pair were 1.56 and 0.94, respectively, for both years combined.
3. Chick survival was higher for those nests hatching earlier in the breeding season and higher for those nests that were farther from the brood's final foraging territory. Chick survival from a Cormack-Jolly-Seber recapture model was 75% for both years combined in this study based on weekly re-sightings throughout each season. 64% of observed hatched chicks in 2008 and 2009 fledged.
4. Adults banded in 2008 had a high second-year return rate (90%) to Onslow Beach in 2009; however only 9.5% of chicks banded in 2008 returned in 2009. Apparent survival of Wilson's plovers banded as adults was very high, at 82%, while apparent survival of plovers banded as chicks was low at 13%. These survival rates for both adults and 1st year birds are very similar to other studies of Piping Plovers on the Atlantic Coast from

populations which were shown to be stable over time. Longer-term work on Wilson's plovers at MCBCL is needed to determine whether this population is stable.

This research contributes valuable information towards evaluating the validity of the population goals for Wilson's Plovers as identified in the U.S. Shorebird Plan for the southeastern coastal plains region (Hunter 2002). The plan set a regional goal to double the Wilson's Plover population over the next 50 years (Hunter 2002), and suggested a 5-yr mean productivity of 1.5 fledglings per breeding pair based on estimates from Piping Plovers (*Charadrius melodus*) and Snowy Plovers (*Charadrius alexandrinus*) (Page et al. 2009). We observed a mean fledging rate over a 2-yr period of only 0.94 fledglings per pair. It may be plausible that 1.5 fledglings per breeding Wilson's Plover pair are unnecessary to maintain a viable population. An increased understanding of Wilson's Plover population demography in this region is needed before setting target productivity values necessary to sustain or increase this population. For instance, target productivity rates for sustaining the Threatened Atlantic Coast Piping Plover population were determined by analyzing 10 years of pooled demographic data collected from areas that accounted for 90% of the breeding coastal population; thus, at this stage in our knowledge of Wilson's Plover demography, it is premature to estimate sustainable productivity levels.

Another research priority outlined in the southeastern regional shorebird conservation plan was to assess the impacts of nest depredation on successful reproduction (Hunter 2002). We identified common mammalian nest predators as the primary cause of nest failures on Onslow Beach using physical signs and camera data at the nest site. Similarly, Corbat (1990) identified raccoons as a common nest predator in her study. We provided this information to MCBCL Land and Wildlife staff in the Environmental Management Division during each year of our study to assist them in targeting and locating raccoons and opossums, thus increasing the efficiency of their seasonal trapping strategies and efforts. It is important to consider that predation is a natural process, and determining appropriate or effective levels of removal (if necessary at all) will depend on the region, predator community, prey community, presence or absence of human activity (i.e., human-attracted predators), and temporal stochastic environmental variables (i.e., storms, temperature, drought). At this point, we cannot definitively say whether predators are the most important factor limiting Wilson's Plover population numbers at Onslow Beach; further study of factors limiting Wilson's Plovers at Onslow Beach are needed to fully justify predator removal activities. For example, data should be collected on Wilson's Plover population numbers before and after well-controlled predator removal activities, holding habitat availability constant, to truly assess the efficacy of predator management at this site.

Factors Affecting Wilson's Plover Nesting and Foraging Habitat Use

1. Sixteen of 20 (80%) nests placed in clumped grasses or mixed vegetation were successful, compared to 9 of 22 (41%) nests in low-growing sparse vegetation or open sand ($\chi^2_1 = 6.66$, $P = 0.01$, $n = 42$ both years combined; not all nests had known fate).
2. Area of a fiddler crab mud flat was the most important habitat feature influencing whether or not a Wilson's Plover brood established a territory on it.
3. Close proximity to water and vegetative cover were important factors in where broods chose to forage on a given fiddler crab mud flat and in all habitats (fiddler flats, interdune sand flats, beach front) combined ≥ 7 days post-hatch.

4. Wilson's Plover broods appeared to peck more and 'run and grab' less in 2009 compared to 2008. This change in foraging behavior may have been a response to changing environmental conditions in 2009. Similarly, broods established final foraging territories in all available foraging habitat (i.e., fiddler flats, interdune sand flats, and beach front) in 2009, but only used fiddler flats in 2008. In 2009, Wilson's Plover access to fiddler crab mud flats was limited due to a coast-wide sea level anomaly; however, sand accretion occurring between the two study seasons increased the beach front foraging opportunities during this same time period. No evidence was found of decreased chick survival between years despite this observed habitat shift by foraging adults and broods.

Management should aim to provide a matrix of potential nesting and foraging sites from the beach front to sound-side mud flats to allow flexible habitat use by breeding Wilson's Plovers and foraging broods. Below we outline some specific management suggestions to support the habitat objectives outlined in the U.S. Shorebird Conservation Plan.

1. This study and previous research suggests that Wilson's Plover hatching success is positively related to the presence of a certain vegetation density around the nest site (i.e., successful nests have 7.9% - 22.4 % vegetated cover within 0.5 - 1 m² of nest bowl) and a gradient of vegetation growth form (i.e., low-growing sparse vegetation and clumped grasses) beginning at the nest bowl and extending up to 1 m²; management for Wilson's plovers should attempt to achieve this density of vegetation in sandflat areas.
2. According to this study, an ideal *Uca* crab mud flat for Wilson's Plover brood territory establishment would be one that is ≥ 1250 m², within 10 m of water, subject to regular tidal inundation, and within approximately 4 m of vegetation cover; management that can maximize the size and number of *Uca* flats will benefit Wilson's plover populations.
3. Result from this field study suggest an optimal range of 11–18% vegetation cover per 1 m² of beach front habitat as favorable for foraging broods. This goal can be achieved by protecting newly formed overwash and beach front sand accumulation that results in habitat relatively free of vegetation, except for sparse low-growing plants adapted to the coastal dynamics of tidal fluctuations, wind, and sand movement (i.e., sea rocket (*Cakile edentula*), new growth seashore-elder (*Iva imbricate*), seaside pennywort (*Hydrocotyle bonariensis*)).

Environmental personnel at MCBCL post symbolic signs and fencing to protect shorebird nesting areas, and we worked with them during our study to identify and safeguard unknown and new nesting habitat. In addition to the specific habitat requirements outlined above, we suggest increased efforts to protect ephemeral and inter-tidal foraging areas beach front and sound-side in the southern portion of Onslow Beach. Flexible management as such will not only provide a matrix of habitats for Wilson's Plovers to use, but also provide resources for other breeding shorebirds like the Atlantic Coast Threatened Piping Plover.

While the Base has met with public objections about restricting access to this area of island during shorebird breeding season, alternative measures to signs and fencing, such as posting interns or technicians during high use periods to conduct educational outreach and monitor critical foraging areas might be a less confrontational, more effective approach to habitat management and conservation.

Future Challenges for Shorebird Conservation at MCBCL

A challenge currently on the horizon for MCBCL land management will be its response to the possible relocation of the New River Inlet, located at the southern end of Onslow Beach. The inlet relocation is part of a stabilization effort to protect North Topsail Beach (across the inlet) communities and its tourism-based economy from ongoing beach erosion. North Topsail Island hosts year-round and vacation residences that have been negatively impacted by beach erosion related to tropical storms and hurricanes over the past 20 years (Federal Register 2010-1810). In 2007, the Town of North Topsail Beach requested that the U.S. Army Corps of Engineers (USACE) submit an Environmental Impact Statement (EIS) to the U.S. Environmental Protection Agency (EPA) to facilitate immediate and ongoing beach nourishment, and to relocate the New River Inlet. These efforts, it is suggested may minimize erosion on North Topsail Beach, but will likely increase erosion on Onslow Beach. The EPA (Region 4) issued a letter of concern to the USACE expressing concerns about the impacts of increased erosion on the southwestern end of Onslow Beach due to the inlet relocation, in particular potentially adverse effects on shorebird habitat. Originally, relocation of the New River inlet was planned to begin in Fall 2010 (Federal Register 2010-1820), however; this has extended at least into 2011. While the permit process is complete, insufficient funds have delayed the project. MCBCL has been involved in the EIS process and is aware of the potential adverse effects of short- and long-term beach loss (Mueller 2010). The potentially adverse effects of inlet relocation on the southwest portion of Onslow Beach may accelerate the erosion process and threaten to diminish existing and newly formed habitat important for breeding and foraging shorebirds (Hubbard and Dugan 2003).

On Onslow Beach, Foxgrover (2009) reported a trend of shoreline erosion over the past 80 years, emphasizing the limited sediment volume from nearshore and fluvial sources necessary naturally to mitigate this loss. While erosion on Onslow Beach is primarily attributed to natural barrier island movement, habitat loss has already occurred and will likely continue even in the absence of inlet relocation (Morton and Miller 2005, Foxgrover 2009). In the face of historical and ongoing large-scale coastal habitat loss and alteration, conserving what remains at a regional scale is of crucial importance. MCBCL should prepare to mitigate for the probability of increased short-term erosion rates as a result of proximate beach stabilization efforts at North Topsail Beach.

It is likely that the newly accreted beach front sand accumulation on the southwestern end of the island will diminish, with or without the inlet relocation (Morton and Miller 2005), as this area is actively undergoing barrier-island rollover (Foxgrover 2009). However, the speed at which this newly accreted habitat is lost may accelerate if the inlet is moved (Griggs 2005, Cooper and McKenna 2008, Defeo et al. 2009). Given Onslow Beach's long term beach erosion trend (Foxgrover 2009) and predictions for ongoing natural habitat loss (Morton and Miller 2005), we suggest that regulators consider recommending North Topsail Beach fund a mitigation effort that would create new shorebird habitat on Onslow Beach and protect the existing sand accretion on the southwestern end of Onslow Beach. Past studies have demonstrated that stabilization structures and efforts can result in erosion on adjacent beach front shorelines (Hall and Pilkey 1991, Griggs 2005).

One possible mitigation effort would be to increase shorebird (specifically Wilson's Plovers as related to this study's findings) monitoring efforts in the Military Buffer Zone where these birds do already nest, and both monitoring and management efforts in the Amphibious Training Zone, where we did not find nests during this study. Since access is restricted and enforced in these areas of the island, management approaches such as posting symbolic fencing would not be as necessary; however, collecting presence/absence, habitat, and reproductive data would be beneficial in ongoing demographic monitoring and contribute to long-term population recovery goals. If monitoring activities determined that habitat in these Zones could be improved for Wilson's Plovers by simple activities such as vegetation thinning or creation of pathways to foraging fiddler flats, the Base could then weigh the costs and benefits of increasing Wilson's Plovers in these areas if the population decreases in the Wildlife Area due to beach erosion. For example, one option would be to create a path from the Amphibious Training Zone beach front to the sound-side intertidal mud flats in the middle of the island. The path could be located between Egresses 10 and 11 where there is already a break in the access roads at this point. Vegetation removal and thinning would most likely be necessary for broods to gain access to the flats since there has been a lack of overwash in the middle of the island. Similarly, vegetation thinning or removal just north of the overwash in the Wildlife Area would be beneficial in making fiddler flats more accessible to foraging Wilson's Plover broods.

Less aggressive, but still invaluable, mitigation would be to re-focus land management efforts to other important existing and ephemeral foraging habitats and nesting areas in the Wildlife Area. In particular, I recommend increased management (i.e., symbolic fencing, patrols, on-site educators) of the fiddler flats and surrounding nesting habitats at the sound-side southwestern end of Onslow Beach (**Figure 12-1**). The largest ($> 14\,000\text{ m}^2$) and most used (by Wilson's Plover broods) fiddler crab mud flat is located in this area sound-side, and is bordered by the New River Inlet and marsh habitat. Additional inter-tidal mud flats (not colonized by fiddler crabs) surround this flat, and provide benthic and terrestrial arthropod prey resources for Wilson's Plovers, and other breeding, migratory, and resident foraging shorebirds, such as Piping Plovers (Federally Threatened), Semi-palmated Plovers (*Charadrius semipalmatus*), Black-bellied Plovers (*Pluvialis squatarola*), Sanderlings (*Calidris alba*), and Ruddy Turnstones (*Arenaria interpres*; Ray, unpublished data, available in the Monitoring and Research Data Information System [MARDIS]). Our behavioral observations of Wilson's Plover broods using this area coupled with regular shorebird surveys (Ray, unpublished data, available in MARDIS) indicate that these intertidal mudflats at the southwestern end of the island are important habitat for breeding, migrating, wintering, foraging, resting, and roosting shorebirds. This would also be an ideal area for North Topsail Beach to work with Base personnel in creating, stabilizing, and protecting critical shorebird habitat that may be lost on the beach front as a result of inlet relocation and island stabilization efforts.

The sound-side habitat on the southwestern end of Onslow Beach is a challenging area to protect as it is easily accessible by recreational boaters and fisherman. During this 2-yr study, recreational users often used the bayside inter-tidal zone within 5-10 m from posted shorebird areas surrounding the fiddler flat to anchor their boats, picnic, and walk. While the inter-tidal zone is a public property, it is apparent that symbolic fencing and signs are not entirely effective in protecting Wilson's Plover nesting pairs and foraging broods using the higher-elevation dry sand (i.e., posted sand flat) and adjacent fiddler crab mud flat. All five nests found in this area of the island over the 2-yr period failed; we confirmed three nest depredations by mammalian

predators, but two (one in each year) were abandoned shortly after the Memorial Day holiday when ≥ 100 people and up to 20 boats were counted in this area. Studies have shown that human disturbance can lead to nest abandonment and increased depredation from human-attracted predators (MacIvor et al. 1990, USFWS 1996, Lord et al. 2001, Cohen et al. 2009). Nest abandonment caused by human disturbance (i.e. physical presence of humans) has been observed in Wilson's Plover studies (Bergstrom 1988, Corbat and Bergstrom 2000, this study), but to a small extent relative to other causes of nest failure.

Considering the predominantly natural, long-term erosion on Onslow Beach and planned relocation of the New River Inlet, increasing and improving shorebird habitat and the monitoring and protection of existing nesting and foraging areas may help to mitigate the likely habitat loss beach front, and provide supplemental resources to sustain and increase Wilson's Plover productivity. Regardless of ever-present natural-caused or imminent human-induced changes to the southwestern end of Onslow Beach, it will be important for the Base's Environmental Management Division to apply flexible management practices to protect newly formed and ephemeral habitats (e.g. overwash, sand accretion, ephemeral tidal pools) supporting Wilson's Plover nesting pairs and broods, and other breeding shorebirds with similar habitat requirements that nest and raise young on Onslow Beach (e.g. Piping Plovers, American Oystercatchers (*Haematopus palliatus*), Least Terns (*Sterna antillarum*), and Willets (*Catoptrophorus semipalmatus*); Ray, unpublished data).

Literature Cited

- Aebischer, A., N. Perrin, M. Krieg, J. Studer, and D.R. Meyer. 1996. The role of territory choice, mate choice and arrival date on breeding success in the Savi's Warbler (*Locustella luscinioides*). *Journal of Avian Biology* 27:134–152.
- Akaike, H. 1973. Information theory as an extension of the maximum likelihood principle. Pages 267–281 in the 2nd International Symposium on Information Theory. Edited by B.N. Petrov, and F. Caski. Akademiai Kiado, Budapest.
- Altmann, J. 1974. Observational study of behavior: Sampling methods. *Behaviour* 49:227–267.
- Anderson, D.R., W.A. Link, D.H. Johnson, and K.P. Burnham. 2001. Suggestions for presenting the results of data analyses. *Journal of Wildlife Management* 65:373–378.
- Arnold, J.M., J.J. Hatch, and I.C.T. Nisbet. 2006. Effects of egg size, parental quality and hatch-date on growth and survival of common tern (*Sterna hirundo*) chicks. *Ibis* 148:98–105.
- Arnold, J.M., J.J. Hatch, and I.C.T. Nisbet. 2004. Seasonal declines in reproductive success of the common tern (*Sterna hirundo*): Timing or parental quality? *Journal of Avian Biology* 35:33–45.
- Backwell, P.R., P.D. O'Hara, and J.H. Christy. 1998. Prey availability and selective foraging in birds. *Animal Behavior* 55:1659–1667.
- Bergstrom, P.W. 1988. Breeding biology of Wilson's Plover (*Charadrius wilsonia*). *Wilson Bulletin* 100:25–35.
- Bergstrom, P.W. 1986. Daylight incubation sex roles in Wilson's Plover. *Condor* 88:113–115.
- Bergstrom, P.W. 1982. *Ecology of Incubation in Wilson's Plover (Charadrius wilsonius)*. Dissertation, University of Chicago, Chicago, IL.
- Bergstrom, P.W., and K. Terwilliger. 1987. Nest sites and aggressive behavior of piping and Wilson's plovers in Virginia: Some preliminary results. *Wader Study Group Bulletin* 50:35–39.
- Botto, F., A. Mendez-Casariago, M. Valiñas, and O. Iribarne. 2008. Spatial heterogeneity created by burrowing crabs affects human Impact on migratory shorebirds. *Estuaries and Coasts* 31:134–143.
- Brosnan, D.M., and L.L. Crumrine. 1994. Effects of human trampling on marine rocky shore communities. *Journal of Experimental Marine Biology and Ecology* 177:79–97.
- Brown, S., C. Hickey, B. Harrington and R. Gills, eds. 2001. *The U. S. Shorebird Conservation Plan* (2nd edition). Manomet Center for Conservation Sciences, Manomet, MA.

- Burger, J., 1998. Effects of motorboats and personal water craft on flight behaviour over a colony of Common Terns. *Condor* 100:528–534.
- Burger, J. 1994. The effect of human disturbance on foraging behavior and habitat use in piping plover (*Charadrius melodus*). *Estuaries* 17:695–701.
- Burger, J. 1989. Least tern populations in coastal New Jersey: Monitoring and management of a regionally endangered species. *Journal of Coastal Research* 5:801–811.
- Burger, J. 1986. The effect of human activity on shorebirds on two coastal bays in Northeastern United States. *Environmental Conservation* 12:123–130.
- Burger, J. 1982. An overview of proximate factors affecting reproductive success in colonial birds: Concluding remarks and summary of panel discussion. *Colonial Waterbirds* 5:58–65.
- Burger, J., C. Jeitner, K. Clark, and L.J. Niles. 2004. The effect of human activities on migrant shorebirds: Successful adaptive management. *Environmental Conservation* 31:283–288.
- Burger, J., M., A. Howe, D.C. Hahn, and J. Chase. 1977. Effects of tide cycles on habitat selection and habitat partitioning by migrating shorebirds. *The Auk* 94:743–758.
- Burnham, K.P., and D.R. Anderson. 2002. *Model Selection and Inference: A Practical Information-Theoretic Approach* (2nd edition). Springer: New York, NY.
- Catlin, D.H. 2009. *Population Dynamics of Piping Plovers (Charadrius melodus) on the Missouri River*. Ph.D. Dissertation, Virginia Tech, Blacksburg, VA.
- Cohen, J.B., L.M. Houghton, and J.D. Fraser. 2009. Nesting density and reproductive success of piping plovers in response to storm- and human-created habitat changes. *Wildlife Monographs* 173:1–24.
- Cohen, J.B., S.M. Karpanty, J.D. Fraser, B.D. Watts, and B.R. Truitt. 2009. Residence probability and population size of red knots during spring stopover in the mid-Atlantic region of the United States. *Journal of Wildlife Management* 73:939–945.
- Cohen, J.B., S. M. Karpanty, D.H. Catlin, J.D. Fraser, and R.A. Fischer. 2008. Winter ecology of piping plovers at Oregon Inlet, North Carolina. *Waterbirds* 30:472–479.
- Collazo, J.A., J.R. Walters, and J.F. Parnell. 1994. *Factors Affecting Reproduction and Migration of Waterbirds on the North Carolina Barrier Islands. III. Effects of Human Disturbance on Shorebird Populations on the Outer Banks of North Carolina*. Final Report to the National Park Service, North Carolina State University, Raleigh, NC.
- Connors, P.G., J.P. Myers, S.W. Connors, and F.A. Pitelka. 1981. Interhabitat movements by sanderlings in relation to foraging profitability and the tidal cycle. *The Auk* 98:49–64.

- Cook, C.W., and C.D. Bonham. 1977. Techniques for vegetation measurements and analysis for a pre- and post-mining inventory. *Colorado State University Range Science Series 28*, Fort Collins, CO.
- Cooper, J.A.G., and J. McKenna. 2008. Social justice in coastal erosion management: The temporal and spatial dimensions. *Geoforum* 39:294–306.
- Corbat, C.A. 1990. *Nesting Ecology of Selected Beach-Nesting Birds in Georgia*. Thesis, University of Georgia, Athens, GA.
- Corbat, C.A., and P.W. Bergstrom. 2000. Wilson's plover (*Charadrius wilsonia*). The Birds of North America Online. Edited by A. Poole. Available at <http://bna.birds.cornell.edu/bna/species/516doi:bna.516>. Accessed 9 July 2010.
- Davenport, J., and J.L. Davenport. 2006. The impact of tourism and personal leisure transport on coastal environments: A review. *Estuarine, Coastal and Shelf Science* 67:280–292.
- Defeo, O., A. McLachlan, D.S. Schoeman, T.A. Schlacher, J. Dugan, A. Jones, M. Lastra, and F. Scapini. 2009. Threats to sandy beach ecosystems: A review. *Estuarine, Coastal and Shelf Science* 81:1–12.
- Di Bitetti, M.S., A. Paviolo, and C. De Angelo. 2006. Density, habitat use and activity patterns of ocelots (*Leopardus pardalis*) in the Atlantic Forest of Misiones, Argentina. *Journal of Zoology* 270:153–163.
- Dikun, K.A. 2008. *Nest-Site Selection of Wilson's Plovers (Charadrius wilsonia) in South Carolina*. Thesis, Coastal Carolina University, Conway, SC.
- Dijak, W.D., and F.R. Thompson, III. 2000. Landscape and edge effects on the distribution of mammalian predators in Missouri. *Journal of Wildlife Management* 64:209–216.
- Dinsmore, S.J., G.C. White, and F.L. Knopf. 2002. Advanced techniques for modeling avian nest survival. *Ecology* 83:3476–3488.
- Elias, S.P., J.D. Fraser, and P.A. Buckley. 2000. Piping plover brood foraging ecology on New York barrier islands. *Journal of Wildlife Management* 64:346–354.
- Elliott-Smith, E., and S.M. Haig. 2004. Piping plover (*Charadrius melodus*). The Birds of North America Online. Edited by A. Poole.
- Erwin, R.M., B.R. Truitt, and J.E. Jiménez. 2001. Ground-nesting waterbirds and mammalian carnivores in the Virginia barrier island region: Running out of options. *Journal of Coastal Research* 17:292–296.

- FAS (Federation of American Scientists). 2000. U.S. Land Warfare Systems. Available at <http://www.fas.org/programs/ssp/man/uswpns/uslandwarfaresystems.html>. Accessed 30 August 2010.
- Folmer, E.O., H. Olff, and T. Piersma. 2010. How well do food distributions predict spatial distributions of shorebirds with different degrees of self-organization? *Journal of Animal Ecology* 79:747–756.
- Foxgrover, A.C. 2009. Quantifying the overwash component of barrier island morphodynamics: Onslow Beach, NC. M.S. thesis, College of William and Mary, Williamsburg, VA.
- Fraser, J.D., S.E. Keane, and P.A. Buckley. 2005. Prenesting use of intertidal habitats by piping plovers on South Monomoy Island, Massachusetts. *Journal of Wildlife Management* 69:1731–1736.
- Galbraith, H., R. Jones, R. Park, J. Clough, S. Herrod-Julius, B. Harrington, and G. Page. 2002. Global climate change and sea level rise: Potential losses of intertidal habitat for shorebirds. *Waterbirds* 25:173–183.
- Graul, W.D. 1979. An evaluation of selected capture techniques for nesting shorebirds. *North American Bird Bander* 4:19–21.
- Griggs, G.B. 2005. The impacts of coastal armoring. *Shore and Beach* 73:13–22.
- Hall, M.J., and O.H. Pilkey. 1991. Effects of hard stabilization on dry beach widths for New Jersey. *Journal of Coastal Research* 7:771–785.
- Higgins, K.F., K.J. Jenkins, G.K. Clambey, D.W. Uressek, D.E. Naugle, J.E. Norland, and W.T. Barker. 2005. Vegetation sampling and measurement. Pp. 524–553 in *Techniques for Wildlife Investigations and Management* (6th edition). Edited by C.E. Braun. Wildlife Society, Bethesda, MD.
- Hood, S.L. 2006. Nesting ecology of snowy and Wilson's plovers in the lower Laguna Madre region of Texas. Thesis, Mississippi State University, Starkville, MS.
- Hosmer, D.W., and S. Lemeshow. 2000. *Applied Logistic Regression* (2nd edition). John Wiley & Sons, Inc.: New York, NY.
- Hubbard, D.M., and J.E. Dugan. 2003. Shorebird use of an exposed sandy beach in southern California. *Estuarine, Coastal and Shelf Science* 58S:41–54.
- Hunter, W.C. 2002. *Southeastern Coastal Plains—Caribbean Region Report, U.S. Shorebird Conservation Plan*. U.S. Fish and Wildlife Service, Atlanta, GA.
- Hylgaard, T., and M.J. Liddle. 1981. The effect of human trampling on a sand dune ecosystem dominated by *Empetrum nigrum*. *Journal of Applied Ecology* 18:559–569.

- Isaksson, D., J. Wallander, and M. Larsson. 2007. Managing predation on ground-nesting birds: The effectiveness of nest enclosures. *Biological Conservation* 136:136–142.
- IPCC (Intergovernmental Panel on Climate Change). 2007. *Climate Change 2007: Synthesis Report*. Available at http://www.ipcc.ch/pdf/assessment-report/ar4/syr/ar4_syr.pdf. Accessed 5 February 2010.
- Karpanty, S.M., J.D. Fraser, J. Berkson, L.J. Niles, A. Dey, and E.P. Smith. 2006. Horseshoe crab eggs determine red knot distribution in Delaware Bay. *Journal of Wildlife Management* 70:1704–1710.
- Kotliar, N.B., and J. Burger. 1986. Colony site selection and abandonment by least terns (*Sterna antillarum*) in New Jersey, USA. *Biological Conservation* 37:1–21.
- Lafferty, K.D. 2001. Disturbance to wintering western snowy plovers. *Biological Conservation* 101:315–325.
- Leary, P. 2009. Wilson's plover (*Charadrius wilsonia*) chick forages on small finfish. *Florida Field Naturalist* 37:151.
- Lebreton, J. D., K. P. Burnham, J. Clobert, and D.R. Anderson. 1992. Modeling survival and testing biological hypotheses using marked animals: A unified approach with case studies. *Ecological Monographs* 62:67–118.
- Lehner, P.N. 1979. *Handbook of Ethological Methods*. Garland STMP Press: New York, NY.
- Lessells, C.M. 1984. The mating system of Kentish plovers (*Charadrius alexandrinus*). *Ibis* 126:474–483.
- Loefering, J.P., and J.D. Fraser. 1995. Factors affecting piping plover chick survival in different brood-rearing habitats. *Journal of Wildlife Management* 59:646–655.
- Long, L.L., and C.J. Ralph. 2001. Dynamics of habitat use by shorebirds in estuarine and agricultural habitats in northwestern California. *Wilson Bulletin* 113:41–52.
- Lord, A., J.R. Waas, J. Innes, M.J. and Whittingham. 2001. Effects of human approaches to nests of northern New Zealand dotterels. *Biological Conservation* 98:233–240.
- Lowther, P.E., D.D. Hector III, and C.L. Gratto-Trevor. 2001. Willet (*Catoptrophorus semipalmatus*). The Birds of North America Online. Edited by A. Poole. Available at <http://bna.birds.cornell.edu/bna/species/579doi:bna.579>. Accessed 17 December 2009.
- Macia, A., I. Quincardete, and J. Paula. 2001. A comparison of alternative methods for estimating population density of the fiddler crab *Uca annulipes* at Saco Mangrove, Inhaca Island (Mozambique). *Hydrobiologia* 449:213–219.

- MCBCL (Marine Corps Base Camp Lejeune). 2007. About the Base. Available at <http://www.lejeune.usmc.mil/about>. Accessed 30 August 2010.
- Mayfield, H.F. 1975. Suggestions for calculating nest success. *The Wilson Bulletin* 87:456–466.
- Mayfield, H.R. 1961. Nesting success calculated from exposure. *The Wilson Bulletin* 73:255–261.
- MacIvor, L.H., S.M. Melvin, and C.R. Griffin. 1990. Effects of research activity on piping plover nest predation. *Journal of Wildlife Management* 54:443–447.
- Møller, A.P. 2001. Heritability of arrival date in a migratory bird. *Proceedings of the Royal Society of London Biological Sciences* 268:203–206.
- Møller, A.P., F. de Lope, and N. Saino. 2004. Parasitism, immunity, and arrival date in a migratory bird, the barn swallow. *Ecology* 85:206–219.
- Moreno, J. 1998. The determination of seasonal declines in breeding success in seabirds. *Etología* 6:17–31.
- Morrier, A., and R. McNeil. 1991. Time-activity budget of Wilson's and semipalmated plovers in a tropical environment. *Wilson Bulletin* 103:598–620.
- Morton, R.A., and T. Miller. 2005. *National Assessment of Shoreline Change: Part 2: Historical Shoreline Changes and Associated Coastal Land Loss Along the U.S. Southeast Atlantic Coast: U.S. Geological Survey Open-file Report 2005-1401*. Available at <http://pubs.usgs.gov/of/2005/1401>. Accessed 4 December 2010.
- Mueller, H.J. 2010. Comments on the Final Environmental Impact Statement (FEIS) for the relocation of New River Inlet ebb tide channel between North Topsail Beach and Onslow Beach, and the placement of the dredged material along the ocean shoreline of North Topsail Beach in Onslow County, NC. CEQ Number: 20100025. ERP Number: COE-E30043-NC. U.S. Environmental Protection Agency, Atlanta, GA.
- Nisbet, I., K.J. Wilson, and W.A. Broad. 1978. Common terns raise young after death of their mates. *Condor* 80:106–109.
- Nol, E., and R.C. Humphrey. 1994. American oystercatcher (*Haematopus palliatus*). The Birds of North America Online. Edited by A. Poole. Available at <http://bna.birds.cornell.edu/bna/species/082doi:10.2173/bna.82>. Accessed 14 May 2010.
- NCWRC (North Carolina Wildlife Resources Commission). 2005. *North Carolina Wildlife Action Plan*. Raleigh, NC. Available at http://www.ncwildlife.org/Portals/0/Conserving/documents/ActionPlan/WAP_complete.pdf.

- Page, G.W., L.E. Stenzel, G.W. Page, J.S. Warriner, J.C. Warriner, and P.W. Paton. 2009. Snowy plover (*Charadrius alexandrinus*). The Birds of North America Online. Edited by A. Poole. Available at <http://bna.birds.cornell.edu/bna/species/154/articles/introduction>. Accessed 23 May 2010.
- Paton, P.W.C. 1994. Survival estimates for snowy plovers nesting at Great Salt Lake, Utah. *Condor* 96:1106–1109.
- Peterson, C.H., and M.J. Bishop. 2005. Assessing the environmental impacts of beach nourishment. *BioScience* 55:887–896.
- Peterson, C.H., M.J. Bishop, G.A. Johnson, L.M. D’Anna, and L.M. Manning. 2006. Exploiting beach filling as an unaffordable experiment: Benthic intertidal impacts propagating upwards to shorebirds. *Journal of Experimental Marine Biology and Ecology* 338:205–221.
- Placyk, Jr., J.S., and B.A. Harrington. 2004. Prey abundance and habitat use by migratory shorebirds at coastal stopover sites in Connecticut. *Journal of Field Ornithology* 75:223–231.
- Ribeiro, P.D., O.O. Iribarne, D. Navarro, and L. Jauregui. 2004. Environmental heterogeneity, spatial segregation of prey, and the utilization of southwest Atlantic mudflats by migratory shorebirds. *Ibis* 146:672–682.
- Roche, E.A., T.W. Arnold, and F.J. Cuthbert. 2010. Apparent nest abandonment as evidence of breeding-season mortality in Great Lakes piping plovers (*Charadrius melodus*). *The Auk* 127:402–410.
- Rotella, J.J., S.J. Dinsmore, and T.L. Shaffer. 2004. Modeling nest-survival data: A comparison of recently developed methods that can be implemented in MARK and SAS. *Animal Biodiversity and Conservation* 27:187–205.
- Sabine, J.B., S.H. Schweitzer, and J.M. Meyers. 2006. Nest fate and productivity of American oystercatchers, Cumberland Island National Seashore, Georgia. *Waterbirds* 29:308–314.
- Sabine, J.B., J.M. Meyers, and S.H. Schweitzer. 2005. A simple, inexpensive video camera setup for the study of avian nest activity. *Journal of Field Ornithology* 76:293–297.
- Safina, C., and J. Burger. 1983. Effects of human disturbance on reproductive success in the black skimmer. *Condor* 85:164–171.
- Schiel, D.R., and D.I. Taylor. 1999. Effects of trampling on a rocky intertidal assemblage in southern New Zealand. *Journal of Experimental Marine Biology and Ecology* 235:213–235.

- Schlacher, T.A., D.S. Schoeman, J. Dugan, M. Lastra, A. Jones, F. Scapini, and A. McLachlan. 2008. Sandy beach ecosystems: Key features, sampling issues, management challenges and climate change impacts. *Marine Ecology* 29:70–90.
- Spruzen, F.L., A.A.M. Richardson, and E.J. Woehler. 2008. Influence of environmental and prey variables on low tide shorebird habitat use within the Robbins Passage wetlands, Northwest Tasmania. *Estuarine, Coastal and Shelf Science* 78:122–134.
- Strauch, Jr., J.G., and L.G. Abele. 1979. Feeding ecology of three species of plovers wintering on the bay of Panama, Central America. *Studies in Avian Biology* 2:217–230.
- Sweet, W., C. Zervas, and S. Gill. 2009. *Elevated East Coast Sea Level Anomaly: June–July 2009*. Technical Report NOS CO-OPS 051. National Oceanic and Atmospheric Administration, Silver Spring, MD.
- Thibault, M., and R. McNeil. 1995. Predator-prey relationship between Wilson’s plovers and fiddler crabs in northeastern Venezuela. *Wilson Bulletin* 107:73–80.
- Thibault, M., and R. McNeil. 1994. Daylight variation in habitat use by Wilson’s plovers in northeastern Venezuela. *Wilson Bulletin* 106:299–310.
- Tomkins, I.R. 1959. Wilson’s plover: Some egg weights. *The Oriole* 1:67–68.
- Tomkins, I.R. 1944. Wilson’s plover in its summer home. *The Auk* 61:259–269.
- Tyler, S. 1979. Time-sampling: A matter of convention. *Animal Behaviour* 27:801–810.
- Warnock, S.E., and J.Y. Takekawa. 1995. Habitat preferences of wintering shorebirds in a temporally changing environment: Western sandpipers in the San Francisco Bay estuary. *The Auk* 112:920–931.
- White, G.C., and K.P. Burnham. 1999. Program MARK—Survival estimation from populations of marked animals. *Bird Study* 46:S120–S138.
- Wilcox, L. 1959. A 20-year banding study of the piping plover. *The Auk* 76:129–152.

[This page intentionally left blank.]

Appendix 12-A
List of Scientific Publications

List of Scientific Publications

Papers

- Ray, K.L., S.M. Karpanty, and J.D. Fraser. In preparation. Demography of Wilson's plovers (*Charadrius wilsonia*) in southeastern North Carolina. To be submitted to the *Journal of Field Ornithology*.
- Ray, K.L., S.M. Karpanty, and J.D. Fraser. In preparation. Habitat characteristics affecting nest hatching success, brood territory establishment, and foraging site selection of Wilson's plovers (*Charadrius wilsonia*) in southeastern North Carolina. To be submitted to *Condor*.

Thesis

- Ray, K. 2011. *Factors Affecting Wilson's Plover (Charadius wilsonia) Demography and Habitat Use at Onslow Beach, Marine Corps Base Camp Lejeune, North Carolina*. M.S. thesis, Virginia Tech, Blacksburg, VA.

Presentations

- Karpanty, S.M., K.L. Ray, and J.D. Fraser. 2011. *Habitat Characteristics Affecting Nest Hatching Success, Brood Territory Establishment, and Foraging Site Selection of Wilson's Plovers (Charadrius wilsonia) in Southeastern North Carolina*. Presented at The Waterbird Society's 35th Annual Meeting, Grand Island, NE. 13–16 March.
- Ray, K.L., Karpanty, S.M., and Fraser, J.D. 2009. *Wilson's Plover Population Ecology and Habitat Use at Marine Corps Base Camp Lejeune, North Carolina*. Presented at The Waterbird Society's 33rd Annual Meeting, Cape May, NJ. 4–8 November. Also presented at the 127th Meeting of the American Ornithologist's Union, Philadelphia, PA. 12–15 August.
- Ray, K.L., S.M. Karpanty, and J.D. Fraser. 2008. *Breeding Ecology of Wilson's Plovers (Charadrius wilsonia) at Marine Corps Base Camp Lejeune, North Carolina*. Poster presented at The Waterbird Society's 32nd Annual Meeting, South Padre Island, TX. 4–8 November.
- Ray, K.L., S.M. Karpanty, and J.D. Fraser. 2008. *Understanding the Top-Down and Bottom-Up Drivers of Shorebird Population Dynamics and Habitat Use on MCBCL*. Lunch and learn presented to the Environmental Management Division, Marine Corps Base Camp Lejeune, NC. 31 July.

Appendix 12-B

List of Students

- Kacy Ray, M.S., Virginia Tech, May 2011

[This page intentionally left blank.]

Chapter 13

Effects of Different Understory Restoration Management Options on Terrestrial Ecosystem Structure and Function

SERDP Project Number: RC-1413

Terrestrial Module

Research Project T-1

Lead Researcher:

Dr. Norman L. Christensen
Duke University
Durham, NC 27708
E-mail: normc@duke.edu

Supporting Researchers:

Dr. Stephen R. Mitchell
Duke University
Durham, NC 27708
E-mail: stephen.mitchell@duke.edu

Dr. Jeff Walters
Virginia Tech
Blacksburg, VA 24060
E-mail: jrwalt@vt.edu

May 10, 2013

Final

This report was prepared under contract to the U.S. Department of Defense (DoD) Strategic Environmental Research and Development Program (SERDP). The publication of this report does not indicate endorsement by DoD, nor should the contents be construed as reflecting the official policy or position of DoD. References herein to any specific commercial product, process, or service by trade name, trademark, manufacturer, or otherwise, do not necessarily constitute or imply its endorsement, recommendation, or favoring by DoD.

Table of Contents

List of Acronyms	13-vi
Abstract.....	13-1
Objectives of the Research Project	13-2
Hypotheses.....	13-2
Background.....	13-3
Materials and Methods.....	13-5
MCBCL Pine Forest Plant Diversity and Composition.....	13-5
Experimental Design and Study Sites.....	13-7
Soil Sampling.....	13-7
Vegetation, Arthropod, and Bird Sampling	13-9
Pre- and Post-Prescribed Burning Fuel Sampling	13-10
Statistical Analyses	13-11
Results and Discussion	13-12
MCBCL Pine Forest Plant Diversity and Composition.....	13-12
Soil Characteristics	13-15
Pre- and Post-Treatment Variation in Vegetation, Arthropod and Bird Communities	13-18
Pre- and Post-Prescribed Burning Fuels	13-27
Conclusions and Implications for Future Research	13-31
Literature Cited	13-33
Appendix 13-A List of Species Encountered in 85 MCBCL Pine Monitoring Plots	13-A-1
Appendix 13-B NMS Axis 1 and Axis 2 Scores for 85 Pine-Dominated Permanent MCBCL Vegetation Monitoring Plots.....	13-B-1
Appendix 13-C Soil Data for 85 Pine-Dominated Permanent MCBCL Vegetation Monitoring Plots	13-C-1
Appendix 13-D r (Correlation Coefficient) and r^2 (Coefficient of Determination) Values for All Species with NMS Axes 1 and 2.....	13-D-1
Appendix 13-E List of Scientific Publications	13-E-1
Appendix 13-F List of Students.....	13-F-1

List of Figures

13-1.	The distribution of georeferenced 0.1-ha sample plots in pine dominated forests of MCBCL.....	13-6
13-2.	Diagram of a CVS permanent sample plot. Intensive plots (cells 2, 3, 8, and 9) are indicated by “I.”	13-6
13-3.	A typical loblolly pine site prior to understory/midstory thinning (top).	13-8
13-4.	The location of experimental blocks and treatment plots for Research Project T-1 on MCBCL.....	13-9
13-5.	The arrangement of vegetation sample plots (the numbered rectangle) and arthropod traps in individual 1-ha experimental plots.	13-10
13-6.	NMS ordination of 85 pine-dominated stands located on MCBCL (see Appendix 13-B for actual stand scores).	13-13
13-7.	Average soil organic matter (%) for each treatment arranged by blocks.	13-18
13-8.	Post-treatment 1–20 cm dbh stem density by block and treatment.	13-20
13-9.	Post-treatment species richness of plants (number/0.1 ha), arthropods (number trapped/site) and birds (number identified/site) by block and treatment. Blocks are ordered left to right as high pocosin (FGE, FGW, and IES), wet mesic (IEN, HA, and MF) and mesic (RBE and RBW).	13-21
13-10.	NMS ordination of plant species composition in 24 Research Project T-1 experimental plots (red, blue, and light blue symbols) and 11 longleaf pine dominated plots (green symbols).	13-22
13-11.	NMS ordination of bird species composition in 24 Research Project T-1 experimental plots (red, blue, and light blue symbols) and 11 longleaf pine dominated plots (green symbols).	13-23
13-12.	NMS ordination of arthropod species composition in 24 Research Project T-1 experimental plots (red, blue, and light blue symbols) and 11 longleaf pine-dominated plots (green symbols).	13-24
13-13.	A structural equation model for 24 Research Project T-1 experimental plots and 11 longleaf pine dominated plots.	13-25
13-14.	Species richness of plants compared to that of birds in 24 Research Project T-1 experimental plots (red, blue, and light blue symbols) and 11 longleaf pine dominated plots (green symbols).	13-26
13-15.	Total pre-burn fuel, total fuel consumed and % pre-burn fuel consumed arrayed by block and treatment.	13-29

List of Tables

13-1.	Significant correlations between soil or stand vegetation characteristics and NMS ordination axes.	13-13-14
13-2.	Averaged values and standard deviations (in parentheses) for soil organic matter (OM%), pH, bulk density (BD, g/cm ³), cation exchange capacity (CEC, milliequivalents/100 gm soil), and extracorthophosphate (PO ₄ -P), calcium (Ca), magnesium (Mg), potassium (K), sulfur (S), boron (B), iron (Fe), manganese (Mn), copper (Cu), zinc (Zn), and aluminum (Al) in each of the experimental treatment plots.....	13-13-16
13-3.	Summary of pre-treatment and post-treatment vegetation data for experimental plots.....	13-13-19
13-4.	Summary of burn dates, estimated maximum soil surface fire temperatures, and fuel moisture index for different fuel categories by block and treatment plot.....	13-13-28
13-5.	Average fuel amounts (g/m ²) by block and treatment prior to and following prescribed burning.	13-13-30

List of Acronyms

χ^2	chi square goodness of fit statistic
$\gamma_{partial}$	partial path coefficient
$\gamma_{semipartial}$	semipartial path coefficient
Al	Aluminum
ANOVA	analysis of variance
Av	Average
B	Boron
BD	bulk density
Blk-Trt	block treatment
C	control treatment
Ca	calcium
CEC	cation exchange capacity
cm	centimeter
Cu	copper
CVS	Carolina Vegetation Survey
D	dormant season thinning treatment
dbh	diameter at breast height (1.5 meters)
DCERP	Defense Coastal/Estuarine Research Project
DF	degrees of freedom
DoD	U.S. Department of Defense
F	F ratio
Fe	iron
G	growing season thinning treatment
K	potassium
m	meter
m ²	square meter
MCBCL	Marine Corps Base Camp Lejeune
Mg	magnesium
mm	millimeter
Mn	manganese
N/A	not applicable
Na	sodium
NMS	nonmetric multidimensional scaling
NS	not significant
P	phosphorus
PB	prescribed burn
PCA	principal components axis

PO ₄ -P	extractable orthophosphate
r	correlation coefficient
r ²	coefficient of determination
RCW	red-cockaded woodpecker
S	sulfur
SEM	structural equation modeling
SERDP	Strategic Environmental Research and Development Program
SOM	soil organic matter
USDA FS	U.S. Department of Agriculture Forest Service
Zn	zinc

[This page intentionally left blank.]

Abstract

Changing patterns of land use, agriculture and forest management have greatly altered forest ecosystems across much of the mid-Atlantic lower coastal plain. In particular, vast areas that were once dominated by open longleaf pine (*Pinus palustris*) savanna now support closed canopy stands of loblolly pine (*Pinus taeda*) with a dense understory and midstory of broadleaved shrubs and trees. The absence of fire on these landscapes has exacerbated this trend. This situation is typical for large parts of Marine Corps Base Camp Lejeune (MCBCL). In recent years, longleaf pine restoration at MCBCL has focused on understory and midstory thinning with HydroAx equipment to produce savanna-like conditions and allow restoration of historical fire regimes using prescribed burning (PB). The objectives of this study were to: (1) determine the effects of different understory/midstory thinning treatments (hereafter simply called thinning) and PB in 50- to 60-year-old loblolly pine stands on plant, arthropod, and avifaunal communities; (2) determine the interrelationships among the vegetation, arthropod, and avifaunal communities across sites representing a wide range of soil conditions and red-cockaded woodpecker (RCW) habitat qualities; and (3) provide data on fuel amounts and characteristics, as well as analytical support, to complement studies by the Atmospheric (Air) team comparing the effects of PB on emissions of gases and aerosols in unthinned control and dormant season thinned loblolly pine stands. These objectives were pursued using a randomized block design field experiment consisting of eight blocks with three treatments in each block. Individual blocks were located on MCBCL so as to represent a range of soil site conditions. Treatments included an unthinned control (C), dormant season thinning (D) and growing season thinning (G). All experimental plots (including controls) received PB 6–18 months following treatment. The density of 1–20 cm diameter at breast height (dbh) understory stems (understory shrubs and midstory trees) was decreased in all treatments following thinning treatment application and PB. However, understory stem density was considerably higher in the C treatment than either D or G thinning treatment. Furthermore, understory stem density was significantly lower in the G treatment than the D treatment. In just a single year following midstory thinning and PB, understory plant species richness was significantly higher in D and G compared to C. No treatment effect was yet evident for arthropods or birds. Nonmetric multidimensional scaling ordinations are consistent with treatment related differences in understory plant, arthropod, and avian species composition. Additional sampling in 2–3 years will be required to confirm any trends. Structural equation modeling reveals very high correlations between a composite of soil characteristics and vegetation composition and between vegetation composition and avian community composition. Correlations with arthropod community composition were considerably weaker. Thinning significantly increased amounts of fine (1-hour) and decreased amounts of very coarse (1,000-hour) fuels. It also diminished canopy cover and increases exposure of understory fuels, resulting in dryer fuels compared to C treatments. As a consequence, greater amounts of forest floor fuel were consumed in thinned than in unthinned plots. Thus, consumption of accumulated litter and forest floor organic matter may be a very important effect of thinning treatments. Taken together, these results indicate that, after a single growing season, thinning treatments are producing changes consistent with restoration objectives. Furthermore, because growing season thinning produces a greater reduction in the growth of the woody understory, it may accelerate the restoration process compared to thinning during the dormant season.

Keywords: Arthropod, bird, and plant species composition and richness, forest management practices, fuels, HydroAx, loblolly pine, longleaf pine, prescribed burning (PB), red-cockaded woodpecker (RCW), randomized block experiment, restoration ecology, understory thinning

Objectives of the Research Project

The research projects of the Terrestrial Module focus on critical knowledge gaps related to efforts to restore longleaf pine ecosystems on sites across Marine Corps Base Camp Lejeune (MCBCL) that have been modified by past land use and forest management activities. Specifically, we examined the effects of alternative understory restoration strategies (dormant and growing season thinning of understory and midstory trees and shrubs) on understory plant, arthropod, and avian communities. Research Project T-1 focused primarily on the plants and arthropods, whereas Research Project T-2 focused on avian communities. Research Project T-1 activities were directed toward three objectives.

1. Determine the effects of different understory/midstory thinning treatments (hereafter simply called thinning treatments) and prescribed burning (PB) aimed at restoring longleaf pine forest habitat in 50- to 60-year-old loblolly pine stands on plant, arthropod, and avifaunal communities.
2. Determine the interrelationships among the vegetation, arthropod, and avifaunal communities across sites representing a wide range of soil conditions and red-cockaded woodpecker (RCW) habitat qualities.
3. Provide data on fuel amounts and characteristics, as well as analytical support, to complement studies in Research Project Air-1 of the Atmospheric Module comparing the effects of PB on emissions of gases and aerosols in unthinned and dormant season thinned loblolly pine stands.

Objectives 1 and 2 were pursued in close collaboration with Jeff Walters and his colleagues working on Research Project T-2. Objective 3 was carried out in collaboration with Karsten Baumann and his colleagues working on Research Project A-1. The following hypotheses were associated with these objectives.

Hypotheses

1. Herbaceous cover and species diversity will increase with thinning to remove understory and midstory hardwood shrubs and trees and subsequent PB.
2. These effects will vary depending on the season of thinning (growing season versus dormant season).
3. Thinning and PB will have their greatest impacts on vegetation species richness and composition in wetter sites compared to drier sites.
4. Changes in the composition and diversity of the herbaceous community will be highly correlated with variations in the composition of insect and bird communities.
5. Unthinned and dormant season thinned loblolly pine stands will provide different amounts and quality of fuel for prescribed fire.

6. Fuel consumption during PB will differ between unthinned and dormant season thinned loblolly pine stands.

Background

The terrestrial vegetation of North Carolina's lower coastal plain is known for its diversity across a wide range of spatial scales. MCBCL lands capture much of that variation. At the landscape scale, geomorphic variations such as relict dune and estuarine deposits and subtle changes (± 1 m) in elevation of the soil surface relative to the shallow water table produce remarkable variations in ecosystem structure, composition and processes. Within a few kilometers of the coast, vegetation composition is heavily influenced by salt aerosol and maritime climatic gradients. In pre-settlement times, inland vegetation varied along a continuum from shrub bog (pocosin) wetlands on deep peat soils to pine-dominated flatwoods with an understory of shrubs on poorly drained mineral soils and longleaf pine savannas on well-drained sands (Christensen, 2000). There was nearly complete turnover of plant species composition from one end of this gradient to the other. Some of these ecosystems display remarkable species richness and high levels of species endemism at very local scales. For example, longleaf pine savannas may support more than 60 vascular plant species per m^2 and more than 120 species per ha (Walker and Peet, 1983).

Ecosystem composition and structure was also heavily influenced by variations in pre-settlement fire regimes along this gradient. Pocosins typically experience intense, crown-killing fires at return intervals of more than 40 years, whereas longleaf pine savannas are maintained by light surface fires at intervals of 1–5 years (Bailey et al., 2007; Christensen, 1981, 1992, and 2000). The relative amount and distribution of pocosin, flatwood and savanna ecosystems on pre-settlement landscapes was heavily influenced by the frequency and behavior of fire. Repeated, low severity fires can maintain savanna on very moist soils with relatively high amounts of organic matter. Indeed, it is just these situations that support the highest plant species richness at small (m^2) spatial scales. It is also these sites that support a number of unique endemic species, including several insectivorous plant species. On all but very well-drained sites, the absence of fire for periods longer than 5–6 years results in the invasion of shrubs and a variety of understory trees. This invasion also changes the amounts and distribution of fuels such that subsequent fires are likely to be severe enough to kill and even consume canopy trees.

Today, post-settlement land use and disturbance influence the mosaic of terrestrial ecosystems on lower coastal plain landscapes such as on MCBCL. Except for the wettest and driest sites, forests on much of this landscape were cleared for agriculture during the eighteenth and nineteenth centuries (Crowley, 1996). Longleaf pine savannas that were not cut were heavily managed for naval stores (Early, 2004). Much of this farmland was abandoned in the years following the Civil War and Reconstruction up to World War II; post abandonment succession generally produced an even-aged overstory of loblolly pine with an understory dominated by shrubs and understory trees on all but the driest sites (Christensen, 2000). Fire was not only excluded from these forests, but the successional changes promoted understory vegetation and fuels that are comparatively difficult to burn (Nowacki and Abrams, 2008). During the period from 1940 to 1960, large tracts of such land were acquired by timber companies who managed them to maintain loblolly pine dominance.

Across the Southeast, this history of land use led to the transformation of more than 95% of the land once dominated by longleaf pine savanna to loblolly pine dominated flatwoods. Even where longleaf pine remained, fire suppression often led to the invasion of woody understory plants and the loss of endemic plant and animal species. In many places longleaf pine ecosystems are represented by relatively small and often isolated stands.

Altered fire regimes and habitat loss and fragmentation have contributed to the significant number of plant and animal species found in communities dominated by longleaf pine that are currently listed as threatened or endangered under the Endangered Species Act. The RCW is probably most notable among these listed species. These listings, along with general concerns about the loss of longleaf pine habitat, have been the impetus for restoration of loblolly pine flatwoods to longleaf pine savannas. Indeed, maintenance and restoration of longleaf pine habitat and, hopefully, associated populations of RCWs have been prominent objectives of forest management over much of the MCBCL landscape.

In some parts of MCBCL, restoration has taken the form of clear-cutting, followed by planting of longleaf pine and eventual re-establishment of an appropriate prescribed fire program. Restoration of mature longleaf pine habitat by this approach will, of course, require many decades. As an alternative strategy to accelerate habitat restoration, MCBCL staff have implemented mechanical thinning treatments (i.e., with HydroAx equipment) to remove understory and midstory hardwoods (generally stems <20 cm diameter at breast height [dbh]) and open savanna-like stand structures and understory composition and fuels that are more typical of longleaf pine ecosystems. Such management is currently being applied to hundreds of MCBCL acres each year. Variations on this management theme include different seasons (growing and dormant) of mechanical control of the woody understory. Restoration of low severity, high frequency fire regimes is a key objective. Therefore, all thinned areas receive a late winter or early spring prescribed fire in the year following treatment.

Dr. Joan Walker of the U.S. Department of Agriculture Forest Service (USDA FS) is currently performing Strategic Environmental Research and Development Program (SERDP)–sponsored research (SI-1474) to examine patterns of establishment of longleaf pine in response to such treatments. The effects of similar understory thinning on avifaunal communities have been examined in longleaf pine forests of the sand hills of northwest Florida (Provencher et al., 2002 and 2003). The specific effects of these treatments on other understory components (e.g., vegetation, forest floor, and fuels), insects, and avifauna have not been studied in loblolly dominated ecosystems such as on MCBCL. Loblolly dominated flatwoods occur on a range of soil site situations, but the variation in the response to such thinning treatments (i.e., restoration success) across this range has not been studied.

The effects of restoration treatments on understory vegetation are especially relevant because the composition of this community is a major determinant of RCW habitat quality (USFWS, 2003). The needs of RCWs are well known, but virtually nothing is known about the relationships between the diversity and composition of the plant communities and the diversity and composition of avian communities (USFWS, 2003). Arthropods play an important role in determining habitat quality for many bird species, but the effects of restoration treatments on arthropod diversity and composition are largely unknown.

Both Research Projects T-1 and T-2 have objectives unique to themselves. For example, in collaboration with Research Project Air-1, evaluation of fuel characteristics and amounts prior to and immediately following prescribed fire was an important objective for T-1 and evaluation of the role of RCW nest cavities for other cavity nesting birds was an important objective for T-2. But Research Projects T-1 and T-2 also constitute an integrated program designed to provide a greater understanding of how forest restoration affects plant and animal communities across the soil-moisture gradient relevant to such management.

Materials and Methods

MCBCL Pine Forest Plant Diversity and Composition

To provide a context for experimental studies, 85 0.1-ha permanent-vegetation monitoring plots were established in pine-dominated forests across MCBCL (**Figure 13-1**). The experimental treatment plots (described below) were included among these monitoring plots. Site location and field sampling were initiated in early 2009 and continued through the growing seasons of 2009 and 2010. Each site was located and permanently marked with heavy steel posts. Each site was subsequently sampled for fuel load, woody and herbaceous vegetation and soil characteristics. The Carolina Vegetation Survey (CVS) protocol (Peet et al., 1998) was used at all sites. Individual plots were located within the sample stands to avoid obvious vegetation transitions and represent relatively uniform environmental conditions. Within a 20 × 50-m (0.1-ha) plot, all living and dead stems (>1-cm dbh) were tallied by species and dbh. For the herbaceous layer, the plot was further subdivided into ten 10 × 10-m plots. Four of these plots were termed as “intensive,” and the other six plots were referred to as “residual.” Each intensive plot was sampled for herbaceous species (recorded as percent cover) with five nested plots that increased in sizes of 0.01 m², 0.09 m², 1.0 m², 9.0 m², and 100.0 m² in two corners of the intensive plot (see **Figure 13-2**). After intensive plots were sampled, the residual plots were surveyed to identify all species not found in any of the four intensive plots. We measured species diversity in terms of richness, the total number of species present in a sample. Species composition refers to identities and relative abundances of the community of species.

In addition to herbaceous vegetation, important legacies, such as rotting logs and woody debris, were assessed by size class using line intercept transects across the plot (e.g., Harmon and Sexton, 1986). Finally, fuel condition was assessed in each plot using standard USDA FS protocols for fuel load estimation for the National Fire Danger Rating System model (Andrews and Bradshaw, 1997).

Forest canopy cover was assessed by analyzing hemispherical canopy photos at each site. Five photos were taken at 10-m intervals along the centerline of each 0.1-ha plot using a Nikon 8-mm fisheye lens and a Nikon D-50 digital camera. Photographs were analyzed for percent canopy cover using MATLAB’s Image Processing Toolbox (Korhonen and Heikkinen, 2009).

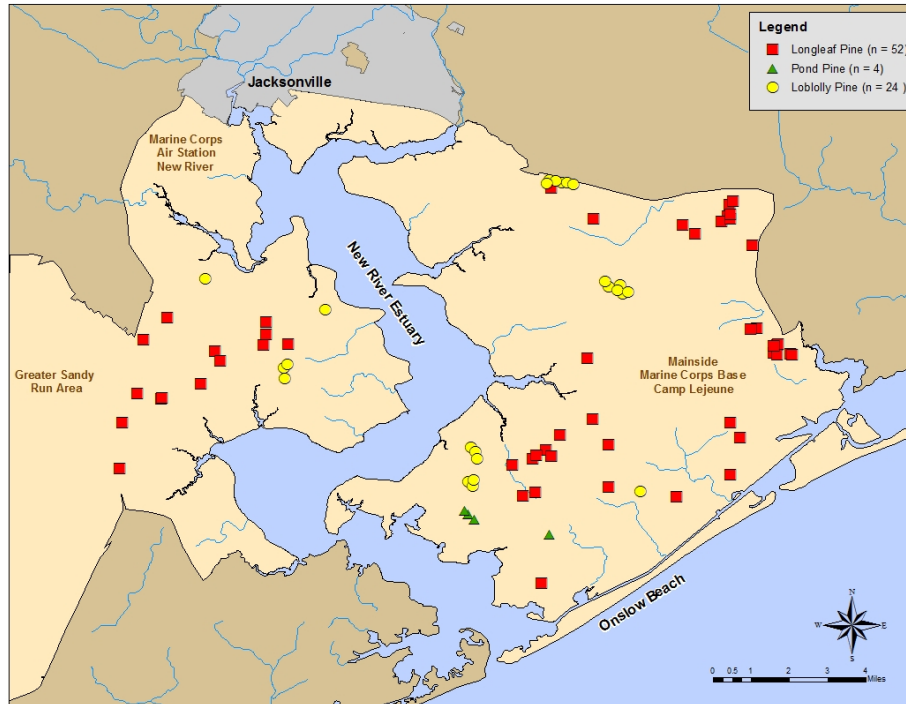


Figure 13-1. The distribution of georeferenced 0.1-ha sample plots in pine dominated forests of MCBCL.

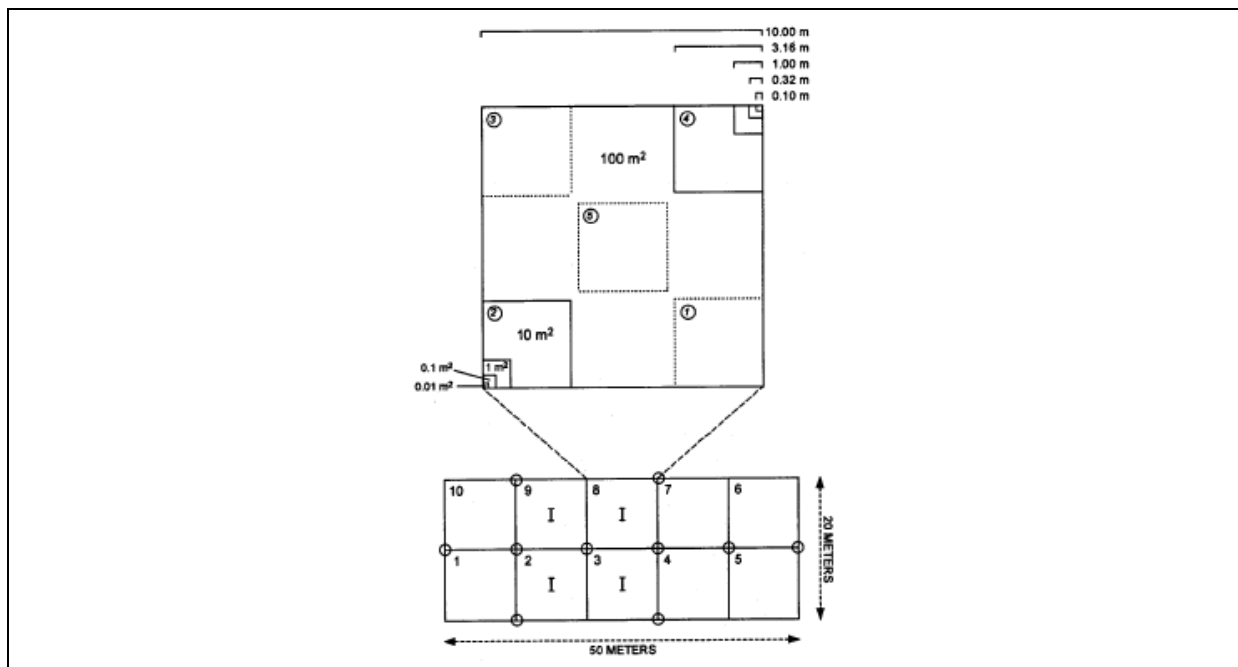


Figure 13-2. Diagram of a CVS permanent sample plot. Intensive plots (cells 2, 3, 8, and 9) are indicated by “I.”

Experimental Design and Study Sites

Working with MCBCL staff, nine stands that were slated for forest management restoration (i.e., mechanical thinning treatment) were identified in late 2008. These stands or restoration treatment units were dominated in the canopy by 50- to 60-year-old loblolly pine, with a dense midstory of woody trees and shrubs. Based on general appearance, soil series, and dominant species, stands had been designated by MCBCL staff as either mesic (well-drained soils, dominated by loblolly pine and some longleaf pine), wet-mesic (moister soils dominated by loblolly pine only), and high pocosin (wet, organic soils dominated by loblolly and with some pond pine).

Restoration treatment units were selected to be sufficiently large (>5 ha) to accommodate experimental treatment blocks as well as simultaneous studies of bird communities undertaken by Research Project T-2. Each experimental treatment block included three 1-ha treatment plots: (1) no woody understory and midstory removal control (C), (2) dormant season mechanical understory and midstory removal (D), and (3) growing season mechanical understory/midstory removal (G). A 25-m treated buffer surrounded each 1 ha treatment plot. Understory/midstory removal was done with a HydroAx mulching device, which typically cuts and mulches all trees <20 cm dbh, leaving behind the shredded biomass (**Figure 13-3**). Dormant season (D) treatments were installed during January and February, and growing season (G) treatments were installed in June and July of 2009. Restoration treatment units were selected so as to establish three blocks in each of the mesic, wet-mesic and high pocosin designations for a total of nine blocks. However, one of the wet-mesic blocks was lost to wildfire in 2009, leaving eight blocks (**Figure 13-4**). All treatments were to receive non-growing season prescribed burns at 3-year intervals. The original plan was to complete the first post-treatment burns between December 2009 and April 2010. However, because of unfavorable weather conditions in 2010, only two of the eight treatment areas could be burned during that year. Post-treatment burns on the remaining plots were completed between February and April 2011.

Soil Sampling

Soil samples were collected from each experimental plot during the growing season following treatment and prescribed burning. Using a 5-cm diameter piston corer, a uniform sample of the top 0–10 cm of mineral soil (soil beneath layers of litter and duff) was collected at each of four points located 10 m from the center point of each experimental plot. Each soil sample was subsequently analyzed by Brookside Laboratories (New Knoxville, OH). Soil pH as measured using a glass electrode in a 1:1 slurry of soil and distilled water (McLean, 1982). Percent soil organic matter (SOM) was determined by weight loss after ignition at 360°C. Phosphorus (P), potassium (K), calcium (Ca), magnesium (Mg), manganese (Mn), zinc (Zn), boron (B), copper (Cu), iron (Fe), aluminum (Al), sulfur (S), and sodium (Na) were extracted according to Mehlich (1984). P concentrations in the Mehlich extractant were measured colorimetrically; concentrations of other elements were determined by plasma emission spectroscopy. Cation exchange capacity (CEC) was measured by summation of all cations as milliequivalents/100 g of soil (Ross, 1995). Several of these soil features have been shown to have a high correlation with the distribution of many coastal plain plant species (Christensen, 2000; Christensen et al., 1988; Peet, 2006; Walker and Peet, 1983). These analyses were considerably more detailed than

originally proposed in order to provide a more complete set of baseline data and to permit direct comparison with other CVS samples on MCBCL and surrounding lands.



Figure 13-3. A typical loblolly pine site prior to understory/midstory thinning (top).
HydroAx device (center) mulching woody stems <20 cm dbh. A typical site following understory/midstory thinning (bottom).

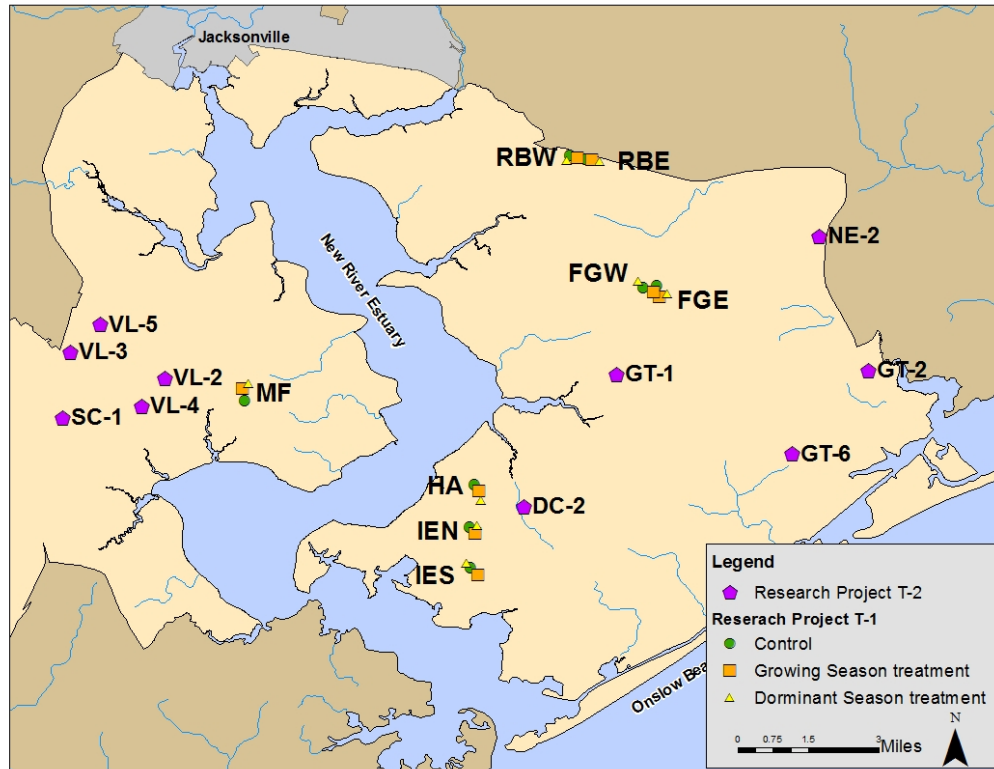


Figure 13-4. The location of experimental blocks and treatment plots for Research Project T-1 on MCBCL.

MCBCL staff had designated blocks IES, FGE, and FGW as high pocosin, blocks MF, IEN, and HA as wet mesic, and Blocks RBE and RBW as mesic.

Vegetation, Arthropod, and Bird Sampling

During December 2008 and January 2009, prior to treatment applications, woody stems 1–20 cm dbh were censused by species and diameter class in each of the three 1-ha experimental plots in each of the eight blocks. The 1–20 cm dbh size range was selected because these are the stems typically removed in the thinning treatment. Within an 8 m radius of each of 5 randomly located points in each plot, dbh and species identity were recorded for each stem ≥ 5 cm dbh. All stems less than 5 cm were recorded by species and dbh along a 1×8 m transect traversing each point.

In the year after treatment and prescribed burning, each experimental plot was censused for vegetation species abundance and diversity, cover of herbs, and biomass of woody plants using the CVS methodology (Peet et al., 1998).

Arthropod (primarily insects and spiders) populations were monitored in pit-fall traps, yellow pan traps and Malaise traps (Malaise, 1937; Provencher et al., 2001a, b). Arthropods were euthanized and identified in the laboratory to the lowest taxon possible. Insect identification was performed in collaboration with Drs. Andy Deans and Matthew Bertone of the Department of Entomology at North Carolina State University in Raleigh, NC. Vegetation and arthropod sampling was also performed on an additional 11 plots corresponding to Research Project T-2

bird sampling plots (also indicated in **Figure 13-4**). The arrangement of vegetation and arthropod samples is shown in **Figure 13-5**. Bird composition and abundance were assessed from point count samples located at the center of each treatment plot at several times throughout the breeding season in conjunction with Research Project T-2. The details of avian sampling methods are described in the final report for Research Project T-2.

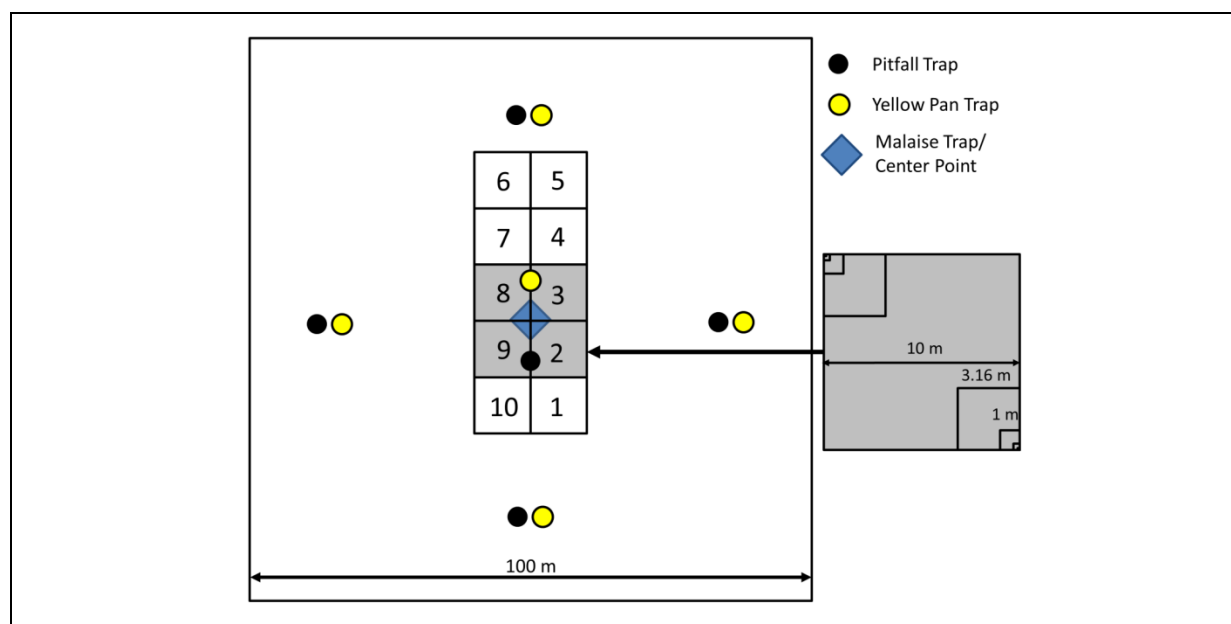


Figure 13-5. The arrangement of vegetation sample plots (the numbered rectangle) and arthropod traps in individual 1-ha experimental plots.

Pre- and Post-Prescribed Burning Fuel Sampling

In addition to standard USDA FS fuel load estimates (Andrews and Bradshaw, 1997) and in collaboration with Research Project Air-1, fuel biomass was intensively sampled before and after PB in each of the treatment plots. All litter and aboveground biomass (living and dead) was gathered from five randomly located 1-m² plots in each treatment area prior to and again immediately following prescribed burning. These samples were returned to the laboratory where living material was separated from dead. Samples were further separated into leaves and stems by size class based on fuel moisture lag times (i.e., the time required for a fuel fragment to come into moisture equilibrium with the relative humidity of the air). Size classes were as follows: 1 hour <0.62 cm, 10 hours = 0.63–2.54 cm, and 100 hours = 2.55–7.62 cm. Fuels were then dried and weighed. In addition, five steel “duff pins” were randomly located in each treatment area and the duff surface marked on the pin prior to burning. This was compared to the height of the duff surface on each pin after prescribed fire.

Pre-fire fuel moistures were estimated using FARSITE 4, the latest version of the FARSITE model series (Finney, 1998). FARSITE uses meteorological driving data (T_{\min} , T_{\max} , RH_{\min} , RH_{\max} , and S_{rad} , and wind speed) and percent canopy cover estimates to provide continuous moisture estimates for different-sized time lag fuel size classes. Fuel was grouped in to three classes: 1 hour (0–0.62 cm), 10 hours (0.62–2.54 cm), and 100 hours (2.54–7.62 cm). We obtained historical meteorological driving data for the 3 months prior to each controlled burn.

Historical meteorological data were obtained from National Oceanic and Atmospheric Administration's online database. Canopy cover was estimated using digitally processed fisheye lens canopy photos, which were subsequently analyzed with an image processing algorithm developed for MATLAB software (Korhonen and Heikkinen, 2009).

Paint pyrometers were used to estimate the maximum fire temperature. Pyrometers were made by painting a piece of steel 4×10 cm with 11 differently colored paints with different melting points (Omega Engineering, Inc.). Paint colors were placed on the pyrometer in a pattern of increasing points for each paint color. Minimum detectable melting point was 93°C (200°F) and increased in 23.3°C increments (50°F) to 350°C (750°F). Prior to each burn, pyrometers were placed on the surface of the forest floor, approximately 2 m from the duff pins (five per plot). After the burn, the pyrometers were recovered from each plot. An estimate of maximum burn temperature was inferred from seeing which paint color did not melt during the prescribed burn, as the maximum temperature could be assumed to have a value between the melting point of the remaining paint and the melting point of the paint that was next to it.

Statistical Analyses

Data for monitoring and experimental plots were analyzed using standard statistical tools for product-moment correlation and analysis of variance (ANOVA) provided in the data analysis and graphics system R (Venables, 2011). Nonmetric multidimensional scaling (NMS) ordination (Kruskal and Wish, 1978) was used to analyze trends in species composition in monitoring and experimental plots. Each NMS axis represents a component of variation in the multivariate data set that is similar to a principal components axis (PCA). However, NMS ordination is much better suited for use with non-normal species composition data than PCA. Plots with similar scores for a particular NMS axis are more similar to one another with respect to the trends in species composition represented by that axis than stands with less similar scores. Our NMS analyses used the Sørensen dissimilarity metric for 1,000 iterations to derive two-dimensional ordination axes, which represent the main axes of compositional variation. We ran PC-ORD for Windows with random starting configurations for 100 runs with real data with a maximum of 1,000 iterations per run, and a stability criterion of 0.00001. Indicator species analysis (Dufrêne and Legendre, 1997), and correlation and regression tree analyses (McCune and Grace, 2002) were used to identify those species and site measures that are most highly correlated to variations in species composition represented in the NMS ordination (McCune and Grace, 2002).

We used structural equation modeling (SEM) to evaluate the correlational relationships among the composition of vegetation, arthropod, and breeding bird communities for experimental plots and the 21 additional Research Project T-2 plots. There are several features of SEM that are different from most classical methods of statistical analyses. First, unlike many classical statistical techniques, SEM is not intended to test and/or reject null hypotheses. Instead, the purpose of SEM is to test theoretical relationships among different variables and competing models. Second, the calculation of the degrees of freedom in the model comes from having more known values (from the covariance matrix of the data) than estimated values (required by the model). Models in which all possible pathways are specified are saturated and possess zero degrees of freedom; nonzero degrees of freedom permit the testing of model structure (Grace et al., 2010). Third, chi square (χ^2) goodness of fit statistics that yield a p-value <0.05 are considered a *poor* model fit, whereas higher p-values are considered a stronger fit. However,

good-fitting structural equation models do not prove causal relationships (Bollen, 1989). Inferences about the sign and strength of directional paths in SEM can only be made if sound theory guides both the model building and the model fitting processes (Grace, 2006). Fourth, SEM allows several correlated variables to be represented collectively as a composite variable. A composite variable is a special type of variable that is completely specified by two or more causal indicators (Grace and Bollen, 2008). We combined soil pH, CEC, and percent SOM (Table 13-1) into a single, composite variable of soil characteristics. Non-composite variables that are directly observed are referred to as manifest variables.

Within SEMs, the strengths of associations between variables are represented as path coefficients, which are standardized regression coefficients (Grace and Bollen, 2005). *Partial* path coefficients (γ_{partial}) represent the change expected if a predictor is varied (in standard deviation units) and are identical to correlation coefficients. Thus, partial coefficients measure the predicted sensitivity of the response variable to one or more predictor variables. *Semipartial* path coefficients ($\gamma_{\text{semipartial}}$) are the square root of the unique variance explanation of a predictor variable on a response variable; they are a measure of covariance between the predictor variable and the response variable that is independent of any other variable (Grace and Keeley, 2006). In other words, the semipartial path coefficient represents the unique influence of a specific variable that is uncorrelated with any other variable.

Results and Discussion

MCBCL Pine Forest Plant Diversity and Composition

A list of all 354 plant taxa encountered in MCBCL pine stands is provided in **Appendix 13-A**. An NMS ordination of 85 pine-dominated stands from across MCBCL produced two prominent axes as displayed in **Figure 13-6 (Appendix 13-B)**. Longleaf pine stands on sandy soils have high first axis scores, whereas stands occurring on organic soils and dominated by a mixture of pond and loblolly pines have low first axis scores. First axis stand scores are positively correlated with soil bulk density, and negatively correlated with % SOM and CEC (**Table 13-1**; soil data for all 85 plots are summarized in **Appendix 13-C**).

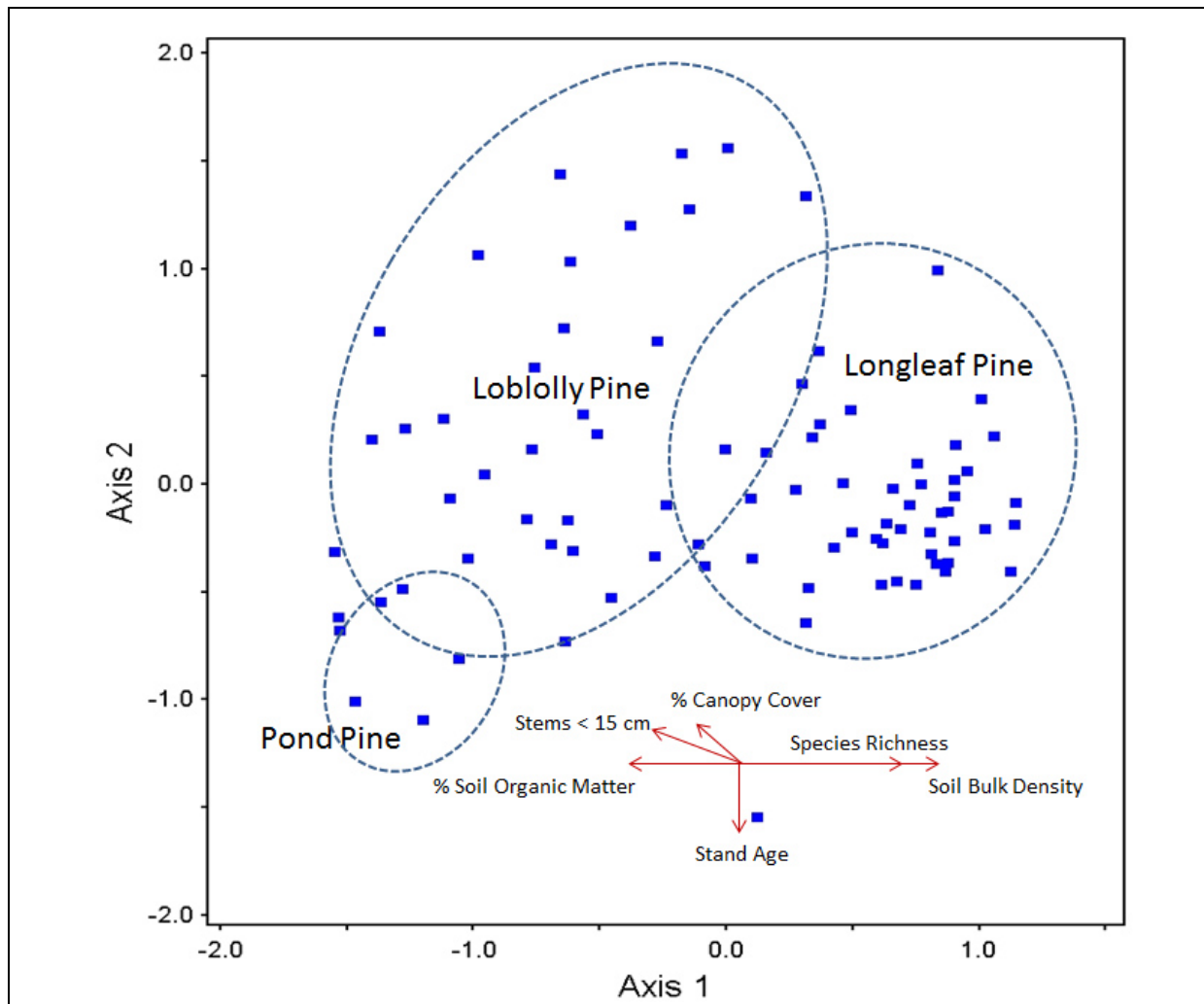


Figure 13-6. NMS ordination of 85 pine-dominated stands located on MCBCL (see Appendix 13-B for actual stand scores).

The distance between individual plots in ordination space is a measure of dissimilarity in species composition. The red vectors relate to the relationships between specific soil or stand characteristics and NMS axes. The vector length reflects the strength of the correlation (see Table 13-1) and vector direction indicates the trajectory in which the characteristic increases in the ordination space.

Table 13-1. Significant correlations between soil or stand vegetation characteristics and NMS ordination axes.

Variables	Correlation with NMS Axis 1 r (p <)	Correlation with NMS Axis 2 r (p <)
Soil bulk density	0.68 (0.0001)	−0.08 (NS)
Cation exchange capacity	−0.36 (0.001)	0.24 (0.05)
% Soil organic matter	−0.51 (0.0001)	−0.03 (NS)
% Canopy cover	−0.39 (0.001)	0.34 (0.01)
Stand age	0.04 (NS)	−0.41 (0.001)
Stem <15 cm dbh	−0.46 (0.001)	0.14 (NS)
Basal area (m ² /ha)	0.21 (0.05)	−0.19 (NS)
Understory species richness	0.53 (0.0001)	−0.03 (NS)

Note: NS = not significant.

Several stand characteristics were also correlated with NMS ordination scores (**Table 13-1**). Understory species richness was, for example, highly positively correlated with NMS Axis 1. Species richness was indeed highest (exceeding 100 species ha^{−1} in some cases) in mature longleaf stands, and lowest (fewer than 15 species ha^{−1}) in pocosins. The density of stems less than 15 cm in dbh (a measure of shrub cover) was negatively correlated with NMS Axis 1. This is indicative of the relative importance of understory shrubs in many loblolly and pond pine dominated stands. Percent canopy cover was negatively correlated with NMS Axis 1 and positively correlated with NMS Axis 2 (i.e., canopy cover generally increased from lower right to upper left in the ordination). Canopy cover was directly related to the density of understory shrubs and trees. Finally, stand age (age of dominant trees) was negatively correlated with NMS Axis 2.

Species with highly significant positive correlations ($r > 0.30$) with the NMS Axis 1 (i.e., indicative of longleaf dominated stands) included *Aristida stricta* (wire grass), *Carphephorus tomentosus* (carphephorus), *Cnidoscolus stimulosus* (cnidoscolus), *Gaylussacia dumosa* (dwarf huckleberry), *Iris verna* (dwarf iris), *Pinus palustris* (longleaf pine), *Sericocarpus tortifolius* (white-topped aster), and *Vaccinium tenellum* (blueberry). Species with highly significant negative correlations with the NMS first axis (i.e., indicative of organic soils) included *Acer rubrum* (red maple), *Lyonia lucida* (fetter-bush), *Osmunda cinnamomea* (cinnamon fern), and *Persea palustris* (red bay). Species with highly significant positive correlations with the NMS second axis included *Coreopsis* spp. (coreopsis), *Dichanthelium* spp. (panic grass), *Eupatorium capillifolium* (dog fennel), *Gelsemium sempervirens* (Carolina jasmine), *Hypericum tenuifolium* (St. John's wort), *Rubus* spp. (blackberry), *Smilax bona-nox* (greenbrier), *Solidago odora* (goldenrod), and *Vitis rotundifolia* (muscadine grape). Nearly all of these species are also common in disturbed locations such as roadsides and recently logged areas. Only two species (i.e., *Pinus palustris* and *Pteridium aquilinum* [bracken fern]) had significant negative correlations with the second axis. (See **Appendix 13-D** for a tally of r (correlation coefficient) and r^2 (coefficient of determination) values for all species with NMS Axes 1 and 2.)

NMS Axis 1 represents vegetation variation that is generally correlated with the prevalent soil gradient across MCBCL from organic soils supporting pocosin vegetation to well-drained sandy soils supporting longleaf pine savanna. NMS Axis 1 scores for stands dominated by loblolly pine (most with relatively dense undergrowth of shrubs and understory trees) are generally less than zero (i.e., they are arrayed on the left side of the ordination). There are three equally likely explanations for this pattern. First, soil moisture conditions for these sites were historically probably more suitable for agriculture and subsequent pine silviculture. This would have favored conversion of longleaf dominated stands to loblolly. Second, the exclusion of fire from these stands favored the invasion of understory shrubs and trees, many of which are more indicative of wetter sites. Third, fire exclusion and ingrowth of woody vegetation favors the accumulation of a deep humus layer and increased SOM. Thus, in presettlement times, many of these sites probably supported vegetation similar to that of longleaf stands with high NMS Axis 1 scores.

NMS Axis 2 is probably related to a complex of disturbances overlaid on soil-site gradient represented in NMS Axis 1. Several of the stands with very high NMS Axis 2 scores had overstory trees in the 10- to 20-years age class, reflecting recent cutting. The high positive correlations with weedy species such as *Eupatorium capillifolium* and *Solidago odora*, and with vines such as *Gelsemium sempervirens* and *Vitis rotundifolia* are consistent with this assertion.

In summary, species composition in MCBCL pine stands is highly correlated with a complex site and soil moisture gradient from comparatively wet, organic soils with low bulk densities to well-drained sandy soils with high bulk densities. Plant species richness also increases along this same gradient. Additional variation in species composition (represented in NMS Axis 2) is related to the effects of disturbance.

Soil Characteristics

Values for soil characteristics in each treatment plot are displayed in **Table 13-2**. In general, values for these various soil characteristics were generally correlated with one another and with SOM and bulk density in particular (compare to **Table 13-1**). As expected, SOM percentages ranged higher for experimental treatment blocks (4.66–85.45%) than for monitoring plots that were dominated by longleaf pine (0.82–17.85%). The range of soil bulk densities for experimental treatment plots was 0.18–1.09 g/cm³; this was considerably lower than the range for longleaf pine monitoring plots (0.85–1.50 g/cm³). These soil differences indicate that loblolly pine stands generally occur on moister sites than longleaf pine stands and that the absence of fire and ingrowth of dense understory vegetation had encouraged accumulation of SOM (which results in lower soil bulk density).

Figure 13-7 displays percent SOM by block and treatment and allows visual comparison of variation within and between treatment blocks. The variation among blocks is generally consistent with the MCBCL staff's a priori classification of these sites. The high pocosin sites (IES, FGE, and FGW) have the highest organic matter, wet mesic sites (IEN, MF, and HA) have intermediate organic matter, and mesic sites (RBE and RBW) have the lowest organic matter. Analysis of variance reveals significant differences among blocks (F ratio [F] = 6.3, degrees of freedom [DF] = 7, P < 0.01) and no a priori difference among treatments (F = 1.25, DF = 2, P > 0.32). However, this graph also reveals that there is considerable within treatment block variation. This was particularly true for blocks FGW and IEN.

Table 13-2. Averaged values and standard deviations (in parentheses) for soil organic matter (OM%), pH, bulk density (BD, g/cm³), cation exchange capacity (CEC, milliequivalents/100 gm soil), and extractable orthophosphate (PO₄-P), calcium (Ca), magnesium (Mg), potassium (K), sulfur (S), boron (B), iron (Fe), manganese (Mn), copper (Cu), zinc (Zn), and aluminum (Al) in each of the experimental treatment plots.

Blk-Trt	OM%	pH	BD	CEC	PO ₄ -P	Ca	Mg	K	S	B	Fe	Mn	Cu	Zn	Al
FGE-C	68.21 (6.31)	3.80 (0.02)	0.21 (0.03)	9.59 (2.66)	2.75 (0.43)	236.00 (86.64)	88.00 (14.40)	44.50 (4.97)	14.00 (1.87)	0.13 (0.05)	43.25 (10.57)	1.00 (0.61)	0.41 (0.11)	1.12 (0.25)	171.00 (68.61)
FGE-D	50.21 (19.32)	3.85 (0.21)	0.33 (0.13)	6.96 (1.29)	7.25 (2.28)	191.25 (33.17)	49.25 (10.52)	51.25 (16.38)	20.00 (1.58)	0.13 (0.05)	78.75 (17.92)	1.13 (0.54)	0.43 (0.07)	0.93 (0.28)	759.50 (182.09)
FGE-G	24.90 (27.40)	3.93 (0.16)	0.67 (0.29)	7.16 (1.28)	3.25 (0.43)	254.25 (99.24)	48.75 (8.26)	23.50 (3.20)	6.75 (0.83)	0.10 (0.00)	41.75 (13.08)	1.50 (1.46)	0.39 (0.03)	1.28 (0.58)	181.75 (19.12)
FGW-C	64.30 (15.6)	3.78 (0.13)	0.24 (0.08)	10.07 (1.65)	3.25 (0.83)	231.75 (0.69)	98.00 (5.34)	53.00 (3.24)	15.75 (1.09)	0.10 (0.00)	62.00 (25.33)	1.00 (0.61)	0.43 (0.06)	1.09 (0.33)	245.75 (100.64)
FGW-D	11.84 (7.43)	3.88 (0.08)	0.81 (0.23)	9.85 (2.01)	3.00 (0.71)	333.25 (68.16)	62.50 (17.39)	31.50 (11.50)	7.00 (0.71)	0.10 (0.00)	29.25 (6.83)	2.00 (0.71)	0.36 (0.03)	1.77 (0.40)	113.75 (15.02)
FGW-G	39.25 (5.95)	4.00 (0.12)	0.39 (0.05)	7.35 (1.66)	2.50 (1.12)	230.25 (47.13)	64.50 (7.57)	30.75 (4.32)	6.75 (0.43)	0.16 (0.06)	45.75 (11.14)	1.75 (0.43)	0.35 (0.13)	1.63 (0.34)	253.50 (137.71)
IES-C	85.45 (6.53)	3.63 (0.04)	0.18 (0.01)	8.27 (1.07)	3.50 (1.12)	109.00 (57.28)	114.00 (6.52)	87.75 (12.50)	7.75 (3.19)	0.14 (0.06)	38.00 (1.41)	0.75 (0.25)	1.22 (0.78)	0.84 (0.11)	121.50 (13.90)
IES-D	68.34 (29.58)	3.83 (0.04)	0.35 (0.22)	9.29 (3.59)	3.25 (0.43)	222.00 (97.31)	94.00 (38.19)	35.75 (8.35)	6.50 (1.12)	0.26 (0.64)	37.75 (11.41)	2.38 (1.63)	0.52 (0.52)	1.84 (0.83)	228.25 (108.05)
IES-G	47.78 (29.64)	3.90 (0.21)	0.37 (0.24)	11.25 (3.91)	3.75 (1.30)	323.00 (92.23)	85.75 (16.45)	47.00 (8.97)	22.75 (19.03)	0.31 (0.04)	116.75 (81.17)	3.75 (0.83)	0.62 (0.06)	2.29 (0.74)	193.75 (81.22)
IEN-C	11.25 (1.87)	3.98 (0.11)	0.70 (0.07)	5.23 (1.52)	13.00 (3.94)	171.50 (58.80)	26.00 (4.74)	28.75 (3.77)	27.50 (13.31)	0.27 (0.10)	113.00 (21.75)	1.13 (0.54)	0.73 (0.08)	0.66 (0.14)	1211.5 (217.0)
IEN-D	18.19 (8.92)	3.85 (0.09)	0.70 (0.09)	7.37 (4.30)	8.00 (1.87)	219.00 (199.25)	44.25 (29.59)	38.00 (8.06)	18.75 (8.95)	0.21 (0.08)	139.50 (39.71)	0.88 (0.65)	0.58 (0.09)	0.65 (0.12)	1003.5 (196.8)
IEN-G	30.14 (20.95)	3.93 (0.10)	0.57 (0.23)	9.44 (2.35)	6.00 (2.16)	295.25 (117.5)	74.25 (13.40)	43.00 (20.90)	8.75 (2.22)	0.23 (0.09)	100.50 (62.69)	1.50 (1.68)	0.53 (0.07)	1.34 (0.49)	524.25 (210.1)

(continued)

Table 13-2. Averaged values and standard deviations (in parentheses) for soil organic matter (OM%), pH, bulk density (BD, g/cm³), cation exchange capacity (CEC, milliequivalents/100 gm soil), and extractable orthophosphate (PO₄-P), calcium (Ca), magnesium (Mg), potassium (K), sulfur (S), boron (B), iron (Fe), manganese (Mn), copper (Cu), zinc (Zn), and aluminum (Al) in each of the experimental treatment plots. (continued)

Blk-Trt	OM%	pH	BD	CEC	PO ₄ -P	Ca	Mg	K	S	B	Fe	Mn	Cu	Zn	Al
HA-C	15.02 (7.29)	4.10 (0.12)	0.68 (0.20)	5.39 (2.52)	5.75 (1.30)	161.75 (82.88)	45.25 (19.32)	35.50 (11.41)	10.00 (1.58)	0.28 (0.04)	167.50 (33.39)	1.25 (0.75)	0.77 (0.09)	1.46 (0.58)	606.50 (115.5)
HA-D	12.60 (8.46)	4.15 (0.23)	0.78 (0.18)	11.48 (2.75)	5.75 (2.17)	518.25 (140.41)	63.75 (24.62)	29.00 (8.97)	8.50 (2.06)	0.10 (0.00)	78.25 (8.38)	4.50 (3.35)	0.48 (0.12)	1.58 (0.56)	350.75 (23.73)
HA-G	9.41 (6.83)	4.47 (0.33)	0.85 (0.19)	5.81 (4.11)	3.00 (0.71)	240.0 (125.8)	54.15 (37.66)	33.75 (12.21)	10.5 (1.80)	0.34 (0.04)	220.50 (96.50)	1.25 (0.75)	0.64 (0.08)	0.55 (0.33)	642.25 (285.5)
MF-C	14.14 (1.99)	3.95 (0.05)	0.72 (0.09)	6.51 (1.02)	14.25 (2.86)	213.00 (41.83)	43.75 (4.66)	29.50 (16.04)	9.75 (0.83)	0.32 (0.05)	240.25 (24.97)	2.00 (0.00)	79.07 (9.79)	58.98 (9.37)	901.50 (270.02)
MF-D	27.92 (10.14)	3.85 (0.05)	0.44 (0.08)	7.02 (2.28)	9.75 (2.38)	174.25 (62.49)	61.50 (61.50)	46.50 (5.85)	14.75 (2.17)	0.26 (0.03)	150.00 (20.94)	2.50 (1.12)	0.83 (0.20)	1.54 (0.46)	732.25 (222.8)
MF-G	31.63 (9.41)	3.88 (0.13)	0.42 (0.17)	5.69 (2.39)	9.75 (3.90)	170.50 (134.65)	42.25 (10.35)	29.00 (2.45)	18.50 (10.31)	0.24 (0.09)	139.00 (71.05)	1.00 (0.61)	1.93 (1.88)	0.98 (0.31)	871.75 (259.08)
RBE-C	17.88 (10.68)	4.55 (0.30)	0.67 (0.17)	10.42 (1.46)	12.00 (4.85)	595.00 (156.18)	75.00 (15.28)	45.00 (6.20)	13.25 (2.68)	0.21 (0.07)	123.75 (48.07)	0.88 (0.22)	0.45 (0.09)	1.56 (0.24)	762.50 (278.43)
RBE-D	6.20 (2.26)	4.28 (0.22)	0.92 (0.16)	7.49 (1.76)	8.75 (2.68)	341.50 (81.13)	52.00 (6.96)	28.50 (7.23)	8.75 (0.83)	0.28 (0.08)	50.25 (13.33)	4.00 (1.58)	0.70 (0.21)	2.73 (0.69)	185.75 (59.99)
RBE-G	8.52 (2.28)	4.20 (0.16)	0.85 (0.12)	8.61 (3.15)	11.50 (2.29)	350.25 (116.00)	64.75 (14.04)	32.25 (1.92)	10.75 (1.48)	0.32 (0.02)	205.00 (37.06)	1.38 (0.65)	0.62 (0.08)	1.55 (0.54)	580.75 (164.73)
RBW-C	4.66 (2.32)	4.55 (0.23)	1.09 (0.10)	5.15 (1.35)	4.50 (1.66)	278.50 (79.94)	37.75 (7.12)	36.00 (4.30)	21.75 (11.52)	0.36 (0.03)	204.25 (78.68)	1.25 (0.75)	0.85 (0.25)	2.90 (2.26)	994.0 (136.4)
RBW-D	7.73 (4.05)	4.68 (0.16)	0.98 (0.16)	7.75 (4.88)	9.50 (5.36)	438.50 (290.70)	68.75 (38.26)	63.00 (57.25)	11.25 (1.48)	0.29 (0.08)	165.25 (28.10)	4.13 (2.56)	1.16 (0.45)	12.12 (11.53)	577.25 (147.91)
RBW-G	5.92 (1.81)	4.18 (0.25)	0.93 (0.10)	7.35 (1.38)	7.00 (2.12)	316.75 (113.51)	55.75 (13.63)	33.50 (3.64)	9.25 (1.09)	0.32 (0.02)	232.75 (49.94)	2.38 (1.63)	0.63 (0.10)	1.71 (0.54)	541.25 (102.38)

Extractable element concentrations are expressed in µg/g. Treatments are designated as control (-C), growing season thinning (-G), and dormant season thinning (-D). Soil samples were collected following treatment applications and dormant season prescribed burns. Note: Blk-Trt = block treatment.

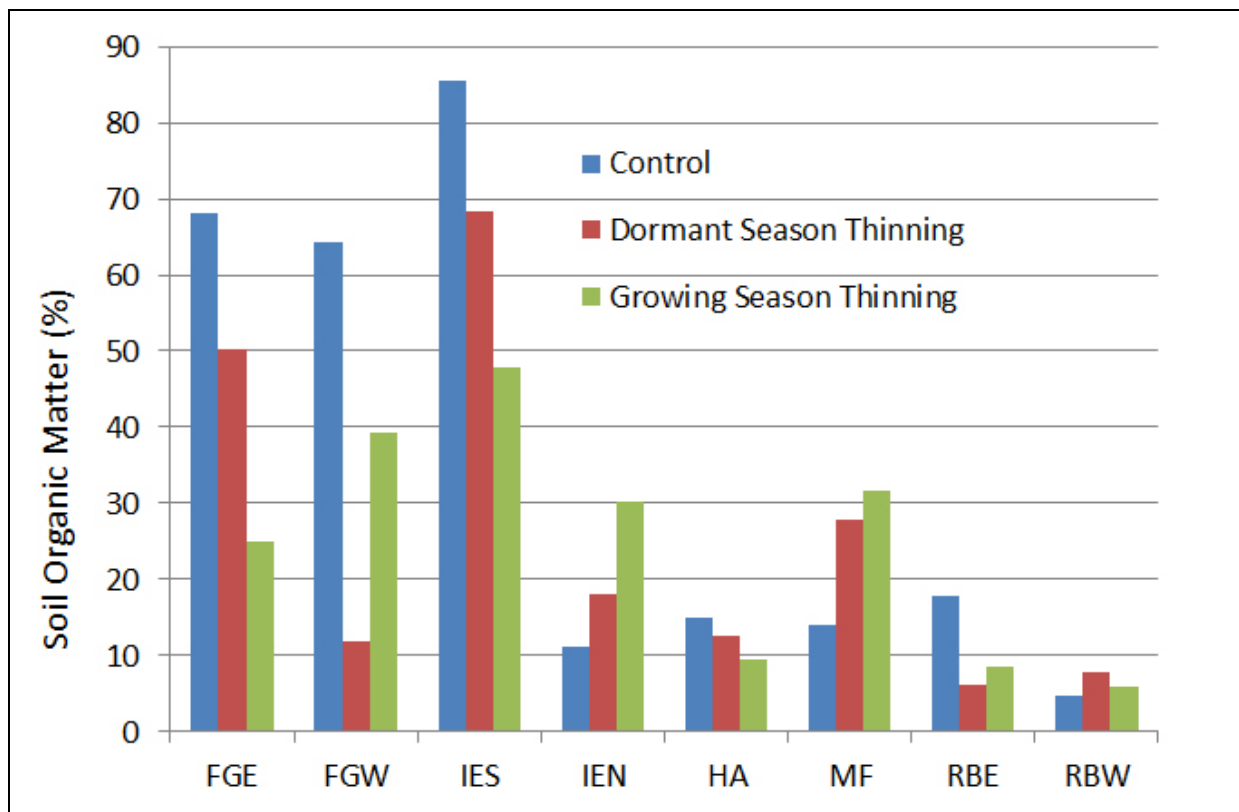


Figure 13-7. Average soil organic matter (%) for each treatment arranged by blocks.

Although there is a significant block effect and no significant treatment effect, there is considerable within block variation within some blocks. Blocks are ordered left to right as high pocosin (FGE, FGW, and IES), wet mesic (IEN, HA, and MF), and mesic (RBE and RBW).

Pre- and Post-Treatment Variation in Vegetation, Arthropod and Bird Communities

Pre- and post-treatment data for stem density and basal area for woody stems, and post-treatment % canopy cover in each treatment plot are displayed in **Table 13-3**. Although stem density varied considerably among treatment plots (5,500 to 57,000 stems/ha for the 1–4 cm dbh size class and 130 to 1,390 stems/ha for the 5–20 cm dbh size class), it was considerably higher than the average for longleaf pine stands that have been prescribe burned at regular intervals (e.g., <1,000 stems/ha for the 1–4 cm dbh size class and <100 stems/ha for the 5–20 cm size class). Basal area for 1–20 cm stems accounted for 15% to more than 70% of total stand basal area; in longleaf stands basal area of 1–20 cm stems generally accounts for less than 15% of total basal area.

As expected, density of 1–20 cm dbh stems was considerably less than pre-treatment density in all post-treatment plots. In nearly all cases, understory stem density was reduced by over 90%. This was true even for control plots because they had been subjected to PB in either 2010 or 2011 along with the thinned plots. There were no significant differences among blocks ($F = 0.98$, $DF = 7$, $P > 0.48$), however there were significant differences among treatments ($F = 47.56$, $DF = 2$, $P < 0.00001$). Specifically, stem density was uniformly highest in control plots, lower in dormant season thinning plots and lowest in growing season thinned plots (**Figure 13-8**).

Table 13-3. Summary of pre-treatment and post-treatment vegetation data for experimental plots.

Blk-Trt	Age (yr)	Pre-Treatment			Post-Treatment			% Canopy Cover	Total Basal Area
		Stems <5 cm	Stems 5–20 cm	Basal Area Stems 1–20 cm dbh	Stems <5 cm	Stems 5–20 cm	Stems >20 cm		
FGE-C	50	N/A	N/A	N/A	1,820	620	220	37.34	26.2
FGE-D	50	10,250	770	6.02	610	130	190	47.45	19.6
FGE-G	50	21,250	190	4.01	110	40	200	100	19.6
FGW-C	50	N/A	N/A	N/A	1,530	640	180	99.99	25.6
FGW-D	50	11,000	520	5.06	650	140	210	54.68	19.6
FGW-G	50	22,000	370	4.64	130	30	190	52.8	19.6
IES-C	60	46,750	510	11.5	300	80	220	100	19.7
IES-D	60	6,000	1,390	11.65	590	180	170	60.92	18.5
IES-G	60	11,750	130	2.46	380	240	120	59.92	13.5
IEN-C	50	57,000	120	13.42	1,730	340	110	61.65	7.6
IEN-D	50	10,750	770	8.2	840	160	120	60.2	10.2
IEN-G	50	16,250	420	4.31	220	0	220	94.48	17.6
HA-C	53	27,750	610	14.52	1,130	300	110	66.75	18.1
HA-D	53	16,500	600	6.06	80	10	80	58.19	8.4
HA-G	53	9,000	340	3.07	350	30	80	79.44	8.4
MF-C	63	34,500	480	8.64	2,100	670	130	68.7	21.3
MF-D	65	6,500	820	7.71	300	50	250	61.95	23.6
MF-G	65	11,500	260	2.53	440	130	190	58.75	16.5
RBE-C	60	12,750	610	9.72	2,060	650	90	96.36	23.8
RBE-D	64	5,500	1,330	9	980	100	140	69.39	18.4
RBE-G	64	10,500	300	2.45	190	10	80	59.88	13.3
RBW-C	56	11,500	380	4.38	1,060	220	230	96.63	26
RBW-D	56	6,000	650	4.63	850	170	120	44.62	22.1
RBW-G	56	9,500	210	2.72	170	20	130	64.63	19.1

Pre-treatment basal area data could not be gathered for treatment plots FGE-C and FGW-C owing to military training activities. Blocks are ordered left to right as high pocosin (FGE, FGW, and IES), wet mesic (IEN, HA, and MF), and mesic (RBE and RBW).

Note: N/A = not applicable.

These results indicate that growing season thinning may be more effective than dormant season thinning in reducing understory hardwood density, at least in the short term. If these differences persist, it would suggest that there is an added restoration benefit to growing season compared to dormant season thinning.

The pattern of change in the IES block is noteworthy. In this block only, post-treatment 1–20 cm stem density was actually lower in the control treatment than in either the dormant or growing season thinning treatments. This was a direct consequence of the fact that the prescribed fire in IES-C was far more severe than in any of the other blocks or treatments.

Canopy cover (%) was uniformly highest in control plots compared to thinned treatment plots. However, there was no significant difference between dormant and growing season thinning in this regard.

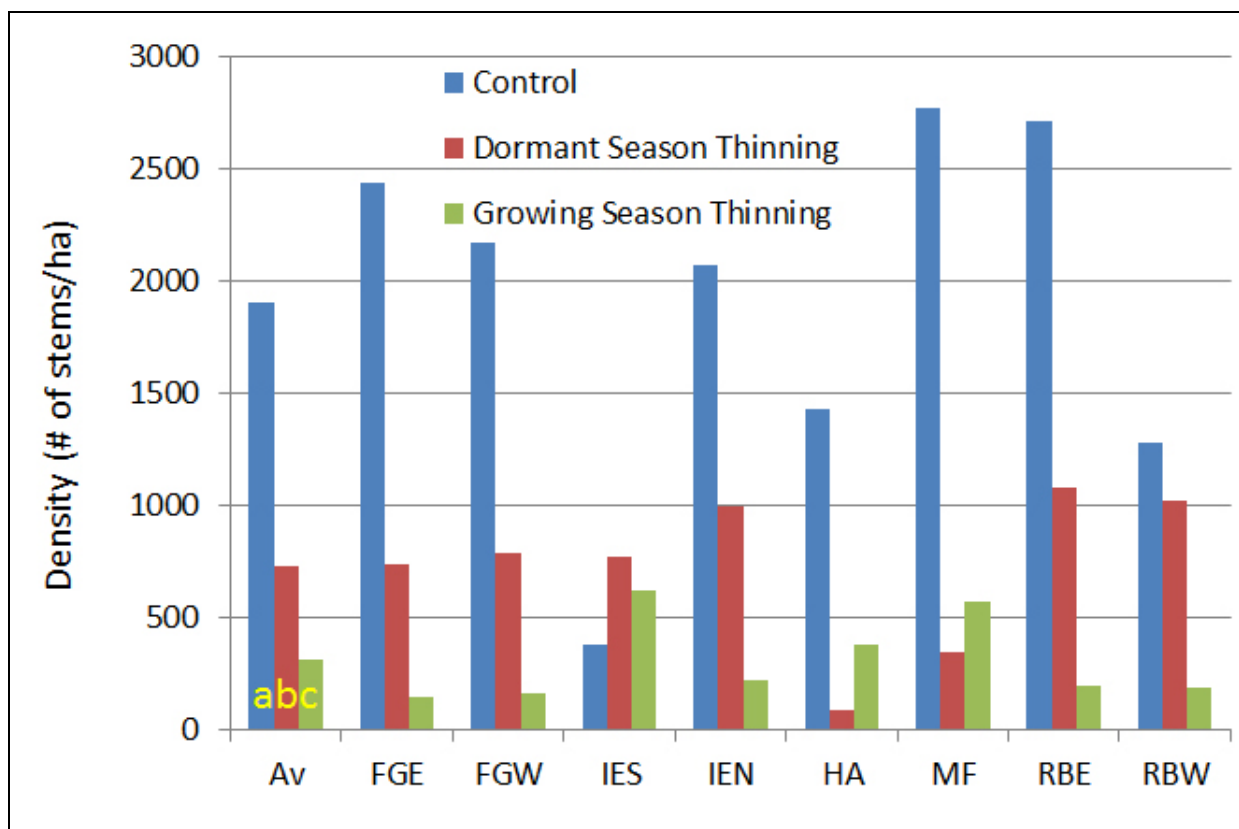


Figure 13-8. Post-treatment 1–20 cm dbh stem density by block and treatment.

Blocks are ordered left to right as high pocosin (FGE, FGW, and IES), wet mesic (IEN, HA, and MF) and mesic (RBE and RBW). There are no significant differences among blocks. Treatments, however, are significantly different from one another ($P < 0.05$, Duncan's Multiple Range Test) as indicated by the lower case yellow letters in the average (Av) bars.

Species richness (number of taxa/0.1 ha) for plants, arthropods and plants is displayed in **Figure 13-9**. Total plant species richness (number of species/0.1 ha) ranged from as low as 7 in FGW-C, a pocosin plot, to as high as 41 in HA-D, a wet-mesic plot. There were significant differences among treatment blocks ($F = 5.43$, $DF = 7$, $P < 0.005$). In general, high pocosin blocks (FGE, FGW, and IES) and one wet mesic block (IEN) had fewer species than other blocks. There was

also a highly significant treatment effect ($F = 14.50$, $DF = 2$, $P < 0.0005$); the control treatments had fewer species than either of the thinning treatments. There was no significant difference between the thinning treatments.

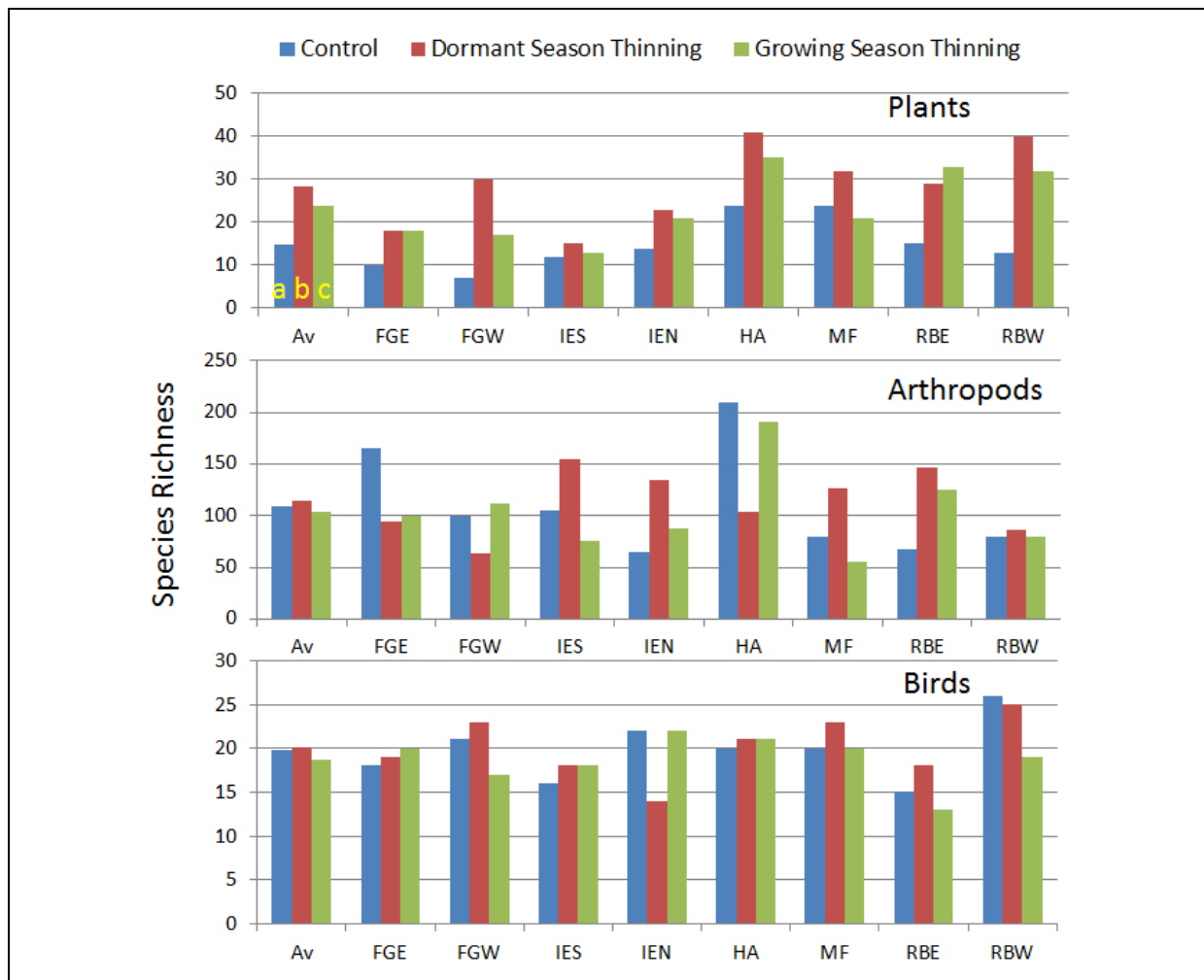


Figure 13-9. Post-treatment species richness of plants (number/0.1 ha), arthropods (number trapped/site) and birds (number identified/site) by block and treatment. Blocks are ordered left to right as high pocosin (FGE, FGW, and IES), wet mesic (IEN, HA, and MF) and mesic (RBE and RBW).

Av represents the average for each treatment across all blocks. There are significant differences in plant species richness among blocks. Furthermore, the control treatment had significantly lower species richness than either of the thinning treatments ($P < 0.05$, Duncan's Multiple Range Test) as indicated by the lower case yellow letters in the average bars. There are no differences among blocks or treatments for either arthropods or birds.

These results support our Hypothesis 1 that understory/midstory thinning will increase herbaceous species diversity. This increase in plant species richness in thinned treatment plots is notable because it occurs in the growing season following treatment applications and PB. It is very likely a consequence of increased light to the understory owing to diminished canopy cover, reduced amounts of litter and diminished competition from understory shrubs. Differences between growing season and dormant season thinning treatments were not evident after 1 year (Hypothesis 2).

There were no significant differences among either blocks or treatments in species richness of either arthropods or birds. However, within and among block variation was much higher for arthropod than for bird species richness. The Malaise, yellow pan and pit-fall traps sample insect populations in a small area (probably within 5–10 m of the traps) compared to the bird point counts that sample populations over a much larger area (>50 m). This is the most likely explanation for the high sample to sample variance among arthropods compared to birds.

Compositional variation in the community of plants among treatment plots based NMS ordination is displayed in **Figure 13-10**. Also included in this graph are the 11 longleaf pine dominated stands that were simultaneously surveyed for arthropods and birds. There is a clear separation of the loblolly dominated experimental plots with generally low NMS Axis 1 scores from the longleaf dominated plots with generally higher NMS Axis 1 scores. Experimental plots are arrayed as a continuum from high pocosin with low NMS Axis 2 scores to wet mesic with intermediate second axis scores and mesic plots with high second axis scores. Species diversity in the wettest block (IES) remains low and none of the species typical of longleaf pine stands occur here. Thus, such very wet areas may be poor candidates for restoration. These results are contrary to our Hypothesis 3 that thinning and PB will have their greatest impacts on vegetation species richness and composition in wetter sites compared to drier sites.

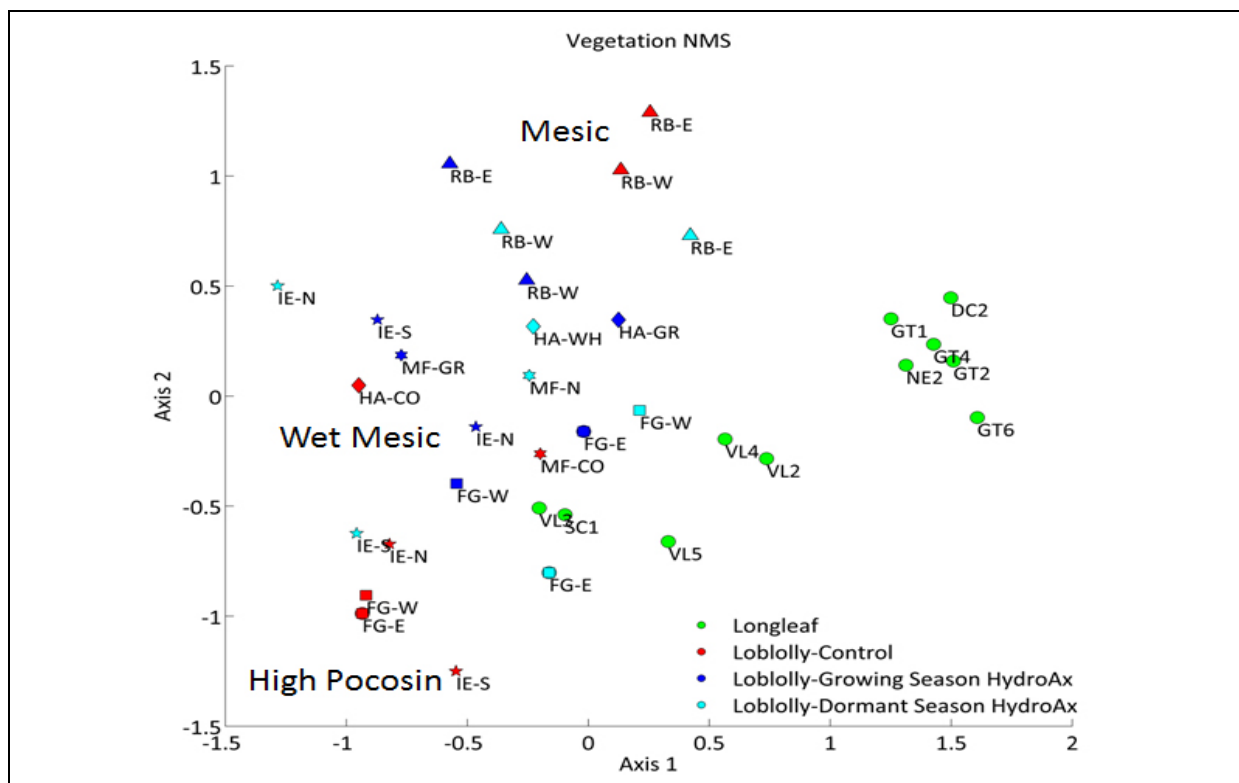
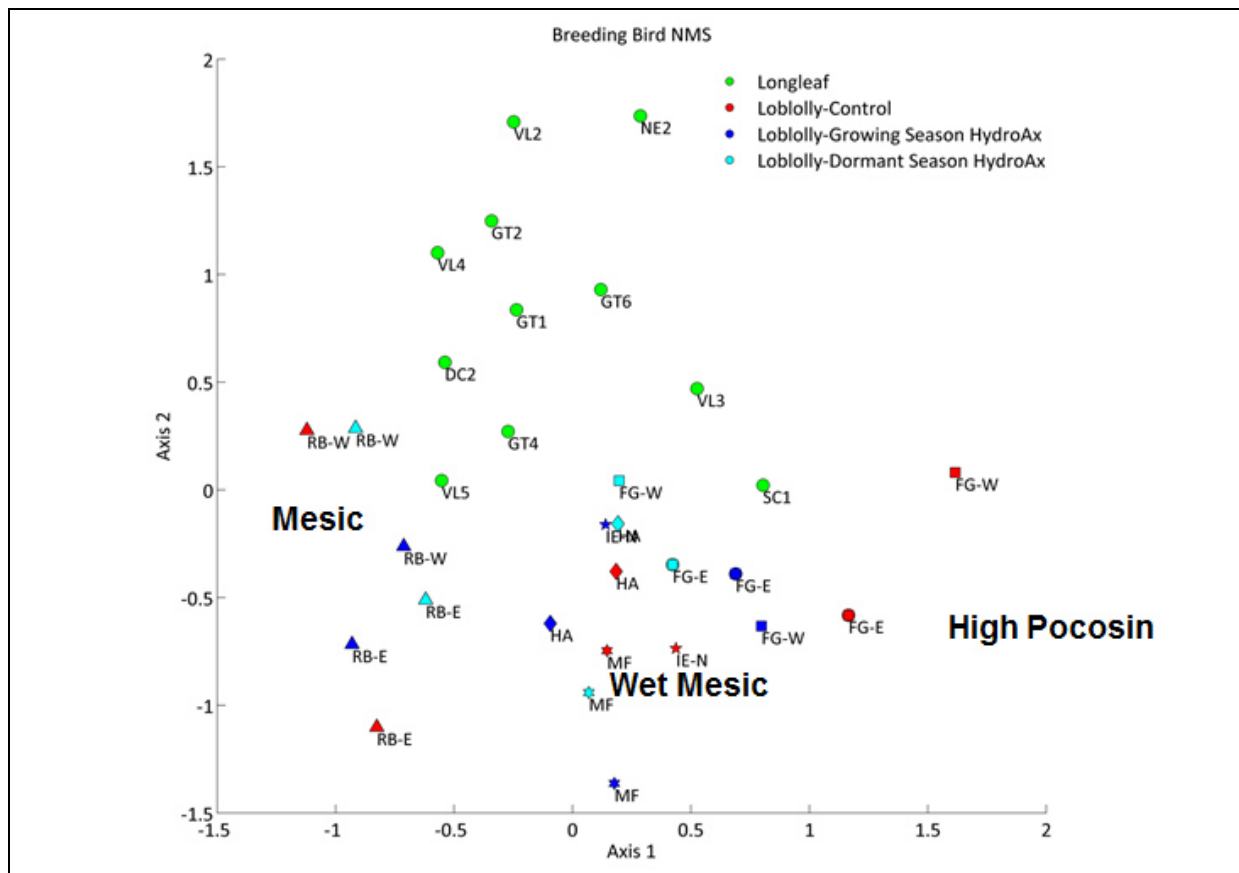


Figure 13-10. NMS ordination of plant species composition in 24 Research Project T-1 experimental plots (red, blue, and light blue symbols) and 11 longleaf pine dominated plots (green symbols).

Each treatment block is represented by a different shape symbol.

For any given block, thinning treatments tend to be located more toward the middle of NMS Axis 2. However, with just a single sample in time, it is not possible to determine if this represents a genuine shift in species composition. Future measurements of these same plots will allow us to plot actual trajectories of change.



Each treatment block is represented by a different shape symbol.

than loblolly dominated stands. Among loblolly pine stands there was no discernible pattern among either blocks or treatments.

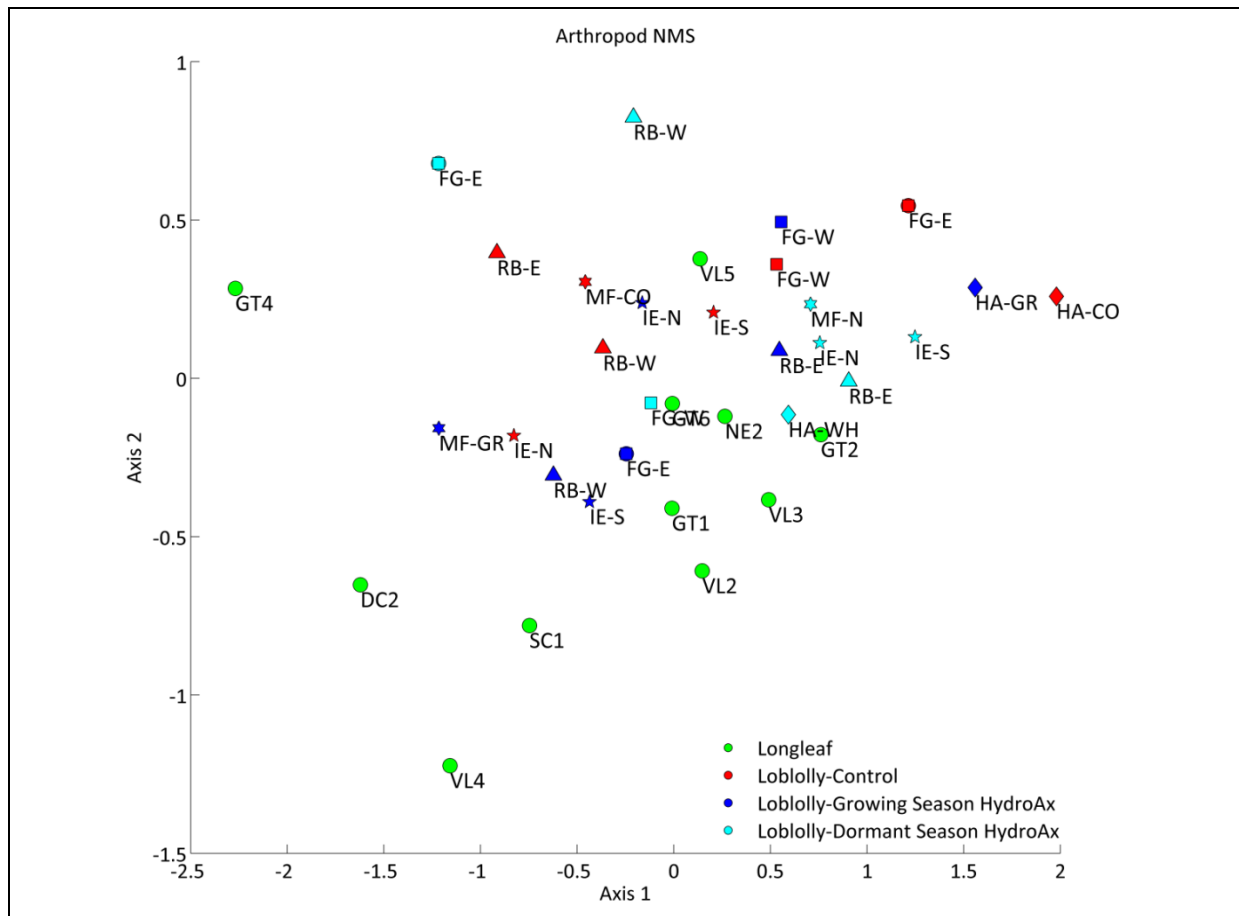


Figure 13-12. NMS ordination of arthropod species composition in 24 Research Project T-1 experimental plots (red, blue, and light blue symbols) and 11 longleaf pine-dominated plots (green symbols).

Each treatment block is represented by a different shape symbol.

We analyzed the relationships among soil characteristics, plant, arthropod, and bird species composition for these same 35 stands (24 Research Project T-1 experimental plots + 11 Research Project T-2 plots) using a structural equation model (**Figure 13-13**). The model provided a good fit to the data ($\chi^2 = 1.99$, $df = 5$, $P = 0.85$); a non-significant p-value indicates that there are no significant deviations between the model and the data. The general rationale for this model is that plant species composition is significantly influenced by the properties of soils, and that both arthropod and avian community composition are influenced by the composition of the plant community. We also hypothesized that avian community composition is influenced by the composition of the arthropod community.

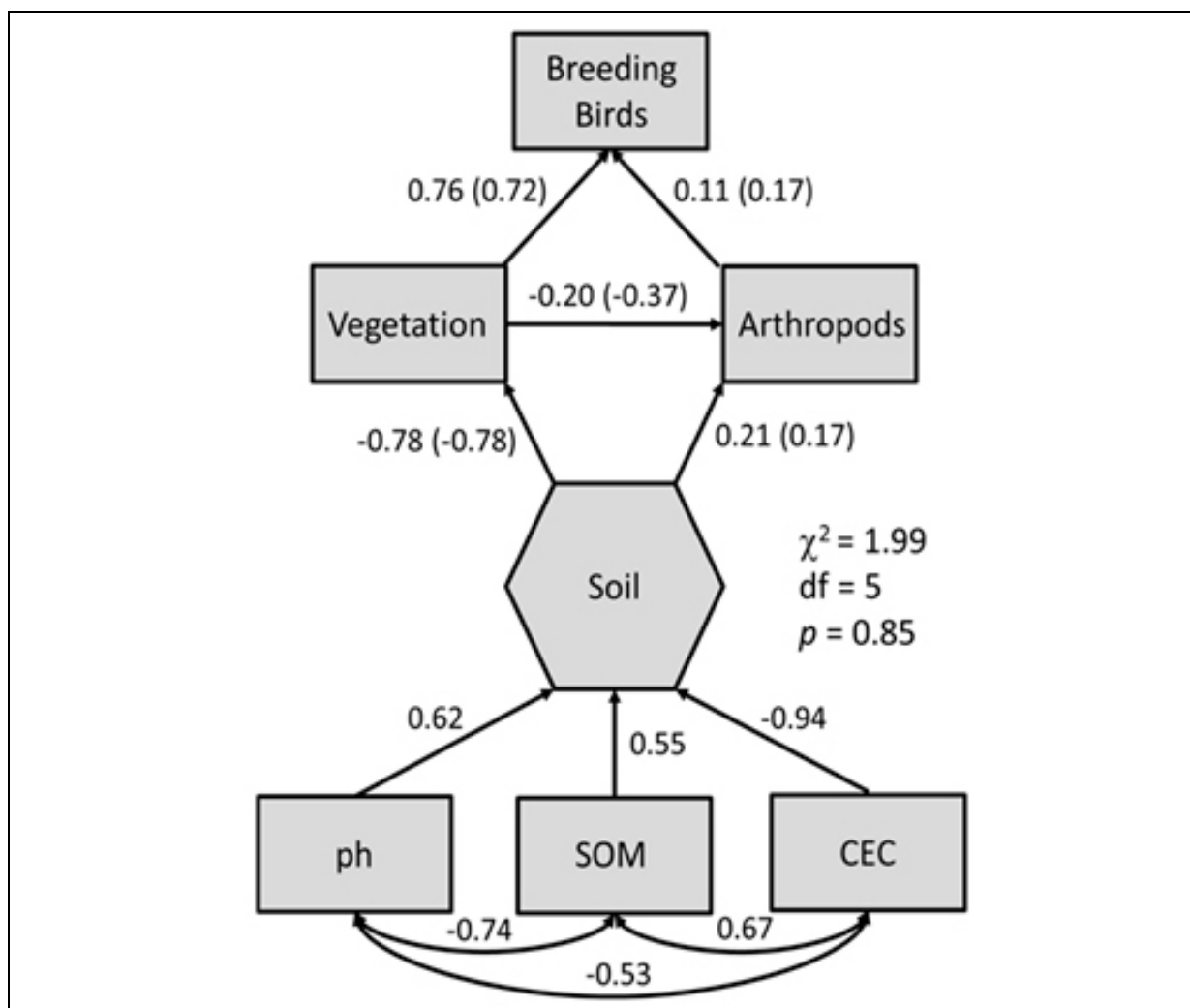


Figure 13-13. A structural equation model for 24 Research Project T-1 experimental plots and 11 longleaf pine dominated plots.

The direction of the arrow is the assumed direction of influence. Numbers indicate partial path coefficients and numbers in parentheses indicate semipartial path coefficients. Positive coefficients indicate positive correlations and negative coefficients indicate negative correlations between model components.

The path coefficient between the composite soil variable and vegetation composition is quite strong ($\gamma_{\text{partial}} = -0.78$). Partial path coefficients (γ_{partial}) represent the change expected in a variable such as vegetation composition if the predicting variable, in this case the composite soil variable, varies; it is equivalent to a correlation coefficient. The path coefficient for vegetation to birds is also quite strong ($\gamma_{\text{partial}} = 0.76$). In structural equation models that included arthropod species composition, path coefficients linking arthropods to soils, vegetation to birds were much weaker. For example, the partial path coefficient for arthropods on birds was only 0.11. The partial path coefficient for vegetation to arthropods is somewhat stronger ($\gamma_{\text{partial}} = -0.20$). The semipartial path coefficient, a measure of the covariance of the response variable independent of any other variable, is even stronger (-0.37).

The correlation between plant community composition and avian community composition is also reflected in the highly significant correlation ($r = 0.49$, $p < 0.0001$) between plant species richness and avian species richness (**Figure 13-14**). Note that for both plants species richness is consistently higher in longleaf pine stands compared to the loblolly dominated treatment plots. Although the richest bird communities were observed in longleaf stands, there is considerably more overlap in bird species richness between longleaf and loblolly dominated stands. There was no significant relationship between arthropod species richness and species richness of either plants or birds.

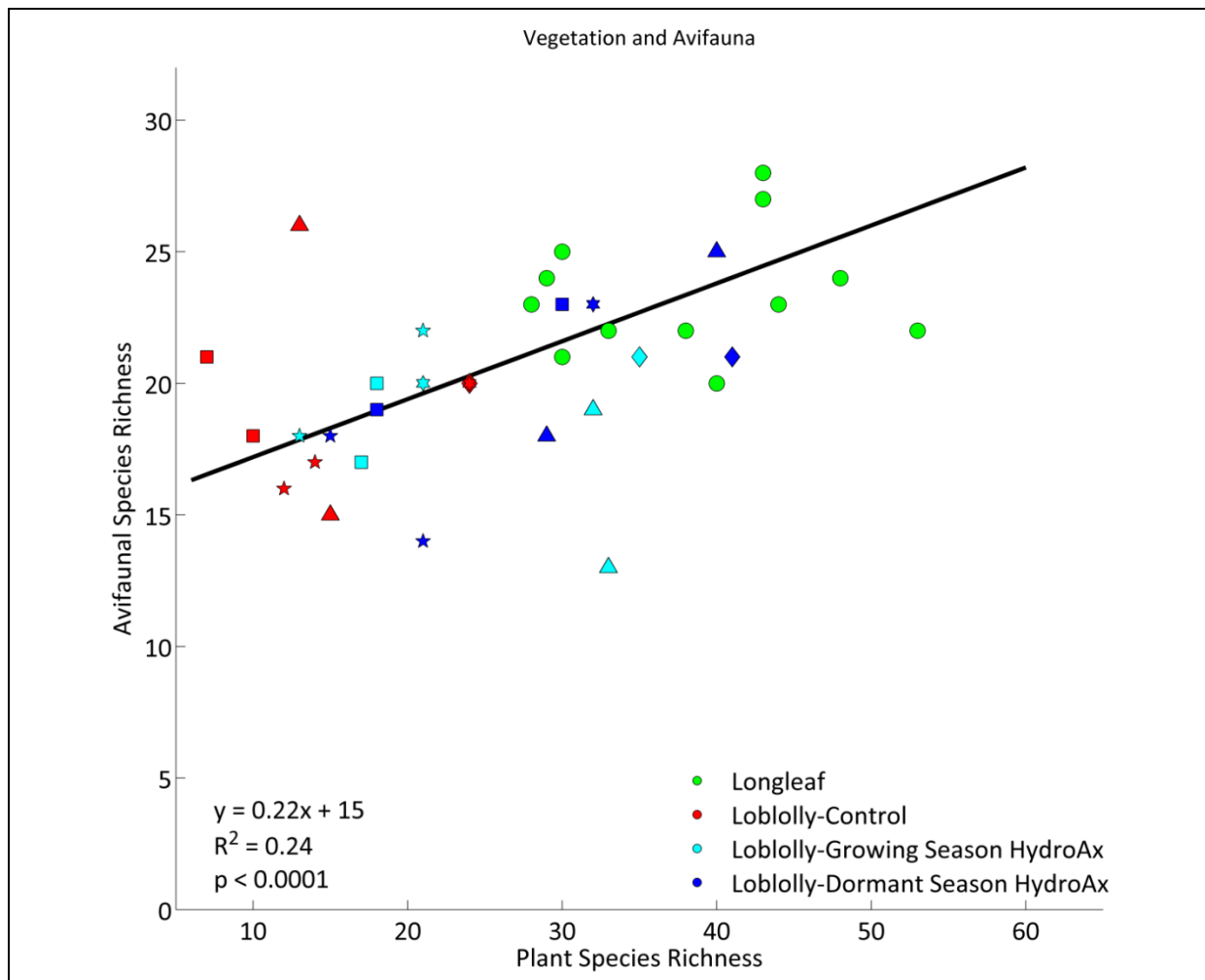


Figure 13-14. Species richness of plants compared to that of birds in 24 Research Project T-1 experimental plots (red, blue, and light blue symbols) and 11 longleaf pine dominated plots (green symbols).

Each treatment block is represented by a different shape symbol.

The weak correlations between arthropod community richness and composition and other ecosystem components may be a consequence of several factors. Although it is possible that the diversity and composition of the assemblage of arthropods are determined by factors other than those influencing the diversity and composition of plants and birds, other issues associated with the sampling and identification of arthropods are undoubtedly important. Sampling procedures

for plants and birds are well established and potential sampling errors are well understood and easily quantified. This is not the case for arthropods. Although we used three rather different trapping methods, it is still likely that we sampled only a portion of the total community of arthropods biased by those species that are most attracted to these trap types. Furthermore, pan, pit-fall, and Malaise traps typically sample the arthropod community from a relatively small area (within 5–10 m) compared to point counts for birds (>50 m). Unfortunately, it is not possible to quantify sampling error or bias for these animals. This is further complicated by the fact that most arthropod identifications were only to the family level.

Our results do signify very strong relationship between soil characteristics and vegetation composition and between vegetation composition and avian community composition, and thus support in part our Hypothesis 4. They are indicative of likely causal relationships among these different model components, and they provide strong assurance that management strategies focused on particular ecosystem components such as the restoration of plant community composition are likely to have favorable effects on other ecosystem components.

Pre- and Post-Prescribed Burning Fuels

Table 13-4 displays the actual dates of the prescribed burn events, average soil surface temperature measurements and moisture indices for different fuel categories. There was no discernible pattern for blocks or treatments in soil surface temperature measurements. This is likely a reflection of the highly variable nature of fire behavior over a range of spatial scales from tens to hundreds of meters, as well as between date differences in fire severity. Fuel moisture indices were highest for the duff and soil surface. Across all fuel categories, fuel moisture was consistently and significantly ($P < 0.01$) lower in thinned (D) than in control (C) treatments. This was a direct consequence of the impacts in the FARSITE model of diminished canopy cover in thinned treatments. Thus, Hypothesis 5 (unthinned and dormant season thinned loblolly pine stands provide different amounts and quality of fuel for prescribed fire) is supported.

Amounts of fuel in stems and leaves before and after prescribed burning are displayed in **Figure 13-15** and **Table 13-5**. With the notable exception of the RBW block, total pre-burn fuel amounts were generally higher in thinned treatments than in the controls ($P < 0.08$). This was largely a consequence of material mulched and redistributed from mechanical thinning. Given these higher fuel amounts, total fuel consumption was also generally higher in thinned plots compared to control plots (again with the exception of RBW, $P < 0.05$). However, the actual fraction of fuel consumed in the fire (% burned) was generally lower in thinned plots compared to unthinned control plots ($P < 0.07$).

These results support Hypothesis 6 that fuel consumption during PB would differ between unthinned and dormant season thinned loblolly pine stands. This is likely due to differences in the vertical distribution of fuels that influence combustion. Fuels in unthinned control areas are distributed vertically allowing more aeration and combustion. Such “ladder fuels” are also likely to increase overall burn severity beyond management prescriptions. Fuels in thinned areas are generally arrayed on the soil surface. This fuel distribution promotes less severe, but uniform surface fires that are more consistent with restoration objectives. The implications of these

differences with respect to gaseous and particulate emissions associated with PB are discussed in the final report for Research Project Air-1.

Table 13-4. Summary of burn dates, estimated maximum soil surface fire temperatures, and fuel moisture index for different fuel categories by block and treatment plot.

Block Treatment	Burn Date	Estimated Temp °C	Duff/Soil Moisture	1-Hour Fuels	10-Hour Fuels	100-Hour Fuels
HA-C	3/19/2010	34	0.722	0.151	0.181	0.166
HA-D	3/19/2010	117	0.687	0.150	0.177	0.161
IEN-C	3/3/2011	10	0.680	0.159	0.189	0.160
IEN-D	3/3/2011	72	0.546	0.109	0.163	0.139
IES-C	3/21/2010	260	0.741	0.190	0.196	0.169
IES-D	3/21/2010	122	0.701	0.179	0.194	0.163
MF-C	2/28/2011	53	0.726	0.172	0.214	0.166
MF-D	2/28/2011	66	0.541	0.112	0.182	0.138
RBW-C	2/28/2011	177	0.726	0.172	0.214	0.167
RBW-D	2/28/2011	104	0.541	0.052	0.179	0.135

The fuel moisture index is expressed on a scale of 0 to 1, where 1 = maximum moisture holding capacity.

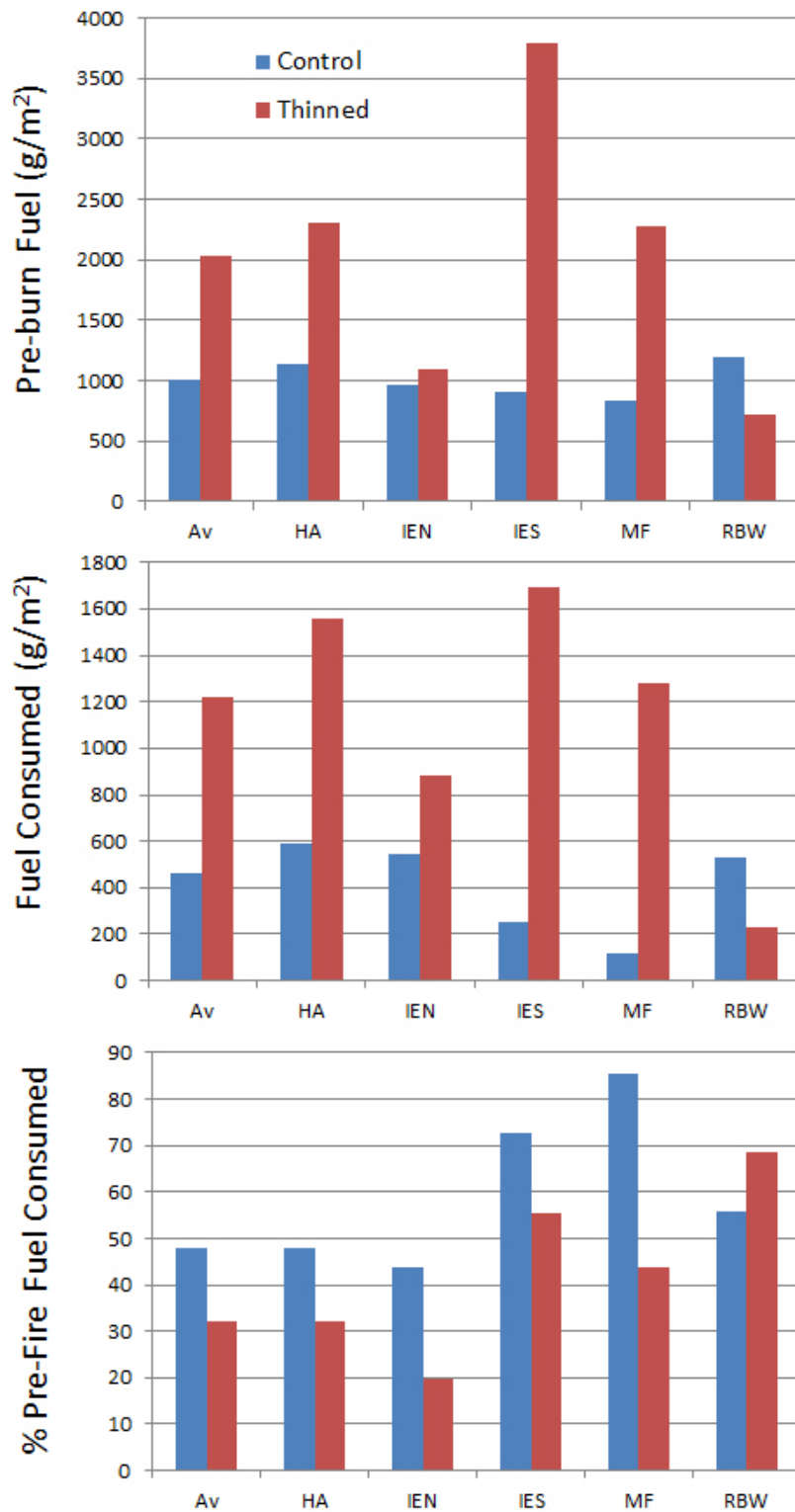


Figure 13-15. Total pre-burn fuel, total fuel consumed and % pre-burn fuel consumed arrayed by block and treatment.

“Av” refers to the average for each treatment across blocks.

Table 13-5. Average fuel amounts (g/m²) by block and treatment prior to and following prescribed burning.

Block-Treatment	Burn Date	Pre-burn Stems	Pre-burn Leaves	Pre-burn Total	Post-burn Stems	Post-burn Leaves	Post-burn Total	Stems Burned	Leaves Burned	Total Burned	% Burned
HA-C	3/19/2010	170.04	961.88	1131.93	128.90	411.88	540.78	41.14	550.01	591.15	47.8
HA-D	3/19/2010	1701.70	596.84	2298.54	267.50	470.12	737.62	1434.21	126.71	1560.92	32.1
IEN-C	3/3/2011	215.34	747.76	963.10	147.35	272.80	420.15	67.99	474.96	542.95	43.6
IEN-D	3/3/2011	405.98	690.34	1096.32	56.19	160.06	216.25	349.79	530.28	880.07	19.7
IES-C	3/21/2010	455.30	451.94	907.24	215.69	441.87	657.56	239.61	10.07	249.68	72.5
IES-D	3/21/2010	2594.71	1189.31	3784.02	1125.98	965.06	2091.04	1468.73	224.25	1692.98	55.3
MF-C	2/28/2011	140.68	689.22	829.90	100.64	608.84	709.48	40.04	80.38	120.43	85.5
MF-D	2/28/2011	1761.36	514.00	2275.36	568.65	423.05	991.70	1192.71	90.95	1283.66	43.6
RBW-C	2/28/2011	321.70	874.84	1196.54	202.63	462.87	665.50	119.07	411.97	531.04	55.6
RBW-D	2/28/2011	217.98	504.72	722.70	138.27	358.33	496.60	79.71	146.39	226.10	68.7

Conclusions and Implications for Future Research

Differences among the Research Project T-1 treatments are expected to become increasingly evident 3–5 years after implementation. We are reporting here the results after only a single growing season. Nevertheless, we can draw a number of important conclusions from these results.

1. On MCBCL, loblolly pine stands with dense woody understories and midstories typically occur on wetter sites with higher amounts of SOM compared to sites that typically support longleaf pine savanna vegetation. This is partly a consequence of the fact that moister sites were historically favored for agricultural and silvicultural development. But it is also due in part to the impacts of this conversion and the exclusion of fires on soils.
2. Variation in plant species composition and diversity among loblolly pine stands is directly correlated with variations in soil characteristics including SOM, bulk density, and CEC. Loblolly sites at the wet end of this gradient share many species in common with pocosins. Sites at the dryer end of this gradient are more likely to support species that are common in longleaf pine savannas.
3. Prescribed burning alone reduces the density of understory/midstory woody plants (1–20 cm dbh) by an average of 88%. However, dormant season thinning results in 63% fewer woody stems (for a total of 95% reduction) and growing season thinning results in 81% fewer understory stems (total of a 98% reduction) than prescribed burning alone. If these differences persist, they would indicate a possible benefit of growing season thinning compared to dormant season thinning.
4. Plant species richness was higher in thinned plots compared to unthinned control plots. However, there was no significant difference between dormant and growing season treatments. No treatment effects were evident for either arthropod or bird species richness.
5. NMS ordinations suggest possible change in plant and bird species composition in thinned treatments compared to unthinned controls. However, future measurements will be required to measure any actual trends.
6. Across treatment plots, there were very strong correlations between soil characteristics and vegetation composition and between vegetation composition and bird community composition. Correlations with arthropod community composition were much weaker.
7. Fuel moisture content is generally lower in thinned compared to unthinned control treatments.
8. Understory thinning generally increases fuel amounts and, therefore, the total amount of fuel consumed in prescribed fires. Furthermore, understory/midstory redistributes fuels to the forest floor and facilitates surface fires that are consistent with overall restoration objectives.
9. Research Project T-1 began a year later than other DCERP research projects, and it was centered on a field experiment that involved large scale manipulations such as thinning treatments and prescribed burning. Weather conditions required that the prescribed

burning program be extended for some of the treatment blocks into winter 2011. Responses among the key independent variables (i.e., plant, arthropod, and avian composition and richness) are expected to occur over several years.

These early results have a number of implications for MCBCL and for other installations with similar restoration programs.

- Understory/midstory thinning followed by prescribed burning produces significant change in plant species richness and composition after a single growing season. These changes are consistent with restoration objectives.
- Understory/midstory thinning of pine stands on moist sites with organic soils may provide benefits for the MCBCL training mission, but such stands appear to have low potential for restoration of plant and animal composition associated with longleaf pine.
- Although prescribed burning without thinning reduces the density of understory shrubs and trees, thinning treatments during the growing season are significantly more effective. In any case, continued suppression of woody growth will depend on the maintenance of regular prescribed burns.
- In the short term, there appear to be no significant differences between growing season and non-growing season thinning treatments with regard to impacts on fuels or on the composition and diversity of plants, arthropods, and birds.
- Management that specifically targets habitat conditions for the RCW has favorable effects on the biodiversity of terrestrial ecosystems in general.

These relatively early results suggest that significant treatment effects are likely to emerge when these plots are resampled in 2–3 years. That said, the unique patterns observed in arthropod species composition and diversity compared to either plants or birds demand further investigation. For example, further analysis of these data may reveal correlations within particular ecological guilds of insects. Such results would be an important guide to the refinement of sampling protocols for these animals.

Although it has not been an objective of this research project, we have gathered vegetation, soil and fuel data in such a way as to provide a basis for the assessment of future changes in carbon storage. Thinning and prescribed burning represent major manipulations of ecosystem carbon pools and likely influence subsequent carbon fluxes. These experimental plots provide an ideal laboratory for future studies of these changes.

Literature Cited

- Andrews, P.L., and L.S. Bradshaw. 1997. *FIRES: Fire Information Retrieval and Evaluation System—A Program for Fire Danger Rating Analysis*. General Technical Report INT-GTR-367. U.S. Department of Agriculture, Forest Service, Intermountain Research Station.
- Bailey, A.D., R. Mickler, and C. Frost. 2007. Presettlement fire regime and vegetation mapping in Southeastern Coastal Plain forest ecosystems. Pp. 275–286 in *The Fire Environment—Innovations, Management, and Policy Conference Proceedings*, Destin, FL. March 26–30. Edited by B.W. Butler, and W. Cook. Proceedings RMRS-P-46CD. Fort Collins, CO: U.S. Department of Agriculture, Forest Service, Rocky Mountain Research Station.
- Bollen K.A. 1989. *Structural Equations with Latent Variables*. John Wiley & Sons: New York.
- Christensen, N.L. 2000. Vegetation of the Coastal Plain of the southeastern United States. Pp. 397–448 in M. Barbour and W. D. Billings (eds.). *Vegetation of North America* (2nd ed.). Cambridge University Press.
- Christensen, N.L. 1992. Variable fire regimes on complex landscapes: Ecological consequences, policy implications, and management strategies. Pp. ix–xiii in *Fire in the Environment*. Edited by T. Waldrop, USDA FS General Technical Report SE-69.
- Christensen, N.L., R.B. Wilbur, and J.S. McLean. 1988. *Soil-Vegetation Correlations in Pocosins of Croatan National Forest, North Carolina*. U.S. Fish and Wildlife Service, Fort Collins, CO.
- Christensen, N.L. 1981. Fire regimes in southeastern ecosystems. Pp. 112–136 in *Fire Regimes and Ecosystem Properties*. Edited by H.A. Mooney, T.M. Bonnicksen, N.L. Christensen, J.E. Lotan, and W.A. Reiniers. U.S. Department of Agriculture Forest Service General Technical Report WO-26. 594 pages.
- Crowley, A.E. 1996. *This Land, This South: An Environmental History*. University of Kentucky Press: Lexington, KY.
- Dufrêne, M., and P. Legendre. 1997. Species assemblages and indicator species: The need for a flexible asymmetrical approach. *Ecological Monographs* 67:345–366.
- Early, L.S. 2004. *Looking for Longleaf*. University of North Carolina Press: Chapel Hill, NC.
- Finney, M.A. 1998. FARSITE: fire area simulation model development and evaluation Research Paper RMRS-4. USDA Forest Service, Rocky Mountain Research Station, Fort Collins, CO. Grace, J.B. 2006. *Structural equation modeling and natural systems*. Cambridge University Press: Cambridge, UK.

- Grace, J., and K. Bollen. 2008. Representing general theoretical concepts in structural equation models: The role of composite variables. *Environmental and Ecological Statistics* 15:191–213.
- Grace J.B., T.M. Anderson, H. Olff, and S.M. Scheiner. 2010. On the specification of structural equation models for ecological systems. *Ecological Monographs* 80:67–87.
- Grace, J.B., and J.E. Keeley. 2006. A structural equation model analysis of postfire plant diversity in California shrublands. *Ecological Applications* 16:503–514.
- Grace, J.B., and K.A. Bollen. 2005. Interpreting the results from multiple regression and structural equation models. *Bulletin of the Ecological Society of America* 86:283–295.
- Harmon, M.E., and J. Sexton. 1996. *Guidelines for measurements of woody detritus in forest ecosystems*. Publication No. 20. U.S. LTER Network Office, University of Washington, Seattle, WA.
- Kruskal, J.B., and M. Wish. 1978. Multidimensional scaling. Sage Publications: Beverly Hills, CA.
- Korhonen, L. and J. Heikkinen. 2009. Automated analysis of in situ canopy images for the estimation of forest canopy cover. *Forest Science* 55(4): 323–334.
- Malaise, R. 1937. A new insect trap. *Entomologisk Tidskrift* 58:257–271.
- McCune, B., and J.B. Grace. 2002. Analysis of ecological communities. MjM Software Design: Gleneden Beach.
- McCune, B., J.B. Grace, and D.L. Urban. 2002. *Analysis of Ecological Communities*. Gleneden Beach, OR: MjM Software Design.
- McLean, E.O. 1982. Soil pH and lime requirement. Pp. 199–223 in *Methods of Soil Analysis, Part 2*. Agronomy Monograph 9, Second edition. Edited by A.L. Page, R.H. Miller, and D.R. Keeney. ASA and SSSA: Madison, WI.
- Mehlich, A. 1984. Mehlich-3 soil test extractant: A modification of Mehlich-2 extractant. *Communications in Soil Science and Plant Analysis* 15:1409–1416.
- Nowacki, G.J., and M.D. Abrams. 2008. The demise of fire and the “mesophication” of forests in the eastern United States. *Bioscience* 58:124–138.
- Peet, R.K. 2006. Ecological classification of longleaf pine woodlands. Pp 51–94 in *Longleaf Pine Ecosystems: Ecology, Management, and Restoration*. Edited by S. Jose, E. Jokela, and D. Miller. Springer: New York, NY.
- Peet, R.K., T.R. Wentworth, and P.S. White. 1998. A flexible, multipurpose method for recording vegetation composition and structure. *Castanea* 63(3):262–274.

- Provencher, L., A.R. Litt, and D.R. Gordon. 2003. Predictors of species richness in northwest Florida longleaf pine sandhills. *Conservation Biology* 17:1660–1671.
- Provencher, L., N.M. Gobris, L.A. Brennan, D.R. Gordon, and J.L. Hardesty. 2002. Breeding bird response to midstory hardwood reduction in Florida sandhill longleaf pine forests. *Journal of Wildlife Management* 66:641–661.
- Provencher, L., B.J. Herring, D.R. Gordon, H.L. Rodgers, G.W. Tanner, J.L. Hardesty, L.A. Brennan, and A.R. Litt. 2001a. Longleaf pine and oak responses to hardwood reduction techniques in fire-suppressed sandhills in northwest Florida. *Forest Ecology and Management* 148:63–77.
- Provencher, L., B.J. Herring, D.R. Gordon, H.L. Rodgers, K.E.M. Galley, G.W. Tanner, J.L. Hardesty, and L.A. Brennan. 2001b. Effects of hardwood reduction techniques on longleaf pine sandhill vegetation in northwest Florida. *Restoration Ecology* 9:13–27.
- Ross, D. 1995. Recommended soil tests for determining exchange capacity. Pp. 62–69 in *Recommended Soil Testing Procedures for the Northeastern United States*. Northeastern Regional Bulletin #493. Edited by J.T. Sims, and A. Wolf. Ag Experiment Station: University of Delaware, Newark. DE. USFWS 2003.
- USFWS (U.S. Fish and Wildlife Service). 2003. *Red-cockaded Woodpecker (Picoides borealis) Recovery Plan: Second Revision*. U.S. Fish and Wildlife Service, Atlanta, GA.
- Venables, W.N. 2011. *An Introduction to R: Version 2.13.2*. Available at <http://cran.r-project.org/doc/manuals/R-intro.pdf>. Accessed June 13, 2012.
- Walker, J., and R.K. Peet, 1983. Composition and species diversity of pine-wire grass savannas of the Green Swamp, North Carolina. *Vegetatio* 55:163–179.

[This page intentionally left blank.]

Appendix 13-A

List of Species Encountered in 85 MCBCL Pine Monitoring Plots

List of Species Encountered in 85 MCBCL Pine Monitoring Plots

Species codes refer to acronyms used in field notes and in various computer analyses.

	Species Name	Species Code
1.	<i>Andropogon ternarius</i> , <i>A. elliottii</i> , <i>Schizachyrium scoparium</i> , <i>A. virginicus</i>	ANDCOM
2.	<i>Acer rubrum</i>	ACERUB
3.	<i>Agalinis fasciculate</i>	AGAFAS
4.	<i>Agalinis setacea</i>	AGASET
5.	<i>Aletris farinose</i>	ALEFAR
6.	<i>Amelanchier Canadensis</i>	AMECAN
7.	<i>Amorpha herbacea</i>	AMOHER
8.	<i>Andropogon capillipes</i>	ANDCAP
9.	<i>Andropogon glaucopsis</i>	ANDGLA
10.	<i>Andropogon glomeratus</i> var. <i>glomeratus</i>	ANDGLO
11.	<i>Andropogon glomeratus</i> var. <i>hirsutior</i>	ANDGLOH
12.	<i>Andropogon mohrii</i>	ANDMOH
13.	<i>Antennaria plantaginifolia</i>	ANTPLA
14.	<i>Aristida stricta</i>	ARISTR
15.	<i>Aristida virgate</i>	ARIVIR
16.	<i>Aronia arbutifolia</i>	AROARB
17.	<i>Aronia melanocarpa</i>	AROMEL
18.	<i>Arundinaria tecta</i>	ARUTEC
19.	<i>Asclepias</i>	ASCSP
20.	<i>Asclepias amplexicaulis</i>	ASCAMP
21.	<i>Asclepias humistrata</i>	ASCHUM
22.	<i>Asclepias pedicellata</i>	ASCPED
23.	<i>Asteraceae</i>	ASTSP
24.	<i>Baccharis halimifolia</i>	BACHAL
25.	<i>Bacopa</i>	BACOPA
26.	<i>Baptisia tinctoria</i>	BAPTIN
27.	<i>Bigelowia nudata</i> var. <i>nudata</i>	BIGNUD
28.	<i>Callicarpa Americana</i>	CALAME
29.	<i>Carex</i>	CARSPP
30.	<i>Carex reniformis</i>	CARREN
31.	<i>Carex striata</i> var. <i>brevis</i>	CARSTR

	Species Name	Species Code
32.	<i>Carphephorus paniculatus</i>	CARSPP
33.	<i>Carphephorus paniculatus</i> + <i>odor</i>	CARTOM
34.	<i>Carphephorus tomentosus</i>	CAROPP
35.	<i>Carya glabra</i>	CARGLA
36.	<i>Carya pallida</i>	CARPAL
37.	<i>Centella erecta</i>	CENERE
38.	<i>Cercis Canadensis</i>	CERCAN
39.	<i>Chamaecrista [nictitans + fasciculata]</i>	CHANPF
40.	<i>Chamaecyparis thyoides</i>	CHATHY
41.	<i>Chasmanthium</i>	CHAMAN
42.	<i>Chasmanthium laxum</i>	CHALAX
43.	<i>Chrysopsis gossypina</i>	CHRGOS
44.	<i>Chrysopsis mariana</i>	CHRMAR
45.	<i>Cirsium</i>	CIRSIU
46.	<i>Cirsium horridulum</i>	CIRHOR
47.	<i>Cirsium lecontei</i>	CIRLEC
48.	<i>Cirsium repandum</i>	CIRREP
49.	<i>Cirsium virginianum</i>	CIRVIR
50.	<i>Cirsium vulgare</i>	CIRVUL
51.	<i>Cleistes [bifaria + divaricata]</i>	CLEBPD
52.	<i>Clethra alnifolia</i>	CLEALN
53.	<i>Cnidoscolus stimulosus</i>	CNISTI
54.	<i>Comptonia</i>	COMPTON
55.	<i>Coreopsis falcate</i>	CORFAL
56.	<i>Coreopsis linifolia</i>	CORLIN
57.	<i>Coreopsis UK*</i>	CORUK
58.	<i>Coreopsis verticillata</i>	CORVER
59.	<i>Crataegus aprica</i>	CRAAPR
60.	<i>Crocianthemum carolinianum</i>	CROCAR
61.	<i>Crotalaria purshii</i>	CROPUR
62.	<i>Ctenium aromaticum</i>	CTEARO
63.	<i>Cuscuta</i>	CUSCUT
64.	<i>Cyperus retrorsus</i>	CYPRET
65.	<i>Cyrilla racemiflora</i>	CYRRAC

	Species Name	Species Code
66.	<i>Desmodium</i>	DESSPP
67.	<i>Desmodium ciliare</i>	DESCIL
68.	<i>Desmodium glabellum</i>	DESGLA
69.	<i>Desmodium lineatum</i>	DESLIN
70.	<i>Desmodium marilandicum</i>	DESMAR
71.	<i>Desmodium obtusum</i>	DESOBT
72.	<i>Desmodium paniculatum</i>	DESPAN
73.	<i>Desmodium perplexum</i>	DESPER
74.	<i>Desmodium tenuifolium</i>	DESTEN
75.	<i>Dichantherium</i>	DICSPP
76.	<i>Dichantherium [longiligulatum + ensifolium]</i>	DICLPE
77.	<i>Dichantherium strigosum</i>	DICSLS
78.	<i>Dichantherium aciculare</i>	DICACI
79.	<i>Dichantherium angustifolium</i>	DICANG
80.	<i>Dichantherium arenicoloides</i>	DICARE
81.	<i>Dichantherium chamaelonche ssp. chamaelonche</i>	DICCHA
82.	<i>Dichantherium commutatum</i>	DICCOM
83.	<i>Dichantherium commutatum var. ashei</i>	DICCOM
84.	<i>Dichantherium consanguineum</i>	DICCON
85.	<i>Dichantherium dichotomum</i>	DICDIC
86.	<i>Dichantherium dichotomum var. dichotomum</i>	DICDID
87.	<i>Dichantherium ensifolium</i>	DICENS
88.	<i>Dichantherium mattamuskeetense</i>	DICMAT
89.	<i>Dichantherium ovale</i>	DICOVA
90.	<i>Dichantherium ovale var. addisonii</i>	DICOVA
91.	<i>Dichantherium ovale var. ovale</i>	DICOPO
92.	<i>Dichantherium portoricense</i>	DICPOR
93.	<i>Dichantherium portoricense ssp. Patulum</i>	DICPSP
94.	<i>Dichantherium portoricense ssp. Portoricense</i>	DICPSO
95.	<i>Dichantherium portoricense X</i>	DICPSX
96.	<i>Dichantherium scoparium</i>	DICSCO
97.	<i>Dichantherium species 2</i>	DICSP2
98.	<i>Dichantherium sphaerocarpon</i>	DICSPH
99.	<i>Dichantherium strigosum</i>	DICSTR

	Species Name	Species Code
100.	<i>Dichanthelium strigosum</i> var. <i>glabrescens</i>	DICSPG
101.	<i>Dichanthelium strigosum</i> var. <i>leucoblepharis</i>	DICSPL
102.	<i>Dichanthelium strigosum</i> var. <i>strigosum</i>	DICSPS
103.	<i>Dichanthelium tenue</i>	DICTEN
104.	<i>Dichanthelium villosissimum</i> var. <i>villosissimum</i>	DICVIL
105.	<i>Diodia virginiana</i>	DIOVIR
106.	<i>Dionaea</i>	DIONAE
107.	<i>Dionaea muscipula</i>	DIOMUS
108.	<i>Dioscorea</i>	DIOSCO
109.	<i>Diospyros virginiana</i>	DIOVIR
110.	<i>Drosera</i> [<i>brevifolia</i> + <i>capillaris</i>]	DROBPC
111.	<i>Drosera brevifolia</i>	DROBRE
112.	<i>Elephantopus nudatus</i>	ELEPHA
113.	<i>Eragrostis refracta</i>	ERAREF
114.	<i>Eragrostis spectabilis</i>	ERASPE
115.	<i>Erigeron strigosus</i> var. <i>strigosus</i>	ERISTR
116.	<i>Erigeron vernus</i>	ERIVER
117.	<i>Eubotrys racemosa</i>	EUBRAC
118.	<i>Eupatorium</i>	EUPSPP
119.	<i>Eupatorium</i> [<i>mohrii</i> + <i>recurvans</i>]	EUPMPR
120.	<i>Eupatorium album</i>	EUPALB
121.	<i>Eupatorium capillifolium</i>	EUPCAP
122.	<i>Eupatorium hyssopifolium</i>	EUPHYS
123.	<i>Eupatorium leucolepis</i>	EUPLEU
124.	<i>Eupatorium linearifolium</i>	EUPLIN
125.	<i>Eupatorium mohrii</i>	EUPMOH
126.	<i>Eupatorium pilosum</i>	EUPPIL
127.	<i>Eupatorium rotundifolium</i>	EUPROT
128.	<i>Euphorbia curtisii</i>	EUPCUR
129.	<i>Euphorbia ipecacuanhae</i>	EUPIPE
130.	<i>Eurybia compacta</i>	EURCOM
131.	<i>Eurybia paludosa</i>	EURPAL
132.	<i>Euthamia caroliniana</i>	EUTCAR
133.	<i>Fimbristylis annua</i>	FIMANN

	Species Name	Species Code
134.	<i>Galactia [regularis + volubilis var. volubilis]</i>	GALRVV
135.	<i>Galactia erecta</i>	GALERE
136.	<i>Galactia regularis</i>	GALREG
137.	<i>Galactia volubilis var. volubilis</i>	GALVPV
138.	<i>Gaylussacia dumosa</i>	GAYDUM
139.	<i>Gaylussacia frondosa</i>	GAYFR
140.	<i>Gaylussacia tomentosa</i>	GAYTOM
141.	<i>Gelsemium sempervirens</i>	GELSEM
142.	<i>Gentiana autumnalis</i>	GENAUT
143.	<i>Gleditsia triacanthos</i>	GLETRI
144.	<i>Gnaphalium</i>	GNAPHA
145.	<i>Gordonia lasianthus</i>	GORLAS
146.	<i>Gymnopogon brevifolius</i>	GYMBRE
147.	<i>Helianthus angustifolius</i>	HELANG
148.	<i>Helianthus atrorubens</i>	HELATR
149.	<i>Helianthus heterophyllus</i>	HELHET
150.	<i>Hexastylis</i>	HEXAST
151.	<i>Hieracium gronovii</i>	HIEGRO
152.	<i>Hieracium marianum</i>	HIEMAR
153.	<i>Hydrocotyle bonariensis</i>	HYDBON
154.	<i>Hypericum cistifolium</i>	HYPCIS
155.	<i>Hypericum crux-andreae</i>	HYPCRU
156.	<i>Hypericum hypericoides</i>	HYPHYP
157.	<i>Hypericum setosum</i>	HYPSET
158.	<i>Hypericum tenuifolium</i>	HYPTEN
159.	<i>Hypoxis hirsuta</i>	HYPHIR
160.	<i>Hypoxis juncea</i>	HYPJUN
161.	<i>Ilex coriacea</i>	ILECOR
162.	<i>Ilex glabra</i>	ILEGLA
163.	<i>Ilex opaca var. opaca</i>	ILEOPA
164.	<i>Ilex vomitoria</i>	ILEVOM
165.	<i>Ionactis linariifolia</i>	IONLIN
166.	<i>Ipomoea</i>	IPOMOE
167.	<i>Iris verna var. verna</i>	IRIVER

	Species Name	Species Code
168.	<i>Juncus</i>	JUNSP
169.	<i>Juncus acuminatus</i>	JUNACU
170.	<i>Juncus biflorus</i>	JUNBIF
171.	<i>Juncus canadensis</i>	JUNCAN
172.	<i>Juncus dichotomus</i>	JUNDIC
173.	<i>Juncus scirpoides</i>	JUNSCI
174.	<i>Kalmia carolina</i>	KALCAR
175.	<i>Lachnocaulon anceps</i>	LACANC
176.	<i>Lactuca canadensis</i>	LACCAN
177.	<i>Lechea [pulchella var. ramosissima + torreyi var. congesta]</i>	LECPRT
178.	<i>Lechea minor</i>	LECMIN
179.	<i>Lechea pulchella var. ramosissima</i>	LECPPR
180.	<i>Lechea tenuifolia</i>	LECTEN
181.	<i>Lespedeza angustifolia</i>	LESA
182.	<i>Lespedeza capitata</i>	LESCAP
183.	<i>Lespedeza hirta</i>	LESHIR
184.	<i>Lespedeza hirta var. curtissii</i>	LESHPC
185.	<i>Lespedeza hirta var. hirta</i>	LESHPH
186.	<i>Lespedeza virginica</i>	LESVIR
187.	<i>Leucothoe axillaris</i>	LECAXI
188.	<i>Liatris [pilosa + virgata]</i>	LIAPPV
189.	<i>Liatris spicata</i>	LIASPI
190.	<i>Liatris spicata var. resinosa</i>	LIASPI
191.	<i>Linum floridanum</i>	LINFLO
192.	<i>Liquidambar styraciflua</i>	LIQSTY
193.	<i>Liriodendron tulipifera</i>	LIRTUL
194.	<i>Lobelia nuttallii</i>	LOBNUT
195.	<i>Ludwigia virgata</i>	LUDVIR
196.	<i>Lycopodiella alopecuroides</i>	LYCALO
197.	<i>Lycopodium</i>	LYCOPO
198.	<i>Lyonia ligustrina</i>	LYOLIG
199.	<i>Lyonia ligustrina var. foliosiflora</i>	LYOLIG
200.	<i>Lyonia lucida</i>	LYOLUC
201.	<i>Lyonia mariana</i>	LYOMAR

	Species Name	Species Code
202.	<i>Lysimachia loomisii</i>	LYSLOO
203.	<i>Magnolia virginiana</i>	MAGVIR
204.	<i>Marshallia graminifolia</i>	MARGRA
205.	<i>Mikania scandens</i>	MIKSCA
206.	<i>Mitchella repens</i>	MITREP
207.	<i>Morella caroliniensis</i>	MORCAR
208.	<i>Morella cerifera</i>	MORCER
209.	<i>Morella pumila</i>	MORPUM
210.	<i>Muhlenbergia expansa</i>	MUHEXP
211.	<i>Nyssa sylvatica</i>	NYSSYL
212.	<i>Orbexilum pedunculatum</i> var. <i>psoralioides</i>	ORBPED
213.	<i>Osmunda cinnamomea</i> var. <i>cinnamomea</i>	OSMCIN
214.	<i>Osmunda regalis</i>	OSMREG
215.	<i>Osmunda regalis</i> var. <i>spectabilis</i>	OSMRPS
216.	<i>Oxypolis denticulata</i>	OXYDEN
217.	<i>Panicum amarum</i>	PANAMA
218.	<i>Panicum anceps</i>	PANANC
219.	<i>Panicum anceps</i> var. <i>rhizomatum</i>	PANAPR
220.	<i>Panicum virgatum</i>	PANVIR
221.	<i>Parthenium</i>	PARSPP
222.	<i>Parthenocissus quinquefolia</i>	PARQUI
223.	<i>Paspalum praecox</i> var. <i>praecox</i>	PASPRA
224.	<i>Paspalum setaceum</i> var. <i>stramineum</i>	PASSET
225.	<i>Persea palustris</i>	PERPAL
226.	<i>Picea</i>	PICSPP
227.	<i>Pinus palustris</i>	PINPAL
228.	<i>Pinus serotina</i>	PINSER
229.	<i>Pinus taeda</i>	PINTAE
230.	<i>Pityopsis graminifolia</i>	PITGRA
231.	<i>Platanthera</i>	PLATAN
232.	<i>Platanthera ciliaris</i>	PLACIL
233.	<i>Pleea tenuifolia</i>	PLETEN
234.	<i>Pluchea baccharis</i>	PLUBAC
235.	<i>Polygala</i> [<i>brevifolia</i> + <i>hookeri</i> + <i>cruciata</i>]	POLBHC

	Species Name	Species Code
236.	<i>Polygala brevifolia</i>	POLBRE
237.	<i>Polygala cruciata</i>	POLCRU
238.	<i>Polygala incarnata</i>	POLINC
239.	<i>Polygala lutea</i>	POLLUT
240.	<i>Potentilla</i>	POTSPP
241.	<i>Prenanthes</i>	PRESPP
242.	<i>Prunus serotina</i>	PRUSER
243.	<i>Pteridium aquilinum</i> var. <i>pseudocaudatum</i>	PTEAQU
244.	<i>Pterocaulon pycnostachyum</i>	PTEPYC
245.	<i>Pycnanthemum flexuosum</i>	PYCFLE
246.	<i>Pyxidanthera barbulata</i>	PYXBAR
247.	<i>Quercus</i>	QUESPP
248.	<i>Quercus falcata</i>	QUEFAL
249.	<i>Quercus geminata</i>	QUEGEM
250.	<i>Quercus hemisphaerica</i>	QUEHEM
251.	<i>Quercus incana</i>	QUEINC
252.	<i>Quercus incana</i> X <i>marilandica</i>	QUEIXM
253.	<i>Quercus laevis</i>	QUELAE
254.	<i>Quercus laevis</i> X <i>marilandica</i>	QUELXM
255.	<i>Quercus margaretta</i>	QUEMAR
256.	<i>Quercus marilandica</i>	QUEMVM
257.	<i>Quercus marilandica</i> var. <i>marilandica</i>	QUEMPM
258.	<i>Quercus michauxii</i>	QUEMIC
259.	<i>Quercus nigra</i>	QUENIG
260.	<i>Quercus stellata</i>	QUESTE
261.	<i>Quercus virginiana</i>	QUEVIR
262.	<i>Quercus xashei</i>	QUEXASH
263.	<i>Quercus xcaduca</i>	QUEXCA
264.	<i>Quercus xincomita</i>	QUEXIN
265.	<i>Rhexia</i> [<i>nashii</i> + <i>mariana</i> var. <i>mariana</i>]	RHENMM
266.	<i>Rhexia alifanus</i>	RHEALI
267.	<i>Rhexia lutea</i>	RHELUT
268.	<i>Rhexia mariana</i>	RHEMAR
269.	<i>Rhexia nashii</i>	RHENAS

	Species Name	Species Code
270.	<i>Rhexia petiolata</i>	RHEPET
271.	<i>Rhizophora</i>	RHIZOP
272.	<i>Rhododendron atlanticum</i>	RHOATL
273.	<i>Rhus copallinum</i>	RHUCOP
274.	<i>Rhynchosia tomentosa</i>	RHYTOM
275.	<i>Rhynchospora</i>	RHYSPP
276.	<i>Rhynchospora baldwinii</i>	RHYBAL
277.	<i>Rhynchospora divergens</i>	RHYDIV
278.	<i>Rhynchospora fascicularis</i> var. <i>distans</i>	RHYFVD
279.	<i>Rhynchospora fascicularis</i> var. <i>fascicularis</i>	RHYFVF
280.	<i>Rhynchospora grayi</i>	RHYGRA
281.	<i>Rhynchospora harveyi</i>	RHYHAR
282.	<i>Rhynchospora plumosa</i>	RHYPLU
283.	<i>Robinia nana</i>	ROBSPP
284.	<i>Rubus</i>	RUBSPP
285.	<i>Sabatia difformis</i>	SABDIF
286.	<i>Saccharum</i>	SACCHA
287.	<i>Salix caroliniana</i>	SALCAR
288.	<i>Sarracenia flava</i>	SARFLA
289.	<i>Sarracenia rubra</i> x <i>flava</i>	SARRXF
290.	<i>Sassafras albidum</i>	SASALB
291.	<i>Schizachyrium scoparium</i>	SCHSCO
292.	<i>Scleria</i> [<i>ciliata</i> var. <i>ciliata</i> + <i>elliottii</i>]	SCLCCE
293.	<i>Scleria</i> [<i>ciliata</i> var. <i>glabra</i> + <i>pauciflora</i> var. <i>pauciflora</i>]	SCLCGP
294.	<i>Scleria</i> [<i>nitida</i> + <i>triglomerata</i>]	SCLNPT
295.	<i>Scleria ciliate</i>	SCLCIL
296.	<i>Scleria ciliata</i> var. <i>ciliata</i>	SCLCVC
297.	<i>Scleria ciliata</i> var. <i>glabra</i>	SCLCVG
298.	<i>Scleria nitida</i>	SCLNIT
299.	<i>Scleria oligantha</i>	SCLOLI
300.	<i>Scleria pauciflora</i> var. <i>pauciflora</i>	SCLPVP
301.	<i>Scleria triglomerata</i>	SCLTRI
302.	<i>Sericocarpus asteroides</i>	SERAST
303.	<i>Sericocarpus linifolius</i>	SERLIN

	Species Name	Species Code
304.	<i>Sericocarpus tortifolius</i>	SERTOR
305.	<i>Seymeria cassioides</i>	SEYCAS
306.	<i>Silphium compositum</i>	SILCOM
307.	<i>Sisyrinchium capillare</i>	SISCAP
308.	<i>Smilax bona-nox</i>	SMIBON
309.	<i>Smilax glauca</i>	SMIGLA
310.	<i>Smilax laurifolia</i>	SMILAU
311.	<i>Smilax rotundifolia</i>	SMIROT
312.	<i>Solidago arguta</i>	SOLARU
313.	<i>Solidago odora</i>	SOLODO
314.	<i>Solidago odora</i> var. <i>odora</i>	SOLOVO
315.	<i>Solidago pulchra</i>	SOLPUL
316.	<i>Solidago stricta</i>	SOLSTR
317.	<i>Sophronanthe pilosa</i>	SOPPIL
318.	<i>Sorbus americana</i>	SORAME
319.	<i>Spiranthes</i>	SPISPP
320.	<i>Spiranthes eatonii</i>	SPIEAT
321.	<i>Spiranthes lacera</i> var. <i>gracilis</i>	SPILVG
322.	<i>Spiranthes praecox</i>	SPIPra
323.	<i>Sporobolus pinetorum</i>	SPOPIN
324.	<i>Stylosanthes biflora</i>	STYBIF
325.	<i>Symphyotrichum concolor</i>	SYMCON
326.	<i>Symphyotrichum concolor</i> var. <i>concolor</i>	SYMVCV
327.	<i>Symphyotrichum dumosum</i> var. <i>dumosum</i>	SYMDVD
328.	<i>Symphyotrichum tenuifolium</i>	SYMTEU
329.	<i>Symphyotrichum walteri</i>	SYMWAL
330.	<i>Symplocos tinctoria</i>	SYMTIN
331.	<i>Tephrosia florida</i>	TEPFLO
332.	<i>Tephrosia hispidula</i>	TEPHIS
333.	<i>Toxicodendron pubescens</i>	TOXPUB
334.	<i>Toxicodendron radicans</i>	TOXRAD
335.	<i>Toxicodendron radicans</i> var. <i>radicans</i>	TOXRVR
336.	<i>Tragia urens</i>	TRAURE
337.	<i>Uvularia puberula</i>	UVUPUB

	Species Name	Species Code
338.	<i>Vaccinium arboreum</i>	VACARB
339.	<i>Vaccinium corymbosum</i>	VACCOR
340.	<i>Vaccinium crassifolium</i>	VACCRA
341.	<i>Vaccinium formosum</i>	VACFOR
342.	<i>Vaccinium fuscatum</i>	VACFUS
343.	<i>Vaccinium stamineum</i>	VASTA
344.	<i>Vaccinium tenellum</i>	VACTEN
345.	<i>Viola primulifolia</i>	VIOPRI
346.	<i>Viola septemloba</i>	VIOSEP
347.	<i>Vitis rotundifolia</i>	VITROT
348.	<i>Vitis rotundifolia</i> var. <i>rotundifolia</i>	VITRVR
349.	<i>Woodwardia areolata</i>	WOOARE
350.	<i>Woodwardia virginica</i>	WOOVIR
351.	<i>Xyris ambigua</i>	XYRAMB
352.	<i>Xyris caroliniana</i>	XYRCAR
353.	<i>Zigadenus glaberrimus</i>	ZIGGLA
354.	<i>Zenobia pulverulenta</i>	ZENPUL

Appendix 13-B

NMS Axis 1 and Axis 2 Scores for 85 Pine-Dominated Permanent MCBCL Vegetation Monitoring Plots

**NMS Axis 1 and Axis 2 Scores for 85 Pine-Dominated Permanent
MCBCL Vegetation Monitoring Plots**

Dominant Pine refers to the most important pine species in each plot: PP = longleaf pine (*Pinus palustris*), PT = loblolly pine (*Pinus taeda*), and PS = pond pine (*Pinus serotina*).

	Plot Name	Dominant Pine	NMS Axis 1	NMS Axis 2
1.	6x-1-53	PP	0.61419	-0.4719
2.	6x-1-54	PP	0.74759	-0.47243
3.	6x-1-58	PP	0.90756	0.17752
4.	6x-2-54	PP	0.86571	-0.41059
5.	6x-2-58	PP	0.69034	-0.21325
6.	6x-2-59	PP	0.1569	0.14158
7.	6x-3-51	PP	0.82855	-0.37238
8.	6x-3-53	PP	0.49165	0.33787
9.	6x-4-53	PP	0.62017	-0.27774
10.	6x-4-54	PP	1.12505	-0.41213
11.	6x-4-56	PP	0.42528	-0.3012
12.	6x-4-57	PP	0.67587	-0.45495
13.	6x-4-58	PP	0.81135	-0.33025
14.	6x-4-59	PP	0.80338	-0.22602
15.	6x-5-54	PP	0.72381	-0.10248
16.	6x-5-55	PP	0.87677	-0.36766
17.	6x-5-58	PP	1.14166	-0.19049
18.	6x-5-59	PP	0.27532	-0.02883
19.	6x-5-60	PP	0.49802	-0.22684
20.	6x-8-1	PP	0.59131	-0.25772
21.	6x-8-2	PP	0.10175	-0.35128
22.	6x-8-3	PP	0.89967	-0.06008
23.	6x-8-4	PP	0.32478	-0.48416
24.	6x-8-5	PP	1.02055	-0.2142
25.	CR1	PP	0.30001	0.45959
26.	CT1	PP	1.14257	-0.08891
27.	CT2	PP	0.85287	-0.13465
28.	CT4	PP	0.9508	0.05422
29.	DC2	PP	0.89926	0.01509
30.	FGE-C	PT	-1.52872	-0.68128

	Plot Name	Dominant Pine	NMS Axis 1	NMS Axis 2
31.	FGW-C	PT	-1.53495	-0.62361
32.	FGE-G	PT	-0.62774	-0.17138
33.	FGW-G	PT	-1.02088	-0.34787
34.	FGE-D	PT	-1.09509	-0.06874
35.	FGW-D	PT	-0.23701	-0.10289
36.	GT1	PP	0.63212	-0.18651
37.	GT2	PP	0.87831	-0.1331
38.	GT3	PP	0.76711	-0.00474
39.	GT4	PP	0.7568	0.09355
40.	GT6	PP	0.90209	-0.26664
41.	HA-C	PT	-1.11971	0.29928
42.	HA-G	PT	-0.51165	0.22852
43.	HA-D	PT	-0.56809	0.32073
44.	IEN-C	PT	-1.28177	-0.49336
45.	IES-C	PS	-1.54982	-0.31862
46.	IEN-G	PT	-0.95642	0.04131
47.	IES-G	PS	-1.40092	0.20367
48.	IEN-D	PT	-1.37066	0.70397
49.	IES-D	PS	-1.3678	-0.55005
50.	MC-C	PT	-0.79124	-0.16841
51.	MF-G	PT	-1.27222	0.25251
52.	MF-D	PT	-0.76833	0.15511
53.	NE2	PP	0.65591	-0.02674
54.	NE4	PP	0.46299	0.00071
55.	PN17	PP	1.00596	0.3882
56.	PN18	PP	0.83674	0.98564
57.	PN19	PS	-0.08364	-0.38343
58.	PN23	PP	1.05941	0.21936
59.	PN33	PP	-0.61837	1.03024
60.	PN34	PP	0.33835	0.21189
61.	PN39	PP	0.36928	0.27189
62.	PN47	PT	0.00458	1.55609
63.	PN51	PP	0.31335	1.33316
64.	PN60	PP	-0.28137	-0.34093

	Plot Name	Dominant Pine	NMS Axis 1	NMS Axis 2
65.	PN62	PT	-0.1462	1.2726
66.	PN65	PP	0.09856	-0.07279
67.	PN66	PT	-0.65647	1.43361
68.	PN69	PP	0.36497	0.61174
69.	RBE-C	PT	-0.37976	1.19608
70.	RBW-C	PT	-0.17899	1.53099
71.	RBE-G	PT	-0.98429	1.05857
72.	RBW-G	PT	-0.75715	0.53483
73.	RBE-D	PT	-0.27122	0.65807
74.	RBW-D	PT	-0.64428	0.71765
75.	SC1	PP	-0.69305	-0.28208
76.	SC2	PP	0.31149	-0.64961
77.	VL2	PP	-0.00372	0.15791
78.	VL3	PP	-0.60865	-0.31306
79.	VL4	PP	-0.11169	-0.28379
80.	VL5	PP	-0.45343	-0.52996
81.	VL6	PP	0.11906	-1.54827
82.	POC11	PS	-1.46645	-1.01023
83.	POC12	PS	-1.20074	-1.09799
84.	POC9	PS	-1.05872	-0.81341
85.	POC10	PS	-0.63862	-0.73411

Appendix 13-C

Soil Data for 85 Pine-Dominated Permanent MCBCL Vegetation Monitoring Plots

For 85 MCBCL pine-dominated monitoring plots, averaged values for species richness (#/0.1 ha), stems <15 cm (#/ha), basal area (m²/ha), cation exchange capacity (CEC, milliequivalents/100 gm soil), bulk density (BD, g/cm³), pH, soil organic matter (SOM%), and extractable sulfur, orthophosphate (PO₄-P), calcium (Ca), magnesium (Mg), potassium (K), and aluminum (Al) in each of the experimental treatment plots. Extractable element concentrations are expressed in µg/g. “N/A” indicates missing data.

Plot Name	Species Richness	Stems <15 cm	Basal Area	CEC	BD	pH	SOM%	P	Ca	Mg	K	Al
1. 6x-01-0053	48	50	10.69	3.78	1.33	4.15	2.15	2.25	140.00	31.00	18.50	110.50
2. 6x-01-0054	46	20	30.34	5.01	1.16	4.28	3.28	1.00	221.75	32.50	24.75	119.75
3. 6x-01-0058	75	160	42.28	2.91	1.40	4.00	1.01	1.00	98.25	18.00	9.00	292.50
4. 6x-02-0054	45	120	56.81	5.22	1.16	4.40	3.97	2.25	228.00	42.25	36.00	186.00
5. 6x-02-0058	68	90	51.94	5.11	1.16	4.18	3.75	3.25	183.50	33.50	54.75	306.50
6. 6x-02-0059	91	50	28.03	3.66	1.24	4.18	2.90	1.50	126.00	23.00	20.75	391.25
7. 6x-03-0051	34	190	72.82	4.85	1.18	4.13	3.67	1.25	183.75	30.75	22.00	101.00
8. 6x-03-0053	118	160	33.05	2.68	1.26	4.18	2.43	1.50	100.50	16.00	20.00	798.00
9. 6x-04-0053	49	130	19.56	4.27	1.30	3.95	3.09	1.00	109.50	40.00	25.75	117.75
10. 6x-04-0054	32	130	11.59	4.23	1.14	4.80	4.46	2.50	254.50	34.00	26.75	89.25
11. 6x-04-0056	57	20	10.59	5.84	1.26	3.80	3.50	1.25	162.50	43.25	22.00	145.50
12. 6x-04-0057	49	130	45.43	2.89	1.36	4.10	1.90	1.00	101.25	20.75	14.75	52.50
13. 6x-04-0058	61	280	42.12	2.33	1.34	4.20	1.75	1.00	88.75	15.00	11.75	578.75
14. 6x-04-0059	68	110	27.10	6.06	1.26	4.30	3.16	2.75	286.75	31.00	31.75	172.75
15. 6x-05-0054	55	250	30.15	3.85	1.39	4.00	2.84	1.00	105.25	35.00	20.75	122.00
16. 6x-05-0055	72	140	26.24	2.55	1.40	4.38	1.45	1.25	121.75	19.50	16.00	401.50
17. 6x-05-0058	32	30	37.99	3.21	1.36	4.08	1.73	4.00	128.50	16.25	13.75	80.50
18. 6x-05-0059	84	190	41.45	3.01	1.14	3.88	4.01	2.75	77.25	21.00	20.25	713.00
19. 6x-05-0060	56	260	41.58	3.20	1.25	4.08	2.36	5.25	111.50	21.50	18.25	233.25
20. 6x-08-0001	91	110	110.88	8.30	0.95	3.85	10.64	2.50	267.50	50.00	37.75	277.75
21. 6x-08-0002	92	50	18.95	9.50	0.96	3.83	10.28	1.50	276.25	65.75	36.50	424.75

Plot Name	Species Richness	Stems <15 cm	Basal Area	CEC	BD	pH	SOM%	P	Ca	Mg	K	Al
22. 6x-08-0003	57	30	20.81	5.40	1.21	4.20	3.52	1.25	218.50	28.25	26.00	149.25
23. 6x-08-0004	60	70	6.38	11.12	1.04	3.73	10.51	1.25	302.50	83.50	56.25	149.75
24. 6x-08-0005	46	160	77.93	5.86	1.11	4.10	3.54	4.25	230.75	45.50	23.50	135.50
25. CR1	37	760	8.11	3.29	1.23	4.68	2.24	6.00	170.00	39.75	13.50	87.00
26. CT1	23	90	9.95	2.07	1.21	4.85	2.10	5.25	116.50	23.75	14.00	76.00
27. CR2	20	250	13.99	N/A	N/A	N/A	N/A	N/A	N/A	N/A	N/A	N/A
28. CT4	38	490	11.19	3.06	1.04	4.60	4.49	4.25	160.25	28.00	12.50	102.25
29. DC2	28	0	12.52	4.17	0.90	4.33	18.35	4.00	159.25	35.75	20.00	89.00
30. FGE-C	10	2,880	26.28	9.57	0.22	3.78	67.83	3.25	216.75	96.00	46.50	231.25
31. FGW-C	7	2,430	25.60	9.88	0.39	3.78	51.44	3.00	251.00	84.75	46.75	208.50
32. FGE-G	18	2,060	19.69	6.89	0.54	3.98	34.27	3.00	243.25	52.75	24.00	198.50
33. FGW-G	17	2,060	19.69	7.36	0.41	4.00	37.39	3.75	235.75	60.25	31.25	400.75
34. FGE-D	18	2,060	19.69	7.19	0.53	3.78	41.19	6.25	196.75	47.50	46.50	574.50
35. FGW-D	30	2,060	19.69	9.47	0.81	4.08	11.91	4.25	351.25	63.25	37.00	118.25
36. GT1	48	280	12.72	3.83	1.09	4.73	2.75	9.00	233.50	36.25	22.50	131.75
37. GT2	38	50	20.28	3.04	1.12	4.63	2.21	7.50	149.75	31.25	21.00	126.25
38. GT4	39	590	8.38	4.46	1.01	4.80	3.74	6.50	272.75	36.75	19.25	167.00
39. GT5	53	110	13.69	7.13	0.98	4.45	7.19	4.25	347.75	59.75	20.50	220.00
40. GT6	30	40	10.96	4.56	1.02	4.50	8.17	4.25	180.50	44.00	28.00	230.25
41. HAC	24	1,580	18.11	6.21	0.69	4.10	13.83	5.50	186.25	56.00	34.50	527.00
42. HAG	35	360	8.48	6.57	0.93	4.45	6.07	4.25	301.25	39.00	25.75	658.50
43. HAD	41	360	8.48	8.60	0.76	4.18	13.37	6.75	390.75	54.75	30.00	640.50
44. IEN-C	14	5,470	7.66	6.68	0.55	3.88	30.33	10.25	172.50	48.25	41.00	868.25
45. IES-C	12	100	19.78	7.93	0.30	3.73	68.12	3.75	93.75	103.00	77.25	167.75

Plot Name	Species Richness	Stems <15 cm	Basal Area	CEC	BD	pH	SOM%	P	Ca	Mg	K	Al
46. IEN-G	21	0	17.66	11.29	0.45	3.85	43.43	6.50	336.75	80.75	48.50	496.00
47. IES-G	13	350	13.59	10.74	0.50	3.93	33.82	5.00	346.75	69.75	43.25	418.75
48. IEN-D	23	1,880	10.23	7.42	0.59	3.85	33.67	6.25	170.50	71.75	41.00	786.00
49. IES-D	15	590	18.51	7.65	0.44	3.85	53.26	6.00	193.25	72.00	29.50	379.25
50. MFC	24	4,940	21.36	5.71	0.74	3.93	14.38	12.25	172.25	42.00	31.75	866.50
51. MFG	21	240	16.50	5.54	0.39	3.90	30.22	10.25	170.00	40.50	30.25	841.75
52. MFD	32	60	23.64	6.98	0.58	3.95	25.49	9.00	193.75	59.25	43.00	626.75
53. NE2	43	230	10.93	4.52	1.07	4.23	3.29	4.75	177.75	33.25	20.25	159.25
54. NE4	41	160	11.74	3.57	0.93	4.25	5.52	4.50	129.75	35.25	20.50	351.25
55. PN17	25	340	3.17	3.42	1.22	4.43	1.41	2.50	170.25	24.50	8.25	70.75
56. PN17	14	800	1.82	4.11	1.34	4.68	1.03	2.50	265.75	22.25	11.00	62.25
57. PN18	32	1,080	4.35	3.86	1.37	4.55	0.91	5.00	226.75	21.75	11.25	60.25
58. PN23	28	870	0.07	8.16	0.98	4.85	4.96	148.50	741.00	48.25	24.00	473.25
59. PN33	30	4,330	39.71	5.75	0.98	4.18	8.98	8.50	229.00	42.00	17.75	504.25
60. PN34	29	270	4.33	4.37	0.97	4.43	5.95	6.75	186.75	40.00	27.75	498.50
61. PN39	30	1,540	8.96	4.20	1.00	4.68	5.10	5.75	215.75	49.00	29.25	352.25
62. PN47	37	630	0.42	4.29	1.13	4.65	2.86	5.25	207.00	57.75	72.25	501.25
63. PN51	33	1,290	8.34	N/A	N/A	N/A	N/A	N/A	N/A	N/A	N/A	N/A
64. PN60	30	100	10.59	4.67	1.00	4.10	5.15	6.00	153.75	41.00	24.00	391.00
65. PN62	39	4,020	7.18	7.59	0.91	4.30	7.91	6.00	309.00	50.25	25.25	579.75
66. PN65	38	280	12.70	10.64	0.82	4.08	9.56	8.75	450.50	57.50	16.75	322.00
67. PN66	19	1,390	1.19	5.17	0.92	4.28	5.26	9.25	231.50	39.25	23.00	220.00
68. PN69	36	290	15.32	3.26	1.11	4.40	4.36	4.50	130.50	33.50	18.25	206.50
69. RBE-C	15	3,660	23.89	8.09	0.80	4.45	16.05	7.00	401.00	56.75	37.75	692.00

Plot Name	Species Richness	Stems <15 cm	Basal Area	CEC	BD	pH	SOM%	P	Ca	Mg	K	Al
70. RBW-C	13	3,340	26.08	4.97	1.01	4.43	5.69	7.50	229.25	47.00	36.00	852.00
71. RBE-G	33	110	13.31	9.64	0.85	4.03	7.95	10.50	369.50	64.50	33.00	545.00
72. RBW-G	32	30	19.07	8.03	0.90	4.23	6.52	7.25	359.00	56.75	30.50	393.75
73. RBE-D	29	910	18.37	4.54	1.05	4.60	5.18	6.50	242.00	40.25	28.50	382.75
74. RBW-D	40	2,920	22.05	10.04	0.66	4.23	17.92	8.25	458.75	83.50	66.50	361.50
75. SC1	29	1,010	9.20	4.82	1.08	4.15	5.96	5.50	171.75	43.00	17.00	232.25
76. SC2	24	1,120	12.86	3.95	1.21	4.30	2.51	3.75	160.75	31.50	16.75	131.00
77. VL2	40	0	13.54	5.26	0.85	4.05	8.05	3.50	176.50	44.25	20.25	254.75
78. VL3	44	50	12.85	4.77	0.90	3.98	9.39	4.75	120.00	53.00	17.00	256.50
79. VL4	43	880	12.64	1.63	0.96	4.10	5.34	3.38	9.13	30.25	12.00	462.75
80. VL5	33	3,530	12.89	3.92	0.86	4.08	6.91	5.50	122.50	36.00	27.25	339.25
81. VL6	30	50	8.77	5.38	0.94	4.05	4.91	6.25	174.75	47.25	27.00	137.25
82. POC11	9	N/A	N/A	3.78	0.71	4.95	21.69	3.50	138.00	98.00	23.75	127.75
83. POC12	10	N/A	N/A	4.38	0.44	4.55	41.41	3.50	167.25	74.25	23.25	174.50
84. POC9	14	N/A	N/A	6.70	0.78	4.58	8.01	9.25	410.50	56.00	30.75	604.25
85. POC10	28	N/A		3.79	0.92	4.70	5.12	3.50	175.75	48.50	17.75	170.00

[This page intentionally left blank.]

Appendix 13-D

**r (Correlation Coefficient) and r^2 (Coefficient
of Determination) Values for All Species
with NMS Axes 1 and 2**

Correlation coefficients (r) and coefficients of determination (r^2) for plant species with NMS Axis 1 and Axis 2 scores for 85 pine-dominated permanent MCBCL vegetation monitoring plots. Species codes correspond to species names listed in Appendix A.

Species Code	NMS Axis 1 r	NMS Axis 1 r^2	NMS Axis 2 r	NMS Axis 2 r^2
ANDCOM	0.266	0.071	0.198	0.039
ACERUB	-0.45	0.203	-0.111	0.012
AGAFAS	0.024	0.001	0.022	0
ANDCAP	0.152	0.023	-0.011	0
ANDGLA	-0.075	0.006	-0.24	0.058
ANDGLO	0.104	0.011	-0.163	0.027
ARISTR	0.708	0.501	-0.258	0.067
AROARB	-0.124	0.015	-0.127	0.016
ARUTEC	-0.09	0.008	-0.142	0.02
ASCAMP	0.123	0.015	-0.038	0.001
ASCPED	0.182	0.033	-0.091	0.008
ASTSPP	0.086	0.007	0.045	0.002
BACHAL	-0.119	0.014	0.033	0.001
CARSPP	-0.161	0.026	-0.044	0.002
CARBEL	0.119	0.014	-0.09	0.008
CAROPP	0.462	0.214	-0.214	0.046
CARTOM	-0.044	0.002	0.285	0.081
CHANPF	0.085	0.007	-0.013	0
CHAMAN	0.076	0.006	-0.199	0.04
CHRGOS	0.174	0.03	-0.087	0.008
CIRREP	0.203	0.041	-0.074	0.005
CIRVUL	0.21	0.044	0.036	0.001
CLEBPD	0.155	0.024	-0.113	0.013
CLEALN	0.041	0.002	-0.131	0.017
CNISTI	0.421	0.178	-0.08	0.006
CORLIN	0.048	0.002	-0.149	0.022
CORUK	-0.074	0.005	0.301	0.091
CROPUR	0.157	0.025	-0.095	0.009
CTEARO	0.055	0.003	-0.128	0.016
CYRRAC	0.015	0	-0.105	0.011
DESSPP	0.017	0	0.27	0.073
DESCIL	0.141	0.02	-0.079	0.006
DESLIN	0.084	0.007	0.085	0.007

Species Code	NMS Axis 1 r	NMS Axis 1 r ²	NMS Axis 2 r	NMS Axis 2 r ²
DESMAR	0.08	0.006	0.105	0.011
DESPAN	0.193	0.037	-0.139	0.019
DESTEN	0.186	0.035	-0.174	0.03
DICSPP	-0.137	0.019	0.351	0.123
DICANG	0.225	0.051	-0.175	0.03
DICCOM	-0.044	0.002	0.234	0.055
DICENS	0.187	0.035	0.127	0.016
DICMAT	0.045	0.002	0.033	0.001
DICOVA	0.117	0.014	-0.036	0.001
DICPOR	0.015	0	0.145	0.021
DICPSP	0.21	0.044	-0.189	0.036
DICTEN	0.13	0.017	-0.073	0.005
DICVIL	0.194	0.038	-0.094	0.009
DIOMUS	-0.038	0.001	-0.266	0.071
DIOVIR	0.166	0.028	0.245	0.06
ELEPHA	-0.025	0.001	0.166	0.028
ERIVER	0.047	0.002	-0.138	0.019
EUBRAC	0.124	0.015	-0.093	0.009
EUPSPP	0.095	0.009	0.039	0.002
EUPALB	0.194	0.038	-0.121	0.015
EUPCAP	-0.098	0.01	0.373	0.139
EUPLEU	0.089	0.008	0.111	0.012
EUPPIL	0.049	0.002	-0.183	0.034
EUPROT	-0.012	0	-0.16	0.025
EUPIPE	0.326	0.107	-0.129	0.017
EURPAL	0.077	0.006	-0.148	0.022
EUTCAR	0	0	-0.113	0.013
GALRVV	0.277	0.077	-0.063	0.004
GALERE	0.174	0.03	-0.095	0.009
GALVPV	0.134	0.018	0.043	0.002
GAYDUM	0.423	0.179	-0.188	0.035
GAYFR	0.156	0.024	-0.086	0.007
GELSEM	-0.097	0.009	0.3	0.09
GENAUT	0.16	0.025	-0.139	0.019
GORLAS	-0.179	0.032	-0.142	0.02
GYMBRE	0.161	0.026	-0.178	0.032

Species Code	NMS Axis 1 r	NMS Axis 1 r ²	NMS Axis 2 r	NMS Axis 2 r ²
HELANG	0.164	0.027	-0.149	0.022
HELHET	0.062	0.004	-0.137	0.019
HIEGRO	0.197	0.039	-0.158	0.025
HIEMAR	0.167	0.028	-0.074	0.005
HYP CRU	0.052	0.003	-0.114	0.013
HYPHYP	0.041	0.002	0.194	0.038
HYPTEN	-0.014	0	0.309	0.096
ILECOR	-0.192	0.037	-0.035	0.001
ILEGLA	0.058	0.003	-0.127	0.016
ILEOPA	-0.13	0.017	-0.006	0
IONLIN	0.323	0.104	-0.152	0.023
IPOMOE	0.122	0.015	-0.084	0.007
IRIVER	0.42	0.176	-0.166	0.028
JUNSCI	0.035	0.001	0.104	0.011
KALCAR	0.05	0.002	-0.121	0.015
LACANC	0.086	0.007	-0.148	0.022
LECMIN	0.158	0.025	-0.047	0.002
LESANG	0.126	0.016	0.038	0.001
LESCAP	-0.024	0.001	0.283	0.08
LESHIR	0.139	0.019	-0.006	0
LESHPC	0.135	0.018	-0.082	0.007
LESVIR	0.215	0.046	-0.181	0.033
LIAPPV	0.394	0.155	0.052	0.003
LIQSTY	-0.182	0.033	0.147	0.022
LOBNUT	0.104	0.011	-0.129	0.017
LUDVIR	0.132	0.017	-0.17	0.029
LYCALO	0.047	0.002	-0.138	0.019
LYOLIG	0.05	0.003	-0.139	0.019
LYOLUC	-0.592	0.35	-0.268	0.072
LYOMAR	0.184	0.034	-0.031	0.001
MAGVIR	0.078	0.006	-0.172	0.029
MORCAR	0.1	0.01	-0.176	0.031
MORCER	0.192	0.037	0.071	0.005
MORPUM	0.266	0.071	-0.186	0.034
MUHEXP	0.068	0.005	-0.057	0.003
NYSSYL	-0.165	0.027	0.046	0.002

Species Code	NMS Axis 1 r	NMS Axis 1 r ²	NMS Axis 2 r	NMS Axis 2 r ²
OSMCIN	-0.3	0.09	-0.215	0.046
OSMREG	-0.136	0.018	0.015	0
PANVIR	-0.091	0.008	0.287	0.082
PARQUI	-0.132	0.017	0.19	0.036
PERPAL	-0.379	0.144	-0.248	0.061
PINPAL	0.573	0.329	-0.304	0.093
PINSER	0.114	0.013	-0.196	0.038
PINTAE	-0.285	0.081	-0.042	0.002
PITGRA	0.311	0.097	0.072	0.005
PLATAN	0.11	0.012	-0.159	0.025
POLINC	0.079	0.006	-0.1	0.01
POLLUT	0.088	0.008	0.215	0.046
PRUSER	0.162	0.026	-0.116	0.013
PTEAQU	0.046	0.002	-0.329	0.109
PTEPYC	0.211	0.045	-0.085	0.007
PYXBAR	0.086	0.007	-0.132	0.017
QUESPP	-0.049	0.002	0.229	0.052
QUEFAL	0.142	0.02	-0.085	0.007
QUEGEM	0.187	0.035	-0.101	0.01
QUEHEM	0.253	0.064	-0.05	0.002
QUEINC	0.299	0.089	-0.143	0.02
QUELAE	0.318	0.101	-0.06	0.004
QUEMAR	0.21	0.044	0.082	0.007
QUEMVM	0.105	0.011	0.038	0.001
QUEMPM	0.187	0.035	-0.069	0.005
QUENIG	0.107	0.011	0.008	0
QUESTE	0.142	0.02	-0.065	0.004
QUEVIR	0.049	0.002	0.096	0.009
QUEXASH	0.206	0.042	-0.042	0.002
RHEALI	0.039	0.002	0.052	0.003
RHELUT	0.041	0.002	-0.098	0.01
RHEMAR	-0.07	0.005	0.254	0.064
RHEPET	-0.01	0	-0.122	0.015
RHOATL	0.098	0.01	-0.12	0.014
RHUCOP	0.131	0.017	0.224	0.05
RHYSPP	-0.026	0.001	-0.058	0.003

Species Code	NMS Axis 1 r	NMS Axis 1 r ²	NMS Axis 2 r	NMS Axis 2 r ²
RHYPLU	0.151	0.023	-0.082	0.007
ROBSPP	0.139	0.019	0.091	0.008
RUBSPP	0.005	0	0.299	0.089
SACCHA	0.082	0.007	-0.159	0.025
SASALB	0.215	0.046	0.069	0.005
SCLCCE	0.163	0.026	-0.089	0.008
SCLCVG	0.147	0.021	-0.089	0.008
SCLNIT	0.261	0.068	-0.059	0.003
SERAST	0.169	0.029	-0.133	0.018
SERLIN	0.068	0.005	-0.139	0.019
SERTOR	0.453	0.205	0.019	0
SILCOM	0.139	0.019	-0.039	0.001
SISCAP	0.101	0.01	-0.158	0.025
SMIBON	-0.034	0.001	0.38	0.144
SMIGLA	-0.032	0.001	0.265	0.07
SMILAU	-0.214	0.046	0.05	0.002
SMIROT	-0.09	0.008	0.106	0.011
SOLARU	0.132	0.017	-0.049	0.002
SOLODO	-0.049	0.002	0.302	0.091
SOLOVO	0.331	0.11	-0.181	0.033
SOLPUL	0.066	0.004	-0.153	0.023
SOLSTR	0.054	0.003	-0.157	0.025
SORAME	-0.037	0.001	-0.022	0
SPILVG	0.227	0.051	-0.153	0.023
SPOPIN	0.054	0.003	-0.112	0.012
STYBIF	0.256	0.065	-0.111	0.012
SYMDVD	0.166	0.028	-0.162	0.026
SYMWAL	0.253	0.064	-0.189	0.036
SYMTIN	0.008	0	-0.006	0
TEPFLO	0.173	0.03	-0.056	0.003
TEPHIS	0.26	0.068	-0.146	0.021
TOXPUB	0.221	0.049	-0.031	0.001
TOXRAD	-0.085	0.007	0.231	0.054
TRAURE	0.315	0.099	-0.124	0.015
VACARB	0.174	0.03	-0.072	0.005
VACCRA	0.227	0.052	-0.132	0.018

Species Code	NMS Axis 1 r	NMS Axis 1 r ²	NMS Axis 2 r	NMS Axis 2 r ²
VACFOR	-0.117	0.014	0.21	0.044
VACFUS	0.046	0.002	0.01	0
VASTA	0.311	0.097	-0.144	0.021
VACTEN	0.458	0.21	-0.012	0
VIOPRI	0.007	0	-0.088	0.008
VITROT	-0.058	0.003	0.327	0.107
WOOVIR	0.041	0.002	-0.083	0.007
XYRAMB	0.106	0.011	-0.169	0.028
XYRCAR	0.166	0.028	-0.06	0.004

[This page intentionally left blank.]

Appendix 13-E

List of Scientific Publications

List of Scientific Publications

Papers in Press

Smart, L., J.J. Swenson, N.L. Christensen, and J.O. Sexton. 2012. Three-dimensional characterization of pine forest type and red-cockaded woodpecker habitat by small-footprint, discrete-return LIDAR. *Forest Ecology and Management*. In press.

Papers in Active Preparation

Mitchell S.R., N.L. Christensen, J.W. Walters, S.A. Cohen, and M. Bertone. Soil properties drive differences in taxonomic groups among pine forests of the Atlantic coastal plain. For *Ecological Applications*.

Mitchell, S.R., N. Christensen, and J.R. Walters. Responses to forest restoration among three trophic levels. For *Conservation Biology*.

Mitchell, S.R., and N.L. Christensen. Dormant and growing season understory thinning to restore herbaceous plant communities typical of longleaf pine ecosystems. For *Forest Ecology and Management*.

Mitchell, S.R., and N.L. Christensen. Vegetation variation among disturbed and managed pine stands on the lower coastal plain of North Carolina. For *Plant Ecology*.

Christensen, N.L., and S. Mitchell. Vegetation variation on the lower coastal plain of North Carolina: The role of environment and disturbance. For *Forest Ecology and Management*.

Appendix 13-F

List of Students

- Lindsey Smart, Master of Environmental Management, Nicholas School of the Environment at Duke University, Durham, NC. Three-dimensional characterization of pine forest type and red-cockaded woodpecker habitat by small-footprint, discrete return radar. Graduated May 2009.
- Kyle Palmquist, Ph.D. candidate, Department of Biology at the University of North Carolina at Chapel Hill, Chapel Hill, NC. Species turnover and compositional shifts of the longleaf pine ecosystem after 18 years. Research Assistant: May–August 2010; expected graduation date: May 2013.

[This page intentionally left blank.]

Chapter 14

**Effects of Habitat Management for Red-Cockaded
Woodpeckers on Bird Communities**

SERDP Project Number: RC-1413

Terrestrial Module

Research Project T-2

Senior Researcher
Dr. Jeffrey R. Walters
Department of Biological Sciences
Virginia Tech
Blacksburg, VA 24061-0406
E-mail: jrwalt@vt.edu

Project Personnel:
Vicki Garcia (Ph.D. Student)
Kevin Rose (Lead Technician)
Lori Blanc (Research Scientist)

May 10, 2013

Final

This report was prepared under contract to the U.S. Department of Defense (DoD) Strategic Environmental Research and Development Program (SERDP). The publication of this report does not indicate endorsement by DoD, nor should the contents be construed as reflecting the official policy or position of DoD. References herein to any specific commercial product, process, or service by trade name, trademark, manufacturer, or otherwise, do not necessarily constitute or imply its endorsement, recommendation, or favoring by DoD.

Table of Contents

List of Acronyms	14-vi
Abstract.....	14-1
Objectives of the Research Project	14-2
Objectives	14-2
Hypotheses	14-2
Background	14-3
Section 1: Effects of Habitat Management for RCWs on Avian Communities	14-5
Materials and Methods.....	14-5
Results and Discussion	14-9
Section 2: Avian Communities of Pond Pine Pocosin, Bottomland Hardwood, and Coastal Scrub Habitats	14-16
Materials and Methods.....	14-16
Results and Discussion	14-17
Section 3: The Cavity-Nesting Bird Community.....	14-19
Materials and Methods.....	14-19
Results and Discussion	14-20
Literature Cited	14-25

List of Figures

14-1. Distribution of avian census points (Point Count Stations) coded by RCW habitat quality score.	14-8
14-2. Average number of species detected per point count stations as a function of RCW habitat quality.	14-10
14-3. Probability that RCWs are present as a function of RCW habitat quality.	14-11
14-4. Density of RCWs as a function of RCW habitat quality.	14-11
14-5. Presence of Bachman's sparrow as a function of RCW habitat quality.	14-12
14-6. Density of Bachman's sparrow as a function of RCW habitat quality.	14-12
14-7. Distribution of avian census points (point count stations) for 2011 in coastal scrub (Coastal), hardwood bottomland (Hwd), and pond pine pocosin (Pocosin) habitats.	14-16
14-8. The 300-m × 300-m cavity-nester study plot design.	14-20
14-9. Cavity nest web at MCBCL, based on data from nest searches 2008–2010.	14-21
14-10. Number of nests found for each species by nesting substrate at MCBCL from 2008–2010.	14-22
14-11. Nest substrate use at Eglin Air Force Base (n=35) and MCBCL (n=59).	14-22
14-12. Nest densities (mean ± standard error) of cavity-nesting birds found during April–July 2010 on 14 plots each at MCBCL (Lejeune, n=43) and Eglin Air Force Base (Eglin, n=21), for both primary cavity excavators (Excavators) and non-excavating secondary cavity nesters (Non-Excavators).	14-23
14-13. Densities of pine and hardwood snags (mean ± standard error) of sufficient size to support nests at MCBCL (Lejeune) and Eglin Air Force Base (Eglin).	14-23

List of Tables

14-1.	RCW foraging habitat scoring criteria, replicated from the USFWS's RCW Matrix application.	14-6
14- 2.	Criteria used to calculate habitat quality scores to select census points.	14-7
14-3.	Final distribution of census points across RCW foraging habitat quality scores.	14-8
14-4.	Relationships of habitat occupancy and density of species in the open longleaf assemblage to RCW habitat quality scores.	14-13
14-5.	Relationships of habitat occupancy and density of widespread species commonly found in longleaf habitat to RCW habitat quality scores.	14-13
14-6.	Relationships of habitat occupancy and density of species commonly associated with hardwood habitats to RCW habitat quality scores.	14-14
14-7.	Relationships of habitat occupancy and density of species associated with shrub vegetation to RCW habitat quality scores. See text for explanation of symbols.	14-15
14-8.	Ten most frequently detected species in three habitat types, listed from most to least frequent.	14-17

List of Acronyms

°C	degrees Celsius
ac	acre
AIC	Akaike Information Criterion
AIC _c	Akaike Information Criterion corrected for small sample sizes
cm	centimeter
dbh	diameter at breast height
DCERP	Defense Coastal/Estuarine Research Program
DoD	U.S. Department of Defense
GIS	geographic information systems
ha	hectare
km/h	kilometers per hour
km ²	square kilometer
m	meter
MCBCL	Marine Corps Base Camp Lejeune
RCW	red-cockaded woodpecker
SERDP	Strategic Environmental Research and Development Program
USFWS	U.S. Fish and Wildlife Service

Abstract

The primary objective of this project was to relate foraging habitat quality for the endangered red-cockaded woodpecker (RCW; *Picoides borealis*) to avian community composition within upland pine savanna and pine flatwood ecosystems to test the hypothesis that improving habitat for RCWs benefits the remainder of the avian community characteristic of these habitats. The two secondary objectives were to: (1) determine avian community composition in three other habitats found on MCBCL (i.e., coastal scrub, bottomland hardwoods, and pond pine pocosins), and (2) examine interactions between avian cavity-nesting species on Marine Corps Base Camp Lejeune (MCBCL) to test the hypotheses developed from previous research on a similar community at Eglin Air Force Base in Florida.

The primary objective was approached through experimental and correlational studies. The experimental study involved altering RCW habitat quality through management and documenting changes in avian community composition over time. There has been insufficient time to determine avian response to treatment in the experimental study. During the correlational study, we censused breeding birds in 2009 and 2010 at 146 points spanning the range of RCW foraging habitat quality on MCBCL, as measured by the RCW foraging habitat matrix tool developed by the U.S. Fish and Wildlife Service. We divided the RCW habitat into four categories, ranging from low to high and analyzed both the occurrence (using occupancy modeling) and abundance (using Program Distance) of bird species as a function of RCW habitat quality. Avian diversity increased with increasing RCW habitat quality and the occurrence and/or density of most species was positively related to RCW habitat quality, supporting our hypothesis. This linkage was particularly strong for the Bachman's sparrow (*Peucaea aestivalis*), a species of special concern on MCBCL, and was true of all species generally considered to be associated with longleaf savannas.

Overall avian diversity is a function of alpha (within habitat) and beta (between habitat) diversity. Coastal scrub contributes little to beta diversity because only one species recorded there is endemic to that habitat, albeit another species of special concern, the painted bunting (*Passerina ciris*). Other species recorded there are associated with adjacent habitats such as marsh and beach, or are widespread birds found in a variety of terrestrial habitats. Most of the species, recorded in pond pine pocosins, including all the most common ones, are also found in the pine uplands into which pocosin grades through distinctive ecotones throughout the MCBCL landscape. A few species are shared with bottomland hardwoods rather than pine uplands, and one unique species (i.e., the gray catbird [*Dumetella carolinensis*]) was recorded there. Relative abundance of particular species is quite different between pocosin and pine uplands however, with some species increasing toward the mesic end of the gradient and others decreasing. Notable in this respect are shrub-associated species, the only group to exhibit negative relationships with the RCW habitat quality score. These species may be pushed toward mesic sites by RCW habitat management, but because they are known to respond positively to fire they likely also benefit from such management to the extent that burning extends into pocosin habitat. We documented two groups of hardwood-associated species occur in bottomland hardwood habitat: those that are restricted to such a habitat and those that are common in both this habitat and pine uplands. Those that are restricted to such a habitat contribute substantially to avian diversity on MCBCL, but are unaffected by RCW habitat management because they rarely use even a poor RCW habitat. The presence and/or abundance of those that are common in both this

habitat and pine uplands are actually positively associated with RCW habitat quality with only a couple of exceptions. Thus, even hardwood-associated species appear to benefit from the management of pine habitat for RCWs.

Species densities of cavity-nesting birds on MCBCL are approximately twice as high as those found on Eglin Air Force Base. Our results indicate that the relative availability of nesting substrates (e.g., live pines, pine snags, hardwood snags) is similar between the two sites, suggesting that cavity nesters are not limited by cavity availability in these longleaf ecosystems. Cavity-nesting species tend to partition themselves among nesting substrates, and a shortage of pine or hardwood snags intensifies competition among species. MCBCL should maintain, whenever possible, the availability of nesting substrates (e.g., live pines, pine snags, hardwood snags) for the wide variety of cavity-nesting avian species because that determines the strength of interactions among species. Specifically, a shortage of pine snags likely would result in negative impacts on RCWs due to increased usurpation of their cavities in live pines by other species.

Objectives of the Research Project

Objectives

1. The primary objective of this project was to measure foraging habitat quality for the endangered red-cockaded woodpecker (RCW) within upland pine savanna and pine flatwood ecosystems and relate RCW foraging habitat quality to avian community composition (see Section 1). The components of this objective are to
 - a. Test experimentally how avian community composition changes in response to changes in RCW foraging habitat quality in association with Research Project T-1
 - b. Measure the relationship between avian community composition and RCW foraging habitat quality broadly across the MCBCL landscape.
2. A secondary objective of the project was to measure avian community composition in ecosystems other than upland pine savannas and pine flatwoods, especially pond pine pocosins (see Section 2).
3. Another secondary objective was to examine interactions between avian cavity-nesting species on MCBCL to test the hypotheses developed from previous research on a similar community at Eglin Air Force Base in Florida (see Section 3).

Hypotheses

1. The hypothesis tested as the primary objective of this research is that improving quality of upland pine savanna and pine flatwood habitats for RCWs also benefits the remainder of the avian community characteristic of these habitats, which will be reflected in increased avian diversity and a net positive change in abundance of birds as habitat quality improves.
2. An alternative hypothesis is that improving habitat quality for RCWs will not benefit the overall avian community, which will be reflected in a neutral or negative relationship

between RCW habitat quality and avian diversity, and reductions in abundance of some species that match or exceed increases in abundance of other species.

Background

Management of species at risk, particularly the red-cockaded woodpecker (RCW; *Picoides borealis*), is a management priority at Marine Corps Base Camp Lejeune (MCBCL). Because the RCW is federally endangered, MCBCL is required by the U.S. Fish and Wildlife Service (USFWS) to recover the RCW, that is, to not just maintain its current numbers but to increase the population toward a recovery goal of 173 active territories (MCBCL, 2006) negotiated between USFWS and MCBCL. One of the requirements imposed by USFWS is to improve the quality of foraging habitat assigned to each RCW group on the Base to meet standards specified in the Recovery Plan for the species (USFWS, 2003). This plan states that each woodpecker group be provided 49 ha of high-quality foraging habitat, defined as open pine stands with moderate densities of large, old pines, a rich herbaceous groundcover, and relatively few midstory hardwoods or medium-sized pines. To satisfy these requirements while maintaining some flexibility in land use, MCBCL is managing 198 foraging areas averaging 81 ha each as RCW habitat. The net result is that more than 16,000 ha are being managed for RCWs, representing essentially all the upland pine savanna and pine flatwood habitat outside of the Greater Sandy Run Area.

The enormous impact the endangered RCW has on management of pine habitat on MCBCL is typical of U.S. Department of Defense (DoD) installations in the Southeast that contain such habitat. Individual family groups of RCWs require large areas for their territories, and a viable population requires a large number of such groups, 100–350 for most installations. As a result, for installations such as Fort Bragg (North Carolina), Fort Benning and Fort Stewart (both in Georgia), Fort Polk (Louisiana), Eglin Air Force Base (Florida), and MCBCL, the primary conservation objectives in the terrestrial environment are to recover the RCW and restore its longleaf pine habitat. These installations are among the most active in the nation with respect to training, and much of that training occurs in the pine habitats managed for RCWs. Therefore training needs must be integrated with RCW recovery, and accomplishing that goal is the highest management priority in the terrestrial environment on these installations.

At the outset of this study there were 79 active RCW territories on MCBCL, representing slightly less than half of the recovery goal of 173, and only 2% of the pine stands on the Base met the USFWS (2003) criteria for high quality RCW habitat. Natural resources staff at MCBCL are actively improving RCW habitat to meet habitat quality standards on existing territories and restore habitat through timber management and prescribed fire programs to provide new territories. Base managers are taking an ecosystem management approach to this activity (MCBCL, 2006) and indeed the features of high quality RCW foraging habitat (open pine stands with diverse groundcover) mimic the characteristics of pristine longleaf ecosystems, and are being produced by similar processes, that is, through use of prescribed fire to mimic historic fire regimes. Thus, on MCBCL (and on other DoD installations in the Southeast) managing for high quality RCW foraging habitat is viewed as ecosystem restoration.

Although this habitat ostensibly is managed for a single species, the RCW, it is widely believed that because of the way habitat is managed, that is, with an ecosystem approach involving

restoration of historic fire regimes and habitat structure, this management will benefit other species characteristic of these ecosystems. That is, the RCW is thought to serve as an umbrella species (Roberge and Angelstam, 2004; Wilcox, 1984). However, the actual effects of habitat restoration for RCWs on other vertebrates are poorly documented. In particular, the impact of this management on the remainder of the avian community is an important knowledge gap. The relationship is expected to be complex as variation in the fire regime interacts with the soil-moisture gradient characteristic of the terrestrial environment on MCBCL to create variation in habitat structure, and thus variation in habitat availability for birds. Previous studies have documented higher diversity and abundance of birds in restored pine habitat compared to fire-suppressed stands unsuitable for RCWs (Allen et al., 2006; Conner et al., 2002; Provencher et al., 2002), but no prior studies have examined the impact of habitat improvements in habitat considered suitable for RCWs. This is the primary objective of this study.

We measured RCW foraging habitat quality according to the criteria outlined in USFWS (2003), and quantified its relationship to the abundance and diversity of other bird species. Our hypothesis was that avian diversity and abundance would increase with RCW habitat quality. We predicted that community composition would change as habitat quality improved, specifically that species associated with midstory hardwoods (Allen et al., 2006) would decline and that species associated with fire-maintained pine savannas (Allen et al., 2006; Engstrom, 1993) such as Bachman's sparrow (*Peucaea aestivalis*; another at-risk species found at MCBCL) would increase. We tested these ideas using both correlational and experimental approaches (see Section 1).

Although pine savannas and flatwoods dominate the terrestrial environment at MCBCL, other habitats of interest occur. A secondary objective of the project was to describe the bird species associated with these other habitats, specifically bottomland hardwoods, coastal scrub and especially pond pine pocosin. The latter represents the mesic extreme of the soil-moisture gradient in pine habitats at MCBCL on which the research and monitoring activities of the terrestrial module were focused. There is particular interest in pond pine pocosin habitat because it is widespread on the base, is poorly studied due to its inaccessibility and is potentially of value to RCWs. The other two habitats are quite distinct from pine habitats, and are of interest because of their potential contribution to avian diversity on MCBCL, particularly beta diversity, that is, diversity across habitat types (Whittaker, 1960). Overall diversity is determined by species diversity within specific habitat types (alpha diversity) and by the extent to which sets of species differ between habitat types (beta diversity). Our sampling is designed to assess alpha diversity in additional habitats as well as beta diversity, and thus measure overall avian diversity on MCBCL (see Section 2). Also, coastal scrub contains an additional species of special interest, the painted bunting (*Passerina ciris*).

Cavity-nesting birds, which include songbirds, ducks, woodpeckers, and raptors, represent a significant portion of avian diversity within longleaf pine forests and can comprise up to 30% of the breeding bird community (Blanc, 2007). Some cavity-nesters in the Southeast have experienced population declines in recent decades and effective conservation and management of these species will require an understanding of factors limiting their populations. Factors limiting RCW populations are well understood (Walters, 1991). However, there is a deficit of knowledge about how the rest of the cavity-nesting bird community is structured and limited by factors such as cavity-nesting resource availability in longleaf pine ecosystems (e.g., RCW cavities in live

pinus and standing dead trees or “snags,” both hardwood and pinus), or how nest resource availability influences interactions between RCWs and other cavity-nesting birds. The need to fill this information gap was specified as a research need in the RCW Recovery Plan (USFWS, 2003).

In an investigation of the cavity-nesting bird community in old growth longleaf forests on Eglin Air Force Base in Florida, Blanc and Walters (2008a and b) described the nesting ecology of cavity-nesting birds, documented heterospecific use of RCW cavities in relation to snag availability, and identified two species (the northern flicker [*Colaptes auratus*] and RCW) that were responsible for creating a disproportionately large number of cavities on the landscape. Their findings were consistent with studies on cavity-nesting bird communities in other ecosystems, in which there were one or two “key” cavity excavators (Bednarz et al., 2004; Huss et al., 2002; Martin et al., 2004; Saab et al., 2004). Research to investigate whether this pattern of nest site selection and cavity excavation holds in second growth longleaf and other younger managed southern pine forests is lacking. Another secondary objective of the project was to examine the cavity-nesting bird community on MCBCL, specifically to: (1) describe the nesting ecology of the avian cavity-nesting community in second growth longleaf pine forests on MCBCL, (2) investigate the role of RCWs in structuring the cavity-nesting bird community and resulting implications for management, and (3) build on the previous studies by Blanc and Walters (2008a and b) at Eglin Air Force Base. Building on these previous studies allowed for comparisons of: (1) cavity-nesting bird community structure and nesting density, and (2) nesting resource availability in second growth longleaf pine forests at MCBCL in comparison to old growth longleaf pine forests at Eglin Air Force Base (see Section 3).

Section 1: Effects of Habitat Management for RCWs on Avian Communities

Materials and Methods

Correlational Study: We selected 146 census point locations for the correlational study of the linkage between RCW habitat quality and bird diversity and abundance in December 2008–January 2009. In selecting the census stations, our goal was to capture the full range of variation in RCW habitat quality at MCBCL. RCW foraging habitat quality was assessed using the RCW Foraging Matrix application, which is available on the USFWS’s Web site at <http://www.fws.gov/rcwrecovery/matrix.html>. This tool was developed by USFWS based on its foraging habitat guidelines articulated in the Recovery Plan (USFWS, 2003; **Table 14-1**). RCW habitat quality scores range from 0 to 5 and are classified as nonhabitat (0), unsuitable (1), potentially suitable (2–3), or suitable (4–5). We used MCBCL’s forest stand and geographic information systems (GIS) data to select census points with a roughly even distribution across scores between 2 and 5.

Table 14-1. RCW foraging habitat scoring criteria, replicated from the USFWS's RCW Matrix application.

Values using inches as units are diameters at breast height.

Stand Characteristics	Score					Weight
	1	2	3	4	5	
Number of pines >14" and ≥60 years old	<5	5–8	9–12	13–17	18+	0.152
Basal area pines >14" and ≥60 years old	<5	5–9	10–14	15–19	20+	0.139
Basal area pines 10–14"	>55	51–55	46–50	41–45	0–40	0.038
Basal area pines <10"	>30	23–29	16–22	10–15	<10	0.025
# pines <10"	>40	33–39	26–32	20–25	<20	0.013
Basal area pines ≥10"	<20	21–26	27–32	33–39	40+	0.051
% herbaceous groundcover	<10	10–19	20–29	30–39	40+	0.101
Hardwood midstory ^a	T–D	M–M	M–S	—	L–S	0.114
	M–D	T–M	T–S	—	L–M	—
	—	—	—	—	L–D	—
% Canopy hardwood (within longleaf stand)	>30	23–29	16–22	10–15	<10	0.063
Stand age	≤30	31–39	40–49	50–59	60+	0.139
Fire return interval (years)	≥7	6	5	4	≤3	0.089
Season of last prescribed burn ^b	—	—	NGS	—	GS	0.076

^a Height: L = low (<7'), M = medium (7'-15'), T = tall (>15'); density: S = sparse, M = medium, D = dense.

^b GS = growing season; NGS = non-growing season.

Our first group of census points was the center points of the Research Project T-1 experimental plots ($n=24$). These were used to study the linkage between changes in habitat and changes in the avian community over time experimentally (see below) as well as being included in the correlational study. We used the center points of the cavity-nesting bird study plots (see Section 3) as additional sampling locations for the correlational study ($n=30$). We also used points from other existing study plots on MCBCL to the extent possible, subject to the criterion that they were located in pine stands ≥60 years of age. These included Terrestrial Module Monitoring plots ($n=14$), MCBCL staff photo points ($n=6$), and Carolina Vegetation Survey sample points ($n=6$).

To select the remaining 66 census locations we randomly generated points throughout longleaf habitat on MCBCL using the Hawth's Analysis Tools for ArcGIS (which is available on the following Web site <http://www.spatial ecology.com/htools>; Beyer, 2004). To ensure independence of sampling stations, all randomly generated points that fell within 200 m of existing points were removed from the sample. Some of the randomly generated points fell within stands for which MCBCL did not have complete data. We collected data for those points in December 2008 using protocols specified within the RCW Foraging Matrix procedures. Briefly, we used 0.1-ac circular plots to collect stem and hardwood midstory data and 0.01-ac circular plots to collect groundcover data. Within each plot, we recorded percent herbaceous

ground cover, percent hardwood canopy, and the number and diameter at breast height of pine stems ≥ 3.5 cm. We used stem data to calculate basal area by diameter classes (**Table 14-2**).

Table 14- 2. Criteria used to calculate habitat quality scores to select census points.

The columns to the left indicate the weighted variables used in the standard USFWS RCW foraging habitat quality calculations. The final column gives the standardized weights used in calculating RCW foraging habitat quality scores for census points in the current study.

Variable	Standard Weight	MCBCL Weight
Total number of pines ≥ 14 " dbh	0.152	—
Basal area of pines ≥ 14 " dbh	0.139	0.175
Basal area of all pines between 10" and 14" dbh	0.038	0.048
Basal area of pines between 4" and 9.9" dbh	0.025	0.032
Total number of pines between 4" and 9.9" dbh	0.013	0.016
Basal area of all pines ≥ 10 " dbh	0.051	—
% Herbaceous groundcover in 10% increments	0.101	0.127
Height and density of midstory	0.114	0.143
Percentage of the canopy comprised of hardwoods	0.063	0.079
Stand age (pine)	0.139	0.175
Number of years since the last burn	0.089	0.111
Season of last burn (growing season/non-growing season)	<u>0.076</u>	<u>0.095</u>
Sum	1.00	1.00

Because available stand data at MCBCL differed from what was required to run the RCW Matrix application, we generated habitat quality scores using a modified version of the Foraging Matrix algorithm during plot selection. This modified algorithm included 10 out of the 12 variables required by the RCW Foraging Matrix application, with similar diameter at breast height size classes for basal area calculations (**Table 14-2**). We standardized the weighted value of these 10 variables to sum to 1, based on the same weight distribution used in the RCW Foraging Matrix (**Table 14-2**). Using the modified algorithm, we calculated habitat quality scores for all potential points and assessed their distribution across five habitat quality score categories (**Table 14-2**). We continued to randomly generate and score additional points until we had sufficient representation of all score classes for quality. The distribution of the 146 points across the RCW habitat quality scale is shown in **Table 14-3**, and their locations in **Figure 14-1**. To validate data points for which pre-existing MCBCL data were used, we ground-truthed 10% of the sample ($n=15$ points).

The census points were sampled in 2009 and again in 2010. We used point counts to census birds following a methodology from Ralph et al. (1995) by Kirkpatrick et al. (2006). Surveys were conducted between April 10 and July 10 starting at sunrise and going no later than 10 a.m. (or 4 hours after dawn), on days without precipitation and with wind speeds less than 12 km/h (Ralph et al., 1995; Rosenstock et al., 2002). We recorded temperature ($^{\circ}\text{C}$), wind speed (km/h), cloud cover, and background noise level. After initially arriving at a point, we waited for a 1-minute silent period, and then recorded any birds seen or heard for an 8-minute period (Farnsworth et

al., 2002; Rosenstock et al., 2002). We estimated the distance to each bird, using a Rangefinder whenever necessary (Buckland, 2001; Rosenstock et al., 2002).

Table 14-3. Final distribution of census points across RCW foraging habitat quality scores.

Quality Score	N
2–3	17
3.01–3.5	33
3.51–4	38
4.01–4.5	39
4.51–5	19
Total	146

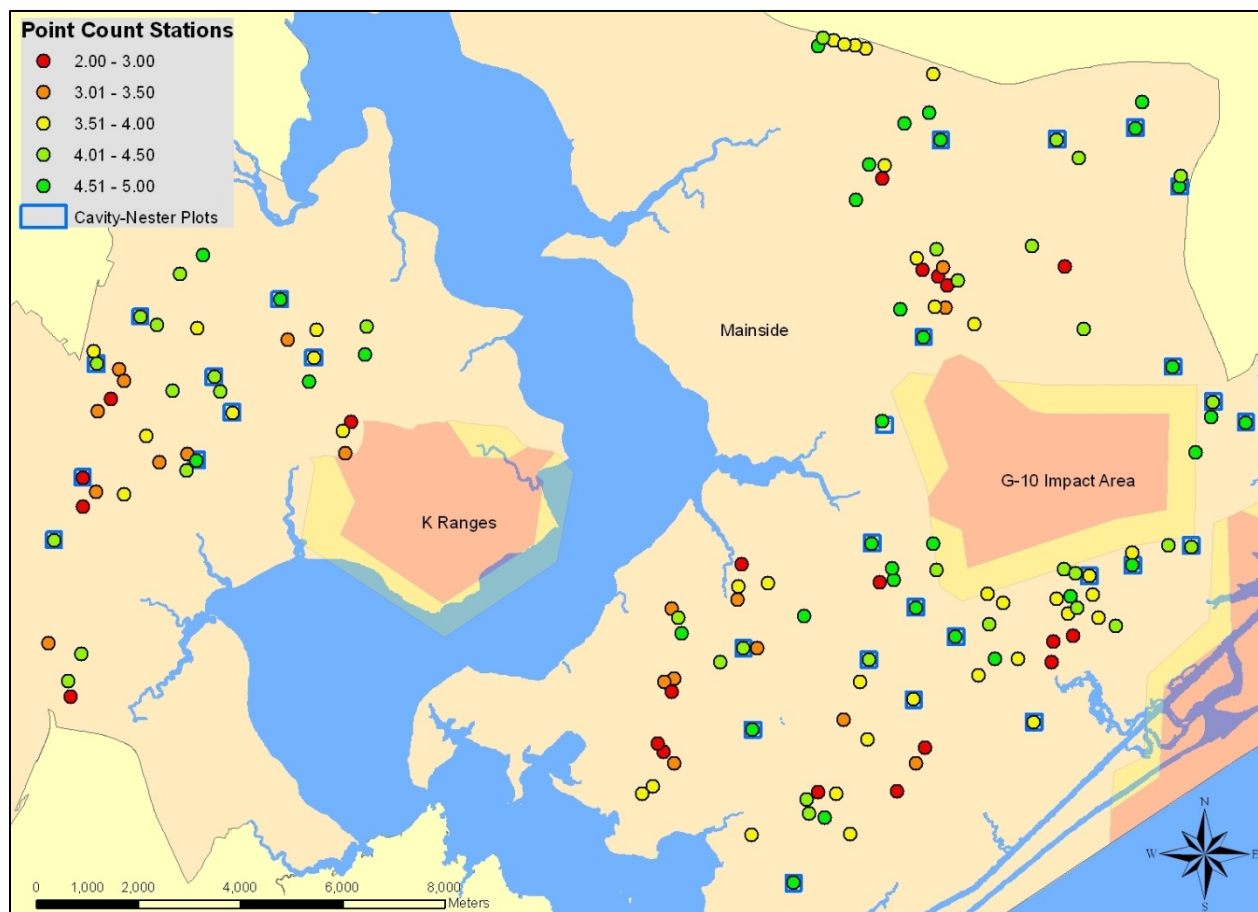


Figure 14-1. Distribution of avian census points (Point Count Stations) coded by RCW habitat quality score.

Points within cavity-nester plots (see Section 3) are indicated by blue boxes.

We analyzed the data in two ways. First, we determined the probability that each species occurs at a point as a function of habitat quality using occupancy models in Program Presence 4.0 (Hines, 2006). Repeated sampling of points is used to estimate detection probability in this

analysis. Second, we used the program Distance 6.0 release 2 (Thomas et al., 2009) to estimate the density of each species at points as a function of habitat quality across the range of habitat conditions in which that species occurred. Thus, our two-stage analysis indicates first how likely a species is to occur, and second how abundant it is where it occurs, as a function of habitat quality.

For the Distance analysis, we created a set of candidate models, including the following covariates: distance (m) to the detected bird, temperature, cloud cover, wind, noise, survey start time, observer, and survey round (1–4; each point was surveyed four times). We then ran each model in Distance 6.0 and chose the model with the lowest AIC_c value (i.e., Akaike Information Criterion corrected for small sample sizes). The data were stratified by RCW habitat score, which yielded separate density and detection probability estimates for each habitat score, along with associated standard errors.

For the occupancy analysis, we also created a set of candidate models including the same covariates, and used a multi-season analysis to determine the best model for each species. Immigration and emigration was modeled as constant between years, and we excluded survey rounds where detections were below normal (i.e., that species had not yet arrived or had already departed). The model with the lowest Akaike Information Criterion (AIC) score was chosen, and occupancy (proportion of sites occupied) and detection probability from that model were estimated, along with standard errors.

Experimental Study: The selection of sites for the experimental study and the features of these sites are described in Chapter 13 (Research Project T-1) of this report. In addition to being included in the correlational study, these sites were analyzed for changes over time as a function of management treatments that were designed to improve RCW foraging habitat quality. These 24 census points were sampled a third time in 2011, as well as in 2009 and 2010, using the same methodology as previously described. Linkages between vegetation, arthropods, and birds were examined as described Chapter 13. There has been insufficient time since treatments were applied for hypothesized changes in the avian community to occur.

Results and Discussion

Correlational Study: The program Distance analyses require that habitat quality be used as a categorical rather than continuous variable, and the original five categories resulted in relatively small sample sizes, particularly for the highest quality habitat. Therefore, for these analyses, we divided the RCW habitat quality scores into four categories: 2.013–2.759; 2.760–3.506; 3.507–4.253; and 4.254–5. We will refer to these categories henceforth as 2, 3, 4, and 5, respectively.

Avian diversity increased as a function of RCW habitat quality. That is, the average number of species detected at a point increased as RCW habitat quality improved (**Figure 14-2**). This suggests that managing pine habitats for RCWs has positive effects on the avian community, supporting our hypothesis.

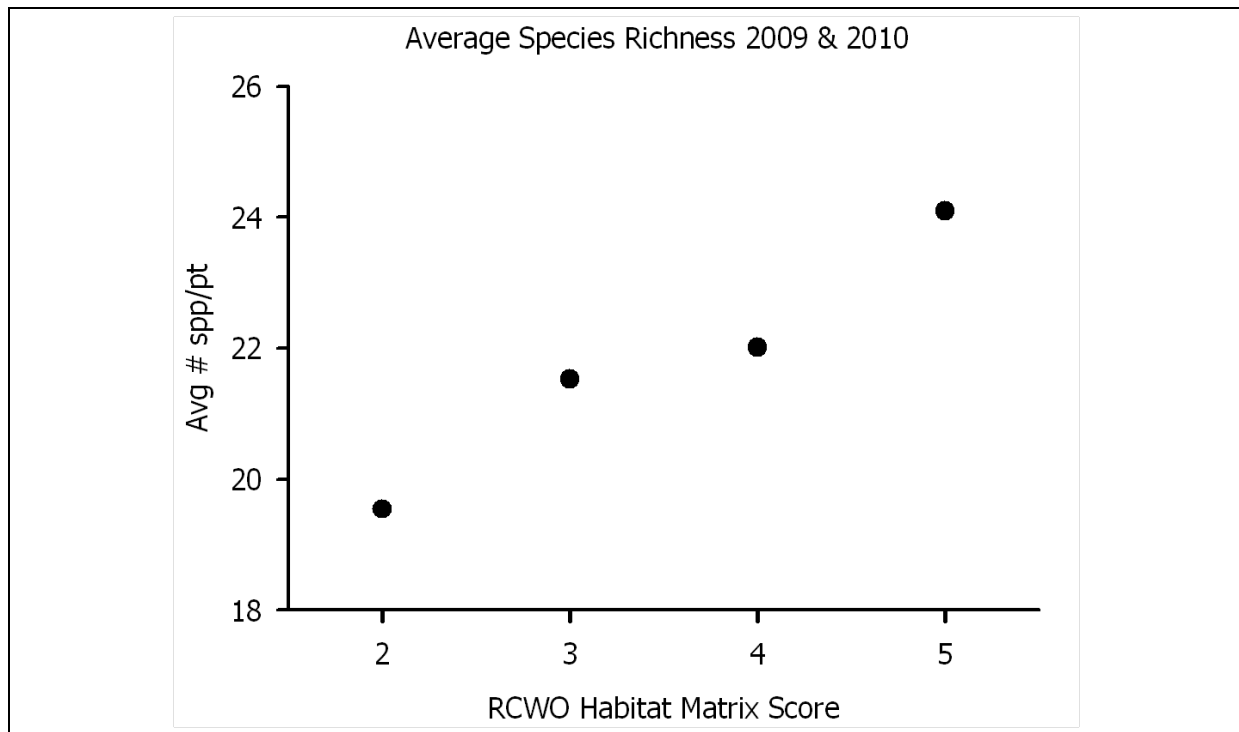


Figure 14-2. Average number of species detected per point count stations as a function of RCW habitat quality.

What was true of the community was generally true of individual species. The relationship of RCW habitat quality to presence and abundance of individual species generally was positive or neutral rather than negative. It is instructive to view these relationships according to previously known habitat associations of the species present at MCBCL. One expects those species known to be associated with open longleaf pine habitat to be especially likely to benefit from management for RCWs and this indeed proved to be the case. Most especially, such management should benefit the RCW itself, and indeed both presence (**Figure 14-3**) and abundance (**Figure 14-4**) of RCWs increased with increasing habitat quality. The open longleaf guild contains another at-risk species of special concern to MCBCL, the Bachman's sparrow (*Peucaea aestivalis*). It is particularly important that management for the RCW, which is designed to produce open pine stands with well-developed ground cover, should also benefit Bachman's sparrow. This is clearly the case: both presence (**Figure 14-5**) and abundance (**Figure 14-6**) of Bachman's sparrow increased dramatically, from zero to very high levels, with increasing RCW habitat quality. Indeed, the RCW habitat quality score appears to function better as an indicator of habitat quality for Bachman's sparrow than for the RCW.

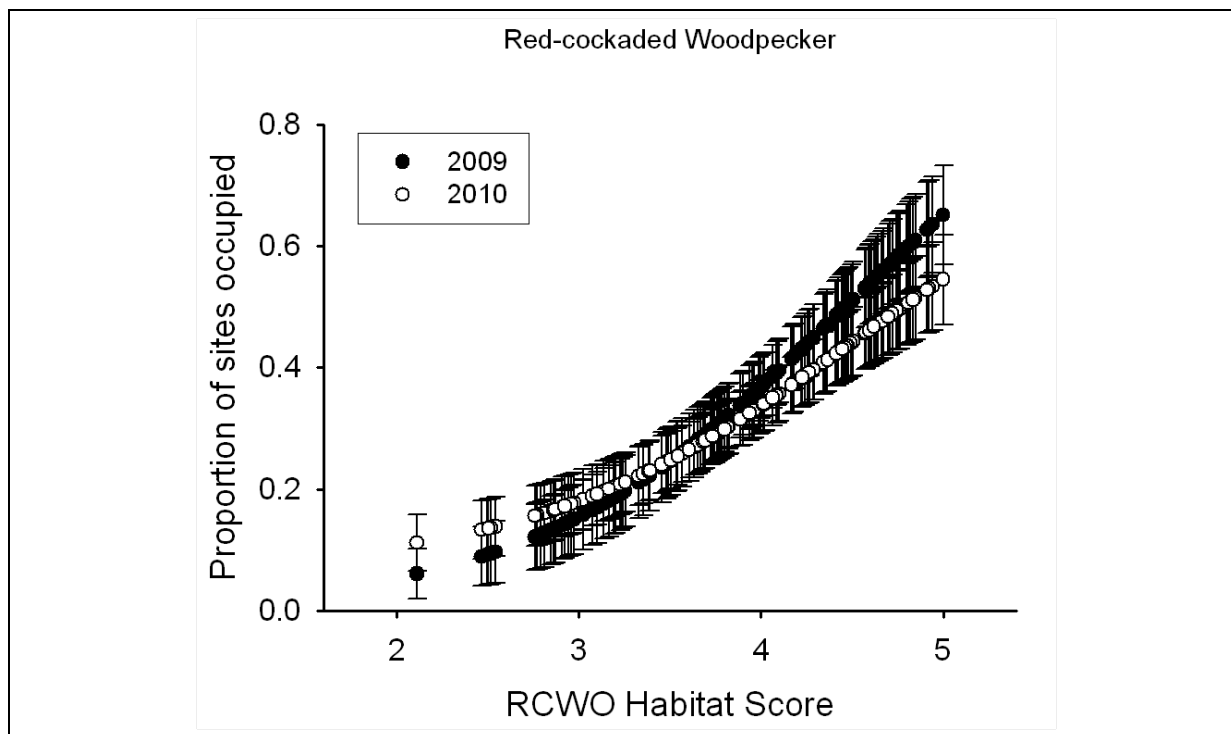


Figure 14-3. Probability that RCWs are present as a function of RCW habitat quality.

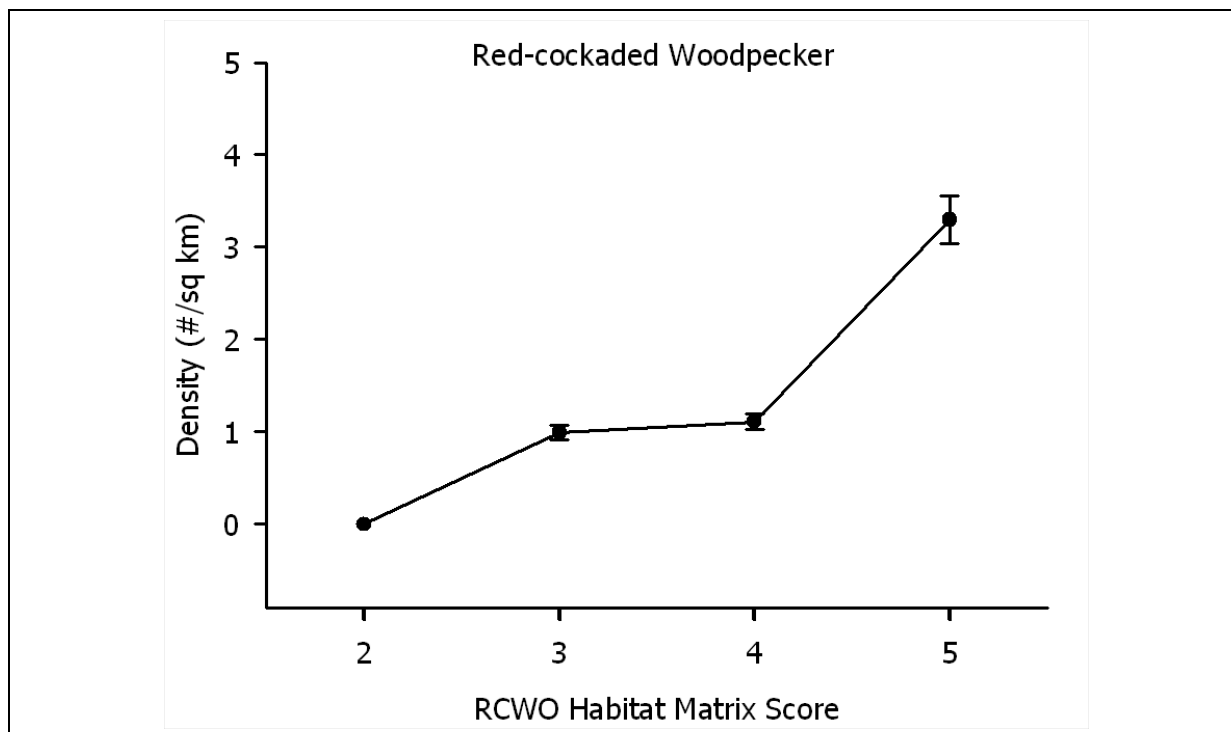


Figure 14-4. Density of RCWs as a function of RCW habitat quality.

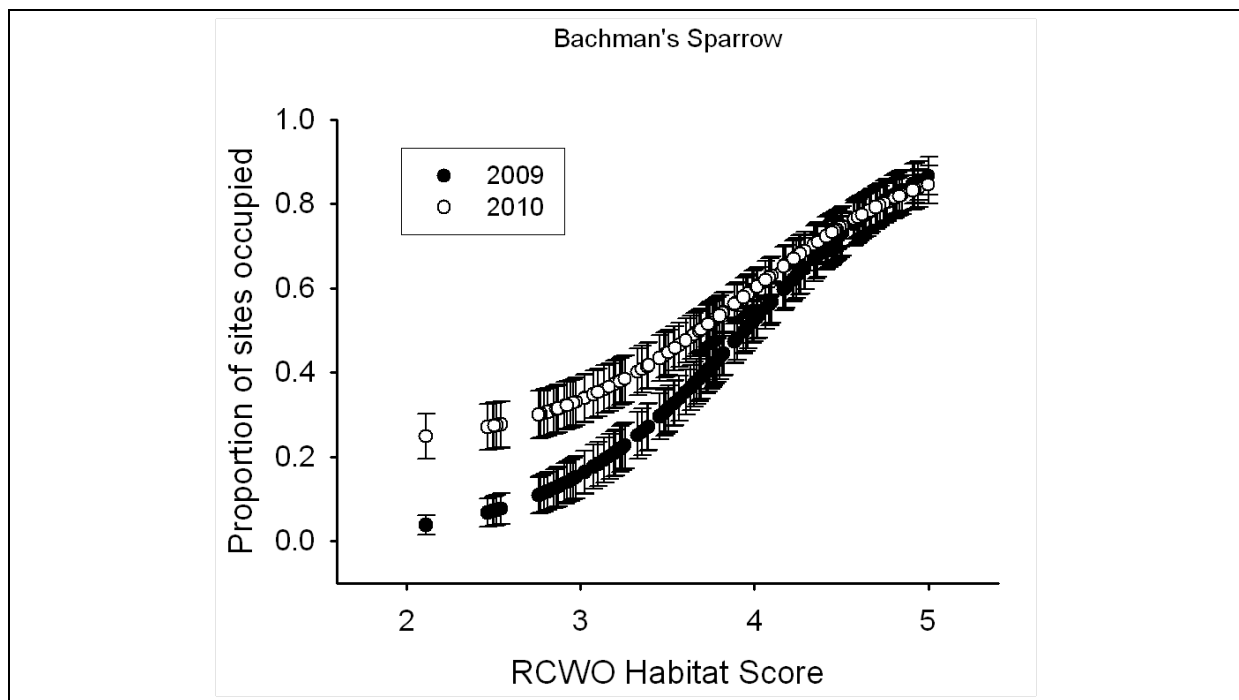


Figure 14-5. Presence of Bachman's sparrow as a function of RCW habitat quality.

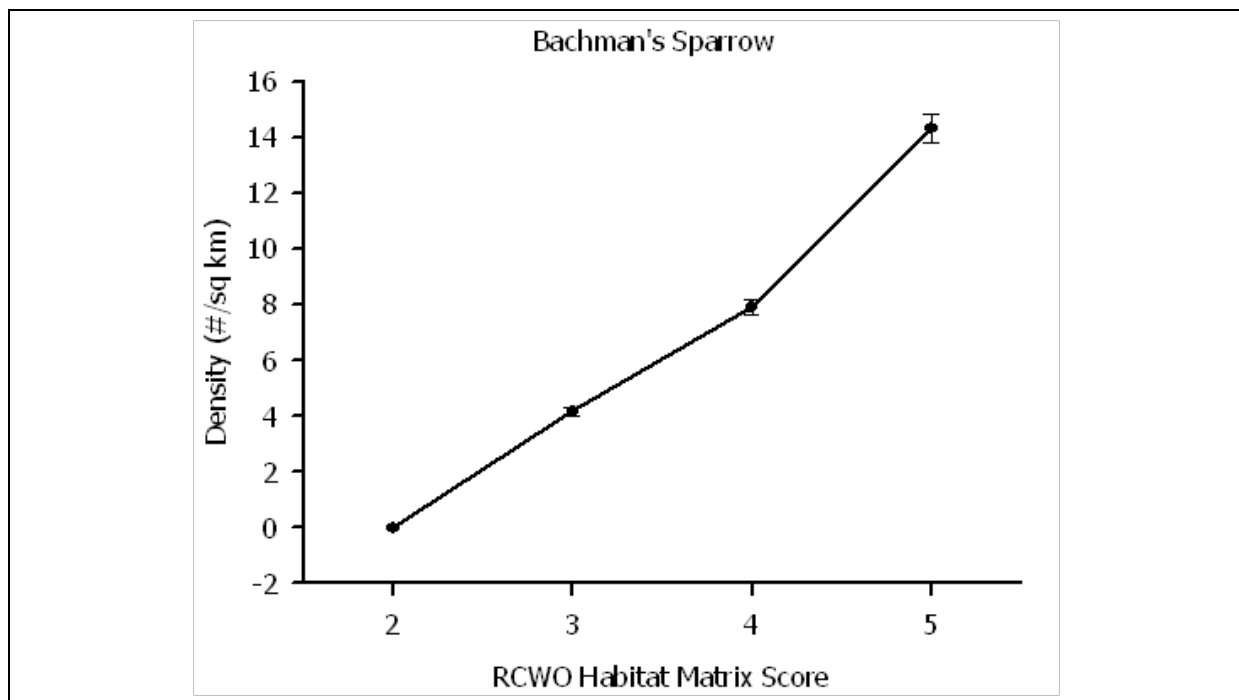


Figure 14-6. Density of Bachman's sparrow as a function of RCW habitat quality.

Results for the open longleaf assemblage are summarized in **Table 14-4**. To facilitate showing the pattern in the results, for this and other guilds below, we indicate whether the trends in occupancy are increasing (+), stable (0), or declining (–) with respect to RCW habitat quality and whether the values are high or low. We used 60% occupancy as the threshold separating low

and high occupancy, and two birds per km² as the threshold separating low and high density. If the values changed across the habitat quality gradient, then this is also indicated. For example, both occupancy and density of RCWs increased from low to high with increasing RCW habitat quality, whereas both occupancy and density of brown-headed nuthatches (*Sitta pusilla*) also increased but were always high, even in low quality RCW habitat (**Table 14-4**). Relationships to RCW habitat quality were all positive within this guild with the exception of a neutral relationship to red-headed woodpecker (*Melanerpes erythrocephalus*) occupancy, which was always high.

Table 14-4. Relationships of habitat occupancy and density of species in the open longleaf assemblage to RCW habitat quality scores.

Species	Occupancy	Density
Eastern bluebird	+ / L–H	+ / L–H
Brown-headed nuthatch	+ / H	+ / H
Red-headed woodpecker	0 / H	+ / L
Bachman’s sparrow	+ / L–H	+ / L–H
Pine warbler	+ / H	+ / L–H
Red-cockaded woodpecker	+ / L–H	+ / L–H

NOTE: In the Occupancy and Density columns, we indicate whether the trends in occupancy are increasing (+) or stable (0).

The next group is constituted of species that are also associated with longleaf habitat but, unlike the first group, are also commonly found in other habitat types including hardwood forests. One does not necessarily expect these widespread species to be positively affected by habitat management for RCWs. Again, however, responses of these species to RCW habitat management are overwhelmingly positive (**Table 14-5**). Occupancy of five of eight species increases from low to high with increasing RCW habitat quality score, and 12 out of 16 trends are positive. Only one trend is negative (i.e., occupancy by Summer Tanagers [*Piranga rubra*]) and that is countered by a positive effect on density in this species.

Table 14-5. Relationships of habitat occupancy and density of widespread species commonly found in longleaf habitat to RCW habitat quality scores.

Species	Occupancy	Density
Indigo bunting	+ / L–H	+ / L
Eastern wood peewee	+ / L–H	+ / L–H
Summer tanager	– / H	+ / L
Great crested flycatcher	0 / H	+ / H
Northern bobwhite	+ / L–H	+ / L
Chipping sparrow	+ / L–H	+ / H
Brown-headed cowbird	+ / L–H	+ / L–H
Northern flicker	0 / H	0 / L

NOTE: In the Occupancy and Density columns, we indicate whether the trends in occupancy are increasing (+), stable (0), or declining (–) with respect to RCW habitat quality.

Several of the species we detected are usually considered birds of hardwood rather than pine forests. One might expect these species to suffer from management for RCWs as such management is designed to reduce hardwood presence in the canopy and greatly reduce the presence of a hardwood midstory layer. This proved not to be the case. There were as many positive relationships (four) with RCW habitat quality score as negative ones (three) among this group of species, and many (five) neutral relationships (**Table 14-6**). Blue-gray gnatcatchers (*Poliophtila caerulea*) and red-bellied woodpeckers (*Melanerpes carolinus*) appear to benefit from RCW management, whereas yellow-throated warblers (*Setophaga dominica*) and blue jays (*Cyanocitta cristata*) are negatively affected and tufted titmouse (*Baeolophus bicolor*) and Carolina chickadees (*Poecile carolinensis*) are unaffected. The negative effect on blue jays may be related to their dependence on acorns, as RCW management is especially geared to reducing oak densities. Our results are consistent with those of Allen et al. (2006) who found that in the North Carolina Sandhills, bird species that are often associated with hardwood habitat and were common in riparian areas did not invade pine uplands in response to increased hardwood presence under fire suppression. Several of the species for which this was true in the Allen et al. (2006) study are the same ones that show neutral or positive relationships to RCW habitat quality in **Table 14-6**. Interestingly the species that are most common in longleaf habitat show positive relationships to RCW habitat score, whereas the species that exhibit negative or neutral relationships are uncommon in this habitat, even when it is in poor condition (**Table 14-6**).

Table 14-6. Relationships of habitat occupancy and density of species commonly associated with hardwood habitats to RCW habitat quality scores.

Species	Occupancy	Density
Tufted titmouse	+ / H	0 / H
Blue-gray gnatcatcher	+ / H	+ / H
Yellow-throated warbler	- / H-L	- / L
Red-bellied woodpecker	+ / L-H	0 / L
Carolina chickadee	0 / H	0 / L
Blue jay	- / H-L	0 / L

NOTE: In the Occupancy and Density columns, we indicate whether the trends in occupancy are increasing (+), stable (0), or declining (-) with respect to RCW habitat quality.

The species most negatively affected by RCW management are those associated with the shrub layer. RCW management favors forbs and grasses over woody vegetation in the ground cover and thus inhibits development of a shrub layer, as well as reducing hardwood midstory. The species in this guild exhibited negative or neutral relationships of occupancy and density with RCW habitat quality (**Table 14-7**). Three of the five species in this group were common in pine habitat of all degrees of quality. Only one, the white-eyed vireo (*Vireo griseus*), declined from common to uncommon as RCW habitat quality increased (**Table 14-7**). All of these species are abundant in other habitat types such as bottomland hardwoods and especially pocosin (see Section 2).

Table 14-7. Relationships of habitat occupancy and density of species associated with shrub vegetation to RCW habitat quality scores. See text for explanation of symbols.

Species	Occupancy	Density
Northern cardinal	– / H	– / H
Eastern towhee	0 / H	0 / H
Carolina wren	– / H	– / H
White-eyed vireo	– / H-L	– / H-L
Common yellowthroat	0 / L	+ / L

NOTE: In the Occupancy and Density columns, we indicate whether the trends in occupancy are increasing (+), stable (0), or declining (–) with respect to RCW habitat quality.

We conclude that our hypothesis that management of pine habitat for RCWs benefits the overall avian community is supported. Improved habitat condition for RCWs results in greater avian diversity and has positive effects on many individual species. Those few species that are negatively affected are common in other habitat types. There is no species characteristic of pine savanna habitat that is negatively affected by management for RCWs. Thus it appears that the RCW functions as an effective umbrella species with respect to the wider avian community inhabiting pine habitat at MCBCL. For species associated with open pine habitats, this is not surprising because the objectives of RCW habitat management are much the same as those of longleaf ecosystem restoration, and the primary means to achieve these objectives is the dominant disturbance in the natural system (i.e., fire). The open pine stands with rich ground cover that management practices are aiming to produce represent the habitat condition to which the pine bird assemblage is adapted, and accordingly this assemblage appears to be responding positively to this management. More surprising is that generalist species and species not linked to pine systems in their distribution also show positive effects, or in some cases at least no negative effects. This suggests that the habitat conditions characterizing poor RCW habitat such as significant hardwood presence in the canopy and a dense hardwood midstory, do not provide niches that are exploited by species associated with such habitat elements elsewhere. That is, there is no indication that habitat degradation provides opportunities for certain species to increase their distribution and abundance. Apparently, the niches of these species in this ecosystem in high-quality habitat that account for their presence in the system are not replicated by conditions characterizing degraded habitat. The exception is the woody understory characteristic of poor RCW habitat, which does appear to benefit shrub-associated species (Table 14-7). Again, however, these species are common in other habitat types on MCBCL.

Finally, the strong patterns in relationships of avian species to RCW habitat quality that we observed indicate that results were not significantly confounded by detection of birds from adjacent habitat types. The species inhabiting the most common other habitat type (pocosin) is the same shrub-associated guild found commonly in pine habitat (see Section 2 of this chapter). Species such as red-eyed vireo (*Vireo olivaceus*) and prothonotary warbler (*Protonotaria citrea*) closely tied to the other common habitat (bottomland hardwood) were almost never recorded in pine habitat. Point count stations were placed to minimize the chances of detecting birds that were actually in other habitat types, and it appears that this was effective.

Section 2: Avian Communities of Pond Pine Pocosin, Bottomland Hardwood, and Coastal Scrub Habitats

Materials and Methods

The goal of our first secondary objective was to describe the avian communities in other significant terrestrial habitat types on MCBCL besides upland pine savannas and pine flatwoods, specifically pond pine pocosin, bottomland hardwoods, and coastal scrub. We established 70 new point count stations in 2011 to sample these habitats, 26 in bottomland hardwood and 22 each in pocosin and coastal scrub (**Figure 14-7**). Potential locations were identified using MCBCL GIS data then verified with site visits. Due to the linear nature of the majority of these sites, census stations were placed approximately 250 m apart along the stands with no two stations less than 200 m apart. Hardwood bottomland points were generally placed by following the stream through the habitat.

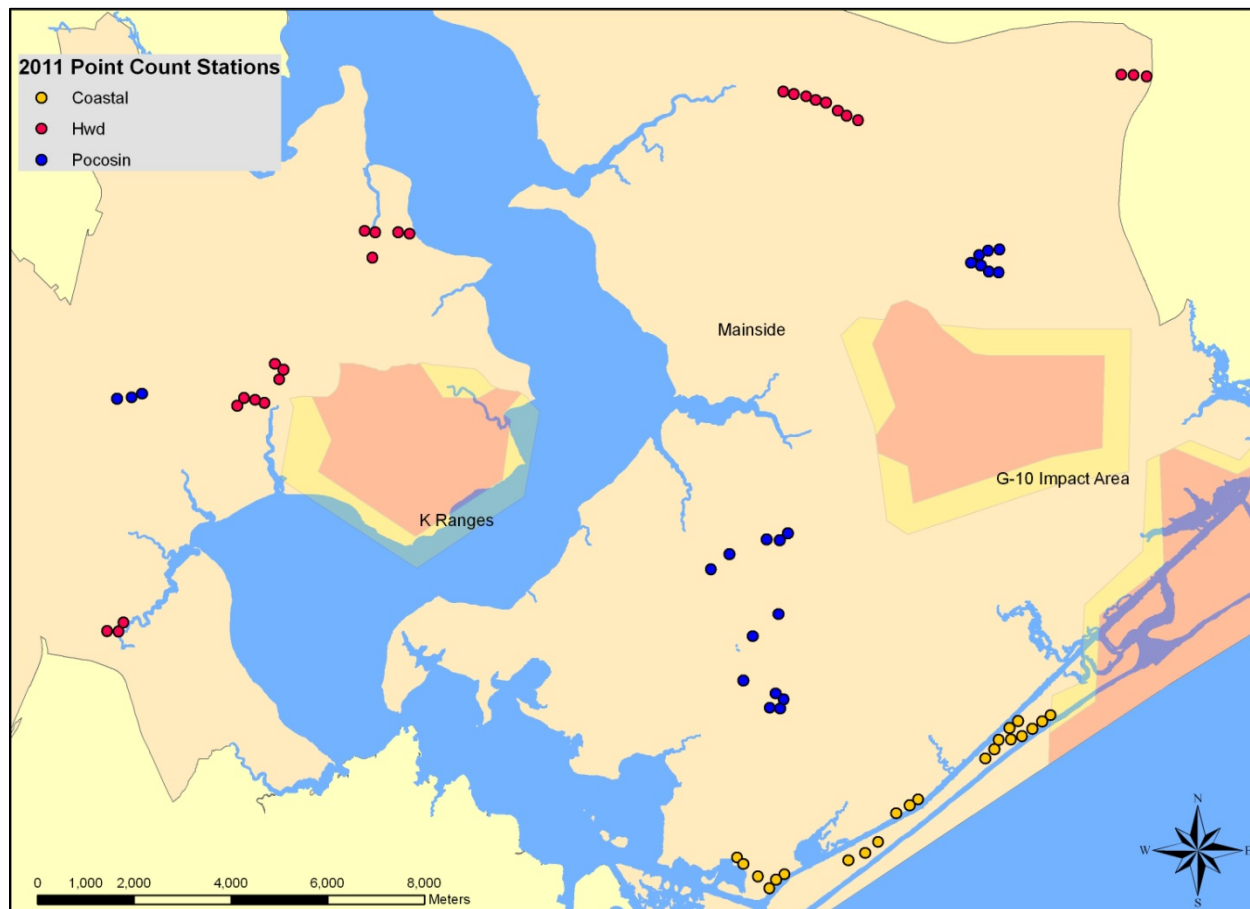


Figure 14-7. Distribution of avian census points (point count stations) for 2011 in coastal scrub (Coastal), hardwood bottomland (Hwd), and pond pine pocosin (Pocosin) habitats.

We made several adjustments to our methodology in sampling these habitats. First, we did not attempt to measure distance to birds detected due to the poor visibility in these habitat types. As a result we could not estimate abundance, but instead focused solely on species presence. Second, we sampled each point only three times rather than four.

Results and Discussion

Several species of passage migrants were observed during the 2011 point counts, most of which were detected only in bottomland hardwoods. This likely is a particularly important habitat for passage migrants on MCBCL. A number of shorebirds and wading birds were also observed, and most of these were seen in the coastal scrub. A couple of these species, Willets and Killdeer, use this habitat while breeding whereas the others merely pass through this habitat in transit to the aquatic and outer beach habitats in which they are normally found.

The remaining species detected are land birds that breed on MCBCL. Fifty such species were detected in coastal scrub, 57 in pocosin and 60 in bottomland hardwoods. Most of these species were detected at least a few times in upland pine habitat as well. This is somewhat deceptive however, as the landscape at MCBCL is characterized by a mosaic of habitat types on relatively small scales, such that birds using one habitat type may be detected from a point located in another habitat type. The exception to this pattern is coastal scrub, which is a distinctive habitat confined to a narrow zone adjacent to the coastal dunes, marshes, and beach (**Figure 14-7**). This habitat, despite its distinctiveness, contributes little to beta diversity. In fact, it contributes just one species (i.e., the painted bunting), which was one of the most frequently detected species in coastal scrub (**Table 14-8**) and was observed in no other habitat. The true affinities of other species we observed primarily or only in coastal scrub habitat are with adjacent habitats such as marshes (seaside sparrows [*Ammodramus maritimus*], red-winged blackbirds [*Agelaius phoeniceus*], various wading birds) and beach (various shorebirds and gulls). Otherwise, the species observed in coastal scrub were also common in one or more other habitat types (Table 8).

Table 14-8. Ten most frequently detected species in three habitat types, listed from most to least frequent.

Pond Pine Pocosin	Bottomland Hardwood	Coastal Scrub
Northern cardinal ^a	Northern parula	Northern cardinal ^a
Prairie warbler ^a	Northern cardinal ^a	Red-winged blackbird
Eastern towhee ^a	Tufted titmouse ^a	Painted bunting
Great crested flycatcher ^a	Great crested flycatcher ^a	Prairie warbler ^a
Brown-headed cowbird ^a	Blue-gray gnatcatcher ^a	Common grackle
Yellow-breasted chat ^a	Red-eyed vireo	Tufted titmouse ^a
Blue-gray gnatcatcher ^a	Red-bellied woodpecker ^a	Indigo bunting ^a
Common yellowthroat ^a	Prothonotary warbler	American crow ^a
Mourning dove ^a	Yellow-throated warbler ^a	Carolina wren ^a
Indigo bunting ^a	Carolina chickadee ^a	Blue grosbeak ^a

^a Indicates species also commonly detected in point counts in pine uplands.

Bottomland hardwood habitat is also distinctive and tends to have narrow, sharp ecotones with pine uplands. Nevertheless, the two habitats occur in close proximity regularly across the MCBCL landscape. Bottomland hardwoods contribute greatly to avian diversity on MCBCL as a number of species found in this habitat, including some of the most common ones (northern parula [*Setophaga americana*], red-eyed vireo [*Vireo olivaceus*], prothonotary warbler

[*Protonotaria citrea*], **Table 14-8**), rarely use pine uplands, even those in poor condition with respect to RCW foraging habitat quality. These species were occasionally detected during point counts in pine habitat, but these instances appeared to be cases in which these species were in or near the edge of adjacent bottomland hardwood habitat. Included in this group are the Acadian flycatcher (*Empidonax virescens*), Louisiana waterthrush (*Parkesia motacilla*), ovenbird (*Seiurus aurocapilla*), Swainson's warbler (*Limnothlypis swainsonii*), and white-breasted nuthatch (*Sitta carolinensis*). Our data suggest that these species do not invade pine uplands that develop a significant hardwood component as occurs under fire suppression, a conclusion also reached by Allen et al. (2006). Thus the species found in bottomland hardwood habitat can be divided into two groups: (1) those that are confined to this habitat and remain so regardless of the condition of the pine uplands and (2) those that occur in both bottomland hardwoods and pine uplands. As previously discussed (see Section 1), most of the latter respond positively to management for RCWs despite their seeming affinity to hardwoods. The two exceptions are yellow-throated warbler and blue jay (**Table 14-6**). These are the only two species characteristic of bottomland hardwoods that can be thought of as profiting from degradation (from the perspective of RCWs) of pine uplands and thus being negatively affected by habitat management for RCWs.

Pond pine pocosins grade into pine uplands through distinctive ecotones throughout the MCBCL landscape. These ecotones are known as areas of high plant diversity and are of great ecological interest. The contribution of pocosins to avian diversity arises through effects on relative abundance of species rather than supporting species endemic to that habitat. Only one species commonly detected in this habitat, the gray catbird (*Dumetella carolinensis*), was not also found in other habitat types. A few species were shared with bottomland hardwoods (prothonotary warbler, Swainson's warbler) or coastal scrub (common grackle [*Quiscalus quiscula*]), but the great majority was shared with pine uplands. Indeed, all of the most common species in pocosin were also regularly detected in pine uplands (**Table 14-8**). It is instructive to think of the birds found in pine habitats on MCBCL, running from xeric longleaf uplands to mesic pond pine pocosins, as a single community. One species, the yellow-breasted chat, appears to thrive in the ecotones between upland and pocosin. For other species, the linkage between RCW habitat score and abundance appears to reflect where along the soil-moisture gradient a point lies. Three of the species we classified as associated with shrubs (**Table 14-7**) are among the 10 most common species in pocosin (**Table 14-8**) and the other two are also common there. These species are more common in more mesic sites where woody vegetation is more prevalent and RCW foraging habitat scores are lower. Although occurrence of these species may be negatively correlated, we suggest this is a result for their preferred locations along the soil-moisture gradient than RCW management per se. Allen et al. (2006) found these same five species to be associated with pocosin-like vegetation in riparian areas on Fort Bragg, NC. However, they also found that fire had positive effects on all of these species. That is, these species were more common in pocosins that burned as a result of prescribed fires set to benefit RCWs than in pocosins in fire-suppressed areas. Thus RCW management, specifically prescribed fire, may actually benefit these species, at least in areas that are too wet to be converted into upland vegetation. There likely are negative effects on these species when RCW management pushes ecotones back toward the mesic end of the gradient, and conversely fire suppression allows woody vegetation and the ecotone to spread farther upland along the gradient.

We conclude that bottomland hardwoods make important contributions to avian diversity on MCBCL by supporting unique species, and that pond pine pocosins do so as part of a larger pine

community spanning the soil-moisture gradient. Coastal scrub contributes a single species of considerable interest, the painted bunting. Habitat management for RCWs does not conflict with promoting avian diversity as species endemic to bottomland hardwoods remain there regardless of how pine habitats are managed, and prescribed fire appears to benefit the entire pine community. Only a handful of species, the yellow-throated warbler, blue jay, and prairie warbler (*Setophaga discolor*; a specialized species we do not discuss), can be viewed as being negatively impacted by RCW habitat management.

Section 3: The Cavity-Nesting Bird Community

Materials and Methods

The methods for this portion of the study are based on a previous study at Eglin Air Force Base in Florida (Blanc, 2007; Blanc and Walters, 2008a and b) to allow for direct comparisons between cavity-nesting avian communities on Eglin and MCBCL and thereby test ideas about the dynamics of this community developed in the Eglin study. From April through July 2009–2011, we searched for nests of cavity-nesting birds on 30 9-ha plots. We selected a set of plots in upland stands dominated by longleaf pine at least 60 years of age that were distributed throughout the Base (**Figure 14-1**) and that reflected the range of RCW cavity tree densities available. Locations of RCW cavity trees within the plots were obtained from the RCW management database on MCBCL. We conducted nest searches between 0900 and 1400 daily, and searched each plot three times each year. The order in which we searched plots was randomized each round, and when possible we searched two plots per day. During each round of nest searching, two field technicians started at opposite corners of the plot and walked transects for one hour until they met in the middle. We ignored RCW cavity trees during nest searching to reduce bias for plots with high RCW tree density. All RCW cavity trees within plots were instead checked separately three times during the season. Contents of cavities were determined with a pole-mounted camera video system (Treetop Peeper Video System, Sandpiper Technologies Inc., Manteca, CA). Data collected for each nest found included diameter at breast height of the cavity tree, tree type (hardwood, live pine, and dead pine; species for pines only), bird species of bird, nest contents, whether cavity entrances were normal or enlarged, species of excavator if known (2009–2010), decay class of dead cavity trees (i.e., snags), cavity height and orientation, and location. Nest trees were assigned a tree number and tagged for future reference. We conducted nest searching only during good weather conditions of no precipitation and little wind. In 2008, a pilot study was conducted using 10 out of the 30 plots to verify protocols in habitat available on MCBCL.

During the 2011 field season, we documented nest success on 20 of the plots. We systematically monitored each nest discovered to determine the fate of the nest. Nests were classified as successful if nestlings were present 1 week prior to the expected fledging. We did not revisit nests after that time to prevent prematurely fledging young.

After nest searching was completed for the season, we estimated the number of snags in each plot using nine 25-m radius vegetation plots (**Figure 14-8**). Snags were defined as dead trees ≥ 10.2 cm dbh and ≥ 1.4 m in height. We classified snags into structural classes based on the presence of branches, amount of bark and stage of decay. The classes were as follows: (1) recently dead (most bark and branches and top of tree intact) (2) dead several years (greater than

50% bark and/or branches intact and top usually [but not necessarily] broken), (3) dead several years (less than 50% bark and/or branches intact and top usually broken), and (4) dead for many years (few to no branches or bark, broken top, and/or extensive decay).

We used nest webs (Blanc and Walters, 2008b; Martin and Eadie, 1999; Martin et al., 2004) to illustrate connections of cavity-nesting species with one another and with nesting substrates. We included in the nest web all nests in cavities with known or reasonably determined excavators. Determination of cavity excavator was based on cavity size and shape if the excavator was not directly known (Blanc, 2007).

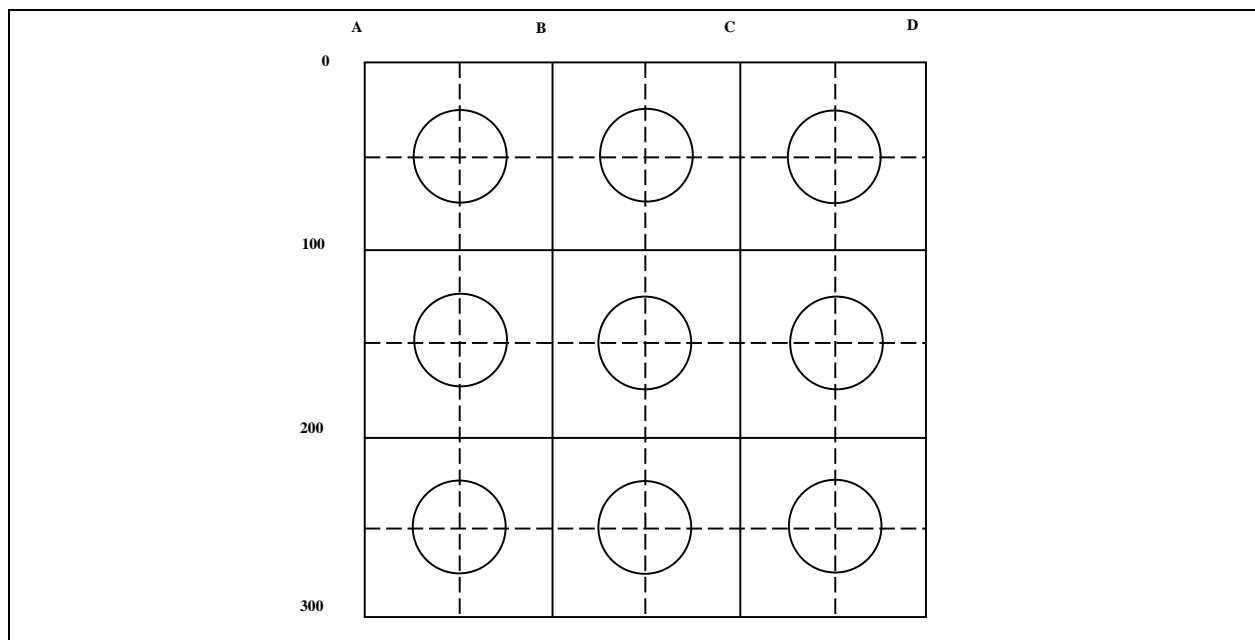


Figure 14-8. The 300-m × 300-m cavity-nester study plot design.

Lines, solid and dotted, indicate transects. Circles indicate 25-m radius vegetation plots.

From April to July 2010, nest searches were conducted for cavity-nesting birds on 14 300-m × 300-m (9-ha) plots on Eglin Air Force Base. The results from these plots were compared to those from 14 of the cavity nesting plots on MCBCL. We selected research plots to contain the same total number of RCW cavity trees in living pine on Eglin Air Force Base as the 14 plots on MCBCL. Nest searching protocols were identical to above. Nest densities were calculated using only those nests that fell within the plot boundaries; however, nests found within 50 m of plot boundaries were included in the analysis of resource selection. We estimated available snag density on each plot by quantifying the number, type and diameter at breast height of all snags within the nine 25-m radius circular vegetation plots in the same manner as on MCBCL as described above. We compared nest and snag densities on Eglin and MCBCL using Wilcoxon rank sum (Mann-Whitney U) tests.

Results and Discussion

Nest searches at MCBCL resulted in 334 nests representing 12 avian species (i.e., the northern flicker, pileated woodpecker [*Dryocopus pileatus*], RCW, red-headed woodpecker, red-bellied

woodpecker, hairy woodpecker [*Picoides villosus*], brown-headed nuthatch, Carolina chickadee, eastern bluebird [*Sialia sialis*], eastern screech owl [*Megascops asio*], great-crested flycatcher [*Myiarchus crinitus*], and tufted titmouse (**Figure 14-9**). The majority of nests occurred in pine snags (n=197, 59%), followed by living pine (in cavities excavated by RCWs; n=93, 27.8%) and finally hardwood snags (n=30, 9%; **Figure 14-9**). The nest web illustrates the importance of RCW cavity trees in this ecosystem (**Figure 14-9**). The eastern bluebird was the most common heterospecific user of RCW cavity trees (n=21) and used unenlarged cavities that could otherwise be occupied by RCWs (**Figure 14-10**). Nesting density (nests/ha) at MCBCL was 0.53 nests per ha. Vegetation surveys indicated that pine snags were more prevalent than hardwood snags.

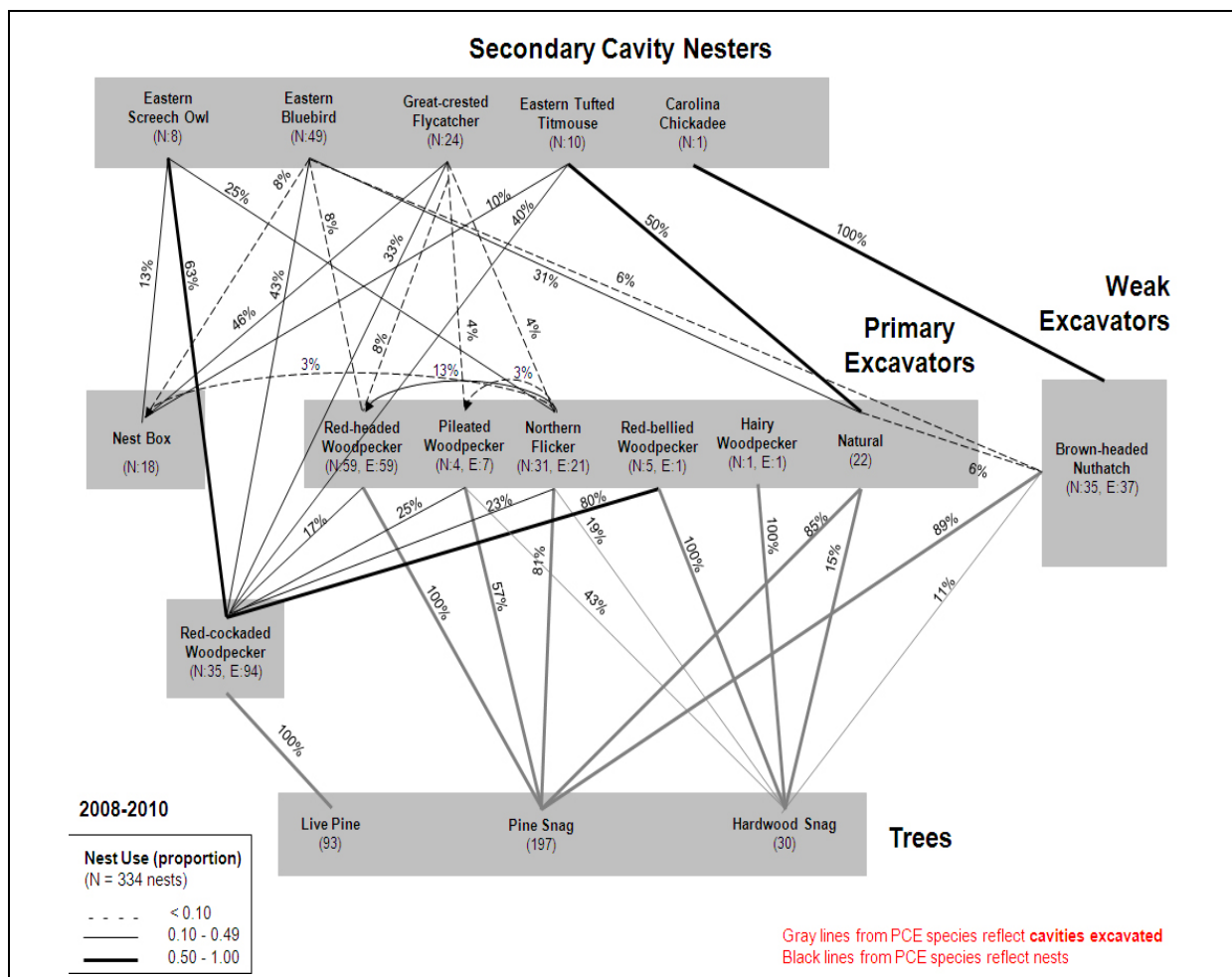


Figure 14-9. Cavity nest web at MCBCL, based on data from nest searches 2008–2010.

The cavity-nesting bird community at MCBCL proved to be remarkably similar to that on Eglin in terms of species composition and richness, as well as nest-site selection, with the majority of nests occurring in pine snags at both sites. The comparative study in 2010 documented this (**Figure 14-11**), but also revealed one notable difference between the two sites, a significantly higher nesting density at MCBCL (0.34 nests/ha in the 14 plots included in this comparative study) that was twice the density observed on Eglin Air Force Base (0.17 nests/ha) (P=0.008). This difference applied to both primary cavity excavators and secondary cavity users (**Figure**

14-12), and occurred despite similar densities of snags at the two sites (MCBCL = 8.7 snags/ha; Eglin = 9.6 snags/ha). Eglin's pine snags were larger on average than those at MCBCL (mean dbh Eglin = 25.9 cm, n=95; MCBCL = 21.2 cm, n=118; $P=0.0001$), but density of usable-size pine snags (i.e., snags large enough to support a cavity-nest) did not differ between the two sites ($P=0.21$; **Figure 14-13**). The mean dbh of available hardwood snags did not differ between Eglin (mean dbh = 17.1 cm, n=99) and MCBCL (mean dbh = 16.0 cm, n=28; $P=0.25$), but Eglin had a higher density of usable-size hardwood snags ($P=0.01$; **Figure 14-13**).

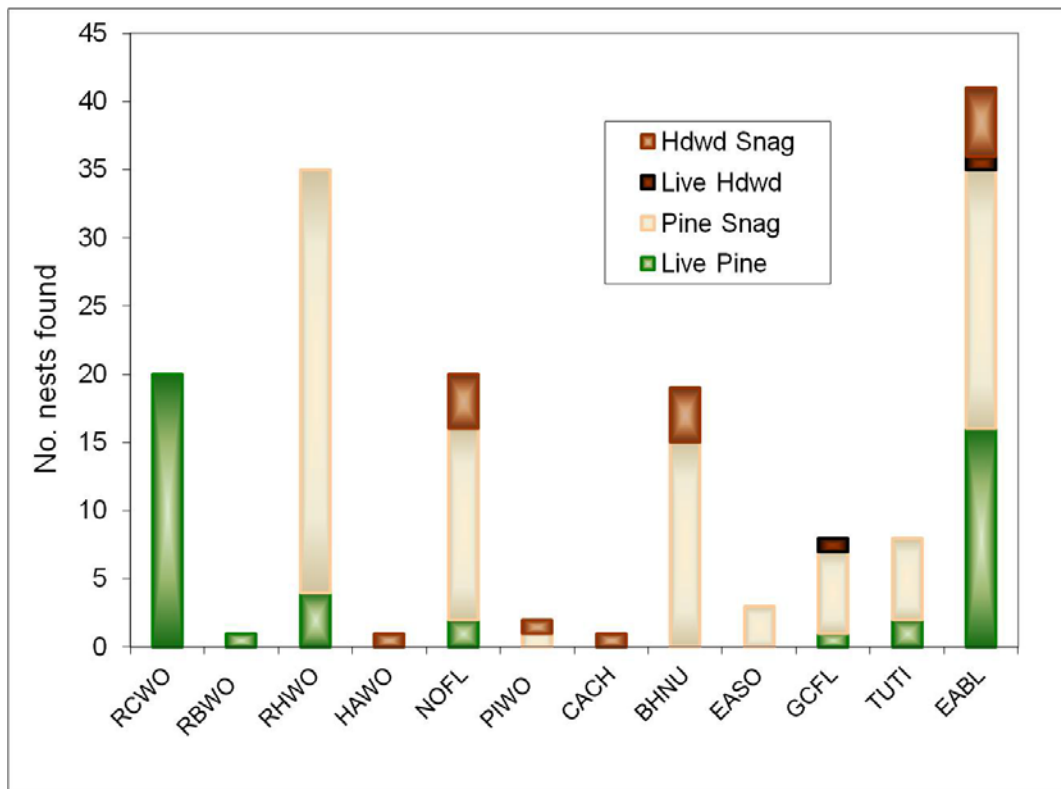


Figure 14-10. Number of nests found for each species by nesting substrate at MCBCL from 2008–2010.

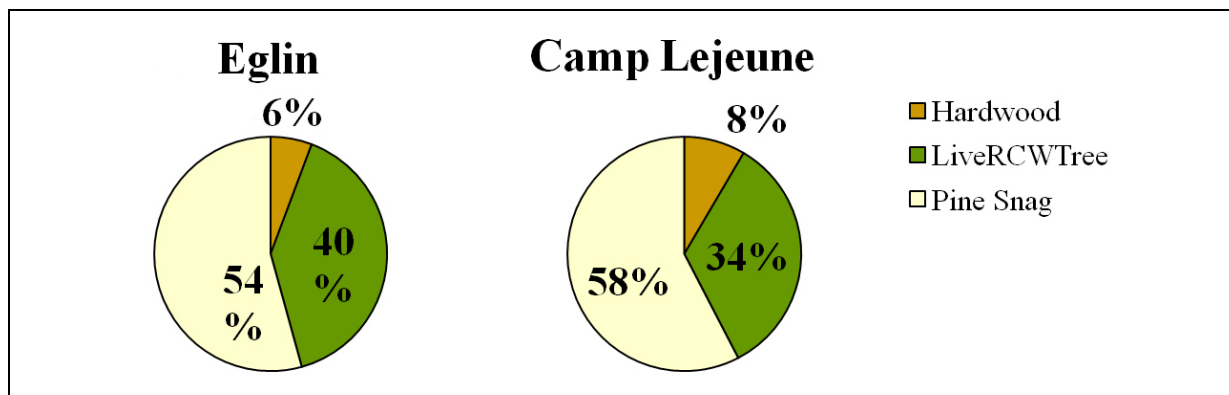


Figure 14-11. Nest substrate use at Eglin Air Force Base (n=35) and MCBCL (n=59). Nest substrates are pine snag, hardwood snag (Hardwood) and live pines with cavities excavated by RCWs (LiveRCWTree). Excludes eight nests from MCBCL in nest boxes.

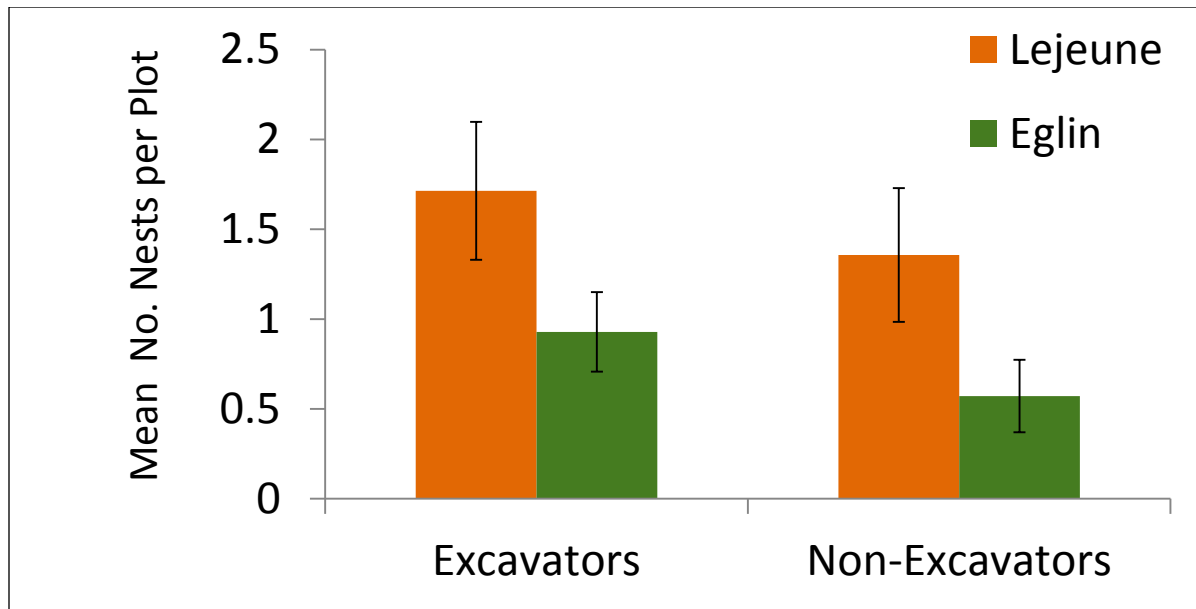


Figure 14-12. Nest densities (mean \pm standard error) of cavity-nesting birds found during April–July 2010 on 14 plots each at MCBCL (Lejeune, n=43) and Eglin Air Force Base (Eglin, n=21), for both primary cavity excavators (Excavators) and non-excavating secondary cavity nesters (Non-Excavators).

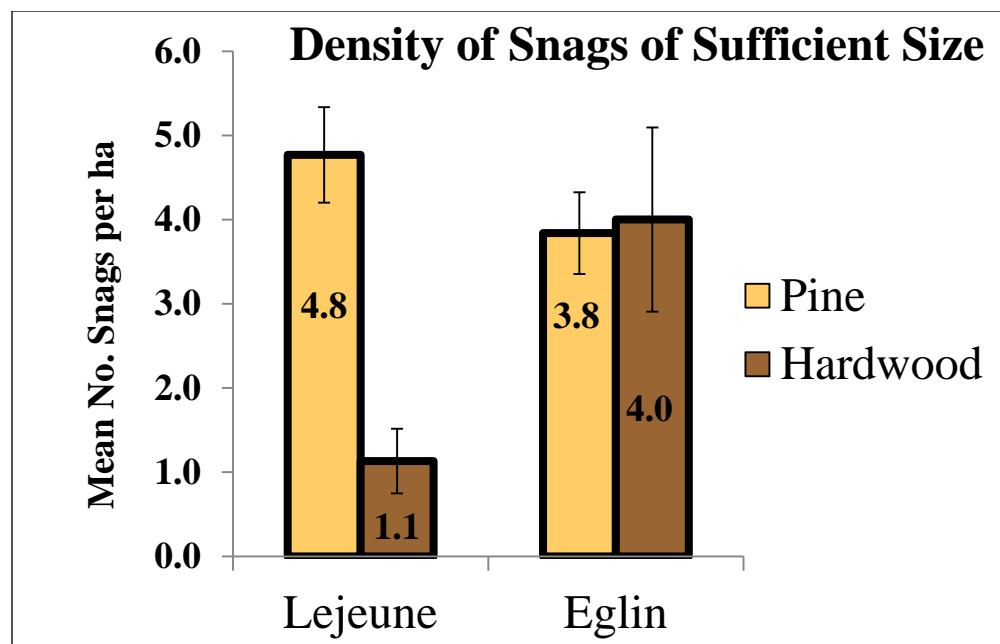


Figure 14-13. Densities of pine and hardwood snags (mean \pm standard error) of sufficient size to support nests at MCBCL (Lejeune) and Eglin Air Force Base (Eglin).

Sufficient size is defined by the smallest diameter at breast height of each tree type (pine = >16.8 cm and hardwood = >12.8 cm) found to contain a nest at either site.

Thus differences in available snags do not appear to explain the higher nesting densities at MCBCL, suggesting that neither snag quantity nor quality is limiting cavity-nester populations in the old-growth forests at Eglin Air Force Base. Cavity and snag availability are often considered to be the main limiting factor for avian cavity-nesting bird populations (Newton, 1994), although other factors such as foraging habitat quality may play a stronger role in limiting cavity-nesting bird populations (Homyack et al., 2011; Miller, 2010), particularly in old growth forests (Wesołowski, 2007). Our results suggest that this may be the case at Eglin. We hypothesize that greater ecosystem productivity and heterogeneous habitat may explain the higher nesting density at MCBCL. The Eglin reservation is dominated by vast areas of Sandhills habitat that is highly xeric. In contrast, the landscape at MCBCL contains a greater proportion of more mesic habitat and is highly heterogeneous (see Section 2), which could lead to a greater abundance and diversity of food sources for cavity-nesting birds. More research is needed to investigate this hypothesis.

The difference between Eglin and MCBCL in hardwood snag density is likely a function of differences in RCW habitat management. Prescribed burning to reduce hardwoods is conducted at both sites; however, herbicide also has been used extensively at Eglin (resulting in many hardwood snags), but not yet at MCBCL. At MCBCL some mechanical hardwood removal is done, which of course does not produce snags.

Literature Cited

- Allen, J.C., S.M. Krieger, J.R. Walters, and J.A. Collazo. 2006. Associations of breeding birds with fire-influenced and riparian-upland gradients in a longleaf pine ecosystem. *Auk* 123:1110–1128.
- Bednarz, J., D. Ripper, and P. Radley. 2004. Emerging concepts and research directions in the study of cavity-nesting birds: Keystone ecological processes. *Condor* 106:1–4.
- Beyer, H.L. 2004. Hawth's Analysis Tools for ArcGIS. Available at <http://www.spatialecology.com/htools>.
- Blanc, L. 2007. *Experimental Study of an Avian Cavity-nesting Community*. Ph.D. dissertation, Virginia Tech, Blacksburg, VA.
- Blanc, L., and J.R. Walters. 2008a. Cavity excavation and enlargement as mechanisms for indirect interactions in an avian community. *Ecology* 89:506–514.
- Blanc, L., and J.R. Walters. 2008b. Cavity-nest webs in longleaf pine ecosystem. *Condor* 110:80–92.
- Buckland, S.T. 2001. *Introduction to Distance Sampling: Estimating Abundance of Biological Populations*. Oxford University Press: New York.
- Conner, R.N., C.E. Shackelford, R.R. Schaefer, D. Saenz, and D.C. Rudolph. 2002. Avian community response to southern pine ecosystem restoration for red-cockaded woodpeckers. *Wilson Bulletin* 114:324–332.
- Engstrom, R.T. 1993. Characteristic mammals and birds of longleaf pine forests. Pages 127–138 in *The Longleaf Pine Ecosystem: Ecology, Restoration and Management*. Edited by S.M. Hermann. *Proceedings of the Tall Timbers Fire Ecology Conference* 18. Tall Timbers Research Station, Tallahassee, FL.
- Farnsworth, G.L., K.H. Pollock, J.D. Nichols, T.R. Simons, J.E. Hines, and J.R. Sauer. 2002. A removal model for estimating detection probabilities from point-count surveys. *Auk* 119:414–425.
- Hines, J.E. 2006. PRESENCE4—Software to estimate patch occupancy and related parameters. USGS-PWRC. Available at <http://www.mbr-pwrc.usgs.gov/software/presence.shtml>.
- Homyack, J., B. Paxton, M. Wilson, B. Watts, and D. Miller. 2011. Snags and cavity-nesting birds within intensively managed pine stands in Eastern North Carolina. *Southern Journal of Applied Forestry* 35:148–154.
- Huss, M., J. Bednarz, D. Juliano, and D. Varland. 2002. The efficacy of inoculating fungi into conifer trees to promote cavity excavation by woodpeckers in managed forests in western Washington. Pages 777–794 in *Proceedings of the Symposium on the Ecology and Management of Dead Wood in Western Forests*. Edited by W. Laudenslayer Jr., P. Shea, B. Valentine, P. Weatherspoon, and T. Lisle. U.S. Department of Agriculture, Forest Service General Technical Report PSW-GR-181.

- Kirkpatrick, C., C.J. Conway, and P.B. Jones. 2006. Distribution and relative abundance of forest birds in relation to burn severity in southeastern Arizona. *Journal of Wildlife Management* 70:1005–1012.
- Martin, K., and J.M. Eadie. 1999. Nest webs: A community-wide approach to the management and conservation of cavity-nesting forest birds. *Forest Ecology and Management* 115:243–257.
- Martin, K., K. Aitken, and K. Wiebe. 2004. Nest sites and nest webs for cavity-nesting communities in interior British Columbia, Canada: Nest characteristics and niche partitioning. *Condor* 106:5–19.
- MCBCL (Marine Corps Base Camp Lejeune). 2006. *Integrated Natural Resource Management Plan(INRMP)*. U.S. Marine Corps Camp Lejeune, NC. Available at <http://www.lejeune.usmc.mil/emd/INRMP/INRMP.htm>.
- Miller, K. 2010. Nest-site limitation of secondary cavity-nesting birds in even-age southern pine forests. *The Wilson Journal of Ornithology* 122:126–134.
- Newton, I. 1994. The role of nest site in limiting the numbers of hole nesting birds: A review. *Biological Conservation* 70:265–276.
- Provencher, L., N.M. Gobris, L.A. Brennan, D.R. Gordon, and J.L. Hardesty. 2002. Breeding bird response to midstory hardwood reduction in Florida sandhill longleaf pine. *Journal of Wildlife Management* 66:641–661.
- Ralph, C.J., S. Droege, and J.R. Sauer. 1995. Managing and monitoring birds using point counts: Standards and applications. Pages 161–168 in *Monitoring Bird Populations by Point Counts*. Edited by C.J. Ralph, S. Droege, and J.R. Sauer. U.S. Department of Agriculture, Forest Service General Technical Report PSW-GTR-149.
- Roberge, J-M., and P. Angelstam. 2004. Usefulness of the umbrella species concept as a conservation tool. *Conservation Biology* 18:76–85.
- Rosenstock, S.R., D.R. Anderson, K.M. Giesen, T. Leukering, M.F. Carter, and F. Thompson III. 2002. Landbird counting techniques: Current practices and an alternative. *Auk* 119:46–53.
- Saab, V., W. Dudley, and W. Thompson. 2004. Factors influencing occupancy of nest cavities in recently burned forests. *Condor* 106:20–36.
- Thomas, L., J.L. Laake, E. Rexstad, S. Strindberg, F.F.C. Marques, S.T. Buckland, D.L. Borchers, D.R. Anderson, K.P. Burnham, M.L. Burt, S.L. Hedley, J.H. Pollard, J.R.B. Bishop, and T.A. Marques. 2009. Distance 6.0 Release 2. Research Unit for Wildlife Population Assessment, University of St. Andrews, UK. Available at <http://www.ruwpa.st-and.ac.uk/distance>.
- USFWS (U.S. Fish and Wildlife Service). 2003. *Red-cockaded Woodpecker (Picoides borealis) Recovery Plan: Second Revision*. U.S. Fish and Wildlife Service, Atlanta, GA.

- Walters, J.R. 1991. Application of ecological principles to the management of endangered species: the case of the red-cockaded woodpecker. *Annual Review of Ecology and Systematics* 22:505-523.
- Wesołowski, T. 2007. Lessons from long-term hole-nester studies in a primeval temperate forest. *Journal of Ornithology* 148: S395–S405.
- Whittaker, R.H. 1960. Vegetation of the Siskiyou Mountains, Oregon and California. *Ecological Monographs* 30:279–338.
- Wilcox, B.A. 1984. In situ conservation of genetic resources: determinants of minimum area requirements. Pages 639–647 in *National Parks, Conservation and Development: The Role of Protected Areas in Sustaining Society*. Edited by J.A. McNeely and K.R. Miller. Smithsonian Institution Press: Washington, DC.

[This page intentionally left blank.]

Chapter 15

Optimization of Prescribed Burning by Considering Mechanical Thinning as a Viable Land Management Option

SERDP Project Number RC-1413

Atmospheric Module

Research Project Air-1

Lead Researcher:

Dr. Karsten Baumann

Atmospheric Research & Analysis, Inc.

1000 Perimeter Park Drive (Suite G), Morrisville, NC 27560

E-mail: kbaumann@atmospheric-research.com

May 10, 2013

Final

This report was prepared under contract to the U.S. Department of Defense (DoD) Strategic Environmental Research and Development Program (SERDP). The publication of this report does not indicate endorsement by DoD, nor should the contents be construed as reflecting the official policy or position of DoD. Reference herein to any specific commercial product, process, or service by trade name, trademark, manufacturer, or otherwise, does not necessarily constitute or imply its endorsement, recommendation, or favoring by DoD.

Table of Contents

Abbreviations.....	15-viii
Abstract.....	15-1
Objectives	15-2
Background.....	15-3
Role of Prescribed Burning in Land Management	15-3
Role of Prescribed Burning in Air Quality	15-6
Materials and Methods.....	15-10
Fuel Characterization and Consumption.....	15-10
PB Emissions Measurements.....	15-12
Ozone (O ₃) Forming Potential	15-17
Secondary Organic Aerosol (SOA) Forming Potential	15-18
Results and Discussion	15-20
Fuel Character and Consumption.....	15-21
Gas-Phase PB Emissions and Emission Factors (EF).....	15-25
Particle-Phase PB Emissions and Emission Factors (EF).....	15-29
Fuel Treatment Effects on Modified Combustion Efficiency (MCE) and Emissions (EF).....	15-37
VOC Profiles and the Potential to Form Ozone and SOA.....	15-44
EF Applications and Comparisons.....	15-50
Local to Regional Air Quality Trends	15-56
Urban PM _{2.5} Sensitivity to Sub-Regional PB Activities.....	15-58
Urban PM _{2.5} Sensitivity to Sub-Regional PB Activities.....	15-59
Summary Conclusions and Implications	15-62
PB Emissions, Fuel Consumption, and Emission Factors	15-62
PB Effect on Nutrient Mobilization.....	15-64
Local to Regional Trends in Ozone, PM _{2.5} , and Rainfall	15-65
PB Influence on PM _{2.5} Relative to Forecast Weather Conditions	15-65
Literature Cited	15-67
Appendix 15-A: Supporting Data	15-A-1
Appendix 15-B: List of Scientific/Technical Presentations.....	15-B-1

List of Figures

15-1.	Nationwide annual total wildland fires burned and occurrence frequency in comparison with annual total PB areas from five major U.S. land management agencies (NIFC, 2012).	15-3
15-2.	Annual total wildfire (WF) occurrences and areas relative to annual acres burned via PB application during the growing season (PB-GS) and the dormant season (PB-DS) at MCBCL.....	15-5
15-3.	Linkage between wildfires and prescribed burns at MCBCL.....	15-6
15-4.	Location of investigated vegetation plots at MCBCL.	15-10
15-5.	Conceptual approach for the comparative measurement of emissions from untreated control and mechanically thinned treated fuels; adapted from <i>The Nature Conservancy Magazine Vol. 58 (3), Autumn 2008</i>	15-13
15-6.	Available and consumed fuel for different fuel types and treatment plots.	15-22
15-7.	Comparison of gaseous species' EF (individual and groups) as weighted average from the different vegetation plots investigated for fuel consumption.....	15-26
15-8.	EF comparison of certain gaseous species and VOC groups from different studies. Here Light Organic Acids (LOA*) comprise only formic and acetic acids.	15-28
15-9.	Comparison of particle phase PM _{2.5} species's EF (individual and groups) as weighted average from the different vegetation plots investigated for fuel consumption.....	15-31
15-10.	Mass fraction of major inorganic compound groups emitted with PM _{2.5} from PB of both fuel types at the five experiment plots at MCBCL.....	15-32
15-11.	Charge balance of emitted PM _{2.5} mass for the two different fuel types in five different fuel beds (plots) at MCBCL.	15-34
15-12.	Comparison of emission profiles relative to PM _{2.5} mass from fuels in California (CA), the southeastern (SE) United States, South Carolina (SC), and Georgia (GA).	15-35
15-13.	Comparison of normalized POC emissions in milligrams of carbon per gram of OC of major organic compound groups.....	15-36
15-14.	EF as a function of MCE for each of the 10 samples from the control (blue diamonds) and treatment (red triangles) plots.	15-38
15-15.	Comparison of correlation coefficients from gaseous species's EF versus MCE regression.	15-40
15-16.	Comparison of correlation coefficients from PM _{2.5} mass and species' EF versus MCE regression.	15-41
15-17.	Comparison of average VOC MR in individual fuel bed emissions.	15-45

15-18. Average ranking of VOCs emitted during PB of control (CTRL) and mechanically thinned (HYAX) fuel beds (15-17), compared to propylene-equivalent ranking R(OH), indicating O ₃ forming potential.	15-46
15-19. Relative contributions of major aromatic and biogenic VOC groups emitted by the PB of different fuel types and beds to the SOA forming potential of the surrounding region.	15-48
15-20. Comparison of our in situ PM _{2.5} , CO, CH ₄ , and NMHC EF from mechanically thinned (HYAX) and control (CTRL) fuel with AP-42 (EPA, 1996).	15-50
15-21. Comparison of main pollutants' annual emissions from fuel-specific PB with those from other MCBCL sources; ECOM = boilers, ICOM = generators, FIRE = training pits, JET = engine test stands.	15-52
15-22. Emission factors as a function of KBDI comparing control (blue diamonds) and treatment (red triangles) plots.	15-55
15-23. Location of atmospheric monitoring stations within the regional study domain.....	15-58
15-24. MCBCL monitoring and research stations with rainfall monitor locations used in Research Project Air-2.....	15-59

List of Tables

15-1. Species percent abundances in investigated plots at MCBCL based on pre-treatment stem density measurements.	15-11
15-2. List of aerosol species measured from discrete PB emissions samples from investigated plots at MCBCL.....	15-14
15-3. OH rate constants (k), the fraction of VOC species reacted with midday OH levels after 5 hours (FR), and the FAC from Grosjean (1992), except as noted.....	15-20
15-4. Available fuel (F), different fuel moisture (FM) and fuel consumption (FC) levels—absolute and relative to what was available, and vegetation composition indicators CCA and NMS for the two different treatment types investigated in the five different vegetation plots.	15-21
15-5. Statistically significant Pearson's correlation coefficients between different fuel parameters from within the two fuel types, CTRL in blue and HYAX in red.....	15-23
15-6a. Statistically significant <i>r</i> -values for relationships between certain fuel parameters and species' EF values, using both flaming and smoldering EF values independently.	15-24
15-6b. Statistically significant <i>r</i> -values for relationships between certain fuel parameters and species's EF values, using combined flaming and smoldering EF values (as weighted average).	15-24
15-7. EF values (all in g/kg except NMHC is in gC/kg) of gaseous species and compound groups for PB emissions from CTRL and HYAX fuel types of the five vegetation plots, in descending order of average EF.	15-26

15-8.	EF of PM _{2.5} species and compound groups, plus other calculated values from MCBCL control (CTRL) and treatment (HYAX) plots (see text).....	15-30
15-9.	Major carbonaceous and ionic compounds in %-mass fraction of PM _{2.5} emissions from PB of the five different vegetation plots with control and treatment fuels.	15-33
15-10.	Statistics for the linear regression of gaseous species' EF as a function of MCE for both fuel types: control [CTRL] and mechanically thinned [HYAX].	15-39
15-11.	Summary of EF-MCE regression statistics derived from Burling et al. (2011).	15-39
15-12.	Statistics for linear regression of PM _{2.5} species's EF as a function of MCE for both control [CTRL] and mechanically thinned [HYAX] fuel types.	15-42
15-13.	Average EF of SOA indicator species in emissions from control (CTRL) and mechanically thinned (HYAX) fuels at MCBCL.	15-44
15-14.	Numerical summary of values depicted in Figure 15-18 as average ranking of VOCs emitted during PB of control (CTRL) and mechanically thinned (HYAX) fuel beds.	15-46
15-15.	Comparison of SOA forming potential for aromatic and biogenic VOCs in PB emissions from mechanically thinned (HYAX) and control (CTRL) fuels at MCBCL.....	15-49
15-16.	Comparison of this study's EF with corresponding AP-42 values, including EF for total N for control (CTRL) and mechanically thinned (HYAX).	15-51
15-17.	Linear regression statistics assuming pollutant species' EF dependence on sub-regional KBDI from routine forecasts for control (CTRL) and mechanically thinned treatments (HYAX).....	15-54
15-18.	Comparison of PB emission and throughfall deposition of major ions for RB (semi-mesic loblolly pine) and HA (wet-mesic loblolly/longleaf pine).	15-56
15-19.	Given periods' total rainfall amounts (mm) from MCBCL sites relative to 30-year normals regionally averaged over the SCP (N30*).	15-58
15-20.	List of parameters and their units as input to PCR analysis (left), and ranking of the parameters' unit-less sensitivity towards PM _{2.5} (right) for the two data sets with values from either morning (A.M., yellow) or prior evening (P.M., blue) forecasts.	15-61
15-A-1.	EF of gaseous species based on weighted average excess MR from successive flaming/smoldering phase measurements for each fuel bed with and without treatment.	15-A-2
15-A-2.	EF of PM _{2.5} species based on weighted average excess MR from successive flaming/smoldering phase measurements for each fuel bed with and without treatment.	15-A-4
15-A-3.	EF of POC species based on weighted average excess MR from successive flaming/smoldering phase measurements for each fuel bed with and without treatment.	15-A-6

15-A-4. Linear regression statistics of gas species' EF as function of MCE for both fuel types.	15-A-9
15-A-5. Linear regression statistics of PM _{2.5} species' EF as a function of MCE for both fuel types.	15-A-11
15-A-6. Linear regression statistics of POC species' EF as a function of MCE for both fuel types.	15-A-13

Abbreviations

$\mu\text{g}/\text{m}^3$	micrograms per cubic meter
$\mu\text{g m}^{-3}$	micrograms per cubic meter
μm	Micron
$^{\circ}\text{C}$	degrees Celsius
ACM	aerosol composition monitoring (system)
ATV	all-terrain vehicle
AVG	Average
BLH	boundary layer mixing height
C_5H_8	isoprene or 2-methyl-1,3-butadiene
CCA	canonical correspondence analysis
CE	combustion efficiency
CH_3Br	methyl bromide
CH_3Cl	methyl chloride
CH_3CN	Acetonitrile
CH_4	Methane
$\text{C}_{10}\text{H}_{16}$	mono-terpenes (e.g., α - and β -pinene, limonene)
Cl^-	Chloride
$\text{C}_{15}\text{H}_{24}$	sesqui-terpenes (e.g., α -cedrene, α -copaene, α -humulene, β -caryophyllene)
CHN	Castle Hayne (site)
$\text{cm}^3/\text{molec}/\text{s}$	units of second order rate constant k
CMB	chemical mass balance
CO	carbon monoxide
CO_2	carbon dioxide
COS	carbonyl sulfide
CTRL	control, untreated fuel
DCERP	Defense Coastal/Estuarine Research Program
diffT	daytime maximum and minimum temperature
DL	detection limit
DoD	U.S. Department of Defense
EC	elemental carbon
ECD	electron capture detection
ECOM	boilers from MCBCL inventory
EF	emission factor

E _n	specie's n emission in mass per unit area
EPA	U.S. Environmental Protection Agency
ESI-MS	electro-spray ionization mass spectrometry
FAC	fractional aerosol coefficients
FC	fuel consumption
FID	flame ionization detection
FIRE	fire training pits from MCBCL inventory
Fn	net emitted mass of pollutant n
FR	fraction of VOC reacted with OH
FS	Forest Service
FWS	U.S. Fish and Wildlife Service
gC/kg	grams of carbon per kilogram
GC-MS	gas chromatography mass spectrometry
GHG	greenhouse gas
ha	Hectare
HAI	Haynes Index
Halo-C	Halocarbons
HAS	Hierarchical Data Storage Access System
HCl	hydrochloric acid
HNO ₃	nitric acid
HNO _x	nitrous and nitric acids
HO ₂	hydroperoxyl radical
HONO	nitrous acid
HS	Holly Shelter Game Land
HYAX	Understory and midstory thinning treatment using HydroAx equipment (i.e., mechanical thinning)
IBT	inversion burn-off temperature
IC	ion chromatography
ICOM	diesel generators at MCBCL
ICP-MS	inductively coupled plasma mass spectrometry
IEPOX	isoprene epoxydiols
ISDN	Integrated Services Digital Network
IVOC	intermediate volatility organic compound
JET	Jet Engine Test stands at MCBCL
JVA	Jacksonville site
K ⁺	water-soluble potassium

K ₂ O	potassium oxide
KBDI	Keetch-Byram Drought Index
kg	Kilogram
kg/m ²	kilogram per square meter
LOAg	light organic acid gases (e.g., acetic, formic, oxalic)
LOAp	light organic acids in the particle phase
m	Meter
m ⁻¹	per meter
MCA	Marine Corps Air Station
MCBCL	Marine Corps Base at Camp Lejeune
MCE	modified combustion efficiency
mg/g	milligrams per gram
mg/m ²	milligrams per square meter
mg-C/g OC	milligrams of carbon per gram of organic carbon
MMO	major metal oxides
MΩ	mega-ohm, measure of water's purity
MR	mixing ratio
N	Nitrogen
N ₂	nitrogen gas
NaCl	sodium chloride
NCDC	National Climatic Data Center
NH ₃	ammonia
NIFC	National Interagency Fire Center
nm	Nanometer
NMHC	non-methane hydrocarbons
NMS	non-metric multidimensional scaling
NO	nitric oxide
NO ₂	nitrogen dioxide
NO ₃ ⁻	Nitrate
NO _x	nitrogen oxides
NO _y	odd nitrogen oxides
NOAA	National Oceanic and Atmospheric Administration
NWS	National Weather Service
O ₃	ozone
OA	organic aerosol
OC	organic carbon

OM	organic mass
OOE	other organic elements
OVOC	oxygenated volatile organic compound
PAH	polycyclic aromatic hydrocarbons
PB	prescribed burning
DS	dormant season
GS	growing season
PBW	particle-bound water
PCA	principal component analysis
PCCD	polychlorinated dibenzo-p-dioxins
PCDF	polychlorinated dibenzofurans
PCR	principal component regression
pDR	personal DataRAM
PM	particulate matter
PM _{2.5}	particulate matter with a diameter less than or equal to 2.5 microns
PMF	positive matrix factorization
PNNL	Pacific Northwest National Laboratory
POA	primary organic aerosol
POC	particulate organic compound
POP	probability of precipitation
ppbv	parts per billion by volume
ppmv	parts per million by volume
PTR-MS	proton transfer reaction mass spectrometry
QA	quality assurance
QC	quality control
RH	relative humidity
RO ₂	organic peroxy radical
ROI	region of interest
S	sulfur
SC	South Carolina
SCP	Southern Coastal Plain
STD	standard deviation
SE	southeastern; standard error
SERDP	Strategic Environmental Research and Development Program
SEUS	southeastern United States
SO ₂	sulfur dioxide

SOA	secondary organic aerosol
SOP	standard operating procedure
SRG	Sandy Run Ground Site
SVOC	semi-volatile organic compound
TEOM	tapered element oscillating microbalance
TOC	total organic carbon
TOT	thermal optical transmittance
TWD	transport wind direction
TWS	transport wind speed
USDA	U.S. Department of Agriculture
UV	ultraviolet
VOC	volatile organic compound
VR	ventilation rate
WF	wildfire
WIA	Wilmington Site
WSOC	water-soluble organic compounds
WUI	Wildland Urban Interface
XRF	X-ray fluorescence

Abstract

Marine Corps Base Camp Lejeune (MCBCL) near Jacksonville, NC, served as a platform for field experiments designed to link fuel condition and consumption with emissions of gaseous and fine particulate (PM_{2.5}, or fine PM) pollutants from prescribed burning (PB), and to compare undisturbed (control) fuels with mechanically thinned fuels. Mechanical thinning of the forest understory and midstory prior to PB is believed to be effective in reducing wildfire risk and restoring longleaf pine savannas in the fire-dependent forest ecosystems of the southeastern United States (SEUS). Forests across the SEUS landscape are managed via PB, with more than 8 million acres being burned every year. As part of the Defense Coastal/Estuarine Research Program (DCERP), in situ measurements of PB emissions from the combustion of pine dominated forest were conducted in conjunction with detailed before and after fuel inventory surveys, yielding actual fuel consumption. Fuel consumption was characterized in experimental research plots that incorporated a understory and midstory thinning treatment by HydroAx followed by PB, capturing the moisture gradient from semi-mesic loblolly pine forest to wet-mesic loblolly–longleaf pine forests to pond pine pocosin. In general, understory and midstory thinning treatment yielded greater availability and consumption of fuels, especially woody material regardless of fuel moisture. Innovative mobile aerosol composition monitors were employed to measure and distinguish emissions from mechanically thinned plots with those from control plots. Measured compounds included reactive gases (ammonia [NH₃], nitrous acid [HONO], nitric acid [HNO₃], hydrochloric acid [HCl], sulfur dioxide [SO₂], light organic acids) and particulate organic compounds (POCs), water-soluble ionic species, organic carbon (OC) and elemental carbon (EC), and total PM_{2.5} mass. More than 100 POC species, including key molecular markers, were quantified and more than 40 volatile organic compounds (VOCs) were measured, including certain aromatic and biogenic compounds that are important PM_{2.5} precursors. Metallic and mineral emission components were determined via energy dispersive X-ray fluorescence and inductively coupled plasma-mass spectrometry. Applying the carbon mass balance, emission factors (EF) were calculated for the suite of aerosol species measured. Our results indicate that site vegetation variation is not driving the observed EF differences, which are therefore not confounded by either soil characteristics or vegetation differences, allowing direct comparison of treatment effects on EF. Gaseous EF averages from the two fuel types are similar, and EF variability is highest for acidic gases and isoprene. However, PM_{2.5} mass and most PM_{2.5} species EF from mechanically thinned fuels are significantly lower than those from untreated control fuels. OC is the dominant PM_{2.5} constituent in emissions from both fuel types, followed by EC, nitrate, potassium, and chloride. More VOCs are being emitted from either fuel type under less efficient (smoldering) combustion conditions, which also promote higher emissions of inorganic constituents such as major ions (especially chloride, nitrate, and sulfate), major metal oxides, and non-sulfate sulfur. Episodic comparison of PB emissions with throughfall-deposition suggests that long-term soil nutrient levels remain unaffected by PB, causing only a short-term disturbance. Combining ambient PM_{2.5} data from the site in Jacksonville, with records of MCBCL PB activities and meteorological parameters, a sensitivity analysis revealed certain weather forecast parameters' importance to local air quality relative to the amount of PB applied on MCBCL.

Objectives

The major objectives of the Atmospheric Module are to

1. Quantify fuel consumption (FC) and correlate with specific fuel conditions
2. Investigate benefits from mechanically thinning fuel prior to prescribed burning (PB) for both FC and emissions reduction
3. Establish links between measured emissions and specific fuel characteristics in collaboration with the Terrestrial Module
4. Improve inventories of emissions from PB with detailed gaseous and particulate species's emissions factors
5. Assess the magnitude and spatio-temporal trends in nutrient deposition across MCBCL and its surrounding aquatic/estuarine ecosystems in contrast to local short-term remobilization and deposition as a result of PB
6. Quantify and compare local fine particulate matter (PM_{2.5}) pollution to local Base-wide PB activities relative to important fire weather forecast parameters used in PB planning
7. Characterize local air quality on MCBCL and within the larger regional context of eastern North Carolina.

These objectives are based on the underlying hypotheses, that ecologically targeted PB decision making will be improved by enhancing fuel models with information on the relationship of fuel consumed and smoke emitted, in connection with innovative management practices to restore longleaf pine. This work will inform further investigations into impacts of forest management practices on specific restoration goals and potential changes in future emissions if restoration targets change. The last objective will be discussed more specifically and detailed in the *DCERP1 Final Baseline Monitoring Report*.

Background

Role of Prescribed Burning in Land Management

Uncontrolled wildfires are a potential threat to life and property across the nation and especially in the central and western territories of the United States. To prevent the occurrence and magnitude of wildfires, prescribed fires are becoming an integral part of public land management practices. For example, the National Interagency Fire Center (NIFC) is the nation's support center for wildland firefighting. The NIFC collaborates with several federal and state agencies to coordinate and support wildland fire and disaster operations. It collects and publishes wildland fire data reported by the various agencies. Although wildfires have been reported since 1960, prescribed burn data have been gathered since 1995 from five major U.S. land management agencies, the U.S. Department of Agriculture's (USDA's) Forest Service (FS), the Bureau of Indian Affairs, the Bureau of Land Management, the National Park Service, and the U.S. Fish and Wildlife Service (FWS). **Figure 15-1** depicts the history of wildland fires in terms of sizes (in acres burned) and frequencies (locations and occurrences) relative to the—more limited—record of acres burned per prescription. Although Figure 1 seems to indicate a trend towards less fire occurrences over time, the variability of total acres burned seems to increase, with particularly large total areas burned in 1996, 2000, and 2004–2007 period, pointing to the occurrence of fewer but larger fires than in the 1960s to early 1980s. Also, the 5-year averaged trend indicates an increase of long-term average total areas burned nationwide between 1995 and 2007. Benefits from employing prescribed burning (PB), causing an overall reduction of the frequency and size of wildfires is not readily discernible, and requires more data for any conclusive statistical evaluation.

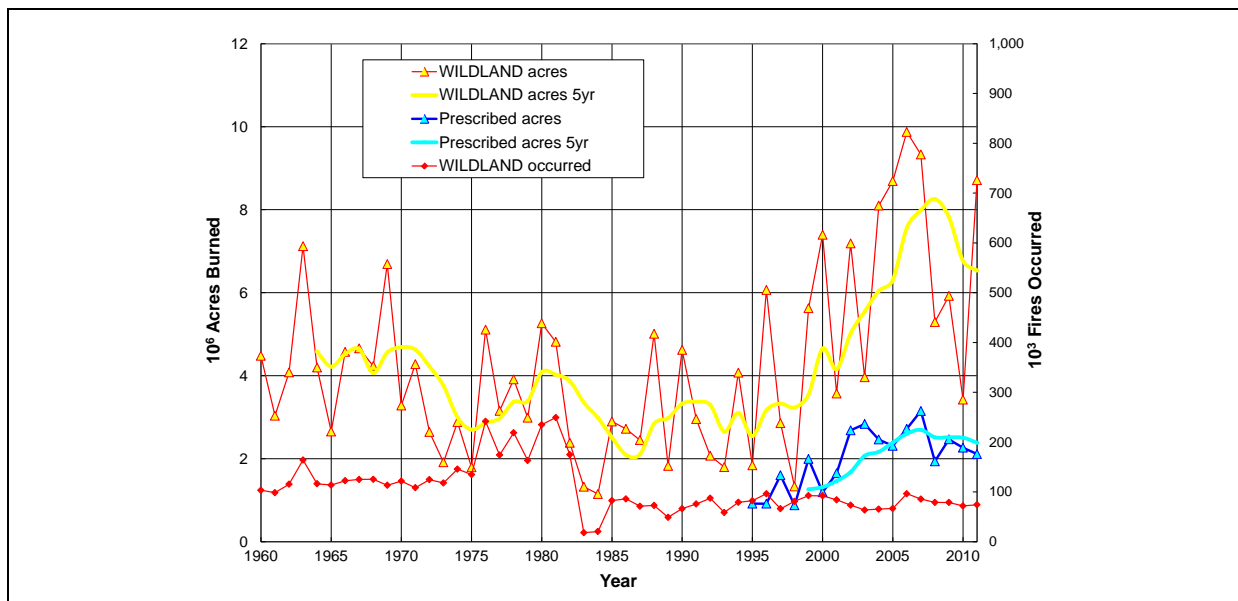


Figure 15-1. Nationwide annual total wildland fires burned and occurrence frequency in comparison with annual total PB areas from five major U.S. land management agencies (NIFC, 2012).

Yellow and light blue traces are 5-year smoothed trend lines.

Large wildfires regularly blazing in California, Arizona, and New Mexico are evidence that the plan to “fireproof” the West’s forests has backfired. Fire suppression, logging, and grazing on fire-prone public land were intended to reduce the risk of fires, but many western forests are now more flammable (Dr. Norman Christensen, Duke University and Terrestrial Module Leader in an Integrated Services Digital Network (ISDN) broadcast interview, May 24, 2004). Current wildfire management practices in the Western United States apparently fail to take into account local conditions such as weather and topography, and do not give top priority to the most hazardous fuel source (i.e., ground fuel such as dry grasses, pine needles, and low shrubs). The attempt to suppress wildfires by indiscriminate logging is considered to aggravate the problem by thinning a fire-prone forest’s canopy and littering its floor with sawdust and other combustible debris, which can accumulate to dangerous levels. The loss of canopy increases wind speed and air temperature, and decreases humidity inside the forest. As a result, ground fuel fires that break out can spread faster and farther than they would normally.

In the southeastern United States (SEUS), preventing wildfires is only one of many objectives for employing PB. Guided by the Endangered Species Act, the U.S. Department of the Interior through the FWS advises land owners in the SEUS to use PB in the recreation of the natural fire regimes needed to maintain the health of its native forest ecosystems. Across the southeastern landscape, more than 8 million acres are burned every year, whereby most PB are conducted between January and June but wildfires occur year round (Haines et al., 2001; Wade et al., 2000). Most of the longleaf pine forests in the SEUS represent the natural habitat of various threatened and endangered species such as the red-cockaded woodpecker. Hence, private land owners and land managers on military installations use PB. Of the 18.6 million acres of forested land in North Carolina, which is approximately 60% of the state’s total land area, 79% are privately owned, 14% are publicly owned (including national forests, federal, and state and local government), and 7% are used in the forest industry (Brown and New, 2012). As part of the Southern Coastal Plain (SCP), holding 5.1 million acres of forests, Onslow County is one of four counties that are more than 75% forested, and most of the 23 counties in the State of North Carolina fall into the greater than 75% forest category are located in the mountains region.

The burning of biomass is essential in creating and maintaining functional ecosystems and achieving other land use objectives (Hardy and Leenhouts, 2001). For example, North Carolina’s economy is heavily supported by agriculture and forestry. Both of these economic uses utilize PB practices to cultivate agriculture, maintain natural forests, protect endangered species, and ultimately protect human lives and property. The State of North Carolina regulates biomass burning to assure air quality, minimize fire danger and protect wildlife species such as red-cockaded woodpecker, bald eagle, piping plover, eastern wild turkey, bobwhite quail, and white tail deer that are designated by state initiatives for wildlife management. Native songbirds and flora such as rough-leaved loosestrife (*Lysimachia asperulifolia*), coastal goldenrod (*Solidago villosicarpa*), and Hirst’s panic grass (*Dichanthelium hirstii*) are also dependent on fire in many of these ecosystems.

The U.S. Department of Defense (DoD) manages more than 25 million acres of federal and state training lands and testing areas on more than 425 major military installations throughout the 50 states (DoD and USFWS, 2001). These installations vary in size from tens of acres to millions of contiguous acres, with the largest installations found in the southwestern and western regions of the nation, as well as in Alaska. The two largest military installations in North Carolina are Fort

Bragg and Marine Corps Base Camp Lejeune (MCBCL), occupying actively managed training land areas of 162,000 and 101,000 acres, respectively. Similar to many other DoD lands, the training areas of these North Carolina installations provide important ecological settings and habitat for a variety of flora and fauna, including the previously mentioned threatened and endangered species.

Similar to the nationwide trend, benefits of PB application at MCBCL in terms of causing a decrease in occurrence or size of wildfires are not obvious as illustrated in **Figures 15-2 and 15-3**. Recent years of data from MCBCL suggest such an opposing relationship (as seen in the growing season PB acres and number of wildfires in Figure 15-2), but a direct second-order regression, between annual total area of wildfires and acres of PB indicate a beneficial decline in wildfires only until a minimum PB up to about 15,000 to 17,000 acres (Figure 15-3). Annual total PB acres exceeding this amount, causes a turnaround and change to an increase in unwanted wildfires. No linkage can be discerned between the growing season PB (PB-GS) and wildfire numbers or acres, thus pointing to the added importance of dormant season PB, in addition to the ecological benefits. The regression curves suggest that if no PB was performed in the dormant season, almost 9,000 acres of wildfires would burn instead. Not performing any PB at all, would leave MCBCL lands at the potential risk of wildfires burning more than 18,000 acres per year.

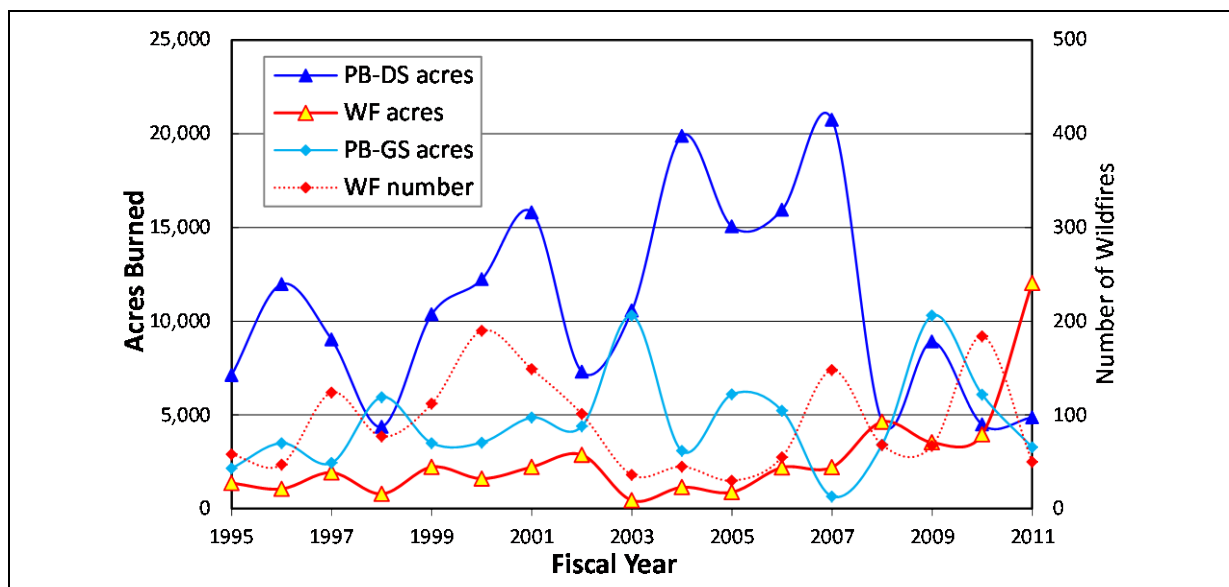


Figure 15-2. Annual total wildfire (WF) occurrences and areas relative to annual acres burned via PB application during the growing season (PB-GS) and the dormant season (PB-DS) at MCBCL.

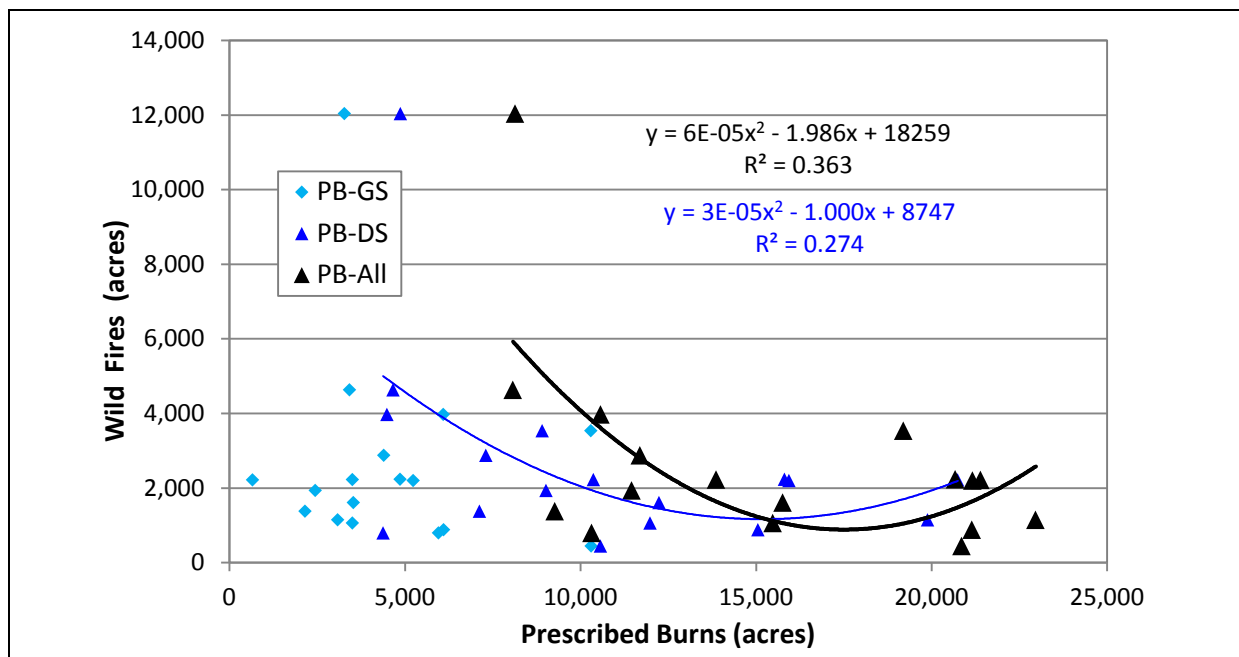


Figure 15-3. Linkage between wildfires and prescribed burns at MCBCL.

Role of Prescribed Burning in Air Quality

The following section provides background information necessary to understand the links between PB (and biomass combustion in general), its emissions as well as direct and indirect impacts on local and regional air quality.

Over the past few decades, the SEUS experienced substantial population growth, causing significant urban sprawl in an otherwise heavily forested region, making the wildland urban interface an important aspect of the forest management. The burning of wildland (wildfires and PB) is the largest single source of directly emitted PM_{2.5} (particulate matter with a diameter of less than or equal to 2.5 microns, also known as fine PM) in the SEUS (EPA, 2000), and PB alone is ranked third largest anthropogenic source of primary PM_{2.5} in the entire United States, emitting 12% of the total PM_{2.5} mass (EPA, 2004). Source apportionment modeling of PM_{2.5} mass concentrations from 24 Speciation Trend Network sites suggests PB may contribute more than 30% of the annual PM_{2.5} mass in the SEUS (Lee et al., 2007). Recent studies show that PB can significantly impact air quality in neighboring urban communities, contributing to both the primary and secondary portions of ambient PM_{2.5} mass (i.e., the directly emitted and atmospherically formed portions [Hu et al., 2008; Lee et al., 2005]). The ecological reliance on PB combined with increased air quality pressure due to tighter regulatory constraints (imposed by federal National Ambient Air Quality Standards) necessitates a better understanding of the dynamic and chemical processes in a PB plume. It is therefore highly desirable to develop tools that can predict air quality impacts of PB, based on the fire behavior, fire spread and amount of fuel consumed. The process of biomass combustion is a sequence of several stages such as ignition, flaming (including relatively minor glowing and pyrolysis), smoldering (post-flaming glowing plus pyrolysis), glowing, and extinction (Andreae and Merlet, 2001). In PB, all combustion types co-exist at any given time as the open vegetation fire moves through the biomass fuel. Therefore, the combined emissions are released into the atmosphere and the

biomass combustion process is typically divided into two phases, a predominantly flaming and a predominantly smoldering stage.

Biomass burning includes wildfires (occurring naturally and mostly in rural to remote areas), PB, burning of agricultural wastes, and domestic fuel–wood (anthropogenic) burning. Biomass burning has raised considerable concern because it is a significant source to regional and global particulate matter (PM) into the atmosphere. Much of the concern comes about the largely unknown interplay between initially emitted (primary) PM and new (secondary) PM formed from precursors during the atmospheric transport and dispersion of the fire emissions. The evolution of fire emissions into the atmosphere due to gas-particle partitioning and photo-oxidation can substantially alter the composition of gas and particle constituents. As emissions are diluted downwind of a fire source, semi-volatile particulate organic compounds (POC) may evaporate, reducing the organic aerosol (OA) concentrations relative to conserved species such as carbon monoxide (CO) (Lipsky and Robinson, 2006). This can be a major source of organic vapors, which can contribute to gas-phase chemical processes such as ozone (O₃) formation. Alternately, gas-phase organic compounds can undergo photo-oxidation reactions and form secondary organic products that may condense (secondary organic aerosol [SOA]) and increase the OA concentration within a plume. Indeed, SOA formation in the transport of PB emissions had the greatest influence on PM_{2.5} concentrations during a severe air quality event in Atlanta, GA (Lee et al., 2008). The atmospheric processes leading to SOA formation are complex and the role that biomass burning emissions play in these processes is discussed in the following paragraphs.

Globally, biomass burning is believed to contribute up to 40% of carbon dioxide (CO₂), 32% of CO, 10% of methane (CH₄), 24% of non-methane hydrocarbons (NMHC), 21% of nitrogen oxides (NO_x), 38% of tropospheric O₃, 39% of organic PM, and 86% of elemental carbon (EC) (Levine et al., 1995). Biomass burning emissions impact global climate by perturbing solar radiation (e.g., via CO₂, CH₄, PM), and by destroying O₃ in the stratosphere (methyl chloride [CH₃Cl], methyl bromide [CH₃Br]) (Cicerone, 1994; Levine et al., 1995). On regional and local scales, biomass burning emissions contribute to photochemical production of O₃ in the troposphere due to the release of precursors (e.g., NO_x, NMHC). Up to 80% of PM_{2.5} from biomass fires are organic, which includes significant amounts of solvent-extractable organic compounds such as carcinogenic, mutagenic polycyclic aromatic hydrocarbons (PAH) and polychlorinated dibenzo-p-dioxins (PCDD) and polychlorinated dibenzofurans (PCDF) (Bacher et al, 1992; Chagger et al., 1998; dos Santos et al., 2002; Freeman and Cattell, 1990; Gullett and Touati, 2003; Hays et al., 2002; Nestruck and Lamparski, 1982). Many studies have been conducted to characterize emissions from the burning of different biomass materials and combustion conditions (e.g., residential fireplaces, wood stoves or open burning), and to determine impacts of biomass burning on the atmosphere. Although many emissions were characterized in laboratory setups, our understanding of the atmospheric effects and impacts on local to regional air quality is still limited. Identifying specific “fingerprint” biomarkers for different burn sources, remains an important task for researchers. In addition, investigations of human exposure to open PB and associated health impacts have begun only recently (Naeher et al., 2006). Exposure to fireplace wood smoke was seen to cause negative effects on respiratory and pulmonary function in children (e.g., Larson and Koenig, 1994).

Despite the many undisputed ecological benefits (described in previous section) PB also reduces the risk of wildfires, but is still a form of biomass burning, producing combustion by-products

that potentially impair visibility and reduce air quality in urban environments (Battye and Battye, 2002; Cheng et al., 1998; Crutzen and Andreae, 1990; Hardy and Leenhouts, 2001), thus contributing to urban air pollution. Quantifying this contribution has been the focus of researchers in recent years. For example, particulate water-soluble potassium (K^+) serves as a diagnostic tracer, because the combustion of plant matter, which contains K^+ as a major electrolyte within its cytoplasm, releases large amounts of submicron particles rich in K^+ , whereas soil- or sea-spray derived submicron aerosol usually is low in K^+ (Andreae et al., 1996; Cachier et al., 1991; Gaudichet et al., 1995). Primary PM (soot) is an aerosol containing EC and is formed by the pyrolysis of biomass. Primary PM is of graphitic nature, but it contains aromatic hydrocarbons, functional groups of various types, as well as chemisorbed water on its surface (Chughtai, 1999a and b; Smith et al., 1989). There is growing evidence from field and laboratory studies that the “aging” (oxidation) of soot may lead to not only hygroscopic (e.g., Kotzick and Niessner, 1999), but also to water soluble organic PM (Decesari et al., 2001). The contribution of EC to PM, however, is highly variable and can range from 4 to 25%, depending on the fire’s level of smoldering to flaming, respectively (Khalil and Rasmussen, 2003). Various organic particulate compounds are also uniquely found in biomass burning emissions and have been used for source apportionment (Lee et al., 2005; Schauer et al., 1996; Zheng et al., 2002). Furthermore, certain gaseous species are considered useful tracers, including acetonitrile (CH_3CN), CH_3Cl , and less uniquely, but especially in conjunction with the sum of odd nitrogen oxides (NO_y) and CO (Blake et al., 1996 and 1999; Reiner et al., 2001).

Although the tracers previously mentioned have atmospheric lifetimes of several days and weeks, even up to 2 months (as in the case of CO), a great variety of reactive gaseous species with much lower lifetimes (e.g., ammonia [NH_3], sesqui-terpenes, oxygenated volatile organic compounds [OVOCs], other organic and inorganic gases) are being emitted that act as potentially effective precursors for the formation of new SOA particles. Due to their reactivity, these gaseous precursors are hard to measure in the field and have been detected mainly in benchmark-type laboratory setups (Christian et al., 2003 and 2004; Goode et al., 1999; Hays et al., 2002; Lobert et al., 1991; Yokelson et al., 1996), or in isolated intensive field campaigns (Andreae et al., 1996; Friedli et al., 2001; Goode et al., 2000; Griffith et al., 1991; Hobbs et al., 2003; Holzinger et al., 1999; Nance et al., 1993; Worden et al., 1997; Yokelson et al., 1997 and 1999). Christian et al. (2003) detected direct biomass burning emissions of acetaldehyde, phenol, acetol, glycolaldehyde, methylvinylether, furan, acetone, CH_3CN , propene-nitrile, and propane-nitrile, most of which are OVOCs, which further reinforces the importance of these reactive compounds in the atmospheric formation of SOA.

Assessing SOA from biomass burning is difficult since the traditional understanding of SOA formation is insufficient to explain OA observations in photochemically aging smoke plumes (Grieshop et al., 2009). Organic matter makes up a significant fraction of the sub-micron aerosol composition in the troposphere (Zhang et al., 2007). This OA consists of thousands of very complex molecules, thus making it very hard to identify its sources and atmospheric transformation processes, and also its effects on human health and climate (Hallquist et al., 2009). OA is emitted directly into the atmosphere by many different combustion processes, such as vehicular engines, industrial boilers, power plants, and residential cooking besides biomass burning. In addition, a significant portion of OA is formed in the atmosphere via secondary processes (hence named SOA) involving gas/particle partitioning of semi-volatile products from the photo-oxidation of reactive organic species.

SOA particles are detected in the atmosphere and laboratory experiments as oxidized OA with a wide range of volatility, hygroscopicity, and reactivity (Jimenez et al., 2009). Recent work suggests that organic gases with lower volatilities than traditional SOA precursors may be an important SOA source not accounted for in atmospheric models (Robinson et al., 2007). Characterizing these intermediate volatility organic compounds (IVOCs) and semi-volatile organic compounds (SVOCs) can help close the gap on SOA model predictions. Quantifying SVOCs and IVOCs is also essential in understanding the gas-particle partitioning of organic emissions as they undergo dynamic processing in the atmosphere. Investigating the variability in IVOC and SVOC emissions as a function of fire behavior and fuel consumption will enhance predictions of PM_{2.5} concentrations in aging PB emissions. This is essential in understanding the impacts of PB on air quality and constructing land management policies accordingly.

Besides the previously mentioned OVOCs, other potential SOA-forming precursors primarily include mono-terpenes (C₁₀H₁₆-ringed structures [e.g., α -, and β -pinene, limonene]) and sesqui-terpenes (C₁₅H₂₄ multi-ringed [e.g., α -cedrene, α -copaene, α -humulene, β -caryophyllene]) from biogenic sources (Altshuller, 1983; Glasius et al., 2000; Hoffmann et al., 1997; Hull, 1981; Jang and Kamens, 1999; Jaoui and Kamens, 2001; Kamens et al., 1999; Noziere et al., 1999; Odum et al., 1997; Wangberg et al., 1997; Yu et al., 1999) and aromatics from anthropogenic sources (Jeffries, 1995; Odum et al., 1996). Atmospheric oxidation reactions of these organic compounds create multi-functional oxygenated or nitrated SVOCs (i.e., organic acids, diacids, and aldehydes from the oxidation of terpenes) and result in SOA formation via self-nucleation processes or gas-particle partitioning on pre-existing PM. Due to their reactivity and extremely short life-time, the sesqui-terpenes, which are believed to have 2 to 3 times higher SOA yields than mono-terpenes, are very difficult to measure directly in the atmosphere. Therefore, PM formation and growth linked to sesqui-terpenes has only been observed in laboratory studies thus far. Jang and Kamens (2001) observed a heterogeneous hemiacetal and acetal formation from the reaction of aldehydes with alcohols in the presence of light and photo-oxidants. The studies showed that for time scales between several minutes to few hours, aldehydes, which can be either photochemically produced in the atmosphere or directly emitted by open burning; undergo heterogeneous reactions accelerated by acid catalysts, similar to sulfuric acid, leading to higher aerosol yields than when the acid compound is absent.

A number of more recent investigations supported these findings, and furthermore found that isoprene (2-methyl-1,3, 3-butadiene [C₅H₈]), the single largest biogenic NMHC emitted into the Earth's atmosphere (Guenther et al., 2006), previously thought to be uninvolved in producing atmospheric aerosols, plays a potentially major role in that process (Carlton et al., 2009 and 2010; Claeys et al., 2004; Limbeck et al., 2003; Surratt et al., 2010). This is especially important in the context of biomass burning, as isoprene not only accounts for up to 50% of the NMHC in the atmosphere, but is also emitted in significant quantities during the open burning of biomass as shown in this study's results.

Isoprene, similar to many other volatile organic compounds (VOCs) emitted by biomass burning, is the primary "fuel" for the atmospheric formation of O₃ in the presence of NO_x (i.e., nitric oxide [NO] + nitrogen dioxide [NO₂]) and sunlight. The VOC oxidation, similar to nearly all atmospheric oxidation processes, is initiated by the hydroxyl radical (OH), which itself is very reactive, and therefore, the path on which it becomes recycled is of critical importance. Under "clean" conditions, it directly oxidizes CO and CH₄ to convert into a hydroperoxyl radical (HO₂),

which in turn is recycled back to OH via reaction with either NO or O₃. In typically polluted urban environments, the NO-recycling path is favored forming NO₂. NO₂ is known to be the only source for O₃ production via its photolysis in the 320–430 nm spectral range, dissociating into NO and O. However, NO immediately reacts with O₃, so that no net O₃ is formed. The oxidation path of OH with alkanes (e.g., CH₄) and most unsaturated, biogenic or anthropogenic NMHC (e.g., alkenes, aromatics, alkynes) leads to alanyl radicals R_n with n–2 carbon atoms, which in turn react explicitly with atmospheric oxygen to form organic peroxy radicals RO₂ (here short for R_nO₂, and sometimes referred to as RO_x=RO₂+HO₂ as the total peroxy radicals). In polluted urban areas, NO is oxidized by RO₂, representing the source for a net O₃ production since NO₂ is formed without consuming O₃. Thus, NO_x are the catalyst for the VOC (fuel) consumption in the process of photochemical O₃ production. Simple methods will be employed to estimate potentials to form both O₃ and SOA from the measured VOC emissions.

Materials and Methods

Fuel Characterization and Consumption

PB emissions were measured from sites that had received an understory and midstory thinning treatment by HydroAx the winter prior to PB and were compared with emissions from sites without treatment (i.e., control) in five experimental blocks. The five blocks were a subset of eight blocks established by the Research Project T-1 research team, assuming their vegetation communities fall along a continuous gradient extending from wet pocosin to semi-mesic longleaf pine.

Research Project T-1 researchers used ordination methods such as non-metric multidimensional scaling (NMS) and canonical correspondence analysis (CCA) to produce plant community results along this gradient that are suitable for correlation with the PB results. The winter prior to PB (i.e., 1 year prior to the experiment), MCBCL foresters mechanically thinned the understory and midstory on 1-ha (100-m × 100-m) plot that met the requirements for comparable emissions measurements from mechanically thinned treatment (HYAX) versus untreated control (CTRL) fuel burnings. Due to the

steep hydrological gradient found in IE and the different burn requirements in its southern versus northern sections, the IE research plots were treated as two independent and different burn experiments (IEs versus IEn), amounting to a total of five PB study sites on a hydrological gradient beginning with the wettest “near pocosin” sites in IEs and ending with well drained “semi-mesic” sites in RB, with IEn, MF, and HA located in between (see **Figure 15-4**).

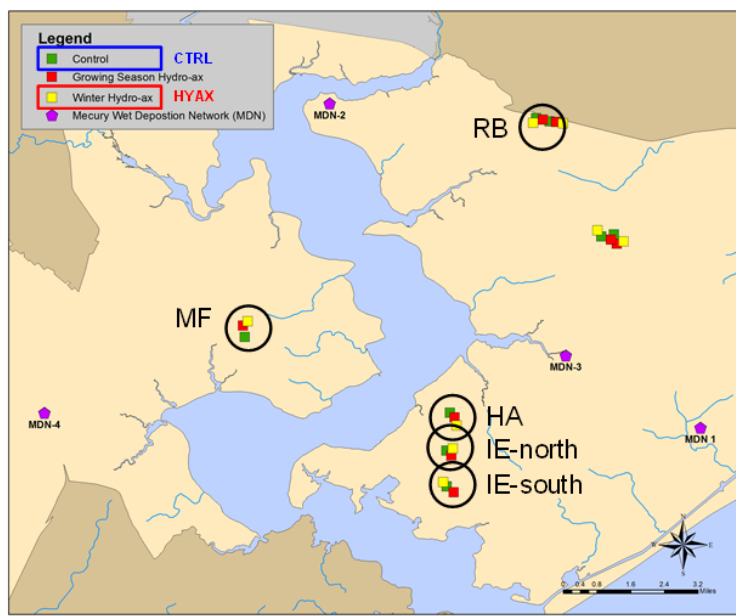


Figure 15-4. Location of investigated vegetation plots at MCBCL.

Significant differences exist in the amount of accumulated fuel and fuel composition, which is largely a function of soil type and its associated moisture gradient. Treatment plots are designed to capture the moisture gradient from semi-mesic loblolly pine forest to wet-mesic loblolly–longleaf pine forest to pond pine pocosins. Consequently, the species specific composition of the fuels varies significantly. Semi-mesic loblolly pines have a fuel composition dominated by red bay (*Persea palustris*), and wet-mesic loblolly pines also contain loblolly bay (*Gordonia laisianthus* and *Lyonia mariana*). Pocosin plots have a lower quantity of red bay but possess a high density of shrubs, including titi (*Cyrilla racemiflora*) and fetterbush (*Lyonia lucida*). **Table 15-1** compares species percent abundances based on pre-treatment stem density measurements. The least pocosin-like, mesic sites were dominated by tulip poplar and red bay, and the more pocosin-like sites were characterized by mostly titi, fetterbush, and loblolly pine. The mechanically thinned plots were generally richer in tulip poplar and red bay, whereas the control plots had more gall berry, black tupelo, green briar, and other species. Following methods established by USDA FS in field instructions for Southern Forest Inventory (Bechtold and Patterson, 2005), the vegetation plots were measured before and after the PB conduct, determining the consumption of above ground fuel biomass of foliage material (mainly leaves and needle litter) separate from woody debris biomass (trunks, branches, sticks, mulch, and duff). Due to inclement weather conditions, only plots HA and IEs could be burned in 2010 (March 19 and 21, respectively), and the other three plots were burned in the 2011 dormant season (February 26 and 28 and March 3 for RB, MF, and IEn, respectively). Soil OM, a surrogate measure of long-term soil moisture, as well as short-term moisture levels of the duff, and above-ground 1-, 10-, and 100-hour fuels were estimated from the FARSITE model (Finney, 1998) and expressed in percent fraction moisture holding capacity. Different hour fuels are defined as fuels with different diameters, ranging from 0–0.62 cm for 1 hour, 0.62–2.54 cm for 10 hours, to 2.54–7.62 cm for 100-hour fuels.

Table 15-1. Species percent abundances in investigated plots at MCBCL based on pre-treatment stem density measurements.

	Common name	Red maple	Titi	Ink berry	Gall berry	American holly	Tulip poplar	Fetterbush	Black tupelo	Red bay	Loblolly pine	Oaks	Green-briar	
	Plot	<i>Acer rubrum</i>	<i>Cyrilla racemiflora</i>	<i>Ilex coriacea</i>	<i>Ilex glabra</i>	<i>Ilex opaca</i>	<i>Liriodendron tulipifera</i>	<i>Lyonia lucida</i>	<i>Nyssa sylvatica</i>	<i>Persea palustris</i>	<i>Pinus taeda</i>	<i>Quercus spp.</i>	<i>Smilax laurifolia</i>	Other
IEs	CTRL	0	0	13.7	4.8	1.2	0	56.6	6.0	8.9	0	0	7.7	1.2
	HYAX	22.7	40.9	0	1.5	1.5	10.6	0	0	21.2	0	1.5	0	0
IEn	CTRL	4.0	0	0	15.9	1.7	7.4	36.4	2.8	12.5	7.4	0	4.0	8.0
	HYAX	8.7	0	0	0	0	13.0	0	0	30.4	47.8	0	0	0
MF	CTRL	0	0	0	32.6	0	12.3	0	0	8.0	24.6	8.0	1.5	13.0
	HYAX	36.2	2.1	0	0	8.5	17.0	0	0	21.3	2.1	8.5	0	4.3
HA	CTRL	1.7	0	0	0	1.7	18.6	0	3.4	67.8	1.7	1.7	0	3.4
	HYAX	0	0	0	0	0	25.0	0	0	75.0	0	0.0	0	0
RB	CTRL	5.0	0	0	0	0	58.3	0	10.0	10.0	0	6.7	0	10.0
	HYAX	0	0	0	0	0	93.6	0	0	2.1	0	2.1	0	2.1

PB Emissions Measurements

The process of biomass combustion is a sequence of several stages such as ignition, flaming (including some glowing and pyrolysis), smoldering (glowing plus pyrolysis), glowing, and extinction (Andreae and Merlet, 2001). In PB, all combustion types exist at any given time because the open vegetation fire moves through the biomass fuel. Therefore, the combined emissions are released into the atmosphere simultaneously. The biomass combustion process is typically divided into a predominantly flaming and a predominantly smoldering stage. The following describes the technical approach for sample collection and methods employed for the chemical analysis of those samples. The burn areas on MCBCL are characterized by dense fuel loads and are difficult to access, requiring deployment of the Research Project Air-1 measurement equipment on a highly mobile platform. To meet the specific requirements of size and mobility, an aerosol composition monitoring (ACM) system was designed and constructed. The ACM concept used in the two experiments performed in March 2010 had proven successful. The measurement methods are briefly summarized in the following paragraphs.

As illustrated by Figure 15-5, the ACM is positioned along the moving flaming front with an all-terrain vehicle (ATV), hence capturing the emissions clearly dominated by flaming processes. Once flaming has ceased, sample media are exchanged and the ACM is left unattended in the middle of the smoldering area (e.g., of the treatment plot). Meanwhile, the ATV is used to position a second ACM unit into the neighboring control burn area, capturing its flaming dominated emissions. A third ACM is deployed upwind to provide important background concentrations. All ACM units are equipped identically, providing real-time meteorological, trace gas and PM mass data, as well as discrete samples being analyzed for aerosol chemical constituents in the gas and particle phase. The suite of measurements (summarized in Table 15-2) made in this study is unique and has never been undertaken before in such a comprehensive manner.

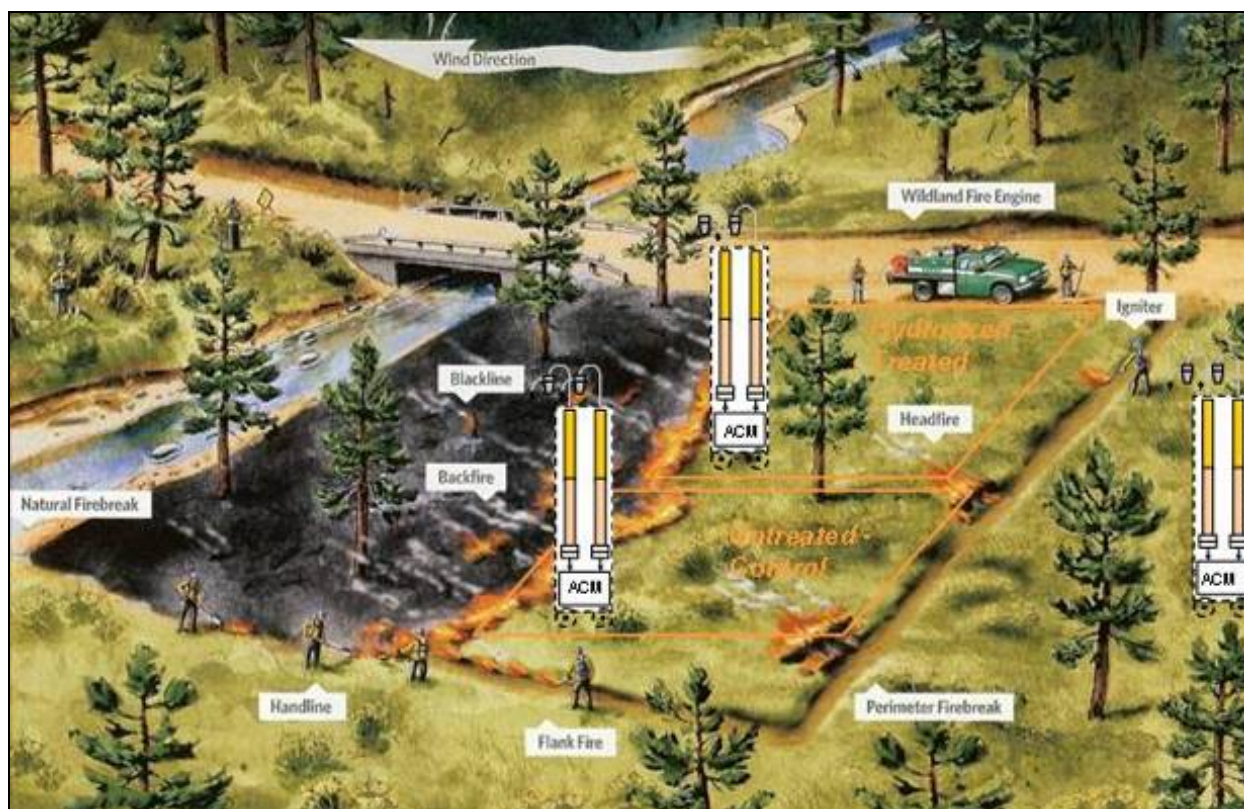


Figure 15-5. Conceptual approach for the comparative measurement of emissions from untreated control and mechanically thinned treated fuels; adapted from *The Nature Conservancy Magazine Vol. 58 (3), Autumn 2008*.

The ACM payload consists of two evacuated and flow controlled stainless steel canisters to measure VOCs and two battery powered membrane pumps providing sample air flow through a cyclone, denuder-pair and filter pack sample train. Cans, denuders, and filters constitute the sample media (substrates) for the integrated measurement of aerosol composition. The front Teflon and quartz filters are used to quantify primary emissions, whereas the quartz backup filters in both channels (QBT and QBQ) are used to assess impacts from semi-volatile species (Baumann et al., 2003). Other important payload components are a nephelometer for continuous $PM_{2.5}$ mass concentration measurement (model pDR-1500 from Thermo-Fisher Scientific) and a handheld CO/CO_2 monitor (model Qtrak-7565 from TSI). The pDR-1500 continuously measures the amount of light (at a wavelength of 880 nm) scattered by particles (scattering coefficient range 1.5×10^{-6} to 0.6 m^{-1}) drawn through an optical chamber at a specific flow rate. The amount of light scattered is converted to particle concentration readings using well-established light scattering theory (Kerker, 1969). The size fraction of $2.5 \mu\text{m}$ is achieved by drawing the sample air through a cyclone with corresponding aerodynamic separation characteristics. The aerosol sample passes through a diffusion drier at the inlet upstream of the cyclone, which otherwise would elevate the in situ particle mass relative to a discrete filter sample because it includes increased particle-bound water (PBW) (i.e., particle mass due to condensational growth of the particles associated with water uptake by hygroscopic PM components (McMurry et al., 1996; Sloane, 1984). The particle mass measured by filter-based methods, which incorporate a filter equilibration step at low relative humidity (RH) for time-integrated samples, will not include

most of the PBW mass. Thus, the personal DataRAM (pDR) operated without a dryer would overestimate PM mass at higher RH.

The Teflon and quartz sample substrates from the two otherwise identical ACM sampling trains undergo different laboratory analytical procedures. First, PM_{2.5} mass is determined from gravimetric measurement of the Teflon filter deposits, employing a robotic weighing system in a clean room environment. The Teflon filter sample is then submitted to the non-destructive energy dispersive X-ray fluorescence (XRF) analysis for the determination of numerous metallic and mineral elements contained in the PM_{2.5} sample matrix, before it is extracted in pure deionized distilled water (with resistivity of approximately 18 MΩ) and further analyzed for ionic content via ion chromatography (IC) and for water-soluble metals via inductively coupled plasma mass spectrometry (ICP-MS).

More than 100 POC, including key molecular markers, such as levoglucosan, pimaric acid, abietic acid, and retene, are analyzed and quantified from quartz filter samples employing different techniques. More than 50 VOC species are measured from the can samples, including ethyne (acetylene) and 1,3-butadiene (potential carcinogen), aromatics and biogenics (isoprene, mono-terpenes) that are important PM precursors, as well as CO, CO₂, and CH₄. The IC analysis of the denuder extracts provides quantitative information on other reactive gases that play an important role in aerosol chemistry (i.e., NH₃, nitrous acid [HONO], nitric acid [HNO₃], sulfur dioxide [SO₂], and certain light organic [carboxylic] acids). The individual analytical methods and techniques have been described in various standard operating procedures (SOPs) developed for DCERP.

Table 15-2. List of aerosol species measured from discrete PB emissions samples from investigated plots at MCBCL.

Group	Species					Spl Medium	Method
Crustals It metals	<i>Be, Na, Mg, Al, Si, P, S, Cl, K, Ca, Sc, Ti, V, Cr, Mn, Fe, Co, Ni, Rb, Sr, Ba, La ^)</i>					T filter	XRF/ICP-MS
Heavy metals	<i>Cu, Zn, Ga, Ge, As, Se, Br, Y, Zr, Mo, Pd, Ag, Cd, In, Sn, Sb, W, Tl, Pb, Bi, U ^)</i>					T filter	XRF/ICP-MS
Ionic PM species	Na ⁺ , K ⁺ , Ca ⁺⁺ , Mg ⁺⁺ , NH ₄ ⁺ , F ⁻ , Cl ⁻ , NO ₃ ⁻ , SO ₄ ⁼ , formate, acetate, oxalate					T filter	IC
Reactive gases	NH ₃ , HONO, HNO ₃ , HCl, SO ₂ , formic, acetic, oxalic acids					Denuder	IC
Carbon-PM	EC, OC, WSOC					Q filter	TOT, TOC
Volatile Organic Compounds	Halo-C	Alkyl-Nitrates	Alkanes	Alkenes *)	Aromatics	Whole-Air Canister	GC-MS/FID/ECD
	CHCl ₃	Methyl-NO ₃	Ethane	Ethene	Benzene		
	CH ₂ Cl ₂	Ethyl-NO ₃	Propane	Ethyne*	Toluene		
	C ₂ HCl ₃	i-Propyl-NO ₃	i-Butane	Propene	Ethylbenzene		
	C ₂ Cl ₄	n-Propyl-NO ₃	n-Butane	1-Butene	m/p-Xylene		
	CH ₃ Cl	2-Butyl-NO ₃	i-Pentane	i-Butene	o-Xylene		
	CH ₃ Br	Biogenic HC	n-Pentane	trans-2-Butene	Isopropylbenzene		
	CH ₃ I	Isoprene	2-Methylpentane	cis-2-Butene	Propylbenzene		
	Other	α-Pinene	3-Methylpentane	1,3-Butadiene*	2/3/4-Ethyltoluene		
	CH ₄	β-Pinene	n-Hexane	1-Pentene	1,3,5-Trimethylbenzene		
	CO	DMS	n-Heptane		1,2,4-Trimethylbenzene		
	CO ₂	COS §)	n-Octane		1,2,3-Trimethylbenzene		

(continued)

Table 15-2. List of aerosol species measured from discrete PB emissions samples from investigated plots at MCBCL (continued).

Group	Species					Spl Medium	Method
Particulate Organic Compounds	n-Alkanes #)	Alkanoic Acids	Dicarbox. Acids	PAH	Arom Carbox Acids	Q filter	GC-MS
	Eicosane	Octanoic A	Succinic A	Fluoranthene	Phthalic A		
	Heneicosane	Decanoic A	Glutaric A	Acephenanthrylene	Isophthalic A		
	Docosane	Dodecanoic A	Adipic A	Pyrene	Terephthalic A		
	Tricosane	Tetradecanoic A	Pimelic A	Benz(a)anthracene	1,2,4-Benzenetricarbox A		
	Tetracosane	Pentadecanoic A	Suberic A	Chrysene/triphenylene	+5 more species detected,		
	Pentacosane	Hexadecanoic A	Azelaic A	Coronene	but below DL in samples		
	Hexacosane	Heptadecanoic A	Sebacic A	Benzo (b)fluoranthene	Alkylcyclohexanes		
	Heptacosane	Octadecanoic A		Benzo(k)fluoranthene	9 species detected,		
	Octacosane	Nonadecanoic A	Resin Acids	Benzo(j)fluoranthene	but below DL in samples		
	Nonacosane	Eicosanoic A	Dehydroabietic A	Benzo(a)pyrene	Hopanes/Steranes		
	Triacontane	Heneicosanoic A	7-Oxo-DHAA	Benzo(e)pyrene	16 species detected,		
	Hentriacontane	Docosanoic A	Isopimaric A	Perylene	but below DL in samples		
	Dotriacontane	Tricosanoic A	Pimaric A	Indeno(cd)pyrene	Phthalates		
	Tritriacontane	Tetracosanoic A	Sandaracopim.A	Dibenz(ah)anthracene	mainly for QA and QC		
	Tetracontane	Pentacosanoic A	Abietic A	Benzo(ghi)perylene	SOA Indicators †)		
	Pentatriacontane	Hexacosanoic A		Cyclopenta(cd)pyrene	Pinic acid (a)		
	Hexatriacontane	Heptacosanoic A	Sterols	Benzo(ghi)fluoranthene	Pinonic acid (a)		
	Heptatriacontane	Octacosanoic A	Cholesterol	1-Methylchrysene	3-Hydroxyglutaric A (a)		
	Octatriacontane	Nonacosanoic A	Stigmasterol	Retene	3-Acetyl hexanedioic A (a)		
	n-Alkenoic A.	Triacantanoic A	b-Sitosterol	Picene	2-Hydroxy-4,4-DMglutaric (a)		
	Palmitoleic A		Campesterol		2-HO-4-isopropyladipic (a)		
	Oleic A		Stigmastanol	Others	2-Methylglyceric A (i)		
	Linoleic A			Levogluconan	2-Methylthreitol (i)		
	Linolenic A				2,3-diHO-4-Opentanoic (t)		

^ Italic elements are below DL in all samples.

* Ethyne (acetylene) and 1,3-butadiene (carcinogen) belong to family of alkynes and dienes, respectively.

Lower alkanes with 11 to 19 carbon atoms were detected but below DL in all samples.

§ Atmospheric carbonyl sulfide (COS) has also anthropogenic sources.

† From precursor reactions with α -pinene (a), isoprene (i), and toluene (t). Water-soluble organic carbon (WSOC) from total organic carbon (TOC) via ultraviolet (UV) oxidation and CO₂ conductivity detection.

One of our main goals was to more accurately determine emission factors (EF_{ni}) for chemical species n and fuel type i , to improve total emission estimates F_n (e.g., in g_n/yr for annual reporting) based on land area burned, fuel loading, carbon fraction of the fuel (assuming 42.6% carbon by mass), and combustion fraction, besides EF_{ni} .

The total net flux F_n of species n can be determined by summing over each vegetation type i as shown in Equation 15-1:

$$F_n = \sum_i \{ m_{fi} \cdot c_{fi} \cdot f_{Ci} \cdot EF_{nCi} \cdot (A_i/T_i) \} \quad (\text{Eq. 15-1})$$

...with $FC_i = m_{fi} \cdot c_{fi} \quad (\text{Eq. 15-2})$

being the fuel type specific fuel consumption in g_{fc}/m², here determined experimentally in Equation 15-2

...and $EF_{ni} = f_{Ci} \cdot EF_{nCi} \quad (\text{Eq. 15-3})$

being the fuel type specific EF for species n in g_n/g_{fc} shown in Equation 15-3.

Thus, the specie's n total emission per unit area for fuel type i in g_n/m^2 can be calculated using Equation 15-4:

$$E_{ni} = EF_{ni} \cdot FC_i \quad (\text{Eq. 15-4})$$

- m_{fi} = Amount of fuel mass available for combustion in $\text{g}_{fuel}/\text{m}^2$
- c_{fi} = Combustion factor (i.e., fraction of actually combusted fuel)
- f_{Ci} = Average carbon-mass fraction of the fuel (here assumed $0.426 \cdot \text{g}_C/\text{g}_{fuel}$)
- EF_{nCi} = Carbon-related EF for species n in g_n/g_C ; see below
- A_i = Fuel type specific area burned in m^2
- T_i = Reference time (single burn, time between burns or inventory period).

Because the selected burn plots fall into specific fuel classes distinguishing the treatment from control, we apply the carbon mass balance method (Batty and Batty, 2002; Radke et al., 1998; Sinha et al., 2004), assuming that all of the combusted fuel carbon is emitted into five measurable forms of carbon (i.e., CO_2 , CO , CH_4 , VOCs, and particulate carbon). For a certain fuel type i , the EF of a species n , is then calculated from the ratio of the mass concentration of that species to the total carbon concentration emitted as shown in Equation 15-5:

$$EF_{ni} = f_{Ci} \cdot EF_{nCi} = f_{Ci} \cdot [n] / ([C]_{\text{CO}_2} + [C]_{\text{CO}} + [C]_{\text{CH}_4} + [C]_{\text{VOC}} + [C]_{\text{PC}}) \quad (\text{Eq. 15-5})$$

Hays et al. (2002) measured the carbon contents of several biomass types obtained from various forests in the SEUS and found it to be 42.6% for aged needles of loblolly pine, which we used here ($f_{Ci}=0.426$). The overall uncertainty in the total emission flux F_n is less uncertain than in other published work thanks to the direct in situ measurement of the amount of fuel consumption (FC) from a series of representative plot surveys conducted by the Terrestrial Module's monitoring field team before and after the burn. The plot surveys provide important parameters that describe the fuel mix and condition, including vegetation classes, dead versus live mass fractions, fuel moisture and soil organic matter content.

An important parameter describing combustion behavior, intensity and completeness is the modified combustion efficiency (MCE) defined in Equation 15-6 as the ratio of the moles of CO_2 to the combined moles of CO_2 plus CO emitted by the fire (Ward and Radke, 1993):

$$\text{MCE} = \Delta[\text{CO}_2] / (\Delta[\text{CO}_2] + \Delta[\text{CO}]) \quad (\text{Eq. 15-6})$$

where $\Delta[\text{CO}_2]$ and $\Delta[\text{CO}]$ are the excess mixing ratios (MR) of CO_2 and CO in the PB emissions relative to the background levels upwind. A more accurate measure would be the combustion efficiency (CE) defined as the fraction of fuel carbon converted to CO_2 (i.e., the ratio of the moles of CO_2 emitted by the fire to the moles of all emitted carbon species). However, due to the difficulties of measuring the entirety of carbon species emitted, CE has not been as widely reported as MCE. MCE is much easier to determine and represents CE fairly well, considering that on a molar basis CO and CO_2 together constitute between 90% and 100% of all carbonaceous compounds emitted (e.g., as shown later, our results ranged from 91% to 99.8%, averaging $97 \pm 2\%$). MCE has the added advantage that other carbonaceous compounds can be plotted and regressed against it as independent variables. CE and MCE are higher when flaming dominates over smoldering combustion. Thus, MCE of 0.98–1.0 indicate *pure* flaming, whereas

pure smoldering usually yields MCE of 0.75–0.85. For the benefits of minimal air quality impact and maximum energy release, both CE and MCE would ideally approach the value of 1.0.

As previously mentioned, our integrative PB emissions measurements in each vegetation plot were divided into a relatively short period (approximately 20 minutes) immediately after ignition, followed by a 2- to 3-hour period presumably dominated by smoldering. Our MCE levels ranged between 0.84 and 0.998, averaging 0.94 ± 0.04 . However, because we could not control the level of flaming versus smoldering occurring in the immediate surroundings of the ACM's sample inlets, MCE from the shorter first periods averaged 0.94 ± 0.02 and from the longer subsequent periods 0.95 ± 0.05 , indicating that our assumption of either flaming or smoldering stage dominating over the other one did not hold. Therefore, a time-weighted average of certain species's excess MR from the short and long period was used to determine its EF value that qualifies to be compared with the experimentally determined fuel consumption, fuel moisture and vegetation composition indicators (NMS and CCA ordination parameters). Except for the MCE related sensitivities of the fuel-type specific EF discussed later, the time-weighted EF averages were used.

Ozone (O₃) Forming Potential

The variety and amounts of VOCs released into the atmosphere from biomass burning is quite large, and so is their reactivity (i.e., individual VOCs have different impacts on the chemical formation of O₃, which are discussed here briefly). Differences in the reactivity of individual VOCs to O₃ formation have been documented in laboratory chambers and other controlled conditions. Consider the function $P(O_3)_j$ defined as the rate of O₃ production from VOC species j . Because VOC oxidation is usually initiated by reaction with OH, $P(O_3)_j$ can be approximated using Equation 15-7:

$$P(O_3)_j = C_j \times C_{OH} \times k_{OH}(j) \times \Phi(j) \quad (\text{Eq. 15-7})$$

where C_j is the concentration of VOC species j , C_{OH} is the OH atmospheric concentration, $k_{OH}(j)$ is the rate constant for the reaction between species j and OH, and $\Phi(j)$ is the O₃ yield, defined as the number of O₃ molecules produced for each carbon atom of species j that is oxidized. Equation 15-8 shows that the relative importance of one VOC species to another will depend upon the relative magnitudes of the product of three variables: C_j , k_{OH} , and Φ . For this reason, a species with a large concentration will not necessarily be an important O₃ precursor if it is unreactive with OH or ineffective in producing O₃. Conversely, a species with a small concentration may still be an important O₃ precursor if it is extremely reactive. Because of the large variability of C_j and k_{OH} compared to Φ these two variables are the dominant factors that determine the relative contribution of VOC species to O₃ production. To account for this combined effect the propylene-equivalent method as defined by Chameides et al. (1992) can be applied. This reactivity-based method is based on the variable *Propyl-Equiv* (j) defined in Equation 15-8 as the following:

$$\text{Propyl} - \text{Equiv}(j) = C_j \frac{k_{OH}(j)}{k_{OH}(C_3H_6)} \quad (\text{Eq. 15-8})$$

Equation 15-8 is a measure of the concentration of species j on an OH-reactivity-based scale normalized to the reactivity of propylene C_3H_6 . Therefore if a VOC species has an ambient concentration of 10 ppb of carbon and it is twice as reactive as propylene, it will have a Propyl-Equiv of 20 ppb of carbon. If, in contrast, the species is half as reactive as propylene, it will have a Propyl-Equiv of 5 ppb of carbon. This method was being applied to the emission measurement results and is discussed relative to the fuel treatment types in the next section.

Secondary Organic Aerosol (SOA) Forming Potential

Like forest fires, or industrial emissions from oil refineries, chemical plants, pulp and paper industries, and vehicular emissions, PB causes smoke. A large fraction of this smoke is primary organic aerosol (POA) directly emitted into the atmosphere. The organic portion is the least understood component of $PM_{2.5}$. However, $PM_{2.5}$ is not only made up of such primary emissions; a secondary aerosol fraction resulting from the reaction of VOCs in the atmosphere is being recognized as an important contributor. This SOA fraction is extremely complex as the precursor VOCs can originate from many different sources. It has been estimated that in California's Los Angeles Basin, SOA can make up to 80% of the observed organic particulate carbon under peak photochemical smog conditions, typically coinciding with periods of non-attainment of O_3 and $PM_{2.5}$ (Turpin and Huntzicker, 1995).

A detailed understanding of SOA formation in the atmosphere is essential to characterize the chemical composition of ambient OAs, to accurately incorporate such processes in air quality models, and to be able to attribute the ambient OA mass to the appropriate man-made and natural sources thus allowing for the development of adequate control strategies (e.g., in urban environments). Although aromatic hydrocarbons and biogenic terpenes are major contributors to SOA in the atmosphere, these two compound classes are not solely responsible for SOA formation. Currently, in fact, other potentially important contributors to SOA formation are subject of intense scientific investigation. In addition, there is a large amount of semi-volatile organic material (direct emissions and photochemical oxidation products of VOC emissions) that has the potential to move into the aerosol phase as climate or atmospheric chemistry undergoes subtle changes. The mass of such material is so large in comparison to amounts of material currently in the aerosol phase, that impacts on $PM_{2.5}$ are potentially significant. Thus, it is important to identify all such SOA precursors, their aerosol-forming potential, and their sources.

The evolution of PB emissions in the atmosphere due to gas-particle partitioning and photo-oxidation can substantially alter the composition of gas and particle constituents. As emissions are diluted downwind of a PB source, SVOCs may evaporate, reducing the OA concentrations relative to conserved species such as CO (Lipsky and Robinson, 2006). This can be a major source of organic vapors, which can contribute to gas-phase chemical processes leading to O_3 formation as previously described. Alternately, gas-phase organic compounds can undergo photo-oxidation reactions and form SOA products that may condense and increase the OA concentration within a plume. Indeed, SOA formation in the transport of PB emissions had the greatest influence on $PM_{2.5}$ concentrations during a severe air quality event in Atlanta, GA (Lee et al., 2008). The formation of SOA from biomass burning emissions may exceed POA emissions from biomass burning globally; however, this estimate is highly uncertain (Hallquist et al., 2009). Assessing SOA from biomass burning is difficult since the traditional understanding of SOA formation is insufficient to explain OA observations in photochemically aging smoke

plumes (Grieshop et al., 2009). Recent work suggests that organic gases with lower volatilities than traditional SOA precursors may be an important SOA source not accounted for in atmospheric models (Robinson et al., 2007). Characterizing these IVOCs and SVOCs can help close the gap on SOA model predictions. Quantifying SVOCs and IVOCs is also essential in understanding the gas-particle partitioning of organic emissions as they undergo dynamic processing in the atmosphere. Unfortunately, the variability in IVOC and SVOC emissions as a function of fire behavior and fuel consumption is currently unknown, making predictions of PM_{2.5} concentrations in aging PB emissions very difficult or highly uncertain. This is essential in understanding the impacts of PB on air quality and constructing land management policies accordingly.

Because of these complexities in SOA reaction pathways, the vast number of products formed by photochemical oxidation of primary aerosol, and the costly analytical methods required for speciation, indirect methods for quantitative assessment of SOA have been developed and become useful to a limited degree. One such method utilizes fractional aerosol coefficients (FAC), developed and first published by Grosjean and Seinfeld (1989).

The FAC approach for determining SOA yield is based on measurements of the total aerosol formed in smog chamber reactions of a specific precursor species and a specific oxidant. Because the reaction mechanism is not known, the kinetics and reaction rate constants are also not known. The smog chamber data are, therefore, used to empirically derive the reaction stoichiometry, that is, to determine the amount of condensed matter formed per gram of reactant, which is the FAC or fractional aerosol yield. The FAC can be expressed on a molar, mass or carbon concentration basis (Grosjean and Seinfeld, 1989). This dimensionless ratio of mass concentration is defined by Grosjean (1992) as shown in Equation 15-9:

$$\text{FAC} = \text{aerosol from VOC } (\mu\text{g m}^{-3}) / \text{initial VOC } (\mu\text{g m}^{-3}) \quad (\text{Eq. 15-9})$$

With this definition, and knowing the VOC emission rate and the fraction of VOC that has reacted in the atmosphere, the amount of aerosol formed from each VOC can be calculated as shown in Equation 15-10:

$$[\text{Aerosol}] \text{ produced} = [\text{VOC}] \text{ emitted} * [\% - \text{VOC}] \text{ reacted} * \text{FAC} \quad (\text{Eq. 15-10})$$

The FAC is a very crude first order approximation to quantify SOA formation P(SOA). It summarizes the complicated oxidation-condensation processes that govern SOA formation into one constant for each precursor VOC species. SOA can be formed by parent VOC species which have a carbon chain greater than six, but generally less than ten ($6 < C < 10$). Species with high molecular weights ($C > 10$) tend to be present only at low concentrations, and those with low molecular weights ($C < 6$) have high saturation vapor pressures. Therefore, from the aromatic species identified in the VOC samples analyzed and presented above, those with $C > 6$ were selected in the following analysis using the FAC approach. It is noteworthy to mention that aerosol formation varies with many factors such as oxidant concentration, temperature, RH, and existing aerosol concentration in the ambient air. Thus, the results obtained from this study are estimates of SOA formation *potentials* rather than quantification of SOA formation. Thus, with the VOC species emissions rate E_{VOC} (in mass per unit burned area; Equation 15-4) for the two

different fuel types, and the fraction of VOC reacted (FR), the SOA forming potential is calculated as shown in Equation 15-11:

$$P(\text{SOA}) = E_{\text{VOC}} * \text{FR} * \text{FAC} \quad (\text{Eq. 15-11})$$

Table 15-3. OH rate constants (k), the fraction of VOC species reacted with midday OH levels after 5 hours (FR), and the FAC from Grosjean (1992), except as noted

VOC	$k \cdot 10^{12}$ $\text{cm}^3/\text{molec/s}$	FR	FAC
n-Heptane	7.15	0.12	0.0006
n-Octane	8.68	0.14	0.007
Benzene	1.3	0.02	0.16 ^a
Toluene	6.12	0.10	0.08 ^a
Ethylbenzene	7.48	0.13	0.054
mp-Xylene	24.4	0.36	0.047
o-Xylene	14.7	0.23	0.05
Isopropylbenzene	6.6	0.11	0.007
Propylbenzene	5.8	0.10	0.007
3-Ethyltoluene	19.2	0.29	0.063
4-Ethyltoluene	24.4	0.36	0.026
2-Ethyltoluene	14.7	0.23	0.026
1,3,5-TMBenzene	57.5	0.64	0.026
1,2,4-TMBenzene	37.2	0.49	0.017
1,2,3-TMBenzene	32.7	0.44	0.014
Isoprene	99.3	0.83	0.031 ^a
α -Pinene	52.6	0.61	0.072 ^a
b-Pinene	76.9	0.75	0.072 ^a

^a The FAC for these compounds are conservative estimates based on Henze et al. (2008).

FR is calculated assuming first-order principles from reaction with OH, midday (OH) of $10^6 \text{ molec cm}^{-3}$, and a 5-hour reaction period; $\text{FR} = 1 - \exp(-kt)$. **Table 15-3** lists the OH rate constants (k) (Atkinson, 1990), the fraction of molecules reacted with OH (FR), and the FAC (Grosjean, 1992) for the aromatic and biogenic species investigated here.

Results and Discussion

In this section, the two investigated fuel types, the mechanically treated (thinned) fuel and untreated control fuel are characterized relative to their position along a hydrological gradient, and observed differences in fuel consumption are presented and discussed first. These differences are then discussed in light of combustion behavior and numerically related to gas and particle phase emissions from a wide host of species on the basis of individual EF. Theoretical models are employed to estimate the potential of certain species to form secondary air pollutants (O_3 and $\text{PM}_{2.5}$) during atmospheric transport and dispersion after emission. Influence of fuel type on the different AP forming potentials is elucidated and discussed. Finally, the newly developed

fuel-specific EF are being compared in different applications that are relevant in the land managers' decision-making process.

Fuel Character and Consumption

Soil OM, which is a surrogate measure of long-term soil moisture, influencing above-ground vegetation composition, increased along the spatial gradient from plot RB being the driest, over HA, MF, IE-north to the wettest IE-south. Short-term moisture levels of the duff and above-ground 1-, 10-, and 100-hour fuels available for combustion were estimated from the FARSITE model and expressed in percent fraction moisture holding capacity. Different hour fuels are defined as fuels with different diameters, ranging 0–0.62 cm for 1-hour, 0.62–2.54 cm for 10-hour, and 2.54–7.62 cm for 100-hour fuels. **Table 15-4** provides an overview of the measured fuel moisture levels, total available and consumed fuel amounts as well as relative fuel consumption for the two main fuel material categories, woody sticks and leaves. Also included are the vegetation composition scores CCA and NMS determined from the ordination method employed by Research Project T-1 researchers. The more negative scores generally indicate more pocosin-like conditions. More details on these scores and how they were determined can be found in Chapter 13 (Final Report for Research Project T-1 Report).

The HYAX/CTRL column shows the ratio of averages from the corresponding five plots of each fuel type. Results indicate that on average and relative to the control, the understory and midstory thinning treatment made about twice as much fuel available for consumption, and almost three times (2.8) more fuel was consumed during PB. Woody fuel consumption was almost nine times higher in absolute terms and two times higher in relative terms (i.e., the fraction of woody fuel consumed relative to what was available on average in the mechanically thinned plots was twice the corresponding fraction of the control). Moisture levels of the mechanically treated fuels (HYAX) were systematically lower than the corresponding control fuels in each plot.

Table 15-4. Available fuel (F), different fuel moisture (FM) and fuel consumption (FC) levels—absolute and relative to what was available, and vegetation composition indicators CCA and NMS for the two different treatment types investigated in the five different vegetation plots.

Fuel Type/ Plot	CTRL ^a					HYAX ^b					CTRL ^c		HYAX ^d		HYAX/ CTRL ^e
Parameter	RB	HA	MF	IE _n	IE _s	RB	HA	MF	IE _n	IE _s	AVG	STD	AVG	STD	
F-Avail_g/m ²	1197	1132	830	963	907	723	2299	2275	1096	3784	1006	154	2035	1203	2.0
FC-Tot_g/m ²	531	591	120	543	250	226	1561	1284	880	1693	407	209	1129	593	2.8
FC-Wd_g/m ²	119	41	40	68	240	80	1434	1193	350	1469	102	84	905	646	8.9
FC-Lvs_g/m ²	412	550	80	475	10	146	127	91	530	224	305	244	224	178	0.7
FC-Rel_%	44	52	15	56	28	31	68	56	80	45	39	18	56	19	1.4
FC-Wd_%	37	24	28	32	53	37	84	68	86	57	35	11	66	21	1.9
FC-Lvs_%	47	57	12	64	2	29	21	18	77	19	36	28	33	25	0.9
Soil-OM_%	5	15	14	11	68	8	9	28	48	18	23	26	22	16	1.0
FM-Duff_%	73	72	73	68	74	54	69	54	55	70	72	2	60	8	0.8
FM-1hr_%	17	15	17	16	19	5	15	11	11	18	17	2	12	5	0.7

(continued)

Table 15-4. Available fuel (F), different fuel moisture (FM) and fuel consumption (FC) levels—absolute and relative to what was available, and vegetation composition indicators CCA and NMS for the two different treatment types investigated in the five different vegetation plots (continued).

Fuel Type/ Plot	CTRL ^a					HYAX ^b					CTRL ^c		HYAX ^d		HYAX/ CTRL ^e
Parameter	RB	HA	MF	IEn	IEs	RB	HA	MF	IEn	IEs	AVG	STD	AVG	STD	
FM-10hr_%	21	18	21	19	20	18	18	18	16	19	20	1	18	1	0.9
FM-100hr_%	17	17	17	16	17	14	16	14	14	16	17	0	15	1	0.9
CCA	-0.9	-1.0	-1.8	-2.0	-1.8	-1.1	-0.5	-0.8	-2.0	-0.7	-1.5	0.5	-1.0	0.6	0.7
NMS	-0.2	-1.2	-0.8	-1.4	-1.7	-0.8	-0.7	-0.9	-1.3	-1.5	-1.1	0.6	-1.0	0.4	1.0

CCA: Canonical Correspondence Analysis, ordination score (the more negative the more pocosin-like).

NMS: Non-metric Multidimensional Scaling, ordination score (the more negative the more pocosin-like).

^a Blue represents control data.

^b Red represents the treated (HYAX) data.

^c Bold blue is the average of the control.

^d Bold red is average of HYAX.

^e Bold black is the average HYAX greater than the average control.

In support of the table, **Figure 15-6** clearly shows that except for site RB, the understory/ midstory thinning treatment yielded greater availability and consumption of all fuels, but especially woody material regardless of fuel moisture. Untreated control plots provided less fuel available for combustion, of which PB also consumed less relative to the fraction consumed in the treated plots, especially for sites MF and IEs control plots, where duff and 1-hour fuels had highest moisture levels.

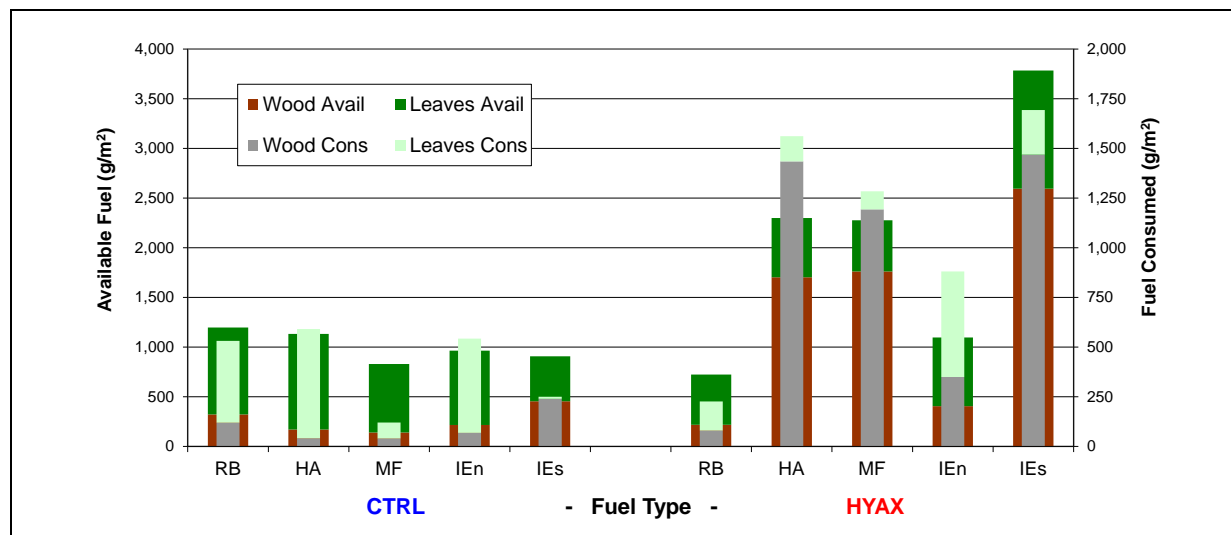


Figure 15-6. Available and consumed fuel for different fuel types and treatment plots.

To investigate the existence and strengths of relationships between the different fuel parameters, a correlation matrix was established assuming linear regressions and calculating Pearson's correlation coefficients r across all parameters shown in **Table 15-5** for the HYAX and CTRL data sets separately. The resulting correlation matrix is presented in **Table 15-5**, but only the statistically significant r -values ($p < 0.05$) are shown; HYAX values in red and CTRL in blue.

Because each correlation was based on only five data pairs (from five plots), r had to be greater than 0.848 for the linear relationship to be statistically significant.

Table 15-5. Statistically significant Pearson's correlation coefficients between different fuel parameters from within the two fuel types, CTRL in blue and HYAX in red.

p<0.05 for r>0.848	CTRL													
	F-Avail_g/m2	FC-Tot_g/m2	FC-Wd_g/m2	FC-Lvs_g/m2	FC-Rel_%	FC-Wd_%	FC-Lvs_%	Soil-OM_%	FM-Duff_%	FM-1hr_%	FM-10hr_%	FM-100hr_%	CCA	NMS
F-Avail_g/m2	1.00												0.89	
FC-Tot_g/m2	0.90	1.00		0.94	0.97		0.92							
FC-Wd_g/m2	0.90	0.96	1.00			0.99		0.85						
FC-Lvs_g/m2				1.00	0.91		0.98			-0.87				
FC-Rel_%					1.00		0.93							
FC-Wd_%					0.98	1.00				0.88				
FC-Lvs_%				0.95			1.00			-0.86				
Soil-OM_%								1.00						
FM-Duff_%									1.00			1.00		
FM-1hr_%	0.90	0.96	0.88						0.86	1.00				
FM-10hr_%											1.00			
FM-100hr_%									1.00	0.89		1.00		
CCA				-0.88			-0.95						1.00	
NMS														1.00
p<0.05 for r>0.84	F-Avail_g/m2	FC-Tot_g/m2	FC-Wd_g/m2	FC-Lvs_g/m2	FC-Rel_%	FC-Wd_%	FC-Lvs_%	Soil-OM_%	FM-Duff_%	FM-1hr_%	FM-10hr_%	FM-100hr_%	CCA	NMS
	HYAX													

Only two linkages are equally important for both fuel types (boxed cells): (1) the fraction of leaves consumed is proportional to its total mass consumed, and (2) fuel moistures of the 100-hour fuels correspond exactly (1:1 ratio) with the moisture levels found in the duff. However, moisture levels of the 1-hour fuels vary differently among the different fuel types. Although HYAX moisture levels strongly increase with the amount of total available fuel, as well as with the amounts of consumed total and woody fuels, they increase only with the fraction of woody CTRL fuel consumed, but decrease for CTRL with the amount and fraction of leaves consumed (i.e., more CTRL leaves material was consumed when 1-hour fuels were drier.) The only other apparently inverse linkage existed between the CCA vegetation community scores and HYAX fuel consumption. The more pocosin-like the stand, the more leaves (total amount and fraction) were consumed from the mechanically thinned plots. Under less pocosin-like conditions, more fuel was available for PB, but in the CTRL plots only. The proportionality between total amount and fraction of fuel consumed was upheld only for CTRL but not for HYAX fuels. However, only HYAX data revealed a strong positive linkage (1) between total fuel consumed and available fuel (i.e., consumption [both total and woody fuel] increased with availability) and (2) between woody and total fuel consumed (i.e., the consumption of woody material scaled linearly with that of all treated materials).

To gauge fuel treatment specific differences (HYAX versus CTRL) in the linkages between measured fuel parameters and species's EF, the EF values entering the linear regression matrix were determined in two different ways: (1) by treating the two EF measurements from the shorter flaming-dominated phase and the subsequent longer smoldering-dominated phase

separately, and (2) by combining the two into a single time-weighted EF average. Considering the same level of significance in r between the two methods, **Tables 15-6a and 15-6b** show that relatively few species's emissions are sensitive to the underlying fuel conditions.

Table 15-6a. Statistically significant r -values for relationships between certain fuel parameters and species' EF values, using both flaming and smoldering EF values independently.

p<0.05 for $r>0.442$	MCE	CO_g/kg	CH ₄ _g/kg	Toluene_g/kg	<8 Carbon Alkanes_g/kg	Halo- C_g/kg	SO ₄ =_g/ kg	NH ₄ +_g/ kg
F-Avail_g/m ²				-0.48				
FC-Tot_g/m ²			-0.45	-0.44	-0.48			
FC-Lvs_g/m ²					-0.46			
FC-Rel_%						-0.47		
FM-Duff_%							-0.51	-0.51
FM-1hr_%	0.46	-0.46	-0.45				-0.52	-0.56
FM-100hr_%							-0.52	-0.53

Table 15-6b. Statistically significant r -values for relationships between certain fuel parameters and species's EF values, using combined flaming and smoldering EF values (as weighted average).

p<0.05 for $r>0.624$	MCE	CO_g/kg	CO ₂ _g/ kg	1,3- Butadiene_g/kg	<8 Carbon Alkanes_g/kg	Halo- C_g/kg	Acetylene _g/kg	EC_g/kg
FC-Tot_g/m ²								0.72
FC-Wd_g/m ²								0.67
FC-Lvs_g/m ²	0.72	-0.72	0.66		-0.69	-0.74		
FC-Rel_%						-0.64		
FC-Lvs_%						-0.64		
FM-Duff_%				-0.67				
FM-1hr_%				-0.74			-0.67	
FM-100hr_%				-0.69				

The two tables show that none of the linear linkages between fuel consumption and fuel moisture with gas and particle-phase species emissions are very strong. Of all the species measured (see **Table 15-2**), only the EF values from the group of alkanes and halocarbons (*Halo-C*) decrease with increasing consumption of leaves and relative consumption of all fuels, respectively. For both methods, species's EF values correlate negatively with fuel parameters except for MCE, which correlates positively albeit very weakly with 1-hour fuel moisture and leaves consumed for the individual and combined EF, respectively. The former may be an artifact of the second (longer) combustion phase, yielding a higher CE due to the drying effect of the preceding first phase, whereas the latter points to an overall effect of more leaves being burned (which are harder to ignite) when the average combustion of the two stages is more intense and subsequently at higher temperature. Higher fuel moisture levels yield lower sulfur (S) and nitrogen (N) emissions in the particle phase (in the form of sulfate and ammonium, respectively) when treated separately, and lower 1,3-butadiene and acetylene emissions on the basis of a

weighted average. There is a weak trend towards lower emissions of gaseous aromatics and alkanes but higher emissions of particle-phase EC when more fuel is being consumed.

In summary, understory and midstory thinning treatment yielded about twice the availability and almost 3 times more consumption of fuels, especially woody material, regardless of fuel moisture. The fuel parameters investigated were the available amount of fuel, the total and relative amount of fuel consumed, and different fuel moistures reflecting both fuel conditions and vegetation composition. Variations in vegetation type as reflected in CCA or NMS scores and variation in soil characteristics as indicated by soil organic matter content showed no linkage to the emissions of most chemical species. Only a few species' emissions correlated weakly with some of the fuel parameters investigated; in particular the total and relative amount of fuel consumed and different fuel moistures reflecting short-term above-ground fuel conditions. The poor correlations of these fuel measures with EF values suggest that site vegetation variation is not the driving factor in explaining the observed variability in EF values for most species. Differences in emissions between treatments (control and HYAX) are therefore not confounded by either soil characteristics (indicated by soil organic matter content) or vegetation differences, allowing direct comparison of treatment effects on emissions factors.

Gas-Phase PB Emissions and Emission Factors (EF)

All aerosol emissions measured via ACM at the burn locations are characterized in terms of reactive gas-phase and particle-phase chemical species EF calculated according to Equation 15-3 and expressed in g-species's mass per kg-fuel mass consumed. All EF values are based on net emissions because the corresponding background concentrations have been subtracted. **Figure 15-7** and **Table 15-7** show the weighted EF averages from each vegetation plot comparing the untreated control fuels (CTRL in blue) with the mechanically thinned fuels (HYAX in red) for gaseous emissions. For clarity, some species have been reduced to groups, especially for the large number of VOC and POC species determined from the whole air canister samples and quartz filter samples, respectively (see **Table 15-2**). The *LOAg* (light organic acids) are mainly formic and acetic acids in the gas-phase with corresponding salts in the particle-phase (*LOAp*). The groups of *<8C-Alkanes*, *<5C-Alkenes* and *<9C-Aromatics* are governed by ethane, ethene plus propene, and benzene plus m/p-xylenes, respectively. Note that the most dominant aromatic specie, toluene, is graphed individually. The group of *Halo-C* is dominated by CH₃Cl, a typical biomass burning marker, towering two orders of magnitude above other *Halo-C* compounds, whereas alkyl-nitrates (*Alkyl-NO₃*) are governed primarily by methyl-nitrate followed by a distant ethyl-nitrate (ca. 20–30% of methyl-nitrate). Units are g/kg except for NMHC, which are in g-carbon per kg-fuel mass burned.

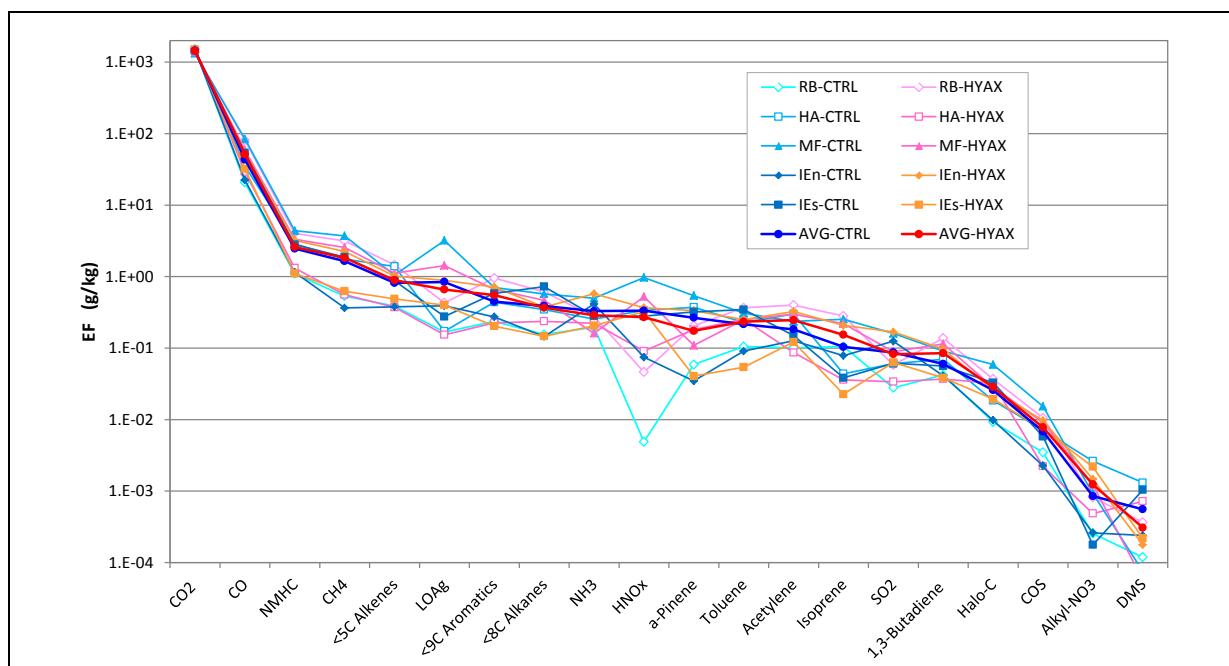


Figure 15-7. Comparison of gaseous species' EF (individual and groups) as weighted average from the different vegetation plots investigated for fuel consumption.
NMHC is in units of gC/kg.

Table 15-7. EF values (all in g/kg except NMHC is in gC/kg) of gaseous species and compound groups for PB emissions from CTRL and HYAX fuel types of the five vegetation plots, in descending order of average EF.

	CTRL ^a					HYAX ^b					CTRL	HYAX	HYAX/CTRL ^c
	RB	HA	MF	IEEn	IEs	RB	HA	MF	IEEn	IEs	AVG ^c	AVG ^d	CTRL ^e
MCE	0.98	0.96	0.91	0.98	0.95	0.91	0.97	0.94	0.94	0.97	0.955	0.946	0.99
CO ₂	1,515	1,460	1,323	1,504	1,448	1,359	1,490	1,410	1,414	1,495	1450	1434	0.99
CO	20.8	35.2	84.3	22.4	53.6	80.6	29.2	59.5	55.1	32.1	43.2	51.3	1.19
NMHC	1.10	2.86	4.39	1.15	2.80	4.03	1.32	3.32	3.20	1.10	2.46	2.59	1.05
CH ₄	0.53	1.76	3.71	0.36	1.87	3.15	0.56	2.55	2.25	0.62	1.65	1.83	1.11
<5C Alkenes	0.39	1.39	1.05	0.38	0.87	1.46	0.37	1.12	1.02	0.49	0.82	0.89	1.09
LOAg	0.17	0.17	3.20	0.39	0.28	0.43	0.15	1.43	0.88	0.40	0.84	0.66	0.78
<9C Aromats	0.24	0.44	0.70	0.27	0.58	0.95	0.23	0.66	0.71	0.20	0.45	0.55	1.24
<8C Alkanes	0.15	0.34	0.57	0.15	0.72	0.61	0.24	0.46	0.37	0.15	0.39	0.37	0.94
NH ₃	0.20	0.26	0.50	0.41	0.28	0.28	0.22	0.16	0.58	0.21	0.33	0.29	0.88
HNO _x	0.00	0.34	0.97	0.07	0.28	0.05	0.09	0.52	0.37	0.32	0.33	0.27	0.81
α-Pinene	0.06	0.37	0.54	0.03	0.32	0.21	0.18	0.11	0.33	0.04	0.27	0.17	0.66
Toluene	0.11	0.23	0.31	0.09	0.34	0.37	0.25	0.25	0.25	0.05	0.22	0.23	1.09
Acetylene	0.10	0.30	0.24	0.13	0.15	0.40	0.09	0.30	0.33	0.12	0.18	0.25	1.35
Isoprene	0.11	0.04	0.25	0.08	0.04	0.28	0.04	0.22	0.21	0.02	0.10	0.15	1.48
SO ₂	0.03	0.06	0.16	0.12	0.06	0.06	0.03	0.09	0.17	0.06	0.09	0.08	0.95
1,3-Butadiene	0.04	0.07	0.09	0.04	0.06	0.14	0.04	0.11	0.10	0.04	0.06	0.08	1.42
Halo-C	0.009	0.018	0.059	0.010	0.033	0.037	0.032	0.028	0.026	0.019	0.026	0.029	1.11
COS	0.003	0.007	0.015	0.002	0.006	0.011	0.002	0.009	0.010	0.007	0.007	0.008	1.14
Alkyl-NO ₃	0.0003	0.0026	0.0009	0.0003	0.0002	0.0008	0.0005	0.0012	0.0015	0.0022	0.0008	0.0012	1.46
DMS	0.0001	0.0013	0.0001	0.0002	0.0010	0.0004	0.0007	0.0001	0.0002	0.0002	0.0006	0.0003	0.55

^a Blue represents control data.

^b Red represents the treated (HYAX) data.

^c Bold blue is the average of the control.

^d Bold red is average of HYAX.

^e Bold black is the average HYAX greater than the average control.

Gaseous emissions of ammonia (NH_3), HNO_x (primarily HONO and HNO_3 secondarily), aromatics (especially *Toluene*), and biogenic organic compounds (α -*Pinene* and *Isoprene*) are significant. All these gas species are reactive and play an important role in the atmospheric formation of ozone and new particles (inorganics and SOA), which is discussed later. It is important to note that these reactive gas species are not necessarily a direct product of combustion, and instead are emitted from the underlying soil and leaves via stomatal transpiration in response to heat exposure to the moving flame. These species' EF values also exhibit the biggest variability among the different vegetation plots relative to the longer lived acetylene, 1,3-butadiene and *Halo-C*.

Excluding the single outliers for OC/EC and OM/organic carbon (OC) in each data set from the five fuel plots in support of the Figures, **Table 15-7** lists the numerical values of the data plotted and quantitatively compares potential treatment effects on average EF by means of the ratio of the HYAX to CTRL average EF values (last column). Although mechanical thinning is relative to the control, it causes significant EF increases in isoprene, alkyl-nitrates, 1,3-butadiene, acetylene, aromatics and CO, significantly less DMS, α -pinene, LOAg, and HNO_x are emitted per unit fuel mass burned. Both formic and acetic acids each make up approximately 50% of the LOAg emissions for both fuel types (0.84 ± 1.3 and 0.66 ± 0.5 g/kg for CTRL and HYAX, respectively, with oxalic acid contributing well below 10%) followed by NH_3 with 0.33 ± 0.12 and 0.29 ± 0.17 g/kg for CTRL and HYAX, and an average NH_3/CO ratio of 15 ± 9 and 10 ± 5 ppbv/ppmv, respectively. NH_3 emissions are associated with smoldering combustion (Lacaux et al., 1996; Griffith et al., 1991), and emanate from the degradation of N compounds in the fuel materials. The large variability reflects the variable influence of smoldering emissions in the individual integrated sample, which is also reflected in the MCE values (top row in **Table 15-7**) and discussed in more detail below. The NH_3/CO range between 4 and 31 ppbv/ppmv confirms the observations from open-path FTIR spectroscopy laboratory experiments of pine needle combustion (Yokelson et al., 1996 and 1997).

To assess plausibility and sensitivity of our results towards fuel mix and conditions, **Figure 15-8** compares some of our gaseous species EF results with values from four different studies cited in the literature (Burling et al., 2011; Lee et al., 2005; Schauer et al., 2001; Sinha et al., 2004). Burling et al. (2011) reported about the most recent PB measurements made in February and March 2010 at the MCBCL, the Holly Shelter Game Land (HS) and airborne onboard a Twin Otter aircraft. HS encompasses 75,000 acres and is located in the southeastern coastal plain of Pender County, NC, just west of MCBCL (see Figure 15-23) and is managed by the North Carolina Wildlife Resources Commission. For our comparison, we used the average from five PB emission samples taken at MCBCL unit ME on March 1, 2010 (in the following abbreviated *PNNL-CL*) and five from the "sand ridge" and adjacent low-lying areas of HS on March 5, 2010 (*PNNL-HS*). The *PNNL-CL* emissions were from (1) recently mechanically thinned fuels with re-sprouted fetterbush shrubs; (2) untreated moderate density midstory of red bay, red maple, gall berry, and fetterbush under a moderate density loblolly pine canopy; and (3) an area of regrown small shrubs of fetterbush and swamp titi with grasses. The *PNNL-HS* emissions were primarily from PB of pine litter and midstory shrubs in a loblolly pine dominated stand. The airborne measurements (*PNNL-TO*) were made in smoke plumes intercepted between 150 and 1,000 m above the flame front of routine PB applications in managed forests in the MCBCL and HS areas (Onslow and Pender Counties) between February 11 and March 5, 2010, including the above burns that were sampled on the ground. Because all reported EF values were based on an

assumed 50% carbon content of the consumed fuel mass, we adjusted them here to reflect our assumed 42.6% fuel-C content.

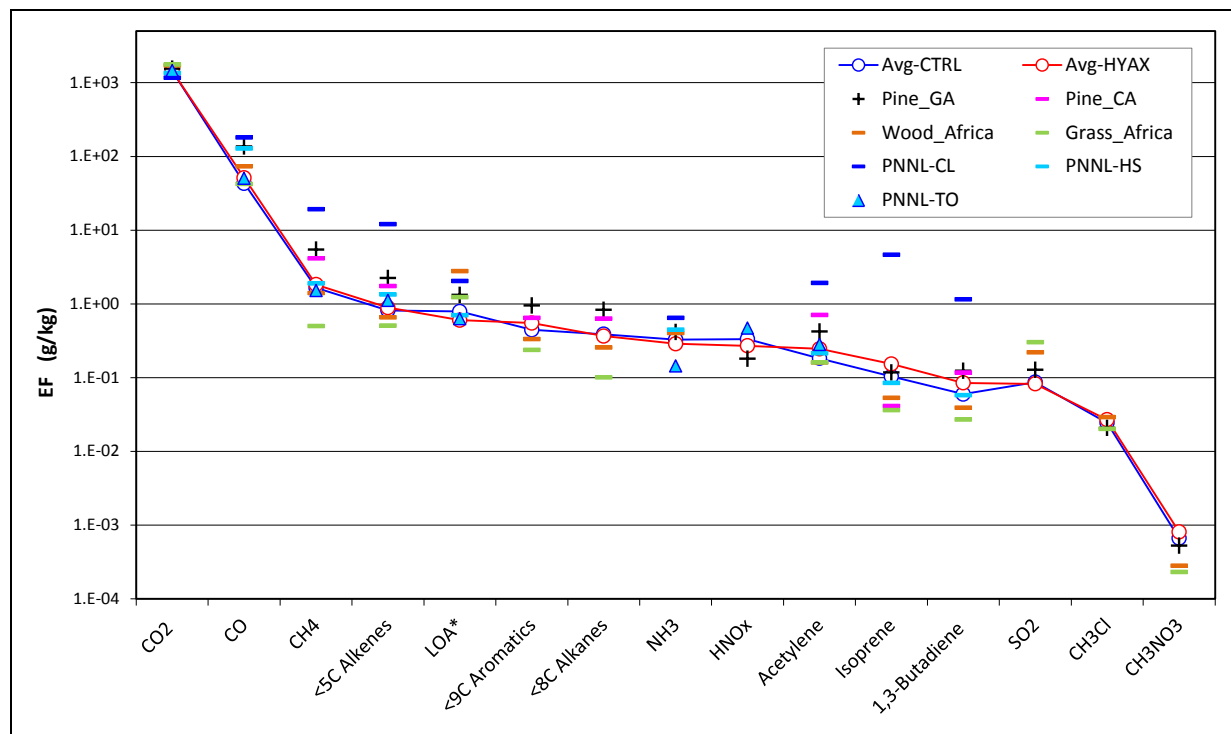


Figure 15-8. EF comparison of certain gaseous species and VOC groups from different studies. Here Light Organic Acids (LOA*) comprise only formic and acetic acids.

The Lee et al. (2005) values (*Pine_GA*) used in our comparison are an average from several ground-based PB experiments carried out in April 2004 at Forts Benning and Gordon in central Georgia. These fuels were dominated by a 50/50 mix of loblolly and long leaf pine midstory of needle litter and shrubs. EF values reported by Sinha et al. (2004) are from prescribed fires in the miombo woodland savanna and the dambo grassland savanna, prevalent savanna types in southern Africa, thus labeled *Wood_Africa* and *Grass_Africa*. Smoke samples were taken aboard an instrumented research aircraft during the dry season (May–October) of 2000, at approximately 300 m above ground and between 0.3 and 14 km downwind of the fires. The Schauer et al. (2001) values (*Pine_CA*) were obtained from fireplace combustion experiments of western pine wood.

The species and compound groups on the abscissa of **Figure 15-8** are sorted in descending order of the HYAX values (in red). The large differences in EF(CO) indicate different combustion intensities and efficiencies, hence it is not surprising that the dead stump smoldering during the PNNL-CL with the highest EF(CO) caused the lowest average MCE of 0.81 followed by 0.87 and 0.88 from the PB of pine litter and shrubs in PNNL-HS and *Pine_GA*. The airborne measurements indicate MCE levels between 0.94 and 0.96, about the same as the average CTRL and HYAX each with 0.95. The fires with the poorest MCE also have the highest average EF values for CH₄, alkenes, acetic acid, NH₃, acetylene, isoprene and 1,3-butadiene. Aircraft derived EF values are lowest for acetic acid, NH₃ and isoprene, which seem to have reacted away in the airborne plumes within the 10 to 30 minutes of average transport times. EF of longer lived

species-like CH₄, acetylene and CH₃Cl agree well between ground and airborne measurements when the combustion intensity (MCE) is similar.

Similar comparisons will be made for particle-phase species in the following section.

Particle-Phase PB Emissions and Emission Factors (EF)

Figures 15-9 and 15-10 and Table 15-8 focus on the particle phase (PM_{2.5}) species EF values (in absolute terms and relative fractions, respectively) resulting from the ACM aerosol measurements made at the burn sites. Similar to the gaseous emissions, the large number of POC species determined from quartz filter samples (see **Table 15-2**) has been reduced to groups.

Figure 15-11 presents absolute results in descending order, corresponding to the above profiles for the gaseous species, and **Figure 15-12** focuses on PM_{2.5} mass contributions from inorganic species. For clarity in presenting the results, some particulate constituents are combined into different groups (e.g., major metal oxides [*MMO*] is the sum of masses of the oxides of Al, Ca, Fe, K, Si, and Ti in their highest oxidation states [i.e., $1.88 \cdot \text{Al} + 2.13 \cdot \text{Si} + 1.21 \cdot \text{K} + 1.4 \cdot \text{Ca} + 1.41 \cdot \text{Fe} + 1.67 \cdot \text{Ti}$]). The group of *Alkali Metals* is comprised of Li + Na + Mg + Rb + Sr + Ba, and the group of *Heavy Metals* reflects the sum of Cr + Mn + Ni + Cu + Zn + As + Se + Cd + Sb + Pb without assuming any oxidation states. As a general rule for either group, values of the less uncertain elements detected via either ICP-MS or XRF were used. For example, Na, Mg, Ti, and Cu detected by XRF were only used to compare with other published EF values and not officially reported, due to low fluorescent yields, broad region of interest (ROI, a sensitivity measure specific to XRF analysis), and/or detection limit issues. Detailed data quality indicators for both XRF and ICP-MS analytical methods were presented in the SOPs.

The quantity other organic elements (OOE) was calculated from the PM_{2.5} mass balance and introduced to account for elements associated with the amount of OC measured. OOE is assumed here to be equal to the amount of unidentified mass (i.e., the difference between the total gravimetric mass and all identified components such as ions, metal oxides, other elements, and EC and OC). In our case, oxygen is the most important OOE due to its abundance and central role in fuel combustion. Hence, assuming the sum of OOE plus OC to be total organic mass (OM), oxygenated carbon species are most likely the ones causing elevated OM in the emitted fine PM. Organic compounds constitute the overwhelming bulk contribution to the fine PM emissions from both fuel types. On average, the OM fraction of total PM_{2.5} mass emitted from both CTRL and HYAX fuels is $96 \pm 2\%$ and $94 \pm 4\%$, respectively.

Table 15-8. EF of PM_{2.5} species and compound groups, plus other calculated values from MCBCL control (CTRL) and treatment (HYAX) plots (see text).

		CTRL					HYAX					CTRL	HYAX	HYAX/
		RB	HA	MF	IE _n	IE _s	RB	HA	MF	IE _n	IE _s	AVG	AVG	CTRL
MCE	—	0.98	0.96	0.91	0.98	0.95	0.91	0.97	0.94	0.94	0.97	0.95	0.95	0.99
PM _{2.5}	g/kg	3.15	10.75	45.54	9.52	5.84	18.58	7.00	16.00	15.56	4.39	14.96	12.30	0.82
OC	g/kg	2.28	8.08	21.93	4.66	3.74	14.34	4.82	10.45	11.60	2.62	8.14	8.77	1.08
sum-POC	gC/kg	0.28	1.29	2.79	0.42	0.48	1.47	0.52	1.18	1.25	0.32	1.05	0.95	0.90
Levogluconan	gC/kg	0.154	0.616	1.175	0.214	0.270	0.598	0.278	0.590	0.546	0.194	0.486	0.441	0.91
Resin Acids	gC/kg	0.044	0.309	0.779	0.055	0.075	0.451	0.098	0.172	0.301	0.039	0.252	0.212	0.84
Alkanoic As	gC/kg	0.049	0.134	0.381	0.083	0.083	0.230	0.067	0.233	0.182	0.053	0.146	0.153	1.05
PAH	gC/kg	0.006	0.145	0.202	0.010	0.007	0.062	0.032	0.024	0.081	0.003	0.074	0.040	0.54
Sterols	gC/kg	0.009	0.020	0.080	0.018	0.014	0.046	0.010	0.046	0.038	0.005	0.028	0.029	1.03
Alkanes	gC/kg	0.010	0.027	0.066	0.023	0.010	0.020	0.017	0.057	0.047	0.010	0.027	0.030	1.11
Alkenoic As	gC/kg	0.004	0.020	0.062	0.006	0.007	0.029	0.005	0.026	0.024	0.001	0.020	0.017	0.87
Dicarbox. As	gC/kg	0.005	0.018	0.022	0.009	0.007	0.019	0.012	0.016	0.018	0.008	0.012	0.015	1.22
LOAp	gC/kg	0.002	0.003	0.023	0.005	0.002	0.009	0.002	0.010	0.009	0.003	0.007	0.007	0.97
Aromatic CAs	gC/kg	0.000	0.002	0.002	0.000	0.000	0.001	0.001	0.001	0.001	0.000	0.001	0.001	0.76
EC	g/kg	0.06	0.50	0.05	0.23	0.17	0.02	0.57	0.25	0.26	0.28	0.20	0.28	1.36
Cl ⁻	g/kg	0.0075	0.0296	0.1599	0.0411	0.0190	0.0643	0.0285	0.0617	0.0960	0.0251	0.051	0.055	1.07
K ⁺	g/kg	0.0058	0.0215	0.0886	0.0236	0.0139	0.0291	0.0372	0.0443	0.1494	0.0182	0.031	0.056	1.81
NO ₃ ⁻	g/kg	0.0083	0.0401	0.0875	0.0162	0.0109	0.0180	0.0250	0.0686	0.0276	0.0208	0.033	0.032	0.98
SO ₄ ⁼	g/kg	0.0055	0.0075	0.0409	0.0162	0.0120	0.0209	0.0095	0.0329	0.0545	0.0094	0.016	0.025	1.55
F ⁻	g/kg	0.0024	0.0110	0.0494	0.0065	0.0053	0.0146	0.0064	0.0177	0.0131	0.0027	0.015	0.011	0.73
NH ₄ ⁺	g/kg	0.0021	0.0136	0.0171	0.0094	0.0045	0.0128	0.0056	0.0236	0.0116	0.0048	0.009	0.012	1.25
nonSO ₄ -S	g/kg	0.0012	0.0042	0.0171	0.0050	0.0005	0.0021	0.0022	0.0058	0.0051	0.0014	0.006	0.003	0.59
MMO	g/kg	0.011	0.037	0.230	0.046	0.025	0.050	0.085	0.103	0.206	0.034	0.070	0.096	1.37
Alkali Ms	g/kg	0.000	0.003	0.019	0.002	0.015	0.004	0.003	0.003	0.021	0.024	0.008	0.011	1.36
Heavy Ms	g/kg	0.001	0.004	0.025	0.005	0.002	0.007	0.004	0.007	0.008	0.004	0.008	0.006	0.79
sumPOC/OC	%	12	16	13	9	13	10	11	11	11	12	12.6	11.0	0.87
nonSO ₄ -S/S	%	40	62	56	48	11	23	41	35	22	31	43	30	0.70
OOE	g/kg	0.77	2.02	22.92	4.47	1.84	4.02	1.43	4.97	3.26	1.36	6.40	3.01	0.47
OM	g/kg	3.05	10.10	44.85	9.14	5.58	18.37	6.25	15.42	14.86	3.98	14.54	11.78	0.81
OM/OC	—	1.34	1.25	2.05	1.96	1.49	1.28	1.30	1.48	1.28	1.52	1.62	1.37	0.85
OC/EC	—	36	16	412	20	22	788	8	41	45	9	101	178	1.76
NH ₃ /CO	ppb/m	15	12	10	31	9	6	13	4	17	11	15	10	0.66

Table 15-8 also compares potential treatment effects on average EF by means of the ratio of the HYAX to CTRL average EF values (last column). Excluding the single outliers for OC/EC and OM/OC in each data set from the five fuel plots listed in **Table 15-8**, similar averages of OC/EC (24 ± 9 and 26 ± 20) and OM/OC (1.5 ± 0.3 and 1.4 ± 0.1) are obtained for CTRL and HYAX fuels, respectively. The single OC/EC outliers for CTRL (412) and HYAX (788) occurred also for the lowest MCE, indicating higher contributions from smoldering emissions, which cause a shift to higher OC and lower EC due to less complete combustion (Khalil and Rasmussen, 2003). Our OC/EC values range from 8 to 45 and encompass a range of values found in previous laboratory simulations (i.e., 6.3 ± 9 from fireplace combustion of loblolly and slash pine materials found by Fine et al. [2002]; 23.2 ± 32 determined by Hays et al. [2002] in laboratory type simulations of the open burning of loblolly pine and wire grass/loblolly pine needle mix, resembling most closely the fuel burned in our study; and 40 ± 3 in pine logs fireplace emissions

from Schauer et al. [2001]). Combustion-dependent relationships of OC/EC and other derived parameters (e.g., OOE, OM, and OM/OC), as well as individual species's EF are being evaluated later more specifically based on measured MCE.

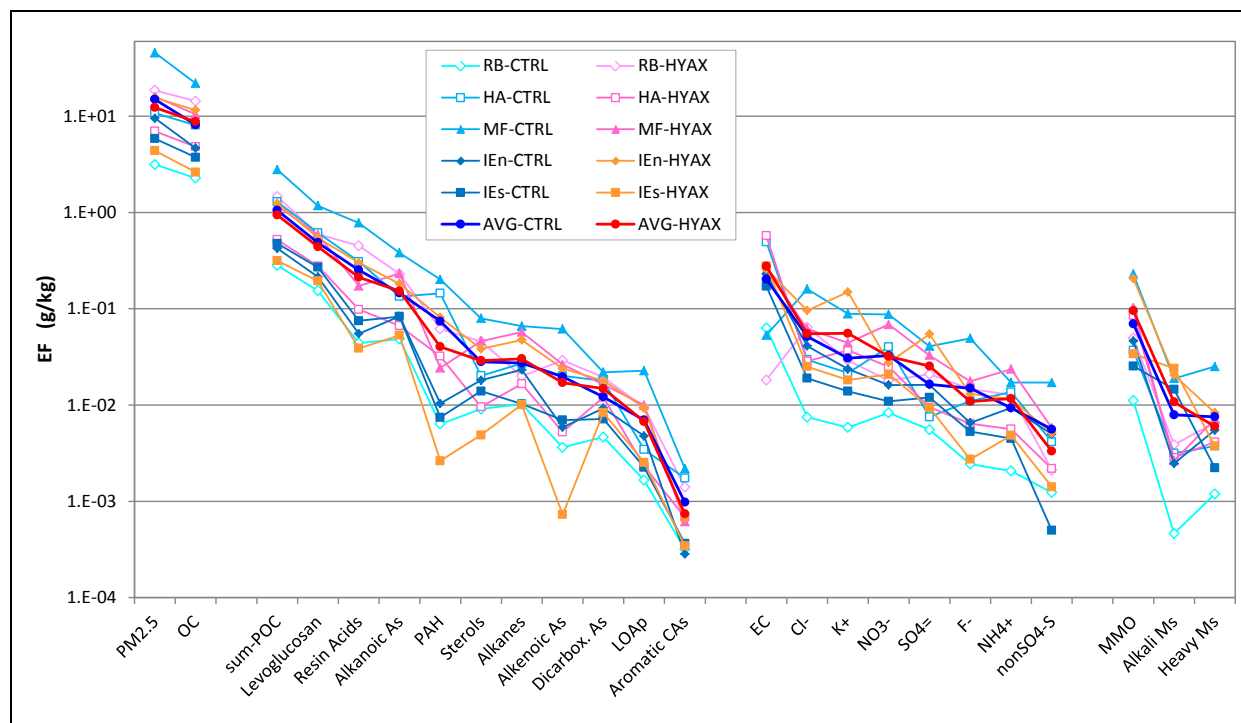


Figure 15-9. Comparison of particle phase $PM_{2.5}$ species's EF (individual and groups) as weighted average from the different vegetation plots investigated for fuel consumption.

Sum-POC and individual POC species and groups are in units of gC/kg for comparison with OC.

The PB of mechanically thinned fuels yields on average 18% less $PM_{2.5}$ emissions (per kg fuel burned) than the PB of control fuels. The lower $PM_{2.5}$ emissions, however, contain ca. 8% more OC, which is the largest contributor to $PM_{2.5}$ mass for both fuel types. The fraction of OC explained by individual POC species (depicted in Figure 9 to the right of OC) is $12.6 \pm 2\%$ and $11.0 \pm 1\%$ for CTRL and HYAX fuel emissions, respectively, assuming that the carbon from all POC species, including that from the *LOAp* species formate, acetate and oxalate have been detected by the thermal optical transmission (TOT) technique employed to measure total OC. Considering the logarithmic scale, the variability and magnitude in differences among the two fuel types and five experiment plots is remarkable, as highlighted by the HYAX/CTRL ratios in the right hand column of **Table 15-8**. Considering absolute emissions relative to CTRL, PB of mechanically treated (HYAX) fuels yield on the one hand significantly lower EF values for OOE, PAH, non-sulfate S, fluoride, aromatic carboxylic acids, heavy metals, OM, $PM_{2.5}$ mass and resin acids (governed by dehydroabietic acid), and on the other hand higher EF values for K^+ , sulfate, MMO, alkali metals, and EC. As shown in **Figure 15-10**, the latter species are even more enhanced in the mass fractions of the $PM_{2.5}$ emitted from HYAX fuels due to the 18% lower EF in $PM_{2.5}$. As previously noted, MMO contains total potassium (as detected by XRF) in its mineral oxidation state as potassium oxide (K_2O), which includes water-soluble K^+ that is therefore omitted in the fine PM mass fraction graph. K_2O is the bulk contributor to MMO mass.

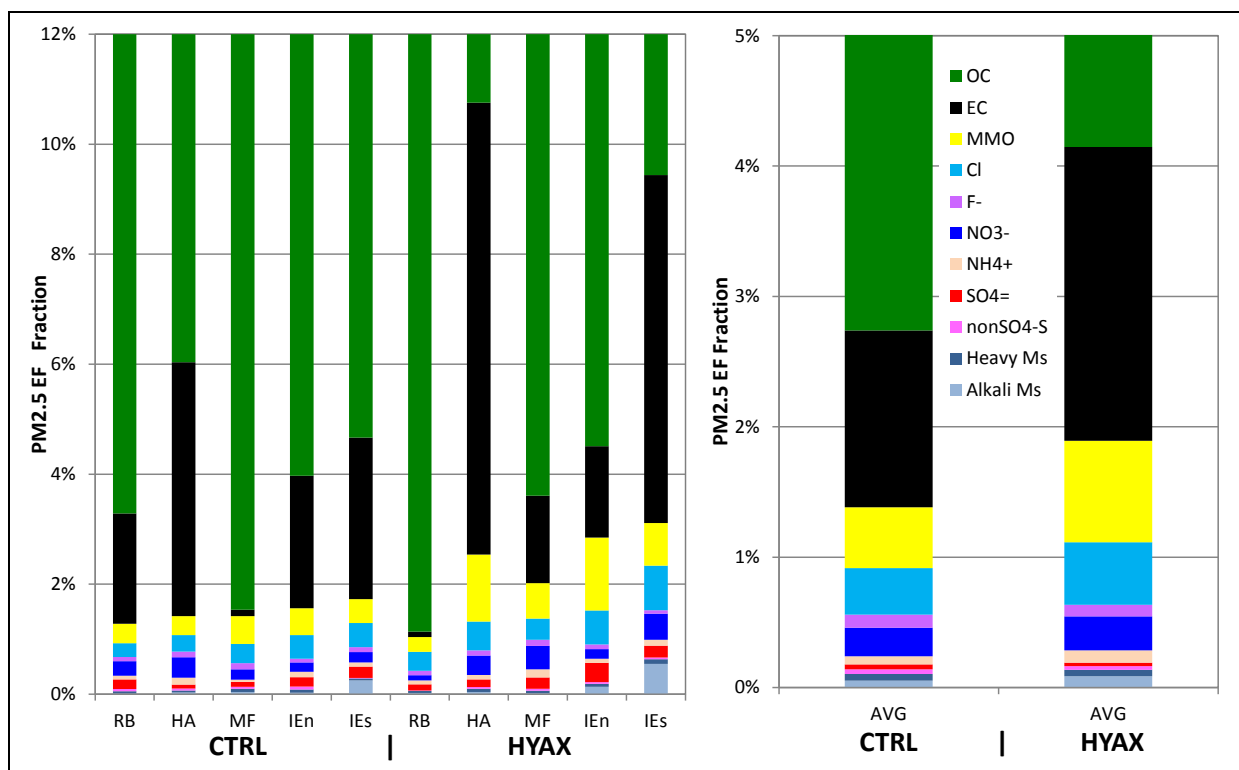


Figure 15-10. Mass fraction of major inorganic compound groups emitted with $PM_{2.5}$ from PB of both fuel types at the five experiment plots at MCBCL.

As previously mentioned, OC is the dominant $PM_{2.5}$ constituent in emissions from all investigated fuels, followed by EC, chloride (Cl^-), K^+ , and nitrate (NO_3^-). The average OC contribution to $PM_{2.5}$ in CTRL emissions are $62 \pm 13\%$ and $69 \pm 7\%$ in HYAX emissions. The various percent-contributions to $PM_{2.5}$ emissions from carbonaceous (EC and OC) and ionic species are listed in **Table 15-9**; however, the individual OC_i ($i=1-4, p$) percentages are fractions of OC (not $PM_{2.5}$), therefore adding up to 100% for each set. The OC_i groups are determined by the TOT method used in the analysis of the quartz filter samples. OC_1 through OC_4 indicate OC species of different volatility, with OC volatilizing from the sample in a pure helium atmosphere as the temperature is stepped from initially approximately $45^\circ C$ to $340^\circ C$, $500^\circ C$, $615^\circ C$ to $900^\circ C$ within approximately 4.5 minutes. However, not all OC species volatilize during this time and instead form EC due to pyrolysis, which is measured by means of a filter transmission reference of a helium/neon laser light at 633 nm and reported as OC_p . The average OC_i fractions are very similar between the two fuel types, but the MF and RB fuel burnings with the lowest MCE cause a notable shift to higher emissions of the more volatile OC_1 and OC_2 species. The OC_p fractions in the HYAX OC emissions appear systematically higher than in those from the control fuel combustion.

Table 15-9. Major carbonaceous and ionic compounds in %-mass fraction of PM_{2.5} emissions from PB of the five different vegetation plots with control and treatment fuels.

	CTRL					HYAX					CTRL	HYAX	HYAX/
	RB	HA	MF	IE _n	IE _s	RB	HA	MF	IE _n	IE _s	AVG	AVG	CTRL
MCE	0.98	0.96	0.91	0.98	0.95	0.91	0.97	0.94	0.94	0.97	0.955	0.946	0.99
EC	2.0	4.6	0.1	2.4	2.9	0.1	8.2	1.6	1.7	6.3	2.4	3.6	1.48
OC	72	75	48	49	64	77	69	65	75	60	62	69	1.12
OC1, 340C	48	42	56	45	44	50	46	52	48	37	47	47	1.00
OC2, 500C	19	29	14	16	25	17	23	15	15	27	21	19	0.94
OC3, 615C	11	9	9	9	10	9	10	8	9	11	9	9	1.00
OC4, 900C	13	9	11	14	8	12	7	11	12	9	11	10	0.95
OC _p	10	11	11	16	12	11	14	13	16	16	12	14	1.17
Acetate ⁻	0.03	0.02	0.03	0.02	0.03	0.04	0.02	0.04	0.03	0.04	0.03	0.04	1.33
Formate ⁻	0.10	0.04	0.10	0.11	0.04	0.10	0.03	0.11	0.12	0.05	0.08	0.08	1.04
Oxalate ⁼	0.05	0.04	0.03	0.05	0.06	0.03	0.06	0.05	0.06	0.09	0.05	0.06	1.29
F ⁻	0.08	0.10	0.11	0.07	0.09	0.08	0.09	0.11	0.08	0.06	0.09	0.09	0.95
Cl ⁻	0.24	0.28	0.35	0.43	0.32	0.35	0.41	0.39	0.62	0.57	0.32	0.47	1.44
SO ₄ ⁻	0.18	0.07	0.09	0.17	0.21	0.11	0.14	0.21	0.35	0.21	0.14	0.20	1.43
NO ₃ ⁻	0.26	0.37	0.19	0.17	0.19	0.10	0.36	0.43	0.18	0.47	0.24	0.31	1.29
NH ₄ ⁺	0.07	0.13	0.04	0.10	0.08	0.07	0.08	0.15	0.07	0.11	0.08	0.10	1.19
Na ⁺	0.01	0.01	0.03	0.01	0.24	0.02	0.03	0.01	0.12	0.51	0.06	0.14	2.31
K ⁺	0.19	0.20	0.19	0.25	0.24	0.16	0.53	0.28	0.96	0.41	0.21	0.47	2.19
Mg ⁺⁺	0.01	0.01	0.01	0.01	0.01	0.00	0.01	0.00	0.01	0.04	0.01	0.01	1.06
Ca ⁺⁺	0.04	0.01	0.05	0.05	0.01	0.02	0.02	0.02	0.01	0.02	0.03	0.02	0.51

Among the water-soluble species, Cl⁻, K⁺, and NO₃⁻, are the major ions comprising on average 0.32 ±0.07%, 0.21 ±0.03%, 0.24 ±0.08% for CTRL fuel emissions, and 0.47 ±0.12%, 0.47 ±0.31%, 0.31 ±0.16% for HYAX, respectively. Total elemental Cl and K are also identified by XRF, agreeing well with the corresponding water soluble fractions within +2 and -3% accuracy and R² of 0.982 and 0.975, respectively. K⁺ often serves as a diagnostic tracer for biomass burning, because the combustion of plant matter, which contains K⁺ as a major electrolyte within its cytoplasm, releases large amounts of submicron particles rich in K⁺, whereas soil- or sea-spray derived submicron aerosol usually is low in K⁺ (Andreae et al., 1996; Cachier et al., 1991; Gaudichet et al., 1995). Assuming that ionic K⁺ is an exclusive signature for wood combustion would then suggest that only approximately 2% of the total K emitted is from soil.

Comparing IC-sulfate with total sulfur from XRF shows that all samples contain a significant amount of water-insoluble sulfur. A significant fraction of total sulfur is non-sulfate (i.e., 43 ±20% in average CTRL versus 30 ±8% in average HYAX fuels emissions [Table 15-9]), pointing to potential emissions of organic sulfate compounds. Ammonium, sulfate, and NO₃⁻ combined contribute less than 1% to the total emitted PM_{2.5} mass concentration from either fuel type under mostly acidic conditions. Figure 15-11 shows the charge balance for the emitted PM_{2.5} in units of milli-equivalents per mass kg fuel burned for (1) the sulfate-nitrate-ammonium system only (SO₄), (2) all inorganic ions (INOrg), and (3) all measured ions, including the three organic ions (TOTAL). When all inorganic ions are included in the charge balance, the emissions

appear more neutralized only for the fuel beds with the highest soil, duff and 1 hour–fuel moistures, namely IEn and IEs, which also indicated significant negative correlations between these fuel parameters and sulfate emissions in **Table 15-6a**. Most other fuel beds caused a significant increase in inorganic acidity of PM_{2.5} due to the exceedingly large Cl⁻ emissions relative to K⁺ (e.g., both MF beds and mechanically thinned RB). Lastly, adding the three main organic acids, increase overall acidity especially in the fine PM emissions from the less efficient fuel combustions in MF and RB and even turn the near-neutral emissions from the “wettest” plots slightly acidic, except for the mechanically thinned fuels in IEs with the highest duff and 1 hour–fuel moisture levels. On average, mechanically thinned fuel combustion yields less acidic fine PM emissions.

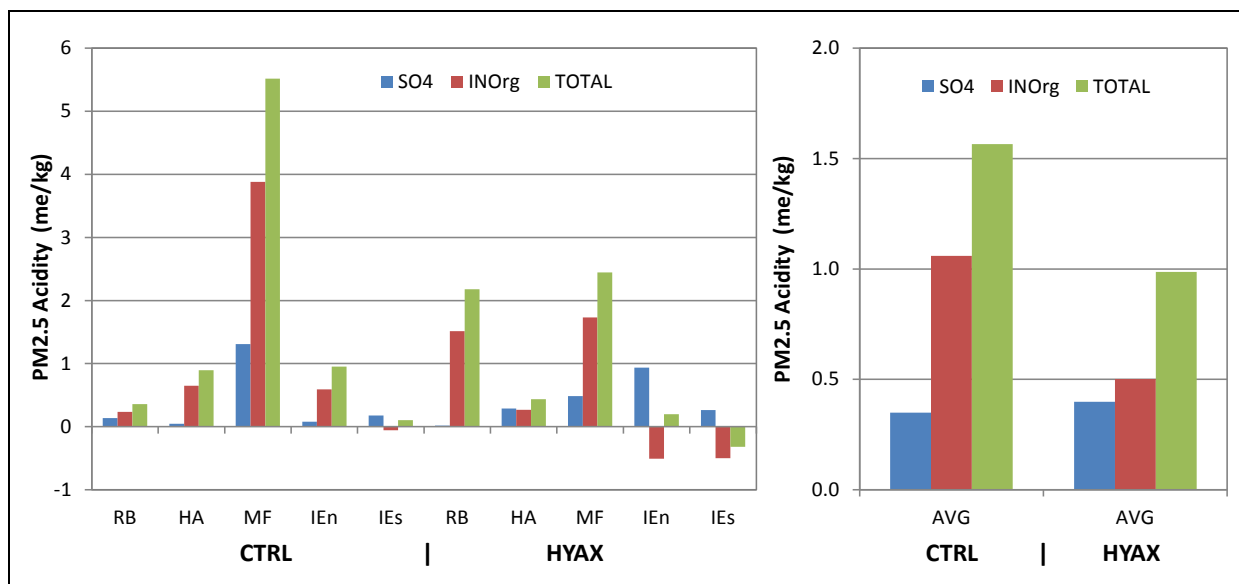


Figure 15-11. Charge balance of emitted PM_{2.5} mass for the two different fuel types in five different fuel beds (plots) at MCBCL.

Figure 15-12 compares the average profile of species emissions relative to PM_{2.5} mass from both fuel types (control and mechanically thinned treatment), with profiles from other fuels, sites and studies (Chow et al., 2004; Fine et al., 2002; Lee et al., 2005; Schauer et al., 2001). The figure is organized in descending order of the HYAX (red) profile and illustrates its systematic difference to the CTRL profile resulting from the different fuel treatment. Most elemental and ionic PM_{2.5} fractions from HYAX fuel emissions are higher than those from CTRL fuels, except for calcium and lead. The comparison of several elements detected using both XRF and IC methods show the before mentioned uncertainties of Na and Mg detection via XRF, but it also shows that mass fractions of other water-soluble elements (i.e., Cl⁻, K⁺, sulfate-S, and calcium ions) are consistently lower than the corresponding XRF totals and are highly correlated across all 20 samples (two per fuel type and plot). This suggests that a significant fraction of those elements is locked up inside the PM matrix, hindering solubility and requiring more rigorous extraction (e.g., by acid microwave digestion and subsequent ICP-MS detection). Reasons for such PM matrix effects are subject to further investigation, helping to inform about certain particle formation during PB.

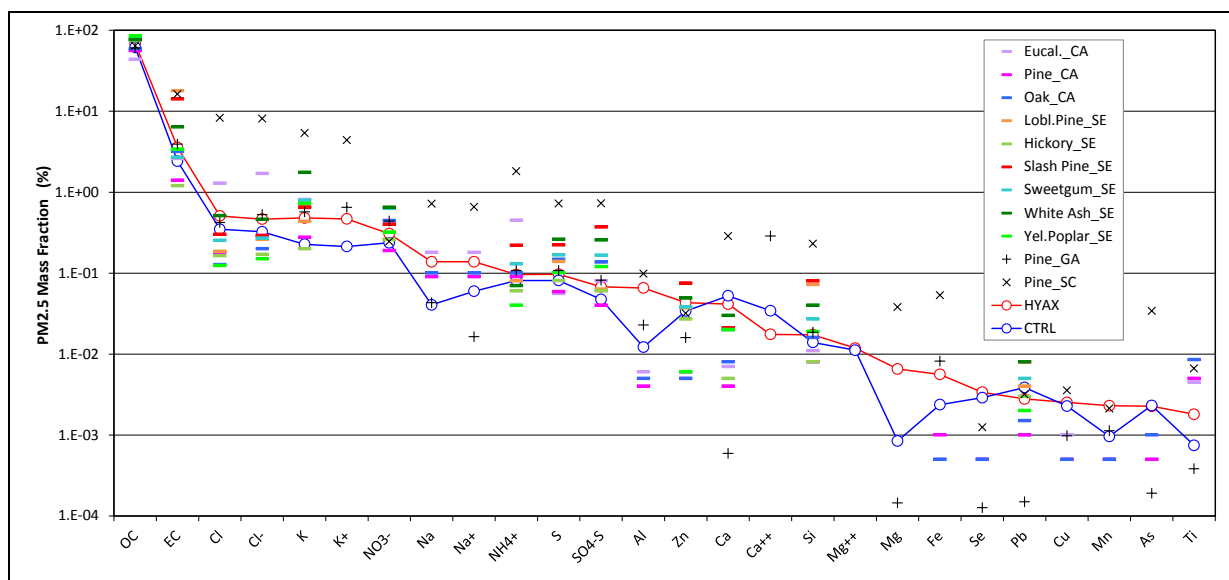


Figure 15-12. Comparison of emission profiles relative to PM_{2.5} mass from fuels in California (CA), the southeastern (SE) United States, South Carolina (SC), and Georgia (GA).

Figure 15-12 compares our HYAX and CTRL PM_{2.5} chemical composition results with those from four other emission tests, three from fireplace burnings and one from in situ PB measurements. Schauer et al. (2001) used three main soft and hard wood fuel types obtained from the western United States (extension CA), whereas Fine et al. (2002) and Chow et al. (2004) measured fireplace emissions from six different fuels of the SEUS (SE) and from South Carolina (SC), respectively. However, similar dilution sampling systems were used by all investigators to simulate cooling and dilution effects of the atmosphere. Lee et al. (2005) measured PB emissions in situ during routine applications in longleaf and loblolly pine dominated forests of central GA. Considering the logarithmic scale, the figure exhibits a large variability in PM_{2.5} composition from these different tests, owing to the different fuels, fuel conditions and combustion environments. Although OC fractions range between 44% and 100%, fractions of other elements vary up to two orders of magnitude. The 62% and 69% OC fraction of our average HYAX and CTRL fuel emissions are in the middle of the overall range but our crustal and mineral PM emissions are higher (excluding K and Si). This points to an important difference in fuel mix relative to the other investigations, in that our fuels contained significantly higher amounts of chlorophyll materials (leaves and needles), where these minerals (especially Cl, Al, Zn, and Ca) are accumulated in higher biomass concentrations during active photosynthesis than in woody material.

The normalized POC emissions (mg-C/g OC) from those studies were calculated for only those compounds measured and reported by all investigators, which were then consolidated in comparable compound groups for the most similar fuels (pine wood, needles and underbrush in pine stands) as shown in **Figure 15-13**. Results from Hays et al. (2002), who measured emissions from open burning simulating the prescribed fire of aged loblolly pine needles, have been added to the figure denoted as *Lobl.Pine_NC* for comparison with the other pine dominated fuels investigated by Schauer et al. (2001) and Fine et al. (2002). Thus, the comparable sums of POC emissions are 311, 74, 126, and 170 mg-C/g OC for Schauer et al. (2001; fireplace *Pine_CA*),

Fine et al. (2002; fireplace *Lobl.Pine_SE*), Hays et al. (2002; laboratory-simulated *Lobl.Pine_NC*), and Lee et al. (2005; in situ *Pine_GA*), respectively. Our corresponding sum of POC emissions for in situ CTRL and HYAX fuels are 117 and 102 mg-C/g OC, respectively, which are close to the needle litter burnings. Our distributions of major POC emissions are also most similar to those measured by Hays et al. (2002) for needle litter, except for the groups of resin acids and PAH. Levoglucosan, a pyrolysis product of cellulose, is the most abundant species and is followed by resin acids for all studies. However, their normalized emissions (mg/g) are very different. Although levoglucosan levels from our study are close to that from Hays et al. (2002) PB laboratory simulation, they are almost a factor of 3 less than Schauer et al. (2001) measured for western pine fireplace emissions. Our resin acid emissions are similar to the two fireplace burnings but about half that of the needle litter burnings. These differences are driven by dehydroabietic acid, which is the most dominant species in all studies. Unlike laboratory simulations or fireplace wood burning studies, the in situ PB emitted sterols, which have been used in source apportionment studies as important species identifying meat cooking. Sterols are common animal steroids and exist in soil due to the presence and activity of soil microorganism and higher living organisms (Puglisi et al., 2003). Thus, the sterols emission process during PB could be similar to steam-stripping and vaporization during meat cooking (Rogge et al., 1991).

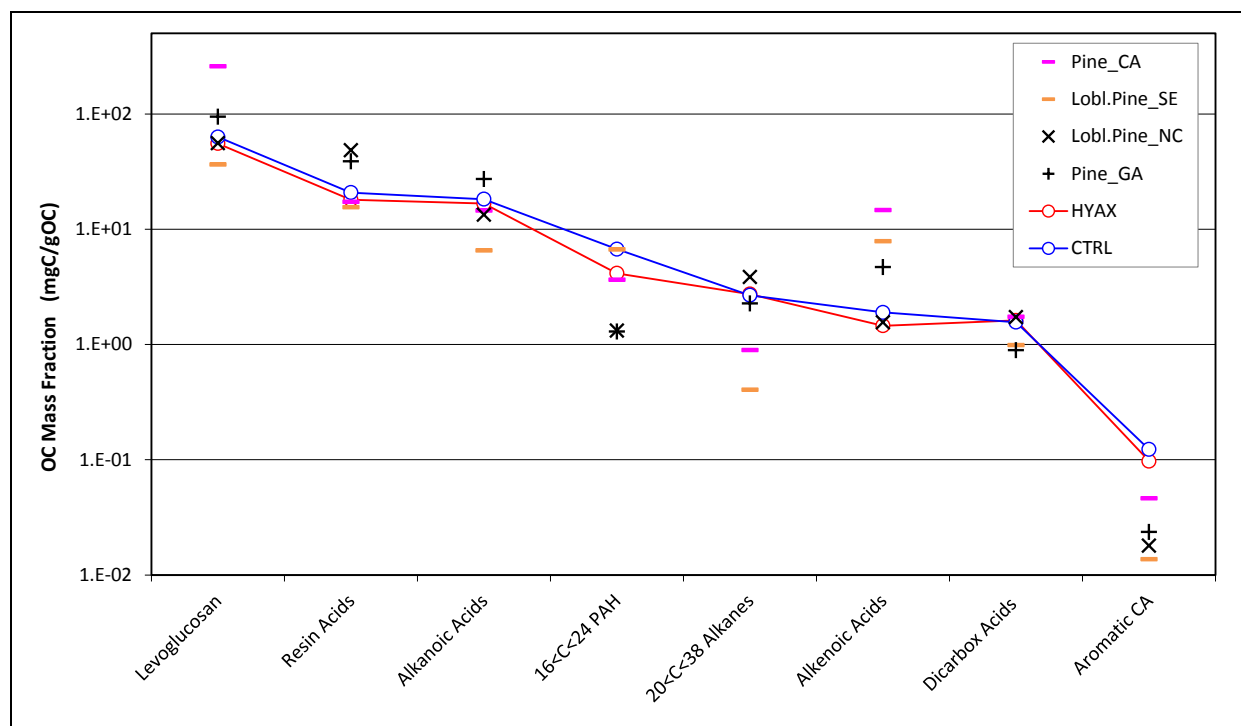


Figure 15-13. Comparison of normalized POC emissions in milligrams of carbon per gram of OC of major organic compound groups.

Emission profiles of this type are of critical importance in the source apportionment of ambient $PM_{2.5}$ at certain receptor sites; particularly locations that have to meet air quality regulations and compliance requirements. These profiles help identify individual sources and their relative contributions to the observed ambient $PM_{2.5}$ mass concentration. **Figures 15-14 and 15-15** suggest that profiles from different fuels and different locations vary significantly, therefore

yielding different results in source apportionment exercises, stressing the importance of using proper source profile data as input to chemical mass balance (CMB) receptor models or as reference for factor profiles from multivariate linear regression models such as positive matrix factorization (PMF) or UNMIX (www.epa.gov/heads/products/unmix/unmix.html). All three models have been developed by the U.S. Environmental Protection Agency (EPA) and are continuously being improved for use in air quality management. CMB fully apportions receptor concentrations to chemically distinct source-types depending upon the source profile database, whereas UNMIX and PMF use ambient data to mathematically generate factor profiles, which have to be interpreted as and associated with real sources.

Fuel Treatment Effects on Modified Combustion Efficiency (MCE) and Emissions (EF)

As described in the PB Emission Measurements section, the MCE is a good and widely used parameter to characterize the level or completeness of oxidation of the carbon in the fuel. When MCE reaches the value of 1.0, fuel-C is completely oxidized in a fully flaming dominated combustion process. However, due to limited oxygen access to the fuel and high fuel moistures encountered in open biomass burning, flaming always coexists with smoldering conditions of less complete oxidation, causing MCE to drop as low as 0.75 (Yokelson et al., 1996).

The following describes the relationships we found between gas and particle-phase species' EF and MCE, comparing effects of the mechanically thinned fuel type with those from the control. These relationships are based on linear regressions of individual species' or species groups' EF values with the coincident MCE values. Because any species' emissions are dependent on MCE, the slope, y-intercept and correlation coefficient will be used to characterize the individual $EF_i=f$ (MCE) relationship for the two fuel types. Chemical species yielding a strong negative slope (anti-correlated with MCE) point to their preferred formation during the smoldering dominated phase of the combustion process. Other species showing a less negative or even positive slope (correlating with MCE) indicate a lower sensitivity to smoldering and instead a greater potential of being formed during flaming. This generalization may not hold for chemical species containing elements other than carbon, hydrogen or oxygen, as the elemental composition of the fuel plays an important role in those species' emissions.

Note that in contrast to the fuel related comparisons, for which we used the time-weighted averages of the EF from the two subsequent measurement periods (20–30 minutes flaming dominated followed by the 2- to 3-hour smoldering dominated phase), here all EF values entered the regressions with MCE individually. Thus, since we are comparing effects from the two different fuel types, each regression is based on 10 data pairs with MCE always assumed to be the abscissa and EF the dependent variable on the ordinate. A linear regression with $n=10$ data pairs is statistically significant ($p < 0.05$) when the Pearson product-moment correlation coefficient r is either greater than 0.625 in case of a positive slope or smaller than -0.625 for a negative slope, or when the coefficient of determination R^2 is greater than 0.391.

Fuel type specific regressions are shown in **Figure 15-14** for a few important gaseous emission species. Explicit regression statistics for the most prevalent species and species's groups are shown in **Table 15-10** in accordance with their ranking in **Table 15-9**. Regressions that are statistically insignificant are faded gray.

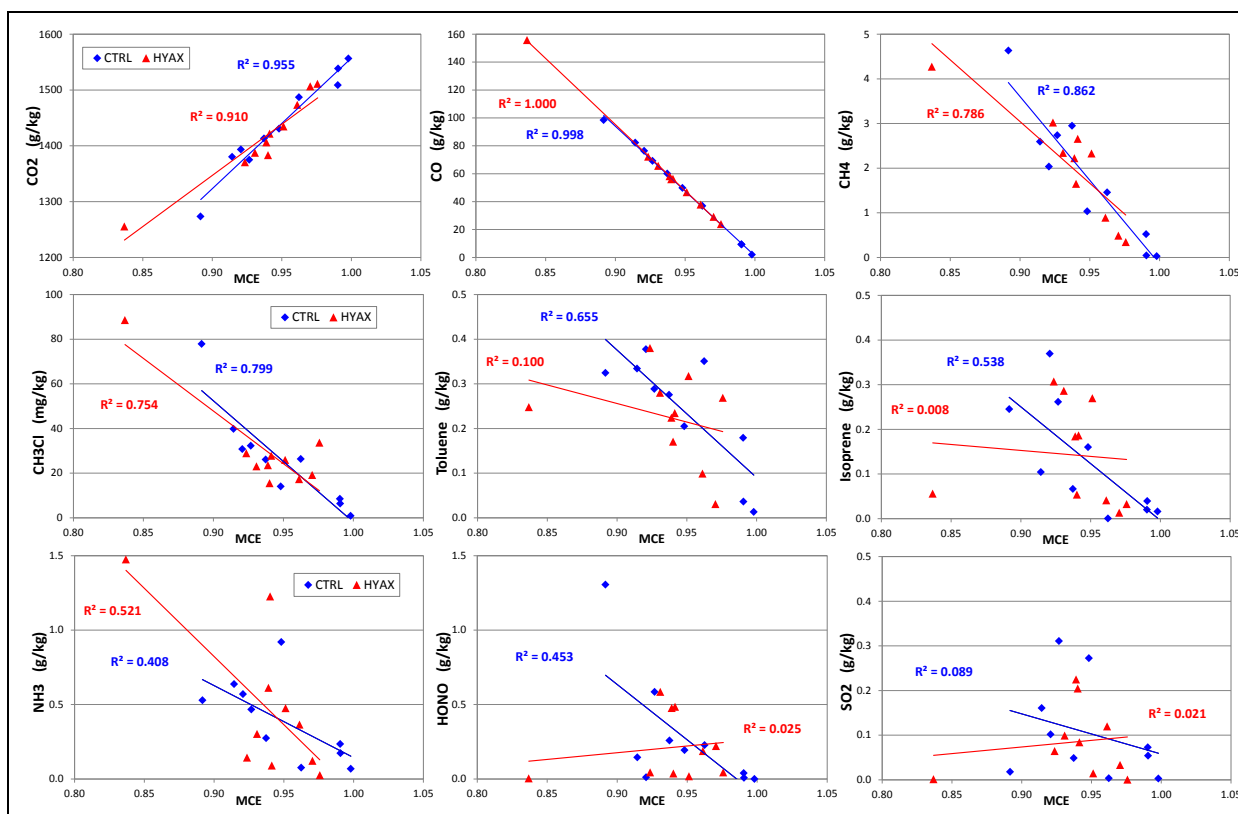


Figure 15-14. EF as a function of MCE for each of the 10 samples from the control (blue diamonds) and treatment (red triangles) plots.

As expected, $EF(CO_2)$ correlates strongly positive with MCE and $EF(CO)$ strongly negative with the latter showing more similar slope and y-intercept for both fuel types. The only other gaseous species showing a positive slope for both fuel types are the alkyl nitrates, suggesting their preferred formation under complete combustion conditions during the flaming stage. Except for alkanes and NH_3 , the HYAX regression slopes are “less negative,” indicating a lower sensitivity of those species’ emissions under combustion conditions that are conducive to smoldering; i.e., most species’ emissions from HYAX fuel increase less during transition from flaming to smoldering than what they do for CTRL fuel. This is especially true for reactive organic species such as α -pinene, toluene, and isoprene, although these slopes lack statistical significance. EF slopes of inorganic species’ such as HONO and SO_2 show a weak trend in change from negative to positive, suggesting that flaming processes may become more important for those species’ emissions when the fuel is mechanically thinned. Many species that show a statistically significant relationship for the control fuel yield less strong relationships when mechanically thinned fuel is combusted. Besides the before mentioned toluene and isoprene, this is also true for the groups of NMHC, LOAg, and aromatics, including carbonyl sulfide (COS), a relatively long-lived unreactive compound. It is currently unclear why COS emissions become less dependent on MCE when burning mechanically thinned fuel. CH_3Cl and the group of *Halo*-Cs in general show similar EF-MCE dependencies for either fuel type.

Table 15-10. Statistics for the linear regression of gaseous species' EF as a function of MCE for both fuel types: control [CTRL] and mechanically thinned [HYAX].

Fuel Type		CTRL						HYAX					
		p-val.	R ²	SLP	SE	y-ICPT	SE	p-val.	R ²	SLP	SE	y-ICPT	SE
CO ₂	g/kg	0.00	0.95	2341	181	-784	171	0.00	0.91	1835	204	-305	191
CO	g/kg	0.00	1.00	-930	14	931	14	0.00	1.00	-948	6	948	5
NMHC	gC/kg	0.00	0.74	-36.2	7.5	37.1	7.1	0.31	0.13	-11.7	10.9	13.7	10.2
CH ₄	g/kg	0.00	0.86	-37.5	5.3	37.4	5.0	0.00	0.79	-27.6	5.1	27.9	4.8
<5C Alkenes	g/kg	0.28	0.14	-6.2	5.5	6.9	5.2	0.26	0.15	-3.8	3.2	4.5	3.0
LOAg	g/kg	0.04	0.42	-26.4	10.9	25.9	10.3	0.34	0.11	-5.0	4.9	5.5	4.6
<9C Aromats	g/kg	0.00	0.76	-6.9	1.4	7.0	1.3	0.80	0.01	-1.0	3.9	1.5	3.7
<8C Alkanes	g/kg	0.02	0.50	-5.2	1.8	5.3	1.7	0.00	0.88	-5.7	0.8	5.8	0.7
NH ₃	g/kg	0.04	0.41	-4.8	2.1	5.0	2.0	0.02	0.52	-9.2	3.1	9.1	2.9
HNO _x	g/kg	0.03	0.44	-7.7	3.0	7.6	2.9	0.55	0.05	1.2	1.9	-0.9	1.8
α -Pinene	g/kg	0.08	0.34	-5.4	2.7	5.4	2.6	0.97	0.00	-0.1	2.8	0.3	2.6
Toluene	g/kg	0.00	0.66	-2.9	0.7	2.9	0.7	0.37	0.10	-0.8	0.9	1.0	0.8
Acetylene	g/kg	0.59	0.04	-1.0	1.7	1.1	1.6	0.89	0.00	-0.2	1.2	0.4	1.2
Isoprene	g/kg	0.01	0.54	-2.5	0.8	2.5	0.8	0.80	0.01	-0.3	1.1	0.4	1.0
SO ₂	g/kg	0.40	0.09	-0.90	1.02	0.96	0.97	0.69	0.02	0.29	0.72	-0.19	0.67
1,3-Butadiene	g/kg	0.08	0.33	-0.80	0.41	0.83	0.39	0.79	0.01	-0.11	0.40	0.18	0.37
Halo-C	g/kg	0.00	0.80	-0.57	0.10	0.57	0.09	0.00	0.76	-0.50	0.10	0.50	0.09
COS	g/kg	0.00	0.87	-0.16	0.02	0.16	0.02	0.47	0.07	-0.02	0.03	0.03	0.03
Alkyl-NO ₃	g/kg	0.55	0.05	0.008	0.013	-0.007	0.013	0.40	0.09	0.007	0.008	-0.006	0.008
DMS	g/kg	0.45	0.07	-0.006	0.008	0.007	0.007	0.93	0.00	0.000	0.005	0.001	0.004

Note: Gray highlights indicate statistical insignificance (p>0.05). SE is standard error

Similar relationships were determined by Burling et al. (2011) for ground-based and airborne measurements described in the previous section discussing **Figure 15-8**. Their results are summarized in **Table 15-11** for comparison with our results above.

Table 15-11. Summary of EF-MCE regression statistics derived from Burling et al. (2011).

MCE-Avg		PNNL-CL			PNNL-HS			PNNL-TO		
		0.806			0.870			0.948		
		R ²	SLP	y-ICPT	R ²	SLP	y-ICPT	R ²	SLP	y-ICPT
CO ₂	g/kg	0.18	-929	1906	1.00	1513	30	0.79	3456	-1826
CO	g/kg	0.97	-1233	1173	1.00	-988	988	0.99	-905	909
CH ₄	g/kg	0.60	223.0	-160.6	0.23	-3.2	4.7	0.04	-16.5	17.2
Alkenes*	g/kg	0.60	396.7	-308.4	0.59	8.5	-6.2	0.54	-26.0	25.8
LOA**	g/kg	0.64	54.4	-41.8	0.29	4.1	-2.9	0.49	-12.9	12.9
NH ₃	g/kg	0.01	-3.9	3.8	0.57	-12.2	11.0	0.00	-0.1	0.3
HONO	g/kg							0.00	0.1	0.4
Acetylene	g/kg	0.56	71.1	-55.4	0.94	2.3	-1.7	0.27	-3.2	3.4
Isoprene	g/kg	0.68	150.9	-117.0	0.33	0.6	-0.4			
1,3-Butadiene	g/kg	0.58	37.04	-28.69	0.30	0.41	-0.30			

Note: Gray highlights indicate statistical insignificance (p>0.05).

* Sum of ethene + propene.

** Acetic acid for ground-based CL and HS, sum of acetic + formic acids for airborne TO.

The smoldering dominated poor combustion in the case of *PNNL-CL* (dead stump smoldering at MCBCL with highest EF(CO) causing lowest average MCE of 0.806) yielded no significant relationship for any species except CO. The CO slope from the other ground-based measurements during *PNNL-HS* (PB of pine litter and shrubs at Holly Shelter yielding average MCE of 0.870) and from the airborne *PNNL-TO* plume intercepts (with average MCE of 0.948) bracket the slopes we found for our CTRL and HYAX fuels. Similarly, our CO₂ slopes lie between these two ground and airborne results. The only other strong relationship is apparent for acetylene, showing an increase with increasing MCE towards flaming dominated combustion on the ground but a weak negative relationship for the plume aloft. Our acetylene emission measurements show no correlation with MCE for either fuel type.

The EF(LOA)-MCE relationship becomes nominally less negative (less steep) when shifting from control to treatment fuels but is strongly positive for the smoldering dominated *PNNL-CL* case. Similar to isoprene, it can be speculated that LOA species are not a direct product of combustion and instead are co-emitted by live vegetation's response to heat exposure and release through their stomates during evapotranspiration. The HS-type burning of ground litter reveals similar NH₃ behavior as in our case. Differences in EF(NH₃) versus MCE regression must be seen in differences in composition and thus N-content of the fuel, which tends to be lower in woody biomass (e.g., logs) than in foliage.

Figure 15-15 highlights the fuel dependent differences in the EF-MCE relationship by ranking the species from **Table 15-12** in descending order of the regression's significance level (p-value) for the control fuel (in blue) and comparing their correlation coefficients r with those from the treatment fuel (in red). For better illustration, CO₂ is plotted at the very left and the ranking starts with CO, showing a near perfect r of -1.00 ($p=0$) for both fuel types. The dashed lines indicate the r for the imposed significance level of $p=0.05$ for either positive or negative correlation. An r -value falling between zero and either dashed line indicates a statistically insignificant relationship. Any r -value above or below the dashed line indicates whether the species' EF strongly correlates (positive) or anti-correlates (negative) with MCE in a statistically robust way.

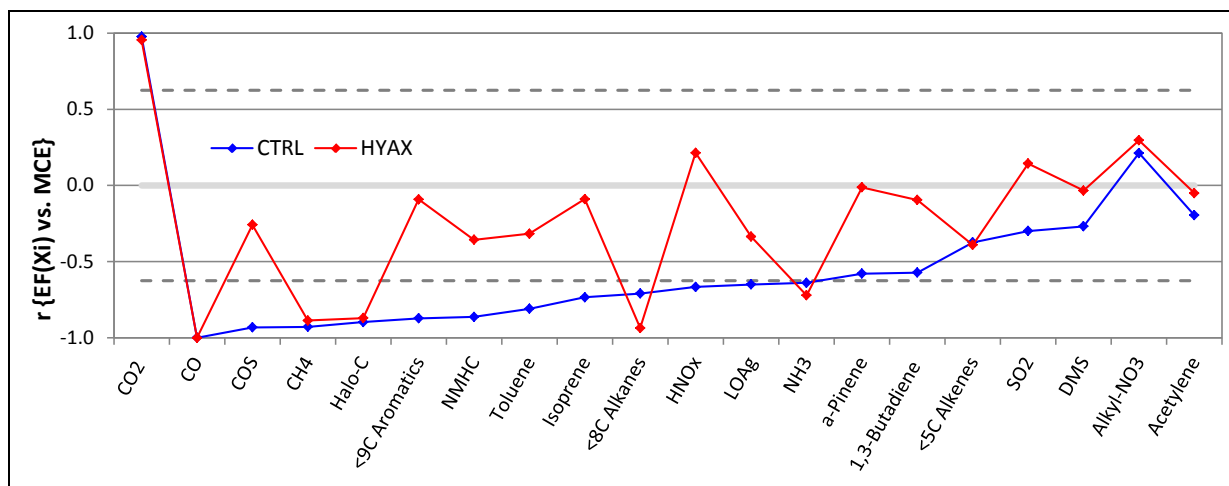


Figure 15-15. Comparison of correlation coefficients from gaseous species's EF versus MCE regression.

Although the burning of control fuel yields strong negative correlations for CO, COS, CH₄, *Halo-Cs*, aromatics, NMHC, toluene, isoprene, alkanes, HONO, HNO₃, light organic acids, and NH₃, equally significant relationships are found only for CO, CH₄, *Halo-Cs*, alkanes, and NH₃ when mechanically thinned fuels are burned (i.e., a largely reduced number of species maintain that strong and consistent decrease in emissions with increasing CE). Emissions of more reactive species such as toluene, isoprene, and light organic and inorganic acids are much more variable and inconsistent among the mechanically thinned fuel beds.

Fuel specific differences in particle-phase species emissions show similar characteristics as depicted in **Figure 15-16**. Similar ranking of control fuel emissions show that levoglucosan, various organic acids, OC, PM_{2.5}, major ions and MMO, as well as calculated quantities OOE (from mass closure) and non-sulfate S exhibit a strong and consistent decline with increasing MCE. For mechanically thinned fuels, however, these linkages are less clear, less consistent and much more variable. Inorganic species and elements tend to even cause a change in slope, showing a trend towards an increase in emissions with increasing MCE, suggesting preferred contributions of these species emissions from flaming combustion of mechanically thinned fuels. Only EC shows a positive (albeit weak) correlation with MCE for both fuel types, pointing to its characteristic formation in flaming combustion (Grisdale, 1953).

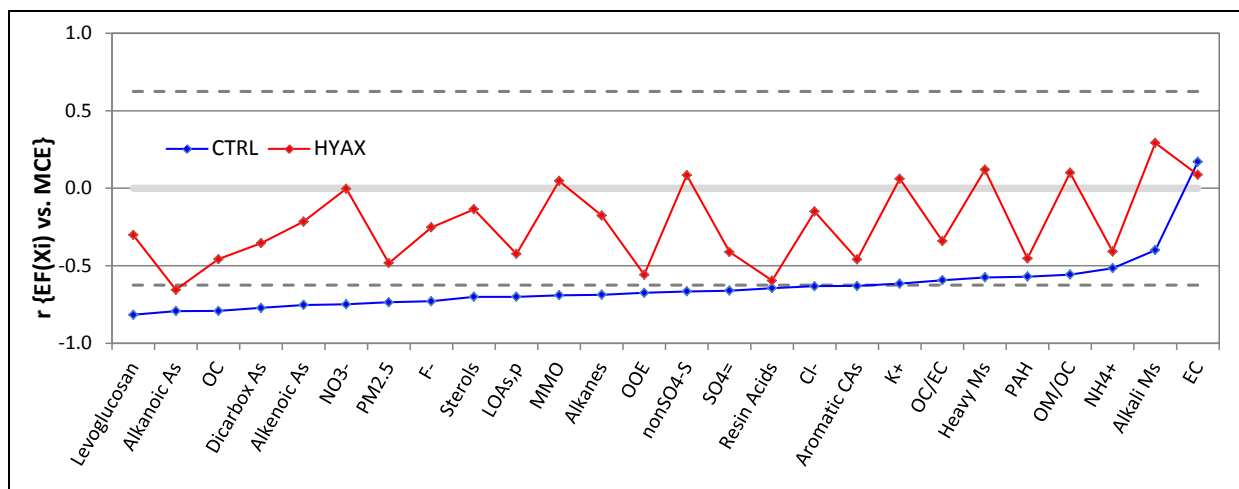


Figure 15-16. Comparison of correlation coefficients from PM_{2.5} mass and species' EF versus MCE regression.

A numeric summary of the depicted correlation levels in the form of the individual regression's slope and y-intercept is given in **Table 15-12**. The species in this table follow the order chosen in **Table 15-8**. The grey faded regression statistics are again not significant at $n-1$ degrees of freedom and 95% confidence level assuming a 2-tailed normal distribution. In accordance with **Table 15-8**, **Table 15-12** also contains correlation statistics from the various calculated quantities, of which OOE, OM, and NH₃:CO ratio show significant correlation with MCE (i.e., because OOE and OM are related [OM=OC+OOE], both decrease with MCE, whereas NH₃/CO increases with increasing CE due to the more rapid decrease of CO than NH₃). Ignoring from the regression the potential outliers from MF and RB for CTRL and HYAX sets, respectively, will nominally reduce the OOE and OM slopes for the remaining four CTRL data pairs and also reduce the strength of the correlation; p equals 0.28 and 0.10, respectively, down from 0.03 and 0.01. Removing the RB outliers from the HYAX data set has the opposite effect in that the OOE

and OM slopes nominally increase (steeper negative) and their correlations with MCE improve in significance with p now well below 0.05 (from 0.09 and 0.11 for OOE and OM, respectively). For given uncertainties expressed in standard errors (SE), any of the listed species's EF can be approximated based on an assumed or measured MCE. A corresponding list of all detected and quantified individual species can be found in **Appendix 15-A**.

Table 15-12. Statistics for linear regression of PM_{2.5} species's EF as a function of MCE for both control [CTRL] and mechanically thinned [HYAX] fuel types.

Fuel Type		CTRL						HYAX					
		p-val.	R ²	SLP	SE	y-ICPT	SE	p-val.	R ²	SLP	SE	y-ICPT	SE
PM _{2.5}	g/kg	0.01	0.54	-376	122	373	116	0.15	0.23	-91.6	59	99.6	55
OC	g/kg	0.01	0.63	-177	48	177	46	0.18	0.21	-64.0	44	69.6	41
sum-POC	gC/kg	0.01	0.59	-23.7	6.9	23.6	6.6	0.08	0.33	-8.5	4.3	9.1	4.1
Levoglucosan	gC/kg	0.00	0.67	-9.53	2.4	9.57	2.3	0.39	0.09	-2.74	3.1	3.07	2.9
Resin acids	gC/kg	0.04	0.41	-7.15	3.0	7.03	2.8	0.07	0.35	-2.77	1.3	2.83	1.2
Alkanoic As	gC/kg	0.01	0.63	-3.06	0.8	3.06	0.8	0.04	0.43	-1.87	0.8	1.93	0.7
PAH	gC/kg	0.08	0.33	-2.04	1.0	2.00	1.0	0.18	0.21	-0.67	0.5	0.68	0.4
Sterols	gC/kg	0.02	0.49	-0.58	0.2	0.58	0.2	0.71	0.02	-0.09	0.2	0.11	0.2
Alkanes	gC/kg	0.03	0.47	-0.45	0.2	0.46	0.2	0.63	0.03	-0.12	0.2	0.15	0.2
Alkenoic As	gC/kg	0.01	0.57	-0.52	0.2	0.52	0.2	0.55	0.05	-0.08	0.1	0.09	0.1
Dicarbox. As	gC/kg	0.01	0.61	-0.18	0.1	0.18	0.0	0.28	0.14	-0.12	0.1	0.13	0.1
LOAp	gC/kg	0.02	0.49	-0.19	0.1	0.19	0.1	0.21	0.19	-0.05	0.0	0.05	0.0
Aromatic CAs	gC/kg	0.05	0.40	-0.02	0.0	0.02	0.0	0.18	0.21	-0.01	0.0	0.01	0.0
EC	g/kg	0.63	0.03	1.31	2.7	-1.00	2.5	0.81	0.01	1.95	7.9	-1.33	7.4
Cl ⁻	g/kg	0.05	0.40	-1.07	0.5	1.08	0.4	0.68	0.02	-0.17	0.4	0.21	0.4
K ⁺	g/kg	0.05	0.38	-0.57	0.3	0.58	0.2	0.87	0.00	0.11	0.7	-0.05	0.6
NO ₃ ⁻	g/kg	0.01	0.56	-0.70	0.2	0.70	0.2	0.99	0.00	0.00	0.2	0.04	0.2
SO ₄ ⁼	g/kg	0.03	0.44	-0.29	0.1	0.29	0.1	0.23	0.17	-0.26	0.2	0.27	0.2
F ⁻	g/kg	0.01	0.53	-0.39	0.1	0.39	0.1	0.48	0.06	-0.06	0.1	0.07	0.1
NH ₄ ⁺	g/kg	0.12	0.27	-0.13	0.1	0.14	0.1	0.24	0.17	-0.08	0.1	0.09	0.1
nonSO ₄ -S	g/kg	0.03	0.44	-0.14	0.1	0.14	0.1	0.82	0.01	0.01	0.0	0.00	0.0
MMO	g/kg	0.02	0.48	-1.70	0.6	1.69	0.6	0.90	0.00	0.17	1.2	-0.04	1.2
Alkali Ms	g/kg	0.25	0.16	-0.09	0.1	0.10	0.1	0.41	0.09	0.13	0.2	-0.11	0.1
Heavy Ms	g/kg	0.08	0.33	-0.16	0.1	0.16	0.1	0.74	0.01	0.02	0.0	-0.01	0.0
sumPOC/OC	%	0.76	0.01	9.90	31.1	3.57	29.5	0.34	0.11	-9.50	9.4	20.30	8.9
nonSO ₄ -S/S	%	0.20	0.19	-289	211	317	200	0.16	0.23	273	177	-221	166
OOE	g/kg	0.03	0.45	-196	76	193	72	0.09	0.31	-29	15	31	14
OM	g/kg	0.01	0.54	-373	121	369	115	0.11	0.29	-93	52	100	49
OM/OC	-	0.09	0.31	-5.8	3.0	7.0	2.9	0.78	0.01	0.4	1.4	1.0	1.3
OM/PM	%	0.14	0.25	-44	27	137	25	0.19	0.20	-52	37	143	35
OC/EC	-	0.07	0.35	-3523	1691	3462	1604	0.33	0.12	-2589	2527	2574	2370
NH ₃ /CO	ppb/m	0.01	0.58	366	110	-325	104	0.66	0.02	-42	93	52	87

Note: Gray highlights indicate statistical insignificance (p>0.05). SE is standard error.

Table 15-12 indicates that emissions (in g/kg as EF) of non-sulfate S, OOE and OM (which is the sum of OC plus OOE) all negatively correlate in a statistical significant way with MCE, suggesting that these compounds are being emitted under smoldering dominated conditions.

Remembering that non-sulfate S is the difference between the total sulfur detected via XRF and the water-soluble (ionic) sulfur from sulfate, and that OOE is calculated from mass balance of all detected PM_{2.5} species including non-sulfate S and oxygen associated with major metals assuming common oxidation states, elements with significant mass such as N and O that have not been explicitly detected must be preferably emitted from the smoldering combustion of both control and mechanically thinned fuels. This trend is slightly less consistent for the mechanically thinned fuels, as suggested by the nominally less negative OOE slope (−29) and lower R² (0.31).

Because such smoldering conditions are conducive for significant emissions in reactive species such as isoprene, α -pinene, and toluene (see **Table 15-12**), the question arises whether certain SOA forming processes are fast enough to be detected in the PB plume. As part of the GCMS analysis of our quartz filter samples, a suite of polar oxygenated compounds were detected in form of hydroxy-dicarboxylic acids, which are indicators of SOA formation from certain precursor species (i.e., here specifically, toluene, isoprene, and α -pinene). As such, the following dicarboxylic acid compounds have been identified as photo-oxidation products of toluene, isoprene and α -pinene: 2,3-dihydroxy-4-oxopentanoic acid (toluene); 2-methylglyceric acid, 2-methylerythritol and 2-methylthreitol (isoprene); pinonic acid, pinic acid, 2-hydroxy-4,4-dimethylglutaric acid, 3-hydroxyglutaric acid, 3-acetyl hexanedioic acid, 2-hydroxy-4-isopropyladipic acid (α -pinene) (Claeys et al., 2004; Edney et al., 2005; Surratt et al., 2006).

Table 15-13 compares the emissions of these precursors (as EF) with those of the SOA-indicator species. Despite abundant precursor concentrations, none of the indicator species were detected except for 2-hydroxy-4-isopropyladipic acid, which is an α -pinene product. Because α -pinene was highly abundant in these PB plumes and no other product compound was detected, other precursor(s) were required to form this particular compound (2-hydroxy-4-isopropyladipic acid) so rapidly. Any of the known sesquiterpene compounds would meet this requirement due to their structural similarity. These compounds are very reactive and presumably highly abundant in such fire plumes, but they are only detectable via very involved cryogenic trapping or by using the proton transfer reaction mass spectrometry (PTR-MS) technique (Kim et al., 2009).

In laboratory chamber experiments, Surratt et al. (2010) were able to create mass spectrometric evidence of isoprene epoxydiols (IEPOX), formed from the photo-oxidation of isoprene, being rapidly taken up and incorporated into acidified sulfate seed aerosols. This evidence was recently hardened by controlled dark chamber studies, providing direct evidence for IEPOX as precursors to isoprene SOA, and demonstrating that IEPOX uptake explains the formation of known isoprene SOA tracers found in ambient aerosols, including 2-methyltetrols, C₅-alkene triols, hemiacetal dimers, and IEPOX-derived organosulfates (Lin et al., 2012). Pending specific chemical analysis of our PB emission samples, rapid formation of organosulfates from the abundant isoprene and non-sulfate S (from XRF-IC difference) will be considered and further investigated in the future.

Table 15-13. Average EF of SOA indicator species in emissions from control (CTRL) and mechanically thinned (HYAX) fuels at MCBCL.

Precursor	SOA Indicator Species	CTRL-EF	STD	HYAX-EF	STD
	(<i>Claeys et al., 2004 and 2007</i>)	mg/kg	mg/kg	mg/kg	mg/kg
Toluene		215	115	234	113
	2,3-Dihydroxy-4-oxopentanoic acid	0	0	0	0
Isoprene		104	88	153	117
	2-Methylglyceric acid	0	0	0	0
	2-Methylerythritol	0	0	0	0
	2-Methylthreitol	0	0	0	0
α -Pinene		266	216	174	110
	Pinonic acid	0	0	0	0
	Pinic acid	0	0	0	0
	2-Hydroxy-4,4-dimethylglutaric acid	0	0	0	0
	3-Hydroxyglutaric acid	0	0	0	0
	3-Acetyl hexanedioic acid	0	0	0	0
α -Pinene?	2-Hydroxy-4-isopropyladipic acid	2.32	2.35	2.82	1.20
SO ₂ ^a	Non-sulfate sulfur	5.60	6.72	3.32	1.98
Isoprene	IEPOX-derived organosulfates	^a	^a	^b	^b
	(<i>Surratt et al., 2010</i>)				

^a Origin of sulfur and form as precursor is unknown.

^b Pending analysis.

VOC Profiles and the Potential to Form Ozone and SOA

The detailed VOC EF profiles for the individual treatment prescribed burns and their fuel bed averages based on weighted average excess MR from successive flaming-smoldering phase measurements are listed in **Table 15-A-1** of the Appendix. The following is an evaluation of the potential impact of the emitted VOC species on atmospheric O₃ formation based on their reactivity with OH. Considering the important role that isoprene, α -pinene and toluene play in both photochemical O₃ and SOA formation mentioned earlier, it seems relevant to note, that on the basis of weighted average excess MR measured in the emissions from the five control fuel beds, α -pinene emissions were approximately twice as high and isoprene emissions approximately 70% lower than the corresponding average from the mechanically thinned fuel emissions, and most aromatics emissions were similar except for the xylenes. However, most averages are based on a standard deviation of approximately 100% due to the large variability from burn to burn as illustrated in **Figure 15-17**. Thus, the average differences are not statistically significant and only indicate a trend. However, the figure suggests that the more pocosin-like fuels (e.g., IEs) tend to cause systematically lower VOC emissions, whereas emissions from the drier mesic-like loblolly pine fuel beds seem systematically above the average level. The species on the abscissa are ranked according to their excess MR found in the average control fuel emissions. The rankings within each individual fuel type, the average excess MR values and HYAX/CTRL ratios are listed in **Table 15-14** for numerical comparison.

Considering the different reactivity that each VOC species has towards photochemical O₃ production in the atmosphere, the propylene-equivalent method mentioned in the Background section earlier, and as defined by Chameides et al. (1992) was applied, which changed the ranking and relative importance of the VOC species as illustrated in **Figure 15-18**, and explicitly in the right half of **Table 15-16**. Most alkenes and all three biogenic hydrocarbons have increased in importance, so that isoprene, α -, and β -pinene now rank second, first, and tenth for CTRL fuels and first, second, and twelfth for HYAX fuels, respectively. Both emission profiles, the absolute and reactivity-based, are similar for most species except for the xylenes and some alkanes (e.g., butanes, heptane, octane), which are significantly higher in the HYAX emissions, whereas some aromatics (e.g., trimethylbenzenes, ethyltoluenes) methylpentanes, pinenes, DMS, and alkyl nitrates are systematically higher in the CTRL fuel emissions. Reactivity-based emissions are similar for both fuel types with ethene, α -pinene, isoprene, ethane, propene, and 1,3-butadiene being the six most important species. The potential to form O₃ from these top six species is higher for HYAX fuel emissions by a factor of 280/276 or 1.5%, whereas for all species combined, this O₃ forming potential is reduced to 345/341 or 1.2% relative to the CTRL fuel emissions' potential.

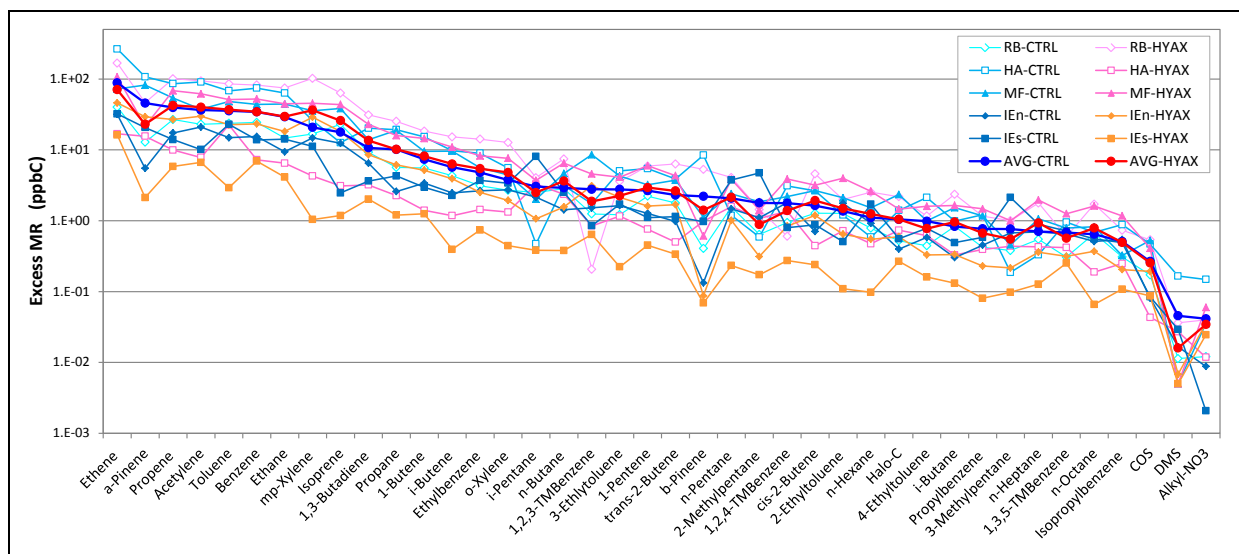


Figure 15-17. Comparison of average VOC MR in individual fuel bed emissions.

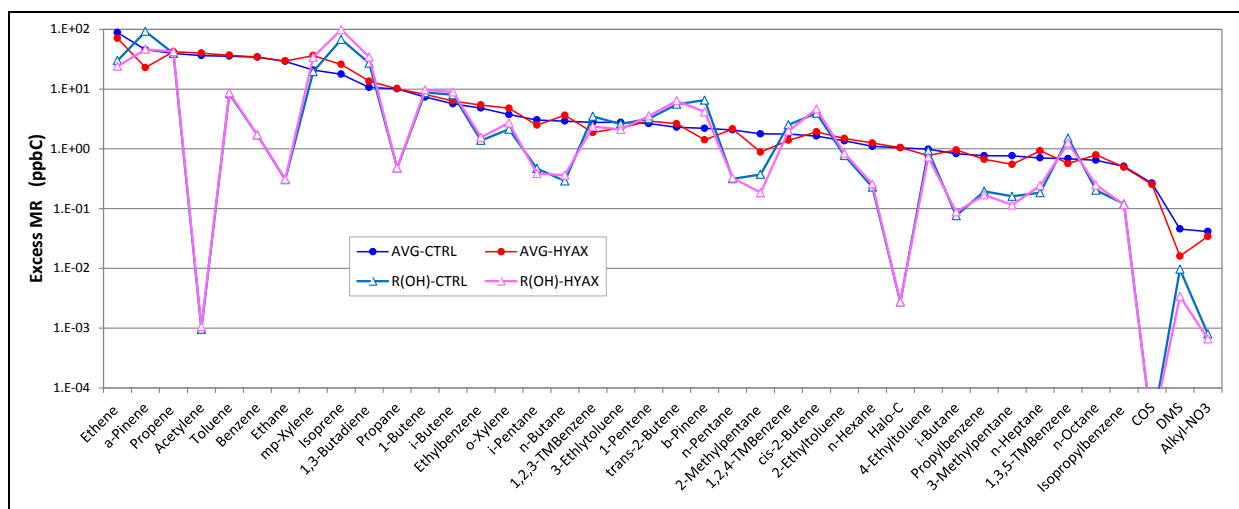


Figure 15-18. Average ranking of VOCs emitted during PB of control (CTRL) and mechanically thinned (HYAX) fuel beds (Figure 15-17), compared to propylene-equivalent ranking R(OH), indicating O₃ forming potential.

Table 15-14. Numerical summary of values depicted in Figure 15-18 as average ranking of VOCs emitted during PB of control (CTRL) and mechanically thinned (HYAX) fuel beds.

VOC	Ranking		Excess MR (ppbC)		HYAX/ CTRL	k(OH) ppb ⁻¹ min ⁻¹	Ranking		R(OH)-MR (ppbC)	
	CTRL	HYAX	CTRL	HYAX			CTRL	HYAX	CTRL	HYAX
Ethene	1	1	88.3	70.8	0.80	13.0	4	6	30.0	24.1
α -Pinene	2	9	45.6	22.9	0.50	77.3	1	2	92.3	46.4
Propene	3	2	39.5	42.4	1.07	38.2	3	3	39.5	42.4
Acetylene	4	3	36.4	40.0	1.10	0.001	38	38	0.001	0.001
Toluene	5	4	35.5	36.9	1.04	9.0	8	9	8.37	8.70
Benzene	6	6	34.3	34.4	1.00	1.9	18	18	1.71	1.71
Ethane	7	7	29.2	29.6	1.01	0.4	27	27	0.31	0.31
mp-Xylene	8	5	20.8	36.3	1.75	35.9	6	5	19.6	34.1
Isoprene	9	8	17.7	25.9	1.46	146.0	2	1	67.8	98.8
1,3-Butadiene	10	10	10.7	13.6	1.27	97.1	5	4	27.2	34.4
Propane	11	11	10.1	10.1	1.00	1.8	23	23	0.48	0.48
1-Butene	12	12	7.34	8.14	1.11	45.6	7	7	8.76	9.72
i-Butene	13	13	5.67	6.33	1.12	54.0	9	8	8.02	8.95
Ethylbenzene	14	14	4.80	5.42	1.13	11.0	20	19	1.38	1.56
o-Xylene	15	15	3.76	4.80	1.28	21.6	17	14	2.13	2.71
i-Pentane	16	19	3.04	2.50	0.82	5.9	24	24	0.47	0.39
n-Butane	17	16	2.91	3.64	1.25	3.8	28	25	0.29	0.36
1,2,3-TMBenzene	18	23	2.78	1.87	0.67	48.2	13	15	3.50	2.36
3-Ethyltoluene	19	20	2.77	2.24	0.81	35.9	15	16	2.60	2.11
1-Pentene	20	17	2.65	2.94	1.11	46.2	14	13	3.21	3.55
trans-2-Butene	21	18	2.30	2.63	1.14	92.4	11	10	5.56	6.37

(continued)

Table 15-14. Numerical summary of values depicted in Figure 15-18 as average ranking of VOCs emitted during PB of control (CTRL) and mechanically thinned (HYAX) fuel beds (continued).

VOC	Ranking		Excess MR (ppbC)		HYAX/	k(OH)	Ranking		R(OH)-MR (ppbC)	
	CTRL	HYAX	CTRL	HYAX	CTRL	ppb ⁻¹ min ⁻¹	CTRL	HYAX	CTRL	HYAX
b-Pinene	22	25	2.21	1.41	0.64	113.0	10	12	6.54	4.17
n-Pentane	23	21	2.07	2.15	1.04	5.8	26	26	0.31	0.33
2-Methylpentane	24	31	1.78	0.88	0.50	8.0	25	31	0.37	0.18
1,2,4-TMBenzene	25	26	1.77	1.39	0.79	54.7	16	17	2.53	1.99
cis-2-Butene	26	22	1.63	1.92	1.18	92.4	12	11	3.95	4.65
2-Ethyltoluene	27	24	1.37	1.49	1.09	21.6	22	21	0.77	0.84
n-Hexane	28	27	1.10	1.25	1.13	7.9	29	28	0.23	0.26
<i>Halo-C</i>	29	28	1.04	1.05	1.00	0.1	37	37	0.00	0.00
4-Ethyltoluene	30	33	0.99	0.77	0.78	35.9	21	22	0.93	0.73
i-Butane	31	29	0.83	0.96	1.16	3.5	35	35	0.08	0.09
Propylbenzene	32	34	0.77	0.67	0.87	9.7	31	32	0.19	0.17
3-Methylpentane	33	36	0.77	0.55	0.72	8.0	33	34	0.16	0.12
n-Heptane	34	30	0.70	0.93	1.32	10.0	32	30	0.18	0.24
1,3,5-TMBenzene	35	35	0.68	0.57	0.83	84.5	19	20	1.51	1.25
n-Octane	36	32	0.65	0.79	1.22	12.0	30	29	0.20	0.25
Isopropylbenzene	37	37	0.51	0.49	0.97	9.0	34	33	0.12	0.12
COS	38	38	0.27	0.25	0.95	0.003	40	40	0.0000	0.0000
DMS	39	40	0.05	0.02	0.35	8.1	36	36	0.010	0.003
Alkyl-NO ₃	40	39	0.04	0.03	0.83	0.7	39	39	0.0008	0.0007

The following compares the SOA forming potential P(SOA) for the most important contributing aromatic and biogenic VOCs introduced in the Materials and Methods section and listed in **Table 15-3**. **Figure 15-19** and **Table 15-15** summarize the P(SOA) of VOC groups for the different fuel bed emissions. P(SOA) values were determined according to Equation 15-9 with VOC species emissions rate E_{VOC} (in mass per unit burned area) determined as the product from the species' EF values and the amount of fuel consumed (FC) according to Equation 15-4. The FC values for each fuel bed are listed in the table as reference and reminder from earlier. To improve the visual presentation of these results, certain VOC species have been lumped into groups. Thus, the figure presents the P(SOA) contributions from these groups as fractions of the total potential atmospheric SOA burden from each fuel type and bed. The group of *Alkanes* here comprises n-heptane and n-octane, *R-toluenes* and *R-benzenes* are single ring aromatic compounds with aliphatic functional groups, and *Xylenes* are the sum of m-, p-, and o-xylene.

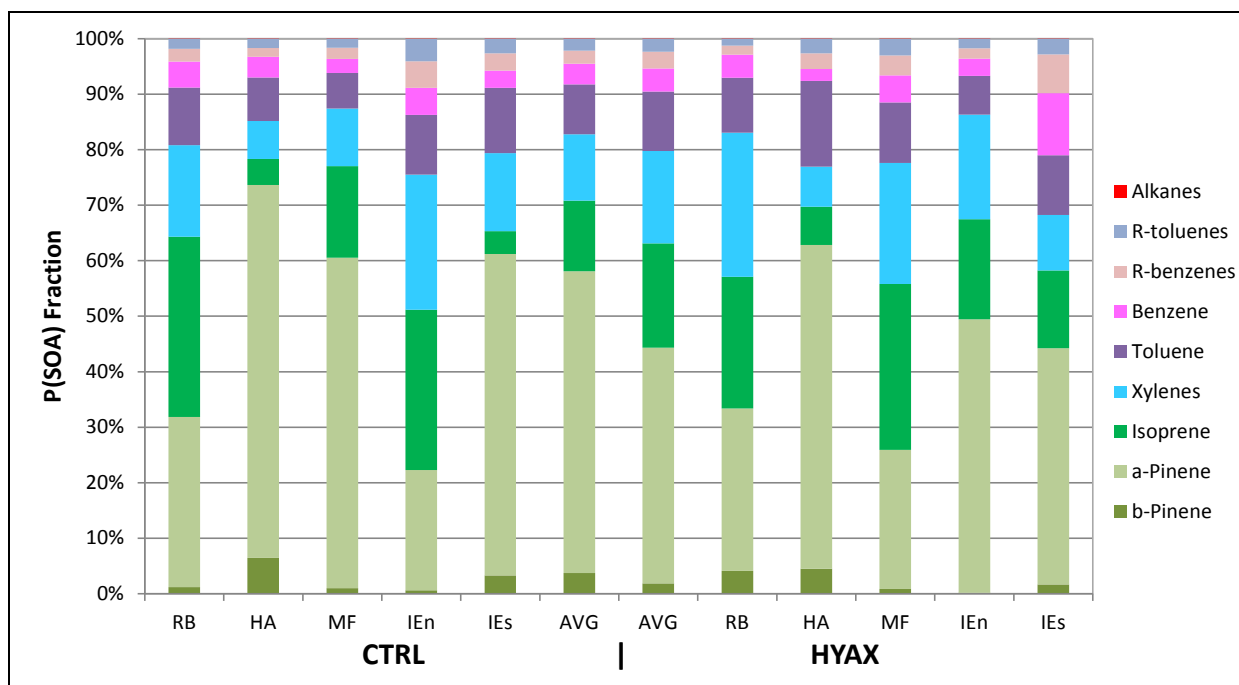


Figure 15-19. Relative contributions of major aromatic and biogenic VOC groups emitted by the PB of different fuel types and beds to the SOA forming potential of the surrounding region.

The center two bars in Figure 19 compare the arithmetic means of the two fuel types, suggesting that P(SOA) contributions from the biogenic VOCs are consistently highest for both fuel types and all fuel beds, averaging $71 \pm 11\%$ for CTRL fuels and $63 \pm 6\%$ for the HYAX fuels. Conversely, the HYAX fuels cause higher contributions from the aromatic VOCs with 17%, 13%, and 7% for the combined xylenes, toluenes, and benzenes, respectively, adding up to $73 \pm 6\%$, and the 69 $\pm 4\%$ from the CTRL fuels split into 12%, 11%, and 6% for the combined xylenes, toluenes, and benzenes, respectively.

Table 15-15 also compares the total (SOA) emission rate between the fuel types and relative to the fuel type specific total $PM_{2.5}$ and POA emissions. Remembering that the P(SOA) calculations were based on the assumption of a 5-hour reaction time and considering that (1) atmospheric lifetime of the aromatic VOC species is longer than 5 hours and (2) emissions likely continue into the next day, the listed P(SOA) emission rates must be regarded as low estimates. We already learned that mechanical thinning of the fuel makes two times more fuel available for combustion and helps consume almost 3 times more fuel relative to control; see average $1.13 \pm 0.6 \text{ kg/m}^2$ HYAX versus $0.41 \pm 0.2 \text{ kg/m}^2$ CTRL in **Table 15-15**. Thus, due to the larger FC, the HYAX emission rates must be expected to be larger by definition. However, relative to the respective POA emissions ($POA = OC + OOE$), the P(SOA) contributions are minuscule (i.e., 0.22% and 0.16% for CTRL and HYAX fuel type, respectively). The listed $PM_{2.5}$, POA and SOA values are being compared again later in the discussion of the 2009 emission inventory reporting example for MCBCL.

Table 15-15. Comparison of SOA forming potential for aromatic and biogenic VOCs in PB emissions from mechanically thinned (HYAX) and control (CTRL) fuels at MCBCL.

		CTRL		HYAX	
		STD	AVG	AVG	STD
Fuel Consumed	kg/m ²	0.21	0.41	1.13	0.59
n-Heptane	mg/m ²	0.000	0.000	0.000	0.000
n-Octane	mg/m ²	0.001	0.002	0.005	0.004
Benzene	mg/m ²	0.164	0.250	0.715	0.352
Toluene	mg/m ²	0.327	0.606	1.850	1.148
mp-Xylene	mg/m ²	0.159	0.705	2.601	2.013
o-Xylene	mg/m ²	0.043	0.100	0.272	0.168
Ethylbenzene	mg/m ²	0.037	0.071	0.189	0.097
Isopropylbenzene	mg/m ²	0.001	0.001	0.003	0.002
Propylbenzene	mg/m ²	0.000	0.001	0.003	0.002
1,3,5-TMBenzene	mg/m ²	0.016	0.027	0.091	0.057
1,2,4-TMBenzene	mg/m ²	0.018	0.032	0.110	0.088
1,2,3-TMBenzene	mg/m ²	0.010	0.027	0.119	0.077
3-Ethyltoluene	mg/m ²	0.054	0.105	0.289	0.180
4-Ethyltoluene	mg/m ²	0.013	0.020	0.057	0.040
2-Ethyltoluene	mg/m ²	0.010	0.018	0.060	0.057
Isoprene	mg/m ²	0.455	0.855	3.238	2.725
α -Pinene	mg/m ²	3.541	3.657	7.315	5.133
b-Pinene	mg/m ²	0.386	0.252	0.325	0.366
P(SOA), sum	mg/m²	4.37	6.73	17.24	9.48
PM _{2.5}	mg/m ²	2,290	4,028	11,355	6,257
OC	mg/m ²	1,525	2,419	7,765	4,166
OOE	mg/m ²	1,097	1,450	2,933	2,057
POA	mg/m²	2,189	3,868	10,699	6,082
POA/PM_{2.5}	%	1.7	96.1	94.1	4.1
P(SOA)/POA	%	0.15	0.22	0.16	0.05

It should be noted here, that the application of the SOA forming potential emphasizes the relative contribution of species for certain samples, for which similar plume rise velocity and fuel consumption rate have been assumed. The P(SOA) estimates must be considered highly uncertain due to the variability of the actual flaming/smoldering burn stage durations and plume rise times. Another uncertainty arises from the possibility of pollutants accumulating during certain burn stages and under conditions of insufficient venting, causing an increase of the local background and/or the smoldering sample itself. In general, if the source profile and emissions data of precursor species are known, the SOA formation potential of those species can be estimated utilizing the empirical FAC approach. Quantification of atmospheric SOA

concentrations, however, is questionable, since the approach neglects important variables such as timescales involved in SOA formation, transport factors, RH influences, competition between VOC species, synergistic reactions of VOC species and other possibilities that exist in ambient gas mixtures that do not exist in controlled chamber studies. Despite these limitations, FACs can be used to compare the relative importance of VOC sources for SOA formation. This study was limited to the amount of aromatic and biogenic VOC species that the employed methods allowed us to determine. A more comprehensive study employing more real-time, but more involved, measurement techniques will have to follow in future investigations.

EF Applications and Comparisons

Comparison with EPA Clearinghouse AP-42

Our new EF values for in situ PB are compared with corresponding data published by the Emission Factor and Inventory Group (EFIG) from EPA's Office of Air Quality Planning and Standards. The AP-42 series is the principal means by which EFIG documents its EF library, and EF for wildfires and PB are published in Chapter 13 of the AP-42 (EPA, 1996), accessible via <http://www.epa.gov/ttn/chief/ap42/ch13/final/c13s01.pdf>. **Figure 15-20** and **Table 15-16** compare the AP-42 EF for PB of a 65/35 short/long pine needle fuel mix assuming a 2/1 smolder/flaming weighted average, with the correspondingly weighted EF average PM_{2.5}, CO, CH₄, and NMHC values for the fuels from our study. Horizontal bars in the figure indicate the range (on a log-scale) of the EF values for both our fuel types and the spectrum of the flaming to smoldering and long to short needle fuel of the AP-42. The circles and x-markers indicate the average EF values of PM_{2.5}, CO, CH₄, and NMHC for CTRL (blue) and HYAX (red) fuels and AP-42 assumed reference fuel, respectively. The means' standard deviations are given in the **Table 15-16**.

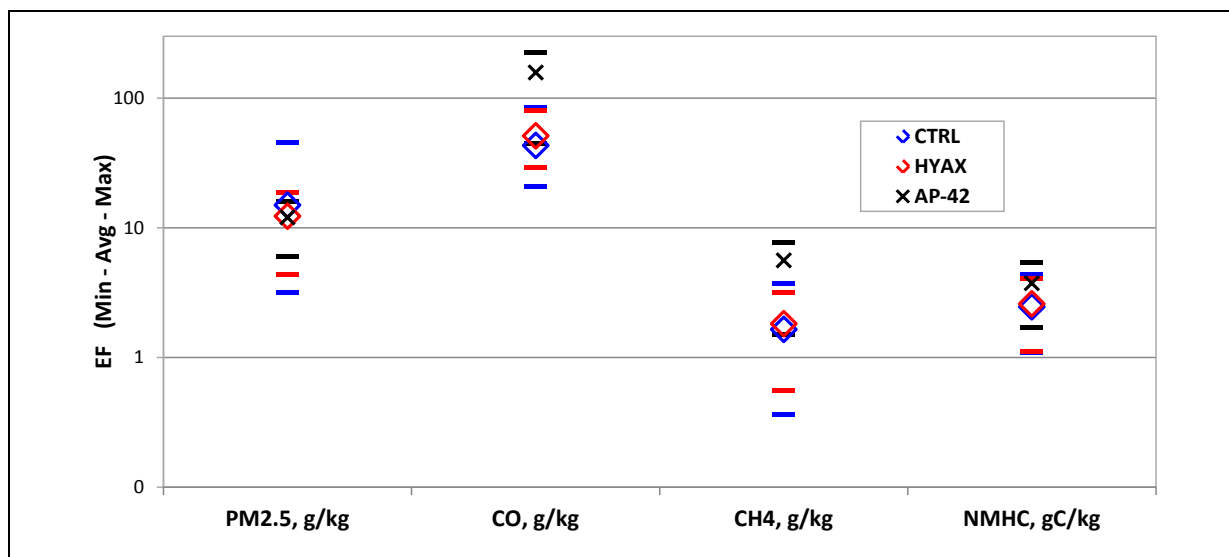


Figure 15-20. Comparison of our in situ PM_{2.5}, CO, CH₄, and NMHC EF from mechanically thinned (HYAX) and control (CTRL) fuel with AP-42 (EPA, 1996).

Table 15-16. Comparison of this study's EF with corresponding AP-42 values, including EF for total N for control (CTRL) and mechanically thinned (HYAX).

EF	AP-42		CTRL		HYAX		HYAX/ CTRL
	AVG	STD	AVG	STD	AVG	STD	
PM _{2.5} , g/kg	12.0	5.0	15.0	17.4	12.3	6.2	0.82
CO, g/kg	158.0	83.8	43.2	26.4	51.3	21.2	1.19
CH ₄ , g/kg	5.6	3.2	1.6	1.3	1.8	1.2	1.11
NMHC, gC/kg	3.7	1.8	2.5	1.4	2.6	1.3	1.05
Total N, g/kg			1.9	0.7	1.7	0.3	0.93

Although the average PM_{2.5} value from our mechanically thinned fuel compares well with AP-42, the value from our control fuel is 18% higher (i.e., in addition to removing three times more fuel, mechanical thinning of the fuel also bears the benefit of emitting 18% less PM_{2.5} per mass fuel removed). Both our CO and CH₄ EF are less than a third of the corresponding AP-42 levels, with treated fuels producing 19% and 11% more CO and CH₄ emissions per mass fuel burned, respectively. The same trend exists for NMHC (here used synonymously with VOC), except that (1) Mechanical thinning produces only approximately 5% higher NMHC emissions per kg fuel, and (2) both our fuel types' EF are within 35% of the AP-42 level.

Although not part of AP-42, EF values for total N are listed at the bottom of the table for comparison of its relative magnitude between fuel types. Total N was determined from the sum of all N-containing gas and particle phase species measured. Because NO_x emissions were not measured, we assumed them from the linear relationship with MCE for similar fuel given by Burling et al. (2011). N emissions are in part caused by the N contained in the fuel, and in part dependent on the combustion parameters governing the access of air (hence nitrogen gas [N₂]) to the combusting fuel and the subsequent dissociation of N₂ forming either thermal or prompt NO. Our EF values for total N average for both fuel types very similarly, between 1.7 and 1.9 g/kg with mechanically thinned fuel generating on average only 7% less total N per kg fuel. However, the variability within fuel type is significant, with a systematic shift to higher total N emissions from more pocosin-like (moister) fuel beds. Because both fuel types combusted on average at very similar MCE levels, the 7% lower N emissions per kg treated fuel may indicate lower concentration or combustibility of fuel-N in the mechanically thinned fuel, which would point to a greater retention of this nutrient in the mechanically treated fuel.

Comparison with Other MCBCL Emission Sources

From January to June 2010, almost 4,400 ha underwent PB at MCBCL. Assuming the average CTRL fuel consumption rate of 0.41 ± 0.21 kg/m², the 4,400 ha yielded almost 18,000 tons of fuel removed in 2010. Applying average EF from untreated CTRL fuel beds, results in annual total emissions, which can be compared to emissions if the same amount of fuel had been removed employing HydroAx treatment. **Figure 15-21** compares these two PB emission scenarios (from untreated control fuels and treated fuels) with 2009 emissions data from other MCBCL combustion sources (personal communication with Lisa L. Gideon, MCBCL Environmental Management Division). Total annual emissions from various species, including PM_{2.5}, CO₂, CO, CH₄, VOC, and total N (as NO₂ and NO₃⁻ in gas and particle phase,

respectively) are reported routinely for each calendar year. The four main reporting source categories include Jet Engine Test (JET) stands at MCBCL, fire training pits (FIRE) from MCBCL inventory, diesel generators (ICOM) at MCBCL, and boilers (ECOM) from MCBCL inventory. Emission values for CO₂, the main greenhouse gas (GHG) are not depicted because most reported sources exceed 1,000 tons annual emissions because state and federal regulations do not yet require the removal (scrubbing) of GHG from combustion emissions. Boilers and generators emit 125,850 and 807 tons of CO₂ annually, whereas Jet and FIRE emit only 301 and 27 tons, respectively. For comparison, the PB removal of almost 18,000 tons of forest fuel employing no particular pre-treatment generates almost 26,000 tons of CO₂. Understory and midstory mechanical thinning of that amount of fuel prior to PB removal would have saved 290 tons of CO₂ emissions, yet another beneficial advantage of pre-treating the fuel in that manner.

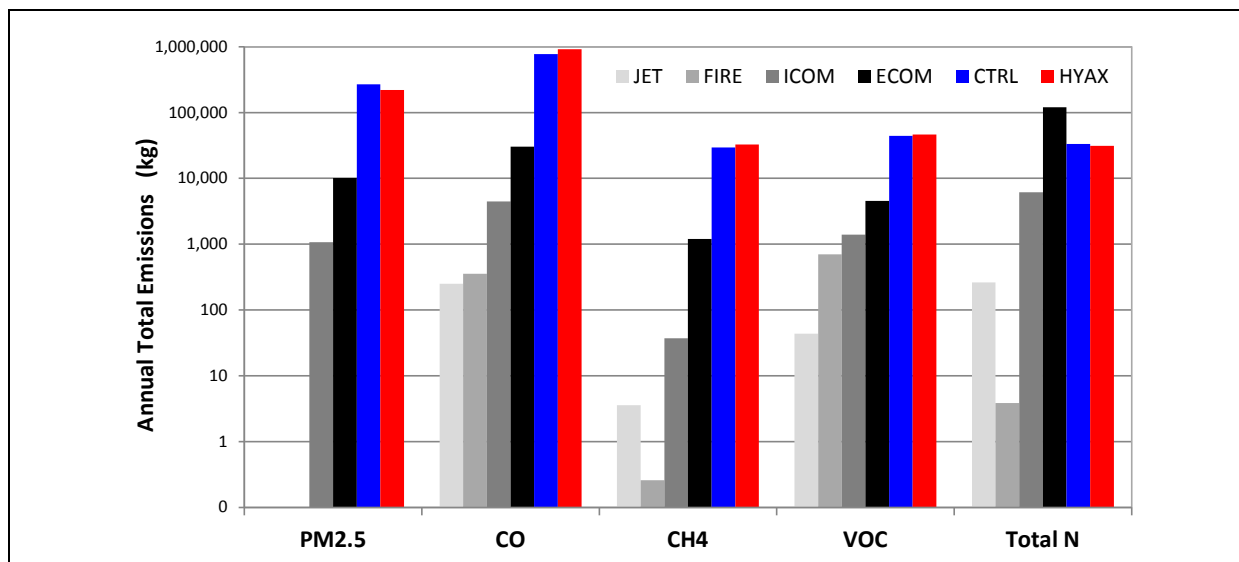


Figure 15-21. Comparison of main pollutants' annual emissions from fuel-specific PB with those from other MCBCL sources; ECOM = boilers, ICOM = generators, FIRE = training pits, JET = engine test stands.

Considering the logarithmic scale, the different sources span a wide range of emission levels for the shown pollutants. The PB emissions of all criteria pollutants (excluding N) are significantly higher on an annual basis than any other combustion source category operated on MCBCL. Relative to the untreated fuel, the mechanically thinned fuel emissions are significantly reduced for PM_{2.5} by almost 48 tons, corresponding to the before mentioned 18%. However, the 19, 11 and 5% increase in HYAX-EF for CO, CH₄, and VOC (=NMHC) over CTRL (see **Table 15-7**) translates into 144, 3.2, and 2.4 additional tons of annual emissions, respectively. The small EF values determined for potential SOA emissions yield only 350 kg from mechanically thinned fuels and 374 kg (6% more) from control, representing only 0.14% and 0.16% of the total primary PM_{2.5} emissions, respectively. But note that the SOA forming potential was calculated for only the first 5 hours after precursors release and not taking into account continued smoldering emissions into any following days. The PB related annual total N emissions are based on the above assumptions and EF values listed in Table 15-16 above. The average annual N emissions from CTRL and HYAX fuels are ca. 33 and 31 tons, differing by only 7% (i.e.,

when the effect from different moisture levels is averaged out), and are in between the ICOM diesel generators category (6 tons) and boilers (120 tons). This comparison illustrates the importance and value of developing and implementing measures to effectively reduce PB emissions relative to other pollution sources on MCBCL.

EF Sensitivity to the Keetch-Byram Drought Index Dryness Index

The Keetch-Byram Drought Index (KBDI) is a continuous reference scale for estimating dryness of soil and duff layers towards the potential of causing unwanted wildfires. The KBDI is an important parameter in the PB decision process of the MCBCL land managers. A higher value indicates a higher risk of a PB turning into a wildfire. This index is based on a daily water balance, where a drought factor is balanced with precipitation and soil moisture (assumed to have a maximum storage capacity of 8 inches) and is expressed in hundredths of an inch of soil moisture depletion. The KBDI ranges from 0 to 800, with 0 representing no moisture depletion, and 800 representing absolutely dry conditions. Without rain, its daily increase depends on daily high temperature and it decreases or is reset when it rains. KBDI values are published twice daily for different State districts as part of the National Weather Service (NWS) fire weather forecasts, where they are calculated from ground based temperature and precipitation measurements and interpolated spatially and temporally (see section on PM_{2.5} sensitivity analysis). The North Carolina Forest Service regularly publishes KBDI maps based on these forecasts providing spatially resolved KBDI values at the sub-regional county level for the following ranges:

- 0-200: Soil moisture and large class fuel moistures are high and do not contribute significantly to fire intensity.
- 201-400: Lower litter and duff layers are drying and beginning to contribute to fire intensity; typical of late spring and early growing season.
- 401-600: Lower litter and duff layers burn intensely, which is typically the case in late summer and early fall.
- 601-800: Live fuels are dry and burn actively and intensely with significant downwind spotting (spread) under severe drought conditions and increased wildfire occurrences.

On the days when the PB experiments were conducted at the individual research plots RB, HA, MF, IEn, and IEs, the corresponding KBDI values fell all into the lowest category and were 107, 56, 79, 94, and 75, respectively. Although the KBDI values apply to untreated (CTRL) fuels, we assume the same values for the mechanically thinned test plots in the following evaluation.

Table 15-17 and **Figure 15-22** show linear regression statistics between EF and KBDI, assuming the EF values of the main pollutant and GHG species emissions (i.e., PM_{2.5}, CO₂, CO, CH₄, NMHC, and total N) being linearly dependent on the sub-regional KBDI fuel conditions.

Table 15-17. Linear regression statistics assuming pollutant species' EF dependence on sub-regional KBDI from routine forecasts for control (CTRL) and mechanically thinned treatments (HYAX).

		CTRL				HYAX			
		p-val.	R ²	SLP	y-ICPT	p-val.	R ²	SLP	y-ICPT
PM _{2.5}	g/kg	0.732	0.043	-0.19	30.2	0.093	0.616	0.25	-8.4
CO ₂	g/kg	0.484	0.165	1.61	1318	0.036	0.762	-2.61	1648
CO	g/kg	0.504	0.152	-0.53	86.9	0.028	0.793	0.97	-28.8
CH ₄	g/kg	0.354	0.267	-0.04	4.6	0.049	0.723	0.05	-2.4
NMHC	gC/kg	0.221	0.412	-0.05	6.2	0.057	0.701	0.06	-2.0
Total N	g/kg	0.906	0.005	-0.003	2.1	0.118	0.569	-0.013	2.8
MCE	—	0.517	0.144	0.001	0.9	0.028	0.792	-0.001	1.0

Note: Grey highlights indicate statistical insignificance (p>0.05).

Surprisingly, all species EF except Total N yield a significant relationship for the mechanically thinned fuel but not for the control fuel. For KBDI values within the lowest category (where high fuel moistures do not contribute significantly to fire intensity), the mechanical thinning causes a KBDI sensitivity in that decreasing fuel moisture yields significantly increasing levels of PM_{2.5}, CO, CH₄, and NMHC per kg consumed fuel. The control fuel shows the opposite trend, although at a level of low statistical significance. Negative slopes are seen for CO₂ and MCE, suggesting that mechanically thinned fuels within that highest fuel moisture range combust less efficiently and therefore yield lower CO₂ emissions with lower fuel moistures. The same negative trend can be seen also for total N, possibly owing to the before mentioned greater N retention in mechanically thinned fuel. As long as PB is performed on untreated fuels, changes in KBDI have very little influence on emissions of the major species including PM_{2.5}. This is in line with the results from the sensitivity analysis presented below, showing little influence on ambient PM_{2.5} relative to other meteorological parameters. However, relatively small changes in KBDI (in the investigated narrow range of 56 to 107) cause significant changes in major species' emissions from mechanically thinned fuels, most notably an increase in PM_{2.5} emissions with increasing KBDI.

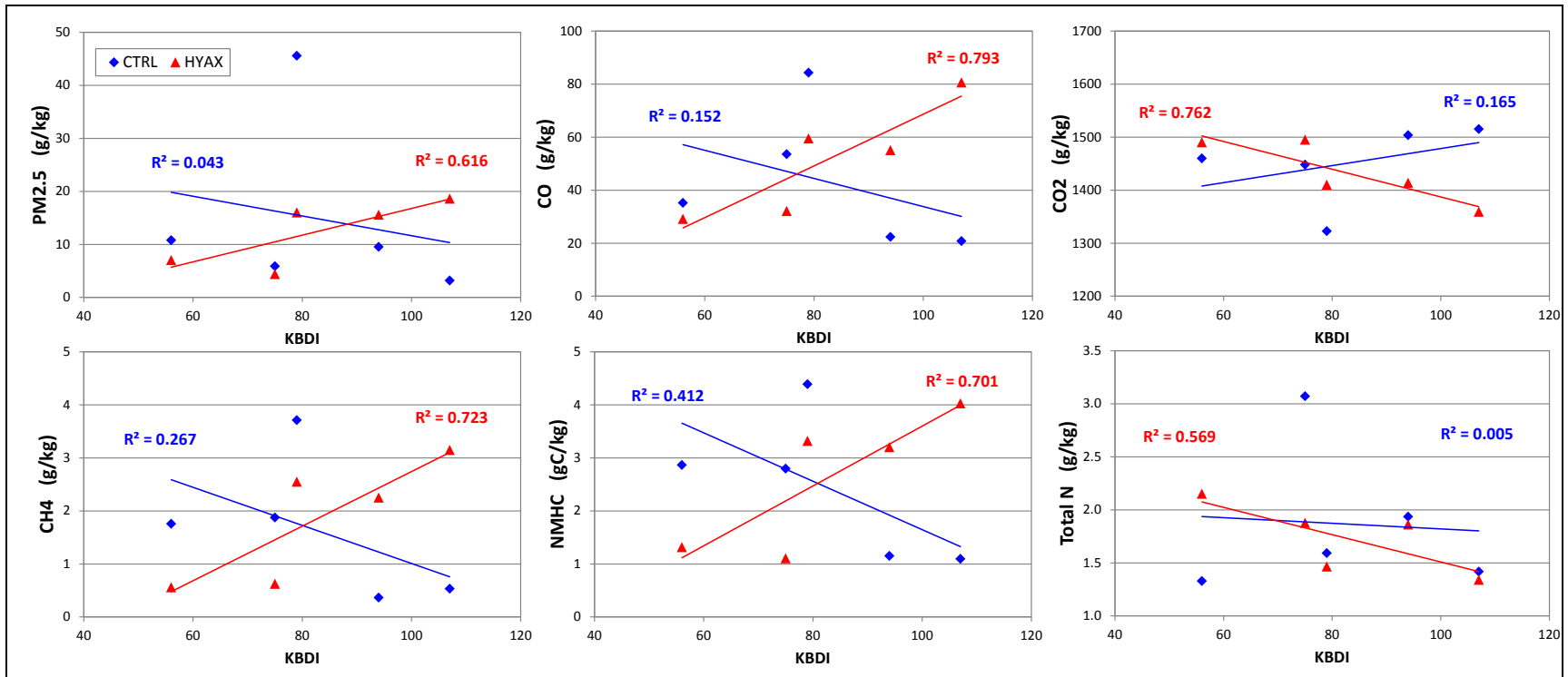


Figure 15-22. Emission factors as a function of KBDI comparing control (blue diamonds) and treatment (red triangles) plots.

Comparison with Through-fall Deposition

In an attempt to compare potential nutrient loss via PB emissions with re-deposition from the forest canopy's retaining effect and washout in subsequent rain events, throughfall samples were collected during two consecutive post-PB rain events. These events were captured during two different field intensive studies in 2010 and 2011. The two study sites were characterized by different stands; one stand contained mesic loblolly/longleaf pine close to the estuary (HA in 2010) and the other semi-mesic loblolly pine farther inland (RB in 2011) with soil moisture levels about half those of the other stand. Due to the ocean water's proximity, more sodium chloride (NaCl) was deposited to the mesic stand close to the estuary, whereas the semi-mesic stand received more K⁺, sulfate, and N (see row *Dep.* in **Table 15-18**). Relative to deposition, emissions of cations from PB on both stands were insignificant except for K⁺ and ammonium (see row *E./D.* in the Table). For both single events, nutrient export via PB emissions was significantly smaller than subsequent nutrient input from throughfall deposition except for reduced N under wetter stand conditions, for which export about equaled input. The 1-ha size mechanically thinned fuel beds were too small to decipher an effect from its potentially greater nutrient retention. Instead, these two single experiments suggest that long-term soil nutrient levels in either type fuel bed would remain unaffected by PB, causing only a short-term disturbance; however, additional observations are needed to develop statistically robust conclusions.

Table 15-18. Comparison of PB emission and throughfall deposition of major ions for RB (semi-mesic loblolly pine) and HA (wet-mesic loblolly/longleaf pine).

Plot		Na	Mg	Ca	K	Cl	SO ₄	NH ₄	NO ₃	K/Cl	Mg/SO ₄
		kg/ha	kg/ha	kg/ha	kg/ha	kg/ha	kg/ha	kgN/ha	kgN/ha	-	-
RB ^a	PB-E.	0.001	0.001	0.006	0.027	0.036	0.026	0.008	0.008	0.75	0.04
	Dep.	0.389	0.094	0.523	0.328	0.728	0.957	0.189	0.238	0.45	0.10
	E./D.	0.00	0.01	0.01	0.08	0.05	0.03	0.04	0.04	—	—
HA ^a	PB-E.	0.005	0.004	0.004	0.070	0.089	0.026	0.027	0.023	0.78	0.14
	Dep.	0.528	0.131	0.527	0.264	1.223	0.348	0.028	0.041	0.22	0.38
	E./D.	0.01	0.03	0.01	0.26	0.07	0.08	0.97	0.56	—	—

^aThe RB site is located away from the estuary, and the HA site is located close to the estuary.

Local to Regional Air Quality Trends

Although the local on-Base measurements did not meet (and were not intended to meet) regulatory requirements, the metrics employed by EPA were applied here as a basis for regional comparison of air quality. Pollutants used to assess air quality are O₃ and PM_{2.5}. A detailed discussion of the analysis of the Atmospheric Module's monitoring data is presented as part of the *DCERP1 Final Monitoring Report*. The following only briefly summarizes the most important findings related to O₃, PM_{2.5}, and rainfall.

The spatial distribution and temporal resolution of O₃ measurements made on MCBCL were adequate to capture both short- and long-term variations and trends in the regional context. The

study domain as shown in **Figure 15-23**, received the highest average O_3 concentration from southeasterly directions, pointing to effects from photochemical production of O_3 under maritime conditions and transport with the sea breeze. Low O_3 levels associated with north and west wind directions indicated that O_3 loss from chemical reactions and surface deposition overwhelmed O_3 production in continental air masses. Using the EPA metrics for regional comparison, spatial O_3 levels recently showed a decreasing trend with increasing distance from the coast. During the past 10 years, O_3 levels declined steadily across the region, being in line with the nation-wide trend attributed mainly to reductions in O_3 precursor emissions NO_x and CH_4 (EPA, 2003).

In contrast to O_3 , average concentration levels of $PM_{2.5}$ increased with increasing distance from the ocean, indicating that secondary (atmospheric) particle formation in maritime air masses played a minor role in the local to sub-regional burden of $PM_{2.5}$. Especially during the colder months of the year, the region's two urban inland sites at Goldsboro and Kinston (DLL and LCC in Figure 15-23) reported fine PM concentrations consistently higher than those registered at the MCBCL's beach site (Risely Pier), likely due to PM emissions from residential heating and wood burning activities in urban areas. Although the on-Base O_3 measurements fit a relatively homogeneous regional character, previous analysis called for an expansion of both fine and coarse PM measurement (coarse PM here being the mathematical difference between measured PM_{10} and $PM_{2.5}$) from only two to four on-Base sites. The measurements from the central Sandy Run Tower 40 m above ground near an artillery training range pointed to a greater local influence from primary emission sources, of which PB as well as movement and operation of heavy military equipment are the most important sources to consider. The spatially more highly resolved PM monitoring that began in October 2010 by adding two sites on-Base fit the more regional trend of increasing $PM_{2.5}$ with increasing distance from the beach.

The spatial and temporal distribution of rainfall on MCBCL is investigated extensively as part of Research Project Air-2 (described in Chapter 16 of this report). **Table 15-19** looks beyond the MCBCL borders and compares accumulated total rainfall data from five sites in the greater study domain off-Base (**Figure 15-23**) with data from two on-Base sites (MCA and SRG in **Figure 15-24**). For comparison with long-term trends, 30-year normals ending in 2008 (N30*) were calculated based on data from the State Climate Office of North Carolina (<http://www.nc-climate.ncsu.edu>), representing regionally averaged rainfall data for the SCP, encompassing our study area. Although rainfall amounts in the second half of 2008 were significantly below normal, the following 2 years averaged above normal annual totals. Although WIA, HOS, and SRG are parallel to the North Carolina coastline (approximately 10–15 km off of the coast), sites SRG, MCA, JVA, and LCC line up with increasing distance to the coast. Average rainfall amounts decreased along this inland gradient during the study period. However, more complex patterns in nutrient deposition were observed in the highly resolved spatial sampling of rainfall amounts and composition across MCBCL.

Table 15-19. Given periods' total rainfall amounts (mm) from MCBCL sites relative to 30-year normals regionally averaged over the SCP (N30*).

Sites SRG and MCA are on MCBCL, JVA, and LCC sites are farthest from the coast at ca. 40 and 100 km, respectively. AVG is coastal average spanning WIA to HOF.

Period	N30*	AVG	WIA	HOS	SRG	MCA	HOF	JVA	LCC
Jul–Dec 2008	711	621	690	572	699	510	634	306	484
Jan–Dec 2009	1,305	1,544	1,564	1,709	1,682	1,343	1,423	1,096	862
Jan–Dec 2010	1,305	1,415	1,596	1,382	1,464	1,191	1,443	721	901

Note: Values in bold italics indicate incomplete records.

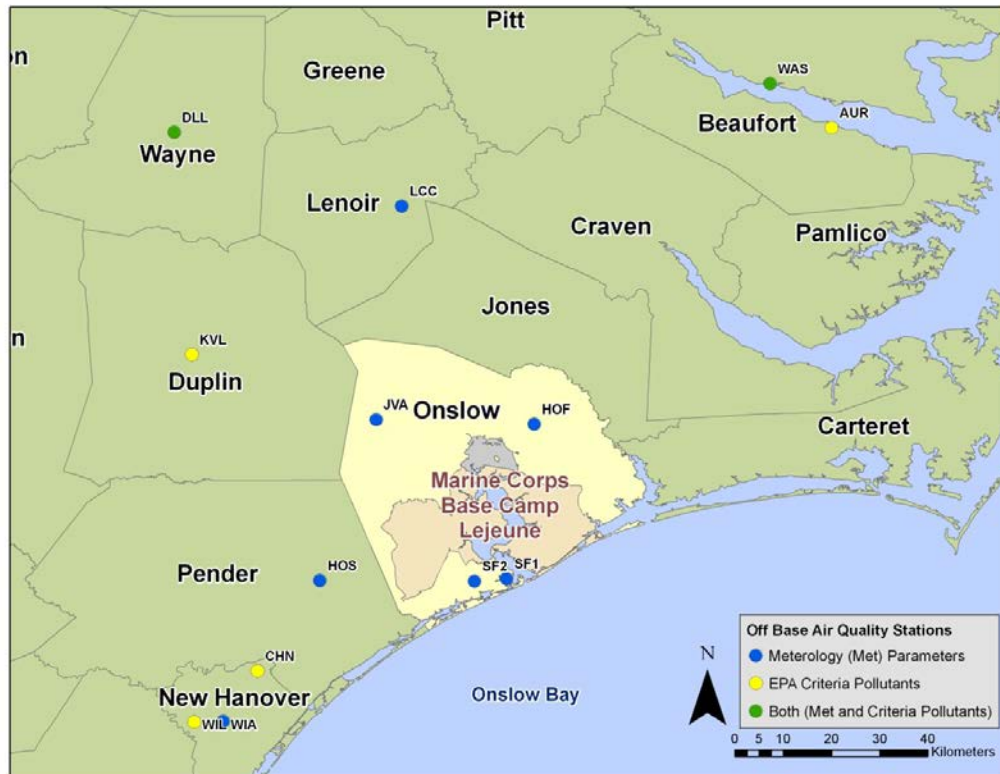


Figure 15-23. Location of atmospheric monitoring stations within the regional study domain.

Urban PM_{2.5} Sensitivity to Sub-Regional PB Activities

To determine the sensitivity of ambient fine PM measured at Jacksonville, NC, to PB activities on the MCBCL relative to different meteorological parameters, we followed an approach combining a principal component analysis (PCA) of partly observed and partly forecasted input variables with a subsequent multivariate regression of the resulting principal components, a method known as principal components regression (PCR) (Fekedulegn et al., 2002). In this exercise, the measured PM_{2.5} is treated as the only dependent variable. Jacksonville (population ca. 67,000 per 2000 Census) required regulatory monitoring of ambient PM_{2.5} from 1999 until 2007, during which time the North Carolina Department of Environment and Natural Resources Division of Air Quality measured 24-hour average PM_{2.5} mass every third day. To maximize the

number of coincidental data points subject to this PCA exercise, the 2 days between each PM measurement have been interpolated in two different ways; one was using a simple linear temporal interpolation, and the other employed an air mass flow dependent spatial correlation with daily averaged $PM_{2.5}$ (from continuous tapered element oscillating microbalance [TEOM]) monitoring data from the State's regulatory site at Castle Hayne (CHN in **Figure 23**) almost 100 km away to the southwest. Details about the different interpolation methods and the applied PCR procedure and the presentation and interpretation of results are currently being prepared for peer-reviewed publication (Balachandran et al., 2012). The following provides a brief overview of this work.

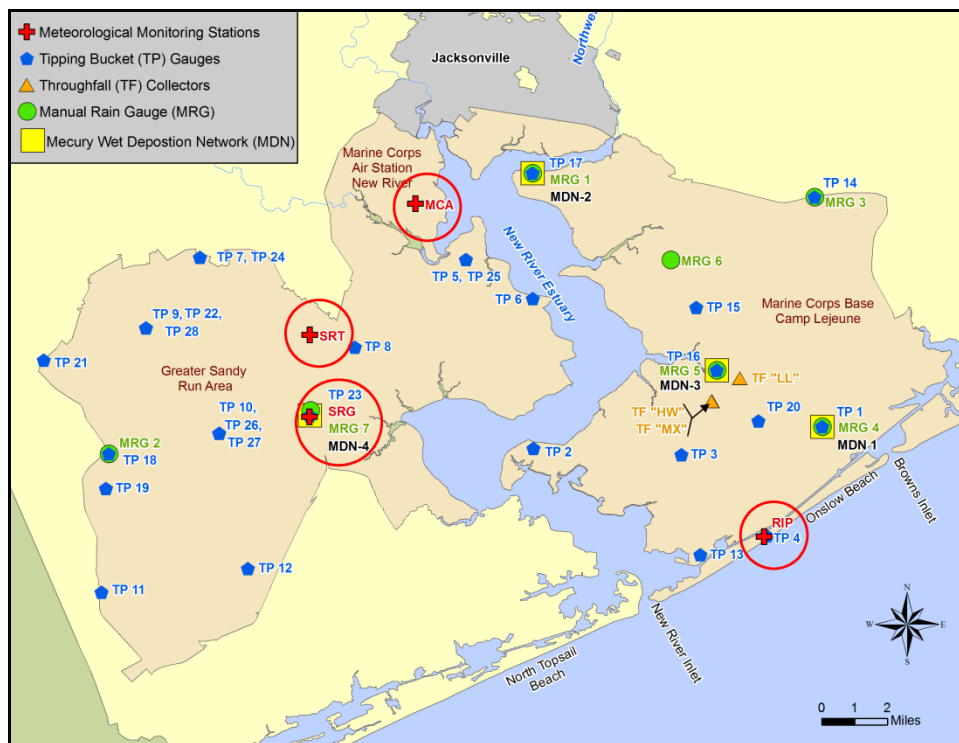


Figure 15-24. MCBCL monitoring and research stations with rainfall monitor locations used in Research Project Air-2.

Circles indicate locations of comprehensive air quality monitoring network.

Urban $PM_{2.5}$ Sensitivity to Sub-Regional PB Activities

To determine the sensitivity of ambient fine PM measured at Jacksonville, NC, to PB activities on the MCBCL relative to different meteorological parameters, we followed an approach combining a principal component analysis (PCA) of partly observed and partly forecasted input variables with a subsequent multivariate regression of the resulting principal components, a method known as principal components regression (PCR) (Fekedulegn et al., 2002). In this exercise, the measured $PM_{2.5}$ is treated as the only dependent variable. Jacksonville (population ca. 67,000 per 2000 Census) required regulatory monitoring of ambient $PM_{2.5}$ from 1999 until 2007, during which time the North Carolina Department of Environment and Natural Resources Division of Air Quality measured 24-hour average $PM_{2.5}$ mass every third day. To maximize the number of coincidental data points subject to this PCA exercise, the 2 days between each PM

measurement have been interpolated in two different ways; one was using a simple linear temporal interpolation, and the other employed an air mass flow dependent spatial correlation with daily averaged PM_{2.5} (from continuous tapered element oscillating microbalance [TEOM]) monitoring data from the State's regulatory site at Castle Hayne (CHN in **Figure 23**) almost 100 km away to the southwest. Details about the different interpolation methods and the applied PCR procedure and the presentation and interpretation of results are currently being prepared for peer-reviewed publication (Balachandran et al., 2012). The following provides a brief overview of this work.

MCBCL's annual PB target is 25,000 acres burned mainly between December and May. The PB activity data used for this analysis were extracted from electronic records provided by the MCBCL's forestry department detailing the total acres burned on given days during both dormant and growing season (as presented in Background section). To minimize the air quality impact on the civilian population in neighboring Jacksonville, land managers routinely consult the fire weather forecast released twice daily by the National Oceanic and Atmospheric Administration's (NOAA's) NWS via <http://fire.boi.noaa.gov/FIREWX/RDUFWFMHX.html>. Although the morning (A.M.) version (released early mornings) provides a 24-hour forecast, the night (P.M.) version (released late afternoon) looks 48 hours ahead. Each posting provides the area-specific ventilation rate (VR) (i.e., the product of wind speed and mixing height) and other important forecast parameters that are considered in the final preparations and decision process of the imminent PB conduct. Among the issued parameters, the probability of precipitation (POP), daytime (maximum) temperature and RH (dayT and dayRH), the difference between daytime maximum and minimum temperature (diffT), the inversion burn-off temperature (IBT), boundary layer mixing height (BLH), transport wind speed and direction (TWS, TWD), and Haines Index (HAI) are considered most important. The HAI is a lower atmospheric stability index used to forecast the potential for large fire growth and/or erratic fire behavior.

The above forecast data are archived at the National Climatic Data Center (NCDC) and can be accessed via NCDC's Service Records Retention System in the Hierarchical Data Storage System Access System (HAS) at <http://has.ncdc.noaa.gov/pls/plhas/has.dsselect>. The HAS allows the downloading of historical forecast data spanning a maximum period of 1 month at a time. Because the data for Jacksonville in Onslow county are deeply embedded in the HAS product, a special program utility had to be created to extract the relevant parameters. The utility was written in C# using Visual Studio 2010, requiring the .Net 3.5 platform. The application is installable and compatible with XP, Vista, and Win7. The installer defaults to the (Program Files)\ARA\ directory and automatically links all platforms so that the only responsibility left for the user is picking the downloaded HAS files.

The left half of **Table 15-20** summarizes the forecast and observed parameters entering the PCA. The observations were made at the on-Base MCA site (see Figure 24) and these parameters are denoted in the table with the prefix "mca" (e.g., *mcaVIS_min* is the daily minimum visibility as detected by the site's ceilometer). Daily values for the KBDI (a continuous reference scale for estimating dryness of soil and duff layers presenting wildfire risks) were available on hard copies of the MCBCL foresters' records and were manually entered into the data matrix from. The complete data matrix consisted of 635 records spanning December 1, 2002, to March 15, 2007. The data matrix had been prepared for three main PCA runs investigating (1) the sensitivity of the spatially interpolated PM_{2.5} to the A.M. reported forecast relative to observed meteorological

conditions, (2) the same but for the temporally interpolated PM_{2.5}, and (3) the sensitivity of the spatially interpolated PM_{2.5} to the P.M. reported forecast relative to observed meteorological conditions. This exercise assessed the importance and merit of the A.M. forecast relative to the P.M. forecast, helping foresters prioritize their decisions in the PB planning phase.

Table 15-20. List of parameters and their units as input to PCR analysis (left), and ranking of the parameters' unit-less sensitivity towards PM_{2.5} (right) for the two data sets with values from either morning (A.M., yellow) or prior evening (P.M., blue) forecasts.

PCA-A.M.	Units	PCA-P.M.	Units	PCA-A.M.	Rank	PCA-P.M.	Rank
PB	acr	PB	acr	PB	0.322	PB	0.295
KBDI	0–800	KBDI	0–800	mcaWD	0.059	dayRH_pm	0.090
mcaT_avg	°C	mcaT_avg	°C	IBT_am	0.033	mcaRH_min	0.084
mcaT_diff	°C	mcaT_diff	°C	mcaPCP	0.032	IBT_pm	0.079
mcaRH_avg	pct	mcaRH_avg	pct	mcaT_avg	0.026	mcaRH_avg	0.077
mcaRH_min	pct	mcaRH_min	pct	dayT_am	0.026	mcaT_avg	0.069
mcaPCP	mm	mcaPCP	mm	mcaT_diff	0.024	mcaPCP	0.065
mcaVIS_min	km	mcaVIS_min	km	dayRH_am	0.023	dayT_pm	0.064
mcaWS	m/s	mcaWS	m/s	mcaRH_min	0.018	POP_pm	0.056
mcaWD	degN	mcaWD	°N	TWD_am	0.014	mcaWD	0.035
POP_am	pct	POP_pm	pct	mcaRH_avg	0.009	KBDI	0.016
dayT_am	F	dayT_pm	F	mcaVIS_min	0.009	mcaT_diff	–0.013
diffT_am	F	diffT_pm	F	POP_am	0.006	TWS_pm	–0.014
IBT_am	F	IBT_pm	F	TWS_am	–0.001	TWD_pm	–0.019
dayRH_am	pct	dayRH_pm	pct	mcaWS	–0.008	mcaWS	–0.022
HAI_am	—	HAI_pm	—	KBDI	–0.014	mcaVIS_min	–0.040
BLH_am	ft	BLH_pm	ft	diffT_am	–0.019	diffT_pm	–0.057
TWS_am	mph	TWS_pm	mph	HAI_am	–0.023	VR_pm	–0.065
TWD_am	23–360	TWD_pm	23–360	VR_am	–0.033	BLH_pm	–0.065
VR_am	ftmph	VR_pm	ftmph	BLH_am	–0.044	HAI_pm	–0.067

PCA is a statistical technique often used to: (1) remove multi, co-linear effects of the original (input) data, and (2) reduce dimensionality of large data sets. The first step in the PCA employed here was to normalize our data matrix, so that all variables have a mean of 0 and standard deviation of 1, yielding a matrix X. Next, singular value decomposition was used to determine the principal components, which are the eigenvectors V of the dispersion matrix, $X^T \cdot X$. The relative strength, or scores Z, of each component, for each record or day are therefore a rotation of the data matrix X (i.e., $Z = X \cdot V$). Because the eigenvectors V are orthonormal, and the resulting scores Z are orthogonal, co-linearities within the data matrix X were effectively removed. The higher the eigenvalue for a particular component, the more variability in X that component explains. Here we identified the components with the highest eigenvalues and chose the ones explaining at least 80% of the variability in PM_{2.5}. Employing PCR, the dependent variable PM_{2.5} was regressed against the PCA scores Z. Performing a few standard matrix transformations yields the relationship $A = V \cdot B$ with A representing the unit-less sensitivity of

PM_{2.5} to the standardized variables, and B being the vector of regression coefficients from the PCR analysis. Physical units were then applied back to the unit-less sensitivities through computational steps as described in Balachandran et al. (2012).

The right half of **Table 15-20** compares the unit-less sensitivity (A) towards PM_{2.5} by ranking the independent variables' importance relative to each other. Doing this for the A.M. forecast variables, PB ranks as the top most positive influence on PM_{2.5} by a big margin over IBT, suggesting that the stronger the nocturnal inversion the more PM_{2.5} has accumulated. The most negative rankings have BLH and VR, reasonably pointing to the diluting effect of a deep well-mixed boundary layer on ambient PM_{2.5} concentration, followed by HAI as third lowest (most negative), implying that the more unstable the atmospheric conditions are the lower the ambient PM_{2.5} levels but also the less is being burned (because foresters sensibly avoid PB actions under high HAI forecasts). A similar comparison of the unit-less PCR scores using the P.M. forecast variables, yields again PB at the top by a large margin over closely ranked forecast RH, measured RH and again IBT, possibly an indication of the greater uncertainty in the IBT forecast from the night before. The biggest negative PM_{2.5} effect has HAI closely followed by BLH and VR (i.e., more or less the same negative effect ranking as for the A.M. case). Thus, land managers can make decisions based on those parameters' evening forecast instead of waiting for A.M. forecast because both yield similar influence on PM_{2.5}.

The unit-based results show similar PM_{2.5} sensitivity to PB activities on MCBCL for both the A.M. case (using variables from same morning forecast) and the P.M. case (using variables from evening before forecast), estimating a PB contribution to local PM_{2.5} levels of 3.6 and 3.3 µg/m³ per 1,000 acres burned on MCBCL, respectively. This result suggests that foresters may plan their PB conduct the evening before yielding basically the same outcome in terms of potential contributions to fine PM air pollution on a local scale.

Summary Conclusions and Implications

PB Emissions, Fuel Consumption, and Emission Factors

Fuel consumption was characterized in experimental research plots that incorporated a understory and midstory removal treatment by HydroAx followed by PB, capturing the moisture gradient from semi-mesic loblolly pine forests to wet-mesic loblolly–longleaf pine forests to pond pine pocosins. In general, the mechanical thinning treatment yielded greater availability and consumption of fuels, especially woody material regardless of fuel moisture. The fuel parameters investigated were the available amount of fuel, the total and relative amount of fuel consumed, and different fuel moistures reflecting both fuel conditions and vegetation composition. Only a few species's emissions correlated weakly with some of these fuel parameters, in particular the total and relative amount of fuel consumed and different fuel moistures reflecting short-term above-ground fuel conditions. The poor correlations of these fuel measures with EF suggest that site vegetation variation is not the driving factor in explaining the observed variability in EF values for most species. Differences in emissions between treatments (control versus treated) are therefore not confounded by either soil characteristics or vegetation differences, allowing direct comparison of treatment effects on EF.

Considering possible effects from the fuel treatment (mechanically thinned and control) alone, average gaseous EF from the two treatment types is similar, and EF variability is highest for acidic gases and isoprene. However, PM_{2.5} mass and most PM_{2.5} species EF from mechanically thinned fuels are significantly lower than those from untreated control fuels. Therefore, removing a certain targeted amount of fuel by employing mechanical thinning prior to PB, bares significant air quality benefits due to lower total PM_{2.5} emissions, although CO, CH₄ and NMHC emissions are slightly enhanced. Comparison with EPA's AP-42 emissions inventory suggests that our in situ PB emission factors are distinctly lower than the laboratory simulation based AP-42, with similar magnitude only for PM_{2.5} emissions from treated fuel and control fuel being almost 20% higher. The distinctly lower CO and CH₄ emissions point to our in situ combustion process being more effective and complete, which is also indicated by the relatively high MCE of 0.95 for both treated and untreated fuels. Combustion efficiencies on which the AP-42 values are based on are lower (MCE <0.92), suggesting that access of combustion air to our in situ fuel might have been significantly better.

Emission levels of ammonia, certain aromatic and biogenic VOCs (α -pinene and isoprene) are significant from all investigated treatment fuels. Ammonia emissions (i.e., EF) are among the largest of all inorganic species, exceeded only by CH₄, CO and CO₂, and α -pinene and isoprene rank second and ninth among all VOCs EF. All of these gas species play an important role in the atmospheric formation of ozone and secondary PM_{2.5} (i.e. secondary organic aerosol, SOA). The potential to form O₃ from these species is 1.5 % higher in emissions from hydro-axed fuel over those from control. Biogenic VOCs contribute the most to the SOA forming potential in emissions from either fuel type, averaging 71 % for control fuels and 63 % for mechanically thinned fuels. Conversely, treated fuel causes higher contributions from the aromatic VOCs with 37 % versus 29 % from control. However, relative to the total primary PM_{2.5} emissions, the potential SOA contributions within the first 5 hours from emission are very small, 0.16 % and 0.14 % for the control and hydro-axed fuel type, respectively.

OC is the dominant PM_{2.5} constituent in emissions from the investigated fuels, followed by EC, nitrate, K⁺, and Cl⁻. More volatile OC compounds are being emitted from either fuel type under less efficient (smoldering) combustion conditions, which also promote higher emissions of inorganic constituents similar to major ions (especially Cl⁻, nitrate sulfate), major metal oxides, and non-sulfate S. Because OOE (i.e., elements that are associated with OC and are part of the emitted PM_{2.5} organic mass [OM=OC+OOE]) also increase with smoldering (i.e., with decreasing CE), it is plausible to assume that such conditions are conducive to the formation of highly oxygenated compounds containing N and S similar to compounds found in photochemically aged polluted air masses (e.g., organosulfates formed by the photo-oxidation of isoprene in the presence of acidified sulfate seed aerosols). Non-sulfate S constitutes a large fraction of total S in PM_{2.5} emitted from both fuel types (average 30% from mechanically thinned fuels and 43% from control), but it is currently unknown how the water-insoluble S is embedded in the PM matrix and whether some of it will ultimately oxidize to its highest oxidation state during atmospheric dilution and transport away from the PB source.

The MCE is a measure of combustion intensity and completeness; it is estimated from the molar ratio of CO₂ over the sum of CO₂+CO. In general, the EF values of all gas and particle phase species correlate better with MCE for control fuels than for mechanically thinned fuels. Furthermore, all but CO₂, alkyl-nitrates, and EC emissions from control fuels correlate

negatively with MCE, indicating a decrease of emissions with increasing CE. Mechanically thinned fuel combustion is more variable yielding nominally less strong EF/MCE linkages with slopes closer to zero and poorer correlation coefficients. For some inorganic species and elements even a change in EF/MCE slope is seen, indicating increasing emissions with increasing MCE, suggesting preferred contributions of these species emissions from the flaming combustion of mechanically thinned fuels. Only EC shows a positive EF/MCE correlation for both fuel types, pointing to its preferred formation during the hot flaming phase.

Similar correlations of main pollutant species' EF with the KBDI drought index revealed a somewhat reverse relationship in that mechanical thinning causes a significant increase in emissions of PM_{2.5}, CO, CH₄, and NMHC per kg fuel consumed when drought levels increase. The control fuel shows the opposite trend, although at a lower level of statistical significance. The KBDI indicates dryness of soil and duff layers towards the potential of causing unwanted wildfires. The values for our test fuel beds ranged between 56 and 107, all falling into the lowest fire danger category with high soil and fuel moistures not contributing significantly to fire intensity. Total N emissions correlate negatively with KBDI in that category for both fuel types but at a steeper slope for mechanically thinned fuel, suggesting that within that highest fuel moisture range mechanically thinned fuel beds potentially retain this nutrient better than control fuel beds.

From a practical land management perspective, the above results suggest to plan and conduct PB towards the goal of minimum primary PM_{2.5} emissions. The mechanisms involved in forming additional (secondary) PM_{2.5} pollution downwind via complex SOA processes are difficult to predict with the currently available tools. Thankfully, our measurements showed that the SOA forming potential of the emitted precursor gases is relatively small and would yield a negligible contribution to the overall PM_{2.5} burden of the local to sub-regional air shed. Thus, the benefit of achieving an almost 20% reduction in primary PM_{2.5} emissions per kg fuel removed when employing mechanical thinning, is significant and important to consider. Our sensitivity analysis showed that the current PB planning tools are adequate to identify conditions that are conducive for effective atmospheric dispersion. Because PB removes effectively three times more mechanically thinned fuel than untreated fuel, such conditions should be exploited and PB applied on scheduled burn areas whose fuel beds had been mechanically thinned. Such a targeted understory and midstory mechanical thinning application will help meet the Base's restoration targets faster.

PB Effect on Nutrient Mobilization

In an attempt to compare potential nutrient loss via PB emissions with re-deposition from the forest canopy's retaining effect and washout in subsequent rain events, throughfall samples were collected during post-PB rain events in two different episodes and at two different locations. One site was a mesic loblolly/longleaf pine stand close to the estuary and the other site stood semi-mesic loblolly pine farther inland with soil moisture levels about half those of the mesic stand. Due to the water's proximity, more NaCl was deposited to the mesic stand close to the estuary, and the semi-mesic stand received more K⁺, sulfate, and N. Relative to deposition, emissions of cations from PB on both stands were insignificant except for K⁺ and ammonium. For both episodes, nutrient export via PB emissions was significantly smaller than subsequent nutrient input from throughfall deposition except for reduced N under wetter stand conditions, for which

export about equaled input. These results suggest that long-term soil nutrient levels remain unaffected by PB, causing only a short-term disturbance; however, additional observations are needed to develop statistically robust conclusions.

Local to Regional Trends in Ozone, PM_{2.5}, and Rainfall

A detailed discussion of the analysis of the Atmospheric Module's monitoring data is presented as part of the *Baseline Monitoring Report*. The following only briefly summarizes the most important conclusions from our O₃, PM_{2.5}, and rainfall observations.

The spatial distribution and temporal resolution of O₃ measurements made at MCBCL were adequate to capture both short- and long-term variations and to compare to regional trends. MCBCL lands received the highest average O₃ concentration from a southeasterly direction, pointing to effects from photochemical production of O₃ in maritime air masses transported by sea breezes. Removal of O₃ via chemical reactions and surface deposition overwhelmed O₃ production in continental air masses. Over the past 10 years, O₃ concentrations declined steadily across the region, in line with the nation-wide trend attributed primarily to reductions in O₃ precursor emissions (NO_x and CH₄).

In contrast to O₃, average concentrations of PM_{2.5} increased with increasing distance from the ocean, indicating that secondary (atmospheric) particle formation in maritime air masses played only a minor role in the local burden of PM_{2.5}. Especially during colder months, fine PM levels farther inland consistently exceeded those at the coast, likely due to residential heating and wood burning in urban areas. The MCBCL PM measurements point to a greater local influence from primary emission sources, of which PB as well as movement and operation of heavy military equipment are the most important. The local, more highly resolved PM monitoring on MCBCL fit the regional trend of increasing PM_{2.5} with increasing distance from the ocean.

The spatial and temporal distribution of rainfall reported over 30 years to the National Weather Service (NWS) repository from hardened rainfall monitors scattered regionally on and around MCBCL, revealed drought conditions during the 2.5-year study period except for a few locations and periods with extreme rainfall amounts, helping to push annual totals above 30-year normals. Based on monthly totals, rainfall amounts regionally across the entire study domain consistently decreased with increasing distance from the coast.

In contrast to the regional, long-term NWS data, spatial patterns on rainfall amounts across MCBCL did not exhibit a consistent gradient from the ocean moving inland based on intensive rainfall monitoring performed as part of Research Project Air-2. For the 2+ years of continuous monitoring of rainfall distribution and amount, less than 30% of the total rainfall for each year occurred within the period of January–June. Without the extreme event (Tropical Storm Nicole) at the end of September 2010, rainfall amounts for that year would have been substantially below the long-term average. Details about the spatial and temporal patterns in rainfall and associated nutrient deposition across MCBCL can be found in the Chapter 16 of this report.

PB Influence on PM_{2.5} Relative to Forecast Weather Conditions

To minimize air quality impacts, land managers routinely consult the fire weather forecast released twice daily by NOAA's NWS. Although the A.M. version (released early mornings)

provides a 24-hour forecast, the P.M. version (released late afternoon) looks 48 hours ahead. Each posting provides the area-specific VR (i.e., the product of wind speed and mixing height), among other forecast parameters that are of critical importance in the PB planning. To determine the sensitivity of ambient $PM_{2.5}$ measured at Jacksonville to PB activities on the MCBCL relative to these different forecast and observed meteorological parameters, we applied the PCR technique to a data set spanning from 1999 to 2007. The PCR analysis yielded a ranking with PB as the top most positive influence on $PM_{2.5}$ by a significant margin over the measured wind direction and the forecasted inversion burn-off temperature (the temperature required to dissolve remnants of the nocturnal inversion layer), suggesting that the stronger the nocturnal inversion, the more $PM_{2.5}$ accumulates. The most negative rankings have mixing height and VR, reasonably pointing to the diluting effect of a deep well-mixed boundary layer on ambient $PM_{2.5}$ concentration. Similarly, the unit-based results showed statistically the same $PM_{2.5}$ sensitivity to PB activities on MCBCL for both the A.M. and P.M. forecasts, estimating a PB contribution to local $PM_{2.5}$ levels of 3.6 and 3.3 $\mu g\ m^{-3}$ per 1,000 acres burned, respectively. This result suggests that forest managers can plan their PB activities the evening before without having to wait for the morning forecast and still meet the objective to conduct the PB with minimal impact on local $PM_{2.5}$ air quality.

Literature Cited

- Altshuller, A.P. 1983. Natural volatile organic substances and their effect on air quality in the United States. *Atmospheric Environment* 17:2131–2165.
- Andreae, M.O., and P. Merlet. 2001. Emission of trace gases and aerosols from biomass burning, *Global Biogeochemical Cycles* 15:955–966.
- Andreae, M.O., E. Atlas, H. Cachier, W.R. Cofer III, G.W.G. Helas, R. Koppmann, J-P. Lacauz, and D.E. Ward. 1996. Trace gas and aerosol emissions from savanna fires. Pp. 278–295 in *Biomass Burning and Global Change (Vol. 1)*. Edited by J.S. Levine. MIT Press: Cambridge, MA.
- Atkinson, R. 1990. Gas-phase tropospheric chemistry of organic compounds—A review. *Atmospheric Environment* 24A:1–41.
- Bacher, R., M. Swerev, and K. Ballshmitter. 1992. Profile and pattern of monochloro- through octachloro-dibenzodioxins and –dibenzofurans in chimney deposits from wood burning. *Environmental Science and Technology* 26(8):1649–1655.
- Balachandran, S., K. Baumann, J. Pachon, J. Mulholland, and A. Russell. 2012. Verification of Fire Weather Forecasts Using PM_{2.5} Sensitivity Analysis. To be presented at the 31st AAAR Annual Conference, Minneapolis, MN. October 8–12.
- Battye, W., and R. Battye. 2002. *Development of Emissions Inventory Methods for Wildland Fire*. Report prepared for the U.S. Environmental Protection Agency, Research Triangle Park, NC. EPA Contract number 68-D-98-046. Available at <http://www.epa.gov/ttnchie1/ap42/ch13/related/firerept.pdf>.
- Baumann, K., F. Ift, J.Z. Zhao, and W.L. Chameides. 2003. Discrete measurements of reactive gases and particle mass and composition during the 1999 Atlanta Supersite Experiment. *Journal of Geophysical Research* 108, 8416. (20 pages).
- Bechtold, W.A., and P.L. Patterson. 2005. *The Enhanced Forest Inventory and Analysis Program: National Sampling Design and Estimation Procedures*. U.S. Department of Agriculture Forest Service General Technical Report SRS-80, Asheville, NC. Available at <http://www.srs.fs.usda.gov/pubs/20371>.
- Blake, N.J., D.R. Blake, O.W. Wingenter, B.C. Sive, L.M. McKenzie, J.P. Lopez, I.J. Simpson, H.E. Fuelberg, G.W. Sachse, B.E. Anderson, G.L. Gregory, M.A. Carroll, G.M. Albercook, and F.S. Rowland. 1999. Influence of southern hemisphere biomass burning on midtropospheric distributions of nonmethane hydrocarbons and selected halocarbons over the remote South Pacific. *Journal of Geophysical Research* 104:16213–16232.
- Blake, N.J., D.R. Blake, B.C. Sive, T-Y. Chen, F.S. Rowland, J.E. Collins Jr., G.W. Sachse, and B.E. Anderson. 1996. Biomass burning emissions and vertical distribution of atmospheric

- methyl halides and other reduced carbon gases in the South Atlantic region *Journal of Geophysical Research* 101:24151–24164.
- Brown, M.J., and B.D. New. 2012. North Carolina, 2010 Forest Inventory and Analysis Factsheet. *e-Science Update SRS-044*. U.S. Department of Agriculture Forest Service, Southern Research Station, Asheville, NC. Available at <http://www.treesearch.fs.fed.us/pubs/40000>.
- Burling, I.R., R.J. Yokelson, S.K. Akagi, S.P. Urbanski, C.E. Wold, D.W.T. Griffith, T.J. Johnson, J. Reardon, and D.R. Weise. 2011. Airborne and ground-based measurements of the trace gases and particles emitted by prescribed fires in the United States. *Atmospheric Chemistry and Physics* 11:12197–12216.
- Cachier, H., J. Ducret, M. Bremond, V. Yoboue, J. Lacaux, A. Gaudichet, and J. Baudet. 1991. Biomass burning aerosols in a savanna region of the Ivory Coast. Pp. 74–180 in *Global Biomass Burning: Atmospheric Climatic and Biospheric Implications*. Edited by J.S. Levine. MIT Press: Cambridge, MA.
- Carlton, A.G., P. Bhawe, S. Napelenok, E.O. Edney, G. Sarwar, R.W. Pinder, G. Pouliot, and M. Houyoux. 2010. Model representation of secondary organic aerosol in CMAQ v4.7. *Environmental Science and Technology* 44(22):8553–8560.
- Carlton, A.G., C. Wiedinmyer, and J.H. Kroll. 2009. A review of secondary organic aerosol (SOA) formation from isoprene. *Atmospheric Chemistry and Physics* 9(14):4987–5005.
- Chagger, H.K., A. Kendall, A. McDonald, M. Pourkashanian, and A. Williams. 1998. Formation of dioxins and other semi-volatile organic compounds in biomass combustion. *Applied Energy* 60(2):101–114.
- Chameides W.L., F. Fehsenfeld, M.O. Rodgers, C. Cardelino, J. Martinez, D. Parrish, W. Lonneman, D.R. Lawson, R.A. Rasmussen, P. Zimmerman, J. Greenberg, P. Middleton, and T. Wang. 1992. Ozone precursor relationships in the ambient atmosphere. *Journal of Geophysical Research* 97, D5:6037–6055.
- Cheng, L., K.M. McDonald, R.P. Angle, and H.S. Sandhu. 1998. Forest fire enhanced photochemical air pollution: A case study. *Atmospheric Environment* 32:673–681.
- Chow, J.C., J.G. Watson, H. Kuhns, V. Etyemezian, D.H. Lowenthal, D. Crow, S.D. Kohl, J.P. Engelbrecht, and M.C. Green. 2004. Source profiles for industrial, mobile, and area sources in the Big Bend Regional Aerosol Visibility and Observational study. *Chemosphere* 54:185–208.
- Christian, T.J., B. Kleiss, R.J. Yokelson, R. Holzinger, P.J. Crutzen, W.M. Hao, T. Shirai, and D.R. Blake. 2004. Comprehensive laboratory measurements of biomass-burning emissions: 2. First intercomparison of open-path FTIR, PTR-MS, and GC-MS/FID/ECD. *Journal of Geophysical Research* 109, D02311 (12 pages).

- Christian, T.J., B. Kleiss, R.J. Yokelson, R. Holzinger, P.J. Crutzen, W.M. Hao, B.H. Saharjo, and D.E. Ward. 2003. Comprehensive laboratory measurements of biomass-burning emissions: 1. Emissions from Indonesian, African, and other fuels. *Journal of Geophysical Research* 108 4719. (13 pages).
- Chughtai, A.R., G.R. Williams, M.M.O. Atteya, N.J. Miller, and D.M. Smith. 1999a. Carbonaceous particle hydration. *Atmospheric Environment* 33(17):2679–2687.
- Chughtai, A.R., N.J. Miller, D.M. Smith, and J.R. Pitts. 1999b. Carbonaceous particle hydration III. *Journal of Atmospheric Chemistry* 34(2):259–279.
- Cicerone, R.J. 1994. Fires, atmospheric chemistry, and the ozone layer. *Nature* 263:1243–1244.
- Claeys, M., R. Szmigielski, I. Kourtchev, P. Van der Veken, R. Vermeylen, W. Maenhaut, M. Jaoui, T.E. Kleindienst, M. Lewandowski, J.H. Offenberg, and E.O. Edney. 2007. Hydroxydicarboxylic acids: Novel markers for SOA from the photooxidation of α -pinene. *Environmental Science and Technology* 41:1628–1634.
- Claeys, M., B. Graham, G. Vas, W. Wang, R. Vermeylen, V. Pashynska, J. Cafmeyer, P. Guyon, M.O. Andreae, P. Artaxo, and W. Maenhaut. 2004. Formation of secondary organic aerosols through photooxidation of isoprene. *Science* 303(5661):1173–1176.
- Crutzen, P.J., and M.O. Andreae. 1990. Biomass burning in the tropics: Impact on atmospheric chemistry and biogeochemical cycles. *Science* 250:1669–1678.
- Decesari, S., M.C. Facchini, S. Fuzzi, G.B. McFiggans, H. Coe, and K.N. Bower. 2001. Chemical features and seasonal trend of water soluble organic compounds in the Po Valley fine aerosol. *Atmospheric Environment* 35:3691–3699.
- DoD and USFWS (U.S. Department of Defense and U.S. Fish and Wildlife Service). 2001. Factsheet titled *The Military and the Endangered Species Act: Interagency Cooperation*. Available at http://www.fws.gov/endangered/esa-library/pdf/military_esa_factsheet.pdf.
- dos Santos, C.Y.M., D.D.A. Azevedo, and F.R.D.A. Neto. 2002. Selected organic compounds from biomass burning found in the atmospheric particulate matter over sugarcane plantation areas. *Atmospheric Environment* 36:3009–3019.
- Edney, E.O., T.E. Kleindienst, M. Jaoui, M. Lewandowski, J.H. Offenberg, W. Wang, and M. Claeys. 2005. Formation of 2-methyltetrols and 2-methylglyceric acid in secondary organic aerosol from laboratory irradiated isoprene/NO_x/SO₂/air mixtures and their detection in ambient PM_{2.5} samples collected in the eastern United States. *Atmospheric Environment* 39:5281–5289.
- Fekedulegn, D., J.J. Colbert, R.R. Hicks Jr. and M.E. Schuckers. 2002. Coping with Multicollinearity: An Example on Theory and Application of Principal Components Regression in Dendroecology. U.S. Department of Agriculture Forest Service,

- Northeastern Research Station. Research Paper NE-721. Available at <http://www.fs.fed.us/ne/morgantown/4557/dendrochron/rpne721.pdf>.
- Fine, P.M., G.R. Cass, and B.R.T. Simoneit. 2002. Chemical characterization of fine particle emissions from the fireplace combustion of woods grown in the Southern U.S. *Environmental Science and Technology* 36:1442–1451.
- Finney, M.A. 1998. FARSITE: Fire area simulator: Model development and evaluation. U.S. Department of Agriculture Forest Service, Rocky Mountain Research Station, Ogden, UT. Research Paper RMRS-RP-4 (revised).
- Freeman, D.J., and C.R. Cattell. 1990. Wood burning as a source of atmospheric polycyclic aromatic hydrocarbons. *Environmental Science and Technology* 24(10):1581–1585.
- Friedli, H.R., E. Atlas, V.R. Stroud, L. Giovanni, T. Campos, and L.F. Radke. 2001. Volatile organic trace gases emitted from North American wildfires. *Global Biogeochemical Cycles* 15(2):435–452.
- Gaudichet, A., F. Echalar, B. Chatenet, J.P. Quisefit, G. Malingre, H. Cachier, P. Buat-Menard, P. Artaxo, and W. Maenhaut. 1995. Trace elements in tropical African savanna biomass burning aerosols. *Journal of Atmospheric Chemistry* 22(1–2):19–39.
- Glasius, M., M. Lahaniati, A. Calogirou, D.D. Bella, N.R. Jensen, J. Hjorth, D. Kotzias. And B.R. Larsen. 2000. Carboxylic acids in secondary aerosols from oxidation of cyclic monoterpenes by ozone. *Environmental Science and Technology* 34:1001–1010.
- Goode, J.G., R.J. Yokelson, D.E. Ward, R.A. Susott, R.E. Babbitt, M.A. Davies, and W.M. Hao. 2000. Measurements of excess O₃, CO₂, CO, CH₄, C₂H₄, C₂H₂, HCN, NO, NH₃, HCOOH, CH₃COOH, HCHO, and CH₃OH in 1997 Alaskan biomass burning plumes by airborne Fourier transform infrared spectroscopy (AFTIR). *Journal Geophysical Research* 105:22147–22166.
- Goode, J.G., R.J. Yokelson, R.A. Susott, and D.E. Ward. 1999. Trace gas emissions from laboratory biomass fires measured by Fourier transform IR spectroscopy: Fires in grass and surface fuels. *Journal of Geophysical Research* 104:21237–21245.
- Grieshop, A.P., J.M. Logue, N.M. Donahue, and A.L. Robinson. 2009. Laboratory investigation of photochemical oxidation of organic aerosol from wood fires 1: Measurement and simulation of organic aerosol evolution. *Atmospheric Chemistry and Physics* 9:1263–1277.
- Griffith, D.W.T., W.G. Mankin, M.T. Coffey, D.E. Ward, and A. Riebau. 1991. FTIR remote sensing of biomass burning emissions of CO₂, CO, CH₄, CH₂O, NO, NO₂, NH₃, and N₂O. Pp. 230–239 in *Global Biomass Burning: Atmospheric, Climatic, and Biospheric Implications*. Edited by J.S. Levine. MIT Press: Cambridge, MA.

- Grisdale, R.O. 1953. The formation of black carbon. *Journal of Applied Physics* 24:1082–1091.
- Grosjean, D. 1992. In situ organic aerosol formation during a smog episode: Estimated production and chemical functionality. *Atmospheric Environment* 26A:953–963.
- Grosjean, D., and J. Seinfeld. 1989. Parameterization of the formation potential of secondary organic aerosols. *Atmospheric Environment* 23:1733–1747.
- Guenther, A., T. Karl, P. Harley, C. Wiedinmyer, P.I. Palmer, and C. Geron. 2006. Estimates of global terrestrial isoprene emissions using MEGAN (Model of Emissions of Gases and Aerosols from Nature). *Atmospheric Chemistry and Physics* 6(11):3181–3210.
- Gullett, B.K., and A. Touati. 2003. PCDD/F emissions from forest fires simulations. *Atmospheric Environment* 37:803–803.
- Haines, T.K., R.L. Busby, and D.A. Cleaves. 2001. Prescribed burning in the South: Trends, purpose, and barriers. *Southern Journal of Applied Forestry* 25(4):149–153.
- Hallquist, M., J.C. Wenger, U. Baltensperger, Y. Rudich, D. Simpson, M. Claeys, J. Dommen, N.M. Donahue, C. George, A.H. Goldstein, J.F. Hamilton, H. Herrmann, T. Hoffmann, Y. Iinuma, M. Jang, M.E. Jenkin, J.L. Jimenez, A. Kiendler-Scharr, W. Maenhaut, G. McFiggans, T.F. Mentel, A. Monod, A.S.H. Prévôt, J.H. Seinfeld, J.D. Surratt, R. Szmigielski, and J. Wildt. 2009. The formation, properties and impact of secondary organic aerosol: Current and emerging issues, *Atmospheric Chemistry and Physics* 9(14):5155–5236.
- Hardy, C.C., and B. Leenhouts. 2001. *Introduction* (Pp. 3–8) to the *2001 Smoke Management Guide for Prescribed and Wildland Fire*. National Wildfire Coordinating Group. NFES-1279. Available at <http://www.nwcg.gov/pms/pubs/SMG/SMG-72.pdf>.
- Hays, M.D., D.D. Geron, K.J. Linna, and N.D. Smith. 2002. Speciation of gas-phase and fine particle emissions from burning of foliar fuels. *Environmental Science and Technology* 36:2281–2295.
- Henze, D.K., J.H. Seinfeld, N.L. Ng, J.H. Kroll, R-M. Fu, D.J. Jacob, and C.L. Heald. 2008. Global modeling of secondary organic aerosol formation from aromatic hydrocarbons: High- vs. low-yield pathways. *Atmospheric Chemistry and Physics* 8:2405–2420.
- Hobbs, P.V., P. Sinha, R.L. Yokelson, T.J. Christian, D.R. Blake, S. Gao, T.W. Kirchstetter, T. Novakov, and P. Pilewskie. 2003. Evolution of gases and particles from a savanna fire in South Africa. *Journal of Geophysical Research* 108, 8485. (20 pages).
- Hoffmann, T., J.R. Odum, F. Bowman, D. Collins, D. Klockow, R.C. Flagan, and J.H. Seinfeld. 1997. Formation of organic aerosol from the oxidation of biogenic hydrocarbons. *Atmospheric Environment* 26:189–222.

- Holzinger, R., C. Warneke, A. Hansel, A. Jordan, W. Lindinger, D.H. Scharffe, G. Schade, P.J. Crutzen. 1999. Biomass burning as a source of formaldehyde, acetaldehyde, methanol, acetone, acetonitrile, and hydrogen cyanide. *Geophysical Research Letters* 26(8):1161–1164.
- Hu, Y., M.T. Odman, M.E. Chang, W. Jackson, S.G. Lee, K. Baumann, and A.G. Russell. 2008. Simulation of air quality impacts from prescribed fires on an urban area. *Environmental Science and Technology* 42:3676–3682.
- Hull, L.A. 1981. Terpene ozonolysis products. Pp. 161–186 in *Atmospheric Biogenic Hydrocarbons (Vol. 2)*. Edited by J.J. Bufalini, and R.R. Arnts. Ann Arbor Science: Michigan.
- Jang, M., and R.M. Kamens. 2001. Atmospheric secondary aerosol formation by heterogeneous reactions of aldehydes in the presence of a sulfuric acid catalyst. *Environmental Science and Technology* 35:4758–4766.
- Jang, M., and R.M. Kamens. 1999. Newly characterized products and composition of secondary aerosols from the reaction of α -pinene with ozone. *Atmospheric Environment* 33:459–474.
- Jaoui, M., and R.M. Kamens. 2001. Mass balance of gaseous and particulate products analysis from α -pinene/ NO_x /air in the presence of natural sunlight. *Journal of Geophysical Research* 106:12541–12558.
- Jeffries, H.E. 1995. Pp. 308–348 in *Photochemical Air Pollution in Composition, Chemistry, and Climate of the Atmosphere*. Edited by H.B. Singh. Van Nostrand Reinhold: New York, NY.
- Jimenez, J.L. M.R. Canagaratna, N.M. Donahue, A.S. Prevot, Q. Zhang, J.H. Kroll, P.F. DeCarlo, J.D. Allan, H. Coe, N.L. Ng, A.C. Aiken, K.S. Docherty, I.M. Ulbrich, A.P. Grieshop, A.L. Robinson, J. Duplissy, J.D. Smith, K.R. Wilson, V.A. Lanz, C. Hueglin, Y.L. Sun, J. Tian, A. Laaksonen, T. Raatikainen, J. Rautiainen, P. Vaattovaara, M. Ehn, M. Kulmala, J.M. Tomlinson, D.R. Collins, M.J. Cubison, E.J. Dunlea, J.A. Huffman, T.B. Onasch, M.R. Alfarra, P.I. Williams, K. Bower, Y. Kondo, J. Schneider, F. Drewnick, S. Borrmann, S. Weimer, K. Demerjian, D. Salcedo, L. Cottrell, R. Griffin, A. Takami, T. Miyoshi, S. Hatakeyama, A. Shimono, J.Y. Sun, Y.M. Zhang, K. Dzepina, J.R. Kimmel, D. Sueper, J.T. Jayne, S.C. Herndon, A.M. Trimborn, L.R. Williams, E.C. Wood, A.M. Middlebrook, C.E. Kolb, U. Baltensperger, and D.R. Worsnop. 2009. Evolution of organic aerosols in the atmosphere. *Science* 326(5959):1525–1529.
- Kamens, R.M., M. Jang, C.J. Chien, and K. Leach. 1999. Aerosol formation from the reaction of α -pinene and ozone using a gas-phase kinetics-aerosol partitioning model. *Environmental Science and Technology* 33:1430–1438.
- Kerker, M. 1969. *The Scattering of Light*. Academic Press: New York, NY.

- Khalil, M.A.K., and R.A. Rasmussen. 2003. Tracers of wood smoke. *Atmospheric Environment* 37:1211–1222.
- Kim, S., T. Karl, D. Helmig, R. Daly, R. Rasmussen, and A. Guenther. 2009. Measurement of atmospheric sesquiterpenes by proton transfer reaction-mass spectrometry (PTR-MS). *Atmospheric Measurement Techniques* 2:99–112.
- Kotzick, T.R., and R. Niessner. 1999. The effects of aging processes on critical supersaturation ratios of ultrafine carbon aerosols. *Atmospheric Environment* 33:2669–2677.
- Lacaux, J.P., R. Delmas, C. Jambert, and T.A.J. Kuhlbusch. 1996. NO_x emissions from African savanna fires. *Journal of Geophysical Research* 101:23585–23595.
- Larson, T.V., and J.Q. Koenig. 1994. Wood smoke: Emissions and non-cancer respiratory effects. *Annual Review of Public Health* 15:133–156.
- Lee, S., H.K. Kim, B. Yan, C.E. Cobb, C. Hennigan, S. Nichols, M. Chamber, E.S. Edgerton, J.J. Jansen, Y. Hu, M. Zheng, R.J. Weber, and A.G. Russell. 2008. Diagnosis of aged prescribed burning plumes impacting an urban area. *Environmental Science and Technology* 42:1438–1444.
- Lee, S., A.G. Russell, and K. Baumann. 2007. Source apportionment of fine particulate matter in the southeastern United States. *Journal of the Air & Waste Management Association* 57:1123–1135.
- Lee, S., K. Baumann, J.J. Schauer, R.J. Sheesley, L.P. Naeher, S. Meinardi, D.R. Blake, E.S. Edgerton, A.G. Russell, and M. Clements. 2005. Gaseous and particulate emissions from prescribed burning in Georgia. *Environmental Science and Technology* 39:9049–9056.
- Levine, J.S., W.R. Cofer III, D.R. Cahoon Jr., and E.L. Winstead. 1995. Biomass burning: A driver for global change. *Environmental Science and Technology* 29(3):A120–A125.
- Limbeck, A., M. Kulmala, and H. Puxbaum. 2003. Secondary organic aerosol formation in the atmosphere via heterogeneous reaction of gaseous isoprene on acidic particles. *Geophysical Research Letters* 30. (4 pages).
- Lin, Y-H., Z. Zhang, K.S. Docherty, H. Zhang, S.H. Budisulistiorini, C.L. Rubitschun, S.L. Shaw, E.N. Knipping, E.S. Edgerton, T.E. Kleindienst, A. Gold, and J.D. Surratt. 2012. Isoprene epoxydiols as precursors to secondary organic aerosol formation: Acid-catalyzed reactive uptake studies with authentic compounds. *Environmental Science and Technology* 46(1):250–258.
- Lipsky, E.M., and A.L. Robinson. 2006. Effects of dilution on fine particle mass and partitioning of semivolatile organics in diesel exhaust and wood smoke. *Environmental Science and Technology* 40:155–162.

- Lobert, J.M., D.H. Scharffe, W.M. Hao, T.A. Kuhlbusch, R. Seuwen, P. Warneck, and P.J. Crutzen. 1991. Experimental evaluation of biomass burning emissions: Nitrogen and carbon containing compounds. Pp. 289–304 in *Global Biomass Burning: Atmospheric, Climatic, and Biospheric Implications*. Edited by J.S. Levine. MIT Press: Cambridge, MA.
- McMurry, P.H., X. Zhang and Q.T. Lee. 1996. Issues in aerosol measurement for optical assessments. *Journal of Geophysical Research* 101:19188–19197.
- Naeher, L.P., G.L. Achtemeier, J.S. Glitzenstein, D.R. Streng, and D. Macintosh. 2006. Real-time and time-integrated PM_{2.5} and CO from prescribed burns in chipped and non-chipped plots: Firefighter and community exposure and health implications. *Journal of Exposure Science and Environmental Epidemiology* 16(4):351–361.
- Nance, J.D., P.V. Hobbs, and L.F. Radke. 1993. Airborne measurements of gases and particles from an Alaskan Wildfire. *Journal of Geophysical Research* 98:14873–14882.
- Nestrick, T.J., and L.L. Lamparski. 1982. Isomer-specific determination of chlorinated dioxins for assessment of formation and potential environmental emission from wood combustion. *Analytical Chemistry* 54(13):2292–2299.
- NIFC (National Interagency Fire Center). *Total Wildland Fires and Acres (1960–2009)*. Available at www.nifc.gov/fireInfo/fireInfo_stats_totalFires.html. Accessed May 7, 2012.
- Noziere, B., I. Barnes, and K.H. Becker. 1999. Product study and mechanisms of the reactions of α -pinene and pinonaldehyde with OH radicals. *Journal of Geophysical Research* 104:23645–23656.
- Odum, J.R., T.P.W. Jungkamp, and J.H. Seinfeld. 1997. The atmospheric aerosol-forming potential of whole gasoline vapor. *Science* 276:96–99.
- Odum, J.R., T. Hoffmann, F. Bowman, D. Collins, R.C. Flagan, and J.H. Seinfeld. 1996. Gas/particle partitioning and secondary organic aerosol yields, *Environmental Science and Technology* 30(8):2580–2585.
- Puglisi, E., M. Nicelli, E. Capri, M. Trevisan, and A.A.M. Del Re. 2003. Cholesterol, β -sitosterol, ergosterol, and coprostanol in agricultural soils. *Journal of Environmental Quality* 32:466–471.
- Radke, L.F., D.A. Hegg, J.H. Lyons, C.A. Brock, and P.V. Hobbs. 1998. Airborne measurements on smokes from biomass burning. Pp. 411–422 in *Aerosols and Climate*. Edited by P.V. Hobbs and M.P. McCormick. Deepak Publishing: Hampton, VA.
- Reiner, T., D. Sprung, C. Jost, R. Gabriel, O.L. Mayol-Bracero, M.O. Andreae, T.L. Campos, and R.E. Shelter. 2001. Chemical characterization of pollution layers over the tropical

- Indian Ocean: Signatures of emission from biomass and fossil fuel burning. *Journal of Geophysical Research* 106, D22:28497–28510.
- Robinson, A.L., N.M. Donahue, M.K. Shrivastava, E.A. Weitkamp, A.M. Sage, A.P. Grieshop, T.E. Lane, J.R. Pierce, and S.N. Pandis. 2007. Rethinking organic aerosols: Semi-volatile emissions and photochemical aging. *Science* 315:1259–1262.
- Rogge, W.F., L.M. Hildemann, M.A. Mazurek, and G.R. Cass. 1991. Sources of fine organic aerosol. 1. Charbroilers and meat cooking operations. *Environmental Science and Technology* 25:1112–1125.
- Schauer, J.J., M.J. Kleeman, G.R. Cass, and B.R.T. Simoneit. 2001. Measurement of emissions from air pollution sources. 3. C₁-C₂₉ organic compounds from fireplace combustion of wood. *Environmental Science and Technology* 35:1716–1728.
- Schauer, J.J., W.F. Rogge, L.M. Hildemann, M.A. Mazurek, and G.R. Cass. 1996. Source apportionment of airborne particulate matter using organic compounds as tracers. *Atmospheric Environment* 30:3837–3855.
- Sinha, P., P.V. Hobbs, R.J. Yokelson, D.R. Blake, S. Gao, and T.W. Kirchstetter. 2004. Emissions from miombo woodland and dambo grassland savanna fires. *Journal of Geophysical Research* 109, D11305.
- Sloane, C.S. 1984. Optical properties of aerosols of mixed composition. *Atmospheric Environment* 18:871–878.
- Smith, D.M., M.S. Akhter, J.A. Jassim, C.A. Sergides, W.F. Welch, and A.R. Chughtai. 1989. Studies of the structure and reactivity of soot. *Aerosol Science and Technology* 10:311–325.
- Surratt, J.D., A.W.H. Chan, N.C. Eddingsaas, M. Chan, C.L. Loza, A.J. Kwan, S.P. Hersey, R.C. Flagan, P.O. Wennberg, and J.H. Seinfeld. 2010. Reactive intermediates revealed in secondary organic aerosol formation from isoprene. *Proceedings of the National Academy of Sciences* 107(15):6640–6645.
- Surratt, J.D., S.M. Murphy, J.H. Kroll, N.L. Ng, L. Hildebrandt, A. Sorooshian, R. Szmigielski, R. Vermeylen, W. Maenhaut, M. Claeys, R.C. Flagan, and J.H. Seinfeld. 2006. Chemical composition of secondary organic aerosol formed from the photooxidation of isoprene. *Journal of Physical Chemistry A* 110:9665–9690.
- Turpin, B.J., and J.J. Huntzicker. 1995. Identification of secondary organic aerosol episodes and quantitation of primary and secondary organic aerosol concentrations during SCAQS. *Atmospheric Environment* 29:3527–3544.
- U.S. EPA (U.S. Environmental Protection Agency). 2004. *Air Quality Criteria for Particulate Matter*. Fourth External Review Draft Report. EPA-600/P-99-002, aD, bD, Office of

- Research and Development, Research Triangle Park, NC. Data from <http://www.epa.gov/ttn/chief/trends>.
- U.S. EPA (U.S. Environmental Protection Agency). 2003. *Latest Findings on National Air Quality: 2002 Status and Trends*. Report 454/K-03-001. Office of Air Quality Planning and Standards; Emissions, Monitoring, and Analysis Division, Research Triangle Park, NC. Available at www.epa.gov/airtrends. August.
- U.S. EPA (U.S. Environmental Protection Agency). 2000. *National Air Pollutant Emission Trends 1900–1998*. Report EPA 454/R-00-002 (NTIS PB2000-108054). Office of Air Quality Planning and Standards, Research Triangle Park, NC. Available at <http://www.epa.gov/ttn/chief/trends/trends98>.
- U.S. EPA (U.S. Environmental Protection Agency). 1996. *AP-42, Fifth Edition, Volume I (13): Miscellaneous Sources*. Section 13.1, *Wildfires and prescribed burning*, Supplement B. October. Available at <http://www.epa.gov/ttnchie1/ap42/ch13>.
- Wade, D.D., B.L. Brock, P.H. Brose, J.B. Grace, G.A. Hoch, and W.A. Patterson III. 2000. Chapter 4, pp. 53–96 in *Wildland Fire in Ecosystems: Effects of Fire on Flora*. Edited by J.K. Brown, and J.K. Smith. U.S. Department of Agriculture Forest Service, Rocky Mountain Research Station.
- Wangberg, I., I. Barnes, and K.H. Becker. 1997. Product and mechanistic study of the reaction of NO₃ radicals with α -pinene. *Environmental Science and Technology* 31:2130–2135.
- Ward, D.E., and L.F. Radke. 1993. Emission measurements from vegetation fires: A comparative evaluation of methods and results. Pp. 53–76 in *Fire in the Environment: The Ecological, Atmospheric, and Climatic Importance of Vegetation Fires*. Edited by P.J. Crutzen. Wiley: Chichester, UK.
- Worden, H., R. Beer, and C.P. Rinsland 1997. Airborne infrared spectroscopy of 1994 western wildfires. *Journal of Geophysical Research* 102:1287–1299.
- Yokelson, R.J., J.G. Goode, D.E. Ward, R.A. Susott, R.E. Babbitt, D.D. Wade, I. Bertschi, D.W.T. Griffith, and W.M. Hao. 1999. Emissions of formaldehyde, acetic acid, methanol, and other trace gases from biomass fires in North Carolina measured by airborne Fourier transform IR spectroscopy. *Journal of Geophysical Research* 104:30109–30125.
- Yokelson, R.J., R. Susott, D.E. Ward, J. Reardon, and D.W.T. Griffith. 1997. Emissions from smoldering combustion of biomass measured by open-path Fourier transform infrared spectroscopy. *Journal of Geophysical Research* 102:18865–18877.
- Yokelson, R.J., D.W.T. Griffith, and D.E. Ward. 1996. Open-path Fourier transform infrared studies of large-scale laboratory biomass fires. *Journal of Geophysical Research* 101:21067–21080.

- Yu, J., D.R. Cocker, R.J. Griffin, R.C. Flagan, and J.H. Seinfeld. 1999. Gas-phase ozone oxidation of monoterpenes: Gaseous and particulate products. *Journal of Atmospheric Chemistry* 34:207–258.
- Zhang, Q., J.L. Jimenez, M.R. Canagaratna, J.D. Allan, H. Coe, I. Ulbrich, M.R. Alfarra, A. Takami, A.M. Middlebrook, Y.L. Sun, K. Dzepina, E. Dunlea, K. Docherty, P.F. DeCarlo, D. Salcedo, T. Onasch, J.T. Jayne, T. Miyoshi, A. Shimono, S. Hatakeyama, N. Takegawa, Y. Kondo, J. Schneider, F. Drewnick, S. Borrmann, S. Weimer, K. Demerjian, P. Williams, K. Bower, R. Bahreini, L. Cottrell, R.J. Griffin, J. Rautiainen, J.Y. Sun, Y.M. Zhang, and D.R. Worsnop. 2007. Ubiquity and dominance of oxygenated species in organic aerosols in anthropogenically influenced Northern Hemisphere midlatitudes. *Geophysical Research Letters* 34, L13801. (6 pages).
- Zheng, M., G.R. Cass, J.J. Schauer, and E.S. Edgerton. 2002. Source apportionment of PM_{2.5} in the Southeastern United States using solvent-extractable organic compounds as tracers. *Environmental Science and Technology* 36:2361–2371.

[This page intentionally left blank.]

Appendix 15-A

Supporting Data

Table 15-A-1. EF of gaseous species based on weighted average excess MR from successive flaming/smoldering phase measurements for each fuel bed with and without treatment.

Gaseous Species		CTRL					HYAX				
		RB	HA	MF	IEn	IEs	RB	HA	MF	IEn	IEs
CO ₂	g/kg	1,515	1,460	1,323	1,504	1,448	1,359	1,490	1,410	1,414	1,495
CO	g/kg	20.8	35.2	84.3	22.4	53.6	80.6	29.2	59.5	55.1	32.1
CH ₄	g/kg	0.53	1.76	3.71	0.36	1.87	3.15	0.56	2.55	2.25	0.62
NMHC	gC/kg	1.10	2.86	4.39	1.15	2.80	4.03	1.32	3.32	3.20	1.10
Ethane	g/kg	0.075	0.242	0.323	0.066	0.244	0.366	0.083	0.248	0.229	0.087
Propane	g/kg	0.028	0.072	0.134	0.018	0.072	0.121	0.028	0.087	0.075	0.025
i-Butane	g/kg	0.004	0.004	0.011	0.002	0.008	0.011	0.004	0.009	0.004	0.003
n-Butane	g/kg	0.014	0.012	0.033	0.010	0.042	0.035	0.029	0.035	0.019	0.008
i-Pentane	g/kg	0.012	0.002	0.014	0.014	0.133	0.019	0.040	0.020	0.013	0.008
n-Pentane	g/kg	0.008	0.004	0.017	0.010	0.062	0.019	0.019	0.021	0.012	0.005
2-Methylpentane	g/kg	0.003	0.002	0.013	0.007	0.078	0.007	0.013	0.007	0.004	0.003
3-Methylpentane	g/kg	0.002	0.001	0.003	0.005	0.035	0.005	0.005	0.005	0.003	0.002
n-Hexane	g/kg	0.004	0.002	0.011	0.006	0.028	0.012	0.006	0.014	0.007	0.002
n-Heptane	g/kg	0.003	0.001	0.007	0.005	0.015	0.008	0.005	0.010	0.004	0.003
n-Octane	g/kg	0.003	0.002	0.006	0.003	0.009	0.008	0.002	0.009	0.004	0.001
Ethene	g/kg	0.190	0.949	0.493	0.207	0.516	0.769	0.202	0.558	0.542	0.320
Ethyne	g/kg	0.101	0.300	0.236	0.127	0.150	0.399	0.087	0.298	0.325	0.122
Propene	g/kg	0.127	0.307	0.366	0.113	0.224	0.463	0.119	0.355	0.315	0.115
1-Butene	g/kg	0.026	0.055	0.065	0.022	0.048	0.084	0.017	0.075	0.061	0.025
i-Butene	g/kg	0.020	0.035	0.065	0.016	0.036	0.070	0.014	0.057	0.046	0.008
trans-2-Butene	g/kg	0.008	0.014	0.025	0.006	0.018	0.029	0.006	0.022	0.020	0.007
cis-2-Butene	g/kg	0.006	0.009	0.018	0.005	0.014	0.021	0.005	0.016	0.014	0.005
1,3-Butadiene	g/kg	0.042	0.070	0.091	0.041	0.056	0.138	0.037	0.115	0.097	0.038
1-Pentene	g/kg	0.011	0.019	0.022	0.008	0.018	0.027	0.009	0.031	0.019	0.009
Benzene	g/kg	0.107	0.246	0.277	0.093	0.206	0.350	0.080	0.253	0.254	0.127
Toluene	g/kg	0.105	0.228	0.307	0.091	0.345	0.367	0.252	0.250	0.249	0.054
Ethylbenzene	g/kg	0.014	0.030	0.036	0.016	0.056	0.061	0.016	0.040	0.028	0.014
mp-Xylene	g/kg	0.075	0.087	0.229	0.091	0.170	0.442	0.048	0.223	0.322	0.019
o-Xylene	g/kg	0.012	0.019	0.029	0.017	0.051	0.055	0.015	0.037	0.022	0.008
Isopropylbenzene	g/kg	0.001	0.003	0.002	0.003	0.008	0.003	0.003	0.006	0.002	0.002
Propylbenzene	g/kg	0.002	0.004	0.008	0.003	0.009	0.005	0.004	0.007	0.003	0.002
3-Ethyltoluene	g/kg	0.005	0.017	0.028	0.010	0.026	0.016	0.013	0.020	0.024	0.004
4-Ethyltoluene	g/kg	0.002	0.007	0.006	0.004	0.012	0.005	0.007	0.008	0.004	0.003
2-Ethyltoluene	g/kg	0.006	0.004	0.014	0.011	0.008	0.009	0.008	0.020	0.007	0.002
1,3,5-TMBenzene	g/kg	0.001	0.003	0.005	0.004	0.011	0.003	0.005	0.006	0.004	0.005
1,2,4-TMBenzene	g/kg	0.004	0.011	0.014	0.011	0.012	0.003	0.015	0.019	0.009	0.005
1,2,3-TMBenzene	g/kg	0.006	0.006	0.055	0.009	0.013	0.001	0.010	0.023	0.035	0.012

Gaseous Species		CTRL					HYAX				
		RB	HA	MF	IEn	IEs	RB	HA	MF	IEn	IEs
CHCl₃	mg/kg	0.002	0.057	0.328	0.139	0.007	0.002	0.111	0.055	0.191	0.119
CH₂Cl₂	mg/kg	0.228	0.138	0.836	0.206	0.049	0.410	0.036	0.625	0.504	0.060
C₂HCl₃	mg/kg	0.039	0.024	0.221	0.017	0.173	0.156	0.093	0.117	0.057	0.057
C₂Cl₄	mg/kg	0.122	0.001	0.120	0.027	0.005	0.035	0.860	0.190	0.025	0.006
CH₃Cl	mg/kg	8.428	17.435	55.738	8.854	31.284	34.890	30.656	26.182	24.194	18.511
CH₃Br	mg/kg	0.365	0.598	1.288	0.461	0.961	1.224	0.413	0.883	0.817	0.348
CH₃I	mg/kg	0.068	0.214	0.270	0.096	0.321	0.215	0.089	0.222	0.160	0.246
MethylNO₃	mg/kg	0.172	2.309	0.478	0.189	0.172	0.623	0.240	0.762	0.755	1.679
EthylNO₃	mg/kg	0.083	0.172	0.313	0.063	0.001	0.115	0.012	0.259	0.289	0.294
i-PropylNO₃	mg/kg	0.000	0.126	0.103	0.006	0.001	0.035	0.231	0.062	0.100	0.001
n-PropylNO₃	mg/kg	0.000	0.011	0.003	0.002	0.001	0.000	0.002	0.002	0.020	0.215
2-ButylNO₃	mg/kg	0.000	0.005	0.030	0.001	0.001	0.041	0.001	0.141	0.306	0.002
COS	mg/kg	3.472	7.165	15.321	2.261	5.788	10.538	2.218	9.107	9.690	7.316
DMS	mg/kg	0.119	1.310	0.075	0.240	1.037	0.367	0.719	0.058	0.177	0.218
Isoprene	g/kg	0.105	0.044	0.253	0.078	0.038	0.282	0.036	0.220	0.207	0.023
α-Pinene	g/kg	0.059	0.372	0.541	0.035	0.322	0.206	0.181	0.109	0.334	0.041
β-Pinene	g/kg	0.002	0.029	0.007	0.001	0.015	0.024	0.011	0.003	0.001	0.001
Acetic	g/kg	0.023	0.082	1.810	0.144	0.097	0.138	0.048	0.777	0.384	0.151
Formic	g/kg	0.111	0.081	1.241	0.203	0.153	0.247	0.091	0.571	0.419	0.182
Oxalic	g/kg	0.034	0.009	0.148	0.044	0.025	0.044	0.014	0.078	0.081	0.066
NH₃	g/kg	0.195	0.255	0.499	0.415	0.282	0.277	0.223	0.161	0.575	0.205
HONO	g/kg	0.003	0.151	0.956	0.068	0.198	0.040	0.043	0.519	0.353	0.210
HNO₃	g/kg	0.002	0.186	0.015	0.007	0.082	0.006	0.048	0.005	0.014	0.115
HCl	g/kg	0.003	0.003	0.001	0.000	0.004	0.005	0.004	0.001	0.005	0.003
SO₂	g/kg	0.028	0.060	0.160	0.125	0.061	0.058	0.034	0.089	0.168	0.063

Table 15-A-2. EF of PM_{2.5} species based on weighted average excess MR from successive flaming/smoldering phase measurements for each fuel bed with and without treatment.

Main		CTRL					HYAX				
		RB	HA	MF	IEn	IEs	RB	HA	MF	IEn	IEs
PM_{2.5}	g/kg	3.15	10.75	45.54	9.52	5.84	18.58	7.00	16.00	15.56	4.39
OC	g/kg	2.28	8.08	21.93	4.66	3.74	14.34	4.82	10.45	11.60	2.62
EC	g/kg	0.06	0.50	0.05	0.23	0.17	0.02	0.57	0.25	0.26	0.28
OC1, 340C	g/kg	1.08	3.43	12.23	2.10	1.65	7.23	2.22	5.48	5.60	0.96
OC2, 500C	g/kg	0.43	2.31	3.03	0.76	0.95	2.41	1.11	1.59	1.72	0.70
OC3, 615C	g/kg	0.24	0.75	1.90	0.41	0.36	1.31	0.47	0.87	0.99	0.29
OC4, 900C	g/kg	0.29	0.72	2.47	0.63	0.31	1.74	0.36	1.17	1.43	0.24
OCp	g/kg	0.23	0.88	2.30	0.77	0.47	1.65	0.67	1.34	1.85	0.43
from IC		RB	HA	MF	IEn	IEs	RB	HA	MF	IEn	IEs
Acetate⁻	mg/kg	0.93	2.49	15.24	2.05	1.64	7.32	1.59	7.16	4.73	1.91
Formate⁻	mg/kg	3.21	4.38	46.27	10.16	2.44	18.13	2.04	18.11	17.97	2.39
Oxalate⁻²	mg/kg	1.56	4.65	15.46	4.49	3.44	6.05	4.15	8.32	9.85	4.11
Na⁺	mg/kg	0.21	1.56	12.16	1.15	13.96	3.25	1.98	1.80	19.06	22.43
NH₄⁺	mg/kg	2.07	13.63	17.13	9.35	4.49	12.75	5.62	23.55	11.57	4.84
K⁺	mg/kg	5.85	21.49	88.57	23.62	13.92	29.11	37.17	44.32	149.37	18.19
Mg⁺⁺	mg/kg	0.20	1.52	6.21	1.17	0.56	0.50	0.71	0.68	1.09	1.54
Ca⁺⁺	mg/kg	1.31	1.39	24.65	4.80	0.74	3.16	1.36	3.04	1.93	0.86
F⁻	mg/kg	2.44	11.00	49.37	6.53	5.30	14.64	6.42	17.66	13.06	2.73
Cl⁻	mg/kg	7.49	29.62	159.90	41.08	18.96	64.30	28.55	61.71	95.98	25.05
SO₄⁻²	mg/kg	5.55	7.52	40.88	16.24	11.99	20.93	9.51	32.88	54.47	9.39
NO₃⁻	mg/kg	8.32	40.14	87.49	16.16	10.91	17.98	24.97	68.64	27.57	20.81
from XRF		RB	HA	MF	IEn	IEs	RB	HA	MF	IEn	IEs
Al	mg/kg	0.21	1.10	6.73	1.29	0.92	1.64	10.30	17.72	5.86	1.02
Si	mg/kg	0.20	0.91	14.62	0.72	0.90	0.99	1.66	2.48	2.04	1.27
S	mg/kg	3.09	6.67	30.80	10.42	4.02	9.11	5.37	16.77	23.33	4.56
Cl	mg/kg	7.92	32.31	150.81	40.57	25.47	50.06	36.65	61.10	86.49	35.52
K	mg/kg	6.70	23.80	83.83	24.55	15.13	24.36	44.53	41.23	139.41	21.35
Ca	mg/kg	0.87	2.86	51.67	5.40	2.21	1.83	5.56	3.78	6.68	2.24
Mn	mg/kg	0.03	0.08	0.57	0.13	0.03	0.01	0.57	0.06	0.17	0.08
Fe	mg/kg	0.07	0.08	1.83	0.09	0.24	0.55	0.46	1.17	0.62	0.31
Zn	mg/kg	0.98	3.23	13.98	4.67	1.73	5.35	3.00	4.96	7.32	2.92
As	mg/kg	0.06	0.12	2.39	0.15	0.11	0.24	0.13	0.52	0.13	0.18
Se	mg/kg	0.07	0.22	0.85	0.37	0.27	0.32	0.29	0.30	0.33	0.31
Pb	mg/kg	0.04	0.04	7.01	0.11	0.06	0.04	0.09	1.19	0.27	0.15
ICP-MS		RB	HA	MF	IEn	IEs	RB	HA	MF	IEn	IEs
Li	mg/kg	0.004	0.010	0.033	0.010	0.009	0.014	0.013	0.014	0.021	0.010
Mg	mg/kg	0.206	0.604	4.503	1.118	0.344	0.380	0.608	0.411	1.027	0.889
Al	mg/kg	0.061	0.124	0.716	0.175	0.094	0.162	2.855	1.259	0.347	0.149
K	mg/kg	6.47	20.45	91.70	26.36	13.71	31.03	36.55	46.94	146.71	17.70
Ca	mg/kg	1.495	0.661	28.609	7.359	0.283	4.470	1.061	4.055	5.808	0.554
Ti	mg/kg	0.001	0.001	0.002	0.002	0.002	0.002	0.001	0.001	0.004	0.002
Cr	mg/kg	0.001	0.000	0.014	0.003	0.001	0.004	0.001	0.007	0.007	0.001
Mn	mg/kg	0.028	0.073	0.334	0.100	0.031	0.041	0.215	0.063	0.150	0.031
Fe	mg/kg	0.012	0.001	0.027	0.008	0.004	0.129	0.003	0.035	0.011	0.005
Ni	mg/kg	0.003	0.002	0.141	0.009	0.004	0.116	0.003	0.014	0.020	0.009
Cu	mg/kg	0.000	0.005	0.017	0.006	0.008	0.013	0.012	0.002	0.008	0.077
Zn	mg/kg	0.737	2.305	13.127	4.603	1.340	5.738	2.196	4.754	7.302	2.289

Main		CTRL					HYAX				
		RB	HA	MF	IEn	IEs	RB	HA	MF	IEn	IEs
As	mg/kg	0.005	0.003	0.022	0.006	0.004	0.011	0.004	0.007	0.010	0.004
Se	mg/kg	0.003	0.010	0.033	0.021	0.010	0.026	0.019	0.014	0.033	0.008
Rb	mg/kg	0.026	0.048	0.244	0.071	0.024	0.063	0.074	0.118	0.266	0.031
Sr	mg/kg	0.003	0.010	0.077	0.028	0.009	0.007	0.016	0.010	0.024	0.009
Cd	mg/kg	0.010	0.048	0.147	0.037	0.023	0.042	0.039	0.086	0.089	0.025
Sb	mg/kg	0.000	0.000	0.005	0.001	0.000	0.001	0.001	0.001	0.002	0.000
Ba	mg/kg	0.010	0.023	0.135	0.045	0.010	0.051	0.060	0.020	0.063	0.015
Pb	mg/kg	0.015	0.046	3.027	0.058	0.024	0.060	0.019	0.622	0.024	0.032

Table 15-A-3. EF of POC species based on weighted average excess MR from successive flaming/smoldering phase measurements for each fuel bed with and without treatment.

	CTRL					HYAX				
PAH	RB	HA	MF	IEn	IEs	RB	HA	MF	IEn	IEs
Fluoranthene	0.23	1.06	2.36	0.96	0.32	2.87	0.45	0.82	2.86	0.09
Acephenanthrylene	0.09	0.18	1.25	0.35	0.12	1.36	0.10	0.35	1.11	0.02
Pyrene	0.22	0.87	2.37	0.90	0.31	2.76	0.42	0.85	2.67	0.08
Benz(a)anthracene	0.09	0.44	1.30	0.30	0.15	0.82	0.25	0.44	1.05	0.08
Chrysene	0.13	0.56	1.55	0.38	0.20	0.89	0.31	0.59	1.34	0.13
Coronene	0.02	0.04	0.16	0.05	0.02	0.12	0.05	0.07	0.13	0.02
Benzo(b)fluoranthene	0.09	0.33	0.97	0.26	0.14	0.64	0.16	0.41	0.70	0.11
Benzo(k)fluoranthene	0.07	0.20	0.85	0.25	0.09	0.58	0.14	0.33	0.82	0.08
Benzo(j)fluoranthene	0.02	0.06	0.35	0.09	0.05	0.23	0.07	0.14	0.25	0.03
Benzo(a)pyrene	0.06	0.24	0.92	0.23	0.08	0.69	0.12	0.32	0.73	0.04
Benzo(e)pyrene	0.06	0.18	0.66	0.16	0.06	0.39	0.10	0.27	0.51	0.06
Perylene	0.02	0.02	0.27	0.05	0.01	0.18	0.03	0.10	0.13	0.01
Indeno(1,2,3-cd)pyrene	0.06	0.28	0.61	0.19	0.11	0.34	0.19	0.23	0.48	0.10
Dibenz(ah)anthracene	0.04	0.00	0.17	0.06	0.00	0.13	0.00	0.00	0.16	0.02
Benzo(GHI)perylene	0.07	0.16	0.57	0.14	0.07	0.30	0.13	0.27	0.37	0.07
Cyclopenta(cd)pyrene	0.06	0.11	0.88	0.17	0.06	0.71	0.08	0.35	0.66	0.02
Benzo(GHI)fluoranthene	0.07	0.19	0.37	0.22	0.08	0.55	0.15	0.31	0.76	0.05
1-Methylchrysene	0.00	0.05	0.00	0.00	0.06	0.00	0.08	0.00	0.00	0.03
Retene	5.45	151.98	202.76	6.30	6.08	52.70	31.99	20.36	72.94	1.79
Picene	0.00	0.00	0.15	0.06	0.00	0.13	0.00	0.00	0.16	0.00
Alkanes	RB	HA	MF	IEn	IEs	RB	HA	MF	IEn	IEs
Eicosane	0.32	0.19	0.00	0.55	0.00	1.66	0.21	0.00	0.98	0.00
Heneicosane	0.47	0.22	1.31	0.75	0.33	2.44	0.37	1.29	1.19	0.17
Docosane	0.65	0.84	3.94	0.86	0.53	2.33	0.47	2.04	1.59	0.36
Tricosane	0.57	2.09	3.58	0.77	0.81	1.70	1.02	2.00	1.63	0.74
Tetracosane	0.23	2.21	2.28	0.43	0.79	0.80	0.91	1.53	0.89	0.60
Pentacosane	0.37	1.88	2.91	0.62	0.80	1.05	0.95	2.06	1.18	0.61
Hexacosane	0.26	1.19	1.98	0.46	0.52	0.57	0.63	1.43	0.79	0.53
Heptacosane	0.49	3.17	3.05	1.04	1.00	0.94	1.97	3.09	2.40	1.02
Octacosane	0.29	1.07	2.58	0.60	0.42	0.75	0.66	2.06	1.28	0.55
Nonacosane	3.27	6.29	13.75	7.18	2.42	3.59	4.14	21.24	22.05	2.22
Triacontane	0.60	1.66	5.31	1.66	0.72	1.57	1.13	3.62	2.66	0.83
Hentriacontane	3.09	6.00	20.21	7.75	2.28	3.97	3.98	21.01	12.47	1.61
Dotriacontane	0.38	1.25	3.73	1.16	0.47	0.84	0.82	1.99	1.81	0.71
Tritriacontane	0.77	1.21	7.36	2.13	0.55	1.20	0.98	3.17	2.61	0.60
Tetratriacontane	0.25	1.00	2.59	0.52	0.03	0.03	0.53	0.72	1.13	0.43
Pentatriacontane	0.00	0.96	1.90	0.36	0.40	0.00	0.36	0.00	0.22	0.36
Hexatriacontane	0.00	0.50	0.96	0.45	0.00	0.00	0.36	0.00	0.30	0.38
Heptatriacontane	0.00	0.00	0.00	0.00	0.00	0.00	0.00	0.00	0.23	0.00
Octatriacontane	0.00	0.00	0.00	0.00	0.00	0.00	0.00	0.00	0.29	0.17
Alkenoic Acids	RB	HA	MF	IEn	IEs	RB	HA	MF	IEn	IEs

	CTRL					HYAX				
Palmitoleic acid	0.00	0.00	0.00	0.00	0.00	0.00	0.00	0.00	0.00	0.00
Oleic acid	2.43	15.68	48.76	3.83	4.49	18.29	3.44	17.29	15.51	0.56
Linoleic acid	2.01	9.99	28.75	3.13	3.81	17.25	2.84	13.98	11.69	0.39
Linolenic acid	0.29	0.58	2.81	0.70	0.80	2.48	0.55	3.14	3.92	0.00
Octanoic acid	0.57	2.23	1.45	0.00	0.83	2.31	2.56	1.43	0.44	1.12
Decanoic acid	0.34	1.09	1.02	0.28	0.46	2.10	0.87	0.50	0.68	0.43
Dodecanoic acid	1.92	3.00	3.08	3.55	1.85	15.90	2.01	1.66	6.13	0.84
Tetradecanoic acid	5.58	8.14	37.49	10.76	7.11	36.84	5.32	20.06	19.93	3.10
Pentadecanoic acid	1.50	3.13	13.88	2.21	2.18	7.39	1.51	5.67	3.94	1.30
Palmitic acid	12.34	33.48	105.71	21.93	18.12	63.22	18.17	61.77	51.71	10.85
Heptadecanoic acid	0.75	2.15	6.24	1.13	1.15	3.68	0.91	3.47	2.51	0.71
Stearic acid	5.56	14.08	41.72	7.34	7.63	23.08	6.38	20.91	18.58	4.86
Nonadecanoic acid	0.60	1.85	4.29	0.74	0.77	2.92	0.71	2.15	1.43	0.53
Eicosanoic acid	2.83	7.63	26.48	5.23	5.31	10.73	3.63	11.84	10.11	2.59
Heneicosanoic acid	0.92	2.51	7.45	1.49	1.62	3.55	1.22	3.99	2.99	1.10
Docosanoic acid	5.28	15.65	42.44	8.11	9.77	21.97	6.35	20.79	16.19	5.95
Tricosanoic acid	2.12	5.68	16.15	3.14	3.46	8.16	2.61	9.53	6.24	2.53
Tetracosanoic acid	9.28	26.03	81.94	13.60	19.39	46.04	11.19	43.99	34.34	11.49
Pentacosanoic acid	0.68	1.97	5.81	1.17	1.22	3.04	1.00	3.55	2.31	0.98
Hexacosanoic acid	3.84	13.25	30.79	5.69	10.35	23.50	5.59	22.19	16.09	6.54
Heptacosanoic acid	0.35	1.40	2.62	0.83	0.69	1.17	0.74	2.12	1.54	0.66
Octacosanoic acid	3.20	19.01	23.05	7.10	6.76	11.12	7.17	24.88	15.89	5.91
Nonacosanoic acid	0.84	1.54	6.61	2.27	1.46	2.18	1.59	5.90	3.88	1.29
Triacontanoic acid	5.01	10.60	38.05	12.12	7.97	13.40	7.49	35.74	22.22	6.07
Aromatic Carboxylic As	RB	HA	MF	IEn	IEs	RB	HA	MF	IEn	IEs
Phthalic acid	0.16	0.70	0.54	0.14	0.09	1.05	0.29	0.25	0.24	0.12
Isophthalic acid	0.10	0.83	1.00	0.19	0.24	0.76	0.26	0.30	0.51	0.18
Terephthalic acid	0.23	0.81	2.00	0.12	0.25	0.56	0.42	0.38	0.38	0.19
1,2,4-Benzenetricarbo. a.	0.07	0.77	0.27	0.04	0.06	0.06	0.23	0.15	0.00	0.12
Dicarboxylic Acids	RB	HA	MF	IEn	IEs	RB	HA	MF	IEn	IEs
Succinic acid	3.41	15.03	15.63	8.07	4.78	17.50	10.26	10.33	14.68	4.59
Glutaric acid	0.70	4.90	4.32	1.16	1.14	4.23	2.03	1.88	2.36	0.67
Adipic acid	0.40	1.41	1.73	0.55	0.54	1.65	0.70	1.01	1.09	0.52
Pimelic acid	0.56	0.64	2.61	0.83	0.48	2.25	1.11	2.18	1.55	0.72
Suberic acid	0.82	1.96	4.01	1.61	1.14	3.05	1.41	3.13	2.78	1.34
Azelaic acid	2.32	6.57	12.66	5.32	4.12	9.76	4.49	10.57	10.14	4.09
Sebacic acid	0.42	0.41	1.15	0.87	0.52	0.25	0.69	1.72	1.26	0.68
2-HO-4-i.propyl Adipic a.	0.76	6.33	2.29	0.55	1.68	1.75	4.20	1.57	2.73	3.87

	CTRL					HYAX				
Sugars and Sterols	RB	HA	MF	IEn	IEs	RB	HA	MF	IEn	IEs
Levoglucozan	347	1,387	2,646	482	608	1,346	627	1,328	1,229	438
Cholesterol	0.09	0.21	1.22	0.17	0.12	0.47	0.26	0.65	0.46	0.05
Stigmasterol	0.00	0.48	3.24	0.46	0.39	0.77	0.37	1.16	1.16	0.17
b-Sitosterol	9.44	19.85	76.68	18.41	13.89	45.92	9.26	46.76	38.81	4.71
Campesterol	0.80	2.28	9.72	1.86	1.53	5.96	1.01	4.51	4.02	0.49
Stigmastanol	0.50	1.20	3.94	0.65	0.69	1.50	0.52	1.95	1.24	0.40
Resin Acids	RB	HA	MF	IEn	IEs	RB	HA	MF	IEn	IEs
Dehydroabietic acid	43.0	245.5	603.7	54.4	68.9	323.7	86.1	152.4	271.9	37.3
7-Oxodehydroabietic a.	4.03	39.59	63.12	3.23	8.12	48.70	8.81	15.08	28.37	3.42
Isopimaric acid	1.40	32.46	71.65	1.85	2.85	45.00	13.79	10.95	15.58	3.28
Pimaric acid	3.99	47.27	81.18	4.35	7.28	39.71	10.23	16.60	33.04	3.57
Sandaracopimaric acid	1.15	11.91	23.48	1.66	2.19	15.45	4.03	5.37	7.09	1.02
Abietic acid	1.95	12.46	136.94	3.67	5.16	95.46	0.94	16.56	22.07	0.26

**Table 15-A-4. Linear regression statistics of gas species' EF as function of MCE
for both fuel types.**

Gaseous Species		CTRL				HYAX			
		Slope	y-Intercept	r	p-val.	Slope	y-Intercept	r	p-val.
CO ₂	g/kg	2341	-784	0.98	0.00	1835	-305	0.95	0.00
CO	g/kg	-930	931	-1.00	0.00	-948	948	-1.00	0.00
CH ₄	g/kg	-38	37	-0.93	0.00	-28	28	-0.89	0.00
NMHC	gC/kg	-36	37	-0.86	0.00	-12	14	-0.36	0.31
Ethane	g/kg	-3.12	3.17	-0.90	0.00	-2.99	3.03	-0.89	0.00
Propane	g/kg	-1.37	1.37	-0.90	0.00	-1.71	1.69	-0.94	0.00
i-Butane	g/kg	-0.12	0.12	-0.88	0.00	-0.22	0.22	-0.96	0.00
n-Butane	g/kg	-0.35	0.36	-0.70	0.02	-0.43	0.43	-0.78	0.01
i-Pentane	g/kg	0.01	0.02	0.01	0.99	-0.04	0.06	-0.10	0.79
n-Pentane	g/kg	-0.09	0.11	-0.13	0.72	-0.16	0.16	-0.55	0.10
2-Methylpentane	g/kg	0.02	0.00	0.02	0.95	0.04	-0.03	0.17	0.63
3-Methylpentane	g/kg	0.02	-0.01	0.04	0.90	0.01	0.00	0.08	0.83
n-Hexane	g/kg	-0.07	0.07	-0.21	0.55	-0.08	0.08	-0.43	0.22
n-Heptane	g/kg	-0.04	0.04	-0.24	0.50	-0.03	0.04	-0.26	0.46
n-Octane	g/kg	-0.05	0.05	-0.45	0.19	-0.10	0.10	-0.81	0.00
Ethene	g/kg	-1.63	2.09	-0.14	0.70	-0.79	1.21	-0.15	0.69
Acetylene	g/kg	-0.95	1.12	-0.20	0.59	-0.18	0.40	-0.05	0.89
Propene	g/kg	-2.89	3.00	-0.69	0.03	-1.91	2.07	-0.57	0.08
1-Butene	g/kg	-0.54	0.57	-0.64	0.04	-0.29	0.32	-0.43	0.21
i-Butene	g/kg	-0.60	0.61	-0.86	0.00	-0.42	0.44	-0.67	0.03
trans-2-Butene	g/kg	-0.24	0.25	-0.89	0.00	-0.19	0.20	-0.76	0.01
cis-2-Butene	g/kg	-0.17	0.18	-0.88	0.00	-0.14	0.14	-0.77	0.01
1,3-Butadiene	g/kg	-0.80	0.83	-0.57	0.08	-0.11	0.18	-0.10	0.79
1-Pentene	g/kg	-0.18	0.18	-0.52	0.12	-0.09	0.10	-0.36	0.31
Benzene	g/kg	-2.14	2.25	-0.65	0.04	-1.81	1.92	-0.74	0.01
Toluene	g/kg	-2.86	2.95	-0.81	0.00	-0.83	1.00	-0.32	0.37
Ethylbenzene	g/kg	-0.38	0.39	-0.70	0.02	-0.06	0.09	-0.13	0.72
mp-Xylene	g/kg	-2.45	2.47	-0.85	0.00	0.36	-0.12	0.05	0.89
o-Xylene	g/kg	-0.35	0.36	-0.65	0.04	0.01	0.02	0.02	0.96
Isopropylbenzene	g/kg	-0.02	0.02	-0.22	0.54	0.01	0.00	0.10	0.77
Propylbenzene	g/kg	-0.09	0.09	-0.85	0.00	0.01	-0.01	0.11	0.77
3-Ethyltoluene	g/kg	-0.32	0.33	-0.82	0.00	0.11	-0.08	0.17	0.64
4-Ethyltoluene	g/kg	-0.09	0.09	-0.67	0.03	0.02	-0.02	0.20	0.58
2-Ethyltoluene	g/kg	-0.16	0.17	-0.60	0.07	0.03	-0.02	0.10	0.79
1,3,5-TMBenzene	g/kg	-0.06	0.06	-0.50	0.14	0.03	-0.03	0.28	0.44
1,2,4-TMBenzene	g/kg	-0.23	0.23	-0.67	0.03	0.08	-0.06	0.21	0.55
1,2,3-TMBenzene	g/kg	-0.59	0.58	-0.70	0.02	0.19	-0.16	0.19	0.59

Gaseous Species		CTRL				HYAX			
		Slope	y-I.cept	r	p-val.	Slope	y-I.cept	r	p-val.
CHCl ₃	mg/kg	-2.46	2.44	-0.49	0.15	1.16	-0.99	0.35	0.31
CH ₂ Cl ₂	mg/kg	-8.50	8.41	-0.73	0.01	-19.47	18.79	-0.91	0.00
C ₂ HCl ₃	mg/kg	-1.91	1.91	-0.70	0.02	0.50	-0.39	0.30	0.40
C ₂ Cl ₄	mg/kg	0.06	-0.01	0.03	0.92	1.46	-1.21	0.18	0.61
CH ₃ Cl	mg/kg	-543.33	541.38	-0.89	0.00	-471.68	472.31	-0.87	0.00
CH ₃ Br	mg/kg	-11.83	12.04	-0.87	0.00	-16.64	16.47	-0.97	0.00
CH ₃ I	mg/kg	-2.71	2.79	-0.72	0.02	1.08	-0.84	0.47	0.16
MethylNO ₃	mg/kg	9.59	-8.35	0.28	0.44	6.60	-5.48	0.36	0.31
EthylNO ₃	mg/kg	-1.47	1.54	-0.31	0.37	1.11	-0.88	0.27	0.45
i-PropylNO ₃	mg/kg	0.02	0.03	0.01	0.98	0.78	-0.67	0.37	0.28
n-PropylNO ₃	mg/kg	0.08	-0.07	0.42	0.22	0.80	-0.72	0.31	0.38
2-ButylNO ₃	mg/kg	-0.08	0.08	-0.15	0.69	-2.17	2.14	-0.56	0.09
COS	g/kg	-0.16	0.16	-0.93	0.00	-0.02	0.03	-0.26	0.47
DMS	g/kg	-0.01	0.01	-0.27	0.45	0.00	0.00	-0.03	0.93
Isoprene	g/kg	-2.54	2.54	-0.73	0.01	-0.27	0.39	-0.09	0.80
α -Pinene	g/kg	-5.40	5.38	-0.58	0.08	-0.10	0.30	-0.01	0.97
b-Pinene	g/kg	-0.14	0.15	-0.30	0.40	-0.01	0.02	-0.06	0.87
Acetic	g/kg	-15.11	14.78	-0.62	0.05	-0.57	0.86	-0.06	0.87
Formic	g/kg	-10.04	9.90	-0.69	0.02	-2.66	2.86	-0.49	0.15
Oxalic	g/kg	-1.21	1.21	-0.71	0.02	-1.74	1.73	-0.78	0.01
NH ₃	g/kg	-4.84	4.98	-0.64	0.04	-9.16	9.07	-0.72	0.02
HONO	g/kg	-7.43	7.32	-0.67	0.03	0.90	-0.64	0.16	0.66
HNO ₃	g/kg	-0.25	0.29	-0.08	0.83	0.30	-0.25	0.24	0.51
HCl	g/kg	-0.02	0.02	-0.29	0.42	0.00	0.00	0.02	0.96
SO ₂	g/kg	-0.90	0.96	-0.30	0.40	0.29	-0.19	0.14	0.69

Table 15-A-5. Linear regression statistics of PM_{2.5} species' EF as a function of MCE for both fuel types.

Main		CTRL				HYAX			
		Slope	y-I.cept	r	p-val.	Slope	y-I.cept	r	p-val.
PM _{2.5}	g/kg	-376.3	373.1	-0.74	0.01	-91.6	99.6	-0.48	0.15
OC	g/kg	-177.0	176.7	-0.79	0.01	-64.0	69.6	-0.46	0.18
EC	g/kg	1.3	-1.0	0.17	0.63	2.0	-1.3	0.09	0.81
OC1, 340C	g/kg	-103.0	102.1	-0.76	0.01	-36.6	38.9	-0.54	0.10
OC2, 500C	g/kg	-23.9	24.3	-0.77	0.01	-10.9	12.0	-0.36	0.30
OC3, 615C	g/kg	-14.0	14.1	-0.78	0.01	-6.4	6.9	-0.48	0.16
OC4, 900C	g/kg	-18.2	18.2	-0.75	0.01	-8.0	8.5	-0.52	0.12
OCp	g/kg	-17.9	18.0	-0.77	0.01	-2.2	3.3	-0.10	0.78
from IC		Slope	y-I.cept	r	p-val.	Slope	y-I.cept	r	p-val.
Acetate ⁻	mg/kg	-125.7	123.9	-0.71	0.02	-38.4	41.2	-0.50	0.14
Formate ⁻	mg/kg	-384.2	378.9	-0.68	0.03	-91.9	99.1	-0.41	0.23
Oxalate ⁻²	mg/kg	-130.8	130.5	-0.73	0.01	-29.9	36.2	-0.21	0.56
Na ⁺	mg/kg	-42.2	45.4	-0.21	0.56	130.4	-111.3	0.30	0.40
NH ₄ ⁺	mg/kg	-132.1	136.0	-0.52	0.12	-78.3	86.0	-0.41	0.24
K ⁺	mg/kg	-574.8	579.6	-0.62	0.05	114.4	-47.4	0.06	0.87
Mg ⁺⁺	mg/kg	-48.3	47.8	-0.64	0.04	1.9	-0.9	0.11	0.76
Ca ⁺⁺	mg/kg	-190.6	187.8	-0.65	0.04	-7.6	9.3	-0.19	0.60
F ⁻	mg/kg	-391.3	387.0	-0.73	0.01	-59.9	68.2	-0.25	0.48
Cl ⁻	mg/kg	-1073.5	1075.1	-0.63	0.05	-167.8	214.1	-0.15	0.68
SO ₄ ⁻	mg/kg	-288.8	292.7	-0.66	0.03	-255.4	267.2	-0.41	0.23
NO ₃ ⁻	mg/kg	-696.1	695.6	-0.75	0.01	-2.0	36.9	0.00	0.99
from XRF		Slope	y-I.cept	r	p-val.	Slope	y-I.cept	r	p-val.
Al	mg/kg	-47.4	47.2	-0.66	0.03	-1.1	13.2	0.00	1.00
Si	mg/kg	-120.0	117.4	-0.63	0.05	8.8	-6.3	0.25	0.48
S	mg/kg	-243.6	243.6	-0.69	0.03	-14.5	26.0	-0.05	0.89
Cl	mg/kg	-980.0	986.6	-0.62	0.05	-58.3	113.7	-0.05	0.90
K	mg/kg	-551.6	557.9	-0.63	0.05	149.9	-78.3	0.08	0.84
Ca	mg/kg	-434.6	425.1	-0.62	0.05	5.1	0.7	0.03	0.94
Mn	mg/kg	-4.0	3.9	-0.57	0.08	1.3	-0.9	0.06	0.87
Fe	mg/kg	-15.0	14.7	-0.65	0.04	-2.7	3.3	-0.15	0.67
Zn	mg/kg	-80.0	81.4	-0.49	0.14	12.5	-7.0	0.13	0.72
As	mg/kg	-16.4	16.1	-0.62	0.05	-0.9	1.1	-0.20	0.58
Se	mg/kg	-5.5	5.6	-0.62	0.05	1.3	-0.7	0.10	0.78
Pb	mg/kg	-47.7	46.7	-0.59	0.07	1.7	-1.3	0.13	0.72

		CTRL				HYAX			
ICP-MS		Slope	y-I.cept	r	p-val.	Slope	y-I.cept	r	p-val.
Li	mg/kg	-0.27	0.28	-0.76	0.01	0.00	0.02	0.00	1.00
Mg	mg/kg	-31.2	31.0	-0.60	0.06	-1.4	2.1	-0.08	0.82
Al	mg/kg	-4.9	4.9	-0.70	0.02	-1.1	3.3	-0.01	0.98
K	mg/kg	-593.7	598.7	-0.61	0.06	102.1	-35.6	0.06	0.88
Ca	mg/kg	-209.2	206.8	-0.61	0.06	-22.4	24.4	-0.40	0.25
Ti	mg/kg	0.00	0.00	0.00	0.99	-0.06	0.06	-0.61	0.06
Cr	mg/kg	-0.07	0.07	-0.43	0.21	-0.01	0.01	-0.09	0.81
Mn	mg/kg	-2.11	2.12	-0.62	0.05	-0.05	0.20	-0.01	0.98
Fe	mg/kg	-0.28	0.28	-0.63	0.05	-0.18	0.20	-0.14	0.71
Ni	mg/kg	-0.53	0.54	-0.23	0.52	-0.11	0.13	-0.11	0.76
Cu	mg/kg	-0.05	0.06	-0.18	0.62	0.38	-0.32	0.23	0.52
Zn	mg/kg	-68.9	70.3	-0.40	0.24	9.1	-4.4	0.11	0.76
As	mg/kg	-0.17	0.17	-0.71	0.02	-0.17	0.17	-0.82	0.00
Se	mg/kg	-0.16	0.17	-0.31	0.37	0.05	-0.03	0.09	0.80
Rb	mg/kg	-1.75	1.75	-0.68	0.03	0.17	-0.04	0.05	0.89
Sr	mg/kg	-0.58	0.58	-0.63	0.05	0.03	-0.01	0.08	0.83
Cd	mg/kg	-0.96	0.97	-0.65	0.04	0.10	-0.04	0.08	0.83
Sb	mg/kg	-0.03	0.03	-0.60	0.06	0.00	0.00	0.05	0.89
Ba	mg/kg	-0.91	0.91	-0.63	0.05	-1.81	1.77	-0.71	0.02
Pb	mg/kg	-20.2	19.7	-0.58	0.07	0.1	0.0	0.02	0.95

Table 15-A-6. Linear regression statistics of POC species' EF as a function of MCE for both fuel types.

		CTRL				HYAX			
PAH		Slope	y-I.cept	r	p-val.	Slope	y-I.cept	r	p-val.
Fluoranthene	mg/kg	-18.2	18.4	-0.63	0.05	-2.5	3.6	-0.07	0.84
Acephenanthrylene	mg/kg	-9.9	9.8	-0.63	0.05	-0.9	1.3	-0.06	0.86
Pyrene	mg/kg	-17.7	17.8	-0.63	0.05	-2.6	3.7	-0.08	0.82
Benz(a)anthracene	mg/kg	-9.7	9.7	-0.72	0.02	-0.1	0.6	-0.01	0.98
Chrysene	mg/kg	-11.2	11.2	-0.72	0.02	-0.5	1.2	-0.03	0.92
Coronene	mg/kg	-1.1	1.1	-0.62	0.05	0.1	0.0	0.05	0.90
Benzo(b)fluoranthene	mg/kg	-6.7	6.8	-0.71	0.02	-0.5	0.9	-0.06	0.86
Benzo(k)fluoranthene	mg/kg	-6.2	6.2	-0.70	0.02	-0.3	0.7	-0.04	0.92
Benzo(j)fluoranthene	mg/kg	-2.5	2.5	-0.66	0.03	0.1	0.0	0.03	0.93
Benzo(a)pyrene	mg/kg	-7.0	6.9	-0.70	0.02	-0.5	0.8	-0.05	0.88
Benzo(e)pyrene	mg/kg	-4.5	4.5	-0.68	0.03	-0.6	0.8	-0.10	0.77
Perylene	mg/kg	-2.1	2.1	-0.68	0.03	0.0	0.1	-0.01	0.98
Indeno(1,2,3-cd)pyrene	mg/kg	-4.1	4.2	-0.68	0.03	0.1	0.2	0.02	0.96
Dibenz(ah)anthracene	mg/kg	-1.8	1.8	-0.59	0.07	0.1	-0.1	0.07	0.85
Benzo(GHI)perylene	mg/kg	-3.8	3.8	-0.68	0.03	-0.7	0.9	-0.15	0.68
Cyclopenta(cd)pyrene	mg/kg	-6.3	6.3	-0.65	0.04	-0.3	0.6	-0.04	0.91
Benzo(GHI)fluoranthene	mg/kg	-1.5	1.6	-0.22	0.55	0.4	0.0	0.05	0.90
1-Methylchrysene	mg/kg	0.0	0.0	-0.02	0.97	0.3	-0.3	0.17	0.63
Retene	mg/kg	-2,090	2,055	-0.55	0.09	-721	724	-0.45	0.19
Picene	mg/kg	-1.3	1.3	-0.49	0.15	0.0	0.0	0.01	0.98
Alkanes		Slope	y-I.cept	r	p-val.	Slope	y-I.cept	r	p-val.
Eicosane	mg/kg	-0.9	1.1	-0.06	0.87	-15.0	14.6	-0.76	0.01
Heneicosane	mg/kg	-15.2	15.2	-0.60	0.06	-20.8	20.7	-0.85	0.00
Docosane	mg/kg	-32.3	32.1	-0.76	0.01	-37.4	36.8	-0.97	0.00
Tricosane	mg/kg	-28.8	29.0	-0.76	0.01	-28.1	28.1	-0.93	0.00
Tetracosane	mg/kg	-15.3	15.8	-0.57	0.08	-10.6	11.2	-0.56	0.09
Pentacosane	mg/kg	-23.8	24.0	-0.79	0.00	-14.0	14.5	-0.69	0.02
Hexacosane	mg/kg	-15.9	16.0	-0.80	0.00	-5.3	5.9	-0.31	0.38
Heptacosane	mg/kg	-20.3	21.2	-0.59	0.07	0.5	1.6	0.01	0.97
Octacosane	mg/kg	-19.0	19.1	-0.74	0.01	-4.7	5.7	-0.19	0.59
Nonacosane	mg/kg	-88.5	91.7	-0.55	0.09	-0.7	11.5	0.00	0.99
Triacontane	mg/kg	-38.1	38.3	-0.70	0.02	-3.8	5.8	-0.08	0.82
Hentriacontane	mg/kg	-125.8	128.4	-0.57	0.08	-8.8	18.0	-0.03	0.93
Dotriacontane	mg/kg	-26.3	26.5	-0.68	0.03	-0.4	1.9	-0.01	0.97
Trtriacontane	mg/kg	-46.7	47.0	-0.57	0.08	-0.9	2.8	-0.02	0.96
Tetratriacontane	mg/kg	-16.6	16.7	-0.61	0.06	1.9	-1.1	0.09	0.80
Pentatriacontane	mg/kg	-11.2	11.4	-0.51	0.12	2.9	-2.4	0.16	0.65
Hexatriacontane	mg/kg	-9.0	8.9	-0.50	0.13	3.3	-2.7	0.18	0.62

		CTRL				HYAX			
Heptatriacontane	mg/kg	0.0	0.0	0.00	1.00	0.9	-0.7	0.13	0.72
Octatriacontane	mg/kg	0.0	0.0	0.00	1.00	1.7	-1.5	0.20	0.58
Alkenoic Acids		Slope	y-I.cept	r	p-val.	Slope	y-I.cept	r	p-val.
Palmitoleic acid	mg/kg	0.0	0.0	0.00	1.00	0.0	0.0	0.00	1.00
Oleic acid	mg/kg	-429.5	423.2	-0.72	0.02	-71.9	78.1	-0.32	0.37
Linoleic acid	mg/kg	-235.0	233.3	-0.77	0.01	-30.8	37.5	-0.14	0.69
Linolenic acid	mg/kg	-14.9	15.3	-0.30	0.40	-3.5	5.2	-0.06	0.88
Octanoic acid	mg/kg	-12.6	13.0	-0.43	0.21	1.2	0.8	0.02	0.95
Decanoic acid	mg/kg	-8.7	9.0	-0.69	0.03	-6.3	6.9	-0.25	0.47
Dodecanoic acid	mg/kg	-41.6	42.9	-0.48	0.15	-48.1	49.7	-0.36	0.31
Tetradecanoic acid	mg/kg	-306.1	306.2	-0.77	0.01	-189.8	195.2	-0.54	0.10
Pentadecanoic acid	mg/kg	-119.7	118.6	-0.76	0.01	-80.2	79.9	-0.89	0.00
Palmitic acid	mg/kg	-802.1	803.3	-0.77	0.01	-410.0	430.4	-0.50	0.14
Heptadecanoic acid	mg/kg	-51.7	51.5	-0.79	0.01	-32.6	33.2	-0.73	0.01
Stearic acid	mg/kg	-329.4	329.1	-0.79	0.01	-178.9	184.5	-0.61	0.06
Nonadecanoic acid	mg/kg	-36.8	36.7	-0.81	0.00	-23.8	24.1	-0.84	0.00
Eicosanoic acid	mg/kg	-216.1	215.4	-0.79	0.01	-98.9	101.7	-0.66	0.04
Heneicosanoic acid	mg/kg	-60.7	60.7	-0.80	0.00	-36.0	36.8	-0.76	0.01
Docosanoic acid	mg/kg	-366.5	365.5	-0.81	0.00	-235.6	237.8	-0.84	0.00
Tricosanoic acid	mg/kg	-134.0	133.8	-0.82	0.00	-68.5	70.9	-0.66	0.04
Tetracosanoic acid	mg/kg	-729.0	724.2	-0.79	0.01	-587.2	586.0	-0.93	0.00
Pentacosanoic acid	mg/kg	-46.5	46.5	-0.79	0.01	-24.2	25.2	-0.64	0.04
Hexacosanoic acid	mg/kg	-274.4	274.4	-0.79	0.01	-291.4	291.0	-0.93	0.00
Heptacosanoic acid	mg/kg	-17.3	17.7	-0.65	0.04	-6.2	7.2	-0.24	0.49
Octacosanoic acid	mg/kg	-111.3	118.8	-0.38	0.28	-63.3	74.3	-0.22	0.53
Nonacosanoic acid	mg/kg	-51.2	51.5	-0.76	0.01	-9.4	12.2	-0.12	0.73
Triacontanoic acid	mg/kg	-269.9	272.9	-0.69	0.02	-50.1	66.0	-0.11	0.76
Aromatic Carboxylic As		Slope	y-I.cept	r	p-val.	Slope	y-I.cept	r	p-val.
Phthalic acid	mg/kg	-4.5	4.6	-0.54	0.11	-2.8	3.1	-0.25	0.49
Isophthalic acid	mg/kg	-9.5	9.5	-0.66	0.03	-7.4	7.4	-0.75	0.01
Terephthalic acid	mg/kg	-17.8	17.6	-0.63	0.05	-5.4	5.6	-0.38	0.28
1,2,4-Benzenetricarbo. a.	mg/kg	-2.9	3.0	-0.26	0.46	-3.8	3.8	-0.36	0.30
Dicarboxylic Acids		Slope	y-I.cept	r	p-val.	Slope	y-I.cept	r	p-val.
Succinic acid	mg/kg	-135.3	138.6	-0.71	0.02	-57.7	67.3	-0.20	0.57
Glutaric acid	mg/kg	-38.4	39.1	-0.63	0.05	-17.6	19.1	-0.29	0.41
Adipic acid	mg/kg	-14.9	15.1	-0.80	0.00	-14.2	14.5	-0.63	0.05
Pimelic acid	mg/kg	-18.5	18.7	-0.66	0.04	-16.8	17.7	-0.48	0.15
Suberic acid	mg/kg	-30.1	30.6	-0.77	0.01	-28.7	29.8	-0.64	0.04
Azelaic acid	mg/kg	-95.5	97.5	-0.78	0.01	-67.2	72.3	-0.50	0.13

		CTRL				HYAX			
Sebacic acid	mg/kg	-9.4	9.7	-0.48	0.15	-12.9	13.3	-0.55	0.10
2-HO-4-i.propyl Adipic a.	mg/kg	-23.7	24.8	-0.29	0.41	-24.2	27.4	-0.18	0.62
Sugars and Sterols		Slope	y-I.cept	r	p-val.	Slope	y-I.cept	r	p-val.
Levoglucozan	mg/kg	-21,472	21,553	-0.82	0.00	-6,175	6,918	-0.30	0.39
Cholesterol	mg/kg	-8.5	8.5	-0.65	0.04	-2.4	2.6	-0.30	0.39
Stigmasterol	mg/kg	-16.7	16.8	-0.42	0.22	0.8	0.0	0.04	0.92
b-Sitosterol	mg/kg	-561.4	564.3	-0.70	0.02	-82.5	105.9	-0.13	0.72
Campesterol	mg/kg	-68.3	68.4	-0.69	0.03	-11.2	13.6	-0.16	0.65
Stigmastanol	mg/kg	-31.6	31.5	-0.77	0.01	-6.3	7.2	-0.32	0.36
Resin Acids		Slope	y-I.cept	r	p-val.	Slope	y-I.cept	r	p-val.
Dehydroabietic acid	mg/kg	-5,421	5,345	-0.65	0.04	-2,396	2,447	-0.60	0.07
7-Oxodehydroabietic a.	mg/kg	-621	612	-0.64	0.04	-350	351	-0.69	0.03
Isopimaric acid	mg/kg	-695	681	-0.60	0.07	-318	317	-0.74	0.01
Pimaric acid	mg/kg	-791	779	-0.61	0.06	-218	228	-0.42	0.23
Sandaracopimaric acid	mg/kg	-224	221	-0.67	0.03	-74	77	-0.62	0.05
Abietic acid	mg/kg	-1,244	1,212	-0.61	0.06	-129	140	-0.16	0.66

[This page intentionally left blank.]

Appendix 15-B
List of Scientific/Technical Presentations

Appendix 15-B

List of Scientific/Technical Presentations

- Baumann, K., J.J. Schauer, D.R. Blake, S.R. Mitchell, N.L. Christensen, J.M. Fort, and E.S. Edgerton. 2012. In situ Measurements of Gas and Fine Particle Species Emissions from Prescribed Burning of Differently Treated Fuels in the Southeastern United States. Presented at the Air Quality Measurement Methods and Technology Conference of the Air & Waste Management Association, Durham, NC. April 24–26.
- Baumann, K., J.J. Schauer, D.R. Blake, S.R. Mitchell, J.M. Fort, and E.S. Edgerton. 2011. Gas and Fine Particle Species Emissions from Prescribed Burning in Managed Forests of the Southeastern United States. Presented at the 10th Annual Community Multiscale Air Quality Conference, Friday Center in Chapel Hill, NC. October 24–26.
- Baumann, K., B.K. Gullett, J. Aurrell, D.R. Blake, A.L. Robinson, J.M. Fort, and E.S. Edgerton. 2011. Chemical Character of Prescribed Burning Emissions at the Ground and Above the Canopy of Managed Forests in the Southeastern United States. Presented at the 30th Annual Conference of the American Association for Aerosol Research, Orlando, FL. October 3–7.
- Baumann, K., J.J. Schauer, D.R. Blake, S.R. Mitchell, W.P. Robarge, J.M. Fort, and E.S. Edgerton. 2011. Primary and Secondary PM Emissions from Prescribed Burning of Differently Treated Fuels in Managed Forests. Presented at the 43rd Annual Air Pollution Workshop and International Symposium, Fort McMurray, Alberta, Canada. May 23–26.
- Baumann, K., J.M. Fort, J.J. Schauer, D.R. Blake, S.R. Mitchell, W.P. Robarge, B.E. Hartsell, and E.S. Edgerton. 2010. Gaseous and Particulate Emissions from Prescribed Burning of Differently Treated Fuels in Managed Forests of Marine Corps Base Camp Lejeune. Presented at the 15th Strategic Environmental Research and Development Program (SERDP) and Environmental Security Technology Certification Program Partners in Environmental Technology Symposium, Washington DC. November 30–December 2.
- Baumann, K., J.M. Fort, J.J. Schauer, D.R. Blake, B.E. Hartsell, and E.S. Edgerton. 2010. Gaseous and Particulate Species Emissions from Different Forest Management Strategies Employing Prescribed Burning. Presented at the 29th Annual Conference of the American Association for Aerosol Research, Portland, OR. October 25–29.
- Baumann, K., S.R. Mitchell, W.P. Robarge, J.M. Fort, J.J. Schauer, D.R. Blake, B.E. Hartsell, and E.S. Edgerton. 2010. Gaseous and Particulate Emissions from Prescribed Burning in Pine Dominated Forest Ecosystems of the Southeastern United States. Presented at the 103rd Annual Conference and Exhibition of the Air and Waste Association, Calgary, Alberta, Canada. June 22–25.

Chapter 16

Nitrogen Deposition to Terrestrial and Aquatic Ecosystems

SERDP Project Number: RC-1413

Atmospheric Module

Research Project Air-2

Lead Researcher:

Dr. Wayne P. Robarge
North Carolina State University
Raleigh, NC
E-mail: wayne_robarge@ncsu.edu

May 10, 2013

Final

This report was prepared under contract to the U.S. Department of Defense (DoD) Strategic Environmental Research and Development Program (SERDP). The publication of this report does not indicate endorsement by DoD, nor should the contents be construed as reflecting the official policy or position of DoD. References herein to any specific commercial product, process, or service by trade name, trademark, manufacturer, or otherwise, do not necessarily constitute or imply its endorsement, recommendation, or favoring by DoD.

Table of Contents

List of Acronyms	16-vi
Abstract.....	16-1
Objectives of the Research Project	16-2
Objectives	16-2
Hypothesis.....	16-2
Background	16-2
Methods and Materials.....	16-4
Rainfall Amounts—Manual Rain Gauge Units	16-4
Rainfall Amounts—Tipping Bucket Gauge Units.....	16-4
Wet Deposition—N Deposition.....	16-5
N Loading to Forest Floor—Throughfall	16-5
Statistical Analyses	16-6
Results and Discussion	16-7
Rainfall Amounts	16-7
Wet Deposition—N Deposition.....	16-11
N Loading to Forest Floor—Throughfall	16-17
Nitrogen Loading to MCBCL.....	16-22
Conclusions and Implications for Future Research	16-25
Temporal and Spatial Trends in N Deposition	16-25
DON in Wet Deposition.....	16-26
Magnitude and Long-Term Temporal Trends in N Deposition.....	16-27
Baseline Estimate of N Deposition to Assess Local Remobilization During PBs	16-27
Literature Cited	16-29
Appendix 16-A Supporting Data	16-A-1
Appendix 16-B List of Scientific Publications	16-B-1

List of Figures

16-1.	Distribution of MDN, MRG, TP, and throughfall (TF) sampling locations across MCBCL along with the location of meteorological monitoring stations located at Risley Pier (RIP), Marine Corps Air Station (MCA), Sandy Run Observation Tower (SRT), and Sandy Run Forestry Offices (SRG).	16-6
16-2.	Average monthly rainfall amounts collected using MRGs dispersed across MCBCL.....	16-8
16-3.	Surface projections of monthly rainfall amounts based on TPs deployed across MCBCL for the period July–December 2008.....	16-9
16-4.	Surface projections of rainfall amounts based on TPs deployed across MCBCL for the periods September 1–26, 2010, and September 27–30, 2010.	16-10
16-5.	Comparison of seasonal averages of wet deposition of total N, NO ₃ -N and NH ₄ -N for the period July 2009–June 2011 at MCBCL to wet deposition data from NTN collector NC29 for the period 2003–2011.	16-11
16-6.	Comparison of seasonal averages of the percent of organic-N in TN and the percent of NH ₄ -N for the sum of DIN in wet deposition at MCBCL for the period July 2009–June 2011 to the percent of NH ₄ -N for the sum of DIN derived from wet deposition data for NTN collector NC29 for the period 2003–2011.	16-13
16-7.	Comparison of seasonal averages of wet deposition of Cl ⁻ , Na ⁺ , and SO ₄ ²⁻ for the period July 2009 June 2011 at MCBCL to wet deposition data from NTN collector NC29 for the period 2003–2011.	16-14
16-8.	Percent distribution of wind direction and rainfall amounts (30 degree arcs) averaged across three locations for winter (Quarter [Q]1), spring (Q2), summer (Q3) and winter (Q4) for the period December 2008–November 2010.	16-14
16-9.	Comparison of seasonal averages of wet deposition of Ca ²⁺ , Mg ²⁺ , and K ⁺ for the period July 2009–June 2011 at MCBCL to wet deposition data from NTN collector NC29 for the period 2003–2011.	16-15
16-10.	Seasonal differences in net throughfall for total N, NO ₃ -N and NH ₄ -N for three individual forested canopies (longleaf pine, mixed pines & hardwoods, hardwoods) calculated as the difference between throughfall and wet deposition as measured by the nearest MDN collector (MDN-3 at French Creek) at MCBCL....	16-19
16-11.	Seasonal differences in net throughfall for Cl ⁻ , Na ⁺ , and SO ₄ ²⁻ for three individual forested canopies (longleaf pine, mixed pines & hardwoods, hardwoods) calculated as the difference between throughfall and wet deposition as measured by the nearest MDN collector (French Creek) at MCBCL.....	16-20
16-12.	Seasonal differences in net throughfall for Ca ²⁺ , Mg ²⁺ , and K ⁺ for three individual forested canopies (longleaf pine, mixed pines & hardwoods, hardwoods) calculated as the difference between throughfall and wet deposition as measured by the nearest MDN collector (French Creek) at MCBCL.....	16-22

List of Tables

16-1.	Annual (December 2009–November 2010) wet deposition of N and other potential nutrient species measured at four locations across MCBCL as compared to comparable estimates derived from the NTN NC29 collector located at the Hofmann Forest, Jacksonville, NC	16
16-2.	Annual deposition (December 2009–November 2010) of N and other potential nutrient species to the forest floor under three individual forested canopies (longleaf pine, mixed pines & hardwoods, hardwoods) measured by throughfall compared to wet deposition of N and other potential nutrient species as measured by the nearest MDN collector (MDN-3 at French Creek) at MCBCL.	17
16-3.	Estimate of annual dry deposition (December 2009–November 2010) of N and other potential nutrient species to three individual forested canopies (longleaf pine, mixed pines & hardwoods, hardwoods) calculated as net throughfall: the difference between throughfall and wet deposition as measured by the nearest MDN collector (MDN-3 at French Creek) at MCBCL.	18
16-4.	Estimated annual loading from wet deposition of total N (Mean = 4.34 kg N ha ⁻¹ , Minimum = 3.70 kg N ha ⁻¹ , Maximum = 5.10 kg N ha ⁻¹) and DIN (Mean = 3.20 kg N ha ⁻¹ , Minimum = 2.80 kg N ha ⁻¹ , Maximum = 3.60 kg N ha ⁻¹) across six combined land covers at MCBCL in 2010.	23
16-5.	Estimated annual loading of total N and DIN to combined land cover classes at MCBCL for 2010 from wet and dry deposition.....	24

List of Acronyms

Ca^{2+}	calcium ion
CASTNET	Clean Air Status and Trends Network
Cl^-	chloride ion
cm	centimeter
DIN	dissolved inorganic nitrogen
DoD	U.S. Department of Defense
DON	dissolved organic nitrogen
HCl	hydrogen chloride
HNO_3	nitric acid
HOF	Hofmann Forest
HW	hardwoods (throughfall site)
JJA	June, July, and August
K^+	potassium ion
kg ha^{-1}	kilograms per hectare
$\text{kg N ha}^{-1} \text{ y}^{-1}$	kilograms of nitrogen per hectare per year
km	kilometer
L	liter
LL	longleaf pine savanna (<i>Pinus palustris</i> ; throughfall site)
MAM	March, April, and May
m^2	square meter
MARDIS	Monitoring and Research Data Information System
MCBCL	Marine Corps Base Camp Lejeune
MDN	Mercury Deposition Network
Mg^{2+}	magnesium ion
mm	millimeter
MRG	manual rain gauge (with wind screen)
MX	mixed pines and hardwoods (throughfall site)
N	nitrogen
Na^+	sodium ion
NADP	National Atmospheric Deposition Program
NH_3	ammonia
NH_4^+	ammonium ion
$\text{NH}_4\text{-N}$	total dissolved inorganic NH_4^+ expressed as N
NO_2	nitrogen dioxide
NO_2^-	nitrite

NO_3^-	nitrate
$\text{NO}_3\text{-N}$	total dissolved inorganic NO_2^- and NO_3^- expressed as N
NRE	New River Estuary
NTN	National Trends Network
PB	prescribed burn
PM	particulate matter
$\text{PM}_{2.5}$	particulate matter with a diameter less than or equal to 2.5 microns
PM_{10}	particulate matter with a diameter less than or equal to 10 microns
PO_4^{3-}	phosphate ion
Pr	detection probability for F-test
Q	quarter
r^2	r-squared value
RSD	relative standard deviation
SAS	Statistical Analysis Software
SERDP	Strategic Environmental Research and Development Program
SO_2	sulfur dioxide
SO_4^{2-}	sulfate ion
SON	September, October, and November
total N	sum of DON and DIN
TP	tipping bucket rain gauge
USGS	U.S. Geological Survey
V	volt

[This page intentionally left blank.]

Abstract

Long-term sustainability of our nation's military training bases is of critical importance to national security. The focus of this project was to attempt to assess and quantify the degree of atmospheric loading of nitrogen (N) and other nutrients arising from wet and dry deposition to the aquatic and terrestrial ecosystems at Marine Corps Base Camp Lejeune (MCBCL). Atmospheric deposition represents a significant source of new N to these ecosystems. Wet deposition (essentially rainfall) was measured from July 2009–June 2011 using approved solar-powered Mercury Deposition Network (MDN) Wet Deposition collectors at four locations across MCBCL. Average annual (2010) wet deposition of total N was $4.3 \pm 0.7 \text{ kg N ha}^{-1} \text{ y}^{-1}$, and for dissolved inorganic nitrogen (DIN), it was $3.2 \pm 0.4 \text{ kg N ha}^{-1} \text{ y}^{-1}$. Wet deposition of DIN at MCBCL in 2010 was comparable to the 9-year average of $3.7 \text{ kg N ha}^{-1} \text{ y}^{-1}$ calculated for the National Trends Network (NTN) collector NC29 located at the nearby Hofmann Forest, NC, location. Highest deposition of DIN wet deposition was in the summer (June, July, and August). Dissolved organic nitrogen (DON; measured as the difference between total N and DIN) in wet deposition was substantial (approximately $1 \text{ kg N ha}^{-1} \text{ y}^{-1}$), with highest percentage (approximately 40%) of inputs observed in the fall. A network of up to 28 tipping bucket rain gauges found no apparent latitudinal gradient in rainfall amounts across MCBCL due to the proximity of the nearby marine environment. There was, however, a measureable gradient in wet and dry deposition of chloride (Cl^-), sodium (Na^+), and sulfate (SO_4^{2-}) moving inland. Throughfall collectors were used to measure inputs of N and other nutrients into the forest floor under the dominant forested canopies at MCBCL: (1) longleaf pine savannah (*Pinus palustris*), (2) mixed pines and hardwoods (loblolly pine [*Pinus taeda*] and predominantly oaks [*Quercus* spp.]), and (3) hardwood (predominantly oak with unidentified deciduous understory). Inputs of total N under forested canopies were approximately 2 times greater than those observed from wet deposition alone, a substantial fraction of which appeared to be in the form of DON. Calculation of net throughfall (throughfall minus wet deposition) indicated the presence of dry deposition of $\text{NO}_3\text{-N}$ and to a lesser extent $\text{NH}_4\text{-N}$, but also loss of N from wet deposition during the summer and fall months due to interaction with the overhead canopy. N loading to different land cover classes (U.S. Geological Survey 2006 National Land Cover Database for the Conterminous United States) at MCBCL was estimated using the combined wet deposition and throughfall data. For 2010, approximately 360 metric tons of total N and approximately 210 metric tons of DIN were received at the Base. These estimates are still biased low due to the absence of measures of dry deposition of N to the New River and other waterways, to residential areas, and to grasses and shrub located within the confines of ranges at MCBCL. Agreement between measured amounts of the wet deposition of N by this project to the nearby NTN collector NC29 indicate that this amount of atmospheric loading of N to MCBCL has been relatively constant for at least the past 10 years.

Keywords: Wet deposition, dry deposition, throughfall, net throughfall, tipping bucket gauge, Mercury Deposition Network collector, DIN, DON, sea salt aerosols, manual rain gauge, rainfall, atmospheric N loading.

Objectives of the Research Project

Objectives

1. To assess the magnitude and temporal and spatial trends in nitrogen (N) deposition (both wet and dry deposition) to the vegetative canopies and underlying soil-groundwater ecosystem across Marine Corps Base Camp Lejeune (MCBCL).
2. To provide baseline estimates of N deposition to contrast to local remobilization and deposition of N as the result of prescribed burning within the confines of MCBCL.
3. To estimate the fraction of dissolved organic nitrogen (DON) prevalent in wet deposition occurring at MCBCL.
4. To estimate the magnitude and long-term temporal trends in N-deposition (wet deposition) to surrounding aquatic ecosystems at MCBCL.

Hypothesis

1. Atmospheric deposition (both wet and dry) represents the dominant source of new N (dissolved inorganic nitrogen and DON) into the terrestrial and aquatic ecosystems of MCBCL. Local influences and national trends in N emissions to the atmosphere suggest that N-loading may continue to increase with time at MCBCL, having a direct impact on the sustainability of the terrestrial and aquatic ecosystems.

Background

Airborne transport crosses watershed and state boundaries. Any impact observed on the habitats of interest must take into account sources of airborne pollutants transporting into and depositing on the area (via wet and dry deposition), as well as sources within Marine Corps Base Camp Lejeune (MCBCL) and subsequent transport of locally derived airborne pollutants. The New River Estuary (NRE), MCBCL, and surrounding coastal waters lie directly east of Sampson and Duplin Counties, NC, which have the highest density of confined animal operations in the United States (McCulloch et al., 1998). Ammonia emissions from these operations have impacted rainfall chemistry in the region (Walker et al., 2000b) and increased nitrogen (N) deposition up to 80 km away (Walker et al., 2000a), which is within range of the NRE, MCBCL, and surrounding waters.

The vegetative cover of the terrestrial ecosystem at the MCBCL represents a large surface area that promotes atmospheric deposition. Atmospheric deposition, in turn, represents an input into both the terrestrial and aquatic ecosystems. Nutrients and pollutants from atmospheric deposition are incorporated into internal nutrient cycles within the respective ecosystems at the Base, exerting their influence on various time scales, depending on the nature of the ecosystem itself and activities undertaken by MCBCL to optimize its primary training mission. The proximity of MCBCL to the near-coastal environment adds another level of complexity because the presence of marine-derived sea salt aerosols imposes a natural gradient of deposition across the Base and also exerts an influence on atmospheric transformations not typically encountered further inland (Andreae et al., 1986; O'Dowd et al., 1997).

Except for N fixation by native plant species, inputs from migrating wildlife, and nutrient release from soil weathering, atmospheric deposition represents the only source of new nutrients into the terrestrial ecosystems at the MCBCL. The amount, composition, and frequency of inputs are necessary to assess the sustainability of current terrestrial ecosystems and to determine long-term sustainability in regards to native flora and fauna, as well as the training mission of MCBCL. Wet deposition can be estimated from rainfall records or measured directly, whereas dry deposition (which may be equal to or exceed wet deposition) must be estimated from on-site measurements. Changes in forest management (such as thinning and clear cutting) will have direct impacts on atmospheric deposition and nutrient inputs. The short-term capabilities of forests to retain nutrients from atmospheric deposition will be influenced by the frequency and acreage of prescribed burns (PBs) and by conversion of current forested stands to meet the existing environmental and training goals of MCBCL.

Measurements of wet deposition are usually expressed in units of mass of a chemical species per unit area per unit time. Determination of mass in wet deposition requires knowledge of both the chemical composition and quantity (volume) of rainfall using collectors of known surface area (mass of chemical species A per unit time = concentration of chemical species A \times volume of rainfall collected per unit time). Extrapolation of single point measurements of rainfall amounts and chemical composition to broader areas can be improved upon by deployment of more collectors and/or deployment of devices dedicated solely to measuring rainfall amount. The costs of chemical analysis of collected rainfall and of individual rainfall collectors limit the practicality of deployment of large numbers of standard wet deposition collectors. It is more cost effective to decrease the uncertainty in wet deposition across a broader area by deployment of lower cost devices dedicated to measuring solely rainfall amounts. The magnitude of wet deposition is thus addressed by selection of point measurements of rainfall composition times the volume of wet deposition over a given area as derived from data from a number of lower cost devices dedicated to measuring rainfall amounts.

Wet deposition as rainfall occurs as discrete events of varying duration. The temporal resolution of rainfall events will increase in cost with the attempt to determine intra- and inter-variability in rainfall composition and amount. In the United States, the standard duration selected by the National Trends Network (NTN; formerly the National Atmospheric Deposition Program; NADP, 2000) to characterize wet deposition is 1 week (7 days). This temporal protocol was adopted by this project to generate a dataset consistent with the NTN program, facilitating comparison of data generated by this project to NTN collectors located within North Carolina. The point measurements of rainfall composition and amount were supplemented by a network of devices dedicated to measuring solely rainfall amounts positioned along transects across MCBCL at approximately the same distance from the ocean as the corresponding rainfall collector. This design was used to assess whether distinct spatial patterns in rainfall amounts exist across MCBCL at different time scales (minimum 1 week) due to its proximity to the marine environment.

Chemical characterization of the composition of wet deposition included dissolved organic nitrogen (DON), which was derived as the difference between total N (the sum of DON and dissolved organic nitrogen [DIN] and DIN in wet deposition. The importance of organic N species in wet deposition has been substantiated by a growing body of research and is now considered a widespread phenomenon (Neff et al., 2002). Initial reports by Whitall and Paerl

(2001) in North Carolina suggested DON on average could account for 30% of the N in wet deposition. Current monitoring of the composition of wet deposition in the United States excludes estimates of DON, suggesting that calculated atmospheric inputs of N loading in rainfall are biased low. This study contributes to further our understanding of both the magnitude and temporal nature of the loading of DON in wet deposition to the aquatic and terrestrial ecosystems at MCBCL.

Dry deposition of atmospheric species to terrestrial canopies was estimated using throughfall. Vegetative canopies represent large exposed collection surfaces for dry deposition. Throughfall represents rainwater (wet deposition) that has interacted with the vegetative canopy. Measurement of the chemical composition of throughfall represents the mass (flux) of soluble nutrients entering the underlying soil-groundwater ecosystem (Böhlmann et al., 2005; Thimonier et al., 2005). Correction for the mass of nutrients in wet deposition (net throughfall) provides an indirect measure of dry deposition of nutrients to the overhead vegetative canopy, which is subsequently washed off during rain or fog events. Measurement of throughfall offers a robust means to measure deposition that has been used in long-term forest ecosystem research (e.g., Swiss Long-Term Forest Ecosystem Research Programme; Schmitt et al., 2005) and in urban and rural environments (Balestrini et al., 2007; Böhlmann et al., 2005; Juknys et al., 2007).

The magnitude of dry deposition will be expressed the same as wet deposition (mass of chemical species per unit area per unit time). The temporal resolution selected is 1 week to be consistent with the measurements of wet deposition. Results from the throughfall measurements under forested canopies combined with the measured wet deposition provide a measure of the magnitude of the total annual loading of N to the confines of MCBCL when combined with geographic information systems-based distributions of different land cover classes at the Base.

Methods and Materials

Rainfall Amounts—Manual Rain Gauge Units

NovaLynx Standard manual rain gauges (MRGs; Model 260-2510) with tripod support (Model 260-2510S) and a windscreen (Model 260-953) were used to provide an accurate measurement of rainfall amount. A total of six MRGs with accompanying windscreens were deployed (**Figure 16-1**) and operated from July 2008–June 2011. Four of these MRGs were co-located with the NTN-approved Mercury Deposition Network (MDN) collectors. A seventh MRG (i.e., MRG7 in **Figure 16-1**) was monitored that was already in use at MCBCL near the Forestry/Wildlife Building (#464) in Greater Sandy Run. This MRG did not have an accompanying windscreen. Rainfall amounts collected on a weekly basis were calculated based on the total mass of rainfall collected divided by the cross-sectional area of the collection surface for a MRG unit.

Rainfall Amounts—Tipping Bucket Gauge Units

Twenty-eight tipping bucket (TP) rain gauges (Model RG3-M HOBO® Data Logging Rain Gauge–Metric Data Logger, Onset Computer Corp.) were eventually deployed across MCBCL from July 2008 to October 2010 (**Figure 16-1**). The accompanying battery operated event loggers were downloaded typically every 3 weeks, but were capable of storing data for extended periods (months) should training activities prevent access to a particular TP unit. When

appropriate, missing data for a TP unit due to a mechanical or logger failure was extrapolated by averaging inputs from the nearest TP units to complete the individual TP datasets. Extrapolated data has been appropriately flagged in the final delivered datasets (i.e., stored in MARDIS). Six TP units were collocated with MRGs to provide calibration data to determine the systematic bias associated with TP units, which are known to underestimate wet deposition. The resulting derived relationship (**Figure 16-A-1, Appendix A**) was used to correct all rainfall estimates derived from the TP units.

Wet Deposition—N Deposition

Four NTN-approved MDN-style collectors (N-CON Systems Company, Inc., Crawford, GA) were used to collect samples of rainfall events at four locations across MCBCL (**Figure 16-1**). Each collector was powered using a combination of an 80-Watt solar panel, 1,000-Watt DC-AC inverter, and two deep-cycle 12-volt marine batteries. All heater circuits within the MDN collector were disconnected, as were the internal fans. Each MDN collector had an accompanying MRG and TP unit to provide information on the week's rainfall total and the number and intensity of rainfall events that comprise the week's rainwater sample (**Figure 16-A-2, Appendix A**). Each collector had a 2-L collection vessel, which provided a sampling capacity of 152.4 mm of rainwater. Samples were analyzed for pH, soluble cations (i.e., ammonium [NH_4^+], magnesium [Mg^{2+}], calcium [Ca^{2+}], sodium [Na^+], and potassium [K^+]; WMO, 2004a), soluble anions (i.e., phosphate [PO_4^{3-}], chloride [Cl^-], nitrite [NO_2^-], nitrate [NO_3^-], sulfate [SO_4^{2-}]; WMO, 2004b), and total N (ASTM, 2008). Sample collection began in July 2009 and ended in May 2011. Initially, a preservative was not used for rainwater collection. Starting in April 2010, thymol (2-isopropyl-5-methylphenol; CAS# 89-83-8) was added to containers to prevent potential microbial destruction of NH_4^+ and DON in the captured rainwater. All results for rainwater analyses were reviewed for potential bird fecal matter contamination, which was evident when sample pH greater than 6 with excessive concentrations of DON, NH_4^+ , and PO_4^{3-} . When found, weekly values for these parameters were replaced by extrapolated values from the remaining MDN collectors deemed not to have been influenced by bird fecal matter. Suspect data has been appropriately flagged in the final delivered datasets (i.e., stored in MARDIS).

N Loading to Forest Floor—Throughfall

Wet deposition to the forest floor under three representative canopies, LL—longleaf pine savannah (*Pinus palustris*); MX—mixed pines and hardwoods (predominately loblolly pine [*Pinus taeda*] and oaks [*Quercus* spp.]); and HW—hardwoods (predominately oaks with unidentified mixed deciduous understory), at MCBCL was determined using throughfall collectors. Three throughfall sites were established (one per each representative forest canopy) using 12 collectors per site (**Figure 16-1**). Each collector assembly consisted of a wooden stand (1-m height) with an attached plastic funnel (25.4 cm in diameter). The funnel was connected by a short section of large-diameter Tygon® tubing to a 10-L plastic jerry can with an accompanying spigot. Both the Tygon tubing and jerry cans are wrapped in opaque duct tape or painted black to block out light (**Figures 16-A-3 and 16-A-4, Appendix A**). Plastic mesh was placed over the funnel to minimize the impact of forest litter on sample collection. Samples were collected weekly to coincide with the collection of MDN rainfall samples and were analyzed for pH, soluble cations (i.e., NH_4^+ , Mg^{2+} , Ca^{2+} , Na^+ , K^+ ; WMO, 2004a), soluble anions (Cl^- , NO_2^- , NO_3^- , SO_4^{2-} ; WMO, 2004b), and total N (ASTM, 2008). Initially, a preservative was not added to the

Statistical Analyses

16-6

[Pr] value 0.076); however, it is recognized that the preponderance of zeros added to the dataset does challenge the typical assumption of normality within the data.

The possibility of a low order polynomial surface effect within the TP data for 2010 was investigated by creating two continuous location variables for each TP unit ($xlat = 100 \times [latitude - 34.5]$; $xlong = 100 \times [longitude - 77.5]$). This was done to avoid artifacts in the analysis and matrix manipulations when using the latitude and longitude of the location of each TP unit across MCBCL. Inclusion of the TP units as a CLASS variable with the newly generated variables demonstrated that all the variability in the dataset was captured in the xlong variable, excluding the need for the TP units, latitude or latitude x longitude cross products or their higher powers from further analysis. Removal of these lack-of-fit terms resulted in the final analysis displayed in **Table 16-A-2 (Appendix A)**. The analysis suggests the presence of a low order polynomial surface as a function of longitude (i.e., moving across MCBCL [e.g., parallel to the coast], rather than moving inland from east to west. This longitudinal gradient may have been driven in part by substantial rain events like Tropical Storm Nicole (September 27–29, 2010) that resulted in a marked uneven distribution of rainfall across MCBCL over a single or several day period.

Results and Discussion

Rainfall Amounts

Rainfall amounts were measured using MRGs at seven locations across MCBCL from July 2008 to June 2011 (**Figure 16-1**). Expressed as monthly summaries, the variation in rainfall collected among the different locations was relatively minor, being the lowest during the winter months and the highest during the summer months or with extreme events (e.g., Tropical Storm Nicole at the end of September 2010) (**Figure 16-2**). The driest periods during 2008–2011 were during the first 6 months of the year when typically less than 30% of the rainfall for the year was recorded. Rainfall amounts increased after June. The apparent driest months observed were April and October 2010 and May and June 2011.

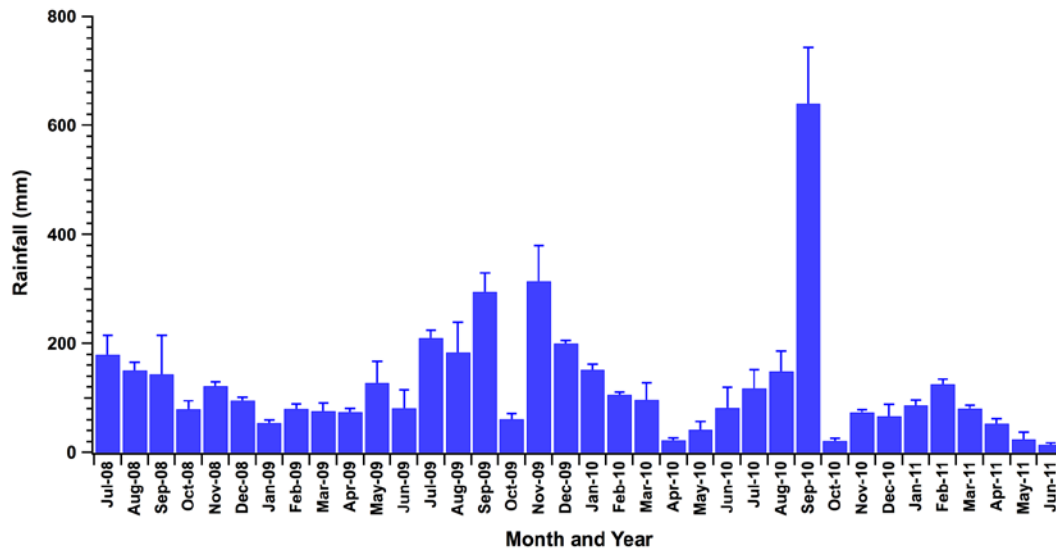


Figure 16-2. Average monthly rainfall amounts collected using MRGs dispersed across MCBCL.

Error bars represent one standard deviation.

Spatial variation in rainfall amounts was further investigated at MCBCL using a network of TPs (**Figure 16-1**). Monthly summaries were prepared in 6-month blocks. The monthly summaries for July–December 2008 are shown in **Figure 16-3**. The remaining summary plots are provided in the **Appendix A (Figures 16-A-5 through 16-A-8)**.

The patterns revealed by the TPs across MCBCL are consistent with the magnitude of the standard deviations provided in **Figure 16-2** associated with the MRGs. For example, for September 2008, the uncertainty around the mean monthly estimate generated by the MRGs is the largest observed in 2008. This is consistent with the actual rainfall pattern across MCBCL, where rainfall totals differed by 50–100 mm, depending on location (**Figure 16-3**). In December 2008, variations in monthly rainfall amounts across MCBCL were much less, generally less than 15 mm. This general pattern is repeated in 2009–2011 (**Figures 16-A-5 through 16-A-8, Appendix A**). Statistical analysis among the TP units failed to detect a latitudinal gradient indicating that the presence of the nearby marine environment at MCBCL is not having a consistent positive or negative influence on observed rainfall patterns.

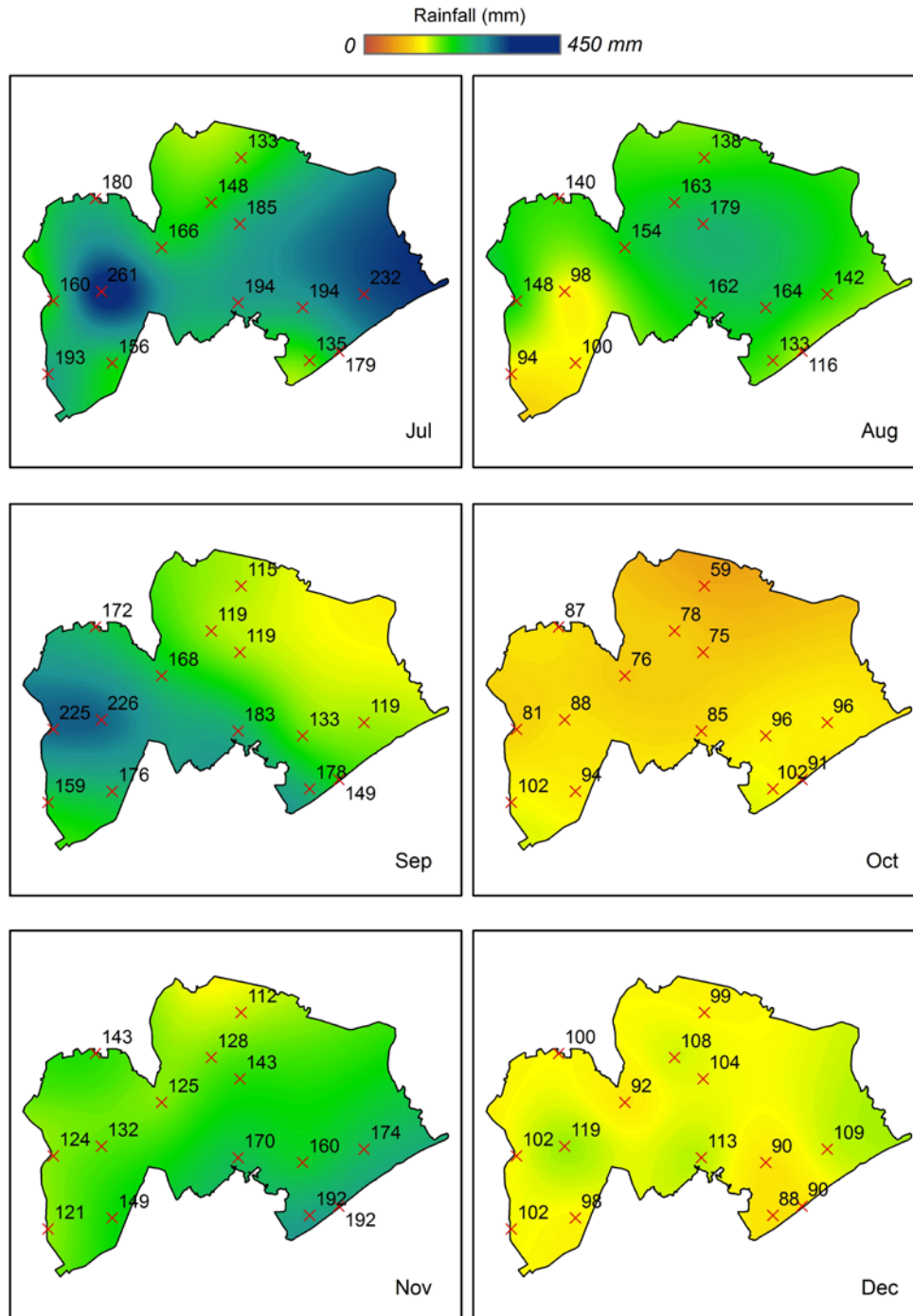


Figure 16-3. Surface projections of monthly rainfall amounts based on TPs deployed across MCBCL for the period July–December 2008.

The location of each TP is marked with an X along with monthly total rainfall amount (mm) recorded at that location.

Comparison of total rainfall amounts in 2009 (1,725 mm \pm 2.5% relative standard deviation [RSD]) and 2010 (1,560 mm \pm 8.7% RSD) suggest that rainfall patterns were similar between years. However, closer inspection of the extreme event in September 2010 (Tropical Storm

Nicole) reveals that this single event accounted for between 20–30% of the rainfall recorded for 2010 (**Figure 16-4**).

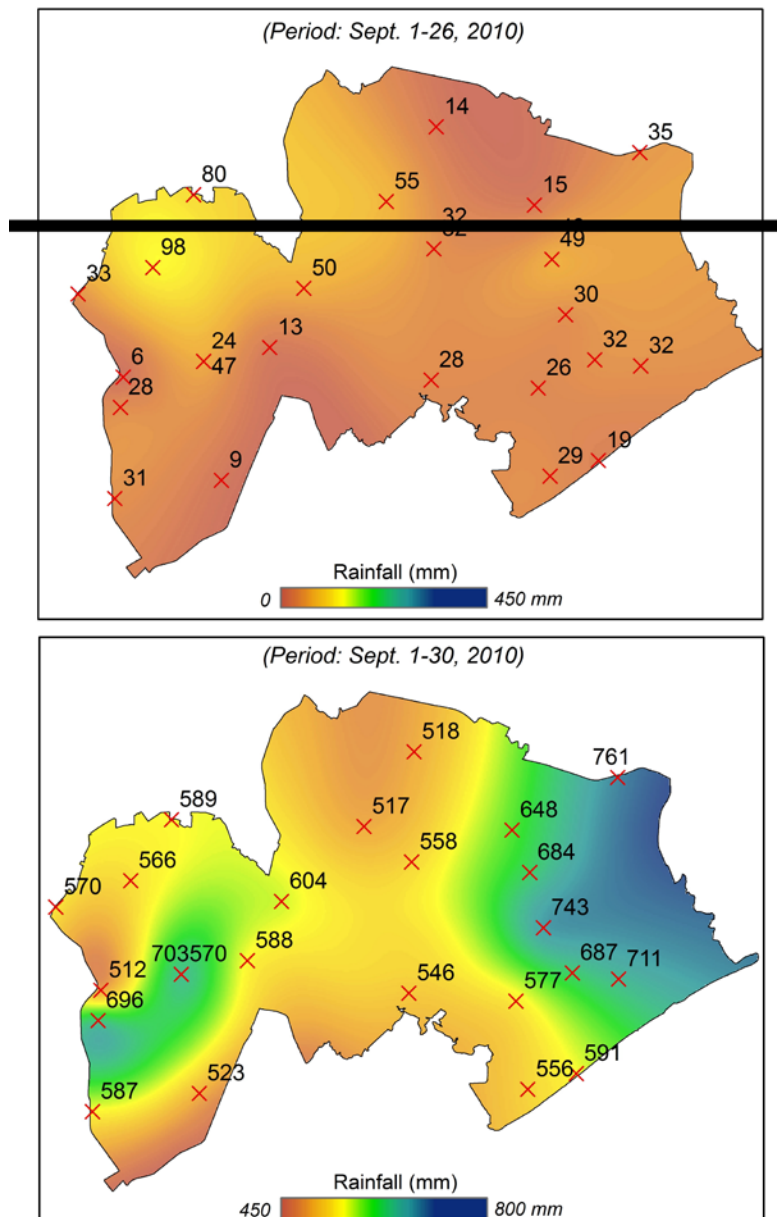


Figure 16-4. Surface projections of rainfall amounts based on TPs deployed across MCBCCL for the periods September 1–26, 2010, and September 27–30, 2010.

The location of each TP is marked with an X along with monthly total rainfall amount (mm) recorded at that location.

In the absence of Tropical Storm Nicole, the total rainfall amount for 2010 was only approximately 1,000 mm. It is also apparent from **Figure 16-4** that September 2010 was the beginning of a downward trend in rainfall amounts at MCBCCL that continued through June 2011, as compared to 2008 and 2009 (**Figure 16-2**).

Wet Deposition—N Deposition

Wet deposition of N and other potential nutrient species from rainfall was determined using four automatic MDN rainfall samplers positioned along an approximate transect across MCBCL (**Figure 16-1; Figure 16-A-9, Appendix A**). Preliminary analysis of the wet deposition data indicated no readily apparent gradient in deposition moving inland except for Cl^- and Na^+ , and possibly SO_4^{2-} . The data from all four MDN collectors was thus combined into seasonal averages to facilitate comparison of wet deposition data derived from NTN collector NC29 located at the Hofmann Forest just north of MCBCL (**Figure 16-A-9, Appendix A**). This NTN site has been in operation since 2003 and is approximately 26.5 km from the Atlantic Ocean. Seasonal summaries for the wet deposition of total N, inorganic NO_2^- and NO_3^- expressed as nitrogen ($\text{NO}_3\text{-N}$), and total dissolved inorganic NH_4^+ expressed as nitrogen ($\text{NH}_4\text{-N}$) for the period July 2009–June 2011 at MCBCL compared to the average of wet deposition of $\text{NO}_3\text{-N}$ and $\text{NH}_4\text{-N}$ for 2003–2011 measured by NTN NC29 are shown in **Figure 16-5**.

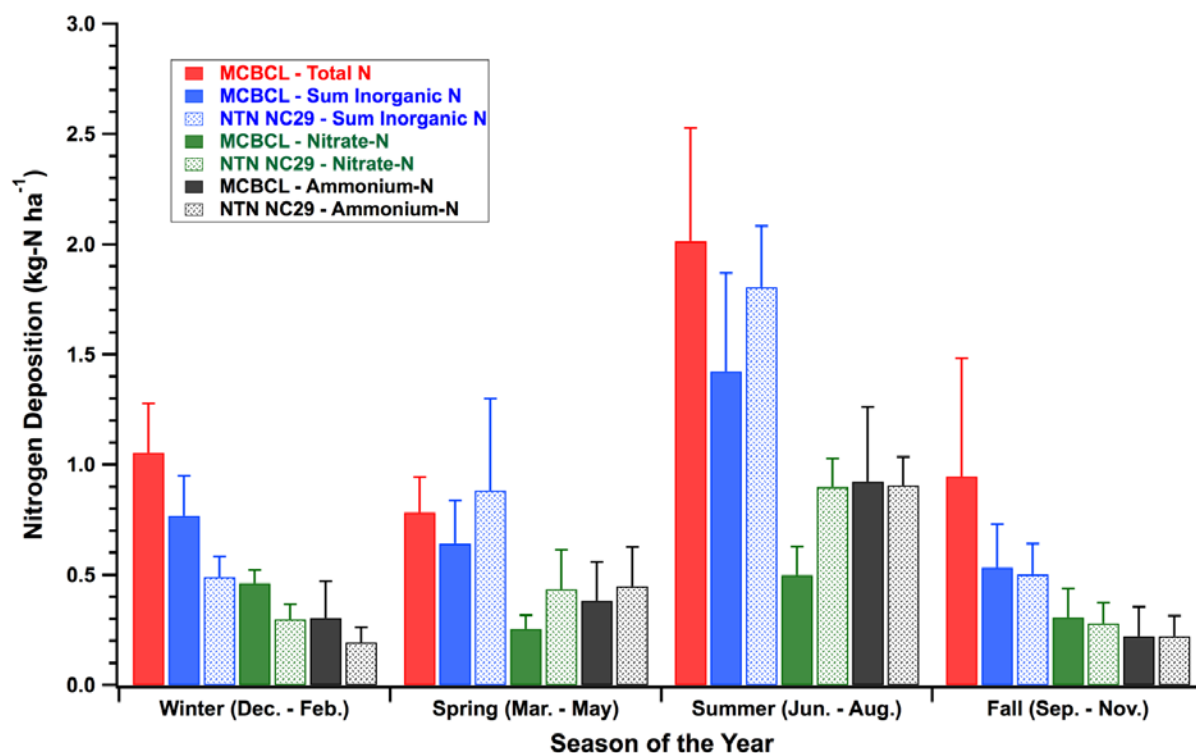


Figure 16-5. Comparison of seasonal averages of wet deposition of total N, $\text{NO}_3\text{-N}$ and $\text{NH}_4\text{-N}$ for the period July 2009–June 2011 at MCBCL to wet deposition data from NTN collector NC29 for the period 2003–2011.

Error bars represent one standard deviation.

Overall, both the relatively recent wet deposition data collected at MCBCL and the average wet deposition estimates calculated for the past 9-years' worth of observations at NTN NC29 show the same trends in N wet deposition, with many of the error bars representing one standard deviation overlapping for the N chemical species presented (**Figure 16-5**). Highest wet deposition of N is in the summer (approximately 2 kg-N ha^{-1}) and is approximately double that

of the remaining seasons of the year. Total N determined for the MCBCL MDN collectors (a total N analysis is not reported for NTN wet deposition data), is greater than the sum of DIN ($\text{NO}_3\text{-N} + \text{NH}_4\text{-N}$) during each season, suggesting a consistent presence of additional organic N in wet deposition. Similar amounts of the sum of inorganic N is observed for the fall, but the sum of DIN species appears higher at MCBCL in the winter and lower than that calculated for the 9-year average at the Hofmann Forest location for NTN NC29 in spring and summer. The larger sum of DIN during winter at MCBCL appears to be due to the presence of higher amounts of both $\text{NH}_4\text{-N}$ and $\text{NO}_3\text{-N}$. Conversely, the greater amounts of DIN calculated for NTN NC29 appears largely due to the presence of $\text{NO}_3\text{-N}$. For the spring, the calculated 9-year average sum of DIN for NTN NC29 actually exceeds the wet deposition of total N measured at MCBCL, although the error bars for both analyses overlap. At MCBCL, $\text{NO}_3\text{-N}$ appears to dominate the DIN species in wet deposition in the fall and winter seasons, whereas $\text{NH}_4\text{-N}$ is dominant in the spring and especially summer, at least for the observation period July 2009–June 2011. In general, for NTN NC29, the calculated wet deposition of $\text{NO}_3\text{-N}$ and $\text{NH}_4\text{-N}$ is approximately equal for the spring and summer months, with $\text{NO}_3\text{-N}$ being dominant in the fall and winter months.

The contribution of DON species to total N wet deposition at MCBCL was investigated further by comparing the seasonal differences in percent N contributed from DON and $\text{NH}_4\text{-N}$ (**Figure 16-6**). Percent DON in wet deposition was calculated as the difference between total N and DIN. **Figure 16-6** illustrates that DON is a significant fraction of wet deposition of N at MCBCL for each season of the year, accounting for approximately 20% or greater of the N loading to both aquatic and terrestrial ecosystems. For the period July 2009–June 2011, the contribution to N wet deposition was the highest in the fall approaching values of near 40%, although the relative uncertainty for the contribution of DON in wet deposition appears greater in the fall months as well. **Figure 16-6** also reinforces the general contributions of $\text{NH}_4\text{-N}$ in wet deposition as measured both across MCBCL and at NTN NC29 at the Hofmann Forest, as noted for **Figure 16-5**. During the fall and winter months, $\text{NH}_4\text{-N}$ is approximately 40% of the DIN in wet deposition. In the spring and summer, $\text{NH}_4\text{-N}$ accounts for 50–60+% of DIN in wet deposition.

Comparison of seasonal trends in wet deposition of Cl^- , Na^+ , and SO_4^{2-} at MCBCL for the period July 2009–June 2011 to the calculated 9-year averages from NTN NC29 is shown in **Figure 16-7**. Cl^- , Na^+ , and SO_4^{2-} exhibited distinct seasonal differences within MCBCL as compared to the 9-year calculated averages from the data collected at NTN NC29. As noted earlier, preliminary analysis of the wet deposition data for MCBCL indicated that both Cl^- and Na^+ , and to some extent SO_4^{2-} , exhibited a gradient in wet deposition moving inland (**Figure 16-1**). However, **Figure 16-7** illustrates that this gradient in deposition is highly seasonal in nature. During the fall and winter months, wet deposition of Cl^- and Na^+ , and to some extent SO_4^{2-} , is substantially higher across MCBCL than at the Hofmann Forest location of NTN NC29. However, these differences for Cl^- and Na^+ are absent for the spring and summer months when the amounts of wet deposition of these two chemical species are essentially the same within MCBCL and at the NTN NC29 site. The trend in wet deposition of SO_4^{2-} actually appears to reverse, with substantially higher amounts of wet deposition of SO_4^{2-} recorded at NTN NC29 than within MCBCL during the spring and summer months.

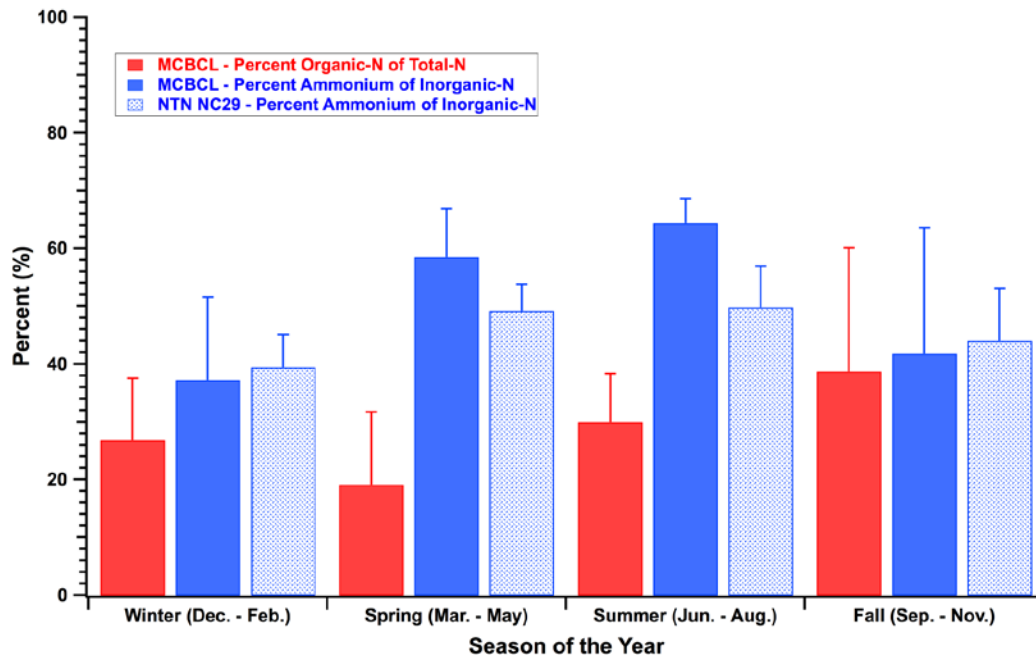


Figure 16-6. Comparison of seasonal averages of the percent of organic-N in TN and the percent of $\text{NH}_4\text{-N}$ for the sum of DIN in wet deposition at MCBCL for the period July 2009–June 2011 to the percent of $\text{NH}_4\text{-N}$ for the sum of DIN derived from wet deposition data for NTN collector NC29 for the period 2003–2011.

Error bars represent one standard deviation.

The presence of Cl^- and Na^+ in wet deposition in winter and fall suggests a marine influence due to the proximity of MCBCL to the Atlantic Ocean. A predominance of winds and rain events from the northeast, east, southeast, and south would include a contribution from the marine environment. A summary was prepared of the percent of wind direction and rain amounts for the delineated seasons of the year for the period December 2008–November 2010 (**Figure 16-8**). For the winter and fall periods, there does appear to be a substantial contribution of rain events originating from the northeast to the south, while the spring period sees more dominance of winds from the west. However, the summer period appears to have experienced a substantial period of time and rainfall amounts from storms originating from the east and southeast, even though this period recorded the lowest amounts of wet deposition of Cl^- and Na^+ . Without further analysis of individual storm events for the period December 2008–November 2010, especially during the summer months, it is not known why the summer period recorded the lowest amounts of the wet deposition of Cl^- and Na^+ for the period July 2009–June 2011. Such an analysis is outside of the scope of the current project.

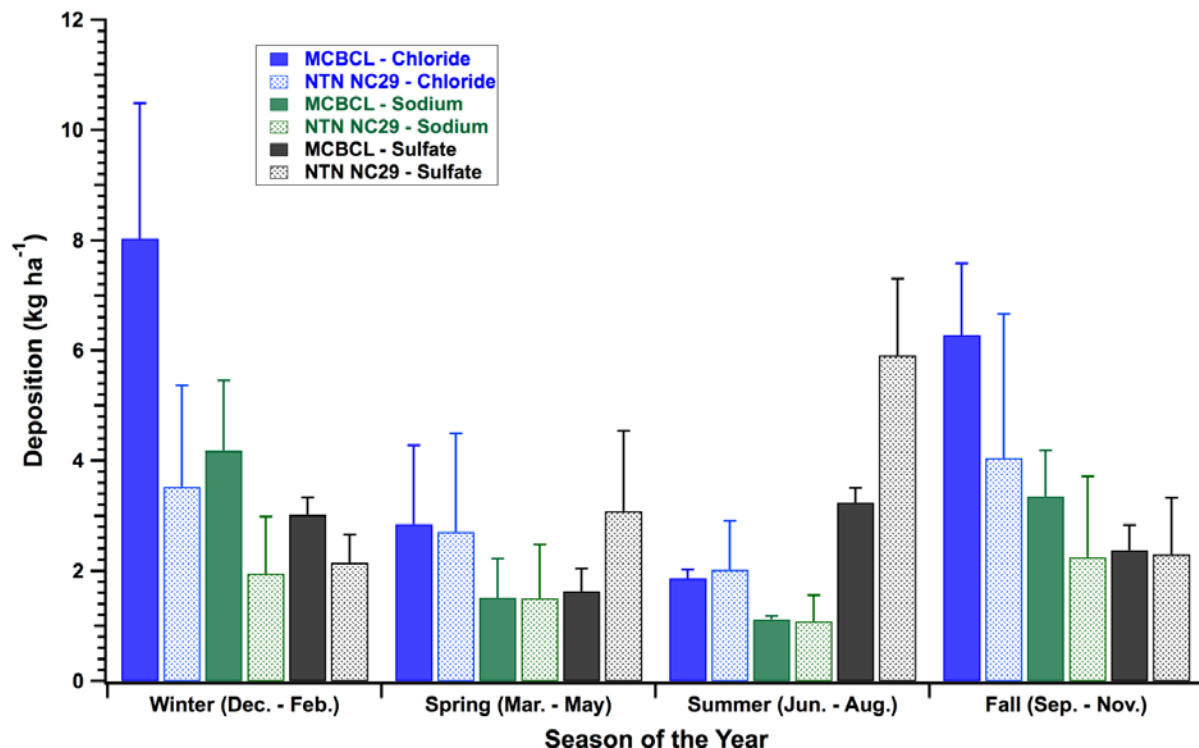


Figure 16-7. Comparison of seasonal averages of wet deposition of Cl^- , Na^+ , and SO_4^{2-} for the period July 2009 June 2011 at MCBCL to wet deposition data from NTN collector NC29 for the period 2003–2011.

Error bars represent one standard deviation.

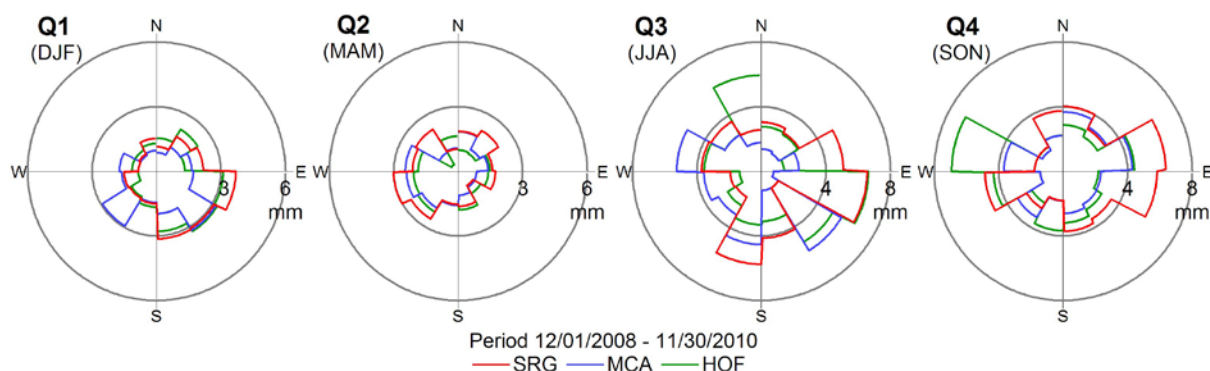


Figure 16-8. Percent distribution of wind direction and rainfall amounts (30 degree arcs) averaged across three locations for winter (Quarter [Q1], spring (Q2), summer (Q3) and winter (Q4) for the period December 2008–November 2010.

HOF = Hofmann Forest, Onslow, Co.; MCA = Marine Corps Air Station, MCBCL; SRG = Sandy Run Forestry Offices, MCBCL; DJF = December, January, February; MAM = March, April, and May; JJA = June, July, and August; SON = September, October, and November.

The apparent shift in SO_4^{2-} wet deposition during the spring and summer in **Figure 16-7** between MCBCL and the NTN NC29 location may in fact be an artifact of averaging SO_4^{2-} wet deposition data across a 9-year period (2003–2011). Nationally, trends in SO_4^{2-} wet deposition have been consistently decreasing due to regulatory actions to reduce sulfur dioxide (SO_2) emissions from industrial sources. Thus it is reasonable to expect 2009–2011 SO_4^{2-} wet deposition estimates from across MCBCL to be lower than the longer 9-year average calculated from the NTN NC29 site. For the period spring 2009–spring 2011, the calculated average SO_4^{2-} wet deposition at the NTN NC29 site is $1.5 \pm 0.7 \text{ kg SO}_4^{2-} \text{ ha}^{-1}$, which corresponds well with the values obtained at MCBCL (**Figure 16-7**). The calculated SO_4^{2-} wet deposition for the summer months for the same period (2009–2011) at NTN NC29 is $5.2 \pm 1.0 \text{ kg SO}_4^{2-} \text{ ha}^{-1}$, which is still substantially higher than that measured at MCBCL. It is not known why the NTN NC29 site continues to demonstrate higher wet deposition of SO_4^{2-} during the summer months than that obtained across MCBCL from July 2009–June 2011.

Comparison of seasonal trends in wet deposition of Ca^{2+} , Mg^{2+} , and K^+ at MCBCL for the period July 2009–June 2011 to the calculated 9-year averages from NTN NC29 is shown in **Figure 16-9**.

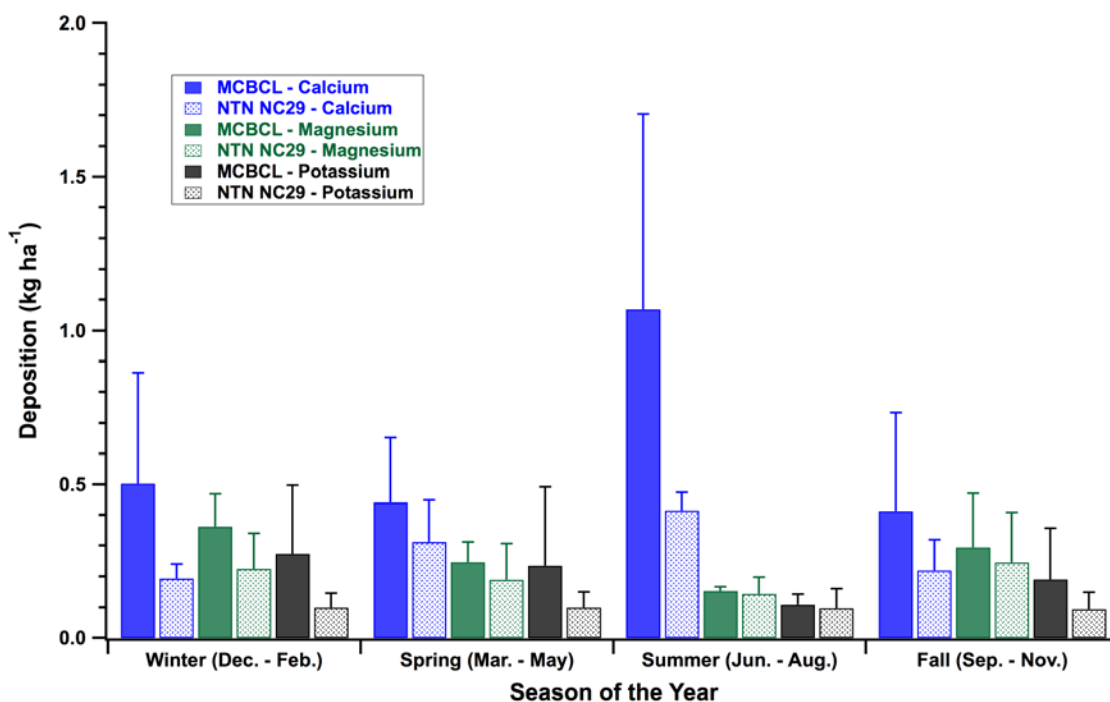


Figure 16-9. Comparison of seasonal averages of wet deposition of Ca^{2+} , Mg^{2+} , and K^+ for the period July 2009–June 2011 at MCBCL to wet deposition data from NTN collector NC29 for the period 2003–2011.

Error bars represent one standard deviation.

Calcium dominated wet deposition among the three cations, with amounts of Ca^{2+} wet deposition in the summer (approximately $1 \text{ kg Ca}^{2+} \text{ ha}^{-1}$) being approximately 2 times that observed during the remaining seasons of the year. A similar trend was mirrored in the calculated NTN NC29 data but at substantially lower absolute amounts of Ca^{2+} wet deposition (**Figure 16-9**). In

general, wet deposition of Ca^{2+} , Mg^{2+} , and K^{+} across MCBCL for the period July 2009–June 2011 was greater than the 9-year calculated wet deposition at the NTN NC29 site. The lowest amounts of the wet deposition of Mg^{2+} and K^{+} were during the summer months, when values were most similar to those derived from the NTN NC29 dataset.

A measure of the annual wet deposition of N and other potential nutrient species measured across MCBCL for 2010 (December 2009–November 2010) is provided in **Table 16-1**. Also included is comparable 2010 data for the NTN NC29 site, as well as the calculated 9-year average for the NTN NC29 site (2003–2011).

Table 16-1. Annual (December 2009–November 2010) wet deposition of N and other potential nutrient species measured at four locations across MCBCL as compared to comparable estimates derived from the NTN NC29 collector located at the Hofmann Forest, Jacksonville, NC.

Chemical Species	MDN-1 Freeman Creek (3.5 km) (kg ha ⁻¹)	MND-3 French Creek (8.1 km) (kg ha ⁻¹)	MDN-4 Sandy Run (15.6 km) (kg ha ⁻¹)	MDN-2 Golf Course (20.3 km) (kg ha ⁻¹)	2010 NTN NC29 (26.5 km) (kg ha ⁻¹)	2003–2011 NTN NC29 (26.5 km) (kg ha ⁻¹)
Total N	5.10	3.70	3.73	4.84	—	—
NH ₄ -N	1.86	1.63	1.70	1.97	1.25	1.77
NO ₃ -N	1.74	1.33	1.10	1.47	1.56	1.91
Cl ⁻	22.9	21.1	18.5	15.9	11.6	12.3
SO ₄ ²⁻	11.0	11.0	9.9	9.7	9.5	13.5
Na ⁺	12.6	11.7	10.7	9.0	6.1	6.8
K ⁺	0.45	0.37	1.25	0.48	0.32	0.40
Mg ²⁺	1.25	1.17	1.40	0.76	0.74	0.80
Ca ²⁺	1.70	1.39	4.27	1.76	0.97	1.14

Values in parentheses reflect distance inland for each sampling location (**Figure 16-A-9, Appendix A**). Total N data is not available for the NTN NC29 dataset.

Highest annual wet deposition of total N, NH₄-N, and NO₃-N was observed at the Freeman Creek (MDN-1) and Golf Course (MDN-2) sampling locations at MCBCL in 2010, whereas the French Creek (MDN-3) and Sandy Run (MDN-4) locations (both located within the middle regions of MCBCL; see **Figure 16-1**) had the lowest annual wet deposition of the three N chemical species measured. The measured wet deposition of NH₄-N and NO₃-N in 2010 was comparable to the 9-year average of the NTN NC29 location, but 2010 wet deposition of NH₄-N at this location was lower than that measured across MCBCL.

The distinct gradient in the wet deposition of Cl⁻ and Na⁺ is evident moving inland across MCBCL, with approximately 2 times the amount of deposition at Freeman Creek versus at NTN NC29 in the Hofmann Forest. In 2010, there is a slight elevation in wet deposition of SO₄²⁻ near the coast, but the values measured are actually less than the 9-year average calculated for the NTN NC29 location.

Comparison among the annual wet deposition estimates for Ca^{2+} , Mg^{2+} , and K^{+} indicates similar amounts for three of the MCBCL locations sampled. Significant higher wet deposition amounts of Ca^{2+} and K^{+} were measured at the Sandy Run (MDN-4) location, as well as a slight increase over the other MCBCL sites in the wet deposition of Mg^{2+} . The higher measured wet deposition of these three cations at the Sandy Run location may reflect the influence from wildfires in the immediate vicinity that occurred in 2010, as well as possible other unknown sources. Overall, the wet deposition of Ca^{2+} and Mg^{2+} was consistently higher across MCBCL in 2010 than measured at the NTN NC29 site. The wet deposition of K^{+} at MCBCL was actually comparable both to the 2010 data and the 9-year average for 2003–2011 for the NTN NC29 location, except for the Sandy Run site.

N Loading to Forest Floor—Throughfall

Throughfall collectors were used under three representative forested canopies at MCBCL (longleaf pine, mixed pines & hardwoods, hardwoods) to derive an indirect estimate of the contribution of dry deposition of N and other potential nutrients to the underlying forest floor. Forest canopies represent relatively large surface areas across MCBCL that can collect various gases (e.g., ammonia [NH_3], nitric acid [HNO_3], nitrogen dioxide [NO_2], hydrogen chloride [HCl]) and aerosol particulates (e.g., PM_{10} [particulate matter with a diameter less than or equal to 10 microns] and $\text{PM}_{2.5}$ [particulate matter with a diameter less than or equal to 2.5 microns]). Removal of these deposited substances by subsequent rainfall events from the surfaces of the overhead canopy represents additional loading of N and other potential nutrients to the underlying forest floor. Throughfall collection at MCBCL in this project was more limited than wet deposition and only results for 2010 (December 2009–November 2010) are presented (Table 16-2).

Table 16-2. Annual deposition (December 2009–November 2010) of N and other potential nutrient species to the forest floor under three individual forested canopies (longleaf pine, mixed pines & hardwoods, hardwoods) measured by throughfall compared to wet deposition of N and other potential nutrient species as measured by the nearest MDN collector (MDN-3 at French Creek) at MCBCL.

Chemical Species	Forest Canopy			Wet Deposition
	Longleaf Pine (kg ha^{-1})	Mixed Pines & Hardwoods (kg ha^{-1})	Hardwoods (kg ha^{-1})	French Creek (kg ha^{-1})
Total N	7.94	6.55	5.61	3.70
$\text{NH}_4\text{-N}$	1.81	0.91	1.24	1.63
$\text{NO}_3\text{-N}$	3.12	1.43	1.03	1.33
Cl^-	97.1	92.7	84.8	21.1
SO_4^{2-}	22.2	20.1	16.3	11.0
Na^+	53.3	47.2	52.1	11.7
K^+	8.58	12.7	12.2	0.37
Mg^{2+}	5.56	6.03	3.98	1.17
Ca^{2+}	13.9	10.2	9.77	1.39

Total N loading to the underlying forest floor in 2010 was approximately 2 times that measured for the closest wet deposition collector (MDN-3; see **Figure 16-1**). The majority of this enhanced N loading appears to be DON, since the loading from $\text{NH}_4\text{-N}$ and $\text{NO}_3\text{-N}$ (except for the longleaf pine stand) was similar in magnitude to inputs from wet deposition (rainfall). Loading to the forest floor of Cl^- , Na^+ , and SO_4^{2-} is substantially higher due to the presence of the overhead canopies than from direct inputs of wet deposition, as are the measured inputs of Ca^{2+} , Mg^{2+} , and K^+ . The potential contribution of N and other nutrient species from dry deposition to the forested canopies was estimated by calculating net throughfall (**Table 16-3**). Net throughfall is here defined as the difference between the measured total loading to the forest floor and an estimate of wet deposition for the chemical species of interest, the latter being obtained from the nearby wet deposition collector located at French Creek (MDN-3, **Figure 16-1**).

Table 16-3. Estimate of annual dry deposition (December 2009–November 2010) of N and other potential nutrient species to three individual forested canopies (longleaf pine, mixed pines & hardwoods, hardwoods) calculated as net throughfall: the difference between throughfall and wet deposition as measured by the nearest MDN collector (MDN-3 at French Creek) at MCBCL.

Chemical Species	Forest Canopy			Wet Deposition
	Longleaf Pine (kg ha^{-1})	Mixed Pines & Hardwoods (kg ha^{-1})	Hardwoods (kg ha^{-1})	French Creek (kg ha^{-1})
Total N	4.24	2.85	1.91	3.70
$\text{NH}_4\text{-N}$	0.18	-0.72	-0.39	1.63
$\text{NO}_3\text{-N}$	1.79	0.10	-0.30	1.33
Cl^-	76.0	71.6	63.7	21.1
SO_4^{2-}	11.2	9.1	5.3	11.0
Na^+	41.6	35.5	40.4	11.7
K^+	8.21	12.3	11.8	0.37
Mg^{2+}	4.39	4.86	2.81	1.17
Ca^{2+}	12.5	8.81	8.38	1.39

Table 16-3 illustrates that in 2010, measureable dry deposition of sources of $\text{NH}_4\text{-N}$ (NH_3) or $\text{NO}_3\text{-N}$ (HNO_3 , NO_2) appeared to be minimal and not significantly greater than inputs from wet deposition alone, except possibly for the longleaf pine stand. The longleaf pine stand was located very near a major highway intersection at MCBCL, and the enhanced $\text{NO}_3\text{-N}$ dry deposition may reflect this nearby source of emissions from passing vehicular traffic. Alternatively, failure to detect substantial amounts of dry deposition of $\text{NH}_4\text{-N}$ or $\text{NO}_3\text{-N}$ may reflect the incorporation of the source species directly into the forest canopy. The majority of total N calculated as net throughfall appears to be DON, whose magnitude appears to be a function of canopy type as well as total canopy surface area. Hardwood stands would drop leaves in the late fall and winter months, decreasing their canopy surface area. The longleaf pine stand would tend to have a more constant canopy surface area all year round. The mixed pine & hardwoods stand would have a combination of both. This enhanced presence of DON loading from the forest canopies probably

reflects a combination of the leaching of organic compounds from the leaves and bark of the individual trees as well as dry deposition of organic compounds containing N.

Seasonal variations in net throughfall calculated for total N, $\text{NO}_3\text{-N}$ and $\text{NH}_4\text{-N}$ across the three canopies are shown in **Figure 16-10**. Differences in net throughfall of total N between the three canopies remain consistent between seasons as suggested by the data in **Table 16-3**. However, the contribution of N sources to total N appears to vary with season and stand. For the longleaf pine stand, $\text{NO}_3\text{-N}$ and to some degree $\text{NH}_4\text{-N}$ contribute a substantial portion of total N in net throughfall in the winter and spring months. This contribution essentially disappears in the summer and fall where DON appears to be the dominant source of total N in net throughfall. For the mixed pines & hardwoods and hardwoods stands, there is relatively little contribution of $\text{NO}_3\text{-N}$ and $\text{NH}_4\text{-N}$ to net throughfall total N for the year, indicating that organic-N is the source of additional N being deposited to the forest floor within these canopies.

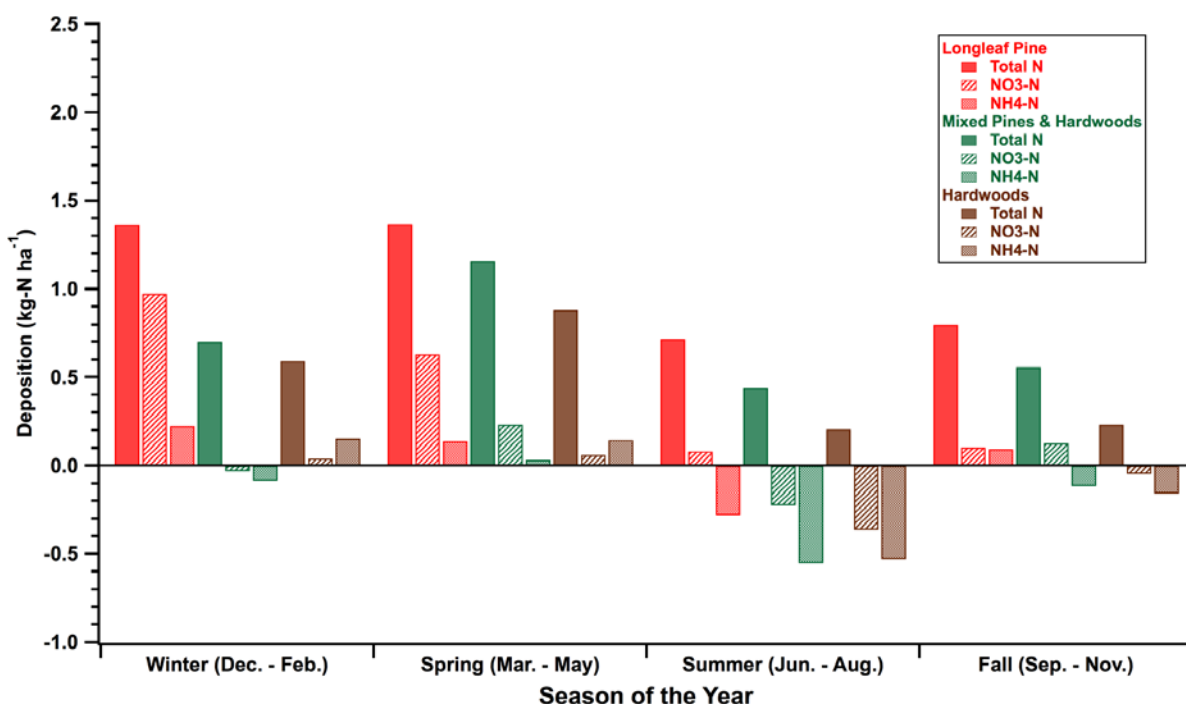


Figure 16-10. Seasonal differences in net throughfall for total N, $\text{NO}_3\text{-N}$, and $\text{NH}_4\text{-N}$ for three individual forested canopies (longleaf pine, mixed pines & hardwoods, hardwoods) calculated as the difference between throughfall and wet deposition as measured by the nearest MDN collector (MDN-3 at French Creek) at MCBCL.

As previously noted, one explanation for the presence of $\text{NO}_3\text{-N}$ in net throughfall at the longleaf pine stand during the winter and spring months is the close proximity of the stand to a major traffic intersection at MCBCL. However, traffic patterns do not deviate substantially with season at MCBCL, suggesting an alternative explanation that the calculated net throughfall for the longleaf pine stands for winter and spring 2010 represents an estimate of the contribution of dry deposition of oxidized and reduced forms of DIN species to forested canopies at MCBCL. The ability to detect the dry deposition of these sources of N over time diminishes due to the increasing interaction and retention of the dry deposited N species within the canopy. This

interaction and retention within the overhead canopy is most pronounced during the summer months, when the apparent demand for N for canopy growth removes N from rainfall as it falls through the canopy (**Figure 16-10**). There is some recovery in the fall season, although the calculated net throughfall values are within the uncertainties associated with the throughfall and wet deposition estimates. To what extent DIN species in dry deposition and retained within the canopy are released back into the measured throughfall as DON is not known.

Seasonal variations in net throughfall calculated for Cl^- , Na^+ , and SO_4^{2-} across the three canopies are shown in **Figure 16-11**.

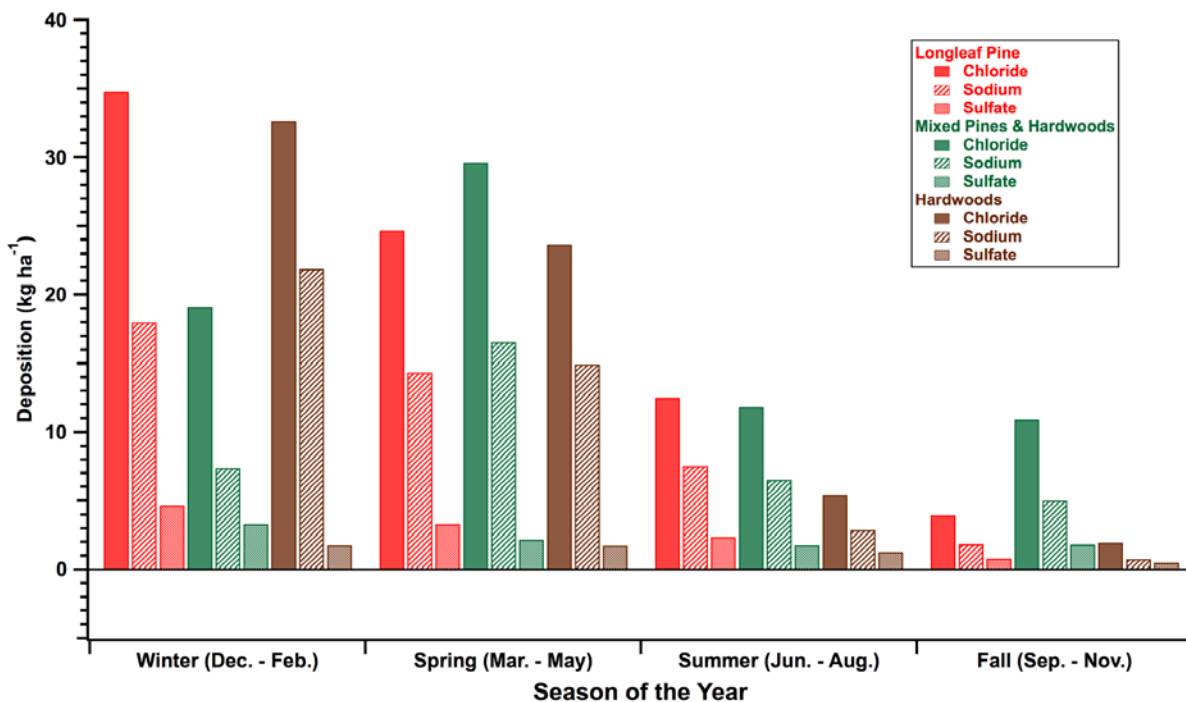


Figure 16-11. Seasonal differences in net throughfall for Cl^- , Na^+ , and SO_4^{2-} for three individual forested canopies (longleaf pine, mixed pines & hardwoods, hardwoods) calculated as the difference between throughfall and wet deposition as measured by the nearest MDN collector (French Creek) at MCBCL.

Figure 16-11 illustrates the definite seasonal trend in the dry deposition of Cl^- , Na^+ , and SO_4^{2-} as calculated by net throughfall (**Table 16-3**). For the longleaf pine and hardwoods stands, highest Cl^- , Na^+ , and SO_4^{2-} dry deposition is in the winter and the lowest is in the fall, somewhat different from that observed in wet deposition (**Figure 16-7**). Highest dry deposition of Cl^- and Na^+ within the mixed pines & hardwoods canopy is in the spring, followed by the winter and then lower but relatively constant inputs during the summer and fall. Highest dry deposition of SO_4^{2-} within the mixed pines & hardwoods canopy is in the winter months, with the values in spring declining slightly and then remaining relatively constant in summer and fall.

The data in **Figure 16-11** suggest that a local source is influencing the dry deposition of Cl^- and Na^+ because the deposition patterns vary from those in wet deposition. The most logical source for this would be sea salt aerosols generated by wave action along the beaches forming the

eastern boundary of MCBCL (**Figure 16-1**). One explanation for the apparent decline in dry deposition over the year would be the gradual shifting in dominant wind patterns, as well as changes in frequency of events generating large amounts of sea salt aerosols.

For SO_4^{2-} , sea salt aerosols constitute only one potential source of dry deposition. The other is dry deposition of SO_2 with subsequent oxidation on the canopy surfaces to form sulfates, which are then removed via subsequent rainfall events. An estimate of the potential dry deposition of $\text{SO}_2 + \text{SO}_4^{2-}$ for the coastal region occupied by MCBCL can be obtained from the Clean Air Status and Trends Network (CASTNET) site BFT142 located near Beaufort, NC, in Carteret County. According to the *2010 Annual CASTNET Report* (CASTNET, 2012), projected annual deposition to the combined sources of $\text{SO}_2 + \text{SO}_4^{2-}$ in the ambient atmosphere is approximately $1.5 \text{ kg-S ha}^{-1} \text{ y}^{-1}$. This translates to approximately $4.5 \text{ kg-SO}_4^{2-} \text{ ha}^{-1} \text{ y}^{-1}$, which is approximately 50% of the projected dry deposition of SO_4^{2-} calculated by net throughfall for the longleaf pine and mixed pines & hardwoods canopies in **Table 16-4**, and slightly less than the total projected dry deposition of SO_4^{2-} for the hardwoods canopy in 2010. This comparison suggests that sea salt aerosols are probably a significant source of dry deposition of SO_4^{2-} to forested canopies at MCBCL.

Seasonal variations in net throughfall calculated for Ca^{2+} , Mg^{2+} , and K^+ across the three canopies are shown in **Figure 16-12**. Highest values for calculated net throughfall for Ca^{2+} and K^+ for all three canopies was during the summer. Potassium is known to be highly mobile in forested canopies, being readily leached from the overhead canopies and then recycled back into the canopy foliar tissue through root uptake. A substantial portion of K^+ in the net throughfall for the three canopies, therefore, is most likely canopy-derived and does not represent substantial amounts of dry deposition of K^+ containing chemical species. Trends in calculated net throughfall for Mg^{2+} are less distinct and can reflect both dry deposition of sea salt aerosols as well as leaching and potential recycling within the forested canopy. Calcium is considered relatively immobile in foliar tissue, yet substantial amounts of Ca^{2+} are present as net throughfall, especially for the longleaf pine canopy. It is possible, therefore, that a significant amount of Ca^{2+} is being recycled within the three-forested canopies selected for observation. An alternative source of Ca^{2+} may arise from $\text{PM}_{2.5}$, as limestone forms a portion of the bedrock at MCBCL. The presence of $\text{PM}_{2.5}$ from limestone would also impact the presence of Mg^{2+} in the net throughfall. It is likely that no one source dominates the presence of Ca^{2+} and Mg^{2+} detected as net throughfall among the three forested canopies observed in 2010.

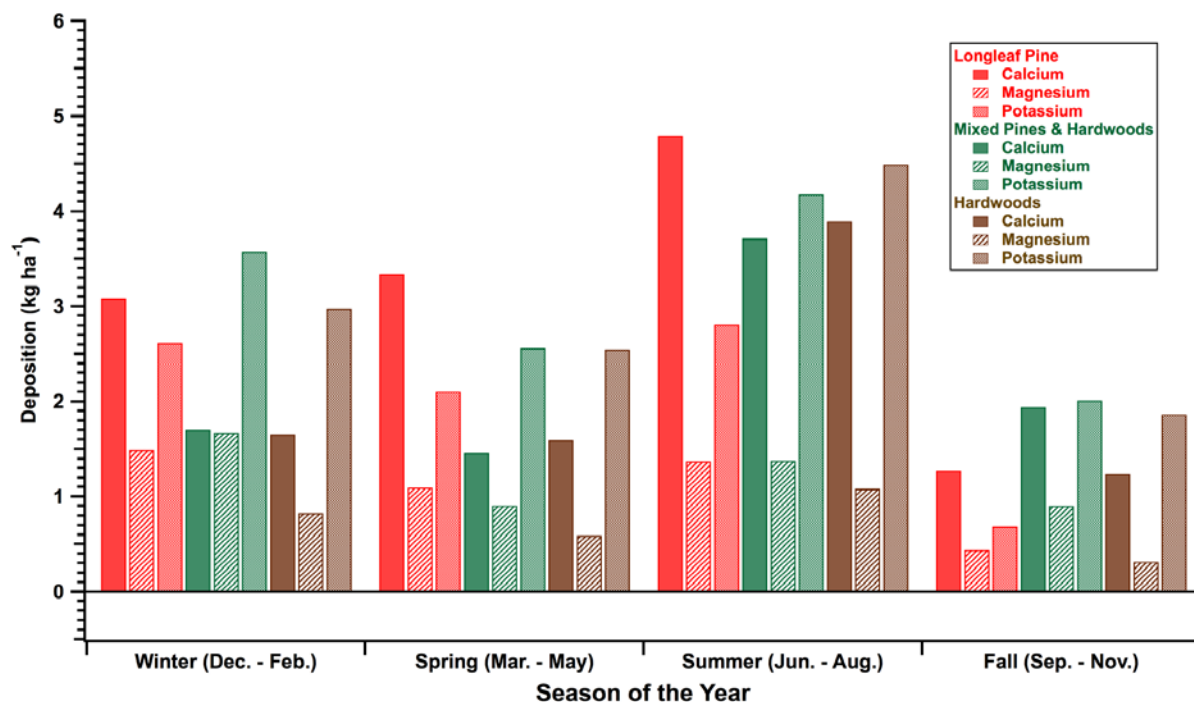


Figure 16-12. Seasonal differences in net throughfall for Ca^{2+} , Mg^{2+} , and K^{+} for three individual forested canopies (longleaf pine, mixed pines & hardwoods, hardwoods) calculated as the difference between throughfall and wet deposition as measured by the nearest MDN collector (French Creek) at MCBCL.

A consistent pattern in **Figures 16-10 through 16-12** is that, in almost all cases, the lowest amount of net throughfall calculated among the different chemical species was for the fall season. Inspection of **Figure 16-2** (and **Figure 16-A-8, Appendix A**) demonstrates that fall 2010 (September–November) contained two of the driest months (September and October 2010) observed from July 2008–June 2011, despite the occurrence of the passage of Tropical Storm Nicole at the end of September 2010. Although the amounts of rainfall delivered by Tropical Storm Nicole were excessive, they essentially were confined to a 3-day period, while the remainder of September and October 2010 experienced less than 30 mm of rainfall each month. November 2010 was relatively dry as well (**Figure 16-A-8, Appendix A**). Significantly lower amounts of rainfall over fall 2010 would result in lower amounts of canopy leaching, and perhaps result in fall 2010 being consistently low in calculated net throughfall for N and the other potential nutrient species.

Nitrogen Loading to MCBCL

N loading to various land cover classes at MCBCL was calculated for 2010 using the data synthesized in **Tables 1 and 2**. The land cover classes were drawn from the 2006 U.S. Geological Survey (USGS) National Land Cover Database for the Conterminous United States (Fry et al., 2011) and, therefore, do not reflect recent changes in land cover at MCBCL especially those associated with the “202k Grow the Force” effort. The USGS database currently lists 13 land cover classes for the area occupied by MCBCL. This number was further reduced to six land cover classes as documented in **Table 16-A-3 (Appendix A)**. These six combined land cover

designations served as the basis for calculating an estimate of N loading from atmospheric deposition.

Table 16-4 contains the calculated atmospheric loading of both total N and DIN from wet deposition in 2010 based on the data summarized in **Table 16-1**. A mean value for total N and the sum of DIN was calculated from the determined annual deposition values for each of the four MDN collectors. The minimum and maximum annual deposition values observed among the four MDN collectors were used to provide an estimate of the uncertainty.

Table 16-4. Estimated annual loading from wet deposition of total N (Mean = 4.34 kg N ha⁻¹, Minimum = 3.70 kg N ha⁻¹, Maximum = 5.10 kg N ha⁻¹) and DIN (Mean = 3.20 kg N ha⁻¹, Minimum = 2.80 kg N ha⁻¹, Maximum = 3.60 kg N ha⁻¹) across six combined land covers at MCBCL in 2010.

Combined Land Cover	Combined Area (ha)	Mean (kg N y ⁻¹)	Range	
			Minimum (kg N y ⁻¹)	Maximum (kg N y ⁻¹)
Source: Wet Deposition Total N				
Business/residential	2,714	11,800	10,000	13,800
Bare/marsh/shrub	8,677	37,700	32,100	44,200
River/stream/waterway	7,600	33,000	28,100	38,800
Pine	21,842	94,800	80,800	111,000
Mixed pine/hardwood	7,316	31,800	27,100	37,300
Hardwood	9,647	41,900	35,700	49,200
Totals	57,796	251,000	213,800	294,000
Source: Wet Deposition DIN (NO ₃ -N + NH ₄ -N)				
Business/residential	2,714	8,700	7,600	9,800
Bare/marsh/shrub	8,677	27,800	24,300	31,200
River/stream/waterway	7,600	24,300	21,300	27,400
Pine	21,842	69,900	61,100	78,600
Mixed pine/hardwood	7,316	23,400	20,500	26,300
Hardwood	9,647	30,900	27,000	34,700
Totals=	57,796	185,000	161,000	208,000

In 2010, approximately 250 metric tons of N was deposited across MCBCL in the form of wet deposition (primarily rainfall). Of this total, approximately 74% was deposited as DIN (approximately 185 metric tons), and the remainder (approximately 65 metric tons) as DON, illustrating again that a substantial percentage of N inputs to the aquatic and terrestrial ecosystems of MCBCL (approximately 26%) is organic in form. The range in wet deposition of N among the four MDN collectors used in this study provides an estimate of the uncertainty in the projected 2010 wet deposition loading of N. For total N, the range produces an uncertainty of ± approximately 40 metric tons; for DIN, the uncertainty is ± approximately 20 metric tons.

Although the estimates of the N loading from wet deposition provided in **Table 16-4** are for a single year (2010), they appear representative of the recent historical wet deposition of DIN at MCBCL. Comparison of the data in **Table 16-1** between annual wet deposition of DIN determined by the four MDN collectors deployed across MCBCL to the 9-year average calculated from NTN NC29 demonstrates excellent agreement, with values differing only by a few tenths of $\text{kg N ha}^{-1} \text{ y}^{-1}$. Thus the calculated deposition values in **Table 16-4** for DIN probably are representative of the yearly average DIN loading, at least for the past 9 years, even though 2010 was a relatively dry year (approximately 1,000 mm), excluding the one 3-day event represented by Tropical Storm Nicole. Assuming that DON has been present in wet deposition at comparable levels to that determined in 2010, terrestrial and aquatic systems at MCBCL have been receiving the equivalent of approximately 250 metric tons of N per year from wet deposition for at least the past 10 years.

Although **Table 16-4** represents N loading due to wet deposition, it does not include N loading attributed to dry deposition. This can be obtained (**Table 16-5**), at least for dominant forested canopies at MCBCL, by the inclusion of the data from **Table 16-2**. However, no estimate of uncertainty is possible because only one forested stand of each type was monitored in this study.

Table 16-5. Estimated annual loading of total N and DIN to combined land cover classes at MCBCL for 2010 from wet and dry deposition.

Combined Land Cover	Combined Area (ha)	Mean (kg N y ⁻¹)	Range	
			Minimum (kg N y ⁻¹)	Maximum (kg N y ⁻¹)
Source: Wet Deposition Total N				
Business/Residential	2,714	11,800	10,000	13,800
Bare/Marsh/Shrub	8,677	37,700	32,100	44,200
River/Stream/Waterway	7,600	33,000	28,100	38,800
Pine	21,842	173,000	—	—
Mixed Pine/Hardwood	7,316	47,900	—	—
Hardwood	9,647	54,100	—	—
Totals=	57,796	358,000	—	—
Source: Wet Deposition DIN (NO ₃ -N + NH ₄ -N)				
Business/Residential	2,714	8,700	7,600	9,800
Bare/Marsh/Shrub	8,677	27,800	24,300	31,200
River/Stream/Waterway	7,600	24,300	21,300	27,400
Pine	21,842	108,000	—	—
Mixed Pine/Hardwood	7,316	17,100	—	—
Hardwood	9,647	21,900	—	—
Totals=	57,796	207,800	—	—

Only the three forested land cover classes include an estimate of wet and dry deposition of N. The remaining land classes are estimated from wet deposition only (**Table 16-4**). Only a single estimate is available for three forested land cover classes in 2010.

Table 16-5 illustrates a modest increase in N loading of DIN due to the presence of forested canopies at MCBCL, with the total estimated input increasing to approximately 210 metric tons

of N per year as opposed to approximately 185 metric tons of N per year from wet deposition alone. There is, however, a substantial increase in total N loading due to the presence of the forested canopies with a value of approximately 360 metric tons of N per year as opposed to approximately 250 metric tons of N per year from wet deposition. This increase in total N deposition is due almost entirely to an increase in DON deposition reaching the forest floor under the forested canopies.

No estimate on dry deposition was made in this project for the combined land classes of Business/Residential, Bare/Marsh/Shrub or River/Stream/Waterway, thus the estimates of N-loading for 2010 for MCBCL in **Table 16-5** are still biased low. In addition, these estimates represent only N-loading reaching the air-land interface across MCBCL. It is not known, for example, how much of the DON measured using the throughfall collectors is in fact recycled within the forested stands on a yearly basis and, thus, does not represent new N actually introduced yearly into the forested ecosystems due to wet and dry deposition. The consistent presence of DON-containing species in wet deposition (**Figure 16-6**), however, supports the assumption that there must also be measureable amounts of dry deposition of these substances, especially to forested canopies with their relatively high surface areas. The observed increase in total N loading measured in this study (**Table 16-5**), the majority of which appears to be DON, is consistent with a yearly addition of new N across MCBCL due to substantial amounts of dry deposition of DON containing compounds to the various forested canopies.

Conclusions and Implications for Future Research

Temporal and Spatial Trends in N Deposition

No latitudinal gradient (moving east to west) in rainfall amounts was detected in this study (July 2008–July 2011) due to the proximity of the nearby marine environment. A potential longitudinal trend (parallel to the coast) in rainfall amounts may be significant, but may also be the result of several major storm events (e.g., Tropical Storm Nicole) that occurred during the study period. Overall no spatial trend was detected in DIN wet deposition, with annual loading in 2010 ($3.2 \text{ kg N ha}^{-1} \text{ y}^{-1}$) being comparable to the 9-year average ($3.7 \text{ kg N ha}^{-1} \text{ y}^{-1}$) derived for nearby NTN collector NC29 at the Hofmann Forest, NC. Differences in wet deposition among the 4 rainfall collectors used in this study (**Figure 16-1**) were more apparent for total N wet deposition (**Table 16-1**). However, total N is not reported by the NTN network, and the variations in total N among the collectors were interpreted as a measure of the uncertainty in N wet deposition within the confines of MCBCL. A distinct temporal trend in N wet deposition (**Figure 16-5**) was apparent, with summer receiving the highest inputs of N. This temporal pattern was also mirrored for DIN in the 9-year seasonal averaged calculated for the NTN NC29 site.

Net throughfall associated with three dominant forested canopies (longleaf pine, mixed pines & hardwoods, hardwoods) was used to assess trends in dry deposition of N (**Figure 16-10**). The presence of dry deposition of $\text{NO}_3\text{-N}$, and to a lesser extent $\text{NH}_4\text{-N}$, was detected in the winter and spring months. Highest dry deposition was a function of canopy coverage, with the longleaf pine stand having the highest magnitude of net throughfall for $\text{NO}_3\text{-N}$ (approximately 1 kg N ha^{-1}) and $\text{NH}_4\text{-N}$ (approximately 0.4 kg N ha^{-1}) in the winter months. Net throughfall values declined throughout the rest of the year and were negative for DIN in the summer and most of

the fall. Negative values reflect a high degree of interaction and retention of wet deposition and dry deposition of N species by the overhead canopy during the growing season. Thus, measures of dry deposition are limited to the winter months, and no estimate in the temporal trends in dry deposition of DIN was derived from this study. Total N derived from net throughfall was positive for all four seasons of the year (**Figure 16-10**). A significant fraction of this total N was DON, especially during the summer and fall months. However, it is not known to what extent the presence of DON species in net throughfall: (1) reflects the conversion of DIN from dry deposition into DON by interaction with the overhead canopy, (2) is simply the leaching of DON-containing species from the overhead canopy, or (3) is an indirect measure of the dry deposition of DON.

This study has documented that DON is a significant fraction of wet deposition at MCBCL. Reliance alone on wet deposition data being collected in the nearby Hofmann Forest by the NTN is not sufficient to quantify total N wet deposition at MCBCL. This study suggests that the %RSD associated with reliance on only one wet deposition collector located at MCBCL as a measure of total N in wet deposition would be approximately 17%. An attempt to estimate dry deposition of DIN at MCBCL in this study was limited to the dominant forested canopies and did not include other land cover classes such as waterways, residential areas, or marsh and shrub lands within ranges. Future efforts to measure temporal and spatial trends in dry deposition of N will require a more intensive combined measurement and modeling effort than was possible in this study, with emphasis on attempts to identify whether organic-N containing species constitute a significant fraction of N dry deposition. However, this study has produced an estimate of N loading to the forest floor under the dominant forested canopies at MCBCL, which include any net impact of the dry deposition of N.

DON in Wet Deposition

A significant amount of DON was detected in wet deposition in this study (**Table 16-1**). DON (determined as the difference between total N and DIN) was also a significant fraction of N-loading to the forest floor as determined using throughfall under forested canopies. The percentage of DON in wet deposition appeared to vary seasonally, with its percent contribution to rainfall being lowest in the spring (approximately 20%) and highest in the fall (approximately 40%) (**Figure 16-6**).

As noted above, future measurements that exclude total N at MCBCL will underestimate N loading via wet deposition. The uncertainty associated with this negative bias on an annual basis can range from 0.7–1.5 kg N ha⁻¹ y⁻¹ (**Table 16-1**). For throughfall the uncertainty associated is even higher ranging from 2–4 kg N ha⁻¹ y⁻¹, depending on the overhead canopy (**Table 16-3**). However, measures of DON in wet deposition are sensitive to potential sources of contamination from bird fecal matter, as well as microbial transformations and conversion of DIN to organic matter within collected samples. Care is needed to limit bird interactions with wet deposition collectors, which are usually located in open areas and do not immediately retract covers after rain events. Deployment of accompanying bird perches away from the collectors and siting collectors away from favored bird areas are highly recommended (Kelly et al., 2012). Use of a preservative, such as thymol, is also highly recommended, both for measurements of wet deposition and throughfall.

Magnitude and Long-Term Temporal Trends in N Deposition

A combination of direct measurements from this study with existing reported land cover classes for MCBCL was used to produce estimates of the magnitude of N deposition at MCBCL. In 2010, MCBCL received approximately 250 metric tons of total N and approximately 185 metric tons of DIN via wet deposition (**Table 16-4**). Inclusion of the indirect estimate of N dry deposition to the dominant forested canopies at MCBCL increases these values to approximately 360 metric tons of total N and approximately 210 metric tons of DIN in 2010 (**Table 16-5**). Implications for long-term temporal trends in N deposition at MCBCL are based on several assumptions. DIN inputs were similar to the 9-year average derived from NTN collector NC29 at the Hofmann Forest, NC (**Table 16-1**), suggesting no marked change in wet deposition of N for the past approximately 10 years. Ammonium-N is becoming a larger fraction of DIN in wet deposition, especially during the spring and summer months (**Figure 16-6**), but this trend is national in scope (Lehmann et al., 2005) and does not immediately reflect an undue influence of the relatively high density animal feeding operations (swine and poultry) located approximately due west of MCBCL in the adjacent counties of Sampson and Duplin, NC. If the assumption that the percent contribution of DON in wet deposition has remained relatively constant is valid (see e.g., Whitall and Paerl, 2001), then the figure of approximately 250 metric tons of total N is a valid approximation of the loading of N to MCBCL for at least the past 10 years, with an uncertainty of ± 40 metric tons of N.

The uncertainty associated with the N loading from both wet and dry deposition is much greater and is still biased low due to the lack of measures of N dry deposition to waterways, residential areas, and marsh and shrub areas within ranges across MCBCL. The figure of approximately 360 metric tons is also based on essentially single measurements of the three representative forested canopies measured at approximately the same location within MCBCL. It is not known to what extent there may be a gradient in N deposition to forested and other vegetative canopies across MCBCL. As detailed in **Table 16-1**, such gradients do exist for other chemical species such as Cl^- , Na^+ , and SO_4^{2-} with strong seasonal trends (**Figure 16-11**), and the presence of an overhead canopy can significantly impact the magnitude of the dry deposition of these species (**Table 16-3**). The type of overhead canopy impacts the amount of N reaching the forest floor, with coniferous canopies (i.e., longleaf pine) having higher amounts of N in throughfall reaching the underlying forest floor, than under deciduous (i.e., hardwood) canopies (**Table 16-3**). A combined measurement and modeling effort would be required to improve the uncertainty associated with the annual value of approximately 360 metric tons of N from wet and dry deposition. However, although it is apparent from this study that conversion of more forested canopies to longleaf pine at MCBCL will tend to increase net N deposition (**Table 16-2**), it is also evident that forest canopies act to buffer N inputs during several seasons of the year (especially summer) (**Figure 16-10**), when inputs from wet deposition are the highest (**Figure 16-5**).

Baseline Estimate of N Deposition to Assess Local Remobilization During PBs

Due to their relatively high surface areas, forested canopies located immediately downwind of PBs represent potential collection surfaces for gas and particulate matter (PM) emissions that occur during the flame and smoldering periods of the burns. Material collected on the overhead canopy would be subsequently incorporated into the underlying forest floor via subsequent rain

events. Net throughfall calculated as part of this study indicates that detection of local remobilization of N and other nutrients from PBs will be difficult using the simple throughfall technique (**Figure 16-10**). This is especially true for mixed pines & hardwoods and hardwood canopies, where lack of leaves may hinder capture of gas and PM released from PBs, which typically are done in late fall or winter months, or interaction within the canopy results in the loss of N in the subsequent collected throughfall. **Figure 16-10** suggests greater success may be had in longleaf pine canopies in the winter months, but background levels during this period are also high, increasing the uncertainty associated with potential measured increases in N in throughfall due to local remobilization during PBs.

This study also illustrates that measurement of other nutrients or chemical species downwind from PBs using throughfall must account for seasonal patterns in deposition (e.g., **Figures 11 and 12**) both in wet and dry deposition, as well as losses from the forest canopies themselves. Antecedent periods between the last significant rainfall and the PB can also have a significant impact on the ability to detect measureable increases in throughfall above baseline. The datasets generated as part of this study can be used to investigate further the uncertainty in weekly throughfall measurements for N and other nutrient species for future studies that attempt to measure local remobilization during PBs.

Literature Cited

- ASTM (American Society for Testing and Materials). 2008. Standard D5176-08, Standard test method for total chemically bound nitrogen in water by pyrolysis and chemiluminescence detection. ASTM International, West Conshohocken, PA.
- Andreae, M.O., R.J. Charlson, F. Bruynseels, H. Storms, R. van Grieken, and W. Maenhaut. 1986. Internal mixture of sea salt, silicates, and excess sulfate in marine aerosols. *Science* 27:1620–1623.
- Balestrini, R., S. Arisci, M.C. Brizzio, R. Mosello, M. Rogora, and A. Tagliaferri. 2007. Dry deposition of particles and canopy exchange: Comparison of wet, bulk and throughfall deposition at five forest sites in Italy. *Atmospheric Environment* 41(4):745–756.
- Böhlmann, N., R. Meissner, S. Bernsdorf, F. Boehme, R. Russow, and U. Wegener. 2005. Studies of atmospheric nitrogen deposition in a mire of the German National Park Hochharz Mountains using two different methods. *Water, Air, & Soil Pollution* 168:17–32.
- CASTNET (Clean Air Status and Trends Network). 2012. *2010 Annual Report*. U.S. Environmental Protection Agency, Washington, DC. EPA Contract No. EP-W-09-028. Available at http://epa.gov/castnet/javaweb/docs/annual_report_2010_v2.pdf. Accessed July 2012.
- Fry, J., G. Xian, S. Jin, J. Dewitz, C. Homer, L. Yang, C. Barnes, N. Herold, and J. Wickham. 2011. Completion of the 2006 National Land Cover Database for the conterminous United States. *Photogrammetric Engineering and Remote Sensing* 77(8):858–864.
- Juknys, R., J. Zaltauskaite, and V. Stakenas. 2007. Ino fluxes with bulk and throughfall deposition along an urban-suburban-rural gradient. *Water, Air, & Soil Pollution* 178:363–372.
- Kelly, V.R., K.C. Weathers, G.M. Lovett, and G.E. Likens. 2012. A comparison of two collectors for monitoring precipitation chemistry. *Water, Air, & Soil Pollution* 223:951–954.
- Lehmann, C.M.B., V.C. Bowersox, and S. Larson. 2005. Spatial and temporal trends of precipitation chemistry in the United States, 1985–2002. *Environmental Pollution* 135(3):347–361.
- McCulloch, R.B., G.S. Few, G.C. Murray Jr., and V.P. Aneja. 1998. Analysis of ammonia, ammonium aerosols and acid gases in the atmosphere at a commercial hog farm in eastern North Carolina, USA. *Environmental Pollution* 102:263–268.
- NADP (National Atmospheric Deposition Program). 2000. *Instruction Manual: NADP/NTN Site Selection and Installation*. Available at <http://nadp.sws.uiuc.edu/lib/manuals/siteinst.pdf>.

- Neff, J.C., E.A. Holland, F.J. Dentener, W.H. McDowell, and K.M. Russell. 2002. The origin, composition and rates of DONitrogen deposition: A missing piece of the nitrogen cycle? *Biogeochemistry* 57/58:99–136.
- O'Dowd, C.D., M.H. Smith, I.E. Consterdine, and J.A. Lowe. 1997. Marine aerosol, sea-salt, and the marine sulphur cycle: A short review. *Atmospheric Environment* 31:73–80.
- Schmitt, M., L. Thoni, P. Waldner, and A. Thimonier. 2005. Total deposition of nitrogen on swiss long-term forest ecosystem research (LWF) plots: Comparison of the throughfall and the inferential method. *Atmospheric Environment* 39:1079–1091.
- Thimonier, A., M. Schmitt, P. Waldner, and B. Rihm. 2005. Atmospheric deposition on Swiss long-term forest ecosystem research (LWF) plots. *Environmental Monitoring and Assessment* 104:81–118.
- Walker, J.T., D. Nelson, and V.P. Aneja. 2000a. Trends in ammonium concentration in precipitation and atmospheric ammonia emissions at a Coastal Plain site in North Carolina, USA. *Environmental Science and Technology* 34:3527–3534.
- Walker, J.T., V.P. Aneja, and D. Dickey. 2000b. Atmospheric transport and wet deposition of ammonium in North Carolina, USA. *Atmospheric Environment* 34:3407–3418.
- Whitall, D.R., and H.W. Paerl. 2001. Spatiotemporal variability of wet atmospheric nitrogen deposition to the Neuse River Estuary, North Carolina. *Journal of Environmental Quality* 30(5):1508–1515.
- WMO (World Meteorological Organization). 2004a. *Manual for the GAW [Global Atmosphere Watch] Precipitation Chemistry Programme: Guidelines, Data Quality Objectives and Standard Operating Procedures*. Edited by M.A. Allan. Prepared by the GAW Precipitation Chemistry Science Advisory Group. Pp. 48–50 in Section 4.4.4, Cation Determination by Ion Chromatography.
- WMO (World Meteorological Organization). 2004b. *Manual for the GAW [Global Atmosphere Watch] Precipitation Chemistry Programme: Guidelines, Data Quality Objectives and Standard Operating Procedures*. Edited by M.A. Allan. Prepared by the GAW Precipitation Chemistry Science Advisory Group. Pp. 45–47 in Section 4.4.3, Anion Determination by Ion Chromatography.

Appendix 16-A

Supporting Data

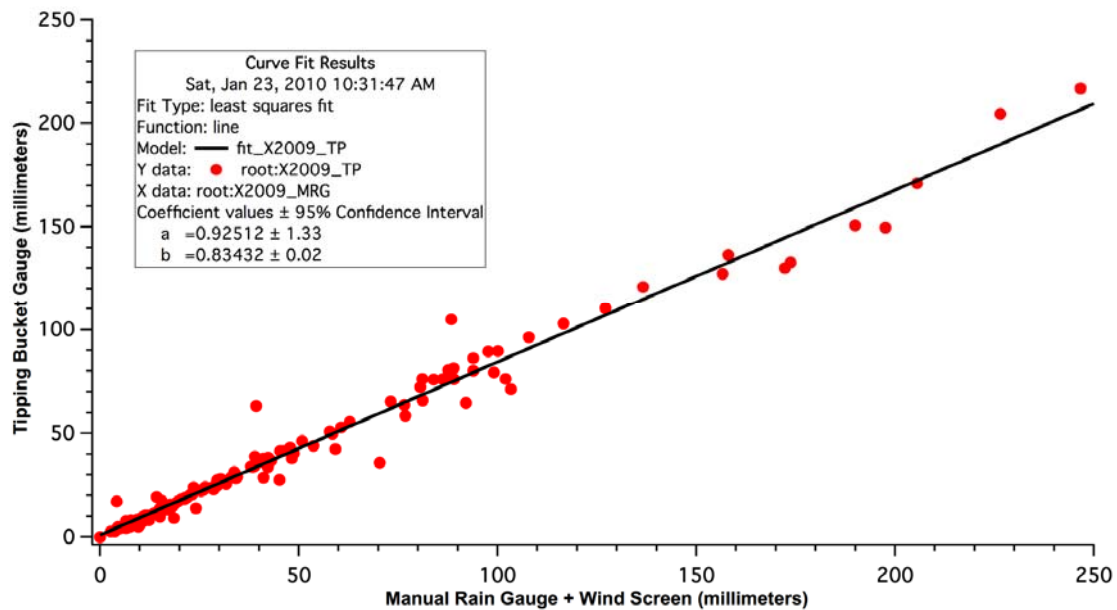


Figure 16-A-1. Relationship between rainfall amounts measured using collocated TP and MRG units. Linear line represents model projection based on least squares fit.



Figure 16-A-2. Example of a deployed MDN collector at Freeman Creek with an associated 80-W solar panel and MRG and TP gauges.



Figure 16-A-3. Example of an assembled throughfall collector.



Figure 16-A-4. Example of deployed throughfall collectors under longleaf pine canopy (TF “LL”).

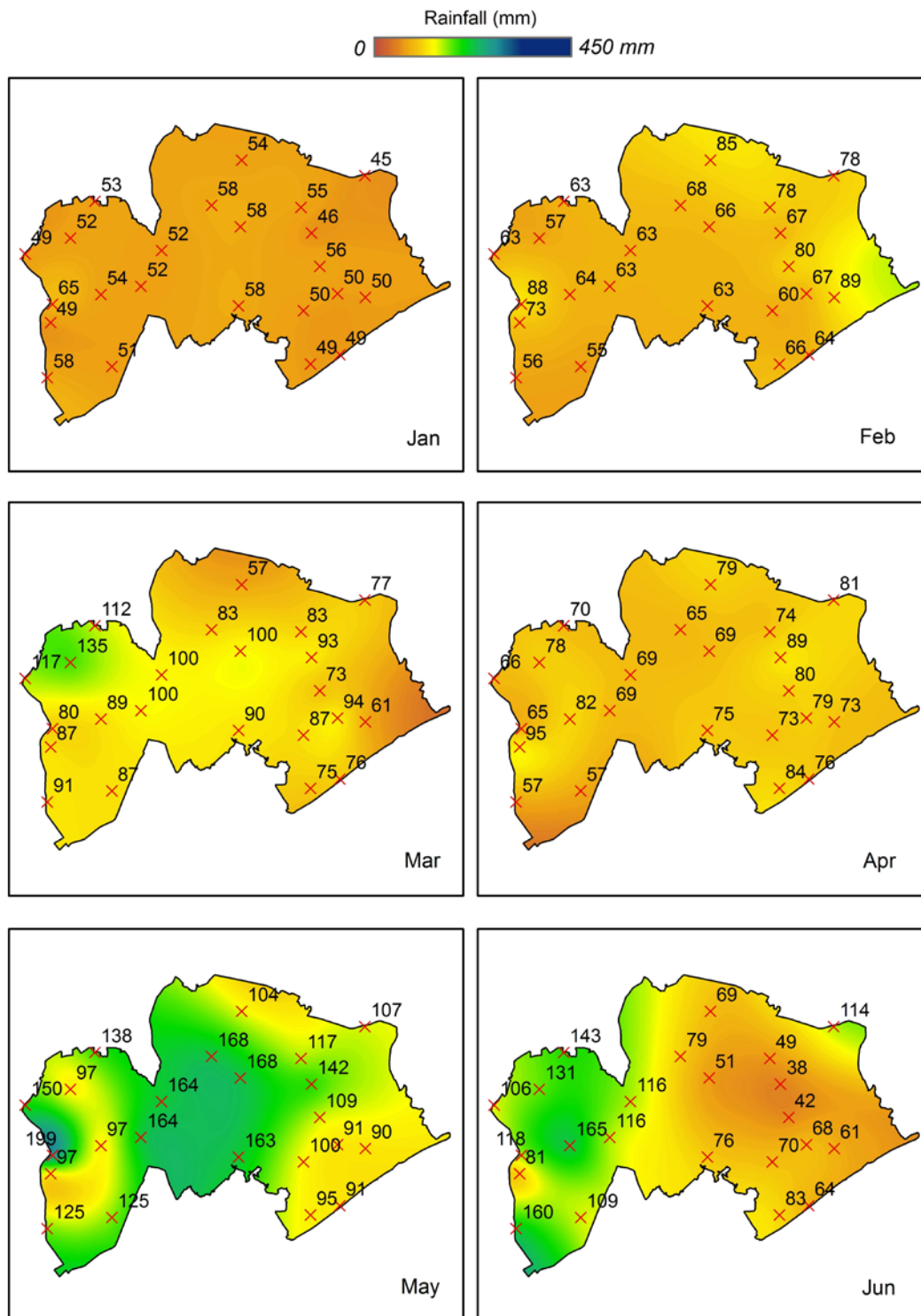


Figure 16-A-5. Surface projections of monthly rainfall amounts based on TPs deployed across MCBCL for the period January–June 2009. The location of each TP is marked with an X along with the monthly total rainfall amount recorded at that location.

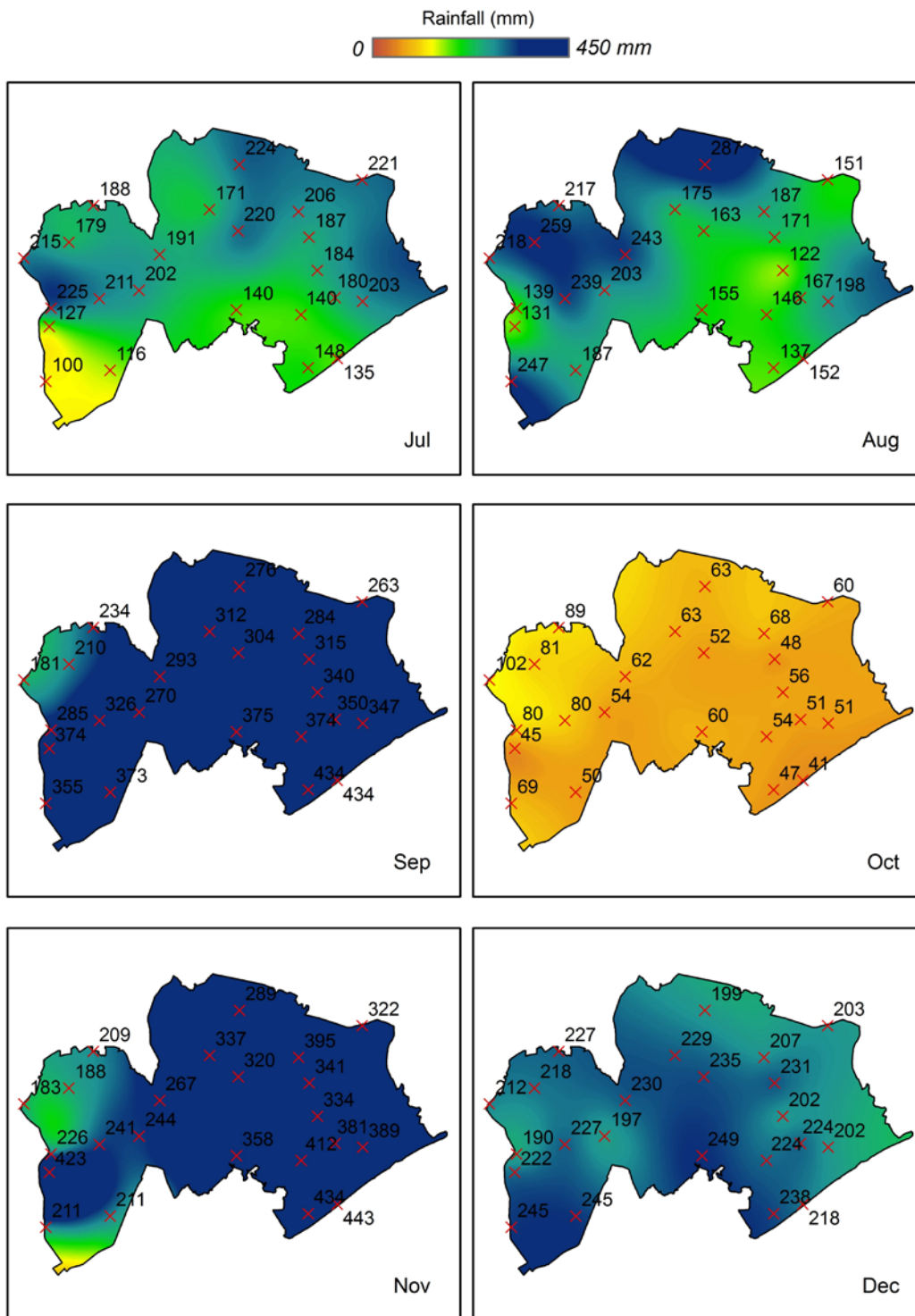


Figure 16-A-6. Surface projections of monthly rainfall amounts based on TPs deployed across MCBCL for the period July–December 2009. The location of each TP is marked with an X along with the monthly total rainfall amount recorded at that location.

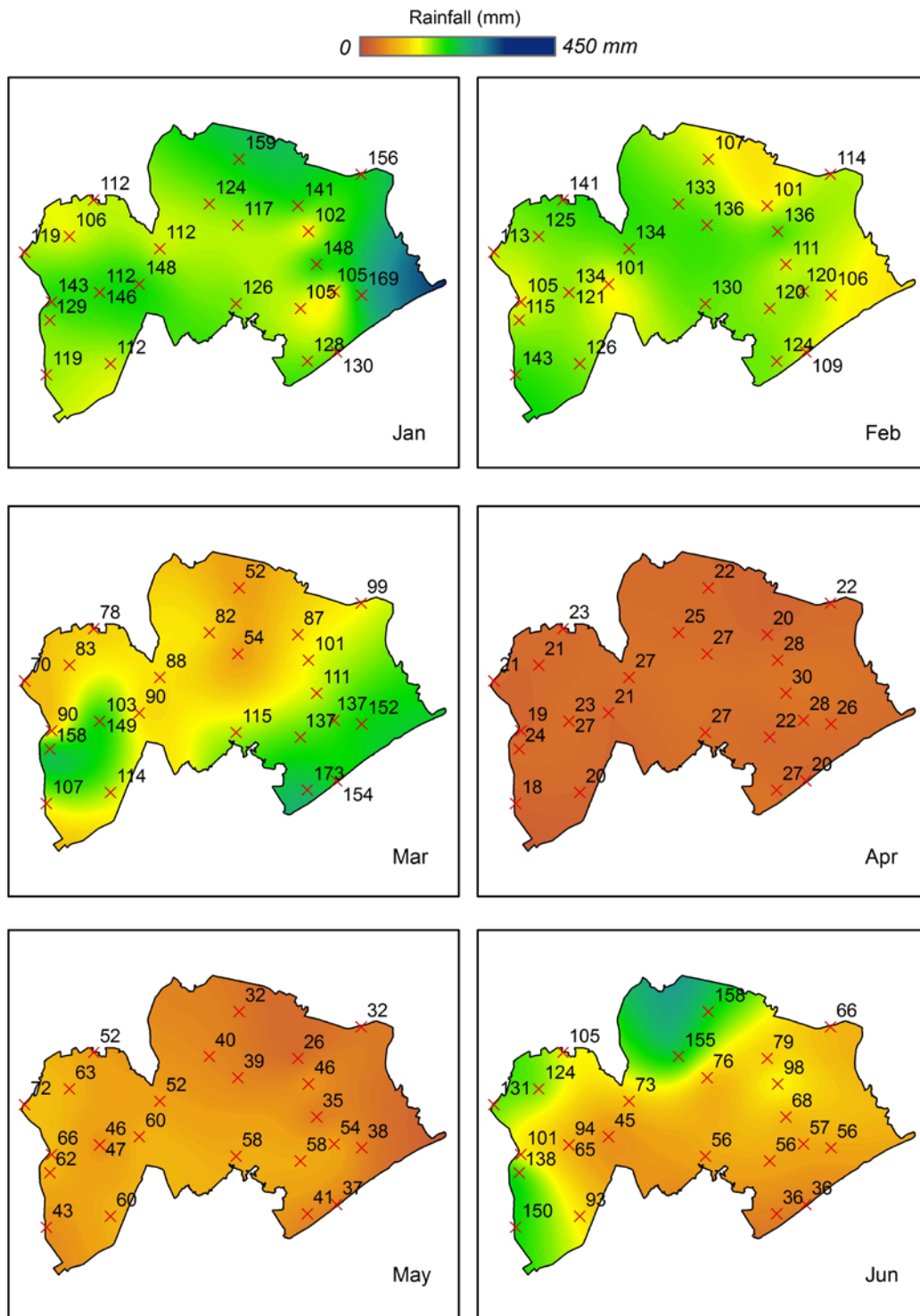


Figure 16-A-7. Surface projections of monthly rainfall amounts based on TPs deployed across MCBCL for the period January–June 2010. The location of each TP is marked with an X along with the monthly total rainfall amount recorded at that location.

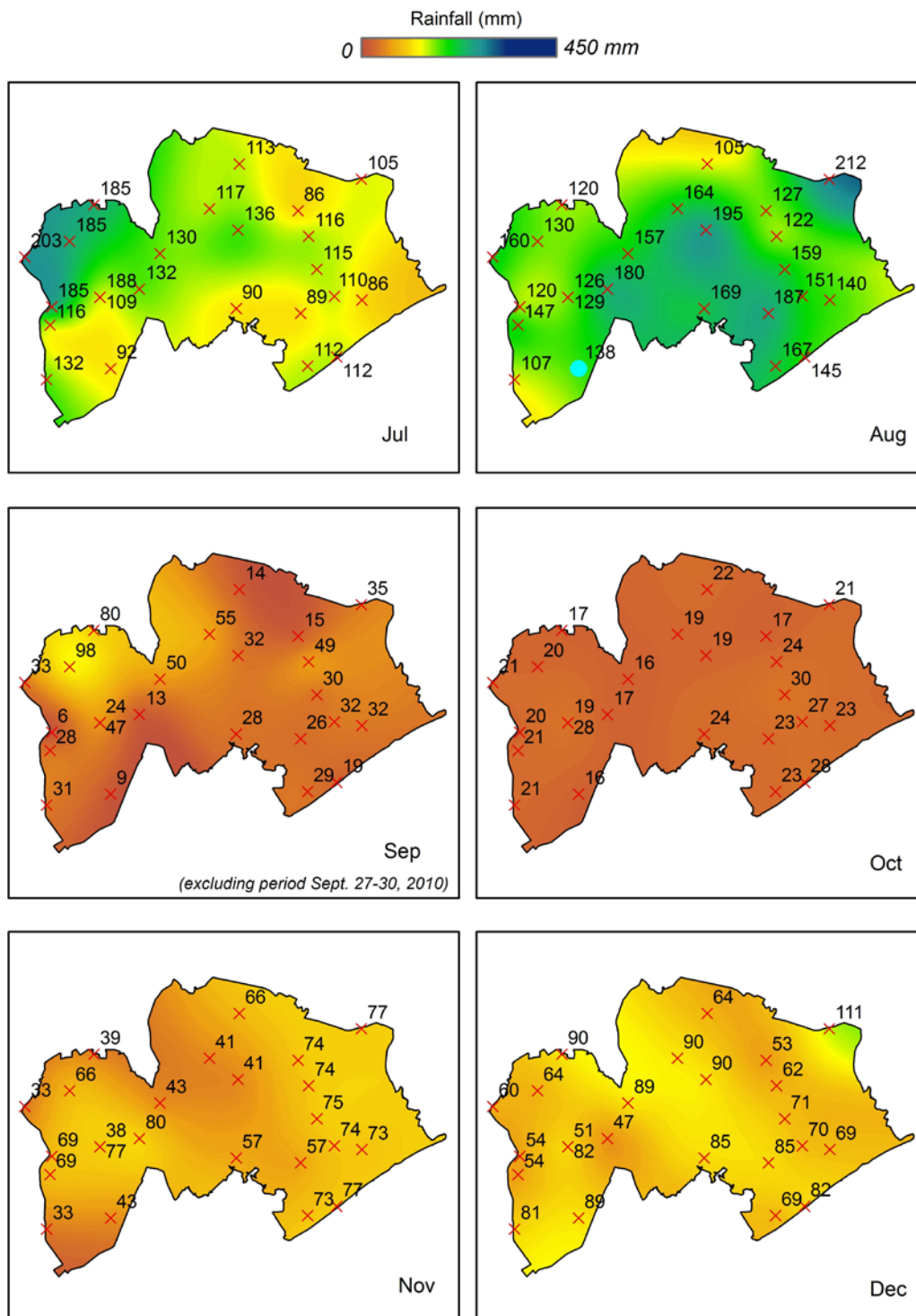


Figure 16-A-8. Surface projections of monthly rainfall amounts based on TPs deployed across MCBCL for the period July–December 2010. The location of each TP is marked with an X along with the monthly total rainfall amount recorded at that location.

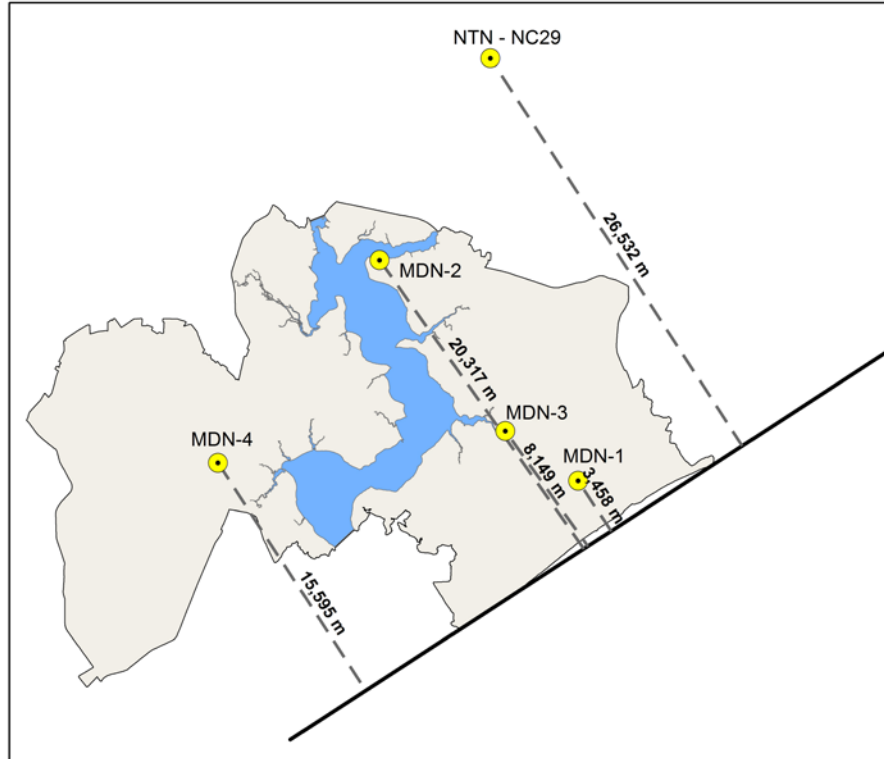


Figure 16-A-9. Distances and positions of MDN collectors and NTN collector NC29 at the Hofmann Forest relative to the shoreline along the eastern boundary of MCBCL.

Table 16-A-1. Output of general liner models analysis (PROC GLM) of TP event data collected at MCBCL. Collector TP 7 was excluded as an outlier due to documented mechanical problems with the TP unit. Zero values were included to create a balanced dataset ($r^2 = 0.906$).

Source	DF	Sum of Squares	Mean Square	F Value	Pr >F
Model	224	49457909.54	220794.24	214.29	<0.0001
Error	4,975	512951.029	1030.34		
Corrected Total	5,199	54583860.83			
Type I Errors					
TP	25	36839.14	1473.57	1.43	0.076
Date	199	49421070.41	248347.09	241.03	<0.0001
Type III Errors					
TP	25	36839.14	1473.57	1.43	0.076
Date	199	49421070.41	248347.09	241.03	<0.0001

Table 16-A-2. Output of quadratic model analysis to determine potential presence of polynomial surface among TP units (excluding unit TP 7). xlong = 100*(longitude–77.5).

Source	DF	Sum of Squares	Mean Square	F Value	Pr >F
Type I Errors					
xlong	1	4638.88	4638.88	4.50	0.034
xlong*xlong	1	10598.00	10598.00	10.29	0.001
Date	199	49421070.41	248347.09	241.13	<0.0001
Type III Errors					
xlong	1	3231.36	3231.36	3.14	0.077
xlong*xlong	1	10598.00	10598.00	10.29	0.001
Date	199	49421070.41	248347.09	241.13	<0.0001
Model Parameters					
Parameter	Standard Estimate	Error	t Value	Pr > t	
Intercept	–1.7397	6.31083	–0.28	0.783	
xlong	0.13831	0.07808	1.77	0.077	
xlong*xlong	0.01467	0.00457	3.21	0.001	
Date	Data varies with date (n=199 coefficients)				

**Table 16-A-3. Combined land covers at MCBCL derived from the 2006 USGS
National Land Cover Database for the Conterminous United States
and used for calculating N-loading for 2010.**

Combined Land Cover	Combined Area (ha)	Original Land Cover	Assigned Area (ha)
Business/residential	2,714	Business of commercial area Residential area	1,972 742
Bare/marsh/shrub	8,677	Bare ground Marshland Shrub or scrub Grasses Cropland	3,941 1,476 3,149 24 86
River/stream/waterway	7,600	River, stream, lake, pond, waterway	7,600
Pine	21,842	Predominantly pine forest Forest plantations under 10 years	19,991 1,851
Mixed pine/hardwoods	7,316	Mixed pine & hardwood forest	7,316
Hardwood	9,647	Upland hardwood forest Bottomland hardwood forest	2,195 7,452
Totals	57,796		57,796

Appendix 16-B

List of Scientific Publications

List of Scientific Publications

Presentations

- Robarge, W.P., K. Baumann, P. Cunningham, and S. Cohen. 2011. *Atmospheric Nitrogen Loading to Marine Corps Base Camp Lejeune (MCBCL): Current and Historical Implications*. Abstract for the SERDP and Environmental Security Technology Certification Program's Partners in Environmental Technology Technical Symposium & Workshop, Washington, DC. November 29–December 1.
- Robarge, W.P., K. Baumann, P. Cunningham, and S. Cohen. 2011. *Nutrient Loading via Atmospheric Deposition to Marine Corps Base Camp Lejeune (MCBCL), Jacksonville, NC*. Presented at the National Atmospheric Deposition Program's Annual Meeting and Scientific Symposium: NADP at the Nexus: Cross System Connections, Renaissance Providence Hotel, Providence, RI. October 24–28.
- Robarge, W.P., R. Austin, K. Baumann, and P. Cunningham. 2009. *Temporal and Spatial Variation in Rainfall at Marine Corps Camp Lejeune, NC, Using Tipping Bucket Gauges*. Presented during Atmospheric Sciences Section A10 of the American Geophysical Union's Fall Meeting, San Francisco, CA. December 14–18.
- Robarge, W.P., R. Austin, K. Baumann, and P. Cunningham. 2009. *Temporal and Spatial Variation in Rainfall at Marine Corps Camp Lejeune (MCBCL), NC, Using Tipping Bucket Gauges*. Presented at the SERDP and Environmental Security Technology Certification Program's Partners in Environmental Technology Symposium, Washington, DC. December 1–3.
- Robarge, W.P., K. Baumann, P. Cunningham, and S. Cohen. 2007. *Assessing the Impact of Wet and Dry Nitrogen Deposition as an Ecosystem Stressor at Marine Corps Base Camp LeJeune (MCBCL), Jacksonville, NC*. Presented at the National Atmospheric Deposition Program's Fall Scientific Meeting, Boulder, CO. September 11–13.